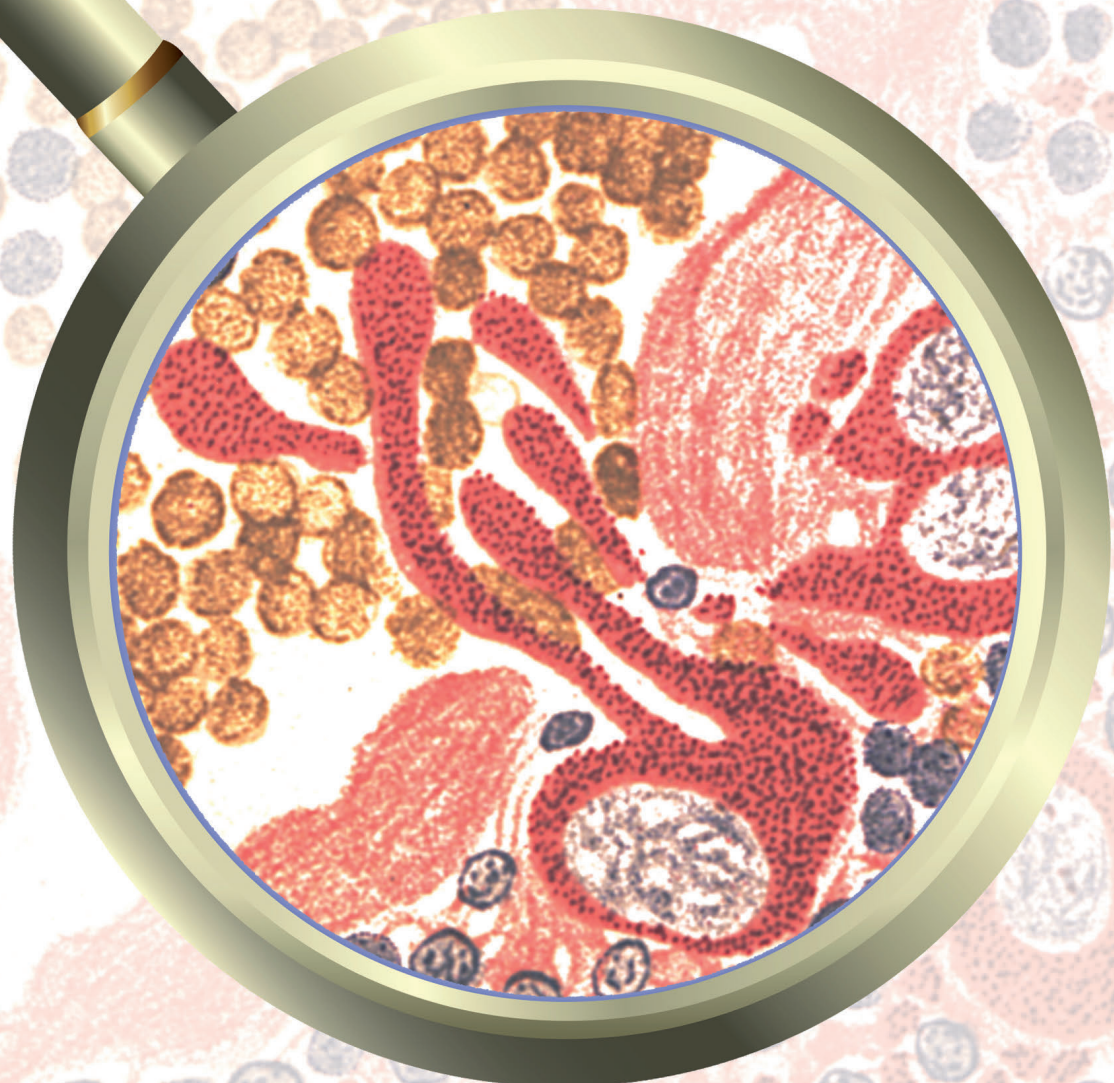




haematologica

Journal of The Ferrata Storti Foundation



ISSN 0390-6078

Volume 105

JUNE

2020 - 06

www.haematologica.org

haematologica

Looking for a definitive source
of information in hematology?

Haematologica is an Open Access
journal: all articles are completely
free of charge

Haematologica
is listed on *PubMed, PubMedCentral,*
DOAJ, Scopus and many other
online directories

5000 / amount of articles read daily

4300 / amount of PDFs downloaded daily

2.20 / gigabytes transferred daily

WWW.HAEMATOLOGICA.ORG

Editor-in-Chief

Luca Malcovati (Pavia)

Deputy Editor

Carlo Balduini (Pavia)

Managing Director

Antonio Majocchi (Pavia)

Associate Editors

Hélène Cavé (Paris), Monika Engelhardt (Freiburg), Steve Lane (Brisbane), PierMannuccio Mannucci (Milan), Simon Mendez-Ferrer (Cambridge), Pavan Reddy (Ann Arbor), Francesco Rodeghiero (Vicenza), Andreas Rosenwald (Wuerzburg), Davide Rossi (Bellinzona), Jacob Rowe (Haifa, Jerusalem), Wyndham Wilson (Bethesda), Swee Lay Thein (Bethesda)

Assistant Editors

Anne Freckleton (English Editor), Britta Dorst (English Editor), Cristiana Pascutto (Statistical Consultant), Rachel Stenner (English Editor),

Editorial Board

Jeremy Abramson (Boston); Paolo Arosio (Brescia); Raphael Bejar (San Diego); Erik Berntorp (Malmö); Dominique Bonnet (London); Jean-Pierre Bourquin (Zurich); Suzanne Cannegieter (Leiden); Francisco Cervantes (Barcelona); Nicholas Chiorazzi (Manhasset); Oliver Cornely (Köln); Michel Delforge (Leuven); Ruud Delwel (Rotterdam); Meletios A. Dimopoulos (Athens); Inderjeet Dokal (London); Hervé Dombret (Paris); Peter Dreger (Hamburg); Martin Dreyling (München); Kieron Dunleavy (Bethesda); Dimitar Efremov (Rome); Sabine Eichinger (Vienna); Jean Feuillard (Limoges); Carlo Gambacorti-Passerini (Monza); Guillermo Garcia Manero (Houston); Christian Geisler (Copenhagen); Piero Giordano (Leiden); Christian Gisselbrecht (Paris); Andreas Greinacher (Greifswald); Hildegard Greinix (Vienna); Paolo Gresele (Perugia); Thomas M. Habermann (Rochester); Claudia Haferlach (München); Oliver Hantschel (Lausanne); Christine Harrison (Southampton); Brian Huntly (Cambridge); Ulrich Jaeger (Vienna); Elaine Jaffe (Bethesda); Arnon Kater (Amsterdam); Gregory Kato (Pittsburg); Christoph Klein (Munich); Steven Knapper (Cardiff); Seiji Kojima (Nagoya); John Koreth (Boston); Robert Kralovics (Vienna); Ralf Küppers (Essen); Ola Landgren (New York); Peter Lenting (Le Kremlin-Bicetre); Per Ljungman (Stockholm); Francesco Lo Coco (Rome); Henk M. Lokhorst (Utrecht); John Mascarenhas (New York); Maria-Victoria Mateos (Salamanca); Giampaolo Merlini (Pavia); Anna Rita Migliaccio (New York); Mohamad Mohty (Nantes); Martina Muckenthaler (Heidelberg); Ann Mullally (Boston); Stephen Mulligan (Sydney); German Ott (Stuttgart); Jakob Passweg (Basel); Melanie Percy (Ireland); Rob Pieters (Utrecht); Stefano Pileri (Milan); Miguel Piris (Madrid); Andreas Reiter (Mannheim); Jose-Maria Ribera (Barcelona); Stefano Rivella (New York); Francesco Rodeghiero (Vicenza); Richard Rosenquist (Uppsala); Simon Rule (Plymouth); Claudia Scholl (Heidelberg); Martin Schrappe (Kiel); Radek C. Skoda (Basel); Gérard Socié (Paris); Kostas Stamatopoulos (Thessaloniki); David P. Steensma (Rochester); Martin H. Steinberg (Boston); Ali Taher (Beirut); Evangelos Terpos (Athens); Takanori Teshima (Sapporo); Pieter Van Vlierberghe (Gent); Alessandro M. Vannucchi (Firenze); George Vassiliou (Cambridge); Edo Vellenga (Groningen); Umberto Vitolo (Torino); Guenter Weiss (Innsbruck).

Editorial Office

Simona Giri (Production & Marketing Manager), Lorella Ripari (Peer Review Manager), Paola Cariati (Senior Graphic Designer), Igor Ebuli Poletti (Senior Graphic Designer), Marta Fossati (Peer Review), Diana Serena Ravera (Peer Review)

Affiliated Scientific Societies

SIE (Italian Society of Hematology, www.siematologia.it)

SIES (Italian Society of Experimental Hematology, www.siesonline.it)

Information for readers, authors and subscribers

Haematologica (print edition, pISSN 0390-6078, eISSN 1592-8721) publishes peer-reviewed papers on all areas of experimental and clinical hematology. The journal is owned by a non-profit organization, the Ferrata Storti Foundation, and serves the scientific community following the recommendations of the World Association of Medical Editors (www.wame.org) and the International Committee of Medical Journal Editors (www.icmje.org).

Haematologica publishes editorials, research articles, review articles, guideline articles and letters. Manuscripts should be prepared according to our guidelines (www.haematologica.org/information-for-authors), and the Uniform Requirements for Manuscripts Submitted to Biomedical Journals, prepared by the International Committee of Medical Journal Editors (www.icmje.org).

Manuscripts should be submitted online at <http://www.haematologica.org/>.

Conflict of interests. According to the International Committee of Medical Journal Editors (<http://www.icmje.org/#conflicts>), "Public trust in the peer review process and the credibility of published articles depend in part on how well conflict of interest is handled during writing, peer review, and editorial decision making". The ad hoc journal's policy is reported in detail online (www.haematologica.org/content/policies).

Transfer of Copyright and Permission to Reproduce Parts of Published Papers. Authors will grant copyright of their articles to the Ferrata Storti Foundation. No formal permission will be required to reproduce parts (tables or illustrations) of published papers, provided the source is quoted appropriately and reproduction has no commercial intent. Reproductions with commercial intent will require written permission and payment of royalties.

Detailed information about subscriptions is available online at www.haematologica.org. Haematologica is an open access journal. Access to the online journal is free. Use of the Haematologica App (available on the App Store and on Google Play) is free.

For subscriptions to the printed issue of the journal, please contact: Haematologica Office, via Giuseppe Belli 4, 27100 Pavia, Italy (phone +39.0382.27129, fax +39.0382.394705, E-mail: info@haematologica.org).

Rates of the International edition for the year 2019 are as following:

	<i>Institutional</i>	<i>Personal</i>
<i>Print edition</i>	<i>Euro 700</i>	<i>Euro 170</i>

Advertisements. Contact the Advertising Manager, Haematologica Office, via Giuseppe Belli 4, 27100 Pavia, Italy (phone +39.0382.27129, fax +39.0382.394705, e-mail: marketing@haematologica.org).

Disclaimer. Whilst every effort is made by the publishers and the editorial board to see that no inaccurate or misleading data, opinion or statement appears in this journal, they wish to make it clear that the data and opinions appearing in the articles or advertisements herein are the responsibility of the contributor or advisor concerned. Accordingly, the publisher, the editorial board and their respective employees, officers and agents accept no liability whatsoever for the consequences of any inaccurate or misleading data, opinion or statement. Whilst all due care is taken to ensure that drug doses and other quantities are presented accurately, readers are advised that new methods and techniques involving drug usage, and described within this journal, should only be followed in conjunction with the drug manufacturer's own published literature.

Direttore responsabile: Prof. Carlo Balduini; Autorizzazione del Tribunale di Pavia n. 63 del 5 marzo 1955.
Printing: Press Up, zona Via Cassia Km 36, 300 Zona Ind.le Settevene - 01036 Nepi (VT)



Associated with USPI, Unione Stampa Periodica Italiana.
Premiato per l'alto valore culturale dal Ministero dei Beni Culturali ed Ambientali

Table of Contents

Volume 105, Issue 6: June 2020

About the cover

- 1467** 100-YEAR-OLD HAEMATOLOGICA IMAGES: THE QUARREL ABOUT THE ORIGIN OF PLATELETS (II)
Carlo L. Balduini

Editorials

- 1468** Keys to drug sensitivity from updated functional work flows
Stephen E. Kurtz and Jeffrey W. Tyner
- 1470** To target the untargetable: elucidation of synergy of APR-246 and azacitidine in *TP53* mutant myelodysplastic syndromes and acute myeloid leukemia
David A. Sallman
- 1472** Peripheral T-cell lymphoma diagnosis: building a molecular tool
Miguel A Piris
- 1474** PIKING the next therapeutic target in multiple myeloma
Jessica L. Caro and Faith E. Davies
- 1475** The increasing complexity of the management of core-binding factor acute myeloid leukemia
Mark R. Litzow

Perspective Article

- 1478** Immunological consequences of extramedullary erythropoiesis: immunoregulatory functions of CD71⁺ erythroid cells
Shokrollah Elahi and Siavash Mashhour

Review Articles

- 1484** Geriatric assessment in older patients with a hematologic malignancy: a systematic review
Ellen R.M. Scheepers et al.
- 1494** The regulation and function of CD20: an “enigma” of B-cell biology and targeted therapy
Gabriela Pavlasova and Marek Mráz

Guideline Article

- 1507** Clinical practice recommendation on hematopoietic stem cell transplantation for acute myeloid leukemia patients with *FLT3*-internal tandem duplication: a position statement from the Acute Leukemia Working Party of the European Society for Blood and Marrow Transplantation
Ali Bazarbachi et al.

Articles

Hematopoiesis

- 1517** *DKC1* is a transcriptional target of GATA1 and drives upregulation of telomerase activity in normal human erythroblasts
Laura A. Richard et al.
- 1527** Multi-parametric single cell evaluation defines distinct drug responses in healthy hematologic cells that are retained in corresponding malignant cell types
Muntasir M. Majumder et al.

Myelodysplastic Syndromes

- 1539** Synergistic effects of PRIMA-1^{Met} (APR-246) and 5-azacitidine in *TP53*-mutated myelodysplastic syndromes and acute myeloid leukemia
Nabih Maslah et al.

Acute Myeloid Leukemia

- 1552** The prevalence of extramedullary acute myeloid leukemia detected by ¹⁸F-FDG-PET/CT: final results from the prospective PETAML trial
Friedrich Stölzel et al.
- 1559** Obesity is a risk factor for acute promyelocytic leukemia: evidence from population and cross-sectional studies and correlation with *FLT3* mutations and polyunsaturated fatty acid metabolism
Luca Mazzarella et al.

Myeloid Neoplasms

- 1567** Oral arsenic trioxide ORH-2014 pharmacokinetic and safety profile in patients with advanced hematologic disorders
Farhad Ravandi et al.

Acute Lymphoblastic Leukemia

- 1575** Low level CpG island promoter methylation predicts a poor outcome in adult T-cell acute lymphoblastic leukemia
Aurore Touzart et al.

Non-Hodgkin Lymphoma

- 1582** Defining signatures of peripheral T-cell lymphoma with a targeted 20-marker gene expression profiling assay
Fanny Drieux et al.
- 1593** The architecture of neoplastic follicles in follicular lymphoma; analysis of the relationship between the tumor and follicular helper T cells
William Townsend et al.
- 1604** *KMT2D* mutations and *TP53* disruptions are poor prognostic biomarkers in mantle cell lymphoma receiving high-dose therapy: a FIL study
Simone Ferrero et al.

Chronic Lymphocytic Leukemia

- 1613** A laboratory-based scoring system predicts early treatment in Rai 0 chronic lymphocytic leukemia
Jared A. Cohen et al.
- 1621** IGHV mutational status and outcome for patients with chronic lymphocytic leukemia upon treatment: a Danish nationwide population-based study
Emelie Curovic Rotbain et al.

Plasma Cell Disorders

- 1630** Hypoxia-induced long non-coding RNA DARS-AS1 regulates RBM39 stability to promote myeloma malignancy
Jia Tong et al.
- 1641** Identification of PIKfyve kinase as a target in multiple myeloma
Cecilia Bonolo de Campos et al.
- 1650** Health-related quality of life in transplant ineligible newly diagnosed multiple myeloma patients treated with either thalidomide or lenalidomide-based regimen until progression: a prospective, open-label, multicenter, randomized, phase 3 study
Lene Kongsgaard Nielsen et al.

Platelet Biology & its Disorders

- 1660** Glycoprotein Ib clustering in platelets can be inhibited by α -linolenic acid as revealed by cryo-electron tomography
Simona Stivala et al.
- 1667** Coactosin-like 1 integrates signaling critical for shear-dependent thrombus formation in mouse platelets
Inga Scheller et al.

Hemostasis

- 1677** LIM-only protein FHL2 attenuates vascular tissue factor activity, inhibits thrombus formation in mice and *FHL2* genetic variation associates with human venous thrombosis
Chantal Kroone et al.
- 1686** Placenta-derived extracellular vesicles induce preeclampsia in mouse models
Cha Han et al.

Coagulation & its Disorders

- 1695** D' domain region Arg782-Cys799 of von Willebrand factor contributes to factor VIII binding
Małgorzata A. Przeradzka et al.
- 1704** Thrombotic biomarkers for risk prediction of malignant disease recurrence in patients with early stage breast cancer
Cinzia Giaccherini et al.
- 1712** Ile73Asn mutation in protein C introduces a new N-linked glycosylation site on the first EGF-domain of protein C and causes thrombosis
Yeling Lu et al.

Stem Cell Transplantation

- 1723** Allogeneic stem cell transplantation in second complete remission for core binding factor acute myeloid leukemia: a study from the Acute Leukemia Working Party of the European Society for Blood and Marrow Transplantation
Kazimierz Halaburda et al.

Cell Therapy & Immunotherapy

- 1731** Yttrium-90-labeled anti-CD45 antibody followed by a reduced-intensity hematopoietic cell transplantation for patients with relapsed/refractory leukemia or myelodysplasia
Phuong Vo et al.

Transfusion Medicine

- 1738** Genetic platelet depletion is superior in platelet transfusion compared to current models
Manuel Salzmann et al.

Letters to the Editor

Letters are available online only at www.haematologica.org/content/105/6.toc

- e264** Clonal hematopoiesis in patients with anti-neutrophil cytoplasmic antibody-associated vasculitis
Christopher Maximilian Arends et al.
<http://www.haematologica.org/content/105/6/e264>
- e268** PIEZO1 gain-of-function mutations delay reticulocyte maturation in hereditary xerocytosis
Pedro L. Moura et al.
<http://www.haematologica.org/content/105/6/e268>
- e272** Hydroxyurea to lower transcranial Doppler velocities and prevent primary stroke: the Uganda NOHARM sickle cell anemia cohort
Robert O. Opoka et al.
<http://www.haematologica.org/content/105/6/e272>
- e276** Myeloid neoplasms with isolated del(5q) and *JAK2* V617F mutation: a "grey zone" combination of myelodysplastic and myeloproliferative features?
Valentina F.I. Sangiorgio et al.
<http://www.haematologica.org/content/105/6/e276>
- e280** Inflammation regulates long non-coding RNA-PTTG1-1:1 in myeloid leukemia
Sébastien Chateauvieux et al.
<http://www.haematologica.org/content/105/6/e284>
- e285** The microRNA miR-196b acts as a tumor suppressor in Cdx2 driven acute myeloid leukemia
Vijay P. S. Rawat, et al.
<http://www.haematologica.org/content/105/6/e285>

- e290** RNAmut: robust identification of somatic mutations in acute myeloid leukemia using RNA-sequencing
Muxin Gu et al.
<http://www.haematologica.org/content/105/6/e290>
- e294** Unique clinico-biological, genetic and prognostic features of adult early T-cell precursor acute lymphoblastic leukemia
Eulàlia Genescà et al.
<http://www.haematologica.org/content/105/6/e294>
- e298** High frequency of chronic lymphocytic leukemia-like low-count monoclonal B-cell lymphocytosis in Japanese descendants living in Brazil
Mariane de Faria-Moss et al.
<http://www.haematologica.org/content/105/6/e298>
- e302** Effect of daratumumab on normal plasma cells, polyclonal immunoglobulin levels, and vaccination responses in extensively pre-treated multiple myeloma patients
Kristine A. Frerichs et al.
<http://www.haematologica.org/content/105/6/e302>
- e307** Safety of using direct oral anticoagulants in the diagnostic workup of outpatients with suspicion of acute venous thromboembolism
Maddie S. Stephen et al.
<http://www.haematologica.org/content/105/6/e307>
- e310** Mental fatigue after allogeneic hematopoietic stem cell transplantation is associated with cognitive dysfunction, but not central nervous system inflammation
Erik Boberg et al.
<http://www.haematologica.org/content/105/6/e310>

Case Reports

Case Reports are available online only at www.haematologica.org/content/105/6.toc

- e315** *IGH* rearrangement in myeloid neoplasms
Amy W. Xiao et al.
<http://www.haematologica.org/content/105/6/e315>
- e318** Genetic heterogeneity highlighted by differential FDG-PET response in diffuse large B-cell lymphoma
Shamzah Araf et al.
<http://www.haematologica.org/content/105/6/e318>
- e322** Excellent proliferation and persistence of allogeneic donor-derived 41-BB based CAR-T cells despite immunosuppression with cyclosporine A
Francis Ayuk et al.
<http://www.haematologica.org/content/105/6/e322>

100-YEAR-OLD HAEMATOLOGICA IMAGES: THE QUARREL ABOUT THE ORIGIN OF PLATELETS (II)

Carlo L. Balduini

*Ferrata-Storti Foundation, Pavia, Italy**E-mail: CARLO L. BALDUINI - carlo.balduini@unipv.it**doi:10.3324/haematol.2020.254011*

At the time of the birth of Haematologica in 1920, the origin of platelets was still a hotly debated topic, as demonstrated by the observation that five of the 31 articles published in the first volume of the journal dealt with the genesis of these corpuscles.¹

The cover of this issue of Haematologica has been taken from one of the figures of the article entitled "Facts and hypotheses on the origin of platelets" published in Haematologica in 1923 by Antonio Cesaris Demel, Professor of Pathology at the University of Pisa, Italy.² The author stimulated megakaryopoiesis in cats with 'fairly rapid asphyxiation' of the animals, and then studied sections of their spleens stained with Giemsa. Cesaris Demel observed that, on stimulation of megakaryopoiesis, megakaryocytes migrate to the vessel, introduce pseudopods into the vascular wall, and sometimes pass in their entirety into the lumen of the vessel. During this process, platelets detach from the surface of the cell in contact with blood. These findings of Cesaris Demel seem to confirm the hypothesis formulated in 1906 by Wright that platelets are produced from megakaryocytes.³ However, unexpectedly, the author concluded that they are not fragments of megakaryocytes, but instead derive from a not clearly defined plasma component

that precipitates in contact with the surface of megakaryocytes "as", he wrote, "fibrin is formed by precipitation of plasma components under specific conditions".

Although this conclusion was wrong, the Cesaris Demel drawings are extraordinary because they describe proplatelet formation exactly as we know it occurs today after nearly a century of studies with increasingly sophisticated technologies.⁴ As already discussed in previous comments to old Haematologica images, knowledge of blood cells a century ago, obtained almost exclusively by observing blood and tissues under a microscope, was much more advanced than is commonly believed.

References

1. Mazzarello P. One hundred years of Haematologica. *Haematologica*. 2020;105(1):12-21.
2. Cesaris Demel A. [Fatti ed ipotesi sulla origine delle piastrine]. *Haematologica*. 1924;5:104-146.
3. Wright JH. The origin and nature of the blood plates. *Boston Medic. Surg. J.* 1906;154:643-645.
4. Italiano JE Jr, Lecine P, Shivdasani RA, Hartwig JH. Blood platelets are assembled principally at the ends of proplatelet processes produced by differentiated megakaryocytes. *J Cell Biol.* 1999;147(6):1299-1312.



Figure 1. Platelet formation in cat spleen as described by Cesaris Demel in Haematologica in 1923. The introduction of long and thin protrusions of megakaryocytes into the lumen of vessel, as well as the migration of the entire megakaryocyte into the vessel, has been 'rediscovered' only recently.

Keys to drug sensitivity from updated functional work flows

Stephen E. Kurtz¹ and Jeffrey W. Tyner^{1,2}

¹Division of Hematology and Medical Oncology and ²Department of Cell, Developmental and Cancer Biology, Knight Cancer Institute, Oregon Health and Science University, Portland, OR, USA

E-mail: JEFFREY W. TYNER - tynerj@ohsu.edu

doi:10.3324/haematol.2020.250662

A primary goal of cancer therapy is to match patients with the most appropriate drug regimens. Identifying characteristics of patients who respond to therapies and devising alternative strategies for non-responsive patients are important clinical considerations. Next generation sequencing (NGS) has provided a central technology to reveal genetic alterations and guide this process. Additionally, the development of cancer therapies that target specific signaling pathways and subcellular components has increased the opportunity for matching patients with molecularly targeted drugs. In practice, however, limitations in understanding the relationship between cancer genotypes and their corresponding phenotypes have hindered this process; somatic cancer mutations do not always reliably suggest therapies. Indeed, in some cases, targeted drugs have shown clinical utility when matched to cell phenotypes rather than somatic genotype. In this way, the use of orthogonal technologies, such as functional testing and immune-profiling, integrated with NGS holds promise to improve outcomes by better matching therapies to individual patients.¹ In addition, lack of durable efficacy of many categories of therapies has sometimes been attributed to inadequate elimination or targeting of leukemic stem/progenitor cells (reviewed by Rossi *et al.*²).

In this issue, Majumder *et al.* report on the manner by which understanding of innate drug sensitivities in healthy hematopoietic cells advances both the identification of lineage-specific anti-cancer therapies as well as off-target drug effects in treating acute myeloid leukemia.³ Underlying this work is the well-characterized biology of hematopoiesis whereby multipotent stem cells and precursors differentiate through distinct signaling pathways to generate a set of blood cell types with discrete phenotypes and functions. The authors surmise that malignant hematopoietic cells use the same signaling pathways; consequently, they leverage specific pathways from normal cells as a means to identify cancer therapies for their malignant counterparts. Conversely, the authors note that drug responses seen in healthy cells may reveal potential adverse effects.

The authors augment their established cell-based screening platform for identifying anti-leukemia drugs⁴ with high capacity flow cytometry (Figure 1A). This technological development permits the simultaneous evaluation of drug responses from multiple hematopoietic cell populations based on their respective surface antigens. Drug responses are mapped to proteome and cell type specific signaling profiles using mass spectrometry and mass cytometry. In this study, sensitivities to 71 small molecules were simultaneously assessed using multi-parametric flow cytometry and then mapped to proteomic and signaling profiles to characterize the spectrum of drug

responses in various hematopoietic cell types. Across healthy cell types for B cells, natural killer (NK) cells, helper T cells, cytotoxic T cells and monocytes, the authors identify cell lineage-specific drug responses to define a global view of response profiles. By comparing drug responses between healthy and neoplastic cells, they show that healthy cell responses predict drug responses in corresponding malignant cells. The authors evaluate this screening approach on a large cohort of primary samples obtained from healthy donors and patients with myeloid and lymphoid leukemias, providing evidence that this method identifies new applications for the tested drugs.

A key highlight of this study is the profile observed for the BCL2 inhibitor, venetoclax, which revealed dose-dependent sensitivities across the hematopoietic cell types (Figure 1B). At the ends of this spectrum, B cells (CD19⁺) were the most sensitive whereas monocytes and granulocytes were the least sensitive to venetoclax. Moderate sensitivities were observed on cytotoxic and helper T cells (CD3⁺CD4⁺ and CD3⁺CD4⁻), NK cells (CD56⁺), and NK-T cells (CD3⁺CD56⁺). Venetoclax had similar cell-specific effects regardless of disease status (healthy vs. malignant) indicating the variable nature of response to venetoclax is lineage specific. In addition, the study found an inverse relationship between venetoclax sensitivity and levels of phosphorylated STAT3. Monocytes and granulocytes have the highest levels of phosphorylated STAT3 and the lowest venetoclax sensitivity, perhaps reflecting the different transcriptional programs defining these two cell types.

Previous work by these authors and others indicated that BCL2 is differentially expressed in subpopulations of AML cells enriched for malignant stem/progenitor cells compared to more differentiated tumor cells⁵ and that venetoclax sensitivity in primary AML cells with a monocytic phenotype is reduced.⁶ These observations led to the hypothesis that clinical features of AML indicative of myeloid differentiation status may correlate with reduced BCL2 dependence in AML patients. Indeed, the venetoclax response profile in this study is consistent with recent findings correlating venetoclax sensitivity with stages of AML disease differentiation as defined by flow cytometry.⁷ In the context of venetoclax-based therapies, phenotypically primitive AML is sensitive whereas monocytic AML is more resistant, due to intrinsic properties of monocytic AML cells including loss of BCL2 expression and reliance on MCL1 to mediate oxidative phosphorylation and survival.

Cumulatively, these findings raise the possibility of new definitions for stem/progenitor cells in hematologic malignancies; definitions that would be based on propensity of cell types of any maturation state to persist in the face of a selective pressure. In some ways, these findings may also call into question the long-held notions that targeting

of more primitive leukemic cell populations will hold the key to durable disease control. It seems possible that most cancer therapeutics utilized to date are simply more active against more mature cell types based on targeting of biological programs that are more prominent in these more mature cells. The identification of drugs that show inversely preferential activity against the more primitive cell states is an example of the enormous benefit that can be derived from this updated platform for flow cytometric drug sensitivity assessment.

Majumder *et al.* speculate that their profiling will open

new opportunities for other disease indications. As examples, they note that dexamethasone and midostaurin targeted NK cells as effectively as B cells, suggesting their potential clinical use in NK-cell malignancies. They further envision incorporating cell lineage specific drug responses into the regimen for preclinical drug development will identify unexpected therapeutic niches for small molecules and enhanced therapeutic precision. Their study provides additional support for the concept of using multiple diagnostic technologies to enhance precision therapy. Indeed, the use of this technology platform to identify

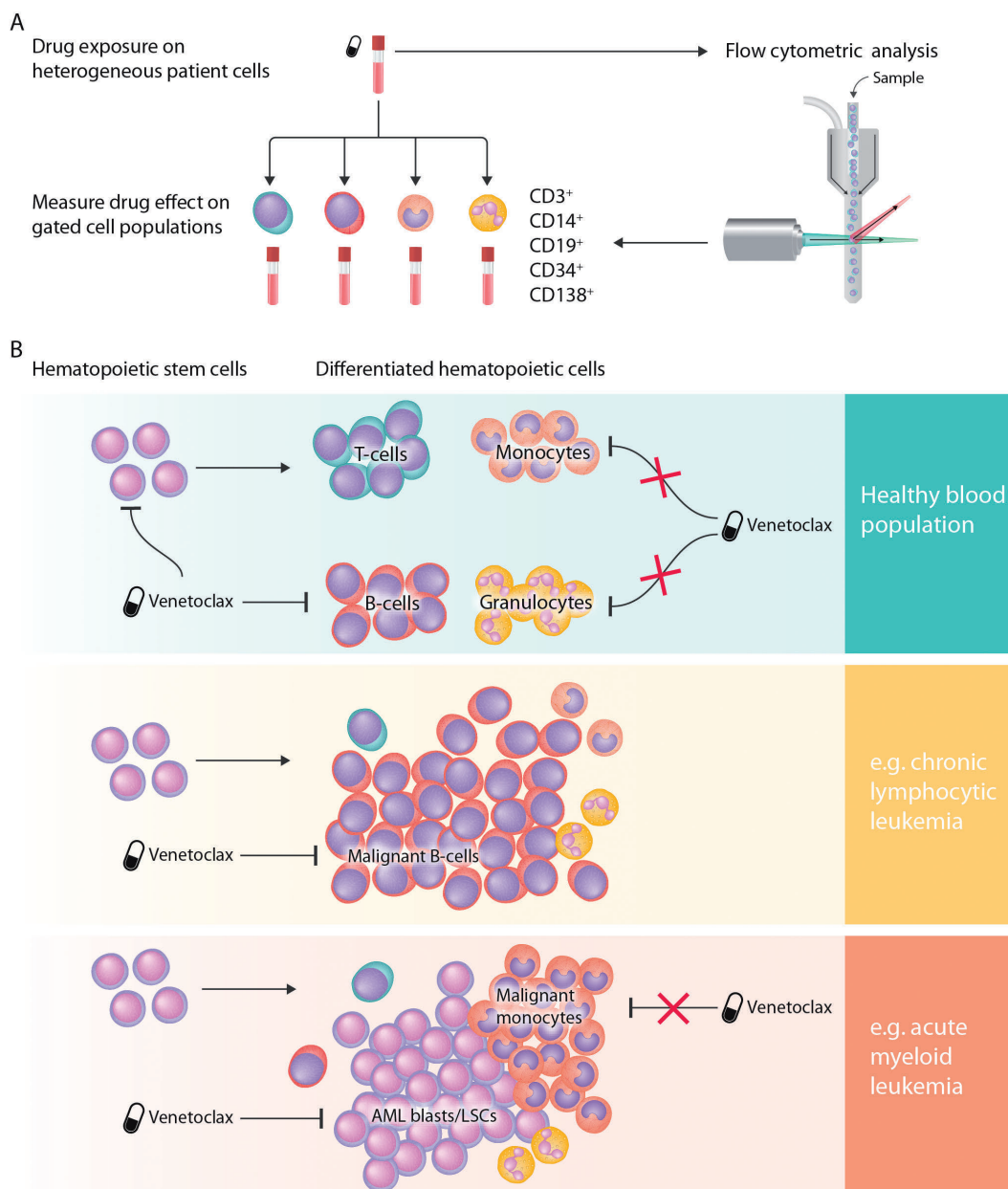


Figure 1. High-throughput flow cytometry functional screening strategy identifies drug effects on discrete cell lineages. (A) Schematic for screening workflow whereby cells from leukemia patient samples are exposed to a library of drugs and then subjected to flow cytometry using antibodies to distinguish discrete cell populations, such as T cells (CD3), B cells (CD19), monocytes (CD14), hematopoietic stem/progenitor cells (CD34), etc. (B) Results from the workflow in (A) have shown that drugs have differential effects on cell lineage states, which are often conserved between malignant and healthy settings. As an example, the BCL2 inhibitor, venetoclax, was shown to have more effect against less differentiated cells as well as mature B cells and less impact on mature monocytes and granulocytes in cells from healthy donors. This observation extended to these same cell states in leukemia patient samples, where venetoclax was more effective in killing mature B cells in chronic lymphocytic leukemia and leukemic progenitor cells in acute myeloid leukemia (AML), but was less effective against malignant monocytes in the same AML samples.

drug combinations that can simultaneously target the undifferentiated leukemic cell populations as well as the more mature myeloid lineages (especially monocytes) may represent a powerful way to prioritize the most promising drug combinations for pre-clinical study and for clinical development. Clearly, this report demonstrates just the beginning of utility of this exciting drug screening platform.

References

1. Friedman AA, Letai A, Fisher DE, Flaherty KT. Precision medicine for cancer with next-generation functional diagnostics. *Nat Rev Cancer*. 2015;15(12):747-756.
2. Rossi DJ, Jamieson CH, Weissman IL. Stems cells and the pathways to aging and cancer. *Cell*. 2008;132(4):681-696.
3. Majumder MM, Leppa AM, Hellesoy M, et al. Multi-parametric single cell evaluation defines distinct drug responses in healthy hematological cells that are retained in corresponding malignant cell types. *Haematologica*. 2020;105(6):1527-1538.
4. Pemovska T, Kontro M, Yadav B, et al. Individualized systems medicine strategy to tailor treatments for patients with chemorefractory acute myeloid leukemia. *Cancer Discov*. 2013;3(12):1416-1429.
5. Lagadinou ED, Sach A, Callahan K, et al. BCL-2 inhibition targets oxidative phosphorylation and selectively eradicates quiescent human leukemia stem cells. *Cell Stem Cell*. 2013;12(3):329-341.
6. Kuusanmaki H, Leppa AM, Polonen P, et al. Phenotype-based drug screening reveals association between venetoclax response and differentiation stage in acute myeloid leukemia. *Haematologica*. 2020;105(3):708-720.
7. Pei S, Pollyea DA, Gustafson A, et al. Monocytic Subclones Confer Resistance to Venetoclax-Based Therapy in Patients with Acute Myeloid Leukemia. *Cancer Discov*. 2020;10(4):536-551.

To target the untargetable: elucidation of synergy of APR-246 and azacitidine in TP53 mutant myelodysplastic syndromes and acute myeloid leukemia

David A. Sallman

Department of Malignant Hematology, H. Lee Moffitt Cancer Center, Tampa, FL, USA

E-mail: DAVID A. SALLMAN - david.sallman@moffitt.org

doi:10.3324/haematol.2020.249060

Mutations of the tumor suppressor gene *TP53* represent a common mutation in myeloid malignancies, occurring in 10-20% of patients with *de novo* myelodysplastic syndromes (MDS) and acute myeloid leukemia (AML) with profound negative impact on outcomes and a median overall survival (OS) of 6-12 months.¹⁻³ Critically, the clonal burden of *TP53*, that is the variant allele frequency (VAF) and/or allelic state of *TP53*, is intimately tied with the clinical trajectory of these patients and is a robust, independent predictor of survival.^{4,7} Given the poor OS and lack of therapeutic options for *TP53* mutant MDS/AML patients, a number of novel agents are being investigated in this patient group.⁸ Of these, APR-246 has evoked considerable excitement based on its robust clinical efficacy in combination with azacitidine in *TP53* mutant MDS/AML patients.^{9,10} In this issue of *Haematologica*,¹¹ Maslah *et al.* describe compelling preclinical synergy of APR-246 in combination with azacitidine in *TP53* mutated MDS and AML and, more importantly, identify a novel molecular mechanism underlying the observed synergy.

Recent elegant work has definitively identified that *TP53* missense mutations in myeloid malignancies result in a dominant-negative effect without evidence of neomorphic gain-of-function activities, ultimately leading to a selection advantage when exposed to DNA damage.¹² Thus, restoring wild-type function in *TP53* mutant clones would be of profound beneficial impact. APR-246, a methylated PRIMA-1 analog, is a novel, first-in-class, small molecule that selectively induces apoptosis in *TP53* mutant cancer cells. Mechanistically, APR-246 is spontaneously converted into the active species methylene quinclidinone (MQ), which is able to covalently bind to cysteine residues in mutant p53 thereby producing thermo-

dynamic stabilization of the protein and shifting equilibrium toward a functional conformation.^{13,14} APR-246 monotherapy was originally investigated in a phase I trial including AML patients with clinical activity and correlative data identifying activation of p53-dependent pathways.^{15,16}

Maslah *et al.* identified in *TP53* mutant cell lines, *in vivo* models, and primary patient samples that the combination of APR-246 and azacitidine results in a synergistic pro-apoptotic effect as well as a dramatic reduction in cell proliferation *via* cell cycle arrest (Figure 1). As the majority of *TP53* mutations are missense and located in the DNA binding domain, synergy experiments were performed with the SKM1 cell line, which harbors a homozygous hotspot mutation of *TP53* (p. R248Q), and thus is an appropriate representation of clinical disease.¹⁷ Combination therapy of APR-246 and azacitidine resulted in a doubling of apoptotic cells *versus* azacitidine alone as well as 83% of cells undergoing cell cycle arrest in G0/G1. This synergistic effect was confirmed in a xenotransplantation model where combination therapy resulted in a pronounced inhibition of disease progression which occurred early and was durable. Subsequently, the authors interrogated differential gene expression profiles of SKM1 cells treated with either drug alone *versus* the combination of APR-246 and azacitidine. As expected, Gene Set Enrichment Analysis (GSEA) and DAVID analyses of APR-246 treated cells showed robust induction of p53-target genes including *CDKN1A*, *CASP1*, *BAX* and *FAS*, which was confirmed by reverse transcription real-time quantitative polymerase chain reaction (RT-qPCR), resulting in activation of an early apoptotic program. Furthermore, GSEA analysis of “synergistic only” genes (i.e. genes differentially expressed only with combination treatment)

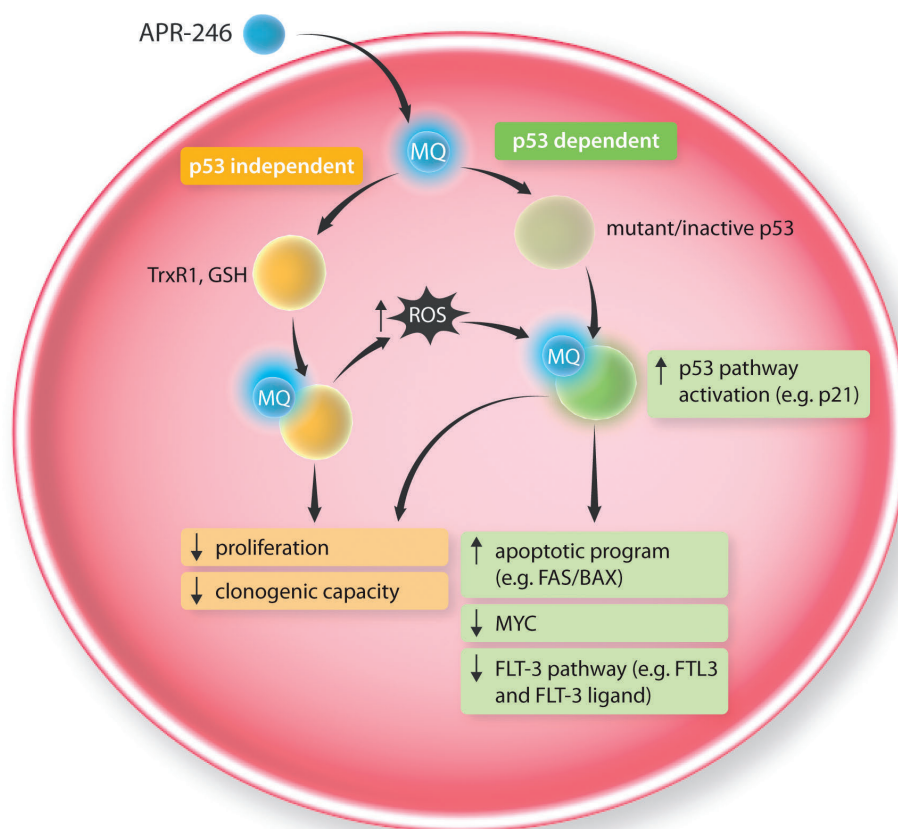


Figure 1. Mechanisms of synergy with APR-246 and azacitidine in *TP53* mutant myelodysplastic syndromes (MDS) / acute myeloid leukemia (AML). GSH: glutathione; MQ: methylene quinuclidinone; ROS: reactive oxygen species; wt: wild-type; TrxR1: thioredoxin reductase 1; FLT-3: fms like tyrosine kinase 3.

identified activation of p53 pathway, induction of apoptosis, and downregulation of *MYC* expression, thus functionally demonstrating restoration of wild-type p53 function. Notably, transcriptome analysis with confirmation by RT-qPCR also identified a novel synergistic mechanism of FLT3 pathway downregulation. Importantly, the inhibition of cell proliferation with combination therapy could be overcome in a dose-dependent fashion in the presence of FLT3 ligand, highlighting a novel therapeutic mechanism of APR-246 that could potentially be exploited in combination with FLT3 inhibitors in future clinical study.

Of importance, synergy was most robust in the presence of *TP53* missense mutations where there is accumulation of misfolded p53 protein, strongly supporting the primary mechanism of APR-246. However, APR-246 also has p53-independent function *via* MQ binding to thioredoxin reductase and glutathione, leading to depletion of glutathione and accumulation of reactive oxygen species (ROS), which can feed forward p53 activation (Figure 1).^{18,19} Indeed, the authors also show synergy in *TP53* knockout mutant cell lines where there is absence of p53, albeit with less synergy than in the missense mutant model. Accordingly, there was significant enrichment of ROS-induced genes with APR-246 treatment. The authors also show data whereby both cell proliferation and clonogenic capacity were strongly inhibited, both in the presence and absence of mutant p53 protein.

Perhaps the most compelling data regarding the synergy of APR-246 and azacitidine originates from the clinical activity in *TP53* mutant MDS/AML patients, where recent

data report an overall and complete remission rate of 87% and 53%, respectively (*clinicaltrials.gov* identifier: NCT03072043).⁹ Similarly, preliminary results from a phase II study of APR-246 and azacitidine by the Groupe Francophone des Myélodysplasies (*clinicaltrials.gov* identifier: NCT03588078) showed comparable response rates.¹⁰ Accordingly, the US Food and Drug Administration has recently granted breakthrough therapy designation for the treatment of patients with *TP53* mutant MDS with the combination of APR-246 and azacitidine and the randomized phase III study of APR-246 and azacitidine *versus* azacitidine is ongoing in MDS patients (*clinicaltrials.gov* identifier: NCT03745716). As *TP53* mutations are strong drivers of negative outcomes in multiple hematologic malignancies, as exemplified by relapsed pediatric acute lymphoblastic leukemia, APR-246 may likely have more broad clinical implications including synergy with traditional cytotoxic agents, as has been recently described.²⁰ Together, shedding light on the synergistic mechanisms underlying APR-246 and azacitidine therapy as presented in this study are critical to continue to advance this novel therapeutic option for patients with the poorest outcomes to traditional treatments.

References

1. Papaemmanuil E, Gerstung M, Malcovati L, et al. Clinical and biological implications of driver mutations in myelodysplastic syndromes. *Blood*. 2013;122(22):3616-3627.
2. Bejar R, Stevenson K, Abdel-Wahab O, et al. Clinical Effect of Point

- Mutations in Myelodysplastic Syndromes. *N Engl J Med.* 2011;364(26):2496-2506.
3. Hunter AM, Sallman DA. Current status and new treatment approaches in TP53 mutated AML. *Best Pract Res Clin Haematol.* 2019;32(2):134-144.
 4. Sallman DA, Komrokji R, Vaupel C, et al. Impact of TP53 mutation variant allele frequency on phenotype and outcomes in myelodysplastic syndromes. *Leukemia.* 2016;30(3):666-673.
 5. Haase D, Stevenson KE, Neuberg D, et al. TP53 mutation status divides myelodysplastic syndromes with complex karyotypes into distinct prognostic subgroups. *Leukemia.* 2019;33(7):1747-1758.
 6. Montalban-Bravo G, Kanagal-Shamanna R, Benton CB, et al. Genomic context and TP53 allele frequency define clinical outcomes in TP53-mutated myelodysplastic syndromes. *Blood Adv.* 2020;4(3):482-495.
 7. Bernard E, Nannya Y, Yoshizato T, et al. TP53 State Dictates Genome Stability, Clinical Presentation and Outcomes in Myelodysplastic Syndromes. *Blood.* 2019;134(Supplement_1):675-675.
 8. Hunter AM, Sallman DA. Targeting TP53 Mutations in Myelodysplastic Syndromes. *Hematol Oncol Clin North Am.* 2020;34(2):421-440.
 9. Sallman DA, DeZern AE, Garcia-Manero G, et al. Phase 2 Results of APR-246 and Azacitidine (AZA) in Patients with TP53 mutant Myelodysplastic Syndromes (MDS) and Oligoblastic Acute Myeloid Leukemia (AML). *Blood.* 2019;134(Supplement_1):676-676.
 10. Cluzeau T, Sebert M, Rahmé R, et al. APR-246 Combined with Azacitidine (AZA) in TP53 Mutated Myelodysplastic Syndrome (MDS) and Acute Myeloid Leukemia (AML). a Phase 2 Study By the Groupe Francophone Des Myéloblastoses (GFM). *Blood.* 2019;134(Supplement_1):677-677.
 11. Maslah N, Salomao N, Drevon L, et al. Synergistic effects of PRIMA-1Met (APR-246) and Azacitidine in TP53-mutated myelodysplastic syndromes and acute myeloid leukemia. *Haematologica.* 2019;xxx
 12. Boettcher S, Miller PG, Sharma R, et al. A dominant-negative effect drives selection of TP53 missense mutations in myeloid malignancies. *Science.* 2019;365(6453):599-604.
 13. Lambert JM, Gorzov P, Veprintsev DB, et al. PRIMA-1 reactivates mutant p53 by covalent binding to the core domain. *Cancer Cell.* 2009;15(5):376-388.
 14. Zhang Q, Bykov VJN, Wiman KG, Zawacka-Pankau J. APR-246 reactivates mutant p53 by targeting cysteines 124 and 277. *Cell Death Dis.* 2018;9(5):439.
 15. Lehmann S, Bykov VJ, Ali D, et al. Targeting p53 in vivo: a first-in-human study with p53-targeting compound APR-246 in refractory hematologic malignancies and prostate cancer. *J Clin Oncol.* 2012;30(29):3633-3639.
 16. Deneberg S, Cherif H, Lazarevic V, et al. An open-label phase I dose-finding study of APR-246 in hematological malignancies. *Blood Cancer J.* 2016;6(7):e447.
 17. Cluzeau T, Dubois A, Jacquel A, et al. Phenotypic and genotypic characterization of azacitidine-sensitive and resistant SKM1 myeloid cell lines. *Oncotarget.* 2014;5(12):4384-4391.
 18. Bykov VJ, Zhang Q, Zhang M, Ceder S, Abrahmsen L, Wiman KG. Targeting of Mutant p53 and the Cellular Redox Balance by APR-246 as a Strategy for Efficient Cancer Therapy. *Front Oncol.* 2016;6:21.
 19. Peng X, Zhang MQ, Conserva F, et al. APR-246/PRIMA-1MET inhibits thioredoxin reductase 1 and converts the enzyme to a dedicated NADPH oxidase. *Cell Death Dis.* 2013;4(10):e881.
 20. Demir S, Boldrin E, Sun Q, et al. Therapeutic targeting of mutant p53 in pediatric acute lymphoblastic leukemia. *Haematologica.* 2020;105(1):170-181.

Peripheral T-cell lymphoma diagnosis: building a molecular tool

Miguel A Piris^{1,2}

¹Department of Pathology, Hospital Universitario, Fundación Jiménez Díaz and ²CIBERONC, Madrid, Spain

E-mail: MIGUEL A PIRIS - mapirispinilla@gmail.com

doi:10.3324/haematol.2020.249052

T-cell lymphoma (TCL) has quite a poor probability of survival (around 25-30% of patients after 5 years), which contrasts with the progress that has recently been made in Hodgkin lymphoma and B-cell lymphoma.¹⁻³ Some recently defined TCL types, such as anaplastic large-cell lymphoma (ALCL), have a better clinical outcome. However, the majority of cases diagnosed with peripheral T-cell lymphoma (PTCL) will eventually die of the disease, and in some specific tumor types, such as intestinal TCL, the prognosis is even more miserable.

Poor survival probability in this context is associated with serious difficulties in lymphoma diagnosis when using routine morphological and immunohistochemistry tools. PTCL classification involves division into multiple subtypes, typically of low frequency and with hazy distinctions (Figure 1). As a consequence, different studies coincide in achieving a very low rate of reproducibility in TCL diagnosis, especially in recognizing ALK-negative ALCL, and distinguishing between PTCL-not otherwise specified (NOS) and PTCL with TFH phenotype or angioimmunoblastic TCL.⁴

An important feature of this situation is that the relative frequencies of the tumor types are quite low, which makes it difficult to design and develop clinical trials, and this hampers the introduction of new drugs for PTCL therapy.

Nevertheless, these difficulties have inspired some research groups to provide essential information about the molecular basis of TCL pathogenesis, and to identify some attractive and challenging therapeutic targets.⁵⁻⁹

Drieux and co-workers,¹⁰ in a joint project involving French, Belgian and Swiss hospitals, are now addressing the radical proposal that molecular diagnosis may give a more precise and reproducible way of classifying TCL cases. Using a technique applicable to paraffin-embedded tissue, they measure the expression of 20 genes, including 17 markers relevant to T-cell classification, one Epstein-Barr virus-related transcript, and frequently mutated variants of RHOA (G17V) and IDH2 (R172K/T). Selected genes allow the identification of several entities: TFH cells, the normal counterparts of angioimmunoblastic TCL; TH1 and TH2 phenotypes, which reflect the diversity of PTCL-NOS; T-regulatory cells, for distinguishing ATLL; the cytotoxic markers, CD30 and ALK, for identifying ALCL; and CD56 and EBER1, to discriminate T/natural killer (NK)-cell lymphomas.

The results validate the solid basis of the currently used PTCL classification scheme, and highlight the similarity between angioimmunoblastic TCL and PTCL-TFH. The findings show a group of cases with simultaneous expression of TFH markers and TH2 (GATA3), and indicate that ALK-negative ALCL is a heterogeneous condition. Cases of PTCL-NOS appear to be extremely heterogeneous,

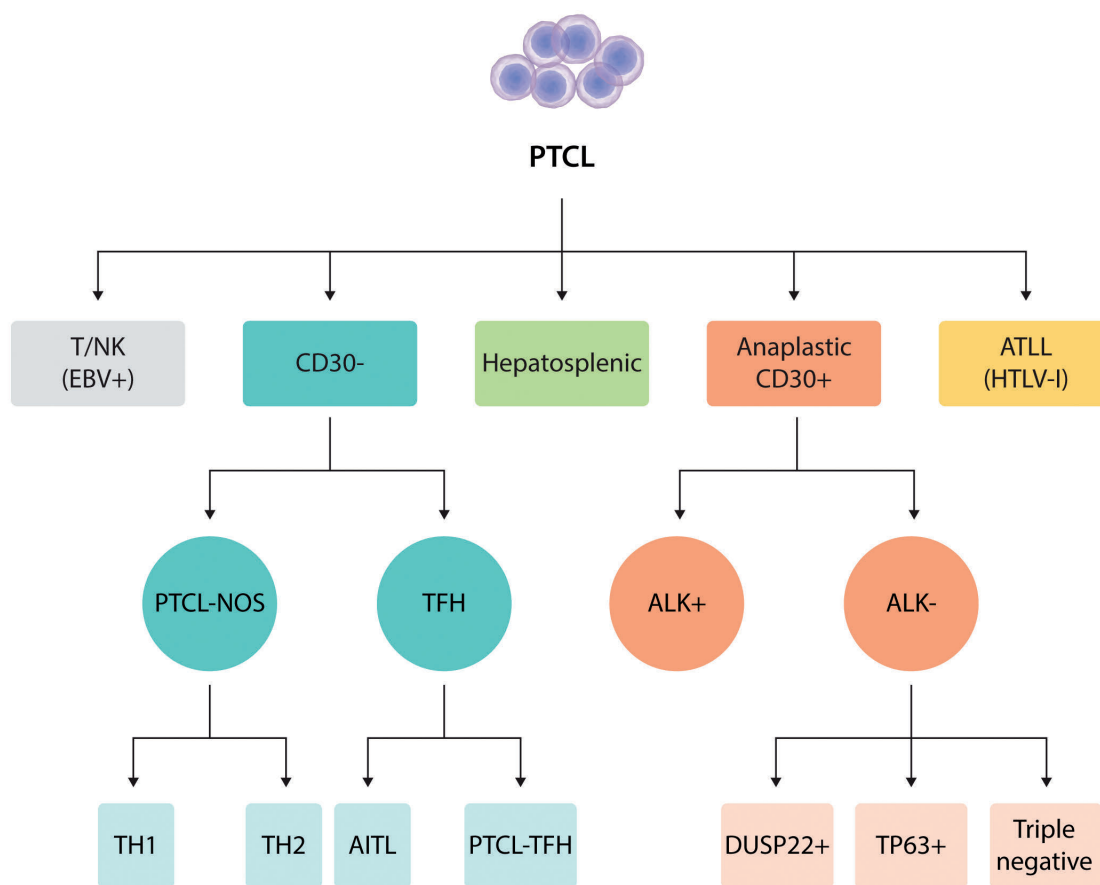


Figure 1. Peripheral T-cell lymphoma classification following the World Health Organization 2017 Lymphoma Classification, here restricted to the tumor types covered in the article. PTCL: Peripheral T-cell Lymphoma. NK: Natural Killer; ATLL: Adult T-cell Leukemia/Lymphoma; NOS: Not otherwise specified; TFH: T-Follicular Helper; ALK: Anaplastic Lymphoma Kinase; TH: T Helper; AITL: Angioimmunoblastic T-cell Lymphoma.

with the cases divided among the different phenotypes. In this study, ALK-negative ALCL had two distinct profiles, with or without expression of cytotoxic genes.

Clinical correlation confirmed the poor prognosis of PTCL (5-year OS=27%), and the better prognosis for ALK⁺ and DUSP22⁺ ALCL, but failed to recognize markers that recognize groups with additional clinical variability. In particular, the division into TH1 and TH2 phenotypes in PTCL-NOS was not found to be clinically significant. It is of particular note that a 90% concordance was obtained between the three centers, thus emphasizing one of the stronger points in this approach, i.e. better reproducibility.

Although this is almost certainly not the last word on the process of creating molecular tools for the routine diagnosis of PTCL, it is an important step forward that establishes the viability of the proposal to integrate gene expression and variant recognition, and raises some questions about the PTCL subclasses as they are currently recognized.

Peripheral T-cell lymphoma diagnosis is an area in which molecular diagnosis can play an important role in the near future. Efforts in this field could prove even more relevant, with the provision, not only of diagnostic markers, but also of predictive therapeutic markers, by which the different lymphoma categories may be associated

with the identification of useful targets that can be exploited for therapeutic purposes.

Funding

This work was supported by grants from the Instituto de Salud Carlos III (ISCIII) of the Spanish Ministry of Economy and Competence (MINECO, RTICC ISCIII and CIBERONC) (SAF2013-47416-R, RD06/0020/0107-RD012/0036/0060 and Plan Nacional I+D+I: PI17/2172, PI16/01294 and PIE15/0081), AECC, and the Madrid Autonomous Community.

References

1. Mak V, Hamm J, Chhanabhai M, et al. Survival of patients with peripheral T-cell lymphoma after first relapse or progression: spectrum of disease and rare long-term survivors. *J Clin Oncol.* 2013;31(16):1970-1976.
2. Federico M, Bellei M, Marcheselli L, et al. Peripheral T cell lymphoma, not otherwise specified (PTCL-NOS). A new prognostic model developed by the International T cell Project Network. *Br J Haematol.* 2018;181(6):760-769.
3. Weisenburger DD, Savage KJ, Harris NL, et al. Peripheral T-cell lymphoma, not otherwise specified: a report of 340 cases from the International Peripheral T-cell Lymphoma Project. *Blood.* 2011;117(12):3402-3408.
4. Laurent C, Baron M, Amara N, et al. Impact of Expert Pathologic Review of Lymphoma Diagnosis: Study of Patients From the French Lymphopath Network. *J Clin Oncol.* 2017;35(18):2008-2017.
5. de Leval L, Rickman DS, Thielen C, et al. The gene expression profile

- of nodal peripheral T-cell lymphoma demonstrates a molecular link between angioimmunoblastic T-cell lymphoma (AITL) and follicular helper T (TFH) cells. *Blood*. 2007;109(11):4952-4963.
6. Piccaluga PP, Agostinelli C, Califano A, et al. Gene expression analysis of peripheral T cell lymphoma, unspecified, reveals distinct profiles and new potential therapeutic targets. *J Clin Invest*. 2007;117(3):823-834.
 7. Cortes JR, Ambesi-Impiombato A, Couronne L, et al. RHOA G17V Induces T Follicular Helper Cell Specification and Promotes Lymphomagenesis. *Cancer Cell*. 2018;33(2):259-273.e7.
 8. Heavican TB, Bouska A, Yu J, et al. Genetic drivers of oncogenic pathways in molecular subgroups of peripheral T-cell lymphoma. *Blood*. 2019;133(15):1664-1676.
 9. Pedersen MB, Hamilton-Dutoit SJ, Bendix K, et al. DUSP22 and TP63 rearrangements predict outcome of ALK-negative anaplastic large cell lymphoma: a Danish cohort study. *Blood*. 2017;130(4):554-557.
 10. Drieux F, Ruminy P, Abdel-Sater A, et al. Defining signatures of peripheral T-cell lymphoma with a targeted 20-marker gene expression profiling assay. *Haematologica*. 2020;105(6):1582-1592.

PIKING the next therapeutic target in multiple myeloma

Jessica L. Caro and Faith E. Davies

Perlmutter Cancer Center, NYU Langone Health, New York, NY, USA

E-mail: FAITH E DAVIES - faith.davies@nyulangone.org

doi:10.3324/haematol.2020.248971

Arguably the most transformative myeloma therapies to date have been those which target essential processes involved in plasma cell function. Although their mechanism of action may not have been entirely obvious when first introduced, it has now become clear from cell-based studies that these therapies target protein degradation via the ubiquitin proteasome pathway, a critical process for plasma cell survival. Examples include proteasome inhibitors (such as bortezomib, carfilzomib, and ixazomib) and the immunomodulatory drugs (such as lenalidomide and pomalidomide), which inhibit the CUL4 E3 ubiquitin ligase, cereblon. Both drug classes are the 'go to' choices in current myeloma treatment.¹ It therefore comes as no surprise that the search for other therapies targeting protein degradation pathways continues.

The key function of a normal plasma cell is to produce immunoglobulins. Studies have shown that myeloma plasma cells, which produce large quantities of M protein, are highly dependent on the multiple pathways that enable a cell to handle excess unfolded or misfolded proteins. Over the last 10 years, cancer researchers have explored many of these pathways with a view to therapeutic exploitation. The rationale is that inhibition of these pathways leads to a build up of unwanted or misfolded proteins, the induction of cellular stress, and ultimately to cancer cell death. Such pathways include not only the ubiquitin proteasome pathway but also the heat shock protein pathway, autophagy pathway, unfolded protein response pathway, and pathways involving lysosomes and aggresomes.² However, translating *in vitro* findings into clinical success has been difficult. It has become clear that some cancer types are dependent on one pathway more than others, the pathways are interlinked, and the crosstalk between pathways enables the development of both primary and drug-induced mechanisms of resistance.

In this edition of *Haematologica*, Bonolo de Campos *et al.* describe a promising new approach for myeloma therapy by perturbing the autophagy and lysosome pathways.³ In autophagy, misfolded and aggregated proteins are sequestered in double-membraned vesicles called autophagosomes that eventually fuse with lysosomes for digestion and recycling. Previous studies have shown that

myeloma cells require tight regulation of the autophagy pathway for cell survival, and genetic or therapeutic manipulation of this pathway induces growth inhibition and/or cell death.^{2,4,5}

Phosphatidylinositol-3-phosphate 5 kinase (PIKfyve) is a phosphoinositide kinase with many diverse functions within the cell, including the generation of phosphorylated substrates critical to the regulation of autophagy.⁶ Inhibition of PIKfyve using the selective inhibitor apilimod has previously been investigated as a potential therapeutic approach for both inflammatory diseases and non-Hodgkin lymphoma.⁷ Using an unbiased chemical screen, Bonolo de Campos *et al.* identified APY0201 and examined its activity along with that of apilimod and another novel PIKfyve inhibitor YM201636 in 25 human myeloma cell lines and 100 *ex-vivo* patient-derived samples. They confirmed dose-dependent inhibition of cell viability in all myeloma cell lines, with APY0201 being the most potent PIKfyve inhibitor. They additionally observed dose-dependent sensitivities in 40% of *ex-vivo* patient-derived samples with APY0201. Mechanistic experiments suggested that exposure to APY0201 resulted in activation of the transcription factor EB (TFEB) leading to upregulation of autophagosome and lysosomal biogenesis. Exposure also disrupted lysosomal function leading to alterations in autophagic flux and a vacuolization phenotype.

As myeloma is a genetically and biologically heterogeneous disease, it is critical to identify which patients would benefit most from a new therapy. The prime example of the need for such an approach is venetoclax, a Bcl-2 inhibitor, which has been shown to be particularly efficacious in patients harboring a t(11;14) translocation.⁸ Although targeting a pathway central to plasma cell survival should theoretically result in universal myeloma cell death, it has become clear that the genetic background of the cell influences response to therapy.⁹ For instance, whereas patients with a t(14;16) translocation tend to respond poorly to proteasome inhibitors, these therapies may be able to overcome some of the adverse outcome associated with the t(4;14) subgroup.¹⁰ Therefore, trying to incorporate genetic information into therapeutic decision-making may allow us to optimize treatment choices and response rates and to provide long-lasting remissions. Importantly, the authors have tried to assess this in their

study using data from the patients' samples. The activity of APY0201 was highest in patient-derived samples with hyperdiploidy (trisomies with one or more odd-numbered chromosomes) and lowest in patients' samples with a t(11;14) translocation. In addition, *ex-vivo* samples with high TFEB levels were sensitive to APY0201. High TFEB levels have been associated with increased autophagic flux suggesting that autophagic flux may be directly related to PIKfyve inhibition. These preliminary results may suggest patient populations that could be enriched for in a future clinical trial.

In conclusion, Bonolo de Campos *et al.* provide exciting data to support the ongoing investigation of therapeutically manipulating targets specific to plasma cell function, particularly protein handling in myeloma.² Although the finer details of the actual mechanisms may differ somewhat between multiple myeloma and non-Hodgkin lymphoma, data from this study and those performed in non-Hodgkin lymphoma provide compelling evidence for the role of PIKfyve inhibition in inducing cell death, with changes seen in the autophagy and lysosomal pathways. Notably, this study demonstrates the importance of the inherent genetic differences in myeloma biology and the potential role of PIKfyve inhibitors in targeting a distinct group of genetically defined myeloma to continue this era of personalized medicine.

References

1. Gay F, Engelhardt M, Terpos E, et al. From transplant to novel cellular therapies in multiple myeloma: European Myeloma Network guidelines and future perspectives. *Haematologica*. 2018;103(2):197-211.
2. Aronson LI, Davies FE. DangER: protein ovERload. Targeting protein degradation to treat myeloma. *Haematologica*. 2012;97(8):1119-1130.
3. Bonolo De Campos C, Zhu YX, Sepetov N, et al. Identification of PIKfyve kinase as a target in multiple myeloma. *Haematologica*. 2020;105(6):1641-1649.
4. Hoang B, Benavides A, Shi Y, Frost P, Lichtenstein A. Effect of autophagy on multiple myeloma cell viability. *Mol Cancer Ther*. 2009;8(7):1974-1984.
5. Aronson LI, Davenport EL, Mirabella F, Morgan GJ, Davies FE. Understanding the interplay between the proteasome pathway and autophagy in response to dual PI3K/mTOR inhibition in myeloma cells is essential for their effective clinical application. *Leukemia*. 2013;27(12):2397-2403.
6. Hessvik NP, Øverbye A, Brech A, et al. PIKfyve inhibition increases exosome release and induces secretory autophagy. *Cell Mol Life Sci*. 2016;73(24):4717-4737.
7. Gayle S, Landrette S, Beeharry N, et al. Identification of apilimod as a first-in-class PIKfyve kinase inhibitor for treatment of B-cell non-Hodgkin lymphoma. *Blood*. 2017;129(13):1768-1778.
8. Kumar S, Kaufman JL, Gasparetto C, et al. Efficacy of venetoclax as targeted therapy for relapsed/refractory t(11;14) multiple myeloma. *Blood*. 2017;130(22):2401-2409.
9. Pawlyn C, Davies FE. Toward personalized treatment in multiple myeloma based on molecular characteristics. *Blood*. 2019 14;133(7):660-675.
10. Qiang YW, Ye S, Chen Y, et al. MAF protein mediates innate resistance to proteasome inhibition therapy in multiple myeloma. *Blood*. 2016;128(25):2919-2930.

The increasing complexity of the management of core-binding factor acute myeloid leukemia

Mark R. Litzow

Division of Hematology and Transplant Center, Mayo Clinic Rochester, Rochester, MN, USA

E-mail: MARK R. LITZOW - litzow.mark@mayo.edu

doi:10.3324/haematol.2020.249110

The core binding factor (CBF) acute myeloid leukemias characterized by the t(8;21) and inv(16)(p13q22)/t(16;16)(p13;q22) cytogenetic abnormalities have long been known to prognostically represent more favorable subcategories of acute myeloid leukemia (AML). These translocations are characterized by the presence of the *RUNX1-RUNX1T1* (*AML1-ETO*) and *CBFB-MYH11* fusion transcripts, respectively. In fact, the t(8;21) was the first cytogenetic abnormality identified in AML in 1973.¹ These CBF-AML subtypes have continued to remain in the favorable risk category in multiple classification systems up to the current time based on their high rate of achievement of complete remission with induction chemotherapy and their relatively low relapse rate.² Clinical trials over the years have demonstrated that these two CBF-AML subtypes are particularly responsive to high doses of cytarabine utilized in consolidation regimens. Addition of the immunconjugate drug, gemtuzumab ozogamicin, to induction chemotherapy further reduces the risk of relapse and improves overall survival in patients with CBF-AML.³ The favorable results of chemotherapy in patients with CBF-AML have led to the widely accepted practice not to perform allo-

genic blood or marrow transplant (alloBMT) in these patients who achieve first remission. This is in contrast to patients with AML with intermediate risk or unfavorable risk features where allogeneic blood or marrow transplant in first remission is a widely accepted practice.

However, the two subtypes of CBF-AML are not the same in all respects. Studies going back 15 years or more have pointed out the difference between these two subtypes.⁴ Use of next-generation sequencing (NGS) and identification of additional gene mutations in patients with AML have begun to further define differences between the two. One of the first mutational abnormalities found in subsets of patients with CBF-AML were *c-KIT* mutations. The *c-KIT* mutation has been suggested to be associated with a poorer prognosis in CBF-AML patients but, here again, this mutation seems to have less of a prognostic impact in patients with inv(16) compared to those with t(8;21).⁵ NGS studies, which are now widely utilized to assess prognosis in many subtypes of AML, have been applied to patients with CBF-AML. Multiple mutations in addition to *c-KIT* have been identified, including genes activating tyrosine kinase signaling, such as *N/KRAS* and *FLT3*. Mutations in genes that regulate

Risk factor	Risk ratio	P
Age	1.031	0.0017
<i>KIT</i> D816V mutation positive (Ref = negative)	4.331	0.0018
<i>KIT</i> D816V mutation non-tested/missing (Ref = negative)	2.567	0.0036
WBC at diagnosis	1.018	0.0361
Number of chromosomes (Ref = non-pseudodiploidy)	2.552	0.0035

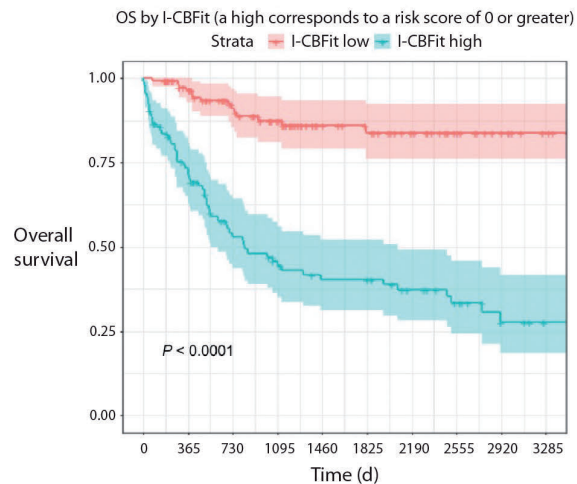


Figure 1. Risk factors and a novel scoring system (I-CBfit) for core-binding acute myeloid leukemia. (A) Risk ratios of risk factors for death or relapse. (B) Overall survival (OS) according to I-CBfit. Ref: reference values; WBC: white blood cell count; d: days.

chromatin conformation or encode members of the cohesin complex have been observed with high frequency in t(8;21) AML, although they are infrequent in inv(16) AML.⁶⁷ These studies all highlight the heterogeneity of the two subtypes of CBF-AML and have added further complexity to their characterization.

Additionally, monitoring for minimal or measurable residual disease (MRD) by quantitative real-time polymerase chain reaction has been shown to risk stratify patients and predict relapse and, as in other subtypes of AML, has been shown to be a powerful prognostic factor.⁸

Despite the favorable risk categorization of CBF-AML, up to 30-40% of these patients can still relapse after standard intensive induction and consolidation chemotherapy. Once they do relapse, additional re-induction chemotherapy is required to put them into second remission and, generally, these patients are then candidates for alloBMT in second remission in order to prevent subsequent relapse and ensure durable second remissions. Fortunately, these patients can achieve a second remission with chemotherapy in up to 80-90% of the cases. In this setting, addition of gemtuzumab ozogamicin can also help to lessen the risk of subsequent relapse.⁹

Thus, the outcome of patients with CBF-AML who have relapsed and achieve a second remission and subsequently undergo alloBMT is of significant importance in the management of these patients. In this issue of *Haematologica*, Halaburda and colleagues from the Acute Leukemia Working Party of the European Society for Blood and Marrow Transplantation report the results of 631 patients reported to the EBMT registry between 2000 and 2014 with CBF-AML.¹⁰ These patients came from 181 transplant centers, and a little over half of them (n=366) had an inv(16) and 265 of them (42%) had a t(8;21). There were more males with t(8;21) than with inv(16), and time from diagnosis to transplantation, and time from diagnosis to first remission, were also longer in the t(8;21) group. Over half of the patients were transplanted between the years 2010 and 2014, and 21% of patients had additional cytogenetic abnormalities found at diagnosis. Molecular

abnormalities were identified, but were reported with low frequency. Leukemia-free survival at 2-5 years was 59% and 54%, respectively, while overall survival probabilities were 65% and 58%, respectively. Relapse risk at two and five years was 20% and 23%, respectively, and non-relapse mortality was 21% and 23% at two and five years, respectively. In multivariate analysis, factors negatively impacting leukemia-free and overall survival were: t(8;21), presence of three or more additional chromosomal abnormalities, and poor Karnofsky performance score of <80%. Furthermore, additional cytogenetic abnormalities and the t(8;21) increased relapse risk. Use of reduced intensity conditioning in the transplant regimen also increased relapse risk. As expected, the presence of MRD assessed by molecular techniques before transplantation was associated with increased relapse risk and inferior leukemia-free survival.

One caveat to keep in mind in studies assessing the results of alloBMT, particularly in patients with second remission, is that these studies do not take into account the outcome of all patients who have relapsed and they thus select for patients who are able to achieve a second remission and move on to transplant. These studies also do not include an analysis of patients who relapse and fail to achieve second remission, die in the attempt to achieve a second remission, or have significant comorbidities develop which preclude them from proceeding to transplant. This has been described as the “myth of the second remission”.¹¹

Given the increasing heterogeneity of CBF-AML as outlined earlier, how are we now to determine which patients with CBF-AML should undergo alloBMT in first remission or continue to not be transplanted in first remission and only to proceed to transplant if they relapse and achieve a second remission? There are increasing numbers of prognostic scoring systems that are under development for multiple diseases, and some of those emerging incorporate the availability of identification of additional genetic abnormalities.¹² In particular, a recent publication has reported a novel scoring system for patients with the

t(8;21) subtype of CBF-AML. This study of 247 patients from the United States and Europe identified older age, a *KIT D816V* mutation, a high white blood count, and pseudodiploidy compared with hyper- or hypodiploidy into a scoring system called the I-CBFit. This scoring system demonstrated a disease-free survival rate at two years of 76% in patients with a low-risk I-CBFit score compared with 36% for those with a high-risk I-CBFit score (Figure 1).¹³

Whereas in the past, CBF-AML has been characterized and treated as a monolithic entity in terms of treatment and prognosis, one must now take into account the multiple clinical and laboratory characteristics in order to more expertly characterize the prognosis of these patients so as to design the most appropriate treatment plan and incorporate decision-making toward use of alloBMT in first or second remission. The study by Halaburda and colleagues from the Acute Leukemia Working Party of the EBMT¹⁰ adds a valuable source of information to help understand the pros and cons of these approaches and the outcomes of patients who undergo transplant with CBF-AML in second remission.

References

- Rowley JD. Identification of a translocation with quinacrine fluorescence in a patient with acute leukemia. *Ann Genet.* 1973;16(2):109-112.
- Dohner H, Estey E, Grimwade D, et al. Diagnosis and management of AML in adults: 2017 ELN recommendations from an international expert panel. *Blood.* 2017;129(4):424-447.
- Hills RK, Castaigne S, Appelbaum FR, et al. Addition of gemtuzumab ozogamicin to induction chemotherapy in adult patients with acute myeloid leukaemia: a meta-analysis of individual patient data from randomised controlled trials. *Lancet Oncol.* 2014;15(9):986-996.
- Marcucci G, Mrozek K, Ruppert AS, et al. Prognostic factors and outcome of core binding factor acute myeloid leukemia patients with t(8;21) differ from those of patients with inv(16): a Cancer and Leukemia Group B study. *J Clin Oncol.* 2005;23(24):5705-5717.
- Ayatollahi H, Shajiei A, Sadeghian MH, et al. Prognostic Importance of C-KIT Mutations in Core Binding Factor Acute Myeloid Leukemia: A Systematic Review. *Hematol Oncol Stem Cell Ther.* 2017;10(1):1-7.
- Duployez N, Marceau-Renaut A, Boissel N, et al. Comprehensive mutational profiling of core binding factor acute myeloid leukemia. *Blood.* 2016;127(20):2451-2459.
- Prieto-Conde MI, Jimenez C, Garcia-Alvarez M, et al. Identification of relapse-associated gene mutations by next-generation sequencing in low-risk acute myeloid leukaemia patients. *Br J Haematol.* 2020 Mar 2. [Epub ahead of print]
- Yin JA, O'Brien MA, Hills RK, Daly SB, Wheatley K, Burnett AK. Minimal residual disease monitoring by quantitative RT-PCR in core binding factor AML allows risk stratification and predicts relapse: results of the United Kingdom MRC AML-15 trial. *Blood.* 2012;120(14):2826-2835.
- Hospital MA, Prebet T, Bertoli S, et al. Core-binding factor acute myeloid leukemia in first relapse: a retrospective study from the French AML Intergroup. *Blood.* 2014;124(8):1312-1319.
- Halaburda K, Labopin M, Mailhol A, et al. Allogeneic stem cell transplantation in second complete remission for core binding factor acute myeloid leukemia: a study from the Acute Leukemia Working Party of the European Society for Blood and Marrow Transplantation. *Haematologica* 2020;105(6):1723-1730.
- Forman SJ, Rowe JM. The myth of the second remission of acute leukemia in the adult. *Blood.* 2013;121(7):1077-1082.
- Gerstung M, Papaemmanuil E, Martincorena I, et al. Precision oncology for acute myeloid leukemia using a knowledge bank approach. *Nat Genet.* 2017;49(3):332-340.
- Ustun C, Morgan E, Moodie EEM, et al. Core-binding factor acute myeloid leukemia with t(8;21): Risk factors and a novel scoring system (I-CBFit). *Cancer Med.* 2018;7(9):4447-4455.



Immunological consequences of extramedullary erythropoiesis: immunoregulatory functions of CD71⁺ erythroid cells

Shokrollah Elahi^{1,2,3,4} and Siavash Mashhour¹

¹School of Dentistry, University of Alberta, Alberta; ²Department of Medical Microbiology and Immunology, University of Alberta, Alberta; ³Department of Medical Oncology, Faculty of Medicine and Dentistry, University of Alberta, Alberta and ⁴Li Ka Shing Institute of Virology, University of Alberta, Edmonton, Alberta, Canada

Haematologica 2020
Volume 105(6):1478-1483

Introduction

Mammalian erythropoiesis occurs in three stages; the primitive, the fetal definitive and the adult definitive stages.¹ After the primitive stage, which takes place in the yolk sac, definitive erythropoiesis moves to the fetal liver and the spleen but is finally restricted to the bone marrow, as adult definitive red blood cells, for the rest of the life.² After birth, the location of erythropoiesis gradually switches to spongy flat bones, such as ilium, sternum, ribs, and cranium, the sites which adults rely on mostly for steady-state erythropoiesis.³ Erythrocytes are constantly produced under a highly orchestrated process regulated by multiple factors in adult bone marrow niches and local tissue microenvironments that control hematopoietic stem cell maintenance/survival.⁴ Nonetheless, stresses such as anemia, chronic infection, pregnancy, cancer, hematologic disorders, and stromal abnormalities disrupt this balance in the bone marrow, causing erythropoiesis to occur outside of the bone marrow (e.g. in spleen and liver).^{5,6} It is worth noting that stress erythropoiesis may be a better reflection of this phenomenon than extramedullary erythropoiesis (EE) in some cases. However, as will be discussed in this perspective, there is a rich body of evidence demonstrating the occurrence of EE under different physiological and pathological conditions.

EE implies the generation of erythrocytes outside of medullary spaces of the bone marrow.⁷ Under these circumstances, EE is considered to be the main cause of the abundance of erythroid precursors in the periphery. This may occur as a result of passive incontinence of hematopoietic cells from the sites of EE, where tissue structure/control of cell egress is less efficient than that of the bone marrow.⁸ However, the clinical implication of the expansion of erythroid precursors outside of the bone marrow has not been well defined. This perspective aims to provide the reader with an overview of the current understanding of the immunological consequences of EE.

Erythroid precursors are the newborn's first-time enemies but lifelong friends

Newborns are highly susceptible to fatal infections. This susceptibility has generally been ascribed to the immaturity of the neonatal immune system. Nevertheless, this old dogma has been challenged with the discovery of the physiological abundance of immunosuppressive erythroid precursors during this developmental stage of life. It has been reported that the spleen of neonatal mice is impressively enriched with erythroid precursors co-expressing the transferrin receptor CD71 and the erythroid lineage marker TER119. The levels of these cells were maximal between days 6-9 but gradually declined to the adult level by day 21 in experiments performed in Cincinnati, USA⁹ and by day 28 in experiments performed in Edmonton, Canada.¹⁰ This difference might be related to geographical factors, such as altitude, or differences in the animals' microbiome. Likewise, human cord blood and placenta accommodate an equally enriched proportion of erythroid precursor cells co-expressing CD71 and the erythroid lineage marker CD235a (glycophorin A). However, these cells are sparse in the peripheral blood of healthy adults.⁹ Since their discovery, we have defined these cells as "CD71⁺ erythroid cells (CEC)".¹¹ CEC are mainly erythroid precursors expressing high levels of CD71, including reticulocytes but excluding mature red blood cells. Neonatal

Correspondence:

SHOKROLLAH ELAHI
elahi@ualberta.ca

Received: November 28, 2019.

Accepted: April 6, 2020.

Pre-published: April 30, 2020.

doi:10.3324/haematol.2019.243063

Check the online version for the most updated information on this article, online supplements, and information on authorship & disclosures: www.haematologica.org/content/105/6/1478

©2020 Ferrata Storti Foundation

Material published in *Haematologica* is covered by copyright. All rights are reserved to the Ferrata Storti Foundation. Use of published material is allowed under the following terms and conditions:

<https://creativecommons.org/licenses/by-nc/4.0/legalcode>.

Copies of published material are allowed for personal or internal use. Sharing published material for non-commercial purposes is subject to the following conditions:

<https://creativecommons.org/licenses/by-nc/4.0/legalcode>, sect. 3. Reproducing and sharing published material for commercial purposes is not allowed without permission in writing from the publisher.



CEC express arginase-2, whose activity is essential for the cells' immunosuppressive properties.⁹ The presence of CEC was found to be associated with increased neonatal susceptibility to infection.⁹ However, CEC-mediated susceptibility to infection was counterbalanced by these cells' protective role against aberrant immune cell activation in the intestine, allowing swift colonization by microbial communities after parturition.⁹ This was shown by increased immune cell activation and production of pro-inflammatory cytokines [interleukin (IL)-6 and tumor necrosis factor (TNF)- α] by antigen-presenting cells in the intestine when CEC were partially depleted in wildtype compared to germ-free mice.⁹ In addition, following studies in a murine model of whooping cough, it was reported that CEC impaired innate immune responses against *Bordetella pertussis* infection.¹⁰ Specifically, depletion of CEC unleashed an innate immune response characterized by enhanced production of protective cytokines [interferon (IFN)- γ , TNF- α , and IL-12] and resulted in the recruitment of natural killer cells and antigen-presenting cells in the lungs of neonatal mice, which restored resistance to *B. pertussis* infection. In contrast, neonatal CEC adoptively transferred into adult recipients by intravenous injection impaired the adults' innate immune response against *B. pertussis* infection.¹⁰ Moreover, the enzymatic activity of arginase-2 secreted by CEC inhibited phagocytosis of *B. pertussis* *in vitro*.¹⁰ These observations challenged the notion of neonatal susceptibility to infection being due to intrinsic defects of immune cells, and instead highlighted active immune suppression mediated by the abundance of CEC in the newborn. These findings provided additional support to the novel concept in neonatal immunology that immunosuppression is essential to dampen costly robust immune responses in newborns. Further studies demonstrated that CEC hindered adaptive cellular and humoral immune responses to infection with *B. pertussis* and vaccination against this pathogen in neonatal mice. Depletion of CEC before vaccination resulted in a substantial increase in the induction of antigen-specific protective cytokines (IFN- γ and IL-17) and antibodies (IgA and IgG) against *B. pertussis*.¹² Similarly, the ablation of CEC before a primary infection resulted in more robust, protective immunity following re-infection with *B. pertussis* in neonatal mice.¹² These observations suggest that the accumulation of CEC in the periphery could have detrimental effects on both the innate and adaptive immune responses to pathogens. Furthermore, CEC from human cord blood and placenta have immunosuppressive effects following stimulation with different bacterial ligands or anti-CD3/CD28 *in vitro*.^{9,12,15} In a complementary study, pre-term labor-derived human cord blood CEC were shown to participate in the suppression of CD4⁺ and CD8⁺ T-cell proliferation and modulate cytokine production by antigen-presenting cells in the presence of heat-killed *Listeria monocytogenes*.¹⁴ These observations raised the possibility that CEC might have immunomodulatory rather than immunosuppressive properties, leading to enhanced pro-inflammatory cytokine production under specific circumstances (e.g., CEC from pre-term versus full-term cord blood). Although CEC impair both innate and adaptive immune responses against pathogens in the neonate, their crucial role in the host's adaptation to microbial communities has lifelong benefits and deserves appreciation (Figure 1).

Future research should be directed at understanding the cross-talk between CEC and microbial communities to determine any therapeutic benefit in human newborns. Such novel studies will establish the scientific framework for more in-depth translational studies in the future.

Immunological benefits of extramedullary erythropoiesis in pregnancy and gut homeostasis

A good pregnancy outcome requires selective silencing of maternal immune effector cells against the father's fetal alloantigens.^{15,16} The fetus is antigenically similar to a semi-allogeneic transplant, with the risk of immunological rejection. As such, the mother's immune response during gestation requires tolerance to alloantigens, preventing potentially damaging immune responses that may result in abortion or preterm delivery.¹⁷ The maintenance of pregnancy does, therefore, represent a major challenge for the maternal immune system, since it has to tolerate a semi-allogeneic fetus and at the same time protect both the mother and the fetus against potential pathogens. Several mechanisms have been reported to be involved in blocking the immunological rejection of the fetus,^{18,19} including those modified by CEC. During pregnancy, especially after mid-gestation, the total red blood cell count increases to meet the increased demand for blood supply by the mother and the fetus. The normal range of erythropoietin concentration in pregnant women is varied, although erythropoietin concentration rises as the demand for blood supply increases.²⁰ This high level of erythropoietin, alongside other factors, such as 27-hydroxycholesterol, the cholesterol metabolite, which induces hematopoietic stem cell mobilization through the estrogen receptor α , is required for EE formation during gestation.²¹ In concert with estradiol, 27-hydroxycholesterol promotes EE by regulating estrogen receptor α function in hematopoietic stem cell mobilization. In agreement with this concept, Delyea *et al.* found physiological expansion of CEC in the spleen and peripheral blood of an allogeneic mouse model of pregnancy.²² Although a moderate expansion of CEC was observed in syngeneic pregnancy, it was significantly lower than that in the allogeneic mice.²² This suggests a potential role for CEC in response to alloantigens. In support of these hypotheses, an abundance of CEC was found at the fetomaternal interface during pregnancy.²² Maternal CEC, like the neonatal CEC, expressed arginase-2 and activity of this enzyme was required for the cells' inhibitory effect against the aggressive allogeneic response at the fetomaternal interface. These CEC from the spleen and placental tissues of pregnant mice, unlike neonatal CEC, expressed substantial levels of programmed death-1/2 ligands (PDL-1/PDL-2) and subsequently suppressed PD-1-expressing T cells at the fetomaternal interface.²² Furthermore, the ablation of CEC in allogeneic mice skewed the immune response toward a Th1 response characterized by upregulation of inflammatory cytokines and chemokines (e.g. TNF- α and IFN- γ , IL-6 and CXCL-1) resulting in fetal resorption.²² Similarly, expansion of CEC was observed in the peripheral blood of pregnant women in the second and third trimesters of pregnancy.¹⁵ CEC from either peripheral blood or cord blood/placental tis-

sues of healthy mothers exhibited immunosuppressive properties. However, the frequency of CEC was lower in mothers with inflammatory bowel disease (IBD) and the cells were functionally impaired when examined *in vitro*.¹³ IBD is associated with intestinal dysbiosis and dysfunctional interaction between the microbiota and the gut mucosal immune system, which results in a dysregulated immune response against commensal microbial antigens.²³ The reduced frequency and/or impaired functionality of CEC during pregnancy may, therefore, predispose patients with IBD to a more pro-inflammatory milieu in their gastrointestinal tract, characterized by lower numbers of regulatory T cells (Treg), higher concentrations of IL-6 and TNF- α , and dysbiosis.¹³ In line with this, in the absence of CEC, upregulation of IL-6 and TNF- α production by residential antigen-presenting cells in the gut was observed in a mouse model of pregnancy.^{13,22} Immune activation following upregulation of TNF- α production may result in excessive tissue damage and disruption of tight junctions in IBD mothers.²⁴ In agreement with this, an increased permeability of the intestinal epithelial barrier was noted in pregnant mice when CEC were depleted.¹³ Compromised intestinal barrier integrity may result in translocation of bacteria and their products, triggering a vicious cycle of inflammatory response.

An inflammatory milieu may influence the diversity and frequency of microbial communities in the gut. As such,

the ablation of CEC was associated with dysbiosis during pregnancy, suggesting a crucial role for these cells in maintaining homeostasis and symbiosis.¹³ The initial establishment of the neonatal microbiome is mainly determined by maternal-newborn exchanges of the microbiota. During normal vaginal delivery, the newborn is exposed to an army of new allies, which colonize the urogenital tract of the mother.²⁵ Delivery via Cesarean section deprives the newborn of these microbial communities.²⁶ Thus, vaginal delivery and subsequent exposure to maternal microbiota via nursing are evolutionarily important to the development of the newborn's immune system. Interestingly, not only was the frequency of CEC observed in the cord blood and placenta of a twin delivered by Cesarean section lower than that of the vaginally delivered twin, but the CEC of the two twins also had a different gene profile.²⁷ It can, therefore, be speculated that lower levels of CEC in IBD patients may result in intestinal dysbiosis and poor pregnancy outcomes.^{28,29} In support of this hypothesis, lower CEC frequency was associated with preterm deliveries and emergency Cesarean sections.³⁰ Therefore, during gestation EE is not only required as a physiological response to the demand for a greater blood supply but it also plays a crucial role in feto-maternal tolerance and symbiosis. However, whether the source of abundant CEC in pregnant women, similar to mice, is splenic EE or due to passive incontinence from the bone marrow is unknown.

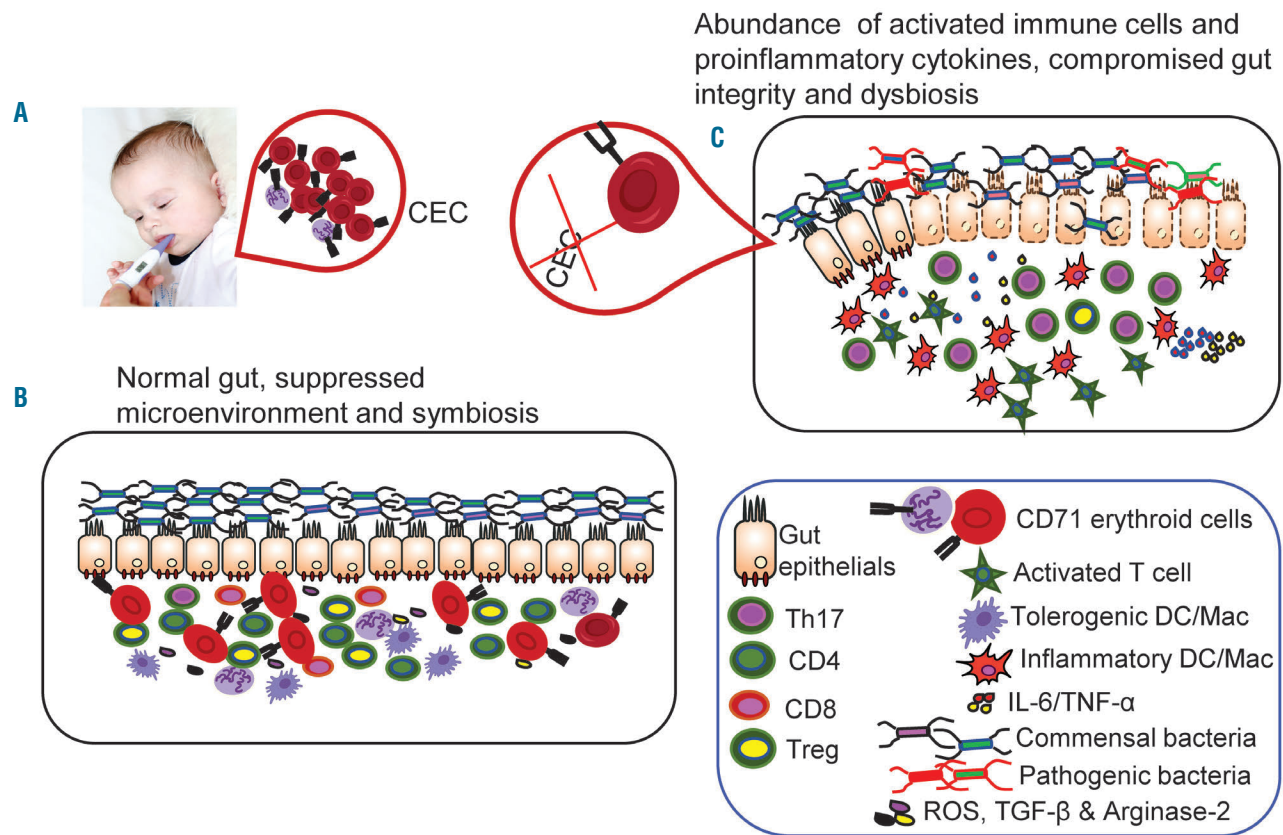


Figure 1. CD71⁺ erythroid cells play an important role in gut homeostasis. (A) Physiological abundance of CD71⁺ erythroid cells (CEC) is associated with increased neonatal susceptibility to infections. (B) Model illustrating the putative role of CEC in providing an immunosuppressive environment upon release of regulatory mediators such as reactive oxygen species, transforming growth factor- β , arginase-2 as well as the induction of regulatory T cells (Treg), which might contribute to maintaining symbiosis with the microbiome and intestinal integrity. (C) An absence or reduction of CEC results in a pro-inflammatory state associated with raised levels of tumor necrosis factor- α and interleukin-6, and hyper-immune activation, but lower numbers of Treg, which results in compromised intestinal integrity and dysbiosis. DC: dendritic cell; Mac; macrophage; IL-6: interleukin-6; TNF- α : tumor necrosis factor- α ; ROS: reactive oxygen species; TGF- β : transforming growth factor- β .

How erythroid precursors modulate immune responses in cancer

Anemia has been described as a primary consequence of tumor development in some oncological patients and animal models of cancer.³¹ The pathogenesis of cancer-related anemia is complicated and can be multifactorial. There are several reports on EE development in malignant solid tumors such as breast and lung cancers.^{32,33} Although the principal explanation for the formation of EE in solid tumors is unknown, it appears that erythropoiesis-stimulating agents may play a pivotal role in the emergence of EE niches in cancer patients.³⁴ A recent study highlighted the expansion of CEC (named Ter-cells in that study) in the spleen of an animal model of hepatocellular carcinoma.³⁵ Han *et al.* reported that tumor-derived transforming growth factor (TGF)- β activates the Smad3 downstream signaling pathway, which induces CEC from erythroid progenitor cells in the spleen. These CEC, by releasing artemin, a member of the glial cell line-derived neurotrophic factor family, directly promote the development and metastasis of hepatocellular carcinoma via an interaction of artemin with its receptor GFR α 3 on tumor cells.³⁵ Although Han *et al.* claimed that these erythroid precursors lacked immunosuppressive properties, a more recent study demonstrated immunosuppressive effects of CEC in advanced cancer.³⁶ The latter study reported an association

between the expansion of immunosuppressive CEC and impaired Epstein-Barr virus-specific CD8⁺ T-cell proliferation in patients with advanced cancer who were anemic.³⁶ This research group also described strongly impaired CD8⁺ and CD4⁺ T-cell proliferation from melanoma-bearing C57BL/6 mice by splenic CEC when co-cultured *in vitro*,³⁶ and that CD45⁺-expressing CEC showed more robust production of reactive oxygen species (ROS) compared to CD45⁻ CEC.³⁶ Accordingly, CD45⁺ CEC exhibited more potent suppression of virus-specific CD8⁺ T-cell proliferation compared to their CD45⁻ counterparts in a mouse model of chronic lymphocytic choriomeningitis virus infection.³⁶

In addition to ROS production, we believe that CEC may utilize other soluble regulatory mediators (e.g. arginase-2, TGF- β , and galectins) or, via cell-cell interactions, modulate the functionality of immune cells in different conditions including cancer (Figure 2). As proof-of-concept, Shahbaz *et al.* found that a subpopulation of neonatal CEC, which express the inhibitory molecule V-domain Ig suppressor of T-cell activation (VISTA), promotes the development of Treg through TGF- β ³⁷ as VISTA⁺ CEC were the major source of TGF- β production compared to CD71⁺ VISTA⁻ erythroid cells.³⁷ Subsequently, CD71⁺ VISTA⁺ cells, via TGF- β , promoted the generation of Treg from naïve CD4⁺ T cells *in vitro*.³⁷ It is, therefore, possible that expanded CEC in chronic

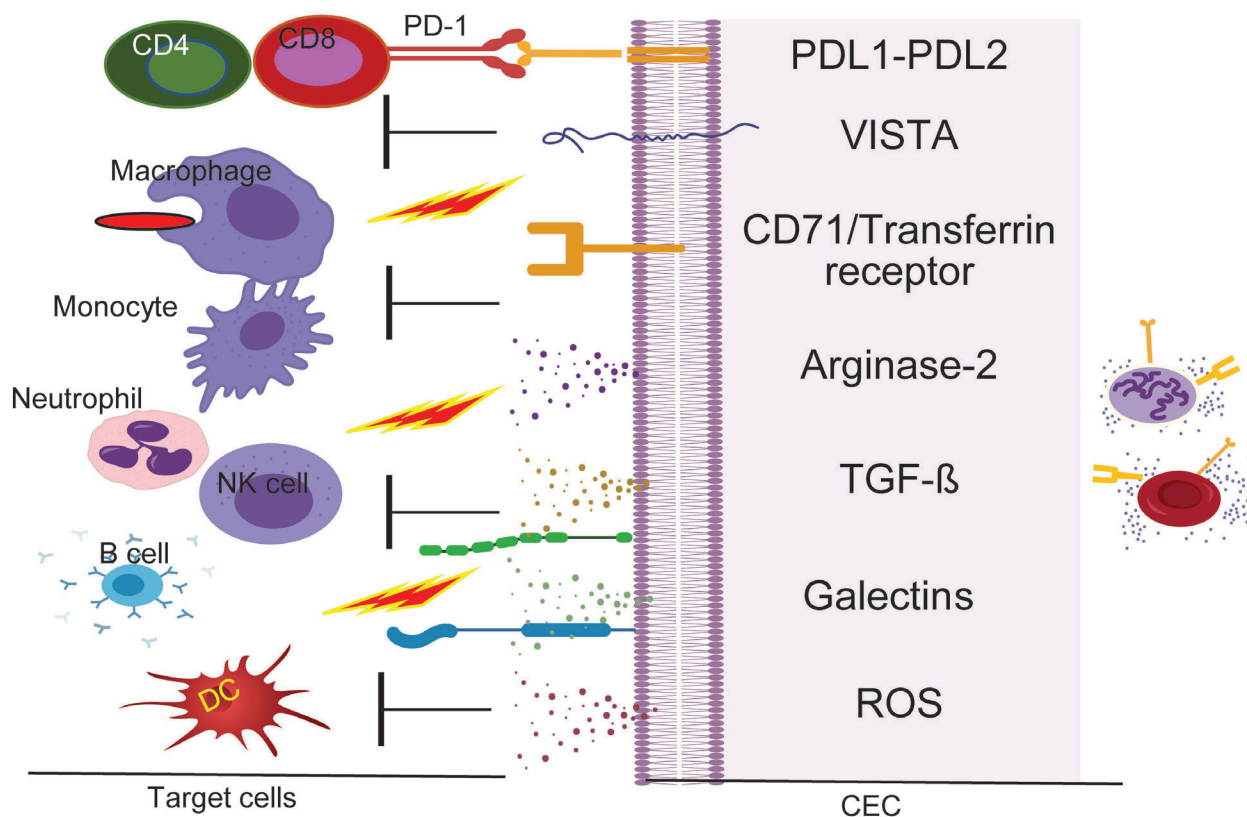


Figure 2. Putative immunoregulatory properties of CD71⁺ erythroid cells. The proposed model hypothesizes that CD71⁺ erythroid cells via cell-cell interactions (VISTA:?, PD-1:PDL1/PDL-2 and Galectins) or via soluble factors (e.g. TGF- β , Arginase-2, ROS and Galectins) suppress or modulate the functionality of different immune cells. PD-1: programmed cell death protein 1; PDL: programmed death ligand; VISTA: V-domain Ig suppressor of T-cell activation; TGF- β : transforming growth factor- β . ROS: reactive oxygen species; DC: dendritic cells; CEC: CD71⁺ erythroid cells.

conditions such as cancer can also promote the development of Treg and indirectly suppress T-cell effector functions.

Human immunodeficiency virus binds to erythroid precursors via CD235a

Although an interaction of human immunodeficiency virus (HIV) with red blood cells via the Duffy antigen receptor for chemokines and complement receptor-1 has been documented,^{38,39} the role of CEC in HIV pathogenicity has not been investigated until now. Expansion of CEC in the blood of HIV-infected and anemic individuals was recently reported.⁴⁰ It was demonstrated that these cells, via ROS, exacerbate HIV replication/infection in CD4⁺ T cells and even make CD4⁺ T cells more permissive to HIV infection. Besides, by binding to CD235a on the surface of CEC, HIV can travel to different parts of the body.⁴⁰ In support of this, a positive correlation between plasma viral load and the frequency of these cells was found in HIV patients. More importantly, it was observed that infective HIV particles reside inside CEC but not inside mature red blood cells. Therefore, by harboring HIV, CEC can play an important role in the pathogenesis of HIV-related disease.

Conclusion

In general, EE is not considered a physiological event in adults but a compensatory mechanism occurring secondary to inadequate medullary function in adults.⁴¹ EE is, therefore, identified as secondary or accessory to another factor that directly affects the bone marrow or to a systemic event that subsequently impacts the bone marrow. For instance, EE can be related to stromal abnormalities in the bone marrow such as osteopetrosis, and marrow fibrosis in which narrow storage becomes limited. Moreover, EE can be prompted by hematologic disorders, chronic infections and cancer.^{41,42} Overall, in terms of clin-

ical relevance, EE should be considered a risk factor for an underlying condition in adults. However, EE may be considered a normal physiological process during pregnancy and in developing newborns.

Regardless of the underlying mechanism, EE results in the development of erythroblastic islands in other organs/tissues, in particular the spleen and liver. EE results in an abundance of erythroid precursors or CEC in the periphery, which can be costly for the host. As we discussed above, erythroid precursors have immunosuppressive or immunomodulatory properties and their expansion can, therefore, have an impact on the effector functions of various different immune cells. CEC compromise neonatal innate immune responses against prenatal pathogens^{9,10} and also impair adaptive immunity in newborns.¹² We and others have demonstrated that CEC, via soluble mediators such as arginase-2, TGF- β , and ROS or through cell-cell interactions (e.g. PD-1:PDL-1, VISTA: ζ), suppress/modulate different immune cells *in vitro* and *in vivo*.^{11,14,36,43} These observations highlight the diverse immunosuppressive and/or immunomodulatory properties of CEC in different scenarios. The immunological consequences of EE in different pathological conditions such as autoimmune diseases, hematologic disorders, chronic infections, malnutrition, anemia, parasitic infections, and cancer should, therefore, be taken into consideration. Moreover, understanding the mechanisms controlling the extramedullary microenvironment might lead to a better comprehension of the rules balancing immunity and tolerance induction contributed by CEC, particularly during pregnancy and in newborns. In conclusion, more in-depth investigations are required to better appreciate the diverse immunological properties of these forgotten cells in different circumstances such as thalassemia, malaria and other hematologic disorders.

Acknowledgments

This work was supported by the Canadian Institutes of Health Research (CIHR), a CIHR New Investigator Salary Award (360929) and a CIHR Foundation Scheme Grant (353953) (all to SE).

References

- Palis J. Ontogeny of erythropoiesis. *Curr Opin Hematol.* 2008;15(3):155-161.
- Baron MH, Isem J, Fraser ST. The embryonic origins of erythropoiesis in mammals. *Blood.* 2012;119(21):4828-4837.
- Dzierzak E, Philipsen S. Erythropoiesis: development and differentiation. *Cold Spring Harb Perspect Med.* 2013;3(4):a011601.
- Morrison SJ, Spradling AC. Stem cells and niches: mechanisms that promote stem cell maintenance throughout life. *Cell.* 2008;132(4):598-611.
- Yamamoto K, Miwa Y, Abe-Suzuki S, et al. Extramedullary hematopoiesis: elucidating the function of the hematopoietic stem cell niche (review). *Mol Med Rep.* 2016;13(4):587-591.
- Kim CH. Homeostatic and pathogenic extramedullary hematopoiesis. *J Blood Med.* 2010;1:13-19.
- Fan N, Lavu S, Hanson CA, Tefferi A. Extramedullary hematopoiesis in the absence of myeloproliferative neoplasm: Mayo Clinic case series of 309 patients. *Blood Cancer J.* 2018;8(12):119.
- Johns JL, Christopher MM. Extramedullary hematopoiesis: a new look at the underlying stem cell niche, theories of development, and occurrence in animals. *Vet Pathol.* 2012;49(3):508-523.
- Elahi S, Ertelt JM, Kinder JM, et al. Immunosuppressive CD71+ erythroid cells compromise neonatal host defence against infection. *Nature.* 2013;504(7478):158-162.
- Dunsmore G, Bozorgmehr N, Delyea C, Koleva P, Namdar A, Elahi S. Erythroid suppressor cells compromise neonatal immune response against Bordetella pertussis. *J Immunol.* 2017;199(6):2081-2095.
- Elahi S. Neglected cells: immunomodulatory roles of CD71(+) erythroid cells. *Trends Immunol.* 2019;40(3):181-185.
- Namdar A, Koleva P, Shahbaz S, Strom S, Gerdts V, Elahi S. CD71+ erythroid suppressor cells impair adaptive immunity against Bordetella pertussis. *Sci Rep.* 2017;7(1):7728.
- Dunsmore G, Koleva P, Ghobakhloo N, et al. Lower abundance and impaired function of CD71+ erythroid cells in inflammatory bowel disease patients during pregnancy. *J Crohns Colitis.* 2019;40(3):181-185.
- Miller D, Romero R, Unkel R, et al. CD71+ erythroid cells from neonates born to women with preterm labor regulate cytokine and cellular responses. *J Leukoc Biol.* 2018;103(4):761-775.
- Kahn DA, Baltimore D. Pregnancy induces a fetal antigen-specific maternal T regulatory cell response that contributes to tolerance. *Proc Natl Acad Sci U S A.* 2010;107(20):9299-9304.
- Rowe JH, Ertelt JM, Aguilera MN, Farrar MA, Way SS. Foxp3(+) regulatory T cell expansion required for sustaining pregnancy compromises host defense against prenatal bacterial pathogens. *Cell Host Microbe.* 2011;10(1):54-64.

17. Levy O. Innate immunity of the newborn: basic mechanisms and clinical correlates. *Nat Rev Immunol.* 2007;7(5):379-390.
18. Rowe JH, Ertelt JM, Xin LJ, Way SS. Pregnancy imprints regulatory memory that sustains anergy to fetal antigen. *Nature.* 2012;490(7418):102-106.
19. Xin L, Ertelt JM, Rowe JH, et al. Cutting edge: committed Th1 CD4⁺ T cell differentiation blocks pregnancy-induced Foxp3 expression with antigen-specific fetal loss. *J Immunol.* 2014;192(7):2970-2974.
20. Cotes PM, Canning CE, Lind T. Changes in serum immunoreactive erythropoietin during the menstrual cycle and normal pregnancy. *Br J Obstet Gynaecol.* 1983;90(4):304-311.
21. Oguro H, McDonald JG, Zhao Z, Umetani M, Shaul PW, Morrison SJ. 27-Hydroxycholesterol induces hematopoietic stem cell mobilization and extramedullary hematopoiesis during pregnancy. *J Clin Invest.* 2017;127(9):3392-3401.
22. Delyea C, Bozorgmehr N, Koleva P, et al. CD71(+) erythroid suppressor cells promote fetomaternal tolerance through arginase-2 and PDL-1. *J Immunol.* 2018; 200(12):4044-4058.
23. Dalal SR, Chang EB. The microbial basis of inflammatory bowel diseases. *J Clin Invest.* 2014;124(10):4190-4196.
24. Grabinger T, Bode KJ, Demgenski J, et al. Inhibitor of apoptosis protein-1 regulates tumor necrosis factor-mediated destruction of intestinal epithelial cells. *Gastroenterology.* 2017;152(4):867-879.
25. Palmer C, Bik EM, DiGiulio DB, Relman DA, Brown PO. Development of the human infant intestinal microbiota. *PLoS Biol.* 2007;5(7):e177.
26. Dominguez-Bello MG, Costello EK, Contreras M, et al. Delivery mode shapes the acquisition and structure of the initial microbiota across multiple body habitats in newborns. *Proc Natl Acad Sci U S A.* 2010;107(26):11971-11975.
27. Dunsmore G, Koleva P, Sutton RT, Ambrosio L, Huang V, Elahi S. Mode of delivery by an ulcerative colitis mother in a case of twins: immunological differences in cord blood and placenta. *World J Gastroenterol.* 2018;24(42):4787-4797.
28. Cornish J, Tan E, Teare J, et al. A meta-analysis on the influence of inflammatory bowel disease on pregnancy. *Gut.* 2007;56(6):830-837.
29. Stephansson O, Larsson H, Pedersen L, et al. Congenital abnormalities and other birth outcomes in children born to women with ulcerative colitis in Denmark and Sweden. *Inflamm Bowel Dis.* 2011;17(3):795-801.
30. Gomez-Lopez N, Romero R, Xu Y, et al. Umbilical cord CD71+ erythroid cells are reduced in neonates born to women in spontaneous preterm labor. *Am J Reprod Immunol.* 2016;76(4):280-284.
31. Kim A, Rivera S, Shprung D, et al. Mouse models of anemia of cancer. *PloS One.* 2014;9(3):e93283.
32. Hsu FI, Filippa DA, Castro-Malaspina H, Downey RJ. Extramedullary hematopoiesis mimicking metastatic lung carcinoma. *Ann Thorac Surg.* 1998;66(4):1411-1413.
33. Redmond J 3rd, Kantor RS, Auerbach HE, Spiritos MD, Moore JT. Extramedullary hematopoiesis during therapy with granulocyte colony-stimulating factor. *Arch Pathol Lab Med.* 1994;118(10):1014-1015.
34. Han Y, Liu Q, Hou J, et al. Tumor-induced generation of splenic erythroblast-like Ter-cells promotes tumor progression. *Cell.* 2018;173(3):634-648.
35. Zhao L, He R, Long H, et al. Late-stage tumors induce anemia and immunosuppressive extramedullary erythroid progenitor cells. *Nat Med.* 2018;24(10):1536-1544.
36. Shahbaz S, Bozorgmehr N, Koleva P, et al. CD71+VISTA+ erythroid cells promote the development and function of regulatory T cells through TGF-beta. *PLoS Biol.* 2018;16(12):e2006649.
37. He W, Neil S, Kulkarni H, et al. Duffy antigen receptor for chemokines mediates trans-infection of HIV-1 from red blood cells to target cells and affects HIV-AIDS susceptibility. *Cell Host Microbe.* 2008;4(1):52-62.
38. Montefiori DC, Graham BS, Zhou JY, Zhou JT, Ahearn JM. Binding of human immunodeficiency virus type 1 to the C3b/C4b receptor CR1 (CD35) and red blood cells in the presence of envelope-specific antibodies and complement. *National Institutes of Health AIDS Vaccine Clinical Trials Networks. J Infect Dis.* 1994;170(2):429-432.
39. Namdar A, Dunsmore G, Shahbaz S, et al. CD71(+) erythroid cells exacerbate HIV-1 susceptibility, mediate trans-infection, and harbor infective viral particles. *mBio.* 2019;10(6).
40. Sohawon D, Lau KK, Lau T, Bowden DK. Extra-medullary haematopoiesis: a pictorial review of its typical and atypical locations. *J Med Imaging Radiat Oncol.* 2012;56(5):538-544.
41. Neiman RS, Barcos M, Berard C, et al. Granulocytic sarcoma: a clinicopathologic study of 61 biopsied cases. *Cancer.* 1981;48(6):1426-1437.
42. Elahi S. New insight into an old concept: role of immature erythroid cells in immune pathogenesis of neonatal infection. *Front Immunol.* 2014;5:376.



Geriatric assessment in older patients with a hematologic malignancy: a systematic review

Ellen R.M. Scheepers,¹ Ariel M. Vondeling,² Noortje Thielen,¹ René van der Griend,¹ Reinhard Stauder³ and Marije E. Hamaker²

¹Department of Internal Medicine, Diaconessenhuis Utrecht, Utrecht, the Netherlands;

²Department of Geriatric Medicine, Diaconessenhuis Utrecht, Utrecht, the Netherlands

and ³Department of Internal Medicine V (Hematology and Oncology), Innsbruck Medical University, Innsbruck, Austria

Haematologica 2020
Volume 105(6):1484-1493

ABSTRACT

The aim of this systematic review is to give an update of all currently available evidence on the relevance of a geriatric assessment in the treatment of older patients with hematologic malignancies. A systematic search in MEDLINE and EMBASE was performed to find studies in which a geriatric assessment was used to detect impaired geriatric domains or to address the association between geriatric assessment and survival or clinical outcome measures. The literature search included 4,629 reports, of which 54 publications from 44 studies were included. Seventy-three percent of the studies were published in the last 5 years. The median age of the patients was 73 years (range, 58-86) and 71% had a good World Health Organization (WHO) performance status. The median prevalence of geriatric impairments varied between 17% and 68%, even in patients with a good WHO performance status. Polypharmacy, nutritional status and instrumental activities of daily living were most frequently impaired. Whereas several geriatric impairments and frailty (based on a frailty screening tool or summarized geriatric assessment score) were predictive for a shorter overall survival, WHO performance status lost its predictive value in most studies. The association between geriatric impairments and treatment-related toxicity varied, with a trend towards a higher risk of (non-)hematologic toxicity in frail patients. During the follow-up, frailty seemed to be associated with treatment non-completion, especially when patients were malnourished. Patients with a good physical capacity had a shorter stay in hospital and a lower rate of hospitalization. Geriatric assessment, even in patients with a good performance status, can detect impaired geriatric domains and these impairments may be predictive of mortality. Moreover, geriatric impairments suggest a higher risk of treatment-related toxicity, treatment non-completion and use of healthcare services. A geriatric assessment should be considered before starting treatment in older patients with hematologic malignancies.

Correspondence:

ELLEN.R.M. SCHEEPERS
escheepers@diakhuis.nl

Received: December 24, 2019.

Accepted: April 2, 2020.

Pre-published: May 7, 2020.

doi:10.3324/haematol.2019.245803

Check the online version for the most updated information on this article, online supplements, and information on authorship & disclosures: www.haematologica.org/content/105/6/1484

©2020 Ferrata Storti Foundation

Material published in *Haematologica* is covered by copyright. All rights are reserved to the Ferrata Storti Foundation. Use of published material is allowed under the following terms and conditions:

<https://creativecommons.org/licenses/by-nc/4.0/legalcode>.

Copies of published material are allowed for personal or internal use. Sharing published material for non-commercial purposes is subject to the following conditions:

<https://creativecommons.org/licenses/by-nc/4.0/legalcode>,

sect. 3. Reproducing and sharing published material for commercial purposes is not allowed without permission in writing from the publisher.



Introduction

Given the increasing life expectancy and aging of the population, there is a growing number of older patients with cancer, including patients with a hematologic malignancy. Worldwide, hematologic malignancies account for approximately 9% of all cancers and are the fourth most frequently diagnosed cancer.¹ At present, 60% of these patients are older than 65 years and this proportion will increase in the future.^{2,3}

Over the last decades, treatment options for hematologic malignancies have progressed. For example, the initial treatment of patients with multiple myeloma changed from cytotoxic chemotherapeutics to better-tolerated agents such as immuno-modulatory drugs or monoclonal antibodies.⁴ Moreover, the proportion of older patients with myelodysplastic syndrome or acute myeloid leukemia undergoing hematopoietic stem cell transplantation has increased, partly due to expansion of age limits.^{5,6}

However, it can be difficult to deliver optimal cancer treatment tailored to individual needs of an older patient, particularly as older patients are frequently excluded from clinical trials.⁷ Older patients constitute a heterogeneous population due to large differences in comorbidity, functional capacity and psychological and physical reserves. As a result, the benefit of treatment can differ and patients with comorbidity or geriatric impairments are particularly at risk of adverse health outcomes. Choosing the optimal treatment for these patients is a challenge.

It is therefore recommended that the degree of frailty of older patients is assessed.⁸ Frailty is a biological syndrome which can exist alongside age, comorbidity or disease characteristics. Over the years, numerous definitions of frailty have been formulated and there is still no consensus on a definition.⁹ There are two commonly used approaches to define frailty. The first defines frailty based on phenotypic criteria including reduced grip strength, walking speed, physical capacity, level of energy and weight loss. Patients are considered frail if three or more criteria are present.¹⁰ The second approach proposes a frailty index which is an accumulation of patient's deficits. These deficits consist of physical or cognitive symptoms, functional impairments, abnormal laboratory values and comorbidities.^{11,12} In daily practice, frailty is a dynamic state which needs a multidimensional approach and might have various implications in different scenarios.

An appropriate method to assess the level of frailty of older patients is a geriatric assessment.^{8,13} This consists of a systematic assessment of an older patient's health status focusing on somatic, psychological, functional and social domains. Different tools can be used to detect geriatric impairments in these domains.¹⁴ Moreover, frailty screening tools were developed in order to identify older patients who require a full geriatric assessment.¹⁵ Nowadays, some form of geriatric assessment is increasingly incorporated in hemato-oncologic care to customize hemato-oncologic treatment.¹⁶

In 2014, we published a systematic review on the value of performing a geriatric assessment in older patients with a hematologic malignancy, demonstrating that such an assessment can detect multiple health issues and has predictive value for clinical outcome in older patients with a hematologic malignancy.¹⁷ However, evidence was limited, especially regarding clinical outcomes such as treatment-related toxicity, treatment completion or physical functioning after treatment. Since then, many new studies have been published on this subject. The aim of this present systematic review is, therefore, to give an update of all currently available data on the association between geriatric impairments and hematologic cancer-related outcomes.

Methods

Search strategy and article selection

Our aim was to identify studies concerning patients with a hematologic malignancy in which a geriatric assessment was used to detect geriatric impairments or which addressed the association between baseline geriatric assessment and outcome.

Geriatric assessment was defined as an assessment composed of at least two of the following domains: cognitive function, mood, nutritional status, activities of daily living (ADL), instrumental activities of daily living (IADL), polypharmacy (using five or more drugs), objectively measured physical capacity (for

instance, gait speed, hand grip strength or balance tests), social support and frailty (assessed with a frailty screening tool or by summarizing the geriatric assessment). As prior medical history/comorbidity and performance status are routine parts of the hematologic work-up, these were not counted as domains of the geriatric assessment for this particular systematic review. The following items were defined as outcomes: prevalence of geriatric impairments, change in oncologic treatment plan, toxicity of chemotherapy, healthcare utilization, physical functioning after treatment, quality of life after treatment and mortality.

The following search was performed on March 4, 2019 and updated on January 20, 2020, in both MEDLINE and EMBASE: (((("Hematologic Neoplasms"[Mesh] OR "Leukemia"[Mesh] OR "Lymphoma"[Mesh] OR "Multiple Myeloma"[Mesh] OR "Myelodysplastic Syndromes"[Mesh] OR leukemia[tiab] OR leukaemia[tiab] OR lymphoma*[tiab] OR hodgkin*[tiab] OR non-hodgkin*[tiab] OR (multiple myeloma[tiab]) OR myelodysplas*[tiab] OR (haematolog* AND malignan*[tiab]) OR (hematolog* AND malignan*[tiab]) OR (myeloid[tiab] OR lymphoid[tiab] AND neoplas*[tiab]) OR myeloproliferative[tiab] OR (plasma cell neoplas*[tiab]) OR plasma cell dyscrasia*[tiab] OR (myeloid[tiab] AND sarcoma*[tiab]) OR waldenstrom[tiab] OR myelofibrosis[tiab] OR mastocytosis[tiab] OR (polycyth* AND vera[tiab]) OR (essential AND thrombocyt*[tiab]))) AND (("frailty"[All Fields] OR "Geriatric Assessment"[Mesh] OR frail*[tiab] OR vulnerabl*[tiab] OR geriatric assessment*[tiab] OR geriatric*[tiab]))

No age or language limitations were applied. All search results until 2013 were reviewed previously by Hamaker *et al.*¹⁷ We therefore limited our search to studies published after January 1, 2013. The titles and abstracts of all studies retrieved by the search were assessed by one reviewer (ES) to determine which warranted further examination. The full texts of all potentially relevant articles were subsequently screened. We excluded studies that did not focus exclusively on hematologic malignancies. Finally, references of included studies were cross-referenced to retrieve any additional relevant citations. Eligible studies from all searches (2013, 2019, 2020) were subsequently combined to form the final study selection.

Data extraction

For each eligible study, data regarding study design and results were independently extracted by two authors (ES and AV). Extracted items included the type of study, study population (number of patients, median age, malignancy subtype, stage, treatment) and the content of the geriatric assessment. Only validated tools from the geriatric assessment were included. If multiple tools were used to assess one geriatric domain, the result of the most commonly used tool was noted. We registered the prevalence of geriatric impairments, and the reported results on the association between the geriatric assessment and outcome measures. If necessary, study authors were contacted to obtain additional data.

Quality assessment

The methodological quality of each of the studies was assessed independently by two reviewers (ES and AV), using the Newcastle-Ottawa scale adapted to this subject (*Online Supplementary Table S1*).¹⁸ As our main focus was on older patients with hematologic malignancies, we classified studies of patients with a median age less than 68 years old, or with more than one third of the patients younger than 65 years old, as not being fully representative of our target population. Disagreements among the reviewers were discussed during a consensus meeting and in the case of persisting disagreement, the assistance of a third reviewer (MH) was enlisted.

Data synthesis and analysis

Due to the heterogeneity in the populations of patients and in study designs, with a wide variety in content of geriatric assessments, a meta-analysis was not considered feasible. We therefore summarized the study results to describe our main outcomes of interest.

Results

Study characteristics

The literature search yielded 4,629 citations (832 from MEDLINE and 3,797 from EMBASE), of which 403 were duplicates and 4,184 were excluded for other reasons

(*Online Supplementary Figure S1*). This resulted in 42 eligible publications from 34 studies. Cross-referencing yielded four additional publications. Eight publications from the 2014 review by Hamaker *et al.*¹⁷ were also eligible. Thus, we ultimately included 54 publications from 44 studies in this review.¹⁹⁻⁷²

The characteristics of these 44 studies are summarized in Table 1. Seventy-three percent were published in the last 5 years. The median sample size of the studies was 100 (range, 25-869), and the median age of included patients ranged from 58 to 86 years. Eight studies focused on acute myeloid leukemia and/or myelodysplastic syndromes,^{19-25,27} two on chronic lymphocytic leukemia,^{28,29} 13 on lymphoma,³⁰⁻⁴² seven on multiple myeloma,⁴²⁻⁴⁸ and

Table 1. Characteristics of studies on the association between the geriatric assessment and outcome measures.

Publication Author	Year	Study population				Treatment	GA		Outcome measures		
		Patient population	Type of malignancy	N. of patients	Me(dia)n age*		N. of domains assessed	Summarized GA score	Prevalence of geriatric conditions	Survival	Other
Aguiar ¹⁹	2020	65+	MDS	79	77 (70-84)	No disease-modifying therapy	3		+		
Corsetti ²⁰	2013	65+ or unfit for aggressive CT	AML; RAEB	31	72 (55-84)	CT	2	+	+	+	
Deschler ²¹	2013	60+	AML; MDS	195	71 (60-87)	BSC; CT	5		+	+	
Holmes ²²	2014	60+	AML; MDS	50	65 (60-73)	HSCT	8	+	+		
Klepin ²³	2013	60+	AML	74	68 (65-74)	CT	5		+	+	
Klepin ²⁴	2020	60+	AML (FLT3)	40	68 (61-83)	CT	7		+	+	
Molga ^{25,26}	2020	65+	AML; MDS	98	77 (66-95)	BSC;CT	7		+	+	Treatment completion
Umit ²⁷	2018	no age limit	AML	372	63 (19-97)	CT	4		+	+	
Goede ²⁸	2016	no age limit	CLL	75	75 (48-87)	CT	3		+	+	Toxicity
Molica ²⁹	2019	65+	CLL	108	71 (65-90)	CT	2	+	+	+	Toxicity
Ribi ³⁰	2017	no age limit	B-cell lymphoma	41	75 (40-94)	Various	4	+	+	+	
Merli ³¹	2020	65+ and unfit	DLBCL	33	82 (68-89)	CT	2		+		
Ong ³²	2019	60+	DLBCL	205	73 (60-97)	CT	2	+	+	+	Health care utilization, toxicity, treatment completion
Spina ³³	2012	70+	DLBCL	100	75 (70-89)	CT	4	+	+	+	Toxicity
Tucci ³⁴	2009	65+	DLBCL	84	73 (66-89)	CT	1	+	+	+	Toxicity
Tucci ³⁵	2015	69+	DLBCL	173	77	Various	2	+	+	+	
Aaldriks ³⁶	2015	70+	NHL	44	78 (70-86)	CT	3		+	+	Treatment completion
Naito ³⁷	2016	65+	NHL	93	77 (65-90)	Various	5		+	+	Toxicity
Park ³⁸	2015	65+	NHL	70	74 (65-92)	CT	4		+	+	Treatment completion
Siegel ³⁹	2006	60+	NHL	25	70 (60-85)	?	3		+		
Soubeyran ⁴⁰	2011	70+, unfit for aggressive CT	NHL	32	79 (70-92)	CT	4		+	+	
Winkelmann ⁴¹	2011	18+	NHL	143	63 (18-88)	CT	2		+	+	
Okuyama ⁴²	2015	65+	Lymphoma; MM	106	74 (65-90)	CT	5	+	+		
Engelhardt ⁴³	2016	no age limit	MM	125	63 (56-71)	CT	2		+	+	
Gavriatopoulou ⁴⁴	2019	80+	MM	110	83 (80-92)	CT	3		+	+	
Palumbo ⁴⁵	2015	70+	MM	869	74 (70-78)	CT	2	+	+	+	Toxicity, Treatment completion
Rosko ⁴⁶	2019	18+	MM; amyloidosis	100	59 (36-75)	HSCT	6		+		Health care utilization
Wildes ⁴⁷	2019	65+	MM	40	71 (66-76)	BSC;HSCT	5		+		
Zhong ⁴⁸	2017	no age limit	MM	628	58 (52-66)	CT	2	+	+	+	Toxicity

continued on the next page

continued from the previous page

Buckstein ⁴⁹	2016	65+	Various	445	71 (65-79)	CT	3		+	+	
Deschler ⁵⁰	2018	60+	Various	106	66 (60-78)	HSCT	5		+	+	
Derman ⁵¹	2019	60+	Various	192	>67 (60-83)	HSCT	5		+		
Dubruille ⁵²	2015	65+	Various	90	74 (65-89)	CT	8	+	+	+	
Dumontier ⁵³	2019	75+	Various	464	80 (76-84)	BSC; CT	3		+	+	Health care utilization
Hamaker ⁵⁴	2016	65+	Various	157	78 (67-99)	Various	7	+	+	+	
Huang ⁵⁵	2020	50+	Various	148	62 (50-76)	HSCT	6		+	+	Health care utilization, toxicity
Lin ⁵⁶	2020	60+	Various	457	66 (60-79)	HSCT	5		+	+	
Liu ⁵⁷	2019	75+	Various	448	80 (76-84)	BSC; CT	2	+	+	+	Health care utilization
Muffly ⁵⁸	2014	50+	Various	203	58 (54-63)	HSCT	3	+	+	+	
Nawas ⁵⁹	2019	50+	Various	184	61 (50-75)	HSCT	5		+	+	Health care utilization, toxicity
Rodrigues ⁶⁰	2020	60+	Various	40	68 (60-76)	HSCT	6	+	+		
Rollot-Trad ⁶¹	2008	75+, geriatric department	Various	54	86 (75-99)	Various	4		+	+	
Silay ⁶²	2015	65+	Various	61	69	?	7		+		Health care utilization
Velghe ⁶³	2014	70+	Various	50	76 (70-87)	Various	6	+	+		

*Reported as mean (\pm standard deviation) or median (range or interquartile range). GA: geriatric assessment; MDS: myelodysplastic syndrome; CT: chemotherapy; AML: acute myeloid leukemia; RAEB: refractory anemia with excess of blasts; FLT3: FMS like tyrosine kinase-3; BSC: best supportive care; HSCT: hematopoietic stem cell transplantation; CLL: chronic lymphocytic leukemia; DLBCL: diffuse large B-cell lymphoma; NHL: non-Hodgkin lymphoma; MM: multiple myeloma.

15 studies included various hematologic malignancies.⁴⁹⁻⁶³

The median number of domains addressed in the geriatric assessment was four (range, 2-9). These included ADL in 30 studies (68%), IADL in 37 (84%), cognition in 29 (66%), mood in 24 (55%) and objectively measured physical capacity in 20 studies (46%). Domains less commonly assessed were nutritional status (11 studies; 25%), social support (8 studies; 18%), polypharmacy (13 studies; 30%) and frailty (8 studies assessed with a frailty screening tool and 17 studies by summarizing the geriatric assessment; 18% and 39%, respectively).

The prevalence of geriatric impairments was assessed in all studies (100%). The association between geriatric impairments and mortality was addressed in 33 studies (75%), treatment-related toxicity in ten studies (23%), treatment completion in five (11%) and healthcare utilization in seven studies (16%). No studies assessed the association of geriatric impairments with physical functioning or quality of life after treatment.

Quality assessment

The results of the quality assessment are shown in Figure 1. Detailed results per study are listed in *Online Supplementary Table S1*. The overall quality of the studies was good. Nine studies included a significant proportion of younger patients (i.e. median age less than 68 years old, or more than one third of the patients younger than 65 years old);^{22,27,41,43,46,48,50,58,59} these studies were assessed as not being fully representative of the target cohort of the average older patients with a hematologic malignancy. Similarly, eight studies focused on a very specific treatment^{20,23,24,31,51,55,56,60} which we considered as not fully representative of our target population. Overall, the duration of follow-up was sufficient but in nine studies the follow-up rate was less than 90%^{24,30,46} or the adequacy of follow-up was not reported.^{27,32,33,56,57,62} There were no other quality concerns.

Prevalence of geriatric impairments

The prevalence of geriatric impairments is shown in Table 2. The most commonly reported issues were polypharmacy (in a median of 51% of patients; range, 17-80%), risk of malnutrition (median 44%; range, 27-82%) and IADL impairments (median 37%; range, 3-85%). Impaired physical capacity (median 27%; range, 3-80%), ADL impairments (median 18%; range, 4-67%), symptoms of depression (median 25%; range, 10-94%), and cognitive impairment (median 17%; range, 0-44%) were less common. Four studies that addressed social support showed impairment in a median of 20% (range, 7-54%). The median proportion of patients seen as frail based on a frailty screening tool was 68% (range, 25-76%). The median proportion of patients screened as frail based on a summarized geriatric assessment score was 45% (range, 10-88%).

Overall, the median proportion of patients with at least one geriatric impairment was 51% (range, 9-82%). By comparison, the median proportion of patients with a World Health Organization (WHO) performance status of 2 or higher was only 29% (range, 1-91%). Even in studies in which the median age of patients was ≤ 65 years old, or a small proportion of patients had a poor WHO performance status, geriatric impairments were quite common. For example, in one study, 93% of included patients had a WHO performance status of 0-1; nonetheless, 45% of patients had impairments in IADL, 39% in physical capacity and 25% were frail based on a frailty screening tool (Table 2).⁴⁹

Association between geriatric impairments and mortality

The association of geriatric impairments with mortality was addressed in 33 studies (Table 3). In univariate analysis, 27 out of 29 studies (93%) showed a significant association between at least one geriatric impairment and mortality. The association between a specific geriatric domain and mortality varied between 0 and 74%.

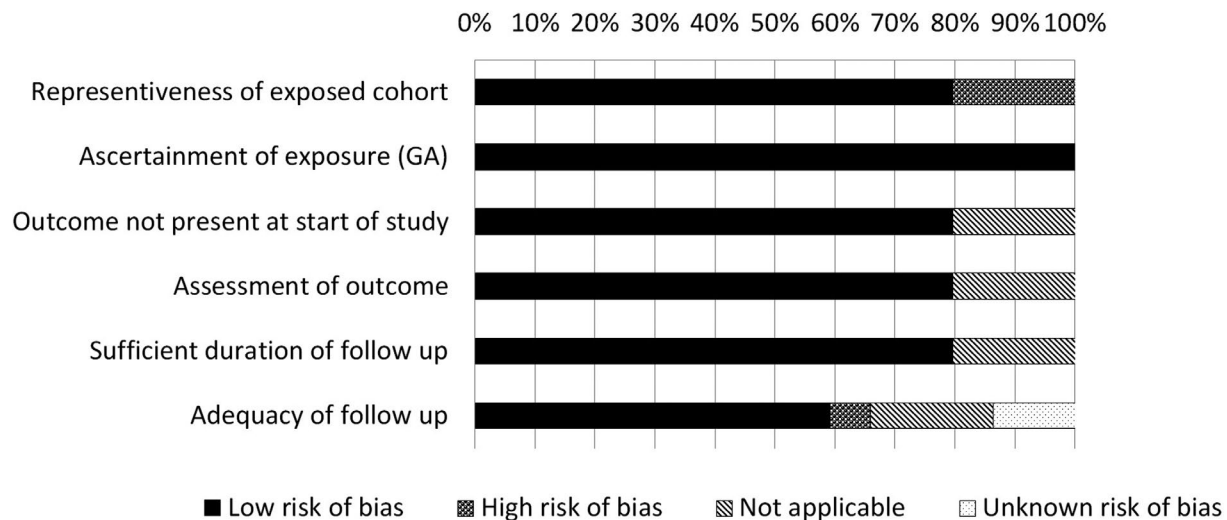


Figure 1. Outcome of the quality assessment. Details are reported in *Online Supplementary Table S1A* (quality assessment questionnaire) and *Online Supplementary Table S1B* (assessment per study).

Polypharmacy was assessed in only two studies and showed no association. For all other geriatric domains except mood, nutritional status and social support, at least 50% of the studies reported a univariate association between impairment and mortality. IADL, ADL, impaired physical capacity and cognition were most frequently associated with mortality (in 74%, 67%, 63% and 55% of the studies, respectively). In multivariable analyses, ADL, IADL, impaired physical capacity and cognition remained associated with mortality (in 40%, 62%, 50% and 50% of the studies, respectively). Moreover, at least 75% of all studies that assessed frailty (with a frailty screening tool or by summarizing the geriatric assessment), demonstrated that this was associated with mortality in multivariable analyses.

Risk factors for mortality commonly used in hematology such as age, WHO performance status and comorbidity were also associated with mortality in univariate analysis (in 79%, 63% and 64% of the studies, respectively). However, in multivariable analyses, this association was no longer present for WHO performance status; age and comorbidity retained their association with mortality in 43% and 47% of the studies, respectively.

Association of geriatric impairments with treatment-related toxicity

Ten studies assessed geriatric impairments in relation to treatment-related toxicity.^{28,29,32-34,37,45,48,55,59} Four out of six studies in which frailty was assessed (based on a summarized geriatric assessment score) reported an association between frailty and treatment-related toxicity.^{33,34,45,48} This included hematologic toxicity in one study,³³ non-hematologic toxicity in two studies^{45,48} and overall toxicity in one study.³⁴ One study showed an association specifically between impaired IADL and treatment-related infections in patients with chronic lymphocytic leukemia.²⁸ In studies in which patients with various hematologic malignancies were included, associations between physical capacity⁵⁵ or cognition⁵⁹ and treatment-related toxicity were demonstrated. No other associations between frailty

(based on a summarized geriatric assessment score) or individual geriatric domains and treatment-related toxicity were found in these ten studies.

Association of geriatric impairments with treatment completion

The association of geriatric impairments with the ability to complete the proposed treatment was studied in five studies.^{25,32,36,38,45} Four out of five studies found an association between geriatric impairments and treatment completion. The risk of treatment non-completion was significantly higher in frail patients (based on a summarized geriatric assessment score or frailty screening tool) than in fit patients.^{25,36,38,45} Three studies showed a significant association between a specifically geriatric domain and treatment non-completion: in two studies that included patients with non-Hodgkin lymphoma, malnutrition was associated with treatment non-completion.^{36,38} Another study, in which patients with acute myeloid leukemia or myelodysplastic syndrome were included, showed an association between impaired IADL, impaired physical capacity or cognitive impairment and treatment non-completion. In this study, no other geriatric impairments or clinical characteristics such as comorbidity or WHO performance status were associated with treatment non-completion.²⁵

Association of geriatric impairments with healthcare utilization

The association of geriatric impairments and health care utilization was addressed in seven studies.^{32,46,53,55,57,59,62} Six out of these studies showed an association between geriatric impairments and health care utilization. In four studies impaired physical capacity was associated with increased use of health care.^{46,55,57,62} In patients with various hematologic malignancies, other geriatric impairments, such as ADL,⁶² IADL,⁵³ cognition⁵⁹ and mood⁴⁶ were also associated with health care utilization. In one study with patients with diffuse large B-cell lymphoma, no association was found between frailty (assessed by a summarized geriatric assessment score) and unplanned admissions.³²

Table 2. Comparison of impaired performance status with impairments in geriatric domains.

Author	Year	Type of malignancy	N	Me(d)ian age*	Poor PS	ADL	IADL	Cognition	Mood	Physical capacity	Nutritional status	Social support	Poly-pharmacy	Frailty screening tool	Summarised GA score
Aguiar ¹⁹	2020	MDS	76	77 (70-84)	-	-	-	-	-	80 %	-	-	61 %	38 %	-
Corsetti ²⁰	2013	AML; RAEB	31	72 (55-84)	38 %	17 %	59 %	-	-	-	-	-	-	-	54 %
Deschler ²¹	2013	AML; MDS	195	71 (60-87)	47 %	34 %	31 %	9 %	14 %	55 %	-	-	-	-	-
Holmes ²²	2014	AML; MDS	50	65 (60-73)	12 %	16 %	-	16 %	10 %	18 %	36 %	54 %	> 28 %	-	66 %
Klepin ²³	2013	AML	74	68 (65-74)	22 %	50 %	41 %	29 %	40 %	50 %	-	-	-	-	-
Klepin ²⁴	2020	AML (FLT3)	40	68 (61-83)	?	?	?	?	?	56 %	-	?	36 %	-	-
Molga ^{25,26}	2020	AML; MDS	98	77 (66-95)	28 %	29 %	34 %	11 %	32 %	31 %	27 %	-	-	68 %	-
Umit ²⁷	2018	AML	372	63 (19-97)	91 %	-	80 %	14 %	79 %	-	-	-	-	70 %	-
Goede ²⁸	2016	CLL	75	75 (48-87)	?	-	19 %	29 %	-	48 %	-	-	-	-	-
Molica ²⁹	2019	CLL	108	71 (65-90)	?	16 %	19 %	-	-	-	-	-	-	-	10 %
Ribi ³⁰	2017	B-cell lymphoma	41	75 (40-94)	15 %	-	-	27 %	20 %	-	73 %	7 %	-	-	39 %
Merli ³¹	2020	DLBCL	33	85 (68-89)	6 %	18 %	3 %	-	-	-	-	-	-	-	-
Ong ³²	2019	DLBCL	205	73 (60-97)	7 %	7 %	36 %	-	-	-	-	-	-	-	38 %
Spina ³³	2012	DLBCL	100	75 (70-89)	26 %	27 %	31 %	?	?	-	-	-	-	-	13 %
Tucci ³⁴	2009	DLBCL	84	73 (66-89)	?	12 %	-	-	-	-	-	-	-	-	50 %
Tucci ³⁵	2015	DLBCL	173	77	?	>4 %; <54 %	>9 %; <54 %	-	-	-	-	-	-	-	38 %
Aaldriks ³⁶	2015	NHL	44	78 (70-86)	6 %	-	-	5 %	-	-	34 %	-	-	43 %	-
Naito ³⁷	2016	NHL	93	77 (65-90)	22 %	28 %	27 %	4 %	15 %	-	51 %	-	-	-	-
Park ³⁸	2015	NHL	70	74 (65-92)	39 %	-	-	37 %	21 %	-	36 %	-	-	47 %	-
Siegel ³⁹	2006	NHL	25	70 (60-85)	12 %	-	-	0 %	16 %	12 %	-	-	-	-	-
Soubeyran ⁴⁰	2011	NHL	32	79 (70-92)	41 %	59 %	81 %	38 %	94 %	-	-	-	-	-	-
Winkelmann ⁴¹	2011	NHL	143	63 (18-88)	16 %	18 %	21 %	-	-	-	-	-	-	-	-
Okuyama ⁴²	2015	Lymphoma; MM	106	74(65-90)	29 %	33 %	45 %	23 %	30 %	-	-	-	17 %	-	50 %
Engelhardt ⁴³	2016	MM	125	63 (56-71)	28 %	48 %	85 %	-	-	-	-	-	-	-	-
Gavriatopoulou ⁴⁴	2019	MM	110	83 (80-92)	> 60 %	18 %	42 %	-	-	-	-	-	-	73 %	-
Palumbo ⁴⁵	2015	MM	869	74 (70-78)	21 %	14 %	18 %	-	-	-	-	-	-	-	30 %
Rosko ⁴⁶	2019	MM; amyloidosis	100	59 (36-75)	48 %	?	?	?	19 %	7 %	-	?	-	-	-
Wildes ⁴⁷	2019	MM	40	71 (66-76)	40 %	-	63 %	10 %	?	40 %	-	-	77 %	-	-
Zhong ⁴⁸	2017	MM	628	58 (52-66)	?	67 %	55 %	-	-	-	-	-	-	-	64 %
Buckstein ⁴⁹	2016	Various	445	71 (65-79)	7 %	-	45 %	-	-	39 %	-	-	-	25 %	-
Deschler ⁵⁰	2018	Various	106	66 (60-78)	60 %	9 %	31 %	12 %	-	3 %	76 %	-	-	-	-
Derman ⁵¹	2019	Various	192	>67(60-83)	< 50 %	-	40 %	7 %	22 %	-	-	?	54 %	-	-
Dubruille ⁵²	2015	Various	90	74 (65-89)	32 %	11 %	39 %	31 %	25 %	4 %	44 %	-	50 %	72 %	80 %
Dumontier ⁵³	2019	Various	464	80 (76-84)	?	11 %	27 %	?	-	-	-	-	-	-	-
Hamaker ⁵⁴	2016	Various	157	78 (67-99)	42 %	22 %	47 %	18 %	29 %	30 %	-	20 %	66 %	-	71 %
Huang ⁵⁵	2020	Various	148	62 (50-76)	28 %	-	39 %	1 %	44 %	8 %	-	?	50 %	-	-
Lin ⁵⁶	2020	Various	457	66 (60-79)	<47 %	4 %	11 %	44 %	18 %	-	-	-	50 %	-	-
Liu ⁵⁷	2019	Various	448	80 (76-84)	47 %	-	-	18 %	-	56 %	-	-	-	-	53 %
Muffly ⁵⁸	2014	Various	203	58 (54-63)	29 %	7 %	40 %	-	-	24 %	-	-	-	-	25 %
Nawas ⁵⁹	2019	Various	184	61 (50-75)	1 %	-	36 %	3 %	35 %	15 %	-	?	-	-	-
Rodrigues ⁶⁰	2020	Various	40	68 (60-76)	75 %	-	10 %	21 %	18 %	16 %	43 %	-	80 %	-	19 %
Rollot-Trad ⁶¹	2008	Various	54	86 (75-99)	56 %	39 %	51 %	27 %	-	-	-	-	39 %	-	-
Silay ⁶²	2015	Various	61	69	?	21 %	26 %	26 %	34 %	16 %	27 %	-	51 %	-	-
Velghe ⁶³	2014	Various	50	76 (70-87)	?	24 %	38 %	4 %	30 %	-	82 %	-	-	76 %	88 %

*Reported as mean (\pm standard deviation) or median (range or interquartile range)? Although geriatric condition was assessed, the proportion of patients with geriatric impairments could not be extracted from the published data. PS: World Health Organization performance status; ADL: activities of daily living; IADL: instrumental activities of daily living; GA: geriatric assessment; MDS: myelodysplastic syndrome; AML: acute myeloid leukemia; RAEB: refractory anemia with excess of blasts; FLT3: FMS-like tyrosine kinase-3; CLL: chronic lymphocytic leukemia; DLBCL: diffuse large B-cell lymphoma; NHL: non-Hodgkin lymphoma; MM: multiple myeloma.

Discussion

This systematic review of 44 studies shows that impairment in geriatric domains is common among older patients with a hematologic malignancy, even in those with a good performance status. The most relevant impairment is frailty (assessed with a frailty screening tool or by summarizing the geriatric assessment), which showed an association with mortality, treatment-related

toxicity and treatment non-completion. Other relevant geriatric impairments were IADL functioning, nutritional status and polypharmacy. Impaired physical capacity was mainly associated with healthcare utilization.

These data should, however, be interpreted with care. The included studies are heterogeneous in study population, design, treatment regimens, content of geriatric assessment and reported outcomes. Various hematologic malignancies can have very different disease courses and

Table 3. The association of geriatric assessment, age, performance status, and comorbidity with mortality.

Publication Author	Year	Number of patients	Type of malignancy	Age	PS	Comorbidity	ADL	Results of univariate and multivariate analysis						Frailty screening tool	Summarized GA score	
								IADL	Cognition	Mood	Physical capacity	Nutritional status	Social support			Polypharmacy
Corsetti ²⁰	2011	31	AML; RAEB					-							-	
Deschler ²¹	2013	195	AML; MDS	--	++	++	++	--	--	-	--					
Klepin ²²	2013	74	AML	--	--	--	--	--	++	--	++					
Klepin ²⁴	2020	40	AML (FLT3)		-	-	-	-	-	-	-		-	-		
Molga ²⁵	2020	98	AML; MDS		--	++	++	++	--	--	--	--				
Umit ²⁷	2018	372	AML	+	+										+	
Goede ²⁸	2016	75	CLL	--		-	-	--	--	--	--					
Molica ²⁹	2019	108	CLL	++	+	++	++	+							++	
Ribi ³⁰	2017	41	B-cell lymphoma			-			-	-		+	-		+	
Ong ³²	2019	205	DLBCL												++	
Spina ³³	2012	100	DLBCL				--	--							++	
Tucci ³⁴	2009	84	DLBCL												+	
Tucci ³⁵	2015	173	DLBCL	+		+	+	+							++	
Aaldriks ³⁶	2015	44	NHL									-			++	
Naito ³⁷	2016	93	NHL	-	-	++	-	+	++	-		-				
Park ³⁸	2015	70	NHL		--				-	-		++			-	
Soubeyran ⁴⁰	2011	32	NHL				+	+	+	+						
Winkelmann ⁴¹	2011	143	NHL	--	--	--	--	++								
Engelhardt ⁴³	2016	125	MM	+		++									++	
Gavriatopoulou ⁴⁴	2019	110	MM												--	
Palumbo ⁴⁵	2015	869	MM	++		--	++	++								
Zhong ⁴⁶	2017	628	MM	--		--	--	--							-	
Buckstein ⁴⁹	2016	445	Various	+	+	++		+			+				++	
Deschler ⁵⁰	2018	106	Various	++	++	-		-			+	-				
Dubruille ⁵²	2015	90	Various	++	--	-			++		-	-		-	-	
Dumontier ⁵³	2019	452	Various	--		--	--	++								
Hamaker ⁵⁴	2016	157	Various	--	--	--									++	
Huang ⁵⁵	2020	148	Various		-			++	-							
Lin ⁵⁶	2020	457	Various	+	++	--		++								
Liu ⁵⁷	2019	448	Various	++					++		++					
Muffly ⁵⁸	2014	203	Various	++	-	++	-	++			++					
Nawas ⁵⁹	2019	184	Various		--			++					+			
Rollot-Trad ⁶¹	2008	54	Various	--	--		--	--	--							
Proportion of studies with a significant association in univariate analysis				79 %	63 %	64 %	67 %	74 %	55 %	14 %	63 %	33 %	33 %	0 %	71 %	67 %
Proportion of studies with a significant association in multivariate analysis				43 %	27 %	47 %	40 %	62 %	50 %	0 %	50 %	50 %	NA	NA	75 %	100 %

+ : association in univariate analysis; - : no association in univariate analysis; ++ : association in multivariate analysis; -- : no association in multivariate analysis; NA : not applicable. PS: World Health Organization performance status; ADL: activities of daily living; IADL: instrumental activities of daily living; GA: geriatric assessment; AML: acute myeloid leukemia; RAEB: refractory anemia with excess of blasts; MDS: myelodysplastic syndrome; FLT3: FMS-like tyrosine kinase-3; CLL: chronic lymphocytic leukemia; DLBCL: diffuse large B-cell lymphoma; NHL: non-Hodgkin lymphoma; MM: multiple myeloma.

require very different intensities of treatment; geriatric impairments that were associated with outcome in one setting may not retain their predictive value in another disease entity. In addition, the content of geriatric assessments, including the definition of frailty (assessed by summarizing the geriatric assessment), was not consistent. Moreover, geriatric impairments were mainly assessed with screening tools (for example, the Mini-Mental State Examination for cognition), and it should be realized that the ensuing results are not the same as an actual diagnosis made by a comprehensive geriatric assessment. Given this heterogeneity, a meta-analysis or a meaningful subgroup analysis (for example, by type of malignancy) could not be performed; and interpretation and extrapolation of results should be done with caution. Another limitation of this review is the procedure used to select the literature. We decided to select only those studies for which a full text is available and which performed a geriatric assessment with validated tools covering at least two geriatric domains. Studies which focused on a single impairment and its relation to outcome were not included, meaning some information on individual associations may have been missed.

Despite these limitations, this review provides a thorough update and overview of all currently available evidence on the relevance of a geriatric assessment for older patients with a hematologic malignancy. At the time of the previous systematic review, by Hamaker *et al.*,¹⁷ the evidence was limited because of a lack of published studies. In the last 5 years, the number of publications concerning the association of geriatric assessment with outcomes in patients with hematologic malignancies has increased greatly, enabling a useful update on the available data.

Performing a geriatric assessment could have an additive value to clinical judgment, treatment allocation and the implementation of non-oncological interventions.

In daily practice, oncologists are able to detect obviously frail patients by clinical judgment. However, estimating the reserve capacity and resilience of the remaining older patients by clinical judgment is difficult, as demonstrated by the discrepancy between performance status and geriatric assessment. In addition, it can be challenging to distinguish whether the detected vulnerabilities are disease-related or patient-related. This may require a more thorough evaluation of the patient's overall health status, including consultation of a geriatrician.

The impact of performing a geriatric assessment on treatment allocation has already been demonstrated in older patients with solid malignancies.^{73,74} In a systematic review, the oncological treatment plan was altered in 28% of patients after geriatric assessment, primarily resulting in a less intensive treatment option. This review showed that using a geriatric assessment to guide treatment decisions

appeared to have a positive effect on clinical outcome, resulting in less treatment-related toxicity, fewer complications, and increased treatment completion.⁷⁵ For example, in patients with cognitive impairments, treatment decisions should be made with great care because of the higher risk of chemotherapy-related progression of cognitive dysfunction, treatment non-compliance and death.^{52,71}

In order to tailor cancer treatment to individual needs, it could be interesting to incorporate patient-reported outcome measures (PROMS) into the treatment decision-making process. PROMS, such as physical functioning and quality of life during and after treatment, were hardly assessed in the studies included in this review, despite quality of life being of primary importance to many older patients.⁷⁶ It is, therefore, highly relevant that future studies address the association between geriatric impairments and PROMS.⁷⁷

In addition to clinical judgment and treatment allocation, a geriatric assessment can be used to introduce non-oncological interventions before and during treatment in the hope of improving the patient's health status, resilience and treatment tolerance. However, evidence concerning the effectiveness of such non-oncological interventions is limited. Previous research suggests that perhaps physiotherapy^{78,79} as well as nutritional counseling⁸⁰⁻⁸² can improve survival, physical functioning and quality of life. Non-oncological interventions in older patients undergoing chemotherapy can improve treatment completion and treatment modifications.⁸³ The process by which a patient's condition can be enhanced before starting treatment is called prehabilitation. Although results of the first studies assessing the effectiveness of prehabilitation in patients with solid malignancies are promising,^{84,85} the level of evidence is weak, making it too early to draw definitive conclusions. Currently, according to clinicaltrials.gov (searched February 5, 2020), there are 29 ongoing trials in which the effect of non-oncological interventions on clinical outcome measures in older cancer patients is being assessed; six out of these 29 trials focus on hematologic malignancies.⁸⁶ Based on these numbers, further data will follow in the coming years.

In conclusion, this review demonstrates the relevance of performing a geriatric assessment in older patients with a hematologic malignancy. Although the results should be interpreted and extrapolated carefully, our review shows that even in patients with a good performance status, a geriatric assessment can detect geriatric impairments that might be predictive of mortality. Moreover, geriatric impairments seem to be associated with a higher risk of treatment-related toxicity, treatment non-completion and utilization of healthcare services. Future research is needed to extend these findings with a focus on reserve capacity, resilience, quality of life and the effectiveness of non-oncological interventions.

References

1. Smith A, Howell D, Patmore R, Jack A, Roman E. Incidence of haematological malignancy by sub-type: a report from the Haematological Malignancy Research Network. *Br J Cancer*. 2011;105(11):1684-1692.
2. National Cancer Institute. Cancer Stat Facts [Internet]. [cited 2019 Jul 21]. Available from: <https://seer.cancer.gov>
3. Bron D, Ades L, Fulop T, Goede V, Stauder R. Aging and blood disorders: new perspectives, new challenges. *Haematologica*. 2015;100(4):415-417.
4. Warren JL, Harlan LC, Stevens J, Little RF, Abel GA. Multiple myeloma treatment transformed: a population-based study of changes in initial management approaches in the United States. *J Clin Oncol*. 2013;31(16):1984-1989.
5. Abel GA, Koreth J. Optimal positioning of hematopoietic stem cell transplantation for older patients with myelodysplastic syndromes. *Curr Opin Hematol*. 2013;20(2):150-156.

6. McClune BL, Weisdorf DJ, Pedersen TL, et al. Effect of age on outcome of reduced-intensity hematopoietic cell transplantation for older patients with acute myeloid leukemia in first complete remission or with myelodysplastic syndrome. *J Clin Oncol.* 2010;28(11):1878-1867.
7. Hamaker ME, Stauder R, van Munster BC. Exclusion of older patients from ongoing clinical trials for hematological malignancies: an evaluation of the National Institutes of Health clinical trial registry. *Oncologist.* 2014;19(10):1069-1075.
8. Extermann M, Aapro M, Bernabei R, et al. Use of comprehensive geriatric assessment in older cancer patients: recommendations from the task force on CGA of the International Society of Geriatric Oncology (SIOG). *Crit Rev Oncol Hematol.* 2005;55(3):241-225.
9. Gobbens RJ, Luijkx KG, Wijnen-Sponselee MT, Schols JM. Toward a conceptual definition of frail community dwelling older people. *Nurs Outlook.* 2010;58(2):76-86.
10. Fried LP, Tangen CM, Walston J, et al. Frailty in older adults: evidence for a phenotype. *J Gerontol A Biol Sci Med Sci.* 2001;56(3):146-156.
11. Mitnitski AB, Mogilner AJ, Rockwood K. Accumulation of deficits as a proxy measure of aging. *ScientificWorldJournal.* 2001;8(1):323-336.
12. Rockwood K, Song X, MacKnight C, et al. A global clinical measure of fitness and frailty in elderly people. *CMAJ.* 2005;173(5):489-495.
13. Mohile SG, Dale W, Somerfield MR, et al. Practical assessment and management of vulnerabilities in older patients receiving chemotherapy: ASCO guideline for geriatric oncology. *J Clin Oncol.* 2018;36(22):2326-2347.
14. Wildiers H, Heeren P, Puts M, et al. International society of geriatric oncology consensus on geriatric assessment in older patients with cancer. *J Clin Oncol.* 2014;32(24):2595-2601.
15. van Walree IC, Scheepers E, van Huis-Tanja LH, et al. A systematic review on the association of the G8 with geriatric assessment, prognosis and course of treatment in older patients with cancer. *J Geriatr Oncol.* 2019;10(6):847-858.
16. Goede V, Stauder R. Multidisciplinary care in the hematology clinic: implementation of geriatric oncology. *J Geriatr Oncol.* 2019;10(3):497-503.
17. Hamaker ME, Prins MC, Stauder R. The relevance of a geriatric assessment for elderly patients with a haematological malignancy - a systematic review. *Leuk Res.* 2014;(38):275-283.
18. Wells GA, Shea B, O'Connell D, et al. The Newcastle-Ottawa Scale (NOS) for assessing the quality of nonrandomised studies in meta-analyses. Ottawa Hospital Research Institute, 2012.
19. Aguiar APN, Mendonça P da S, Ribeiro-Júnior HL, et al. Myelodysplastic syndromes: an analysis of non-hematological prognostic factors and its relationship to age. *J Geriatr Oncol.* 2020;(11):125-127.
20. Corsetti MT, Salvi F, Perticone S, et al. Hematologic improvement and response in elderly AML/RAEB patients treated with valproic acid and low-dose Ara-C. *Leuk Res.* 2011;35(8):991-997.
21. Deschler B, Ihorst G, Platzbecker U, et al. Parameters detected by geriatric and quality of life assessment in 195 older patients with myelodysplastic syndromes and acute myeloid leukemia are highly predictive for outcome. *Haematologica.* 2013;98(2):208-216.
22. Holmes H, Des Bordes JKA, Kebraie P, et al. Optimal screening for geriatric assessment in older allogeneic hematopoietic cell transplantation candidates. *J Geriatr Oncol.* 2014;5(4):422-430.
23. Klepin HD, Geiger AM, Tooze JA, et al. Geriatric assessment predicts survival for older adults receiving induction chemotherapy for acute myelogenous leukemia. *Blood.* 2013;121(21):4287-4294.
24. Klepin HD, Ritchie E, Major-Elechi B, et al. Geriatric assessment among older adults receiving intensive therapy for acute myeloid leukemia: report of CALGB 361006 (Alliance). *J Geriatr Oncol.* 2020;(11):107-113.
25. Molga A, Wall M, Chhetri R, et al. Comprehensive geriatric assessment predicts azacitidine treatment duration and survival in older patients with myelodysplastic syndromes. *J Geriatr Oncol.* 2020;(11):114-120.
26. Molga A, Wall M, Wee LYA, et al. Screening for deficits using the G8 and VES-13 in older patients with myelodysplastic syndromes. *J Geriatr Oncol.* 2020;(11):128-130.
27. Umüt EG, Baysal M, Demir AM. Frailty in patients with acute myeloid leukaemia, conceptual misapprehension of chronological age. *Eur J Cancer Care (Engl).* 2018;27(2):e12810.
28. Goede V, Bahlo J, Chataline V, et al. Evaluation of geriatric assessment in patients with chronic lymphocytic leukemia: results of the CLL9 trial of the German CLL study group. *Leuk Lymphoma.* 2016;57(4):789-796.
29. Molica S, Giannarelli D, Levato L, et al. A simple score based on geriatric assessment predicts survival in elderly newly diagnosed chronic lymphocytic leukemia patients. *Leuk Lymphoma.* 2019;60(3):845-847.
30. Ribi K, Rondeau S, Hitz F, et al. Cancer-specific geriatric assessment and quality of life: important factors in caring for older patients with aggressive B-cell lymphoma. *Support Care Cancer.* 2017;25(9):2833-2842.
31. Merli F, Cavallo F, Salvi F, et al. Obinutuzumab and miniCHOP for unfit patients with diffuse large B-cell lymphoma. A phase II study by Fondazione Italiana Linfomi. *J Geriatr Oncol.* 2020;(11):37-40.
32. Ong DM, Ashby M, Grigg A, et al. Comprehensive geriatric assessment is useful in an elderly Australian population with diffuse large B-cell lymphoma receiving rituximab-chemotherapy combinations. *Br J Haematol.* 2019;(187):73-81.
33. Spina M, Balzarotti M, Uziel L, et al. Modulated chemotherapy according to modified comprehensive geriatric assessment in 100 consecutive elderly patients with diffuse large B-cell lymphoma. *Oncologist.* 2012;17(6):838-846.
34. Tucci A, Ferrari S, Bottelli C, Borlenghi E, Drera M, Rossi G. A comprehensive geriatric assessment is more effective than clinical judgment to identify elderly diffuse large cell lymphoma patients who benefit from aggressive therapy. *Cancer.* 2009;115(19):4547-4553.
35. Tucci A, Martelli M, Rigacci L, et al. Comprehensive geriatric assessment is an essential tool to support treatment decisions in elderly patients with diffuse large B-cell lymphoma: a prospective multicenter evaluation in 173 patients by the Lymphoma Italian Foundation (FIL). *Leuk Lymphoma.* 2015;56(4):921-926.
36. Aaldriks A, Giltay E, Nortier J, et al. Prognostic significance of geriatric assessment in combination with laboratory parameters in elderly patients with aggressive non-Hodgkin lymphoma. *Leuk Lymphoma.* 2015;56(4):927-935.
37. Naito Y, Sasaki H, Takamatsu Y, Kiyomi F, Tamura K. Retrospective analysis of treatment outcomes and geriatric assessment in elderly malignant lymphoma patients. *J Clin Exp Hematop.* 2016;56(1):43-49.
38. Park S, Hong J, Hwang I, et al. Comprehensive geriatric assessment in elderly patients with newly diagnosed aggressive non-Hodgkin lymphoma treated with multi-agent chemotherapy. *J Geriatr Oncol.* 2015;6(6):470-478.
39. Siegel AB, Lachs M, Coleman M, Leonard JP. Lymphoma in elderly patients: novel functional assessment techniques provide better discrimination among patients than traditional performance status measures. *Clin Lymphoma Myeloma.* 2006;7(1):65-69.
40. Soubeyran P, Khaled H, MacKenzie M, et al. Diffuse large B-cell and peripheral T-cell non-Hodgkin's lymphoma in the frail elderly. A phase II EORTC trial with a progressive and cautious treatment emphasizing geriatric assessment. *J Geriatr Oncol.* 2011;2(1):36-44.
41. Winkelmann N, Petersen I, Kiehnopf M, Fricke HJ, Hochhaus A, Wedding U. Results of comprehensive geriatric assessment effect survival in patients with malignant lymphoma. *J Cancer Res Clin Oncol.* 2011;137(4):733-738.
42. Okuyama T, Sugano K, Iida S, Ishida T, Kusumoto S, Akechi T. Screening performance for frailty among older patients with cancer: a cross-sectional observational study of two approaches. *J Natl Compr Cancer Netw.* 2015;13(12):1525-1531.
43. Engelhardt M, Dold SM, Ihorst G, et al. Geriatric assessment in multiple myeloma patients: Validation of the International Myeloma Working Group (IMWG) score and comparison with their common comorbidity scores. *Haematologica.* 2016;101(9):1110-1119.
44. Gavriatopoulou M, Fotiou D, Koloventzou U, et al. Vulnerability variables among octogenarian myeloma patients: a single-center analysis of 110 patients. *Leuk Lymphoma.* 2019;60(3):619-628.
45. Palumbo A, Bringhen S, Mateos MV, et al. Geriatric assessment predicts survival and toxicities in elderly myeloma patients: an International Myeloma Working Group report. *Blood.* 2015;125(13):2068-2074.
46. Rosko AE, Huang Y, Benson DM, et al. Use of a comprehensive frailty assessment to predict morbidity in patients with multiple myeloma undergoing transplant. *J Geriatr Oncol.* 2019;10(3):479-85.
47. Wildes TM, Tuchman SA, Klepin HD, et al. Geriatric assessment in older adults with multiple myeloma. *J Am Geriatr Soc.* 2019;67(5):987-991.
48. Zhong YP, Zhang YZ, Liao AJ, Li SX, Tian C, Lu J. Geriatric assessment to predict survival and risk of serious adverse events in elderly newly diagnosed multiple myeloma patients: A multicenter study in China. *Chin Med J (Engl).* 2017;130(2):130-134.
49. Buckstein R, Wells RA, Zhu N, et al. Patient-related factors independently impact overall survival in patients with myelodysplastic syndromes: an MDS-CAN prospective study. *Br J Haematol.* 2016;174(1):88-101.
50. Deschler B, Ihorst G, Schnitzler S, Bertz H,

- Finke J. Geriatric assessment and quality of life in older patients considered for allogeneic hematopoietic cell transplantation: a prospective risk factor and serial assessment analysis article. *Bone Marrow Transplant.* 2018;53(5):565-575.
51. Derman BA, Kordas K, Ridgeway J, et al. Results from a multidisciplinary clinic guided by geriatric assessment before stem cell transplantation in older adults. *Blood Adv.* 2019;3(22):3488-3498.
 52. Dubruille S, Libert Y, Roos M, et al. Identification of clinical parameters predictive of one-year survival using two geriatric tools in clinically fit older patients with hematological malignancies: major impact of cognition. *J Geriatr Oncol.* 2015;6(5):362-369.
 53. DuMontier C, Liu MA, Murillo A, et al. Function, survival, and care utilization among older adults with hematologic malignancies. *J Am Geriatr Soc.* 2019;(67):889-897.
 54. Hamaker ME, Augschoell J, Stauder R. Clinical judgement and geriatric assessment for predicting prognosis and chemotherapy completion in older patients with a hematological malignancy. *Leuk Lymphoma.* 2016;57(11):2560-2567.
 55. Huang LW, Sheng Y, Andreadis C, et al. Functional status as measured by geriatric assessment predicts inferior survival in older allogeneic hematopoietic cell transplantation recipients: functional status predicts post-alloHCT survival. *Biol Blood Marrow Transplant.* 2020;(26):189-196.
 56. Lin RJ, Elko TA, Devlin SM, et al. Impact of geriatric vulnerabilities on allogeneic hematopoietic cell transplantation outcomes in older patients with hematologic malignancies. *Bone Marrow Transplant.* 2020;(55):157-164.
 57. Liu MA, DuMontier C, Murillo A, et al. Gait speed, grip strength, and clinical outcomes in older patients with hematologic malignancies. *Blood.* 2019;134(4):374-382.
 58. Muffy LS, Kocherginsky M, Stock W, et al. Geriatric assessment to predict survival in older allogeneic hematopoietic cell transplantation recipients. *Haematologica.* 2014;99(8):1373-1379.
 59. Nawas MT, Andreadis C, Martin TG, et al. Limitation in patient-reported function is associated with inferior survival in older adults undergoing autologous hematopoietic cell transplantation. *Biol Blood Marrow Transplant.* 2019;25(6):1218-1224.
 60. Rodrigues M, de Souza PMR, de Oliveira Muniz Koch L, Hamerschlag N. The use of comprehensive geriatric assessment in older patients before allogeneic hematopoietic stem cell transplantation: a cross-sectional study. *J Geriatr Oncol.* 2020;(11):100-106.
 61. Rollet-Trad F, Lahjibi H, Lazarovici C, Bauer C, Saint-Jean O, Gisselbrecht M. Haematological malignancies in older adults: experience in a geriatric acute care department. *Rev Med Interne.* 2008;29(7):541-549.
 62. Silay K, Akinci S, Silay YS, et al. Hospitalization risk according to geriatric assessment and laboratory parameters in elderly hematologic cancer patients. *Asian Pacific J Cancer Prev.* 2015;16(2):1783-1786.
 63. Velghe A, Petrovic M, De Buyser S, Demuyneck R, Noens L. Validation of the G8 screening tool in older patients with aggressive haematological malignancies. *Eur J Oncol Nurs.* 2014;18(6):645-648.
 64. Klepin HD, Geiger AM, Tooze JA, et al. The feasibility of inpatient geriatric assessment for older adults receiving induction chemotherapy for acute myelogenous leukemia. *J Am Geriatr Soc.* 2011;59(10):1837-1846.
 65. Klepin HD, Tooze JA, Pardee TS, et al. Effect of intensive chemotherapy on physical, cognitive, and emotional health of older adults with acute myeloid leukemia. *J Am Geriatr Soc.* 2016;64(10):1988-1995.
 66. Isaacs A, Fiala M, Tuchman S, Wildes TM. A comparison of three different approaches to defining frailty in older patients with multiple myeloma. *J Geriatr Oncol.* 2020;11(2):311-315.
 67. Hamaker ME, Mitrovic M, Stauder R. The G8 screening tool detects relevant geriatric impairments and predicts survival in elderly patients with a haematological malignancy. *Ann Hematol.* 2014;93(6):1031-1040.
 68. Hofer F, Koinig KA, Nagl L, Borjan B, Stauder R. Fatigue at baseline is associated with geriatric impairments and represents an adverse prognostic factor in older patients with a hematological malignancy. *Ann Hematol.* 2018;97(11):2235-2243.
 69. Lin RJ, Shahrokni A, Dahi PB, et al. Pretransplant comprehensive geriatric assessment in hematopoietic cell transplantation: a single center experience. *Bone Marrow Transplant.* 2018;53:1184-1187.
 70. Lin RJ, Dahi PB, Shahrokni A, et al. Feasibility of a patient-reported, electronic geriatric assessment tool in hematopoietic cell transplantation—a single institution pilot study. *Leuk Lymphoma.* 2019;60(13):3308-3311.
 71. Hsieh TT, Jung WF, Grande LJ, et al. Prevalence of cognitive impairment and association with survival among older patients with hematologic cancers. *JAMA Oncol.* 2018;4(5):686-693.
 72. Muffy LS, Boulukos M, Swanson K, et al. Pilot study of comprehensive geriatric assessment (CGA) in allogeneic transplant: CGA captures a high prevalence of vulnerabilities in older transplant recipients. *Biol Blood Marrow Transplant.* 2013;19(3):429-434.
 73. Corre R, Greillier L, Le Caër H, et al. Use of a comprehensive geriatric assessment for the management of elderly patients with advanced non-small cell lung cancer: the phase III randomized ESOGLA-GFPC-GECP 08-02 study. *J Clin Oncol.* 2016;34(13):1476-1483.
 74. Kirkhus L, Benth JS, Rostoft S, et al. Geriatric assessment is superior to oncologists' clinical judgement in identifying frailty. *Br J Cancer.* 2017;117(4):470-477.
 75. Hamaker ME, te Molder M, Thielen N, van Munster BC, Schiphorst AH, van Huis LH. The effect of a geriatric evaluation on treatment decisions and outcome for older cancer patients – a systematic review. *J Geriatr Oncol.* 2018;9(5):430-440.
 76. Van Leeuwen KM, Van Loon MS, Van Nes FA, et al. What does quality of life mean to older adults? A thematic synthesis. *PLoS One.* 2019;14(3):1-39.
 77. Stauder R, Lambert J, Desruol-Allardin S, et al. Patient-reported outcome measures in studies of myelodysplastic syndromes and acute myeloid leukemia: literature review and landscape analysis. *Eur J Haematol.* 2020 Jan 27. [Epub ahead of print]
 78. Meneses-Echávez JF, González-Jiménez E, Ramírez-Vélez R. Supervised exercise reduces cancer-related fatigue: a systematic review. *J Physiother.* 2015;61(1):3-9.
 79. Buffart LM, Kalter J, Sweegers MG, et al. Effects and moderators of exercise on quality of life and physical function in patients with cancer: an individual patient data meta-analysis of 34 RCTs. *Cancer Treat Rev.* 2017;52:91-104.
 80. Baldwin C, Spiro A, Ahern R, Emery PW. Oral nutritional interventions in malnourished patients with cancer: a systematic review and meta-analysis. *J Natl Cancer Inst.* 2012;104(5):371-385.
 81. Schuetz P, Fehr R, Baechli V, et al. Individualised nutritional support in medical inpatients at nutritional risk: a randomised clinical trial. *Lancet.* 2019;393(10188):2312-2321.
 82. Caillet P, Liuu E, Raynaud Simon A, et al. Association between cachexia, chemotherapy and outcomes in older cancer patients: a systematic review. *Clin Nutr.* 2017;36:1473-1482.
 83. Kalsi T, Babic-Illman G, Ross PJ, et al. The impact of comprehensive geriatric assessment interventions on tolerance to chemotherapy in older people. *Br J Cancer.* 2015;112(9):1435-1444.
 84. Bruns ERJ, van den Heuvel B, Buskens CJ, et al. The effects of physical prehabilitation in elderly patients undergoing colorectal surgery: a systematic review. *Color Dis.* 2016;18(8):267-277.
 85. Driessen EJ, Peeters ME, Bongers BC, et al. Effects of prehabilitation and rehabilitation including a home-based component on physical fitness, adherence, treatment tolerance, and recovery in patients with non-small cell lung cancer: a systematic review. *Crit Rev Oncol Hematol.* 2017;114:63-76.
 86. ClinicalTrials.gov. U.S. National Library of Medicine [Internet]. [cited 2020 Feb 5]. Available from: <https://clinicaltrials.gov/>



The regulation and function of CD20: an “enigma” of B-cell biology and targeted therapy

Gabriela Pavlasova^{1,2} and Marek Mraz^{1,2}

¹Central European Institute of Technology, Masaryk University, Brno and ²Department of Internal Medicine, Hematology and Oncology, University Hospital Brno and Faculty of Medicine, Masaryk University, Brno, Czech Republic

Haematologica 2020
Volume 105(6):1494-1506

ABSTRACT

The introduction of anti-CD20 monoclonal antibodies such as rituximab, ofatumumab, or obinutuzumab improved the therapy of B-cell malignancies even though the precise physiological role and regulation of CD20 remains unclear. Furthermore, CD20 expression is highly variable between different B-cell malignancies, patients with the same malignancy, and even between intraclonal subpopulations in an individual patient. Several epigenetic (EZH2, HDAC1/2, HDAC1/4, HDAC6, complex Sin3A-HDAC1) and transcription factors (USF, OCT1/2, PU.1, PiP, ELK1, ETS1, SP1, NFκB, FOXO1, CREM, SMAD2/3) regulating CD20 expression (encoded by *MS4A1*) have been characterized. CD20 is induced in the context of microenvironmental interactions by CXCR4/SDF1 (CXCL12) chemokine signaling and the molecular function of CD20 has been linked to the signaling propensity of B-cell receptor (BCR). CD20 has also been shown to interact with multiple other surface proteins on B cells (such as CD40, MHCII, CD53, CD81, CD82, and CBP). Current efforts to combine anti-CD20 monoclonal antibodies with BCR signaling inhibitors targeting BTK or PI3K (ibrutinib, acalabrutinib, idelalisib, duvelisib) or BH3-mimetics (venetoclax) lead to the necessity to better understand both the mechanisms of regulation and the biological functions of CD20. This is underscored by the observation that CD20 is decreased in response to the “BCR inhibitor” ibrutinib which largely prevents its successful combination with rituximab. Several small molecules (such as histone deacetylase inhibitors, DNA methyl-transferase inhibitors, aurora kinase A/B inhibitors, farnesyltransferase inhibitors, FOXO1 inhibitors, and bryostatin-1) are being tested to upregulate cell-surface CD20 levels and increase the efficacy of anti-CD20 monoclonal antibodies. Herein, we review the current understanding of CD20 function, and the mechanisms of its regulation in normal and malignant B cells, highlighting the therapeutic implications.

Correspondence:

MAREK MRAZ
marek.mraz@email.cz

Received: November 22, 2019.

Accepted: April 15, 2020.

doi:10.3324/haematol.2019.243543

Check the online version for the most updated information on this article, online supplements, and information on authorship & disclosures: www.haematologica.org/content/105/6/1494

©2020 Ferrata Storti Foundation

Material published in *Haematologica* is covered by copyright. All rights are reserved to the Ferrata Storti Foundation. Use of published material is allowed under the following terms and conditions:

<https://creativecommons.org/licenses/by-nc/4.0/legalcode>.

Copies of published material are allowed for personal or internal use. Sharing published material for non-commercial purposes is subject to the following conditions:

<https://creativecommons.org/licenses/by-nc/4.0/legalcode>,

sect. 3. Reproducing and sharing published material for commercial purposes is not allowed without permission in writing from the publisher.



Introduction

The approval of the anti-CD20 antibody rituximab by the Food and Drug Administration in 1997 was a conceptual breakthrough in the treatment of B-cell malignancies. Rituximab improved progression-free survival and overall survival rates when added to chemotherapy in “mature” B-cell leukemias and lymphomas such as chronic lymphocytic leukemia (CLL), follicular lymphoma, and diffuse large B-cell lymphoma (DLBCL), and this proved that monoclonal antibodies could be used in cancer treatment.¹ Additionally, rituximab maintenance therapy has been introduced for some of these diseases. Based on the success of rituximab, new engineered anti-CD20 monoclonal antibodies, namely ofatumumab and obinutuzumab, were developed. Preclinical studies suggest that these new anti-CD20 monoclonal antibodies are superior to rituximab for some mechanisms of action.² Anti-CD20 monoclonal antibodies might act through several mechanisms (Figure 1) including complement-dependent cytotoxicity (CDC), complement-dependent cellular cytotoxicity, antibody-dependent cellular cytotoxicity (ADCC), antibody-

dependent cellular phagocytosis, and direct apoptosis induction, as has been elegantly reviewed by others.^{3,4} All these mechanisms were observed *in vitro* and/or in animal models, and likely act *in vivo* in patients as well, but their relative contribution to the clinical effects of the different anti-CD20 monoclonal antibodies is still debated. It is also unclear why the application of novel engineered monoclonal antibodies provides clinical benefit in comparison to rituximab in some B-cell malignancies, but not in others. For example in CLL patients, obinutuzumab is superior to rituximab when combined with chlorambucil, as judged by the number of complete remissions and prolonged progression-free survival.⁵ A much less significant improvement in progression-free survival has also been demonstrated in previously untreated follicular lymphoma patients treated with obinutuzumab-based chemoimmunotherapy compared to rituximab-based chemoimmunotherapy.^{6,7} Finally, a phase III clinical study demonstrated no improvement in progression-free survival in a large cohort of treatment-naïve DLBCL patients when comparing obinutuzumab plus CHOP (cyclophos-

phamide, adriamycin, vincristine and prednisone) versus rituximab plus CHOP.⁸ It is important to note that in these trials, obinutuzumab was used at doses and schedules quite different from those of rituximab. For example, in the CLL trial⁵ a flat obinutuzumab dose of 1000 mg/patient was used (on days 1, 8, and 15 of cycle 1 and on day 1 of cycles 2-6), while rituximab was used at a dose of 375 mg/m² on day 1 of cycle 1 and 500 mg/m² on day 1 of cycles 2-6. Overall, in this CLL trial the median cumulative rituximab dose per patient was 64% of the obinutuzumab dose (these two monoclonal antibodies have a nearly identical molecular weight).

Currently, efforts have shifted from adding anti-CD20 monoclonal antibodies to chemotherapy to combining them with novel drugs, such as B-cell receptor (BCR) signaling inhibitors (ibrutinib, idelalisib, etc.)⁹ or BH3-mimetics inhibiting BCL2 (venetoclax),¹⁰ and also the development of CD20 targeting chimeric antigen receptor T cells.¹¹ It is essential to understand the mechanism of CD20 regulation and function thoroughly and to elucidate the mechanism of action of monoclonal antibodies in

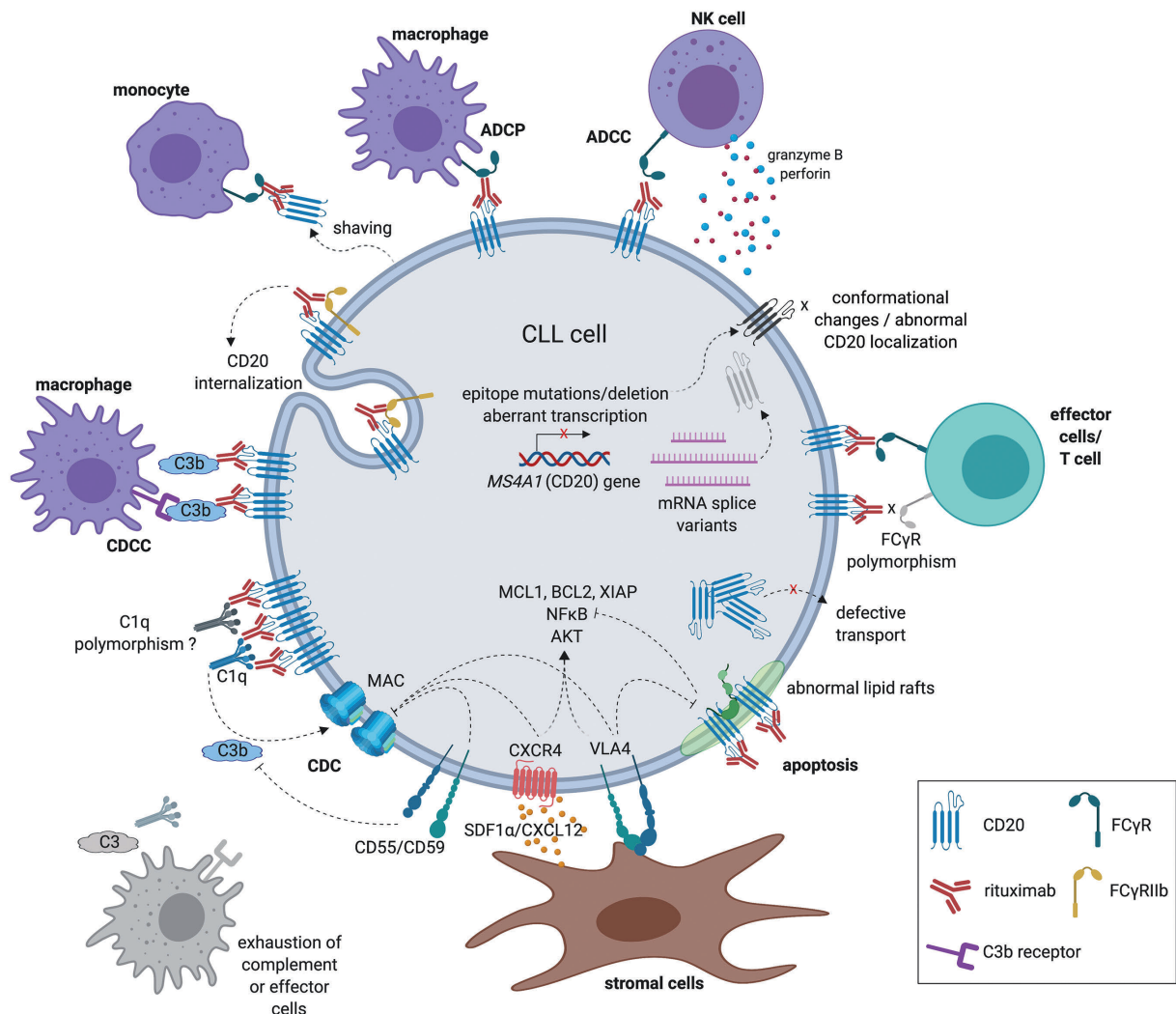


Figure 1. Summary of the known mechanisms of action of anti-CD20 monoclonal antibodies and an overview of potential factors affecting resistance to anti-CD20 therapy in malignant B cells. Anti-CD20 monoclonal antibodies act through several mechanisms, including complement-dependent cytotoxicity (CDC), complement-dependent cellular cytotoxicity (CDCC), antibody-dependent cellular phagocytosis (ADCP), antibody-dependent cellular cytotoxicity (ADCC), and induction of direct apoptosis.

order to fully exploit their therapeutic potential. This is underscored by the recent disappointing results of clinical trials testing rituximab's addition to the BTK inhibitor ibrutinib in CLL, which showed practically no benefit of such a combination.¹² Here we summarize the research describing the regulation and function of CD20 in normal and malignant B cells, and the therapeutic implications of these observations, including the relevance for the combination of "BCR inhibitors" with anti-CD20 monoclonal antibodies.

CD20 gene and protein structure

CD20 is a 33-37 kDa non-glycosylated protein expressed on the surface of normal and malignant B lymphocytes, and belongs to the MS4A (membrane-spanning 4-domain family A) protein family.¹³ To date, 18 MS4A family members have been identified, besides *MS4A1* (encoding CD20), also the high-affinity immunoglobulin E receptor β subunit (*MS4A2/Fc ϵ RI β*) or *HtM4* gene (*MS4A3*) (reviewed by Eon Kuek¹⁴). MS4A proteins are transmembrane molecules and they are predicted to share a similar polypeptide sequence and overall topological structure. The majority of *MS4A* genes, including *MS4A1*, are localized within a cluster on chromosome 11q12 in humans (chromosome 19 in mice), and two members

from a closely related *TMEM176* gene family were identified in chromosome region 7q36.1.¹⁴

The *MS4A1* gene is 16 kb long, comprises eight exons, and several different CD20 mRNA transcripts have been annotated.¹⁵ The dominant CD20 mRNA variant is 2.8 kb long and uses all eight exons, whereas the second most common form is 263 bases shorter, as it skips exon II. A minor 3.5 kb mRNA results from splicing exons in the upstream region into an internal 3' splice site located in exon I. However, all three transcripts are translated into identical full-length CD20 protein as the translation start codon is localized within exon III. Moreover, other alternative transcripts were identified in malignant B cells, some of them encoding truncated forms of CD20 protein leading to impaired binding of anti-CD20 monoclonal antibodies.^{15,16}

CD20 protein consists of four hydrophobic transmembrane domains, one intracellular and two extracellular domains (large and small loops) with both N- and C-termini residing within the cytosol.¹⁴ Three CD20 isoforms (33, 35 and 37 kDa) resulting from different phosphorylation have been identified, and CD20 phosphorylation was reported to be higher in proliferating malignant B cells than in resting B cells.¹⁷ Normally, CD20 does not form hetero-oligomers,¹⁸ but exists on the cell surface as homo-

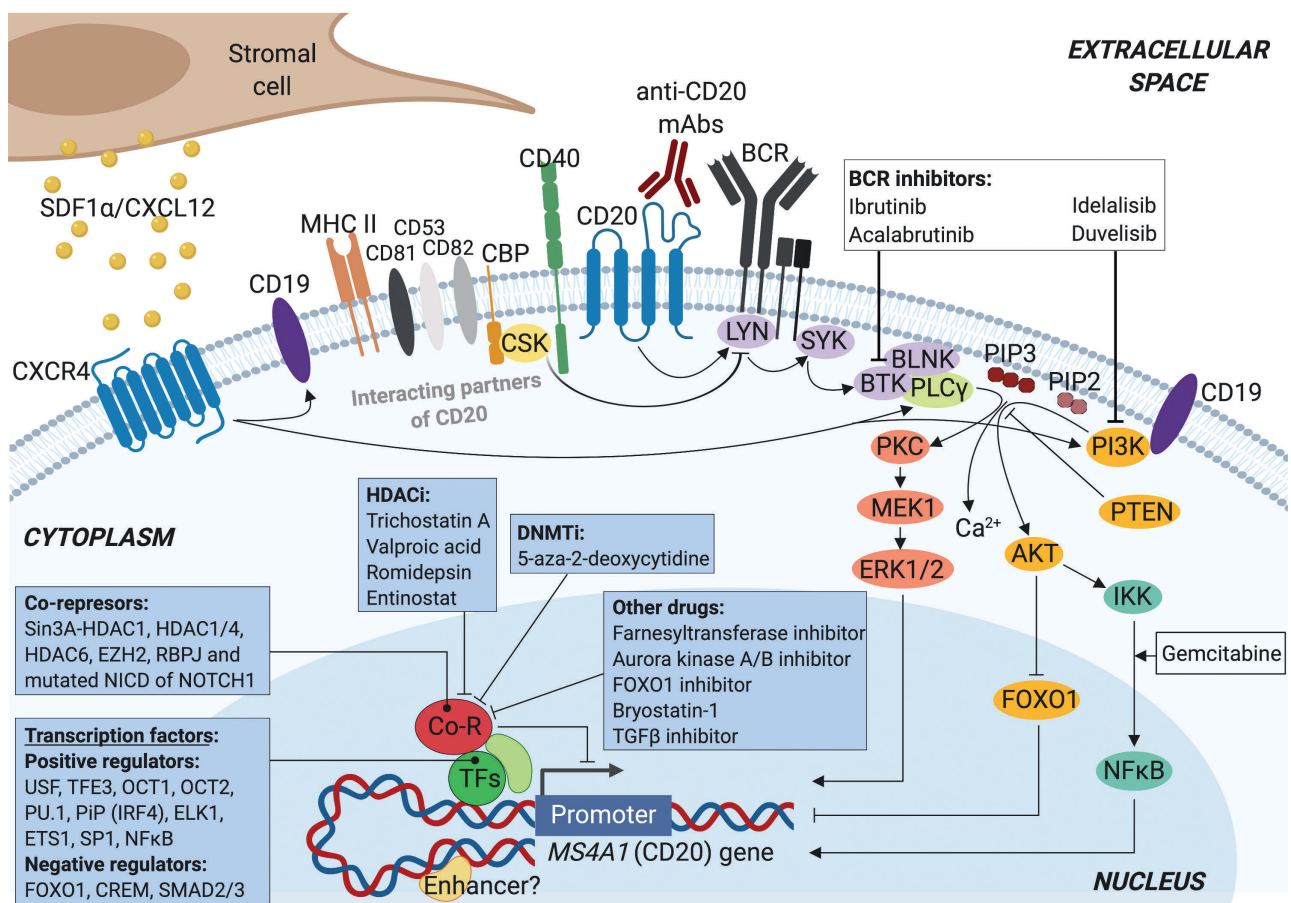


Figure 2. A schematic view of interacting partners of CD20 on cell membrane and mechanisms of CD20 gene (*MS4A1*) regulation in malignant B cells. mAbs: monoclonal antibodies; BCR: B-cell receptor; HDACi: histone deacetylase inhibitors; DNMTi: DNA methyl-transferase inhibitors; NICD: NOTCH1 intracellular domain; TGF β : transforming growth factor β .

dimeric and homo-tetrameric oligomers associated with other cell-surface and cytoplasmic proteins contributing to the signal transduction.^{17,19,20} Tetraspanin proteins tend to associate with multiple other proteins in membrane microdomains (Figure 2).²¹ Energy transfer experiments indicate that CD20 is in close proximity to other tetraspanin molecules, such as CD53, CD81, and CD82, forming supramolecular complexes (Figure 2).²² CD20 is also known to be physically coupled to major histocompatibility complex class II (MHCII), CD40 molecule, BCR, and the C-terminal src kinase-binding protein (CBP) that interacts with Src kinases such as LYN, FYN, and LCK (Figure 2).^{20,23,24} Besides the transmembrane form of CD20, circulating CD20 was reported in CLL patients' plasma;²⁵ however, this is likely to be part of a larger protein complex or a cell membrane fragment originating from cell breakdown.

CD20 is a general B-cell marker expressed by the majority of B cells starting from late pre-B lymphocytes (it is not expressed by pro-B lymphocytes), and its expression is lost in terminally differentiated plasmablasts and plasma cells. Recently, a subset of CD20⁺ T cells with immunoregulatory and pro-inflammatory activity has been described; however, the clinical relevance of this remains to be determined.²⁶ In B-cell malignancies, the level of CD20 expression is extremely variable depending on the specific neoplasm, with the lowest CD20 expression usually being observed in patients with CLL and the highest CD20 cell-surface expression on DLBCL and hairy cell leukemia cells.^{27,28} Within CLL, it was noted that CD20 expression was also relatively higher in a disease subtype with a mutated variable region of immunoglobulin gene (IGHV) than in the subtype with unmutated IGHV.²⁹ Some studies described that higher CD20 expression levels correlate with longer overall survival in patients with B-cell lymphomas treated with rituximab,^{30,31} although this remains controversial.^{32,33} Notably, CD20 levels are heterogeneous not only among patients with the same malignancy, but also within the intraclonal cell subpopulations in an individual patient.³⁴

CD20 function: a link to B-cell receptor signaling and microenvironmental interactions

The biological function of CD20 in B cells and its physiological ligand, if any, remain unclear. Some light on CD20 function has been shed by a case report of a patient with a common variable immunodeficiency and CD20 loss caused by a homozygous mutation in an exon 5 splicing site of *MS4A1*. The mutation led to alternative splicing with complete deletion of exon 5 and insertion of intron sequences and thus a truncated form of *MS4A1* mRNA.³⁵ Due to this homozygous mutation, the patient completely lacked cell-surface CD20. This did not disturb precursor B-cell differentiation in the bone marrow, as the patient had normal serum IgM levels and normal B-cell numbers. However, CD20 deficiency resulted in a reduced number of circulating memory B cells, reduced isotype switching of Ig, and decreased IgG antibody levels. In agreement with this observation, challenging the patient's primary B cells *in vitro* using T-dependent and T-independent antigens led to the normal proliferation and secretion of IgM but reduced production of IgG. Given these data it is surprising that after repeated vaccinations the patient displayed a reduced ability to respond to T-independent antigens (pneumococcal polysaccharide vac-

cine), but a normal reaction to T-dependent antigens (anti-tetanus toxoid IgG).

Cases of a homozygous mutation in the *MS4A1* gene in humans are extremely rare, which prompted the generation of mouse models. This is a reasonable approach, since human and mice CD20 proteins share most structural features and a conserved amino acid sequence (~75% homology) with only a few structural modifications in the transmembrane and N- and C-terminal cytoplasmic domains.³⁶ CD20 in both humans and mice is B-cell specific, being first expressed by late pre-B cells in the bone marrow, predominantly after Ig heavy chain rearrangement. Uchida *et al.* created a mouse model with a homozygous mutation in the *MS4A1* gene.³⁶ These CD20-less mice had normal B-cell differentiation, isotype switching, maturation, mitogen-induced proliferation, and tissue localization. Similarly, CD20 deletion was not observed to have any effect on proliferation and differentiation in mice with *MS4A1* disruption, generated by Neuberger's group.³⁷ CD20^{-/-} mice immunized with T-dependent antigens showed impaired humoral immunity and primary and secondary immune responses connected with reduced numbers of germinal center B cells.³⁸ Altogether, these studies in human and murine CD20-deficient B cells suggest that CD20 is required for both optimal T-independent humoral immunity, and also for a response to T-dependent antigens. However, it should be taken into consideration that the T-dependent immune response might be impaired due to the loss of CD20 in a small CD20⁺ population of T cells whose specific role in the immune system remains unclear.²⁶ Overall, the relatively mild phenotype resulting from CD20 loss in humans and mice is somewhat surprising since CD20 was reported to be physically and functionally coupled to MHCII and CD40 (Figure 2),²³ which are both critical for B- and T-cell interactions.

The development of humoral immunity requires a functional BCR signaling pathway, and CD20 was reported to be co-localized in lipid rafts³⁹ and to interact directly physically with BCR.²⁰ Additionally, it has been observed that CD20 becomes heavily phosphorylated after mitogen stimulation, and it has been proposed that it might function as a calcium channel and be involved in B-cell activation.^{17,19} This is in line with *in vitro* data showing that BCR-activated calcium flux was reduced after siRNA-mediated CD20 down-modulation in human B-cell lines.^{34,40} Moreover, direct CD20 crosslinking induces acute signaling similar to BCR crosslinking, including calcium flux, and overlapping transcription patterns in human lymphoma cell lines.^{41,42} Kheirallah *et al.* also demonstrated that pretreatment of lymphoma cell lines with rituximab interferes with BCR signaling cascade stimulation, suggesting that both cell-surface proteins might share the same signaling pathway components and activate negative feedback regulatory mechanisms, including BCR downmodulation.⁴³ We and others have shown that levels of cell-surface CD20 on primary CLL cells are correlated (and possibly co-regulated) with cell-surface BCR expression.³⁴ Additionally, we observed *in vivo* that CLL cells that have recently exited the lymph node microenvironment to the peripheral blood are characterized by a marked upregulation of CD20 levels.⁴⁴ This stems from the activation of CXCR4 by SDF1 chemokine, which leads to transcriptional activation of CD20 expression. Moreover, CD20 cell-surface levels are

induced in CLL cells treated by microenvironmental factors such as IL4, TNF α , INF α or GM-CSF *in vitro*⁴⁵⁻⁴⁷ (and our unpublished data).

CD20 silencing in malignant B cells revealed that CD20 affects the phosphorylation of multiple BCR-associated kinases and proteins after BCR-ligation (LYN, SYK, GAB1, and ERK).³⁴ This suggests that both CD20 and BCR are induced in immune niches³⁴ to allow effective and strong BCR activation by an antigen or CD20 might also be involved in some form of "tonic" BCR signaling.⁴⁸ This has important implications for combining BCR inhibitors with antibodies targeting CD20. We have shown that inhibiting BTK interferes with CXCR4 signaling in CLL cells and thus leads to very significant repression of CD20 expression in CLL cells. This might partially explain the lack of clinical benefit from adding rituximab to ibrutinib.¹² Ibrutinib was recently tested and approved in combination with a more potent anti-CD20 monoclonal antibody, namely obinutuzumab,⁴⁹ whose efficacy is less affected by lower levels of CD20 on the cell-surface. We also suggest that PI3K inhibition, like BTK inhibition, might lead to the downmodulation of CD20, but this remains to be formally proven, and the implications for the therapeutic combination of rituximab with PI3K inhibitors (including idelalisib) or other BTK inhibitors (such as acalabrutinib) are unclear.

Altogether, functional studies suggest that CD20 is physiologically directly required for efficient BCR signaling in B cells. This is also in line with some data from the CD20 mouse models. In Uchida's CD20^{-/-} mice model, cell-surface IgM expression on both mature and immature B cells was 20 – 30% lower than that on B cells from wild-type littermates, which was connected with reduced BCR- and CD19-dependent intracellular calcium mobilization.⁵⁶ In a study by Morsy *et al.*, the reduction in BCR-associated calcium mobilization in CD20^{-/-} murine B cells was proposed to be caused by a defect in calcium transport rather than in its release from intracellular stores.⁵⁸ In our opinion, there is a sufficient body of evidence suggesting that CD20 is involved in BCR signaling, but it is unclear whether this is related to its putative function as a calcium channel and/or other function(s). Similarly, it is not clear if other molecular pathways or B-T-cell interactions might be affected by CD20 levels on the cell-surface of B cells.

Regulation of CD20 transcription and its "therapeutic modulation"

Rituximab is one of the most effective and widely used therapeutic monoclonal antibodies, but malignant B cells can become relatively resistant to such therapy. Mechanisms of malignant B cells' resistance to anti-CD20 monoclonal antibodies include insufficient CDC activity due to increased expression of regulatory proteins CD55, CD59 or factor H,^{50,51} less effective ADCC in cases with specific Fc γ RIII polymorphism,⁵² exhaustion of cytotoxic mechanisms (such as complement/effector cells),^{53,54} polymorphism in the complement component C1qA,⁵⁵ or abnormal composition and localization of lipid rafts and thus impaired rituximab-induced apoptosis (Figure 1).⁵⁶ Nevertheless, one of the most straightforward and frequent causes of resistance to anti-CD20 monoclonal antibodies is reduced CD20 expression, which can be due to (de)regulation of transcriptional, post-transcriptional, or post-translational mechanisms (including CD20 protein transport to the cell surface⁵⁷).

Regarding transcriptional regulation, the *MS4A1* gene lacks several regulatory elements typical of other B-cell specific genes, including TATA and CAAT box. The

Table 1. Positive and negative regulators of *MS4A1* (CD20 gene) transcription.

Positive regulators ^{Ref}	Negative regulators ^{Ref}
Transcription factors	
USF, TFE3 ⁵⁹	FOXO1 ⁷⁰
OCT1, ⁵⁸ OCT2 ⁵⁸	CREM ⁶⁹
PU.1/PI3 (IRF4) ⁵⁹	SMAD2/3 ⁶⁹
ELK1, ⁶⁴ ETS1 ⁶⁴	MYC ⁶⁷
SP1 ⁶⁵	
NF κ B ⁶⁵	
CHD4, ^{69*} MBD2 ^{69*}	
Epigenetic regulators	
Unknown	Sin3A-HDAC1 ⁶⁶
	EZH2 ⁶⁸
	HDAC1/4 ⁸¹
	HDAC6 ⁶²
	RBPJ and mutated NICD of NOTCH1 ⁸⁵

* The DNA binding site in the *MS4A1* promoter has not been defined. NICD: NOTCH1 intracellular domain.

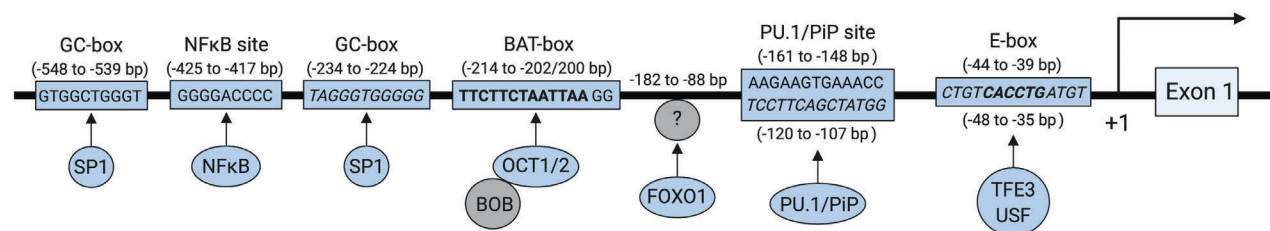


Figure 3. A schematic of the proximal region of *MS4A1* promoter with transcription factor binding sites. Several regulatory elements differ in nucleotide sequence when comparing data from literature and the TRANSFAC database. Shimizu *et al.*⁵⁵ described the GC-box binding SP1 as being located in a region between bases -548 and -539, but the TRANSFAC database identified a GC-box in a position -234 to -224 bp [based on the SP1 chromatin immunoprecipitation sequencing data (ENCODE ID: ENCSR000BHK)]. A BAT-box was identified by Thévenin *et al.*⁵⁸ in the proximal promoter region located between bases -214 and -202 (in bold), while others describe it between bases -214 and -200.^{59,65} The PU.1/PI3 binding site was originally defined as a sequence between -161 and -148 bp,⁵⁹ but TRANSFAC predicts it in the region from -120 to -107 bp (in italics). The E-box sequence is usually described as the CACCTG sequence between -44 and -39 bp (in bold)^{59,62,65} but the TRANSFAC database suggests (based on ENCODE ID: ENCSR000BGI) a longer sequence from -48 to -35 bp (in italics). FOXO1 was suggested as being recruited to the *MS4A1* promoter indirectly by the DNA-binding element between bases -182 and -88.⁷⁰ NF κ B binds into the region of the *MS4A1* promoter between -425 and -417 bp.⁶²

known positive regulatory elements present in the *MS4A1* promoter include an E-box motif (binding μ E3-specific transcription factors such as USF and TFE3), “PU.1/PiP” binding site and a BAT box (Figure 3, Table 1).^{58,59} The BAT box is a sequence element present in the most proximal region and serves as a binding site for the transcription factors OCT1 and OCT2 with a B-cell restricted co-activator BOB (Figure 3, Table 1).^{58,60} The BAT element is important for the high constitutive expression of CD20 in mature B cells and the induction of CD20 in pre-B cells.⁵⁸ The “PU.1/PiP” binding site is a putative site for transcription factors belonging to the ETS family (e.g. PU.1) and protein PiP (IRF4) (Figure 3, Table 1). PiP is recruited to this DNA binding site indirectly by phosphorylated PU.1⁵⁹ and a “PU.1/PiP” binding site seems to be critical for CD20 expression as it is occupied only in CD20-positive B cells. Additionally, PU.1/PiP are downregulated during plasma cell differentiation,⁶¹ and mutations in this binding site nearly completely abolished the promoter activity of *MS4A1*.⁵⁹ Moreover, transcriptional CD20 activation in primary CLL and non-Hodgkin lymphoma (NHL) B cells was associated with increased PU.1 and OCT2 binding to the *MS4A1* promoter in response to farnesyltransferase inhibition.⁶² Downregulating PU.1 expression by overexpression of its negative regulator, namely FLT3, also led to lower CD20 expression in CLL cells and *vice versa*.⁶³

Several transcription factors from the ETS family, such as ELK1 and ETS1, were observed to be activated in an ERK-dependent manner and enhance CD20 cell-surface expression in B-NHL cell lines and primary CLL cells after bryostatin-1 treatment *in vitro* (which activates the MEK1/ERK-1/2 pathway via PKC) (Figure 2, Table 1).⁶⁴ Furthermore, it was proposed that NF κ B might positively regulate CD20 expression^{62,65} and gemcitabine treatment of DLBCL cell lines augmented CD20 expression together with NF κ B signaling activation (Figures 2 and 3, Table 1).⁶⁶ Chromatin immunoprecipitation sequencing analysis also revealed *MS4A1* as a direct MYC target gene in Burkitt lymphoma cell lines (Table 1), and MYC silencing resulted in CD20 upregulation.⁶⁷ The repression of CD20 by MYC is surprising and remains to be confirmed in other lymphoma cell types, since B-cell activation (also leading to MYC expression) is generally known to induce CD20 expression in B cells.⁶⁸ To reveal other factors regulating CD20 expression, Slabicki *et al.*⁶⁹ performed a genome-wide RNA interference screening using a library of small hairpin RNAs delivered into Raji cells (Burkitt lymphoma cell line) by lentiviral vectors. They identified 37 potential CD20 repressors and 51 activators, among them CHD4 and MBD2 as novel *MS4A1* inducers (Table 1). Both CHD4 and MBD2 are members of the nucleosome remodeling deacetylase complex, which plays an important role in the regulation of gene transcription. This screening also revealed CREM as the top candidate for CD20 repression, and the presence of three half-cAMP response elements in *MS4A1* promoter sites (TGACG) led to the notion that cAMP-mediated signal transduction plays a role in CD20 transcriptional repression. Most recently, FOXO1 transcription factor was described as a negative *MS4A1* transcription regulator in lymphoma B cells (Figures 2 and 3, Table 1).⁷⁰ This is in agreement with the observation that DLBCL patients with activating FOXO1 mutations have shorter overall survival upon rituximab-based therapy.⁷¹ As the exact

localization of the putative FOXO1 binding site in the *MS4A1* promoter was not determined, it is believed that FOXO1 binds indirectly to the DNA-binding element between -182 and -88 bp (Figure 3).⁷⁰ These data (and our unpublished data) suggest that FOXO1 inhibitors might theoretically be combined with anti-CD20 antibodies to induce CD20 expression and potentiate the effect of the monoclonal antibodies. Similarly, other groups have proposed that inhibiting aurora kinase A/B could also lead to upregulation of CD20 and potentiation of rituximab's clinical efficacy.^{72,73}

It is not surprising that several recent studies suggested that CD20 is at least partially regulated by epigenetic mechanisms. Tomita *et al.* demonstrated that treating a CD20-negative B-cell line with the histone deacetylase (HDAC) inhibitor trichostatin A resulted in robust upregulation of CD20 mRNA and protein.⁷⁴ *In vitro* treatment of primary cells obtained from relapsed CD20-negative B-NHL patients using the DNA methyl-transferase (DNMT) inhibitor 5-aza-2-deoxycytidine also led to the stimulation of *MS4A1* mRNA and cell-surface expression within 3 days, and restoration of rituximab sensitivity.⁷⁵ Despite the fact that CD20 stimulation by DNMT inhibitors was described both *in vitro*^{75,76} and *in vivo* in patients with B-cell malignancies,⁷⁷ CD20 is less likely to be regulated by CpG (de)methylation as its promoter region does not contain any CpG islands up to ~5 kb upstream from the transcription start site.⁷⁶ However, it is plausible that DNMT inhibition regulates the methylation status of transcription factors critical for *MS4A1* transcription, or some more distant genomic regions (enhancers) are involved in *MS4A1* transcription. Furthermore, it was reported that a Sin3A-HDAC1 co-repressor complex is recruited to the *MS4A1* promoter in CD20-negative B-cell lines (Figure 2, Table 1).⁷⁶ This complex dissociates from the promoter with 5-aza-2-deoxycytidine and trichostatin A treatment, resulting in histone acetylation and partial restoration of CD20 expression. Shimizu *et al.* showed that HDAC inhibitors (valproic acid or romidepsin) are able to induce CD20 expression in B-cell lines through *MS4A1* promoter hyperacetylation and recruit the SP1 transcription factor within 48 hours (Figures 2 and 3, Table 1).⁶⁵ At the moment, several ongoing clinical trials are evaluating the efficacy of epigenetic modulators in combination with rituximab (Table 2). In the VALFRID study, pretreatment with valproic acid before first-line therapy with CHOP plus rituximab in DLBCL patients resulted in histone acetylation, CD20 upregulation at the mRNA and cell-surface levels⁷⁸ and improved overall survival.⁷⁹ In contrast, the analysis of three CLL patients from the PREVAIL study showed no CD20 induction upon pretreatment with valproic acid.⁸⁰ A plausible explanation might be that valproic acid induces a bivalent *MS4A1* promoter status in primary CLL cells *in vivo* as it induces histone acetylation, but also transient recruitment of the transcriptional repressor EZH2 to the *MS4A1* promoter (Figure 2, Table 1). Administering a DNMT inhibitor and pan-HDAC inhibitor (valproic acid, romidepsin, trichostatin A, SAHA) stimulates CD20 expression and might improve anti-CD20 therapy *in vivo*, at least in some patients with B-NHL. However, the clinical use of pan-HDAC inhibitors is hindered by adverse effects^{77,79} and thus the involvement of individual HDAC molecules and selective HDAC inhibitors are undergoing pre-clinical studies. Recently, entinostat, a selective HDAC1/4 inhibitor, was

Table 2. List of novel drugs combined with anti-CD20 monoclonal antibodies in B-cell malignancies.

Drugs	Pre-clinical studies	Phase I: trial ID* and status	Phase II: trial ID* and status	Phase III: trial ID* and status	FDA approvals and comments	
BCR inhibitors	Ibrutinib	↓CD20 in CLL cells <i>in vitro</i> and <i>in vivo</i> ^{44,100}		NCT02007044 (active) ¹²	NCT02264574 (completed) ⁴⁹ NCT02165397 (active) ¹¹⁸	FDA approved (2019) ibrutinib plus obinutuzumab for treatment-naïve CLL. No benefit from combination of ibrutinib and rituximab in CLL (NCT02007044). ¹² FDA approved (2018) ibrutinib in combination with rituximab for Waldenström's macroglobulinemia.
	Idelalisib	Unknown			NCT01539512 (completed) ¹¹⁰ NCT01659021 (terminated) ¹¹¹	FDA approved (2014) idelalisib in combination with rituximab for relapsed CLL.
	Duvelisib	Unknown		NCT02391545 (terminated)	NCT02204982 (terminated)	-
	Acalabrutinib	BTK inhibition ↓CD20 in CLL cells <i>in vitro</i> and <i>in vivo</i> ^{44,100}			NCT02475681 (active) ¹⁰⁹	-
BCL2 inhibitor	Venetoclax	Unknown	NCT02296918 (active) ¹¹⁹	NCT02950051 (active) NCT02005471 (active) ¹⁰ NCT02242942 (active) ¹¹⁶	FDA approved (2018) venetoclax in combination with rituximab for CLL/SLL patients, with or without 17p deletion, who have received at least one prior therapy. FDA approved (2019) venetoclax in combination with obinutuzumab for previously untreated CLL/SLL.	
Chromatin modulators	Valproic acid	↑CD20 in B-cell lines <i>in vitro</i> ⁶⁵ and in DLBCL patients <i>in vivo</i> ⁷⁸	NCT01622439 (completed) ⁷⁹			
			NCT02144623 (completed) ⁸⁰			
	5-Azacitidine, 5-aza-2-deoxycytidine	↑CD20 <i>in vitro</i> ^{75,76} and <i>in vivo</i> ⁷⁷	NCT01004991 (completed)			
			NCT00901069 (completed)			
	Trichostatin A	↑CD20 in B-cell lines <i>in vitro</i> ⁷⁴				
Romidepsin	↑CD20 in B-cell lines <i>in vitro</i> ⁶⁵					
Entinostat	↑CD20 in B-cell lines <i>in vitro</i> ⁸¹					
Other drugs	Bryostatin-1	↑CD20 in B-cell lines <i>in vitro</i> ⁶⁴			NCT00087425 (completed)	
	Gemcitabine	↑CD20 in B-cell lines <i>in vitro</i> ⁶⁶			NCT00169195 (completed) ¹²⁰ NCT02750670 (active)	
	CpG oligodeoxynucleotides	↑CD20 in CLL cells <i>in vitro</i> ¹²¹			NCT00251394 (completed) ¹²²	
Other drugs	Aurora kinase A/B inhibitor (alisertib)	↑CD20 in immunotherapy-resistant cell lines <i>in vitro</i> ¹²³	NCT01397825 (completed) ⁷²			
			NCT01695941 (active)			
	Farnesyltransferase inhibitor (L-744, 832)	↑CD20 in B-cell lines <i>in vitro</i> ⁶²				
TGFβ inhibitor (LY364947)	inhibits the suppression of CD20 mediated by TGFβ <i>in vitro</i> ⁶⁹					
FOXO1 inhibitors (AS1842856)	↑CD20 expression <i>in vitro</i> and <i>in vivo</i> ⁷⁰					

↑: induction of expression; ↓: repression of expression; -: no decision; *: ID on clinicaltrials.gov; ID: identity; FDA: Food and Drug Administration; CLL: chronic lymphocytic leukemia; BCR: B-cell receptor; BTK: Bruton tyrosine kinase; SLL: small lymphocytic lymphoma; DLBCL: diffuse large B-cell lymphoma; TGFβ: transforming growth factor-β.

reported to upregulate CD20 and improve rituximab efficacy both *in vitro* and in a mouse model (Figure 2, Table 1).⁸¹ Additionally, Bobrowicz *et al.* identified HDAC6 as a novel repressor of CD20 expression in B-cell lines and primary CLL cells (Figure 2, Table 1).⁸² HDAC6 was shown to be overexpressed in CLL cells and its inhibition augmented the efficacy of anti-CD20 monoclonal antibodies *in vitro* and improved survival of complement-, NK cell- and macrophage-competent mice (SCID Fox Chase mice) injected with Raji cells and treated with rituximab.⁸² However, it seems that HDAC6 inhibitor does not induce *MS4A1* transcription, but only increases *MS4A1* mRNA translation. Its potential clinical use is, therefore, likely limited to malignancies that have highly active *MS4A1* transcription but escape anti-CD20 antibodies by preventing its translation. This is not likely in most CLL cases, although, one report has suggested that *MS4A1* mRNA might be repressed post-transcriptionally by microRNAs in CLL.⁸³

Regulation of CD20 levels on the cell-surface during therapy

Besides transcriptional and epigenetic regulation, several studies have demonstrated CD20 downmodulation on the B-cell surface in response to anti-CD20 therapy (Figure 1). One of these mechanisms is called “shaving”. Monocytes and macrophages recognize rituximab binding to CD20 and remove this complex from the B-cell surface via the FcγRI-dependent process of endocytosis called trogocytosis⁵³ and this was observed in CLL patients treated with rituximab *in vivo* (Figure 1).^{53,84,85} Alternatively, the acute change in CD20 levels in the malignant B-cell population after rituximab infusion might be partially due to elimination of those cells with the highest CD20 levels. Indeed, we have shown that after rituximab infusion *in vivo*, the antibody primarily targets and eliminates a subpopulation of CLL cells with the highest levels of CD20 via CDC, whereas many CLL cells with pre-therapy low CD20 levels survive.³⁴ Importantly, the CLL cells with the highest cell-surface CD20 levels are also those with the highest BCR signaling propensity and also represent the vast majority of Ki67-positive cells in peripheral blood.³⁴ This “targeting” of the most aggressive intraclonal CLL cell subpopulation at least partially explains the good clinical efficacy of rituximab. It remains to be determined whether rituximab is also targeting specific intraclonal cell subpopulations in diseases such as follicular lymphoma and DLBCL, in which malignant cells have relatively homogeneously higher CD20 cell-surface levels.

Another mechanism reducing CD20 expression on B cells in response to anti-CD20 therapy is known as antigenic modulation (Figure 1).⁸⁶ This refers to the active internalization and subsequent degradation of CD20/monoclonal antibody complexes demanding energy and cytoskeleton remodeling. Importantly, only type I anti-CD20 monoclonal antibodies induce marked antigenic modulation. These anti-CD20 monoclonal antibodies (e.g. rituximab and ofatumumab) recognize and bind CD20 epitope in a different orientation than type II antibodies (obinutuzumab) and are able to redistribute CD20 into lipid rafts on the plasma membrane.^{87,88} Type I anti-CD20 monoclonal antibodies also have an approximately two-fold higher capacity to bind CD20 epitope, which makes them prone to internalization and proteolytic

degradation.^{86,89} Moreover, the extent of antigenic modulation depends on the type of B-cell malignancy. The most rapid internalization can be seen in CLL cells, followed by mantle cell lymphoma cells, while follicular lymphoma and DLBCL cells show relatively lower rates of antigen internalization.⁸⁶ Lim *et al.* suggested that different rates of internalization in B-cell malignancies are due to different levels of inhibitory FcγRIIb on B cells (predominantly expressed on CLL and mantle cell lymphoma cells).⁹⁰ Rituximab was proposed to crosslink CD20 and FcγRIIb on the same B cell, resulting in FcγRIIb phosphorylation, and internalization of these complexes into lysosomes for their degradation.

The selection pressure caused by rituximab therapy can also lead to the emergence of malignant B-cell clones that are relatively or fully negative for cell-surface CD20 expression (Figure 1). In some DLBCL patients, mutations in the *MS4A1* coding sequence were identified; however, mutations involving rituximab epitope are extremely rare.⁹¹ Terui *et al.* analyzed CD20 mutations in samples obtained from patients with previously untreated or relapsed/refractory B-NHL and found *MS4A1* mutations in 11 out of 50 patients (22%).⁹² Importantly, in four cases (8%), such mutations resulted in a C-terminal truncated form of CD20 protein and reduced its cell-surface expression. Nakamaki *et al.* also reported a case of a relapsed DLBCL patient with a homozygous *MS4A1* gene deletion after rituximab-based therapy.⁹³

Notably, some recurrent genetic mutations in patients with B-cell malignancies might affect CD20 levels, and be favored during therapy. In a clinical trial comparing fludarabine and cyclophosphamide treatment with fludarabine, cyclophosphamide and rituximab treatment, it was found that *NOTCH1* mutations are associated with a relative resistance to the anti-CD20 therapy.⁹⁴ Pozzo *et al.* showed that *NOTCH1*-mutated CLL cells are characterized by a lower CD20 expression in comparison to that of *NOTCH1*-wildtype CLL cells.⁹⁵ Mutations in *NOTCH1* intracellular domain (NICD) result in dysregulation of HDAC-mediated epigenetic repression of CD20 through interactions with the RBPJ transcription factor. RBPJ acts as a negative regulator when forming a complex with HDAC1/2; however, accumulation of mutated *NOTCH1* in the nucleus results in the preferential formation of NICD-RBPJ activating complex and higher HDAC1/2 levels available for interactions with an *MS4A1* promoter.

Recently, microenvironmental interactions in various B-cell malignancies were brought into focus as these provide essential pro-proliferative and pro-survival signals and promote drug resistance (reviewed by Seda & Mraz⁹⁶). Interactions between mesenchymal stromal cells and CLL cells were shown to protect the leukemic cells from rituximab-induced CDC⁹⁶ and direct apoptosis,⁹⁷ and this can be therapeutically targeted by integrin inhibition (Figure 1).⁹⁷ These observations led to the coining of the term “cell adhesion-mediated antibody resistance” as an analogy to the long-known “cell adhesion-mediated drug resistance”, which refers to resistance to classical chemotherapy. CD20 down-modulation in response to microenvironmental stimuli might be a theoretical explanation for cell adhesion-mediated antibody resistance. This is supported by the observation that stimulating normal B cells by co-culture with CD40L-expressing fibroblasts results in rapid CD20 endocytosis and thus reduces the cell-surface levels of CD20.⁹⁸ Additionally, Kawabata

et al. observed in the Ramos cell line that TGF β signaling led to SMAD2/3 binding directly to the *MS4A1* transcription start site, resulting in CD20 repression.⁹⁹ However, we and others have shown that in CLL, the chemokine CXCL12 (also known as SDF1) produced by stromal cells in immune niches induces CD20 expression, and that the intracлонаl CLL cell subpopulation that recently exited the lymph nodes is characterized by high levels of CD20.³⁴ This has an important consequence for the mechanism of rituximab's action since, *in vivo*, rituximab infusion leads to rapid and preferential elimination of this aggressive, proliferative CLL cell subpopulation. The remaining large proportion of CLL cells can survive the rituximab therapy because of relatively weak cell-surface levels of CD20, but these cells have a gene-expression profile of non-activated CLL cells, which are relatively less able to activate the BCR pathway, and do not proliferate. It remains unclear which molecular pathways provide CLL cells in the lymph node microenvironment with resistance to rituximab, despite having high levels of CD20.⁹⁷ The resistance to rituximab in the microenvironment seems to be limited to rituximab-mediated apoptosis and CDC.

Combinatorial therapy of novel drugs and anti-CD20 monoclonal antibodies

For over a decade, scientists and clinicians have become accustomed to the empirical experience that adding rituximab to other therapies leads to increased therapeutic efficacy in B-cell malignancies. This also prompted studies for strategies to induce higher CD20 levels on the B-cell surface to potentially sensitize malignant cells to anti-CD20 monoclonal antibodies (summarized in Table 2). Several of these "CD20 inducers" are being explored in preclinical or phase I/II clinical trials, including aurora kinase inhibitors, FOXO1 inhibitors, and chromatin modulators. For example, it has been shown that in lymphomas, the aurora kinase inhibitor alisertib can be safely and successfully used in combination with vincristine and rituximab (phase I/II trial).⁷² Nevertheless, none of the "CD20 inducers" has been prioritized for phase III trials yet (see Table 2). Combining the BTK inhibitor ibrutinib with rituximab was expected to increase the BTK inhibitor's clinical efficacy. This hypothesis was supported by the observation that CLL/lymphoma cells become more sensitive to apoptosis and anti-CD20 monoclonal antibodies when mobilized from immune niches (a typical effect of BCR inhibitors).^{96,97} However, results from a phase II study¹² demonstrated no benefit from adding rituximab to ibrutinib. Recent studies have shown that CD20 levels are repressed during ibrutinib therapy and that ibrutinib affects cells responsible for effector mechanisms such as T/NK cells and macrophages. The reduction of CD20 levels by ibrutinib has a clear impact on rituximab-mediated CDC and apoptosis. However, CD20 is not completely lost, which still allows for anti-CD20 monoclonal antibodies to bind to cells. Skarzynski *et al.*¹⁰⁰ also suggested that ibrutinib reduces complement inhibitor CD55 levels, which might partially counterbalance the effects of lower CD20, but it seems that in the sum of all effects, rituximab or ofatumumab efficacy decreases during ibrutinib therapy.

CD20 levels appear to play an essential role in CDC induced by rituximab, but they seem to be less relevant for ADCC.¹⁰¹ Unfortunately, ibrutinib also affects the

functions of T cells and NK cells by inhibiting their BTK or a related ITK. BTK is critical for regulating the functions of NK cells as BTK-less NK cells have impaired cytotoxic activity.¹⁰² ITK signals downstream of the T-cell receptor and is required to activate NK cells through Fc γ RIII.¹⁰³ Inhibiting BTK or ITK impairs the cytotoxic functions of NK cells (degranulation, cytokine secretion) and ADCC mediated by type I and II anti-CD20 monoclonal antibodies.^{104,105} Thus ibrutinib may impair T- and NK-cell functions through either BTK or ITK, or both.¹⁰⁴ It has also been suggested that phagocytosis by macrophages is affected by ibrutinib, but it is unclear if this is due to BTK inhibition in these cells or an off-target effect.¹⁰⁴⁻¹⁰⁶ Based on the results from the iLLUMINATE study,⁴⁹ the Food and Drug Administration has already approved the combination of ibrutinib plus obinutuzumab for treatment-naïve patients with CLL (Table 2). However, the control arm of the study with chlorambucil plus obinutuzumab did not allow a conclusion on whether obinutuzumab provided a real benefit. Alternatively, sequential ibrutinib administration after the anti-CD20 monoclonal antibody could conceivably allow for better antibody effects. However, a clinical trial in CLL showed that sequential treatment with ofatumumab before ibrutinib was inferior to starting ibrutinib first, followed by the administration of ibrutinib and ofatumumab.¹⁰⁷ Since obinutuzumab acts in part through mechanisms different from those of type I antibodies (rituximab, ofatumumab), its combination with ibrutinib may lead to different effects and increased clinical efficacy. Alternatively, other BTK inhibitors, such as acalabrutinib, are more selective with less off-target activity and likely do not interfere with antibody-dependent cellular phagocytosis or ADCC.¹⁰⁸ It needs to be determined whether acalabrutinib is more suitable than ibrutinib for therapeutic combination with anti-CD20 monoclonal antibodies. Recently, a phase III study showed that acalabrutinib combined with obinutuzumab is highly efficient in prolonging progression-free survival when compared to obinutuzumab and chlorambucil in patients with previously untreated CLL.¹⁰⁹

An interesting case is also the PI3K δ inhibitor idelalisib, which is currently approved for use in combination with rituximab to treat relapsed CLL based on a comparison to rituximab alone (Table 2).¹¹⁰ A similar phase III study showed that the progression-free survival of participants treated with a combination of idelalisib and ofatumumab was significantly longer than that of the group treated with ofatumumab only (Table 2).¹¹¹ However, it is unclear whether adding rituximab or ofatumumab to idelalisib actually provides any clinical benefit, and based on the understanding of CD20 regulation, it is very likely that PI3K inhibitors also repress CD20 expression. In fact, data indicate that any inhibitor repressing Akt or NF κ B or CXCR4 activity in B cells, such as a SYK inhibitor, BTK inhibitor, PI3K δ inhibitor, or CXCR4 antagonist, also reduces CD20 expression, leading to decreased binding of anti-CD20 monoclonal antibodies.^{44,70,100,112,113} Notably, SRC inhibitors such as dasatinib also repress CD20 transcription and impair NK cell functions.¹¹² Additionally, PI3K δ plays a critical role in maturation, development, and effector functions of NK cells, which would indicate that it might impair ADCC. However, some studies indicate that this might be less prominent than ibrutinib's effects¹¹⁴ or that idelalisib does not reduce ADCC at all.¹¹⁵

Idelalisib was also shown to decrease IFN γ production by NK cells, and reduce secretion of various cytokines by T cells (IL6, IL10, TNF α , and CD40L).¹¹⁵ More studies will be needed to determine whether other BTK or PI3K inhibitors have a better profile in terms of affecting ADCC/antibody-dependent cellular phagocytosis, but it seems inevitable that they will all lead to reduced levels of CD20.

The BH3-mimetic venetoclax was also tested in combination with anti-CD20 monoclonal antibodies. It seems that in contrast to “BCR inhibitors”, there are no obvious biological reasons preventing an additive or synergistic effect of such a combination. The Food and Drug Administration granted approval for the use of venetoclax in combination with obinutuzumab for patients with previously untreated CLL/small lymphocytic lymphoma and in combination with rituximab to treat patients with CLL/ small lymphocytic lymphoma who have received at least one prior therapy (Table 2).¹¹⁶ The biological rationale for such combinations in CLL is provided, among others, by a study showing that combining venetoclax and anti-CD20 monoclonal antibodies overcomes microenvironment-mediated resistance of CLL cells to venetoclax monotherapy *in vitro*.¹¹⁷

Conclusion

Although CD20 is considered to be an ideal therapeutic target and rituximab-based immunotherapy has become a standard of care for a majority of B-cell malignancies, it is still unclear what all the functions of CD20 are, and

how its expression is regulated. The main reason is the large heterogeneity of patients with B-cell malignancies and the lack of mouse models with an evident phenotype which makes CD20 analysis *in vivo* more difficult. A full understanding of the complexity of regulation of CD20, its physiological function and the exact mechanism of action of anti-CD20 monoclonal antibodies is of pivotal importance to develop new modified anti-CD20 monoclonal antibodies and their therapeutic combination that would yield better clinical efficacy and/or less toxicity. Recently, the possible role of CD20 in microenvironmental interactions was underscored by the observation that CD20 is upregulated in the context of immune niches. This is likely to be of physiological importance, especially for BCR signaling; however, it is unclear if this is related to the putative function of CD20 as a regulator of calcium flux triggered by BCR or any potential role in T-cell interactions or some additional function(s). Further investigation of the physiological function of CD20 is required, including the identification of molecules that interact with CD20, since this has implications for the development of rational therapeutic combinations and strategies.

Acknowledgments

Supported by the Ministry of Health of the Czech Republic, grant No. NU20-03-00292. All rights reserved. This project has received funding from the European Research Council (ERC) under the European Union's Horizon 2020 research and innovation programme (grant agreement n. 802644). Figures were created using BioRender graphical tool. We would like to thank Prof. Jiri Mayer, MD (University Hospital Brno) for inspiring discussions about anti-CD20 monoclonal antibodies.

References

- Salles G, Barrett M, Foà R, et al. Rituximab in B-cell hematologic malignancies: a review of 20 years of clinical experience. *Adv Ther*. 2017;34(10):2232-2273.
- Mössner E, Brünker P, Moser S, et al. Increasing the efficacy of CD20 antibody therapy through the engineering of a new type II anti-CD20 antibody with enhanced direct and immune effector cell-mediated B-cell cytotoxicity. *Blood*. 2010;115(22):4393-4402.
- Boross P, Leusen JHW. Mechanisms of action of CD20 antibodies. *Am J Cancer Res*. 2012;2(6):676-690.
- Smith MR. Rituximab (monoclonal anti-CD20 antibody): mechanisms of action and resistance. *Oncogene*. 2003;22(47):7359-7368.
- Goede V, Fischer K, Busch R, et al. Obinutuzumab plus chlorambucil in patients with CLL and coexisting conditions. *N Engl J Med*. 2014;370(12):1101-1110.
- Marcus R, Davies A, Ando K, et al. Obinutuzumab for the first-line treatment of follicular lymphoma. *N Engl J Med*. 2017;377(14):1331-1344.
- Hiddemann W, Barbui AM, Canales MA, et al. Immunochemotherapy with obinutuzumab or rituximab for previously untreated follicular lymphoma in the GAL-LIUM study: influence of chemotherapy on efficacy and safety. *J Clin Oncol*. 2018;36(23):2395-2404.
- Vitolo U, Trněný M, Belada D, et al. Obinutuzumab or rituximab plus cyclophosphamide, doxorubicin, vincristine, and prednisone in previously untreated diffuse large B-cell lymphoma. *J Clin Oncol*. 2017;35(31):3529-3537.
- Burger JA, Keating MJ, Wierda WG, et al. Safety and activity of ibrutinib plus rituximab for patients with high-risk chronic lymphocytic leukaemia: a single-arm, phase 2 study. *Lancet Oncol*. 2014;15(10):1090-1099.
- Seymour JF, Kipps TJ, Eichhorst B, et al. Venetoclax-rituximab in relapsed or refractory chronic lymphocytic leukemia. *N Engl J Med*. 2018;378(12):1107-1120.
- Wang Y, Zhang W, Han Q, et al. Effective response and delayed toxicities of refractory advanced diffuse large B-cell lymphoma treated by CD20-directed chimeric antigen receptor-modified T cells. *Clin Immunol*. 2014;155(2):160-175.
- Burger JA, Sivina M, Jain N, et al. Randomized trial of ibrutinib vs ibrutinib plus rituximab in patients with chronic lymphocytic leukemia. *Blood*. 2019;133(10):1011-1019.
- Tedder TF, Klejman G, Schlossman SF, Saito H. Structure of the gene encoding the human B lymphocyte differentiation antigen CD20 (B1). *J Immunol*. 1989;142(7):2560-2568.
- Eon Kuek L, Leffler M, Mackay GA, Hulett MD. The MS4A family: counting past 1, 2 and 3. *Immunol Cell Biol*. 2016;94(1):11-23.
- Henry C, Deschamps M, Rohrlich P-S, et al. Identification of an alternative CD20 transcript variant in B-cell malignancies coding for a novel protein associated to rituximab resistance. *Blood*. 2010;115(12):2420-2429.
- Gamonet C, Bole-Richard E, Delherme A, et al. New CD20 alternative splice variants: molecular identification and differential expression within hematological B cell malignancies. *Exp Hematol Oncol*. 2016;5:7.
- Tedder TF, Schlossman SF. Phosphorylation of the B1 (CD20) molecule by normal and malignant human B lymphocytes. *J Biol Chem*. 1988;263(20):10009-10015.
- Zuccolo J, Deng L, Unruh TL, et al. Expression of MS4A and TMEM176 genes in human B lymphocytes. *Front Immunol*. 2013;4:195.
- Bubien JK, Zhou LJ, Bell PD, Frizzell RA, Tedder TF. Transfection of the CD20 cell surface molecule into ectopic cell types generates a Ca²⁺ conductance found constitutively in B lymphocytes. *J Cell Biol*. 1993;121(5):1121-1132.
- Polyak MJ, Li H, Shariat N, Deans JP. CD20 homo-oligomers physically associate with the B cell antigen receptor. Dissociation upon receptor engagement and recruitment of phosphoproteins and calmodulin-binding proteins. *J Biol Chem*. 2008;283(27):18545-18552.

21. Levy S, Shoham T. Protein-protein interactions in the tetraspanin web. *Physiology*. 2005;20(4):218-224.
22. Szöllösi J, Horejsi V, Bene L, Angelisová P, Damjanovich S. Supramolecular complexes of MHC class I, MHC class II, CD20, and tetraspan molecules (CD53, CD81, and CD82) at the surface of a B cell line JY. *J Immunol*. 1996;157(7):2939-2946.
23. Léveillé C, AL-Daccak R, Mourad W. CD20 is physically and functionally coupled to MHC class II and CD40 on human B cell lines. *Eur J Immunol*. 1999;29(1):65-74.
24. Deans JP, Kalt L, Ledbetter JA, Schieven GL, Bolen JB, Johnson P. Association of 75/80-kDa phosphoproteins and the tyrosine kinases Lyn, Fyn, and Lck with the B cell molecule CD20. Evidence against involvement of the cytoplasmic regions of CD20. *J Biol Chem*. 1995;270(38):22632-22638.
25. Manshour T, Do K, Wang X, et al. Circulating CD20 is detectable in the plasma of patients with chronic lymphocytic leukemia and is of prognostic significance. *Blood*. 2003;101(7):2507-2513.
26. Schuh E, Berer K, Mulazzani M, et al. Features of human CD3+CD20+ T cells. *J Immunol*. 2016;197(4):1111-1117.
27. Prevodnik VK, Lavrenak J, Horvat M, Novakovi BJ. The predictive significance of CD20 expression in B-cell lymphomas. *Diagn Pathol*. 2011;6:33.
28. Olejniczak SH, Stewart CC, Donohue K, Czuczman MS. A quantitative exploration of surface antigen expression in common B-cell malignancies using flow cytometry. *Immunol Invest*. 2006;35(1):93-114.
29. Fang C, Zhuang Y, Wang L, et al. High levels of CD20 expression predict good prognosis in chronic lymphocytic leukemia. *Cancer Sci*. 2013;104(8):996-1001.
30. Johnson NA, Boyle M, Bashashati A, et al. Diffuse large B-cell lymphoma: reduced CD20 expression is associated with an inferior survival. *Blood*. 2009;113(16):3773-3780.
31. Horvat M, Kloboves Prevodnik V, Lavrencak J, Jezersek Novakovic B. Predictive significance of the cut-off value of CD20 expression in patients with B-cell lymphoma. *Oncol Rep*. 2010;24(4):1101-1107.
32. Perz J, Topaly J, Fruehauf S, Hensel M, Ho AD. Level of CD 20-expression and efficacy of rituximab treatment in patients with resistant or relapsing B-cell prolymphocytic leukemia and B-cell chronic lymphocytic leukemia. *Leuk Lymphoma*. 2002;43(1):149-151.
33. Hsi ED, Kopecky KJ, Appelbaum FR, et al. Prognostic significance of CD38 and CD20 expression as assessed by quantitative flow cytometry in chronic lymphocytic leukaemia. *Br J Haematol*. 2003;120(6):1017-1025.
34. Pavlasova G, Borsky M, Svobodova V, et al. Rituximab primarily targets an intra-clonal BCR signaling proficient CLL subpopulation characterized by high CD20 levels. *Leukemia*. 2018;32(9):2028-2031.
35. Kuijpers TW, Bende RJ, Baars PA, et al. CD20 deficiency in humans results in impaired T cell-independent antibody responses. *J Clin Invest*. 2010;120(1):214-222.
36. Uchida J, Lee Y, Hasegawa M, et al. Mouse CD20 expression and function. *Int Immunol*. 2004;16(1):119-129.
37. O'Keefe TL, Williams GT, Davies SL, Neuberger MS. Mice carrying a CD20 gene disruption. *Immunogenetics*. 1998;48(2):125-132.
38. Morsy DED, Sanyal R, Zaiss AK, Deo R, Muruve DA, Deans JP. Reduced T-dependent humoral immunity in CD20-deficient mice. *J Immunol*. 2013;191(6):3112-3118.
39. Petrie RJ, Deans JP. Colocalization of the B cell receptor and CD20 followed by activation-dependent dissociation in distinct lipid rafts. *J Immunol*. 2002;169(6):2886-2891.
40. Li H, Ayer LM, Lyttton J, Deans JP. Store-operated cation entry mediated by CD20 in membrane rafts. *J Biol Chem*. 2003;278(43):42427-42434.
41. Franke A, Niederfellner GJ, Klein C, Burtcher H. Antibodies against CD20 or B-cell receptor induce similar transcription patterns in human lymphoma cell lines. *PLoS One*. 2011;6(2):e16596.
42. Walshe CA, Beers SA, French RR, et al. Induction of cytosolic calcium flux by CD20 is dependent upon B cell antigen receptor signaling. *J Biol Chem*. 2008;283(25):16971-16984.
43. Kheirallah S, Caron P, Gross E, et al. Rituximab inhibits B-cell receptor signaling. *Blood*. 2010;115(5):985-994.
44. Pavlasova G, Borsky M, Seda V, et al. Ibrutinib inhibits CD20 upregulation on CLL B cells mediated by the CXCR4/SDF-1 axis. *Blood*. 2016;128(12):1609-1613.
45. Venugopal P, Sivaraman S, Huang XK, Nayini J, Gregory SA, Preisler HD. Effects of cytokines on CD20 antigen expression on tumor cells from patients with chronic lymphocytic leukemia. *Leuk Res*. 2000;24(5):411-415.
46. Sivaraman S, Venugopal P, Ranganathan R, et al. Effect of interferon-alpha on CD20 antigen expression of B-cell chronic lymphocytic leukemia. *Cytokines Cell Mol Ther*. 2000;6(2):81-87.
47. Sivaraman S, Deshpande CG, Ranganathan R, et al. Tumor necrosis factor modulates CD 20 expression on cells from chronic lymphocytic leukemia: a new role for TNF alpha. *Microsc Res Tech*. 2000;50(3):251-257.
48. Seda V, Mraz M. B-cell receptor signalling and its crosstalk with other pathways in normal and malignant cells. *Eur J Haematol*. 2015;94(3):193-205.
49. Moreno C, Greil R, Demirkan F, et al. Ibrutinib plus obinutuzumab versus chlorambucil plus obinutuzumab in first-line treatment of chronic lymphocytic leukaemia (ILLUMINATE): a multicentre, randomised, open-label, phase 3 trial. *Lancet Oncol*. 2019;20(1):43-56.
50. Hörl S, Bánki Z, Huber G, et al. Reduction of complement factor H binding to CLL cells improves the induction of rituximab-mediated complement-dependent cytotoxicity. *Leukemia*. 2013;27(11):2200-2208.
51. Golay J, Lazzari M, Facchinetti V, et al. CD20 levels determine the in vitro susceptibility to rituximab and complement of B-cell chronic lymphocytic leukemia: further regulation by CD55 and CD59. *Blood*. 2001;98(12):3383-3389.
52. Ahlgrimm M, Pfreundschuh M, Kreuz M, Regitz E, Preuss K-D, Bittenbring J. The impact of Fc-gamma receptor polymorphisms in elderly patients with diffuse large B-cell lymphoma treated with CHOP with or without rituximab. *Blood*. 2011;118(17):4657-4662.
53. Kennedy AD, Beum PV, Solga MD, et al. Rituximab infusion promotes rapid complement depletion and acute CD20 loss in chronic lymphocytic leukemia. *J Immunol*. 2004;172(5):3280-3288.
54. Capuano C, Romanelli M, Pighi C, et al. Anti-CD20 Therapy acts via Fc-gammaRIIIA to diminish responsiveness of human natural killer cells. *Cancer Res*. 2015;75(19):4097-4108.
55. Racila E, Link BK, Weng W-K, et al. A polymorphism in the complement component C1qA correlates with prolonged response following rituximab therapy of follicular lymphoma. *Clin Cancer Res*. 2008;14(20):6697-6703.
56. Janas E, Priest R, Wilde JI, White JH, Malhotra R. Rituxan (anti-CD20 antibody)-induced translocation of CD20 into lipid rafts is crucial for calcium influx and apoptosis. *Clin Exp Immunol*. 2005;139(3):439-446.
57. Tsai P-C, Hernandez-Ilizaliturri FJ, Bangia N, Olejniczak SH, Czuczman MS. Regulation of CD20 in rituximab-resistant cell lines and B-cell non-Hodgkin lymphoma. *Clin Cancer Res*. 2012;18(4):1039-1050.
58. Thévenin C, Lucas BF, Kozlow EJ, Kehrl JH. Cell type- and stage-specific expression of the CD20/B1 antigen correlates with the activity of a diverged octamer DNA motif present in its promoter. *J Biol Chem*. 1993;268(8):5949-5956.
59. Himmelmann A, Riva A, Wilson GL, Lucas BF, Thevenin C, Kehrl JH. PU.1/Pip and basic helix loop helix zipper transcription factors interact with binding sites in the CD20 promoter to help confer lineage- and stage-specific expression of CD20 in B lymphocytes. *Blood*. 1997;90(10):3984-3995.
60. Gstaiger M, Knoepfel L, Georgiev O, Schaffner W, Hovens CM. A B-cell coactivator of octamer-binding transcription factors. *Nature*. 1995;373(6512):360-362.
61. Nagy M, Chapuis B, Matthes T. Expression of transcription factors Pu.1, Spi-B, Blimp-1, BSAP and oct-2 in normal human plasma cells and in multiple myeloma cells. *Br J Haematol*. 2002;116(2):429-435.
62. Winiarska M, Nowis D, Bil J, et al. Prenyltransferases regulate CD20 protein levels and influence anti-CD20 monoclonal antibody-mediated activation of complement-dependent cytotoxicity. *J Biol Chem*. 2012;287(38):31983-31993.
63. Mankaï A, Bordron A, Renaudineau Y, et al. Purine-rich box-1-mediated reduced expression of CD20 alters rituximab-induced lysis of chronic lymphocytic leukemia B cells. *Cancer Res*. 2008;68(18):7512-7519.
64. Wojciechowski W, Li H, Marshall S, Dell'Agnola C, Espinoza-Delgado I. Enhanced expression of CD20 in human tumor B cells is controlled through ERK-dependent mechanisms. *J Immunol*. 2005;174(12):7859-7868.
65. Shimizu R, Kikuchi J, Wada T, Ozawa K, Kano Y, Furukawa Y. HDAC inhibitors augment cytotoxic activity of rituximab by upregulating CD20 expression on lymphoma cells. *Leukemia*. 2010;24(10):1760-1768.
66. Hayashi K, Nagasaki E, Kan S, et al. Gemcitabine enhances rituximab-mediated complement-dependent cytotoxicity to B cell lymphoma by CD20 upregulation. *Cancer Sci*. 2016;107(5):682-689.
67. Seitz V, Butzhammer P, Hirsch B, et al. Deep sequencing of MYC DNA-binding sites in Burkitt lymphoma. *PLoS One*. 2011;6(11):e26837.
68. Filip D, Mraz M. The role of MYC in the transformation and aggressiveness of 'indolent' B-cell malignancies. *Leuk Lymphoma*. 2020;61(3):510-524.
69. Ślabicki M, Lee KS, Jethwa A, et al. Dissection of CD20 regulation in lymphoma using RNAi. *Leukemia*. 2016;30(12):2409-2412.

70. Pyrzynska B, Dwojak M, Zerrouqi A, et al. FOXO1 promotes resistance of non-Hodgkin lymphomas to anti-CD20-based therapy. *Oncoimmunology*. 2018;7(5): e1423183.
71. Trinh DL, Scott DW, Morin RD, et al. Analysis of FOXO1 mutations in diffuse large B-cell lymphoma. *Blood*. 2013;121(18):3666-3674.
72. Kelly KR, Friedberg JW, Park SI, et al. Phase I study of the investigational Aurora A kinase inhibitor alisertib plus rituximab or rituximab/vincristine in relapsed/refractory aggressive B-cell lymphoma. *Clin Cancer Res Off J Am Assoc Cancer Res*. 2018;24(24):6150-6159.
73. Manfredi M. Combination of Aurora kinase inhibitors and anti-CD20 antibodies. *US20100183601A1*.
74. Tomita A, Hiraga J, Kiyoi H, et al. Epigenetic regulation of CD20 protein expression in a novel B-cell lymphoma cell line, RRBL1, established from a patient treated repeatedly with rituximab-containing chemotherapy. *Int J Hematol*. 2007;86(1):49-57.
75. Hiraga J, Tomita A, Sugimoto T, et al. Down-regulation of CD20 expression in B-cell lymphoma cells after treatment with rituximab-containing combination chemotherapies: its prevalence and clinical significance. *Blood*. 2009;113(20):4885-4893.
76. Sugimoto T, Tomita A, Hiraga J, et al. Escape mechanisms from antibody therapy to lymphoma cells: downregulation of CD20 mRNA by recruitment of the HDAC complex and not by DNA methylation. *Biochem Biophys Res Commun*. 2009;390(1):48-53.
77. Tsutsumi Y, Ohigashi H, Ito S, Shiratori S, Teshima T. 5-Azacytidine partially restores CD20 expression in follicular lymphoma that lost CD20 expression after rituximab treatment: a case report. *J Med Case Rep*. 2016;10:27.
78. Damm JK, Gordon S, Ehinger M, et al. Pharmacologically relevant doses of valproate upregulate CD20 expression in three diffuse large B-cell lymphoma patients in vivo. *Exp Hematol Oncol*. 2015;4:4.
79. Drott K, Hagberg H, Papworth K, Relander T, Jerkeman M. Valproate in combination with rituximab and CHOP as first-line therapy in diffuse large B-cell lymphoma (VALFRID). *Blood Adv*. 2018;2(12):1386-1392.
80. Scialdone A, Hasni MS, Damm JK, Lennartsson A, Gullberg U, Drott K. The HDAC inhibitor valproate induces a bivalent status of the CD20 promoter in CLL patients suggesting distinct epigenetic regulation of CD20 expression in CLL in vivo. *Oncotarget*. 2017;8(23):37409-37422.
81. Frys S, Simons Z, Hu Q, et al. Entinostat, a novel histone deacetylase inhibitor is active in B-cell lymphoma and enhances the anti-tumour activity of rituximab and chemotherapy agents. *Br J Haematol*. 2015;169(4):506-519.
82. Bobrowicz M, Dwojak M, Pyrzynska B, et al. HDAC6 inhibition upregulates CD20 levels and increases the efficacy of anti-CD20 monoclonal antibodies. *Blood*. 2017;130(14):1628-1638.
83. Gagez A-L, Duroux-Richard I, Leprêtre S, et al. miR-125b and miR-532-3p predict the efficiency of rituximab-mediated lymphodepletion in chronic lymphocytic leukemia patients. A French Innovative Leukemia Organization study. *Haematologica*. 2017;102(4):746-754.
84. Williams ME, Densmore JJ, Pawluczko AW, et al. Thrice-weekly low-dose rituximab decreases CD20 loss via shaving and promotes enhanced targeting in chronic lymphocytic leukemia. *J Immunol*. 2006;177(10):7435-7443.
85. Baig NA, Taylor RP, Lindorfer MA, et al. Induced resistance to ofatumumab-mediated cell clearance mechanisms, including complement-dependent cytotoxicity, in chronic lymphocytic leukemia. *J Immunol*. 2014;192(4):1620-1629.
86. Beers SA, French RR, Chan HTC, et al. Antigenic modulation limits the efficacy of anti-CD20 antibodies: implications for antibody selection. *Blood*. 2010;115(25):5191-5201.
87. Niederfellner G, Lammens A, Mundigl O, et al. Epitope characterization and crystal structure of GA101 provide insights into the molecular basis for type I/II distinction of CD20 antibodies. *Blood*. 2011;118(2):358-367.
88. Deans JP, Robbins SM, Polyak MJ, Savage JA. Rapid redistribution of CD20 to a low density detergent-insoluble membrane compartment. *J Biol Chem*. 1998;273(1):344-348.
89. Chan HTC, Hughes D, French RR, et al. CD20-induced lymphoma cell death is independent of both caspases and its redistribution into triton X-100 insoluble membrane rafts. *Cancer Res*. 2003;63(17):5480-5489.
90. Lim SH, Vaughan AT, Ashton-Key M, et al. Fc gamma receptor IIb on target B cells promotes rituximab internalization and reduces clinical efficacy. *Blood*. 2011;118(9):2530-2540.
91. Johnson NA, Leach S, Woolcock B, et al. CD20 mutations involving the rituximab epitope are rare in diffuse large B-cell lymphomas and are not a significant cause of R-CHOP failure. *Haematologica*. 2009;94(3):423-427.
92. Terui Y, Mishima Y, Sugimura N, et al. Identification of CD20 C-terminal deletion mutations associated with loss of CD20 expression in non-Hodgkin's lymphoma. *Clin Cancer Res*. 2009;15(7):2523-2530.
93. Nakamaki T, Fukuchi K, Nakashima H, et al. CD20 gene deletion causes a CD20-negative relapse in diffuse large B-cell lymphoma. *Eur J Haematol*. 2012;89(4):350-355.
94. Stilgenbauer S, Schnaiter A, Paschka P, et al. Gene mutations and treatment outcome in chronic lymphocytic leukemia: results from the CLL8 trial. *Blood*. 2014;123(21):3247-3254.
95. Pozzo F, Bittolo T, Arruga F, et al. NOTCH1 mutations associate with low CD20 level in chronic lymphocytic leukemia: evidence for a NOTCH1 mutation-driven epigenetic dysregulation. *Leukemia*. 2016;30(1):182-189.
96. Buchner M, Brantner P, Stickel N, et al. The microenvironment differentially impairs passive and active immunotherapy in chronic lymphocytic leukaemia - CXCR4 antagonists as potential adjuvants for monoclonal antibodies. *Br J Haematol*. 2010;151(2):167-178.
97. Mraz M, Zent CS, Church AK, et al. Bone marrow stromal cells protect lymphoma B-cells from rituximab-induced apoptosis and targeting integrin alpha-4-beta-1 (VLA-4) with natalizumab can overcome this resistance. *Br J Haematol*. 2011;155(1):53-64.
98. Anolik J, Looney RJ, Bottaro A, Sanz I, Young F. Down-regulation of CD20 on B cells upon CD40 activation. *Eur J Immunol*. 2003;33(9):2398-2409.
99. Kawabata KC, Ehata S, Komuro A, Takeuchi K, Miyazono K. TGF- β induced apoptosis of B-cell lymphoma Ramos cells through reduction of MS4A1/CD20. *Oncogene*. 2013;32(16):2096-2106.
100. Skarzynski M, Niemann CU, Lee YS, et al. Interactions between ibrutinib and anti-CD20 antibodies: competing effects on the outcome of combination therapy. *Clin Cancer*. 2016;22(1):86-95.
101. van Meerden T, van Rijn RS, Hol S, Hagenbeek A, Ebeling SB. Complement-induced cell death by rituximab depends on CD20 expression level and acts complementary to antibody-dependent cellular cytotoxicity. *Clin Cancer Res*. 2006;12(13):4027-4035.
102. Bao Y, Zheng J, Han C, et al. Correction: Tyrosine kinase Btk is required for NK cell activation. *J Biol Chem*. 2020;295(10):3389.
103. Khurana D, Arneson LN, Schoon RA, Dick CJ, Leibson PJ. Differential regulation of human NK cell-mediated cytotoxicity by the tyrosine kinase Itk. *J Immunol*. 2007;178(6):3575-3582.
104. Da Roit F, Engelberts PJ, Taylor RP, et al. Ibrutinib interferes with the cell-mediated anti-tumor activities of therapeutic CD20 antibodies: implications for combination therapy. *Haematologica*. 2015;100(1):77-86.
105. Kohrt HE, Sagiv-Barfi I, Rafiq S, et al. Ibrutinib antagonizes rituximab-dependent NK cell-mediated cytotoxicity. *Blood*. 2014;123(12):1957-1960.
106. Chu CC, Pinney JJ, VanDerMeid KR, et al. Anti-CD20 therapy reliance on antibody-dependent cellular phagocytosis affects combination drug choice. *Blood*. 2019;134(Supplement_1):682-682.
107. Jaglowski SM, Jones JA, Nagar V, et al. Safety and activity of BTK inhibitor ibrutinib combined with ofatumumab in chronic lymphocytic leukemia: a phase 1b/2 study. *Blood*. 2015;126(7):842-850.
108. Golay J, Ubiali G, Intronna M. The specific Bruton tyrosine kinase inhibitor acalabrutinib (ACP-196) shows favorable in vitro activity against chronic lymphocytic leukemia B cells with CD20 antibodies. *Haematologica*. 2017;102(10):e400-e403.
109. Sharman JP, Banerji V, Fogliatto LM, et al. ELEVATE TN: Phase 3 study of acalabrutinib combined with obinutuzumab (O) or alone vs o plus chlorambucil (Clb) in patients (Pts) with treatment-naive chronic lymphocytic leukemia (CLL). *Blood*. 2019;134(Suppl 1):31.
110. Furman RR, Sharman JP, Coutre SE, et al. Idelalisib and rituximab in relapsed chronic lymphocytic leukemia. *N Engl J Med*. 2014;370(11):997-1007.
111. Jones JA, Robak T, Brown JR, et al. Efficacy and safety of idelalisib in combination with ofatumumab for previously treated chronic lymphocytic leukaemia: an open-label, randomised phase 3 trial. *Lancet Haematol*. 2017;4(3):e114-e126.
112. Winiarska M, Bojarczuk K, Pyrzynska B, et al. Inhibitors of SRC kinases impair anti-tumor activity of anti-CD20 monoclonal antibodies. *mAbs*. 2014;6(5):1300-1313.
113. Bojarczuk K, Siemicka M, Dwojak M, et al. B-cell receptor pathway inhibitors affect CD20 levels and impair anti-tumor activity of anti-CD20 monoclonal antibodies. *Leukemia*. 2014;28(5):1163-1167.
114. Guo H, Samarakoon A, Vanhaesebroeck B, Malarkannan S. The p110 delta of PI3K plays a critical role in NK cell terminal maturation and cytokine/chemokine generation. *J Exp Med*. 2008;205(10):2419-2435.
115. Herman SEM, Gordon AL, Wagner AJ, et al. Phosphatidylinositol 3-kinase- δ inhibitor CAL-101 shows promising preclinical activity in chronic lymphocytic leukemia by antagonizing intrinsic and extrinsic cellular survival signals. *Blood*. 2010;116(12):2078-2088.
116. Fischer K, Al-Sawaf O, Bahlo J, et al.

- Venetoclax and obinutuzumab in patients with CLL and coexisting conditions. *N Engl J Med.* 2019;380(23):2225-2236.
117. Thijssen R, Slinger E, Weller K, et al. Resistance to ABT-199 induced by microenvironmental signals in chronic lymphocytic leukemia can be counteracted by CD20 antibodies or kinase inhibitors. *Haematologica.* 2015;100(8):e302-e306.
118. Dimopoulos MA, Tedeschi A, Trotman J, et al. Phase 3 trial of ibrutinib plus rituximab in Waldenström's macroglobulinemia. *N Engl J Med.* 2018;378(25):2399-2410.
119. Woyach JA, Blachly JS, Rogers KA, et al. Acalabrutinib plus obinutuzumab in treatment-naïve and relapsed/refractory chronic lymphocytic leukemia. *Cancer Discov.* 2020;10(3):394-405.
120. Mounier N, El Gnaoui T, Tilly H, et al. Rituximab plus gemcitabine and oxaliplatin in patients with refractory/relapsed diffuse large B-cell lymphoma who are not candidates for high-dose therapy. A phase II Lymphoma Study Association trial. *Haematologica.* 2013;98(11):1726-1731.
121. Mankai A, Buhé V, Hammadi M, et al. Improvement of rituximab efficiency in chronic lymphocytic leukemia by CpG-mediated upregulation of CD20 expression independently of PU.1. *Ann N Y Acad Sci.* 2009;1173:721-728.
122. Friedberg JW, Kim H, McCauley M, et al. Combination immunotherapy with a CpG oligonucleotide (1018 ISS) and rituximab in patients with non-Hodgkin lymphoma: increased interferon- α/β -inducible gene expression, without significant toxicity. *Blood.* 2005;105(2):489-495.
123. Kozlova V, Ledererova A, Doubek M, Mayer J, Pospisilova S, Smida M. Epigenetic drug screen on resistant CLL cells reveals aurora kinase inhibitors as enhancers of CD20 expression and sensitizers to treatment with CD20 monoclonal antibodies. *Blood.* 2018;132(Suppl 1):4407.



Clinical practice recommendation on hematopoietic stem cell transplantation for acute myeloid leukemia patients with *FLT3*-internal tandem duplication: a position statement from the Acute Leukemia Working Party of the European Society for Blood and Marrow Transplantation

Ali Bazarbachi,^{1,2} Gesine Bug,³ Frederic Baron,⁴ Eolia Brissot,⁵ Fabio Ciceri,⁶ Iman Abou Dalle,¹ Hartmut Döhner,⁷ Jordi Esteve,⁸ Yngvar Floisand,^{9,10} Sebastian Giebel,¹¹ Maria Gillece,¹² Norbert-Claude Gorin,¹³ Elias Jabbour,¹⁴ Mahmoud Aljurf,¹⁵ Hagop Kantarjian,¹⁴ Mohamed Kharfan-Dabaja,¹⁶ Myriam Labopin,^{17,5} Francesco Lanza,¹⁸ Florent Malard,⁵ Zinaida Peric,¹⁹ Thomas Prebet,²⁰ Farhad Ravandi,¹⁴ Annalisa Ruggeri,²¹ Jaime Sanz,²² Christoph Schmid,²³ Roni Shouval,²⁴ Alexandros Spyridonidis,²⁵ Jurjen Versluis,²⁶ Norbert Vey,²⁷ Bipin N Savani,²⁸ Arnon Nagler²⁹ and Mohamad Mohty⁵

¹Bone Marrow Transplantation Program, Department of Internal Medicine, American University of Beirut Medical Center, Beirut, Lebanon; ²Department of Anatomy, Cell Biology, and Physiological Sciences, American University of Beirut, Beirut, Lebanon; ³Department of Medicine 2, Hematology and Oncology, University Hospital, Goethe University Frankfurt, Frankfurt am Main, Germany; ⁴GIGA-I3, University and CHU of Liège, Liège, Belgium; ⁵Sorbonne Universités, UPMC University of Paris 06, INSERM, Centre de Recherche Saint-Antoine (CRSA), Hematology Department, AP-HP, Saint Antoine Hospital, Paris, France; ⁶Vita-Salute San Raffaele University of Milan, Milan, Italy; Hematology and Bone Marrow Transplantation Unit, IRCCS San Raffaele Scientific Institute, Milan, Italy; ⁷Department of Internal Medicine III, Ulm University Hospital, Ulm, Germany; ⁸Hematology Department, Hospital Clínic of Barcelona, IDIBAPS, University of Barcelona, Barcelona, Spain; ⁹Department of Hematology, Oslo University Hospital - Rikshospitalet, Oslo, Norway; ¹⁰Center for Cancer Cell Reprogramming, Institute for Cancer Research, Oslo University Hospital, Montebello, Oslo, Norway; ¹¹Department of Bone Marrow Transplantation and Oncohematology, Maria Skłodowska-Curie Institute – Oncology Center, Gliwice Branch, Gliwice, Poland; ¹²Department of Haematology, Leeds Teaching Hospitals Trust, Leeds, UK; ¹³Department of Hematology and Cell Therapy, European Society for Blood and Marrow Transplantation, Paris Office, Hôpital Saint-Antoine, Paris, France; ¹⁴Department of Leukemia, The University of Texas MD Anderson Cancer Center, Houston, TX, USA; ¹⁵Department of Hematology King Faisal Specialist Hospital & Research Center, Riyadh, Saudi Arabia; ¹⁶Division of Hematology-Oncology and Blood and Marrow Transplantation and Cellular Therapies Program, Mayo Clinic, Jacksonville, FL, USA; ¹⁷Acute Leukemia Working Party, Paris Study Office, European Society for Blood and Marrow Transplantation, Paris, France; ¹⁸Romagna Transplant Network, Ravenna, Italy; ¹⁹University Hospital Center Zagreb, School of Medicine, University of Zagreb, Zagreb, Croatia; ²⁰Section of Hematology, Department of Internal Medicine, Yale University School of Medicine, New Haven, CT, USA; ²¹Department of Pediatric Hematology and Oncology, IRCCS Bambino Gesù Children's Hospital, Roma, Italy; Eurocord, Hôpital Saint Louis, Paris, France; ²²Hematology Department, Hospital Universitari i Politècnic La Fe. Instituto de Investigación Sanitaria La Fe, Valencia, CIBERONC, Instituto Carlos III, Madrid, Spain; ²³Department of Hematology and Oncology, Augsburg University Hospital, Augsburg, Germany; ²⁴Adult Bone Marrow Transplantation Service, Memorial Sloan Kettering Cancer Center, New York, NY, USA; ²⁵BMT Unit, University of Patras, Patras, Greece; ²⁶Erasmus University Medical Center Cancer Institute, Rotterdam, the Netherlands; ²⁷Department of Hematology, Institut Paoli-Calmettes, Marseille, France; ²⁸Department of Hematology-Oncology, Vanderbilt University Medical Center, Nashville, TN, USA and ²⁹Hematology and Bone Marrow Transplantation Division, Chaim Sheba Medical Center, Tel-Hashomer, Sackler School of Medicine, Tel Aviv University, Israel

ABSTRACT

The *FMS*-like tyrosine kinase 3 (*FLT3*) gene is mutated in 25-30% of patients with acute myeloid leukemia (AML). Because of the poor prognosis associated with *FLT3*-internal tandem duplication mutated AML, allogeneic hematopoietic stem-cell transplantation (SCT) was commonly performed in first complete remission. Remarkable progress

Haematologica 2020
Volume 105(6):1507-1516

Correspondence:

ALI BAZARBACHI,
bazarbac@aub.edu.lb

Received: November 19, 2019.

Accepted: March 19, 2020.

Pre-published: April 2, 2020

doi:10.3324/haematol.2019.243410

Check the online version for the most updated information on this article, online supplements, and information on authorship & disclosures: www.haematologica.org/content/105/6/1507

©2020 Ferrata Storti Foundation

Material published in *Haematologica* is covered by copyright. All rights are reserved to the Ferrata Storti Foundation. Use of published material is allowed under the following terms and conditions:

<https://creativecommons.org/licenses/by-nc/4.0/legalcode>.

Copies of published material are allowed for personal or internal use. Sharing published material for non-commercial purposes is subject to the following conditions:

<https://creativecommons.org/licenses/by-nc/4.0/legalcode>, sect. 3. Reproducing and sharing published material for commercial purposes is not allowed without permission in writing from the publisher.



has been made in frontline treatments with the incorporation of FLT3 inhibitors and the development of highly sensitive minimal/measurable residual disease assays. Similarly, recent progress in allogeneic hematopoietic SCT includes improvement of transplant techniques, the use of haplo-identical donors in patients lacking an HLA matched donor, and the introduction of FLT3 inhibitors as post-transplant maintenance therapy. Nevertheless, current transplant strategies vary between centers and differ in terms of transplant indications based on the internal tandem duplication allelic ratio and concomitant nucleophosmin-1 mutation, as well as in terms of post-transplant maintenance/consolidation. This review generated by international leukemia or transplant experts, mostly from the European Society for Blood and Marrow Transplantation, attempts to develop a position statement on best approaches for allogeneic hematopoietic SCT for AML with *FLT3*-internal tandem duplication including indications for and modalities of such transplants and on the potential optimization of post-transplant maintenance with FLT inhibitors.

Introduction

FMS-like tyrosine kinase 3 (FLT3) is a transmembrane ligand-activated receptor tyrosine kinase that is normally expressed by hematopoietic stem cells and early myeloid and lymphoid progenitor cells, and is involved in the proliferation, differentiation and apoptosis of hematopoietic cells¹ through various signaling pathways, including phosphatidylinositol 3-kinase (PI3K) and rat sarcoma (RAS) signal-transduction cascades.^{2,7} *FLT3* is mutated in about 25-30% of newly diagnosed cases of acute myeloid leukemia (AML),⁸⁻¹⁰ either by internal tandem duplications (*FLT3*-ITD) of the juxtamembrane domain (19-25%), and/or by a point mutation, usually involving the tyrosine kinase domain (TKD) at D835 or I836 in the activating loop (7-10%).¹¹⁻¹⁵ Both mutations are more frequent in cytogenetically normal AML and both constitutively activate *FLT3* causing dimerization in a ligand-independent manner, resulting in proliferation and survival of leukemia cells.^{14,15}

FLT3-ITD mutations in newly diagnosed AML are associated with a greater disease burden, manifesting as an elevated white blood cell count and a high percentage of blasts at the time of diagnosis as well as a tendency to early relapse and a poor overall prognosis.^{8,10-12,16,17} Both European LeukemiaNet (ELN) recommendations and National Comprehensive Cancer Network (NCCN) guidelines incorporate *FLT3*-ITD mutations in risk-stratifying patients based on allelic burden and nucleophosmin-1 (*NPM1*) co-mutation.^{18,19} In cytogenetically normal patients, *FLT3*-ITD mutations in the presence of a concomitant *NPM1* mutation, mainly when the *FLT3*-ITD allele ratio is low (<0.5), fare better than those with wild-type *NPM1*.^{8,10,16,17,20-22} Despite the great effort to harmonize and cross-validate the FLT3 assays within clinical trials,²³ there is still no consensus on the *FLT3*-ITD allele ratio threshold and there is considerable variability between centers in the assessment of the *FLT3*-ITD ratio according to the technique used, if one is available. Furthermore, in addition to *NPM1* mutations, a significant overlap with other mutations (*WT1*, *IDH1*, *DNMT3A*) as well as *NUP98/NSD1* fusions modify outcome as well as response to therapy. Although patients with *FLT3*-ITD AML respond to conventional induction chemotherapy with remission rates similar to those seen in other subtypes of AML, they are much more likely to relapse and to relapse quickly.^{11,12,24-28} The prognostic impact of *FLT3*-TKD is less clear,²⁹⁻³² but it, too, is influenced substantially by *NPM1* co-mutation which confers a better prognosis.³³⁻³⁵

The availability of active FLT3 inhibitors that are able to disrupt the oncogenic signaling initiated by FLT3 has improved the overall survival (OS) of patients with *FLT3*-mutated AML.³⁶ Midostaurin, a multikinase inhibitor, was granted Food and Drug Administration (FDA) and European Medicines Agency (EMA) approval for the treatment of patients with newly diagnosed *FLT3*-mutated AML, in combination with intensive chemotherapy, and by the EMA in addition as maintenance treatment after conventional consolidation therapy. This approval was based on the results of the RATIFY trial, which demonstrated that the combination of midostaurin with standard induction therapy resulted in significantly prolonged OS (not censored for transplant) for AML with either *FLT3*-ITD or *FLT3*-TKD mutations.³⁷ The benefit was particularly remarkable in patients who went on to receive allogeneic hematopoietic stem cell transplantation (allo-SCT) in first complete remission (CR1). Following the results of the ADMIRAL trial, gilteritinib, a second-generation FLT3 inhibitor, was recently approved for relapsed/refractory *FLT3*-mutated AML with *FLT3*-ITD and *FLT3*-TKD mutations.³⁸ Promising data were also reported for quizartinib and crenolanib.^{39,40} Finally, because of its long-time availability, sorafenib has been tested, alone or in combination, in various settings in *FLT3*-ITD AML, such as first-line therapy^{41,42} or for the treatment of disease relapse,⁴³⁻⁴⁵ including after failure of allo-SCT.⁴⁵⁻⁵⁷ However, recent data appear to support incorporating sorafenib into the treatment of patients with *FLT3*-mutated AML, possibly with induction therapy^{41,58,59} as well as maintenance therapy after allo-SCT.^{43,60-65}

Because of the diversity in *FLT3*-mutated AML, which depends on the type of *FLT3* mutation, *FLT3*-ITD allelic burden, insertion site and co-occurring mutations, the decision regarding whether to perform allo-SCT in CR1 is becoming more challenging.⁶⁶⁻⁷⁵ With the use of more effective therapies, especially with the incorporation of FLT3 inhibitors, deeper responses are being achieved. The assessment of minimal/measurable residual disease (MRD) at the time of response has enabled prediction of outcomes in AML, and tailoring of post-remission therapeutic strategies accordingly.⁷⁶⁻⁷⁸ Additionally, substantial progress has been made in allo-SCT in recent years, including improvement of transplant techniques, the use of haplo-identical donors in patients lacking an HLA-matched donor,⁷⁹⁻⁸¹ and post-transplant preventive strategies, such as prophylactic or preemptive use of FLT3 inhibitors.^{63,82-85} Nevertheless, current transplant strategies

vary between centers and differ in terms of indications for the transplants and treatments following them. This review provides a consensus from European Society for Blood and Marrow Transplantation (EBMT) experts on best approaches to allo-SCT in AML with *FLT3*-ITD including the indications for and modalities of allo-SCT and on potential optimization of post-transplant maintenance therapy with *FLT3* inhibitors.

The consensus process

Two chairpersons (AB and MM) appointed a panel of 32 physicians (hereafter referred to as the Panel) selected mostly from the EBMT for their expertise in research and clinical practice in AML and allo-SCT. A physician with expertise in clinical epidemiology (ML) ensured the methodological correctness of the process. The objective of the Panel was to identify practical issues pertinent to all physicians involved in the therapeutic management of patients undergoing allo-SCT for AML with *FLT3* mutations and to generate best practice recommendations on indications for and modalities of allo-SCT and on potential optimization of post-transplant maintenance with *FLT3* inhibitors. This was done through a number of questions according to the Delphi technique.³⁶ A search for relevant literature in English was performed in the MEDLINE, EMBASE and PubMed databases (up to August 2019). Most of the studies used for these recommendations are retrospective cohort studies or phase II trials, with only a few prospective randomized trials. Three panelists drafted statements that addressed the key questions identified, and the remaining panelists scored their agreement with those statements and provided suggestions for rephrasing them.

The evaluation of evidence and the subsequent recommendations were graded according to the system used by Couriel.³⁷ The strength of the recommendations (*Online Supplementary Table S1*) and evidence levels (*Online Supplementary Table S2*) were rated by all participants of the consensus process.

Overview of prognosis and current indications for allogeneic stem-cell transplantation in *FLT3*-mutated acute myeloid leukemia

The indication for allo-SCT in *FLT3*-ITD AML depends largely on *FLT3* variables (allelic burden, insertion site and co-occurring mutations), on disease status (including MRD), and on the use of *FLT3* inhibitors during induction/consolidation treatment, in addition to other patient-, donor- and graft-related factors. Unfortunately, there are no prospective randomized trials evaluating the best post-remission therapeutic strategy in *FLT3*-mutated AML, taking in consideration all the diverse combinations.

Several recent reports have suggested that allelic burden might affect prognosis of *FLT3*-ITD AML treated with standard induction chemotherapy.^{17,22,88,89} Indeed, the presence of a high allelic burden of *FLT3*-ITD mutations (≥ 0.5) confers a poor prognosis.^{12,27,90,91} Several studies have demonstrated that allo-SCT significantly improves survival outcomes in this category^{69,92-95} and that the negative impact of high allelic burden might be overcome when patients undergo allo-SCT in CR1.¹⁷ Therefore, all patients with *FLT3*-ITD^{high} should be considered for allo-SCT in CR1.^{66,69,92-96} These patients still face higher rates of early

relapse and poor responses to further therapy and eventually poor long-term survival.^{92,97} The worst prognosis is observed in patients who relapse after allo-SCT, who have predicted 1-year OS rates below 20%.⁹⁸ However, a subcategory of patients with *FLT3*-ITD^{high}/*NPM1* mutation of the ELN intermediate-risk group treated with *FLT3* inhibitors, and who achieve MRD negativity, may be offered the possibility of post-remission consolidation with longitudinal MRD monitoring of *NPM1*.⁹¹ This approach should be undertaken with caution, and preferably within a clinical trial, since recent data suggest the possible extinction of the *NPM1* clone after chemotherapy while the *FLT3*-ITD clone persists.

Additional mutations may, however, influence the prognosis of AML with *FLT3*-ITD. For example, the co-existence of *NPM1* mutation with *FLT3*-ITD is associated with improved outcomes, particularly in patients with a low *FLT3* allelic ratio (< 0.5).^{8,10,16,20} According to the 2017 ELN recommendations, this subcategory is stratified as favorable risk, advocating against the need for allo-SCT.⁹¹ Nonetheless, the good prognosis of a low allelic ratio is not universally recognized, with data suggesting better outcome for allografted patients regardless of *NPM1* mutation status.⁹⁹ A threshold for *FLT3* allelic burden is also controversial and differs according to studies. It was mainly based on the median of the mutant-to-wildtype ratio found in different retrospective studies. For example, in one study evaluating the prognostic factors of newly diagnosed AML, a *FLT3* ratio above 0.78 was associated with worse survival, whereas in another study the threshold was 0.51.^{11,17} Therefore, the allelic burden has a continuous effect on survival outcomes and a ratio of 0.5 is a chosen threshold based on maximum clinical prognostic data. With the advent of *FLT3* inhibitors in the frontline treatment of *FLT3*-mutated AML, the OS has improved regardless of the allelic burden and the use of allo-SCT. Whether *NPM1*-mutant *FLT3*-ITD^{low} AML warrants post-remission allo-SCT in CR1 or not is still debatable. Although some studies analyzing the effect of allo-SCT in patients with *NPM1*-mutant *FLT3*-ITD^{low} found no improvement in OS or relapse risk, we must take into consideration the retrospective nature of the analysis and the small number of patients with a non-statistically significant improvement in OS and relapse risk.^{17,22} Interestingly, patients with newly diagnosed AML with *NPM1*-mutant *FLT3*-ITD^{low} treated with frontline midostaurin and intensive chemotherapy, had a 3-year OS rate of around 75%. In a retrospective subgroup analysis, the benefit of allo-SCT was only seen in the adverse ELN subgroup [hazard ratio (HR)=0.39; $P=0.003$], but not in the favorable (HR=0.78; $P=0.62$) and intermediate risk subgroups (HR=0.81; $P=0.53$).⁹¹ These findings should, however, be interpreted with caution as the RATIFY trial was not powered to demonstrate a difference of benefit of allo-SCT among diverse *FLT3*-ITD/*NPM1* genotypes. For example, the total number of patients in the favorable ELN subgroup was 85 and these patients were divided into four small groups according to whether they did or did not receive midostaurin and/or allo-SCT in CR1.⁹¹

The deleterious effect of *FLT3*-ITD was most clinically relevant in patients with concomitant *NPM1* and *DNMT3A* mutations, suggesting that AML patients with *NPM1*, *FLT3*-ITD and *DNMT3A* mutations (triple-positive AML) should be transplanted regardless of the *FLT3*-ITD allelic ratio.⁸ A recent study conducted on 147 patients

found that *NPM1*-positive AML with low allelic *FLT3*-ITD still had an unfavorable outcome, with an OS rate of only 41%, but with significant improvements in both relapse-free survival (RFS) and OS for those allografted in CR1.⁹⁹ This challenges the notion of withholding transplant for patients with supposedly favorable outcomes. In that sense, a recent study from the MD Anderson Cancer Center showed that allo-SCT improved leukemia-free survival (LFS) and OS independently of the *FLT3*-ITD allelic ratio and *NPM1* mutation status.¹⁰⁰ This fits with recent NCCN guidelines still offering allo-SCT for all patients with *FLT3*-ITD mutations regardless of allelic ratio or *NPM1* mutation status.¹⁸

On the other hand, patients with a low allelic ITD ratio lacking an *NPM1* mutation (and lacking other adverse risk mutations) are currently considered intermediate risk, hence in a gray prognostic area with no proper consensus on optimal treatment strategy. There is conflict regarding the current practice between proceeding to allo-SCT for these patients or limiting allo-SCT only to those who do not achieve MRD negativity by multiparametric flow cytometry. Indeed, technical limitations prevent the use of *FLT3* mutation for assessment of MRD which must therefore rely on multiparametric flow cytometry.¹⁰¹ Finally, Versluis *et al.* reported that in patients with wildtype *NPM1* AML without *FLT3*-ITD or with a low allelic ratio of *FLT3*-ITD, reduced intensity conditioning allo-SCT resulted in better OS and RFS rates as compared with chemotherapy or autologous SCT.⁸⁹

Overall, limitations to the universal incorporation of *FLT3*-ITD allelic ratio into routine clinical practice and the treatment algorithm include the lack of a clear cut-off (0.5 in the ELN recommendations, 0.7 in the RATIFY study) and the potential variability of the allelic ratio over time. A global effort is needed to standardize the technique for determining the *FLT3*-ITD allelic ratio, making it universal with calibration of all laboratories, reminiscent of the global exercise the world did for *BCR/ABL1*. Similarly, the definition of high and low allelic ratio should also be standardized with a clear consensus on a cut-off level. Until these technical challenges are addressed, the transplant indication remains controversial in patients with *FLT3*-ITD who belong to the ELN favorable risk group (low allelic ratio <0.5 with concomitant *NPM1* mutation) and who achieve MRD negativity. Many European cooperative groups follow the ELN algorithm, deferring allo-SCT in patients with *NPM1*-mutant *FLT3*-ITD^{low}, unless there is molecular persistence of *NPM1*. Thus, performing MRD assessment regularly to decide on allo-SCT timing is crucial when selecting this approach. Conversely, the NCCN guidelines are still advocating allo-SCT in CR1 in this setting.

Finally, data on the prognosis of *FLT3*-TKD AML remain conflicting, with some studies suggesting a negative impact of TKD mutations on LFS and OS,^{11,25,30} while others suggesting no prognostic effect, or even a benefit when a *NPM1* mutation is present.^{29,32,34,35}

Hematopoietic stem cell transplantation and factors predictive of outcome

As stated above, because of the poor prognosis associated with *FLT3*-ITD mutated AML, allo-SCT was most frequently performed in patients in CR1^{66-74,102} including fit patients ≥ 60 years of age.¹⁰³ In most studies, the LFS rate at 2 years ranges between 50 to 60% in that setting,^{66,92,97,104}

although a wide variation from 20%^{70,105} to 70%⁶⁹ has been reported. There are knowledge gaps about the factors that can predict outcome after allo-SCT.

A previous EBMT study⁹⁷ reported that patients with *FLT3*-ITD mutated AML with concomitant mutated *NPM1* had better post-transplant outcomes compared to those with wildtype *NPM1*. Similarly, other studies reported that the presence of active disease or MRD before allo-SCT results in poor post-transplant outcomes.^{106,107}

A recent, large EBMT registry study assessed outcomes in 462 allografted *FLT3*-mutated AML patients with a median follow-up of 39 months for alive patients.⁶⁵ Forty percent received allo-SCT from matched related donors, 49% from matched unrelated donors and 11% from haploidentical donors. Two-year cumulative incidence of relapse (CIR) and non-relapse mortality rates were 34% and 15%, respectively, whereas LFS, OS and graft-*versus*-host disease (GvHD)-free, relapse-free survival (GRFS) rates were 51%, 59% and 38%, respectively. On multivariable analysis, the need for more than one induction treatment negatively affected outcome, while prescribing an allo-SCT in CR1 resulted in improved CIR, LFS and OS. Presence of an *NPM1* mutation was also associated with better outcomes, including better CIR, LFS, OS and GRFS. Post-transplant maintenance therapy with sorafenib significantly reduced the CIR and improved LFS, OS and GRFS. Outcomes were not affected by the type of donor or conditioning intensity. An important finding from this study was that *in vivo* T-cell depletion with antithymocyte globulin decreased chronic GvHD and significantly improved LFS, OS and GRFS, without an apparent increase in the risk of relapse. This indicates that, even in the setting of *FLT3*-mutated AML, *in vivo* T-cell depletion does not appear to abrogate the graft-*versus*-leukemia effect. Finally, the use of haplo-identical donors was associated with improved GRFS compared to that achieved with other types of donors. Given the high risk of rapid relapse of patients with *FLT3*-mutated AML in CR1 and the poor outcome of allo-SCT in CR2 or beyond,^{11,12,108} these results and those of a recent EBMT study suggest that, in the absence of a matched sibling donor, performing haplo-identical transplants in CR1 may be considered.¹⁰⁹ Furthermore, in another large EBMT study on more than 6,500 adult AML patients allografted in CR1, multivariate analysis confirmed the lack of a statistically significant difference in OS following transplants from matched related donors or 10/10 matched unrelated donors, or haplo-SCT.¹¹⁰ Finally, the results of a CIBMTR, EUROCORD and EBMT collaborative analysis demonstrated that outcomes after umbilical cord blood transplantation are similar to those after allo-SCT from sibling donors for patients with *FLT3*-ITD AML.¹¹⁰

Post-transplant maintenance in *FLT3*-mutated acute myeloid leukemia

Even after allo-SCT, *FLT3*-mutated AML is associated with a higher risk of early relapse (30%-59%) compared to *FLT3*-wildtype AML.^{82,92} Indeed, in a CIBMTR analysis of 511 patients (158 with *FLT3* mutations), there was an increase in relapse rates in *FLT3*-mutated AML (38% vs. 28%; $P=0.04$; relative risk 1.60; 95% CI: 1.15-2.22).⁷⁴ Satisfactory treatment of patients with *FLT3*-mutated AML who relapse or progress after allo-SCT, is an unmet need. Chemotherapy or *FLT3* inhibitors alone or com-

bined with donor lymphocyte infusions are rarely effective in the long term,^{45,50} even though a small proportion of patients who relapse after allo-SCT can achieve long-lasting responses with sorafenib.^{52,54,55,57} A second allo-SCT can be offered to only a small percentage of patients and is associated with a rather high non-relapse mortality rate.¹¹¹ Several studies have, therefore, investigated the use of post-transplant maintenance with *FLT3* inhibitors as a strategy aimed to reduce relapse after allo-SCT.¹¹²

Midostaurin was not offered as maintenance therapy to recipients of allo-SCT in the RATIFY study,¹¹³ but the RADIUS phase II randomized trial compared post-transplant midostaurin maintenance with standard care in 60 adult patients.¹¹⁴ Estimated relapse rates at 18 months were 24% in the standard care group and 11% in the midostaurin group ($P=0.27$).¹¹⁴ In another prospective phase II study, maintenance midostaurin was also offered to *FLT3*-mutated AML patients undergoing allo-SCT in CR1. In a landmark analysis in patients who were event free at day 100 after transplant ($n=116$), those who started maintenance therapy within 100 days after their transplant ($n=72$) had a significantly better OS than those who did not.¹¹⁵ The main cause of early discontinuation of maintenance midostaurin after allo-SCT (23%) was poor tolerability, mainly as a result of gastrointestinal toxicity.¹¹⁴

Sorafenib has been studied as maintenance therapy following allo-SCT, demonstrating benefit with regards to survival and improved outcomes in a phase I study, a pilot study, a single-center study, a multicenter study, a registry study and a randomized study.^{60-65,116} A phase I trial (NCT01398501) was conducted in which 22 *FLT3*-ITD AML patients received twelve 28-day cycles of sorafenib 45-120 days after allo-SCT.⁶¹ The maximum tolerated dose was established at 400 mg twice daily. The 1-year progression-free survival (PFS) rate was 85% with a corresponding 1-year OS of 95%. In a pilot study, six patients with *FLT3*-ITD AML received sorafenib ($n=5$ maintenance, $n=1$ salvage) after allo-SCT with similarly encouraging results.¹¹⁶ Five of these patients developed cutaneous corticosteroid-sensitive GvHD within a few days after sorafenib initiation, suggesting a possible immunomodulatory effect, and remarkably all patients had sustained molecular remissions.

In a single-institution, observational study on *FLT3*-ITD AML patients transplanted in CR1, 26 patients who received sorafenib as maintenance treatment after allo-SCT were compared to 55 historical controls who did not.⁶² The sorafenib cohort had a better 2-year OS rate (81% vs. 62%), improved PFS (82% vs. 53%), and lower relapse incidence (8% vs. 38%).

In a multicenter study, 27 *FLT3*-mutated AML patients (aged 15-57 years) received maintenance therapy with sorafenib as a single agent after allo-SCT.⁶⁰ At a median follow-up of 18 months, 25 patients were in complete remission with full donor chimerism, with 1-year PFS and OS rates reaching 92%. Updated results after a median follow-up of 40 months further demonstrated favorable long-term outcomes in patients receiving sorafenib maintenance therapy, with 2-year PFS and OS rates reaching 73% and 80%, respectively, with an acceptable toxicity profile.⁶⁵

A recent large EBMT registry study assessed outcomes in 462 allografted *FLT3*-mutated AML patients over a median follow-up of 39 months for surviving patients.⁶³

Twenty-eight patients received post-transplant sorafenib maintenance treatment, initiated at a median of 55 days after transplantation (range, 1-173) at a median dose of 800 mg/day (range, 200-800 mg/day). Thirteen patients in the sorafenib group had chronic GvHD at a median time of 76 days after the initiation of sorafenib (range, 9-194 days). Chronic GvHD was limited in seven patients and extensive in six. On multivariate analysis, post-transplant maintenance with sorafenib significantly reduced the relapse incidence (HR=0.39; $P=0.05$), and improved LFS (HR=0.35; $P=0.01$), OS (HR=0.36; $P=0.03$) and GFRS (HR=0.44; $P=0.02$). Matched-pair analysis was also performed on 52 patients (26 in the sorafenib group and 26 controls) who engrafted and survived after allo-SCT with no relapse or grade II-IV acute GvHD until sorafenib initiation. The 2-year LFS and OS rates were 79% and 83%, respectively, in the sorafenib group ($P=0.02$) versus 54% and 62%, respectively, in the controls ($P=0.007$).

More recently, preliminary conclusions of a double-blind, prospective trial (SORMAIN) that randomized patients to either maintenance treatment with sorafenib or placebo introduced during the first 60-100 days after allo-SCT provided further support for the use of this drug in this high-risk setting.⁶⁴ Eighty transplanted *FLT3*-ITD adult AML patients were randomized 1:1 to receive either sorafenib (up to 400 mg twice daily) or placebo for up to 24 months. After a median follow-up of 42 months, the median RFS was 31 months in the placebo group whereas it was 'not reached' in the sorafenib group (corresponding to a 2-year RFS of 53% vs. 85%; HR 0.39; $P=0.01$). Sorafenib was well-tolerated with toxicities that were generally manageable, mostly by dose reduction. These findings build on previously reported data and confirm that sorafenib maintenance therapy after allo-SCT in *FLT3*-ITD AML patients is both safe and efficient in significantly reducing CIR and improving survival.

In addition to sorafenib's direct anti-leukemic effect, a possible synergism between the drug and alloreactive donor T cells in facilitating long-term disease control has been suggested,¹¹⁷ and has also been proposed in murine models in which sorafenib apparently exacerbated GvHD.¹¹⁸ A recent study demonstrated that sorafenib promotes graft-versus-leukemia activity in mice and humans through interleukin-15 production in *FLT3*-ITD leukemia cells.¹¹⁹

Gilteritinib is also currently being prospectively assessed for maintenance use in *FLT3*-ITD AML after allo-SCT in a phase III, randomized, double-blind, placebo-controlled multicenter trial (NCT02997202).¹²⁰ This study aims to enroll 346 adult patients with AML in CR1, randomized 1:1, to receive either gilteritinib 120 mg or placebo for 2 years. In addition, a large phase III randomized study (NCT04027309) by a consortium of several cooperative study groups, including HOVON, AMLSG, SAKK, ALFA, CETLAM, PETHEMA, FILO and ALLG, is anticipated to start enrolling by the end of 2019: patients will be randomized to midostaurin or gilteritinib added to standard induction and consolidation treatment. Patients who achieve complete remission will continue maintenance with either midostaurin or gilteritinib.

Finally, the recent approval of midostaurin for frontline treatment of *FLT3*-mutated AML in the USA and Europe may challenge the role of post-transplant maintenance therapies, including sorafenib. Accordingly, new data should be generated in this setting.^{121,122} Most *FLT3*-mutat-

ed AML patients, however, are not currently receiving midostaurin, at least outside the USA and some other countries; therefore, for the foreseeable future, patients may still benefit from sorafenib maintenance treatment after allo-SCT.

Summary of position statement (Table 1)

1- Indications for allogeneic stem-cell transplantation in *FLT3*-internal tandem duplication acute myeloid leukemia

- The indication for allo-SCT is controversial in patients with *FLT3*-ITD who belong to the ELN favorable risk group (low allelic ratio <0.5 with concomitant *NPM1* mutation) and who achieve MRD negativity. Allo-SCT may be delayed until first relapse as recommended by the ELN or performed in CR1 as allowed by NCCN guidelines. Grade level C-II

- In general, all other patients with *FLT3*-ITD AML should be considered for allo-SCT in CR1 if feasible. Grade level B-II

2- Modalities of hematopoietic stem cell transplantation

- Donors should be selected according to EBMT general guidelines⁸³ including the potential use of cord blood grafts whenever indicated. Grade level B-II

- *In vivo* T-cell depletion decreases the risk of chronic GvHD, without apparently increasing the risk of relapse, in *FLT3*-ITD AML and is therefore an option in this setting. Grade level B-II

- The choice of conditioning has no direct link with *FLT3*-ITD mutation and should be adapted to other individual risk factors such as age, disease status at transplant, and donor type. Grade level B-II

3- Post-transplant maintenance for *FLT3*-internal tandem duplication acute myeloid leukemia

- Post-transplant maintenance therapy with a *FLT3* inhibitor for patients who have undergone allo-SCT for *FLT3*-ITD AML is recommended (except for patients with active acute GvHD). In the absence of an appropriate clinical trial, sorafenib could be considered as the preferred option, but other *FLT3* inhibitors are attractive and war-

Table 1. Summary of the European Society for Blood and Marrow Transplantation position statement on allogeneic hematopoietic stem-cell transplantation in *FLT3*-internal tandem duplication acute myeloid leukemia.

Indication for allo-SCT in <i>FLT3</i> mutated AML	Transplant indication is controversial in patients with <i>FLT3</i> -ITD who belong to the ELN favorable risk group (low allelic ratio <0.5 with concomitant <i>NPM1</i> mutation) and who achieve MRD negativity. Allo-SCT may be delayed until first relapse as recommended by the ELN or performed in CR1 as allowed by NCCN guidelines.
	In general, all other patients with <i>FLT3</i> -ITD should be considered for allo-SCT in CR1 if feasible.
Modalities of allo-SCT	Donor selection according to EBMT general guidelines. <i>In vivo</i> T-cell depletion decreases the risk of chronic GVHD without an apparent increase in the risk of relapse in <i>FLT3</i> mutated AML and is therefore an option in this setting.
	The choice of conditioning has no direct link with <i>FLT3</i> mutation and should be adapted to other individual risk factors such as age, disease status at transplant, and donor type.
Post-transplant maintenance	Post-transplant systemic maintenance therapy with a <i>FLT3</i> inhibitor for patients who underwent allo-SCT for <i>FLT3</i> -ITD AML is recommended (except for patients with active acute GvHD).
	In the absence of an appropriate clinical trial, sorafenib could be considered as the preferred option, but the role of other <i>FLT3</i> inhibitors warrants investigation.
	Maintenance treatment should be initiated as soon as possible after disease evaluation, including MRD assessment, especially in patients with MRD-positive AML before or after allo-SCT, provided there is adequate hematologic reconstitution.
	The recommended post-transplant maintenance is sorafenib at a dose of 400 mg/day in two divided doses. Patients with MRD-positive disease may receive 800 mg/day in two divided doses, to be adapted according to tolerance. Sorafenib should be transiently discontinued in the case of GvHD requiring systemic treatment with corticosteroids, but may be cautiously resumed once remission of GvHD is documented.
	Ongoing studies will determine whether midostaurin, gilteritinib or other <i>FLT3</i> inhibitors will become additional alternatives in this setting.
	Maintenance therapy duration is not firmly established, but a minimum of 2 years is recommended, depending on tolerance.

Allo-SCT: allogeneic hematopoietic stem cell transplantation; *FLT3*: FMS-like tyrosine kinase 3; AML: acute myeloid leukemia; *FLT3*-ITD: *FLT3*-internal tandem duplication; ELN: European LeukemiaNet; *NPM1*: Nucleophosmin 1; MRD: minimal residual disease; CR1: first complete remission; NCCN: National Comprehensive Cancer Network; EBMT: European Society for Blood and Marrow Transplantation; GvHD: graft-versus-host disease.

rant further investigation in larger prospective studies. Grade level B-II

- Maintenance therapy should be initiated as soon as possible after disease evaluation, including MRD assessment (whenever feasible), especially in patients with MRD-positive AML before or after allo-SCT, provided there is adequate hematologic reconstitution. Grade level B-II

- Sorafenib should be transiently discontinued in the case of GvHD requiring systemic treatment with corticosteroids, but may be cautiously resumed once remission of GvHD is documented. Grade level B-III

- If choosing sorafenib, the recommended post-transplant maintenance dose is 400 mg/day in two divided doses. Patients with MRD-positive disease may receive 800 mg/day in two divided doses, to be adapted according to tolerance. Grade level B-III

- One potential challenge is the lack of approval of sorafenib for AML and its off-label use may not be reimbursed in many/most countries. Ongoing studies will determine the role and modalities of use of midostaurin, gilteritinib or other FLT3 inhibitors in this setting.

- The duration of maintenance therapy is not firmly established, but a minimum of 2 years is recommended, depending on tolerance. Grade level B-III

- Monitoring is recommended for potential drug-drug interactions and long-term side effects.

Aspects to be resolved

- Standardization of *FLT3*-ITD allelic ratio in terms of technique and cut-off level

- Indication for allo-SCT in patients with *FLT3*-ITD AML who belong to the ELN intermediate risk group (high allelic ratio ≥ 0.5 with concomitant *NPM1* mutation) and who achieve MRD negativity.

- Time of withdrawal of immunosuppression

- Pre-emptive versus prophylactic donor lymphocyte infusion

- Post-transplant maintenance with FLT3 inhibitors outside *FLT3*-ITD AML (immunomodulatory and off-target effects)

- Impact of post-transplant maintenance therapy on immune reconstitution and environment

- Combination of post-transplant FLT3 inhibitors with other drugs such as hypomethylating agents

- Monitoring of patients receiving post-transplant FLT3 inhibitors for potential extramedullary relapse or aggressive clone selection.

References

- Gilliland DG, Griffin JD. The roles of FLT3 in hematopoiesis and leukemia. *Blood*. 2002;100(5):1532-1542.
- Griffith J, Black J, Faerman C, et al. The structural basis for autoinhibition of FLT3 by the juxtamembrane domain. *Mol Cell*. 2004;13(2):169-178.
- Mizuki M, Fenski R, Halfter H, et al. Flt3 mutations from patients with acute myeloid leukemia induce transformation of 32D cells mediated by the Ras and STAT5 pathways. *Blood*. 2000;96(12):3907-3914.
- Hayakawa F, Towatari M, Kiyoi H, et al. Tandem-duplicated Flt3 constitutively activates STAT5 and MAP kinase and introduces autonomous cell growth in IL-3-dependent cell lines. *Oncogene*. 2000;19(5):624-631.
- Roux PP, Blenis J. ERK and p38 MAPK-activated protein kinases: a family of protein kinases with diverse biological functions. *Microbiol Mol Biol Rev*. 2004;68(2):320-344.
- Manning BD, Cantley LC. AKT/PKB signaling: navigating downstream. *Cell*. 2007;129(7):1261-1274.
- Weisberg E, Roesel J, Furet P, et al. Antileukemic effects of novel first- and second-generation FLT3 inhibitors: structure-affinity comparison. *Genes Cancer*. 2010;1(10):1021-1032.
- Papaemmanuil E, Gerstung M, Bullinger L, et al. Genomic classification and prognosis in acute myeloid leukemia. *N Engl J Med*. 2016;374(23):2209-2221.
- Cancer Genome Atlas Research Network; Ley TJ, Miller C, Ding L, et al. Genomic and epigenomic landscapes of adult de novo acute myeloid leukemia. *N Engl J Med*. 2013;368(22):2059-2074.
- Patel JP, Gonen M, Figueroa ME, et al. Prognostic relevance of integrated genetic profiling in acute myeloid leukemia. *N Engl J Med*. 2012;366(12):1079-1089.
- Thiede C, Steudel C, Mohr B, et al. Analysis of FLT3-activating mutations in 979 patients with acute myelogenous leukemia: association with FAB subtypes and identification of subgroups with poor prognosis. *Blood*. 2002;99(12):4326-4335.
- Kottaridis PD, Gale RE, Frew ME, et al. The presence of a FLT3 internal tandem duplication in patients with acute myeloid leukemia (AML) adds important prognostic information to cytogenetic risk group and response to the first cycle of chemotherapy: analysis of 854 patients from the United Kingdom Medical Research Council AML 10 and 12 trials. *Blood*. 2001;98(6):1752-1759.
- Nagel G, Weber D, Fromm E, et al. Epidemiological, genetic, and clinical characterization by age of newly diagnosed acute myeloid leukemia based on an academic population-based registry study (AMLSEG BiO). *Ann Hematol*. 2017;96(12):1993-2003.
- Nakao M, Yokota S, Iwai T, et al. Internal tandem duplication of the flt3 gene found in acute myeloid leukemia. *Leukemia*. 1996;10(12):1911-1918.
- Yamamoto Y, Kiyoi H, Nakano Y, et al. Activating mutation of D835 within the activation loop of FLT3 in human hematologic malignancies. *Blood*. 2001;97(8):2434-2439.
- Schlenk RF, Dohner K, Krauter J, et al. Mutations and treatment outcome in cytogenetically normal acute myeloid leukemia. *N Engl J Med*. 2008;358(18):1909-1918.
- Schlenk RF, Kayser S, Bullinger L, et al. Differential impact of allelic ratio and insertion site in FLT3-ITD-positive AML with respect to allogeneic transplantation. *Blood*. 2014;124(23):3441-3449.
- Tallman MS, Wang ES, Altman JK, et al. Acute myeloid leukemia, version 3. 2019, NCCN clinical practice guidelines in oncology. *J Natl Compr Canc Netw*. 2019;17(6):721-749.
- Döhner H, Estey E, Grimwade D, et al. Diagnosis and management of AML in adults: 2017 ELN recommendations from an international expert panel. *Blood*. 2017;129(4):424-447.
- Garg M, Nagata Y, Kanojia D, et al. Profiling of somatic mutations in acute myeloid leukemia with FLT3-ITD at diagnosis and relapse. *Blood*. 2015;126(22):2491-2501.
- Thiede C, Koch S, Creutzig E, et al. Prevalence and prognostic impact of NPM1 mutations in 1485 adult patients with acute myeloid leukemia (AML). *Blood*. 2006;107(10):4011-4020.
- Pratcorona M, Brunet S, Nomdedeu J, et al. Favorable outcome of patients with acute myeloid leukemia harboring a low-allelic burden FLT3-ITD mutation and concomitant NPM1 mutation: relevance to post-remission therapy. *Blood*. 2013;121(14):2734-2738.
- Thiede C, Prior TW, Lavorgna S, et al. FLT3 mutation assay laboratory cross validation: results from the CALGB 10603/ratify trial in patients with newly diagnosed FLT3-mutated acute myeloid leukemia (AML). *Blood*. 2018;132(Suppl 1):2800.
- Kiyoi H, Naoe T, Nakano Y, et al. Prognostic implication of FLT3 and N-RAS gene mutations in acute myeloid leukemia. *Blood*. 1999;93(9):3074-3080.
- Yanada M, Matsuo K, Suzuki T, Kiyoi H, Naoe T. Prognostic significance of FLT3 internal tandem duplication and tyrosine kinase domain mutations for acute myeloid leukemia: a meta-analysis. *Leukemia*. 2005;19(8):1345-1349.
- Whitman SP, Archer KJ, Feng L, et al. Absence of the wild-type allele predicts poor prognosis in adult de novo acute myeloid

- leukemia with normal cytogenetics and the internal tandem duplication of FLT3: a Cancer and Leukemia Group B study. *Cancer Res.* 2001;61(19):7233-7239.
27. Frohling S, Schlenk RF, Breitnick J, et al. Prognostic significance of activating FLT3 mutations in younger adults (16 to 60 years) with acute myeloid leukemia and normal cytogenetics: a study of the AML Study Group Ulm. *Blood.* 2002;100(13):4372-4380.
 28. Kayser S, Schlenk RF, Londono MC, et al. Insertion of FLT3 internal tandem duplication in the tyrosine kinase domain-1 is associated with resistance to chemotherapy and inferior outcome. *Blood.* 2009;114(12):2386-2392.
 29. Mead AJ, Linch DC, Hills RK, Wheatley K, Burnett AK, Gale RE. FLT3 tyrosine kinase domain mutations are biologically distinct from and have a significantly more favorable prognosis than FLT3 internal tandem duplications in patients with acute myeloid leukemia. *Blood.* 2007;110(4):1262-1270.
 30. Whitman SP, Ruppert AS, Radmacher MD, et al. FLT3 D835/I836 mutations are associated with poor disease-free survival and a distinct gene-expression signature among younger adults with de novo cytogenetically normal acute myeloid leukemia lacking FLT3 internal tandem duplications. *Blood.* 2008;111(3):1552-1559.
 31. Moreno I, Martin G, Bolufer P, et al. Incidence and prognostic value of FLT3 internal tandem duplication and D835 mutations in acute myeloid leukemia. *Haematologica.* 2003;88(1):19-24.
 32. Bacher U, Haferlach C, Kern W, Haferlach T, Schnittger S. Prognostic relevance of FLT3-TKD mutations in AML: the combination matters—an analysis of 3082 patients. *Blood.* 2008;111(5):2527-2537.
 33. Voso MT, Larson RA, Prior T, et al. Ratify (Alliance 10603): prognostic impact of FLT3 tyrosine kinase domain (TKD) and NPM1 mutation status in patients with newly diagnosed acute myeloid leukemia (AML) treated with midostaurin or placebo plus standard chemotherapy. *Blood.* 2018;132 (Suppl 1):2668.
 34. Boddur P, Kantarjian H, Borthakur G, et al. Co-occurrence of FLT3-TKD and NPM1 mutations defines a highly favorable prognostic AML group. *Blood Adv.* 2017;1 (19):1546-1550.
 35. Perry M, Bertoli S, Rocher C, et al. FLT3-TKD mutations associated with NPM1 mutations define a favorable-risk group in patients with acute myeloid leukemia. *Clin Lymphoma Myeloma Leuk.* 2018;18(12):e545-e550.
 36. Short NJ, Kantarjian H, Ravandi F, Daver N. Emerging treatment paradigms with FLT3 inhibitors in acute myeloid leukemia. *Ther Adv Hematol.* 2019;10:2040620719827310.
 37. Stone RM, Mandrekar SJ, Sanford BL, et al. Midostaurin plus chemotherapy for acute myeloid leukemia with a FLT3 mutation. *N Engl J Med.* 2017;377(5):454-464.
 38. Perl AE, Martinelli G, Cortes JE, et al. Gilteritinib or chemotherapy for relapsed or refractory FLT3-mutated AML. *N Engl J Med.* 2019;381(18):1728-1740.
 39. Cortes JE, Khaled S, Martinelli G, et al. Quizartinib versus salvage chemotherapy in relapsed or refractory FLT3-ITD acute myeloid leukaemia (QuANTUM-R): a multicentre, randomised, controlled, open-label, phase 3 trial. *Lancet Oncol.* 2019;20(7):984-997.
 40. Wang ES, Tallman MS, Stone RM, et al. Low relapse rate in younger patients \leq 60 years old with newly diagnosed FLT3-mutated acute myeloid leukemia (AML) treated with crenolanib and cytarabine/anthracycline chemotherapy. *Blood.* 2017;130(Suppl 1):566.
 41. Rollig C, Serve H, Huttmann A, et al. Addition of sorafenib versus placebo to standard therapy in patients aged 60 years or younger with newly diagnosed acute myeloid leukaemia (SORAML): a multicentre, phase 2, randomised controlled trial. *Lancet Oncol.* 2015;16(16):1691-1699.
 42. Serve H, Krug U, Wagner R, et al. Sorafenib in combination with intensive chemotherapy in elderly patients with acute myeloid leukemia: results from a randomized, placebo-controlled trial. *J Clin Oncol.* 2013;31 (25):3110-3118.
 43. Antar A, Otrock ZK, El-Cheikh J, et al. Inhibition of FLT3 in AML: a focus on sorafenib. *Bone Marrow Transplant.* 2017;52(3):344-351.
 44. Macdonald DA, Assouline SE, Brandwein J, et al. A phase I/II study of sorafenib in combination with low dose cytarabine in elderly patients with acute myeloid leukemia or high-risk myelodysplastic syndrome from the National Cancer Institute of Canada Clinical Trials Group: trial IND.186. *Leuk Lymphoma.* 2013;54(4):760-766.
 45. Borthakur G, Kantarjian H, Ravandi F, et al. Phase I study of sorafenib in patients with refractory or relapsed acute leukemias. *Haematologica.* 2011;96(1):62-68.
 46. Metzelder SK, Schroeder T, Lubbert M, et al. Long-term survival of sorafenib-treated FLT3-ITD-positive acute myeloid leukaemia patients relapsing after allogeneic stem cell transplantation. *Eur J Cancer.* 2017;86:233-239.
 47. Cortes JE, Kantarjian H, Foran JM, et al. Phase I study of quizartinib administered daily to patients with relapsed or refractory acute myeloid leukemia irrespective of FMS-like tyrosine kinase 3-internal tandem duplication status. *J Clin Oncol.* 2013;31(29):3681-3687.
 48. Levis MJ, Perl AE, Altman JK, et al. Results of a first-in-human, phase I/II trial of ASP2215, a selective, potent inhibitor of FLT3/Axl in patients with relapsed or refractory (R/R) acute myeloid leukemia (AML). *J Clin Oncol.* 2015;33(15_suppl):7003.
 49. Leung AY, Man CH, Kwong YL. FLT3 inhibition: a moving and evolving target in acute myeloid leukaemia. *Leukemia.* 2013;27(2):260-268.
 50. Thol F, Schlenk RF, Heuser M, Ganser A. How I treat refractory and early relapsed acute myeloid leukemia. *Blood.* 2015;126(3):319-327.
 51. Winkler J, Rech D, Kallert S, et al. Sorafenib induces sustained molecular remission in FLT3-ITD positive AML with relapse after second allogeneic stem cell transplantation without exacerbation of acute GVHD: a case report. *Leuk Res.* 2010;34(10):e270-272.
 52. Sharma M, Ravandi F, Bayraktar UD, et al. Treatment of FLT3-ITD-positive acute myeloid leukemia relapsing after allogeneic stem cell transplantation with sorafenib. *Biol Blood Marrow Transplant.* 2011;17(12):1874-1877.
 53. Metzelder SK, Schroeder T, Finck A, et al. High activity of sorafenib in FLT3-ITD-positive acute myeloid leukemia synergizes with allo-immune effects to induce sustained responses. *Leukemia.* 2012;26(11):2353-2359.
 54. Rautenberg C, Nachtkamp K, Dienst A, et al. Sorafenib and azacitidine as salvage therapy for relapse of FLT3-ITD mutated AML after allo-SCT. *Eur J Haematol.* 2017;98(4):348-354.
 55. Bazarbachi A, Labopin M, Battipaglia G, et al. Sorafenib improves survival of FLT3-mutated acute myeloid leukemia in relapse after allogeneic stem cell transplantation: a report of EBMT Acute Leukemia Working Party. *Haematologica.* 2019;104(9):e398-e401.
 56. Ravandi F, Alattar ML, Grunwald MR, et al. Phase 2 study of azacitidine plus sorafenib in patients with acute myeloid leukemia and FLT-3 internal tandem duplication mutation. *Blood.* 2013;121(23):4655-4662.
 57. Sid S, Rey J, Charbonnier A, et al. Treatment of post-transplant relapse of FLT3-ITD mutated AML using 5-azacytidine and sorafenib bitherapy. *Clin Lymphoma Myeloma Leuk.* 2017;17(4):241-242.
 58. Sasaki K, Kantarjian HM, Kadia T, et al. Sorafenib plus intensive chemotherapy improves survival in patients with newly diagnosed, FLT3-internal tandem duplication mutation-positive acute myeloid leukemia. *Cancer.* 2019;125(21):3755-3766.
 59. Yalniz F, Abou Dalle I, Kantarjian H, et al. Prognostic significance of baseline FLT3-ITD mutant allele level in acute myeloid leukemia treated with intensive chemotherapy with/without sorafenib. *Am J Hematol.* 2019;94(9):984-991.
 60. Battipaglia G, Ruggeri A, Massoud R, et al. Efficacy and feasibility of sorafenib as a maintenance agent after allogeneic hematopoietic stem cell transplantation for Fms-like tyrosine kinase 3-mutated acute myeloid leukemia. *Cancer.* 2017;123(15):2867-2874.
 61. Chen YB, Li S, Lane AA, et al. Phase I trial of maintenance sorafenib after allogeneic hematopoietic stem cell transplantation for fms-like tyrosine kinase 3 internal tandem duplication acute myeloid leukemia. *Biol Blood Marrow Transplant.* 2014;20(12):2042-2048.
 62. Brunner AM, Li S, Fathi AT, et al. Hematopoietic cell transplantation with and without sorafenib maintenance for patients with FLT3-ITD acute myeloid leukaemia in first complete remission. *Br J Haematol.* 2016;175(3):496-504.
 63. Bazarbachi A, Labopin M, Battipaglia G, et al. Allogeneic stem cell transplantation for FLT3-mutated acute myeloid leukemia: in vivo T-cell depletion and posttransplant sorafenib maintenance improve survival. A retrospective acute Leukemia Working Party-European Society for Blood and Marrow Transplant Study. *Clin Hematol Int.* 2019;1(1):58-74.
 64. Burchert A. Sorafenib As Maintenance therapy post allogeneic stem cell transplantation for FLT3-ITD positive AML: results from the randomized, double-blind, placebo-controlled multicentre sormain trial. *Blood.* 2018;132(Suppl 1):661.
 65. Battipaglia G, Massoud R, Ahmed SO, et al. Efficacy and feasibility of sorafenib as a maintenance agent after allogeneic hematopoietic stem cell transplantation for Fms-like tyrosine kinase 3 mutated acute myeloid leukemia: an update. *Clin Lymphoma Myeloma Leuk.* 2019;19(8):506-508.
 66. Bornhauser M, Illmer T, Schaich M, et al. Improved outcome after stem-cell transplantation in FLT3/ITD-positive AML. *Blood.* 2007;109(5):2264-2265; author reply 2265.
 67. Gale RE, Hills R, Kottaridis PD, et al. No evidence that FLT3 status should be considered

- as an indicator for transplantation in acute myeloid leukemia (AML): an analysis of 1135 patients, excluding acute promyelocytic leukemia, from the UK MRC AML10 and 12 trials. *Blood*. 2005;106(10):3658-3665.
68. Meshinchi S, Arcenci RJ, Sanders JE, et al. Role of allogeneic stem cell transplantation in FLT3/ITD-positive AML. *Blood*. 2006;108(1):400; author reply 400-401.
 69. DeZern AE, Sung A, Kim S, et al. Role of allogeneic transplantation for FLT3/ITD acute myeloid leukemia: outcomes from 133 consecutive newly diagnosed patients from a single institution. *Biol Blood Marrow Transplant*. 2011;17(9):1404-1409.
 70. Sengsayadeth SM, Jagasia M, Engelhardt BG, et al. Allo-SCT for high-risk AML-CR1 in the molecular era: impact of FLT3/ITD outweighs the conventional markers. *Bone Marrow Transplant*. 2012;47(12):1535-1537.
 71. Kayser S DK, Krauter J, Kohne C, et al. Allogeneic transplantation from matched related and unrelated donors in first complete remission in younger adult AML patients with FLT3 internal tandem duplications. *Bone Marrow Transplant*. 2011;18(6):395-400.
 72. Hemmati P TT, Vuong LG, le Coutre PD, Dorken B, Arnold R. Allogeneic stem cell transplantation for cytogenetically normal acute myeloid leukemia: impact of FLT3 and NPM1 mutational status. *Blood*. 2013;122(21):2104.
 73. Liegel J, Courville E, Sachs Z, Ustun C. Use of sorafenib for post-transplant relapse in FLT3/ITD-positive acute myelogenous leukemia: maturation induction and cytotoxic effect. *Haematologica*. 2014;99(11):e222-224.
 74. Deol A, Sengsayadeth S, Ahn KW, et al. Does FLT3 mutation impact survival after hematopoietic stem cell transplantation for acute myeloid leukemia? A Center for International Blood and Marrow Transplant Research (CIBMTR) analysis. *Cancer*. 2016;122(19):3005-3014.
 75. DeZern AE, Sung A, Kim S, et al. Patients with FLT3/ITD AML may benefit from allogeneic transplant in first remission: outcomes from a consecutive series of patients at a single institution. *Blood*. 2010;116(21):2172.
 76. Ivey A, Hills RK, Simpson MA, et al. Assessment of minimal residual disease in standard-risk AML. *N Engl J Med*. 2016;374(5):422-433.
 77. Terwijn M, van Putten WLJ, Kelder A, et al. High prognostic impact of flow cytometric minimal residual disease detection in acute myeloid leukemia: data from the HOVON/SAKK AML 42A study. *J Clin Oncol*. 2013;31(31):3889-3897.
 78. Schuurhuis GJ, Heuser M, Freeman S, et al. Minimal/measurable residual disease in AML: a consensus document from the European LeukemiaNet MRD Working Party. *Blood*. 2018;131(12):1275-1291.
 79. Chang Y-J, Huang X-J. Haploidentical stem cell transplantation: anti-thymocyte globulin-based experience. *Semin Hematol*. 2016;53(2):82-89.
 80. McCurdy SR, Kasamon YL, Kanakry CG, et al. Comparable composite endpoints after HLA-matched and HLA-haploidentical transplantation with post-transplantation cyclophosphamide. *Haematologica*. 2017;102(2):391-400.
 81. Zhang Y-Y, Mo X-D, Zhang X-H, et al. FLT3 internal tandem duplication does not impact prognosis after haploidentical allogeneic hematopoietic stem cell transplantation in AML patients. *Bone Marrow Transplant*. 2019;54(9):1462-1470.
 82. Schiller GJ, Tuttle P, Desai P. Allogeneic hematopoietic stem cell transplantation in FLT3-ITD-positive acute myelogenous leukemia: the role for FLT3 tyrosine kinase inhibitors post-transplantation. *Biol Blood Marrow Transplant*. 2016;22(6):982-990.
 83. Shouval R, Fein JA, Labopin M, et al. Outcomes of allogeneic haematopoietic stem cell transplantation from HLA-matched and alternative donors: a European Society for Blood and Marrow Transplantation registry retrospective analysis. *Lancet Haematol*. 2019;6(11):e573-e584.
 84. Xuan L, Wang Y, Huang F, et al. Effect of sorafenib on the outcomes of patients with FLT3 ITD acute myeloid leukemia undergoing allogeneic hematopoietic stem cell transplantation. *Cancer*. 2018;124(9):1954-1963.
 85. Bazarbachi AH, Al Hamed R, Malard F, Mohty M, Bazarbachi A. Allogeneic transplant for FLT3-ITD mutated AML: a focus on FLT3 inhibitors before, during, and after transplant. *Ther Adv Hematol*. 2019;10:2040620719882666.
 86. Williams PL, Webb C. The Delphi technique: a methodological discussion. *J Adv Nurs*. 1994;19(1):180-186.
 87. Couriel DR. Ancillary and supportive care in chronic graft-versus-host disease. *Best Pract Res Clin Haematol*. 2008;21(2):291-307.
 88. Ho AD, Schetelig J, Bochtler T, et al. Allogeneic stem cell transplantation improves survival in patients with acute myeloid leukemia characterized by a high allelic ratio of mutant FLT3-ITD. *Biol Blood Marrow Transplant*. 2016;22(3):462-469.
 89. Versluis J, In 't Hout FE, Devillier R, et al. Comparative value of post-remission treatment in cytogenetically normal AML subclassified by NPM1 and FLT3-ITD allelic ratio. *Leukemia*. 2017;31(1):26-33.
 90. Rombouts WJ, Blokland I, Lowenberg B, Ploemacher RE. Biological characteristics and prognosis of adult acute myeloid leukemia with internal tandem duplications in the FLT3 gene. *Leukemia*. 2000;14(4):675-683.
 91. Döhner K, Thiede C, Jahn N, et al. Impact of NPM1/FLT3-ITD genotypes defined by the 2017 European LeukemiaNet in patients with acute myeloid leukemia. *Blood*. 2020;135(5):371-380.
 92. Brunet S, Labopin M, Esteve J, et al. Impact of FLT3 internal tandem duplication on the outcome of related and unrelated hematopoietic transplantation for adult acute myeloid leukemia in first remission: a retrospective analysis. *J Clin Oncol*. 2012;30(7):735-741.
 93. Ma Y, Wu Y, Shen Z, Zhang X, Zeng D, Kong P. Is allogeneic transplantation really the best treatment for FLT3/ITD-positive acute myeloid leukemia? A systematic review. *Clin Transplant*. 2015;29(2):149-160.
 94. Doubek M, Muzik J, Szotkowski T, et al. Is FLT3 internal tandem duplication significant indicator for allogeneic transplantation in acute myeloid leukemia? An analysis of patients from the Czech Acute Leukemia Clinical Register (ALERT). *Neoplasma*. 2007;54(1):89-94.
 95. Lin PH, Lin CC, Yang HI, et al. Prognostic impact of allogeneic hematopoietic stem cell transplantation for acute myeloid leukemia patients with internal tandem duplication of FLT3. *Leuk Res*. 2013;37(3):287-292.
 96. Canaani J, Labopin M, Huang XJ, et al. T-cell replete haploidentical stem cell transplantation attenuates the prognostic impact of FLT3-ITD in acute myeloid leukemia: a report from the Acute Leukemia Working Party of the European Society for Blood and Marrow Transplantation. *Am J Hematol*. 2018;93(6):736-744.
 97. Schmid C, Labopin M, Socie G, et al. Outcome of patients with distinct molecular genotypes and cytogenetically normal AML after allogeneic transplantation. *Blood*. 2015;126(17):2062-2069.
 98. Thanarajasingam G, Kim HT, Cutler C, et al. Outcome and prognostic factors for patients who relapse after allogeneic hematopoietic stem cell transplantation. *Biol Blood Marrow Transplant*. 2013;19(12):1713-1718.
 99. Sakaguchi M, Yamaguchi H, Najima Y, et al. Prognostic impact of low allelic ratio FLT3-ITD and NPM1 mutation in acute myeloid leukemia. *Blood Adv*. 2018;2(20):2744-2754.
 100. Oran B, Cortes J, Beitinjaneh A, et al. Allogeneic transplantation in first remission improves outcomes irrespective of FLT3-ITD allelic ratio in FLT3-ITD-positive acute myelogenous leukemia. *Biol Blood Marrow Transplant*. 2016;22(7):1218-1226.
 101. Zhao X, Wang Z, Ruan G, et al. Impact of pre-transplantation minimal residual disease determined by multiparameter flow cytometry on the outcome of AML patients with FLT3-ITD after allogeneic stem cell transplantation. *Ann Hematol*. 2018;97(6):967-975.
 102. Popescu B, Sheela S, Thompson J, et al. Timed sequential salvage chemotherapy for relapsed or refractory acute myeloid leukemia. *Clin Hematol Int*. 2019;2(1):27-31.
 103. Poire X, Labopin M, Maertens J, et al. Allogeneic stem cell transplantation in adult patients with acute myeloid leukaemia and 17p abnormalities in first complete remission: a study from the Acute Leukemia Working Party (ALWP) of the European Society for Blood and Marrow Transplantation (EBMT). *J Hematol Oncol*. 2017;10(1):20.
 104. Laboure G, Dulucq S, Labopin M, et al. Potent graft-versus-leukemia effect after reduced-intensity allogeneic SCT for intermediate-risk AML with FLT3-ITD or wild-type NPM1 and CEBPA without FLT3-ITD. *Biol Blood Marrow Transplant*. 2012;18(12):1845-1850.
 105. Gale RE, Green C, Allen C, et al. The impact of FLT3 internal tandem duplication mutant level, number, size, and interaction with NPM1 mutations in a large cohort of young adult patients with acute myeloid leukemia. *Blood*. 2008;111(5):2776-2784.
 106. Gaballa S, Saliba R, Oran B, et al. Relapse risk and survival in patients with FLT3 mutated acute myeloid leukemia undergoing stem cell transplantation. *Am J Hematol*. 2017;92(4):331-337.
 107. Kayser S, Benner A, Thiede C, et al. Pretransplant NPM1 MRD levels predict outcome after allogeneic hematopoietic stem cell transplantation in patients with acute myeloid leukemia. *Blood Cancer J*. 2016;6(7):e449-e449.
 108. Pfeiffer T, Schleunig M, Mayer J, et al. Influence of molecular subgroups on outcome of acute myeloid leukemia with normal karyotype in 141 patients undergoing salvage allogeneic stem cell transplantation in primary induction failure or beyond first relapse. *Haematologica*. 2013;98(4):518-525.
 109. Gorin NC, Labopin M, Blaise D, et al. Stem cell transplantation from a haploidentical donor versus a genoidentical sister for adult male patients with acute myelogenous

- leukemia in first remission: a retrospective study from the Acute Leukemia Working Party of the European Society for Blood and Marrow Transplantation. *Cancer*. 2019;126(5):1004-1015.
110. Versluis J, Labopin M, Ruggeri A, et al. Alternative donors for allogeneic hematopoietic stem cell transplantation in poor-risk AML in CR1. *Blood Adv*. 2017;1(7):477-485.
111. Kharfan-Dabaja MA, Labopin M, Polge E, et al. Association of second allogeneic hematopoietic cell transplant vs donor lymphocyte infusion with overall survival in patients with acute myeloid leukemia relapse. *JAMA Oncol*. 2018;4(9):1245-1253.
112. Levis MJ, Chen Y-B, Hamadani M, et al. FLT3 inhibitor maintenance after allogeneic transplantation: is a placebo-controlled, randomized trial ethical? *J Clin Oncol*. 2019;37(19):1604-1607.
113. Stone RM, Mandrekar SJ, Sanford BL, et al. The addition of midostaurin to standard chemotherapy decreases cumulative incidence of relapse (CIR) in the international prospective randomized, placebo-controlled, double-blind trial (CALGB 10603 / RATIFY [Alliance]) for newly diagnosed acute myeloid leukemia (AML) Patients with FLT3 mutations. *Blood*. 2017;130(Suppl 1):2580.
114. Maziarz RTT, Patnaik MM, Scott BL, et al. Radius: a phase 2 randomized trial investigating standard of care ± midostaurin after allogeneic stem cell transplant in FLT3-ITD-mutated AML. *Blood*. 2018;132(Suppl 1):662.
115. Schlenk RF, Weber D, Fiedler W, et al. Midostaurin added to chemotherapy and continued single-agent maintenance therapy in acute myeloid leukemia with FLT3-ITD. *Blood*. 2019;133(8):840-851.
116. Antar A, Kharfan-Dabaja MA, Mahfouz R, Bazarbachi A. Sorafenib maintenance appears safe and improves clinical outcomes in FLT3-ITD acute myeloid leukemia after allogeneic hematopoietic cell transplantation. *Clin Lymphoma Myeloma Leuk*. 2015;15(5):298-302.
117. Tschan-Plessl A, Halter JP, Heim D, Medinger M, Passweg JR, Gerull S. Synergistic effect of sorafenib and cGvHD in patients with high-risk FLT3-ITD+AML allows long-term disease control after allogeneic transplantation. *Ann Hematol*. 2015;94(11):1899-1905.
118. Yokoyama H, Lundqvist A, Su S, Childs R. Toxic effects of sorafenib when given early after allogeneic hematopoietic stem cell transplantation. *Blood*. 2010;116(15):2858-2859.
119. Mathew NR, Baumgartner F, Braun L, et al. Sorafenib promotes graft-versus-leukemia activity in mice and humans through IL-15 production in FLT3-ITD-mutant leukemia cells. *Nat Med*. 2018;24(3):282-291.
120. Levis MJ, Hamadani M, Logan B, et al. A phase 3, trial of gilteritinib, as maintenance therapy after allogeneic hematopoietic stem cell transplantation in patients with FLT3-ITD+ AML. *J Clin Oncol*. 2018;36(15_Suppl):TPS7075.
121. Canaani J. Management of AML Beyond "3+ 7" in 2019. *Clin Hematol Int*. 2019;1(1):10-18.
122. Culos K, Byrne M. Salvage therapy after allogeneic hematopoietic cell transplantation: targeted and low-intensity treatment options in myelodysplastic syndrome and acute myeloid leukemia. *Clin Hematol Int*. 2019;1(2):94-100.

DKC1 is a transcriptional target of GATA1 and drives upregulation of telomerase activity in normal human erythroblasts

Laura A. Richards,^{1*} Ashu Kumari,^{1*} Kathy Knezevic,² Julie Al Thoms,^{2,3} Georg von Jonquieres,¹ Christine E. Napier,¹ Zara Ali,⁴ Rosemary O'Brien,¹ Jonathon Marks-Bluth,² Michelle F. Maritz,¹ Hilda A Pickett,⁵ Jonathan Morris,⁶ John E. Pimanda^{2,3} and Karen L. MacKenzie^{1,4,7,8}

¹Children's Cancer Institute Australia, Randwick; ²Adult Cancer Program, Prince of Wales Clinical School, Lowy Cancer Research Centre, UNSW, Sydney; ³School of Medical Sciences, UNSW, Sydney; ⁴Cancer Research Unit, Children's Medical Research Institute, Westmead; ⁵Telomere Length Regulation Unit, Children's Medical Research Institute, Westmead; ⁶The University of Sydney School of Medicine, Kolling Institute of Medical Research, St Leonards; ⁷School of Women's and Children's Health, UNSW, Sydney and ⁸Faculty of Medicine and Health, University of Sydney, Sydney, New South Wales, Australia

*LAR and AK contributed equally as co-first authors



Haematologica 2020
Volume 105(6):1517-1526

ABSTRACT

Telomerase is a ribonucleoprotein complex that maintains the length and integrity of telomeres, and thereby enables cellular proliferation. Understanding the regulation of telomerase in hematopoietic cells is relevant to the pathogenesis of leukemia, in which telomerase is constitutively activated, as well as bone marrow failure syndromes that feature telomerase insufficiency. Past studies showing high levels of telomerase in human erythroblasts and a prevalence of anemia in disorders of telomerase insufficiency provide the rationale for investigating telomerase regulation in erythroid cells. Here it is shown for the first time that the telomerase RNA-binding protein dyskerin (encoded by *DKC1*) is dramatically upregulated as human hematopoietic stem and progenitor cells commit to the erythroid lineage, driving an increase in telomerase activity in the presence of limiting amounts of *TERT* mRNA. It is also shown that upregulation of *DKC1* was necessary for expansion of glycophorin A⁺ erythroblasts and sufficient to extend telomeres in erythroleukemia cells. Chromatin immunoprecipitation and reporter assays implicated GATA1-mediated transcriptional regulation of *DKC1* in the modulation of telomerase in erythroid lineage cells. Together these results describe a novel mechanism of telomerase regulation in erythroid cells which contrasts with mechanisms centered on transcriptional regulation of *TERT* that are known to operate in other cell types. This is the first study to reveal a biological context in which telomerase is upregulated by *DKC1* and to implicate *GATA1* in telomerase regulation. The results from this study are relevant to hematopoietic disorders involving *DKC1* mutations, *GATA1* deregulation and/or telomerase insufficiency.

Introduction

Telomerase is a ribonucleoprotein complex that maintains the length and integrity of chromosomal-end structures called telomeres and thereby enables continuous cellular proliferation.¹ The minimum essential components of the human telomerase holoenzyme are a specialized reverse transcriptase (TERT) and a non-coding RNA (TERC) that includes an RNA template domain for priming synthesis of telomeric repeats. Active human telomerase ribonuclear proteins also include the RNA binding and modifying protein, dyskerin. Dyskerin, encoded by *DKC1*, augments telomerase activity by directly binding to TERC to confer the structural rigidity and stability necessary for its accumulation and function.^{2,3}

Telomerase enzyme activity underpins the unrestricted proliferation of cancer cells in approximately 80-90% of malignancies, including acute leukemias and lym-

Correspondence:

KAREN L. MACKENZIE
kmackenzie@cmri.org.au

Received: January 4, 2019.

Accepted: August 13, 2019.

Pre-published: August 14, 2019.

doi:10.3324/haematol.2018.215699

Check the online version for the most updated information on this article, online supplements, and information on authorship & disclosures: www.haematologica.org/content/105/6/1517

©2020 Ferrata Storti Foundation

Material published in *Haematologica* is covered by copyright. All rights are reserved to the Ferrata Storti Foundation. Use of published material is allowed under the following terms and conditions:

<https://creativecommons.org/licenses/by-nc/4.0/legalcode>.

Copies of published material are allowed for personal or internal use. Sharing published material for non-commercial purposes is subject to the following conditions:

<https://creativecommons.org/licenses/by-nc/4.0/legalcode>, sect. 3. Reproducing and sharing published material for commercial purposes is not allowed without permission in writing from the publisher.



phomas.^{4,7} It also plays an important role in the function of normal hematopoietic stem and progenitor cells (HSPC).⁸ Telomerase activity is low in quiescent hematopoietic stem cells, and is upregulated by self-renewal cytokines that promote cell cycling.^{11,12} It is then downregulated to undetectable levels as HSPC differentiate into granulocytes, monocytes and macrophages.^{9,11,12} Telomerase is similarly upregulated in lymphoid cells upon exposure to mitogens but is barely detectable in mature resting lymphocytes and peripheral blood mononuclear cells.^{9,13} Studies of telomerase in erythroid lineage cells are limited; however, our previous investigation demonstrated that in contrast to the downregulation of telomerase observed during myelomonocytic differentiation, telomerase was robustly upregulated as umbilical cord blood (CB)-derived HSPC underwent commitment and expansion along the erythroid lineage.¹⁴ Supporting the functional significance of this finding, a strong correlation was demonstrated between the level of telomerase in human HSPC and the proliferative potential of erythroblasts. In contrast, there was no correlation between telomerase in HSPC and expansion along granulocytic or monocytic lineages. A recent study demonstrating that telomerase knockout mice have more pronounced defects in erythroid progenitors than in granulocyte-macrophage progenitors further supports an important role for telomerase in the erythroid lineage.¹⁵ The mechanism responsible for the upregulation of telomerase during erythropoiesis is currently unknown.

Insufficient telomerase due to mutations in telomerase-associated genes is causally involved in inherited bone marrow failure syndromes including dyskeratosis congenita.¹⁶ Dyskeratosis congenita manifests with mucocutaneous symptoms and multiple organ dysfunction; however, anemia is prevalent and bone marrow failure is the most common cause of death among patients with telomerase mutations.¹⁷ Patients with telomerase insufficiency syndromes exhibit pancytopenias and have fewer circulating hematopoietic progenitors than do healthy individuals.¹⁸ Understanding the mechanisms that regulate telomerase activity in human hematopoietic cells is a crucial step toward the development of effective treatment of hematologic conditions associated with insufficient telomerase. Past studies along these lines have attributed the modulation of telomerase activity in hematopoietic cells to transcriptional regulation of TERT, the rate-limiting component of the telomerase holoenzyme.^{19,21} These studies focused on telomerase regulation in progenitors, lymphoid and myelomonocytic cells. There is no prior study of telomerase regulation in normal erythroid lineage cells. The prevalence of anemia in telomerase insufficiency syndromes and the need for new treatments for these disorders, provided the impetus for investigation in this area.

Here we show that the increase in telomerase activity that occurs as human HSPC commit to the erythroid lineage is a result of upregulation of the *DKC1* gene in the presence of limiting amounts of TERT mRNA. It is shown for the first time that the *DKC1* gene is a direct transcriptional target of the erythroid-specific transcription factor GATA1 and that high expression of *DKC1* is required for efficient production of glycoprotein A-positive (GLYA⁺) erythroblasts. These results provide a novel mechanistic explanation for high levels of telomerase in GLYA⁺ erythroblasts and the heightened vulnerability of the erythroid compartment to telomerase insufficiency.

Methods

Cord blood cell isolation and culture of CD34⁺ and glycoprotein A⁺ cells

CB was obtained from the Royal North Shore Hospital and the Australian Cord Blood Bank. Ethical approval for the use of CB was obtained from the Human Research Ethics Committees of the relevant hospitals and the University of New South Wales (approval numbers: HREC 05188, NSCCH 0602-004M, SESIAHS 08/190). Bone marrow mononuclear cells were obtained from Lonza (Mt Waverly Australia). CB processing and isolation of CD34⁺ HSPC and GLYA⁺ cells are described in the *Online Supplementary Methods*. CD34⁺ HSPC were expanded for 1 week in Isocove modified Dulbecco media (Life Technologies, Carlsbad, CA, USA) with 20% fetal bovine serum (Trace Scientific, Melbourne, Australia), 100 ng/mL stem cell factor (SCF, Amgen, Thousand Oaks, CA, USA), 100 ng/mL thrombopoietin (Peprotech, Rocky Hill, NJ, USA), 100 ng/mL Flt-3 ligand (FLT-3L, Amgen) (STF), 50 µg/mL gentamycin and 200 mM glutamine. The cells were then cultured in cytokine combinations that force expansion and differentiation along specific lineages as described in our previous study (*Online Supplementary Table S1*).¹⁴ Differentiation was assessed by fluorescence activated cell sorting (FACS) analysis after staining cells with the conjugated antibodies detailed in *Online Supplementary Table S2*. Green fluorescent protein-positive (GFP⁺), GLYA⁺ and CD13⁺ subpopulations were purified by FACS using a FACS Diva (Becton Dickinson).

DKC1 gene suppression and overexpression

The viral vectors and methods used for suppression and overexpression of *DKC1* are described in the *Online Supplementary Methods*.

Telomerase enzyme assays and telomere length measurements

Telomerase enzyme activity was quantified using the real-time polymerase chain reaction (PCR)-based telomeric amplification protocol (qTRAP) as described elsewhere.²² Mean telomeric restriction fragment length was measured using the TeloTAGGG Telomere Length Assay kit (Roche, Mannheim, Germany) as previously described and detailed in the *Online Supplementary Methods*.²³

Gene and protein expression analyses

Quantitative real-time PCR (qRT-PCR) and western blot analysis were performed according to standard protocols described in the *Online Supplementary Methods*.

Chromatin immunoprecipitation and reporter assays

Chromatin immunoprecipitation (ChIP) assays were performed as previously described.²⁴ Briefly, 2 × 10⁷ cells were treated with 1% formaldehyde, then cross-linked chromatin was sonicated to obtain 300-500 bp fragments. Chromatin was immunoprecipitated with antibodies detailed in *Online Supplementary Table S2* and subjected to qRT-PCR using Express SYBR Green (Life Technologies) and the primers described in *Online Supplementary Table S3*. Values were normalized to products from immunoprecipitation with control IgG antibody.

A *DKC1* promoter reporter construct (pGL2-DKC1L) was made by cloning a *DKC1* sequence spanning +211 to -1113 bp from the *DKC1* transcription start site into XhoI and HindIII sites of the pGL2 vector encoding luciferase. Two proximal GATA sites were mutated by site-directed mutagenesis using the QuikChange Site-directed Mutagenesis Kit (Stratagene, La Jolla, CA, USA) with the primers listed in *Online Supplementary Table S3*. The mutated

nucleotides were verified by Sanger sequencing. Luciferase assays were performed using HEL 92.1.7 cells as described in the *Online Supplementary Methods*.

Statistics

All statistics were performed using GraphPad Prism 6.0b (La Jolla, CA, USA). Results were considered statistically significant when $P < 0.05$.

Results

DKC1 is upregulated with erythroid lineage commitment

It was previously shown that telomerase activity is upregulated when CB-derived HSPC were switched to conditions promoting erythroid differentiation.¹⁴ To verify this finding in a pure population of erythroid cells, GLYA⁺ cells were sorted by FACS from cultures generated by *ex vivo* expansion of HSPC. CD34⁺ cells were first expanded in medium supplemented with STF for 1 week, then switched to medium containing SCF and erythropoietin (SE) for a further 2 weeks. FACS analysis using antibodies for GLYA and CD34 confirmed differentiation of HSPC and enrichment for GLYA⁺/CD34⁺ erythroid cells (>80% of the viable population) at week 2 and week 3 (Figure 1A and *Online Supplementary Figure S1*). Erythroid cell popula-

tions were further purified from week 2 cultures by FACS sorting cells based on either low or high expression of GLYA and lack of expression of the myeloid cell marker CD13. CD13⁺/GLYA⁻ myeloid cells were also purified from the week 2 cultures for comparison with the erythroid cells (Figure 1B). Telomerase activity was quantified in the FACS-sorted populations of GLYA^{high}, GLYA^{low} erythroid cells and CD13⁺ myeloid cells, as well as CD34⁺ cells and an unsorted population of cells cultured in SE. The results demonstrated that telomerase activity was upregulated in GLYA^{high} erythroblasts relative to both uncultured CD34⁺ HSPC and unsorted SE-cultured cells (Figure 1C). In contrast, no significant telomerase activity was detected in CD13⁺ myeloid cells. These data confirm that telomerase activity was confined to the GLYA⁺ erythroid subset of cells in the SE culture, and was downregulated in differentiated myeloid cells.

To investigate the regulation of telomerase during erythroid commitment, telomerase enzyme activity and expression of *TERT*, *TERC* and *DKC1* was assessed at weekly time points over the 3-week culture period. As previously reported, telomerase was modestly upregulated upon initial cytokine stimulation with STF,^{11,12} then further increased during the second week of culture after switching to SE ($P < 0.01$) (Figure 2A).¹⁴ In parallel with the initial induction of telomerase activity, there was a measurable increase in *TERT* expression during the first week

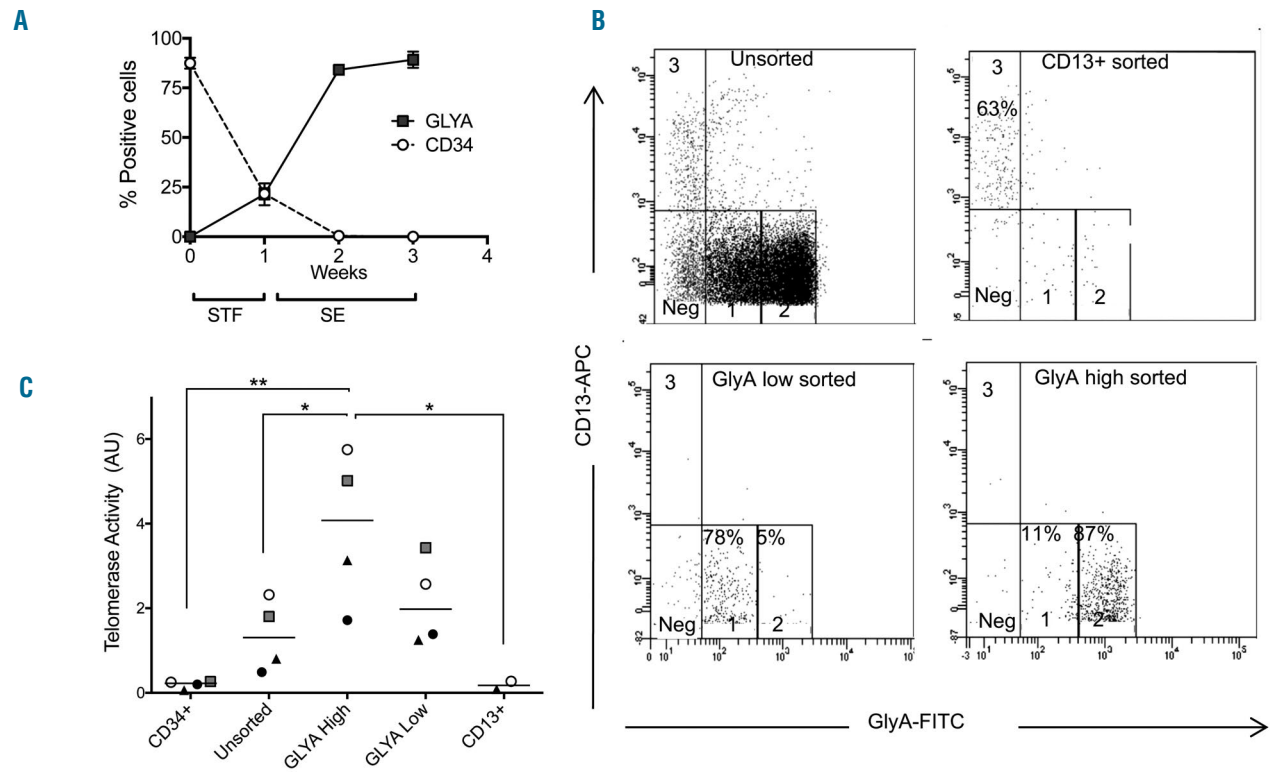


Figure 1. Telomerase enzyme activity is upregulated in glyphorin A⁺ erythroblasts. Cord blood (CB)-derived CD34⁺ hematopoietic stem and progenitor cells (HSPC) were expanded for 7 days in medium supplemented with stem cell factor, thrombopoietin and Flt-3 ligand (STF), then cultured for an additional 2 weeks in medium with stem cell factor plus erythropoietin (SE). (A) Graphical representation of the proportions of CD34⁺ and glyphorin-positive (GLYA⁺) cells in the total viable cell fraction, shown as the mean \pm standard error of the mean (SEM) calculated from nine independent CB cultures. (B) Cell populations enriched for erythroblasts with high or low GLYA expression, or CD13⁺ myeloid cells were isolated from SE cultures by fluorescence activated cell sorting (FACS). Panels show gates used for sorting cell subsets expressing low (1) or high (2) levels of GLYA and CD13 before and after FACS. (C) qTRAP measurement of telomerase enzyme activity in uncultured HSPC cells (CD34⁺), unfractionated cells from SE cultures (Unsorted) and FACS-sorted cell populations. Each symbol represents the mean from three measures of telomerase activity in independent assays of cells from four CB cultures. * $P < 0.05$, ** $P < 0.01$, Dunnett multiple comparisons test.

of culture in STF. *TERT* expression then returned to the low basal levels detected in unstimulated HSPC when the culture was switched to SE (weeks 2-3). In contrast to *TERT*, *DKC1* expression was induced after cultures were switched to SE. The kinetics of *DKC1* upregulation varied among the CB cultures established from different individuals, but invariably increased after the switch to erythroid conditions at week 1 and peaked at either week 2 or 3 of culture (*Online Supplementary Figure S2*). The *DKC1* expression pattern closely paralleled erythroid commit-

ment and expansion, as indicated by expression of *GLYA*⁺ (Figure 1A). Expression of *TERC* did not alter dramatically over the time course, apart from a modest increase from week 1 to 2 of culture.

To determine whether the upregulation of *DKC1* expression was specific for the erythroid lineage, *DKC1* expression was analyzed in cell populations enriched for monocytic, granulocytic and megakaryocytic cells. Cultures enriched for these lineages were produced by switching STF cultures at week 1 from STF to SCE, FLT-3L

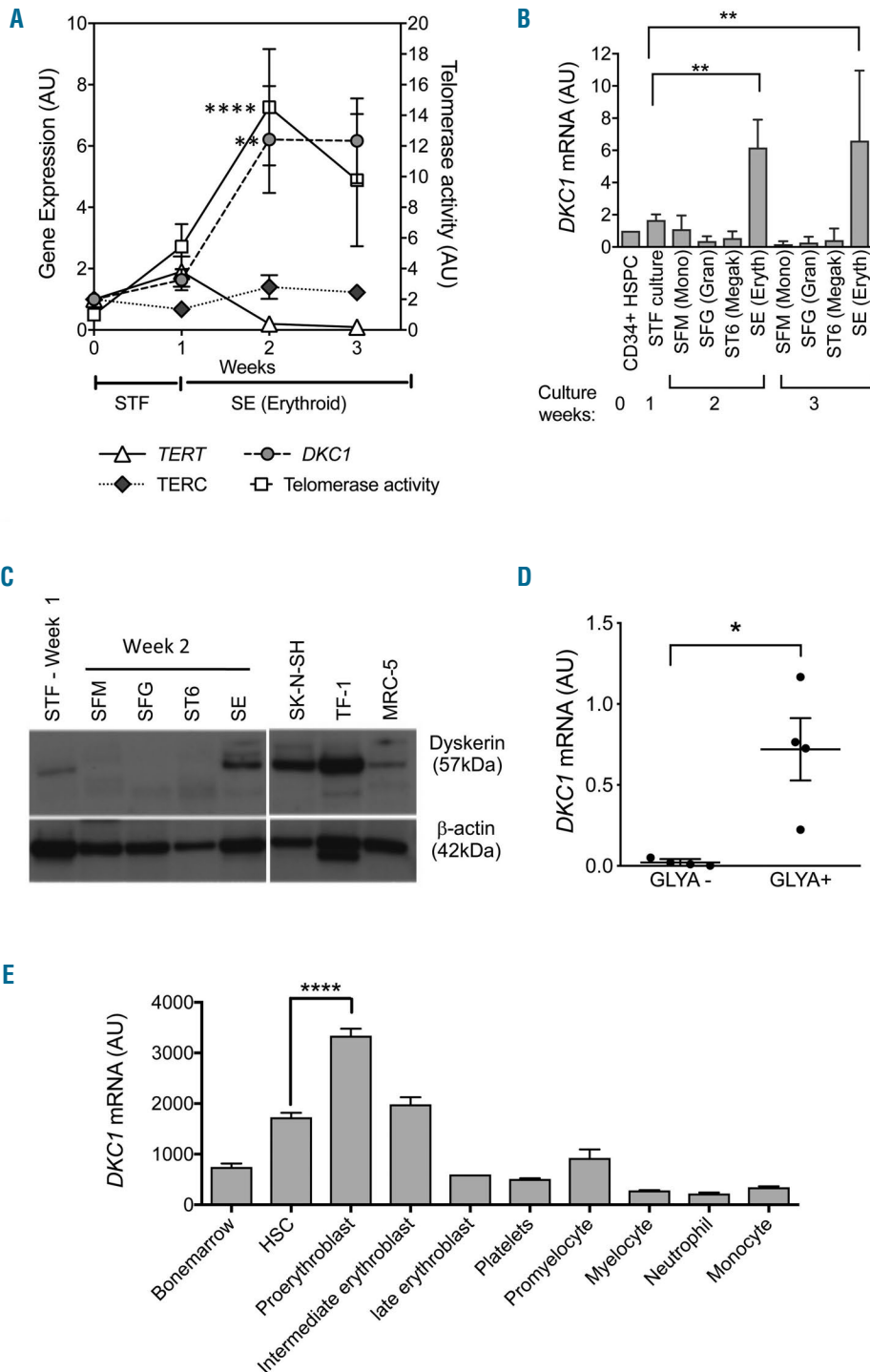


Figure 2. *DKC1* expression is high in erythroblasts relative to the levels in other myeloid cell types. (A) Cord blood (CB) hematopoietic stem and progenitor cells (HSPC) were expanded for 7 days in medium supplemented with stem cell factor, thrombopoietin and Flt-3 ligand (STF), and then for 2 weeks in medium supplemented with stem cell factor and erythropoietin (SE) to induce erythroid differentiation. Expression of genes encoding telomerase components was measured by quantitative real-time polymerase chain reaction (qRT-PCR) (left axis) and telomerase enzyme activity was measured by qTRAP over the 3-week culture period (right axis). Values are presented as means \pm standard error of mean (SEM) from five to nine independent CB expansion experiments. The results show statistically significant upregulation of telomerase activity ($P < 0.0001$) and *DKC1* expression ($P < 0.01$) when cells were switched from STF to erythroid differentiation (SE) conditions (two-way analysis of variance with the Dunnett multiple comparison test). (B, C) CB CD34⁺ HSPC were expanded in STF for 1 week, then split into media supplemented with cytokines that promote expansion and differentiation along specific myeloid lineages. S: stem cell factor; T: thrombopoietin; F: FLT-3L; M: monocyte colony-stimulating factor; G: granulocyte colony-stimulating factor; 6: interleukin 6; E: erythropoietin. (B) *DKC1* mRNA was quantified by qRT-PCR analysis of cells harvested from five to nine independent CB cultures. Each assay was performed three times and results were normalized to those of uncultured CD34⁺ HSPC (week 0). Values are means \pm SEM. $**P < 0.01$ Dunnett multiple comparisons. (C) Western blot of dyskerin protein with actin used as a loading control. The image represents samples run on a single gel, with consistent exposure for all samples. The gap between lanes 5 and 6 represents deletion of a failed sample. SK-N-SH neuroblastoma cell line and MRC-5 mortal human myfibroblasts were used as controls. (D) *DKC1* mRNA quantified by qRT-PCR analysis of glyco-phorin A (GLYA)-positive and -negative cells isolated from uncultured CB or bone marrow by magnetic bead separation. Values are means \pm SEM from four independent samples. $P < 0.05$ paired Student *t* test. (E) *DKC1* gene expression data from the BioGPS Primary Cell Atlas. $****P < 0.0001$ Dunnett multiple comparisons test of proerythroblast and hematopoietic stem cells from bone marrow mononuclear cells. AU: arbitrary units.

and monocyte colony-stimulating factor (SFM) for monocytic differentiation, to SCF, FLT-3L and granulocyte colony-stimulating factor (SFG) for granulocytic expansion and to SCF, thrombopoietin and interleukin-6 (ST6) to promote megakaryocyte differentiation (*Online Supplementary Figure S2*). qRT-PCR analysis showed that in contrast to the upregulation of *DKC1* observed in cells cultured with SE ($P < 0.01$), there was no significant induction of *DKC1* expression in cells grown under conditions favoring monocytic, granulocytic or megakaryocytic differentiation (Figure 2B). Western blot analysis further demonstrated high expression of dyskerin protein only in cell populations produced under erythroid conditions (Figure 2C).

Upregulation of *DKC1* bolsters telomerase activity and promotes telomere lengthening

To confirm that *DKC1* expression was upregulated in erythroblasts produced *in vivo* as well as in *ex vivo*-generated erythroid cultures, *DKC1* expression was assessed in GLYA⁺ cells isolated from uncultured CB and bone marrow mononuclear cells. Results from qRT-PCR analysis consistently showed higher *DKC1* mRNA in the GLYA⁺ fraction than in the GLYA⁻ fraction of cells isolated from four samples (Figure 2D). Consistent with these results, gene expression data, collected through meta-analysis of multiple independent studies (available through the BioGPS Primary Cell Atlas dataset), showed *DKC1* expression to be upregulated in proerythroblasts relative to hematopoietic stem cells and myeloid lineage cells (Figure 2E).²⁵ The upregulation of *DKC1* mRNA in bone marrow proerythroblasts appeared to be transient, as *DKC1* levels in intermediate erythroblasts were similar to those in hematopoietic stem cells. Collectively these data provide strong evidence of *DKC1* upregulation during erythroid commitment of human HSPC.

To test whether induction of *DKC1* was sufficient for the upregulation of telomerase activity observed in erythroblasts, HSPC were transduced with lentiviral vectors encoding *DKC1* cDNA plus GFP (MSCV-DKC1) or GFP alone (MSCV-GFP). Robust upregulation of *DKC1* mRNA in MSCV-DKC1-transduced cells was demonstrated by qRT-PCR analysis of GFP⁺ cells isolated by FACS ($P < 0.01$, Student *t* test) (Figure 3A). Telomerase enzyme activity was also substantially increased in MSCV-DKC1 cells relative to control vector-transduced cells ($P < 0.01$, Student *t* test) (Figure 3B). There were no significant differences in the expression of *TERT* and *TERC* between MSCV-DKC1 and control vector-transduced cells (Figure 3A), although *TERC* expression tended to be higher in the MSCV-DKC1 cells.

To enable analysis of the effect of *DKC1* upregulation over a time course sufficient for assaying telomere length changes, we also overexpressed *DKC1* in the immortal erythroleukemia cell line, HEL 92.1.7 (Figure 3C). Consistent with the CB experiments, overexpression of *DKC1* in HEL 92.1.7 cells caused a substantial elevation of telomerase activity without an apparent change in *TERT* mRNA expression (Figure 3C, D). Southern blot-based analysis of telomere length showed that ectopic expression of *DKC1* resulted in telomere lengthening at a rate of approximately 500 bp over a 2-month period, and 900 bp over 7 months (Figure 3E). To verify that *DKC1* upregulation is sufficient for telomere extension, we also overexpressed *DKC1* in HL-60 cells. Consistent results were obtained, showing that *DKC1* overexpression resulted in

robust upregulation of telomerase and elongated telomeres (*Online Supplementary Figure S4*). These data show that upregulation of *DKC1* results in an accumulation of functional telomerase complexes capable of telomere elongation.

High expression of *DKC1* is necessary for erythroblast proliferation

We next tested whether elevated expression of *DKC1* was necessary for erythroid cell proliferation and differentiation. For these investigations CB-derived HSPC were transduced with retroviral vectors encoding one of two different shRNA targeting *DKC1* mRNA (D2 and D3) or a non-silencing shRNA (NS) plus GFP. HSPC were pre-stimulated and transduced in medium supplemented with STF and then FACS-sorted for GFP⁺ cells, which were then cultured in SE. qRT-PCR analysis confirmed effective suppression of *DKC1* and corresponding downregulation of telomerase activity in erythroid cells transduced with D2 and D3 vectors relative to control vector-transduced cells (Figure 4A, B). The suppression of telomerase activity was not attributable to reduced expression of *TERT*, which was expressed at equivalent levels in D2-, D3- and NS-transduced cells (Figure 4C). *TERC* levels varied among the independent experiments, although they tended to be lower in D2- and D3-transduced cells relative to control cells (Figure 4D), consistent with the known role of dyskerin as a stabilizing scaffold for *TERC*.

Weekly counts of transduced cells revealed that shRNA-mediated suppression of *DKC1* expression inhibited proliferation in SE-driven cultures (Figure 4E). Since there was no apparent difference in the proportion of GLYA⁺ cells in D2 and D3 cultures compared to NS cultures, the reduction in GLYA⁺ cell number did not appear to be due to impaired erythroid differentiation (Figure 4F). When plated in methylcellulose, D2- and D3-transduced cells formed erythroid colonies with normal burst-forming unit-erythroid (BFU-E) size and morphology; however, significantly fewer colonies were generated by D2 and D3 cultures than by NS (Figure 4G). In contrast to the effect of *DKC1* knockdown on BFU-E colony numbers, there was no discernible effect on colony-forming units of granulocyte-monocyte or granulocyte-erythrocyte-macrophage-megakaryocyte. Together, the results demonstrate a critical role for *DKC1* expression in erythroblast proliferation that is independent of differentiation.

GATA1 contributes to transcriptional regulation of *DKC1* in erythroblasts

The *DKC1* promoter was previously shown to be a target of *MYC* family oncoproteins in *MYC*-driven cancers.^{26,27} Since *MYC* is also expressed in erythroid progenitors,²⁸ we next investigated whether *MYC* or other erythroid transcription factors, namely GATA1 and TAL1, play a role in the regulation of *DKC1*. Western blot analysis of uncultured CB CD34⁺ HSPC and *ex vivo*-expanded CB cells revealed *MYC* expression in unstimulated CB HSPC and in cells harvested from STF, STM and SE cultures (Figure 5A). In contrast, expression of GATA1 and TAL1 was confined to cells cultured in SE. Consistent with the qRT-PCR results (Figure 2B), dyskerin protein was detectable in undifferentiated cells cultured in STF and erythroid cells at weeks 2 and 3, but was not detected in cells from monocyte-enriched cultures (Figure 5A).

Canonical E-boxes have previously been identified in

the *DKC1* promoter.^{26,27} ChIP sequencing data from peripheral blood erythroblasts made available through ENCODE on the UCSC browser also provide evidence of GATA 1 binding at the *DKC1* promoter, in the vicinity of -1097 to -493 relative to the transcription start site (chrX: 153,991,030, hg19) (Figure 5B). Guided by these data, we identified putative GATA sites at positions: -679 to -668 and -453 to -468 and designed PCR primers to interrogate the transcription factor binding by ChIP. First, using antibodies to trimethylated H3K4 (H3K4me3), which occupies transcriptionally active chromatin, and H3K27me3, which identifies repressed sites, we verified that chromatin at the *DKC1* promoter was in an open configuration conducive to transcriptional activation in both STF-stimulated cells and erythroblastic cells (Figure 5C).²⁹ ChIP analysis also confirmed MYC binding to the *DKC1* promoter, although this appeared to diminish progressively as undifferentiated CB cells underwent erythroid differentiation in SE culture. Conversely, GATA1 binding at the *DKC1* promoter appeared most robust at week 3, corresponding with the accumulation of ery-

throblasts expressing high levels of GLYA (*Online Supplementary Figure S5*) and peak expression of *DKC1* in six out of nine CB cultures (*Online Supplementary Figure S2*). Consistent with GATA1 binding in GLYA^{high} CB-derived erythroblasts (Figure 5C), ChIP sequencing results from three independent investigations, accessed using CistromeDB, showed GATA1 binding at the *DKC1* promoter of erythroblasts derived from bone marrow and peripheral blood (*Online Supplementary Figure S6*).³⁰⁻³² Although TAL1 can bind DNA via E-boxes, no TAL1 binding at the *DKC1* promoter was detected in CB cells at any stage of culture. Collectively, these data suggest a model whereby MYC binds the *DKC1* promoter in undifferentiated cells and is replaced by GATA1 during erythroid differentiation.

Since GATA1 regulation of *DKC1* has not previously been described, a luciferase reporter assay was conducted to confirm that GATA sites contribute to *DKC1* transcription. Mutations were induced in two potential GATA1 binding sites of the *DKC1* promoter construct by site-directed mutagenesis and luciferase activity was measured

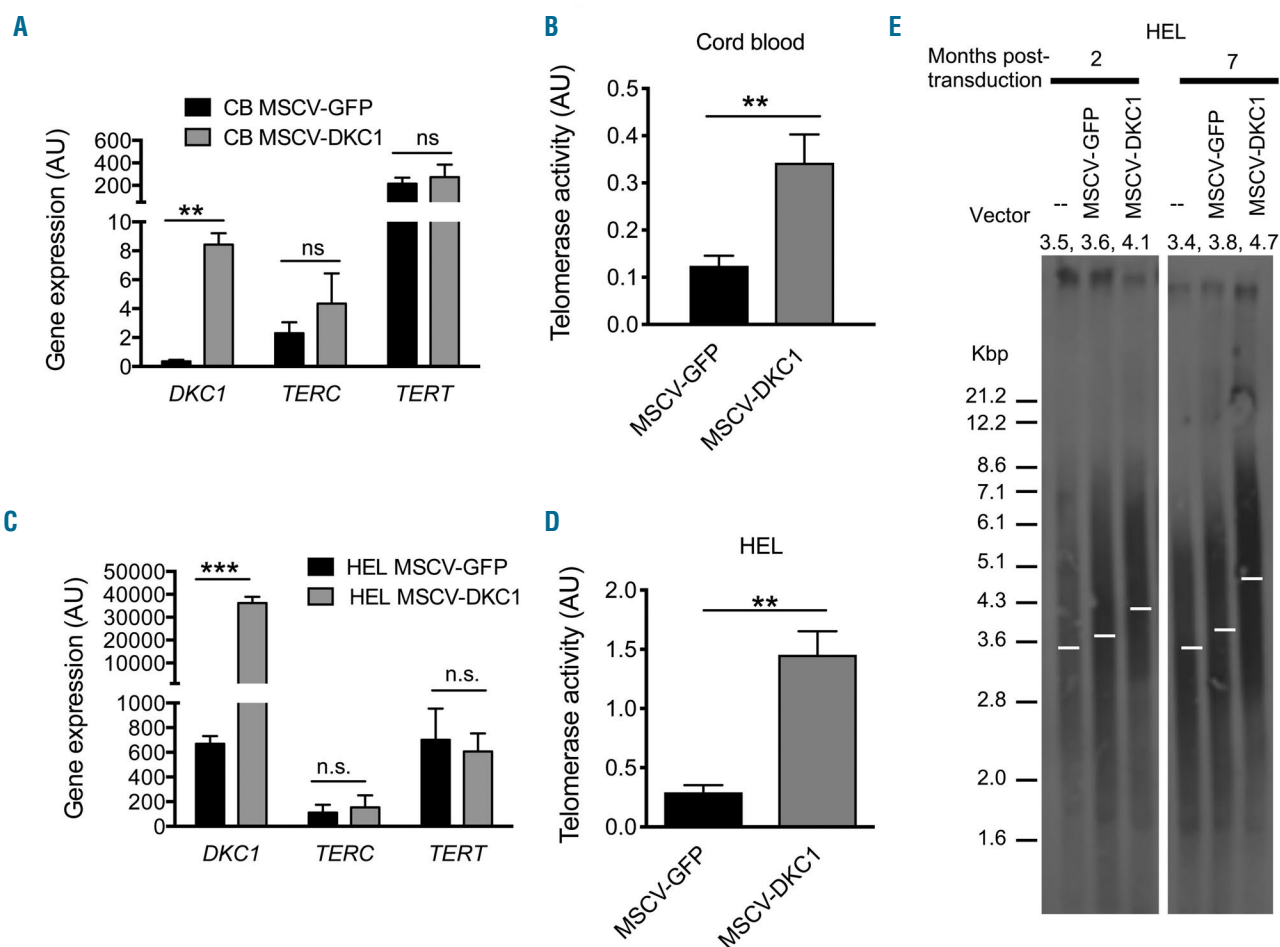


Figure 3. Upregulation of *DKC1* is sufficient for induction of telomerase activity in normal cord blood progenitors and erythroleukemia cells. (A-D) Cord blood (CB) CD34⁺ hematopoietic stem and progenitor cells (HSPC) (A, B) and HEL 92.1.7 leukemia cells (HEL) (C, D) were transduced with a lentiviral vector encoding *DKC1* and green fluorescence protein (GFP) (MSCV-DKC1) or a control vector expressing GFP alone (MSCV-GFP). Transduced cells were enriched by fluorescence activated cell sorting (FACS) for GFP expression 72 h after the last round of lentiviral infection. (A) Quantitative real-time polymerase chain reaction (qRT-PCR) analysis of *DKC1*, *TERC* and *TERT* expression in transduced CB cells collected immediately after FACS. (B) Telomerase activity in transduced CB cells measured using the qTRAP assay. (C) qRT-PCR analysis of *DKC1* mRNA, *TERC* and *TERT* mRNA in HEL 92.1.7 cells. (D) Telomerase activity in transduced HEL 92.1.7 cells measured in cells harvested 7 days after FACS using the qTRAP assay. Results for (A-D) are mean values \pm standard error of mean calculated from three assays from each of two to four independent lentiviral transduction experiments. ** $P < 0.01$, *** $P < 0.001$ from a two-tailed paired Student *t* test. (E) Telomeric restriction fragment Southern blot showing telomere lengths in transduced HEL 92.1.7 cells at 2 months and 7 months after transduction.

in transfected HEL 92.1.7 erythroleukemia cells. The results demonstrated that both GATA sites contributed to promoter activity, and that concurrent ablation of the two GATA sites substantially diminished promoter activity (Figure 5D). Collectively the results provide strong evidence that the erythroid-restricted transcription factor GATA1 contributes to the regulation of *DKC1*.

Discussion

This report is the first to implicate GATA1 in the regulation of telomerase and to describe a biological context in which telomerase activity is upregulated by induction of *DKC1*. Here it is shown that GATA1 binds the *DKC1* promoter and contributes to the upregulation of *DKC1*,

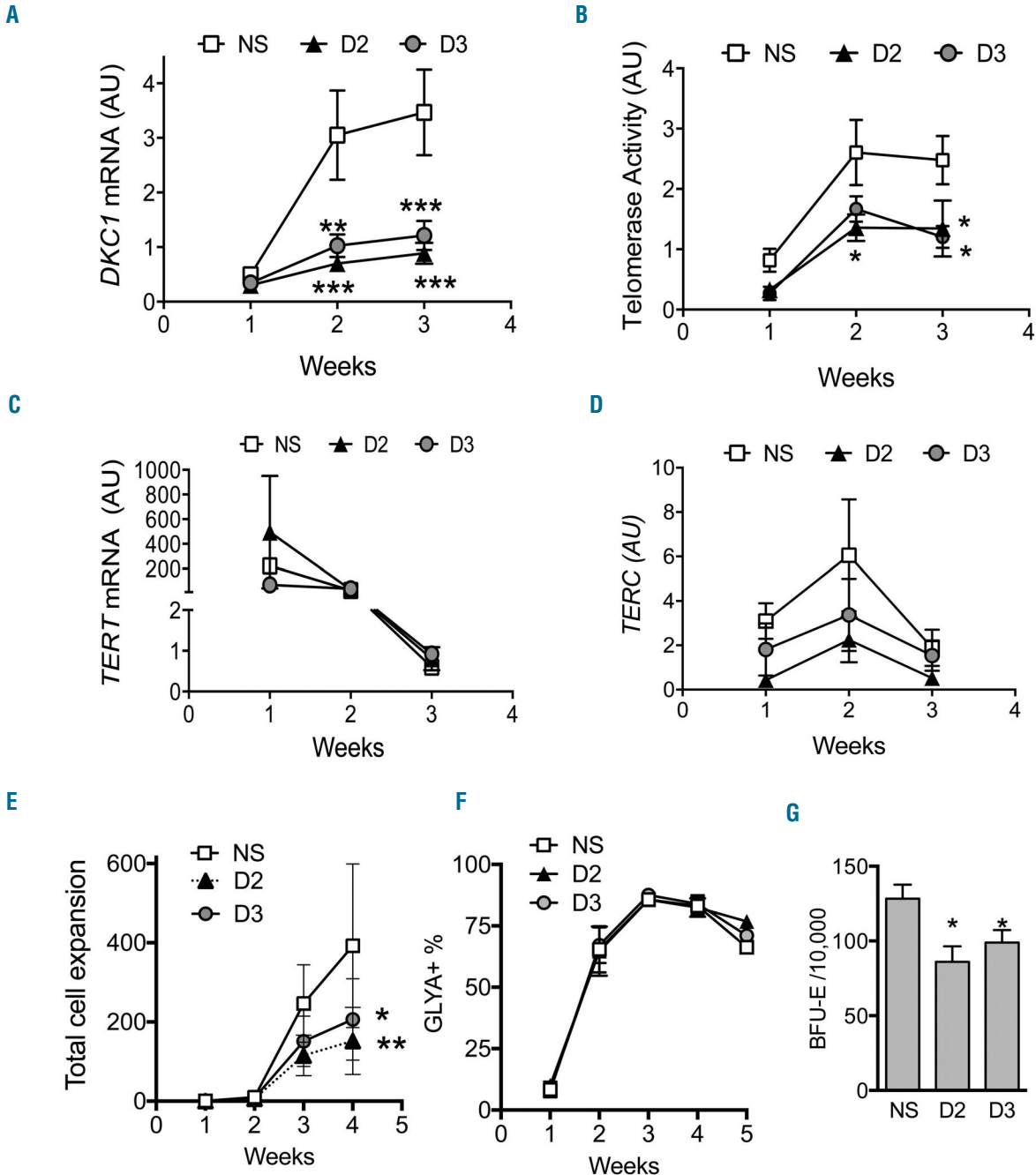


Figure 4. Downregulation of *DKC1* expression suppresses telomerase activity and inhibits erythroid cell proliferation but not differentiation. Cord blood-derived CD34⁺ hematopoietic stem and progenitor cells were transduced with retroviral vectors encoding *DKC1*-targeted shRNA (D2 and D3) or non-silencing RNA (NS) and green fluorescent protein (GFP). GFP⁺ cells were sorted by fluorescent activated cell sorting (FACS) (week 1), then cultured with stem cell factor plus erythropoietin (SE) for a further 2 weeks. Expression of telomerase genes and telomerase enzyme activity were measured by quantitative real-time polymerase chain reaction and the qTRAP assay, respectively. (A) *DKC1* mRNA, (B) telomerase enzyme activity, (C) *TERT* mRNA and (D) *TERC* abundance. (E) Expansion of FACS-sorted GFP⁺ cells determined from cell counts using trypan blue exclusion of dead cells. (F) Percentage of glycoprotein A-positive cells in cultures determined by weekly FACS analysis. (G) Erythroid progenitors in the GFP⁺ sorted fraction were quantified as burst-forming units-erythroid in methylcellulose assays. Values are means ± standard error of mean from six independent experiments. **P*<0.05, ***P*<0.01, *****P*<0.0001 from the Dunnett multiple comparison of D2 and D3 to NS. AU: arbitrary units; BFU-E: burst-forming unit-erythroid; GLYA⁺: glycoprotein A-positive cells.

which drives telomerase activity levels in erythroid cells. These results are notable in relation to past studies that established the paradigm of TERT transcriptional regulation as the primary determinant of telomerase regulation in hematopoietic and cancer cells.^{19,20,33-35}

Past investigations of telomerase regulation in hematopoietic cells focused on lymphoid cells, myeloid progenitors and myeloid leukemia cell lines.^{11-13,36} These studies revealed that mitogen-induced upregulation of telomerase was followed by telomerase downregulation during differentiation. Studies of lymphoid and myeloid cells also established a direct role for MYC in the transcriptional regulation of *TERT* and telomerase re-activation in hematopoietic cells.^{19,37} Consistent with this paradigm, the present study found parallel upregulation of *TERT* and telomerase activity in the presence of MYC protein in CB progenitor cells stimulated with STF. However,

there was a clear dissociation of this pathway when cultures were switched to erythroid conditions. Upon switching cultures from STF to SE, the abundance of MYC protein was sustained, but *TERT* expression declined to an apparently rate-limiting level while telomerase enzyme activity escalated. Rather than correlating with *TERT* expression, the increase in telomerase activity detected in erythroblastic cells correlated with upregulation of endogenous *DKC1* mRNA. Modulation of *DKC1* expression by overexpression or targeting with shRNA confirmed that *DKC1* regulated telomerase activity in erythroid cells without altering *TERT* gene expression. The functional significance of these observations was further supported by evidence of telomere lengthening following upregulation of *DKC1* in the HEL 92.1.7 erythroid cell line. *DKC1* mRNA was shown to be abundant in CB-derived CD34/GLYA⁺ erythroid cells irrespective of

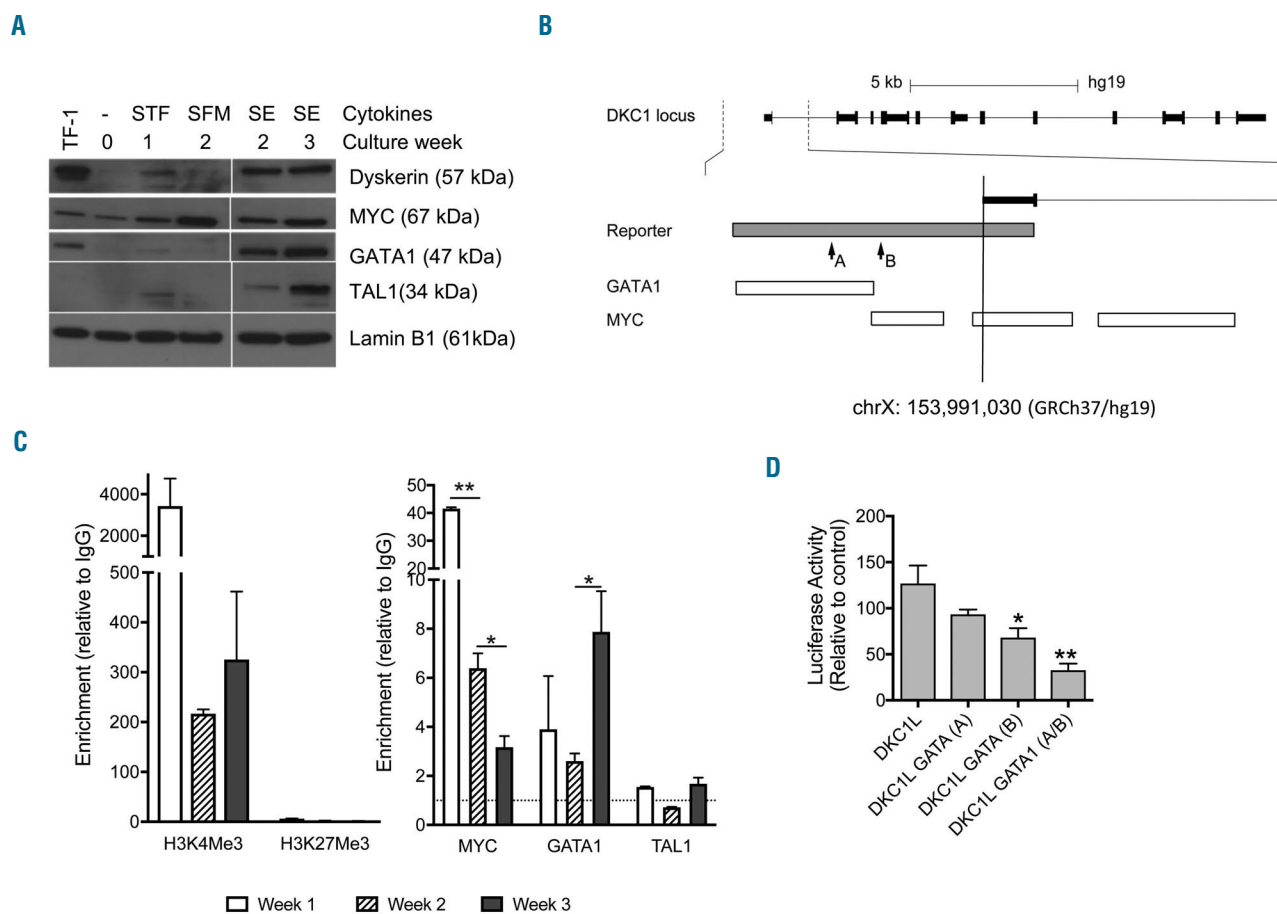


Figure 5. GATA1 interaction and regulation of the *DKC1* promoter in erythroid cells. (A) Immunoblot of nuclear extracts showing expression of dyskerin and the transcription factors MYC, GATA1 and TAL1 in cord blood (CB) cells cultured for 1 week in medium supplemented with stem cell factor (SCF), thrombopoietin and Flt-3 ligand, followed by culture with SCF plus erythropoietin or SCF, Flt-3 ligand and monocyte colony-stimulating factor. The erythroleukemia cell line TF-1 was used as a control for dyskerin expression. The immunoblot was hybridized to Lamin B1 antibody as a loading control. The image shows samples run on a single gel, with consistent exposure for all samples. The gap between lanes 4 and 5 represents deletion of a failed sample. (B) Schematic figure of the *DKC1* promoter showing the region included in the pGL2-*DKC1L* reporter construct, as well as canonical GATA motifs (indicated by arrows labeled A and B), and regions of GATA1 and MYC binding in peripheral blood erythroblasts and other cell types as reported in ENCODE chromatin immunoprecipitation sequencing traces (UCSC browser GRCh37/hg19). (C) Chromatin immunoprecipitation was performed on *ex vivo*-expanded CB cells using antibodies to MYC, GATA1, TAL1 and trimethylated histones or a control IgG antibody. Transcription factor binding was quantified as fold-enrichment of quantitative real-time polymerase chain reaction (qRT-PCR) products amplified from the region of interest relative to control region in an unrelated gene. Data were normalized to results from the IgG control antibody. * $P < 0.05$, ** $P < 0.01$, analysis of variance followed by the Bonferroni multiple comparisons test. (D) Site-directed mutagenesis was performed to introduce point mutations at canonical GATA sites within a pGL2-*DKC1L* luciferase reporter construct. HEL 92.1.7 cells were co-transfected with the reporter constructs and control vector pEFBOS-LacZ for normalization. Promoter activity was detected as luciferase activity and measured 48 h after transfection. Values are means \pm standard error of mean from three independent experiments. * $P < 0.05$, ** $P < 0.01$, ns, not significant, from the Dunnett multiple comparisons test. STF: stem cell factor, thrombopoietin and Flt-3 ligand; SE: stem cell factor plus erythropoietin; SFM: stem cell factor, Flt-3 ligand and monocyte colony-stimulating factor.

whether they were generated *ex vivo* or *in vivo*. Consistent with these findings, publicly available microarray data from fractionated bone marrow showed high levels of *DKC1* expression in proerythroblasts.

In addition to regulating *TERT*, *MYC* has been shown to bind and activate the *DKC1* promoter in tumor cell lines.^{26,27} The present study adds to this knowledge by demonstrating that *MYC* binds the *DKC1* promoter in primary human hematopoietic cells. Notably however, *MYC* binding at the *DKC1* promoter appeared to decline, while *DKC1* was upregulated during erythroid commitment and expansion. These results suggest that *MYC* plays a less prominent role in driving *DKC1* expression in erythroblasts compared with undifferentiated HSPC. Instead, our study highlights a potential role for *GATA1* in the regulation of *DKC1* in the erythroid lineage. This was evidenced by enrichment of *GATA1* at the *DKC1* promoter in *GLYA*⁺ erythroblasts, and an apparent transcriptional requirement for *GATA* binding sites in the proximal region of the *DKC1* promoter.

Consistent with the known role of dyskerin in stabilizing *TERC*,³⁸ we consistently observed an increase in *TERC* in parallel with upregulation of endogenous *DKC1*. The magnitude of this effect was moderate, yet consistent with results from ectopic overexpression of *DKC1*, and converse to the observed effect of shRNA-mediated downregulation of *DKC1*. Overexpression of *TERT* was previously shown to be sufficient to elevate telomerase and hyper-extend telomeres.³⁹⁻⁴¹ Nevertheless it seems unlikely that the modest elevation in endogenous *TERC* observed in primary erythroblasts was the singular cause of the dramatic increase in telomerase activity observed in the erythroblasts. In addition to stabilizing *TERC*, dyskerin may hyperactivate telomerase through its intrinsic pseudouridine synthase activity. This could involve targeting and enzymatically modifying *TERC* moieties with structural or functional roles, or indirectly through functional modification of rRNA or splicesomal RNA.⁴²⁻⁴⁶ There is also scope for dyskerin to modulate telomerase activity through direct interactions with H/ACA box RNA that have been ascribed roles in post-transcriptional regulation of gene expression.⁴⁷⁻⁵³ Clarification of the functional significance of pseudouridylation of *TERC* and other non-coding RNA that interact with dyskerin will be valuable in understanding the full extent of dyskerin's influence on telomerase activity.

Gene suppression experiments reported here demonstrate that high *DKC1* expression is required for proliferation of erythroblasts but is dispensable for erythroid differentiation. The apparent requirement for high expression of *DKC1* to sustain erythroblast proliferation may

reflect dependence on telomerase as well as the telomerase-independent function of dyskerin in ribosome biogenesis.² During erythropoiesis, erythroblasts undergo a period of intense ribosome biogenesis that is necessary for synthesis of large quantities of hemoglobin.⁵⁴ An abundance of dyskerin may be necessary to support this process. Consistent with this possibility, zebra fish and murine models have shown that hypomorphic *DKC1* mutations impaired rRNA processing.⁵⁰⁻⁵³ Ribosomal stress has also been demonstrated in *MYC*-transformed cancer cells subjected to shRNA-mediated suppression of dyskerin.²⁷ The implications of dyskerin's function in ribosome biogenesis are yet to be fully elucidated in relation to the pathogenesis of dyskeratosis congenita when *DKC1* is mutated. However, it is worth noting that the hematologic deficiencies observed in dyskeratosis congenita are also primary characteristics of the bone marrow failure disorders referred to as ribosomopathies, which feature impaired ribosome biogenesis as an underlying cause.⁵⁵ Ribosome dysfunction in these disorders is usually attributed to mutations in genes with known roles in ribosome biogenesis. However, the discovery of *GATA1* mutations in the ribosomopathy Diamond Blackfan anemia raises the possibility that dyskerin insufficiency may contribute to the pathogenesis of this genetic subtype.⁵⁶

Collectively the results from these investigations reveal a novel mechanism of telomerase regulation in primary human erythroblasts which contrasts with the established paradigm centered on *MYC*-mediated regulation of *TERT* expression in HSPC, lymphocytes and myelomonocytic cells. Notwithstanding the requirement for a rate-limiting amount of *TERT* for telomerase activity,⁵⁷ this study shows that *DKC1* expression levels are a critical determinant of telomerase enzyme levels in proliferating erythroblasts. Evidence provided herein that *GATA1* contributes to the regulation of *DKC1* has implications in hematopoietic disorders that feature *DKC1* mutations, *GATA1* deregulation and/or telomerase insufficiency.

Acknowledgments

We thank midwives, mothers and neonates at Royal North Shore Hospital and Royal Hospital for Women for cord blood donations to this project. We also thank Prof Emery Bresnick from University of Wisconsin School of Medicine and Public Health for the *GATA1* antibody, and Prof Inderjeet Dokal, Queen Mary University of London, for the pCL10.1-DKC1 lentiviral vector. This project was funded by the National Health and Medical Research Council (1007911, 510378, RG150480, RG170246), Cancer Council NSW (RG08-03), Cancer Institute NSW and the Anthony Rothe Memorial Fund.

References

1. Arndt GM, MacKenzie KL. New prospects for targeting telomerase beyond the telomere. *Nat Rev Cancer*. 2016;16(8):508-524.
2. Meier UT, Blobel G. NAP57, a mammalian nucleolar protein with a putative homolog in yeast and bacteria. *J Cell Biol*. 1994;127(6 Pt 1):1505-1514.
3. Hamma T, Ferre-D'Amare AR. Pseudouridine synthases. *Chem Biol*. 2006;13(11):1125-1135.
4. Kim NW, Piatyszek MA, Prowse KR, et al. Specific association of human telomerase activity with immortal cells and cancer. *Science*. 1994;266(5193):2011-2015.
5. Maritz MF, Napier CE, Wen VW, MacKenzie KL. Targeting telomerase in hematologic malignancy. *Future Oncol*. 2010;6(5):769-789.
6. Engelhardt M, Mackenzie K, Drullinsky P, Silver RT, Moore MA. Telomerase activity and telomere length in acute and chronic leukemia, pre- and post-ex vivo culture. *Cancer Res*. 2000;60(3):610-617.
7. Ohyashiki JH, Ohyashiki K, Iwama H, Hayashi S, Toyama K, Shay JW. Clinical implications of telomerase activity levels in acute leukemia. *Clin Cancer Res*. 1997;3(4):619-625.
8. Lee HW, Blasco MA, Gottlieb GJ, Homer JW 2nd, Greider CW, DePinho RA. Essential role

- of mouse telomerase in highly proliferative organs. *Nature*. 1998;392(6676):569-574.
9. Hiyama K, Hirai Y, Kyoizumi S, et al. Activation of telomerase in human lymphocytes and hematopoietic progenitor cells. *J Immunol*. 1995;155(8):3711-3715.
 10. Broccoli D, Young JW, de Lange T. Telomerase activity in normal and malignant hematopoietic cells. *Proc Natl Acad Sci U S A*. 1995;92(20):9082-9086.
 11. Engelhardt M, Kumar R, Albanell J, Pettengell R, Han W, Moore MA. Telomerase regulation, cell cycle, and telomere stability in primitive hematopoietic cells. *Blood*. 1997;90(1):182-193.
 12. Chiu CP, Dragowska W, Kim NW, Vaziri H, Yui J, Thomas TE, et al. Differential expression of telomerase activity in hematopoietic progenitors from adult human bone marrow. *Stem Cells*. 1996;14(2):239-248.
 13. Yamada O, Motoji T, Mizoguchi H. Up-regulation of telomerase activity in human lymphocytes. *Biochim Biophys Acta*. 1996;1314(3):260-266.
 14. Schuller CE, Jankowski K, Mackenzie KL. Telomere length of cord blood-derived CD34(+) progenitors predicts erythroid proliferative potential. *Leukemia*. 2007;21(5):983-991.
 15. Raval A, Behbehani GK, Nguyen le XT, et al. Reversibility of defective hematopoiesis caused by telomere shortening in telomerase knockout Mice. *PLoS One*. 2015;10(7):e0131722.
 16. Balakumaran A, Mishra PJ, Pawelczyk E, et al. Bone marrow skeletal stem/progenitor cell defects in dyskeratosis congenita and telomere biology disorders. *Blood*. 2015;125(5):793-802.
 17. Barbaro PM, Ziegler DS, Reddel RR. The wide-ranging clinical implications of the short telomere syndromes. *Intern Med J*. 2016;46(4):393-403.
 18. Kirwan M, Vulliamy T, Beswick R, Waite AJ, Casimir C, Dokal I. Circulating haematopoietic progenitors are differentially reduced amongst subtypes of dyskeratosis congenita. *Br J Haematol*. 2008;140(6):719-722.
 19. Wu KJ, Grandori C, Amacker M, et al. Direct activation of TERT transcription by c-MYC. *Nat Genet*. 1999;21(2):220-224.
 20. Xu D, Gruber A, Bjorkholm M, Peterson C, Pisa P. Suppression of telomerase reverse transcriptase (hTERT) expression in differentiated HL-60 cells: regulatory mechanisms. *Br J Cancer*. 1999;80(8):1156-1161.
 21. Uchida N, Otsuka T, Shigematsu H, et al. Differential gene expression of human telomerase-associated protein hTERT and TEP1 in human hematopoietic cells. *Leuk Res*. 1999;23(12):1127-1132.
 22. Maritz MF, Richards LA, Mackenzie KL. Assessment and quantification of telomerase enzyme activity. *Methods Mol Biol*. 2013;965:215-231.
 23. Taylor LM, James A, Schuller CE, Brce J, Lock RB, Mackenzie KL. Inactivation of p16INK4a, with retention of pRB and p53/p21cip1 function, in human MRC5 fibroblasts that overcome a telomere-independent crisis during immortalization. *J Biol Chem*. 2004;279(42):43634-43645.
 24. Beck D, Thoms JA, Perera D, et al. Genome-wide analysis of transcriptional regulators in human HSPCs reveals a densely interconnected network of coding and noncoding genes. *Blood*. 2013;122(14):e12-22.
 25. Wu C, Orozco C, Boyer J, et al. BioGPS: an extensible and customizable portal for querying and organizing gene annotation resources. *Genome Biol*. 2009;10(11):R130.
 26. Alawi F, Lee MN. DKC1 is a direct and conserved transcriptional target of c-MYC. *Biochem Biophys Res Commun*. 2007;362(4):893-898.
 27. O'Brien R, Tran SL, Maritz MF, et al. MYC-driven neuroblastomas are addicted to a telomerase-independent function of dyskerin. *Cancer Res*. 2016;76(12):3604-3617.
 28. Bondurant MC, Yamashita T, Muta K, Krantz SB, Koury MJ. C-myc expression affects proliferation but not terminal differentiation or survival of explanted erythroid progenitor cells. *J Cell Physiol*. 1996;168(2):255-263.
 29. Shilatfard A. Molecular implementation and physiological roles for histone H3 lysine 4 (H3K4) methylation. *Curr Opin Cell Biol*. 2008;20(3):341-348.
 30. Xu J, Shao Z, Glass K, Bauer DE, et al. Combinatorial assembly of developmental stage-specific enhancers controls gene expression programs during human erythropoiesis. *Dev Cell*. 2012;23(4):796-811.
 31. Hu G, Schones DE, Cui K, et al. Regulation of nucleosome landscape and transcription factor targeting at tissue-specific enhancers by BRG1. *Genome Res*. 2011;21(10):1650-1658.
 32. Zheng R, Wan C, Mei S, et al. Cistrome Data Browser: expanded datasets and new tools for gene regulatory analysis. *Nucleic Acids Res*. 2019;47(D1):D729-D35.
 33. Koyanagi Y, Kobayashi D, Yajima T, et al. Telomerase activity is down regulated via decreases in hTERT mRNA but not TEP1 mRNA or hTERC during the differentiation of leukemic cells. *Anticancer Res*. 2000;20(2A):773-778.
 34. Chang JT, Chen YL, Yang HT, Chen CY, Cheng AJ. Differential regulation of telomerase activity by six telomerase subunits. *Eur J Biochem*. 2002;269(14):3442-3450.
 35. Liu K, Schoonmaker MM, Levine BL, June CH, Hodes RJ, Weng NP. Constitutive and regulated expression of telomerase reverse transcriptase (hTERT) in human lymphocytes. *Proc Natl Acad Sci U S A*. 1999;96(9):5147-5152.
 36. Sharma HW, Sokolowski JA, Perez JR, et al. Differentiation of immortal cells inhibits telomerase activity. *Proc Natl Acad Sci U S A*. 1995;92(26):12343-12346.
 37. Xu D, Popov N, Hou M, et al. Switch from Myc/Max to Mad1/Max binding and decrease in histone acetylation at the telomerase reverse transcriptase promoter during differentiation of HL60 cells. *Proc Natl Acad Sci U S A*. 2001;98(7):3826-3831.
 38. Mitchell JR, Wood E, Collins K. A telomerase component is defective in the human disease dyskeratosis congenita. *Nature*. 1999;402(6761):551-555.
 39. Kirwan M, Beswick R, Vulliamy T, et al. Exogenous TERC alone can enhance proliferative potential, telomerase activity and telomere length in lymphocytes from dyskeratosis congenita patients. *Br J Haematol*. 2009;144(5):771-781.
 40. Napier CE, Veas LA, Kan CY, et al. Mild hyperoxia limits hTR levels, telomerase activity, and telomere length maintenance in hTERT-transduced bone marrow endothelial cells. *Biochim Biophys Acta*. 2010;1803(10):1142-1153.
 41. Cao Y, Huschtscha LI, Nouwens AS, et al. Amplification of telomerase reverse transcriptase gene in human mammary epithelial cells with limiting telomerase RNA expression levels. *Cancer Res*. 2008;68(9):3115-3123.
 42. Kim NK, Theimer CA, Mitchell JR, Collins K, Feigon J. Effect of pseudouridylation on the structure and activity of the catalytically essential P6.1 hairpin in human telomerase RNA. *Nucleic Acids Res*. 2010;38(19):6746-6756.
 43. Meier UT. The many facets of H/ACA ribonucleoproteins. *Chromosoma*. 2005;114(1):1-14.
 44. Jack K, Bellodi C, Landry DM, et al. rRNA pseudouridylation defects affect ribosomal ligand binding and translational fidelity from yeast to human cells. *Mol Cell*. 2011;44(4):660-666.
 45. Heiss NS, Knight SW, Vulliamy TJ, et al. X-linked dyskeratosis congenita is caused by mutations in a highly conserved gene with putative nucleolar functions. *Nat Genet*. 1998;19(1):32-38.
 46. Watkins NJ, Gottschalk A, Neubauer G, et al. Cbf5p, a potential pseudouridine synthase, and Nhp2p, a putative RNA-binding protein, are present together with Gar1p in all H BOX/ACA-motif snoRNPs and constitute a common bipartite structure. *RNA*. 1998;4(12):1549-1568.
 47. Ender C, Krek A, Friedlander MR, et al. A human snoRNA with microRNA-like functions. *Mol Cell*. 2008;32(4):519-528.
 48. Scott MS, Ono M. From snoRNA to miRNA: dual function regulatory non-coding RNAs. *Biochimie*. 2011;93(11):1987-1992.
 49. Yoon A, Peng G, Brandenburger Y, et al. Impaired control of IRES-mediated translation in X-linked dyskeratosis congenita. *Science*. 2006;312(5775):902-906.
 50. Mochizuki Y, He J, Kulkarni S, Bessler M, Mason PJ. Mouse dyskerin mutations affect accumulation of telomerase RNA and small nucleolar RNA, telomerase activity, and ribosomal RNA processing. *Proc Natl Acad Sci U S A*. 2004;101(29):10756-10761.
 51. Ruggero D, Grisendi S, Piazza F, et al. Dyskeratosis congenita and cancer in mice deficient in ribosomal RNA modification. *Science*. 2003;299(5604):259-262.
 52. Ge J, Rudnick DA, He J, et al. Dyskerin ablation in mouse liver inhibits rRNA processing and cell division. *Mol Cell Biol*. 2010;30(2):413-422.
 53. Pereboom TC, van Weele LJ, Bondt A, MacInnes AW. A zebrafish model of dyskeratosis congenita reveals hematopoietic stem cell formation failure resulting from ribosomal protein-mediated p53 stabilization. *Blood*. 2011;118(20):5458-5465.
 54. Zivot A, Lipton JM, Narla A, Blanc L. Erythropoiesis: insights into pathophysiology and treatments in 2017. *Mol Med*. 2018;24(1):11.
 55. Raiser DM, Narla A, Ebert BL. The emerging importance of ribosomal dysfunction in the pathogenesis of hematologic disorders. *Leuk Lymphoma*. 2014;55(3):491-500.
 56. Parrella S, Aspesi A, Quarello P, et al. Loss of GATA-1 full length as a cause of Diamond-Blackfan anemia phenotype. *Pediatr Blood Cancer*. 2014;61(7):1319-1321.
 57. Liu Y, Snow BE, Hande MP, et al. The telomerase reverse transcriptase is limiting and necessary for telomerase function in vivo. *Curr Biol*. 2000;10(22):1459-1462.

Multi-parametric single cell evaluation defines distinct drug responses in healthy hematologic cells that are retained in corresponding malignant cell types



Muntasir M. Majumder,¹ Aino-Maija Leppä,¹ Monica Hellesøy,² Paul Dowling,³ Alina Malyutina,¹ Reidun Kopperud,⁴ Despina Bazou,⁵ Emma Andersson,⁶ Alun Parsons,¹ Jing Tang,¹ Olli Kallioniemi,^{1,7} Satu Mustjoki,^{6,8} Peter O'Gorman,⁵ Krister Wennerberg,^{1,9} Kimmo Porkka,^{8,10} Bjørn T. Gjertsen^{2,4} and Caroline A. Heckman¹

¹Institute for Molecular Medicine Finland FIMM, Helsinki Institute of Life Science, University of Helsinki, Helsinki, Finland; ²Hematology Section, Department of Internal Medicine, Haukeland University Hospital, Bergen, Norway; ³Department of Biology, National University of Ireland, Maynooth, Ireland; ⁴Centre for Cancer Biomarkers CCBC, Department of Clinical Science, University of Bergen, Bergen, Norway; ⁵Department of Hematology, Mater Misericordiae University Hospital, Dublin, Ireland; ⁶Department of Clinical Chemistry and Hematology, University of Helsinki, Finland; ⁷Science for Life Laboratory, Department of Oncology and Pathology, Karolinska Institute, Solna, Sweden; ⁸Hematology Research Unit Helsinki, University of Helsinki, Helsinki, Finland; ⁹BRIC-Biotech Research and Innovation Centre, University of Copenhagen, Copenhagen, Denmark and ¹⁰Department of Hematology, Helsinki University Hospital Comprehensive Cancer Center, Helsinki, Finland

Haematologica 2020
Volume 105(6):1527-1538

ABSTRACT

Innate drug sensitivity in healthy cells aids identification of lineage specific anti-cancer therapies and reveals off-target effects. To characterize the diversity in drug responses in the major hematopoietic cell types, we simultaneously assessed their sensitivity to 71 small molecules utilizing a multi-parametric flow cytometry assay and mapped their proteomic and basal signaling profiles. Unsupervised hierarchical clustering identified distinct drug responses in healthy cell subsets based on their cellular lineage. Compared to other cell types, CD19⁺/B and CD56⁺/NK cells were more sensitive to dexamethasone, venetoclax and midostaurin, while monocytes were more sensitive to trametinib. Venetoclax exhibited dose-dependent cell selectivity that inversely correlated to STAT3 phosphorylation. Lineage specific effect of midostaurin was similarly detected in CD19⁺/B cells from healthy, acute myeloid leukemia and chronic lymphocytic leukemia samples. Comparison of drug responses in healthy and neoplastic cells showed that healthy cell responses are predictive of the corresponding malignant cell response. Taken together, understanding drug sensitivity in the healthy cell-of-origin provides opportunities to obtain a new level of therapy precision and avoid off-target toxicity.

Introduction

During hematopoiesis, multipotent stem cells and pluripotent precursors undergo a complex differentiation program to generate a diverse set of blood cell types with wide-ranging phenotypes and functions.¹ This process is initiated and driven by distinct signaling pathways linked to the different cellular lineages.² It is likely that malignant hematopoietic cells exploit many of the signaling pathways essential for maintaining survival and specific functions of normal cells. Identification and understanding of normal hematopoietic cell type specific pathways could, therefore, be leveraged therapeutically as anti-cancer strategies against their malignant counterparts. For example, targeting B-cell antigen receptor (BCR) signaling with ibrutinib or idelalisib has proven highly effective in treating chronic lymphocytic leukemia (CLL).^{3,4} Conversely, modulating molecular targets shared between malignant and

Correspondence:

CAROLINE A. HECKMAN
caroline.heckman@helsinki.fi

MUNTASIR MAMUN MAJUMDER
muntasir.mamun@helsinki.fi

Received: January 24, 2019.

Accepted: August 22, 2019.

Pre-published: August 22, 2019.

doi:10.3324/haematol.2019.217414

Check the online version for the most updated information on this article, online supplements, and information on authorship & disclosures: www.haematologica.org/content/105/6/1527

©2020 Ferrata Storti Foundation

Material published in *Haematologica* is covered by copyright. All rights are reserved to the Ferrata Storti Foundation. Use of published material is allowed under the following terms and conditions:

<https://creativecommons.org/licenses/by-nc/4.0/legalcode>.

Copies of published material are allowed for personal or internal use. Sharing published material for non-commercial purposes is subject to the following conditions:

<https://creativecommons.org/licenses/by-nc/4.0/legalcode>,

sect. 3. Reproducing and sharing published material for commercial purposes is not allowed without permission in writing from the publisher.



healthy cells may give rise to untoward effects related to these entities. Although seminal studies have contributed to the understanding of signaling diversities across blood cells,⁵⁻⁸ a detailed characterization of cell-type specific vulnerabilities within the hematopoietic hierarchy is still lacking.

Cell-based phenotypic screens of primary cells have shown tremendous potential to identify novel therapeutics in leukemia and to explore novel indications for approved drugs.^{9,10} However, classical drug screening methods that assess the sum of all cellular effects in the bone marrow (BM) or blood restrict the ability to evaluate drug responses in populations affected by rare diseases and is influenced by the more abundant cell types in the sample. Flow cytometry presents a functional platform for dissecting the complexity of hematopoiesis, allowing characterization of the different cell populations. Applying flow cytometry in functional screens allows for a higher throughput (HTS) assessment of vulnerabilities to a large set of oncology drugs in leukemic cells with improved precision, and to compartmentalize drug responses between malignant and healthy cell subsets. However, preclinical flow cytometric-based high throughput functional screens are still limited by numerous washing steps and small cell population numbers, which can compromise the robustness of the assay.

In this study, we developed a high throughput no-wash flow cytometry assay that enabled us to monitor dose responses of 71 oncology compounds simultaneously on multiple hematopoietic cell populations defined by their surface antigen expression. To map the drug responses to the proteome and basal signaling profiles of the different cell types, we utilized mass spectrometry (MS) and mass cytometry (CyTOF) in both healthy and malignant hematologic samples. Finally, we compared inhibition profiles for those small molecules in a cohort of 281 primary samples representing a diverse set of hematologic malignancies to assess whether healthy cell-specific responses can be exploited in a leukemic context. A graphical overview of the study and cohorts is provided in Figure 1. Our results strongly suggest that drug responses are highly specific to cell lineages and often linked to intrinsic cell signaling present in those cell types. We provide evidence that cell-specific responses could potentially be applied to identify new clinical applications of therapies and discover relevant non-oncogenic-dependent activities of small molecules.

Methods

Patient specimens and cohorts

Bone marrow and peripheral blood (PB) samples from 332 donors were collected after written informed consent (Studies: 239/13/03/00/2010, 303/13/03/01/2011, REK2016/253 and REK2012/2247) following protocols approved by local institutional review boards (Helsinki University Hospital Comprehensive Cancer Center and Haukeland University Hospital) in compliance with the Declaration of Helsinki. Samples were allocated to four patient cohorts (I-IV). Cohort I included three healthy PB samples used for flow cytometry screening with 71 drugs, plus three acute myeloid leukemia (AML) and ten multiple myeloma (MM) samples which were tested with bortezomib, clofarabine, dexamethasone, omipalisib, venetoclax and navitoclax. Cohort II included 17 samples from two healthy, eight AML with (n=5) or without FLT3-ITD mutations (n=3), and seven CLL patients tested against

midostaurin, trametinib and dasatinib. Cohort III (n=281) included 231 BM aspirates from a diverse collection of leukemia and 50 MM patients (CD138⁺ enriched). Four healthy BM aspirates subjected to magnetic bead-based enrichment using EasySep™ human CD138, CD3, CD19, CD14 and CD34 positive selection kits (StemCell Technologies), served as healthy cell-of-origin samples for comparison against the malignant cell counterparts. CyTOF was performed on 14 samples in Cohort IV. PB from healthy donors (n=3), AML (n=6), B-cell acute lymphoblastic leukemia (B-ALL) (n=2), and matched BM samples from the same healthy donors were included. An overview of the cohorts and experimental design is provided in Figure 1.

Proteome analysis

10 µg of whole cell protein lysates, prepared from purified CD3, CD19 and CD14 fractions from healthy (n=2) and MM (n=4) samples, were digested and loaded (500 ng) on to a Q-Exactive mass spectrometer connected to a Dionex Ultimate 3000 (RSLCnano) chromatography system (Thermo Scientific). Protein identification and label-free quantification (LFQ) normalization of tandem mass spectrometry (MS/MS) data were performed using MaxQuant v1.5.2.8.

Mass cytometry

For mass cytometry (CyTOF), the 14 samples described in cohort IV were fixed, barcoded (Fluidigm), pooled into a single sample and stained with the antibody panels (*Online Supplementary Table S1*). Acquisition of samples was performed using a Helios mass cytometer (Fluidigm). Data were analyzed using FlowJo v.10.2 and Cytobank (Cytobank Inc.).

High throughput flow cytometry and cell viability assay

High throughput flow cytometry (HTFC) assays were performed in both 384-well (n=3, 71 drugs, 5 concentrations) and 96-well plate formats (n=33) using IntelliCyt iQue Screener PLUS. A detailed optimization protocol is provided in the *Online Supplementary Methods*. A list of the antibodies is provided in *Online Supplementary Table S1*. Data were analyzed using ForeCyt software (Intellicyt). The gating strategy, cell composition and list of compounds are provided in *Online Supplementary Figures S1-S3*. CellTiter-Glo® luminescent viability assay was used based on a previously described method.^{9,16}

Statistical analysis of drug sensitivity data

Cell counts (HTFC) or luminescence intensity were used as input for Dotmatics (Dotmatics Ltd.) or Graphpad Prism 8.0 to generate dose response graphs, which were subsequently applied to calculate drug sensitivity score (DSS) as described by Yadav *et al.*¹⁶ Comparisons between groups were tested with ANOVA and with Tukey's multiple comparison test to derive significance. A two-tailed $P < 0.05$ was considered significant.

Results

Distinct drug response profiles in hematologic cell subsets are tied to cell lineages

To simultaneously monitor drug effects on a large collection (n=71) of samples in multiple cell types, we applied a multiplexed, no-wash flow cytometry-based assay (detailed in the *Online Supplementary Methods*). We first tested *ex vivo* response to the 71 compounds (*Online Supplementary Table S2* and *Online Supplementary Figure S3*) in B (CD19⁺), natural killer (NK, CD56⁺), T-helper cells (THC, CD3⁺CD4⁺), cytotoxic T lymphocytes (CTL,

CD3⁺CD8⁺), NK-T cells (NK-T, CD3⁺CD56⁺), and monocytes (CD14⁺) using three healthy blood samples to generate a global view of response profiles. Unsupervised hierarchical clustering of DSS of the screened samples segregated in three major clusters based on cellular lineages (Figure 2A). Monocytes formed a single cluster and displayed selective sensitivity to MEK/ERK inhibitors and the kinase inhibitor dasatinib (Figure 2A). The MEK inhibitor

trametinib was similarly active in BM derived CD14⁺ cells from healthy and AML samples (*Online Supplementary Figure S4A*). However, reduced efficacy of dasatinib in BM monocytes was noted compared to those derived from blood (*Online Supplementary Figure S4B*). B and NK cells showed similar drug response profiles with higher sensitivity to the glucocorticoid dexamethasone, BCL2 inhibitor venetoclax and pan-kinase inhibitor midostaurin

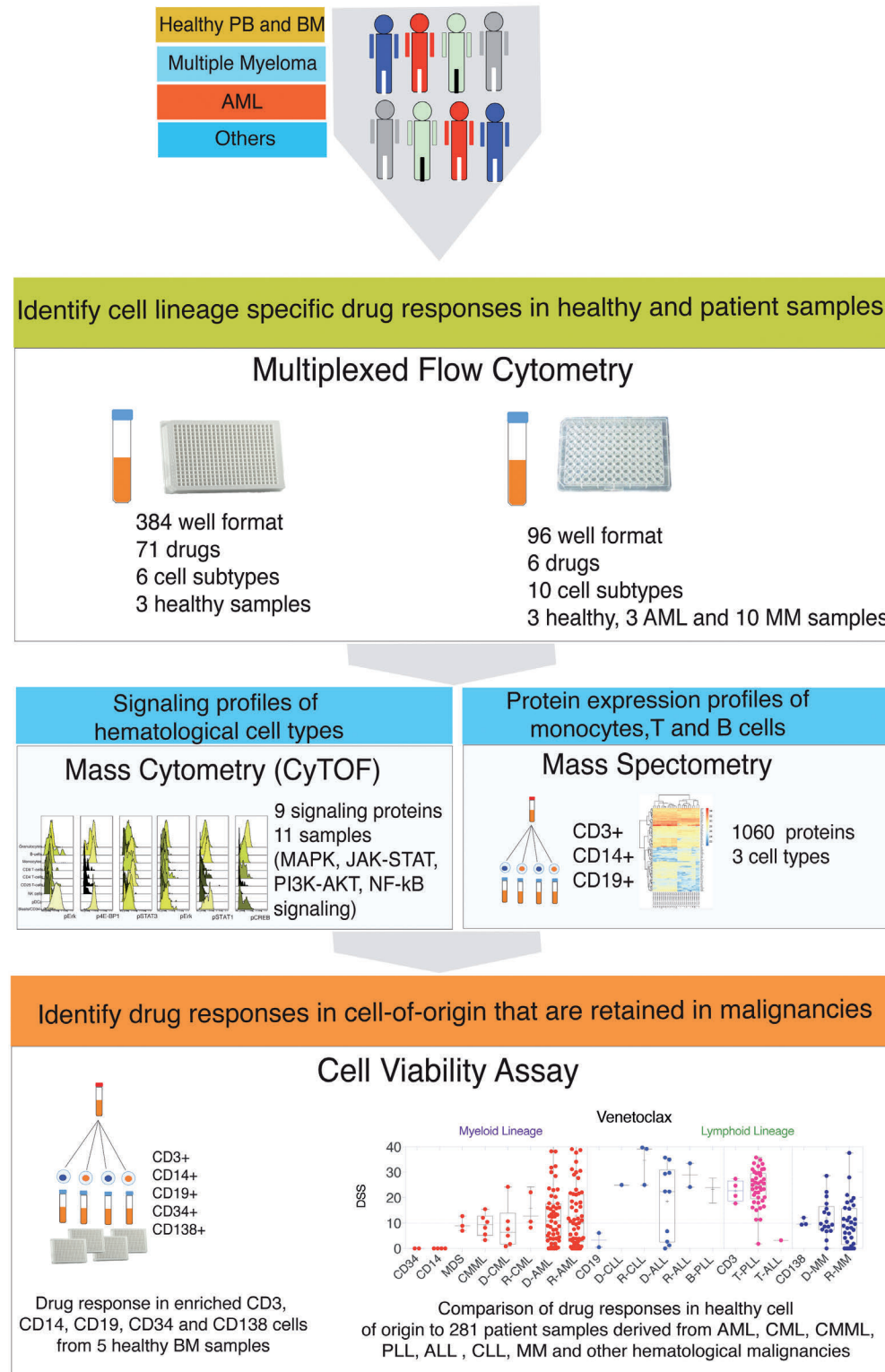


Figure 1. Overview of the study. Schematic diagram summarizing the study design, datasets and analytical framework of the study. Bone marrow (BM) and peripheral blood (PB) samples from both healthy individuals and cancer patients were subjected to drug sensitivity assessment. Single cell drug sensitivity assay using the iQue® Screener PLUS flow cytometer was performed in 96- and 384-well plates to monitor drug effects on ten and six hematopoietic cell subtypes, respectively. Immunophenotypic details and cellular proportions of the analyzed cell types are provided in *Online Supplementary Figure S1A-D*, *Figure S2* and *Online Supplementary Table S3*, respectively. 71 drugs in 384-well plates and six drugs in 96-well plates were tested. Proteomic analysis was performed on three cell subsets (monocytes, T and B cells) from two healthy individuals and four myeloma patients. Basal phosphorylation of nine signaling proteins involved in MAPK, JAK-STAT, PI3K-AKT-mTOR and NF-κB signaling was monitored in 14 samples. Healthy BM samples from four healthy individuals were subjected to CD34, CD3, CD14, CD19 and CD138 cell enrichment and tested against 71 small molecules with cell viability as the end point readout using the CellTiter-Glo® assay. A comparison of ex vivo drug response in healthy and corresponding malignant cell types was performed for six drugs in 281 primary patient samples representing different hematologic malignancies. Samples included both published and unpublished datasets from chronic myeloid leukemia (CML, n=13),^{11,12} chronic myelomonocytic leukemia (CMML, n=11),¹² myelodysplastic syndromes (MDS, n=4), acute myeloid leukemia (AML, n=145),^{21,22} B-cell acute lymphoblastic leukemia (B-ALL, n=14),¹³ chronic lymphocytic leukemia (CLL, n=4),¹² T-cell prolymphocytic leukemia (T-PLL, n=40),¹⁴ multiple myeloma (MM, n=50),¹⁵ and other hematologic malignancies (n=6). PLL: prolymphocytic leukemia.

compared to other cell types. Except for NK-T cells from one donor, all T-cell subsets formed a distinct cluster.

Based on observations from the primary screen, we focused our in-depth analysis on six compounds displaying either non-selective (proteasome inhibitor bortezomib

and nucleoside analog clofarabine) or cell-selective (dexamethasone, venetoclax, pan-BCL2 inhibitor navitoclax and PI3K/mTOR inhibitor omipalisib) responses. Sixteen samples (Cohort I) derived from 10 MM, 3 AML and 3 healthy donors were tested utilizing two antibody panels

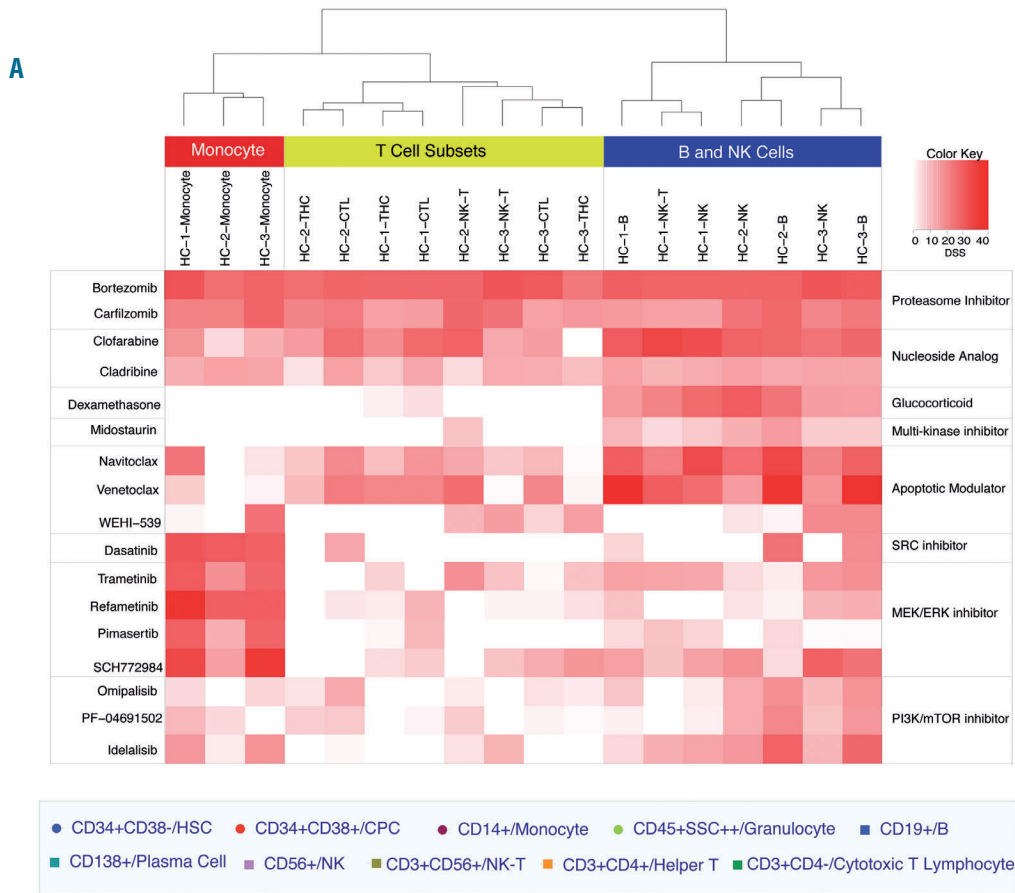
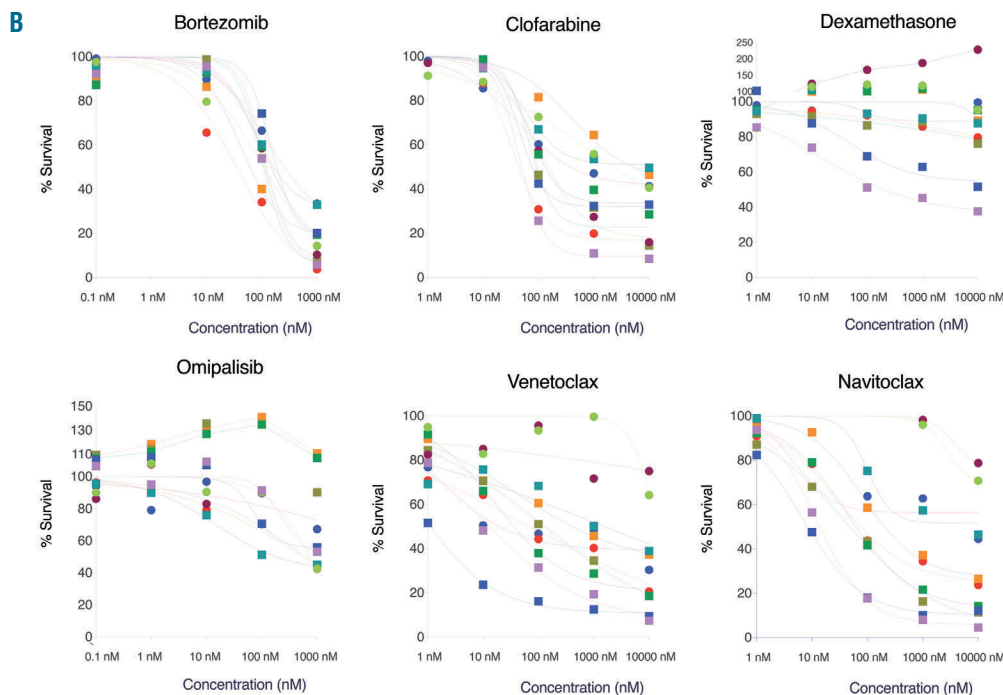


Figure 2. Distinct drug responses observed in immune subsets are tied to cell lineages. (A) A drug sensitivity score (DSS),¹⁶ which is a modified form of the area under the curve (AUC) calculation, was used to quantitate drug responses among the different detected cell populations. Higher DSS values (DSS>10) indicate higher sensitivity to the individual drug. The heatmap displays a summary view of hierarchical clustering analysis with DSS scores for six cell subsets in three peripheral blood (PB) samples from healthy controls (marked as HC-1, 2 and 3). Immunophenotyping of hematopoietic cell types was performed on the basis of their known surface antigen expression profiles (see also *Online Supplementary Figure S1A*). Monocytes and T-cell subsets formed two separate clusters. B and natural killer (NK) cells had similar drug response patterns. Small molecules that were tested along with their functional classes are displayed in *Online Supplementary Figure S3*. DSS scores and IC50 values for all 71 drugs are provided in *Online Supplementary Table S2*. (B) Differential effect of bortezomib, dexamethasone, clofarabine, venetoclax, navitoclax and omipalisib on hematopoietic cell subsets presented as mean values from 16 samples derived from three healthy, three acute myeloid leukemia (AML) and ten multiple myeloma (MM) patients (Cohort I). Highest variation was observed for BCL2 inhibitors (venetoclax and navitoclax) and dexamethasone between myeloid and lymphoid lineages. Monocytes were resistant to both of these drug classes. A concentration-dependent increase in numbers of CD3⁺ cells was observed for omipalisib at 10 and 100 nM. The proportion of cells detected in these analyzed samples are presented in *Online Supplementary Table S3*.



(Online Supplementary Table S1) in 96-well plates to provide a direct comparison between cell types derived from healthy donors and those derived from patients with identical immunophenotypes. Moreover, this enabled detection of drug responses in rare cell subsets, such as plasma cells (CD138⁺) and progenitor cells (CD34⁺CD38⁻ or CD34⁺CD38⁺).

While *ex vivo* response to the proteasome inhibitor bortezomib was detected in most cell types (Figure 2B), CD138⁺CD38⁻ plasma cells were resistant compared to CD138⁺CD38⁺ or other cells (Online Supplementary Figure S5). A higher response to the nucleoside analog clofarabine was noted for CD3⁺CD4⁺ and CD34⁺CD38⁺ cells compared to CD3⁺CD4⁻ or CD34⁺CD38⁻ cells. Dexamethasone depleted CD19⁺ and CD56⁺ cells and induced a dose-dependent increase in the CD14⁺ cell count (Figure 2B). T-cell subsets were insensitive to PI3K/mTOR inhibitor omipalisib. A similar effect for several molecules targeting the PI3K-mTOR signaling axis was observed in CD3⁺ enriched cells tested with a cell viability assay (Online Supplementary Figure S6). Surprisingly, an increase in CD3⁺ cell count was noted at concentrations of 10 and 100 nM (Figure 2B). Apart from individual variations, distinct drug efficacies associated with healthy cell

lineages were detected equally in all patient specimens (Figure 2B and Online Supplementary Figure S7).

Venetoclax shows variable dose-dependent efficacy on hematopoietic cell types

Preclinical and clinical activity of venetoclax has been well documented for several B-cell malignancies.¹⁷⁻²⁰ We measured the response to venetoclax, which is highly selective for BCL2, and navitoclax, which targets BCL2, BCL-W and BCL-XL. Both inhibitors were similarly effective against lymphocytes (Figure 2B). Within the lymphocyte compartment, the highest sensitivity to venetoclax was detected for CD19⁺ cells (Figures 2B, and 3A and B) with the majority of samples (Cohort I) responding at subnanomolar concentrations (IC₅₀, 0.4-12 nM). Activity towards CD3⁺CD4⁺ cells was observed at 10-100-fold higher concentrations (IC₅₀, 8-140 nM). A further reduction in response (Figure 3B) was observed for CD56⁺, CD3⁺CD4⁺ and CD3⁺CD56⁺ cells (IC₅₀, ≈100 nM to 1 μM). Monocytes and granulocytes were sensitive to BCL2 inhibitors only at the highest concentration (10 μM) and were considered largely resistant (Figure 2B). This dose-dependent effect on cell types is particularly relevant when treating elderly patients, with frequent age-related

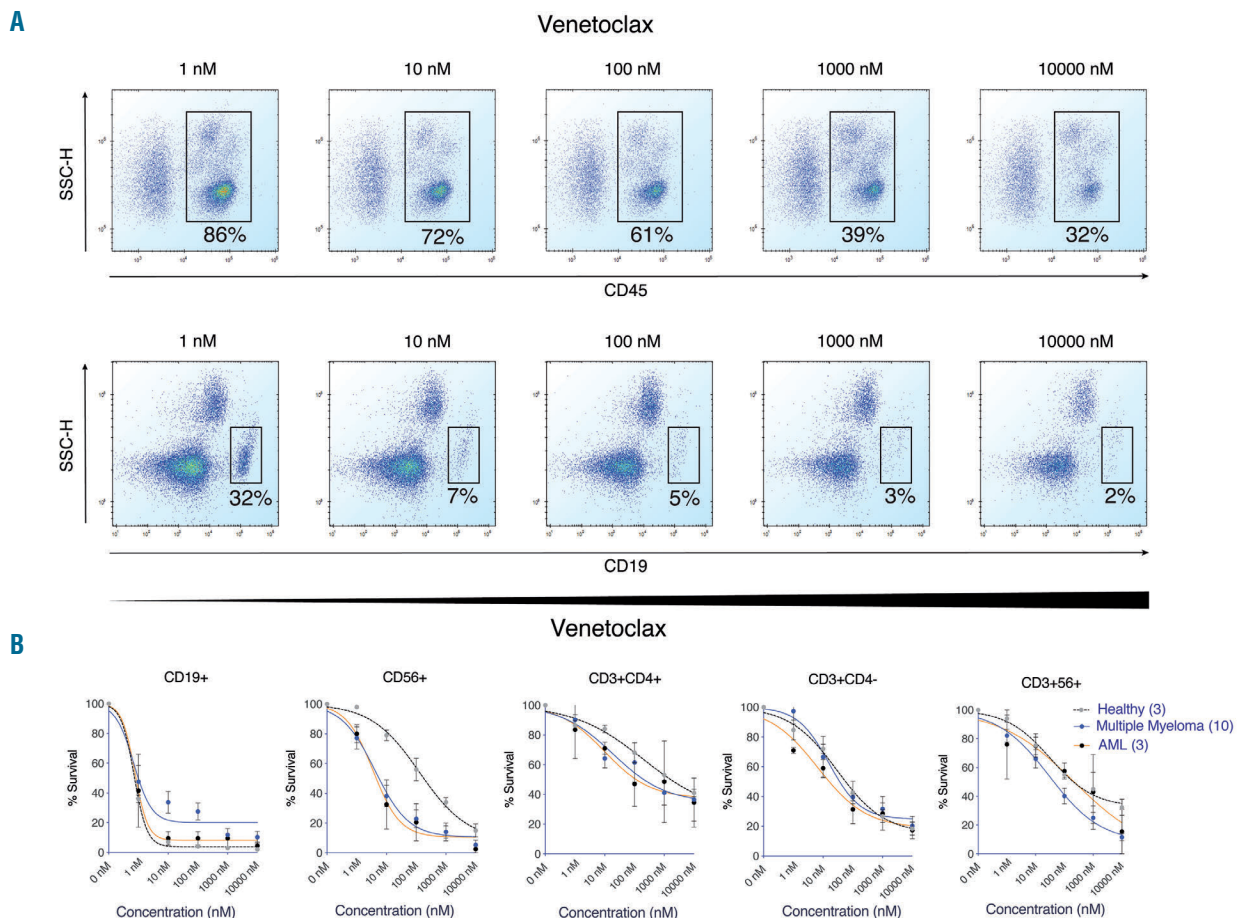


Figure 3. Variable dose-dependent activity of venetoclax on leukocytes. (A) Scatter diagram displaying dose-dependent cytotoxicity of venetoclax (1-10,000 nM) in CD45⁺ (upper panel) and CD45⁺CD19⁺ (lower panel) cells for a single patient. (B) Averaged dose response graphs generated for different immune cell subtypes derived from healthy (n=3), acute myeloid leukemia (AML) (n=3), and multiple myeloma (MM) (n=10) samples showed venetoclax sensitivity in CD19⁺/B cells with an IC₅₀ <1 nM. CD3⁺CD4⁺ cytotoxic T cells were more sensitive compared to CD3⁺CD4⁺ T-helper cells. Data are presented as mean±standard error of mean responses for the tested samples in each disease group. Mean IC₅₀ values for the analyzed samples are listed in Online Supplementary Table S4.

decline in drug metabolism and excretion,^{21,22} which can result in drug accumulation leading to unintended effects on other immune cells. Venetoclax displayed similar cell-specific effects in all tested samples, whether healthy or malignant, suggesting the variation in response is purely lineage specific.

Lineage specific effect of midostaurin on CD19⁺ cells is comparable to FLT3-mutated acute myeloid leukemia cells

In our primary screen, we observed selective depletion of B and NK cells in PB samples (n=3) treated with midostaurin (Figure 2A and *Online Supplementary Figure S8A*), which is approved for treating *FLT3*-mutated AML and systemic mastocytosis.^{23,24} To evaluate CD19⁺ cell specificity in malignant cells such as in CLL and to compare the response to *FLT3*-ITD-mutated AML cells, we tested midostaurin in 17 additional samples (Cohort II) derived from healthy (n=2), CLL (n=7), and AML patients with wild-type (WT) *FLT3* (n=3) or harboring the *FLT3*-ITD mutation (n=5). Variable sensitivity was noted in the CD34⁺CD38⁻ population, presumably leukemic stem cells, from all tested AML samples regardless of *FLT3* mutation status (Figure 4A). CD34⁺CD38⁺/blast cells from all *FLT3*-ITD mutated AML samples were sensitive (median IC₅₀, 554 nM) (Figure 4B). Remarkable sensitivity (IC₅₀, 16 nM) was detected in the CD34⁺CD38⁺ fraction from one of the

three WT samples (*Online Supplementary Figure S8B*). While CD34⁺CD38⁻ cells from healthy donors were insensitive, CD34⁺CD38⁺ cells from one healthy individual responded similarly to *FLT3*-ITD-mutated AML samples (*Online Supplementary Figure S8B*). Importantly, we observed high efficacy against CD19⁺ cells in all tested samples including those derived from CLL patients (Figure 4C, D and *Online Supplementary Figure S8C*) indicating a lineage specific effect. The effect on CD19⁺/B cells (median IC₅₀, 314 nM) was comparable to *FLT3*-ITD mutated AML CD34⁺CD38⁺ (blast) cells (Figure 4B and C). Our results suggest a need for further investigation to evaluate midostaurin efficacy in diseases affecting B-cell lineages such as CLL.

Characterizing protein abundance and basal cell signaling contributing to innate cellular response to therapies

Having determined lineage specificity of the tested small molecules, we next explored whether protein abundance or basal signaling profiles of specific cell populations could explain the innate cellular responses. We also investigated whether healthy cells share identical basal activity for signaling proteins as patient-derived cells or whether basal intracellular signaling was deregulated during malignant transformation. To characterize and compare the proteomic background of healthy hematopoietic

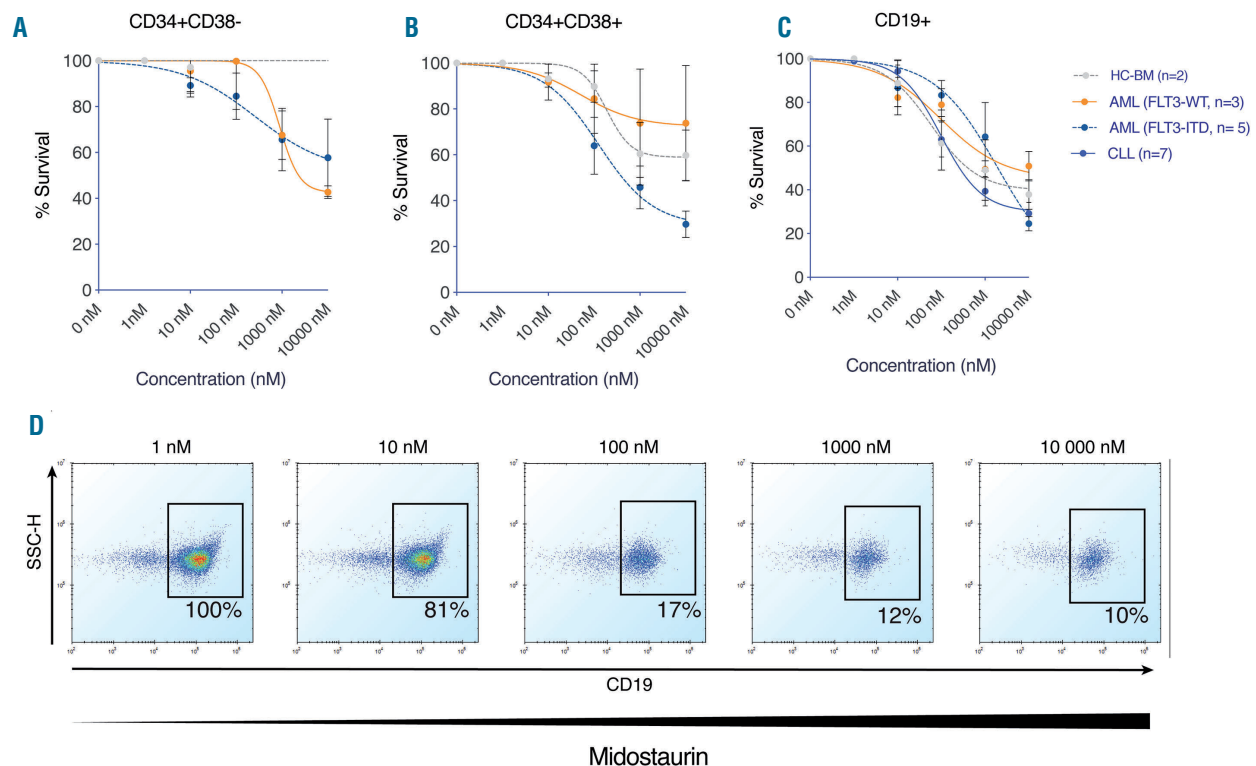


Figure 4. Effect of midostaurin on the viability of CD34⁺CD38⁻, CD34⁺CD38⁺ and CD19⁺ cells derived from healthy donors, and acute myeloid leukemia (AML) or chronic lymphocytic leukemia (CLL) patients. Averaged dose response curves for disease categories are presented as mean±standard error of mean. (A) While midostaurin treatment had no effect on CD34⁺CD38⁻ cells from healthy individuals, variable sensitivity was detected in AML samples. (B) CD34⁺CD38⁺ cells derived from *FLT3*-ITD-mutated AML samples displayed similar sensitivity (median IC₅₀, 554nM). (C) CD19⁺ cells derived from healthy donor or patient samples showed comparable sensitivity at a median IC₅₀ of 319 nM. Individual dose response curves are provided in *Online Supplementary Figure S8C*. (D) Scatter plot showing dose responses for midostaurin in CD19⁺ cells from a CLL patient. The percentage of CD19⁺ live cells present in midostaurin-treated wells compared to untreated cells is displayed numerically on the plot. Cellular proportions for these samples are provided in *Online Supplementary Table S5*. Related IC₅₀ values are provided in *Online Supplementary Table S6*.

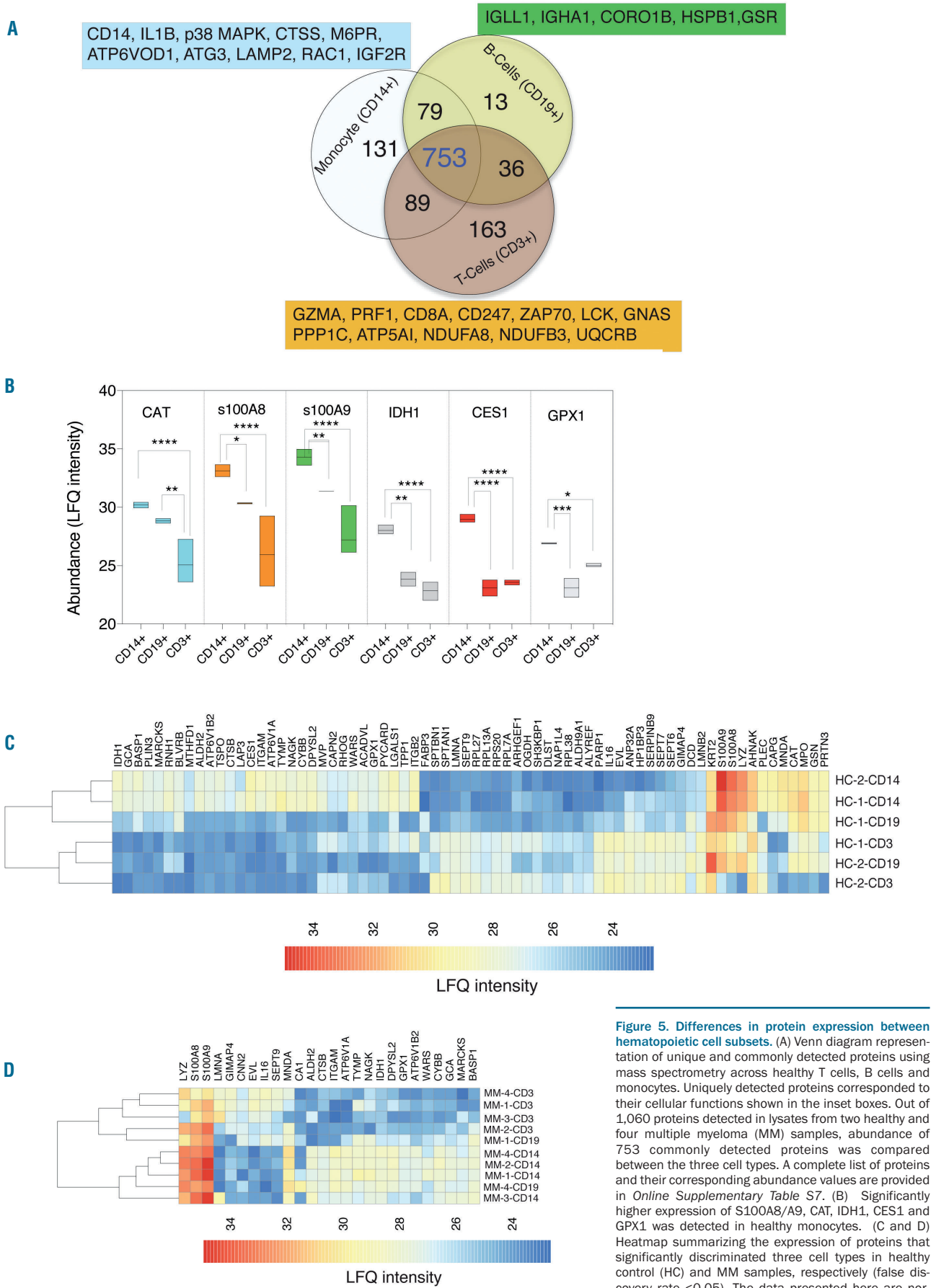


Figure 5. Differences in protein expression between hematopoietic cell subsets. (A) Venn diagram representation of unique and commonly detected proteins using mass spectrometry across healthy T cells, B cells and monocytes. Uniquely detected proteins corresponded to their cellular functions shown in the inset boxes. Out of 1,060 proteins detected in lysates from two healthy and four multiple myeloma (MM) samples, abundance of 753 commonly detected proteins was compared between the three cell types. A complete list of proteins and their corresponding abundance values are provided in *Online Supplementary Table S7*. (B) Significantly higher expression of S100A8/A9, CAT, IDH1, CES1 and GPX1 was detected in healthy monocytes. (C and D) Heatmap summarizing the expression of proteins that significantly discriminated three cell types in healthy control (HC) and MM samples, respectively (false discovery rate <0.05). The data presented here are normalized label-free quantification (LFQ) intensity values for the proteins.

cells, we utilized a mass spectrometry-based quantitative proteomics approach to profile B cells (CD19⁺), T cells (CD3⁺) and monocytes (CD14⁺) derived from two healthy donors (Figure 5). We then employed CyTOF to compare the basal activity of nine proteins (in healthy and leukemic cell subsets) involved in MAPK, JAK-STAT, NF- κ B and PI3K-mTOR signaling, which are commonly activated in many hematologic malignancies²⁵⁻²⁸ (Figure 6). By sample barcoding and subsequent pooling prior to antibody staining, CyTOF allows for direct comparison of the phosphorylation level of target proteins between multiple donors with high fidelity.^{19,20}

Monocytes show higher expression of calprotectin (S100A8/S100A9), which is associated with dexamethasone resistance - By quantitative mass spectrometry-based proteomics, a total of 1,060 proteins were detected. Among these, 163, 131 and 13 proteins were only identified in CD3, CD14 and CD19 lysates, respectively (Figure 5A, *Online Supplementary Table S7*). The uniquely expressed proteins were associated with biological processes consistent with the functional differences between these cell types (*Online Supplementary Figure S9*). For instance, the proteome signature in monocytes was enriched in biological processes related to phagosome maturation (ATP6V0D1, CTSS, M6PR), autophagy (ATG3, LAMP2), PPAR- α /RAR α activation (IL1 β , p38 MAPK, GPD2, PLCG2), and STAT3 signaling (IGF2R, RAC1, p38 MAPK). Immunoglobulins (IGLL1, IGHA1) were identified in B-cell fractions. T cells expressed proteins related to T-cell receptor signaling (CD8A, CD247, LCK, ZAP70), granzyme signaling (GZMA, PRF1), and oxidative phosphorylation (ATP5I, NDUFA8, NDUFB3, UQCRCB). Besides observed differences in the abundance of proteins, variable expression in commonly detected proteins was noted (Figure 5B and C). Enzymes associated with scavenging reactive oxygen species such as catalase (CAT) and glutathione peroxidase 1 (GPX1) were expressed at a significantly higher ($P < 0.001$) level in monocytes (Figure 5B). In addition, monocytes exhibited elevated expression of isocitrate dehydrogenase 1 (IDH1), carboxylesterase 1 (CES1), and inflammatory protein calprotectin, a heterodimer of two proteins S100A8/S100A9 that can mediate dexamethasone resistance in patients.^{29,30} We further compared the protein expression profiles for these cell subsets between healthy and four MM patients, and found an identical pattern of expression for CAT, GPX1 and S100A8/9 proteins (Figure 5D). While expression of 16 proteins differed between healthy and MM samples [false discovery rate (FDR) < 0.05], no significant differences were noted for CD14⁺ and CD3⁺ lysates (< 3 proteins).

Mapping shared signaling activities in healthy and leukemic hematopoietic cell subsets - NF- κ B phosphorylation was detected in most cell types. Compared to other cell types, higher pNF- κ B was detected in T/CD3 cells (*Online Supplementary Figure S10*). Significantly higher mTOR signaling, as measured by p4E-BP1 and pPLC- γ 1, was observed in healthy CD34⁺CD38⁺ cells, monocytes, granulocytes (neutrophils) and B cells (Figure 6A-C). These cell types also tended to have elevated sensitivity to omipalisib (PI3K/mTOR inhibitor) compared to other cell types in healthy or malignant samples (Figure 2B and Figure 7E). T cells lacking sensitivity to PI3K/mTOR inhibitors showed reduced mTOR signaling activity (Figure 6A-C).

CD34⁺CD38⁺ cells also exhibited high levels of ERK phosphorylation (Figure 6A-C). ERK phosphorylation status, however, did not correlate to increased trametinib sensitivity in monocytes. An inverse relation between pSTAT3 levels and venetoclax sensitivity was observed among the different cell populations. Heightened levels of pSTAT3 were detected in monocytes and granulocytes, which lacked sensitivity to venetoclax (Figure 6A-D). In contrast, a lower level of pSTAT3 was observed in venetoclax sensitive B and NK cells. Two related but distinct cell types, CD3⁺CD4⁺ and CD3⁺CD8⁺ T cells, exhibited a difference in the level of pSTAT3 (Figure 6B) that might explain their subtle difference in sensitivity to venetoclax (Figure 6D). Comparison of signaling patterns detected in healthy PB or BM cells to corresponding leukemic cells expressing identical surface markers revealed remarkable similarity (Figure 6A-C), strengthening their association with cellular phenotypes. Furthermore, monitoring changes in signaling pattern for these proteins upon treatment with increasing concentrations (0 nM, 10 nM and 10 μ M) of venetoclax in healthy PB (n=3), revealed that the directionality or magnitude of signaling changes for some of these proteins (i.e. pPLC- γ 1 and pCREB) were also similar across these cell types (*Online Supplementary Figure S11*).

Innate drug sensitivities in cell subsets are retained in their malignant counterparts in different hematologic malignancies

To further confirm the similarity in drug responses between healthy and patient-derived cell subsets observed using the single cell assay, we compared *ex vivo* drug responses detected in bead-enriched healthy cells (CD3⁺, CD14⁺, CD19⁺, CD34⁺ and CD138⁺) to a cohort of 281 primary samples derived from multiple hematologic malignancies. For these analyses, we generated data using the CellTiter-Glo[®] viability assay. In agreement with non-selective effects detected on healthy cell types, bortezomib activity was detected in a wide range of hematologic malignancies (Figure 7A). The highest clofarabine efficacy was observed in CD3⁺ T cells and in the T-cell prolymphocytic leukemia (T-PLL) patient subset (Figure 7B), which is reflective of the clinical success observed with other purine analogs (fludarabine or cladribine) in T-PLL. Reduced activity of the purine analog clofarabine was detected in both healthy and myeloma derived CD138⁺ cells. Although dexamethasone was found to be most effective in B-ALL and CLL, modest *ex vivo* effects were observed in other lymphocytic and plasma cell malignancies, including T-ALL, T-PLL, B-PLL, and MM (Figure 7C). Disease-specific acquisition of sensitivity was also noted in a subset of AML patients, which was undetectable in healthy CD34⁺ (Figure 7C) or CD34⁺CD38⁺ (Figure 4B) cells. T-cell malignancies, similar to healthy T cells, showed no response to omipalisib. Consistent with responses observed in healthy B cells, a higher response to venetoclax was detected in malignant B-cell types (Figure 7F). T-PLL samples also exhibited sensitivity to venetoclax, which has been tested more recently in two T-PLL patients with measurable clinical benefit.³² Venetoclax response agreed with navitoclax responses in B-cell diseases (Figure 7F). Increased sensitivity to navitoclax compared to venetoclax was detected in CML, T-ALL, and MM samples (Figure 7E and F). B-cell specific responses to midostaurin were detected in CLL and ALL samples (Figure 4C and *Online*

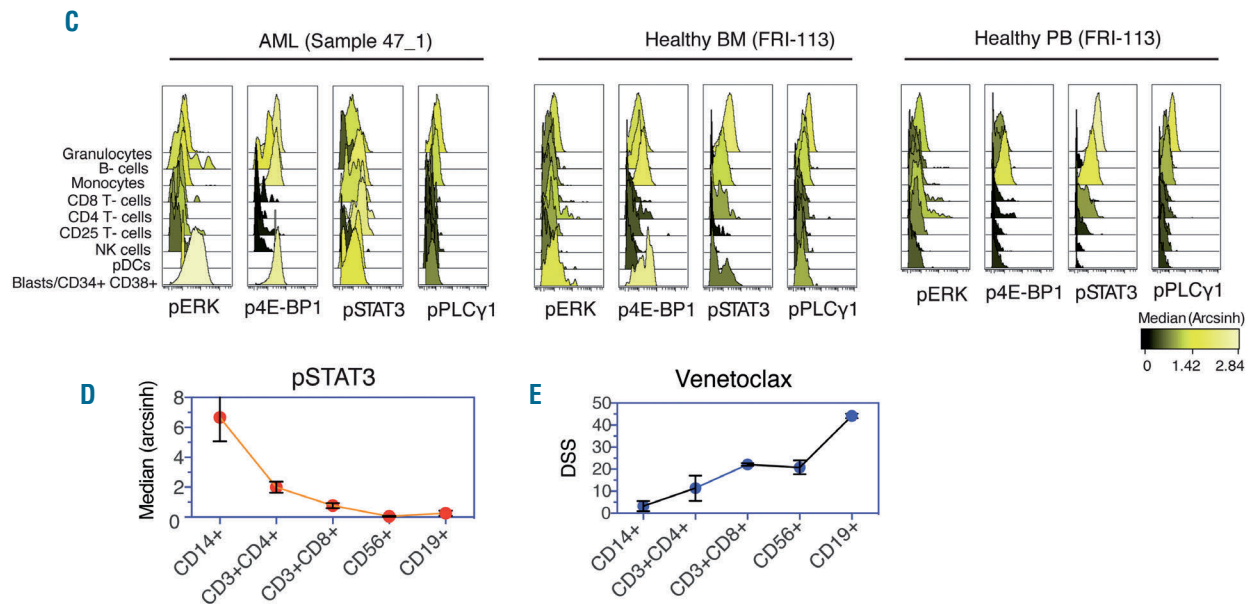


Figure 6. (continued from the previous page) (C) Stacked histogram representations of pERK, p4E-BP1, pSTAT3 and pPLC γ 1 phosphorylation status across cell types in an AML patient and healthy donor samples (paired BM and PB). Immunophenotype of the presented samples are provided in *Online Supplementary Figure S1B*. (D) Phosphorylation of STAT3 in five healthy cell types from three healthy individuals presented as mean \pm standard error of mean (SEM) arcsinh values derived from mass cytometry analysis. (E) Venetoclax response in cell types displayed as SEM of drug sensitivity score (DSS) values for three healthy donors. A higher response to venetoclax correlated with reduced phosphorylation of STAT3. PDC: plasmacytoid dendritic cells; NK: natural killer.

Discussion

Applying a high throughput, multi-parametric single-cell assay, we aimed to assess the diversity in drug effects on multiple cell populations in individual donor samples. Therapeutic efficacy was determined *ex vivo* using complex mixtures of cells to more realistically recapitulate the native environment. Our results demonstrate that cell subtypes are drastically different from each other with respect to macromolecule abundance, signaling profiles and drug-response patterns against a diverse collection of anticancer drugs. As such, this study provides a comprehensive portrait of the drug sensitivity landscape in hematologic cell subsets and reveals drug responses that are tied to specific cell lineages. Importantly, cell subset-specific sensitivity and resistance mechanisms were clearly reflected in their malignant counterpart.

Variation in drug responses can arise in healthy hematologic cell subsets due to differences in signaling state and transcriptional programs attributed to their cellular function or phenotype. Many of the signaling events are tightly regulated in cellular subsets² and may often determine their innate sensitivity to drug treatment. For example, the basal state of pSTAT3 could explain the diversity of the *ex vivo* responses to BCL2 inhibitors observed between healthy cell subsets. In relation to this, we have previously reported a critical role of the JAK-STAT pathway in venetoclax resistance in AML, which could be reversed using a combination of the JAK1/2 inhibitor ruxolitinib, and venetoclax.³² Although changes in signaling behaviors are commonly detected in malignant cells,⁷ understanding basal signaling in the cell-of-origin is fundamental to identify cancer vulnerabilities or off target effects that are lineage specific.

Profiling healthy and malignant cells (from multiple

hematologic malignancies) revealed that the cell-of-origin associated signaling events and drug responses were also retained in the disease context of the affected cell type. Hence, the profiling presented here provides new targeting opportunities in previously unexplored disease indications. Venetoclax sensitivity in B cells may reflect its efficacy in CLL and other B-cell malignancies,³³ which could also be exploited in diseases where B-cell depletion is considered, i.e. in rheumatoid arthritis. Similar to other studies,^{34,35} we demonstrated midostaurin efficacy in CLL and ALL, which may be ascribed to the intrinsic response detected in CD19⁺ cells. Efficacy was also detected in CD34⁺CD38⁺ cells from AML (n=1) with WT *FLT3*. This observation may reflect its efficacy reported in AML with WT *FLT3*.²⁴ Although NK-cell malignancies are rare, they are often highly aggressive and refractory in nature.³⁶ We found that dexamethasone and midostaurin targeted NK cells with similar efficacy as B cells, implicating a potential clinical utility of these drugs for NK-cell malignancies.

Expression of antioxidant enzymes and calprotectin (S100A8/S100A9) is associated with drug resistance, including resistance to dexamethasone, which has been documented in both hematologic and solid tumors.^{29,37-40} We noted that healthy monocytes displaying elevated expression of these proteins are intrinsically resistant to dexamethasone. Dexamethasone induced apoptosis of lymphocytes is attributed to free radical generation, an effect that can be counteracted by antioxidant enzymes such as catalase, which may itself confer in monocytes resistance to steroids.^{30,41} Furthermore, the monocyte expansion observed with dexamethasone treatment could be explained by its ability to mimic IL1 β activation of IL1R,⁴² which stimulates their proliferation. This phenomenon had previously been observed in murine

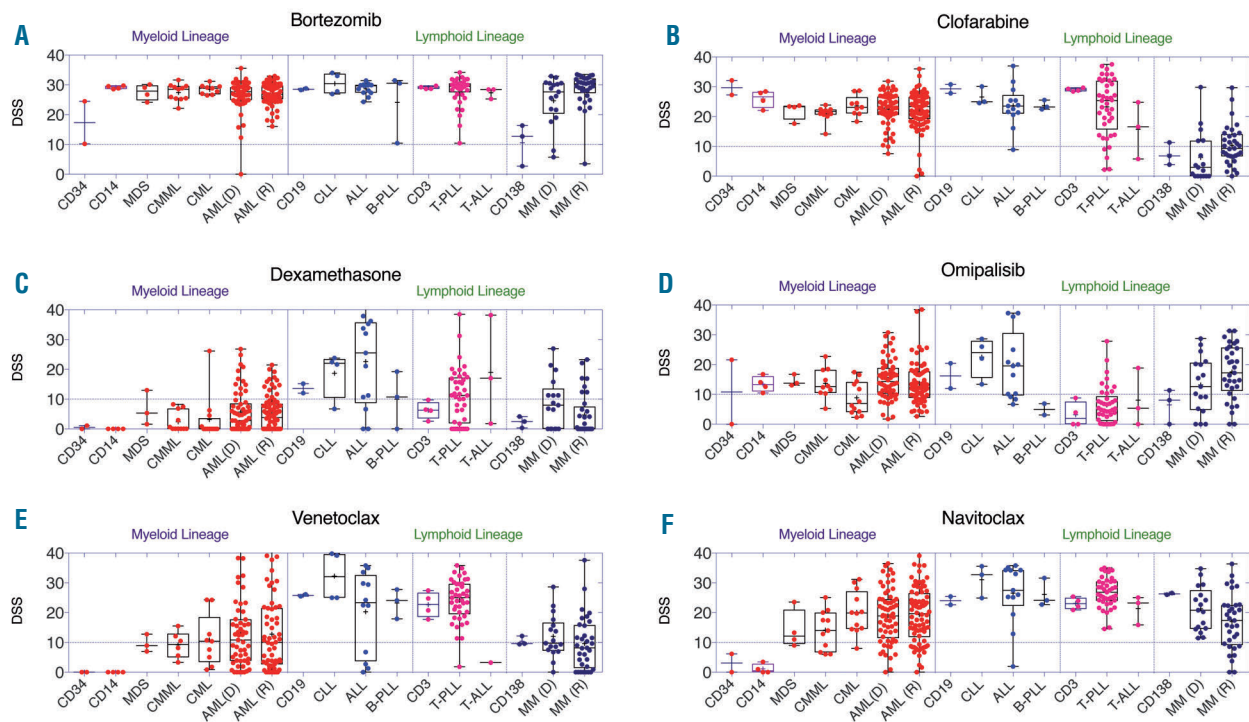


Figure 7. Systematic comparison of drug responses in healthy cell-of-origin and corresponding cell types from hematologic malignancies. (A-F) *Ex vivo* drug responses presented as drug sensitivity scores (DSS) of healthy cell types (CD3, n=4; CD14, n=4; CD19, n=2; CD34, n=2; and CD138, n=3) were compared to malignant counterparts in a cohort of 281 primary samples for bortezomib, clofarabine, dexamethasone, omipalisib, venetoclax and navitoclax. Samples included both published and unpublished datasets generated at our facility for chronic myeloid leukemia (CML) (n=13),^{10,11} chronic myelomonocytic leukemia (CMML) (n=11),¹² myelodysplastic syndromes (MDS) (n=4), acute myeloid leukemia (AML) (n=145),^{9,12} B-cell acute lymphoblastic leukemia (B-ALL) (n=14),¹³ chronic lymphocytic leukemia (CLL) (n=4),¹² T-cell prolymphocytic leukemia (T-PLL) (n=40),¹⁴ multiple myeloma (MM) (n=50)¹⁵ and other hematologic malignancies (n=6). AML and MM samples were subdivided depending on whether they were derived from newly diagnosed (D) and relapsed (R) samples. T-PLL and MM samples were tested with enriched CD3⁺ and CD138⁺ cells. Results provide evidence that response in healthy cell subsets is predictive of responses observed in the malignant cell counterparts. A comparison between drug effects on CD14⁺ and CD34⁺ cells derived from healthy individuals and AML samples are displayed in *Online Supplementary Figure S13 and S14*. B-PLL: B-cell prolymphocytic leukemia.

monocytes,⁴³ as well in acute monocytic leukemia [AML, French-American-British (FAB) subtype M5] where glucocorticoid treatment may further lead to an increase in blast population, fueling disease progression.⁴⁴ Therefore, understanding the cytoprotective mechanisms operating in healthy cell subsets could also provide crucial insights into drug resistance mechanisms in patients.

Cancer immunotherapies and drugs modulating the immune system are emerging as important treatment modalities for hematologic and solid tumors.^{45,46} Preserving cytotoxic lymphocytes is critical for their efficacy and may have significant consequences on long-lasting anti-tumor adaptive immunity, likely responsible for durable clinical responses. In our study, few inhibitors showed a selective effect on a single cell type; instead, effects were either directed to multiple cell types or in a non-selective manner to all exposed cells. For example, dexamethasone and midostaurin depleted CD19⁺ B cells and CD56⁺ NK cells. Similarly, venetoclax depleted CD3⁺CD4⁺ cytotoxic T cells, among other cell types. Reduction of immune effector cells (mainly cytotoxic T cells and NK cells) are particularly relevant because of their key role in cancer immunosurveillance and immunotherapy.⁴⁷ Therefore, profiling the unintended effects of small molecules on effector cells, which are used in combination with immunotherapies, is fundamental to the selection of

rational combination partners, and to preserve the quality and quantity of immune cells in patients.

In summary, the findings presented in this study suggest that dissecting drug responses in hematologic cell lineages could represent an invaluable tool to reveal the full spectrum of cellular effects, identify novel drug resistance mechanisms, and to predict off target effects of small molecules. We envision that incorporating the assessment of cell lineage-specific drug responses into routine procedures in preclinical drug development holds great promise in identifying new therapeutic niches of small molecules and improve precision in therapies, particularly for hematologic malignancies.

Acknowledgments

The authors thank the patients, healthy donors and participating clinics for their generous contributions. Members of the High Throughput Biomedicine Unit at FIMM, Flow Cytometry Core Facility at UiB, and Mass Spectrometry Facility at Maynooth University, are greatly appreciated for their support and expertise. Special appreciation to Minna Suvola and Siv Knaappila for their excellent technical support. The Bergen Research Foundation is acknowledged for support of the Helios CyTOF instrumentation. MH and BTG were supported by the Norwegian Cancer Society project n. 144345. The study was supported by funding from the Cancer Society of Finland.

References

- Jassinskaja M, Johansson E, Kristiansen TA, et al. Comprehensive Proteomic Characterization of Ontogenic Changes in Hematopoietic Stem and Progenitor Cells. *Cell Rep.* 2017;21(11):3285-3297.
- Bendall SC, Simonds EF, Qiu P, et al. Single-cell mass cytometry of differential immune and drug responses across a human hematopoietic continuum. *Science.* 2011;332(6030):687-696.
- Compagno M, Wang Q, Pighi C, et al. Phosphatidylinositol 3-kinase delta blockade increases genomic instability in B cells. *Nature.* 2017;542(7642):489-493.
- Robak T, Robak P. BCR signaling in chronic lymphocytic leukemia and related inhibitors currently in clinical studies. *Int Rev Immunol.* 2013;32(4):358-376.
- Irish JM, Hovland R, Krutzik PO, et al. Single cell profiling of potentiated phospho-protein networks in cancer cells. *Cell.* 2004;118(2):217-228.
- Bodenmiller B, Zunder ER, Finck R, et al. Multiplexed mass cytometry profiling of cellular states perturbed by small-molecule regulators. *Nat Biotechnol.* 2012;30(9):858-867.
- Irish JM, Kotecha N, Nolan GP. Mapping normal and cancer cell signalling networks: towards single-cell proteomics. *Nat Rev Cancer.* 2006;6(2):146-155.
- Krutzik PO, Crane JM, Clutter MR, Nolan GP. High-content single-cell drug screening with phosphospecific flow cytometry. *Nat Chem Biol.* 2008;4(2):132-142.
- Pemovska T, Kontro M, Yadav B, et al. Individualized Systems Medicine Strategy to Tailor Treatments for Patients with Chemorefractory Acute Myeloid Leukemia. *Cancer Discov.* 2013;3(12):1416-1429.
- Pietarinen PO, Pemovska T, Kontro M, et al. Novel drug candidates for blast phase chronic myeloid leukemia from high-throughput drug sensitivity and resistance testing. *Blood Cancer J.* 2015;5:e309.
- Pietarinen PO, Eide CA, Ayuda-Duran P, et al. Differentiation status of primary chronic myeloid leukemia cells affects sensitivity to BCR-ABL1 inhibitors. *Oncotarget.* 2017;8(14):22606-22615.
- Kontro M, Kumar A, Majumder MM, et al. HOX gene expression predicts response to BCL-2 inhibition in acute myeloid leukemia. *Leukemia.* 2017;31(2):301-309.
- Eldfors S, Kuusanmaki H, Kontro M, et al. Idelalisib sensitivity and mechanisms of disease progression in relapsed TCF3-PBX1 acute lymphoblastic leukemia. *Leukemia.* 2017;31(1):51-57.
- Andersson EI, Putzer S, Yadav B, et al. Discovery of novel drug sensitivities in T-PLL by high-throughput ex vivo drug testing and mutation profiling. *Leukemia.* 2018;32(3):774-787.
- Majumder MM, Silvennoinen R, Anttila P, et al. Identification of precision treatment strategies for relapsed/refractory multiple myeloma by functional drug sensitivity testing. *Oncotarget.* 2017;8(34):56338-56350.
- Yadav B, Pemovska T, Sz wajda A, et al. Quantitative scoring of differential drug sensitivity for individually optimized anticancer therapies. *Sci Rep.* 2014;4:5193.
- Cang S, Iragavarapu C, Savooji J, Song Y, Liu D. ABT-199 (venetoclax) and BCL-2 inhibitors in clinical development. *J Hematol Oncol.* 2015;8:129.
- Edelmann J, Gribben JG. Managing Patients with TP53-Deficient Chronic Lymphocytic Leukemia. *J Oncol Pract.* 2017;13(6):371-377.
- Leonard JT, Rowley JS, Eide CA, et al. Targeting BCL-2 and ABL/LYN in Philadelphia chromosome-positive acute lymphoblastic leukemia. *Sci Transl Med.* 2016;8(354):354ra114.
- Rosenthal A. Small Molecule Inhibitors in Chronic Lymphocytic Lymphoma and B Cell Non-Hodgkin Lymphoma. *Curr Hematol Malig Rep.* 2017;12(3):207-216.
- Mangoni AA, Jackson SH. Age-related changes in pharmacokinetics and pharmacodynamics: basic principles and practical applications. *Br J Clin Pharmacol.* 2004;57(1):6-14.
- ElDesoky ES. Pharmacokinetic-pharmacodynamic crisis in the elderly. *Am J Ther.* 2007;14(5):488-498.
- Garcia JS, Percival ME. Midostaurin for the treatment of adult patients with newly diagnosed acute myeloid leukemia that is FLT3 mutation-positive. *Drugs Today (Barc).* 2017;53(10):531-543.
- Stone RM, Manley PW, Larson RA, Capdeville R. Midostaurin: its odyssey from discovery to approval for treating acute myeloid leukemia and advanced systemic mastocytosis. *Blood Adv.* 2018;2(4):444-453.
- Kawauchi K, Ogasawara T, Yasuyama M, Otsuka K, Yamada O. Regulation and importance of the PI3K/Akt/mTOR signaling pathway in hematologic malignancies. *Anticancer Agents Med Chem.* 2009;9(9):1024-1038.
- Yamada O, Kawauchi K. The role of the JAK-STAT pathway and related signal cascades in telomerase activation during the development of hematologic malignancies. *JAKSTAT.* 2013;2(4):e25256.
- Ward AF, Braun BS, Shannon KM. Targeting oncogenic Ras signaling in hematologic malignancies. *Blood.* 2012;120(17):3397-3406.
- Springuel L, Renauld JC, Knoops L. JAK kinase targeting in hematologic malignancies: a sinuous pathway from identification of genetic alterations towards clinical indications. *Haematologica.* 2015;100(10):1240-1253.
- Spijkers-Hagelstein JA, Schneider P, Hulleman E, et al. Elevated S100A8/S100A9 expression causes glucocorticoid resistance in MLL-rearranged infant acute lymphoblastic leukemia. *Leukemia.* 2012;26(6):1255-1265.
- Tome ME, Baker AF, Powis G, Payne CM, Briehl MM. Catalase-overexpressing thymocytes are resistant to glucocorticoid-induced apoptosis and exhibit increased net tumor growth. *Cancer Res.* 2001;61(6):2766-2773.
- Boidol B, Kornauth C, van der Kouwe E, et al. First-in-human response of BCL-2 inhibitor venetoclax in T-cell prolymphocytic leukemia. *Blood.* 2017;130(23):2499-2503.
- Karjalainen R, Pemovska T, Popa M, et al. JAK1/2 and BCL2 inhibitors synergize to counteract bone marrow stromal cell-induced protection of AML. *Blood.* 2017;130(6):789-802.
- Dauids MS, Roberts AW, Seymour JF, et al. Phase I First-in-Human Study of Venetoclax in Patients With Relapsed or Refractory Non-Hodgkin Lymphoma. *J Clin Oncol.* 2017;35(8):826-833.
- Gallooly MM, Lazarus HM. Midostaurin: an emerging treatment for acute myeloid leukemia patients. *J Blood Med.* 2016;7:73-83.
- Ganeshaguru K, Wickremasinghe RG, Jones DI, et al. Actions of the selective protein kinase C inhibitor PKC412 on B-chronic lymphocytic leukemia cells in vitro. *Haematologica.* 2002;87(2):167-176.
- Cheung MM, Chan JK, Wong KF. Natural killer cell neoplasms: a distinctive group of highly aggressive lymphomas/leukemias. *Semin Hematol.* 2003;40(3):221-232.
- Reeb AN, Li W, Sewell W, et al. S100A8 is a novel therapeutic target for anaplastic thyroid carcinoma. *J Clin Endocrinol Metab.* 2015;100(2):E232-242.
- Wang Y, Guo A, Liang X, et al. HRD1 sensitizes breast cancer cells to Tamoxifen by promoting S100A8 degradation. *Oncotarget.* 2017;8(14):23564-23574.
- Yang M, Zeng P, Kang R, et al. S100A8 contributes to drug resistance by promoting autophagy in leukemia cells. *PLoS One.* 2014;9(5):e97242.
- Yang XY, Zhang MY, Zhou Q, et al. High expression of S100A8 gene is associated with drug resistance to etoposide and poor prognosis in acute myeloid leukemia through influencing the apoptosis pathway. *Onco Targets Ther.* 2016;9:4887-4899.
- Tome ME, Jaramillo MC, Briehl MM. Hydrogen peroxide signaling is required for glucocorticoid-induced apoptosis in lymphoma cells. *Free Radic Biol Med.* 2011;51(11):2048-2059.
- Dubois CM, Neta R, Keller JR, Jacobsen SE, Oppenheim JJ, Ruscetti F. Hematopoietic growth factors and glucocorticoids synergize to mimic the effects of IL-1 on granulocyte differentiation and IL-1 receptor induction on bone marrow cells in vivo. *Exp Hematol.* 1993;21(2):303-310.
- Trottier MD, Newsted MM, King LE, Fraker PJ. Natural glucocorticoids induce expansion of all developmental stages of murine bone marrow granulocytes without inhibiting function. *Proc Natl Acad Sci U S A.* 2008;105(6):2028-2033.
- Klein K, Haarman EG, de Haas V, Zwaan Ch M, Creutzig U, Kaspers GL. Glucocorticoid-Induced Proliferation in Untreated Pediatric Acute Myeloid Leukemia Blasts. *Pediatr Blood Cancer.* 2016;63(8):1457-1460.
- Deligne C, Milcent B, Josseume N, Teillaud JL, Siberil S. Impact of Depleting Therapeutic Monoclonal Antibodies on the Host Adaptive Immunity: A Bonus or a Malus? *Front Immunol.* 2017;8:950.
- Gandhi AK, Kang J, Havens CG, et al. Immunomodulatory agents lenalidomide and pomalidomide co-stimulate T cells by inducing degradation of T cell repressors Ikaros and Aiolos via modulation of the E3 ubiquitin ligase complex CRL4(CRBN). *Br J Haematol.* 2014;164(6):811-821.
- Longwe H, Phiri KS, Mbeye NM, Gondwe T, Jambo KC, Mandala WL. Proportions of CD4+, CD8+ and B cell subsets are not affected by exposure to HIV or to Cotrimoxazole prophylaxis in Malawian HIV-uninfected but exposed children. *BMC Immunol.* 2015;16:50.

Synergistic effects of PRIMA-1^{Met} (APR-246) and 5-azacitidine in TP53-mutated myelodysplastic syndromes and acute myeloid leukemia

Nabih Maslah,^{1,2,3} Norman Salomao,³ Louis Drevon,³ Emmanuelle Verger,^{1,3} Nicolas Partouche,⁴ Pierre Ly,¹ Philippe Aubin,¹ Nadia Naoui,¹ Marie-Helene Schlageter,^{1,3} Cecile Bally,⁵ Elsa Miekoutima,⁵ Ramy Rahmé,⁵ Jacqueline Lehmann-Che,^{2,6} Lionel Ades,^{2,3,5} Pierre Fenaux,^{2,3,5} Bruno Cassinat^{1,3#} and Stephane Giraudier^{1,2,3#}

¹APHP, Service de Biologie Cellulaire, Hôpital Saint-Louis, Paris; ²Faculté de Médecine Université Paris Diderot Paris 7, Paris; ³INSERM UMR-S 1131, Hôpital Saint-Louis, Paris; ⁴Faculté de Médecine Paris 12-UPEC, Hôpital Henri Mondor, APHP, Créteil; ⁵APHP, Service d'Hématologie Senior, Hôpital Saint-Louis, Paris and ⁶Unité d'Oncologie Moléculaire, Hôpital Saint-Louis, APHP, Paris, France

[#]BC and SG contributed equally as co-senior authors



Haematologica 2020
Volume 105(6):1539-1551

ABSTRACT

Myelodysplastic syndromes and acute myeloid leukemia with TP53 mutations are characterized by frequent relapses, poor or short responses, and poor survival with the currently available therapies including chemotherapy and 5-azacitidine (AZA). PRIMA-1^{Met} (APR-246, APR) is a methylated derivative of PRIMA-1, which induces apoptosis in human tumor cells through restoration of the transcriptional transactivation function of mutant p53. Here we show that low doses of APR on its own or in combination with AZA reactivate the p53 pathway and induce an apoptosis program. Functionally, we demonstrate that APR exerts these activities on its own and that it synergizes with AZA in TP53-mutated myelodysplastic syndromes (MDS) / acute myeloid leukemia (AML) cell lines and in TP53-mutated primary cells from MDS / AML patients. Low doses of APR on its own or in combination with AZA also show significant efficacy *in vivo*. Lastly, using transcriptomic analysis, we found that the APR + AZA synergy was mediated by downregulation of the FLT3 pathway in drug-treated cells. Activation of the FLT3 pathway by FLT3 ligand reversed the inhibition of cell proliferation by APR + AZA. These data suggest that TP53-mutated MDS / AML may be better targeted by the addition of APR-246 to conventional treatments.

Introduction

Myelodysplastic syndromes (MDS) are malignant bone marrow disorders characterized by ineffective hematopoiesis leading to refractory cytopenias, and by an increased risk of progression to acute myeloid leukemia (AML).¹ They are prognostically stratified on the basis of the percentage of blasts in the bone marrow, the karyotype, and the number of cytopenias present according to an International Prognostic Scoring System (IPSS),² which was recently revised (revised IPSS, IPSS-R).² Current studies are integrating data on somatic gene mutations into prognostic indices to further refine risk stratification.³⁻⁶ At the genetic level, it is now widely recognized that most of the clinical and pathological features of MDS and AML are the direct result of recurrent acquired somatic genetic lesions. Among these, TP53 gene mutations have been shown to occur in 5-10% of all MDS and AML cases,^{3,5,7,9} including 20-25% of the low-risk MDS with isolated del 5q,⁷ and 40-50% of the MDS and AML with complex karyotypes.⁸⁻¹⁰ Among MDS with complex karyotypes, the presence of TP53 mutations has been correlated with a lower number of other mutations and a poorer outcome.¹¹ Furthermore, the allelic burden of the TP53 mutations has been

Correspondence:

STEPHANE GIRAUDIER
stephane.giraudier@aphp.fr

Received: February 4, 2019.

Accepted: September 4, 2019.

Pre-published: September 5, 2019.

doi:10.3324/haematol.2019.218453

Check the online version for the most updated information on this article, online supplements, and information on authorship & disclosures: www.haematologica.org/content/105/6/1539

©2020 Ferrata Storti Foundation

Material published in Haematologica is covered by copyright. All rights are reserved to the Ferrata Storti Foundation. Use of published material is allowed under the following terms and conditions:

<https://creativecommons.org/licenses/by-nc/4.0/legalcode>. Copies of published material are allowed for personal or internal use. Sharing published material for non-commercial purposes is subject to the following conditions: <https://creativecommons.org/licenses/by-nc/4.0/legalcode>, sect. 3. Reproducing and sharing published material for commercial purposes is not allowed without permission in writing from the publisher.



shown to be a strong predictor of poor overall survival.¹² Mutations of p53 proteins generally result in a loss of their normal functions (including cell cycle and apoptosis control), but can also result in a deleterious “gain of function”. In addition, at least in case of complex karyotypes, *TP53*-mutated MDS/AML generally acquire del17p, i.e. loss of the remaining *TP53* allele. *TP53* mutations correlate with poor overall outcomes in MDS and AML, independently^{4,5,13} or not independently¹⁴ of a complex karyotype. *TP53*-mutated MDS/AML are associated with resistance to treatment, including anthracycline + aracytine combinations, low-dose cytarabine,¹⁴ and allogeneic bone marrow transplantation (BMT),¹⁵ while the hypomethylating agents (HMA) 5-azacitidine (AZA)^{7,15} and decitabine¹⁶ yield somewhat better, albeit transient, results. For this reason, HMA are generally considered to be the first-line treatment of MDS/AML with a *TP53* mutation.

As with many other types of cancer, mutated p53 protein, therefore, appears to be one of the most important therapeutic targets in MDS and AML, and restoration of its biological function could prove to be highly beneficial. PRIMA-1^{Met} (APR-246, APR) is a methylated derivative of PRIMA-1, a compound that induces apoptosis in human tumor cells through restoration of the transcriptional transactivation function to mutant p53.¹⁷ Mechanistically, APR is a prodrug that forms an active moiety that covalently binds to thiol groups of the core domain of mutated p53 protein,¹⁸ thereby resulting in a structural change that restores its active conformation. APR induces dose-dependent apoptosis in various tumor models, mostly in combination with other drugs.^{19,20} A phase I/II clinical trial combining AZA and APR in *TP53*-mutated MDS/AML is ongoing at US centers and at our center.²⁹⁻³¹

In this study, we show that APR is efficient on its own, while it also synergizes with AZA in *TP53*-mutated MDS/AML cell lines and in *TP53*-mutated primary cells from MDS/AML patients. We also identified a functional pathway involved in the synergy between these two drugs.

Methods

Reagents and drugs

APR was provided by Aprea Therapeutics AB, Stockholm, Sweden, and kept frozen (-20°C) as a stock solution. AZA was provided by Celgene Corporation (Summit, NJ, USA) and was kept frozen at -80°C as a stock solution. As previously described,³² AZA was added once at day 0 of cell culture and APR was used in the same manner. FLT3 ligand (FLT3-L) was from PeproTech (Neuilly-sur-Seine, France).

Cell lines and primary cells

The MDS cell line SKM1 (kindly provided by Thomas Cluzeau, University Hospital of Nice, France) is an MDS-derived cell line that has undergone detailed characterization in terms of its phenotype and genotype.³³ We confirmed the presence of a homozygous mutation of *TP53* (p.R248Q). SKM1 cells were grown in RPMI 1640 medium (GIBCO; Life Technologies Corporation, Carlsbad, CA, USA) supplemented with 10% FBS (GIBCO), 1% Penicillin/Streptomycin (P/S), and 1% GlutaMAX. All of the other leukemic cell lines (K562, KG1a, THP-1, and HL60) were cultured under the same conditions. Cells in the logarithmic phase of growth that had been seeded at a density of 2×10^5 /mL were used for all of the experiments.

Primary cells from MDS and AML patients with complex karyotypes, del5q, or known or suspected to have mutated *TP53* were provided by the Service d'Hématologie of the Hôpital Saint-Louis, Paris, France, after informed consent had been received. Finally, primary cells were isolated from healthy blood donors as controls. This study was approved by the Groupe Francophone des Myélodysplasies (GFM) review board.

Cytotoxicity assay

The following concentrations were used for each drug: APR from 10^{-8} M to 10^{-5} M and AZA from 10^{-8} M to 10^{-5} M. Proliferating cells were plated, incubated for three days, and then counted. Experiments were performed at least in triplicate. FLT3-ligand was added at final concentrations varying from 0.1 to 100 ng/mL for specific experiments.

Clonogenic assays

Due to partial blastic infiltration in the majority of samples, as generally reported in MDS/AML with a complex karyotype and *TP53* mutation,⁹ liquid cultures were not consistently successful. We used semi-solid cultures to test for the impact of drugs on progenitor clonogenicity. Briefly, 3×10^5 peripheral blood mononuclear cells (PBMC) or 1×10^5 bone marrow-derived mast cells (BMDC) were cultured in cytokine-containing methylcellulose (MethoCult[™], 84434, STEMCELL Technologies) in the presence of the IC₅₀ of each drug (0.5 μM APR or 3 μM AZA) on their own or in combination. After 14 days at 37°C, the erythroid and myeloid colonies were counted. For patients with *TP53* mutations, isolated colonies were picked, and the DNA was extracted and Sanger sequenced to determine the *TP53* genotype at the single progenitor level.

Statistical analysis

All of the results are expressed as mean ± standard deviation (SD). All of the single-parameter measurement comparisons were determined using the Mann-Whitney test (PRISM 18964 software, GraphPad, La Jolla, CA, USA). All tests were two-sided; $P < 0.05$ was considered statistically significant. Combination indices were calculated by CompuSyn software according to the Chou-Talalay method for drug synergy studies.

Results

APR inhibits the proliferation of myeloid cell lines

To evaluate the efficacy of APR-mediated growth inhibition of MDS/AML cells, we tested increasing doses of the drug on a series of MDS/AML cell lines with mutant forms of the *TP53* gene (i.e. SKM1, K562, KG1a, THP-1, and HL60 cells). We first verified that all of these cell lines harbor *TP53* mutations. The SKM1 cell line derived from an MDS patient carries the recurrent homozygous *TP53* mutation p.R248Q (c.743G>A). The four other cell lines carry a frameshift or a splicing mutation (K562: c.406dupC, HL60: c.1_1182del1182, KG1a: c.672+1G>A, or THP-1: c.520_545del26). The p53 protein was detectable in the SKM1 cell line only (*Online Supplementary Figure S1*). Treatment with APR led to a pronounced and dose-dependent reduction in cell proliferation of all of the cell lines tested (Figure 1A), with 50% inhibitory concentrations (IC₅₀) that were in the micromolar range (Figure 1B). Of note, the IC₅₀ was at least 2-fold lower for the SKM1 cell line compared to the other AML lines (Figure 1B and *Online Supplementary Table S1*).

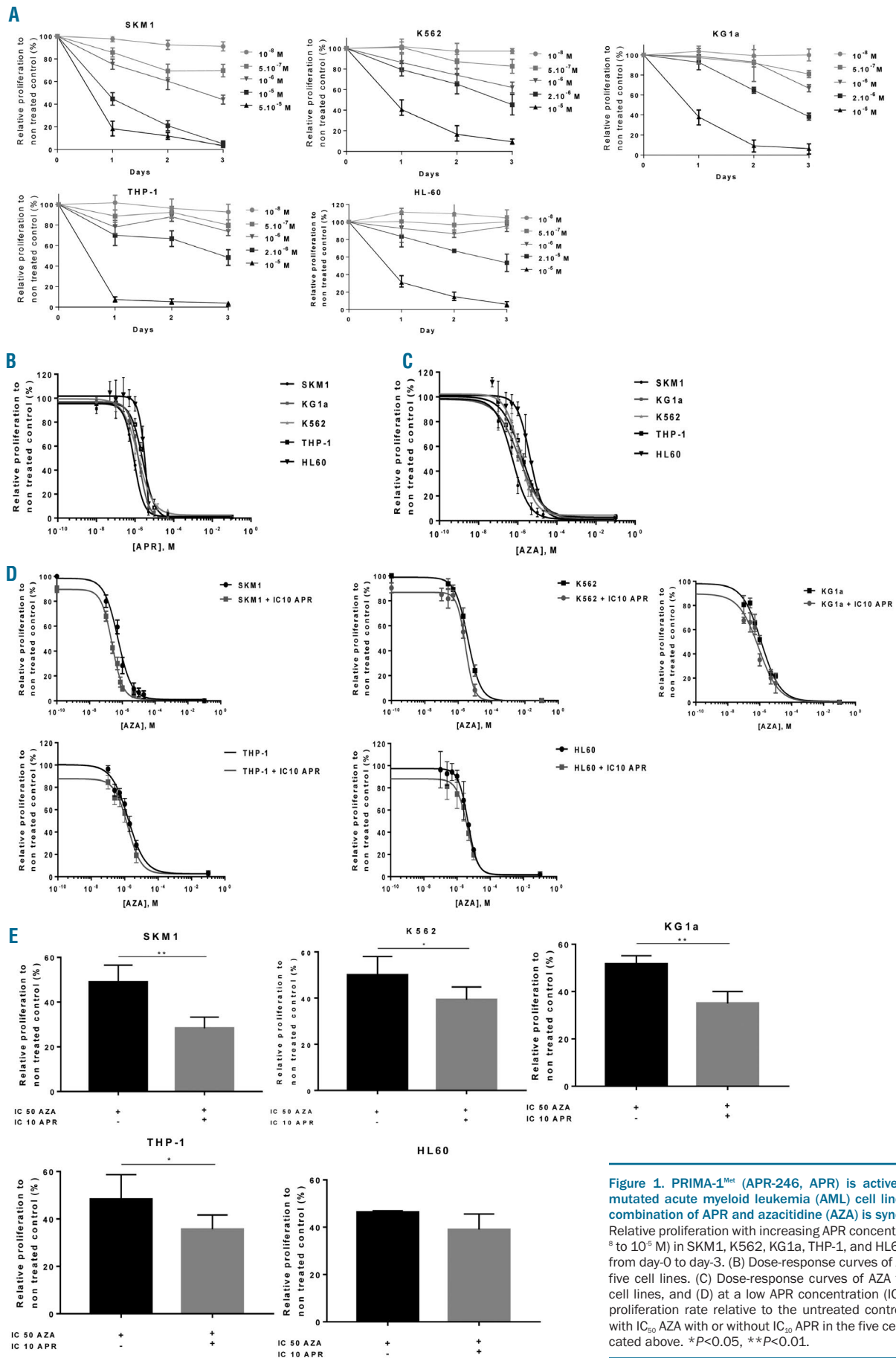


Figure 1. PRIMA-1^{Met} (APR-246, APR) is active on TP53-mutated acute myeloid leukemia (AML) cell lines and the combination of APR with azacitidine (AZA) is synergistic. (A) Relative proliferation with increasing APR concentrations (10⁻⁸ to 10⁻⁵ M) in SKM1, K562, KG1a, THP-1, and HL60 cell lines from day-0 to day-3. (B) Dose-response curves of APR for the five cell lines. (C) Dose-response curves of AZA for the five cell lines, and (D) at a low APR concentration (IC₁₀). (E) The proliferation rate relative to the untreated control at day 3 with IC₅₀ AZA with or without IC₁₀ APR in the five cell lines indicated above. *P<0.05, **P<0.01.

The combination of APR and AZA synergistically reduces the proliferation of myeloid cell lines

AZA is considered to be a first-line treatment for most patients with high-risk MDS, but its effect is relatively limited in MDS patients who have *TP53* mutations. After we evaluated the activity of AZA on *TP53*-mutated AML lines (IC₅₀ ranging from 0.54x10⁻⁶ M for SKM1 to 4.5x10⁻⁶ M for HL60 cells) (Figure 1C), we investigated whether its efficacy could be enhanced by combination with APR. The addition of low doses of APR (IC₁₀) (*Online Supplementary Table S1*) to increasing doses of AZA reduced the proliferation of the five cell lines compared to AZA on its own, with the exception of HL60 cells (Figure 1D and E). SKM1 cells were the most sensitive to the combination, as the IC₅₀ of AZA in these cells was significantly reduced in the presence of low doses of APR. This synergistic effect was confirmed at different concentrations of each drug by calculating the combination index (CI < 1) for all of the tested cell lines, but not at low concentrations of both drugs (i.e. both drugs at their IC₁₀) (*Online Supplementary Table S1*).

The combination of APR and AZA promotes G0/G1 cell cycle arrest and apoptosis

To elucidate the mechanisms underlying the antiproliferative effect of the combination compared with each drug on their own, we performed apoptosis and cell cycle studies using low dose APR (i.e. at the IC₁₀) with a standard dose of AZA (i.e. at the IC₅₀). Other associations are shown in the *Online Supplementary Figures S2-S4*. Under these conditions, APR alone did not induce apoptosis, while AZA on its own induced low levels of apoptosis in some of the cell lines. The combination of APR with AZA significantly increased apoptosis compared to the individual drugs in every cell line that was tested. This effect was more pronounced in SKM1 cells (39% apoptotic cells with APR + AZA vs. 19% with AZA alone, *P*<0.01) (Figure 2A-E).

We then analyzed the cell cycle distribution after treatment with IC₁₀ APR, IC₅₀ AZA, or the combination of these two drugs at these concentrations. At this low concentration, APR on its own did not affect the cell cycle distribution of the various cell lines tested, while AZA tended to increase the proportion of cells in the G0/G1 phase. However, SKM1 cells treated with the combination of AZA and APR underwent cell cycle arrest in G0/G1 as early as 24 hours after exposure (83% of the cells were in G0/G1 phase following APR + AZA treatment vs. 62% for APR-treated cells, *P*<0.01). In parallel, the proportion of cells in the S and G2/M phases was significantly reduced (Figure 2A). Similar results, although less pronounced, were observed in the other cell lines (Figure 2B-E), while various combinations of these drugs confirmed the observed synergism between the two drugs in terms of cell cycle arrest and the induction of apoptosis (*Online Supplementary Figures S2-S4*). Altogether, although the effect is more pronounced on apoptosis than on cell cycle, these results suggest that the addition of APR to AZA in various *TP53*-mutated cell lines potentiates the AZA antiproliferative effect by increasing G0/G1 arrest and a pro-apoptotic effect.

APR is active on primary cells of *TP53*-mutated MDS/AML samples

We then investigated the effect of these drugs on primary cells from MDS/AML patients. Of the 34 patients

included in our study, 15 patients had mutations in the *TP53* gene (10 had a complex karyotype, 2 had an isolated 5q deletion, and 14 had deletion of the other *TP53* allele). All mutations were located in the DNA-binding domain hotspots (DBD) (Table 1).

We performed clonogenic assays in semi-solid medium using the previously determined IC₅₀ for SKM1 cells. AZA on its own at 3 μM induced only a modest reduction (30%) of myeloid and erythroid colony growth, while APR at 0.5 μM significantly inhibited colony growth by approximately 60% (Figure 3A and B).

We then sought to determine whether there was a targeted effect on cells from patients with mutated *TP53*. When compared to AZA on its own, the drug combination always had a greater inhibitory effect on the growth of myeloid or erythroid progenitor colonies, irrespective of the *TP53* genotype of the patients (*Online Supplementary Figure S5*). However, when compared to APR on its own, the APR + AZA combination significantly reduced the number of myeloid and erythroid colonies formed by progenitors derived from patients with mutated *TP53*, while this was not observed with wild-type *TP53* patients (Figure 3C and D). This indicates that the drug combination may be more beneficial to patients with *TP53* mutations. However, the molecular analysis of the residual colonies from four patients with mutated *TP53*, irrespective of the treatment conditions, only revealed mutant *TP53* colonies (Table 2 and *data not shown*), thus making it impossible to conclude that cells with mutated p53 are targeted specifically. To further study the specificity of the combination, we performed liquid cultures of CD34⁺ cells isolated from *TP53*-mutated or wild-type MDS/AML patients and studied proliferation and apoptosis when treated by APR and/or AZA. A significant efficacy of the combination compared to drugs given alone was observed in *TP53*-mutated patients only (Figure 4A-D). Accordingly, CD34⁺ cells isolated from healthy blood donors did not show increased sensitivity to the combination compared to isolated drugs (Figure 4E and F).

In vivo efficacy of APR and AZA in a xenotransplantation model

In order to evaluate the *in vivo* antiproliferative effect of APR and AZA, we developed a xenograft model of SKM1-Luciferase cells in NSG mice that allowed us to use bioluminescence to measure tumor volumes before and after APR and AZA treatment. Intravenous injections of 10⁷ cells yielded highly reproducible tumor engraftment and growth over time (100% of the mice had engraftment) (Figure 5A). The mice were treated with the drugs as soon as the tumor bioluminescence signal reached 10⁶ p/sec/cm²/sr.

Treatment with low doses of APR in combination with AZA resulted in pronounced inhibition of disease progression as early as four days after starting the drug treatment compared to APR or AZA treatment on their own (median tumor volume: 91.1x10⁶ p/sec/cm²/sr in untreated mice, 64.4x10⁶ p/sec/cm²/sr with APR on its own, 103.2x10⁶ p/sec/cm²/sr with AZA on its own vs. 18.9x10⁶ p/sec/cm²/sr mm³ in the APR + AZA group; *P*<0.05) (Figure 5A). There was still a beneficial impact of the drug combination after eight days of treatment (Figure 5B). These results confirmed *in vivo* the efficacy of the combination of a low dose of APR with standard AZA doses that we had previously shown *in vitro*.

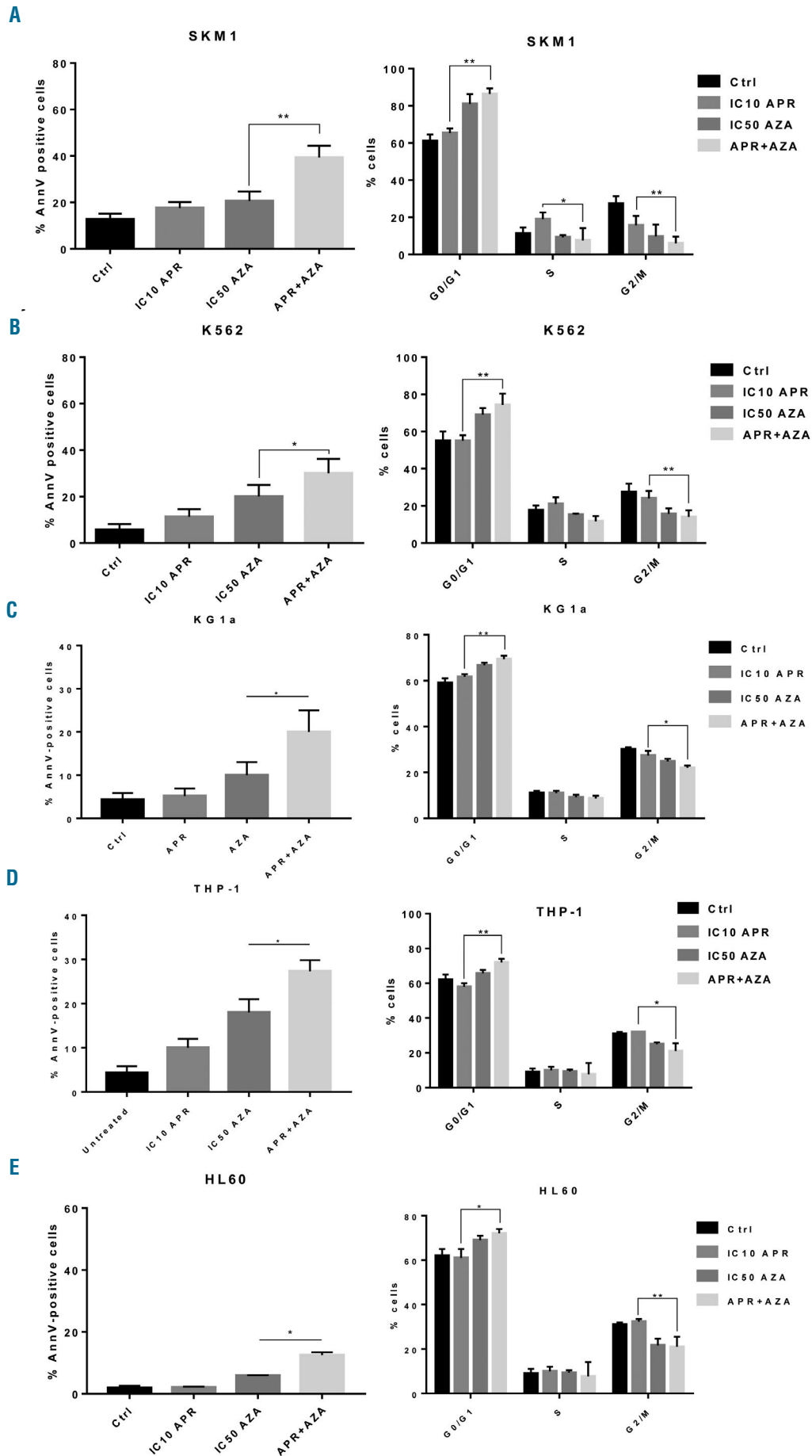


Figure 2. The combination of PRIMA-1^{Met} (APR-246, APR) and azacitidine (AZA) promotes G0/G1 arrest and apoptosis in various TP53-mutated acute myeloid leukemia (AML) cell lines. (Left) Percentage of Annexin V-positive cells at day 3 post treatment with IC₁₀ APR, IC₅₀ AZA, or the combination of these two drugs at these same concentrations. (Right) Proportion of cells in G0/G1, S, or G2/M phase 24 hours after treatment with IC₁₀ APR, IC₅₀ AZA or the combination of these two drugs at these same concentrations. (A) SKM1, (B) K562, (C) KG1a, (D) THP-1, and (E) HL60 cell lines. *P<0.05, **P<0.01.

Treatment with the APR + AZA combination is characterized by a specific gene expression profile

We conducted a transcriptomic analysis of the SKM1 cell line following treatment with APR, AZA, or a combination of these two drugs. A large number of genes were differentially expressed ($P < 0.05$) under treatment by AZA on its own or by APR + AZA ($n = 4,620$ and $n = 4,672$, respectively), while the number of genes differentially expressed under APR alone was relatively small ($n = 691$) (Figure 6A). Accordingly, the number of genes deregulated in common for APR and APR + AZA treatments was small ($n = 201$) while this was very high for the AZA and the APR + AZA treatments ($n = 3,461$). As expected, the Gene Set Enrichment Analysis (GSEA) (Figure 6B) and DAVID analyses of the genes differentially expressed by APR identified the p53 pathway as one of the main deregulated pathways [Normalized Enrichment Score (NES) = 1.2; false discovery rate (FDR) = 0.15], with increased expression of p53-target genes such as *CDKN1A*, *CASP1*, *BAX*, and *FAS*. These differential expression patterns were confirmed by real-time quantitative polymerase chain reaction (RT-qPCR) analysis (Figure 6D). In accordance with the involvement of some of these genes in apoptosis, the GSEA analysis also revealed activation of an early apoptotic program (NES = 1.1; FDR = 0.2) (Figure 6B). Importantly, similar results on p53 and pro-apoptotic pathways were found to occur when AZA was added to APR (Figure 6C and E), thus suggesting that AZA did not suppress the transcriptional modifications associated with APR treatment. Of note, enrichment of ROS-induced genes was found to occur with APR on its own (FDR = 0.06; NES = 1.2) (Online Supplementary Figure S6A) and APR + AZA (FDR = 0.02; NES = 1.52) (Online Supplementary Figure S6B), possibly confirming a p53-independent mechanism of action of APR on oxidative stress, as has already

been described in other tumor models.^{27,34,35} Using Interpretative Phenomenological Analysis (IPA) analysis and a selection of genes with a significant level of differential expression ($P < 0.05$) (Online Supplementary Table S2) on the basis of the difference in fold change (FC), we found 5,428 transcriptionally-regulated genes with APR + AZA treatment compared to untreated cells. Eight hundred and seventy-five genes appeared to be up- or down-regulated with the combined treatment only ("synergistic only" genes) and not by either drug on their own. GSEA analysis of the "synergistic only" genes revealed activation of the p53 pathway, induction of an apoptotic program, and downregulation of the MYC pathway (Online Supplementary Table S3). Surprisingly, in this group of "synergistic only" genes, we identified decreased expression of several FLT3-pathway genes, including FLT3 and FLT3-L (Online Supplementary Table S2). This finding was confirmed using the comparative GSEA analysis, which similarly revealed downregulation of the FLT3 pathway (Valk, FLT3-ITD representative of activation of the FLT3 pathway) (Figure 7A) with the combination treatment compared to either of the drugs on their own. Using RT-qPCR, we were able to confirm the significant downregulation of both the *FLT3* and the *FLT3-L* gene with the combined treatment (Figure 7B).

Downregulation of the FLT3 pathway contributes to the APR + AZA-induced anti-proliferative effect

To analyze the relevance of downregulation of the FLT3 signaling pathway to the synergistic effect of the APR + AZA combination, SKM1 cells were cultured with these drugs in the presence or absence of FLT3-L at different concentrations. The addition of FLT3-L on its own did not affect SKM1 cell proliferation, but, when increasing amounts of FLT3-L were added to the APR + AZA combi-

Table 1. World Health Organization classification of cytogenetic and molecular characteristics of TP53-mutated myelodysplastic syndromes / acute myeloid leukemia patients.

Patient	TP53 mutation	Karyotype	Colonies sequenced	Variant allele frequency (VAF, %)
1	p.V157F	45,XX,add(1)(q4?3),del(5)(q1?3q3?3),der(6)t(6;14)(p2?2;q1?2)x2,-11,-14,+?15,der(16)t(?;16)(?;p1?1)[11q13?],-17,+r(11)[24]	71	90%
2	p.P190L	45,XX,-7,add(3)(p2?6),del(4)(q2?4),del(5)(q1?3q3?3),del(12)(p13)[10]/47,XX,del(4)(q2?4),del(5)(q1?3q3?3),del(12)(p13),+21[6]/47,XX,del(4)(q2?4),del(5)(q1?3q3?3),del(12)(p13),+21,+r(?) [4]	72	92%
3	p.C238F	45,XX,-7[4]/46,XX[6]	71	22%
4	p.R248Q	44,XY,del(5)(q1?3q3?3),-7,add(17)(p1?1),-19[11]/44,idem,del(11)(p1?4p1?5)/46,XY[3]	50	30%
5	p.V216M + p.R248Q	46,XX,del(5)(q1?3q3?3)[11]/46,XX[13]	ND	NA
6	p.S241C	45,XX,t(4;13)(p1?3;q1?2),del(5)(q15q34),del(7)(q21),dic(12;16)(p11;?p1?2),-18,der(?21)(?),+r(?) [cp21]	ND	NA
7	p.R248Q	46,XX,ins(3;12)(p2?1;q13q2?4),del(12)(q1?3),-17,+mar1 [cp10]/46,idem,-7,+mar2,+min [cp7]/46,XX[6]	ND	NA
8	p.M246R	47,XY,+8[21]/46,XY[1]	ND	NA
9	p.R248Q	43,XX,del(5)(q1?4q3?3),del(7)(q2?1),der(12)t(12;13)(p1?1;q1?3),der(13)t(7;13)(q21;q13),del(18)(q21)[21]	ND	77%
10	p.A276T	46,XX,del(5)(q1?3q3?3)[15]/46,XX[7]	ND	NA
11	p.R248T + p.L330R	46,XY,i(17)(q10)[25]	ND	NA
12	p.C275Y	44-47,XY,del(5)(q13q33),+8,+9,del(9)(q2?2),t(12;15)(p13;q1?2),-13,-17,+r(?) [3], +1-4mar [cp19]/46,XY[3]	ND	9%
13	p.R273C46,XY,del(2)(q1?1),add(10)(p1?1),del(11)(q2?1),del(16)(p1?1)[19]/46,idem,add(17)(q2?5)[3]/46,XY,-12,-17,+2mar[3]	ND	NA	
14	p.C238Y	44,XX,-5,del(7)(q2?1),add(8)(q2?4),-18,?der(21)t(8;21)(q?13;q2?1)[21]	ND	NA
15	c.675-2A>G	45,XY,der(1;5)(q10;p10),del(4)(q2?4q2?1),add(17)(p1?1),-21,+r(?) [21]	ND	NA

ND: not determined; NA: not available.

nation, we observed a dose-dependent reversal of the inhibition of cell proliferation (Figure 7C). The relative proliferation of APR + AZA treated cells at day 3 was significantly higher when FLT3-L was added ($P < 0.01$) (Figure

7D). This reversal of the inhibitory effect on proliferation was associated with a decrease in apoptosis, since 40% of the cells stained positive for Annexin V with the drug combination treatment without FLT3-L compared with

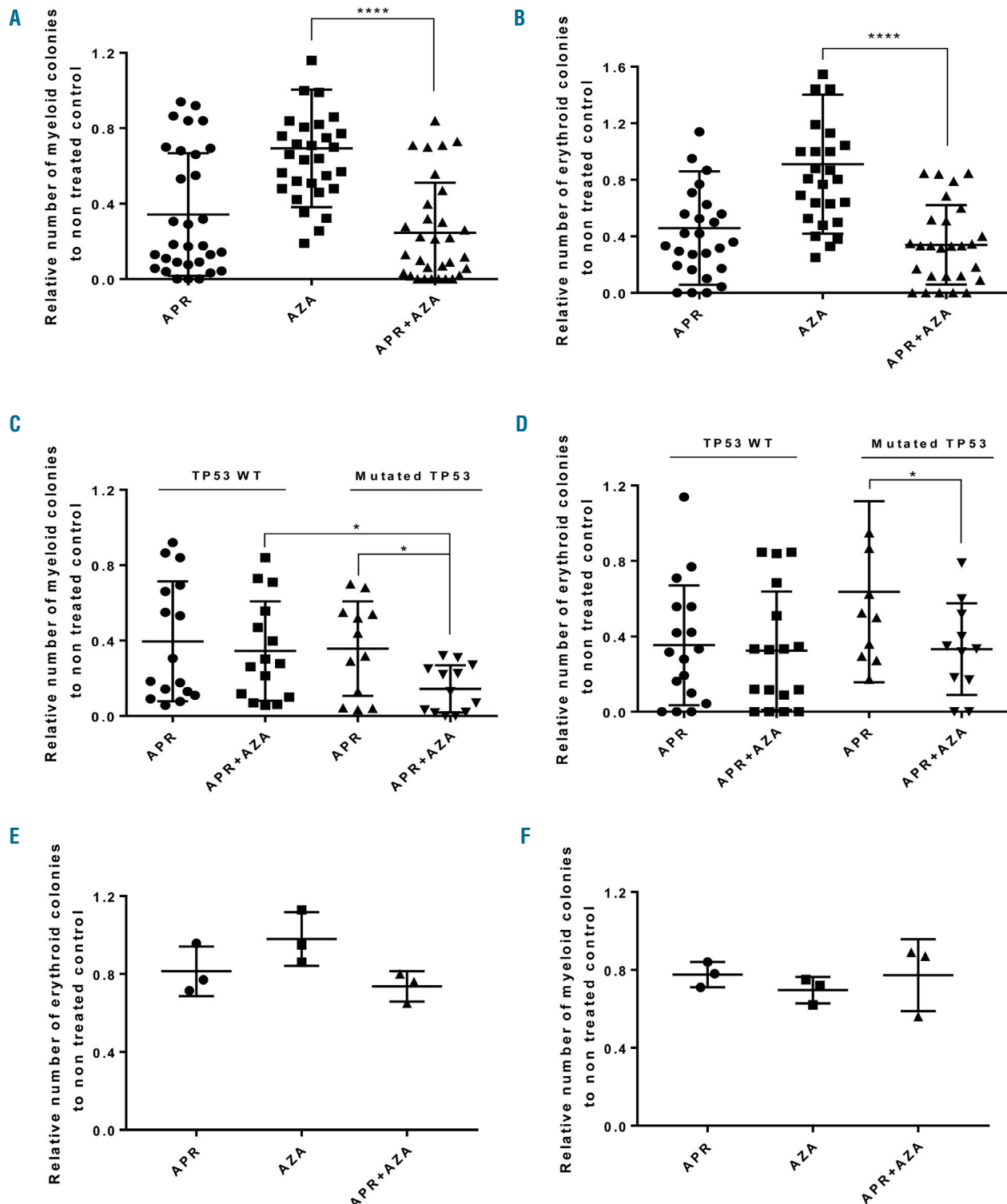


Figure 3. Effects of PRIMA-1^{Met} (APR-246, APR) on primary cells from TP53-mutated myelodysplastic syndromes (MDS) / acute myeloid leukemia (AML) patients and healthy donors. The median numbers of (A) myeloid and (B) erythroid colonies relative to the untreated control for 34 bone marrow samples from MDS/AML patients treated with APR, azacitidine (AZA), or the combination APR + AZA in semi-solid medium (methylcellulose). Relative numbers of (C) myeloid and (D) erythroid colonies according to the TP53 status (WT: wild-type) treated with APR or the combination of APR + AZA. Median numbers of (E) myeloid and (F) erythroid colonies relative to untreated control for 3 CD34⁺ cells from healthy donors treated with APR, AZA or the combination APR + AZA. * $P < 0.05$, **** $P < 0.0001$.

only 26% when FLT3-L was added (Figure 7E). These results suggest that the synergistic effect observed with the APR + AZA combination on proliferation and apoptosis correlates with downregulation of the FLT3 pathway.

Discussion

APR has been shown to have efficacy on its own as well as when combined with other drugs in solid tumors^{19,20,23-25} and lymphoid tumors.^{21,27,28,36} In this study, we observed that APR inhibited the proliferation of several TP53-mutated myeloid cell lines, as previously sug-

gested by other studies on myeloid^{26,34} and lymphoid cell lines.^{27,28} Of note, the additive/synergistic impact of the combination was more robust with regards to apoptosis compared to cell cycle arrest, suggesting that most of the anti-proliferative effect may be mediated by hypomethylating agent (AZA) while the pro-apoptotic effects of the combination was clearly due to APR.

These inhibitory effects were more pronounced in the TP53-mutated MDS-derived SKM1 cell line, and may be related to the structure of the mutant protein in the different cell lines. Indeed, APR binding to the cysteine residues of the DBD has been associated with the reformation of an active structure by p.R175H and p.R273H mutant p53

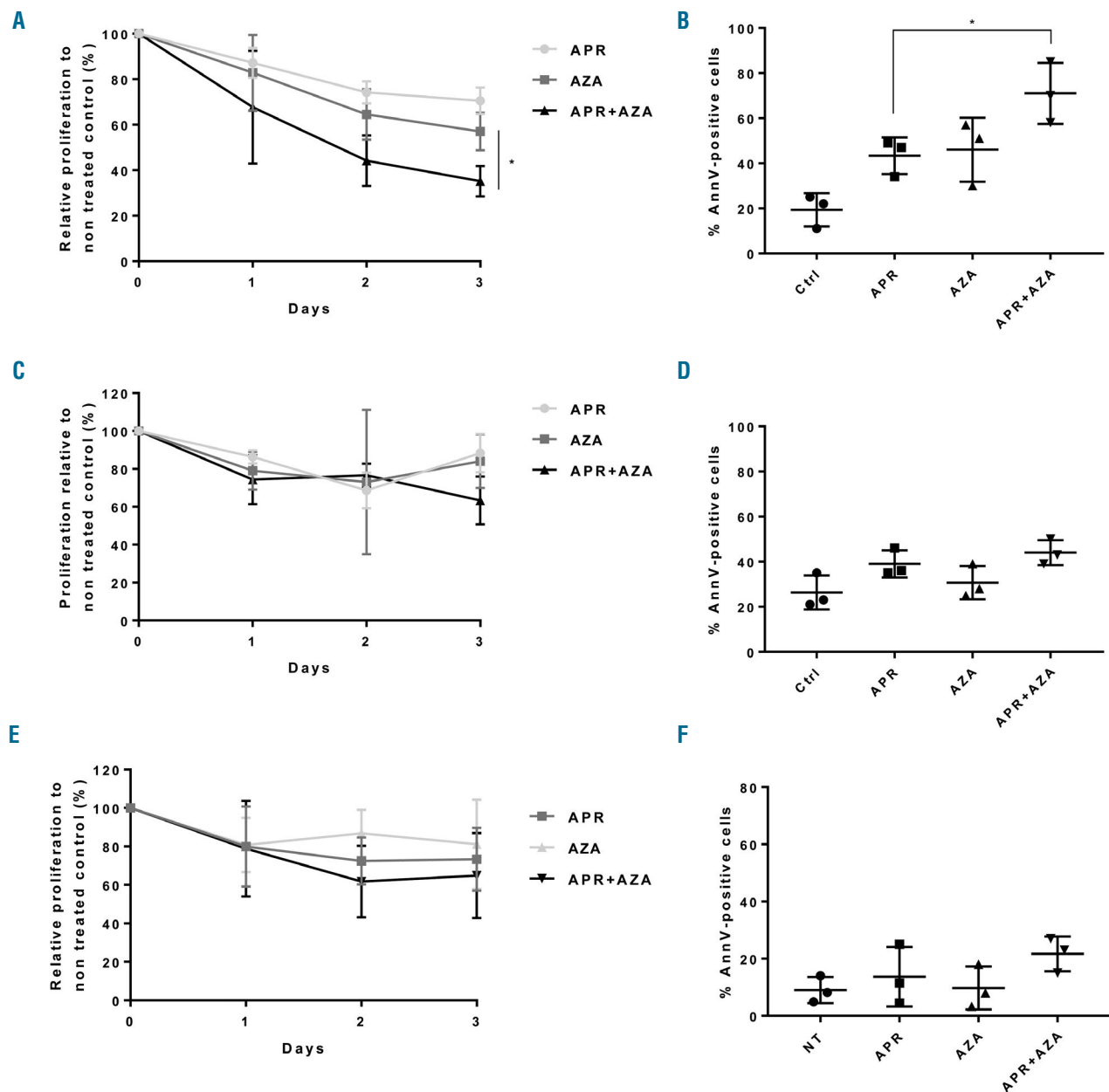


Figure 4. Effects of PRIMA-1^{Met} (APR-246, APR) on primary cells from TP53 wild-type or mutated myelodysplastic syndromes (MDS) / acute myeloid leukemia (AML) patients and healthy donors. (Left) Relative proliferation of CD34⁺ cells treated with 1 μM APR, 1 μM AZA or the combination APR + AZA at these concentrations. (Right) Percentages of Annexin V-positive cells at day 3 post treatment with 1 μM APR, 1 μM of AZA or the combination APR + AZA at these concentrations. (A) TP53-mutated MDS/AML samples (n=3), (B) Wild-type TP53 MDS/AML samples (n=3), and (C) healthy donors (n=3). *P<0.05.

proteins.³⁷ The SKM1 cell line has a p.R248Q mutation located in the DBD, while the other myeloid cell lines tested in this study have various TP53 truncation mutations that result in a lack of detectable p53 protein in all four cell lines.^{38,39} APR may not be able to restore an active conformation to the truncated p53 protein in these cell lines, thereby explaining the lower efficacy of APR compared with SKM1 cells. This also suggests that the effects of APR in these cell lines may be due in part to p53-independent processes.²⁷ We then demonstrated that the inhibitory effect of the APR + AZA combination was synergistic in the five TP53-mutated cell lines that were tested,

although, again, this effect was more pronounced in the SKM1 cells for presumably the same reason. To confirm this efficacy, we showed that APR + AZA combination significantly antagonized development of the disease in an *in vivo* model.

APR exhibited a pronounced anti-clonogenic effect on hematopoietic progenitor cells from MDS/AML patients irrespective of the TP53 mutational status. This suggests that APR on its own targets not only TP53-mutated cells (at least at the doses that we used in our experiments), and that its inhibitory effects are partly p53-independent, as had already been shown previously.^{27,34,35,40} On the other

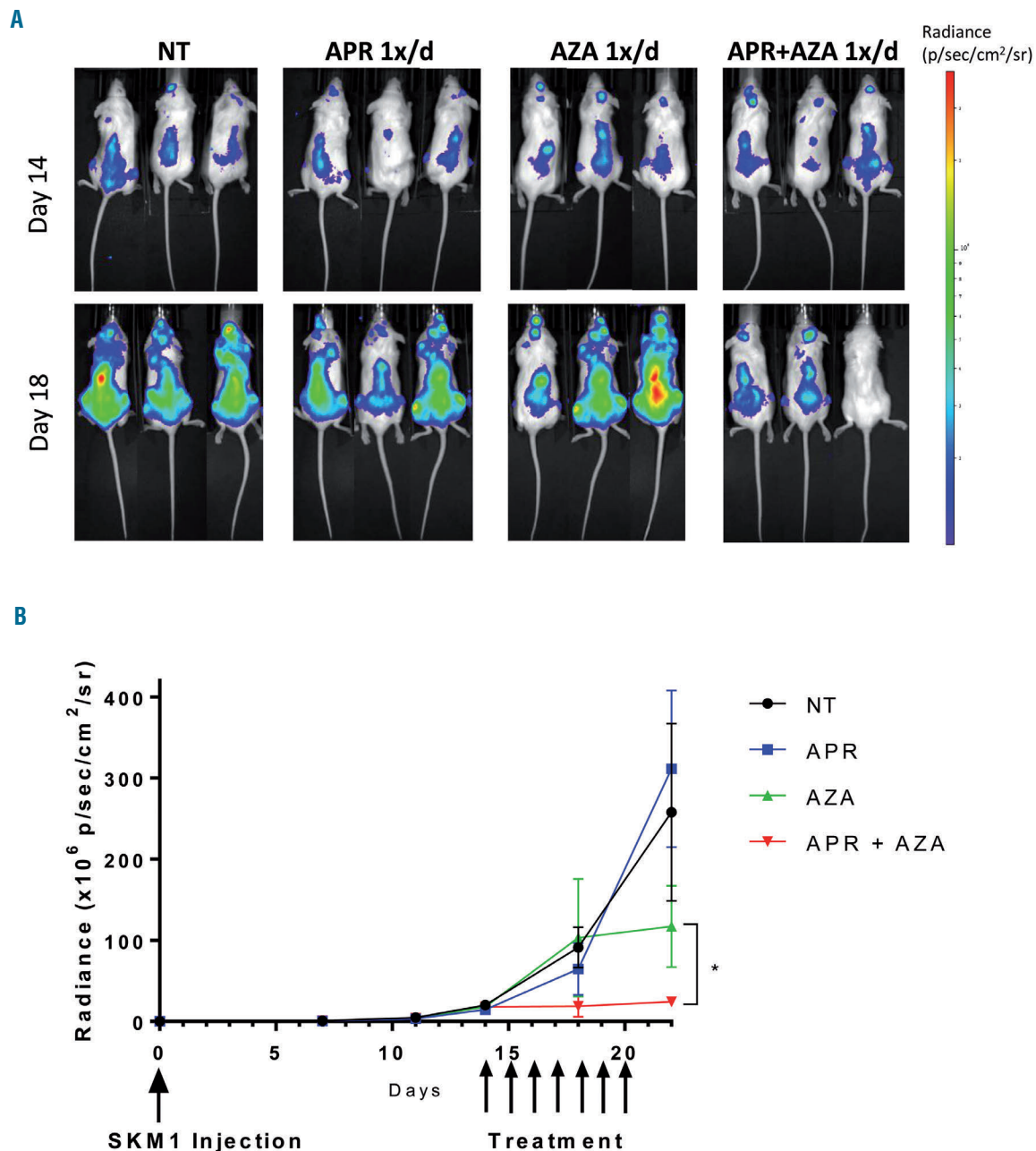


Figure 5. *In vivo* efficacy of PRIMA-1^{Met} (APR-246, APR) and azacitidine (AZA) in a xenotransplantation model. (A) Disease development monitored by luciferase activity and bioluminescence imaging. Images of untreated mice at day 14 (day 1 of treatment) and treated mice at day 18 (day 5 of treatment) following injection of SKM1-Luc cells. (B) The tumor volume (p/sec/cm²/sr) during and after treatment with PBS, APR, AZA, or the APR + AZA combination (treatment days are indicated by the solid arrows). The drug treatments were started when the tumor volume had reached 10⁶ p/sec/cm²/sr. **P*<0.05.

hand, the combination of the two drugs (APR + AZA) had a similar effect as APR on its own in progenitor cells from patients with WT *TP53*, whereas the combination had a significantly more pronounced effect than APR on its

own on progenitor cells from patients with mutant *TP53*. This strongly suggests a selective effect on mutant p53 cells, although we were unable to demonstrate the formation of wild-type *TP53* colonies under treatment, which

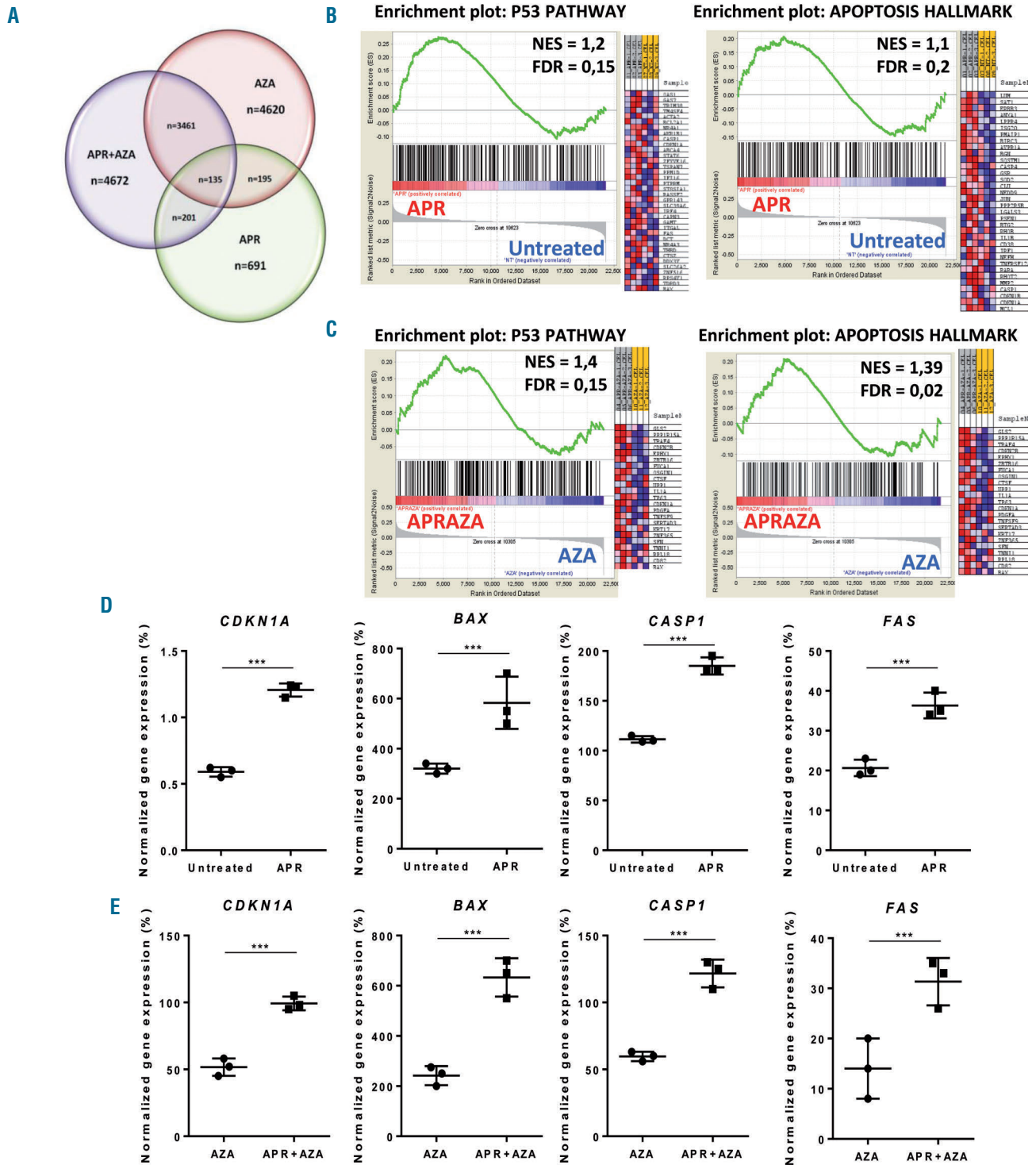


Figure 6. Changes in gene expression induced by treatment with PRIMA-1^{Met} (APR-246, APR) + azacitidine (AZA). (A) A Venn diagram representing the number of deregulated genes with APR on its own, AZA on its own, or the combination of APR + AZA. (B) Gene enrichment plots and associated heatmaps showing reactivation of the p53 pathway and induction of an apoptosis program in SKM1 cells treated with IC₁₀ APR compared to untreated cells. (C) Gene enrichment plots and associated heatmaps showing reactivation of the p53 pathway and induction of an apoptosis program in SKM1 cells treated with the combination of APR IC₁₀ + AZA IC₅₀ (APR + AZA) compared to AZA on its own (AZA). (D) RT-qPCR expression of the main p53 targets (*CDKN1A* and *BAX*) and pro-apoptotic factors (*CASP1* and *FAS*) in SKM1 cells treated with APR compared to untreated cells. (E) RT-qPCR expression of the main p53 targets (*CDKN1A* and *BAX*) and pro-apoptotic factors (*CASP1* and *FAS*) in SKM1 cells treated with the combination of APR + AZA versus AZA on its own. ****P*<0.001. NES: Normalized Enrichment Score; FDR: False Discovery Rate.

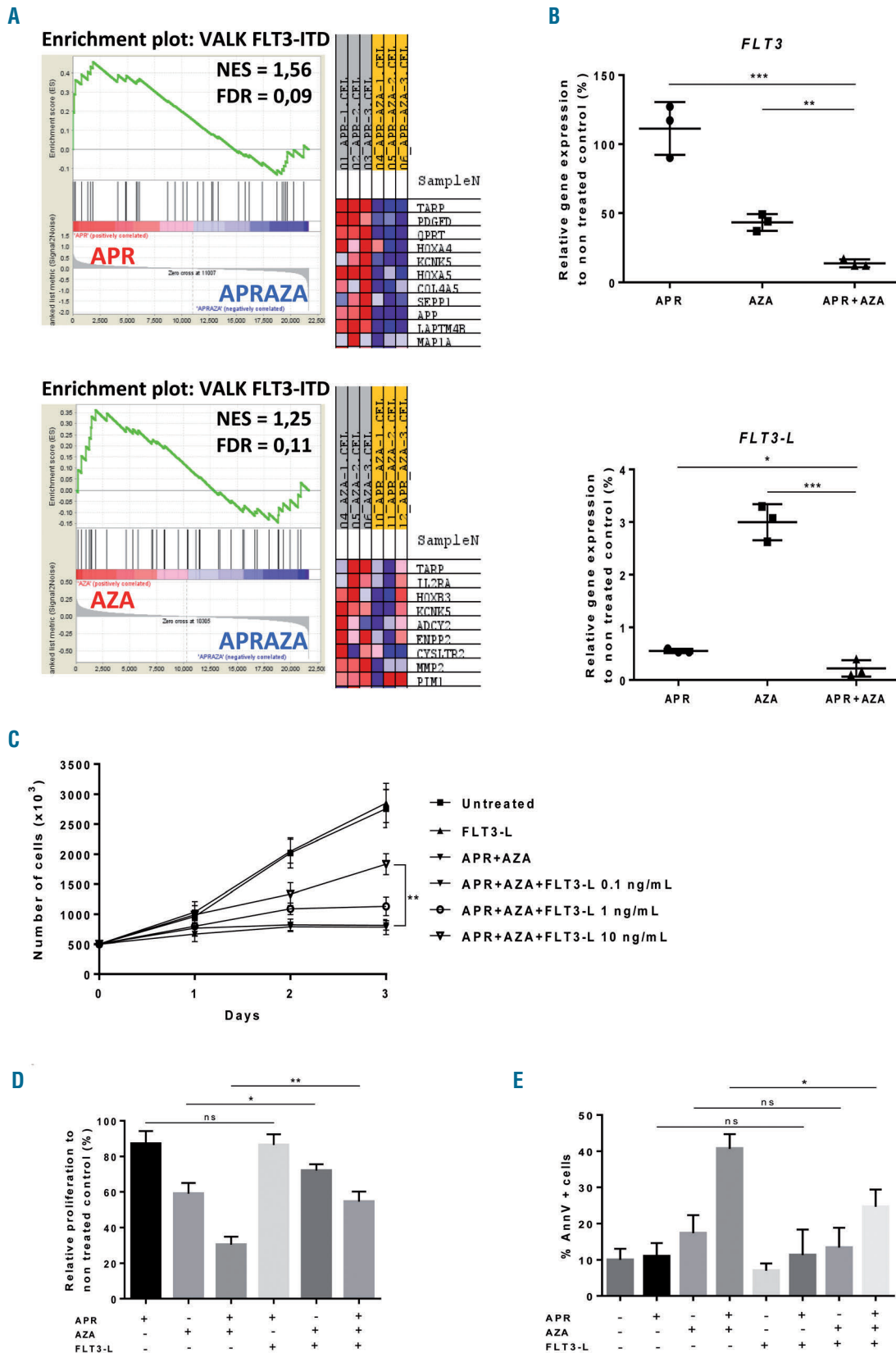


Figure 7. The antiproliferative effect of PRIMA-1^{Met} (APR-246, APR) + azacitidine (AZA) combination is related to downregulation of the FLT3 pathway. (A) Gene enrichment plots and heatmaps representing the FLT3 activated pathway (Valk, FLT3-ITD) in APR versus untreated SKM1 cells and APR + AZA versus AZA-treated cells. (B) Real-time quantitative polymerase chain reaction analysis of gene expression by *FLT3* and *FLT3-L* with APR, AZA, or APR + AZA relative to the untreated control. (C) Absolute numbers of untreated and APR + AZA-treated SKM1 cells exposed to increasing concentrations of FLT3-L. (D) Proliferation of SKM1 cells treated with APR, AZA, or the combination APR + AZA relative to controls, without or with 10 ng/mL FLT3 ligand (FLT3-L). (E) Proportion of Annexin V-positive SKM1 cells at day 3 following treatment with APR, AZA, or the combination of APR + AZA, with or without FLT3L. * $P < 0.05$, ** $P < 0.01$, *** $P < 0.001$.

was probably due to the very high proportion of mutant progenitor cells that grew in these conditions, as no wild-type colonies could be discerned even in the absence of treatment. An *in vivo* evaluation of the change in the *TP53* allelic burden in patients treated by the combination would be relevant to address the question of mutant *TP53* selectivity. A clinical trial (*clinicaltrials.gov* identifier: 03745716) testing the association of APR and AZA in *TP53*-mutant MDS/AML is ongoing and may help answer this question.

The molecular mechanism underlying the efficacy of the association between AZA and APR remains unknown. AZA is a DNA demethylating agent and APR is an agent that reactivates the transcription factor p53. Both drugs may act by modulating gene expression. Thus, we sought to study differences in gene expression profiles between cells treated by the single agents or with the drug combination. The results of the transcriptomic analysis provide further evidence that APR, even at low doses, reactivates the p53 pathway and that it results in activation of an apoptotic program. We also found that genes involved in FLT3 signaling were down-regulated by the combination of APR and AZA. The relevance of this observation was confirmed as the addition of FLT3 ligand reversed the inhibition of cell proliferation by the APR + AZA combination. Interestingly none of the cell lines tested had *FLT3*

mutations or duplications,⁴¹ suggesting that the drug combination effect is not dependent on the presence of such molecular alterations. However, it would be interesting to test this drug combination in cell lines with *FLT3* mutations or duplications. In addition to providing clues for a specific mechanism of action of the drug combination through a synthetic lethality process involving the FLT3 pathway, our observations indicate that the addition of FLT3-inhibitors to the APR + AZA combination could be of relevance in *TP53*-mutated MDS/AML.⁴²

In conclusion, our results suggest that APR exhibits promising synergistic effects when combined with conventional AZA therapy in the high-risk subgroup of *TP53*-mutated MDS/AML. Promising preliminary results of a phase I/II clinical trial combining AZA and APR in *TP53*-mutated MDS/AML, and activated at US centers and our center, have been reported.²⁹

Acknowledgments

We thank the animal facility of the Institut Universitaire d'Hématologie of Hôpital Saint-Louis, Paris, for technical assistance and the Genomic Platform at the Cochin Institute for assistance with the transcriptomic analysis. This study was supported by the Groupe Francophone des Myélodysplasies (GFM). We are indebted to Aprea Therapeutics and Celgene for supplying the APR and AZA, respectively.

References

- Adès L, Itzykson R, Fenaux P. Myelodysplastic syndromes. *Lancet* 2014; 383(9936):2239-2252.
- Greenberg PL, Tuechler H, Schanz J, et al. Revised international prognostic scoring system for myelodysplastic syndromes. *Blood* 2012;120(12):2454-2465.
- Haferlach C, Dicker F, Herholz H, Schnittger S, Kern W, Haferlach T. Mutations of the *TP53* gene in acute myeloid leukemia are strongly associated with a complex aberrant karyotype. *Leukemia* 2008;22(8):1539-1541.
- Bejar R, Levine R, Ebert BL. Unraveling the molecular pathophysiology of myelodysplastic syndromes. *J Clin Oncol Off J Am Soc Clin Oncol* 2011;29(5):504-515.
- Bejar R, Stevenson K, Abdel-Wahab O, et al. Clinical effect of point mutations in myelodysplastic syndromes. *N Engl J Med* 2011;364(26):2496-2506.
- Bejar R, Stevenson KE, Caughey BA, et al. Validation of a prognostic model and the impact of mutations in patients with lower-risk myelodysplastic syndromes. *J Clin Oncol Off J Am Soc Clin Oncol* 2012;30(27):3376-3382.
- Jädersten M, Saft L, Smith A, et al. *TP53* mutations in low-risk myelodysplastic syndromes with del(5q) predict disease progression. *J Clin Oncol Off J Am Soc Clin Oncol* 2011;29(15):1971-1979.
- Preudhomme C, Vanrumbeke M, Lai JL, Lepelletier P, Wattel E, Fenaux P. Inactivation of the p53 gene in leukemias and myelodysplastic syndrome (MDS) with 17p monosomy. *Leukemia* 1994;8(12):2241-2242.
- Lai JL, Preudhomme C, Zandecki M, et al. Myelodysplastic syndromes and acute myeloid leukemia with 17p deletion. An entity characterized by specific dysgranulopoiesis and a high incidence of *P53* mutations. *Leukemia* 1995;9(3):370-381.
- Soenen V, Preudhomme C, Roumier C, Daudignon A, Lai JL, Fenaux P. 17p Deletion in acute myeloid leukemia and myelodysplastic syndrome. Analysis of breakpoints and deleted segments by fluorescence in situ. *Blood* 1998;91(3):1008-1015.
- Haase D, Stevenson KE, Neuberg D, et al. *TP53* mutation status divides myelodysplastic syndromes with complex karyotypes into distinct prognostic subgroups. *Leukemia* 2019;33(7):1747-1758.
- Sallman DA, Komrokji R, Vaupel C, et al. Impact of *TP53* mutation variant allele frequency on phenotype and outcomes in myelodysplastic syndromes. *Leukemia* 2016;30(3):666-673.
- Kulasekararaj AG, Smith AE, Mian SA, et al. *TP53* mutations in myelodysplastic syndrome are strongly correlated with aberrations of chromosome 5, and correlate with adverse prognosis. *Br J Haematol* 2013; 160(5):660-672.
- Wattel E, Preudhomme C, Hecquet B, et al. p53 mutations are associated with resistance to chemotherapy and short survival in hematologic malignancies. *Blood* 1994;84(9):3148-3157.
- Lindsley RC, Saber W, Mar BG, et al. Prognostic Mutations in Myelodysplastic Syndrome after Stem-Cell Transplantation. *N Engl J Med* 2017;376(6):536-547.
- Welch JS, Petti AA, Miller CA, et al. *TP53* and Decitabine in Acute Myeloid Leukemia and Myelodysplastic Syndromes. *N Engl J Med* 2016;375(21):2023-2036.
- Bykov VJN, Issaeva N, Shilov A, et al. Restoration of the tumor suppressor function to mutant p53 by a low-molecular-weight compound. *Nat Med* 2002;8(3): 282-288.
- Lambert JMR, Gorzov P, Vepintsev DB, et al. PRIMA-1 reactivates mutant p53 by covalent binding to the core domain. *Cancer Cell* 2009;15(5):376-388.
- Mohell N, Alfredsson J, Fransson Å, et al. APR-246 overcomes resistance to cisplatin and doxorubicin in ovarian cancer cells. *Cell Death Dis* 2015;6:e1794.
- Zandi R, Selivanova G, Christensen CL, Gerds TA, Willumsen BM, Poulsen HS. PRIMA-1Met/APR-246 induces apoptosis and tumor growth delay in small cell lung cancer expressing mutant p53. *Clin Cancer Res Off J Am Assoc Cancer Res* 2011;17(9):2830-2841.
- Saha MN, Jiang H, Yang Y, Reece D, Chang H. PRIMA-1Met/APR-246 displays high antitumor activity in multiple myeloma by induction of p73 and Noxa. *Mol Cancer Ther* 2013;12(11):2331-2341.
- Liu DSH, Read M, Cullinane C, et al. APR-246 potentially inhibits tumour growth and overcomes chemoresistance in preclinical models of oesophageal adenocarcinoma. *Gut* 2015;64(10):1506-1516.
- Li X-L, Zhou J, Chan Z-L, Chooi J-Y, Chen Z-R, Chng W-J. PRIMA-1met (APR-246) inhibits growth of colorectal cancer cells with different p53 status through distinct mechanisms. *Oncotarget* 2015;6(34): 36689-36699.
- Krayem M, Joume F, Wiedig M, et al. p53 Reactivation by PRIMA-1(Met) (APR-246) sensitises (V600E/K)BRAF melanoma to vemurafenib. *Eur J Cancer Oxf Engl* 1990 2016;5598-110.

25. Fransson Å, Glaessgen D, Alfredsson J, Wiman KG, Bajalica-Lagercrantz S, Mohell N. Strong synergy with APR-246 and DNA-damaging drugs in primary cancer cells from patients with TP53 mutant High-Grade Serous ovarian cancer. *J Ovarian Res* 2016;9(1):27.
26. Ali D, Jönsson-Videsäter K, Deneberg S, et al. APR-246 exhibits anti-leukemic activity and synergism with conventional chemotherapeutic drugs in acute myeloid leukemia cells. *Eur J Haematol* 2011;86(3):206-215.
27. Tessoulin B, Descamps G, Moreau P, et al. PRIMA-1Met induces myeloma cell death independent of p53 by impairing the GSH/ROS balance. *Blood* 2014;124(10):1626-1636.
28. Sobhani M, Abdi J, Manujendra SN, Chen C, Chang H. PRIMA-1Met induces apoptosis in Waldenström's Macroglobulinemia cells independent of p53. *Cancer Biol Ther* 2015;16(5):799-806.
29. Sallman D. Phase 1b/2 Combination Study of APR-246 and Azacitidine (AZA) in Patients with TP53 mutant Myelodysplastic Syndromes (MDS) and Acute Myeloid Leukemia (AML). *ASH; Blood*. 2018;132 (Supplement 1):3091.
30. Lehmann S, Bykov VJN, Ali D, et al. Targeting p53 in vivo: a first-in-human study with p53-targeting compound APR-246 in refractory hematologic malignancies and prostate cancer. *J Clin Oncol Off J Am Soc Clin Oncol* 2012;30(29):3633-3639.
31. Deneberg S, Cherif H, Lazarevic V, et al. An open-label phase I dose-finding study of APR-246 in hematological malignancies. *Blood Cancer J* 2016;6(7):e447.
32. Laine E, Wolfromm A, Marie N, et al. Azacytidine and erlotinib exert synergistic effects against acute myeloid leukemia. *Oncogene* 2013;32(37):4331-4342.
33. Cluzeau T, Dubois A, Jacquelin A, et al. Phenotypic and genotypic characterization of azacitidine-sensitive and resistant SKM1 myeloid cell lines. *Oncotarget* 2014;5(12):4384-4391.
34. Ali D, Mohammad DK, Mujahed H, et al. Anti-leukaemic effects induced by APR-246 are dependent on induction of oxidative stress and the NFE2L2/HMOX1 axis that can be targeted by PI3K and mTOR inhibitors in acute myeloid leukaemia cells. *Br J Haematol* 2016;174(1):117-126.
35. Yoshikawa N, Kajiyama H, Nakamura K, et al. PRIMA-1MET induces apoptosis through accumulation of intracellular reactive oxygen species irrespective of p53 status and chemo-sensitivity in epithelial ovarian cancer cells. *Oncol Rep* 2016;35(5):2543-2552.
36. Saha MN, Abdi J, Yang Y, Chang H. MiRNA-29a as a tumor suppressor mediates PRIMA-1Met-induced anti-myeloma activity by targeting c-Myc. *Oncotarget* 2016;7(6):7149-7160.
37. Zhang Q, Bykov VJN, Wiman KG, Zawacka-Pankau J. APR-246 reactivates mutant p53 by targeting cysteines 124 and 277. *Cell Death Dis* 2018;9(5):439.
38. Lübbert M, Miller CW, Crawford L, Koeffler HP. p53 in chronic myelogenous leukemia. Study of mechanisms of differential expression. *J Exp Med* 1988;167(3):873-886.
39. Akashi M, Hachiya M, Osawa Y, Spirin K, Suzuki G, Koeffler HP. Irradiation Induces WAF1 Expression through a p53-independent Pathway in KG-1 Cells. *J Biol Chem* 1995;270(32):19181-19187.
40. Peng X, Zhang M-Q-Z, Conserva F, et al. APR-246/PRIMA-1MET inhibits thioredoxin reductase 1 and converts the enzyme to a dedicated NADPH oxidase. *Cell Death Dis* 2013;4e881.
41. Quentmeier H, Reinhardt J, Zaborski M, Drexler HG. FLT3 mutations in acute myeloid leukemia cell lines. *Leukemia* 2003;17(1):120-124.
42. Lieberman E, Lahortiga I, Van Miegroet H, Mentens N, Marynen P, Cools J. The ability of sorafenib to inhibit oncogenic PDGFRbeta and FLT3 mutants and overcome resistance to other small molecule inhibitors. *Haematologica* 2007;92(1):27-34.



Ferrata Storti Foundation

The prevalence of extramedullary acute myeloid leukemia detected by ¹⁸F-DG-PET/CT: final results from the prospective PETAML trial

Friedrich Stölzel,¹ Tors Lür,¹ Steffen Löck,² Stefani Parmentier,³ Friederike Kuithan,⁴ Michael Kramer,¹ Nael S. Alakel,¹ Katja Sockel,¹ Franziska Taube,¹ Jan M. Middeke,¹ Johannes Schetelig,¹ Christoph Röllig,¹ Tobias Paulus,⁵ Jörg Kotzerke,⁶ Gerhard Ehninger,¹ Martin Bornhäuser,^{1,7,8} Markus Schaich^{3#} and Klaus Zoepfel^{6#}

¹Department of Internal Medicine I, University Hospital Carl Gustav Carus Dresden, Technische Universität Dresden, Dresden, Germany; ²OncoRay - National Center for Radiation Research in Oncology, University Hospital Carl Gustav Carus, Technische Universität Dresden, Helmholtz Zentrum, Dresden Rossendorf, Germany; ³Department of Haematology and Oncology, Rems-Murr-Hospital, Winnenden, Germany; ⁴Department of Pathology, University Hospital Carl Gustav Carus Dresden, Technische Universität Dresden, Dresden, Germany; ⁵Department of Radiology, Städtisches Klinikum Dresden, Dresden, Germany; ⁶Department of Nuclear Medicine, University Hospital Carl Gustav Carus, Technische Universität Dresden, Dresden, Germany; ⁷National Center for Tumor Diseases NCT, Partner site Dresden, Dresden, Germany; ⁸Department of Haematological Medicine, The Rayne Institute, King's College London, London, UK

[#]MS and KZ contributed equally as co-senior authors.

Haematologica 2020
Volume 105(6):1552-1558

ABSTRACT

Extramedullary (EM) disease in patients with acute myeloid leukemia (AML) is a known phenomenon. Since the prevalence of EM AML has so far only been clinically determined on examination, we performed a prospective study in patients with AML. The aim of the study was to determine the prevalence of metabolically active EM AML using total body ¹⁸Fluorodesoxy-glucose positron emission tomography / computed tomography (¹⁸FDG-PET/CT) imaging at diagnosis prior to initiation of therapy. In order to define the dynamics of EM AML throughout treatment, PET-positive patients underwent a second ¹⁸FDG-PET/CT imaging series during follow up by the time of remission assessment. A total of 93 patients with AML underwent ¹⁸FDG-PET/CT scans at diagnosis. The prevalence of PET-positive EM AML was 19% with a total of 65 EM AML manifestations and a median number of two EM manifestations per patient (range, 1-12), with a median maximum standardized uptake value of 6.1 (range, 2-51.4). When adding those three patients with histologically confirmed EM AML who were ¹⁸FDG-PET/CT negative in the ¹⁸FDG-PET/CT at diagnosis, the combined prevalence for EM AML was 22%, resulting in 77% sensitivity and 97% specificity. Importantly, 60% (6 of 10) patients with histologically confirmed EM AML still had active EM disease in their follow up ¹⁸FDG-PET/CT. ¹⁸FDG-PET/CT reveals a high prevalence of metabolically active EM disease in AML patients. Metabolic activity in EM AML may persist even beyond the time point of hematologic remission, a finding that merits further prospective investigation to explore its prognostic relevance. (Trial registered at [clinicaltrials.gov](https://clinicaltrials.gov/ct2/show/study/01278069) identifier: 01278069.)

Correspondence:

FRIEDRICH STÖLZEL
friedrich.stoelzel@uniklinikum-dresden.de

Received: March 31, 2019.

Accepted: August 27, 2019.

Pre-published: August 29, 2019.

doi:10.3324/haematol.2019.223032

Check the online version for the most updated information on this article, online supplements, and information on authorship & disclosures: www.haematologica.org/content/105/6/1552

©2020 Ferrata Storti Foundation

Material published in *Haematologica* is covered by copyright. All rights are reserved to the Ferrata Storti Foundation. Use of published material is allowed under the following terms and conditions:

<https://creativecommons.org/licenses/by-nc/4.0/legalcode>.

Copies of published material are allowed for personal or internal use. Sharing published material for non-commercial purposes is subject to the following conditions:

<https://creativecommons.org/licenses/by-nc/4.0/legalcode>, sect. 3. Reproducing and sharing published material for commercial purposes is not allowed without permission in writing from the publisher.



Introduction

Acute myeloid leukemia (AML) may present with either concomitant or isolated extramedullary (EM) AML, also termed myeloid sarcoma (MS). EM AML is defined by infiltrating AML blasts effacing normal tissue as demonstrated by histological evaluation.¹ Data on the prevalence of EM AML are based on retrospective or clinical analyses, and they possibly under-estimate the true prevalence,

since they rely on findings from physical examination only or on coincidental findings in standard imaging procedures. Others have performed retrospective analyses from autopsy series, which might over-estimate the prevalence of EM AML, since these series accumulate data on AML patients succumbing to their disease. So far, EM AML prevalence has been seen to range from 2.5% to 9.1%.^{2,3} Previous studies and AML treatment recommendations identified EM AML as an adverse prognostic factor in patients with AML.⁴ In contrast, a recent retrospective analysis based on clinical data from a large number of AML patients included in clinical trials revealed a high proportion of patients with EM AML (23.7%), but could not identify EM AML as an independent prognostic factor.⁵ Nevertheless, this analysis and others also included patients with, for example, hepatomegaly and/or splenomegaly, gingival hyperplasia based on clinical examination, suggesting these represent EM AML or leukemic meningitis. These findings *per se* do not fulfill the criteria for EM AML.^{5,6} However, without a precise assessment of EM AML, valid risk factor analyses cannot be performed. ¹⁸Fluorodesoxy-glucose positron emission tomography/computed tomography (¹⁸FDG-PET/CT) is able to detect highly metabolic tissue and has proven efficacy in imaging studies for various types of malignant diseases. We and others have demonstrated the utility of ¹⁸FDG-PET/CT imaging in AML patients with histologically proven EM AML.⁷⁻¹⁵ We were able to demonstrate a sensitivity of 90% using ¹⁸FDG-PET/CT imaging and found additional EM sites in 60% of the patients.⁸ Another study in ten unselected AML patients using ¹⁸Fluorodeoxythymidine-PET discovered EM AML in 4 of 10.¹⁴ Prospective studies to assess the prevalence of EM disease in AML in unselected patients have, so far, not been performed. The aim of this prospective, observational study was to use ¹⁸FDG-PET/CT to determine the prevalence of EM AML in patients prior to initiation of AML therapy.

Methods

This open, prospective observational study was approved by the institutional review board (EK309102009) and registered at clinicaltrials.gov identifier: 01278069. Informed consent was collected prior to the first PET scan. Patients with AML aged 18-80 years underwent baseline total body ¹⁸FDG-PET/CT scans before initiation of therapy. Patients were included only if a delay of ≤ 5 days of initiation of treatment was clinically justifiable in order to perform the study.¹⁵ Hydroxyurea for disease control was admissible before the ¹⁸FDG-PET/CT. The primary objective of this study was to determine the prevalence of EM AML at diagnosis. The sample size was calculated such that the width of the 95% confidence interval (CI) would stay within 20%. Assuming a prevalence of 40% EM AML, 93 patients would need to be studied. The prevalence of 40% was based on the only data available at the time from a case series of ten unselected patients undergoing PET/CT scanning, demonstrating existence of EM AML in 4 of those 10 patients.¹⁴ This trial was not powered to compare survival differences in EM AML as compared to AML patients without EM. Since there is no evidence to indicate that the treatment of AML patients with EM manifestation of AML needs to be intensified or modified, the presence of EM AML was not part of the decision-making process for treatment of these patients.

In total, 106 patients were screened for the study between February 2011 and July 2013 in the Department of Haematology of the University Hospital Dresden. Of those, 13 patients were considered to be screening failures and were not considered for further analyses, such that the planned sample size of 93 patients was reached. Reasons for screening failure were: age >80 years or ¹⁸FDG-PET/CT not feasible due to the clinical condition of the patient (n = 7) or other (n=6). Interestingly, two of these 13 patients had EM AML (histologically confirmed diagnosis in one patient and clinical diagnosis in the other). Patients with PET-positive EM AML at baseline underwent a second ¹⁸FDG-PET/CT scan after therapy initiation either at the date of complete remission or until day 60 in case of not achieving CR. A complete diagram of screened and included patients is shown in Figure 1. Hybrid ¹⁸FDG-PET/CT scans were performed as recently published using a Siemens Sensation 16 as part of a biograph (Siemens, Knoxville, TN, USA) with intravenous application of ¹⁸FDG and 120 mL contrast media Ultravist 370 (Bayer Schering Pharma, Leverkusen, Germany).⁸ PET 3-dimensional emission scans were conducted with a median activity of 367 MBq (range, 223-433 MBq), as recently published.⁸ For assessment of ¹⁸FDG-PET/CT imaging, no specific threshold or metabolic activity (e.g. maximum standardized uptake value, SUVmax) was applied. Instead, subtle correlation of any ¹⁸FDG-positive lesion with the fused CT images was performed to detect a corresponding tissue proliferation before suspecting an EM manifestation of AML. In cases in which no morphological correlate was apparent, ¹⁸FDG-positive lesions were declared to be unspecific. The estimated prevalence of EM AML was ascertained by calculating the specificity of baseline ¹⁸FDG-PET/CT positivity in relation to those EM AML lesions confirmed positive for EM AML upon histology. Thereafter, the total number of baseline ¹⁸FDG-PET/CT positive EM AML patients was multiplied by this specificity to derive an estimate for the prevalence in the total sample of 93. A CI with at least 95% coverage was derived by calculating the exact Clopper-Pearson-Confidence Intervals. Complete remission (CR) was defined according to the standard consensus criteria.¹⁶ The Mann-Whitney U-test was used to compare continuous variables between patient groups, while the χ^2 -test was applied to categorical variables. All statistical analyses were performed using SPSS version 25 (SPSS Inc., Chicago, IL, USA); two-sided tests were applied. $P < 0.05$ was considered statistically significant.

Results

Patient population and safety

A total of 93 patients with AML (n=9 with relapsed AML) underwent total body ¹⁸FDG-PET/CT scans at diagnosis after giving informed consent. Median age of all patients was 61 years (range, 27-79 years). Clinical characteristics of the patient population are shown in Table 1. The majority were diagnosed with *de novo* AML (n=53, 57%) while 22 patients (23%) had secondary AML after preceding myelodysplastic syndrome (MDS) / myeloproliferative neoplasm (MPN), and n=18 (19%) patients had therapy-related AML (tAML) / therapy-related MPN (tMN). Median follow up of alive patients is 46 months (range, 5-60 months). There were no adverse reactions due to the application of intravenous ¹⁸FDG and intravenous contrast media. No deterioration in renal function, as determined by measurement of creatinine serum levels and estimation of GFR (eGFR) by Cockcroft-Gault, was observed after ¹⁸FDG-PET/CT imaging.

Prevalence and sites

Total body ¹⁸F-DG-PET/CT imaging detected highly metabolic manifestations suggestive of EM AML in 23% of the enrolled patients (n=21). Of these ¹⁸F-DG-PET positive patients, 11 (52%) had *de novo* AML, while 7 (33%) had tAML and 3 (14%) secondary AML with preceding MDS/MPN. In total, 65 EM AML manifestations were identified with ¹⁸F-DG-PET/CT in these 21 patients. The median SUVmax was 6.1 (range, 2-51.4). Patients with EM AML as per ¹⁸F-DG-PET/CT had a median of two EM AML manifestations (range, 1-12) with only six patients having only one EM AML manifestation; exemplary ¹⁸F-DG-PET/CT imaging is depicted in Figures 2A and B and 3A and 3B. Sites of EM AML as detected per ¹⁸F-DG-PET/CT were connective tissue (n=4, one patient paravertebral, one paraaortic, one next to the jaw angle, and one at the base of the tongue), parenchymal tissues (n=8, with manifestations in adrenal glands, kidneys, liver, and spleen), and lymph nodes (n=15). A total of 9% of patients presented with clinically overt EM AML (n=8). Applying ¹⁸F-DG-PET/CT, additional EM manifestations were detected in 62% (n=5) of these patients. In 12 of the 21 patients who were diagnosed with EM AML as per ¹⁸F-DG-PET/CT, biopsies from EM sites were obtained in order to assess the provenance of the diagnosed tumor and to assess the sensitivity of ¹⁸F-DG-PET/CT. In ten patients, histology review confirmed the occurrence of EM AML in these sites, indicating a sensitivity of 77% for ¹⁸F-DG-PET/CT. Interestingly, in the two remaining patients in whom histology could not confirm EM AML, concomitant tumors were found (one patient with Castleman's disease and one patient with a solid fibrous tumor). Extrapolating these results onto the entire cohort, and applying the positive predictive value of 83.3%, the prevalence of EM AML in our AML patient cohort was 17% (95%CI: 11-29%).

When only analyzing patients with newly diagnosed AML, 16 (19%) patients were identified with EM AML as per ¹⁸F-DG-PET/CT. Characteristics of patients with or without EM AML as per ¹⁸F-DG-PET/CT and histological confirmation are shown in *Online Supplementary Table S1*. In comparison with PET-negative patients, those with PET-positive EM AML as per ¹⁸F-DG-PET/CT had a higher percentage of bone marrow infiltrating blasts, higher white blood cell (WBC) count in the peripheral blood, and higher C-reactive protein serum levels. Furthermore, in the cohort of AML patients with EM disease, there were no patients with favorable cytogenetic risk and a higher fraction of patients with relapsed AML.

In addition, in three patients of the ¹⁸F-DG-PET/CT negative group (n=72), EM AML was identified on examination and diagnosed through histological confirmation after biopsy. Two of these patients had a skin manifestation (chloroma) while one patient developed cervical lymphadenopathy during induction chemotherapy and then underwent biopsy and an additional, unscheduled ¹⁸F-DG-PET/CT, both confirming the diagnosis of EM AML. When these patients were added to our extrapolated prevalence of EM AML, the combined prevalence of EM AML in this study was 22%. Thus, the specificity for ¹⁸F-DG-PET/CT to detect EM AML is 97%. An overview of patients undergoing biopsy for diagnosis in both cohorts is available in the *Online Supplementary Table S2*. When we analyzed only the largest subgroup of our study cohort of patients with newly diagnosed AML, the combined prevalence of EM AML was 17%.

A total of 18 patients (19%) in this study were treated with hydroxyurea prior to ¹⁸F-DG-PET/CT and thus prior to initiation of chemotherapy. Four of the 21 patients

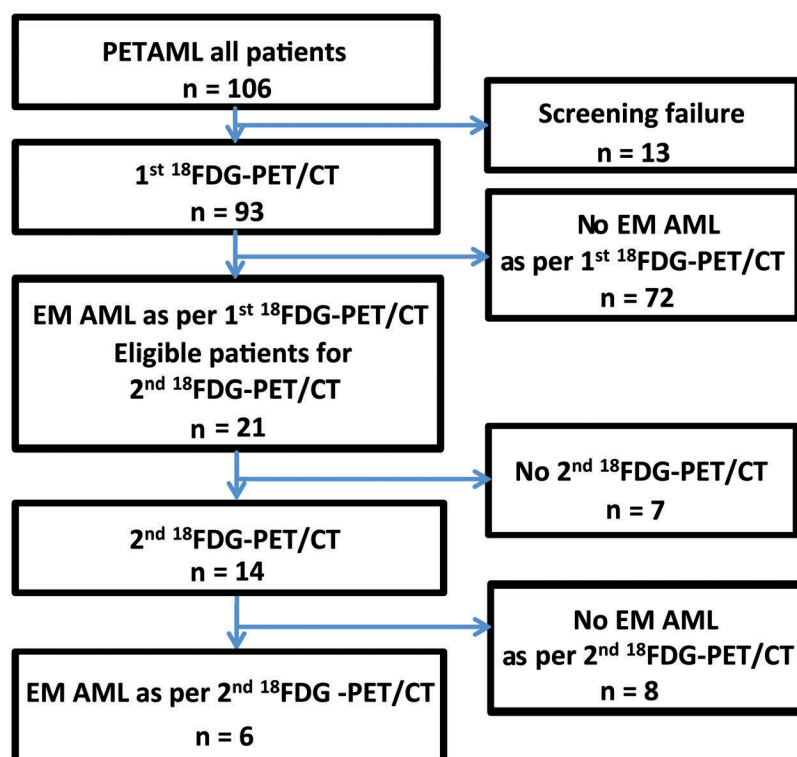


Figure 1. Modified CONSORT diagram demonstrating screening, patient selection and analysis for the complete patient cohort. PETAML: PET-CT in AML for Detection of Extramedullary AML Manifestations study; n: number; ¹⁸F-DG-PET/CT: ¹⁸Fluorodesoxy-glucose positron emission tomography/computed tomography; EM: extramedullary; AML: acute myeloid leukemia.

(19%) who were diagnosed with EM AML as per ^{18}F FDG-PET/CT were treated with hydroxyurea prior to ^{18}F FDG-PET/CT imaging.

Follow-up ^{18}F FDG-PET/CT

Patients with EM diagnosed by ^{18}F FDG-PET/CT underwent a second ^{18}F FDG-PET/CT scan at confirmation of CR or, at the latest, until day 60 after initiation of therapy in case no CR was achieved. A total of 14 of 21 patients with EM AML as per baseline ^{18}F FDG-PET/CT at diagnosis underwent a second ^{18}F FDG-PET/CT. The remaining patients did not undergo a second ^{18}F FDG-PET/CT because of severe disease and intensive care treatment (n=3), mental distress (n=1), palliative care in a hospice (n=1), and withdrawal of study consent for the second ^{18}F FDG-PET/CT (n=2). When we analyzed only the follow up

^{18}F FDG-PET/CT of those patients who were ^{18}F FDG-PET/CT positive and had a positive confirmatory biopsy (n=10 patients), 60% of these patients (n=6) were still positive for EM AML as diagnosed per the second ^{18}F FDG-PET/CT. Exemplary ^{18}F FDG-PET/CT imaging of a responding and a non-responding patient (who both underwent intensive induction chemotherapy) is available in Figures 2C and 3C-E. Interestingly, of the six patients who still had EM AML (as per ^{18}F FDG-PET/CT imaging) at the time of their second ^{18}F FDG-PET/CT, four patients with EM AML and AML bone marrow infiltration at diagnosis were in CR as determined by bone marrow cytomorphology at the time of second ^{18}F FDG-PET/CT. Of those four patients who still had EM AML in their second ^{18}F FDG-PET/CT, but who were in CR as per bone marrow cytomorphology, three patients subsequently relapsed. The other two (of the six patients with persistent metabolic disease) had isolated EM AML as per ^{18}F FDG-PET/CT: one patient had unchanged EM AML manifestations in the second ^{18}F FDG-PET/CT, while the other had a progression of EM AML manifestations in the second ^{18}F FDG-PET/CT. The metabolic and numerical dynamics of EM AML manifestations in patients with histologically confirmed EM AML from baseline to follow up ^{18}F FDG-PET/CT are shown in *Online Supplementary Figure 1A* and *B*.

Table 1. Patients' characteristics at diagnosis.

	PETAML n = 93
Median age at diagnosis (range)	61 (27-79)
Gender, n. (%)	
Female	42 (44)
Male	51 (55)
Median percentage of bone marrow blasts (range)	47.5 (3 - 96.5)
Median WBC count at diagnosis $\times 10^9/\text{L}$ (range)	6.3 (0.4 - 222.4)
Median platelet count at diagnosis $\times 10^9/\text{L}$ (range)	55 (3 - 278)
Median hemoglobin level at diagnosis in g/dL (range)	9 (4 - 14.8)
FAB subtypes, n. (%)	
M0	7 (8)
M1	17 (18)
M2	36 (39)
M4	9 (10)
M5 a,b	12 (13)
M6	4 (4)
M7	3 (3)
other	5 (5)
Cytogenetic risk groups, n. (%) ¹	
adverse	22 (24)
intermediate	64 (69)
favorable	6 (7)
<i>FLT3</i> -ITD status, n. (%) ²	
<i>FLT3</i> -ITD	13 (15)
<i>FLT3</i> -wildtype	74 (85)
<i>NPM1</i> status, n. (%) ³	
wildtype <i>NPM1</i>	72 (82)
mutated <i>NPM1</i>	16 (18)
<i>CEBPA</i> status, n. (%) ⁴	
no biallelic mutated <i>CEBPA</i>	75 (99)
biallelic mutated <i>CEBPA</i>	1 (1)
AML status, n. (%)	
<i>de novo</i> AML	53 (57)
secondary AML	22 (23)
tAML/tMN	18 (19)
relapsed AML	9

¹Assignment to cytogenetic risk-group was not possible for n=1 patient. ²*FLT3*-ITD mutational status could not be obtained for n=6 patients. ³*NPM1* mutational status could not be obtained for n=5 patients. ⁴*CEBPA* mutational status could not be obtained for n=17 patients. AML: acute myeloid leukemia; WBC: white blood cell; FAB: French-American-British classification; *FLT3*: *Fms-Like-Tyrosine Kinase 3*; ITD: internal tandem duplication; *NPM1*: *nucleophosmin 1*; *CEBPA*: *CCAAT/enhancer-binding protein alpha*; tAML/tMN: therapy-related AML/therapy-related myeloid neoplasia; secondary AML: AML after preceding myelodysplastic syndrome or myeloproliferative neoplasia.

Discussion

Our study is the first to prospectively evaluate ^{18}F FDG-PET/CT imaging for the diagnosis of EM AML in patients with AML. Furthermore, this is the first prospective study combining ^{18}F FDG-PET/CT imaging, clinical findings, and histological examination after biopsy to systematically estimate EM AML. According to our results, ^{18}F FDG-PET/CT is a useful and safe tool to detect EM AML with a high sensitivity and specificity of 77% and 97%, respectively. While the prevalence of EM AML as per baseline ^{18}F FDG-PET/CT was 23%, we found an estimated prevalence of EM AML of 19% using ^{18}F FDG-PET/CT when including the sensitivity of ^{18}F FDG-PET/CT after histological examination of biopsied lesions. When also adding the three patients with histologically confirmed EM AML, who were initially ^{18}F FDG-PET/CT negative, the combined prevalence of the whole study cohort is 22%. An analysis of only patients with newly diagnosed AML led to a combined prevalence of EM AML of 17% in our study. This is 3- to 11-fold higher than previously reported^{2,3} but lower than in other reported studies.^{5,17,18} Some reports over-estimated the prevalence of EM AML since data were derived from autopsy studies, which have a natural selection in favor of relapsed and/or refractory patients, or because a positive selection in favor of myelomonocytic AML subtypes occurred, as these are known to have a higher likelihood of presenting with EM AML.^{17,18} Other studies under-estimate the prevalence of EM AML because they rely on the clinical findings of EM AML, which only represents the tip of the iceberg.^{3,5} Some reports also include EM AML sites in their calculation, such as gingival hyperplasia, splenomegaly or leukemic meningitis, which does not *per se* fulfill the World Health Organization (WHO) criteria for EM AML and therefore might over-estimate the prevalence of EM AML.^{5,6,17,19} A recent retrospective analysis by Ganzel *et al.* reported a clinical prevalence of 24% and argued that with a PET-based screening the rate

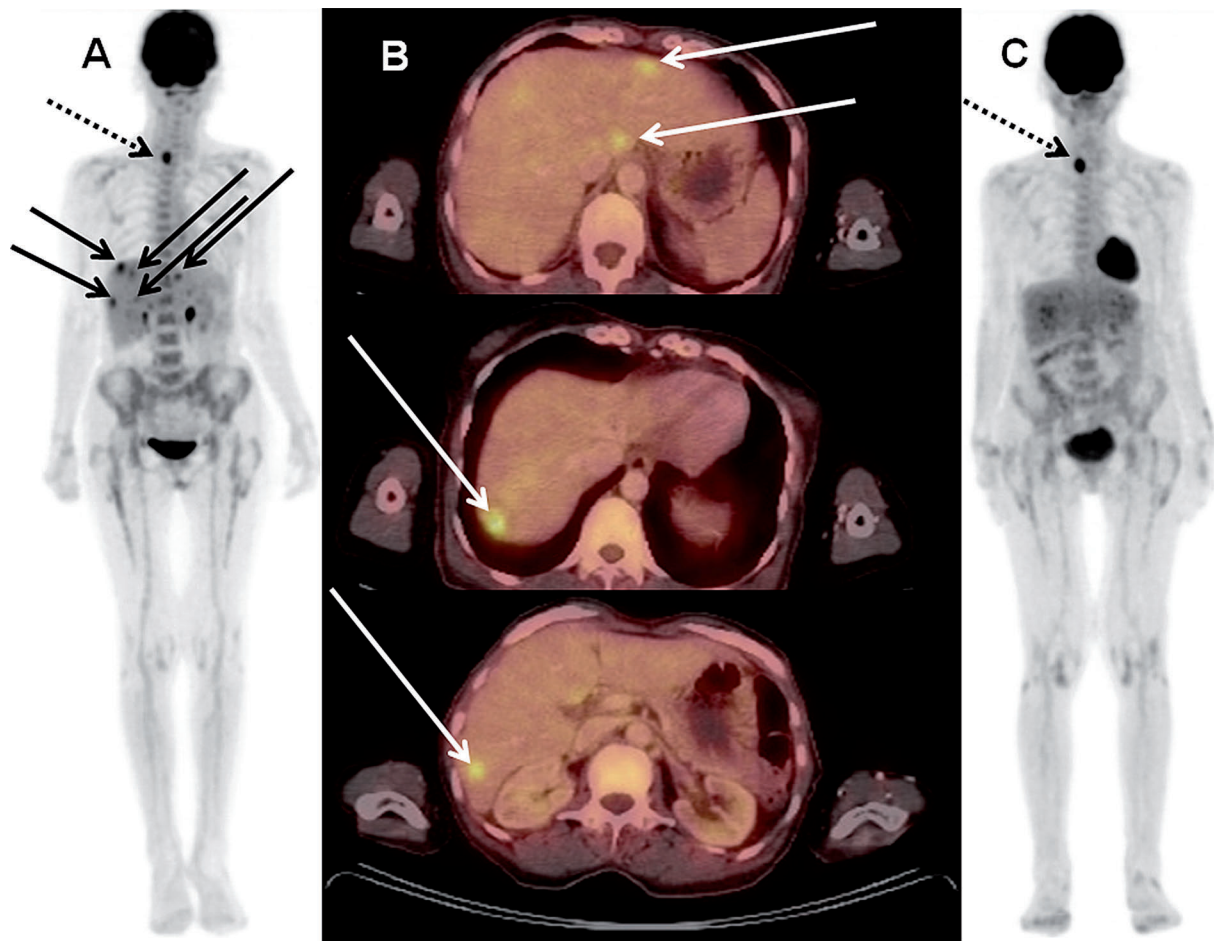


Figure 2. Images of a 69-year old female patient with histologically confirmed extramedullary (EM), bilobular hepatic manifestations of acute myeloid leukemia (AML) (continuous arrows) who underwent intensive induction chemotherapy. (A) Maximum intensity projection (MIP) and (B) three representative slices of the fused multiplanar reconstructions (MPR) of the pre-therapeutic ^{18}F Fluorodesoxy-glucose positron emission tomography/computed tomography (^{18}F FDG-PET/CT). Maximum standardized uptake value (SUVmax) ranged from 5.2 to 7.4. (C) MIP of the post-therapeutic ^{18}F FDG-PET/CT confirming a complete metabolic remission of all hepatic lesions. Note the hypermetabolic focus (SUVmax 8.9) in the right thyroid lobe (dotted arrows, see also (A) at baseline) which does not reflect AML but rather a thyroid adenoma that was still present in the post-therapeutic scan (SUVmax 8.1).

of extramedullary AML would be even higher.⁵ The prevalence of EM AML in our study remains in that range; however, our study and the analysis by Ganzel *et al.* describe and discuss different EM AML characteristics. Whether leukemic meningitis, gingival hyperplasia, and splenomegaly fulfill the WHO criteria for extramedullary disease remains highly debatable. Disrupted tissue architecture by AML cells (or effaced tissue architecture) cannot be considered exclusively responsible for leukemic meningitis (but as rather resembling blood-brain-barrier migration), gingival hyperplasia (resembling indirect hyperplasia), and splenomegaly (resembling leukemic infiltration not effacing spleen architecture).^{1,20} Whether clinical assessment is sufficient, and whether it is necessary to biopsy EM AML, has been the subject of much discussion and controversy.⁵ However, our data show that a non-negligible proportion of AML patients with EM still harbor ^{18}F FDG-avid manifestations despite being in CR at the same time, as per bone marrow assessment. Since the definition of a CR of AML includes resolution of EM AML, this provides a further argument to perform sensitive ^{18}F FDG-PET/CT imaging in these patients.

Furthermore, incidental findings of other hematologic malignancies such as multicentric Castleman's disease at initial presentation of AML diagnosed in parallel in our study seem to argue for histological confirmation whenever possible. The observation that many patients with EM AML harbor more than one EM site has been suggested in our pilot study and others, and could be confirmed by this study.^{5,8} The phenomenon observed here that isolated EM AML of the skin (chloroma) is not necessarily ^{18}F FDG-PET-avid and thus cannot be visualized by ^{18}F FDG-PET/CT imaging has already been reported in our pilot study.⁸ For these patients ^{18}F FDG-PET/CT imaging might only be useful in identifying additional EM AML sites.

However, all imaging methods have limitations. ^{18}F FDG-PET/CT is limited by the size of an EM AML mass required to emit an ^{18}F FDG-PET signal. Theoretically, a cluster of at least 10^6 FDG avid cells is needed to meet the spatial resolution of a commercially available human PET machine and to generate a detectable PET signal. Furthermore, an objective of this trial was to include a representative AML patient cohort, since it was designed to estimate the prevalence of EM AML, and not survival

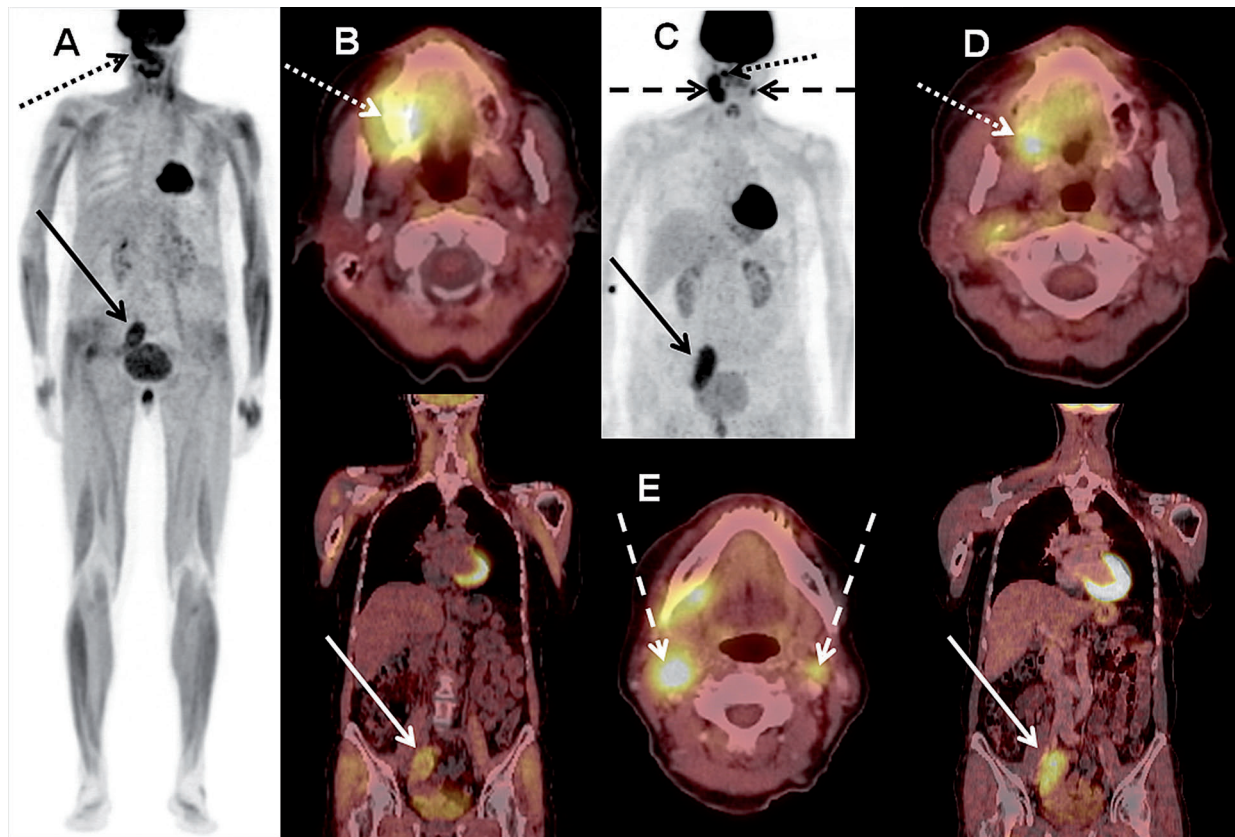


Figure 3. Images of a 63-year old female patient with histologically confirmed extramedullary (EM) manifestation of acute myeloid leukemia (AML) in the oral cavity (dotted arrows) who underwent intensive induction chemotherapy. (A) Maximum intensity projection (MIP) and (B) fused multiplanar reconstruction (MPR) of the pre-therapeutic ^{18}F Fluorodesoxy-glucose positron emission tomography/computed tomography (^{18}F FDG-PET/CT). Maximum standardized uptake value (SUVmax) was 9.1. ^{18}F FDG-PET detected a further right iliac EM AML (SUVmax 5.6; continuous arrows). (C) MIP of the post-therapeutic follow up ^{18}F FDG-PET/CT confirming the slightly regressive EM AML of the oral cavity (SUVmax 7.4) but also the progressive right iliacal EM AML (SUVmax 8.1). (D) MPR of this scan. New bicervical EM AML (dashed arrows) was also detected (E), see also (C) (SUVmax up to 9.5).

differences between patients with EM AML as compared to patients without EM AML. However, 3 of the 9 relapsed AML patients who were included in the trial harbored EM AML as per ^{18}F FDG-PET/CT. In spite of this, the National Comprehensive Cancer Network and others recommend ^{18}F FDG-PET/CT when EM AML is suspected in an AML patient, while the European LeukemiaNet provides no recommendations for doctors treating patients with EM AML.^{2,6,21,22}

In summary, our study demonstrates a higher prevalence of EM AML than previously reported and assumed, while the clinical prevalence was in the range of previously published reports. We were able to demonstrate that ^{18}F FDG-PET/CT is feasible and safe in patients with AML at diagnosis. Furthermore, we were able to confirm that, in most patients, more than one metabolically active EM AML manifestation could be detected with ^{18}F FDG-PET/CT. Interestingly, six patients who were PET-positive at baseline and who had histologically confirmed EM AML were in hematologic CR but still had detectable ^{18}F FDG-avid EM AML depicting heterogeneity after treatment (Online Supplementary Figure S1A). When analyzing those four patients who presented with EM AML at diag-

nosis (as per initial ^{18}F FDG-PET/CT) and frank bone marrow AML, all four were still positive for EM AML as per ^{18}F FDG-PET/CT but in a CR as per bone marrow aspirate; furthermore, three of these four patients eventually relapsed, despite consolidation therapy. The dynamics of PET-positivity with regard to concurrent bone marrow involvement, therefore, seem to be heterogeneous and the prognostic relevance of this has to be studied in further prospective trials. Hence, this study allows further trials to be designed and calculated for a prospective evaluation of the impact of EM AML using ^{18}F FDG-PET/CT.

Funding

This study was supported by the German Cancer Aid Foundation (109575 to FS, KZ, and MS). Open Access funding by the Publication Funds of the TU Dresden.

Acknowledgments

We would like to thank Katrin Rosenow and Gabriele Kotzerke for co-ordinating the ^{18}F FDG-PET/CT procedures. We would like to thank Annett Engmann, Katrin Peschel, and Catrin Theuser for data management. We would like to thank the patients, nurses, and doctors who contributed to this study.

References

- Vardiman JW, Thiele J, Arber DA, et al. The 2008 revision of the World Health Organization (WHO) classification of myeloid neoplasms and acute leukemia: rationale and important changes. *Blood*. 2009;114(5):937-951.
- Bakst RL, Tallman MS, Douer D, Yahalom J. How I treat extramedullary acute myeloid leukemia. *Blood*. 2011;118(14):3785-3793.
- Avni B, Rund D, Levin M, et al. Clinical implications of acute myeloid leukemia presenting as myeloid sarcoma. *Hematol Oncol*. 2012;30(1):34-40.
- Comelissen JJ, Gratwohl A, Schlenk RF, et al. The European LeukemiaNet AML Working Party consensus statement on allogeneic HSCT for patients with AML in remission: an integrated-risk adapted approach. *Nat Rev Clin Oncol*. 2012;9(10):579-590.
- Ganzel C, Manola J, Douer D, et al. Extramedullary Disease in Adult Acute Myeloid Leukemia Is Common but Lacks Independent Significance: Analysis of Patients in ECOG-ACRIN Cancer Research Group Trials, 1980-2008. *J Clin Oncol*. 2016;34(29):3544-3553.
- Dohner H, Estey E, Grimwade D, et al. Diagnosis and management of AML in adults: 2017 ELN recommendations from an international expert panel. *Blood*. 2017;129(4):424-447.
- Karlin L, Itti E, Pautas C, et al. PET-imaging as a useful tool for early detection of the relapse site in the management of primary myeloid sarcoma. *Haematologica*. 2006;91(12 Suppl):ECR54.
- Stölzel F, Rollig C, Radke J, et al. (1)(8)F-FDG-PET/CT for detection of extramedullary acute myeloid leukemia. *Haematologica*. 2011;96(10):1552-1556.
- Aschoff P, Hantschel M, Oksuz M, et al. Integrated FDG-PET/CT for detection, therapy monitoring and follow-up of granulocytic sarcoma. Initial results. *Nuklearmedizin*. 2009;48(5):185-191.
- Kuenzle K, Taverna C, Steinert HC. Detection of extramedullary infiltrates in acute myelogenous leukemia with whole-body positron emission tomography and 2-deoxy-2-[18F]-fluoro-D-glucose. *Mol Imaging Biol*. 2002;4(2):179-183.
- Makis W, Hickeson M, Derbekyan V. Myeloid sarcoma presenting as an anterior mediastinal mass invading the pericardium: Serial Imaging With F-18 FDG PET/CT. *Clin Nucl Med*. 2010;35(9):706-709.
- Mantzariides M, Bonardel G, Fagot T, et al. Granulocytic sarcomas evaluated with F-18-fluorodeoxyglucose PET. *Clin Nucl Med*. 2008;33(2):115-117.
- Ueda K, Ichikawa M, Takahashi M, Momose T, Ohtomo K, Kurokawa M. FDG-PET is effective in the detection of granulocytic sarcoma in patients with myeloid malignancy. *Leukemia Res*. 2010;34(9):1239-1241.
- Buck AK, Bommer M, Juweid ME, et al. First demonstration of leukemia imaging with the proliferation marker 18F-fluorodeoxythymidine. *J Nucl Med*. 2008;49(11):1756-1762.
- Sekeres MA, Elson P, Kalaycio ME, et al. Time from diagnosis to treatment initiation predicts survival in younger, but not older, acute myeloid leukemia patients. *Blood*. 2009;113(1):28-36.
- Cheson BD, Bennett JM, Kopecky KJ, et al. Revised recommendations of the International Working Group for Diagnosis, Standardization of Response Criteria, Treatment Outcomes, and Reporting Standards for Therapeutic Trials in Acute Myeloid Leukemia. *J Clin Oncol*. 2003;21(24):4642-4649.
- Cribe AS, Steenhof M, Marcher CW, Petersen H, Frederiksen H, Friis LS. Extramedullary disease in patients with acute myeloid leukemia assessed by 18F-FDG PET. *Eur J Haematol*. 2013;90(4):273-278.
- Liu PI, Ishimaru T, McGregor DH, Okada H, Steer A. Autopsy study of granulocytic sarcoma (chloroma) in patients with myelogenous leukemia, Hiroshima-Nagasaki 1949-1969. *Cancer*. 1973;31(4):948-955.
- Zhou WL, Wu HB, Wang LJ, Tian Y, Dong Y, Wang QS. Usefulness and pitfalls of F-18-FDG PET/CT for diagnosing extramedullary acute leukemia. *Eur J Radiol*. 2016;85(1):205-210.
- Pileri SA, Ascani S, Cox MC, et al. Myeloid sarcoma: clinico-pathologic, phenotypic and cytogenetic analysis of 92 adult patients. *Leukemia*. 2007;21(2):340-350.
- O'Donnell MR, Tallman MS, Abboud CN, et al. Acute Myeloid Leukemia, Version 3.2017, NCCN Clinical Practice Guidelines in Oncology. *J Natl Compr Cancer Netw*. 2017;15(7):926-957.
- Cunningham I, Kohno B. 18 FDG-PET/CT: 21st century approach to leukemic tumors in 124 cases. *Am J Hematol*. 2016;91(4):379-384.

Obesity is a risk factor for acute promyelocytic leukemia: evidence from population and cross-sectional studies and correlation with FLT3 mutations and polyunsaturated fatty acid metabolism



Luca Mazzarella,^{1,2} Edoardo Botteri,³ Anthony Matthews,⁴ Elena Gatti,¹ Davide Di Salvatore,⁵ Vincenzo Bagnardi,⁶ Massimo Breccia,⁷ Pau Montesinos,⁸ Teresa Bernal,⁹ Cristina Gil,¹⁰ Timothy J Ley,¹¹ Miguel Sanz,⁸ Krishnan Bhaskaran,⁴ Francesco Lo Coco^{12*} and Pier Giuseppe Pelicci^{1,13}

¹Department of Experimental Oncology, European Institute of Oncology IRCCS, Milan, Italy; ²Division of Early Drug Development for Innovative Therapies, European Institute of Oncology IRCCS, Milan, Italy; ³Cancer Registry of Norway, Oslo, Norway; ⁴London School of Hygiene and Tropical Medicine, London, UK; ⁵IFOM-FIRC Institute of Molecular Oncology, Milan, Italy; ⁶University of Milan-Bicocca, Milan, Italy; ⁷Division of Hematology, Department of Cellular Biotechnologies and Hematology, Sapienza University, Rome, Italy; ⁸Hematology Department, Hospital Universitario y Politécnico La Fe, Valencia, Spain; ⁹Hospital Central de Asturias, Oviedo, Spain; ¹⁰Hospital General, Alicante, Spain; ¹¹Department of Medicine, Division of Oncology, Washington University in St. Louis, Saint Louis, MO, USA; ¹²Department of Hematology, University Tor Vergata, Roma, Italy and ¹³Department of Oncology and Hemato-Oncology, University of Milan

Haematologica 2020
Volume 105(6):1559-1566

ABSTRACT

Obesity correlates with hematologic malignancies including leukemias, but risk of specific leukemia subtypes like acute promyelocytic leukemia and underlying molecular mechanisms are poorly understood. We explored multiple datasets for correlation between leukemia, body mass index (BMI) and molecular features. In a population-based study (n=5.2 million), we correlated BMI with promyelocytic leukemia, and other acute myeloid, lymphoid or other leukemias. In cross-sectional studies, we tested BMI deviation in promyelocytic leukemia trial cohorts from that expected based on national surveys. We explored The Cancer Genome Atlas for transcriptional signatures and mutations enriched in promyelocytic leukemia and/or obesity, and confirmed a correlation between body mass and FLT3 mutations in promyelocytic leukemia cohorts by logistic regression. In the population-based study, hazard ratio per 5 kg/m² increase was: promyelocytic leukemia 1.44 (95% CI: 1.0-2.08), non-promyelocytic acute myeloid leukemias 1.17 (95% CI: 1.10-1.26), lymphoid leukemias 1.04 (95% CI: 1.0-1.09), other 1.10 (95% CI: 1.04-1.15). In cross-sectional studies, body mass deviated significantly from that expected (Italy: $P < 0.001$; Spain: $P = 0.011$; USA: $P < 0.001$). Promyelocytic leukemia showed upregulation of polyunsaturated fatty acid metabolism genes. Odds of FLT3 mutations were higher in obese acute myeloid leukemias (odds ratio=2.4, $P = 0.007$), whether promyelocytic or not, a correlation confirmed in the pooled promyelocytic leukemia cohorts (OR=1.22, 1.05-1.43 per 5 kg/m²). These results strengthen the evidence for obesity as a *bona fide* risk factor for myeloid leukemias, and in particular APL. FLT3 mutations and polyunsaturated fatty acid metabolism may play a previously underappreciated role in obesity-associated leukemogenesis.

Introduction

The etiology of acute myeloid leukemia (AML) remains poorly understood. Genetic predisposition or clear exposure to environmental mutagenic agents (smoking, benzene, radiation, prior chemotherapy) can be demonstrated only in a minority of cases.¹ Age is an independent risk factor, probably linked to the pro-

This paper is dedicated to the memory of our wonderful colleague, Prof. Francesco Lo Coco, who recently passed away

Correspondence:

LUCA MAZZARELLA
luca.mazzarella@ieo.it

PIER GIUSEPPE PELICCI
piergiuseppe.pelicci@ieo.it

Received: April 5, 2019.

Accepted: September 11, 2019.

Pre-published: September 12, 2019.

doi:10.3324/haematol.2019.223925

Check the online version for the most updated information on this article, online supplements, and information on authorship & disclosures: www.haematologica.org/content/106/6/1559

©2020 Ferrata Storti Foundation

Material published in *Haematologica* is covered by copyright. All rights are reserved to the Ferrata Storti Foundation. Use of published material is allowed under the following terms and conditions:

<https://creativecommons.org/licenses/by-nc/4.0/legalcode>.

Copies of published material are allowed for personal or internal use. Sharing published material for non-commercial purposes is subject to the following conditions:

<https://creativecommons.org/licenses/by-nc/4.0/legalcode>, sect. 3. Reproducing and sharing published material for commercial purposes is not allowed without permission in writing from the publisher.



gressive mutation accumulation and clonal stem cell expansion that accompanies aging.² Although obesity has recently emerged as a prominent risk factor for a variety of solid tumors,³ its impact on hematologic neoplasms has received less attention. A moderate but consistently positive correlation between body mass index (BMI) and incidence of leukemias has been identified in observational studies,^{4,6} yet none of the collected evidence has been considered sufficiently strong to consider obesity as a *bona fide* risk factor for AML.^{5,7} Most studies did not distinguish between myeloid/lymphoid and acute/chronic forms, nor between genetic subtypes within each form. AML is recognized as a highly heterogeneous disease with genetically diverse subtypes.⁸ Subtypes have radically different outcomes and, similarly, their risk may be differentially affected by environmental factors. Identification of subtype-specific risk associations, however, is made difficult by their rarity.

A genetic subset of AML, acute promyelocytic leukemia (APL), is characterized by a specific chromosomal translocation (t15;17), homogeneous biology and response to clinical agents all-trans retinoic acid (ATRA) and arsenic trioxide, which have made it the most curable form of AML to date.⁹ We previously demonstrated that the risk of relapse after ATRA/idarubicin is significantly increased in overweight/obese APL patients.¹⁰ In the present report, we investigated the association of overweight/obesity with the risk of developing APL and other leukemias. We describe the results of multiple studies across four western populations with significantly different dietary regimens and prevalence of obesity. All the studies demonstrated increased risk of developing APL in overweight/obesity subjects. In an effort to generate mechanistic hypotheses to explain this relationship, we analyzed transcriptomic and mutational data from the AML project in The Cancer Genome Atlas (TCGA)¹¹ and identified alterations selectively associated with obesity and/or APL which may be involved in obesity-associated leukemogenesis.

Methods

UK population-based study: data collection and statistical methods

Full details of the methods for the UK population study were described previously.⁶ The study was approved by the London School of Hygiene and Tropical Medicine Ethics Committee. To identify outcomes of specific leukemia sub-types, Clinical Practice Research Datalink (CPRD) clinical records were searched for codes relating to specific leukemia subgroups. We controlled for multiple co-variables at time of the BMI record(s): age, smoking status, alcohol use, previous diabetes diagnosis, index of multiple deprivation, calendar period, and stratified by gender. We excluded people with missing smoking [49,206 of 5.24 million (0.9%)] and alcohol [394,196 of 5.24 million (7.5%)] status. Confidence intervals (CI) in Figure 1 are presented at the 99% level; all other CIs are presented at the 95% level.

Cross-sectional studies: data collection and statistical methods

Acute promyelocytic leukemia cases from Spain were extracted from the PETHEMA database to include 414 cases diagnosed between 1998 and 2012. APL cases from Italy, where 134 adult patients were treated under the AIDA protocol, were included in the previously described cohort.¹⁰ APL cases from the USA includ-

ed the entire cohort of the published AML The Cancer Genome Atlas (TCGA) project¹¹ (n=20) plus 22 additional APL cases, unselected for any clinical variable, diagnosed at Washington University, St. Louis, MO, USA (Expanded TCGA cohort). For all case cohorts, BMI was measured at the time of diagnosis.

Data collection was approved by the Research Ethics Board of each participating institution, as referenced.¹¹⁻¹⁴ Data sources for expected BMI in the local population are described in the *Online Supplementary Appendix*.

We compared the distribution of BMI observed in the three APL case cohorts to the distribution of BMI expected in the general population of the same countries. Specifically, to calculate the expected distribution of BMI in Italy, we used data from the Italian National Institute of Statistics,¹⁴ and we selected the area of Lazio, where the APL cases were diagnosed, in the years 2000-2010. For Spain, we used data from the Eurostat,¹⁵ and we selected the general population of Spain in the year 2008, the only year available. For both Italy and Spain, the expected BMI distribution was calculated using the available age- and gender-specific BMI distribution of the general population classified into three categories (<25, 25-29.9, ≥30). For the USA, we used the 2009-2010 data from the American National Health and Nutrition Examination Survey.¹⁶ The expected BMI distribution was calculated using the available race-, age-, and gender-specific BMI distribution of the general population classified into four categories (<25, 25-29.9, 30.0-34.9, ≥35).

The global null hypothesis that the observed counts did not differ from the expected ones across the BMI categories was tested in a null Poisson regression model, where the observed counts were considered as dependent variable and the expected counts as the offset. BMI was included in the model as an ordinal variable to test the log-linear relationship between BMI and the observed to expected ratio (i.e. to test for linear trend). Pearson's χ^2 goodness of fit test *P*-value was reported.

Expression data analysis

Expression data (RPKM matrix) were downloaded from the AML TCGA data portal. Cases with available RNAseq, BMI and French-American-British (FAB) classification data (177 of 200) were used in the present study. Cases were classified by FAB in "APL" (FAB="M3") and "non-APL" (FAB ≠ "M3"), and by BMI in "obese" (BMI ≥ 30) and "non-obese" (BMI < 30). Genes with < 0.2 reads per kilo base per million mapped reads (RPKM) in at least 75% of patients were removed.¹¹ The Quantitative Set Analysis for Gene Expression method, as implemented in the quSAGE package¹⁵ in the R programming language (v3.2.3), was used to conduct supervised gene set enrichment analysis. For each expressed gene, the quSAGE algorithm calculates a probability density function (PDF) of differential expression between two groups of samples. For each gene set, it then calculates "activity", i.e. the mean difference in log-expression of individual genes included in a gene set. Gene sets with False Discovery Rate (FDR) < 0.05 were considered significant. We focused on the Kyoto Encyclopedia of Genes and Genomes (KEGG) and chemical and genetic perturbations (CGP) gene set collections, downloaded from MSigDB (<http://software.broadinstitute.org/gsea/msigdb/>). The CGP collection was used to confirm enrichment of previously identified APL-specific gene signatures¹⁶ (*Online Supplementary Table S1*). We focused on the KEGG collection, as it is enriched for metabolism-associated gene annotations.¹⁶ The script to generate the present results is available on request.

Mutational data analysis

For the analysis of the TCGA data, mutational data were retrieved from the TCGA AML paper,¹¹ and AML driver genes (restricted to those with at least 2 mutations in the dataset) were

down-loaded from IntOGen.¹⁷ For each gene, different mutations were conflated so that gene status in each patient was either "mutated" or "wild-type". For each gene, we then calculated the number of mutated or wild-type patients in the obese or non-obese groups, and calculated odds ratios (OR), 95% confidence intervals (CI), and *P*-values by Fisher's test with Benjamini-Hochberg correction. Only genes with >1 mutation in the dataset were considered, using the *fdsm* package in R.

For the analysis of the retrospective cohort, FLT3 Internal Tandem Duplication (ITD) mutational data were provided by the referring centers. Logistic regression was used to calculate OR with 95% CI.

Further details of the methods used are provided in the *Online Supplementary Appendix*.

Results

Population-based cohort study in the UK

Overall characteristics of the 5.24 million UK adults included in this study have been described previously.⁶ A total of 5,833 subjects with a diagnosis of "leukemia" over the observational time were included in the present analy-

sis. These events were further classified in the following groups: "APL" (n=26), "non APL-AML" (n=1,012), lymphoid leukemias ("LL"; n=2,823), and "other" (n=1,972). Median time lapse between BMI measurement and diagnosis was similar across subgroups (APL: 1,810 days; AML: 2,280 days; LL: 1,928 days; other: 1,894 days).

We fit BMI as a three-knot cubic spline and as a linear term. There was no evidence of non-linearity (*P*=0.94), suggesting that the relationship was best described by the linear model. After adjusting for co-variates, per each 5 kg/m² increase we obtained hazard ratios (HR) of 1.44 for

Table 1. Hazard ratios from the UK population study.

Disease	N. of events	Adjusted HR (per 5 kg/m ² increase in BMI)	95% CI
APL	26	1.44	1.00, 2.08
AML	1,012	1.17	1.10, 1.26
LL	2,823	1.04	1.00, 1.09
Other	1,972	1.10	1.04, 1.15

N: number; HR: hazard ratio; BMI: body mass index; CI: confidence interval; APL: acute promyelocytic leukemia; AML: acute myeloid leukemia; LL: lymphoid leukemias.

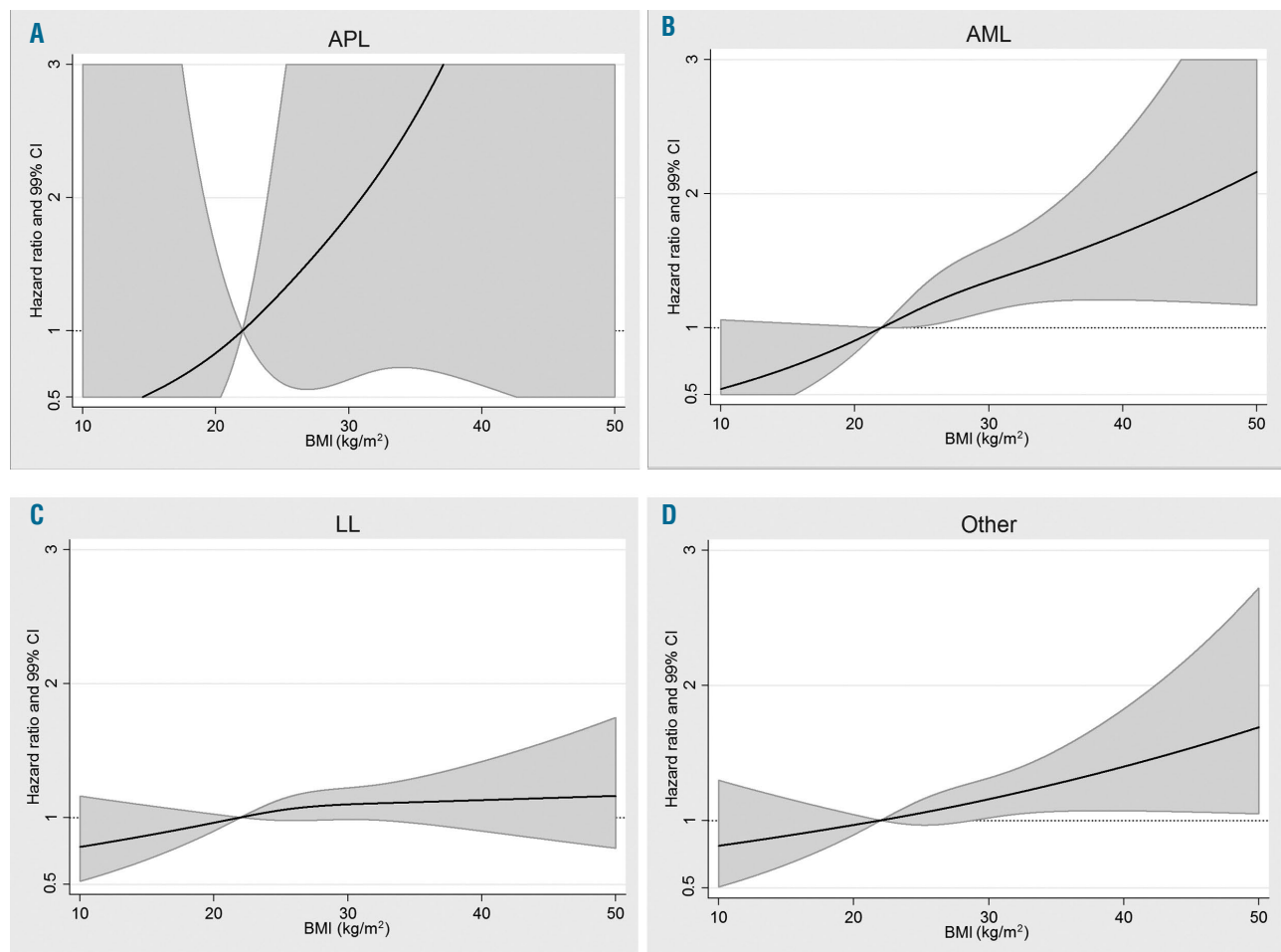


Figure 1. Relationship between body mass index (BMI) and log-hazard ratio (HR) for leukemias in the UK population. (A) Acute promyelocytic leukemia (APL); (B) other acute myeloid leukemia (AML); (C) lymphoid leukemias; (D) all leukemias. Plots show mean (dark line) \pm 95% confidence intervals (shaded area).

APL (95%CI: 1.0-2.08), 1.17 for non APL-AML (95%CI: 1.10-1.26), 1.04 for LL (95%CI: 1.0-1.09), and 1.10 for other leukemias (95%CI: 1.04-1.15) (Table 1 and Figure 1). Stratification by gender suggested a stronger effect for male gender in APL (HR 1.82, 95%CI: 1.10-3.00 vs. female HR 1.19, 95%CI: 0.67-1.98), although the sample size becomes very small (n=13 each). Together, these results suggest that higher BMI is associated with increased risk of all sub-types of leukemia, particularly APL.

Cross-sectional studies in Italian, Spanish and US trial cohorts

Though APL showed the strongest association with higher BMI in the cohort analysis described above, results were not conclusive due to the small number of cases identified (n=26) and the consequently wide confidence intervals. To strengthen the evidence, we carried out retrospective case-control studies using cohorts of APL

patients from national registries of clinical trials from Spain (PETHEMA) and Italy (GIMEMA), and patients from the US-based AML genome sequencing study (the AML TCGA cohort with 22 additional cases characterized at Washington University, St Louis, MO). In all three groups, APL diagnosis was established using gold standard diagnostic procedures.

Demographic characteristics of the three case cohorts (Italy n=134, Spain n=414 and USA n=42) are described in Table 2. Gender (female 53.0%, 55.2%, 50%, respectively) and age (median of 45, 45, 47 years, respectively) were similarly represented. Information on ethnicity was unavailable for the Spanish and Italian cohorts, whereas white, black and hispanic ethnicities were represented in the US cohort.

To generate control groups for comparison, we obtained anthropometric data from epidemiological surveys of the general population in the different countries. As the prevalence of obesity has increased dramatically in most coun-

Table 2. Description of the cross-sectional cohorts.

		Italy n=134	Spain n=414	USA n=42
Age	18 - 35	46 (34.3%)	113 (27.3%)	13 (31.0%)
	36 - 50	34 (25.4%)	145 (35.0%)	12 (28.6%)
	51 - 65	40 (29.9%)	102 (24.6%)	11 (26.2%)
	> 65	14 (10.4%)	54 (13.0%)	6 (14.3%)
	Median (IQR)	45 (31-57)	45 (34-57)	47 (33-60)
Gender	Male	63 (47.0%)	227 (54.8%)	21 (50.0%)
	Female	71 (53.0%)	187 (45.2%)	21 (50.0%)
Year of diagnosis	Median (range)	2002 (1997-2010)	2003 (1996-2012)	2007 (2001-2011)
Race	White	-	-	36 (85.7)
	Black	-	-	5 (11.9)
	Hispanic	-	-	1 (2.4)
BMI	Median (IQR)	26 (23-28)	26 (23-29)	34 (28-39)

IQR: interquartile range; BMI: body mass index; n: number.

Table 3. Observed body mass index (BMI) distribution in acute promyelocytic leukemia (APL) cases and expected BMI distribution in general population (percentages in brackets).

Italy	BMI	Obs	All Exp ^a	P	Obs	Males Exp ^b	P	Obs	Females Exp ^d	P
	<25.0	48 (35.8%)	77.8 (58.0%)	<0.001	16 (25.4%)	29.0 (46.0%)	<0.001	32 (45.1%)	48.8 (68.7%)	<0.001
	25.0-29.9	71 (53.0%)	44.8 (33.4%)		42 (66.7%)	28.0 (44.5%)		29 (40.8%)	16.8 (23.6%)	
	≥30.0	15 (11.2%)	11.4 (8.5%)		5 (7.9%)	6.0 (9.5%)		10 (14.1%)	5.5 (7.7%)	
	Total	134	134		63	63		71	71	
Spain	BMI	Obs	Exp ^a	P	Obs	Exp ^b	P	Obs	Exp ^d	P
	<25.0	172 (41.5%)	189.9 (45.9%)	0.011	79 (34.8%)	85.0 (37.4%)	0.130	93 (49.7%)	104.9 (56.1%)	0.033
	25.0-29.9	156 (37.7%)	158.1 (38.2%)		99 (43.6%)	103.2 (45.5%)		57 (30.5%)	55.9 (29.4%)	
	≥30.0	86 (20.8%)	66.0 (15.9%)		49 (21.6%)	38.8 (17.1%)		37 (19.8%)	27.2 (14.6%)	
	Total	414	414		227	227		187	187	
USA	BMI	Obs	Exp ^a	P	Obs	Exp ^b	P	Obs	Exp ^d	P
	<25.0	2 (4.8%)	12.8 (30.6%)	<0.001	1 (4.8%)	5.3 (25.4%)	0.002	1 (4.8%)	7.5 (35.7%)	0.003
	25.0-29.9	13 (31.0%)	13.7 (32.6%)		5 (23.8%)	7.9 (37.7%)		8 (38.1%)	5.8 (27.6%)	
	30.0-34.9	12 (28.6%)	8.6 (20.5%)		9 (42.9%)	4.8 (23.0%)		3 (14.3%)	3.8 (18.0%)	
	≥35.0	15 (35.7%)	6.9 (16.3%)		6 (28.6%)	2.9 (13.9%)		9 (42.9%)	3.9 (18.8%)	
	Total	42	42		21	21		21	21	

Expected frequencies were obtained from the body mass index (BMI) distribution in the general population of the area of the acute promyelocytic leukemia (APL) cases, period of APL diagnosis and in addition: ^aage class and gender; ^bage class, gender and race; ^cage class; ^dage class and race. Obs: observed.

tries in the last decades (especially in the USA), we obtained data that were as close as possible to the median year of diagnosis (2002 for Italy, 2003 for Spain, 2007 for the USA) (Table 3; see also Methods section).

In all three cohorts, there was strong evidence that the observed BMI distribution for cases across World Health Organization (WHO) BMI classes was different from that expected under the null hypothesis of no association (Italy: $P < 0.001$; Spain: $P = 0.011$; USA: $P < 0.001$) (Table 3) in gender-, age-, and ethnicity- (for USA) matched controls. In particular, in all three datasets, there were more cases than expected in the higher BMI groups, irrespective of gender in all cohorts apart from Spain, in which significance was not reached for males ($P = 0.130$) despite a similar trend (Table 3).

Correlation of TCGA transcriptomics data with body mass index and acute myeloid leukemia subtype

The availability of the TCGA dataset prompted us to search for signatures that could suggest a mechanistic rationale for the association between APL and obesity. We interrogated available AML transcriptomes with supervised gene set enrichment analysis using quSage.¹⁵ Focusing on the KEGG gene set collection, APL was associated with increased activity of 13 and decreased activity of 64 out of 186 gene sets (Table 4, Figure 2A and *Online Supplementary Table S2*). Intriguingly, among significantly up-regulated gene sets, we found pathways associated with the metabolism of long-chain unsaturated fatty acids (linoleic and arachidonic), which are precursors of eicosanoids mediating inflammation-associated cancers.¹⁸

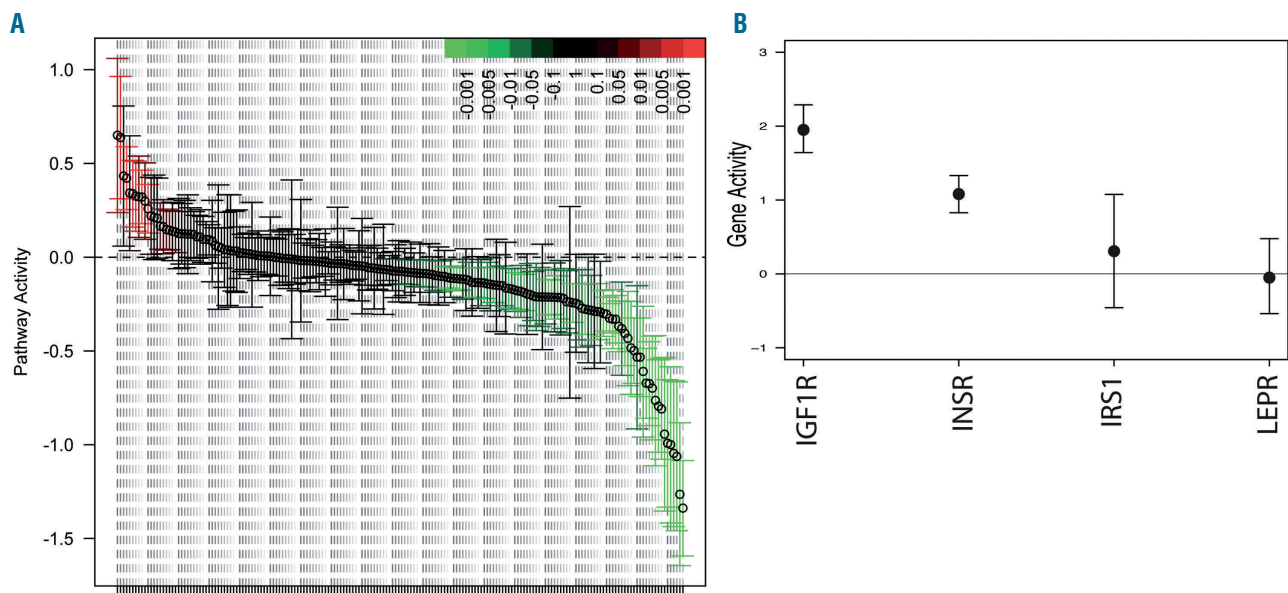


Figure 2. Differential activities of Kyoto Encyclopedia of Genes and Genomes (KEGG) pathways and insulin/leptin receptors in the M3 versus non-M3 quSage comparison in The Cancer Genome Atlas (TCGA). (A) Activity score with 95% Confidence Intervals (CI) of 186 KEGG gene sets; significant gene sets are color-coded in red (if up-regulated) or green (if down-regulated). (B) Insulin/IGF1 receptor pathway and leptin receptors. Mean \pm 95% confidence interval are plotted.

Table 4. Significantly up-regulated Kyoto Encyclopedia of Genes and Genomes (KEGG) pathways in acute promyelocytic leukemia versus acute myeloid leukemia in The Cancer Genome Atlas (TCGA).

pathway.name	log.fold.change	P	FDR
KEGG_RENIN_ANGIOTENSIN_SYSTEM	0.6503	0.0023	0.0093
KEGG_LINOLEIC_ACID_METABOLISM	0.6381	0.0002	0.0010
KEGG_GLYCOSAMINOGLYCAN_BIOSYNTHESIS_HEPARAN_SULFATE	0.4217	0.0000	0.0000
KEGG_GLYCOSPHINGOLIPID_BIOSYNTHESIS_LACTO_AND_NEOLACTO_SERIES	0.3391	0.0003	0.0017
KEGG_ALANINE_ASPARTATE_AND_Glutamate_METABOLISM	0.3258	0.0009	0.0039
KEGG_ARACHIDONIC_ACID_METABOLISM	0.3221	0.0037	0.0130
KEGG_GLYCOSAMINOGLYCAN_DEGRADATION	0.3208	0.0000	0.0001
KEGG_HISTIDINE_METABOLISM	0.2996	0.0044	0.0148
KEGG_ARGININE_AND_PROLINE_METABOLISM	0.2582	0.0001	0.0008
KEGG_LIMONENE_AND_PINENE_DEGRADATION	0.1662	0.0087	0.0250
KEGG_CARDIAC_MUSCLE_CONTRACTION	0.1475	0.0084	0.0245
KEGG_PROTEIN_EXPORT	0.1439	0.0066	0.0204
KEGG_PATHWAYS_IN_CANCER	0.1346	0.0169	0.0428

Also noticeable was the APL-associated upregulation of insulin and insulin-like growth factor (IGF1) receptors, but not leptin receptor (Figure 2B); insulin signaling-associated pathways were also specifically up-regulated in obese *versus* non-obese APL patients ("type II diabetes mellitus" and "insulin signaling") (Online Supplementary Table S2).

No pathway was significantly enriched in obese *versus* non-obese patients among non-M3 cases.

Correlation of mutational data with body mass index

We then asked whether obesity is associated with specific driver mutations in AML in the TCGA cohort. Out of 23 established driver genes mutated at least twice in the cohort, mutations in FLT3 were positively associated with obesity (33 of 88 obese *vs.* 22 of 110 non-obese; OR=2.4, FDR=0.16, $P=0.007$) (Figure 3 and Online Supplementary Table S3). The correlation remained statistically significant both in non-APL AML (27 of 49 obese *vs.* 22 of 102 non-obese; OR=2, $P=0.04$), and in APL (6 of 12 obese *vs.* 0 of 8 non-obese; $P=0.04$). When we analyzed the two main classes of FLT3 mutations separately [tyrosine kinase domain (TKD) and internal tandem duplication (ITD)], the association held statistically significant for ITD (24 of 88 obese *vs.* 14 of 110 non-obese; OR=2.6, $P=0.01$) but not for TKD (9 of 88 obese *vs.* 8 of 110 non-obese; $P=0.6$). In APL, where all FLT3 mutations were ITD, the correlation remained statistically significant (6 of 12 obese *vs.* 0 of 8 non-obese; $P=0.04$). In non-APL AML, with 32 ITD and 17 TKD, overall FLT3 mutations were still significantly enriched in obese patients (27 of 49 obese *vs.* 22 of 102 non-obese; OR=2, $P=0.04$) but not when analyzed separately ($P=0.11$ for ITD and 0.44 for TKD).

We then attempted to validate this finding in the APL cohorts, for which data on the most representative FLT3ITD mutation (ITD) were available (Table 5). In the pooled analysis (163 mutated patients, of a total 569), OR of having a FLT3 ITD was 1.22 (95%CI: 1.05-1.43) per each 5 kg/m² increase. In the individual cohorts, results were significant in the Italian (30 of 114 mutated, OR=2.35, 95%CI: 1.25-4.42) and US (14 of 41 mutated, OR=1.44, 95%CI: 0.93-2.24) cohorts, but not in the Spanish (119 of 414 mutated, OR=1.09, 95%CI: 0.89-1.33).

Discussion

Here we provide substantial evidence for an association between elevated BMI and risk of developing AML. The risk was particularly high with the APL subtype, with an estimated 44% HR increase per each 5 kg/m². This was qualitatively confirmed by comparing expected *versus* observed BMI distributions in APL cohorts across three western countries (the USA, Spain and Italy) with different

obesity prevalence and dietary habits. In addition, we provide hypothesis-generating evidence for molecular mechanisms underlying such an association, in particular, the possible involvement of pro-inflammatory fatty acid metabolism and mutations of the tyrosin kinase FLT3.

Our epidemiological results expand a growing body of literature identifying overweight/obesity as a *bona fide* risk factor for leukemias. The most recent meta-analysis reported an adjusted relative risk of 1.14 (95%CI: 1.04-1.26; $P=0.008$) for AML overall.⁵ Despite the growing evidence, the notion of obesity as a risk factor for leukemia remains widely overlooked.⁷ Among the highly heterogeneous AML subtypes, APL is the most clinically and biologically coherent. We and others previously showed that in APL, but not in other AML, an elevated BMI significantly affects outcome.^{10,19} This is also in line with the few retrospective studies that have assessed APL as a separate disease entity.^{20,21} No study had addressed this question prospectively, a task made difficult by the rarity of the disease, but made possible in our case by the very large study

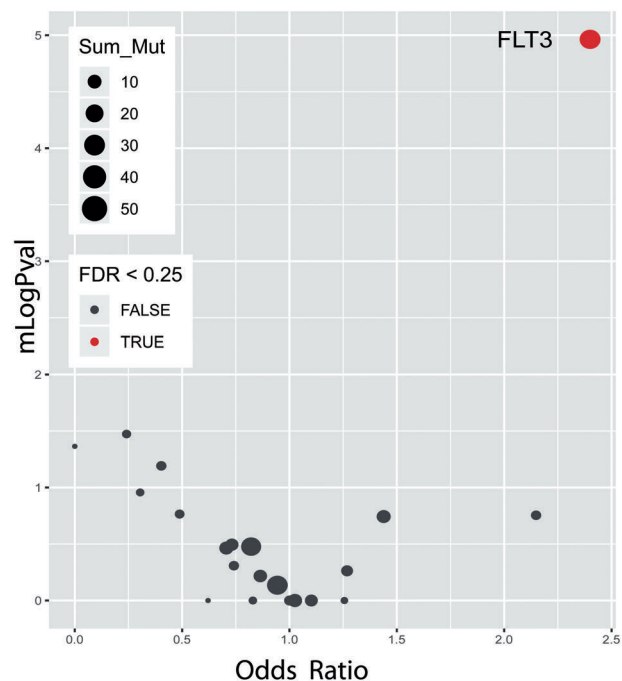


Figure 3. Association between obesity and FLT3 mutations. (A) Bubble plot representing Odds Ratio versus $-\log P$ value (mLogPval) of any mutation in 23 driver genes in The Cancer Genome Atlas (TCGA) acute myeloid leukemia cohort. FLT3 (in red) is the only gene with False Discovery Rate (FDR) < 0.25. Bubble size reflects the number of obese patients with a mutation. Data are tabulated in Online Supplementary Table S3.

Table 5. Logistic regression of body mass index (BMI) and FLT3 ITD mutations.

BMI	All 3 cohorts 163/569 ^a OR (95% CI)	ITALY 30/114 ^a OR (95% CI)	SPAIN 119/414 ^a OR (95% CI)	USA 14/41 ^a OR (95% CI)
5 unit increase	1.22 (1.05-1.43)	2.35 (1.25-4.42)	1.09 (0.89-1.33)	1.44 (0.93-2.24)
≥ 25 <i>vs.</i> <25 ^b	-	4.40 (1.63-11.9)	1.15 (0.75-1.78)	-
≥ 30 <i>vs.</i> <30 ^b	-	-	-	6.46 (1.21-34.5)

^aMutations / All patients. ^bGiven the small number of obese patients in Italy and Spain, we compared overweight/obese patients *versus* normal weight patients (i.e. BMI ≥ 25 *vs.* <25). Given the small number of normal weight patients in the USA, we compared obese patients *versus* non-obese patients (i.e. BMI ≥ 30 *vs.* <30). OR: odds ratios; CI: confidence intervals.

population (5.2 million). The largest prospective study to date (EPIC), which revealed a statistically significant higher risk only in female AML, but not in other gender and biological subgroups,⁴ was based on a relatively small number of incident cases: only 671 out of 375,021 participants over 11.5 years of median follow up. The use of orthogonal epidemiological approaches is a strength of the study, as it attempts to mitigate some weaknesses of each design. Registry-based studies have little patient selection bias, providing results that are more comparable to real-life scenarios. However, the quality of case identification is likely to be sub-optimal; erroneous assignment of APL to the general AML ICD code might "deplete" incident cases and further reduce statistical power. Case-control studies in the context of clinical trials, on the other hand, offer the advantage of gold standard diagnosis but might be affected by significant patient selection biases. This may have counter-selected obese patients in the present study, since the correlated comorbidities may be associated with limited access to clinical trials.

Another limitation of the study is that we could not provide the same degree of geographical homogeneity for control subjects in the case-control studies. This may be particularly relevant for the USA, known to have wide state-specific differences in BMI distribution. However, this variation is mainly due to demographic parameters,²² such as age, gender and race, and is, therefore, at least partly accounted for in our multivariate analysis. We also note that our US APL cohort includes a single patient of hispanic ethnicity. Hispanics are considered at higher incidence of APL, although some large studies based on Surveillance, Epidemiology, and End Results (SEER) data dispute this commonly held conclusion.²³

Understanding the molecular mechanism causing increased cancer risk in obese subjects is crucial for adequate nutritional management in disease prevention, given the sustained rise of obesity worldwide, particularly in emerging economies. The possibility of matching transcriptional and mutational profiles from TCGA to patient clinical and BMI data provided an opportunity to generate hypotheses grounded on actual data. However, extracting biological significance from large molecular datasets remains challenging. Shifting the analytical focus from single genes to gene sets or pathways may allow signals to be captured even when the changes affecting individual genes are minimal, provided they are coherent. The gene set-based method we used here for transcriptional analysis does not assume equal variances, resulting in improved sensitivity and specificity over similar competing methods.¹⁵ Our main finding is the upregulation of several genes involved in the metabolism of pro-inflammatory ω -6 polyunsaturated fatty acids (PUFA, linoleic and arachidonic) in APL. These molecules are increased in the plasma of metabolically impaired subjects, including the obese,²⁴

and may lead to elevated production of derivative molecules with multiple effects in signaling and inflammation, enhancing leukemogenesis through several independent mechanisms: direct growth promotion, generation of genotoxic oxidative stress, immune modulation,^{18,25} and generation of endogenous agonists for Peroxisome proliferator-activated receptors (PPAR).²⁶ PPAR are known insulin sensitizers²⁷ and their transcriptional targets are up-regulated in APL (*Online Supplementary Table S2*); APL expressed higher levels of insulin and IGF1 receptors, and its growth may thus be favored by the increased insulin/IGF1 levels in obese subjects.^{3,28} Elevated generation of PUFA-derived eicosanoids by APL cells may also explain the association between obesity and ATRA differentiation syndrome (DS),¹⁰ as eicosanoids strongly promote leukocyte adhesion and chemokine release in the lungs.²⁹

Finally, the association between FLT3 mutations and a higher BMI, although unconfirmed in the larger Spanish cohort, is an intriguing finding that we think deserves additional research. FLT3 mutations are associated with specific metabolic dependencies which may be differentially affected according to the systemic nutritional status.³⁰ It cannot be entirely ruled out that geographical differences in dietary composition may account for the discrepancies in the association between BMI and APL risk (weakest in Spain) and FLT3 mutations (null in Spain). Consistent with this highly speculative view, a recent EPIC substudy revealed marked differences in nutritional patterns between European nations. Despite sharing a theoretical propensity for "Mediterranean" diets, Italy and Spain were highly polarized, especially in terms of average polyunsaturated fatty acid consumption (3% vs. 38% of the participants in the highest quintile, respectively).³¹ More mechanistic studies are needed to clarify whether FLT3 mutations are favored by specific nutritional components.

In conclusion, based on evidence provided here, we propose including obesity among environmental factors increasing risk for myeloid neoplasms and in particular APL. Additional studies with experimental models will clarify the molecular determinants of this relationship, and test whether and how specific nutritional components like PUFA can determine specific mutational and transcriptional alterations able to influence the natural history of the disease.

Acknowledgments

AIRC-Cariplo Foundation, Italian Ministry of Health, European Hematology Association, Wellcome Trust and Royal Society

Role of the funding source

Funding sources had no role in study design, collection, analysis, and interpretation of data; report writing nor decision to submit the paper for publication.

References

- Mazzarella L, Riva L, Luzi L, Ronchini C, Pelicci PG. The genomic and epigenomic landscapes of AML. *Semin Hematol*. 2014;51(4):259-272.
- Shlush LI, Zandi S, Itzkovitz S, Schuh AC. Aging, clonal hematopoiesis and preleukemia: not just bad luck? *Int J Hematol*. 2015;102(5):513-522.
- Lauby-Secretan B, Ph D, Scoccianti C, Ph D, Loomis D, Ph D. Body Fatness and Cancer — Viewpoint of the IARC Working Group. *N Engl J Med*. 2016;375(8):794-798.
- Saber Hosnijeh F, Romieu I, Gallo V, et al. Anthropometric characteristics and risk of lymphoid and myeloid leukemia in the European Prospective Investigation into Cancer and Nutrition (EPIC). *Cancer Causes Control*. 2013;24(3):427-438.
- Li S, Chen L, Jin W, et al. Influence of body mass index on incidence and prognosis of acute myeloid leukemia and acute promyelocytic leukemia: A meta-analysis. *Sci Rep*. 2017;7(1):17998.
- Bhaskaran K, Douglas I, Forbes H, dos-

- Santos-Silva I, Leon DA, Smeeth L. Body-mass index and risk of 22 specific cancers: a population-based cohort study of 5.24 million UK adults. *Lancet*. 2014;384(9945):755-765.
7. American Cancer Society. Leukemia–Acute Myeloid (Myelogenous). <http://www.cancer.org/cancer/leukemia-acutemyeloidaml/detailedguide/leukemia-acute-myeloid-myelogenous-risk-factors>.
 8. Komanduri K V, Levine RL. Diagnosis and Therapy of Acute Myeloid Leukemia in the Era of Molecular Risk Stratification. *Annu Rev Med*. 2016;67:59-72.
 9. Coombs CC, Tavakkoli M, Tallman MS. Acute promyelocytic leukemia: where did we start, where are we now, and the future. *Blood Cancer J*. 2015;5:e304.
 10. Breccia M, Mazzarella L, Bagnardi V, et al. Increased BMI correlates with higher risk of disease relapse and differentiation syndrome in patients with acute promyelocytic leukemia treated with the AIDA protocols. *Blood*. 2012;119(1):49-54.
 11. Ley TJ, Miller C, Ding L, et al. Genomic and epigenomic landscapes of adult de novo acute myeloid leukemia. *N Engl J Med*. 2013;368(22):2059-2074.
 12. Avvisati G, Lo-Coco F, Paoloni FP, et al. AIDA 0493 protocol for newly diagnosed acute promyelocytic leukemia: very long-term results and role of maintenance. *Blood*. 2011;117(18):4716-4725.
 13. Lo-Coco F, Avvisati G, Vignetti M, et al. Front-line treatment of acute promyelocytic leukemia with AIDA induction followed by risk-adapted consolidation for adults younger than 61 years: results of the AIDA-2000 trial of the GIMEMA Group. *Blood*. 2010;116(17):3171-3179.
 14. Adès L, Sanz MA, Chevret S, et al. Treatment of newly diagnosed acute promyelocytic leukemia (APL): a comparison of French-Belgian-Swiss and PETHEMA results. *Blood*. 2008;111(3):1078-1084.
 15. Yaari G, Bolen CR, Thakar J, Kleinstein SH. Quantitative set analysis for gene expression: A method to quantify gene set differential expression including gene-gene correlations. *Nucleic Acids Res*. 2013;41(18):1-11.
 16. Morishima K, Tanabe M, Furumichi M, Kanehisa M, Sato Y. KEGG: new perspectives on genomes, pathways, diseases and drugs. *Nucleic Acids Res*. 2016;45(D1):D353-D361.
 17. Gonzalez-Perez A, Perez-Llamas C, Deu-Pons J, et al. IntOGen-mutations identifies cancer drivers across tumor types. *Nat Methods*. 2013;10(11):1081-1082.
 18. Wang D, Dubois RN. Eicosanoids and cancer. *Nat Rev Cancer*. 2010;10(3):181-193.
 19. Castillo JJ, Mulkey F, Geyer S, et al. Relationship between obesity and clinical outcome in adults with acute myeloid leukemia: A pooled analysis from four CALGB (alliance) clinical trials. *Am J Hematol*. 2016;91(2):199-204.
 20. Wong O, Harris F, Yiyang W, Hua F. A hospital-based case-control study of acute myeloid leukemia in Shanghai: Analysis of personal characteristics, lifestyle and environmental risk factors by subtypes of the WHO classification. *Regul Toxicol Pharmacol*. 2009;55(3):340-352.
 21. Estey E, Thall P, Kantarjian H, Pierce S, Kornblau S, Keating M. Association between increased body mass index and a diagnosis of acute promyelocytic leukemia in patients with acute myeloid leukemia. *Leukemia*. 1997;11(10):1661-1664.
 22. Flegal KM, Carroll MD, Kit BK, Ogden CL. Prevalence of obesity and trends in the distribution of body mass index among US adults, 1999-2010. *JAMA*. 2012;307(5):491-497.
 23. Matasar MJ, Ritchie EK, Consedine N, Magai C, Neugut AI. Incidence rates of acute promyelocytic leukemia among Hispanics, blacks, Asians, and non-Hispanic whites in the United States. *Eur J Cancer Prev*. 2006;15(4):367-370.
 24. Caspar-Bauguil S, Fioroni A, Galinier A, et al. Pro-inflammatory phospholipid arachidonic acid/eicosapentaenoic acid ratio of dysmetabolic severely obese women. *Obes Surg*. 2012;22(6):935-944.
 25. Trabanelli S, Chevalier MF, Martinez-Usatorre A, et al. Tumour-derived PGD2 and NKp30-B7H6 engagement drives an immunosuppressive ILC2-MDSC axis. *Nat Commun*. 2017;8(1):593.
 26. Kliewer SA, Lenhard JM, Willson TM, Patel I, Morris DC, Lehmann JM. A prostaglandin J2 metabolite binds peroxisome proliferator-activated receptor γ and promotes adipocyte differentiation. *Cell*. 1995;83(5):813-819.
 27. Peters JM, Shah YM, Gonzalez FJ. The role of peroxisome proliferator-activated receptors in carcinogenesis and chemoprevention. *Nat Rev Cancer*. 2012;12(3):181-195.
 28. Poloz Y, Stambolic V. Obesity and cancer, a case for insulin signaling. *Cell Death Dis*. 2015;6:e2037.
 29. Dahlén SE, Björk J, Hedqvist P, et al. Leukotrienes promote plasma leakage and leukocyte adhesion in postcapillary venules: in vivo effects with relevance to the acute inflammatory response. *Proc Natl Acad Sci U S A*. 1981;78(6):3887-3891.
 30. Stockard B, Garrett T, Guingab-Cagmat J, Meshinchi S, Lamba J. Distinct Metabolic features differentiating FLT3-ITD AML from FLT3-WT childhood Acute Myeloid Leukemia. *Sci Rep*. 2018;8(1):5534.
 31. Moskal A, Pisa PT, Ferrari P, et al. Nutrient Patterns and Their Food Sources in an International Study Setting: Report from the EPIC Study. *PLoS One*. 2014;9(6):e98647.

Oral arsenic trioxide ORH-2014 pharmacokinetic and safety profile in patients with advanced hematologic disorders



Farhad Ravandi,¹ Iphigenia Koumenis,² Anandhi Johri,² Martin Tallman,³ Gail J. Roboz,⁴ Stephen Strickland,⁵ Guillermo Garcia-Manero,¹ Gautam Borthakur,¹ Kiran Naqvi,¹ Meghan Meyer,¹ Madhu Pudipeddi,² Sirish Nidarmarthy,² Kris Vaddi² and Hagop Kantarjian¹

¹M.D. Anderson Cancer Center, Houston, TX; ²Olsenix, Wilmington, DE; ³Memorial Sloan Kettering Cancer Center, New York, NY; ⁴Weill Cornell Medicine, New York, NY and ⁵Vanderbilt University Medical Center, Nashville, TN, USA

Haematologica 2020
Volume 105(6):1567-1574

ABSTRACT

Daily intravenous arsenic trioxide administered with all-trans retinoic acid, the standard-of-care for acute promyelocytic leukemia, is costly and challenging to administer. ORH-2014 is a novel, oral arsenic trioxide formulation, consisting of micron-size drug particles with rapid dissolution and high bioavailability. We conducted a multicenter phase 1 dose-escalating study in patients with advanced hematologic malignancies. Twelve patients received ORH-2014 at 5 mg (n=3), 10 mg (n=6), or 15 mg (n=3) orally once a day (fasted state). Objectives were to assess the safety, tolerability and pharmacokinetics of ORH-2014 to support a dose recommendation for future trials. The median age of the patients was 77 years (range: 45-81) and they had received a median of two (range: 1-5) prior therapies. There were no dose limiting toxicities and no drug-related severe adverse events, except one grade III QT prolongation occurring beyond the dose limiting toxicity assessment period and resolving after treatment interruption. ORH-2014 steady-state plasma concentration was reached on day 15. ORH-2014, 15 mg C_{max} was comparable to the calculated approved dose of intravenous arsenic trioxide (mean [% coefficient of variation]: 114 [21%] vs. 124 [60%] ng/mL) and area under the curve from 0 to 24 hours was 2,140 (36%) versus 1,302 (30%) h*ng/mL. These results indicate that ORH-2014 at 15 mg is safe, bioavailable, and provides the required arsenic exposure compared to intravenous arsenic trioxide at the approved dose (0.15 mg/kg); this ORH-2014 dose is recommended for future trials. (NCT03048344; www.clinicaltrials.gov).

Introduction

As a rare subtype of acute myeloid leukemia (AML), acute promyelocytic leukemia (APL) accounts for 10 to 15% of approximately 21,450 new cases of adults with AML per year in the USA.¹ APL leukemic cells typically harbor a t(15:17) chromosomal translocation resulting in the expression of the promyelocytic leukemia-retinoic acid receptor (*PML-RARα*) gene fusion, which blocks the normal cell differentiation processes. Clinically, the disease often presents with coagulopathy that can lead to catastrophic hemorrhage. Until recently, the standard-of-care for patients with newly diagnosed with APL involved the combination of all-trans-retinoic acid (ATRA) plus anthracycline-based chemotherapy for induction and consolidation.² In general, patients receive two to three cycles until complete molecular remission is achieved. After consolidation, patients receive ATRA with or without low-dose chemotherapy for 1 to 2 years for maintenance.

Arsenic has been used to treat a variety of diseases such as the plague and malaria for more than 2 millennia.³ In the late 1900s arsenic was found to have anti-leukemic activity and was used for ~70 years to treat various leukemias. In the 1990s, three teams of Chinese researchers found that intravenous (IV) arsenic trioxide (ATO) was effective in patients with APL, with complete responses (CR)

Correspondence:

FARHAD RAVANDI
fravandi@mdanderson.org

Received: June 13, 2019.

Accepted: September 24, 2019.

Pre-published: September 26, 2019.

doi:10.3324/haematol.2019.229583

Check the online version for the most updated information on this article, online supplements, and information on authorship & disclosures: www.haematologica.org/content/106/6/1567

©2020 Ferrata Storti Foundation

Material published in *Haematologica* is covered by copyright. All rights are reserved to the Ferrata Storti Foundation. Use of published material is allowed under the following terms and conditions:

<https://creativecommons.org/licenses/by-nc/4.0/legalcode>. Copies of published material are allowed for personal or internal use. Sharing published material for non-commercial purposes is subject to the following conditions: <https://creativecommons.org/licenses/by-nc/4.0/legalcode>, sect. 3. Reproducing and sharing published material for commercial purposes is not allowed without permission in writing from the publisher.



observed in 66% of patients in one study.⁴ In other studies, up to 90% of relapsed patients with APL and over 70% of newly diagnosed patients achieved responses.^{5,6} Following this success, several clinical studies conducted in the USA established the safety and efficacy of IV ATO in patients with APL who had relapsed after prior ATRA + anthracycline therapy. In the first pilot study, 92% of the 12 patients treated achieved a CR with IV ATO alone, and 67% had undetectable PML-RAR transcripts.⁷ In a larger trial (n=40), 85% of patients with relapsed APL achieved CR; more than three-quarters of the patients were alive after 2 years.⁸ This trial formed the basis for the approval of IV ATO, Trisenox[®], in the USA in 2000 and in Europe in 2002 for second line therapy of patients with APL who are refractory to - or have relapsed from - ATRA + anthracycline chemotherapy.⁹ Since 2000, ATO has been used as the standard-of-care for relapsed APL, with remission rates greater than 80% as a single agent after two 25-day cycles.

Several investigators have examined the role of IV ATO in frontline therapy of patients with newly diagnosed APL and have demonstrated that this approach is feasible.¹⁰⁻¹⁵ Recently, two large randomized trials have shown that the combination of ATRA and IV ATO for induction is superior to ATRA + chemotherapy in the treatment of APL patients with standard-risk disease.^{14,15} Moreover, long-term follow-up of these patients showed that patients treated with ATRA + IV ATO had a significantly higher event-free and overall survival and a significantly lower cumulative relapse rate compared with the ATRA + chemotherapy cohort.¹⁶ These findings have led to new recommendations for the use of IV ATO as a first-line therapy in combination with ATRA for the management of patients with standard-risk APL (white blood cell [WBC] count $\leq 10 \times 10^9/L$), with additional chemotherapy reserved for patients with high-risk disease (WBC count $> 10 \times 10^9/L$).^{17,18} The combination of IV ATO + ATRA is also safe and effective in patients who are not suitable candidates for anthracycline-based chemotherapy, such as those with significant cardiac disease or older adults.^{14,15}

As a front-line therapy for APL, ATO needs to be administered IV daily for over 100 doses, which is inconvenient, costly, and leads to a decreased quality of life for the patients. Therefore, the introduction of an oral ATO formulation could improve patients' quality of life, and drug compliance, while reducing costs.

Two oral formulations of ATO have been developed in Hong Kong. One is a liquid formulation of As₂O₃ at 1 mg/mL (pH 7.2), which was found to be highly bioavailable.¹⁹ In relapsed APL patients, the formulation was highly active, showing an efficacy comparable to IV ATO.²⁰ As a maintenance regimen in APL patients with first complete remission, the formulation was effective in the long term, with a 3-year leukemia-free-survival, event-free survival, and overall-survival of 87.7%, 83.7%, and 90.6%, respectively.²¹ Oral ATO incorporation into frontline treatment with ATRA and chemotherapy in newly diagnosed APL is safe and reduces relapses.²² This oral liquid formulation did not induce QT prolongation or cardiac arrhythmias,^{20,21,23} and the severity and incidence of other side effects (leucocytosis, LFT abnormalities, and skin rashes) was comparable to that of IV ATO.²⁰

However, commercializing a liquid oral formulation intended to be self-administered by patients could represent a safety challenge in handling and dosing. Therefore,

a solid oral formulation of ATO is preferable. The other oral formulation developed in China is a pill termed RIF containing Realgar, a naturally occurring mixture containing tetra arsenic tetra sulfide (As₄S₄; 30 mg per pill), *Indigo naturalis*, *Radix salvia miltiorrhizae*, and *Radix pseudostellariae*.²⁴ In a phase 2 clinical trial conducted in China, the formulation demonstrated a CR rate of 96.7% and a reasonable safety profile in newly diagnosed APL patients.²⁵ In a phase 3 study, RIF + ATRA was not inferior to IV ATO + ATRA as first-line treatment for APL, and adverse events (AE) were similar in the two arms.²⁶ RIF has been commercialized and is available in China.

However, these oral ATO formulations are not available in Western markets. Therefore, a unique oral powder capsule formulation of ATO, ORH-2014, was developed, for the treatment of APL and other hematologic malignancies. Herein we report the results of the first-in-human study with ORH-2014 in subjects with relapsed advanced hematological disorders. ORH-2014 safety profile, recommended dose, pharmacokinetic profile, and preliminary efficacy data are reported and discussed.

Methods

For ORH-2014 formulation development and physical properties, see the *Online Supplementary Materials and Methods*.

We conducted a multicenter phase 1 open-label, dose-escalating study to evaluate the safety, tolerability, pharmacokinetics and to determine the recommended dose and preliminary efficacy of oral ORH-2014 in patients with advanced hematologic malignancies. ORH-2014 dose-escalation was designed as 5-mg increments starting from 5 mg and could potentially go up to 50 mg, in a standard 3x3 dose-escalation scheme (described below). The starting dose (5 mg) was chosen to be approximately half of the IV ATO approved dose of 0.15 mg/kg for a 70-kg person (i.e. 5.25 mg). ORH-2014 was administered orally once daily (QD) in the fasted state. Dose-escalation was to be stopped when the mean area under the concentration-time curve from 0 to 24 hours (AUC₀₋₂₄) and/or the maximum observed concentration (C_{max}) of total arsenic in plasma at a given dose of ORH-2014 was $\geq 30\%$ higher than that for IV ATO at the approved dose or if the maximum tolerated dose (MTD) was reached. Anticancer agents other than ORH-2014 (including systemic chemotherapy, radiation therapy, or biologic response modifiers) were not permitted during the study, except for the temporary use of hydroxyurea. Supportive care was allowed, including antibiotics, IV electrolytes, platelet transfusions, and steroids.

Male and non-pregnant female subjects ≥ 18 years of age with the following advanced hematological disorders and no available therapies were eligible for enrolment: (i) Relapsed or refractory AML with nucleophosmin-1 (*NPM1*) mutations; (ii) relapsed or refractory APL; (iii) relapsed or refractory intermediate or high-risk myelodysplastic syndrome (MDS); (iv) relapsed or refractory chronic myelomonocytic leukemia (CMML) and other MDS/myeloproliferative neoplasm (MPN) overlapping syndromes; or (v) relapsed or refractory mantle cell lymphoma (MCL). Subjects were excluded if they had an Eastern Cooperative Oncology Group performance status > 3 ; absolute myeloblast count $\geq 20,000/mm^3$; remaining toxicities ($>$ grade I) due to previous chemotherapy; abnormal liver function tests (above specified limits); impaired cardiac function; or had received any antineoplastic therapy (except hydroxyurea) within < 5 half-lives before ORH-2014 administration. All participants gave written informed consent before entering the study.

First, a cohort of three subjects received ORH-2014 at the dose 5 mg QD, and dose-limiting toxicities (DLT) were observed for four weeks (DLT definition in the *Online Supplementary Materials and Methods*). If none of the three subjects exhibited a DLT in the four-week period, then the study could advance to the next higher dose level. At any dose level, if 1 of 3 subjects exhibited a DLT, the cohort was to be expanded to six subjects. If 1 of 6 subjects exhibited a DLT, the next subject was to be enrolled at the next higher dose level. If ≥ 1 of 3 or 6 subjects exhibited a DLT, then the dose level below was considered the maximum tolerated dose (MTD). Subjects with no DLT continued to receive ORH-2014 at the same dose for an additional eight weeks, followed by bone marrow evaluation to analyze response. Subjects achieving CR or partial remission (PR) at the end of the 12-week treatment period were eligible to receive an additional 12 weeks of therapy. The study was approved by the institutional review board affiliated with each study site.

Results

ORH-2014 physical properties

ORH-2014 molecular formula is As_2O_3 , As_4O_6 in form (Figure 1), and its relative molecular mass is 197.8 g/mol. ORH-2014 oral capsule formulation was developed by a lyophilization process (see the *Online Supplementary Materials and Methods*), which significantly reduces the ATO particle size and increases the particle surface area

(Table 1). The aggregate particle size of the Lyopremix (see the *Online Supplementary Materials and Methods*) was about 5-10-fold smaller than that of the unprocessed ATO. The specific surface area of the Lyopremix was also significantly higher than that of the unprocessed ATO. Figure 2A shows the structure of ORH-2014 Lyopremix, which consists of a matrix of sodium lauryl sulfate with microscopic ATO crystals with well-defined morphology. The small particle size and the large surface area of the ATO Lyopremix in ORH-2014 allows rapid drug dissolution in the simulated gastric media of 0.1 N HCl (80% of the compound dissolved in 10 minutes; Figure 2B), potentially enhancing oral bioavailability.

Patient characteristics

The trial enrolled 12 patients (eight males; four females) with advanced hematologic malignancies: six with advanced MDS, four with refractory AML with NPM1

Table 1. ORH-2014 particle size and surface area.

	Unprocessed ATO	Lyophilized ATO (ORH-2014)*
Particle size (D90)	139 μ m	~16-30 μ m
Particle surface area	0.05 m ² /g	~2-8 m ² /g

*Range of values for nine batches of Lyopremix. See *Online Supplementary Materials and Methods* for ORH-2014 physical properties assessment. ATO: arsenic trioxide.

Table 2. Subjects' demographic and baseline characteristics.

	5 mg n=3	10 mg n=6	15 mg n=3	All subjects n=12
Age, years				
Mean (SD)	67.0 (19.1)	73.0 (9.6)	66.0 (16.1)	69.8 (12.9)
Median (min, max)	78.0 (45, 78)	76.5 (55, 81)	71.0 (48, 79)	76.5 (45, 81)
Sex, n (%)				
Female	1 (33.3%)	1 (16.7%)	2 (66.7%)	4 (33.3%)
Male	2 (66.7%)	5 (83.3%)	1 (33.3%)	8 (66.7%)
Race, n (%)				
White	3 (100%)	5 (83.3%)	2 (66.7%)	10 (83.3%)
Black/African American	–	–	1 (33.3%)	1 (8.3%)
Asian	–	1 (16.7%)	–	1 (8.3%)
All other*	–	–	–	–
Ethnicity, n (%)				
Hispanic/Latino	2 (66.7%)	–	–	2 (16.7%)
Not Hispanic/Latino	1 (33.3%)	6 (100%)	3 (100%)	10 (83.3%)
Weight, kg				
Mean (SD)	87.50 (15.43)	72.83 (12.59)	88.43 (6.25)	80.40 (13.60)
Median (min, max)	84.80 (73.6, 104.1)	73.95 (56.0, 91.0)	86.60 (83.3, 95.4)	81.50 (56.0, 104.1)
Type of hematologic malignancy				
AML	1 (33.3%)	3 (50.0%)	0	4 (33.3%)
APL	0	0	0	0
MDS	2 (66.7%)	3 (50.0%)	1 (33.3%)	6 (50.0%)
CMML/MPN	0	0	2 (66.7%)	2 (16.7%)
MCL	0	0	0	0

* All other races included Native Hawaiian or Pacific Islander, American Indian or Alaska Native, and other. AML: acute myeloid leukemia; APL: acute promyelocytic leukemia; MDS: myelodysplastic syndrome; CMML: chronic myelomonocytic leukemia; MPN: MDS/myeloproliferative neoplasm; MCL: mantle cell lymphoma.

Table 3. Common drug-related adverse events (observed in ≥ 2 subjects).

	5 mg n=3	10 mg n=6	15 mg n=3	All subjects n=12
Number of subjects with ≥ 1 drug-related AE	2 (66.7%)	4 (66.7%)	4 (66.7%)	8 (66.7%)
Nausea	2	2	1	5 (41.6%)
Diarrhea	1	1	2	4 (33.3%)
Headache	1	1	1	3 (25.0%)
Dizziness	0	1	1	2 (16.6%)
Anorexia	0	1	1	2 (16.6%)

Data are n (%) of subjects.

mutation, and two with CMML (Table 2). The median patient age was 76.5 years (range: 45-81), (83.3%) were white, the median weight was 81.5 kg (range: 56.0-104.1) and patients had a median of two prior therapies (range: 1-5).

ORH-2014 safety profile

All 12 patients were included in the safety analysis set. No DLT was reported during the four-week DLT observation period. Eight subjects (66.7%) had drug-related AE; the incidence of AE was identical in the three dose groups (66.3%) (Table 3). The most common drug-related AE were nausea (n=5), diarrhea (n=4), and headache (n=3). All but one drug-related AE were mild or moderate (grade I-II). Grade III AE of QTcF prolongation occurred in one subject (8.3%) outside of the DLT observation period (on day 68), and was attributed to ORH-2014 and concomitant levofloxacin (Levaquin[®]; a fluoroquinolone antibiotic). Since both levofloxacin and ATO are known to induce QT prolongation,^{9,30} both were stopped. The AE resolved, and treatment with ORH-2014 alone was resumed at the same dose (5 mg), without any further occurrence of QT prolongation. The patient was able to receive ORH-2014 at 5 mg QD for a total of 171 days. There were very few renal, hepatic, and hematologic AE related to the underlying disease state, with the exception of grade I transaminitis attributed to ORH-2014; this event resolved on its own without treatment interruption or any medications. Two deaths occurred (on days 35 and 40 post dose) due to progression of the disease, both unrelated to ORH-2014.

ORH-2014 pharmacokinetic profile

Total plasma arsenic

Following single and repeated oral administration of 5, 10 or 15 mg of ORH-2014 QD, the median T_{max} for total plasma arsenic occurred between 1 and 12 hours (Table 4). On day 15, C_{max} and AUC₀₋₂₄ geometric means increased by 3.4- and 2.9-fold, respectively, over the 3-fold dose increase (5-15 mg), indicating that systemic exposure was nearly dose-proportional (Figure 3). There was a low correlation (below 0.2) between total the arsenic exposure and patients' BMI, suggesting that a flat dose of ORH-2014 (rather than mg/kg dose) is adequate.

On days 15 and 22, between-subject variability (geometric % CV) was generally moderate with % CV ranging from 17% to 37% for C_{max}, and from 34% to 41% for AUC₀₋₂₄ (Table 4)

The mean extent of accumulation (AR, which is based on AUC₀₋₂₄) was approximately 3- to 4-fold on Day 5, 4- to 5-fold (excluding a patient receiving 5 mg ORH-2014 who had a 7-fold accumulation) on Day 15, and 4- to 5-

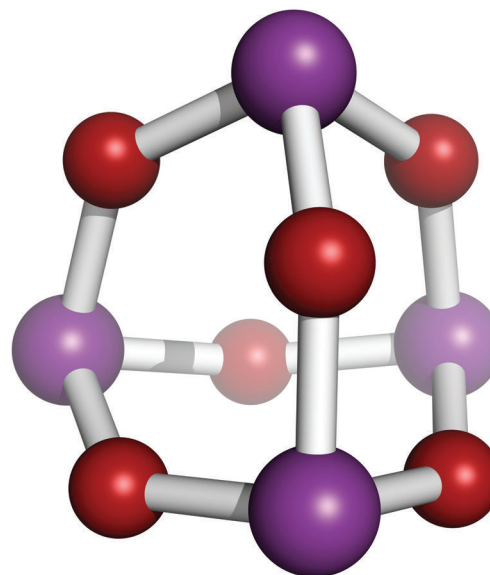


Figure 1. Arsenic oxide structural formula. Atoms are represented as spheres, with oxygen in red and arsenic in purple.

fold on Day 22 (Table 4). The approximately 5-fold accumulation indicated an effective half-life of three days. Visual inspection of trough total arsenic concentrations also indicated that a steady-state reached by day 15 (Figure 3). The observed time to reach steady-state (15 days) is consistent with an effective half-life of three days, since 97% of steady-state is achieved after five half-lives (5x3 days = 15 days).

ORH-2014 at the 15 mg dose is comparable to the IV ATO approved dose (0.15 mg/kg) for adult patients. Exposure to 15 mg ORH-2014 was compared to exposure to IV ATO at the approved dose, using IV ATO historical data (Table 4). After daily administration of 10 mg ORH-2014 for 15 days, ORH-2014 C_{max} was about half of IV-ATO C_{max} at day 8 (mean: 66 vs. 124 ng/mL, respectively) but its AUC₀₋₂₄ was similar (1,340 vs. 1,302 h*ng/mL, respectively). At 15 mg, ORH-2014's C_{max} was similar to IV-ATO's (mean: 114 vs. 124 ng/mL, respectively) but its AUC₀₋₂₄ was higher (2,140 vs. 1,302 h*ng/mL).

Pharmacokinetics of arsenical species

The pharmacokinetic (PK) of arsenical species ([AsIII], [AsV], [MMAV], [DMAV]) was determined for all subjects in this study (see the *Online Supplementary Materials and*

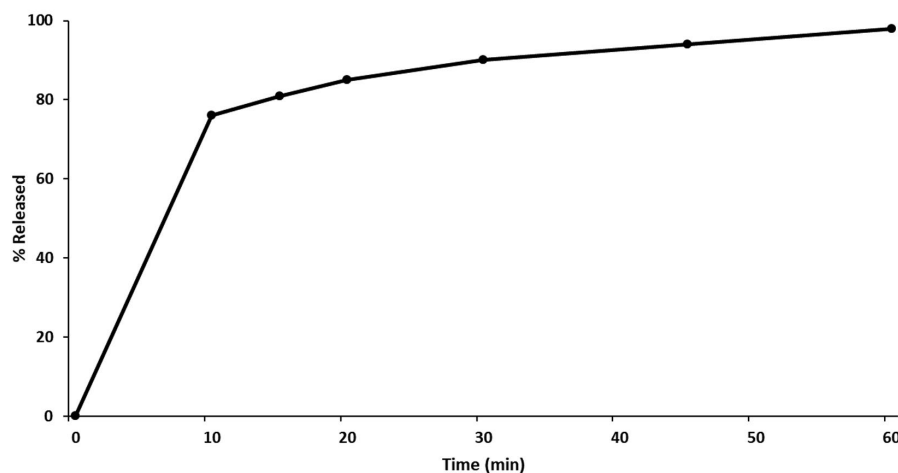
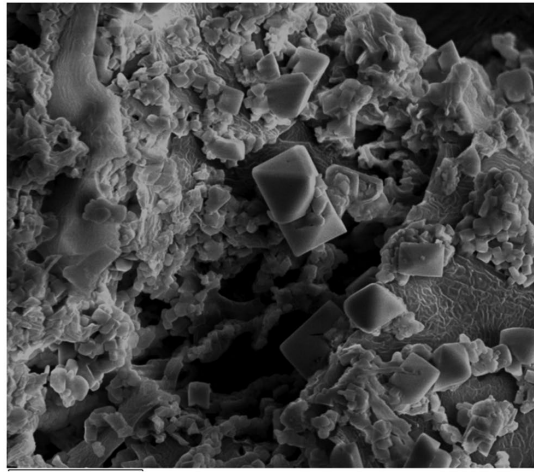


Figure 2. ORH-2014 particles and dissolution profile. A: ORH-2014 Lyopremix by scanning electron microscopy; bar represents 5 μm . B: ORH-2014 capsule dissolution kinetic. See the *Online Supplementary Materials and Methods* for ORH-2014 particle size and dissolution assessments.

Methods). Peak plasma concentrations of AsIII, the primary active species, were reached at approximately two hours across all doses (range: 1-4 hours). Plasma concentration of AsIII declined in a biphasic manner with a mean elimination half-life of 7 to 16 hours and is characterized by an initial rapid distribution phase followed by a slower terminal elimination phase. Twenty-two days after daily administration of ORH-2014 at 15 mg, AsIII C_{max} was 25 ng/mL (42% CV) and AUC was 354 ng*hr/mL (47% CV), which is comparable to the AUC of Trisenox (332 ng*hr/mL; n=6; on Day 25).⁹ After administration at 5, 10 or 15 mg on a daily regimen, accumulation of AsIII ranged from 1.05 to 1.44 compared to a single dose. The primary pentavalent metabolites, MMAV and DMAV, were slow to appear in plasma (approximately 4 to 24 hours after first administration of ORH-2014), but, due to their apparent longer half-life, accumulate more upon multiple dosing than does AsIII. The extent of accumulation of these metabolites is dependent on the dosing regimen. Accumulation ranged from 1.4- to 11-fold following multiple dosing as compared to single dose administration. AsV is present in plasma only at relatively low levels. ORH-2014 AUC of As₃ species, is comparable to the AsIII AUC of IV ATO.⁹

Efficacy

Although this phase 1 study was not intended to formally determine efficacy of ORH-2014, disease improve-

ments were observed in two patients with advanced MDS. One patient had complete marrow remission observed approximately 12 and 27 weeks after starting ORH-2014. The patient took 171 doses and was on the study for 187 days of ORH-2014 at 5 mg daily. Another patient had improvement in peripheral counts and became eligible for bone marrow transplant after 110 days of ORH-2014 dosing at 15 mg daily (this patient did not have any bone marrow procedures performed beyond the 30-day timepoint, to avoid an invasive procedure).

Discussion

In the past 5 years, the standard-of-care for non-high-risk APL patients has shifted from the combination of ATRA plus anthracycline chemotherapy to the combination of IV ATO plus ATRA, triggering new treatment guidelines.² However, IV ATO plus ATRA treatment regimen consists of daily IV administration of ATO for over 100 days, which represents an important burden to patients and caregivers, and can be associated with low treatment compliance, low quality of life, and high costs. Poor compliance is an important issue with IV ATO treatment due to the burden of attending lengthy daily clinic visits for months, particularly for patients who live far from the treatment center, who work, and/or have family obligations, which is common in relatively younger AML

Table 4. Pharmacokinetic parameters for total arsenic.

	ORH-2014 5 mg**		ORH-2014 10 mg			ORH-2014 15 mg			IV ATO 0.15 mg/kg
	Day 1 (n=3)	Day 15 (n=3)	Day 1 (n=6)	Day 15 (n=5)	Day 22 (n=2)	Day 1 (n=3)	Day 15 (n=3)	Day 22 (n=3)	Day 8
C_{max} , ng/mL	7.22 (9.5)	34.0 (16.9)	19.9 (36.8)	65.6 (37.2)	109 (37.0)	24.5 (39.6)	114 (21.1)	111 (29.5)	124 (60)
AUC_{0-24} , ng•h/mL	125 (1.3) [‡]	729 (21.9)	329 (32.7)	1340 (37.6)	2210 (41.2)	454 (36.1)	2140 (35.8)	2240 (40.4)	1302 (30)
T_{max} , h [†]	12.00 [12.0, 24.0]	8.10 [4.0, 8.18]	2.13 [2.00, 24.3]	2.02 [1.00, 8.08]	1.02 [0.97, 1.07]	3.85 [0.98, 24.0]	1.00 [0.90, 1.13]	1.00 [0.00, 1.95]	–
RA	NA	5.14 (1.4) [‡]	NA	4.19 (20.7)	5.27 (40.3)	NA	4.72 (5.9)	4.92	(5.5) –

See the *Online Supplementary Materials and Methods* for PK sampling and data analyses. Geometric mean (%CV) data are presented, unless otherwise noted. *Bolted cells are historical values for IV ATO (Trisenox®) calculated from data in NDA #21-248. ** protocol was amended to add a day 22 after the second dose cohort. †Median [min, max]. ‡N = 2. C_{max} : maximum observed concentration; AUC_{0-24} : area under the plasma drug concentration-time curve from 0 to 24 hours; T_{max} : amount of time that the drug is present at the maximum concentration in serum, RA: ratio of accumulation; NA: not analyzed.

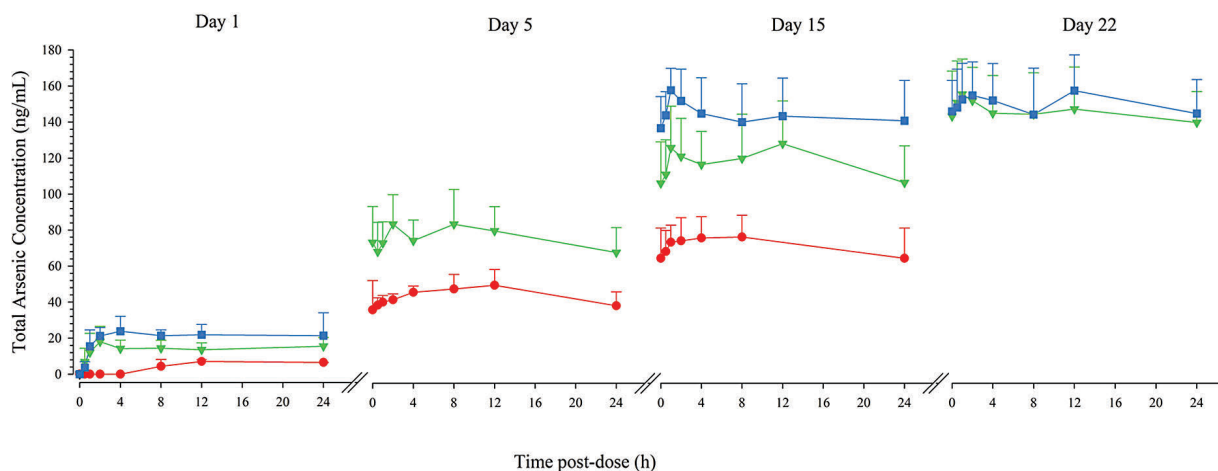


Figure 3. Plasma arsenic concentration-time curves at days 1, 5, 15, and 22. Red curves: 5 mg ORH-2014 QD (n=3); green curves: 10 mg ORH-2014 QD (n=6); blue curves: 15 mg ORH-2014 QD (n=3). Data are arithmetic mean \pm standard deviation (SD) total arsenic (ng/mL plasma). See the *Online Supplementary Materials and Methods* for pharmacokinetic (PK) data analyses. h: hours.

population. Therefore, the development and approval of an oral ATO formulation would greatly improve APL treatment by offering patients the ability to conveniently self-administer the entire treatment at home (since ATRA is also an oral drug) while carrying on their normal daily life. Oral ATO drugs are available in the Chinese market, but not approved in Western countries. To meet the need of Western countries, an oral powder capsule formulation, ORH-2014, was developed using a novel lyophilization process which results in micron-size drug particles with a large surface area that enable rapid dissolution in an acidic environment. The rapid dissolution of ORH-2014 results in a high bioavailability of arsenic, as indicated by the AUC.

ORH-2014 C_{max} and AUC for total arsenic were dose-proportional, indicating linear absorption. Treatment with ORH-2014 at 10 or 15 mg (which is equivalent to IV ATO approved dose for an adult person) resulted in an exposure (AUC_{0-24}) similar to IV ATO at the approved dose. Correlation between total arsenic exposure and patient body weight was found to be very low (less than 0.2),

implying that dose adjustment based on body mass index (BMI) (e.g. dosing in mg/kg) is not necessary. ORH-2014 15 mg AUC and C_{max} for As_3 , the most active species, was also similar to that of IV ATO, which provides additional confidence that the 15 mg dose will be safe and potentially as effective as Trisenox. The liquid ATO formulation in Kumana *et al.* study also reported similar AUC and C_{max} than IV ATO for total arsenic.¹⁹ ORH-2014 also resulted in small inter-patient variations in exposure, indicating reliable dosing. At 15 mg ORH-2014, administration for 25 days yielded an AUC_{0-24} greater than IV ATO, which fulfilled the protocol second stopping rule. (Dose-escalation was to be stopped if MTD was observed, however MTD was not reached or if ORH-2014's mean AUC_{0-24} and/or C_{max} was $\geq 30\%$ higher as calculated in IV ATO at the approved dose). ORH-2014 and IV ATO have a similar elimination half-life of three days and 80 to 100 hours, respectively.⁹

ORH-2014 administration yielded no DLT up to a dose of 15 mg in the 12 patients with hematologic malignancies who had relapsed from prior treatments. Therefore, we recommend using the 15 mg ORH-2014 dose for future

clinical trials with ORH-2014. The most common drug-related AE (observed in ≥ 3 [25%] patients) were nausea, diarrhea, and headache, which were grade I-II (mild and moderate). ORH-2014 did not induce any clinically significant hepatic toxicities which are reported with IV ATO at a great frequency (16-23% and 44%, respectively).⁹ Many of the adverse reactions observed with IV ATO are serious (grade \geq III): in a phase 2 study with IV ATO, 25% of patients had QTc interval ≥ 500 msec (grade III-IV), and the rates of grade III-IV differentiation syndrome, hyperleukocytosis, atrial dysrhythmias, and hyperglycemia were 5% to 7.5% with ORH-2014, only one drug-related AE (grade III) of QT prolongation was observed in one (8.3%) patient who was taking both ORH-2014 5 mg and fluoroquinolone, an antibiotic known to induce QT prolongation. The event was transient and reversible upon interruption of both drugs, and the patient was able to resume treatment with ORH-2014, at a 5 mg dose alone with no further cardiac conduction issues, for a total duration of 187 days on study. The fewer side effects observed with ORH-2014 could be attributed to its lower C_{max} and steadier exposure profile³ prior to steady state (~day 15). Altogether, the findings of this phase 1 study indicate that ORH-2014 oral formulation may be safer than the approved IV ATO formulation. The convenient oral dosing could make it suitable for the treatment of APL and other hematologic malignancies at home without the need of daily hospital visits for IV administration.

Of note ORH-2014 also resulted in a lower incidence of AE, especially lower liver toxicity, compared to the other two oral arsenic formulations. Indeed, liver toxicity was observed in 48% of the patients (26% of whom had grade III-IV toxicities) with the liquid formulation,²² and 45% (all grade I-II) with the Realgar-Indigo naturalis Formula (RIF) formulation,²⁶ while only one (8.3%) transient grade I liver toxicity occurred with ORH-2014, albeit this was observed in a smaller sample population (n=12).

Although this phase 1 study was not formally intended to demonstrate ORH-2014 efficacy, disease improvement was observed in one patient and another patient became eligible for bone marrow transplant with MDS. Additional studies will need to be conducted in MDS and other hematologic malignancies.

This first-in-human phase 1 study in patients with advanced hematological malignancies was intended to determine the safety profile, PK profile, and dose of ORH-2014. Therefore, in this study we did not conduct a side-by-side comparison of ORH-2014 and IV ATO, and used IV ATO historical data for comparison. A parallel comparison with IV ATO may be performed in the next planned study in patients with APL in whom IV ATO is approved. While data from a crossover design may add value to the study, it requires the drug to be held for over one week for an adequate washout of ATO, which is not acceptable in patients with advanced hematological malignancies who require ongoing treatment.

Oral formulations of ATO, including ORH-2014, could represent safer and similarly active alternatives to IV ATO and could have great utility for the treatment of patients with APL by improving the patients' quality of life and treatment compliance, while reducing the patient burden and treatment costs. Based on the findings of the present study, a flat dose of 15 mg daily ORH-2014, administered daily (like IV ATO), appears to be adequate for the induction and consolidation therapy in adult patients with hematologic malignancies in future trials. Additional studies may be conducted with alternate treatment regimen if deemed necessary. In pediatric patients, however, a per-weight dose is recommended.

Acknowledgments

The authors thank Florence Paillard for her editorial assistance, and Stuart Hossack and Mary Sherman for the expert analysis in pharmacokinetics.

References

1. NIH, National Cancer Institute; Surveillance, Epidemiology, and End Results Program (SEER). 2019 data. Available at: <https://seer.cancer.gov/>
2. Sanz MA, Grimwade D, Tallman MS, et al. Management of acute promyelocytic leukemia: recommendations from an expert panel on behalf of the European LeukemiaNet. *Blood*. 2009;113(9):1875-1891.
3. Emadi A, Gore SD. Arsenic trioxide – An old drug rediscovered. *Blood Rev*. 2010; 24(4-5):191-199.
4. Sun HD, Ma L, Hu XC, Zhang TD. Arsenic trioxide [Ai-lin 1] treated 32 cases of acute promyelocytic leukemia. *Chin J Integrated Tradit West Med*. 1992;12:170-172.
5. Shen ZX, Chen GQ, Ni JH, et al. Use of arsenic trioxide (As₂O₃) in the treatment of acute promyelocytic leukemia (APL): II. Clinical efficacy and pharmacokinetics in relapsed patients. *Blood*. 1997;89(9):3354-3360.
6. Zhang P, Wang SY, Hu XH. Arsenic trioxide treated 72 cases of acute promyelocytic leukemia. *Chin J Hematol*. 1996;17:58-62.
7. Soignet SL, Maslak P, Wang ZG, et al. Complete remission after treatment of acute promyelocytic leukemia with arsenic trioxide. *N Engl J Med*. 1998;339:1341-1348.
8. Soignet SL, Frankel SR, Douer D, et al. United States multicenter study of arsenic trioxide in relapsed acute promyelocytic leukemia. *J Clin Oncol*. 2001;19(18):3852-3860.
9. Trisenox® arsenic trioxide injection [Prescribing Information]. Teva Pharmaceuticals, Inc. 2000-2018. https://www.accessdata.fda.gov/drugsatfda_docs/label/2018/021248s0151bl.pdf. Accessed 13 May 2019.
10. Ravandi F, Estey E, Jones D, et al. Effective treatment of acute promyelocytic leukemia with all-trans-retinoic acid, arsenic trioxide, and gemtuzumab ozogamicin. *J Clin Oncol*. 2009;27(4):504-510.
11. Ghavamzadeh A, Alimoghaddam K, Rostami S, et al. Phase II study of single-agent arsenic trioxide for the front-line therapy of acute promyelocytic leukemia. *J Clin Oncol*. 2011;29(20):2753-2757.
12. Mathews V, George B, Lakshmi KM, et al. Single-agent arsenic trioxide in the treatment of newly diagnosed acute promyelocytic leukemia: durable remissions with minimal toxicity. *Blood*. 2006;107(7):2627-2632.
13. Abaza Y, Kantarjian H, Garcia-Manero G, et al. Long-term outcome of acute promyelocytic leukemia treated with all-trans-retinoic acid, arsenic trioxide, and gemtuzumab. *Blood*. 2017;129(10):1275-1283.
14. Lo-Coco F, Avvisati G, Vignetti M, et al. Retinoic acid and arsenic trioxide for acute promyelocytic leukemia. *N Engl J Med*. 2013;369(2):111-121.
15. Burnett AK, Russell NH, Hills RK, et al.; UK National Cancer Research Institute Acute Myeloid Leukaemia Working Group. Arsenic trioxide and all-trans retinoic acid treatment for acute promyelocytic leukaemia in all risk groups (AML17): results of a randomised, controlled, phase 3 trial. *Lancet Oncol*. 2015;16(13):1295-1305.
16. Platzbecker U, Avvisati G, Cicconi L, et al. Improved outcomes with retinoic acid and arsenic trioxide compared with retinoic acid and chemotherapy in non-high-risk acute promyelocytic leukemia: final results of the randomized Italian-German APL0406 trial. *J Clin Oncol*. 2017;35(6):605-612.
17. Iland HJ, Wei A, Seymour JF. Have all-trans retinoic acid and arsenic trioxide replaced all-trans retinoic acid and anthracyclines in APL as standard of care. *Best Pract Res Clin*

- Haematol. 2014;27(1):39-52.
18. Sanz MA, Fenaux P, Tallman MS, et al. Management of acute promyelocytic leukemia: updated recommendations from an expert panel of the European LeukemiaNet. *Blood*. 2019;133(15):1630-1643.
 19. Kumana CR, Au WY, Lee NS, et al. Systemic availability of arsenic from oral arsenic-trioxide used to treat patients with hematological malignancies. *Eur J Clin Pharmacol*. 2002;58(8):521-526.
 20. Au WY, Kumana CR, Kou M, et al. Oral arsenic trioxide in the treatment of relapsed acute promyelocytic leukemia. *Blood*. 2003;102(1):407-408.
 21. Au WY, Kumana CR, Lee HK, et al. Oral arsenic trioxide-based maintenance regimens for first complete remission of acute promyelocytic leukemia: a 10-year follow-up study. *Blood*. 2011;118(25):6535-6543.
 22. Gill H, Yim R, Lee H, et al. Long-term outcome of relapsed acute promyelocytic leukemia treated with oral arsenic trioxide-based reinduction and maintenance regimens: A 15-year prospective study. *Cancer*. 2018;124(11):2316-2326.
 23. Siu CW, Au WY, Yung C, et al. Effects of oral arsenic trioxide therapy on QT intervals in patients with acute promyelocytic leukemia: implications for long-term cardiac safety. *Blood*. 2006;108(1):103-106.
 24. Zhu HH, Wu DP, Jin J, et al. Oral tetra-arsenic tetra-sulfide formula versus intravenous arsenic trioxide as first-line treatment of acute promyelocytic leukemia: a multicenter randomized controlled trial. *J Clin Oncol*. 2013;31(33):4215-4221.
 25. Qian L. Phase II clinical trial of compound Huangdai tablet in newly diagnosed acute promyelocytic leukemia. *Chin J Hematol*. 2006;27:801-804.
 26. Zhu HH, Wu DP, Du X, et al. Oral arsenic plus retinoic acid versus intravenous arsenic plus retinoic acid for non-high-risk acute promyelocytic leukaemia: a non inferiority, randomised phase 3 trial. *Lancet Oncol*. 2018;19(7):871-879.
 27. Brunauer S, Emmett PH, Teller E. Adsorption of gases in multimolecular layers. *J Am Chem Soc*. 1938;60(2):309-319.
 28. Cheson BD, Greenberg PL, Bennett JM, et al. Clinical application and proposal for modification of the International Working Group (IWG) response criteria in myelodysplasia. *Blood*. 2006;108(2):419-425.
 29. Platzbecker U, Fenaux P, Adès L, et al. Proposals for revised IWG 2018 hematological response criteria in patients with MDS included in clinical trials. *Blood*. 2019;133(10):1020-1030.
 30. Levaquin (levofloxacin) [Prescribing Information]. Ortho-McNeil-Janssen Pharmaceuticals, Inc. 2008. https://www.accessdata.fda.gov/drugsatfda_docs/label/2008/021721s020_020635s57_020634s52_lbl.pdf. Accessed 13 May 2019.

Low level CpG island promoter methylation predicts a poor outcome in adult T-cell acute lymphoblastic leukemia

Aurore Touzart,¹ Nicolas Boissel,² Mohamed Belhocine,^{1,3,4} Charlotte Smith,¹ Carlos Graux,⁵ Mehdi Latiri,¹ Ludovic Lhermitte,¹ Eve-Lyne Mathieu,^{3,4} Françoise Huguet,⁶ Laurence Lamant,⁷ Pierre Ferrier,⁸ Norbert Ifrah,⁹ Elizabeth Macintyre,¹ Hervé Dombret,² Vahid Asnafi¹ and Salvatore Spicuglia^{3,4}

¹Université Paris Descartes Sorbonne Cité, Institut Necker-Enfants Malades (INEM), Institut national de recherche médicale (INSERM) U1151, and Laboratory of Onco-Hematology, Assistance Publique-Hôpitaux de Paris (AP-HP), Hôpital Necker Enfants-Malades, Paris, France; ²Université Paris Diderot, Institut de Recherche Saint-Louis, EA-3518, Assistance Publique-Hôpitaux de Paris, University Hospital Saint-Louis, Hematology Department, Paris, France; ³Aix-Marseille University, INSERM, TAGC, UMR 1090, Marseille, France; ⁴Equipe Labéllisée Ligue Contre le Cancer, Marseille, France; ⁵Department of Hematology, Mont-Godinne University Hospital, Yvoir, Belgium; ⁶Centre Hospitalier Universitaire de Toulouse, Institut Universitaire du Cancer de Toulouse Oncopole, Toulouse, France; ⁷Institut Universitaire du Cancer Toulouse Oncopole, Toulouse, France; ⁸Centre d'Immunologie de Marseille-Luminy, Aix-Marseille Université UM2, Inserm, U1104, CNRS UMR7280, Marseille, France and ⁹PRES LUNAM, CHU Angers service des Maladies du Sang et INSERM U 892, Angers, France

ABSTRACT

Cancer cells undergo massive alterations in their DNA methylation patterns which result in aberrant gene expression and malignant phenotypes. Abnormal DNA methylation is a prognostic marker in several malignancies, but its potential prognostic significance in adult T-cell acute lymphoblastic leukemia (T-ALL) is poorly defined. Here, we performed methylated DNA immunoprecipitation to obtain a comprehensive genome-wide analysis of promoter methylation in adult T-ALL (n=24) compared to normal thymi (n=3). We identified a CpG hypermethylator phenotype that distinguishes two T-ALL subgroups and further validated it in an independent series of 17 T-lymphoblastic lymphoma. Next, we identified a methylation classifier based on nine promoters which accurately predict the methylation phenotype. This classifier was applied to an independent series of 168 primary adult T-ALL treated accordingly to the GRAALL03/05 trial using methylation-specific multiplex ligation-dependent probe amplification. Importantly hypomethylation correlated with specific oncogenic subtypes of T-ALL and identified patients associated with a poor clinical outcome. This methylation-specific multiplex ligation-dependent probe amplification based methylation profiling could be useful for therapeutic stratification of adult T-ALL in routine practice. The GRAALL-2003 and -2005 studies were registered at <http://www.clinicaltrials.gov> as #NCT00222027 and #NCT00327678, respectively.

Introduction

T-cell acute lymphoblastic leukemias (T-ALL) are aggressive and heterogeneous malignancies which are predominated by the 10-39-year age group where they account for 20% of acute lymphoblastic leukemias (ALL).¹ T-ALL is associated with a wide range of acquired genetic abnormalities that contribute to developmental arrest and abnormal proliferation of malignant lymphoid progenitors.^{2,3} Despite the diversity of observed mutations and deletions, genome wide expression^{4,6} assays led to the identification of few oncogenic T-ALL subgroups, namely the imma-



Haematologica 2020
Volume 105(6):1575-1581

Correspondence:

SALVATORE SPICUGLIA
salvatore.spicuglia@inserm.fr

VAHID ASNAFI
vahid.asnafi@nck.aphp.fr

Received: April 4, 2019.

Accepted: September 19, 2019.

Pre-published: September 19, 2019.

doi:10.3324/haematol.2019.223677

Check the online version for the most updated information on this article, online supplements, and information on authorship & disclosures: www.haematologica.org/content/106/6/1575

©2020 Ferrata Storti Foundation

Material published in *Haematologica* is covered by copyright. All rights are reserved to the Ferrata Storti Foundation. Use of published material is allowed under the following terms and conditions:

<https://creativecommons.org/licenses/by-nc/4.0/legalcode>.
Copies of published material are allowed for personal or internal use. Sharing published material for non-commercial purposes is subject to the following conditions:
<https://creativecommons.org/licenses/by-nc/4.0/legalcode>, sect. 3. Reproducing and sharing published material for commercial purposes is not allowed without permission in writing from the publisher.



ture/early thymic precursor (ETP) (Lyl1, MEF2C), late cortical (TAL1), early cortical (TLX1/3 and NKX2.1) and HOXA clusters. Although cancer is typically considered a genetic disease, epigenetic aberrations also play important roles in tumor potentiation, initiation, and progression.⁷ Epigenetics is defined as changes in gene expression that are not due to changes in gene sequence, and include DNA methylation, histone modifications, microRNA (miRNA) and nucleosome positioning. Unlike genetic alterations, epigenetic changes are reversible by enzymatic activity and pharmacological treatment with small molecule inhibitors, like those targeting enzymes involved in DNA methylation or chromatin modifications. Altered epigenetic states are a common feature of all cancer types and the most studied epigenetic modification in primary cancer samples is DNA methylation, which is known to display characteristic changes in malignant cells compared to normal tissue. These include diffuse hypomethylation and focal hypermethylation changes at discrete loci potentially associated with repression of specific genes related to cancer pathogenesis.

In the field of ALL, DNA methylation studies have mostly focused on pediatric B-cell precursor ALL (BCP-ALL) describing promoter hypermethylation and specific methylation signatures according to the cytogenetic subgroup.⁸ In pediatric T-ALL, DNA methylation was analyzed by Infinium 27 K and 450 K arrays and two distinct CpG island methylator phenotype (CIMP) groups were identified. Patients with a CIMP-negative profile displayed a significantly higher cumulative incidence of relapse (CIR) compared to CIMP-positive patients suggesting a prognostic relevance of aberrant DNA methylation profiles in T-ALL.^{9,10} Furthermore, it has more recently been shown in a pediatric series that CIMP status correlates with known oncogenic subgroups, for instance, with higher expression of TAL1 in a CIMP-negative subgroup (11). However such data for adult T-ALL are still lacking. In this work, we report genome-wide promoter methylation profiling by methylation-dependent immunoprecipitation (MeDIP) in a cohort of adult T-ALL. Subsequently, a nine-promoter classifier was applied to a large series of 168 adult T-ALL included in the GRAALL 03/05 trial that distinguished two subgroups with highly significant differences in the clinical outcome. Thus, MeDIP profiling is a potential candidate for risk stratification of adult T-ALL and could provide important information in treatment decision making and therapeutic targeting.

Methods

Patients and treatments

Adult patients (15-60 years old) included in two successive French ALL cooperative group trials (GRAALL-2003 and GRAALL-2005) with T-ALL, and defined according to the 2008 World Health Organisation classification, were analyzed. The GRAALL-2003 protocol was a multicenter phase 2 trial, which enrolled 76 adults with T-ALL between November 2003 and November 2005 of whom 50 had sufficient diagnostic tumor material available.¹² The multicenter randomized GRAALL-2005 phase 3 trial was very similar to the GRAALL-2003 trial, with the addition of a randomized evaluation of an intensified sequence of hyperfractionated cyclophosphamide during induction and late intensification.¹³ Between May 2006 and May 2010, 337 adults with T-ALL were randomized in the GRAALL-2005, of which 185

had available diagnostic material. All samples contained >80% blasts. Phenotypic and oncogenetic characteristics were as described.¹⁴⁻¹⁶ Informed consent was obtained from all patients at enrollment. All trials were conducted in accordance with the Declaration of Helsinki and approved by local and multicenter research ethical committees.

MeDIP-assay

Global DNA methylation was assessed by a MeDIP assay on an initial series of 24 T-ALL and three human thymi and a second (confirmatory series) of 17 T-lymphoblastic lymphomas (T-LBL) and three human thymi. Briefly, methylated DNA was immunoprecipitated as described previously¹⁷ using 2 µg of sonicated genomic DNA. MeDIP samples were directly subjected to labeling and hybridization to previously described custom human promoter arrays (Agilent, Santa Clara, CA, USA) covering either 17,970 promoters¹⁷ (T-ALL series) or 25,490 promoters¹⁸ (T-LBL series), following the manufacturer's instructions. The median-normalized log₂ enrichment ratios (MeDIP/Input) were calculated for each probe using the CoCAS software¹⁹ and visualized using the IGB tool (<http://bioviz.org/igb>). Finally, a methylation score was computed for each promoter by calculating the median enrichment ratio of overlapping probes. A summary of the methylation scores per promoter in T-ALL and T-LBL samples is provided in the *Online Supplementary Tables S1-2*, respectively.

Clustering of methylation profiles

Hierarchical clustering analysis (Average Linkage) based on the methylation signal of the top 5% genes with highest variance was performed with the TIGR MeV v. 4.9.0 program,²⁰ using the -1 Spearman rank correlation method. Analysis of the differential methylation signal between the groups was performed using the significant analysis of microarrays (SAM) algorithm (threshold value: FDR<0.121 and delta=2.144). The graphical clustering representation of the clustering was done with the GenePattern software.²¹ The list of differentially methylated promoters in T-ALL and T-LBL is provided in *Online Supplementary Table S3*.

Validation of DNA methylation signature

Direct methylation levels were analyzed by methylation-specific multiplex ligation-dependent probe amplification (MS-MLPA) with custom probes (*Online Supplementary Table S4*) and, SALSA[®] MLPA[®] P200 Reference-1 probemix and EK1 reagent kits from MRC-Holland (Amsterdam, the Netherlands), according to manufacturer's recommendations. Data were analyzed with the Coffalyser software (MRC-Holland, Amsterdam, the Netherlands). In addition, the promoter methylation patterns were verified by quantitative PCR (qPCR) analysis of MeDIP samples and by bisulfite sequencing using specific primers for the MEIS1 gene promoter.

Results

DNA methylation signatures in T-ALL/T-LBL

Global promoter regions DNA methylation by MeDIP-array was performed in a training series of 24 adult T-ALL. Unsupervised hierarchical clustering defined two major groups (group 1 and group 2) with distinct methylation profiles (Figure 1A). The supervised signature of differential methylation (FDR<0.121) between these two groups resulted in 300 unique differentially methylated gene promoters with a vast majority of hypermethylated (hyperM) promoters (297 of 300) in the so-called hyperM group. The second group displayed an intermediate methylation

(interM) profile compared to the normal thymic tissue (Figure 1B and *Online Supplementary Figure S1*). Interestingly, all the TLX⁺ cases without exception (including six TLX1⁺ and two TLX3⁺ cases) clustered in the hyperM group. Conversely, the two SIL-TAL1⁺ cases belonged to the interM group; suggesting a role of oncogenic abnormalities in the observed methylation profiles.

A very similar differential methylation signature (Figure 2A-B) was observed in an independent series of 17 T-LBL. One TLX1⁺ and five TLX3⁺ T-LBL, as in T-ALL, were clustered in the group with a hyperM promoter profile (253 of 255 hyperM gene promoters). T-ALL and T-LBL promoter methylation signatures displayed a highly significant overlap ($P < 0.0001$) with 97 common gene promoters differentially methylated (Figure 2C and *Online Supplementary Table S2*). Among them, the differential methylation of MEIS1 promoter was confirmed with two different targeted methods, MeDIP-QPCR (*Online Supplementary Figure S2A*) and bisulfite sequencing (*Online Supplementary Figure S2B*).

Driver oncogenes defined distinct aberrant methylation profiles

In an effort to explore the DNA methylation profiles in a larger T-ALL series, a minimal robust signature able to

predict the methylation state was defined with a remaining error risk inferior to 0.05. This predictor contained the following nine gene promoters: *BMP4*, *HOXB7*, *KCNA1*, *LHX1*, *MEIS1*, *PROX1*, *PSD3*, *RUNX2*, *SEMA6A* (Figure 3A). A MS-MLPA panel was designed to explore the methylation status of these nine gene promoters and a methylation ratio corresponding to the methylation average of these nine differentially methylated regions (DMR) was calculated. As expected, this predictor allowed the separation of hyperM and interM T-ALL from the training cohort ($P = 0.0016$) (Figure 3B-C). We then performed this analysis on a series of 168 primary adult T-ALL uniformly treated according to the GRAALL03-05 trial (Figure 3D). The methylation ratio was widely ranged (mean=0.62, min=0.04, max=1.1) and major oncogenetic drivers (TLX1, TLX3, SIL-TAL1, HOXA overexpression) defined distinct methylation profiles. TLX1⁺ and TLX3⁺ T-ALL displayed significantly hyperM promoters compared to the HOXA subgroup ($P = 0.03$ and $P = 0.02$ respectively), to the SIL-TAL1 subgroup ($P < 0.0001$) or the others T-ALL ($P < 0.0001$). Conversely, SIL-TAL1⁺ cases and others T-ALL expressing high level of TAL1 had significantly hypomethylated (hypoM) promoters ($P < 0.0001$) compared to TLX1/3⁺, HOXA⁺ or others T-ALL. Unlike oncogenic status, immature early thymic progenitor-ALL

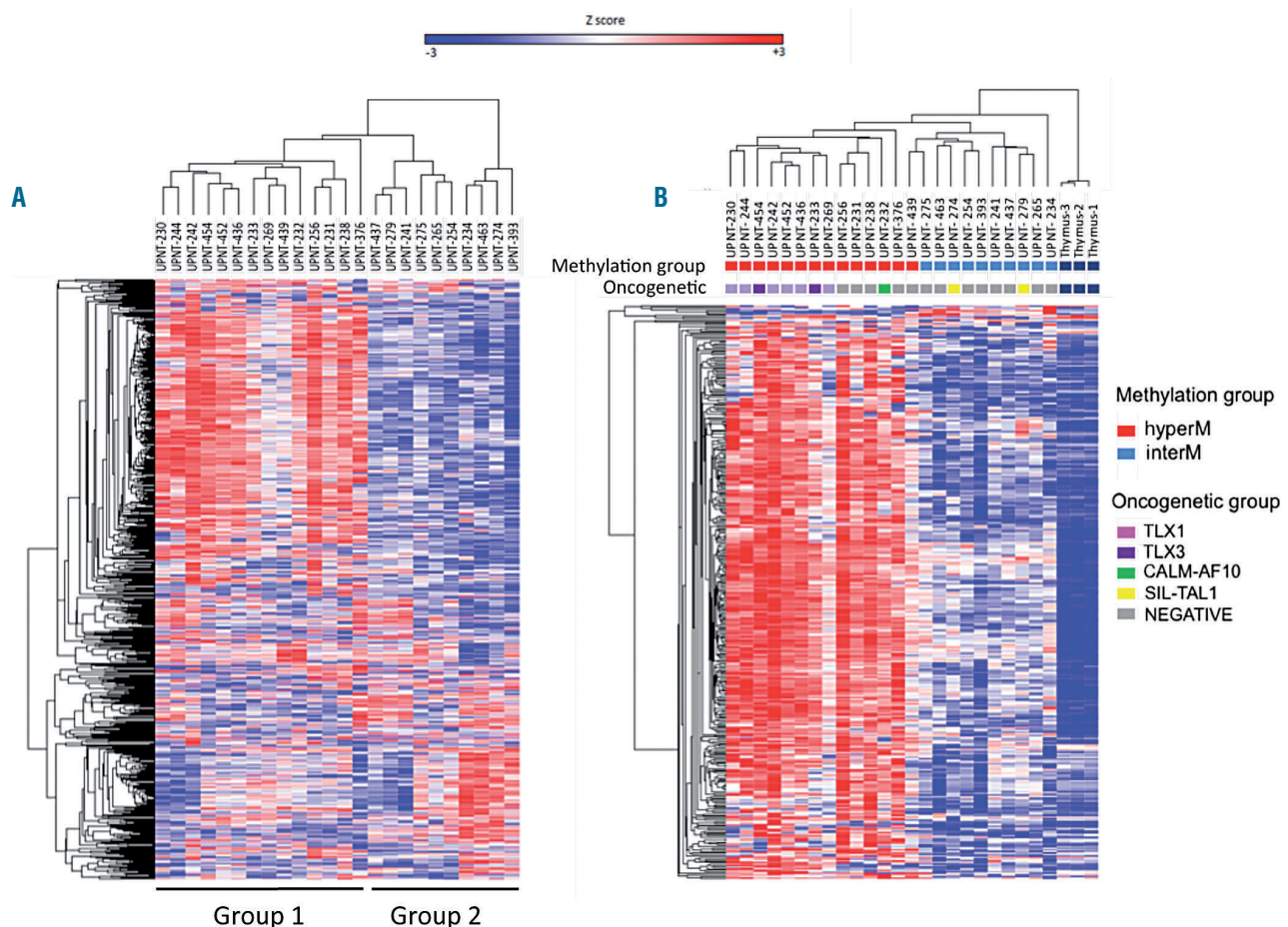


Figure 1. Genome-wide promoter methylation-array hierarchical clustering in T-cell acute lymphoblastic leukemias. (A) Unsupervised hierarchical clustering of 24 adult T-cell acute lymphoblastic leukemias (T-ALL) based on the genome-wide promoter methylation (MeDIP-array). The hypermethylated (hyperM; group 1) and intermediate methylated (interM; group 2) clusters are indicated. (B) Supervised clustering of T-ALL samples along with three human thymi using the differentially methylated signature obtained between groups 1 and 2 (panel A).

(ETP-ALL) lacked a significant distinct methylation signature compared to non-ETP-ALL (Figure 3E).

Low level of promoter methylation predicted a poor outcome subgroup of adult T-ALL

T-ALL patients with the lowest methylation level (Q1, n=42/168) were significantly more men, were younger, and had a higher white blood cell (WBC) count at diagnosis than patients with higher methylation levels (Table 1). Moreover, hypoM T-ALL demonstrated a significantly more frequent mature phenotype (TCRαβ⁺) and were associated with SIL-TAL1 rearrangement. They were also

significantly associated with a low rate of NOTCH1 pathway mutations and a high risk NOTCH1/FBXW7/RAS/PTEN molecular classifier.²² In detail, we observed a significantly lower incidence of *NOTCH1/FBXW7* mutations and also a greater incidence of *PTEN* alterations (mutation and/or deletion) in the hypoM subgroup (CIMP-neg) as compared to the Int/High methylated cases (*Online Supplementary Table S5*). Despite a better bone marrow response at D8 (M1 status) in patients with low methylation, we did not observe any impact of methylation on complete remission (CR) rate or post-induction minimal residual disease (MRD) level. In univariate analysis,

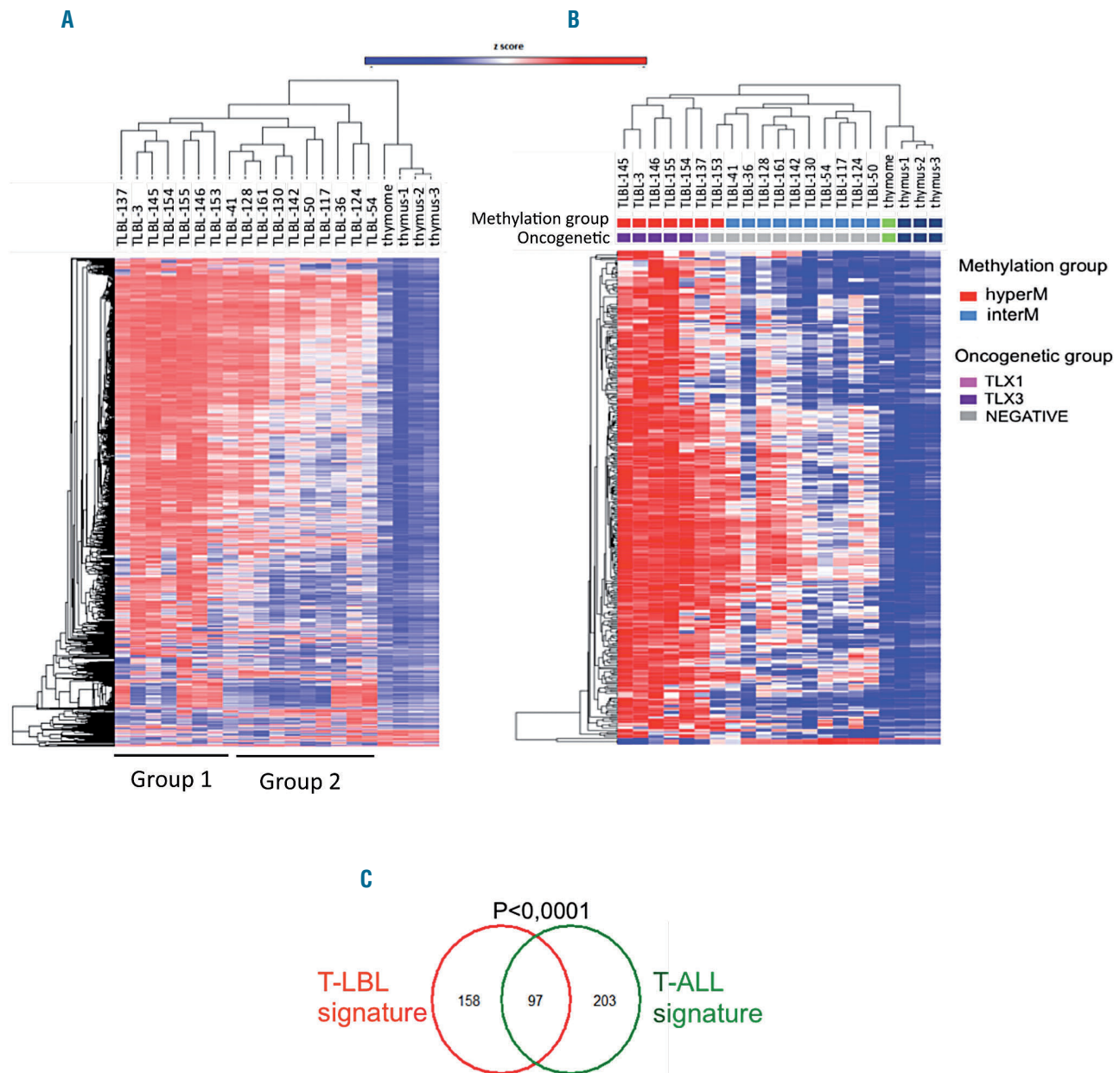


Figure 2. Genome-wide promoter methylation-array hierarchical clustering in T-lymphoblastic lymphomas. (A) Unsupervised hierarchical clustering of 17 T-lymphoblastic lymphomas (T-LBL) based on genome-wide promoter methylation (MeDIP-array). The hypermethylated (hyperM; group 1) and intermediate methylated (interM; group 2) methylated clusters are indicated. (B) Supervised clustering of T-LBL samples, one thymoma and three thymi, using the differentially methylated signature obtained between groups 1 and 2 (panel A). (C) Venn diagram representing the overlap between the differentially methylated promoters between hyperM and interM subgroups found in T-ALL and T-LBL samples. Statistical significance was assessed by a Hypergeometric test.

patients with low methylation levels had higher CIR (sub-distribution hazard ratio [SHR] 1.87, 95% CI: 1.03-3.38, $P=0.04$; Table 2 and Figure 4A) and a shorter overall survival (OS) (hazard ratio [HR] 1.78, 95% CI: 1.06-2.98, $P=0.03$; Table 2 and Figure 4B). In multivariate analysis for CIR, the only prognostic factor to be significantly associated with a reduced CIR was the NOTCH1/FBXW7/RAS/PTEN molecular classifier. However, in multivariate analysis for OS, including age, WBC at diagnosis, central nervous system (CNS) involvement, prednisone response, the molecular classifier, and the methylation level as covariates, a low methylation was still independently associated with a higher risk of death (HR 1.79, 95% CI: 1.00-3.19, $P=0.05$; Table 2).

Discussion

Despite recent insights into the molecular and cellular mechanisms responsible for T-ALL onset and progression, survival rates remain around 50% in adults, justifying the search for novel therapeutic options or more adapted/personalized regimens. The present study focused on promoter DNA methylation in a large series of adult T-ALL. As previously reported in pediatric T-ALL,⁹⁻¹¹ we showed that DNA methylation status is also a prognostic factor in adult T-ALL. Similarly, patients with a hypoM profile dis-

play an unfavorable outcome compared to hyperM patients. Importantly, even if hypoM status is associated with the molecular high-risk classifier,²² methylation level remains an independent prognostic factor. Moreover, methylation status does not seem to influence the initial clinical response to therapy since there were no significant differences regarding the glucocorticoids and initial chemotherapy responses (chemosensitivity or MRD) between hypoM and hyperM patients. Methylation status could therefore represent a relevant additional prognostic factor for adult T-ALL. Nevertheless, further validation by another independent series is needed. Moreover, it would be interesting to study the prognostic impact of this methylation signature in T-LBL, which displayed similar methylation distortion patterns.

We used the relatively new methodology of methylation specific-multiplex ligation-dependent probe amplification (MS-MLPA) to evaluate the promoter DNA methylation level. MS-MLPA is a powerful and easy-to-perform PCR-based technique and we demonstrated that MS-MLPA could provide an attractive alternative way to assess methylation classification compared to array analysis. This approach permits methylation analysis of multiple targets in a single experiment and has been successfully used to evaluate the diagnostic relevance of different markers in several tumor types including lung,²³ rectal,²⁴ breast,²⁵ bladder,²⁶ prostate,²⁷ and adrenocortical cancer.²⁸

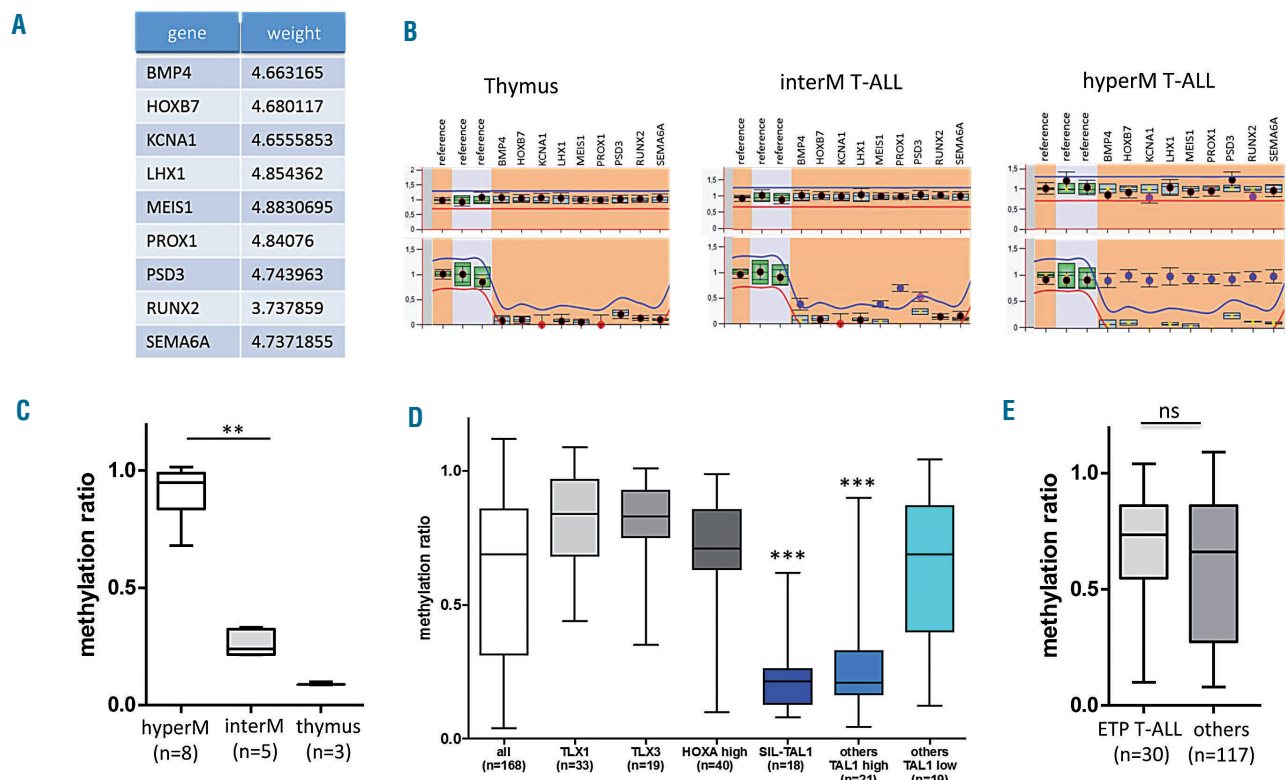


Figure 3. Targeted promoter methylation analysis in GRAALL 03/05 T-cell acute lymphoblastic leukemias series. (A) List of the nine gene promoters classifier allowing methylation status prediction. (B) Representative ratio charts of methylation specific-multiplex ligation-dependent probe amplification (MS-MLPA) analysis for one normal thymus and two T-cell acute lymphoblastic leukemias (T-ALL) from the training series belonging to the intermediate methylated (interM) subgroup and the hypermethylated (hyperM) subgroup respectively. Top panels refer to the MLPA (undigested) reference panel and the bottom panel the MS-MLPA (digested with HhaI restriction enzyme) panel. (C) Methylation ratio was assessed by MS-MLPA for T-ALL from the training series and according to their methylation subgroup and for three normal thymi. (D) Methylation ratio assessed by MS-MLPA for 168 adult T-ALL included in GRAALL03/05 trial and according to the driver oncogene involved (TLX1, TLX3, HOXA, SIL-TAL1). (E) Methylation ratio according to the early thymic precursor (ETP) phenotype.

Table 1. Patients' characteristics and outcome according to methylation status.

	Low methylation N=42 (Q1)	Int/High methylation N= 126 (Q2-Q4)	P†
TCR subsets analyzed			
Immature (IM0, IMδ, IMγ)	4/36 (11%)	32/111 (29%)	0.04
IMβ/pre-αβ	20/36 (56%)	60/111 (54%)	0.99
TCRαβ+	11/36 (31%)	5/111 (5%)	<0.0001
TCRγδ+	1/36 (3%)	14/111 (13%)	0.12
ETP immunophenotype			
<i>NOTCH1/FBXW7</i> ^{mutated}	18/42 (43%)	99/126 (79%)	<0.0001
<i>High Risk Classifier</i> *	29/42 (69%)	43/125 (34%)	0.0001
Oncogenetic Category			
<i>TLX1</i>	0/41 (0%)	35/120 (29%)	<0.0001
<i>TLX3</i>	0/41 (0%)	21/120 (18%)	0.0022
<i>SIL-TALI</i>	16/41 (39%)	2/120 (2%)	<0.0001
<i>CALM-AF10</i>	0/41 (0%)	8/120 (7%)	0.2
<i>None of the above</i>	25/41 (61%)	54/120 (45%)	0.1
<i>HOXA</i> deregulation	3/39 (8%)	40/112 (36%)	0.0008
Clinical Subsets Analyzed			
Age, median (range)	23.2 (16.6-56.2)	33.4 (16.3-59.1)	<0.001
Sex ratio, M/F	35/7	85/41	0.05
WBC (G/L), median (range)	80 (4-604)	30 (1-645)	0.003
CNS involvement	7/42 (17%)	17/126 (13%)	0.616
Early Response			
Prednisone response	23/42 (55%)	68/126 (55%)	1
Bone marrow response	29/39 (74%)	66/126 (52%)	0.02
Complete remission	38/42 (90%)	117/126 (93%)	0.739
MRD (TP1) <10 ⁻⁴	16/19 (84%)	48/73 (66%)	0.164
Long-term outcome			
5-year CIR (95% CI)	45% (31-62)	27% (20-36)	0.04
5-year OS (95% CI)	50% (34-64)	68% (59-76)	0.03

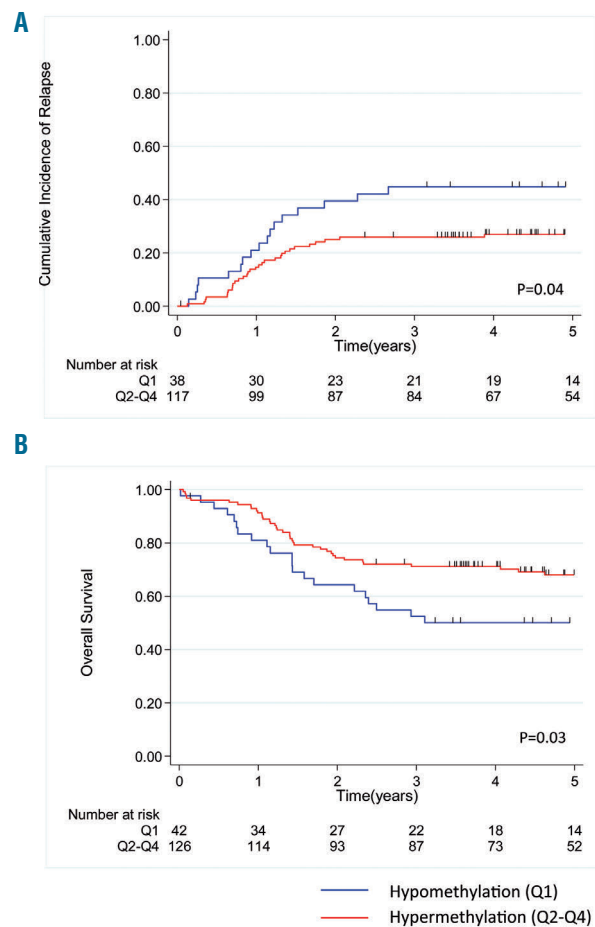
IM: immature; WBC (g/L): white blood cells; CNS: central nervous system; MRD (TP1): post-induction minimal residual disease; CIR: cumulative incidence of relapse; OS: overall survival; 95%CI: 95% confidence interval; TCR: Tcell receptor; ETP: early thymic precursor. * The unfavorable classifier includes NOTCH1, FBXW7, RAS and PTEN (Trinquand, et al. 2013). †χ² or Mann-Whitney tests were used where appropriate.

Table 2. Univariate and multivariate analysis for cumulative incidence of relapse and overall survival.

CIR	Univariate			Multivariate		
	SHR	95%CI	P	SHR	95%CI	P
Age*	1.00	0.97 – 1.03	0.90	–	–	–
WBC**	1.00	0.98 – 1.04	0.29	–	–	–
CNS involvement	1.55	0.75 – 3.21	0.23	–	–	–
Unfavorable risk classifier	3.77	2.04 – 6.98	<0.001	3.53	1.85 – 6.73	<0.001
Prednisone responder	0.71	0.40 – 1.25	0.24	–	–	–
Bone marrow responder	0.76	0.43 – 1.35	0.35	–	–	–
Low methylation (Q1)	1.87	1.03 – 3.38	0.04	1.25	0.67 – 2.34	0.49

OS	Univariate			Multivariate		
	HR	95%CI	P	HR	95%CI	P
Age*	1.03	1.01 – 1.06	0.01	1.04	1.02 – 1.06	0.001
WBC**	1.01	1.00 – 1.03	0.12	–	–	–
CNS involvement	2.14	1.18 – 3.88	0.01	2.32	1.24 – 4.35	0.01
Favorable risk classifier	3.81	2.24 – 6.50	<0.001	2.93	1.65 – 5.21	<0.001
Prednisone responder	0.64	0.39 – 1.05	0.08	0.69	0.41 – 1.16	0.16
Bone marrow responder	0.78	0.47 – 1.27	0.31	–	–	–
Low methylation (Q1)	1.78	1.06 – 2.98	0.03	1.79	1.00 – 3.19	0.05

WBC: white blood cell; CNS: central nervous system; CIR: cumulative incidence of relapse; OS: overall survival; HR: hazard ratio; SHR: sub-distribution hazard ratio; 95% CI: 95% confidence interval. *Age as continuous variable, SHR/HR for 1-year increment. ** WBC as continuous variable, SHR/HR for 10 g/L increment



Additionally, MS-MLPA has the advantage of requiring little DNA and does not require DNA bisulfite conversion or immunoprecipitation. MS-MLPA is readily compatible with clinical routine and could enhance prognostication and precision medicine.

However, array analysis or methylation analysis at the whole genome level would be relevant in T-ALL to gain information and investigate how aberrant methylation patterns are involved in leukemogenesis. We have observed that aberrant methylation profiles were mostly associated with the driver oncogene involved. In particular, a hypoM subgroup with unfavorable outcome is mainly enriched in SIL-TAL1+ cases and also in cases negative for the main oncogenes TLX1, TLX3, SIL-TAL1 and HOXA. Deciphering the molecular mechanism of aberrant methylation and the relationship with driver oncogenes could identify new deregulated pathways for adapted-therapy.

Acknowledgments

We thank all French, Swiss and Belgian participants, clinicians, biologists and clinical research assistants, in the LALA-94 and GRAALL 2003-2005 trials, for collecting and providing data and samples.

Funding

MeDIP experiments were supported by the INCA-project PAIR-Lymphomes. Work in SS laboratory was supported by Ligue contre le Cancer (Equipe labellisée). Work in the Necker hematology department and SS laboratory was supported by grants from ITMO (Institut Thématique Multi-Organisme) épigénétique et cancer. The GRAALL was supported by grants P0200701 and P030425/AOM03081 from Le Programme Hospitalier de Recherche Clinique, Ministère de l'Emploi et de la Solidarité, France and the Swiss Federal Government in Switzerland. AT was supported by a grant from the French program CARPEM (CAncer Research for PErsonalized Medicine).

References

- Chessells JM, Hall E, Prentice HG, et al. The impact of age on outcome in lymphoblastic leukaemia; MRC UKALL X and XA compared: a report from the MRC Paediatric and Adult Working Parties. *Leukemia*. 1998; 12(4):463-473.
- Teitell MA, Pandolfi PP. Molecular genetics of acute lymphoblastic leukemia. *Ann Rev Pathol*. 2009;4:175-198.
- Van Vlierberghe P, Pieters R, Beverloo HB, Meijerink JP. Molecular-genetic insights in paediatric T-cell acute lymphoblastic leukaemia. *Br J Haematol*. 2008;143(2):153-168.
- Ferrando AA, Neuberg DS, Staunton J, et al. Gene expression signatures define novel oncogenic pathways in T cell acute lymphoblastic leukemia. *Cancer Cell*. 2002; 1(1):75-87.
- Homminga I, Pieters R, Langerak AW, et al. Integrated transcript and genome analyses reveal NKX2-1 and MEF2C as potential oncogenes in T cell acute lymphoblastic leukemia. *Cancer Cell*. 2011;19(4):484-497.
- Soulier J, Clappier E, Cayuela JM, et al. HOXA genes are included in genetic and biologic networks defining human acute T-cell leukemia (T-ALL). *Blood*. 2005; 106(1):274-286.
- Flavahan WA, Gaskell E, Bernstein BE. Epigenetic plasticity and the hallmarks of cancer. *Science*. 2017;357(6348).
- Nordlund J, Backlin CL, Wahlberg P, et al. Genome-wide signatures of differential DNA methylation in pediatric acute lymphoblastic leukemia. *Genome Biol*. 2013; 14(9):r105.
- Borssen M, Haider Z, Landfors M, et al. DNA methylation adds prognostic value to minimal residual disease status in pediatric T-cell acute lymphoblastic leukemia. *Pediatr Blood Cancer*. 2016;63(7):1185-1192.
- Borssen M, Palmqvist L, Karrman K, et al. Promoter DNA methylation pattern identifies prognostic subgroups in childhood T-cell acute lymphoblastic leukemia. *PLoS One*. 2013;8(6):e65373.
- Haider Z, Larsson P, Landfors M, et al. An integrated transcriptome analysis in T-cell acute lymphoblastic leukemia links DNA methylation subgroups to dysregulated TAL1 and ANTP homeobox gene expression. *Cancer Med*. 2019;8(1):311-324.
- Huguet F, Leguay T, Raffoux E, et al. Pediatric-inspired therapy in adults with Philadelphia chromosome-negative acute lymphoblastic leukemia: the GRAALL-2003 study. *J Clin Oncol*. 2009;27(6):911-918.
- Mauray S, Chevret S, Thomas X, et al. Rituximab in B-lineage adult acute lymphoblastic leukemia. *N Engl J Med*. 2016; 375(11):1044-1053.
- Asnafi V, Buzyn A, Le Noir S, et al. NOTCH1/FBXW7 mutation identifies a large subgroup with favorable outcome in adult T-cell acute lymphoblastic leukemia (T-ALL): a Group for Research on Adult Acute Lymphoblastic Leukemia (GRAALL) study. *Blood*. 2009;113(17):3918-3924.
- Bergeron J, Clappier E, Radford I, et al. Prognostic and oncogenic relevance of TLX1/HOX11 expression level in T-ALLs. *Blood*. 2007;110(7):2324-2330.
- Bond J, Marchand T, Touzart A, et al. An early thymic precursor phenotype predicts outcome exclusively in HOXA-overexpressing adult T-cell acute lymphoblastic leukemia: a Group for Research in Adult Acute Lymphoblastic Leukemia study. *Haematologica*. 2016;101(6):732-740.
- Jia J, Pekowska A, Jaeger S, et al. Assessing the efficiency and significance of Methylated DNA Immunoprecipitation (MeDIP) assays in using in vitro methylated genomic DNA. *BMC Res Notes*. 2010;3:240.
- Cornen S, Guille A, Adelaide J, et al. Candidate luminal B breast cancer genes identified by genome, gene expression and DNA methylation profiling. *PLoS One*. 2014;9(1):e81843.
- Benoukraf T, Cauchy P, Fenouil R, et al. CoCAS: a ChIP-on-chip analysis suite. *Bioinformatics*. 2009;25(7):954-955.
- Saeed AI, Sharov V, White J, et al. TM4: a free, open-source system for microarray data management and analysis. *Biotechniques*. 2003;34(2):374-378.
- Reich M, Tabor T, Liefeld T, et al. The GenePattern Notebook environment. *Cell Syst*. 2017;5(2):149-151.
- Trinquand A, Tanguy-Schmidt A, Ben Abdelali R, et al. Toward a NOTCH1/FBXW7/RAS/PTEN-based oncogenetic risk classification of adult T-cell acute lymphoblastic leukemia: a group for research in adult acute lymphoblastic leukemia study. *J Clin Oncol*. 2013; 31(34):4333-4342.
- Castro M, Grau L, Puerta P, et al. Multiplexed methylation profiles of tumor suppressor genes and clinical outcome in lung cancer. *J Transl Med*. 2010;8:86.
- Molinari C, Casadio V, Foca F, et al. Gene methylation in rectal cancer: predictive marker of response to chemoradiotherapy? *J Cell Physiol*. 2013;228(12):2343-2349.
- Moelans CB, de Groot JS, Pan X, van der Wall E, van Diest PJ. Clonal intratumor heterogeneity of promoter hypermethylation in breast cancer by MS-MLPA. *Mod Pathol*. 2014;27(6):869-874.
- Garcia-Baquero R, Puerta P, Beltran M, et al. Methylation of tumor suppressor genes in a novel panel predicts clinical outcome in paraffin-embedded bladder tumors. *Tumour Biol*. 2014;35(6):5777-5786.
- Gurioli G, Salvi S, Martignano F, et al. Methylation pattern analysis in prostate cancer tissue: identification of biomarkers using an MS-MLPA approach. *J Transl Med*. 2016;14(1):249.
- Jouinot A, Assie G, Libe R, et al. DNA Methylation is an independent prognostic marker of survival in adrenocortical cancer. *J Clin Endocrinol Metab*. 2017;1 02(3):923-932.



Ferrata Storti Foundation

Defining signatures of peripheral T-cell lymphoma with a targeted 20-marker gene expression profiling assay

Fanny Drieux,^{1,2,3*} Philippe Ruminy,^{1*} Ahmad Abdel-Sater,¹ François Lemonnier,^{3,4} Pierre-Julien Viailly,¹ Virginie Fataccioli,³ Vinciane Marchand,¹ Bettina Bisig,⁵ Audrey Letourneau,⁵ Marie Parrens,⁶ Céline Bossard,⁷ Julie Bruneau,⁸ Pamela Dobay,⁵ Liana Veresezan,^{1,2} Aurélie Dupuy,³ Anaïs Pujals,^{3,9} Cyrielle Robe,³ Nouhoum Sako,³ Christiane Copie-Bergman,^{3,9} Marie-Hélène Delfau-Larue,^{3,10} Jean-Michel Picquenot,^{1,2} Hervé Tilly,¹ Richard Delarue,¹¹ Fabrice Jardin,^{1*} Laurence de Leval^{5#} and Philippe Gaulard^{3,9#}

¹INSERM U1245, Centre Henri Becquerel, Rouen, France; ²Service d'Anatomie et Cytologie Pathologiques, Centre Henri Becquerel, Rouen, France; ³INSERM U955 and Université Paris-Est, Créteil, France; ⁴Unité Hémopathies Lymphoïdes, Groupe Hospitalier Henri Mondor, AP-HP, Créteil, France; ⁵Institut de Pathologie, Centre Hospitalier Universitaire Vaudois (CHUV), Lausanne, Switzerland; ⁶Service d'Anatomie et Cytologie Pathologiques, Hôpital Haut-Lévêque, CHU de Bordeaux, France; ⁷Service d'Anatomie et Cytologie Pathologiques, CHU de Nantes, France; ⁸Service d'Anatomie et Cytologie Pathologiques, Hôpital Universitaire Necker - Enfants Malades, Assistance Publique - Hôpitaux de Paris (APHP), Paris, France; ⁹Département de Pathologie, Groupe Hospitalier Henri Mondor, AP-HP, Créteil, France; ¹⁰Département d'Hématologie et Immunologie Biologique, Groupe Hospitalier Henri Mondor, AP-HP, Créteil, France and ¹¹Service Hématologie Adultes, Hôpital Universitaire Necker - Enfants Malades, Assistance Publique - Hôpitaux de Paris (APHP), Paris, France

*FD and PR contributed equally as co-first authors.

#FJ, LdL and PG contributed equally as co-senior authors.

Haematologica 2020
Volume 105(6):1582-1592

Correspondence:

PHILIPPE GAULARD
philippe.gaulard@aphp.fr

PHILIPPE RUMINY
philippe.ruminy@chb.unicancer.fr

Received: May 9, 2019.

Accepted: September 2, 2019.

Pre-published: September 5, 2019.

doi:10.3324/haematol.2019.226647

Check the online version for the most updated information on this article, online supplements, and information on authorship & disclosures: www.haematologica.org/content/105/6/1582

©2020 Ferrata Storti Foundation

Material published in Haematologica is covered by copyright. All rights are reserved to the Ferrata Storti Foundation. Use of published material is allowed under the following terms and conditions:

<https://creativecommons.org/licenses/by-nc/4.0/legalcode>.

Copies of published material are allowed for personal or internal use. Sharing published material for non-commercial purposes is subject to the following conditions:

<https://creativecommons.org/licenses/by-nc/4.0/legalcode>,

sect. 3. Reproducing and sharing published material for commercial purposes is not allowed without permission in writing from the publisher.



ABSTRACT

Peripheral T-cell lymphoma comprises a heterogeneous group of mature non-Hodgkin lymphomas. Their diagnosis is challenging, with up to 30% of cases remaining unclassifiable and referred to as “not otherwise specified”. We developed a reverse transcriptase-multiplex ligation-dependent probe amplification gene expression profiling assay to differentiate the main T-cell lymphoma entities and to study the heterogeneity of the “not specified” category. The test evaluates the expression of 20 genes, including 17 markers relevant to T-cell immunology and lymphoma biopathology, one Epstein-Barr virus-related transcript, and variants of *RHOA* (G17V) and *IDH2* (R172K/T). By unsupervised hierarchical clustering, our assay accurately identified 21 of 21 ALK-positive anaplastic large cell lymphomas, 16 of 16 extranodal natural killer (NK)/T-cell lymphomas, 6 of 6 hepatosplenic T-cell lymphomas, and 13 of 13 adult T-cell leukemia/lymphomas. ALK-negative anaplastic lymphomas (n=34) segregated into one cytotoxic cluster (n=10) and one non-cytotoxic cluster expressing Th2 markers (n=24) and enriched in *DUSP22*-rearranged cases. The 63 T_{HH}-derived lymphomas divided into two subgroups according to a predominant T_{HH} (n=50) or an enrichment in Th2 (n=13) signatures. We next developed a support vector machine predictor which attributed a molecular class to 27 of 77 not specified T-cell lymphomas: 17 T_{HH}, five cytotoxic ALK-negative anaplastic and five NK/T-cell lymphomas. Among the remaining cases, we identified two cell-of-origin subgroups corresponding to cytotoxic/Th1 (n=19) and Th2 (n=24) signatures. A reproducibility test on 40 cases yielded a 90% concordance between three independent laboratories. This study demonstrates the applicability of a simple gene expression assay for the classification of peripheral T-cell lymphomas. Its applicability to routinely-fixed samples makes it an attractive adjunct in diagnostic practice.

Introduction

Peripheral T-cell lymphomas (PTCL) are a diverse group of neoplasms representing 10-15% of all lymphomas worldwide, with large geographic variation. According to the 2017 revision of the World Health Organization (WHO) classification of lymphoid neoplasms, PTCL comprise up to 30 entities derived from various subsets of mature T or natural killer (NK) cells.¹ The heterogeneity and rarity of these tumors, combined with their complex immunophenotypic profile and partially overlapping features across different entities, make their diagnosis particularly challenging. In addition, there is a high variability in the diagnostic workup among pathologists, which may account for relatively poor reproducibility of the diagnoses.²⁻⁴ Although most cases can be ascribed to specific disease entities, approximately one-third of PTCL not fulfilling the criteria for other entities remain unclassifiable and are categorized “by default” as PTCL-not otherwise specified (NOS).

The classification of PTCL has undergone major changes over the past years with the incorporation of much new information on their genetic background and taking into account the notion that PTCL arise from discrete subsets of normal T cells. In recent years, the description of the signature and mutational landscape of PTCL has generated novel molecular biomarkers to refine the diagnostic criteria for some entities. Notably, the expression of T_H markers and the presence of genetic lesions associated with angio-immunoblastic T-cell lymphoma (AITL) (such as *RHOA*, *TET2*, *DNMT3A*, and *IDH2* mutations), found in a significant proportion of PTCL-NOS,⁵⁻¹⁰ led to the reclassification of these as “nodal PTCL with a T_H phenotype” (T_H-PTCL) in the revised WHO classification.¹ Among anaplastic large cell lymphoma (ALCL), the identification of recurrent rearrangements of the *ALK* gene led to ALK-positive ALCL being referred to as a definitive separate entity (ALCL ALK⁺), and to reconsider ALCL without ALK rearrangement as a distinct but genetically heterogeneous group comprising subtypes characterized by alterations of the *DUSP22/IRF4* or *TP63* genes with distinct clinical, pathological and biological features.¹¹ Among the remaining PTCL-NOS category, two molecular subgroups defined by the expression of the *TBX21* and *GATA3* transcription factors have been proposed,^{12,13} with a worse prognosis suggested for *GATA3*-positive cases.¹³⁻¹⁶ In daily diagnostic practice, however, high-throughput technologies are difficult to integrate. Moreover, the immunohistochemical surrogates are not fully validated and require an increasingly large panel of antibodies, and their evaluation may be problematic or present limitations.^{3,17}

Here, we designed a simple targeted mRNA expression profiling assay based on reverse transcriptase-multiplex ligation-dependent probe amplification (RT-MLPA), using a panel of molecular markers relevant to the characterization of PTCL. We first assessed the accuracy of this assay in the classification of PTCL entities other than PTCL-NOS, and then used the assay to study the heterogeneity of PTCL-NOS. Our findings support this RT-MLPA assay as a robust and useful tool, suitable for the routine classification of PTCL and, therefore, promoting an optimal clinical management of PTCL patients.

Methods

Patients and tumor samples

A series of 270 lymphoma samples were selected within the framework of the multicentric T-cell lymphoma consortium (TENOMIC) of the Lymphoma Study Association (LYSA). All cases had been reviewed by at least two expert hematopathologists, according to the criteria of the recently up-dated WHO classification.¹ The series was enriched in nodal T_H-PTCL (T_H-PTCL) defined by the expression of at least two TFH markers among *CD10*, *BCL6*, *CXCL13*, *PD1*, *ICOS* and in PTCL-NOS defined as a diagnosis of exclusion of any well-defined entity. The design of the study is summarized in *Online Supplementary Figure S1*. Briefly, a classification cohort (n=230) was used to train a support vector machine (SVM) classifier and a diagnostic cohort (n=40) was used to evaluate its inter-laboratory reproducibility on formalin-fixed paraffin-embedded (FFPE) samples. The study was approved by the local ethics committee (CPP Ile de France IX 08-009).

RT-MLPA assay gene expression profiling

RNA extracted from frozen and/or FFPE tumor samples was applied to RT-MLPA, as described¹⁸ (*Online Supplementary Methods*). Briefly, this targeted multiplex assay consists of the hybridization and ligation of specific probes on cDNA, followed by PCR amplification. We designed 41 probes (Eurofins MWG Operon, Ebersberg, Germany) targeting 20 genes, selected for their relevance to PTCL classification (Table 1). RT-MLPA results were compared to Affymetrix HG-U133-plus-2.0 gene expression data in 72 previously reported cases.^{18,19}

Bioinformatic analysis

A web interface was developed for the complete analysis of the RT-MLPA results (<https://bioinfo.calym.org/RTMLPA>). An SVM was developed to classify PTCL samples: two-thirds of the 184 PTCL of the classification cohort, which clustered in defined molecular branches according to the clustering (n=230), were randomly selected to train the classifier, which was validated in the remaining one-third of cases. A bootstrap resampling process was used to build 100 independent training and validation series. A definitive SVM predictor was thus developed using the 184 cases. This supervised learning model assigns a class to every PTCL sample. Therefore, we integrated the distance to the centroid of the predicted class for each sample to avoid classifying distant samples into the same group. The analytical process is detailed in the *Online Supplementary Methods*.

Histopathology and molecular validation

RT-MLPA signatures were correlated to immunochemical data, including expression of *GATA3* and *TBX21*. The cut off for positive immunohistochemical staining was 10% of presumed neoplastic cells (*Online Supplementary Methods*). Fluorescence *in situ* hybridization (FISH) for *DUSP22/IRF4* rearrangement was performed in 20 ALCL. Mutations were validated using polymerase chain reaction (PCR) allele-specific and/or targeted deep sequencing.^{20,21} Technical details are presented in the *Online Supplementary Methods*.

Data analysis

Affymetrix and RT-MLPA gene expression values were correlated using Spearman's correlation test. Correlations between immunohistochemical results and RT-MLPA gene expression values were evaluated using Wilcoxon's rank-sum test. Unsupervised hierarchical analysis was performed using the Ward method.

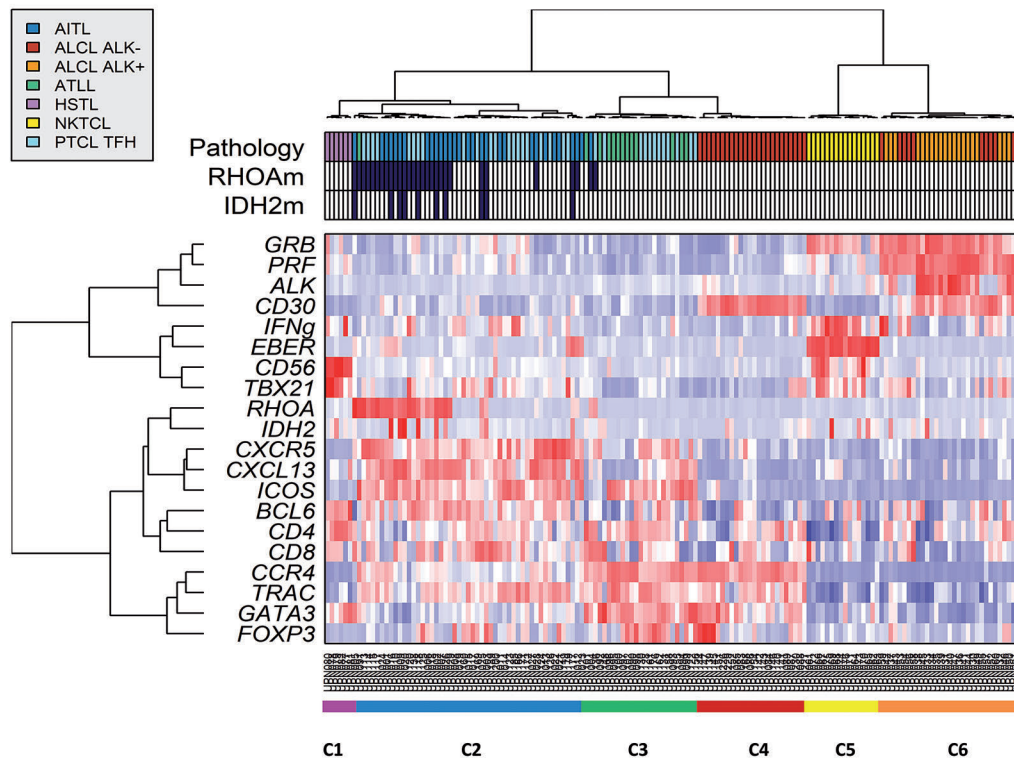


Figure 1. Unsupervised hierarchical clustering of peripheral T-cell lymphoma (PTCL) entities other than PTCL-not otherwise specified (NOS) using reverse transcriptase-multiplex ligation-dependent probe amplification (RT-MLPA) (n=153). The assay was used to classify angioimmunoblastic T-cell lymphomas (AITL) (n=30), PTCL with T-follicular helper phenotype (TFH) (n=33), anaplastic large cell lymphomas (ALCL) (n=55), adult T-cell lymphomas (ATLL) (n=13), hepatosplenic T-cell lymphoma (HSTL) (n=6), and natural killer (NK)-TCL (n=16). Differential gene expression is depicted according to a red (positive) to blue (negative) color scale, and concordance with histopathological diagnosis (Pathology). Two main branches were observed: the left branch divided in 6 HTSL (C1), 50 T_{FH}-PTCL/AITL (C2), 12 ATLL with 13 TFH-PTCL (C3), and 24 ALK-negative ALCL (C4), and the right branch contained two clusters of 16 NKTCL (C5) and 31 cytotoxic ALCL (C6).

Overall and progression-free survival analysis was performed using the Kaplan-Meier method and the log-rank test. The Mann-Whitney test was used to analyze continuous data and the Fisher exact test to analyze categorical data.

Results

Design and validation of the RT-MLPA assay

The study design is presented in *Online Supplementary Figure S1*. The gene set and sequences of the RT-MLPA probes are shown in *Table 1* and *Online Supplementary Table S1*, respectively. The panel was designed to include several genes encoding immunohistochemical or genetic markers routinely used for the diagnosis of PTCL and genes of interest selected from previous transcriptomic and genomic studies.^{9,10,12,13,18} It includes genes related to the major CD4 and CD8 T-cell subsets, genes defining the main subsets of Th cells [T_{FH} (CXCL13, CXCR5, ICOS, BCL6), Th1 (TBX21, IFN γ), Th2 (GATA3, CCR4), and Treg (FOXP3)], as well as genes encoding cytotoxic molecules (PRF, GZMB). CD30 and ALK were chosen to identify ALCL and CD56 and EBER1 (Epstein-Barr virus encoding small RNA) were selected to identify hepatosplenic T-cell lymphoma (HSTL) and NKTCL. We also included the *RHOAG17V* and *IDH2R172K/T* variants, as the most prevalent hotspot mutations of T_{FH}-derived PTCL.

We obtained RT-MLPA profiles for all 230 PTCL of the classification cohort. Representative RT-MLPA profiles for each entity are shown in *Online Supplementary Figure S2*.

Table 1. Gene panel designed for the reverse transcriptase-multiplex ligation-dependent probe amplification assay.

Family genes and other targets	Genes	Detection method in the routine practice
Main T-cell subsets	<i>CD4</i>	Immunohistochemistry
	<i>CD8</i>	Immunohistochemistry
	<i>TCRα</i>	Not applicable
T _{FH}	<i>CXCL13</i>	Immunohistochemistry
	<i>CXCR5</i>	Not applicable
	<i>BCL6</i>	Immunohistochemistry
	<i>ICOS</i>	Immunohistochemistry
Th1	<i>TBX21</i>	Immunohistochemistry
	<i>IFN</i>	Not applicable
Th2	<i>GATA3</i>	Immunohistochemistry
	<i>CCR4</i>	Not applicable
Treg	<i>FOXP3</i>	Immunohistochemistry
NK-associated	<i>CD56</i>	Immunohistochemistry and cytotoxic
	<i>PRF</i>	Immunohistochemistry
	<i>GZB</i>	Immunohistochemistry
Activation	<i>CD30</i>	Immunohistochemistry
Virus	<i>EBER</i>	<i>In situ</i> hybridization
Mutations	<i>RHOAm G17V</i>	AS-PCR, other sequencing methods
	<i>IDH2m R172K/T</i>	AS-PCR, other sequencing methods, immunohistochemistry
Other	<i>ALK</i>	Immunohistochemistry, FISH

AS-PCR: allele-specific polymerase chain reaction; NK: natural killer; FISH: fluorescence *in situ* hybridization.

T_{FH} -PTCL profiles were characterized by the expression of a combination of T_{FH} genes (*CXCL13*, *CXCR5*, *ICOS*, and *BCL6*), together with frequent *RHOA* and/or *IDH2* variants. ATLL expressed Th2 markers (*GATA3* and *CCR4*) and *ICOS*, with variable levels of *FOXP3*. NKTCL showed high expression of *EBER1* and *GZMB*, as well as Th1 markers (*TBX21* and *IFN γ*). HSTL expressed *CD56*, *GATA3*, *TBX21*, and *BCL6*. ALK-positive ALCL expressed *ALK*, *CD30*, *PRF*, and *GZMB*. ALK-negative ALCL comprised two distinct profiles, with or without expression of *PRF* and *GZMB*. The non-cytotoxic ALCL showed high expression of *CD30* and Th2 markers (*GATA3* and *CCR4*) but not *PRF* or *GZMB*. Unexpectedly, RT-MLPA identified *ALK* expression in a case of ALCL initially considered ALK-negative (based on negative immunostaining with the ALK1 clone), leading to reclassification to ALK-positive ALCL. This was further confirmed by IHC using an alternative antibody (D5F3 clone) (Online Supplementary Figure S3).

Paired RT-MLPA profiles and Affymetrix gene expression data available in 72 cases (23 AITL and 49 PTCL-NOS) were compared.^{18,19} There were significant correlations for each evaluable gene (*TNFRSF8/CD30*, *PRF*, *GZMB*, *GATA3*, *CXCL13*, *ICOS*, *CD8*, *BCL6*, *CD4*,

FOXP3, *CCR4*, *CXCR5*, and *TBX21*) (Online Supplementary Figure S4). RT-MLPA and immunohistochemical data scores also showed significant correlations for the 12 evaluable markers (Online Supplementary Figure S5). There was also a good correlation with the *EBER in situ* hybridization results, showing the capacity of the assay to correctly detect EBV infection. RT-MLPA profiles performed in duplicates in 20 PTCL on RNA extracted from both frozen and FFPE samples, showed a strong correlation ($\rho > 0.7$, Spearman correlation test) (Online Supplementary Figure S6).

RT-MLPA identified 33 of 33 *RHOA*G17V and 9 of 10 *IDH2* R172K/T mutations, detected by either AS-quantitative PCR and/or next-generation sequencing (NGS) studies. The only RT-MLPA failure corresponded to an AITL with an *IDH2*R172K mutant with a 2.8% allele frequency, which was only detected by NGS (Online Supplementary Table S2).

Unsupervised analysis highlights heterogeneity among ALK-negative ALCL and T_{FH} -PTCL

Given the expected heterogeneity of PTCL-NOS, we first restricted our analyses to specified PTCL entities (not taking into account PTCL-NOS). Unsupervised hierarchi-

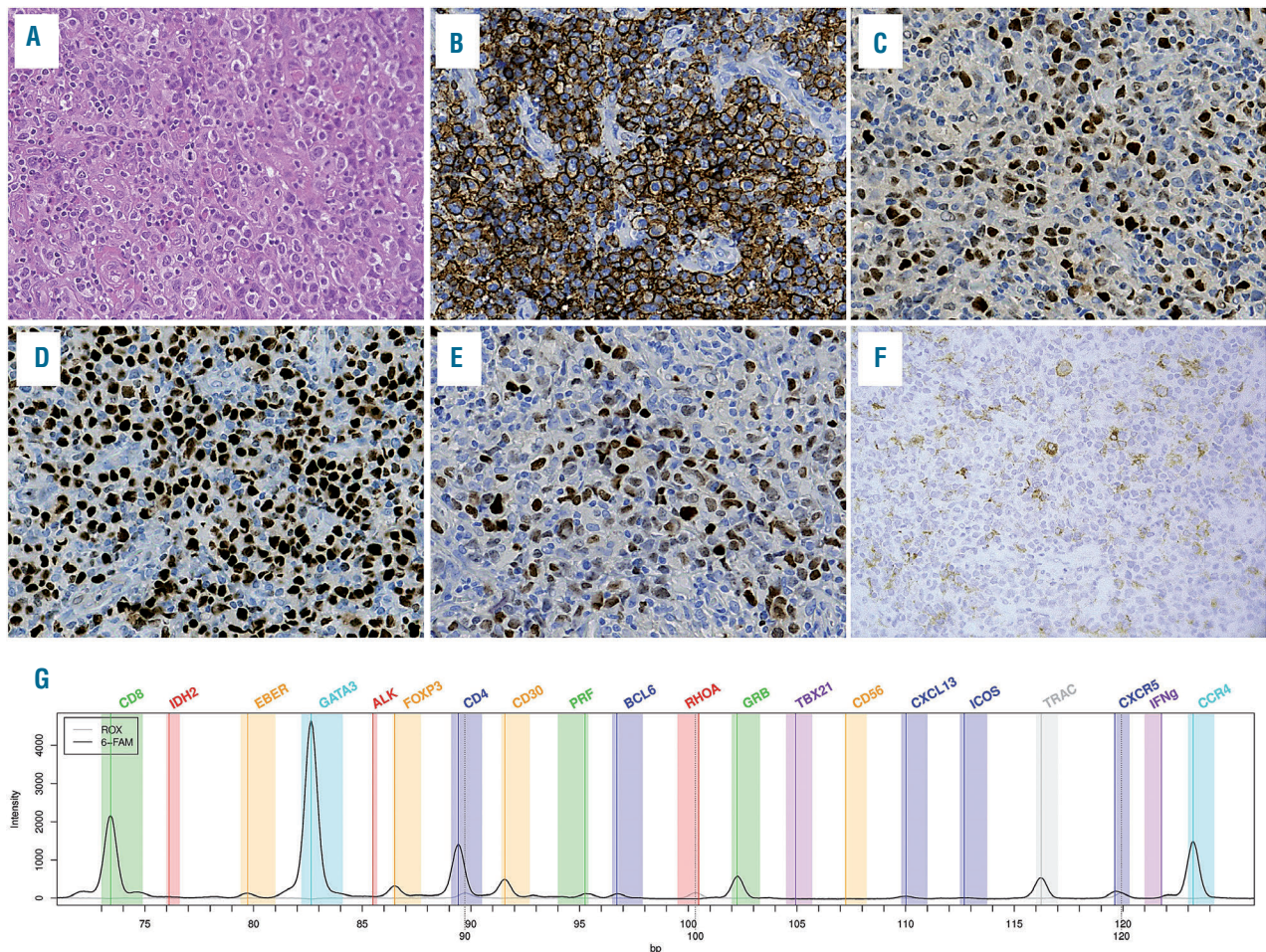


Figure 2. Nodal peripheral T-cell lymphomas (PTCL) with a double T_{FH} /Th2 phenotype and a molecular Th2 signature. (A) Diffuse proliferation of large pleomorphic cells; this case would be classified as T_{FH} PTCL according to the World Health Organization 2017, based on the expression of 2 T_{FH} markers, i.e. PD1 (B) and BCL6 (C), but disclosed strong nuclear staining for GATA3 in virtually all tumor cells (D) and, although less uniform, FOXP3 (E). Few tumor cells also expressed CD30 (F). Reverse transcriptase-multiplex ligation-dependent probe amplification (RT-MLPA) profile showed a Th2 signature and classified in the Th2 class by the support vector machine (SVM).

cal clustering performed on 153 such cases (30 AITL, 33 T_{HH}-PTCL, 16 NKTCL, 13 ATLL, 6 HSTL, 21 ALK-positive ALCL, and 34 ALK-negative ALCL) identified two main branches separating cytotoxic and non-cytotoxic entities (Figure 1).

The cytotoxic branch is divided into two clusters, one very homogeneous cluster (C5) comprising the 16 NKTCL, and a second cluster (C6) composed of 31 cytotoxic ALCL (21 ALK-positive and 10 ALK-negative). The other branch is divided into four clusters (C1-4). The C1 cluster contained the six HSTL. The 63 PTCL with a T_{HH} phenotype (AITL and T_{HH}-PTCL) distributed along the two clusters C2 and C3. The C2 cluster comprised a major group of AITL/T_{HH}-PTCL characterized by a T_{HH} signature (C2, n=50). In addition to 12 ATLL, 13 T_{HH}-PTCL and one AITL in the C3 cluster showed an enrichment in T_{HH} and Th2 markers. Interestingly, *RHOA* mutations were identified in 26 of 50 (52%) and 2 of 13 (15%) of the C2 and C3 clusters, respectively ($P=0.027$). By immunohistochemistry, these T_{HH}-PTCL in the C3 cluster showed expression of GATA3 (in more than 50% of tumor cells) in 9 of 12 (75%) contributive cases (Figure 2). The C4 cluster contained 24 ALK-negative non-cytotoxic ALCL with Th2 signature, with 8 of 16 contributive cases showing *DUSP22* rearrangement by FISH.

PTCL-NOS distribute among distinct clusters using unsupervised clustering

When applied to all 230 PTCL samples (including 77 PTCL-NOS), unsupervised clustering showed that the majority of PTCL-NOS (n=48 of 77, 62.3%) clustered within four of the six previous clusters as they showed gene signatures in common with molecular T_{HH}-PTCL (C2, n=6), T_{HH}/Th2 PTCL (C3, n=19), NKTCL (C5, n=5), and cytotoxic ALCL (C6, n=18) (Figure 3). Despite a variable expression of CD30 by immunohistochemistry, 18 PTCL-NOS distributed within the cluster of cytotoxic ALCL based on the expression of cytotoxic markers plus *TBX21* and *IFN*, consistent with a possible Th1 origin. Accordingly, 8 of 12 of these cases tested for *TBX21* by immunohistochemistry were positive. This molecular subgroup is further referred to as “cytotoxic/Th1 PTCL” according to its signature. In addition, 19 other PTCL-NOS cases, all with negative HTLV-1 serologies, clustered with ATLL, based on an enrichment in Th2 molecules GATA3 and *CCR4*, and are referred to as molecular “Th2 PTCL”. Finally, 29 PTCL-NOS did not cluster within any of the defined branches, and segregated with 19 other cases (4 AITL, 12 T_{HH}-PTCL, 1 ATLL).

Support vector machine classifier accurately classifies specified PTCL and identifies subgroups within PTCL-NOS

We next built a support vector machine (SVM) model to assign each case to a class based on the RT-MLPA data (Figure 4A). One hundred and eighty-four PTCL corresponding to the molecular groups defined according to the latter clustering (Figure 3) were used for the construction of the model and to define the molecular classes: 45 T_{HH}-PTCL/AITL, 21 NKTCL, 42 Th2 PTCL-NOS/ATLL, 50 cytotoxic-ALCL, 20 non-cytotoxic ALCL, and the six HSTL. The 46 PTCL which did not cluster within these six defined branches were not considered to develop the classifier. The SVM algorithm accurately assigned 140 of 153 specified PTCL to the correct categories: 16 of 16

Table 2. Clinical, pathological and molecular features of the two subgroups of TFH-peripheral T-cell lymphomas (PTCL).

	TFH signature n=50	TFH and Th2 signatures n=13	P
Clinical data			
Age median (range)	64.4 (54-74.6)	67.4 (56.7-74.7)	0.79
IPI>=3	71.8% (28/39)	75% (9/12)	1
PIT>=2	71% (27/38)	63.6% (7/11)	0.72
Extranodal site>=2	50% (22/44)	58.3% (7/12)	0.75
Stage>=3	100% (44/44)	91.7% (11/12)	0.21
PS>=2	40% (16/40)	8.3% (1/12)	0.076
LDH>1N	64% (25/39)	50% (6/12)	0.5
B signs	70.7% (29/41)	45.5% (5/11)	0.16
Hypergammaglobulinemia	37.5% (12/32)	12.5% (1/8)	0.24
Coombs	46% (12/26)	0% (0/2)	0.49
Anemia	61.5% (24/39)	41.6% (5/12)	0.32
Cutaneous rash	23.8% (10/42)	33% (4/12)	0.48
BM	48.8% (21/43)	33.3% (4/12)	0.51
Complete response	50% (20/40)	41.7% (5/12)	0.75
OS median (range)	22 (5.5-77)	30.5 (6-50.5)	0.91
PFS median (range)	10 (3-39)	12 (5.5-38)	0.42
Pathological data			
Clear cells	65.2% (30/46)	36% (4/11)	0.1
B blasts	90% (44/49)	66% (8/12)	0.07
EBV positivity	70.2% (33/47)	58.3% (7/12)	0.5
EBV extent >5 large blast-cells/high power field	29.5% (13/44)	0% (0/12)	0.049
Molecular data			
TET2 mutation	60.6% (20/33)	14.3% (1/7)	0.039
DNMT3A mutation	25% (8/32)	0% (0/6)	0.31
RHOA mutation	52% (26/50)	15.4% (2/13)	0.027
IDH2 mutation	20% (10/50)	0% (0/13)	0.1

IPI: International Prognostic Index; EBV: Epstein-Barr virus; PIT: Prognostic Index for PTCL-not otherwise specified; PS: Performance Status; LDH: lactate dehydrogenase; BM: bone marrow; OS: overall survival; PFS: progression-free survival.

NKTCL, 13 of 13 ATLL, 6 of 6 HSTL, 31 of 31 cytotoxic ALCL, 24 of 24 non-cytotoxic ALK-negative ALCL cases, and 50 of 63 AITL/T_{HH}-PTCL. Interestingly, 11 T_{HH}-PTCL without *RHOA* mutation were classified as molecular Th2 PTCL, one as molecular cytotoxic/Th1, and one AITL was distant from the barycenter of the T_{HH}/AITL class and not classified. Of the 77 remaining PTCL-NOS, 70 (91%) were classified by the SVM as T_{HH}/AITL (C2, n=17), cytotoxic/Th1 PTCL (C6, n=19), ALK-negative ALCL (C6, n=5), NKTCL (C5, n=5), while 24 cases were molecularly designated Th2 PTCL (C3). Finally, seven cases, which were distant to the barycenter of their predicted SVM class (2 Th2, 3 T_{HH}/AITL, 2 cytotoxic/Th1), could not be attributed a molecular class by the SVM. Figure 4B illustrates the subgroups of PTCL-NOS as evidenced in the principal component analysis (PCA). A correlation of the SVM class with the histopathological data of the 77 PTCL-NOS is presented in *Online Supplementary Figure S7*.

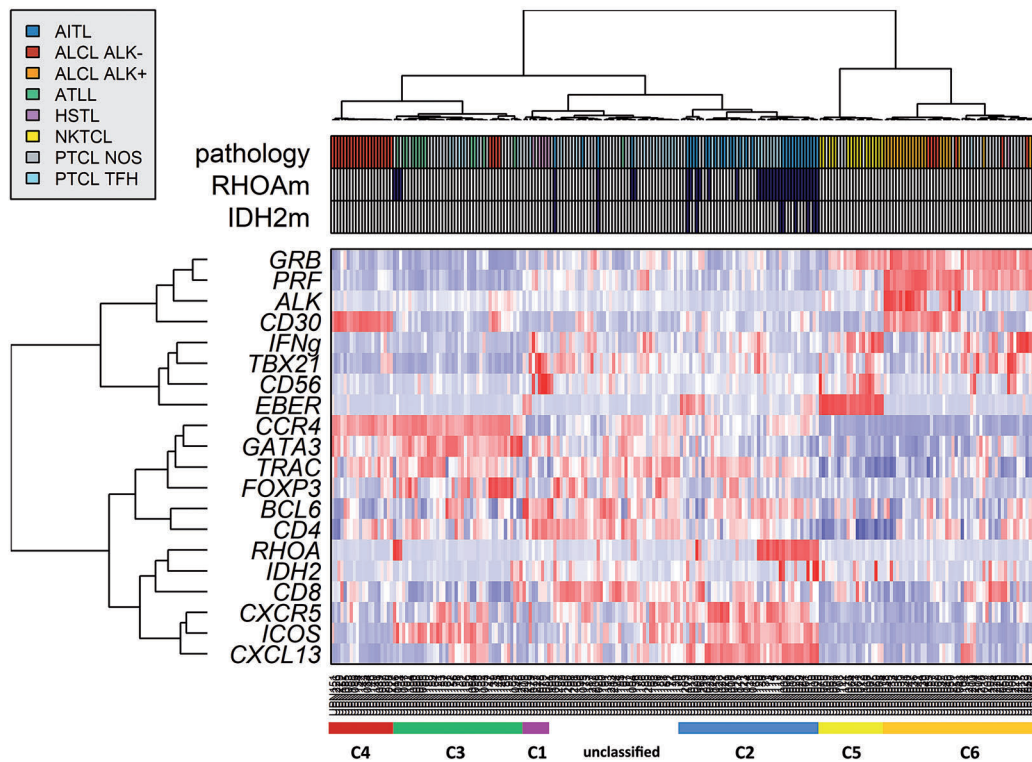


Figure 3. Unsupervised hierarchical clustering of peripheral T-cell lymphomas (PTCL) including PTCL-not otherwise specified (NOS) (n=230). PTCL-NOS distributed among six defined clusters represented by colored bars under the heat map (from left to right): C1 (red), C2 (green), C3 hepatosplenic T-cell lymphoma (HSTL) (purple), C4 angioimmunoblastic T-cell lymphomas AITL/TFH-derived PTCL (blue and light blue), C5 natural killer (NK)-TCL (yellow), and “cytotoxic anaplastic large cell lymphomas (ALCL)” (orange and red). The 77 PTCL-NOS (gray in Pathology) are distributed among the subgroups.

Clinico-pathological correlations of the support vector machine classes

Survival data were available for 88.7% (204 of 230) of the patients. Median duration of follow up was 122 months [interquartile range (IQR) = 80.5-173]. Among the 132 of 175 patients with follow-up data available who received anthracyclin-based chemotherapy, the median overall survival (OS) and progression-free survival (PFS) were 15 months (IQR=6-51.5) and nine months (IQR=3-36), respectively. The outcome of PTCL patients was poor (5-year OS=27%), except for those with ALK-positive ALCL (5-year OS=70%) (Figure 5A).

Considering the two clusters observed among PTCL with a TFH phenotype (Figure 1), we failed to demonstrate any significant clinical difference (Table 2). Interestingly, *RHOAG17V* mutations were found in 52% and 15.4% respectively among the C2 (TFH) and C3 (Th2) clusters ($P=0.02$). *TET2* mutations were observed in 60.6% and 14.3% of the C2 and C3 clusters ($P=0.039$). *DNMT3A* and *IDH2* mutations were found respectively in 25% and 20% of the C2 cluster but none within the C3 (P =not significant, n.s).

Among ALCL, non-cytotoxic ALK-negative ALCL were characterized by the expression of Th2 mRNA (*GATA3* and *CCR4*) and *GATA3* expression by immunohistochemistry in 11 of 12 informative cases. Non-cytotoxic and cytotoxic ALK-negative ALCL disclosed similar PFS and OS (Figure 5A). However, despite similar main clinical characteristics (Online Supplementary Table S3), patients with a *DUSP22*-rearrangement (n=8) tended to

have a favorable outcome (5-year OS=62.5%) close to that of ALK-positive ALCL patients (70% 5-year OS), compared to the very poor prognosis of patients without *DUSP22* rearrangement (n=8) (5-year OS=12.5%; $P=0.07$) (Figure 5B). No *TP63* rearrangement was detected in this series.

Finally, within the limitations of size of the current series, among PTCL-NOS, there was no significant difference in patient's outcome with respect to their “Th1/cytotoxic” or “Th2” molecular signatures (Figure 5C) or immunohistochemical profiles (Figure 5D).

Reproducibility of the RT-MLPA assay among three centers in routine practice

We evaluated the reproducibility of the RT-MLPA assay in the diagnostic setting by testing 40 FFPE PTCL samples in three independent centers. A concordance in the diagnostic class proposed by the classifier was observed between the three centers for 36 (90%) samples (Table 3), with a strong correlation between the RT-MLPA values for each gene (Online Supplementary Table S4). Among the 36 concordant samples, the SVM class was in accordance with the pathological diagnosis for 32 cases (89%). The four discrepancies consisted of two tumor-cell rich AITL assigned to the Th2/ATLL-like group, as previously observed in the classification cohort, one AITL with a prominent cytotoxic T-cell environment assigned to the cytotoxic/Th1-like group, and one ATLL with a double CD4/CD8 phenotype that was not classified.

Table 3. Reproducibility of the reverse transcriptase-multiplex ligation-dependent probe amplification (RT-MLPA) assay among three laboratories (Center 1, Center 2, and Center 3).

	Pathology	RT-MLPA Classification			RHOAG17V/ IDH2 R172 status by RTMLPA (m=mutated, wt= wild-type)	Mutations detected by targeted NGS
		Center 1	Center 2	Center 3		
Concordant samples						
Case1	AITL	AITL	AITL	AITL	m/wt	ND
Case2	AITL	AITL	AITL	AITL	m/wt	RHOA, IDH2 (R712S), TET2, DNMT3a
Case3	AITL	AITL	AITL	AITL	wt/wt	ND
Case4	AITL	AITL	AITL	AITL	m/wt	RHOA, IDH2 (R712S), TET2, DNMT3a
Case5	AITL	AITL	AITL	AITL	wt/wt	ND
Case6	AITL	AITL*	AITL*	AITL*	m/wt	RHOA, IDH2 (R712T), TET2
Case7	AITL	AITL*	AITL*	AITL*	wt/wt	ND
Case8	AITL [†]	TH2	TH2	TH2	wt/wt	IDH2(R172S), TET2, CD28
Case9	AITL [†]	TH2	TH2	TH2	wt/wt	TET2, FYN
Case10	AITL**	Cytotoxic/Th1	Cytotoxic/Th1	Cytotoxic/Th1	m/wt	RHOA, TET2
Case11	AITL**	Cytotoxic/Th1	Cytotoxic/Th1	AITL	m/wt	ND
Case12	AITL**	AITL*	TH2	AITL	m/wt	ND
Case13	AITL	Cytotoxic/Th1*	Cytotoxic/Th1	Cytotoxic/Th1	wt/wt	ND
Case14	ALCL ALK-	ALCL ALK-	ALCL ALK-	ALCL ALK-	wt/wt	ND
Case15	ALCL ALK-	ALCL ALK-	ALCL ALK-	ALCL ALK-	wt/wt	ND
Case16	ALCL ALK-	ALCL ALK-	ALCL ALK-	ALCL ALK-	wt/wt	ND
Case17	ALCL ALK-	CD30TH2*	CD30TH2*	CD30TH2*	wt/wt	TET2, TP53
Case18	ALCL ALK+	ALCL ALK+	ALCL ALK+	ALCL ALK+	wt/wt	ND
Case19	ALCL ALK+	ALCL ALK+	ALCL ALK+	ALCL ALK+	wt/wt	ND
Case20	ALCL ALK+	ALCL ALK+	ALCL ALK+	ALCL ALK+	wt/wt	ND
Case21	ALCL ALK+	ALCL ALK+	ALCL ALK+	ALCL ALK+	wt/wt	ND
Case22	ALCL ALK+	ALCL ALK+	ALCL ALK+	ALCL ALK+	wt/wt	ND
Case23	ALCL ALK+	ALCL ALK+	ALCL ALK+	ALCL ALK+	wt/wt	ND
Case24	ATLL	TH2	TH2	TH2	wt/wt	ND
Case25	ATLL	TH2	TH2	TH2	wt/wt	ND
Case26	ATLL	TH2	TH2	TH2	wt/wt	ND
Case27	ATLL	TH2	TH2	TH2	wt/wt	ND
Case28	ATLL	unclassified	unclassified	unclassified	wt/wt	ND
Case29	ATLL**	Failure	Failure	TH2	wt/wt	ND
Case30	NKTCL	NKTCL	NKTCL	NKTCL	wt/wt	ND
Case31	NKTCL	NKTCL	NKTCL	NKTCL	wt/wt	ND
Case32	NKTCL	NKTCL	NKTCL	NKTCL	wt/wt	ND
Case33	NKTCL	NKTCL	NKTCL	NKTCL	wt/wt	ND
Case34	NKTCL	NKTCL	NKTCL	NKTCL	wt/wt	ND
Case35	NKTCL	NKTCL	NKTCL	NKTCL	wt/wt	ND
Case36	NKTCL	NKTCL	NKTCL	NKTCL	wt/wt	ND
Case37	NKTCL	NKTCL	NKTCL	NKTCL	wt/wt	ND
Case38	NKTCL	NKTCL	NKTCL	NKTCL	wt/wt	ND
Case39	PTCL-NOS	Cytotoxic/Th1	Cytotoxic/Th1	Cytotoxic/Th1	wt/wt	ND
Case40	PTCL-NOS (EBV+)	NKTCL	NKTCL	NKTCL	wt/wt	ND

NGS: next-generation sequencing; m: mutated; wt: wild-type; ND: not determined. Evaluated on 40 formalin-fixed paraffin-embedded (FFPE) samples: six ALK-positive anaplastic large cell lymphomas (ALCL-ALK⁺), four ALCL ALK⁻, 13 angioimmunoblastic T-cell lymphomas (AITL), nine natural killer (NK)/T-cell lymphomas (NKTCL), six adult T-cell lymphomas (ATLL), and two peripheral T-cell lymphomas not otherwise specified (PTCL-NOS). [†]AITL tumor cell rich. *Distant of the samples of the predicted support vector machine (SVM) class. [‡]Among the four discrepant samples, the SVM resulted in concordance between two centers for two cases, one case showed discordant results between the three centers, and one ATLL sample had no interpretable profile in two centers whereas the other determined a Th2 profile concordant with the diagnosis.

Discussion

The classification of PTCL is often challenging and poorly reproducible, with a recent study showing a 31.5% rate of discrepancy between the referral and expert diagnoses,⁴ likely due to the complexity of these rare neoplasms and the wide range of practices among pathologists and laboratories.³ Hsi *et al.* pointed out the limited number of immunohistochemical markers assessed in routine prac-

tice, especially the T_H markers, resulting in a poor characterization of PTCL and a high frequency of PTCL-NOS diagnosed in the US.²² The ligation-dependent RT-PCR assay has been reported to be a simple and robust assay applicable to FFPE samples that can be used to classify DLBCL into GCB or ABC subtypes.^{23,24} Here, we expanded on this as RT-MLPA can contribute to classify the main specified categories of non-cutaneous PTCL in routine practice. This assay, which can be performed relatively

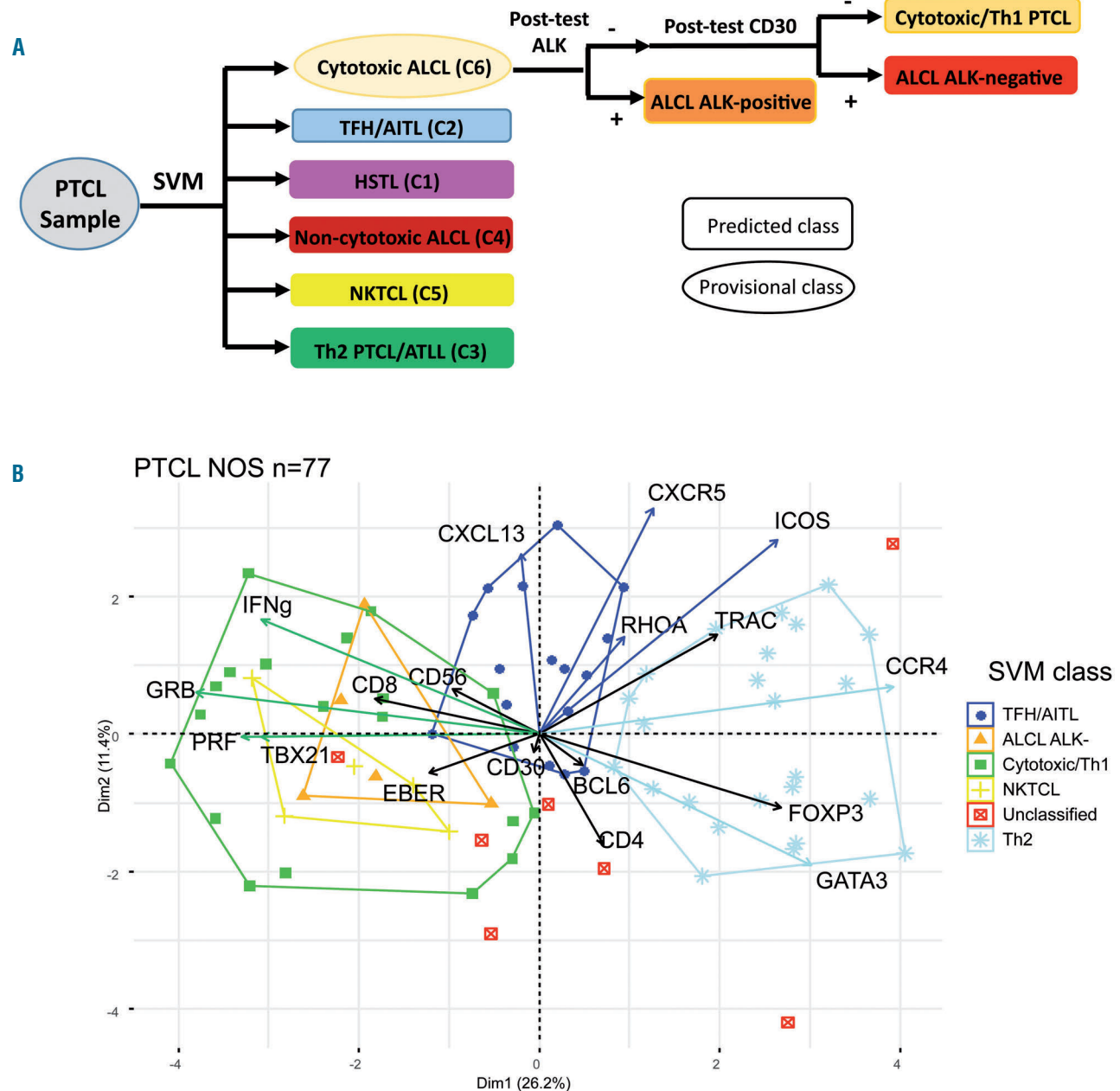


Figure 4. Bioinformatic model for the analysis of reverse transcriptase-multiplex ligation-dependent probe amplification (RT-MLPA) data. (A) The support vector machine (SVM) model attributes a predicted (rectangle) or provisional (oval) class for each peripheral T-cell lymphoma (PTCL) sample. Post-tests based on ALK and CD30 were designed to distinguish between the subgroups in the heterogeneous “cytotoxic/ALCL-like” category. (B) principal component analysis (PCA) plot of the SVM classification for PTCL-not otherwise specified (NOS) (n=77) showed three main molecular categories among: T_H/angiimmunoblastic T-cell lymphomas (AITL) (blue), Th2 (light blue), and cytotoxic/Th1 (green). The latter also comprised NKTCL-like (yellow) and anaplastic large cell lymphomas (ALCL)-like (orange) subgroups. Seven cases were unclassified (red).

quickly (48 hours), only requires equipment already in regular use, including a thermocycler and genetic fragment size analyzer. The profiles are publicly accessible and easy to interpret through a dedicated website. Finally, the assay is cost-effective (approximately \$5 per sample).²⁵ RT-MLPA is a useful tool in combination with pathological evaluation to characterize PTCL, especially when immunohistochemistry is flawed or incomplete. In addition to evaluating the expression of Th-differentiation antigens and markers suitable for immunohistochemistry, the current RT-MLPA assay also provides genetic information, such as *RHOA* and *IDH2* mutations, which are highly relevant for the diagnosis of PTCL of T_{H1} origin,¹⁹ even though the *RHOA* G17V mutation has also been reported in a small minority of ATLL,²⁵ as observed in one case of our series. The accurate classification of specified PTCL other than NOS entities in most cases corroborates the relevance of the designed gene panel. Altogether, although some markers in our RT-MLPA assay might not be useful in every PTCL case, this “one fits all” assay evaluates diag-

nostic markers covering the different PTCL entities in a systematic and cost-effective way.

In addition, the RT-MLPA assay highlighted the heterogeneity in the gene signature of ALK-negative ALCL and PTCL of T_{H1} origin, as defined in the up-dated WHO classification. We observed that a significant proportion of ALK-negative ALCL display a distinct signature, with expression of CD30 and Th2 genes, but no cytotoxic markers. These cases showed a dense and cohesive pattern of CD30-positive anaplastic large cells but, in contrast to common ALCL, only a few hallmark cells, an absence of EMA, and a frequently preserved T-cell program with most T-cell antigens being retained. Genetically, this group appeared heterogeneous but was enriched in cases of *DUSP22/IRF4* rearrangement (in 8 of 16 non-cytotoxic cases vs. in only 1 of 10 cytotoxic ALK- ALCL; $P=0.09$). Despite the absence of any significant morphological or immunophenotypic difference between cases with or without *DUSP22* rearrangement, we further hypothesize that *DUSP22* status is of clinical relevance with better sur-

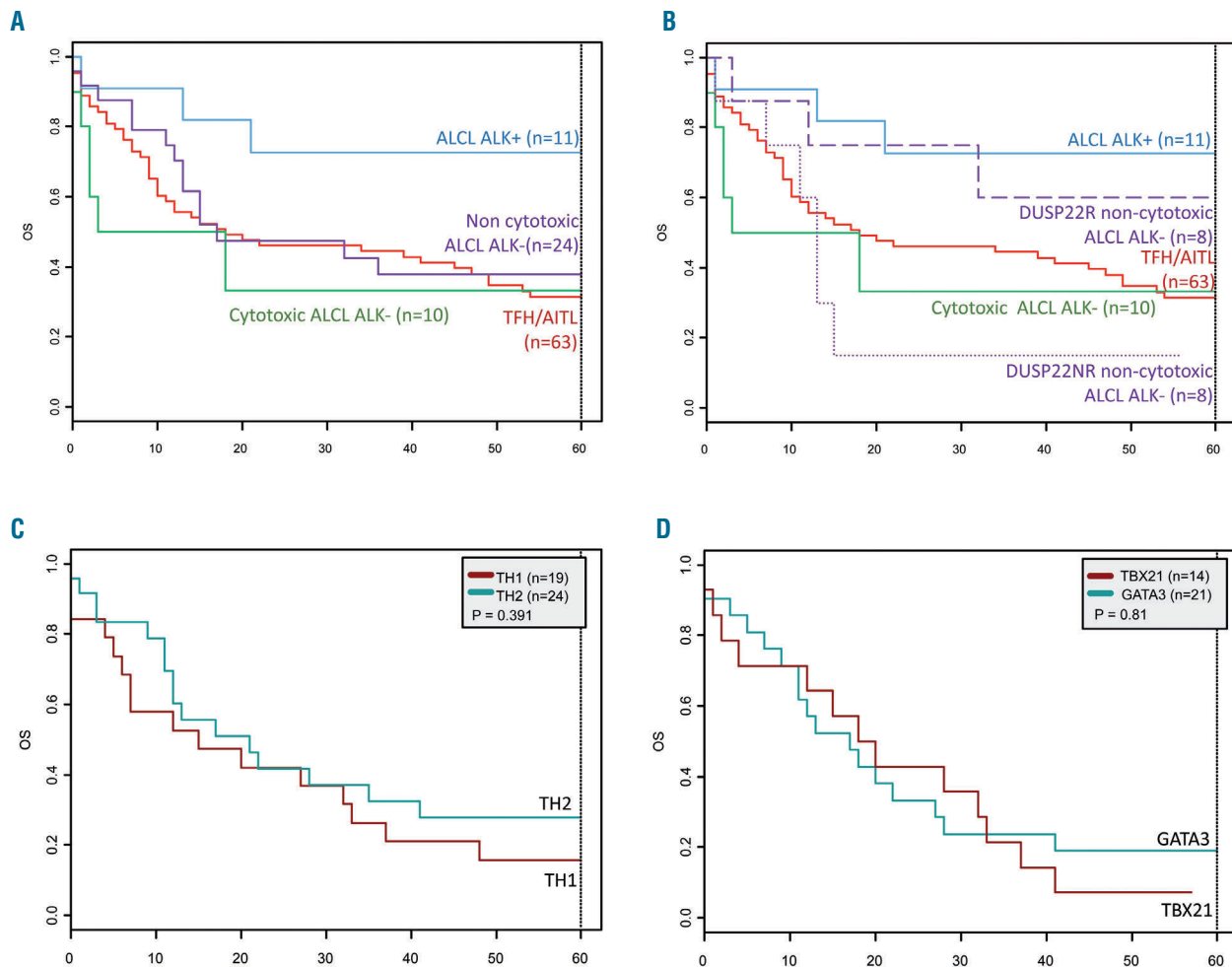


Figure 5. Kaplan-Meier survival analysis. (A) Overall survival of the 108 patients corresponding of the main reverse transcriptase-multiplex ligation-dependent probe amplification (RT-MLPA) subgroups: 11 anaplastic large cell lymphomas (ALCL) ALK⁺, 10 cytotoxic ALCL ALK⁻, 24 non-cytotoxic ALCL ALK⁻, and 63 T_{H1}/angiimmunoblastic T-cell lymphomas (AITL). (B) Overall survival of the main RT-MLPA subgroups according to the *DUSP22* status within the non-cytotoxic ALCL ALK⁻ category. (C) Overall survival of 43 peripheral T-cell lymphomas (PTCL)-not otherwise specified (NOS) according to the molecular status by RT-MLPA (19 cytotoxic/TH1 and 24 TH2). (D) Overall survival of 30 PTCL-NOS according to the immunohistochemistry data (19 GATA3, 11 TBX21).

vival of *DUSP22*-rearranged ALCL.^{11,26} In the absence of *TP63* rearrangement (*data not shown*), further investigations are needed to explore the genetic abnormalities in the *DUSP22*-non rearranged cases.

Within the umbrella category of nodal PTCL of T_H derivation, comprising AITL and a number of nodal PTCL previously classified under PTCL-NOS but expressing two or more T_H markers, our study interrogates the biological and clinical significance of two subgroups.¹ Indeed, whereas the majority (79%) were attributed to the T_H/AITL class by the molecular classifier, a minority disclosed, in addition to T_H markers, enrichment in Th2 genes. We confirmed a “mixed” T_H/Th2 immunophenotype for nine T_H-PTCL showing a Th2 signature by RT-MLPA. It has been reported that Th1 and Th2 cells can express TFH markers, and conversely that T_H cells have the capacity to express Th1 or Th2 cytokines.^{23,24} It has also been suggested that a subset of TFH cells may originate from Th2 lymphocytes in the presence of B cells and that T_H cells can acquire GATA3 expression.^{25,26} Overall, these data raise the question of Th cell plasticity and the specificity of the criteria required to assess T_H-derived PTCL. Indeed, the current definition of a T_H phenotype based on two or more T_H markers may have some limitations in certain cases,¹ and the integration of genetic markers, made possible by the RT-MLPA assay, may be helpful. In this respect, when comparing the “TFH/AITL” class to the other SVM classes, it appeared that, among the four TFH genes in our RT-MLPA panel (*BCL6*, *CXCL13*, *CXCR5*, *ICOS*), *ICOS* and then *BCL6* appeared less specific than *CXCL13* and *CXCR5* (*data not shown*). Further studies, however, are needed to determine whether cases with a “mixed” T_H-Th2 RNA profile or immunophenotype should be considered to be T_H-PTCL or Th2 PTCL-NOS with associated T_H markers. The almost complete absence of *RHOA* and *TET2* mutation in the cases with a Th2-like profile may support the latter hypothesis.

Our targeted RT-MLPA panel confirmed two subgroups among PTCL-NOS, based on the expression of *TBX21* and cytotoxic markers or *GATA3* and *CCR4* in 39% and 31% of cases, respectively, expanding the findings of previous studies.^{13,14} The prognostic relevance of these two groups is controversial.²⁷ Within the limits of our retrospective study, we failed to demonstrate any significant correlation with outcome between the Th1 and Th2 molecular or phenotypic subgroups. In addition, all *TBX21* cases in our series had a cytotoxic profile by RT-MLPA and immunohistochemistry. Among PTCL-NOS with a cytotoxic phenotype, the RT-MLPA assay highlighted a small group of cases with an EBV signature, now referred to as “nodal T/NK lymphoma EBV-positive” according to the revised WHO classification.¹ Whether these cases, confirmed to be EBV-positive in almost all neoplastic cells by EBER ISH, are related to extranodal NK/T lymphoma nasal-type warrants further investigation. Of note, the Th2 signature based on the expression of *GATA3* and *CCR4* in our panel was characteristic, although not specific, of ATLL. The expression of *GATA3* and *CCR4* together with variable expression of *FOXP3* in ATLL is in accordance with a recent study showing that the HBZ transcript induces *CCR4* expression in CD4 T cells by enhancing *GATA3* expression, whereas *FOXP3* expression was inconsistent in ATLL. However, the distinction between PTCL-NOS with a Th2-like signature and ATLL requires an investigation into HTLV1 serology and/or viral integration.^{28,29}

Finally, our SVM model proposed a class for most cases, with few discrepancies. It may be a useful tool in combination with pathological evaluation, especially when immunohistochemistry is not conclusive or not available. In this series, 23% of cases diagnosed by default as PTCL-NOS due to incomplete or failure in immunohistochemistry were classified as T_H/AITL by our assay. Unclassified or misclassified cases by RT-MLPA were limited to T_H-PTCL or AITL rich in reactive CD8-positive cytotoxic cells known to be abundant in a proportion of AITL,³⁰ or cytotoxic PTCL with various reactive T_H cells. These cases illustrate the contribution of the microenvironment to the molecular signature, especially when tumor cell content is low or heterogeneous, a common problem encountered in all gene-expression methods. Therefore, RT-MLPA results should be interpreted in the light of clinical context, as well as biological and histopathological findings. It is worthy of note that our assay does not provide a final solution for PTCL classification, but rather a step forward that requires extensive reworking.

Overall, this study demonstrates the applicability of a robust and dedicated RT-MLPA assay which is easily transposable to the diagnostic workflow. It is simple to use, can be applied to FFPE and frozen samples, integrates genetic features, and is cost-effective; these all make it an attractive alternative to high-throughput technologies in routine practice. Implementation of RT-MLPA in large studies in the future, especially in the setting of clinical trials, may confirm how this adjunct tool can help better classify PTCL and therefore improve the management of these patients in the era of personalized medicine.

Acknowledgments

The authors would like to thank the LYSA-Pathology and the Plateforme de Ressources Biologiques from Henri Mondor Hospital for its technical assistance and the participants of the Tenomic consortium (see Online Supplementary Appendix). This work was supported in part by institutional grants from the Institut National du Cancer (INCA), the Fondation pour la Recherche Médicale (FRM, Equipe Labellisée DEQ20160334875), the Leukemia Lymphoma Society (LLS), the Fondation Force Hématologique and the Institut Carnot (CALYM), MEDIC Foundation.

Appendix

Participants of the Tenomic consortium

A. Martin, Hôpital Avicenne, Bobigny, France; I. Soubeyran, P. Soubeyran, Institut Bergonié, Bordeaux, France; A. Pilon, O. Tournilhac, CHU Estaing, Clermont-Ferrand, France; P. Gaulard, C. Copie-Bergman, M.H. Delfau, J. Moroch, E. Pouillot, F. Lemonnier, F. Le Bras, J. Dupuis, C. Haioun, Hôpital Henri Mondor, Créteil, France; T. Petrella, L. Martin, JN. Bastié, O. Casanovas CHU, Dijon, France; B. Fabre, R. Gressin, CHU, Grenoble, France; L. de Leval, B. Bisig, E. Missiaglia, MP Dobay, A. Cairoli, CHUV, Lausanne, Suisse; C. Bonnet, J. Somja, CHU Sart-Tilman, Liège, Belgique; M.C. Copin, B. Bouchindhomme, F. Morschhauser, CHU, Lille, France; B. Petit, M. Delage, A. Jaccard, Hôpital Dupuytren, Limoges, France; F. Berger, B. Coiffier, A. Traverse-Glehen, L. Genestier, E. Bachy, CHU Sud, Lyon, France; T. Rousset, G. Cartron, V. Szablewski, Hôpital Gui de Chaumié-St Eloi, Montpellier, France; S. Thiebault, B. Drenou, Hôpital E. Muller, Mulhouse, France; K. Montagne, C. Bastien, S. Bologna, CHU de Brabois, Nancy, France; C. Bossard, S. Le Gouill, Hôtel-Dieu, Nantes, France; J. Brière, V. Meignin, C. Gisselbrecht, J. Soulier, Hôpital St Louis, Paris, France; B.

Fabiani, A.Aline-Fardin, P. Coppo, Hôpital Saint-Antoine, Paris, France; F. Charlotte, J. Gabarre, Hôpital Pitié-Salpêtrière, Paris, France; T. Molina, J. Bruneau, D. Canioni, E. Macintyre, V. Asnafi, D. Sibon, R. Delarue, JP Jaïs, Hôpital Necker, Paris, France; M. Parrens, J.P.Merlio, K. Bouabdallah, Hôpital Haut Lévêque, Bordeaux, France; S. Maugendre-Caulet, P. Tas, F. Llamas-Gutierrez T. Lamy, CHU Pontchaillou, Rennes, France; J.M. Picquenot, E.L Veresezan, F. Drieux, P. Ruminy, F. Jardin, C. Bastard, Centre H Becquerel, Rouen, France; M. Peoch, J. Cornillon, CHU, Saint Etienne, France; L. Lamant, C. Laurent, L. Ysebaert, Hôpital Purpan, Toulouse, France; J. Bosq, P. Dartigues, V. Ribrag, P. Dessen, G. Meurice, Institut G Roussy, Villejuif, France; M. Patey, A. Delmer, Hôpital R. Debré, Reims, France; J.F. Emile, K. Jondeau, Hôpital Ambroise Paré, Boulogne, France; M.C. Rousselet, M. Hunault, A. Clavert, CHU, Angers, France; C. Legendre, S. Castaigne, A.L. Taksin, CH Versailles, Le Chesnay, France; J. Vadrot, B. Joly, A. Devidas, CH Sud Francilien, Corbeil, France; G. Damaj, CHU Caen, France; F. Radvanyi, E. Chapeaublanc, Institut Curie, Paris, France; S. Spicuglia, CIML, Marseille, France; C. Thibault, IGBMC, Illkirch, France; V. Fataccioli, project coordinator, Hôpital Henri Mondor, Créteil, France.

References

- Swerdlow S., Campo E., Harris N.L et al. WHO Classification of Tumours of Haematopoietic and Lymphoid Tissues (IARC WHO Classification of Tumours). Revised 4th Edition. Vol. 2. 2017.
- Herrera AF, Crosby-Thompson A, Friedberg JW, et al. Comparison of referring and final pathology for patients with T-cell lymphoma in the National Comprehensive Cancer Network: Second-Opinion Pathology Review of TCL. *Cancer*. 2014;120(13):1993-1999.
- Hsi ED, Said J, Macon WR, Rodig SJ, et al. Diagnostic Accuracy of a Defined Immunophenotypic and Molecular Genetic Approach for Peripheral T/NK-cell Lymphomas: A North American PTCL Study Group Project. *Am J Surg Pathol*. 2014;38(6):768-775.
- Laurent C, Baron M, Amara N, et al. Impact of Expert Pathologic Review of Lymphoma Diagnosis: Study of Patients From the French Lymphopath Network. *J Clin Oncol*. 2017;35(18):2008-2017.
- Lemonnier F, Couronne L, Parrens M, et al. Recurrent TET2 mutations in peripheral T-cell lymphomas correlate with TFH-like features and adverse clinical parameters. *Blood*. 2012;120(7):1466-1469.
- Couronné L, Bastard C, Bernard OA. TET2 and DNMT3A mutations in human T-cell lymphoma. *N Engl J Med*. 2012;366(1):95-96.
- Cairns RA, Iqbal J, Lemonnier F, et al. IDH2 mutations are frequent in angioimmunoblastic T-cell lymphoma. *Blood*. 2012;119(8):1901-1903.
- Manso R, Sánchez-Beato M, Monsalvo S, et al. The RHOA G17V gene mutation occurs frequently in peripheral T-cell lymphoma and is associated with a characteristic molecular signature. *Blood*. 2014;123(18):2893-2894.
- Palomero T, Couronné L, Khiabani H, et al. Recurrent mutations in epigenetic regulators, RHOA and FYN kinase in peripheral T cell lymphomas. *Nat Genet*. 2014;46(2):166-170.
- Sakata-Yanagimoto M, Enami T, Yoshida K, et al. Somatic RHOA mutation in angioimmunoblastic T cell lymphoma. *Nat Genet*. 2014;46(2):171-175.
- Parrilla Castellar ER, Jaffe ES, Said JW, et al. ALK-negative anaplastic large cell lymphoma is a genetically heterogeneous disease with widely disparate clinical outcomes. *Blood*. 2014;124(9):1473-1480.
- Iqbal J, Weisenburger DD, Greiner TC, et al. Molecular signatures to improve diagnosis in peripheral T-cell lymphoma and prognostication in angioimmunoblastic T-cell lymphoma. *Blood*. 2010;115(5):1026-1036.
- Iqbal J, Wright G, Wang C, et al. Gene expression signatures delineate biological and prognostic subgroups in peripheral T-cell lymphoma. *Blood*. 2014;123(19):2915-2923.
- Wang T, Feldman AL, Wada DA, et al. GATA-3 expression identifies a high-risk subset of PTCL, NOS with distinct molecular and clinical features. *Blood*. 2014;123(19):3007-3015.
- Zhang W, Wang Z, Luo Y, Zhong D, Luo Y, Zhou D. GATA3 expression correlates with poor prognosis and tumor-associated macrophage infiltration in peripheral T cell lymphoma. *Oncotarget*. 2016;7(40):65284-65294.
- Heavican TB, Bouska A, Yu J, et al. Genetic drivers of oncogenic pathways in molecular subgroups of peripheral T-cell lymphoma. *Blood*. 2019;133(15):1664-1676.
- de Jong D, Rosenwald A, Chhanabhai M, et al. Immunohistochemical Prognostic Markers in Diffuse Large B-Cell Lymphoma: Validation of Tissue Microarray As a Prerequisite for Broad Clinical Applications—A Study From the Lunenburg Lymphoma Biomarker Consortium. *J Clin Oncol*. 2007;25(7):805-812.
- de Leval L, Rickman DS, Thielen C, et al. The gene expression profile of nodal peripheral T-cell lymphoma demonstrates a molecular link between angioimmunoblastic T-cell lymphoma (AITL) and follicular helper T (TFH) cells. *Blood*. 2007;109(11):4952-4963.
- Dobay MP, Lemonnier F, Missiaglia E, et al. Integrative clinicopathological and molecular analyses of angioimmunoblastic T-cell lymphoma and other nodal lymphomas of follicular helper T-cell origin. *Haematologica*. 2017;102(4):e148-151.
- Alirkilicarslan AL, Dupuy A, Pujals A, et al. Expression of TFH markers and detection of RHOA p. G17V and IDH2 p. R172K/S mutations in cutaneous localizations of angioimmunoblastic T-cell lymphomas. *Am J Surg Pathol*. 2017;41(12):1581-1592.
- Dupuy A, Lemonnier F, Fataccioli V, et al. Multiple ways to detect IDH2 mutations in angioimmunoblastic T cell lymphoma: from immunohistochemistry to Next Generation Sequencing. *J Mol Diagn*. 2018;20(5):677-685.
- Hsi ED, Horwitz SM, Carson KR, et al. Analysis of Peripheral T-cell Lymphoma Diagnostic Workup in the United States. *Clin Lymphoma Myeloma Leuk*. 2017;17(4):193-200.
- Mareschal S, Ruminy P, Bagacean C, et al. Accurate Classification of Germinal Center B-Cell-Like/Activated B-Cell-Like Diffuse Large B-Cell Lymphoma Using a Simple and Rapid Reverse Transcriptase-Multiplex Ligation-Dependent Probe Amplification Assay: A CALYM Study. *J Mol Diagn*. 2015;17(3):273-283.
- Bobée V, Ruminy P, Marchand V, et al. Determination of Molecular Subtypes of Diffuse Large B-Cell Lymphoma Using a Reverse Transcriptase Multiplex Ligation-Dependent Probe Amplification Classifier: a CALYM Study. *J Mol Diagn*. 2017;19(6):892-904.
- Nagata Y, Kontani K, Enami T, et al. Variegated RHOA mutations in adult T-cell leukemia/lymphoma. *Blood*. 2016;127(5):596-604.
- Pedersen MB, Hamilton-Dutoit SJ, Bendix K, et al. DUSP22 and TP63 rearrangements predict outcome of ALK-negative anaplastic large cell lymphoma: a Danish cohort study. *Blood*. 2017;130(4):554-557.
- Maura F, Agnelli L, Leongamornlert D, et al. Integration of transcriptional and mutational data simplifies the stratification of peripheral T cell lymphoma. *Am J Hematol*. 2019;94(6):628-634.
- Matutes E. Adult T-cell leukaemia/lymphoma. *J Clin Pathol*. 2006;60(12):1373-1377.
- Licata MJ, Janakiram M, Tan S, et al. Diagnostic challenges of adult T-cell leukemia/lymphoma in North America – a clinical, histological, and immunophenotypic correlation with a workflow proposal. *Leuk Lymphoma*. 2018;59(5):1188-1194.
- Gaulard P, de Leval L. The microenvironment in T-cell lymphomas: Emerging themes. *Semin Cancer Biol*. 2014;24:49-60.

The architecture of neoplastic follicles in follicular lymphoma; analysis of the relationship between the tumor and follicular helper T cells

William Townsend,^{1,2} Marta Pasikowska,¹ Deborah Yallop,^{1,3} Elizabeth H. Phillips,¹ Piers E.M. Patten,^{1,3} Jonathan R. Salisbury,⁴ Robert Marcus,³ Andrea Pepper,^{5#} and Stephen Devereux^{1,3#}

¹Department of Haematological Medicine, Rayne Institute, King's College London, London; ²Department of Haematology, University College London Hospitals NHS Foundation Trust, London; ³Department of Haematology, King's College Hospital, London; ⁴Department of Histopathology, King's College Hospital, London and ⁵Department of Clinical and Experimental Medicine, Brighton and Sussex Medical School, Brighton, UK

*AP and SD are senior co-authors.



Haematologica 2020
Volume 105(6):1593-1603

ABSTRACT

CD4⁺ T-follicular helper cells are essential for the survival, proliferation, and differentiation of germinal center B cells and have been implicated in the pathogenesis of follicular lymphoma (FL). To further define the role of these cells in FL, we used multiparameter confocal microscopy to compare the architecture of normal and neoplastic follicles and next generation sequencing to analyze the T-cell receptor repertoire in FL lymph nodes (LN). Multiparameter analysis of LN showed that the proportion of T-follicular helper cells (T_{FH}) in normal and neoplastic follicles is the same and that the previously reported increase in T_{FH} numbers in FL is thus due to an increase in the number and not content of follicles. As in normal germinal centers, T_{FH} were shown to have a close spatial correlation with proliferating B cells in neoplastic follicles, where features of immunological synapse formation were observed. The number of T_{FH} in FL correlate with the rate of B-cell proliferation and T_{FH} co-localized to activation induced cytidine deaminase expressing proliferating B cells. T-cell receptor repertoire analysis of FL LN revealed that follicular areas are significantly more clonal when compared to the rest of the LN. These novel findings show that neoplastic follicles and germinal centers share important structural features and provide further evidence that T_{FH} may play a role in driving B-cell proliferation and genomic evolution in T_{FH} . Our results also suggest that targeting this interaction would be an attractive therapeutic option.

Introduction

Follicular lymphoma (FL) is a neoplasm of germinal center B cells that is usually characterized by the t(14;18) translocation and over-expression of BCL2.^{1,2} The clinical course is variable, prognosis is difficult to predict, and it is typically incurable.^{3,4} The tumor is infiltrated by numerous subsets of non-malignant T cells.⁵⁻⁸ Gene expression profiling (GEP) studies have shown that prognosis in FL can be correlated with the signature of non-malignant T cells of the microenvironment rather than the tumor itself, indicating that the microenvironment is important in the pathogenesis of this disease.^{9,10} The relationship between FL B cells and their microenvironment is complex; non-malignant T cells may either promote or inhibit tumor growth whilst the tumor itself can influence the composition of the microenvironment.^{11,12} Many groups have investigated the impact of microenvironment-related factors on outcome.^{10,13-16} These studies have, however, yielded contradictory

Correspondence:

WILLIAM TOWNSEND
william.townsend@nhs.net

Received: March 4, 2019.

Accepted: September 18, 2019.

Pre-published: September 19, 2019.

doi:10.3324/haematol.2019.220160

Check the online version for the most updated information on this article, online supplements, and information on authorship & disclosures: www.haematologica.org/content/106/6/1593

©2020 Ferrata Storti Foundation

Material published in Haematologica is covered by copyright. All rights are reserved to the Ferrata Storti Foundation. Use of published material is allowed under the following terms and conditions:

<https://creativecommons.org/licenses/by-nc/4.0/legalcode>.
Copies of published material are allowed for personal or internal use. Sharing published material for non-commercial purposes is subject to the following conditions:
<https://creativecommons.org/licenses/by-nc/4.0/legalcode>, sect. 3. Reproducing and sharing published material for commercial purposes is not allowed without permission in writing from the publisher.



results, most likely because of differences in patient populations studied, therapy administered and technical limitations of single parameter immunohistochemistry (IHC) that preclude accurate identification of cell subsets.

In normal germinal centers (GC), B cells are critically dependent on interactions with CD4^{pos} follicular helper T cells (T_{FH}),¹⁷⁻²⁰ which are characterized by expression of PD-1, ICOS, CXCR5, CXCL13, IL-21 and IL-4 and the transcription factor BCL6.^{19,21,22} T_{FH} provide signals necessary for the survival and proliferation of GC B cells and induce expression of activation induced cytidine deaminase (AID), a DNA modifying enzyme that initiates somatic hypermutation (SHM) and class switch recombination (CSR) leading to a class-switched, high-affinity antibody response.^{17,19,20,23}

FL follicles and normal GC share a number of features; FL B cells have a similar phenotype and GEP as their normal counterparts and neoplastic follicles contain both follicular dendritic cells (FDC) and T cells. Studies performed on disaggregated FL lymph nodes (LN) have previously demonstrated an enrichment of IL-4-producing T_{FH} in FL with a distinct gene expression profile and the ability to support FL B-cell growth and modify stromal cell function *in vitro*.²⁴⁻²⁸ The anatomic relationship between T_{FH} and FL B cells and how closely this mimics the situation in normal GC has, however, not previously been studied.

In this study we compared the architecture of normal GC and neoplastic follicles, specifically focusing on the spatial relationship between B cells and T_{FH} using multiparameter confocal immunofluorescence microscopy and semi-automated image analysis. We found that T_{FH} - as identified by surface expression of CD4, PD1, and ICOS - constitute a similar proportion of CD4^{pos} T cells in FL as they do in normal GC. They colocalize and form synapses with proliferating neoplastic B cells, which also express the DNA modifying enzyme AID. Finally, T-cell receptor (TCR) repertoire analysis revealed that T cells in neoplastic follicles are significantly more clonal than those in interfollicular areas, suggesting a role for antigen stimulation in this process. Overall, our findings further highlight the role of the microenvironment in FL and are relevant to the mode of action of new therapies such as those targeting antigen receptor signaling and the PD1/PDL1 axis.²⁹⁻³²

Methods

Patient samples

Formalin fixed paraffin embedded (FFPE) LN biopsies were obtained from 25 patients with histologically confirmed untreated or relapsed FL including three cases of grade IIIb FL, and eight patients with reactive lymphadenopathy. Patients with relapsed FL had not received any treatment for at least 12 months. Clinical details are presented in the *Online Supplementary Tables S1-2*. Ethical approval was obtained from the UK national research ethics committee, reference 13/NW/0040.

Immunofluorescent confocal microscopy

FFPE LN sample preparation steps including deparaffinization, antigen retrieval, and staining are described in the *Online Supplementary Materials and Methods*. All images were acquired on a Nikon Eclipse Ti-E microscope and analyzed using Nikon elements NIS Advanced Research software. Full descriptions of imaging and analysis techniques including the use of binary layers for image analysis are presented in the *Online Supplementary Materials*

and *Methods* and further explained in the *Online Supplementary Figure S1*.

Laser micro-dissection, DNA extraction, and TCR sequencing

Follicles were highlighted by conventional IHC staining for BCL6. Follicular and interfollicular areas were dissected from sequential 10 µm FL sections using a laser capture microscope (PALM, Carl Zeiss MicroImaging, Jena, Germany). After DNA extraction, TCR sequences were subject to multiplex PCR amplification prior to next generation sequencing (Adaptive Biotechnologies, Seattle, WA, USA).³³ TCRV CDR3 regions and their component V, D and J segments were identified using the IMGT definitions.³⁴ Sequences not corresponding to a CDR3 were discarded and unique clones defined by the presence of more than one identical productive CDR3 DNA sequence. The number and size of each clone was determined and the richness, clonality and overlap of the follicular and interfollicular TCR repertoires determined (see the *Online Supplementary Materials and Methods*).

Statistical analysis

Statistical analysis was performed using GraphPad Prism software v5 (GraphPad Software Inc, La Jolla, CA, USA). Normally distributed values are presented as the mean (+/- standard deviation), non-normally distributed values are presented as median (+/- interquartile range). Further details of the statistical analysis are presented in the *Online Supplementary Materials and Methods*.

Results

Normal and neoplastic follicles contain similar numbers of T_{FH}

CD4^{pos} T cells were predominantly located in the interfollicular areas of reactive and FL LN but discrete populations were also present within the GC and malignant follicles. We investigated the phenotype of these by staining for CD4, PD-1 and ICOS simultaneously. Within GC of reactive LN 33.05% (24.7-43.7) of CD4^{pos} T cells co-expressed PD-1 and ICOS (T_{FH} phenotype) and these were distributed predominantly in the light zones (Figure 1A). In FL, 25.0% (18.5-28.7) of follicular CD4^{pos} T cells expressed both PD-1 and ICOS and were located at the follicular border or diffusely distributed within the follicles (Figure 1B). The proportion of CD4^{pos} cells co-expressing PD-1 and ICOS was not significantly different between FL follicles and GC (Figure 1C). CD4^{pos}PD-1^{pos}ICOS^{pos} cells were tightly restricted to the GC of reactive LN and FL follicles with only 0.34% (0.26-1.13) and 3.63% (1.89-6.15) of non-GC or interfollicular FL CD4^{pos} cells co-expressing PD-1 and ICOS respectively.

In FL, although 46.9% (34.7-51.9) of follicular CD4^{pos} cells expressed PD-1, only about 50% of these co-expressed ICOS indicating that there are at least two distinct populations of CD4^{pos}PD-1^{pos} cells within FL follicles, highlighting the importance of using all three parameters for identification of T_{FH}. There was no difference in the proportion of CD4^{pos} cells that co-expressed PD-1 and ICOS by histological grade in FL (*Online Supplementary Figure S8*), however, as the number and size of neoplastic follicles increase with histological grade, so must the absolute number of T_{FH}.

To investigate differences in T cells located in the follicles and interfollicular areas of FL, the intensity of CD4 and PD-1 expression were measured. CD4 expression was

30.7% lower in follicular CD4^{pos} T cells than in their inter-follicular counterparts suggesting that these represent a distinct population of T cells (*Online Supplementary Figure S2*). Whilst CD4^{pos}PD-1^{pos}ICOS^{pos} cells were restricted to the follicles, CD4^{pos}PD-1^{pos}ICOS^{neg} cells were present in

the interfollicular area where 9.3% (5.1-26.4) of CD4^{pos} cells expressed PD-1. The intensity of PD-1 expression was significantly higher in follicular PD-1^{pos} T cells than interfollicular PD-1^{pos} T cells (*Online Supplementary Figure S2*) consistent with them being T_{HH}.⁵⁵ Additional co-stain-

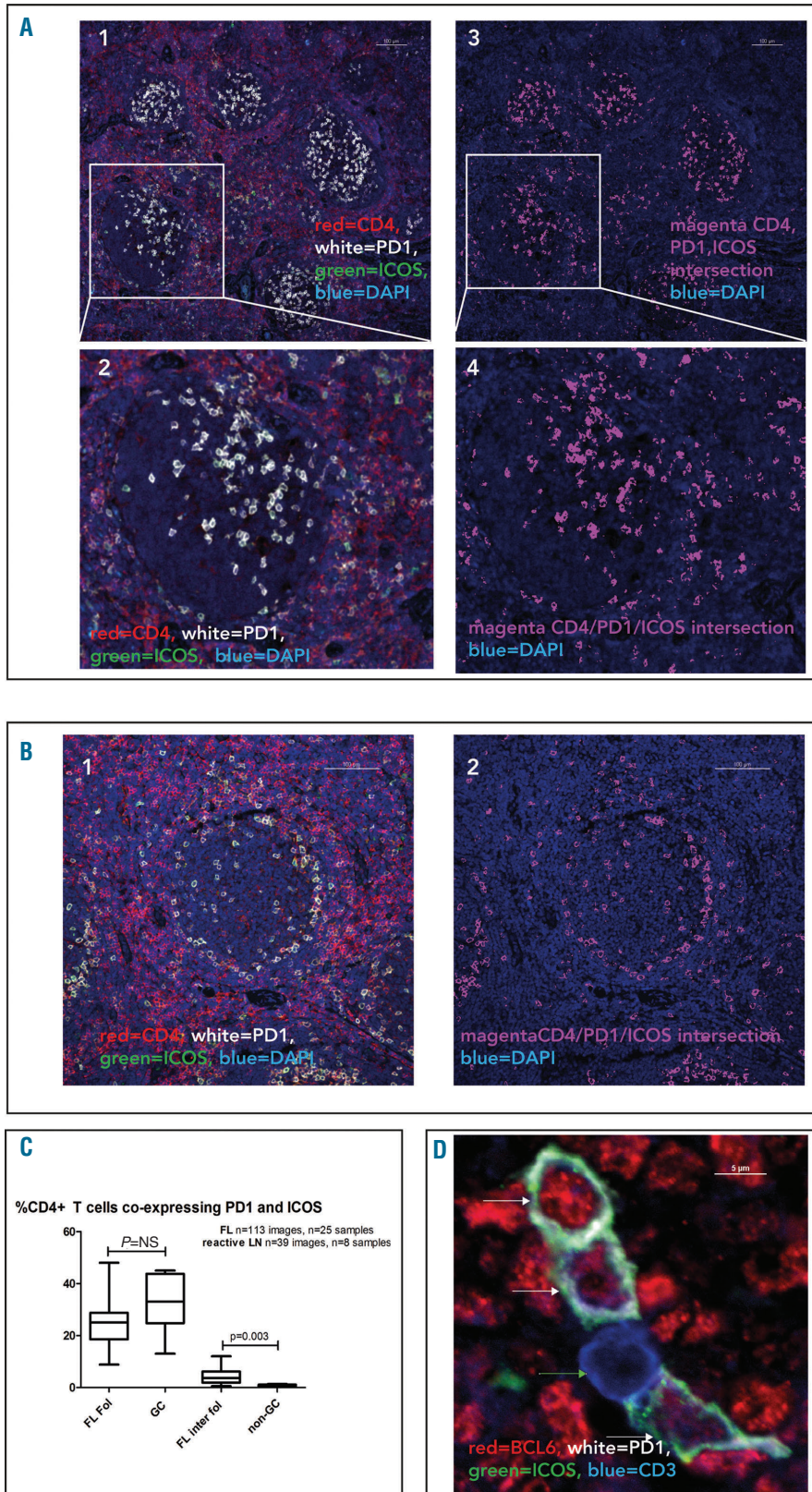


Figure 1. Distribution of CD4^{pos}PD-1^{pos}ICOS^{pos} cells in normal germinal centers and follicular lymphoma. (A1) Low power view of germinal centers (GC) in a reactive lymph node (LN) showing CD4^{pos} (red) T-cells mainly outside the GC. A population of cells within the GC co-express PD-1 (white) and ICOS (green). (A2) The area highlighted by the white rectangle has been enlarged showing the distribution of CD4/PD1/ICOS^{pos} cells in a normal GC where they are mainly polarized to the light zone (A3) Intersecting binary layer of image (A1) showing CD4/PD-1/ICOS^{pos} cells (magenta) in GC. DAPI staining (blue) highlights cell nuclei. (A4) High power view of the intersecting CD4/PD-1/ICOS^{pos} binary layer. (B1) Representative image of follicular lymphoma (FL) lymph node (LN) showing CD4^{pos} (red) T cells mainly outside the follicles but a population within the follicles co-express PD-1 (white) and ICOS (green). (B2) Same image as (B1) showing only DAPI (blue) and the intersecting binary layer of CD4/PD-1/ICOS^{pos} cells (magenta) which are restricted to the follicles where they are located predominantly in a peri-follicular pattern. Scale bars represent 100 μ m. (C) There was no significant difference in the proportion of CD4^{pos} cells co-expressing PD-1 and ICOS in normal and neoplastic follicles. There was a small but significant increase in CD4/PD-1/ICOS^{pos} cells in the inter-follicular compartment of FL compared to the same area zone of reactive LN. Horizontal lines represent median, boxes represent interquartile range, 'whiskers' represent range. (D) Representative, magnified image showing BCL6 expression in T cells in neoplastic follicles. Four CD3^{pos} (blue) cells are shown, three are positive for the transcription factor BCL6 (red) and these are also PD-1^{pos} (white) and ICOS^{pos} (green), indicated with white arrows. One CD3^{pos} cell is negative for BCL6 (green arrow), and this cell does not express PD-1 or ICOS. Overall 89.6% (88.3-91.8) of CD3^{pos}PD1^{pos}ICOS^{pos} cells express BCL6.

ing experiments demonstrated that these cells had a composite CD3^{pos}, CD8^{neg}, PD-1^{pos}, ICOS^{pos}, BCL6^{pos}, CXCR5^{pos}, TBET^{neg} phenotype further confirming their identity as T_{FH} (Figure 1D and *Online Supplementary Figure S2C*). Although CXCR5 has frequently been used to identify T_{FH} by flow cytometry, we found that it was unhelpful in identifying this cellular subset by microscopy since most T cells present within these structures were CXCR5^{pos} and it therefore did not help to distinguish them from other GC/follicularly located cells (*Online Supplementary Figure S2C*). It was not possible to use CD4 in these experiments as the antibody is the same species as the BCL6. No BCL6^{pos} cells

were found to be CD8^{pos} therefore the substitution for CD3 was acceptable (*Online Supplementary Figure S2D*). The intensity of BCL6 staining in T_{FH} was lower than that observed in FL B-cells but higher than in other T cells (*Online Supplementary Figure S2B*). Although 25.0% (6.028.0) of ICOS^{pos} T cells and 4.0% (1.0-8.0) of PD-1^{pos} T cells within FL follicles were FOXP3^{pos}, only a minority of dual PD-1^{pos}ICOS^{pos} T cells expressed FOXP3, (*Online Supplementary Figure S3*). In comparison to FL, very few FOXP3^{pos} T cells were identified within the GC of reactive LN where they were exclusively located outside the GC (*Online Supplementary Figure S3B*).

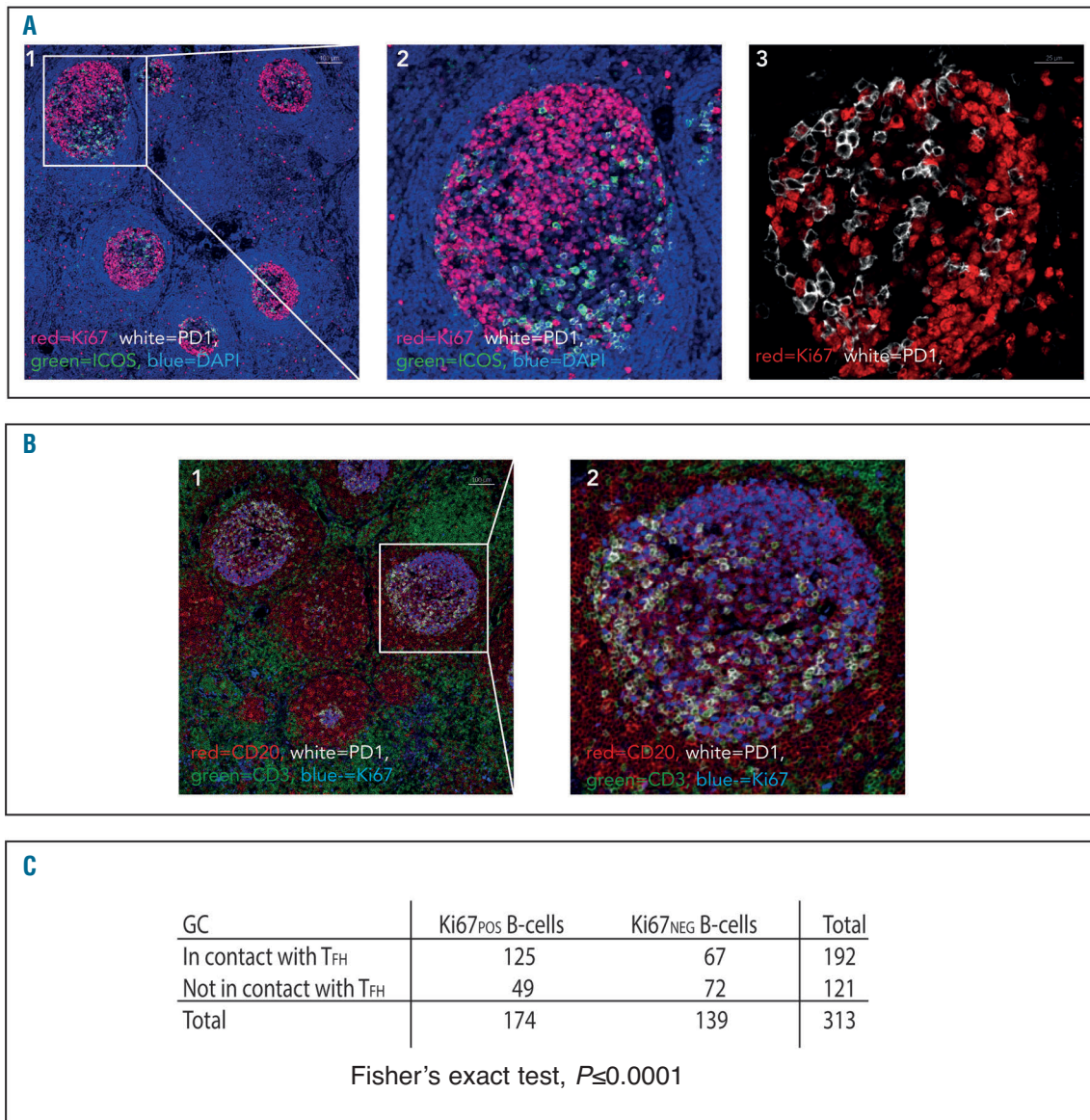


Figure 2. Close physical association between Ki67^{pos} B cells and follicular helper T cells in normal germinal center light zones. (A1) Representative low power image showing polarization of Ki67^{pos} cells to the dark zones of normal germinal centers. Ki67 (red), PD-1 (white), ICOS (green), DAPI (blue). Scale bar represents 100 μ m. The area highlighted by the white rectangle is shown in high power in (A2). (A3) The close association between Ki67^{pos} FL cells (red) and PD-1^{hi} cells (white) is shown in the light zone of another follicle whereas in the dark zone there is less interaction between Ki67^{pos} cells and PD-1^{hi} T cells. The scale bar represents 25 μ m. (B1) Using a different four-color panel, the Ki67^{pos} cells (blue) were confirmed as CD20^{pos} B cells (red) and the PD-1^{hi} cells (white) were confirmed as CD3^{pos} T cells (green). The scale bar represents 100 μ m and the area highlighted by the white rectangle has been magnified in (B2). Images representative of n=13 images from n=4 reactive lymph node (LN) samples. (C) Contingency table showing that Ki67^{pos} B cells are significantly more likely to be in contact with follicular helper T cells (T_{FH}) than Ki67^{neg} B cells in normal germinal center (GC) light zones, as quantified by manual visual assessment. For all samples analyzed together (n=5, Fisher's exact test $P < 0.0001$).

These findings confirm that the majority of GC or follicular CD4^{pos} cells that strongly express PD-1 and ICOS are T_{FH} and constitute the same proportion of CD4⁺ cells in normal and neoplastic follicles.

T_{FH} co-localize with proliferating B cells

Next, we investigated if there is a spatial relationship between proliferating B cells and T_{FH} in reactive and neoplastic follicles. An ideal panel of CD20, Ki67, CD4, PD-1 and ICOS was not possible for technical reasons. However, co-staining for CD20, Ki67, and CD3 (Online Supplementary Figure S4) showed that in both normal GC

and neoplastic follicles the majority of Ki67^{pos} cells are CD20^{pos} B cells. Also, as most PD-1^{hi} cells were ICOS^{pos}, it enabled T_{FH} to be identified using just two parameters; CD4 and high PD1 expression.

In normal GC a close spatial correlation between Ki67^{pos} cells and CD4^{pos}PD-1^{hi} cells was evident in the light zone of all cases (Figure 2A). Automated image analysis showed that 63.1% ±15.9 of Ki67^{pos} cells in the light zones were in direct contact with CD4^{pos}PD-1^{hi} cells, furthermore, the high density of T_{FH} in this compartment meant that the majority of Ki67^{pos} B cells were in close proximity to ≥1 T_{FH}. The majority of these PD-1^{hi} cells were also

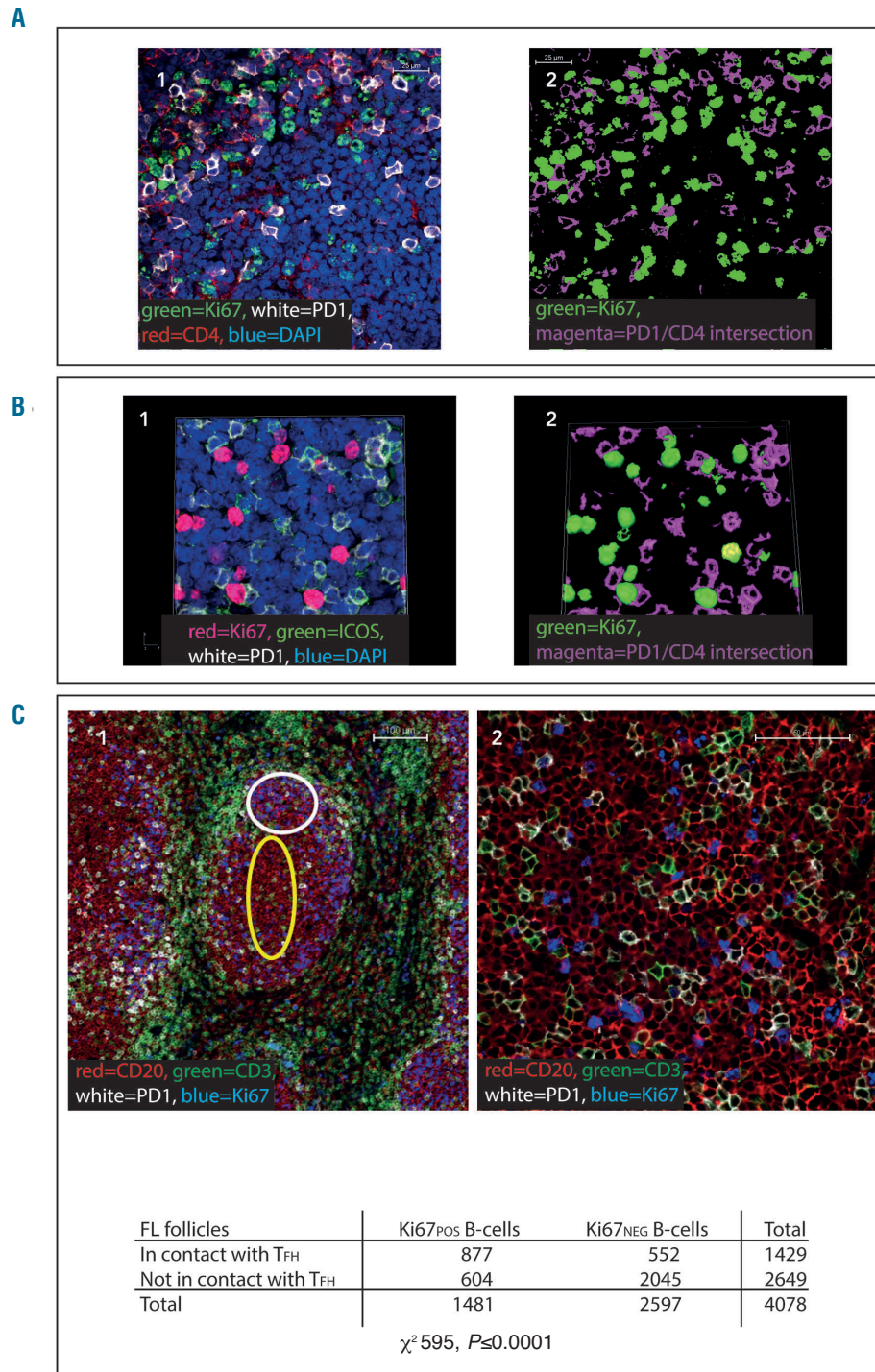


Figure 3. Ki67^{pos} cells are in close proximity to follicular helper T cells (T_{FH}) in follicular lymphoma lymph nodes. (A1) Representative image of a neoplastic follicle showing Ki67^{pos} cells (green) in close proximity to CD4^{pos} (red), PD-1^{hi} (white) T cells. The scale bar represents 25 μm. (A2) Binary image of (A1), the binary layers of Ki67 (green) and the CD4-PD-1^{hi} intersection (magenta) are shown highlighting the close association of Ki67^{pos} cells to PD-1^{hi} T cells. (B1) Representative image demonstrating that the majority of the PD-1^{hi} cells in contact with Ki67^{pos} cells (red) are also positive for ICOS (green). (B2) This is highlighted in the binary layer 3D reconstruction of the same image, PD-1/ICOS^{pos} (magenta) and Ki67 (green). Images representative of n=100 images from n=23 follicular lymphoma (FL) samples (4A), n=43 images from n=13 samples (4B). (C1) Ki67=blue, CD20=red, PD-1=white, CD3=green. Low power image (x10) showing Ki67^{pos} and Ki67^{neg} CD20^{pos} B-cell co-localisation with PD1^{hi} CD3^{pos} T cells in FL. Within the follicles there are areas of low proliferation (low Ki67=blue) where there are few PD1^{hi} (white) CD3^{pos} T cells (green) - area highlighted by yellow oval, whereas in areas where there is high Ki67, there are more PD1^{hi}, CD3^{pos} T cells (area highlighted by white circle) and they are frequently in contact with Ki67^{pos} CD20^{pos} FL B cells. Scale bar represents 100 μm. (C2) High power image (x60) in which the close correlation of Ki67^{pos} (blue) B cells with PD1^{hi} (white) CD3^{pos} (green) cells can be seen, whilst the CD20^{pos} (red), Ki67^{neg} cells are less frequently in contact with follicular helper T cells (T_{FH}). Scale bar represents 50 μm. (C3) contingency tables showing that Ki67^{pos} B cells are significantly more likely to be in contact with T_{FH} than Ki67^{neg} B-cells in FL (for all samples analyzed together [n=25 images from n=7 follicular lymphoma specimens] χ^2 595, $P < 0.0001$).

ICOS^{pos} with 53.9% ± 14.2 of Ki67^{pos} cells in contact with PD-1^{pos}ICOS^{pos} cells. In GC light zones, Ki67^{pos} B cells were significantly more likely than Ki67^{neg} B cells to be in contact with T_{FH} in all cases studied ($P < 0.005$ in each GC examined) (Figure 2C).

In the highly proliferative dark zones, there were few T_{FH} and a very high number of Ki67^{pos} B cells. The closely packed Ki67^{pos} B cells could not be separated by automated image analysis and therefore accurate calculation of the proportion of Ki67^{pos} cells in contact with T_{FH} could not be performed in the dark zones. It is clear from visual inspec-

tion, however, that the degree of spatial correlation between these cells is much lower in the dark zones than in the light zones (Figure 2B).

A close spatial relationship between Ki67^{pos} B cells and CD4^{pos}PD-1^{hi} T cells was also found in FL and, in contrast to normal GC, all areas with high Ki67 also had increased numbers of T_{FH} cells. In FL 41.0% ± 13.6 of CD20^{pos}Ki67^{pos} cells were found to be in direct contact with CD4^{pos}PD-1^{hi} cells, although the level of co-localization was significantly lower than in GC ($P = 0.003$), there was a high level of co-localization in both settings

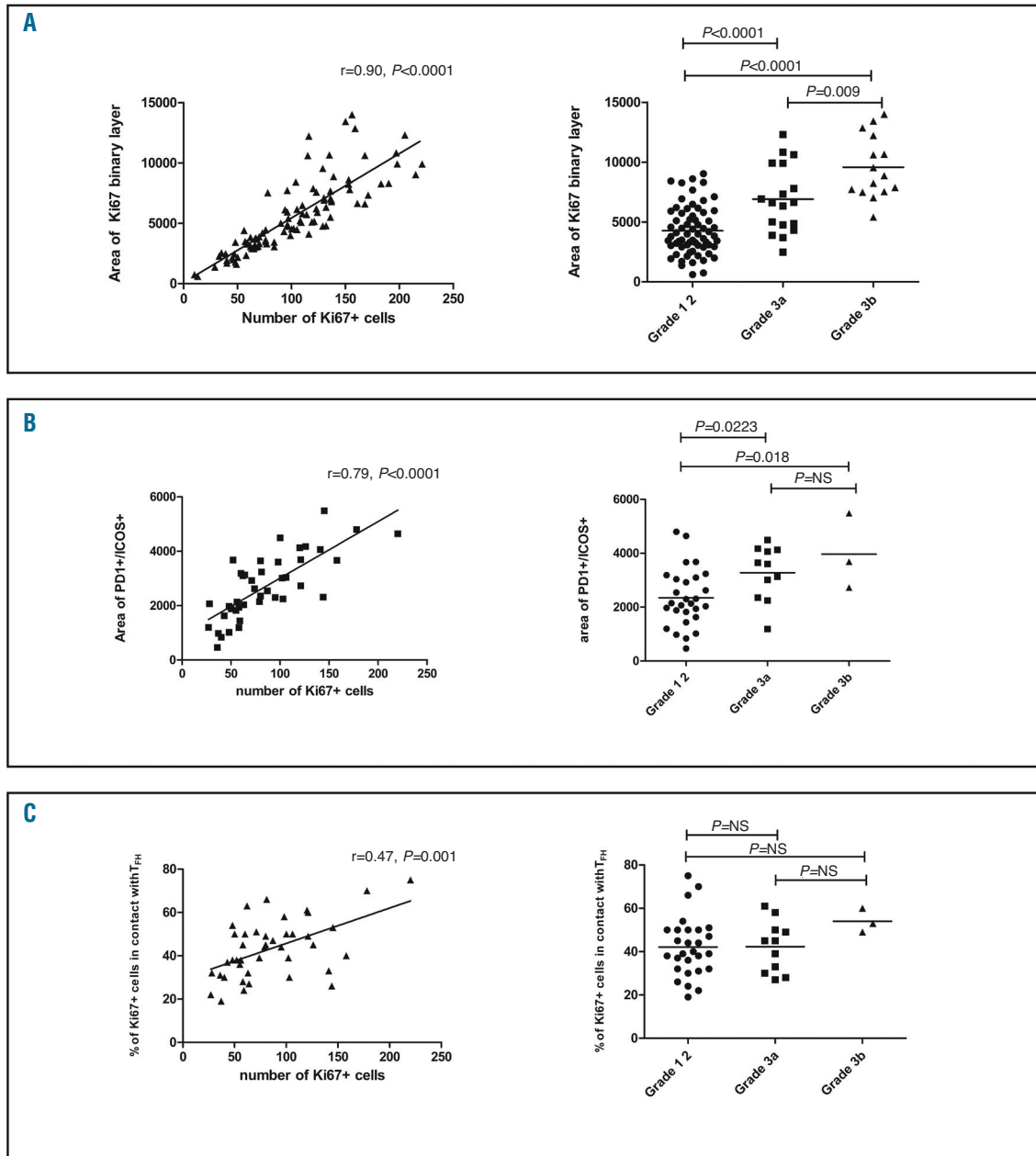


Figure 4. Association between Ki67 and number of follicular helper T cells in follicular lymphoma. (A) The area of the Ki67 binary layer correlates closely with the number of Ki67^{pos} cells automatically counted (left) and the area of the Ki67 binary layer is significantly higher in grade IIIa or IIIb disease than in grade I-II disease (right), n=99 images from n=23 samples. (B) The number of Ki67^{pos} cells correlates closely with the number of PD1^{pos}ICOS^{pos} cells (left) and there are significantly more follicular helper T cells (T_{FH}) (as represented by increased area of PD1/ICOS intersection) in grade IIIa and IIIb disease than in grade I-II disease (right), n=42 images from n=13 samples. (C) The degree of T_{FH} - Ki67 interaction is weakly associated with the number of Ki67^{pos} cells (left), and the proportion of Ki67^{pos} cells in contact with T_{FH} does not differ significantly according to histological grade disease (right) (n=42 images from n=13 samples).

(Figure 3A). High power images and 3D Z-stack reconstructions revealed that there was very close contact between these cells, and Ki67^{pos} cells were frequently observed to be in contact with more than one CD4^{pos}PD-1^{hi} cell simultaneously. Staining for Ki67, PD-1, and ICOS revealed that 84.7% ± 11.1 of the PD-1^{hi}CD4^{pos} cells in

contact with Ki67^{pos} cells were also ICOS^{pos} and therefore likely to be T_{FH} (Figure 3B).

Ki67^{pos}CD20^{pos} FL B cells were significantly more likely than Ki67^{neg}CD20^{pos} FL B cells to be in direct contact with T_{FH} in each case examined, ($P < 0.0001$ for each specimen) (Figure 3C).

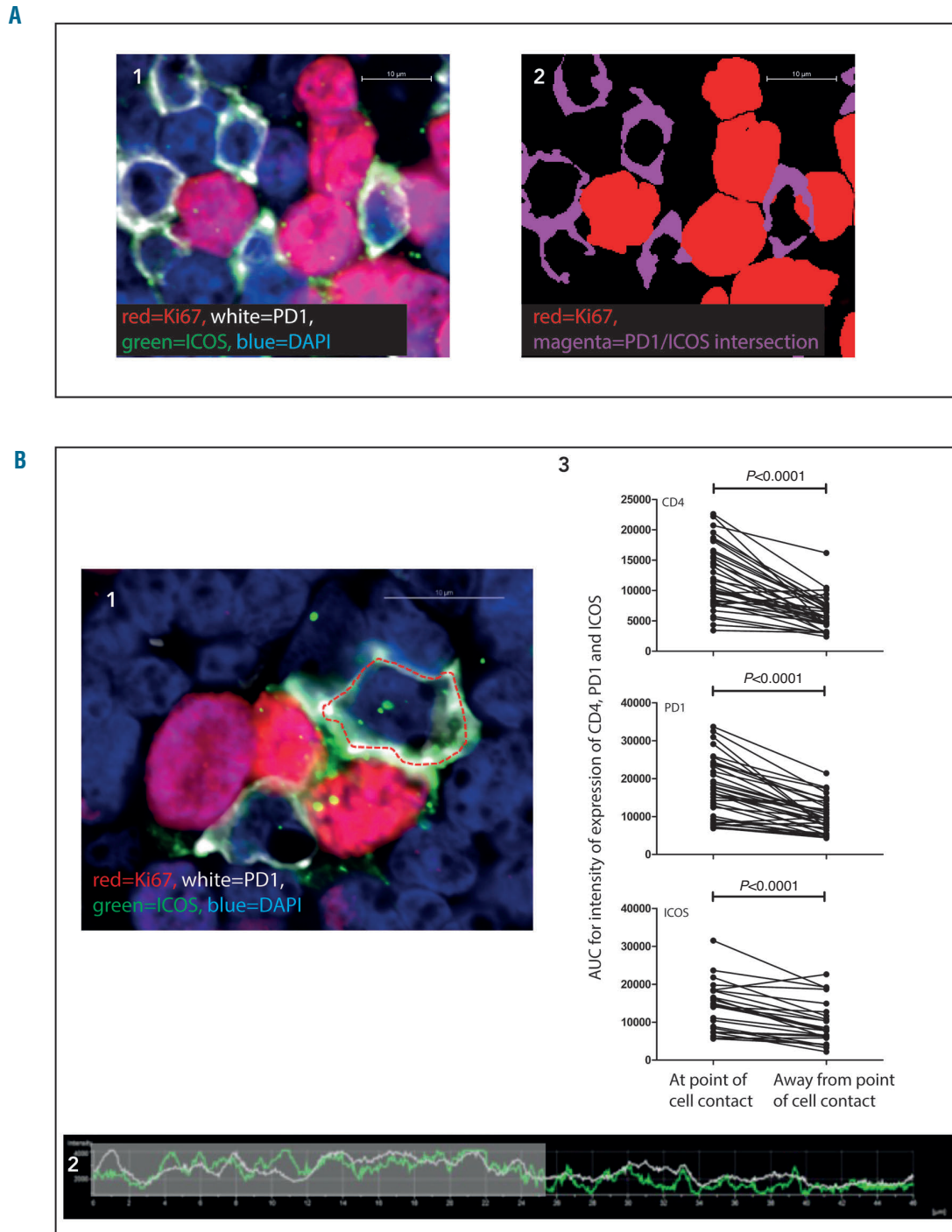


Figure 5. Close contact between Ki67^{pos} cells and follicular helper T cells in follicular lymphoma: evidence for immune synapse formation. (A1) A Ki67^{pos} cell (red) is seen to be in contact with 4 PD-1^{pos} (white) ICOS^{pos} (green) cells simultaneously. The PD-1^{pos}ICOS^{pos} cells are closely associated with the Ki67^{pos} cell. (A2) Binary layer image of A1, the binary layers of Ki67 (red) and PD-1/ICOS intersection (magenta) are shown highlighting the close spatial association. Scale bars represent 10 μ m. (B1) The follicular helper T cells (T_{fh}) form projections encompassing the Ki67^{pos} cells. Scale bar represents 10 μ m. The perimeter of the T_{fh} has been highlighted by the red dotted line and the intensity of CD4, PD-1 and ICOS have been measured around this line, the area of cell contact is highlighted in the shaded area (B2). (B3) CD4, PD1, and ICOS all have significantly higher intensity of expression at the sites of cell contact than at the opposite pole, paired t-tests, n=61 cell contacts, from highly magnified images in nine follicular lymphoma specimens stained with CD4/PD-1/Ki67, or PD-1/ICOS/Ki67. AUC: area under the curve.

Relationship between Ki67, T_{FH} cells and histological grade

The area of the Ki67 binary layer and the corresponding number of Ki67^{pos} cells counted by automated analysis increased with histological grade (Figure 4A). The area of the PD-1^{pos}ICOS^{pos} intersection was closely correlated with the number of Ki67^{pos} cells and histological grade demonstrating that, in higher grade cases with a higher proliferation rate, the absolute number of T_{FH} is increased (Figure

4B). The degree of colocalization between Ki67⁺ B-cells and T_{FH} was, however, similar across all histological grades. Thus, in cases with low Ki67 there were few T_{FH} and in cases with high Ki67 there were more T_{FH}, but the extent of co-localization remained relatively constant (Figure 4C). There was also a correlation between the number of Ki67^{pos} cells and the number of T_{FH} in normal GC ($r=0.55$, $P=0.019$, $n=17$ GC from $n=4$ samples; *Online Supplementary Figure S7*).

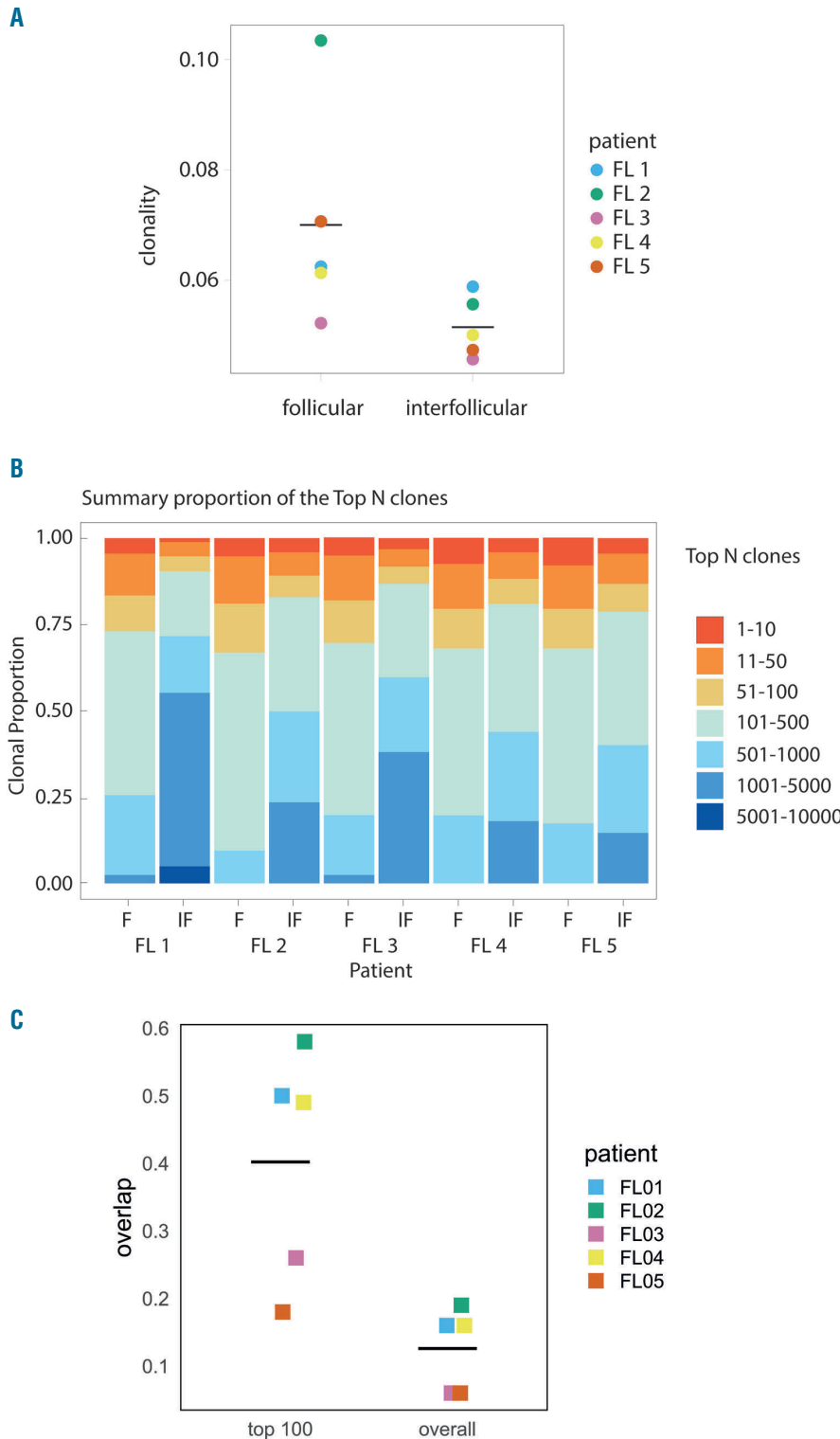


Figure 6. Evidence of T-cell receptor repertoire restriction in follicular lymphoma. (A) The clonality of the T-cell receptors (TCR) in intrafollicular areas was higher than in the interfollicular compartment in all cases examined, horizontal bars represent mean of all samples, median clonality 0.062 versus 0.049 respectively, Mann Whitney, $P=0.0317$. (B) Summary of TCR repertoire data showing the proportion of the total population accounted for by high frequency clones in the follicular and interfollicular regions of follicular lymphoma lymph nodes. In each case, the more frequent clones predominate in the follicular regions compared to the interfollicular areas. (C) The level of overlap of clonotypes between follicular and interfollicular compartments for all clones in paired samples (all clones) and for the 100 most frequent clones (top 100 clones). Horizontal bars represent the mean overlap (0.125 for all clones and 0.22 for top 100 clones)

Proliferating cells in contact with T_{FH} express AID

Since T_{FH} have been implicated in initiating SHM and CSR through induction of AID in GC,²⁰ we investigated if there was a spatial relationship between T_{FH} and AID^{pos} cells. AID was restricted to Ki67^{pos} cells in FL, 63% ±8.8 of which were AID^{pos} and 39.8% ±9.7 of AID^{pos}Ki67^{pos} cells were in direct contact with PD-1^{Hi} cells. As we had established that most PD-1^{Hi} cells in contact with Ki67^{pos} cells were ICOS^{pos}, we can predict that the majority of PD-1^{Hi} cells in contact with AID^{pos}Ki67^{pos} cells were T_{FH} (*Online Supplementary Figure S5*). AID was similarly restricted to Ki67^{pos} cells of GC where close association with PD-1^{Hi} cells was evident in the light zones (*Online Supplementary Figure S5C*).

PD-L1

PD-L1 has previously been reported to be absent from the surface of FL B-cells³⁶ and we found no evidence that PD-L1 was strongly expressed on the Ki67^{pos} cells in contact with PD-1^{Hi} cells. Instead, PD-L1 was expressed mainly on interfollicular CD23^{neg} cells (*Online Supplementary Figure S6*). The identity of these cells was not further investigated in this study.

Features of synapse formation

The close spatial relationship between Ki67^{pos} FL B cells and T_{FH} was further investigated in high power images where morphological features indicating the formation of immunological synapses were identified. Features included: T_{FH} cell membrane projections encompassing the Ki67^{pos} cells, overlapping of the B- and T-cell membranes, distortion of T-cell nuclei away from points of cell contact and significantly increased intensity of CD4, PD-1, and ICOS expression at points of cell contact (Figure 5).³⁷ The intensity of expression of CD4, PD-1, and ICOS at points where T_{FH} were in contact with Ki67^{pos} cells was formally quantified by defining the perimeter of the T-cell membrane and measuring the intensity of fluorescence at each pixel around the perimeter. The area under the curve for intensity at the point of cell contact was compared with an equivalent length of cell membrane at the opposite pole (Figure 5B). Similar features indicating synapse formation were identified in GC light zones but the high number of closely-packed Ki67^{pos} cells and T_{FH} in GC precluded the same analytic method being used because T_{FH} in GC were usually in contact with more than one Ki67^{pos} cell simultaneously.

TCR repertoire within follicles shows evidence of antigen restriction

In view of the close spatial relationship observed between T cells and proliferating tumor cells, we investigated whether T cells within the follicles show evidence of antigen restriction by performing TCRV next generation sequencing of genomic DNA from laser dissected follicular and interfollicular areas from five FL samples. The degree of restriction of the TCRV repertoires in FL neoplastic follicles and interfollicular areas was assessed in several ways. First, we estimated the richness of the repertoire in each compartment by determining the number of different clones present per ng of input DNA which, since we were analysing genomic DNA, was proportionate to the total cell number. The interfollicular areas contained more T-cell clones per ng of input DNA than the intrafollicular regions, however, this did not quite reach statistical significance ($P=0.06$, *Online Supplementary Table S4*). We

also calculated the clonality index³⁸ (see the *Online Supplementary Materials and Methods* for further details). In each of the five cases examined, the clonality of the follicular T cells was greater than in the interfollicular areas ($P=0.0317$, Figure 6A). We also calculated the proportion of the TCR repertoire in each compartment that was accounted for by high frequency clones.³⁹ Compared to the interfollicular areas, the follicular regions were dominated by high frequency clones (Figure 6B). For example, the top 50 most frequent clones made up a mean of 19% of all clones in the follicular areas (95% CI: 17-21) compared to 9.8% in the interfollicular region (95% CI: 6.1-13.4) $P=0.0002$, $n=5$.

As expected from their different phenotypes, the clones present in the follicular and interfollicular areas of the same sample were markedly different, indicating that the TCR repertoires of the follicular and interfollicular areas are distinct (Figure 6C).

Discussion

In this study we compared the structure of neoplastic follicles in FL with GC in reactive LN, focusing on T_{FH}, their relationship with proliferating B cells and TCR repertoire. Although T_{FH} have previously been reported to be present in the FL microenvironment,²⁴⁻²⁷ these studies were performed on disaggregated LN and this is the first time that their spatial organization has been investigated in situ in this way. Using multi-parameter immunofluorescent confocal microscopy, we demonstrated that T_{FH} – as identified by surface expression of CD4, PD1, and ICOS – constitute a similar proportion of CD4^{pos} T cells in FL as in reactive LN and form synapses with proliferating Ki67^{pos} tumor cells which express the DNA modifying enzyme AID. The number of T_{FH} in neoplastic follicles correlates with the level of tumor proliferation and histological grade, and there is evidence for antigen restriction, as supported by the more clonal TCR repertoire found within neoplastic follicles compared to interfollicular areas.

These findings are novel and of significance for a number of reasons. First, in contrast to previous work on disaggregated FL LN, which showed an increase in the total number of T_{FH},^{24,25,40} we found that FL follicles contain T_{FH} in similar proportions to normal reactive GC. This discrepancy likely relates to the fact that in FL, LN architecture is usually effaced by many closely packed follicles, whereas in normal tissues the interfollicular areas, which contain many fewer T_{FH}, are more extensive. Thus, although the overall T_{FH} content of FL LN is increased compared to normal,²⁵ this is because of the larger number of follicles in the tumor and when neoplastic and normal follicles are compared directly, the numbers are the same. This finding underlines the need to complement data obtained from disaggregated tissues with anatomic studies.

Our use of multiparameter microscopy permitted the spatial relationship between T_{FH} and B cells to be closely investigated and this also provided new insights. T_{FH} are essential for providing normal GC B cells with signals necessary for their survival, proliferation and maturation.^{19,41} To our knowledge, this is the first time that the intimate relationship between Ki67^{pos} B cells and T_{FH} has been demonstrated in situ in human LN in this way and our observations are in keeping with the pivotal role they play in the normal GC reaction. Importantly, we also found that the

close spatial association of Ki67^{pos} B cells and T_{HH} is recapitulated in FL, as 41% of Ki67^{pos} FL B cells were in direct contact with T_{HH} and were significantly more likely to be in direct contact with T_{HH} than non-proliferating cells. The observed close spatial correlation between the two cell types is thus not due to chance and suggests that T_{HH} are involved in functionally important interactions with the tumor. This corroborates and advances findings from previous *in vitro* experiments which showed that FL T_{HH} provide signals for B-cell survival.^{25,27}

We also found a correlation between the numbers of T_{HH} and Ki67^{pos} B cells in both normal GC and neoplastic follicles and that, in FL, the number of T_{HH} increase with histological grade. The relationship between number of T_{HH} and rate of B-cell proliferation observed in our study has not been reported previously in FL but is consistent with previous data showing that the regulation of GC size and B-cell number is critically dependent on the number of T_{HH}.^{17,19,23} This adds to the evidence that T_{HH} are central to the pathogenesis of FL, just as they are essential in the normal GC reaction. Furthermore, the degree of co-localization (the proportion of Ki67^{pos} B cells in contact with one or more T_{HH}) remained constant as histological grade increased, with no significant change in the proportion of Ki67^{pos} cells in contact with T_{HH} in grade IIIa or IIIb disease compared to grade I-II disease, suggesting that interaction with T_{HH} remains important regardless of histological grade.

Our studies also underline the crucial importance of using a multi-parameter approach to define and quantify the complex T-cell subsets present in the FL microenvironment. No single antigen or transcription factor specifically identifies T_{HH} and this is the first study reporting the presence of T_{HH} in FL *in situ* using techniques that overcome the limitations of traditional IHC. By using co-staining for ICOS and BCL6 we were able to show that only half of the PD1 expressing cells neoplastic follicles are T_{HH}. Single parameter analysis of PD1 would therefore lead to significant overestimate of T_{HH} numbers perhaps explaining, at least in part, why previous IHC studies have yielded divergent results with regards to the impact of different T-cell infiltrates on prognosis.^{10,13-16}

Previous *in vitro* studies have shown that peripheral blood T cells in FL are dysfunctional and form impaired synapses with B cells.^{40,42} In the present study, however, we found features that suggest normal synapse formation between Ki67^{pos} tumor cells and T_{HH} within the LN.⁴³ This divergence from previous research may be because we examined the interactions between T_{HH} and Ki67^{pos} cells *in situ* in human tissue rather than in an *ex vivo* system using peripheral blood derived cells. It also remains possible that there are other subsets of non T_{HH} cells in the FL microenvironment that are dysfunctional and have an impaired ability to form immunological synapses.

In addition to promoting GC B-cell proliferation, interaction with T_{HH} cells also induces AID expression which induces somatic hypermutation and class switch recombination. Off-target action of AID has previously been proposed to lead to the accumulation of mutations required for germinal center-derived lymphomas to develop or progress and has been associated with transformation of FL.^{44,45} The close spatial association between T_{HH} and AID^{pos}Ki67^{pos} FL B cells observed in the present study is compatible with this theory.

Finally, next generation sequencing analysis of the TCR repertoire of follicular and interfollicular areas of FL LN showed that the neoplastic follicles are significantly more clonal and dominated by high frequency clones compared to the interfollicular regions. As expected from their divergent phenotype, very little repertoire overlap between the two compartments was present. PCR-based analyses of TCR repertoire on small samples are known to suffer from a number of potential limitations including sampling effects and errors introduced during the amplification process, which may lead to apparent skewing.⁴⁶ Whilst we cannot completely exclude these possibilities, we minimized the risk by direct, intra-patient comparison in the same assay run, and, of note, our findings were consistent in all five cases studied. Another possibility is that the demonstrated differences in TCR repertoire relate to the greater number of T cells found in the interfollicular regions compared to the follicles. Whilst T-cell numbers undoubtedly do differ between these two areas, significant difference in the clonality index, which takes into account the number of unique clones present, were observed (Figure 6A). Furthermore, the repertoire of the intrafollicular area was strikingly dominated by high frequency clones; for example, the top 50 clones accounted for a mean of 19% (CI: 17-21%) of all clones present, compared to 9.7% (CI: 6.1-13.4%) in the interfollicular areas ($P=0.0002$).

Taken together, these findings suggest that the interactions between B cells and activated T_{HH} that induce B-cell proliferation and differentiation and lead to the generation of high affinity antibody in normal GC may be recapitulated within the follicles of FL.^{19,41} Since T_{HH} may be involved in processes fundamental to disease progression, such as clonal expansion and genomic evolution of the tumor, our results suggest that they would be an attractive target for novel therapies. This is especially relevant in the era of drugs that target antigen receptor signaling such as PI3-kinase inhibitors, which affect both B- and T-cell receptor pathways. Our results are also relevant to understanding the mechanism of action of drugs that target PD-1 expressing cells, which have been shown to be effective in FL and other lymphomas.²⁹⁻³¹ It is clear that whilst some of the PD-1 expressing cells in the FL LN are indeed T_{HH}, many are not and these may represent exhausted effector cells. Blockade of PD-1 in the latter case may unmask antitumor immunity and lead to disease regression. The impact of interrupting PD-1 function in T_{HH} is, however, less clear as the role of the PD-1 axis in T_{HH} function is not fully established. These findings add another level of complexity to our understanding of the FL tumor microenvironment and underline the necessity of using multi-dimensional methods in future studies.

Funding

This research was funded by grants from the British Society of Haematology in partnership with the Roger Counter Foundation, and Bloodwise.

Acknowledgments

We are grateful for the technical assistance and advice of Adaptive Biotechnologies and of Jon Harris and Jan Soetaert from the Nikon Imaging Centre at Kings' College London.

References

- Harris N, Swerdlow S, Jaffe E, et al. WHO Classification of Tumours of Haematopoietic and Lymphoid Tissues, 4th edn. 4th ed. Lyon: International Agency for Research on Cancer, 2008.
- Marafioti T, Copie-Bergman C, Calaminici M, et al. Another look at follicular lymphoma: immunophenotypic and molecular analyses identify distinct follicular lymphoma subgroups. *Histopathology*. 2013;62(6):860-875.
- Ardeshtna KM, Smith P, Norton A, et al. Long-term effect of a watch and wait policy versus immediate systemic treatment for asymptomatic advanced-stage non-Hodgkin lymphoma: a randomised controlled trial. *Lancet*. 2003;362(9383):516-522.
- Montoto S, Davies AJ, Matthews J, et al. Risk and clinical implications of transformation of follicular lymphoma to diffuse large B-cell lymphoma. *J Clin Oncol*. 2007;25(17):2426-2433.
- Ame-Thomas P, Tarte K. The yin and the yang of follicular lymphoma cell niches: role of microenvironment heterogeneity and plasticity. *Semin Cancer Biol*. 2014;24:23-32.
- de Jong D, Koster A, Hagenbeek A, et al. Impact of the tumor microenvironment on prognosis in follicular lymphoma is dependent on specific treatment protocols. *Haematologica*. 2009;94(1):70-77.
- Farinha P, Al-Tourah A, Gill K, Klasa R, Connors JM, Gascoyne RD. The architectural pattern of FOXP3-positive T-cells in follicular lymphoma is an independent predictor of survival and histologic transformation. *Blood*. 2010;115(2):289-295.
- Farinha P, Masoudi H, Skinnider BF, et al. Analysis of multiple biomarkers shows that lymphoma-associated macrophage (LAM) content is an independent predictor of survival in follicular lymphoma (FL). *Blood*. 2005;106(6):2169-2174.
- Dave SS, Wright G, Tan B, et al. Prediction of survival in follicular lymphoma based on molecular features of tumor-infiltrating immune cells. *N Engl J Med*. 2004;351(21):2159-2169.
- Glas AM, Knoops L, Delahaye L, et al. Gene-expression and immunohistochemical study of specific T-cell subsets and accessory cell types in the transformation and prognosis of follicular lymphoma. *J Clin Oncol*. 2007;25(4):390-398.
- Yang ZZ, Novak AJ, Stenson MJ, Witzig TE, Ansell SM. Intratumoral CD4+CD25+ regulatory T-cell-mediated suppression of infiltrating CD4+ T-cells in B-cell non-Hodgkin lymphoma. *Blood*. 2006;107(9):3639-3646.
- Kiaii S, Clear AJ, Ramsay AG, et al. Follicular lymphoma cells induce changes in T-cell gene expression and function: potential impact on survival and risk of transformation. *J Clin Oncol*. 2013;31(21):2654-2661.
- Lee AM, Clear AJ, Calaminici M, et al. Number of CD4+ cells and location of forkhead box protein P3-positive cells in diagnostic follicular lymphoma tissue microarrays correlates with outcome. *J Clin Oncol*. 2006;24(31):5052-5059.
- Wahlin BE, Aggarwal M, Montes-Moreno S, et al. A unifying microenvironment model in follicular lymphoma: outcome is predicted by programmed death-1-positive, regulatory, cytotoxic, and helper T-cells and macrophages. *Clin Cancer Res*. 2010;16(2):637-650.
- Carreras J, Lopez-Guillermo A, Roncador G, et al. High numbers of tumor-infiltrating programmed cell death 1-positive regulatory lymphocytes are associated with improved overall survival in follicular lymphoma. *J Clin Oncol*. 2009;27(9):1470-1476.
- Richendollar BG, Pohlman B, Elson P, Hsi ED. Follicular programmed death 1-positive lymphocytes in the tumor microenvironment are an independent prognostic factor in follicular lymphoma. *Hum Pathol*. 2011;42(4):552-557.
- Rolf J, Bell SE, Kovacs D, et al. Phosphoinositide 3-kinase activity in T-cells regulates the magnitude of the germinal center reaction. *J Immunol*. 2010;185(7):4042-4052.
- King C. New insights into the differentiation and function of T follicular helper cells. *Nat Rev Immunol*. 2009;9(11):757-766.
- Crotty S. T follicular helper cell differentiation, function, and roles in disease. *Immunity*. 2014;41(4):529-542.
- Linterman MA, Liston A, Vinuesa CG. T-follicular helper cell differentiation and the co-option of this pathway by non-helper cells. *Immunol Rev*. 2012;247(1):143-159.
- Fazilleau N, Mark L, McHeyzer-Williams LJ, McHeyzer-Williams MG. Follicular helper T-cells: lineage and location. *Immunity*. 2009;30(3):324-335.
- Yu D, Rao S, Tsai LM, et al. The transcriptional repressor BCL6 directs T follicular helper cell lineage commitment. *Immunity*. 2009;31(3):457-468.
- Allen CD, Okada T, Cyster JG. Germinal-center organization and cellular dynamics. *Immunity*. 2007;27(2):190-202.
- Pangault C, Ame-Thomas P, Ruminy P, et al. Follicular lymphoma cell niche: identification of a preeminent IL-4-dependent T(FH)-B cell axis. *Leukemia*. 2010;24(12):2080-2089.
- Ame-Thomas P, Le Priol J, Yssel H, et al. Characterization of intratumoral follicular helper T-cells in follicular lymphoma: role in the survival of malignant B cells. *Leukemia*. 2012;26(5):1053-1063.
- Yang ZZ, Grote DM, Ziesmer SC, Xiu B, Novak AJ, Ansell SM. PD-1 expression defines two distinct T-cell sub-populations in follicular lymphoma that differentially impact patient survival. *Blood Cancer J*. 2015;5:e281.
- Ame-Thomas P, Hoeller S, Artchounin C, et al. CD10 delineates a subset of human IL-4 producing follicular helper T-cells involved in the survival of follicular lymphoma B cells. *Blood*. 2015;125(15):2381-2385.
- Pandey S, Mourcin F, Marchand T, et al. IL-4/CXCL12 loop is a key regulator of lymphoid stroma function in follicular lymphoma. *Blood*. 2017;129(18):2507-2518.
- Ansell SM, Lesokhin AM, Borrello I, et al. PD-1 blockade with nivolumab in relapsed or refractory Hodgkin's lymphoma. *N Engl J Med*. 2015;372(4):311-319.
- Hawkes EA, Grigg A, Chong G. Programmed cell death-1 inhibition in lymphoma. *Lancet Oncol*. 2015;16(5):e234-245.
- Westin JR, Chu F, Zhang M, et al. Safety and activity of PD1 blockade by pidilizumab in combination with rituximab in patients with relapsed follicular lymphoma: a single group, open-label, phase 2 trial. *Lancet Oncol*. 2014;15(1):69-77.
- Gopal AK, Kahl BS, de Vos S, et al. PI3Kdelta inhibition by idelalisib in patients with relapsed indolent lymphoma. *N Engl J Med*. 2014;370(11):1008-1018.
- Robins HS, Campregher PV, Srivastava SK, et al. Comprehensive assessment of T-cell receptor beta-chain diversity in alphabeta T-cells. *Blood*. 2009;114(19):4099-4107.
- Yousfi Monod M, Giudicelli V, Chaume D, Lefranc MP. IMGT/Junction Analysis: the first tool for the analysis of the immunoglobulin and T-cell receptor complex V-J and V-D-J JUNCTIONS. *Bioinformatics*. 2004;20 Suppl 1:i379-385.
- Haynes NM, Allen CDC, Lesley R, Ansel KM, Killeen N, Cyster JG. Role of CXCR5 and CCR7 in follicular Th cell positioning and appearance of a programmed cell death gene-1 high germinal center-associated subpopulation. *J Immunol*. 2007;179(8):5099-5108.
- Andorsky DJ, Yamada RE, Said J, Pinkus GS, Betting DJ, Timmerman JM. Programmed death ligand 1 is expressed by non-hodgkin lymphomas and inhibits the activity of tumor-associated T-cells. *Clin Cancer Res*. 2011;17(13):4232-4424.
- Kupfer A, Kupfer H. Imaging immune cell interactions and functions: SMACs and the Immunological Synapse. *Semin Immunol*. 2003;15(6):295-300.
- Sherwood AM, Emerson RO, Scherer D, et al. Tumor-infiltrating lymphocytes in colorectal tumors display a diversity of T-cell receptor sequences that differ from the T-cells in adjacent mucosal tissue. *Cancer Immunol Immunother*. 2013;62(9):1453-1461.
- Nazarov VI, Pogorelyy MV, Komech EA, et al. TcR: an R package for T-cell receptor repertoire advanced data analysis. *BMC Bioinformatics*. 2015;16:175.
- Myklebust JH, Irish JM, Brody J, et al. High PD-1 expression and suppressed cytokine signaling distinguish T-cells infiltrating follicular lymphoma tumors from peripheral T-cells. *Blood*. 2013;121(8):1367-1376.
- Victoria GD, Nussenzweig MC. Germinal centers. *Annu Rev Immunol*. 2012;30:429-457.
- Ramsay AG, Clear AJ, Kelly G, et al. Follicular lymphoma cells induce T-cell immunologic synapse dysfunction that can be repaired with lenalidomide: implications for the tumor microenvironment and immunotherapy. *Blood*. 2009;114(21):4713-4720.
- Barcia C, Thomas CE, Curtin JF, et al. In vivo mature immunological synapses forming SMACs mediate clearance of virally infected astrocytes from the brain. *J Exp Med*. 2006;203(9):2095-2107.
- Pasqualucci L, Bhagat G, Jankovic M, et al. AID is required for germinal center-derived lymphomagenesis. *Nat Genet*. 2008;40(1):108-112.
- Pasqualucci L, Khiabanian H, Fangazio M, et al. Genetics of follicular lymphoma transformation. *Cell Rep*. 2014;6(1):130-140.
- Best K, Oakes T, Heather JM, Shawe-Taylor J, Chain B. Computational analysis of stochastic heterogeneity in PCR amplification efficiency revealed by single molecule barcoding. *Sci Rep*. 2015;5:14629.



Ferrata Storti Foundation

KMT2D mutations and TP53 disruptions are poor prognostic biomarkers in mantle cell lymphoma receiving high-dose therapy: a FIL study

Simone Ferrero,^{1,2*} Davide Rossi,^{3,4*} Andrea Rinaldi,^{4*} Alessio Brusca, ⁴ Valeria Spina,⁴ Christian W. Eskelund,^{5,6} Andrea Evangelista,⁷ Riccardo Moia,⁸ Ivo Kwee,^{4,9,10} Christina Dahl,¹¹ Alice Di Rocco,¹² Vittorio Stefoni,¹³ Fary Diop,⁸ Chiara Favini,⁸ Paola Ghione,¹ Abdurraouf Mokhtar Mahmoud,⁸ Mattia Schipani,⁸ Arne Kolstad,¹⁴ Daniela Barbero,¹ Domenico Novero,¹⁵ Marco Paulli,¹⁶ Alberto Zamò,^{17,18} Mats Jerkeman,¹⁹ Maria Gomes da Silva,²⁰ Armando Santoro,²¹ Annalia Molinari,²² Andres Ferreri,²³ Kirsten Grønbaek,^{5,6} Andrea Piccin,²⁴ Sergio Cortelazzo,²⁵ Francesco Bertoni,^{4#} Marco Ladetto^{26#} and Gianluca Gaidano^{8#}

¹Department of Molecular Biotechnologies and Health Sciences - Hematology Division, Università di Torino, Torino, Italy; ²Hematology Division, AOU Città della Salute e della Scienza di Torino, Torino, Italy; ³Hematology, Oncology Institute of Southern Switzerland, Bellinzona, Switzerland; ⁴Università della Svizzera italiana, Institute of Oncology Research, Bellinzona, Switzerland; ⁵Department of Hematology, Rigshospitalet, Copenhagen, Denmark; ⁶Biotech Research and Innovation Centre, Copenhagen, Denmark; ⁷Clinical Epidemiology, Città della Salute e della Scienza and CPO Piemonte, Torino, Italy; ⁸Division of Hematology, Department of Translational Medicine, University of Eastern Piedmont, Novara, Italy; ⁹Swiss Institute of Bioinformatics (SIB), Lausanne, Switzerland; ¹⁰Dalle Molle Institute for Artificial Intelligence (IDSIA), Manno, Switzerland; ¹¹Danish Cancer Society Research Center, Copenhagen, Denmark; ¹²Department of Cellular Biotechnologies and Hematology, Policlinico Umberto I, "Sapienza" University of Rome, Roma, Italy; ¹³Institute of Hematology "L. e A. Seràgnoli", University of Bologna, Bologna, Italy; ¹⁴Department of Oncology, Oslo University Hospital, Oslo, Norway; ¹⁵First Unit of Pathology, AOU Città della Salute e della Scienza di Torino, Torino, Italy; ¹⁶Unit of Anatomic Pathology, Department of Molecular Medicine, Fondazione IRCCS Policlinico San Matteo and Università degli Studi di Pavia, Pavia, Italy; ¹⁷Department of Oncology, Università di Torino, Torino, Italy; ¹⁸Department of Diagnostics and Public Health, University of Verona, Verona, Italy; ¹⁹Department of Oncology, Lund University Hospital, Lund, Sweden; ²⁰Department of Hematology, Instituto Português de Oncologia de Lisboa, Lisboa, Portugal; ²¹Humanitas Cancer Center, Humanitas Clinical and Research Center, Rozzano, Italy; ²²Hematology, Ospedale degli Infermi, Rimini, Italy; ²³Lymphoma Unit, Department of Onco-Haematology, IRCCS San Raffaele Scientific Institute, Milano, Italy; ²⁴Department of Hematology, Ospedale Generale, Bolzano, Italy; ²⁵Oncology Unit, Humanitas/Gavazzeni Clinic, Bergamo, Italy and ²⁶SC Ematologia, Azienda Ospedaliera Santi Antonio e Biagio e Cesare Arrigo, Alessandria, Italy

*SF, DR and AR contributed equally as co-first authors.

#FB, ML and GG contributed equally as co-senior authors.

Haematologica 2020
Volume 105(6):1604-1612

Correspondence:

SIMONE FERRERO
simone.ferrero@unito.it

Received: December 24, 2018.

Accepted: September 19, 2019.

Pre-published: September 19, 2019.

doi:10.3324/haematol.2018.214056

Check the online version for the most updated information on this article, online supplements, and information on authorship & disclosures: www.haematologica.org/content/105/6/1604

©2020 Ferrata Storti Foundation

Material published in Haematologica is covered by copyright. All rights are reserved to the Ferrata Storti Foundation. Use of published material is allowed under the following terms and conditions:

<https://creativecommons.org/licenses/by-nc/4.0/legalcode>.

Copies of published material are allowed for personal or internal use. Sharing published material for non-commercial purposes is subject to the following conditions:

<https://creativecommons.org/licenses/by-nc/4.0/legalcode>, sect. 3. Reproducing and sharing published material for commercial purposes is not allowed without permission in writing from the publisher.



ABSTRACT

In recent years, the outcome of mantle cell lymphoma (MCL) has improved, especially in younger patients, receiving cytarabine-containing chemoimmunotherapy and autologous stem cell transplantation. Nevertheless, a proportion of MCL patients still experience early failure. To identify biomarkers anticipating failure of intensive chemotherapy in MCL, we performed target resequencing and DNA profiling of purified tumor samples collected from patients enrolled in the prospective *FIL-MCL0208 phase 3 trial* (high-dose chemoimmunotherapy followed by autologous transplantation and randomized lenalidomide maintenance). Mutations of *KMT2D* and disruption of *TP53* by deletion or mutation associated with an increased risk of progression and death, both in univariate and multivariate analysis. By adding *KMT2D* mutations and *TP53* disruption to the MIPI-c backbone, we derived a new prognostic index, the “MIPI-genetic” (“MIPI-

g"). The "MIPI-g" improved the model discrimination ability compared to the MIPI-c alone, defining three risk groups: i) low-risk patients (4-year progression free survival and overall survival of 72.0% and 94.5%); ii) intermediate-risk patients (4-year progression free survival and overall survival of 42.2% and 65.8%) and iii) high-risk patients (4-year progression free survival and overall survival of 11.5% and 44.9%). Our results: i) confirm that *TP53* disruption identifies a high-risk population characterized by poor sensitivity to conventional or intensified chemotherapy; ii) provide the pivotal evidence that patients harboring *KMT2D* mutations share the same poor outcome as patients harboring *TP53* disruption; and iii) allow to develop a tool for the identification of high-risk MCL patients for whom novel therapeutic strategies need to be investigated. (Trial registered at clinicaltrials.gov identifier: NCT02354313).

Introduction

The introduction of high dose cytarabine-containing chemoimmunotherapeutic regimens and autologous transplantation (ASCT) have considerably improved the outcome of young fit mantle cell lymphoma (MCL) patients. Nonetheless, approximately 20-25% of MCL patients demonstrate inadequate efficacy of intensified chemoimmunotherapy as they are either primary refractory or relapse within 2 years from ASCT.¹⁻⁵

Clinical and pathological scores, including the MCL international prognostic index (MIPI),⁶ the Ki-67 proliferative index,⁷ and their combination in the MIPI-c score, stratify MCL patients in groups at different risk of relapse.⁸ However, none of these tools has sufficient positive predictive value to trigger the development of tailored schedules specifically designed for high risk patients.⁹

Several recurrent mutations have been described in MCL, affecting DNA repair genes and cell cycle regulators (*TP53*, *ATM*, *CCND1*), epigenetic regulation genes (*KMT2D*, *WHSC1*) and cell-signaling pathways genes (*NOTCH1-2*, *BIRC3*, *TRAF2*).¹⁰⁻¹² The proof of principle that MCL genetics can impact on disease outcome stems from studies that have focused on the *TP53* tumor suppressor gene, including both mutations and 17p deletions.¹³⁻¹⁷

We prospectively assessed the clinical impact of a panel of genomic alterations in a cohort of young MCL patients treated with high dose chemoimmunotherapy and ASCT from the Fondazione Italiana Linfomi (FIL) MCL0208 phase 3 trial.¹⁸ The results document that *KMT2D* mutations associate with poor outcome in MCL and, along with *TP53* mutations and 17p deletions, might be integrated in a new prognostic score to segregate a subgroup of patients who obtain minimal or no benefit from intensive chemoimmunotherapy. The prognostic score was validated in an independent series of cases.

Methods

Patients series

The FIL-MCL0208 (NCT02354313) is a phase 3, multicenter, open-label, randomized, controlled study, designed to determine the efficacy of lenalidomide as maintenance *versus* observation in young (18-65 years old), fit, advanced stage (Ann arbor II-IV) MCL patients after first line intensified and high-dose chemoimmunotherapy followed by ASCT. Cases of non-nodal MCL were excluded.¹⁹ The clinical trial, as well as the ancillary mutational study, were approved by the Ethical Committees of all the enrolling Centers. All patients provided written informed consent for the use of their biological samples for research purposes, in

accordance with Institutional Review Boards requirements and the Helsinki's declaration. Clinical results of the first interim analysis of the trial were already presented.¹⁸ Further information are supplied in the *Online Supplementary Materials and Methods*.

Biological samples

Tumor cells were sorted from the baseline bone marrow (BM) samples by immunomagnetic beads (CD19 MicroBeads, human-Miltenyi Biotec GmbH, Bergisch Gladbach, Germany) and stocked as dry pellets.

Tumor DNA was extracted according to DNAzol protocol (Life Technologies). Germline DNA was obtained from peripheral blood (PB) mononuclear cells collected under treatment and proven to be tumor free by minimal residual disease (MRD) analysis. Further information are supplied in the *Online Supplementary Materials and Methods*.

Next generation sequencing (NGS)

A targeted resequencing panel (target region: 37'821 bp) (*Online Supplementary Table S1*) including the coding exons and splice sites of seven genes (*ATM*, *TP53*, *CCND1*, *WHSC1*, *KMT2D*, *NOTCH1* exon 34, *BIRC3*) that are recurrently mutated in $\geq 5\%$ of MCL tumors was specifically designed.¹⁰⁻¹² We also included in the panel *TRAF2*²⁰ and *CXCR4*.²¹ NGS libraries preparation was performed using TruSeq Custom Amplicon sequencing assay according to manufacturer's protocol (Illumina, Inc., San Diego, CA, USA). Multiplexed libraries (n=48 per run) were sequenced using 300-bp paired-end runs on an Illumina MiSeq sequencer, (median depth of coverage 2,356x). A robust and previously validated bioinformatics pipeline was used for variant calling (*Online Supplementary Materials and Methods*). Copy number variation analysis methods^{22,23} are supplied in the *Online Supplementary Materials and Methods*.

MRD analysis

For MRD purposes, MCL diagnostic BM and PB samples were investigated for immunoglobulin heavy chain (IGH) gene rearrangements and *BCL1/IGH* MTC by qualitative PCR.²⁴⁻²⁶ Both BM and PB samples were analyzed for MRD at specific time points during and after treatment. Further information are supplied in the *Online Supplementary Materials and Methods*.

Statistical analysis

The primary outcome of the clinical study was progression-free survival (PFS) and secondary outcomes included overall survival (OS).²⁷ The adjusted effects of mutations and exposure variables (MIPI-c and blastoid variant) on PFS and OS were estimated by Cox regression. To compare clinical baseline features between patients enrolled in the molecular study and patients not included in the analysis, we used Mann-Whitney test for continuous variables and Pearson's χ^2 test for categorical variables. Statistical analyses were performed using Stata 13.0 and R 3.4.1. Further information are supplied in the *Online Supplementary Materials and Methods*.

Validation set

The Nordic Lymphoma Group MCL2 and MCL3, phase 2, prospective trials¹⁷ were used for independent validation of our findings. In particular, the raw sequencing data of the study by Eskelund *et al.* were reanalyzed according to our bioinformatics pipeline (detailed before), to get a uniform mutation calling.

Results

Patients characteristics

Out of the 300 patients enrolled in the FIL-MCL0208 clinical trial, 186 (62%) were provided with CD19⁺ sorted tumor cells from the BM and were evaluable for both mutations and copy number abnormalities. Moreover, four more patients were provided with the copy number

abnormalities data only. Baseline features of the cases included in the molecular study overlapped with those cases not included in the molecular analysis because of a lack of tumor material in the BM aspirates. As expected, tumor cells were obtained more frequently in cases with BM infiltration documented by morphological or flow-cytometry analysis (Table 1). Overall, this observation did not introduce a selection bias, since cases evaluable for genomic studies showed a similar outcome to cases not analyzed, both in terms of PFS and OS (*Online Supplementary Figure S1*).

Description of genomic alterations

At least one somatic non-synonymous mutation affecting genes of the target region was observed in 69.8% of patients (130 of 186) (Figure 1, *Online Supplementary Figure*

Table 1. Clinical and biological baseline characteristics of the patients included and not included in the molecular analysis.

Characteristics	Patients analysed for mutations and/or CNV (n=190)	Patients not analysed for mutations and CNV (n=110)	P
Median age	57	58	0.987
Sex			0.090
Female	47 (24.7%)	18 (16.4%)	
Male	143 (75.3%)	92 (83.6%)	
Ki-67			0.210
<30%	126 (71.6%)	61 (64.2%)	
≥30%	50 (28.4%)	34 (35.8%)	
Median WBC	74500/uL	75000/uL	0.567
ECOG			0.722
0	144 (75.8%)	87 (79.2%)	
1	40 (21.1%)	19 (17.3%)	
2	6 (3.2%)	4 (3.6%)	
Median LDH	275.5 UI/L	298	0.848
Risk class MIPI			0.562
Low	114 (60.0%)	66 (60.0%)	
Intermediate	49 (25.8%)	24 (21.8%)	
High	27 (14.2%)	20 (18.2%)	
Risk class MIPI-c			0.685
Low	88 (50.0%)	45 (47.4%)	
Low-Intermediate	49 (27.8%)	30 (31.6%)	
Intermediate/High	25 (14.2%)	10 (10.5%)	
High	14 (8.0%)	10 (10.5%)	
BM invasion			<0.001
No	26 (13.9%)	37 (33.9%)	
Yes	161 (86.1%)	72 (66.1%)	
Median BM invasion by flow (%)	10%	0.8%	<0.0001
Histology			0.842
MCL Classic	174 (91.6%)	100 (90.9%)	
MCL blastoid variant	16 (8.4%)	10 (9.1%)	
Bulky mass			0.315
No	124 (65.3%)	78 (70.9%)	
Yes	66 (34.7%)	32 (29.1%)	

CNV: copy number variation analysis; WBC: white blood cells; ECOG: Eastern Cooperative Oncology Group; LDH: lactate dehydrogenase; MIPI: mantle cell international prognostic index; MIPI-c: combined MIPI; BM: bone marrow; MCL: mantle cell lymphoma.

S2 and Online Supplementary Table S2). Mutated genes were ATM (41.9%), followed by WHSC1 (15.6%), KMT2D (12.4%), CCND1 (11.8%), TP53 (8.1%), NOTCH1 (7.5%), BIRC3 (5.9%) and TRAF2 (1.1%). KMT2D deletion occurred in 1.6% of patients (3 of 190) and TP53 deletion in 13.2% patients (25 of 190). TP53 was inactivated by mutations or deletions in 31 of 186 (16.6%) cases, including 8 of 186 (4.3%) mutated/deleted cases, 16 of 186 (8.6%) deleted but not mutated cases, and 7 of 186 (3.7%) mutated but not deleted cases. KMT2D was inactivated by mutations or deletions in 25 of 186 (13.4%) cases, including 1 of 186 (<1%) mutated/deleted case, 2 of 186 (<1%) deleted but non mutated cases, and 22 of 186 (11.8%) mutated but not deleted cases.

KMT2D mutations and TP53 disruption associate with poor outcome in MCL

By univariate analysis, mutations of KMT2D were associated with poor clinical outcome in terms of both PFS and OS. At 4 years, the PFS of KMT2D mutated patients was 33.2% versus 63.7% (P<0.001) in wild-type (WT) cases (Figure 2A). The OS of KMT2D mutated patients was 62.3% versus 86.8% (P=0.002) in WT patients (Figure 2B). Consistent with previous reports, both TP53 mutations and deletion associated with shorter PFS and OS at 4 years (Figure 2C-D and Figure 3). In detail, the negative prognostic impact for TP53 disruption was equal for all the three inactivation modalities, which were then considered as a single group for further analyses (Online Supplementary Figure S3). No further survival analysis was performed on KMT2D deletions, given the low frequency of this genetic lesion. All the other investigated mutations did not show a strong association with PFS or OS (Online Supplementary Figure S4-6 and Online Supplementary Table S3).

Patients harboring TP53 disruption were significantly enriched in known high-risk features of MCL. Indeed, 48.3% of the TP53 disrupted patients had Ki-67 ≥30%, 37.9% scored in the higher MIPI-c risk classes (i.e. “intermediate-high” and “high”), and 22.6% showed blastoid

morphology. Conversely, 45.5% of cases harboring KMT2D mutations scored in the higher MIPI-c risk classes but did not associate with Ki-67 expression or blastoid morphology (Online Supplementary Table S4). Moreover, KMT2D mutated patients showed slightly higher beta-2 microglobulin (B2M) median values, as well as higher prevalence of B symptoms and bulky disease (>5 cm) than WT patients (all P<0.05). Interestingly, also TP53 disrupted patients showed slightly higher B2M median values (P<0.05) than WT patients (Online Supplementary Table S4) and were associated with a high rate of disease progression during treatment (9 of 31 patients, 29%). Moreover, TP53 disrupted patients reached lower levels of MRD negativity after ASCT, if compared with WT ones: 35% versus 58% in BM (P=0.06) and 58% versus 80% in PB (P=0.04), respectively. Similar trends were seen for KMT2D mutated patients (46% vs. 55% in BM and 58% vs. 79%), albeit not statistically significant (Online Supplementary Table S5). Analogous to the Nordic Lymphoma Group MCL2 and MCL3 trials,¹⁷ also in our study morphological BM involvement was significantly associated with the presence of mutations in any of the genes analysed (P<0.05). However, both TP53 disruptions and KMT2D mutations were equally distributed in patients with and without BM involvement (P=0.26 and P=0.32, respectively).

By multivariate analysis adjusted for the validated risk factors MIPI-c and blastoid variant, both KMT2D mutations and TP53 disruptions maintained an independent increased hazard of progression and death (Table 2 and Online Supplementary Table S6). Patients carrying at least one of these genetic lesions, namely KMT2D mutations, TP53 mutations or deletion (n=49/186, 26.3%), had a 4-year PFS of 32.0% versus 69.9% of WT patients (P<0.0001) and a 4-year OS of 65.1% versus 90.3% (P<0.0001), respectively (Figure 4).

Integration of a genetic score into the MIPI-c: the “MIPI-g” model

In order to integrate the clinical impact of KMT2D

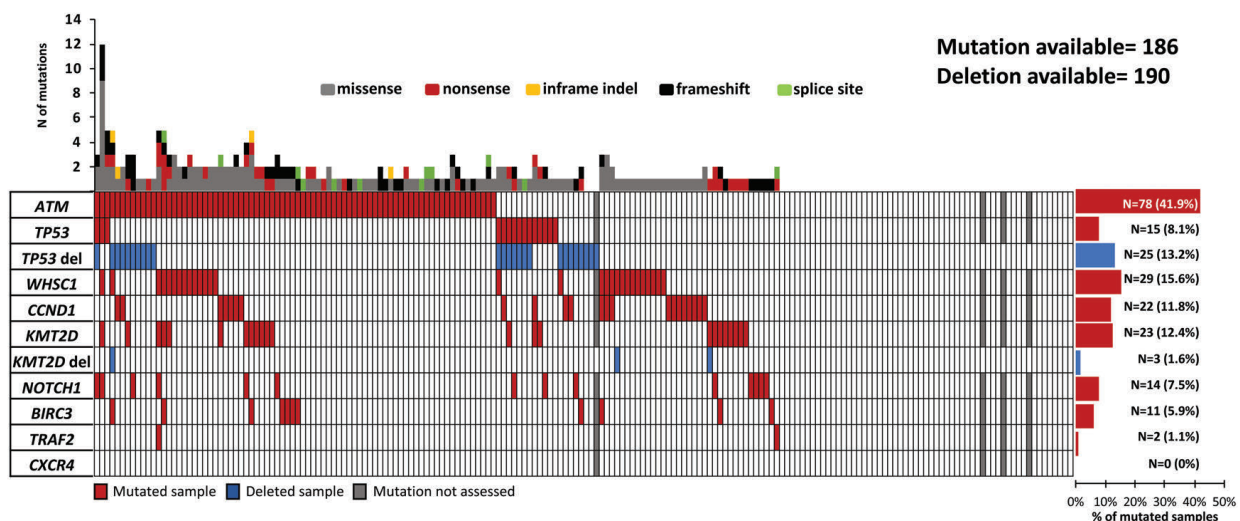


Figure 1. Overview on prevalence and molecular spectrum of non-synonymous somatic mutations discovered in patients' tumor DNA. Heatmap representing the mutational profiles of 186 mantle cell lymphoma (MCL) cases, genotyped on tumor DNA (and four additional patients with copy number abnormalities data only). Each column represents one patient, each row represents one gene. The fraction of patients with mutations in each gene is plotted on the right. The number of aberrations in a given patient is plotted above the heatmap.

mutations and *TP53* disruptions into the MIPI-c prognostic index (complete data available for 172 patients), we assigned a score to each of the single variables, based on the multivariate Cox regression analysis. MIPI-c low, low-intermediate and intermediate-high risk classes scored 0 points, MIPI-c high-risk class scored 1 point, while *KMT2D* mutations as well as *TP53* disruption scored 2 points (Table 3). Patients were then grouped into three risk classes, according to their total score, in the “MIPI-g” index, namely: i) 0 points, low risk group (LR 121 patients, 70.3%); ii) 1-2 points, intermediate risk group (IR 38 patients, 22.1%); iii) ≥ 3 points, high risk group (HR 13 patients, 7.6%). PFS and OS at 4-years for low-, intermediate-, and high-risk groups were 72.0%, 42.2%, 11.5% ($P < 0.0001$) and 94.5%, 65.8%, 44.9% ($P < 0.0001$), respectively (Figure 5). The MIPI-g index improved the model discrimination ability, with a C-statistics of 0.675 for PFS (bootstrapping corrected 0.654) and 0.776 for OS (bootstrapping corrected 0.747), as compared to MIPI-c alone (C-statistics 0.592 and 0.7, respectively).

Validation set

Most *KMT2D* variants considered in the Nordic study have been removed by our mutational calling, since these were missense variants not reported in COSMIC. At the end of the re-analysis, from the original 28 mutations, 21

were excluded. Two previously unrecognized frameshift mutations have been identified by our bioinformatics pipeline, overall accounting for a total of nine *KMT2D* mutations (all disrupting, as expected for *KMT2D*) in the Nordic validation series. In the Nordic validation series, *KMT2D* mutated patients showed a similar increased risk for OS, with a median OS of 12.7 years (95% confidence interval [CI] not evaluable) for WT *versus* 8.4 (95% CI: 0-17.6) for mutated cases. The Nordic validation series also replicated the MIPI-g score. The re-analysis of *TP53* mutations confirmed the original data of Eskelund *et al.*, with median OS of 12.7 (95% CI not evaluable) for WT cases and 2.0 years (95% CI: 1.2-2-8) for mutated cases. Consistently, also the MIPI-g validation on the Nordic series showed similar results: 4-year OS for LR (n=103), IR (n=36) and HR (n=13) MIPI-g groups were 91.3%, 72.2%, 15.4%.

Discussion

To identify new molecular predictors in MCL, we performed targeted resequencing and DNA profiling of purified tumor samples collected from young patients enrolled in the ASCT-based prospective FIL-MCL0208 phase 3 trial (NCT02354313). Our study documents that: i) *KMT2D*

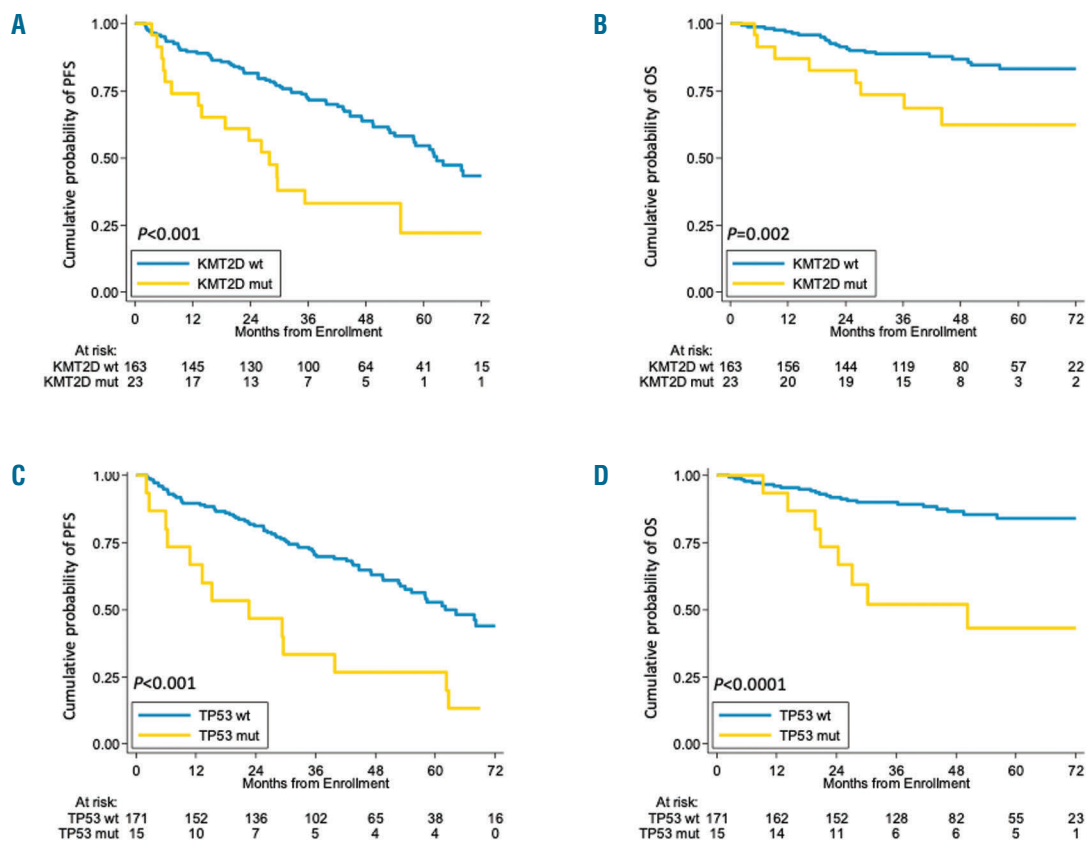


Figure 2. Prognostic impact of *KMT2D* and *TP53* mutations. Kaplan-Meier estimates of progression free survival and overall survival of *KMT2D* (A, B), and *TP53* (C, D) mutated versus wild-type (WT) patients. Cases harboring mutations (mut) in these genes are represented by the yellow line. Cases WT for these genes are represented by the blue line. The Log-rank statistics *P*-values are indicated adjacent curves.

mutations are a novel, independent, adverse genetic biomarker in MCL, impacting both on PFS and OS (Figure 2A-B); ii) TP53 disruptions (both mutations and deletion) prospectively confirm their adverse prognostic value in young MCL patients receiving high-dose chemo-immunotherapy followed by ASCT, both in terms of PFS and OS (Figures 2C-D and Figure 3); iii) identification of either KMT2D mutations or TP53 disruption (or both) defines a HR group of young MCL patients whose outcome is still not satisfactory despite intensive immunochemotherapy and ASCT (Figure 4); iv) these biomarkers may be incorporated into a “MIPI-g” model, accounting for three risk classes (Figure 5), that improves the C-statistics discrimination ability on survival, if compared to MIPI-c alone.

The adverse prognostic value of TP53 mutations in MCL has been already observed in some retrospective series,¹³⁻¹⁷ and has been recently confirmed in a combined series from two, ASCT-based, phase 2 trials of the Nordic Lymphoma Group.¹⁷ TP53 deletions impacted on both PFS

and OS in the randomized, phase 3 European MCL Network “Younger” trial,¹⁶ while these data were not confirmed by multivariate analysis in the Nordic study, due to the high association with TP53 mutations.¹⁷ Our prospective study performed in a similar patient population of young MCL patients demonstrates that the presence of either TP53 mutations or deletions or both associates with poor prognosis. Importantly, although TP53 aberrations associated with elevated Ki-67, higher MIPI-c classes and blastoid morphology, their impact on survival was independent of these known risk factors. Moreover, TP53 disrupted patients show higher levels of MRD positivity after ASCT, as described in the *Online Supplementary Table S5*. Finally, some previous studies reported also a negative impact of NOTCH1 mutations in univariate analysis,^{10,17} however in our cohort these mutations were not an independent predictor of survival, as most of them co-occurred with TP53 mutations.

In the FIL-MCL0208 trial, KMT2D mutations emerged as a novel biomarker heralding chemo-immunotherapy

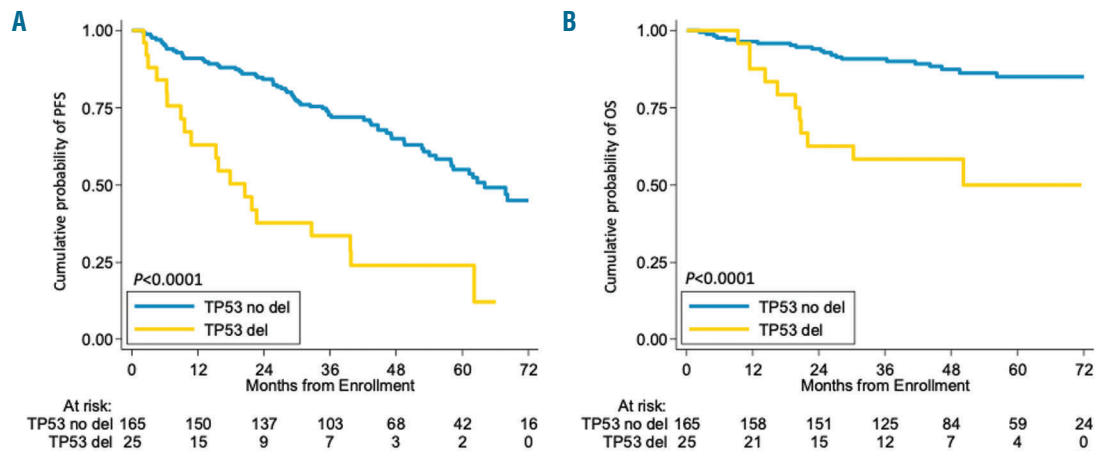


Figure 3. Prognostic impact of TP53 deletion. Kaplan-Meier estimates of progression free survival (PFS) (A) and overall survival (OS) (B) of TP53 deleted versus wild-type patients. Cases with TP53 deletion are represented by the yellow line. Cases without TP53 (del) deletion are represented by the blue line. The Log-rank statistics P-values are indicated adjacent curves.

Table 2. Univariate and multivariate Cox-regression analysis in terms of progression free survival and overall survival.

Genes	Progression free survival						Overall survival					
	Univariate			Multivariate (MIPI-c and blastoid variant adjusted)			Univariate			Multivariate (MIPI-c and blastoid variant adjusted)		
	HR	95% CI	P	HR	95% CI	P	HR	95% CI	P	HR	95% CI	P
ATM mut	1.29	0.84-1.97	0.245	1.19	0.77-1.83	0.432	1.52	0.62-2.51	0.527	1.05	0.52-2.12	0.887
WHSC1 mut	1.53	0.90-2.60	0.119	1.51	0.87-2.61	0.140	0.85	0.30-2.41	0.755	0.741	0.25-2.15	0.581
CCND1 mut	0.83	0.41-1.66	0.595	0.94	0.46-1.92	0.860	0.75	0.23-2.48	0.643	1.01	0.29-3.53	0.980
KMT2D mut	2.59	1.50-4.48	0.001	2.74	1.55-4.84	0.001	3.20	1.48-6.92	0.003	2.48	1.12-5.46	0.024
TP53 mut	2.84	1.57-5.13	0.001	2.55	1.36-4.78	0.003	5.28	2.44-11.45	<0.0001	2.78	1.09-7.06	0.032
NOTCH1 mut	1.86	0.93-3.72	0.078	1.57	0.76-3.24	0.226	1.34	0.41-4.40	0.629	0.61	0.17-2.12	0.609
BIRC3 mut	0.88	0.32-2.41	0.807	0.70	0.25-1.96	0.500	1.84	0.56-6.08	0.315	1.15	0.33-3.98	0.822
TP53 del	3.51	2.09-5.88	<0.0001	3.13	1.73-5.68	<0.001	4.46	2.14-9.29	<0.0001	2.65	1.06-6.59	0.036
TP53 dis	3.39	2.10-5.45	<0.0001	3.17	1.87-5.38	<0.0001	4.26	2.09-8.67	<0.0001	2.65	1.10-6.37	0.030

Del: deleted; dis: disrupted; HR: hazard ratio; CI: confidence interval.

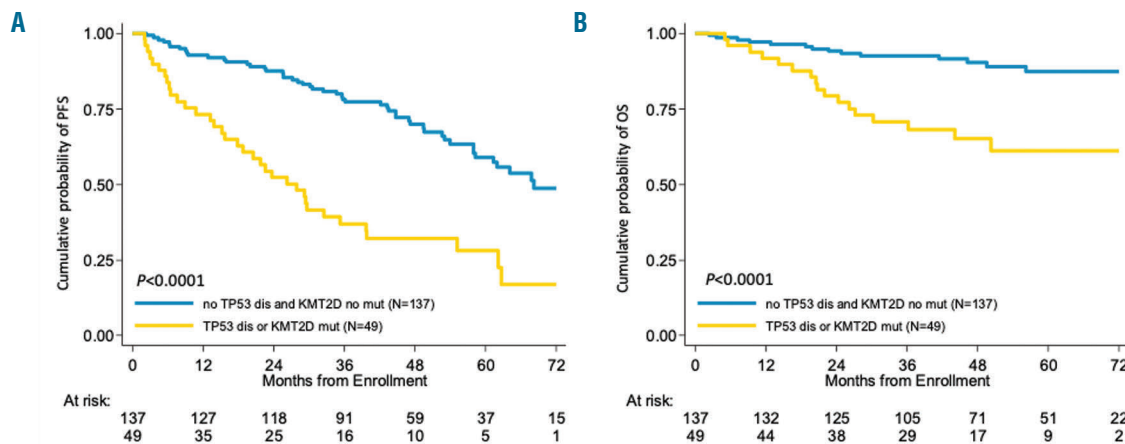


Figure 4. Prognostic impact of combined *KMT2D* mutations and *TP53* disruption. Kaplan-Meier estimates of (A) progression free survival (PFS) and (B) overall survival (OS) of patients harboring *KMT2D* mutations and/or *TP53* disruption (mutations and/or deletions). Cases harboring at least 1 of these 3 genetic lesions are represented by the yellow line. Cases without these genes are represented by the blue line. The Log-rank statistics *P*-values are indicated adjacent curves.

failure, with a predictive value similar to that of *TP53* aberrations. *KMT2D* (lysine methyltransferase 2D), also known as *MLL2*, acts as a tumor suppressor gene mutated in several B-cell lymphoma types, including 10-15% of MCL.²⁸⁻³¹ Even though *KMT2D* mutated patients of the FIL-MCL0208 trial scored in the HR MIPI-c classes, they showed neither elevated Ki-67 nor blastoid morphology, suggesting that *KMT2D* mutations capture high-risk patients not otherwise identifiable through conventional pathologic parameters.

To the best of our knowledge, the adverse impact on cancer survival of *KMT2D* mutations has not been documented to date. No impact on survival was found for *KMT2D* mutations in the Nordic study.¹⁷ The lack of impact on survival of *KMT2D* mutations in the Nordic MCL series might be related to two main reasons. First, in the Nordic series, most *KMT2D* mutations were missense sequence variants (15 of 28) not reported as somatic variants in the COSMIC database, and therefore not fulfilling the criteria of “true” mutations. Conversely, in our series 74% of *KMT2D* mutations were protein truncating events, as expected.²⁸⁻³¹ Second, since Eskelund *et al.* performed mutational analysis in unsorted BM samples, the low or absent tumor content of many cases might lead to underestimate²⁸ “true” mutations. By applying our bioinformatics pipeline to the raw sequencing data of the MCL2 and MCL3 Nordic Lymphoma Group trials, we validated the poor prognostic role of *KMT2D* mutations in an independent prospective cohort.

The independent adverse prognostic value of *TP53* and *KMT2D* aberrations prompted us to integrate the molecular results into the MIPI-c,⁸ aiming at further improving its ability to discriminate high-risk patients. The “MIPI-g” was able to divide patients into three risk classes, on the basis of a simple score given to each variable (namely: MIPI-c class, *TP53* disruption and *KMT2D* mutations). Patients in the HR “MIPI-g” groups may deserve new treatments, and a simple tool like the MIPI-g might be proposed in a future, “tailored” trial to select HR MCL patients for targeted experimental strategies.

Our study suffers from some limitations. The analyses were performed only on CD19⁺ sorted BM cells and no tis-

Table 3. The MIPI-g score.

Variables	Beta-coefficients	Points
<i>KMT2D</i> mutations	1,035,607	2
<i>TP53</i> disruption	1,113,875	2
MIPI-c		
Low	–	0
Low-Intermediate	–	0
Intermediate-High	–	0
High	0.6847757	1

MIPI-c: combined mantle cell international prognostic index.

sue control is available at the moment; this issue might represent a limit for the extrapolation of the results to lymph-node samples, as across-compartment heterogeneity of the mutational landscape is described in MCL.¹⁰ However, the CD19⁺ selection approach we used, increasing the purity of tumor cells and, consequently, the sensitivity of our mutational approach, ensured that all the analyzed samples are representative of MCL. Therefore, we set a variant allele frequency (VAF) threshold of 10% to call a mutation, accordingly to ERIC guidelines for the mutational analysis of the *TP53* gene in chronic lymphocytic leukemia.³² Although we acknowledge that the present validation relies on a limited number of *KMT2D* mutated patients, we noted that the Nordic trials are currently the only prospective studies with prompt available mutational data, adequate clinical follow-up and similar characteristics (*i.e.* patients age and treatment schedule), to validate our original findings from the FIL-MCL0208 trial.

The impact of lenalidomide maintenance in the FIL-MCL0208 trial on the described genetic aberrations has not been addressed, as complete data on randomization are not available yet. However, it should be noted that due to the high number of progressive diseases in the aberrant *TP53/KMT2D* group, 27 patients have been finally randomized but only nine actually started lenalidomide maintenance. Therefore, it is unlikely that lenalidomide might play a clear role in driving the outcome of these

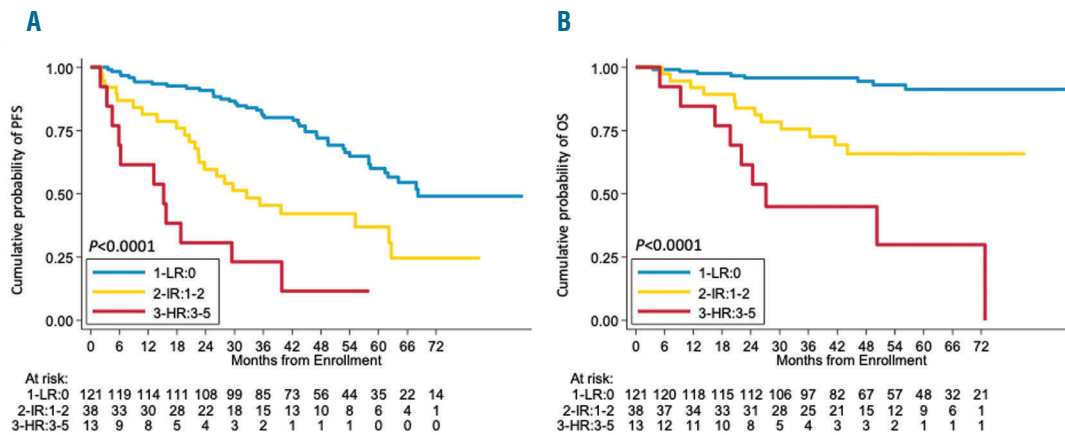


Figure 5. The “MIPI-g” model. Kaplan-Meier estimates of (A) progression free survival (PFS) and (B) overall survival (OS) of patients harboring *KMT2D* mutations and/or *TP53* disruption (mutations and/or deletions) integrated into the MIPI-c. Low MIPI-g risk cases are represented by the blue line, intermediate MIPI-g cases by the yellow line and high MIPI-g cases by the red line. The Log-rank statistics *P*-values are indicated for adjacent curves.

patients and the trial will probably not be able to fully address this issue even with a longer follow-up.

In conclusion, our results show that *KMT2D* mutated and/or *TP53* disrupted younger MCL patients are a HR population, characterized by poor sensitivity even to intensified chemo-immunotherapy. Given the negative prognostic impact of these genetic lesions, they might be used to select HR patients for novel therapeutic approaches that can circumvent these detrimental genetic lesions. As in other lymphoid disorders, novel non-chemotherapeutic strategies specifically designed for HR patients need to be investigated in MCL. Besides the approved drugs lenalidomide and ibrutinib, new molecules such as the BCL-2 inhibitor venetoclax might be very promising for these chemorefractory patients, especially for *TP53* disrupted cases.^{33,34} Moreover, as the majority of *KMT2D* mutated and/or *TP53* disrupted patients of our series actually achieve a response, though short-lasting after ASCT, an alternative consolidation with allogeneic transplantation deserves investigation.

Funding

This work was supported by: Progetto di Rilevante Interesse Nazionale (PRIN2009) from the Ministero Italiano

dell'Università e della Ricerca (MIUR), Roma, Italy [7.07.02.60 AE01]; Progetto di Ricerca Sanitaria Finalizzata 2009 [RF-2009-1469205] and 2010 [RF-2010-2307262 to S.C.], A.O.S. Maurizio, Bolzano/Bozen, Italy; Fondi di Ricerca Locale, Università degli Studi di Torino, Italy; Fondazione Neoplasie Del Sangue (Fo.Ne.Sa), Torino, Italy; Fondazione CRT (project codes: 2016.0677 and 2018.1284), Torino, Italy; Associazione DaRosa, Torino, Italy; Molecular bases of disease dissemination in lymphoid malignancies to optimize curative therapeutic strategies, (5x1,000 No. 21198), Associazione Italiana per la Ricerca sul Cancro Foundation, Milan, Italy; Progetto Ricerca Finalizzata RF-2011-02349712, Ministero della Salute, Rome, Italy; and PRIN 2015ZMRFEA_004, MIUR, Rome, Italy; Partially funded by the AGING Project – Department of Excellence – DIMET, Università del Piemonte Orientale, Novara, Italy; Grant No. KFS-3746-08-2015, Swiss Cancer League, Bern, Switzerland; Grant No. KLS-3636-02-2015, Swiss Cancer League, Bern, Switzerland; Grant No. 320030_169670/1 Swiss National Science Foundation, Berne, Switzerland; iCARE No. 17860, Associazione Italiana per la Ricerca sul Cancro and Unione Europea, Milan, Italy; Fondazione Fidinam, Lugano, Switzerland; Nelia & Amadeo Barletta Foundation, Lausanne, Switzerland; Fondazione Ticinese per la Ricerca sul Cancro, Bellinzona, Switzerland and Novara-AIL Onlus, Novara, Italy.

References

- Eskelund CW, Kolstad A, Jerkeman M, et al. 15-year follow-up of the Second Nordic Mantle Cell Lymphoma trial (MCL2): prolonged remissions without survival plateau. *Br J Haematol.* 2016;175(3):410-418.
- Hermine O, Hoster E, Walewski J, et al. Addition of high-dose cytarabine to immunochemotherapy before autologous stem-cell transplantation in patients aged 65 years or younger with mantle cell lymphoma (MCL Younger): a randomised, open-label, phase 3 trial of the European Mantle Cell Lymphoma Network. *Lancet.* 2016;388(10044):565-575.
- Delarue R, Haioun C, Ribrag V, et al. CHOP and DHAP plus rituximab followed by autologous stem cell transplantation in mantle cell lymphoma: a phase 2 study from the Groupe d'Etude des Lymphomes de l'Adulte. *Blood.* 2013;121(1):48-53.
- Romaguera JE, Fayad LE, Feng L, et al. Ten-year follow-up after intense chemoimmunotherapy with Rituximab-HyperCVAD alternating with Rituximab-high dose methotrexate/cytarabine (R-MA) and without stem cell transplantation in patients with untreated aggressive mantle cell lymphoma. *Br J Haematol.* 2010;150(2):200-208.
- Le Gouill S, Thieblemont C, Oberic L, et al. Rituximab after autologous stem-cell transplantation in mantle-cell lymphoma. *N Engl J Med.* 2017;377(13):1250-1260.
- Hoster E, Dreyling M, Klapper W, et al. A new prognostic index (MIPI) for patients with advanced-stage mantle cell lymphoma. *Blood.* 2008;111(2):558-565.
- Hoster E, Klapper W, Hermine O, et al. Confirmation of the mantle-cell lymphoma International Prognostic Index in randomized trials of the European Mantle-Cell Lymphoma Network. *J Clin Oncol.* 2014;32(13):1338-1346.
- Hoster E, Rosenwald A, Berger F, et al. Prognostic value of Ki-67 index, cytology, and growth pattern in mantle-cell lymphoma: Results from randomized trials of the European mantle cell lymphoma network. *J Clin Oncol.* 2016;34(12):1386-1394.
- Dreyling M, Ferrero SE. The role of targeted treatment in mantle cell lymphoma: Is transplant dead or alive? *Haematologica.* 2016;101(2):104-114.
- Beà S, Valdés-Mas R, Navarro A, et al. Landscape of somatic mutations and clonal

- evolution in mantle cell lymphoma. *Proc Natl Acad Sci U S A*. 2013;110(45):18250-18255.
11. Zhang J, Jima D, Moffitt AB, et al. The genomic landscape of mantle cell lymphoma is related to the epigenetically determined chromatin state of normal B cells. *Blood*. 2014;123(19):2988-2996.
 12. Rahal R, Frick M, Romero R, et al. Pharmacological and genomic profiling identifies NF- κ B-targeted treatment strategies for mantle cell lymphoma. *Nat Med*. 2014;20(1):87-92.
 13. Kumar A, Yang W, Bantilan KS, et al. Prognostic significance of genomic alterations in mantle cell lymphoma. *Blood*. 2016;128(22):4115.
 14. Nordström L, Sembo S, Eden P, et al. SOX11 and TP53 add prognostic information to MIPI in a homogeneously treated cohort of mantle cell lymphoma - a Nordic Lymphoma Group study. *Br J Haematol*. 2014;166(1):98-108.
 15. Halldórsdóttir AM, Lundin A, Murray F, et al. Impact of TP53 mutation and 17p deletion in mantle cell lymphoma. *Leukemia*. 2011;25(12):1904-1908.
 16. Delfau-Larue MH, Klapper W, Berger F, et al. High-dose cytarabine does not overcome the adverse prognostic value of CDKN2A and TP53 deletions in mantle cell lymphoma. *Blood*. 2015;126(5):604-611.
 17. Eskelund CW, Dahl C, Hansen JW, et al. TP53 mutations identify younger mantle cell lymphoma patients who do not benefit from intensive chemioimmunotherapy. *Blood*. 2017;130(17):1903-1910.
 18. Cortelazzo S, Martelli M, Ladetto M, et al. High dose sequential chemotherapy with rituximab and ASCT as first line therapy in adult MCL patients: clinical and molecular response of the MCL0208 trial, a FIL study. *Haematologica*. 2015;100(s1):3-4.
 19. Swerdlow SH, Campo E, Pileri SA, et al. The 2016 revision of the World Health Organization classification of lymphoid neoplasms. *Blood*. 2016;127(20):2375-2390.
 20. Meissner B, Kridel R, Lim RS, et al. The E3 ubiquitin ligase UBR5 is recurrently mutated in mantle cell lymphoma. *Blood*. 2013;121(16):3161-3164.
 21. Roccaro AM, Sacco A, Jimenez C, et al. C1013G/CXCR4 acts as a driver mutation of tumor progression and modulator of drug resistance in lymphoplasmacytic lymphoma. *Blood*. 2014;123(26):4120-4131.
 22. Rinaldi A, Kwee I, Young KH, et al. Genome-wide high resolution DNA profiling of hairy cell leukaemia. *Br J Haematol*. 2013;162(4):566-569.
 23. Kwee IW, Rinaldi A, de Campos CP, et al. Fast and robust segmentation of copy number profiles using multi-scale edge detection. *BioRxiv*. 2016. <https://doi.org/10.1101/056705>.
 24. Voena C, Ladetto M, Astolfi M, et al. A novel nested-PCR strategy for the detection of rearranged immunoglobulin heavy-chain genes in B cell tumors. *Leukemia*. 1997;11(10):1793-1798.
 25. Stamatopoulos K, Kosmas C, Belessi C, et al. Molecular analysis of bcl-1/IgH junctional sequences in mantle cell lymphoma: potential mechanism of the t(11;14) chromosomal translocation. *Br J Haematol*. 1999;105(1):190-197.
 26. Pott C. Minimal residual disease detection in mantle cell lymphoma: technical aspects and clinical relevance. *Semin Hematol*. 2011;48(3):172-184.
 27. Cheson BD, Pfistner B, Juweid ME, et al. Revised response criteria for malignant lymphoma. *J Clin Oncol*. 2007;25(5):579-586.
 28. Froimchuk E, Jang Y, Ge K. Histone H3 lysine 4 methyltransferase KMT2D. *Gene*. 2017;627:337-342.
 29. Varettoni M, Zibellini S, Defrancesco I, et al. Pattern of somatic mutations in patients with Waldenström macroglobulinemia or IgM monoclonal gammopathy of undetermined significance. *Haematologica*. 2017;102(12):2077-2085.
 30. Spina V, Khiabani H, Messina M, et al. The genetics of nodal marginal zone lymphoma. *Blood*. 2016;128(10):1362-1373.
 31. Pasqualucci L, Trifonov V, Fabbri G, et al. Analysis of the coding genome of diffuse large B-cell lymphoma. *Nat Genet*. 2011;43(9):830-837.
 32. Malcikova J, Tausch E, Rossi D, et al. ERIC recommendations for TP53 mutation analysis in chronic lymphocytic leukemia-update on methodological approaches and results interpretation. *Leukemia*. 2018;32(5):1070-1080.
 33. Davids MS, Roberts AW, Seymour JF, et al. Phase I first-in-human study of venetoclax in patients with relapsed or refractory non-hodgkin lymphoma. *J Clin Oncol*. 2017;35(8):826-833.
 34. Tam CS, Anderson MA, Pott C, et al. Ibrutinib plus venetoclax for the treatment of mantle-cell lymphoma. *N Engl J Med*. 2018;378(13):1211-1223.

A laboratory-based scoring system predicts early treatment in Rai 0 chronic lymphocytic leukemia



Jared A. Cohen,¹ Francesca Maria Rossi,¹ Antonella Zucchetto,¹ Riccardo Bomben,¹ Lodovico Terzi-di-Bergamo,² Kari G. Rabe,³ Massimo Degan,¹ Agostino Steffan,⁴ Jerry Polesel,⁵ Enrico Santinelli,⁶ Idanna Innocenti,⁷ Giovanna Cutrona,⁸ Giovanni D'Arena,⁹ Gabriele Pozzato,¹⁰ Francesco Zaja,¹⁰ Annalisa Chiarenza,¹¹ Davide Rossi,^{12,13} Francesco Di Raimondo,¹¹ Luca Laurenti,⁷ Massimo Gentile,^{14,15} Fortunato Morabito,^{15,16} Antonino Neri,¹⁷ Manlio Ferrarini,¹⁸ Christopher D. Fegan,¹⁹ Christopher J. Pepper,^{19,20} Giovanni Del Poeta,⁶ Sameer A. Parikh,²¹ Neil E. Kay²¹ and Valter Gattei¹

¹Clinical and Experimental Onco-Haematology Unit, Centro di Riferimento Oncologico, I.R.C.C.S., Aviano (PN), Italy; ²Institute of Oncology Research, Bellinzona, Switzerland; ³Division of Biomedical Statistics and Informatics, Department of Health Sciences Research, Mayo Clinic, Rochester, MN, USA; ⁴Immunopathology and Cancer Biomarkers, Centro di Riferimento Oncologico, I.R.C.C.S., Aviano (PN), Italy; ⁵Unit of Cancer Epidemiology, Centro di Riferimento Oncologico, I.R.C.C.S., Aviano (PN), Italy; ⁶Division of Haematology, S. Eugenio Hospital and University of Tor Vergata, Rome, Italy; ⁷Hematology Institute, Catholic University of the Sacred Heart, Fondazione Policlinico A. Gemelli, Rome, Italy; ⁸UO Molecular Pathology, Ospedale Policlinico San Martino IRCCS, Genova, Italy; ⁹Onco-Haematology Department, Centro di Riferimento Oncologico della Basilicata, I.R.C.C.S., Rionero in Vulture, Italy; ¹⁰Department of Internal Medicine and Haematology, Maggiore General Hospital, University of Trieste, Trieste, Italy; ¹¹Division of Haematology, Ferrarotto Hospital, Catania, Italy; ¹²Hematology, Oncology Institute of Southern Switzerland, Bellinzona, Switzerland; ¹³Universita' della Svizzera Italiana, Lugano, Switzerland; ¹⁴Hematology Unit, AO, Cosenza, Italy; ¹⁵Biotechnology Research Unit, Aprigliano, Cosenza, Italy; ¹⁶Hematology Department and Bone Marrow Transplant Unit, Cancer Care Center, Augusta Victoria Hospital, East Jerusalem, Israel; and ¹⁷Hematology Unit, Fondazione IRCCS Cà Granda Ospedale Maggiore Policlinico and University of Milan, Milan, Italy; ¹⁸Department of Experimental Medicine, University of Genova, Genova, Italy; ¹⁹Division of Cancer and Genetics, Cardiff University, School of Medicine, Heath Park, Cardiff, UK; ²⁰University of Sussex, Brighton and Sussex Medical School, Brighton, UK and ²¹Division of Hematology, Department of Medicine, Mayo Clinic, Rochester, MN, USA

Haematologica 2020
Volume 105(6):1613-1620

ABSTRACT

We present a laboratory-based prognostic calculator (designated CRO score) to risk stratify treatment-free survival in early stage (Rai 0) chronic lymphocytic leukemia (CLL) developed using a training-validation model in a series of 1,879 cases from Italy, the United Kingdom and the United States. By means of regression analysis, we identified five prognostic variables with weighting as follows: deletion of the short arm of chromosome 17 and unmutated immunoglobulin heavy chain gene status, 2 points; deletion of the long arm of chromosome 11, trisomy of chromosome 12, and white blood cell count $>32.0 \times 10^3$ /microliter, 1 point. Low-, intermediate- and high-risk categories were established by recursive partitioning in a training cohort of 478 cases, and then validated in four independent cohorts of 144 / 395 / 540 / 322 cases, as well as in the composite validation cohort. Concordance indices were 0.75 in the training cohort and ranged from 0.63 to 0.74 in the four validation cohorts (0.69 in the composite validation cohort). These findings advocate potential application of our novel prognostic calculator to better stratify early-stage CLL, and aid case selection in risk-adapted treatment for early disease. Furthermore, they support immunocytogenetic analysis in Rai 0 CLL being performed at the time of diagnosis to aid prognosis and treatment, particularly in today's chemo-free era.

Correspondence:

JARED A. COHEN
jcoen781@gmail.com

VALTER GATTEI
vgattei@cro.it

Received: June 3, 2019.

Accepted: October 2, 2019.

Pre-published: October 3, 2019.

doi:10.3324/haematol.2019.228171

Check the online version for the most updated information on this article, online supplements, and information on authorship & disclosures: www.haematologica.org/content/105/6/1613

©2020 Ferrata Storti Foundation

Material published in Haematologica is covered by copyright. All rights are reserved to the Ferrata Storti Foundation. Use of published material is allowed under the following terms and conditions:

<https://creativecommons.org/licenses/by-nc/4.0/legalcode>. Copies of published material are allowed for personal or internal use. Sharing published material for non-commercial purposes is subject to the following conditions: <https://creativecommons.org/licenses/by-nc/4.0/legalcode>, sect. 3. Reproducing and sharing published material for commercial purposes is not allowed without permission in writing from the publisher.



Introduction

Clinical staging using the Binet and Rai classification systems provides a simple and inexpensive approach to assess prognosis in chronic lymphocytic leukemia (CLL).^{1,2} However, most patients today are diagnosed in early stages of the disease (Binet A or Rai 0) when these prognosticators fail to provide adequate risk stratification.³ Although similarly classified as early-stage CLL, Binet A and Rai 0 patients demonstrate heterogeneous clinical courses ranging from normal life expectancy in the absence of any treatment to unexpectedly short progression-free intervals rapidly requiring clinical intervention.⁴

To overcome the inherent weakness of clinical staging systems, other parameters have been sought and proposed by several studies as reliable prognosticators in CLL, including immunocytogenetic and molecular markers such as deletions of the short arm of chromosome 17 (del17p) and mutations of the *TP53* gene, deletions of the long arm of chromosome 11 (del11q), and trisomy of chromosome 12 (tris12), the immunoglobulin heavy chain (IGHV) gene mutational status as well as biochemical parameters such as beta-2-microglobulin (B2M) and thymidine kinase (TK) and cell surface receptors such as the integrin CD49d.⁵⁻¹⁰

Novel prognostic indices and model systems have been developed to integrate these markers into comprehensive scoring systems, such as the CLL International Prognostic Index (CLL-IPI), the German CLL Study Group (GCLLSG) index, and the MD Anderson Cancer Center (MDACC) score.¹¹⁻¹⁴ Although validations in the setting of early-stage CLL and/or treatment-free-survival (TFS) prediction have been undertaken, these indices were originally generated to predict overall survival operating across all stages of disease.^{11,13,15,16}

Here we present a novel laboratory-based prognostic index specifically developed to predict TFS in Rai 0 CLL, thus allowing clinicians and researchers to uniformly and more accurately identify cases with higher risk for needing early treatment.

Methods

We applied a training-validation strategy using 1,879 cases of phenotypically confirmed Rai 0 CLL¹⁷ collected in the context of an international effort from Italy, the United Kingdom and the United States (Figure 1). The training cohort included 478 Rai 0 cases identified from a consecutive series of Italian multicenter patients (1,201 cases) referred to a single center (Clinical and Experimental Onco-Hematology Unit of the Centro Riferimento Oncologico in Aviano, Italy) for immunocytogenetic analyses between 2006 and 2017. Four independent Rai 0 cohorts were used for external validation made up of three ‘real world’ cohorts from single centers, i) Gemelli Hospital in Rome, Italy (144 cases, Gemelli cohort), ii) Cardiff University Hospital in Wales, UK (395 cases, Cardiff cohort), iii) Mayo Clinic in Rochester, MN, USA (540 cases, Mayo cohort), and one investigational cohort from the multicenter O-CLL1-GISL Italian prospective observational study (O-CLL cohort; *clinicaltrials.gov* identifier: 00917540; 322 cases) (Figure 1). Cases of monoclonal B lymphocytosis were excluded, and the TFS was defined as time from diagnosis to treatment, according to the revised 2018 International Workshop on Chronic Lymphocytic Leukemia (IWCLL) guidelines.¹⁸ Patient information was obtained from the participating centers in accordance with the Declaration of Helsinki and local ethics committee approvals (Approvals n. IRB-05-2010, LREC #02/4806, IRB-12-000969 and NCT00917540).

Deletions at chromosomes 13q14 (del13q), 11q23 (del11q), 17p13 (del17p), and trisomy 12 (tris12), and IGHV gene status were determined at the different participating centers, as reported previously.^{5,19} Cytogenetic thresholds were set at 5% for del13q, del11q, and tris12, and 10% for del17p, and cases were categorized according to the hierarchical model proposed by Dohner *et al.*⁷ The positive fluorescence *in situ* hybridization (FISH) threshold of 10% for del17p was selected in accordance with the European Research Initiative on CLL (ERIC) recommendations and previous clinical studies.²⁰⁻²² IGHV status was considered unmutated (UM) at ≥98%,⁶ and CD49d positivity (only determined in the training cohort) was set at >30%, as reported previously.¹⁹ Investigation of mutations for *TP53* (exons 2–11) and *NOTCH1* (exon 34) (determined in 304 of 478 cases in the training cohort) was performed

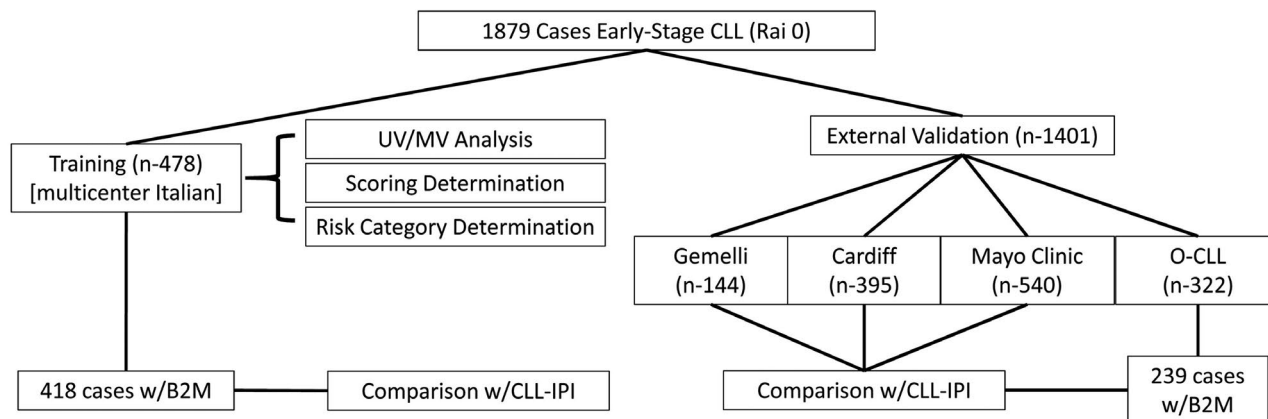


Figure 1. Study design. Training cohort: 478 cases included for univariable (UV) and multivariable (MV) analyses, scoring determination and risk category determination; 418 of 478 cases with beta-2-microglobulin (B2M) data (w/B2M) were employed for comparison with chronic lymphocytic leukemia International Prognostic Index (CLL-IPI) (w/CLL-IPI). Validation cohorts included 1,401 Rai 0 cases. The Italian prospective observational study (O-CLL) cohort had 239 of 322 cases available for comparison to CLL-IPI. In the remaining validation cohorts, all cases were available for comparison with CLL-IPI. n: number.

by a next-generation sequencing (NGS) approach, as previously reported.^{5,23-26} In the case of *TP53* mutation, cases were defined as *TP53* mutated if the variant allele frequency was >10% according to ERIC recommendations.²⁷

The Cox proportional hazards regression model was chosen to assess the independent effect of co-variables on TFS, with a step-wise procedure for selecting significant variables. All co-variables, apart from FISH categories,⁷ were treated as dichotomous and evaluated at diagnosis. Independent variables were internally validated using bootstrapping procedures and weighted based on the proportion of their normalized hazard ratios (HR) rounded to the nearest whole integer (Table 1). Risk-categories were determined by recursive partitioning (*Online Supplementary Figure S1*), and Kaplan-Meier analyses were used to generate survival curves.

In the training cohort, five cases died without treatment and were censored at the date of death. A sensitivity analysis for competitive risk, conducted on the training cohort according to the Fine-Gray model,²⁸ reported no substantial modification in level of risk (*data not shown*).

The concordance index (C-index) was used to compare our model with the CLL-IPI¹¹ in 418 of 478 (training cohort), 144 of 144 (Gemelli cohort), 395 of 395 (Cardiff cohort), 540 of 540 (Mayo cohort), 239 of 322 (O-CLL cohort), and 1,318 of 1,401 (composite validation cohort) cases with available B2M data. In all cases, the statistical significance between C-indices was evaluated by applying the Student *t*-test and internally validated by applying a bootstrapping procedure. The Akaike information criterion (AIC) was also employed as an estimator of the relative quality of the model proposed in this study in comparison to the CLL-IPI as TFS predictors. When applicable, $P < 0.05$ was considered statistically significant. Statistical calculations were made using MedCalc or the open source R package (<http://www.r-project.org/>) statistics software.

Results

Identification of the training cohort and construction of a scoring system

The TFS curves of a consecutive series of 1,201 cases from a single center, split according to Rai staging, are reported in Figure 2A. As expected, the median [95% confidence interval (CI)] TFS of the 478 Rai 0 cases was significantly longer at 124 months (m) (104-183 m) compared to that of Rai I-IV cases, with a median (95%CI) follow up of 62 m (57-68 m 95%CI). The baseline characteristics of this Rai 0 cohort are summarized in *Online Supplementary Table S1*. When Dohner's hierarchical model⁷ was applied to this Rai 0 cohort, cases bearing either *del17p*, *del11q* or *tris12* experienced the shortest TFS, with no difference among these three cytogenetic categories, while similarly longer TFS intervals were observed for *del13q* cases and cases lacking the four major chromosomal abnormalities (Figure 2B).

Therefore, the presence of these three chromosomal aberrations were included, along with white blood cell (WBC) counts, IGHV gene status, CD49d expression, gender and age in a univariate analysis. For the purposes of the present study, WBC counts were dichotomized according to the cut off of $>32 \times 10^3$ cells/ μL (32K), as established by a maximally selected log rank analysis carried out in the training cohort (*Online Supplementary Figure S2*). In patients with WBC counts $\leq 32\text{K}$ and $>32\text{K}$, median (95%CI, $\times 10^3$ cell/ μL) counts were 15.3 (15.0-16.8) versus 54.7 (49.8-58.0), respectively, without clustering around the threshold value (*Online Supplementary Figure S3*).

Apart from age and gender, all of the tested variables

associated with a shorter TFS, and five of them (*del17p*, *del11q*, *tris12*, WBC and IGHV gene status) emerged as independent predictors of short TFS by multivariate analysis (Table 1).

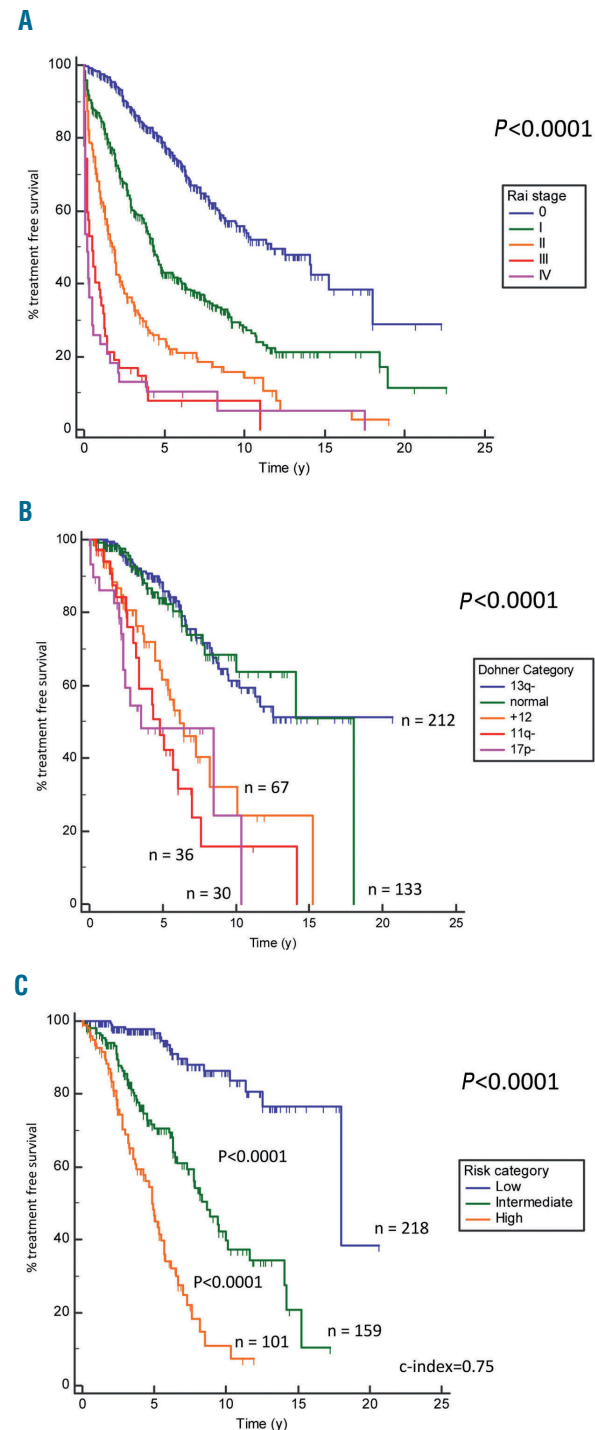


Figure 2. Determination of the Rai 0 training cohort and laboratory-based prognostic calculator (CRO) scoring. Kaplan-Meier curves demonstrating % treatment-free survival (TFS) for (A) a consecutive series of 1,201 cases of chronic lymphocytic leukemia (CLL) referred to our center between 2006 and 2017 from which our training cohort was derived; stratified by Rai stage. The training cohort of 478 Rai 0 cases organized according to (B) Dohner's hierarchical model and (C) CRO score. n: number; y: years. c-index: concordance index.

To construct a scoring system (hereafter designated as the CRO score) using these five independent predictors, a point value of 1 or 2 was assigned to variables according to their respective normalized hazard ratios as follows: i) 2 points to del17p, and UM IGHV; ii) 1 point to del11q, tris12, and WBC count >32K (Table 1). Then, three risk groups, based on point cut offs of 0 (low risk, 218 cases), 1-2 (intermediate risk, 159 cases), and 3-5 (high risk, 101 cases) were established by recursive partitioning analysis (Online Supplementary Figure S1). The median TFS (95%CI) was 216 m (216-216 m), 104 m (93-140 m) and 58 m (44-68 m) ($P<0.0001$) for the low-, intermediate-, and high-risk groups, respectively, with a C-index of 0.75 (Figure 2C). A comparison with the CLL-IPI (possible in 418 of 478 cases with available B2M data) indicated a C-index of 0.76 for the CRO score compared to 0.69 when patient risk groups were split according to the CLL-IPI ($P<0.0001$) (Online Supplementary Figure S4A).

External validation of the CRO score

The CRO score was then validated in four independent cohorts of Rai 0 CLL; baseline patient characteristics are reported in Online Supplementary Table S1. These cohorts demonstrated similar TFS survival curves when compared to each other and the training series (Online Supplementary Figure S5). Results were as follows (see also Figure 3):

i) the 144 cases of the Gemelli cohort (Figure 3A) had a median (95%CI) follow up of 91 m (83-103 m). Overall, median (95% CI) TFS was 86 m (80-94 m) (Online Supplementary Figure S5), while median (95%CI) TFS for the low- (96 cases), intermediate- (36 cases) and high-risk (12 cases) groups was 239 m (range, 239-239 m), 98 m (92-132 m) and 85 m (60-109 m), respectively ($P=0.002$ between low- and intermediate-risk groups, $P=0.09$ between intermediate- and high-risk groups). In this cohort, the C-indices were 0.64 and 0.61 for the CRO score and the CLL-IPI, respectively ($P<0.0001$) (Online Supplementary Figure S4B);

ii) the Cardiff cohort (395 cases) had a median (95%CI) follow up of 94 m (83-104 m). Median (95%CI) TFS was 74 m (67-81 m) overall (Online Supplementary Figure S5), and not reached (NR), 111 m (97-146 m) and 70 m (29-114 m) for the low- (206 cases), intermediate- (136 cases), and high-risk (53 cases) groups, respectively ($P<0.001$ between low- and intermediate-risk groups, $P=0.009$ between intermediate- and high-risk groups) (Figure 3B); C-index

was 0.63 for both the CRO score and the CLL-IPI (P =not significant, ns) (Online Supplementary Figure S4C);

iii) the Mayo cohort (540 cases) had a median (95%CI) follow up of 77 m (68-88 m). Median (95%CI) TFS was 127 m (96 m-NR) overall (Online Supplementary Figure S5), and NR, 76 m (range, 64 m-NR) and 36 m (range, 31-59 m) for the low- (278 cases), intermediate- (168 cases) and high-risk (94 cases) groups, respectively ($P<0.0001$) (Figure 3C); C-indices were 0.72 and 0.68 for the CRO score and the CLL-IPI, respectively ($P<0.0001$) (Online Supplementary Figure S4D);

iv) the multicenter O-CLL cohort (322 cases) had a median (95%CI) follow up of 89 m (85-95 m), while median (95%CI) TFS was NR overall (Online Supplementary Figure S5), and NR, 96 m (83-110 m) and 48 m (39-67 m) for the low- (189 cases), intermediate- (84 cases) and high-risk (49 cases) groups, respectively ($P<0.001$ between low- and intermediate-risk groups, $P=0.003$ between intermediate- and high-risk groups; C-index 0.74) (Figure 3D). In the 239 cases with available B2M data, the C-indices were 0.71 and 0.70 for the CRO score and the CLL-IPI, respectively ($P<0.001$) (Online Supplementary Figure S4E).

The composite TFS curve included 1,401 Rai 0 cases by combining cases from the four validation cohorts. Median (95%CI) TFS was 175 m (143-201 m) overall and NR, 106 m (96-134 m) and 45 m (39-60 m) for the low-, intermediate- and high-risk groups, respectively ($P<0.0001$; C-index 0.69) (Figure 3E). In the 1,318 cases with available B2M data, the C-indices were 0.68 for the CRO score and 0.66 for the CLL-IPI ($P<0.0001$) (Online Supplementary Figure S6). In this context, AIC was 4,881 for the CRO score versus 4,912 for the CLL-IPI, in keeping with a relative better quality of the former as a TFS predictor.

Sub-analyses of the CRO score high-risk group

By combining the training and four validation cohorts, 309 of 1,879 cases (16%) were identified as having relatively higher risk of early progression and treatment according to the CRO score (scores 3, 4 or 5). In this subset, the vast majority of cases had a CRO score of 3 (223 cases, 72%) or 4 (72 cases, 23%); however, a small minority of patients (14 cases, 4.5%) had a CRO score of 5, i.e. presented with a WBC count >32K in the context of disease bearing both del17p and an UM IGHV gene status (Online Supplementary Table S2). Although the median TFS of cases with CRO scores 3 and 4 was similar, a significantly shortened median TFS was demonstrated in

Table 1. Univariable and reduced multivariable analysis of six factors used to generate our risk calculator.

Factor	Univariable analysis			Reduced multivariable analysis			Weight
	P	HR	95% CI	P	HR	95% CI	
WBC>32K cells/L	<0.0001	2.96	2.10-4.16	<0.0001	2.39	1.69 - 3.38	1
FISH category							
del17p	<0.0001	4.38	2.46 - 7.80	0.0002	3.03	1.69 - 5.44	2
del11q	<0.0001	4.02	2.45 - 6.19	0.0049	2.13	1.26 - 3.62	1
tris12	<0.0001	2.85	1.84 - 4.42	0.025	1.7	1.07 - 2.71	1
UM IGHV	<0.0001	4.08	2.86 - 5.80	<0.0001	2.91	1.97 - 4.29	2
CD49d+	0.001	1.78	1.27 - 2.51				
Age>65 years	0.0536	1.4	0.99 - 1.98				
Male	0.9232	0.98	0.70 - 1.38				

Fluorescence *in situ* hybridization (FISH) categories were as reported by Dohner *et al.* Weights were determined using the proportion of normalized hazard ratios rounded to the nearest whole integer. HR: hazard ratio; CI: confidence interval; WBC: white blood cell; UM: unmutated.

patients classified as high-risk with a CRO score of 5 (27.6 m, 95%CI: 14.4-28.8; $P=0.01$) (Online Supplementary Table S2 and Online Supplementary Figure S7).

Application of the CRO score in Rai I patients

To assess the generalizability of the CRO score in patients beyond Rai 0 disease, we applied our scoring system to a consecutive series of Italian multicenter patients with Rai I CLL (375 cases) referred to our center for

immunocytogenic analyses between 2006 and 2017. Our prognostic calculator demonstrated excellent predictive performance in this cohort (c-index 0.67) with a median (95%CI) TFS of 37 m (47-57 m) (Online Supplementary Figure S8).

CRO score variables and TP53 and NOTCH1 mutations

Data of TP53 and NOTCH1 mutations were available in 304 of 478 cases from the training cohort. Therefore, a

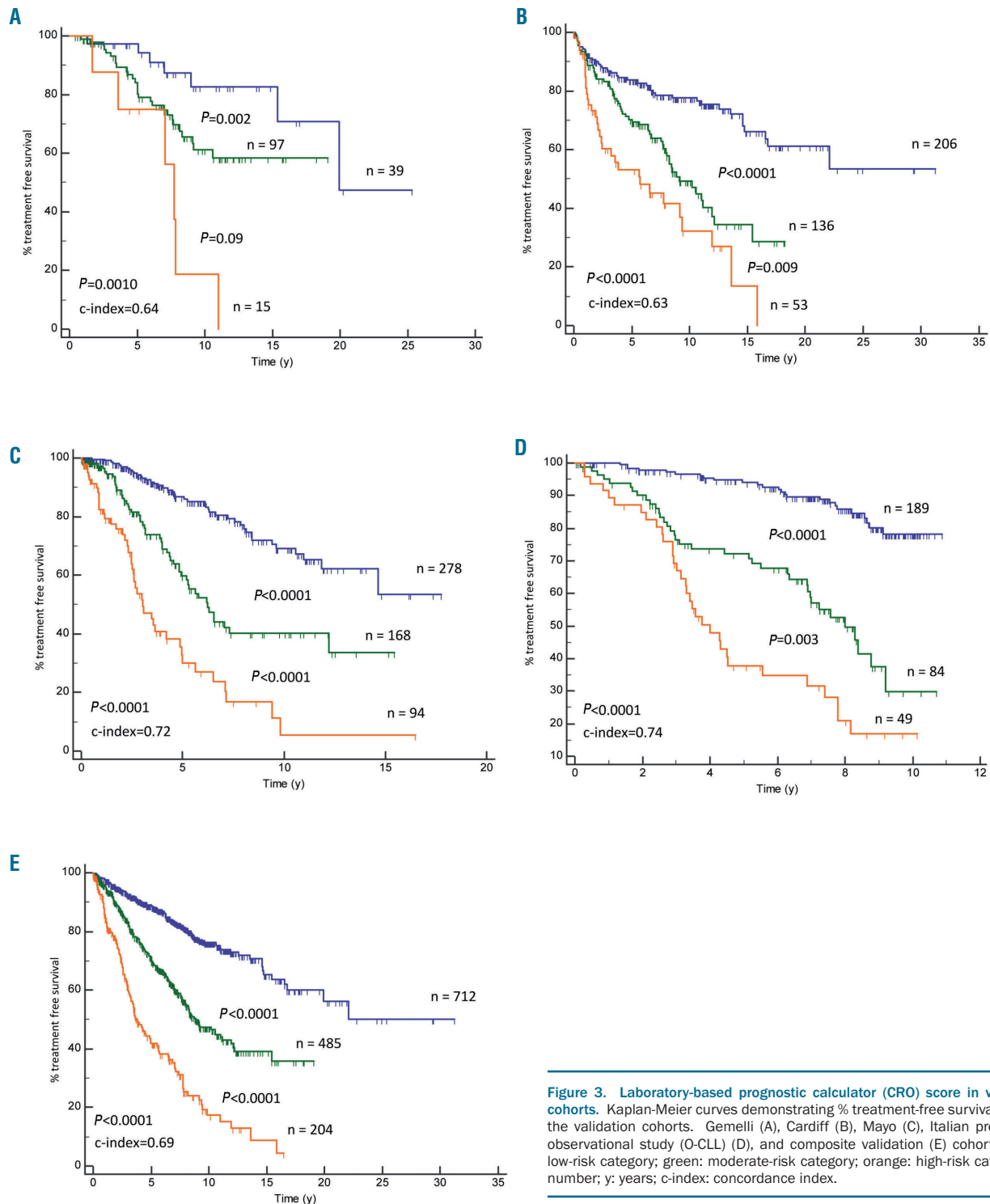


Figure 3. Laboratory-based prognostic calculator (CRO) score in validation cohorts. Kaplan-Meier curves demonstrating % treatment-free survival (TFS) in the validation cohorts. Gemelli (A), Cardiff (B), Mayo (C), Italian prospective observational study (O-CLL) (D), and composite validation (E) cohorts. Blue: low-risk category; green: moderate-risk category; orange: high-risk category. n: number; y: years; c-index: concordance index.

multivariable analysis was performed in these cases by including the same variables (WBC count, del11q, tris12, IGHV gene status, CD49d, age and gender), adding *NOTCH1* and *TP53* mutations and re-classifying del17p and/or *TP53* mutated cases as *TP53* disrupted.^{5,29-31} As shown in *Online Supplementary Table S3*, the CRO score variables WBC count, del11q, tris12, and IGHV gene status maintained the ability to independently predict short TFS along with *TP53* disruption, in a model that included *TP53* and *NOTCH1* gene mutations.

Discussion

The clinical staging systems for CLL, described by Rai and Binet approximately 40 years ago, are still used in clinical practice today to inform prognosis and guide treatment decisions.^{1,2} However, their predictive powers are limited.³ For example, Pflug *et al.* reported C-indices of 0.56 and 0.58 for Rai and Binet systems, respectively, when applied to a cohort of 1,948 patients.¹⁵ Novel model scoring systems developed in recent years have significantly improved the accuracy of prognostication by incorporating new biomarkers and hold the potential for the development of more individualized treatment strategies,^{11-14,26} especially in the age of an increasing sophistication of novel agents alone or in combination. In this regard, the CLL-IPI was developed as an integrative tool to evaluate overall survival for all clinical stages of disease, and although it demonstrated consistency in subgroup analyses circumscribed to early-stage disease,^{15,32} it was not developed specifically to predict TFS.

To our knowledge, this study represents one of the largest attempts to integrate novel biomarkers with traditional clinical factors, with the specific aim of predicting TFS in the setting of Rai 0 CLL. Given the multiplicity of new biomarkers, our goals were: i) to determine which ones individually influence TFS; and ii) to develop a scoring system to stratify risk in patients traditionally thought to harbor indolent disease.

Our training cohort was selected from a consecutive series of 1,201 CLL cases referred to a single center for immunocytogenetic analyses between 2006 and 2017. With respect to TFS, this cohort was stratified into independent risk groups using Rai staging; however, a satisfactory further sub-stratification of Rai 0 cases was not demonstrated using the canonical Dohner's hierarchical classification alone.⁷ This observation provided the stimulus to investigate the potential prognostic significance of additional biomarkers in early-stage disease. One of our main strategies was to integrate known prognostic markers that are commonly used in clinical practice today to increase the accessibility and cost-effectiveness of the risk tool.

Our results demonstrate that the CRO score is a powerful tool for guiding treatment prediction in patients with Rai 0 CLL. Notably, a subset analysis of the so-called high-risk category according to the CRO score (i.e. scores 3-5), revealed that a very small subset of cases (14 cases) in a composite cohort of 1,879 training and validation cases, characterized by high WBC counts in the setting of del17p and UM IGHV gene status (i.e. CRO score 5), progressed within two years, significantly more rapidly than the other so-called high-risk cases with CRO scores of 3 or 4. Conversely, in low-risk patients, the CRO score predicted

TFS at 10 years of approximately 85%, arguing for its expanded utility in allowing clinicians to confidently provide reassurance of disease quiescence to such patients. Furthermore, in comparison to the CLL-IPI,¹¹ our model demonstrated superior performance in the training cohort and in 3 out of the 4 validation cohorts, lending credence to its role in the current compendium of comprehensive risk tools in the setting of Rai 0 CLL.

We observed significant heterogeneity in patient characteristics among the five cohorts included in our study (*Online Supplementary Table S4*). For example, 64% of patients in the Gemelli cohort were aged ≥ 65 years compared to 30% in the O-CLL cohort, and only one patient in the O-CLL had a B2M >3.5 mg, compared to 23% of the patients in the Cardiff cohort. We attribute these differences to the heterogeneity of clinical settings from which each cohort was derived, as has been observed in previous studies comparing 'real world' *versus* observational study patients, single *versus* multicenter registries, and cases from community *versus* tertiary/referral centers.³³⁻³⁵ In contrast to the results in these studies, which show inconsistent performance of several prognostic indexes across dissimilar cohorts, our scoring system retained powerful predictive capacity throughout, showcasing its generalizability and strength as a clinically useful decision-making tool.

In the training, composite and two out of the four validation cohorts, the proposed prognostic score approached or exceeded C-index values of 0.7, a threshold necessary to confer utility at the individual patient level.³⁶ In this regard, however, a more precise evaluation of the individual predictive potential may require the application of complex statistical methods, as recently proposed.^{37,38}

This study raises questions regarding the appropriate timing of immunocytogenetic analysis in early-stage disease, which today is often postponed until the time of disease progression and first treatment. We appreciate the cost-effectiveness of a 'watch-and-wait' approach, particularly since studies investigating the early use of chlorambucil and fludarabine monotherapy as well as FCR regimens (fludarabine/cyclophosphamide + rituximab) have failed to demonstrate improved outcomes in CLL patients.^{18,39,40} However, the role of the novel inhibitors in this setting remains to be elucidated,⁴¹ and the results of this study support the notion that early testing can aid risk-adapted treatment strategies and early intervention, particularly in the modern chemo-free era. In this regard, the CLL12 trial (a phase III clinical study currently underway in Germany) is evaluating the efficacy and safety of ibrutinib compared to a 'watch-and-wait' approach in Binet A CLL using a similar comprehensive scoring system to identify high-risk patients.³⁶ Another randomized phase II study currently underway at the Mayo Clinic is comparing the efficacy of the BTK inhibitor acalabrutinib alone and in combination with the anti-CD20 obinutuzumab in treating patients with early-stage CLL who are classified as high- or very high-risk according to the CLL-IPI (Sameer Parikh *et al.*, 2018, NCT03516617). Further clinical studies are needed to aid identification of progressive cases of early-stage disease who may benefit from risk-adapted treatment approaches. An important caveat to the approach of up-front testing is that cytogenetic and *TP53* mutational analysis must be repeated at the time of disease progression and/or treatment particularly in previously so-called "TP53 non-disrupted" cases to identify

those that have undergone clonal evolution which could affect treatment decisions.

We recognize that our study has several limitations. For example, we did not include *TP53* gene mutation, an important adverse prognostic factor that, together with del17p, recapitulates the so-called “TP53 disrupted” cases.³¹ While the established cut off of 10% for del17p has little biological substantiation, its selection helps mitigate false positive rates. In the era of next generation sequencing, however, *TP53* mutational analysis is admittedly preferred. Despite the exclusion of *TP53* mutational analysis in this study, we were able to achieve superior prognostic power with respect to the CLL-IPi, in keeping with the notion that the majority of del17p cases also bear *TP53* mutations in the undeleted allele,^{29,30} and that the clinical impact of subclonal *TP53* mutations,³¹ especially if detected alone in early-stage disease, is still not completely understood. Furthermore, subgroup analysis of 304 cases from the training cohort demonstrated the preservation of CRO score variables even in the presence of *TP53* and *NOTCH1* gene mutations (*Online Supplementary Table S3*). We also excluded from our analysis other gene mutations usually associated with disease progression, namely *BIRC3* and *SF3B1*⁴²⁻⁴⁵ although, notably, these mutations have mainly failed to operate as independent predictors when tested in large cohorts.^{5,46} Similarly, we did not include in our panel of biomarkers the evaluation of serum thymidine kinase levels, that, according to some studies, is a test with independent clinical relevance as a predictor of overall survival.¹⁵ This assay, however, is of limited application in CLL and is currently not routinely employed in many US or European clinical laboratories.

We have not overlooked the uniqueness of including WBC count as a prognostic biomarker in this study. More commonly, B-cell lymphocyte count is employed in the diagnosis and response to therapy in CLL.¹⁸ However, we demonstrate here that, commensurate with previously

published studies,⁴⁷ WBC count may deserve consideration as a clinically useful surrogate marker of disease burden particularly in the setting of untreated disease where, alongside del17p and unmutated IGHV gene status, it appears to demonstrate prognostic significance. This observation is consistent with previous data demonstrating WBC count, along with IGHV, as independent predictors of TFS in Binet A CLL.⁴⁸

Finally, CD49d, a well-proven independent prognosticator in CLL,^{19,49} including in cases of early-stage disease,⁵⁰ failed, perhaps surprisingly, to emerge in multivariable analysis as an independent factor in our Rai 0 training cohort. We hypothesize that the dropout of CD49d in multivariate analysis was due to the close relationship between CD49d and tris12,⁵¹ the latter maintained in the final multivariable model; this idea is supported by bivariate analysis of these two variables wherein CD49d lost significance (*data not shown*).

In conclusion, we present here a novel laboratory-based scoring system for Rai 0 CLL to aid clinical decision making in cases of early-stage disease. These findings advocate a role for immunocytogenetic analysis in Rai 0 CLL at the time of diagnosis to aid prognosis, particularly in today's chemo-free era where early intervention is acquiring momentum in the investigative setting. Further investigation is needed to definitively validate its utility in risk-adapted treatment.

Acknowledgements

The study was supported by the Associazione Italiana Ricerca Cancro (AIRC), Investigator Grants IG-21687; Progetto Ricerca Finalizzata PE 2016-02362756, Ministero della Salute, Rome, Italy; Associazione Italiana contro le Leucemie, Linfomi e Mielomi (AIL), Venezia Section, Pramaggiore Group, Italy; Linfo-check - Bando ricerca - contributo art. 15, comma 2, lett b) LR 17/2014; “5x1000 Intramural Program”, Centro di Riferimento Oncologico, Aviano, Italy. SAP is a Scholar in the Mayo Clinic Paul Calabresi Program in Translational Research (K12 CA090628).

References

- Binet JL, Lepage M, Dighiero G, et al. A clinical staging system for chronic lymphocytic leukemia: prognostic significance. *Cancer*. 1977;40(2):855-864.
- Rai KR, Sawitsky A, Cronkite EP, et al. Clinical staging of chronic lymphocytic leukemia. *Blood*. 1975;46(2):219-234.
- Letestu R, Levy V, Eclache V, et al. Prognosis of Binet stage A chronic lymphocytic leukemia patients: the strength of routine parameters. *Blood*. 2010;116(22):4588-4590.
- Gribben JG, O'Brien S. Update on therapy of chronic lymphocytic leukemia. *J Clin Oncol*. 2011;29(5):544-550.
- Dal Bo M, Bulian P, Bomben R, et al. CD49d prevails over the novel recurrent mutations as independent prognosticator of overall survival in chronic lymphocytic leukemia. *Leukemia*. 2016 10;30(10):2011-2018.
- Damle RN, Wasi T, Fais F, et al. Ig V gene mutation status and CD38 expression as novel prognostic indicators in chronic lymphocytic leukemia. *Blood*. 1999;94(6):1840-1847.
- Dohner H, Stilgenbauer S, Benner A, et al. Genomic aberrations and survival in chronic lymphocytic leukemia. *N Engl J Med*. 2000;343(26):1910-1916.
- Hallek M, Wanders L, Ostwald M, et al. Serum beta(2)-microglobulin and serum thymidine kinase are independent predictors of progression-free survival in chronic lymphocytic leukemia and immunocytoma. *Leuk Lymphoma*. 1996;22(5-6):439-447.
- Hamblin TJ, Davis Z, Gardiner A, et al. Unmutated Ig V(H) genes are associated with a more aggressive form of chronic lymphocytic leukemia. *Blood*. 1999;94(6):1848-1854.
- Zenz T, Eichhorst B, Busch R, et al. TP53 mutation and survival in chronic lymphocytic leukemia. *J Clin Oncol*. 2010;28(29):4473-4479.
- An international prognostic index for patients with chronic lymphocytic leukaemia (CLL-IPi): a meta-analysis of individual patient data. *Lancet Oncol*. 2016;17(6):779-790.
- Bulian P, Rossi D, Forconi F, et al. IGHV gene mutational status and 17p deletion are independent molecular predictors in a comprehensive clinical-biological prognostic model for overall survival prediction in chronic lymphocytic leukemia. *J Transl Med*. 2012;10:18.
- Pflug N, Bahlo J, Shanafelt TD, et al. Development of a comprehensive prognostic index for patients with chronic lymphocytic leukemia. *Blood*. 2014;124(1):49-62.
- Wierda WG, O'Brien S, Wang X, et al. Prognostic nomogram and index for overall survival in previously untreated patients with chronic lymphocytic leukemia. *Blood*. 2007;109(11):4679-4685.
- Gentile M, Shanafelt TD, Rossi D, et al. Validation of the CLL-IPi and comparison with the MDACC prognostic index in newly diagnosed patients. *Blood*. 2016;128(16):2093-2095.
- Molica S, Shanafelt TD, Giannarelli D, et al. The chronic lymphocytic leukemia international prognostic index predicts time to first treatment in early CLL: Independent validation in a prospective cohort of early stage patients. *Am J Hematol*. 2016;91(11):1090-1095.
- Matutes E, Owusu-Ankomah K, Morilla R,

- et al.* The immunological profile of B-cell disorders and proposal of a scoring system for the diagnosis of CLL. *Leukemia*. 1994;8(10):1640-1645.
18. Hallek M, Cheson BD, Catovsky D, *et al.* iwCLL guidelines for diagnosis, indications for treatment, response assessment, and supportive management of CLL. *Blood*. 2018;131(25):2745-2760.
 19. Bulian P, Shanafelt TD, Fegan C, *et al.* CD49d is the strongest flow cytometry-based predictor of overall survival in chronic lymphocytic leukemia. *J Clin Oncol*. 2014;32(9):897-904.
 20. Else M, Wade R, Oscier D, *et al.* The long-term outcome of patients in the LRF CLL4 trial: the effect of salvage treatment and biological markers in those surviving 10 years. *Br J Haematol*. 2016;172(2):228-237.
 21. Oscier D, Wade R, Davis Z, *et al.* Prognostic factors identified three risk groups in the LRF CLL4 trial, independent of treatment allocation. *Haematologica*. 2010;95(10):1705-1712.
 22. Pospisilova S, Gonzalez D, Malcikova J, *et al.* ERIC recommendations on TP53 mutation analysis in chronic lymphocytic leukemia. *Leukemia*. 2012;26(7):1458-1461.
 23. D'Agaro T, Bittolo T, Bravin V, *et al.* NOTCH1 mutational status in chronic lymphocytic leukaemia: clinical relevance of subclonal mutations and mutation types. *Br J Haematol*. 2018;182(4):597-602.
 24. Pozzo F, Bittolo T, Arruga F, *et al.* NOTCH1 mutations associate with low CD20 level in chronic lymphocytic leukemia: evidence for a NOTCH1 mutation-driven epigenetic dysregulation. *Leukemia*. 2015;30(1):182-189.
 25. Rossi D, Spina V, Bomben R, *et al.* Association between molecular lesions and specific B-cell receptor subsets in chronic lymphocytic leukemia. *Blood*. 2013;121(24):4902-4905.
 26. Rossi D, Rasi S, Spina V, *et al.* Integrated mutational and cytogenetic analysis identifies new prognostic subgroups in chronic lymphocytic leukemia. *Blood*. 2013;121(8):1403-1412.
 27. Malcikova J, Tausch E, Rossi D, *et al.* ERIC recommendations for TP53 mutation analysis in chronic lymphocytic leukemia: af_ update on methodological approaches and results interpretation. *Leukemia*. 2018;32(5):1070-1080.
 28. Fine JP, Gray RJ. A proportional hazards model for the subdistribution of a competing risk. *J Am Stat Ass*. 1999;94(446):496-509.
 29. Gonzalez D, Martinez P, Wade R, *et al.* Mutational status of the TP53 gene as a predictor of response and survival in patients with chronic lymphocytic leukemia: results from the LRF CLL4 trial. *J Clin Oncol*. 2011;29(16):2223-2229.
 30. Rossi D, Cerri M, Deambrogi C, *et al.* The prognostic value of TP53 mutations in chronic lymphocytic leukemia is independent of Del17p13: implications for overall survival and chemorefractoriness. *Clin Cancer Res*. 2009;15(3):995-1004.
 31. Rossi D, Khiabani H, Spina V, *et al.* Clinical impact of small TP53 mutated subclones in chronic lymphocytic leukemia. *Blood*. 2014;123(14):2139-2147.
 32. Molica S, Giannarelli D, Levato L, *et al.* A prognostic algorithm including a modified version of MD Anderson Cancer Center (MDACC) score predicts time to first treatment of patients with clinical monoclonal lymphocytosis (cMBL)/Rai stage 0 chronic lymphocytic leukemia (CLL). *Int J Hematol*. 2014;100(3):290-295.
 33. Bulian P, Tarnani M, Rossi D, *et al.* Multicentre validation of a prognostic index for overall survival in chronic lymphocytic leukaemia. *Hematol Oncol*. 2011;29(2):91-99.
 34. Shanafelt TD, Jenkins G, Call TG, *et al.* Validation of a new prognostic index for patients with chronic lymphocytic leukemia. *Cancer*. 2009;115(2):363-372.
 35. Shanafelt TD, Kay NE, Rabe KG, *et al.* Hematologist/oncologist disease-specific expertise and survival: lessons from chronic lymphocytic leukemia (CLL)/small lymphocytic lymphoma (SLL). *Cancer*. 2012;118(7):1827-1837.
 36. Langerbeins P, Bahlo J, Rhein C, *et al.* The CLL12 trial protocol: a placebo-controlled double-blind Phase III study of ibrutinib in the treatment of early-stage chronic lymphocytic leukemia patients with risk of early disease progression. *Future Oncol*. 2015;11(13):1895-1903.
 37. Gerstung M, Papaemmanuil E, Martincorena I, *et al.* Precision oncology for acute myeloid leukemia using a knowledge bank approach. *Nat Genet*. 2017;49(3):332-340.
 38. Grinfeld J, Nangalia J, Baxter EJ, *et al.* Classification and Personalized Prognosis in Myeloproliferative Neoplasms. *N Engl J Med*. 2018;379(15):1416-1430.
 39. Dighiero G, Maloum K, Desablens B, *et al.* Chlorambucil in indolent chronic lymphocytic leukemia. French Cooperative Group on Chronic Lymphocytic Leukemia. *N Engl J Med*. 1998;338(21):1506-1514.
 40. Hoehstetter MA, Busch R, Eichhorst B, *et al.* Early, risk-adapted treatment with fludarabine in Binet stage A chronic lymphocytic leukemia patients: results of the CLL1 trial of the German CLL study group. *Leukemia*. 2017;31(12):2833-2837.
 41. Hallek M. On the architecture of translational research designed to control chronic lymphocytic leukemia. *Hematology Am Soc Hematol Educ Program*. 2018;2018(1):1-8.
 42. Dal Bo M, Del Principe MI, Pozzo F, *et al.* NOTCH1 mutations identify a chronic lymphocytic leukemia patient subset with worse prognosis in the setting of a rituximab-based induction and consolidation treatment. *Ann Hematol*. 2014;93(10):1765-1774.
 43. Fabbri G, Rasi S, Rossi D, *et al.* Analysis of the chronic lymphocytic leukemia coding genome: role of NOTCH1 mutational activation. *J Exp Med*. 2011;208(7):1389-1401.
 44. Rossi D, Brusca A, Spina V, *et al.* Mutations of the SF3B1 splicing factor in chronic lymphocytic leukemia: association with progression and fludarabine-refractoriness. *Blood*. 2011;118(26):6904-6908.
 45. Rossi D, Fangazio M, Rasi S, *et al.* Disruption of BIRC3 associates with fludarabine chemorefractoriness in TP53 wild-type chronic lymphocytic leukemia. *Blood*. 2012;119(12):2854-2862.
 46. Baliakas P, Hadzidimitriou A, Sutton LA, *et al.* Recurrent mutations refine prognosis in chronic lymphocytic leukemia. *Leukemia*. 2015;29(2):329-336.
 47. Rossi D, Gaidano G. Lymphocytosis and ibrutinib treatment of CLL. *Blood*. 2014;123(12):1772.
 48. Del Giudice I, Mauro FR, De Propriis MS, *et al.* White blood cell count at diagnosis and immunoglobulin variable region gene mutations are independent predictors of treatment-free survival in young patients with stage A chronic lymphocytic leukemia. *Haematologica*. 2011;96(4):626.
 49. Shanafelt TD, Geyer SM, Bone ND, *et al.* CD49d expression is an independent predictor of overall survival in patients with chronic lymphocytic leukaemia: a prognostic parameter with therapeutic potential. *Br J Haematol*. 2008;140(5):537-546.
 50. Rossi D, Zucchetto A, Rossi FM, *et al.* CD49d expression is an independent risk factor of progressive disease in early stage chronic lymphocytic leukemia. *Haematologica*. 2008;93(10):1575-1579.
 51. Zucchetto A, Caldana C, Benedetti D, *et al.* CD49d is overexpressed by trisomy 12 chronic lymphocytic leukemia cells: evidence for a methylation-dependent regulation mechanism. *Blood*. 2013;122(19):3317-3321.

IGHV mutational status and outcome for patients with chronic lymphocytic leukemia upon treatment: a Danish nationwide population-based study

Emelie Curovic Rotbain,^{1,2,3,4} Henrik Frederiksen,^{1,3,5} Henrik Hjalgrim,^{2,4} Klaus Rostgaard,⁴ Gudrun Jakubsdottir Egholm,¹ Banafsheh Zahedi,² Christian Bjørn Poulsen,⁶ Lisbeth Enggard,⁷ Caspar da Cunha-Bang^{#2} and Carsten Utoft Niemann^{#2}

¹Department of Hematology, Odense University Hospital, Odense; ²Department of Hematology, Rigshospitalet, Copenhagen; ³Department of Clinical Research, University of Southern Denmark, Odense; ⁴Department of Epidemiology Research, Statens Serum Institut, Copenhagen; ⁵Academy of Geriatric Cancer Research (AgeCare), Odense University Hospital, Odense; ⁶Department of Hematology, Zealand University Hospital, Roskilde and ⁷Department of Hematology, Herlev Hospital, Herlev, Denmark.

[#]CdC-B and CU contributed equally as co-senior authors.

ABSTRACT

Patients with chronic lymphocytic leukemia and unmutated immunoglobulin heavy-chain variable region gene (IGHV) have inferior survival from time of treatment in clinical studies. We assessed real-world outcomes based on mutational status and treatment regimen in a nationwide population-based cohort, comprising all 4,135 patients from the Danish chronic lymphocytic leukemia registry diagnosed between 2008 and 2017. In total, 850 patients with known mutational status received treatment: 42% of patients received intensive chemoimmunotherapy consisting of fludarabine, cyclophosphamide plus rituximab, or bendamustine plus rituximab; 27% received chlorambucil in combination with anti-CD20 antibodies or as monotherapy, and 31% received other, less common treatments. No difference in overall survival from time of first treatment according to mutational status was observed, while treatment-free survival from start of first treatment was inferior for patients with unmutated IGHV. The median treatment-free survival was 2.5 years for patients treated with chlorambucil plus anti-CD20, and 1 year for those who received chlorambucil monotherapy. The 3-year treatment-free survival rates for patients treated with fludarabine, cyclophosphamide plus rituximab, and bendamustine plus rituximab were 90% and 91% for those with mutated IGHV, and 76% and 53% for those with unmutated IGHV, respectively, and the 3-year overall survival rates were similar for the two regimens (86–88%). Thus, it appears that, in the real-world setting, patients progressing after intensive chemoimmunotherapy as first-line therapy can be rescued by subsequent treatment, without jeopardizing their long overall survival. Intensive chemoimmunotherapy remains a legitimate option alongside targeted agents, and part of a personalized treatment landscape in chronic lymphocytic leukemia, while improved supportive care and treatment options are warranted for unfit patients.

Introduction

Chronic lymphocytic leukemia (CLL) is the most common type of leukemia in the Western world and half of the patients with this condition require treatment within 5 years of diagnosis.¹ According to Danish national CLL guidelines,^{2,3} standard first-line treatment includes fludarabine, cyclophosphamide plus rituximab (FCR) for younger, fit patients,^{4,5} and bendamustine plus rituximab (BR) for patients above 65 years old.^{6,7} Furthermore, chlorambucil, either as monotherapy or com-



Haematologica 2020
Volume 105(6):1621-1629

Correspondence:

CARSTEN UTOFT NIEMANN
carsten.utoft.niemann@regionh.dk

Received: February 22, 2019.

Accepted: September 26, 2019.

Pre-published: October 3, 2019.

doi:10.3324/haematol.2019.220194

Check the online version for the most updated information on this article, online supplements, and information on authorship & disclosures: www.haematologica.org/content/105/6/1621

©2020 Ferrata Storti Foundation

Material published in *Haematologica* is covered by copyright. All rights are reserved to the Ferrata Storti Foundation. Use of published material is allowed under the following terms and conditions:

<https://creativecommons.org/licenses/by-nc/4.0/legalcode>.

Copies of published material are allowed for personal or internal use. Sharing published material for non-commercial purposes is subject to the following conditions:

<https://creativecommons.org/licenses/by-nc/4.0/legalcode>, sect. 3. Reproducing and sharing published material for commercial purposes is not allowed without permission in writing from the publisher.



bined with anti-CD20 antibodies (CD20-chlorambucil), is recommended for unfit patients with significant comorbidity.⁸ Patients with del(17p)/*TP53* mutations are treated with targeted agents (ibrutinib, idelalisib-rituximab or venetoclax).^{9,10} The Danish guidelines are updated biannually and the changes over time have been described previously.³

Immunoglobulin heavy-chain variable region gene (IGHV) mutational status is an acknowledged prognostic factor in CLL and is included in the disease-specific International Prognostic Index (CLL-IPI).^{11,12} In previous studies, patients with unmutated IGHV (U-CLL) had shorter survival from diagnosis compared with patients with mutated IGHV (M-CLL), and inferior remission duration and survival from the start of chemoimmunotherapy.^{5,6,12-18}

We present data on the impact of IGHV mutational status on overall survival (OS) and treatment-free survival (TFS) from the time of treatment in the world's largest, nationwide, population-based cohort of consecutive, unselected patients with CLL receiving different treatment regimens.

Methods

Data sources and study population

The Danish CLL registry contains data on all patients diagnosed with CLL in Denmark since 2008.¹⁹ As of August 2017, the registry contained information on 4,135 CLL patients, who were included in the present study (Figure 1A). The CLL registry contains data on sex, dates of birth, diagnosis, and treatment, type of treatment, IGHV mutational status, and other disease characteristics including cytogenetics, *TP53* mutations, and β_2 -microglobulin levels at the time of diagnosis. Information on vital status is included in the CLL registry through regular linkage with the Danish Civil Registration System.^{20,21} Patients with missing data regarding key variables were excluded from the study. Patients were followed from the date of diagnosis in 2008-2017, until the time of death, emigration, or August 2017, whichever came first. All treatments of minimum one series were considered. For the subset of patients who had received first-line treatment at Odense University Hospital, in the Capital Region, or in the Zealand Region between 2008-2016, detailed information on second-line treatment was collected through review of the patients' clinical records. Together, these regions cover over half of the Danish population. These patients were followed from the date of diagnosis in 2008-2016, until the time of death, emigration, or mid-2018 (ranging from May-November, depending on the date of the patients' record review), whichever came first.

Statistical analysis

The patients' characteristics are reported for those with U-CLL and M-CLL and for treatment groups, and compared using parametric or non-parametric descriptive statistics, depending on the data distribution. Kaplan-Meier survival analyses were used to assess survival. TFS from the time of diagnosis (TFS_d) was defined as the time to first treatment, end of follow-up, or death, whichever came first. OS was determined starting from either the time of diagnosis (OS_d) or the time of first-line treatment initiation (OS_i), until death, or end of follow-up, whichever came first. TFS_i, defined as the time from initiation of first-line treatment to initiation of second-line treatment, death or end of follow-up, whichever came first, was studied for the sub-popu-

lation with detailed information on second-line treatment from medical record review. OS, and TFS, were the primary endpoints of the study, while OS_d and TFS_d were secondary endpoints. We explored the prognostic significance of IGHV status, treatment regimen, del(17p) status, elevated β_2 -microglobulin level, sex, age, and Binet stage for risk of death or treatment, using multi-variable Cox regression models to calculate hazard ratios (HR). All HR presented have been adjusted for these variables, except for TFS_i, which was adjusted for sex, age, del(17p)/*TP53*-mutation, and Binet stage. Unadjusted HR were calculated but are not presented in this paper as they were not of clinical relevance. Log-rank tests were used to test for homogeneity of outcomes between exposures. Data analysis was performed using STATA (StataCorp. 2015. Stata Statistical Software: Release 15.1 College Station: StataCorp LP, TX, USA)

Ethics

The study was approved by the Danish Health and Medicine Authorities (jr. n. 3-3013-1141/1) and the Danish Data Protection Agency (jr. n. RH-2015-96 03856). Results for subgroups including fewer than five patients were reported as "less than five" to ensure anonymity of individual patients, in accordance with Danish legislation.

Results

Characteristics at time of diagnosis of chronic lymphocytic leukemia

In total, 4,135 patients with a median follow-up time of 3.5 years were available for analysis, of whom two were excluded because of incomplete data. Information on IGHV mutational status was available for 3,197 (77%) patients, of whom 1,017 (32%) had U-CLL and 2,180 (68%) had M-CLL (Figure 1A). The characteristics of the patients, divided according to mutational status, are listed in Table 1. Among patients with unknown IGHV status, 255 (27%) received treatment during follow-up, compared with 481 (47%) of U-CLL and 369 (17%) of M-CLL patients. Distributions of sex and age at diagnosis were comparable between U-CLL and M-CLL patients, whereas prognostic factors were unevenly distributed, with del(13q) found in 28% of U-CLL patients and 53% of M-CLL patients. The prevalences of del(17p) (7%), del(11q) (16%) and trisomy(12) (16%) were higher among U-CLL patients than among M-CLL patients (4%, 2% and 11%, respectively). Of the U-CLL patients, 30% were categorized as having Binet stage B/C, compared with 13% of M-CLL patients, and 19% had a high level of β_2 -microglobulin (>4.0 mg/L), compared with 10% of M-CLL patients.

IGHV status and prognosis from the time of diagnosis

Patients with unmutated IGHV had shorter OS_d [HR=1.23, 95% confidence interval (95% CI): 1.01-1.50], compared with patients with M-CLL, and shorter TFS_d (HR=2.24, 95% CI: 1.95-2.57) (Figure 2A, B). The 5-year OS_d was 71% (95% CI: 68-74) for U-CLL patients and 81% (95% CI: 79-83) for those with M-CLL. The 5-year TFS_d for U-CLL patients was 31% (95% CI: 27-35), compared with 68% (95% CI: 65-70) for those with M-CLL. Patients with unknown IGHV status had a shorter 5-year OS_d (61%, 95% CI: 57-64) than patients with U-CLL or M-CLL, while the 5-year TFS_d (45%, 95% CI: 41-49) in this group was between that of U-CLL and M-CLL patients (*data not shown*). Overall, 92 (9%) patients with U-

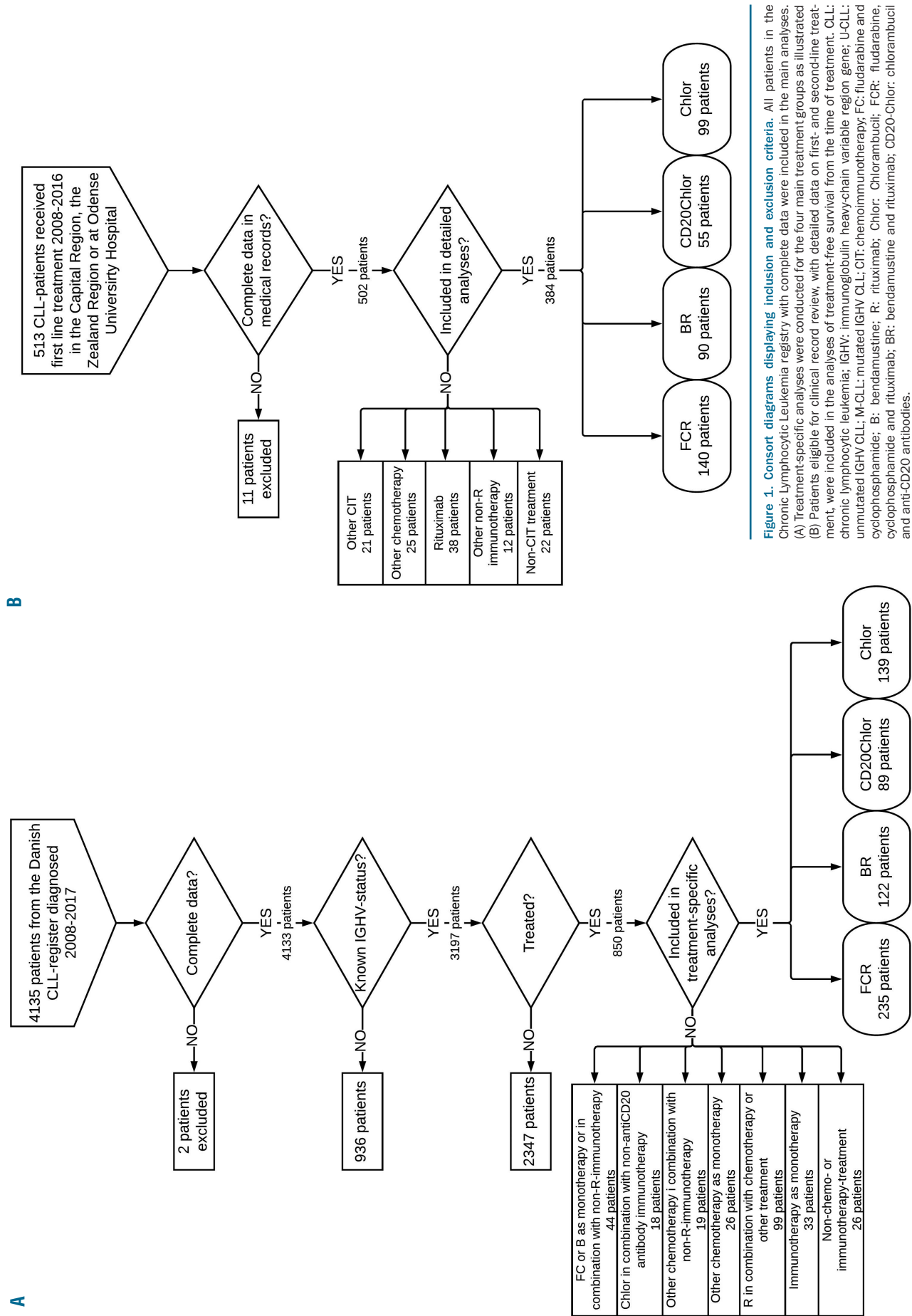


Figure 1. Consort diagrams displaying inclusion and exclusion criteria. All patients in the Chronic Lymphocytic Leukemia registry with complete data were included in the main analyses. (A) Treatment-specific analyses were conducted for the four main treatment groups as illustrated (B) Patients eligible for clinical record review, with detailed data on first- and second-line treatment, were included in the analyses of treatment-free survival from the time of treatment. CLL: chronic lymphocytic leukemia; IGHV: immunoglobulin heavy-chain variable region gene; U-CLL: unmutated IGHV CLL; M-CLL: mutated IGHV CLL; CIT: chemoimmunotherapy; FC: fludarabine and cyclophosphamide; B: bendamustine; R: rituximab; Chlor: Chlorambucil; FCR: fludarabine, cyclophosphamide and rituximab; BR: bendamustine and rituximab; CD20-Chlor: chlorambucil and anti-CD20 antibodies.

CLL, 263 (12%) patients with M-CLL, and 227 (24%) patients with unknown IGHV status died without receiving CLL treatment, while the numbers of events for OS_d, and TFS_d, were, respectively, 263 and 573 for patients with U-CLL, 384 and 632 for patients with M-CLL, and 360 and 482 for patients with unknown IGHV status.

Characteristics of treatment groups

Among the 850 treated patients with known IGHV status, 235 (28%) received FCR, 122 (14%) BR, 89 (10%) CD20-chlorambucil, 139 (16%), chlorambucil alone and 265 (31%) other, less common, treatments. Outcome was assessed separately for subgroups of patients treated with one of the four main treatment regimens (FCR, BR, CD20-chlorambucil and chlorambucil), as illustrated in Figure 1A. Patients who received other types of treatment were not studied in detail because of their small numbers. A subgroup of 99 patients received rituximab in combination with either an undefined type of chemotherapy, or other treatment: these patients were not, therefore, included in the detailed analyses. Baseline characteristics for treatment subgroups are detailed in Table 2. The median time of follow-up from treatment was 3.9 years for patients given FCR, 2.8 years for those given chlorambucil, and 2.1 years for patients treated with BR or CD20-chlorambucil. Patients treated with FCR were younger at the time of treatment (median 62 years) than patients treated with BR (median 70 years), while patients treated with CD20-chlorambucil (median 78 years) or chlorambucil (median 80 years) were the oldest. Binet B/C and U-CLL were more common among FCR-treated patients (56% and 64%, respectively) than among patients treated with BR, CD20-chlorambucil, or chlorambucil (34-42% and 52-58%, respectively). A smaller proportion of FCR-treated patients had a high β₂-microglobulin level or high/very high CLL-IPi score, compared with the other treatment groups (Table 2).

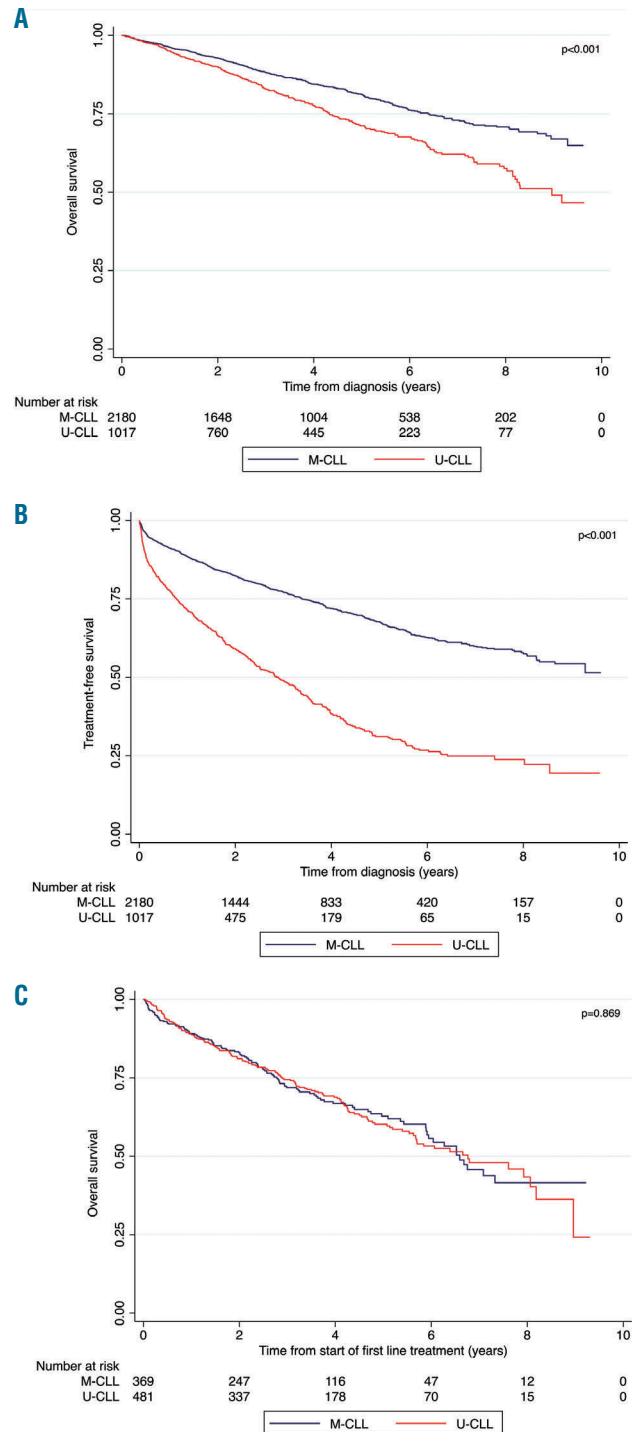
Table 1. Baseline characteristics and demographics at time of diagnosis for patients with chronic lymphocytic leukemia with unmutated, mutated and unknown IGHV mutational status from the Danish CLL registry.

Mutational status	U-CLL	M-CLL	Unknown IGHV
Number of patients	1017	2180	936
Treated	481 (47%)	369 (17%)	255 (27%)
Median age (IQR), years	69 (62-76)	70 (63-77)	74 (66-82)
Male	651 (64%)	1292 (59%)	560 (60%)
Cytogenetic abnormalities			
Del(17p)	70 (7%)	91 (4%)	44(8%)
Del(11q)	152 (16%)	50 (2%)	47 (9%)
Trisomy 12	157 (16%)	219 (11%)	60 (11%)
Normal FISH	313 (33%)	613 (30%)	147 (28%)
Del(13q)	269 (28%)	1088 (53%)	236 (44%)
B2M >4.0 mg/L	151 (19%)	174 (10%)	116 (19%)
Binet stage B/C	308 (30%)	292 (13%)	216 (23%)
Number of events OS _d	263	384	360
Number of events TFS _d	573	632	482
Number of events OS _t	171	121	133

The figures are numbers and percentages within each column unless stated otherwise. *Patients with missing data excluded. CLL: chronic lymphocytic leukemia; IGHV: immunoglobulin heavy-chain variable region gene; U-CLL: unmutated IGHV CLL; M-CLL: mutated IGHV CLL; IQR: interquartile range; FISH; fluorescence *in situ* hybridization; B2M: beta-2-microglobulin; OS_d: overall survival from time of diagnosis; TFS_d: treatment-free survival from time of diagnosis; OS_t: overall survival from time of first-line treatment.

Overall survival after first-line treatment

The median follow-up time from first-line treatment was 2.9 years. No difference in OS_t was observed between patients with U-CLL (171 deaths) and those with M-CLL



(121 deaths) [3-year OS, 74% (95% CI: 70-78) and 72% (95% CI: 66-77), respectively] (Figure 2C). Patients with unknown IGHV status had an inferior OS_t compared with U-CLL and M-CLL patients (133 deaths) [3-year OS, 59% (95% CI: 53- 65)] (*data not shown*). No impact on OS_t was observed based on unmutated IGHV status (HR=0.99, 95% CI: 0.75-1.32), Binet stage B/C at diagnosis (HR 1.01, 95% CI: 0.76-1.35), or male sex (HR=0.97, 95% CI: 0.73-1.29). Age above 65 years at the time of treatment (HR=3.18, 95% CI: 2.12- 4.77), high β₂-microglobulin level (HR=1.92, 95% CI: 1.42-2.60), and del(17p) (HR=1.79,

95% CI: 1.21-2.65) were statistically significantly associated with shorter OS_t.

During follow-up, 40 patients treated with FCR, 11 with BR, 37 with CD20-chlorambucil and 94 with chlorambucil, died. No difference was observed in 3-year OS_t rates between patients treated with FCR (88%, 95% CI: 83-92%) and BR (86%, 95% CI: 75-93%) (Figure 3A), or between those treated with CD20-chlorambucil (59%, 95% CI: 47-70%) and chlorambucil monotherapy (53%, 95% CI: 45-61%) (Figure 3B). No statistically significant variation by IGHV-status was found for OS_t, regardless of

Table 2. Baseline characteristics of chronic lymphocytic leukemia patients from the Danish CLL registry divided by treatment group.

Treatment regimen	FCR	BR	CD20-C1b	C1b	Other
Number of patients	235	122	89	139	265
Median FU time, years ^a	3.9	2.1	2.1	2.8	3.1
Median age (IQR) ^a	62 (55–67)	70 (66–75)	78 (74–82)	80 (74–84)	71 (65–78)
Male	155 (66%)	87 (71%)	60 (67%)	80 (58%)	162 (61%)
U-CLL	150 (64%)	64 (52%)	47 (53%)	80 (58%)	140 (53%)
Del(17p) ^b	10 (4%)	6 (6%)	<5 (-)	9 (4%)	40 (16%)
B2M >4.0 mg/L ^b	25 (15%)	22 (24%)	20 (31%)	30 (31%)	37 (18%)
Clinical stage					
A	103 (44%)	81 (66%)	54 (61%)	90 (65%)	154 (58%)
B/C	132 (56%)	41 (34%)	35 (39%)	49 (35%)	111 (42%)
CLL-IPI ^b					
High/very high	35 (21%)	25 (28%)	22 (34%)	32 (34%)	71 (36%)
Intermediate	82 (50%)	34 (38%)	28 (44%)	42 (44%)	80 (41%)
Low	48 (29%)	31 (34%)	14 (22%)	21 (22%)	45 (23%)
Number of events OS _t , U-CLL	26	6	18	58	63
Number of events OS _t , M-CLL	14	5	19	36	47

Data are from time of diagnosis, and figures are numbers and percentages within each column unless otherwise stated.

^aFrom time of treatment. ^bPatients with missing data excluded. FCR, fludarabine, cyclophosphamide and rituximab; BR: bendamustine and rituximab; CD20-C1b: chlorambucil and anti-CD20 antibodies; C1b: chlorambucil; FU: follow-up; IQR: interquartile range; U-CLL: chronic lymphocytic leukemia with unmutated immunoglobulin heavy-chain variable region gene; B2M: beta-2-microglobulin; CLL-IPI: chronic lymphocytic leukemia international prognostic index; OS_t: overall survival from time of first-line treatment; M-CLL: chronic lymphocytic leukemia with mutated immunoglobulin heavy-chain variable region gene.

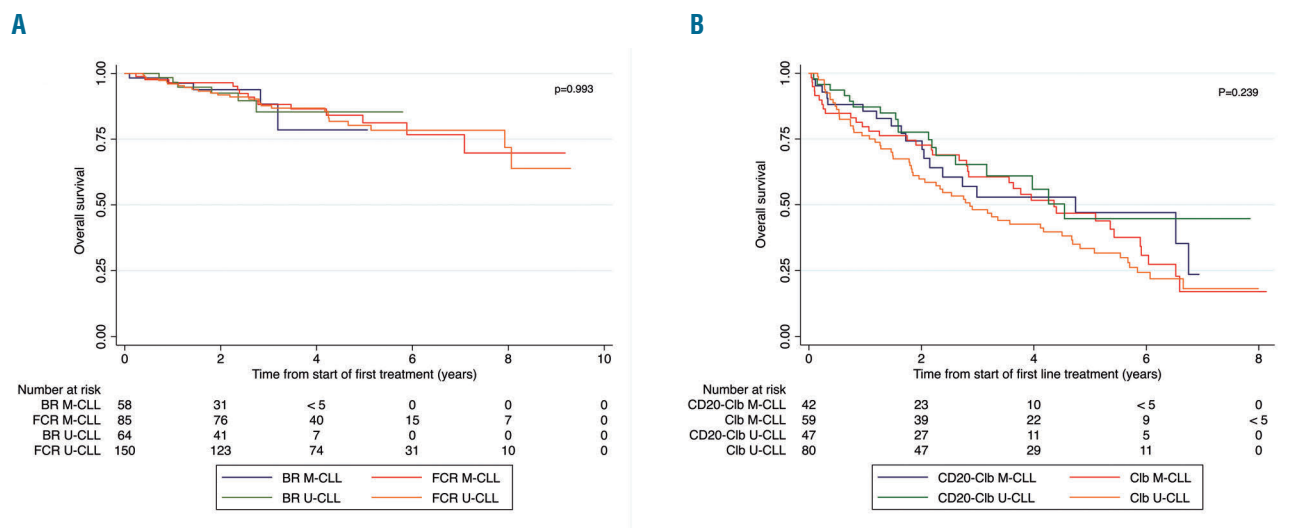


Figure 3. Overall survival of patients in the Danish CLL registry from the start of first-line treatment according to treatment group and immunoglobulin heavy-chain variable region gene mutational status. (A) Overall survival of patients treated with fludarabine, cyclophosphamide and rituximab (FCR), or bendamustine and rituximab (BR). (B) Overall survival of patients treated with chlorambucil and anti-CD20 antibodies (CD20-C1b) or chlorambucil monotherapy (C1b). M-CLL: chronic lymphocytic leukemia with mutated immunoglobulin heavy-chain variable region gene; U-CLL: chronic lymphocytic leukemia with unmutated immunoglobulin heavy-chain variable region gene.

whether the treatment regimens were pooled or separate [pooled: HR=1.15 (95% CI: 0.80-1.66), FCR-treated: HR=1.21 (95% CI: 0.53-2.77), BR-treated: HR=0.78 (95% CI: 0.14-4.15), CD20-chlorambucil-treated: HR=0.86 (95% CI: 0.38-1.91) and chlorambucil-treated: HR=1.31 (95% CI: 0.75-2.28)].

Treatment-free survival after first-line treatment

Among 513 patients eligible for record review, 11 were excluded because of incomplete data. Of the remaining 502 patients, 384 patients received one of the four major treatment regimens, which were studied in detail (Figure 1B). Comparing the four main treatment regimens, also including patients with unknown IGHV status, FCR produced the longest median TFS_t (6.0 years, 95% CI: 4.5-6.7 years), followed by BR (3.9 years, 95% CI: 3.4-5.1 years) (Figure 4A). The median TFS_t for chlorambucil-treated patients was 1 year (95% CI: 0.8-1.3 years), and that for CD20-chlorambucil-treated patients was 2.5 years (95% CI: 1.8-3.3) (Figure 4A). There were 39, 27, 11, and 36 events among U-CLL patients and 9, 7, 11, and 26 events among M-CLL patients, treated with FCR, BR, CD20-

chlorambucil, and chlorambucil, respectively. TFS_t was significantly shorter for patients with U-CLL than for those with M-CLL, following both intensive (FCR or BR) (HR=3.46, 95% CI: 1.93-6.19) and non-intensive (CD20-chlorambucil or chlorambucil) (HR=2.04, 95% CI: 1.24-3.37) treatment (Figure 4B). The 3-year TFS_t for U-CLL patients treated with intensive regimens (68%, 95% CI: 58-76) was inferior compared with that of M-CLL patients (91%, 95% CI: 81-96), also when treatments were assessed separately (FCR: HR=2.56, 95% CI: 1.19-5.50; BR: HR=7.50, 95% CI: 2.80-20.1) (Figure 4C). This was most evident for patients treated with BR, who had an estimated 3-year TFS_t of 91% (95% CI: 74-97%) for those with M-CLL and 53% (95% CI: 36-68%) for those with U-CLL, while the difference for FCR-treated patients was smaller (90%, 95% CI: 76-96%) and 76% (95% CI: 64-84%), respectively (Figure 4C). For CD20-chlorambucil- and chlorambucil-treated patients, no statistically significant difference according to IGHV status was observed when treatments were assessed separately (HR=2.19, 95% CI: 0.77-6.28 and HR=1.74, 95% CI: 0.97-3.12, respectively) (Figure 4D). Out of the 502 patients studied,

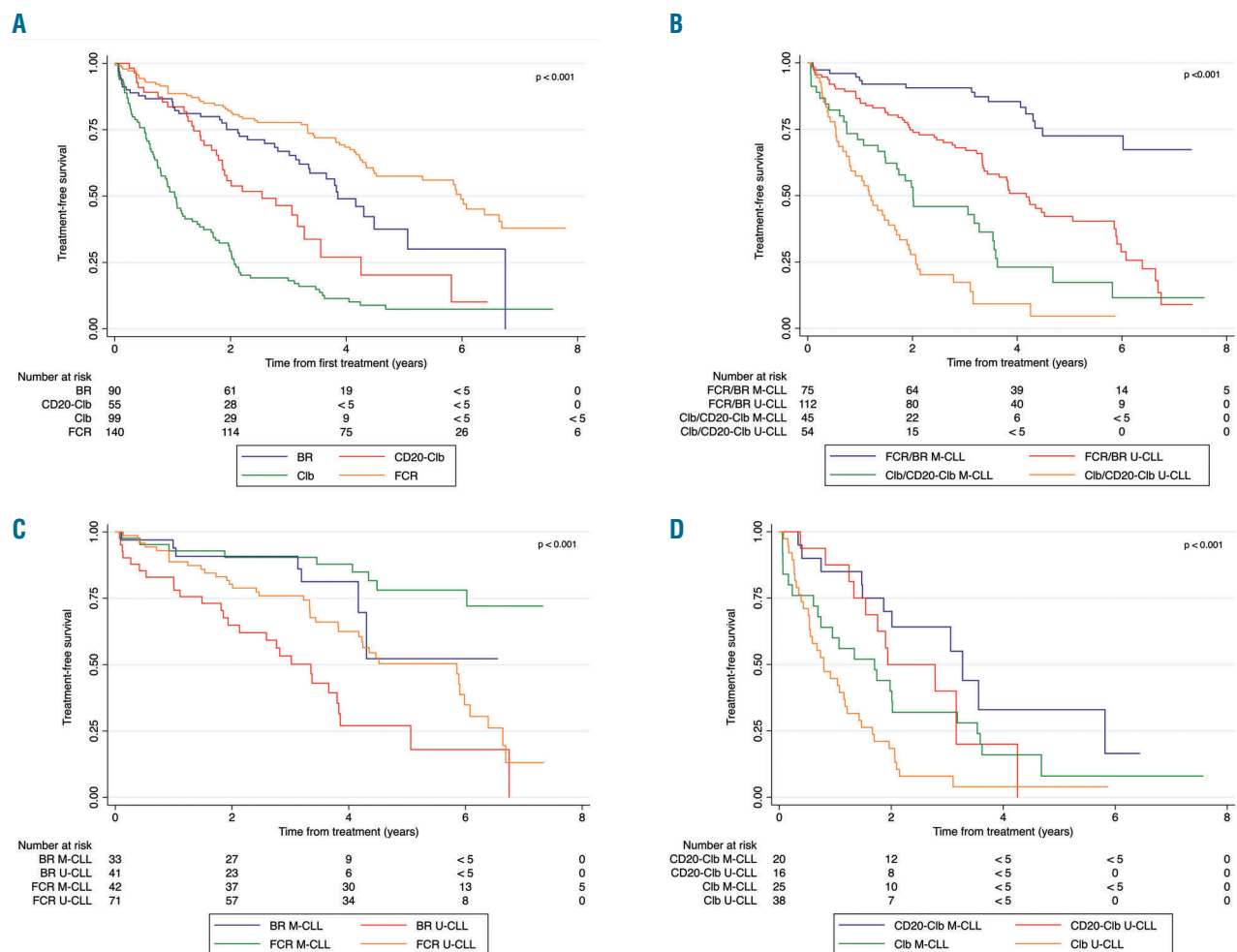


Figure 4. Treatment-free survival from the start of first-line treatment according to treatment group and immunoglobulin heavy-chain variable region gene mutational status. (A) Patients treated with fludarabine, cyclophosphamide and rituximab (FCR), bendamustine and rituximab (BR), chlorambucil (Cib), or chlorambucil and anti-CD20 antibodies (CD20-Cib), including patients with both known and unknown immunoglobulin heavy-chain variable region gene (IGHV) mutational status. (B) Patients fit for intensive treatment with FCR of BR, or unfit patients treated with Cib or CD20-Cib, and with IGHV mutated (M-CLL) or unmutated (U-CLL) CLL. (C) Patients treated with FCR or BR with U-CLL or M-CLL. (D) Patients treated with CD20-Cib or Cib with U-CLL or M-CLL.

233 received second-line treatment during follow-up. Among patients who received second-line treatment, the mutational status was known for 167 (72%), of whom 117 (70%) had U-CLL. Of these unmutated cases, 33 (28%) received targeted treatment, compared with six (12%) of mutated patients.

Discussion

We present real-world data on the prognosis of CLL, from diagnosis and from time of first-line treatment, based on IGHV mutational status from the hitherto largest nationwide, population-based cohort. The main novel finding is the lengthy OS_i of both M-CLL and U-CLL patients treated with either FCR or BR, despite inferior TFS_i of U-CLL patients; reflecting U-CLL patients' response to salvage treatment. We confirm previous findings of U-CLL being associated with shorter OS_d and TFS_d compared with M-CLL.¹²⁻¹⁴

In clinical trial reporting, progression-free survival (PFS), defined as the time until death or disease progression, is commonly used to evaluate treatment outcome. Previous studies have reported superior PFS for M-CLL patients compared with U-CLL,^{5,6,16,17} and M-CLL patients without del(17p) or del(11q) in particular have long PFS upon chemoimmunotherapy.¹⁷ The 3-year PFS rates reported in previous clinical trials with FCR (66-83%)^{5,6,16,22-24} or BR (77% for M-CLL)^{6,25} and in the real-world setting with FCR (60-80%),^{17,26} are high, but inferior to those achieved with ibrutinib-based treatment (83-96%).^{22,25,27,28} Upon chlorambucil treatment the median PFS was 9 months in a Swedish real-world setting²⁶ and 11 months in clinical trials,^{29,30} compared with 1.3-2.4 years upon CD20-chlorambucil treatment in clinical trials.²⁹⁻³²

Here we report the data for treatment-free survival, which can be clinically more relevant as many patients do not meet the International Workshop on CLL criteria for treatment at disease progression.³³ Our results reveal a superior TFS_i for M-CLL patients compared with U-CLL patients, when treated with FCR, BR, or non-intensive treatment regimens. We observed high 3-year TFS_i rates for M-CLL patients treated with FCR (90%) or BR (91%) and for U-CLL patients treated with FCR (76%), similar to the findings of a smaller retrospective study of BR-treated patients who had a 3-year TFS_i of 90%.³⁴ This is especially impressive considering the median age of 70 years of the patients treated with BR in our study. Only 6% of M-CLL patients in our study had high-risk cytogenetics, consistent with the long TFS_i of M-CLL patients that we observed.

A 3-year OS_i of 86-88% was demonstrated for patients treated with either FCR or BR. These findings are comparable with those from randomized clinical trials of FCR (84-91%)^{5,6,16,22-24} and BR (89-92%),^{6,25,35} and other real-world studies of FCR-treated patients (83-95%).^{17,26} However, the overall superior OS_i for M-CLL patients previously reported as a dichotomous variable^{4-6,16,17} and as a continuous variable,³⁶ was not observed in our study. This could reflect that the follow-up time in our study may have been too short for differences in OS_i to manifest, and that factors such as comorbidity and subsequent lines of treatment may have been unevenly distributed across groups. Furthermore, a tendency to favor FCR over other treatment options for patients with U-CLL was

observed. This might reflect physicians' choice of treatment intensification based on recognition of the inferior prognosis for this group of patients. More than twice as many U-CLL patients received second-line treatment and more than five times as many were given targeted agents compared with M-CLL patients. This is likely due to the shorter TFS_i of U-CLL patients, again in recognition of their inferior prognosis, and may in part explain why no difference in OS_i was observed.

A previous study demonstrated that the prognostic impact of IGHV status upon chemoimmunotherapy is not driven by a difference in complete remission rate, but rather by earlier relapse due to the aggressiveness of the disease in U-CLL patients.¹⁸ The long OS_i after treatment with FCR or BR for both U-CLL and M-CLL patients in our study emphasizes that patients who progress after first-line chemoimmunotherapy may be salvaged with targeted treatment, or even repeated chemoimmunotherapy. A recent conference presentation described superior PFS, improved OS, and less toxicity with ibrutinib plus rituximab compared with FCR; however, subgroup analyses indicated that the benefit was mainly for U-CLL patients.²² The findings were similar, also mainly with impact on U-CLL patients, for ibrutinib-based regimens in comparison with BR, although without a difference in OS.²⁵ Cross-over was not allowed in these studies; thus, it remains to be systematically assessed in a clinical trial whether patients with progressive disease may be salvaged with targeted agents in second-line treatment. In view of the long period off treatment in general, and the possibility of a clinical cure for a substantial subgroup of M-CLL patients, chemoimmunotherapy remains a legitimate treatment option with robust data on safety and long-term outcome in the era of targeted agents. Thus, we suggest that intensive chemoimmunotherapy should be part of a personalized treatment landscape in CLL alongside targeted treatment, with treatment options adapted based on shared decision-making, guided by robust data from clinical trials and real-world evidence.

We found that patients treated with chlorambucil as monotherapy had a poor TFS_i regardless of IGHV status. Within 1 year of initiation of first-line treatment with chlorambucil, 50% of the patients had had an event. Patients treated with CD20-chlorambucil, with a median age of 78 years and representing a frail patient population, had a median TFS_i of 2.5 years. A similar median TFS_i of 3.4 years was observed in patients of comparable age receiving CD20-chlorambucil in randomized controlled trials.³⁷ The superior outcome of patients treated with CD20-chlorambucil, compared with chlorambucil suggests that chlorambucil as monotherapy must be considered obsolete. As baseline characteristics were similar between the groups in our study, our findings indicate that chlorambucil should be replaced by CD20-chlorambucil or by more effective and less toxic novel treatments. Considering the results of our study, as well as those of clinical trials, new treatment options and improved supportive care are warranted for patients unfit for intensive chemoimmunotherapy. The recently published studies on venetoclax plus obinutuzumab and ibrutinib-based frontline therapy, compared with CD20-chlorambucil, broaden the options for these patients. Subgroup findings indicate that mainly U-CLL patients benefit from targeted therapy, as also seen when compared with intensive chemoimmunotherapy regimens.^{25,32,38,39}

In contrast to a clinical trial setting, inclusion of patients above 65 years and more patients with significant comorbidities in our cohort^{40,41} may have reduced the impact of IGHV status as a prognostic factor.⁴²⁻⁴⁴ Clinical trial populations in CLL studies exploring IGHV status and chemoimmunotherapy had a median age of 57-73 years,^{5,6,16,32} compared with 62-80 years in our study, further emphasizing the importance of assessing real-world data. The higher prevalence of elevated β_2 -microglobulin levels in the treatment groups with a higher median age in our study may reflect decreased renal function^{45,46} and thus the comorbidity of these patients, rather than more aggressive CLL. The impact of comorbidity and frailty in the real-world population reported here is also reflected by a 3-year OS_i of 59% for patients treated with CD20-chlorambucil compared with over 80% in the CLL11 trial.⁸

Cancer patients for whom data registration is incomplete have previously been found to have poorer outcome,⁴⁷ which was also seen for patients with unknown IGHV status in the present study, when comparing both OS_d and OS_i in these patients with those of patients with mutated or unmutated IGHV. Patients with unknown IGHV status had a superior TFS_d compared with that of U-CLL patients. This reflects that many patients with unknown IGHV status die, probably due to CLL-unrelated causes, without ever receiving treatment for CLL.

The main strength of this study is its nationwide cohort, without the selection bias introduced in clinical trials, and the near completeness of data. Inherent in the retrospective design of the study, patients were assigned therapy by the treating physicians based on clinical assessment of fitness and clinical guidelines, in line with the described age distribution. The discrepancy in baseline characteristics between the treatment groups is a weakness of our study, although we have adjusted for known dissimilarities between the groups. However, as stated above, factors such as number and type of subsequent lines of treat-

ments, and distribution of comorbidities across groups of patients, are unknown. Uneven distribution of these factors could in part explain the discrepancy between our results and those of previous studies regarding the significance of IGHV status in relation to OS_i. More patients were diagnosed with CLL during the latter half of the study period, likely due to earlier detection of CLL, leading to a shorter follow-up time than anticipated. The short median follow-up time was also driven by the high mortality in this population, resulting in over half of the treated patients dying during follow-up.

Conclusions

This population-based study demonstrates excellent OS_i with FCR or BR for both U-CLL and M-CLL patients, indicating that patients who progress after first-line chemoimmunotherapy may be salvaged with second- or later-line treatments. In view of the long treatment-free period and the possibility of clinical cure for a substantial subgroup of M-CLL patients, intensive chemoimmunotherapy remains a valid treatment option and part of a personalized treatment landscape in CLL alongside targeted agents. Patients treated with chlorambucil-based regimens have a poor outcome; thus, improved supportive care and targeted treatment options, as seen in recent randomized controlled trials, are warranted for patients who are unfit for intensive chemoimmunotherapy.

Acknowledgments

We would like to thank Fanny Kullberg for her work in collecting information from medical records. This study was supported in part by grants from Janssen and Novo Nordisk Foundation. The funding sources had no role in the study design, collection, analysis or interpretation of the data, writing the manuscript, or the decision to submit the paper for publication.

References

- Nabhan C, Chaffee KG, Slager SL, et al. Analysis of racial variations in disease characteristics, treatment patterns, and outcomes of patients with chronic lymphocytic leukemia. *Am J Hematol.* 2016;91(7):677-680.
- Danish Lymphoma Group. National guidelines for chronic lymphocytic leukaemia. Available at <http://www.lymphoma.dk/retningslinjer/2018>.
- da Cunha-Bang C, Simonsen J, Rostgaard K, et al. Improved survival for patients diagnosed with chronic lymphocytic leukemia in the era of chemo-immunotherapy: a Danish population-based study of 10455 patients. *Blood Cancer J.* 2016;6(11):e499.
- Hallek M, Fischer K, Fingerle-Rowson G, et al. Addition of rituximab to fludarabine and cyclophosphamide in patients with chronic lymphocytic leukaemia: a randomised, open-label, phase 3 trial. *Lancet.* 2010;376(9747):1164-1174.
- Fischer K, Bahlo J, Fink AM, et al. Long-term remissions after FCR chemoimmunotherapy in previously untreated patients with CLL: updated results of the CLL8 trial. *Blood.* 2016;127(2):208-215.
- Eichhorst B, Fink AM, Bahlo J, et al. First-line chemoimmunotherapy with bendamustine and rituximab versus fludarabine, cyclophosphamide, and rituximab in patients with advanced chronic lymphocytic leukaemia (CLL10): an international, open-label, randomised, phase 3, non-inferiority trial. *Lancet Oncol.* 2016;17(7):928-942.
- Cramer P, Isfort S, Bahlo J, et al. Outcome of advanced chronic lymphocytic leukemia following different first-line and relapse therapies: a meta-analysis of five prospective trials by the German CLL Study Group (GCLLSG). *Haematologica.* 2015;100(11):1451-1459.
- Goede V, Fischer K, Engelke A, et al. Obinutuzumab as frontline treatment of chronic lymphocytic leukemia: updated results of the CLL11 study. *Leukemia.* 2015;29(7):1602-1604.
- Farooqui MZ, Valdez J, Martyr S, et al. Ibrutinib for previously untreated and relapsed or refractory chronic lymphocytic leukaemia with TP53 aberrations: a phase 2, single-arm trial. *Lancet Oncol.* 2015;16(2):169-176.
- Byrd JC, Furman RR, Coutre SE, et al. Targeting BTK with ibrutinib in relapsed chronic lymphocytic leukemia. *N Engl J Med.* 2013;369(1):32-42.
- International C. L. L. I. P. I. Working Group. An international prognostic index for patients with chronic lymphocytic leukaemia (CLL-IPi): a meta-analysis of individual patient data. *Lancet Oncol.* 2016;17(6):779-790.
- da Cunha-Bang C, Christiansen I, Niemann CU. The CLL-IPi applied in a population-based cohort. *Blood.* 2016;128(17):2181-2183.
- Damle RN, Wasil T, Fais F, et al. Ig V gene mutation status and CD38 expression as novel prognostic indicators in chronic lymphocytic leukemia. *Blood.* 1999;94(6):1840-1847.
- Hamblin TJ, Davis Z, Gardiner A, Oscier DG, Stevenson FK. Unmutated Ig V(H) genes are associated with a more aggressive form of chronic lymphocytic leukemia. *Blood.* 1999;94(6):1848-1854.
- Stilgenbauer S, Schnaiter A, Paschka P, et al. Gene mutations and treatment outcome in chronic lymphocytic leukemia: results from the CLL8 trial. *Blood.* 2014;123(21):3247-3254.
- Thompson PA, Tam CS, O'Brien SM, et al. Fludarabine, cyclophosphamide, and ritux-

- imab treatment achieves long-term disease-free survival in IGHV-mutated chronic lymphocytic leukemia. *Blood*. 2016;127(3):303-309.
17. Rossi D, Terzi-di-Bergamo L, De Paoli L, et al. Molecular prediction of durable remission after first-line fludarabine-cyclophosphamide-rituximab in chronic lymphocytic leukemia. *Blood*. 2015;126(16):1921-1924.
 18. Lin KI, Tam CS, Keating MJ, et al. Relevance of the immunoglobulin VH somatic mutation status in patients with chronic lymphocytic leukemia treated with fludarabine, cyclophosphamide, and rituximab (FCR) or related chemoimmunotherapy regimens. *Blood*. 2009;113(14):3168-3171.
 19. da Cunha-Bang C, Geisler CH, Enggaard L, et al. The Danish National Chronic Lymphocytic Leukemia Registry. *Clin Epidemiol*. 2016;8:561-565.
 20. Pedersen CB. The Danish Civil Registration System. *Scand J Public Health*. 2011;39(7 Suppl):22-25.
 21. Schmidt M, Pedersen L, Sorensen HT. The Danish Civil Registration System as a tool in epidemiology. *Eur J Epidemiol*. 2014;29(8):541-549.
 22. Shanafelt TD, Wang V, Kay NE, et al. A Randomized phase III study of ibrutinib (PCI-32765)-based therapy vs. standard fludarabine, cyclophosphamide, and rituximab (FCR) chemoimmunotherapy in untreated younger patients with chronic lymphocytic leukemia (CLL): a trial of the ECOG-ACRIN Cancer Research Group (E1912). *Blood*. 2018;132(Suppl 1):LBA-4-LBA-4.
 23. Lepretre S, Aurran T, Mahe B, et al. Excess mortality after treatment with fludarabine and cyclophosphamide in combination with alemtuzumab in previously untreated patients with chronic lymphocytic leukemia in a randomized phase 3 trial. *Blood*. 2012;119(22):5104-5110.
 24. Munir T, Howard DR, McParland L, et al. Results of the randomized phase IIB ADMIRE trial of FCR with or without mitoxantrone in previously untreated CLL. *Leukemia*. 2017;31(10):2085-2093.
 25. Woyach JA, Ruppert AS, Heerema NA, et al. Ibrutinib regimens versus chemoimmunotherapy in older patients with untreated CLL. *N Engl J Med*. 2018;379(26):2517-2528.
 26. Sylvan SE, Askild A, Johansson H, et al. First-line therapy in chronic lymphocytic leukemia: a Swedish nation-wide real-world study on 1053 consecutive patients treated between 2007 and 2013. *Haematologica*. 2019;104(4):797-804.
 27. Robak T, Burger JA, Tedeschi A, et al. Single-agent ibrutinib versus chemoimmunotherapy regimens for treatment-naïve patients with chronic lymphocytic leukemia: a cross-trial comparison of phase 3 studies. *Am J Hematol*. 2018;93(11):1402-1410.
 28. O'Brien S, Furman RR, Coutre S, et al. Single-agent ibrutinib in treatment-naïve and relapsed/refractory chronic lymphocytic leukemia: a 5-year experience. *Blood*. 2018;131(17):1910-1919.
 29. Goede V, Fischer K, Busch R, et al. Obinutuzumab plus chlorambucil in patients with CLL and coexisting conditions. *N Engl J Med*. 2014;370(12):1101-1110.
 30. Hillmen P, Robak T, Janssens A, et al. Chlorambucil plus ofatumumab versus chlorambucil alone in previously untreated patients with chronic lymphocytic leukaemia (COMPLEMENT 1): a randomised, multicentre, open-label phase 3 trial. *Lancet*. 2015;385(9980):1873-1883.
 31. Goede V, Fischer K, Dyer MJ, et al. Overall survival benefit of obinutuzumab over rituximab when combined with chlorambucil in patients with chronic lymphocytic leukemia and comorbidities: final survival analysis of the CLL11 study. *EHA Learning Center*, 2018; 215923.S151.
 32. Moreno C, Greil R, Demirkan F, et al. Ibrutinib plus obinutuzumab versus chlorambucil plus obinutuzumab in first-line treatment of chronic lymphocytic leukaemia (iLLUMINATE): a multicentre, randomised, open-label, phase 3 trial. *Lancet Oncol*. 2019;20(1):43-56.
 33. Hallek M, Cheson BD, Catovsky D, et al. iwCLL guidelines for diagnosis, indications for treatment, response assessment, and supportive management of CLL. *Blood*. 2018;131(25):2745-2760.
 34. Laurenti L, Innocenti I, Autore F, et al. Bendamustine in combination with rituximab for elderly patients with previously untreated B-cell chronic lymphocytic leukemia: a retrospective analysis of real-life practice in Italian hematology departments. *Leuk Res*. 2015;39(10):1066-1070.
 35. Fischer K, Cramer P, Busch R, et al. Bendamustine in combination with rituximab for previously untreated patients with chronic lymphocytic leukemia: a multicenter phase II trial of the German Chronic Lymphocytic Leukemia Study Group. *J Clin Oncol*. 2012;30(26):3209-3216.
 36. Jain P, Noguera Gonzalez GM, Kanagal-Shamanna R, et al. The absolute percent deviation of IGHV mutation rather than a 98% cut-off predicts survival of chronic lymphocytic leukaemia patients treated with fludarabine, cyclophosphamide and rituximab. *Br J Haematol*. 2018;180(1):33-40.
 37. Al-Sawaf O, Bahlo J, Robrecht S, et al. Outcome of patients aged 80 years or older treated for chronic lymphocytic leukaemia. *Br J Haematol*. 2018;183(5):727-735.
 38. Fischer K, Al-Sawaf O, Bahlo J, et al. Venetoclax and obinutuzumab in patients with CLL and coexisting conditions. *N Engl J Med*. 2019;380(23):2225-2236.
 39. Jain N, Keating M, Thompson P, et al. Ibrutinib and venetoclax for first-line treatment of CLL. *N Engl J Med*. 2019;380(22):2095-2103.
 40. Hutchins LF, Unger JM, Crowley JJ, Coltman CA Jr, Albain KS. Underrepresentation of patients 65 years of age or older in cancer-treatment trials. *N Engl J Med*. 1999;341(27):2061-2067.
 41. Lewis JH, Kilgore ML, Goldman DP, et al. Participation of patients 65 years of age or older in cancer clinical trials. *J Clin Oncol*. 2003;21(7):1383-1389.
 42. Goede V, Cramer P, Busch R, et al. Interactions between comorbidity and treatment of chronic lymphocytic leukemia: results of German Chronic Lymphocytic Leukemia Study Group trials. *Haematologica*. 2014;99(6):1095-1100.
 43. Wieringa A, Boslooper K, Hoogendoorn M, et al. Comorbidity is an independent prognostic factor in patients with advanced-stage diffuse large B-cell lymphoma treated with R-CHOP: a population-based cohort study. *Br J Haematol*. 2014;165(4):489-496.
 44. Zhao H, Wang T, Wang Y, et al. Comorbidity as an independent prognostic factor in elderly patients with peripheral T-cell lymphoma. *Onco Targets Ther*. 2016;9:1795-1799.
 45. Foster MC, Coresh J, Hsu CY, et al. Serum beta-trace protein and beta2-microglobulin as predictors of ESRD, mortality, and cardiovascular disease in adults with CKD in the Chronic Renal Insufficiency Cohort (CRIC) study. *Am J Kidney Dis*. 2016;68(1):68-76.
 46. Delgado J, Pratt G, Phillips N, et al. Beta2-microglobulin is a better predictor of treatment-free survival in patients with chronic lymphocytic leukaemia if adjusted according to glomerular filtration rate. *Br J Haematol*. 2009;145(6):801-805.
 47. Rostgaard K, Vaeth M, Rootzen H, et al. Do changes in lymph node status distribution explain trends in survival of breast cancer patients in Denmark? *Eur J Cancer Prev*. 2006;15(5):398-404.



Hypoxia-induced long non-coding RNA DARS-AS1 regulates RBM39 stability to promote myeloma malignancy

Jia Tong,^{1,*} Xiaoguang Xu,^{1,*} Zilu Zhang,¹ Chengning Ma,² Rufang Xiang,¹ Jia Liu,¹ Wenbin Xu,¹ Chao Wu,¹ Junmin Li,¹ Fenghuang Zhan,³ Yingli Wu² and Hua Yan^{1,4}

¹Department of Hematology, Affiliated Ruijin Hospital of Shanghai Jiao Tong University School of Medicine, Shanghai, China; ²Hongqiao International Institute of Medicine, Shanghai Tongren Hospital, Key Laboratory of Cell Differentiation and Apoptosis of the Chinese Ministry of Education, Shanghai Jiao Tong University School of Medicine, Shanghai, China; ³Division of Hematology, Oncology, and Blood and Marrow Transplantation, Department of Internal Medicine, University of Iowa, Iowa City, IA, USA and ⁴Department of General Practice, Ruijin Hospital, Shanghai Jiao Tong University School of Medicine, Shanghai, China.

*JA and XX contributed equally as co-first authors.

Haematologica 2020
Volume 105(6):1630-1640

ABSTRACT

Multiple myeloma is a malignant plasma-cell disease, which is highly dependent on the hypoxic bone marrow microenvironment. However, the underlying mechanisms of hypoxia contributing to myeloma genesis are not fully understood. Here, we show that long non-coding RNA DARS-AS1 in myeloma is directly upregulated by hypoxia inducible factor (HIF)-1. Importantly, DARS-AS1 is required for the survival and tumorigenesis of myeloma cells both *in vitro* and *in vivo*. DARS-AS1 exerts its function by binding RNA-binding motif protein 39 (RBM39), which impedes the interaction between RBM39 and its E3 ubiquitin ligase RNF147, and prevents RBM39 from degradation. The overexpression of RBM39 observed in myeloma cells is associated with poor prognosis. Furthermore, knockdown of DARS-AS1 inhibits the mammalian target of rapamycin signaling pathway, an effect that is reversed by RBM39 overexpression. We reveal that a novel HIF-1/DARS-AS1/RBM39 pathway is implicated in the pathogenesis of myeloma. Targeting DARS-AS1/RBM39 may, therefore, represent a novel strategy to combat myeloma.

Correspondence:

HUA YAN
yanhua_candy@163.com

YINGLI WU
wuyingli@shsmu.edu.cn

Received: February 1, 2019.

Accepted: July 5, 2019.

Pre-published: July 9, 2019.

doi:10.3324/haematol.2019.218289

Check the online version for the most updated information on this article, online supplements, and information on authorship & disclosures: www.haematologica.org/content/105/6/1630

©2020 Ferrata Storti Foundation

Material published in Haematologica is covered by copyright. All rights are reserved to the Ferrata Storti Foundation. Use of published material is allowed under the following terms and conditions:

<https://creativecommons.org/licenses/by-nc/4.0/legalcode>.

Copies of published material are allowed for personal or internal use. Sharing published material for non-commercial purposes is subject to the following conditions:

<https://creativecommons.org/licenses/by-nc/4.0/legalcode>,

sect. 3. Reproducing and sharing published material for commercial purposes is not allowed without permission in writing from the publisher.



Introduction

Multiple myeloma (MM) is characterized by abnormal accumulation of monoclonal plasma cells in the bone marrow and broad clinical and pathophysiological heterogeneity leading to a fatal outcome. Hypoxia in specific bone marrow niches induces numerous changes in the expression of genes that contribute to the maintenance of myeloma cells and the progression of myeloma, leading to drug resistance and cancer recurrence.¹ Focusing on the hypoxia-related pathogenic mechanisms in myeloma may facilitate the optimization of the choice of therapeutic regimen and improve clinical outcomes.

Long non-coding RNA (lncRNA) are mRNA-like transcripts that are longer than 200 nucleotides.^{2,3} Accumulating evidence indicates that lncRNA are crucial molecules that participate in gene regulation at the epigenetic, transcriptional, and post-transcriptional levels.^{3,4} Aberrant expression of lncRNA can promote the development and progression of malignant tumors through contributing to proliferation, invasion and metastasis.^{5,7} lncRNA may, therefore, serve as potential diagnostic biomarkers and therapeutic targets for cancers. However, few lncRNA have been functionally studied in MM. Many hypoxia inducible factor (HIF)-dependent protein-coding genes contribute to adaptation to hypoxia. Whether lncRNA are involved in the response to hypoxia in myeloma and the determination of their regulatory roles is important for a better understanding of the development and progression of myeloma.

RNA-binding motif protein 39 (RBM39) is a transcriptional coactivator for the steroid nuclear receptors ESR1/ER- α and ESR2/ER- β as well as for JUN/AP-1 and NF- κ B. RBM39 is also involved in the pre-mRNA splicing process.^{9,11} Previous studies have pinpointed RBM39 as a proto-oncogene with important roles in the development and progression of numerous types of malignancies.^{8,12,13} However, the role of RBM39 in MM is largely unknown.

By analysis of high-throughput RNA sequencing results, we identified that lncRNA DARS-AS1 was significantly upregulated in myeloma cells under hypoxic conditions. We evaluated its biological role and clinical significance in tumor progression and revealed that the novel HIF-1/DARS-AS1/RBM39 signaling pathway is implicated in the tumorigenesis of MM.

Methods

Cell culture and transfection

RPMI 8226, LP-1, U266, H929, and HEK293T cells were obtained from the Cell Resource Center of Shanghai Institute for Biological Science, Chinese Academy of Science. All the cell lines have been authenticated using short tandem repeat genotype detection. Myeloma cell lines were grown in RPMI 1640 (Gibco, CA, USA) containing 1% penicillin and streptomycin (Fisher Scientific, MA, USA), supplemented with 10% fetal bovine serum (Sigma-Aldrich, MO, USA). The hypoxic environment (1% O₂) was generated by flushing a 94% N₂/5% CO₂ mixture into the incubator. Retroviral particles were produced in HEK293T cells by transient co-transfection of target gene expression vectors, Gag-pol, and VSVG packaging plasmid, while lentiviral particles were produced by transient co-transfection of target gene expression vectors, psPAX2 and pMD2.G packaging plasmid, using lipofectamine 2000 (Invitrogen, MA, USA), according to the manufacturer's instructions. Cells were infected in culture medium supplemented with polybrene (8 μ g/mL) and 24 h later the medium was changed to RPMI 1640 with 10% fetal bovine serum. Studies were conducted in accordance with the Declaration of Helsinki, and approval was received from the relevant ethics committees.

Luciferase assay

For DARS-AS1 promoter luciferase reporter assays, luciferase reporter constructs (100 ng) containing the potential HIF response element (HRE) sequence [wildtype, (WT) or mutant (MUT)], together with pSV40-renilla (10 ng), and HIF-1 α overexpression plasmids (800 ng) were transfected into HEK293T cells in 24-well plates. Luciferase activity assays were performed 48 h after transfection (Promega, Madison, USA). Firefly luciferase activity was normalized to the corresponding renilla luciferase activity by using the Dual-Luciferase Reporter Assay System. All experiments were performed three times.

Co-immunoprecipitation

Corresponding antibody or IgG was added to cell lysate that was treated with A+G agarose beads (Thermo Fisher Scientific, MA, USA). The mixture was rotated for 6 h and precipitated beads were washed three times with phosphate-buffered saline containing a protease inhibitor cocktail.

RNA immunoprecipitation

RNA immunoprecipitation experiments were performed using a Magna RIP RNA-Binding Protein Immunoprecipitation Kit (Millipore, Darmstadt, Germany) according to the manufac-

turer's instructions. Supernatants were incubated with 1-2 μ g of anti-Flag (Sigma, MO, USA) or mouse IgG (Invitrogen, MA, USA) for 6 h at 4°C followed by precipitation with protein A/G agarose (Pierce, Rockford, IL, USA). The co-precipitated RNA were detected by quantitative real-time reverse transcription polymerase chain reaction (Q-PCR).

RNA pulldown and mass spectrometry analysis

Full-length DARS-AS1 were constructed by subcloning the gene sequences into a pcDNA3.1 (+) backbone. Biotin-labeled DARS-AS1 was synthesized using Biotin RNA Labeling Mix (Roche; Basel, Switzerland) by T7 RNA polymerase (Promega; WI, USA), treated with RNase-free DNase I (Promega) and purified with an RNeasy Mini Kit (QIAGEN). Thirty micrograms of biotinylated RNA were used in each pulldown assay. The proteins with biotin-labeled DARS-AS1 were pulled down with streptavidin magnetic beads (Thermo, Fisher Scientific, MA, USA) after incubation overnight. The samples were separated by electrophoresis and the specific bands were identified using mass spectrometry and a human proteomic library.

Chromatin immunoprecipitation

HEK293T cells with HIF-1 α overexpression (2 \times 10⁷) were harvested and chromatin immunoprecipitation experiments were performed using a SimpleChIP® Enzymatic Chromatin IP Kit (Agarose Beads) (CST, MA, USA) according to the manufacturer's instructions. The primers used are listed in *Online Supplementary Table S3*.

Bioinformatics analysis

Uniprot (<https://www.uniprot.org/>) was used to analyze the protein-protein interactions.

Statistics

Continuous variables are expressed as the mean \pm standard error (SE). For comparisons of two groups, a *t*-test was used. When comparing more than two groups, analysis of variance with the Tukey test for multiple comparisons was used. Statistical significance is defined as: **P*<0.05, ***P*<0.01 and ****P*<0.001.

Results

DARS-AS1 is upregulated under hypoxia in myeloma cells

To identify hypoxia-regulated lncRNA, we analyzed the difference in the RNA-sequencing data of U266 cells in normoxic and hypoxic culture environments (*Online Supplementary Table S4*). Twenty-two upregulated lncRNA in U266 cells were successfully identified (Figure 1A). Q-PCR revealed that two lncRNA, DARS-AS1 and MIR210HG, were significantly upregulated under the hypoxic condition (Figure 1B). The modulation of MIR210HG did not have significant effects on myeloma cell proliferation or apoptosis (*Online Supplementary Figure S1A-D*). Thus, we mainly studied the function of DARS-AS1 in myeloma.

First, we assessed the expression of DARS-AS1 in myeloma cell lines. We found that the hypoxic environment (1% oxygen concentration) caused a significant increase in the level of expression of DARS-AS1 in the MM cell lines (Figure 1C). The expression of DARS-AS1 in CD38⁺ cells derived from bone marrow of patients with active myeloma was significantly higher than that of nor-

mal human bone marrow mononuclear cells after culture in a hypoxic environment for 24 h (Figure 1D). These data suggest that hypoxia leads to upregulation of DARS-AS1.

DARS-AS1 participates in the proliferation of myeloma cells, inhibits their apoptosis and accelerates tumorigenesis

We next investigated the role of DARS-AS1 in myeloma cells. Importantly, we found that the expression of short hairpin RNA (shRNA) against DARS-AS1 in the MM cell lines RPMI 8226 and LP-1 substantially inhibited cell proliferation in the hypoxic environment (Figure 2A, B, *Online Supplementary Figure S2A*), whereas the overexpression of DARS-AS1 promoted cell proliferation (Figure 2C, D, *Online Supplementary Figure S2B*). Furthermore, the knockdown of DARS-AS1 resulted in a substantial increase in the percentages of apoptotic cells in the hypoxic environment (Figure 2E), and DARS-AS1 overexpression reduced

the rate of apoptosis of cells starved of glucose (glucose 1 mM) (*Online Supplementary Figure S2C*), as evidenced by both the increased annexin V⁺ cell population and the cleavage of caspase-3/PARP1 (Figure 2F, *Online Supplementary Figure S2D, E*). At the same time, DARS-AS1 overexpression attenuated the sensitivity of myeloma cells to bortezomib (2.5 nM) (*Online Supplementary Figure S2F*). However, knockdown of DARS-AS1 did not have significant effects on cell migration (*Online Supplementary Figure S2G*), invasion (*Online Supplementary Figure S2H*) or cell-cycle distribution (*Online Supplementary Figure S3A-C*) of myeloma cells in the hypoxic environment. Next, we injected RPMI 8226 cells with stable knockdown/overexpression of DARS-AS1 into the back flank of NOD-SCID mice. We found that stable knockdown of DARS-AS1 in RPMI 8226 cells remarkably inhibited the tumorigenesis of these cells *in vivo*, whereas overexpression of DARS-AS1 significantly enhanced tumor growth (Figure 2G, I,

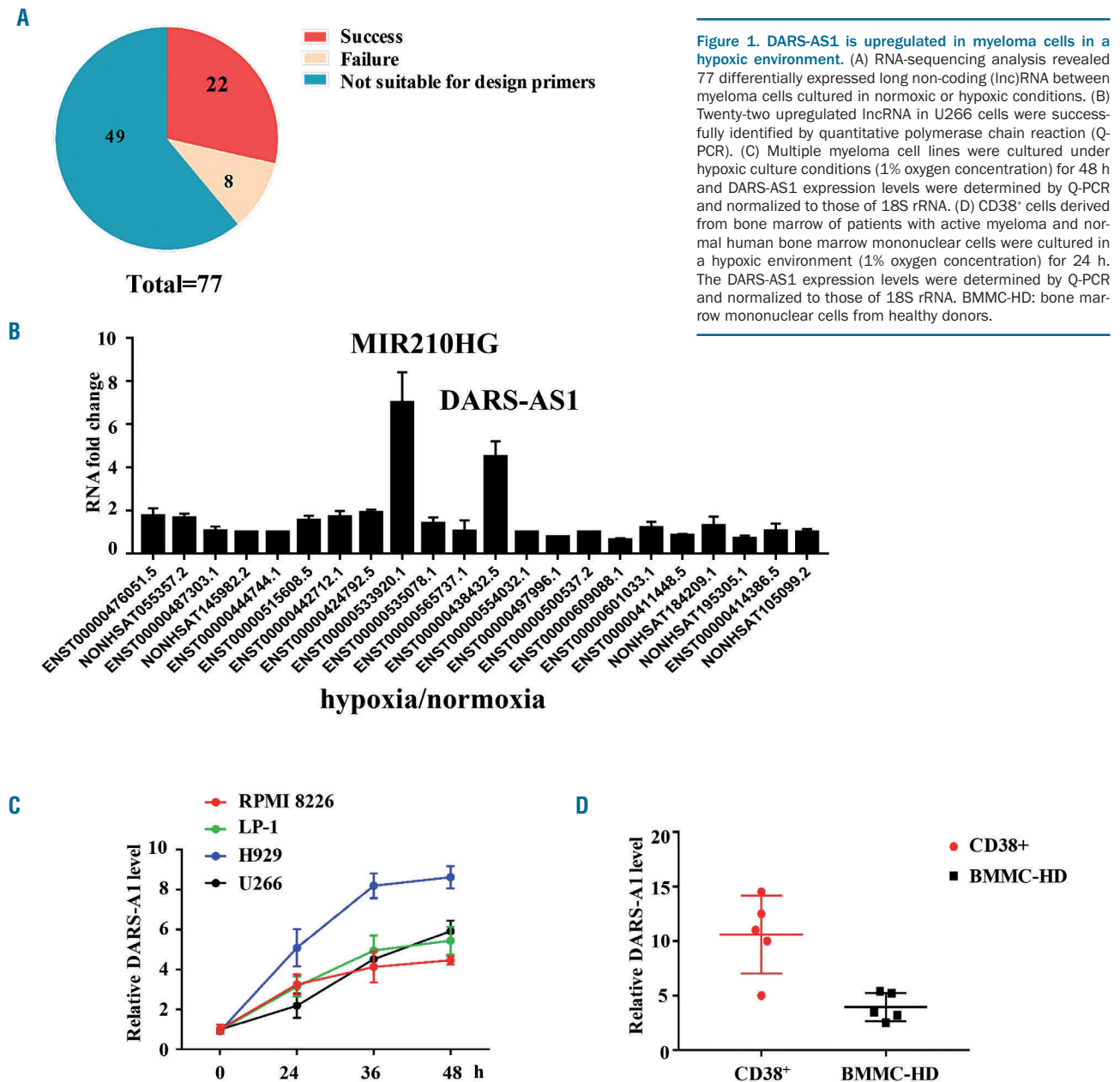


Figure 1. DARS-AS1 is upregulated in myeloma cells in a hypoxic environment. (A) RNA-sequencing analysis revealed 77 differentially expressed long non-coding (lnc)RNA between myeloma cells cultured in normoxic or hypoxic conditions. (B) Twenty-two upregulated lncRNA in U266 cells were successfully identified by quantitative polymerase chain reaction (Q-PCR). (C) Multiple myeloma cell lines were cultured under hypoxic culture conditions (1% oxygen concentration) for 48 h and DARS-AS1 expression levels were determined by Q-PCR and normalized to those of 18S rRNA. (D) CD38⁺ cells derived from bone marrow of patients with active myeloma and normal human bone marrow mononuclear cells were cultured in a hypoxic environment (1% oxygen concentration) for 24 h. The DARS-AS1 expression levels were determined by Q-PCR and normalized to those of 18S rRNA. BMMC-HD: bone marrow mononuclear cells from healthy donors.

Online Supplementary Figure S3D). Ki67 and TUNEL staining of xenografts further confirmed these findings (Figure 2H, J, Online Supplementary Figure S3F). These results indicate that DARS-AS1 promotes MM cell growth and survival, and inhibits apoptosis both *in vitro* and *in vivo*.

Identification of DARS-AS1-interacting proteins

Recent studies have uncovered the involvement of many lncRNA in signal transduction regulation through their interactions with proteins.^{14,15} To explore the molecular mechanism by which DARS-AS1 exerts its effects on

MM cells, we performed biotin-labeled RNA pulldown, followed by mass spectrometry assays to identify the DARS-AS1-interacting proteins in RPMI 8226 and LP-1 cells (Figure 3A, B). After exclusion of the non-specifically binding proteins present in both the sense and antisense of DARS-AS1 precipitate, six potential target proteins were identified, among which RBM39 and PCBP1 were of predominant interest (Online Supplementary Figure S5A). Only RBM39 binding with DARS-AS1 in three myeloma cell lines was detected by western blotting in three independent RNA pulldown assays (Figure 3C). The specific inter-

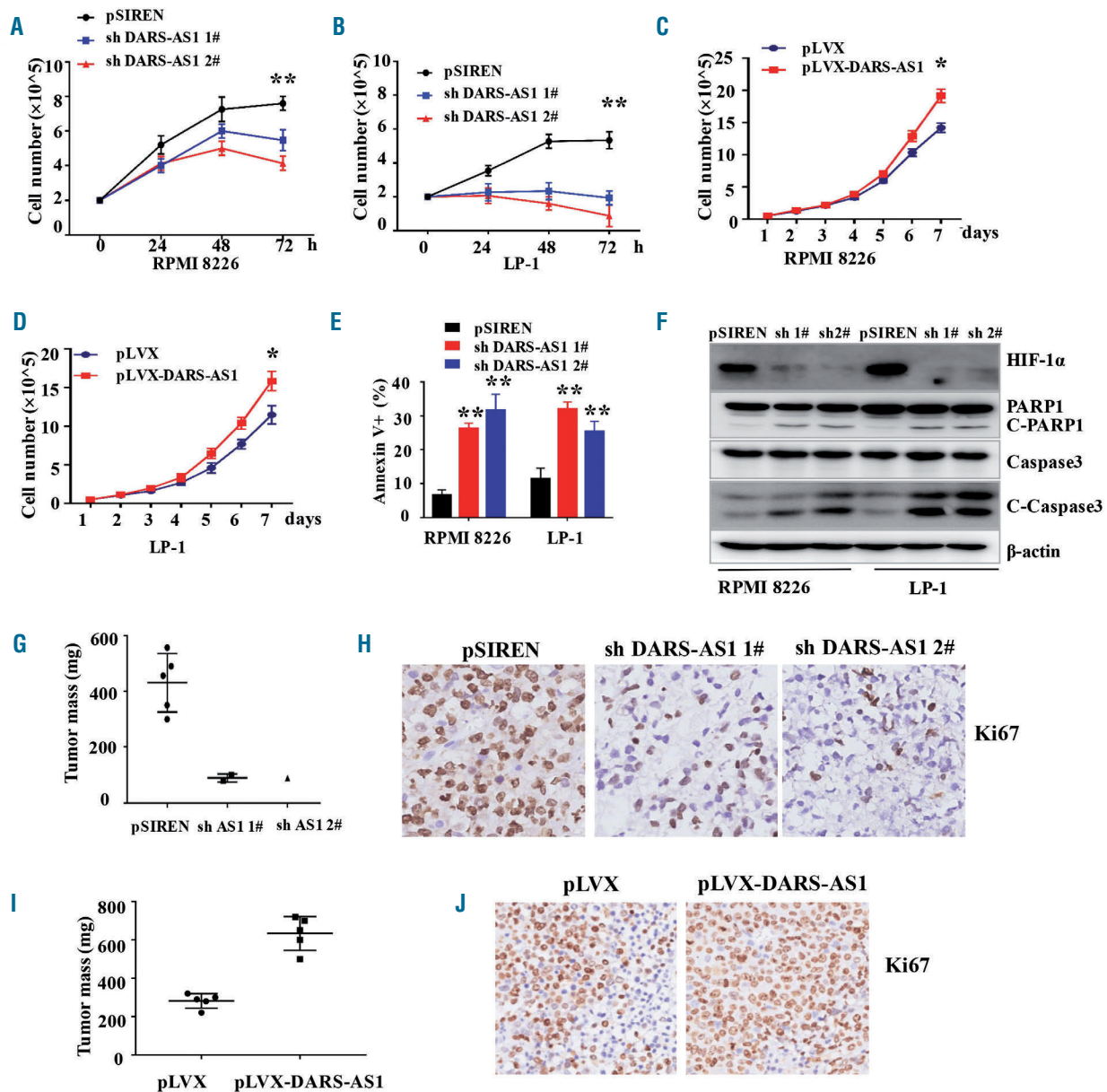


Figure 2. DARS-AS1 participates in proliferation and inhibits apoptosis of myeloma cells in a hypoxic environment. (A, B) Cell growth of RPMI 8226 and LP-1 cells with DARS-AS1 knockdown in a hypoxic environment was determined every 24 h for 72 h using an automated cell counter (Countstar). (C, D) Cell growth of RPMI 8226 and LP-1 cells with DARS-AS1 overexpression was determined every day for 7 days using an automated cell counter (Countstar). (E) The rates of annexin V⁺ cells in myeloma cells with DARS-AS1 knockdown and control cells were determined by flow cytometry. (F) Cleaved caspase-3 and cleaved PARP were demonstrated by western blotting of RPMI 8226 and LP-1 cells with DARS-AS1 knockdown. (G, I) Xenograft mouse models of myeloma cells with DARS-AS1 overexpression or DARS-AS1 knockdown in NOD-SCID mice. (H, J) Ki67 staining of xenografts of DARS-AS1 overexpressing or DARS-AS1 knockdown cells. * $P < 0.05$ and ** $P < 0.01$, compared with the control. Data are presented as the mean \pm standard error of mean from three experiments.

action between DARS-AS1 and RBM39 was also confirmed by an RNA immunoprecipitation assay. Plasmid-overexpressing RBM39 with a Flag-tag was transferred into HEK293T cells and then cultured in the hypoxic environment for 24 h. We observed DARS-AS1 enrichment (but not actin mRNA enrichment) using the Flag antibody compared with a nonspecific antibody (IgG control) (Figure 3D).

RBM39 promotes myeloma cell proliferation and inhibits cell apoptosis in the hypoxic environment

According to the Oncomine database, the transcription levels of RBM39 were significantly higher in patients with smoldering myeloma (n=12) than those of bone marrow mononuclear cells from healthy donors (n=22) ($P < 10^{-4}$). Data from another 74 myeloma patients also led to an identical conclusion (Figure 4A). Consistently with the aforementioned results, RBM39 was more highly expressed in the tested myeloma cell lines (Figure 4B). Importantly, patients with high expression of RBM39 had a poor response to treatment (Figure 4C). To further elucidate the biological functions of RBM39 in MM cells, we stably knocked down RBM39 using two independent shRNA in MM cells. The downregulation of RBM39 significantly inhibited MM cell growth and survival, and induced apoptosis (Figure 4D-F) under the hypoxic environment. Of note, cell apoptosis and the inhibition of MM cell proliferation that resulted from the downregulation of DARS-AS1 were partially reversed by the overexpression of RBM39 in the hypoxic environment (Figure 4G-I). These results indicate that RBM39 may mediate the bio-

logical functions of DARS-AS1 in MM in a hypoxic environment.

DARS-AS1 regulates mammalian target of rapamycin signaling via RBM39 under the hypoxic environment

The mammalian target of rapamycin (mTOR) signaling pathway plays critical roles in regulating myeloma cell proliferation and apoptosis. Previous reports suggested that RBM39 might be involved in these pathways.¹⁶ We, therefore, investigated the impact of RBM39 silencing on the mTOR signaling pathway. Knockdown of RBM39 resulted in a substantial decrease in p-mTOR, p-4EBP1, and p-P70 levels in the hypoxic environment compared to the levels in control cells (Figure 5A, B). Similar results were obtained in DARS-AS1-silenced cells. It is worth noting that the inhibition of mTOR signaling that resulted from DARS-AS1 knockdown was rescued by overexpression of RBM39 (Figure 5C, D), which suggests that the effects of DARS-AS1 are mediated mainly by RBM39. Our hypothesis was further supported by the increase of p-mTOR, p-4EBP1, p-P70 and RBM39 levels (Figure 5E, F) after DARS-AS1 overexpression in myeloma cells.

DARS-AS1 inhibits RBM39 degradation in the hypoxic environment

To further understand the mechanism of regulation between RBM39 and DARS-AS1, we stably downregulated DARS-AS1 and RBM39 in MM cells. The downregulation of the RBM39 protein did not affect the level of DARS-AS1 in either RPMI 8226 or LP-1 cells in the hypoxic environment (*Online Supplementary Figure S5B,C*).

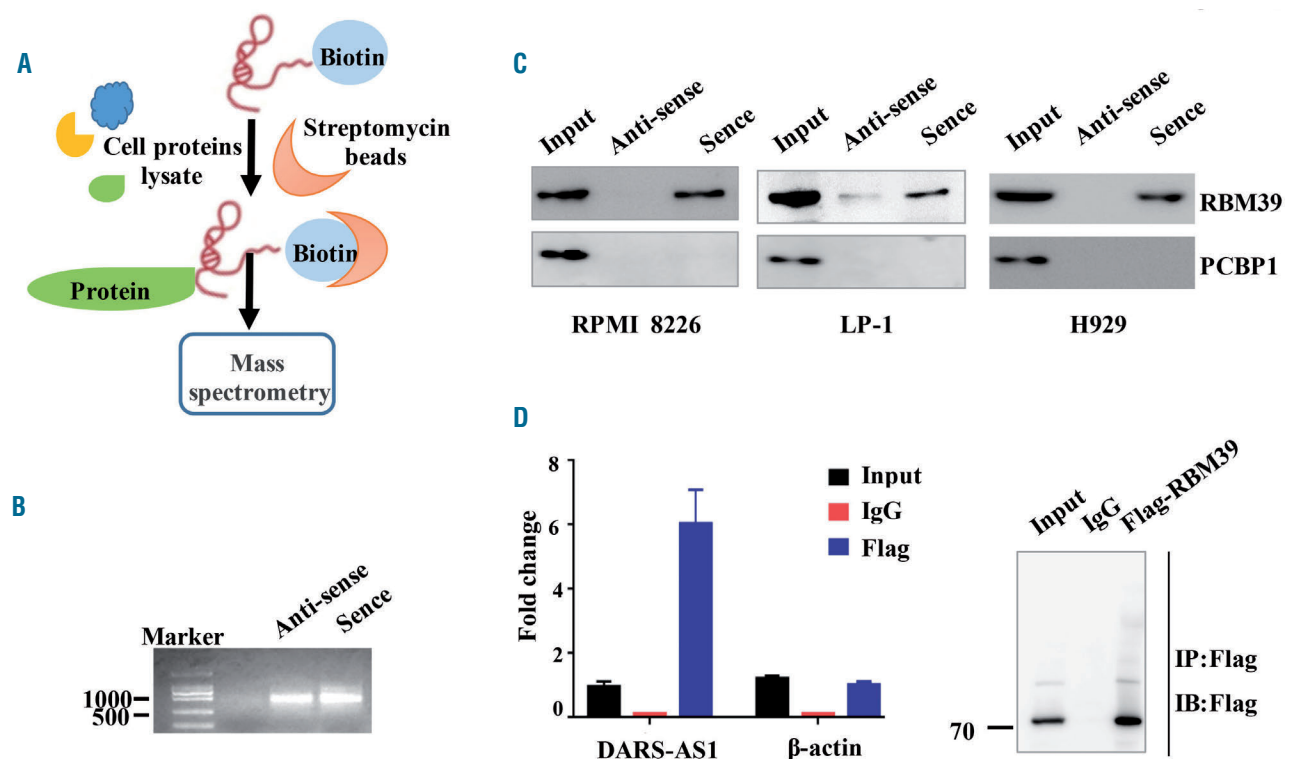


Figure 3. DARS-AS1 interacts with RBM39. (A) Schematic of the RNA DARS-AS1 pull-down experiment. (B) RNA electrophoresis showed the sense and antisense DARS-AS1 *in vitro*. (C) Western blotting analysis of the proteins from the proteomics screen after pull-down. (D) RNA immunoprecipitation experiments were performed using a Flag antibody (exogenous RBM39 protein with Flag-tag), and specific primers to detect DARS-AS1 or β -actin.

Intriguingly, the knockdown of DARS-AS1 caused down-regulation of the level of RBM39 protein without decreasing the level of mRNA in both RPMI 8226 and LP-1 cells in the hypoxic environment (Figure 6A). However, the change in the RBM39 protein level was abolished by the presence of the proteasome inhibitor MG132 (Figure 6B), suggesting that DARS-AS1 may regulate the degradation of RBM39 in hypoxia. We also treated the DARS-AS1-knockdown and control MM cells with the protein synthesis inhibitor cycloheximide. As shown in *Online Supplementary Figure S5D*, the degradation rate of RBM39 was significantly accelerated in DARS-AS1 knockdown

myeloma cells in a hypoxic environment. Moreover, the knockdown of DARS-AS1 increased the ubiquitination of RBM39 in hypoxia (Figure 6C). In contrast, the overexpression of DARS-AS1 reduced the ubiquitination of RBM39 (Figure 6D). These findings indicate that DARS-AS1 regulates the stability of RBM39 via the ubiquitin-proteasome pathway in a hypoxic environment.

The RBM39 protein is composed of an arginine-serine domain at the N terminus, followed by three predicted RNA recognition motifs (RRM) (Figure 6E). We next constructed a series of RBM39 truncations (1-240, 241-400, 400-530, 1-400, and 241-530) to map its binding domains

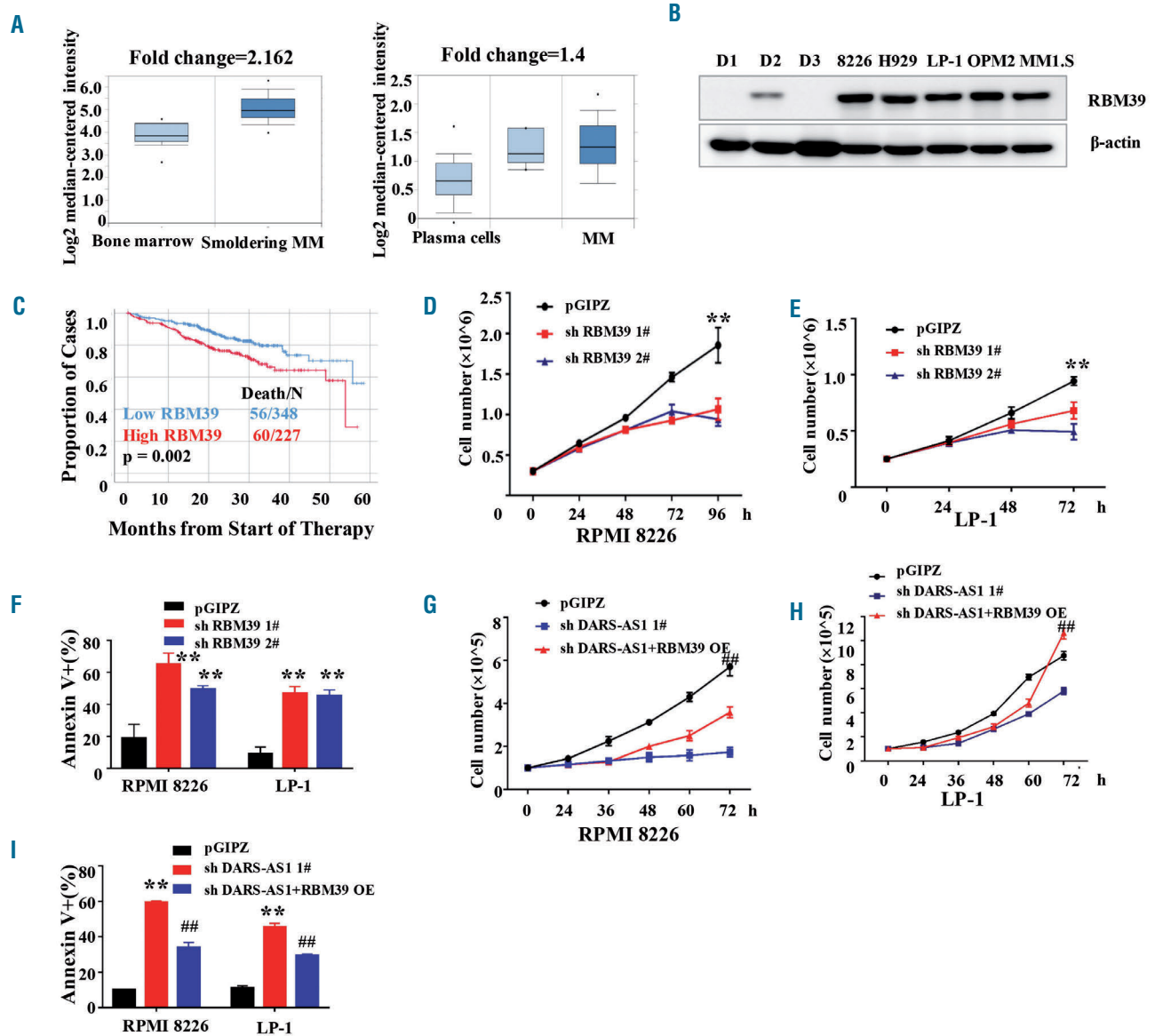


Figure 4. Role of RBM39 in myeloma cells under hypoxia. (A) OncoPrint data showing the mRNA levels of RBM39 in myeloma cells and plasma cells. (B) Western blotting analysis of RBM39 in myeloma cell lines and mononuclear cells from healthy donors. D1/D2/D3: healthy donor 1/2/3. (C) Data from the Multiple Myeloma Research Foundation (MMRF) showing the survival rate after treatment in patients with high/low expression of RBM39. (D, E) Numbers of myeloma cells transfected with short hairpin (sh)RNA targeting RBM39 were determined by an automated cell counter (Countstar). ** $P < 0.01$, compared with the control. (F) Annexin V⁺ cells in RPMI 8226 and LP-1 cells transfected with shRNA targeting RBM39 or control shRNA were assessed using flow cytometry. ** $P < 0.01$, compared with the control. (G, H) The growth of RPMI 8226 and LP-1 cells under hypoxia was assessed by an automated cell counter (Countstar). Results are expressed as the mean \pm standard error of mean (SEM) (n=3). shDARS-AS1: DARS-AS1 was knocked down in myeloma cells. shDARS-AS1+RBM39 overexpression (OE): DARS-AS1 was knocked down and then RBM39 overexpressed in myeloma cells. ** $P < 0.01$, shDARS-AS1+RBM39 OE compared with the shDARS-AS1. (I) Cell apoptosis was assessed by flow cytometry analysis. Results are expressed as the mean \pm SEM (n=3). shDARS-AS1: DARS-AS1 was knocked down in myeloma cells. shDARS-AS1+RBM39 OE: DARS-AS1 was knocked down and then RBM39 overexpressed in myeloma cells. ** $P < 0.01$, compared with the control. ## $P < 0.01$, shDARS-AS1+RBM39 OE compared with shDARS-AS1.

with the DARS-AS1. The deletion-mapping analyses identified the 1-240 amino acid sequence (corresponding to the RRM1 of RBM39) of RBM39 as required for its association with DARS-AS1 (Figure 6E). The truncated proteins con-

taining the 1-240 amino acid fragment were downregulated, whereas the truncated RBM39 without amino acids 1-240 could not be degraded after the knockdown of DARS-AS1 under the hypoxic conditions (Figure 6F). These

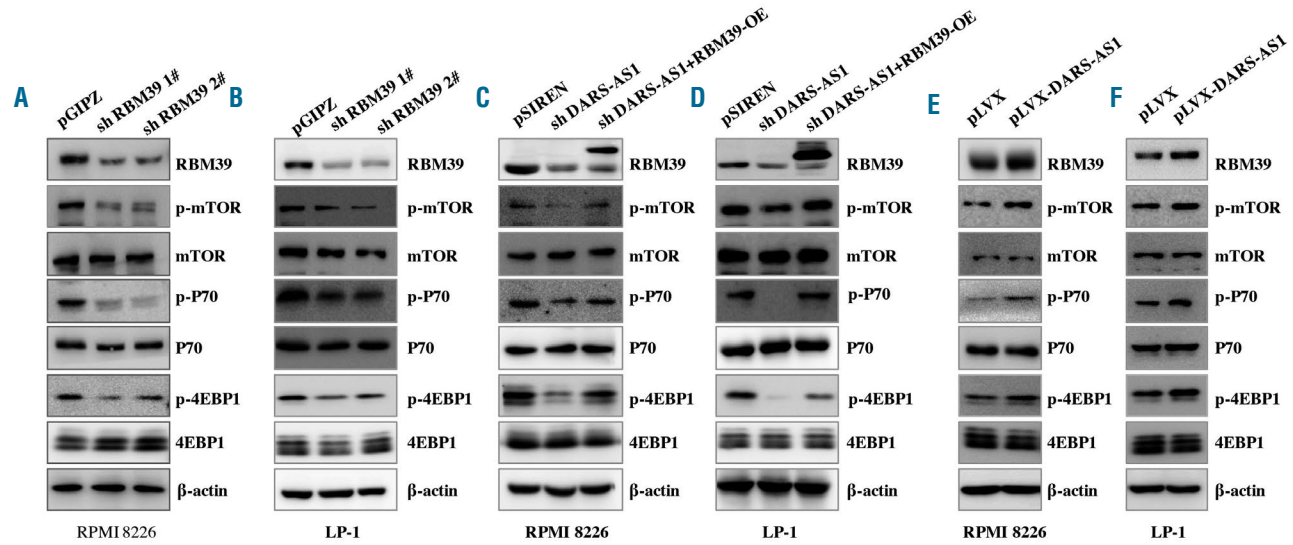


Figure 5. DARS-AS1 regulates the RBM39-related signaling pathway in hypoxic conditions. (A, B) Immunoblot analysis of total and phosphorylated mammalian target of rapamycin (mTOR) and downstream pathway proteins in RPMI 8226 and LP-1 cells expressing RBM39 short hairpin (sh)RNA or control shRNA. (C, D) mTOR signaling was analyzed in RPMI 8226 and LP-1 cells with DARS-AS1 silencing or DARS-AS1 silencing and RBM39 overexpression (OE). (E, F) mTOR signaling was analyzed in RPMI 8226 and LP-1 cells with DARS-AS1 OE.

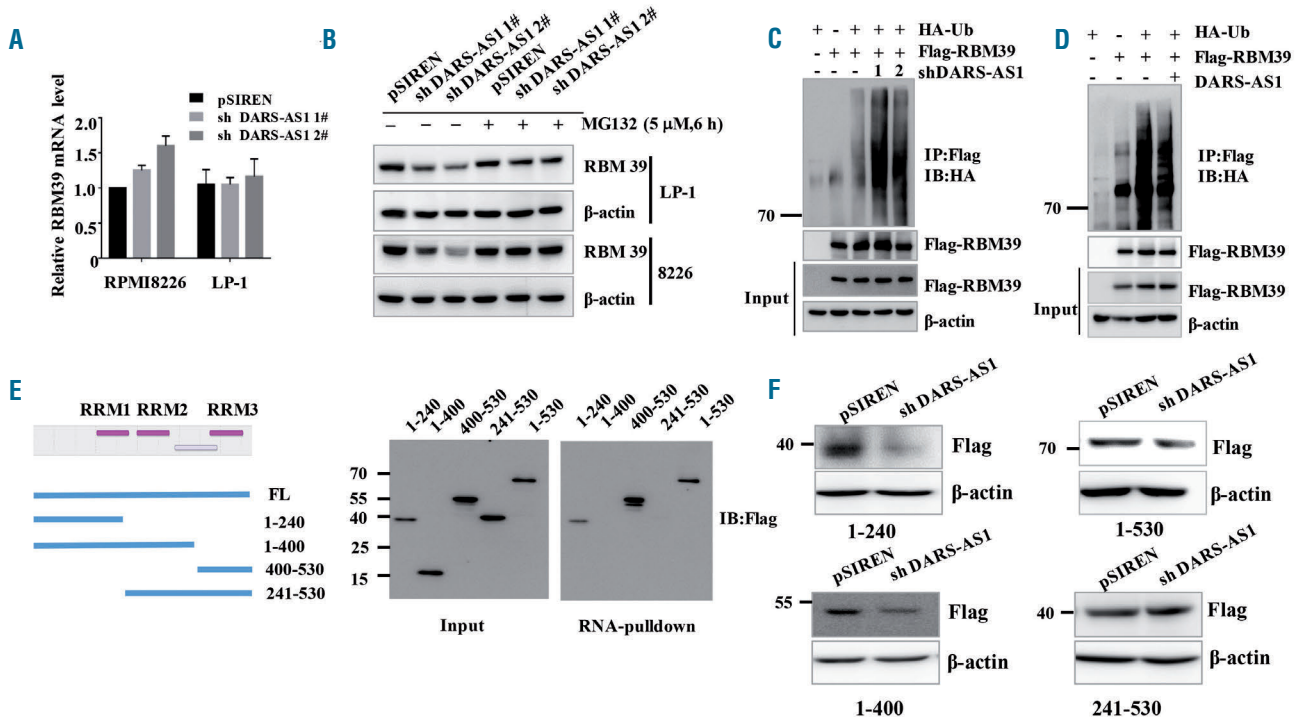


Figure 6. DARS-AS1 interacts with and inhibits RBM39 degradation in a hypoxic environment. (A) Reverse transcriptase polymerase chain reaction analysis of RBM39 mRNA (mean ± standard deviation) in DARS-AS1 knockdown cells in a hypoxic environment. (B) DARS-AS1-silenced myeloma cells were treated with dimethylsulfoxide (DMSO, 1:1000) or MG-132 (5 μM) for 6 h under hypoxic conditions. (C) HEK293T cells overexpressing Flag-RBM39 only, overexpressing HA-Ub only, overexpressing both Flag-RBM39 and HA-Ub, and with simultaneously silenced DARS-AS1 and overexpressed Flag-RBM39/HA-Ub were cultured in a hypoxic environment for 24 h, and then cell lysates were immunoprecipitated with anti-Flag antibody, followed by western blotting with anti-HA antibody. All cells were treated with MG132 (10 μM) for 12 h before collection. (D) Cell lysates from HEK293T cells overexpressing Flag-RBM39 only, overexpressing HA-Ub only, overexpressing both Flag-RBM39 and HA-Ub, and overexpressing DARS-AS1/Flag-RBM39/HA-Ub were immunoprecipitated with Flag antibody, followed by western blotting with anti-HA antibody. All cells were treated with MG132 (10 μM) for 12 h before collection. (E) Immunoblot analysis of Flag-tagged RBM39 [wildtype (WT) and truncation fragments] retrieved by *in vitro*-transcribed, biotinylated DARS-AS1. (F) The changes of truncated RBM39 after silencing DARS-AS1 were assessed using immunoblot analysis.

results suggest that the 1–240 amino acid sequence of RBM39 is essential for its binding to DARS-AS1.

The interaction of DARS-AS1 with RBM39 inhibits the degradation of RBM39 through RNF147

Currently, the E3 ligases responsible for the ubiquitination of RBM39 are not clear. Several E3 ligases, including CHIP, RNF2, RNF147, and RNF113A, have been reported as possible RBM39-interacting proteins. Intriguingly, among the interacting proteins, the knockdown of RNF147 increased RBM39 protein levels and the overexpression of RNF147 decreased RBM39 protein levels in the hypoxic environment (Figure 7A, *Online Supplementary S6B-D*). A direct association between endogenous RBM39 and RNF147 was also revealed by the co-immunoprecipitation assays (Figure 7B). Using RNA pull-down assays, we further verified the association of DARS-AS1 with both RBM39 and RNF147 (Figure 7C). The immunoprecipitation assay showed that DARS-AS1 deficiency promoted endogenous RBM39 binding to RNF147, thereby increasing RNF147-mediated RBM39 ubiquitination in the hypoxic environment (Figure 7D, E). Additionally, in the hypoxic environment, RNF147 bound to the RRM1 domain of RBM39 which contains possible ubiquitin-modified lysines (Figure 7F, *Online Supplementary Figure S6A*). Together, these results indicate that DARS-AS1 may function as a mediator, which weakens the RBM39-RNF147 interaction, thereby diminishing RNF147-mediated ubiquitination and degradation of RBM39.

HIF-1 α directly upregulates the expression of long non-coding RNA-DARS-AS1

To uncover the mechanisms of hypoxia-induced upregulation of DARS-AS1, we knocked down and overexpressed two well-known hypoxia-responsible transcriptional factors in HEK293T cells, HIF-1 α and HIF-2 α (*Online Supplementary Figure S7A*). Overexpression of HIF-1 α , but not of HIF-2 α , enhanced the expression of DARS-AS1; in the meantime, knockdown of HIF-1 α substantially attenuated the hypoxia-induced DARS-AS1 upregulation (Figure 8A). HIF-1 acts by binding to an HRE upon hypoxia. There are two possible HRE in the promoter region of DARS-AS1 (<http://jaspar.genereg.net>) (*Online Supplementary Figure S7B*). To determine whether HIF regulates the expression of DARS-AS1 through these HRE, we constructed luciferase expression plasmids containing the promoter region (2000 bp) of DARS-AS1. As expected, HIF-1 α strongly increased luciferase expression from the wildtype, but not the mutant HRE reporters (Figure 8B). At the same time, we used a chromatin immunoprecipitation assay to certify the binding of HIF-1 with the predicted two HRE regions (Figure 8C). Additionally, RNA immunoprecipitation assays showed that DARS-AS1 did not interact directly with HIF-1 α (Figure 8D). Interestingly, the overexpression of DARS-AS1 upregulated the HIF-1 α protein, whereas the knockdown of DARS-AS1 reduced the level of HIF-1 α protein which could not be abolished by the proteasome inhibitor MG132 in the hypoxic environment (Figure 8E, F). Moreover, DARS-

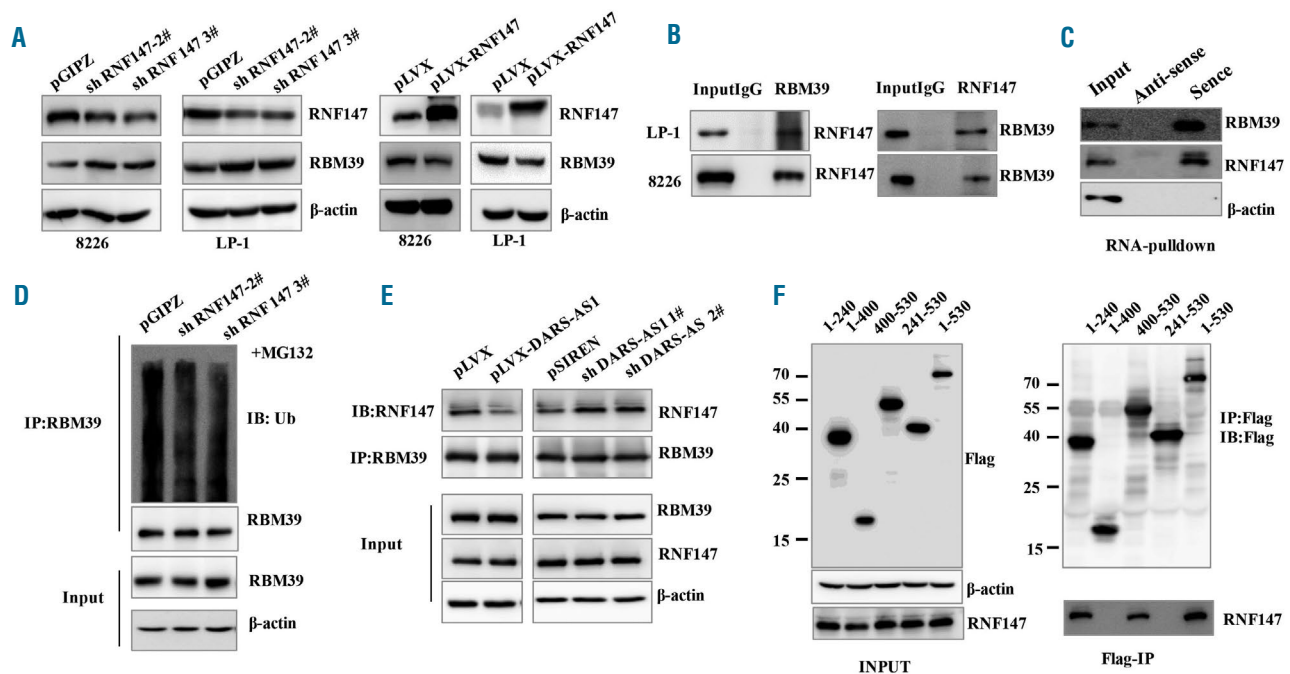


Figure 7. DARS-AS1 inhibits RBM39 ubiquitination by weakening the RBM39-RNF147 interaction in a hypoxic environment. (A) The expression of RBM39 in RNF147 silenced/overexpressing myeloma cells in a hypoxic environment. (B) Cell lysates from myeloma cells were immunoprecipitated with RBM39/RNF147 antibody, followed by western blotting with antibody against RNF147/RBM39. (C) Cell lysates from RPMI 8226 cells cultured under hypoxic conditions were incubated with *in vitro*-synthesized, biotin-labeled sense or antisense DARS-AS1 for pull-down followed by immunoblot analysis. (D) HEK293T cells with stable knockdown of RNF147 were cultured in a hypoxic environment for 24 h, then treated with MG132 (10 μ M) for 12 h. Cell lysates were immunoprecipitated with anti-RBM39 antibody, followed by western blotting with anti-ubiquitin antibody. (E) HEK293T cells with stable overexpression of DARS-AS1 or knockdown of DARS-AS1 were treated with MG132 (10 μ M) for 12 h. Cell lysates were immunoprecipitated with antibody against RBM39. The precipitates and input were analyzed by immunoblotting. (F) Constructs for Flag-tagged RBM39 (wildtype and truncation fragment) were transfected into HEK293T cells, and then cultured in a hypoxic environment for 24 h. Immunoprecipitation was performed using anti-Flag M2 beads, and precipitates and input were analyzed by immunoblotting with anti-RNF147 and anti-Flag antibodies.

AS1 could not influence the HIF-1 α mRNA level in RPMI 8226 cells (*Online Supplementary Figure S7C*). We speculated that the DARS-AS1 silencing inhibited the translation of HIF-1 α by suppression of the mTOR pathway.^{17,18} Altogether, HIF-1 enhanced the transcription activity of DARS-AS1; in turn, DARS-AS1 might accelerate the translation rate of HIF-1 α expression via the mTOR pathway.

Discussion

Hypoxia-responsive genes are involved in the malignant progression and poor prognosis of human cancers.¹⁹ Numerous lncRNA have been reported to show abnormal expression in cancers.²⁰ In the present work, we found that hypoxic-regulated DARS-AS1 was required for the survival and tumorigenicity of myeloma cells *in vitro* and *in*

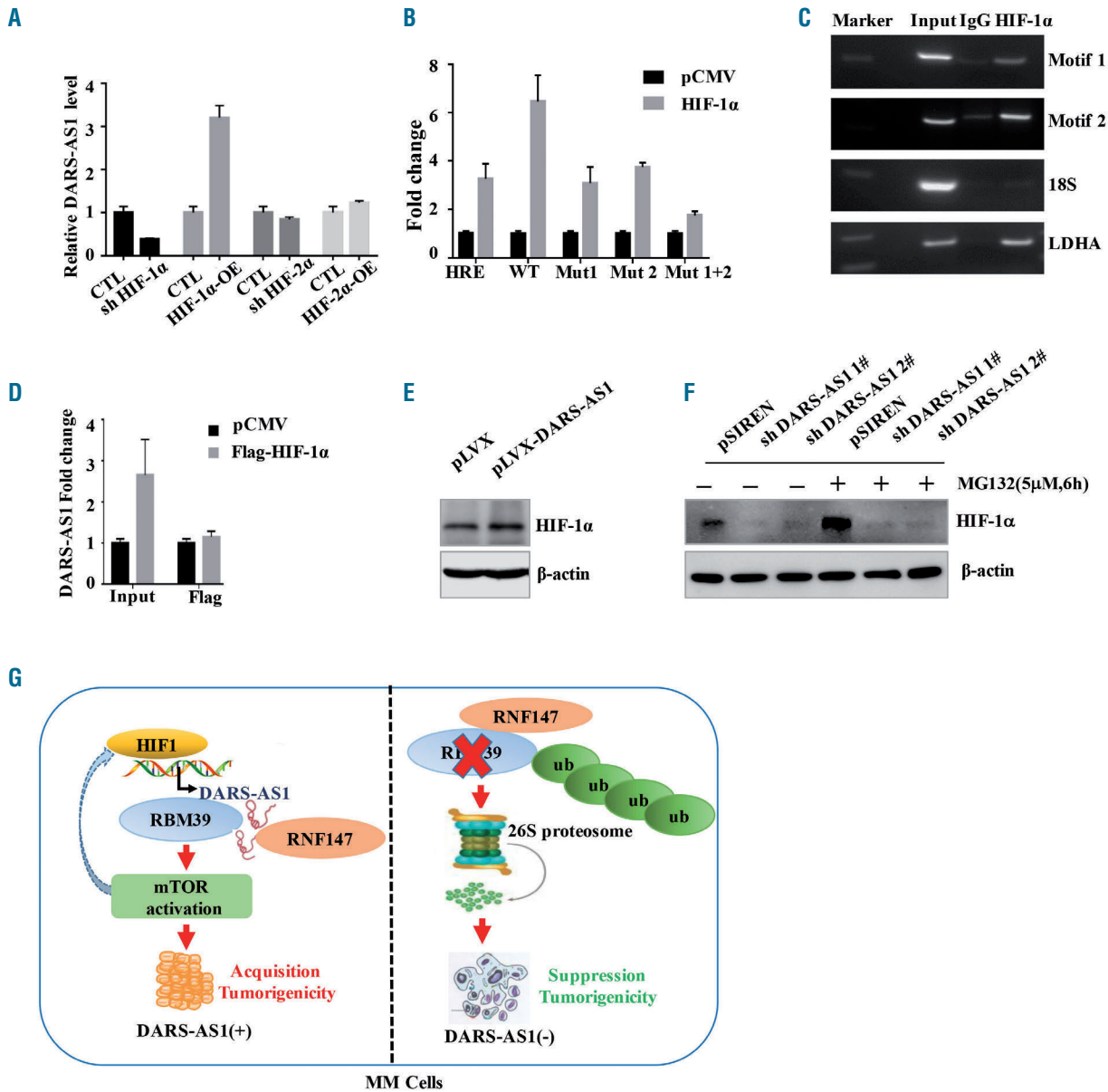


Figure 8. HIF-1 directly upregulates the expression of DARS-AS1, which may, in turn, enhance the expression of HIF-1 α . (A) HIF-1 α or HIF-2 α was knocked down or overexpressed in 293T cells. DARS-AS1 expression levels were determined by quantitative polymerase chain reaction analysis and normalized to 18S rRNA. (B) Transient transfection of a DARS-AS1 promoter [wildtype (WT) or mutant] luciferase transcriptional reporter and plasmid overexpressing HIF-1 α /control vector. The luciferase values were determined from cell lysates by normalization to renilla luciferase. The pGL3 control vector containing the HRE promoter was used as a positive control. The data represent the average and standard deviation of three independent experiments. (C) Chromatin immunoprecipitation assay certified the binding of HIF-1 with the predicted two HIF response element (HRE) regions; LDHA was used as a positive control. (D) RNA immunoprecipitation experiments were performed using a Flag-antibody (exogenous HIF-1 α protein with Flag-tag), and specific primers to detect DARS-AS1. (E) The expression of HIF-1 α in the RPMI 8226 cells overexpressing DARS-AS1 in a hypoxic environment was analyzed by immunoblotting. (F) DARS-AS1-knockdown RPMI 8226 cells were treated with dimethyl-sulfoxide (DMSO, 1:1000) or MG132 (5 μ M) for 6 h. The expression of HIF-1 α under hypoxic conditions was analyzed by immunoblotting. (G) Proposed mode of action of DARS-AS1 in modulating myeloma tumorigenesis in a hypoxic environment. DARS-AS1 is directly regulated by HIF-1 and, in turn, promotes the expression of HIF-1 α in myeloma. RBM39 mediates DARS-AS1-induced activation of mammalian target of rapamycin (mTOR) signaling. DARS-AS1 stabilizes the RBM39 by interfering with E3 ligase RNF147-mediated ubiquitination. HIF-1/DARS-AS1/RBM39 signaling pathways are involved in the tumorigenesis of myeloma.

vivo. We propose that the HIF-1 α -DARS-AS1-RBM39 axis is a potential target for MM treatment.

DARS-AS1 is close to DARS in the genome (*Online Supplementary Figure S4A*). Numerous antisense lncRNA participate in physiological or pathological cellular processes through the regulation of the expression of its adjacent gene.^{21,22} By contrast, we found that the downregulation of DARS-AS1 was not associated with the expression of DARS at either transcriptional or protein levels (*Online Supplementary Figure S4B-E*). The DARS-AS1 gene has two annotated transcripts, NR_110199.1 and NR_110200.1, in the National Center for Biotechnology Information database (<https://www.ncbi.nlm.nih.gov/>), with limited protein-coding potential (<http://cpc.cbi.pku.edu.cn/>) (*Online Supplementary Figure S4E, F*). The transcript of DARS-AS1 #2 (NR_110200.1) is not detectable in the myeloma cells. We, therefore, focused on DARS-AS1 #1 isoform in our gain- and loss-of-function studies.

Nutritional deficiency is common in the microenvironment of tumors. HIF-1, the protein that responds to low O₂ concentrations, apparently leads to increased glycolysis, angiogenesis and drug resistance.¹ In culture with low levels of glucose, the overexpression of DARS-AS1 suppressed myeloma cell apoptosis (*Online Supplementary Figure S2D, E*). More importantly, DARS-AS1 can promote the expression of HIF-1 α . Thus, DARS-AS1 and HIF-1 α may create a positive feedback, increasing the ability of myeloma cells to survive, although the underlying mechanism is not fully known. In addition, it would be interesting to examine the impact of DARS-AS1 on the prognosis of myeloma patients through the analysis of data from large numbers of samples.

The mass spectrometry and RNA pull-down data revealed that DARS-AS1 interacts directly with RBM39, suppressing the ubiquitination and subsequent degradation of RBM39 protein, an RNA-binding protein. Dysregulation of these types of proteins, which can lead to aberrant expression of cancer-related genes, has been widely observed in cancer cells.^{23,24} Previous studies suggested that *RBM39* is a proto-oncogene in multiple cancer types. Our results extend this notion, indicating that *RBM39* is a novel oncogene in myeloma. First, a significantly higher mortality risk was observed in patients with high expression of *RBM39* than in those with lower expression. Second, activation of the mTOR signaling pathway reportedly plays a critical role in the pathogenesis of myeloma. Our results showed that the knockdown of RBM39 inhibited mTOR signaling, thus suggesting that RBM39 is critical for the proliferation and tumorigenesis of MM cells and may serve as a prognostic predictor for patients with MM. However, further investigations will be necessary to reveal the mechanisms of the regulation of the mTOR pathway by RBM39. Furthermore, similar results were observed in DARS-AS1 knockdown cells. The overexpression of RBM39 reversed the inhibition of mTOR signaling induced by the knockdown of DARS-AS1. Based on these data, we propose that the aberrant

expression of DARS-AS1 in cells may increase the levels of RBM39, thereby triggering continuous activation of mTOR signaling.

Previous studies showed that sulfonamides have anti-cancer effects by promoting an interaction between RBM39 and the E3 ubiquitin ligase DCAF15, leading to the degradation of RBM39.¹² However, RBM39 is not the endogenous substrate of DCAF15. To the best of our knowledge, in the present study we, for the first time, discovered that RBM39 is a substrate of the E3 ubiquitin ligase RNF147. RNF147 is a member of the tripartite motif protein (TRIM) family and contains an N-terminal RING-domain, one or two B-boxes, and a coiled-coil region.²⁵ We found that the RRM1 domain of RBM39, which contains the ubiquitin binding site domain (<http://ubibrowser.ncpsb.org/>, <http://cplm.biocuckoo.org/>), was responsible for the interaction with both DARS-AS1 and RNF147. Our results raise the possibility that DARS-AS1 may inhibit ubiquitination of RBM39 by competing with E3 ubiquitin ligase RNF147 for binding to RBM39. In fact, accumulating evidence shows that lncRNA can protect proteins from proteasome-mediated degradation. For instance, NKILA is a lncRNA that directly masks the phosphorylation motifs of I κ B, thereby inhibiting the degradation of I κ B and subsequently activating the NF- κ B pathway.²⁶ UPAT was found to inhibit the ubiquitination of epigenetic factor UHRF1 and play a critical role in the survival and tumorigenicity of tumor cells.²⁷ In addition, LINC00673, as a cancer suppressor, was able to promote PTPN11 degradation, which weakened SRC-ERK signaling and increased STAT1-dependent antitumor effects.²⁸ Our findings, together with the aforementioned earlier results, indicate that there is a class of lncRNA that regulate protein ubiquitination and degradation.

In conclusion, we demonstrate that DARS-AS1 has important functions in the hypoxic microenvironment of myeloma and may serve as a prognostic predictor for patients with MM. Our results indicate that the HIF-1/DARS-AS1/RBM39 pathway might provide a positive feedback loop that augments the HIF-1 response in myeloma, and that targeting this pathway may be pivotal in the prevention or treatment of myeloma. Our findings shed new light on the orchestrated interactions between HIF-1 and lncRNA in maintaining myeloma cell survival under hypoxia.

Acknowledgments

We thank Guoqiang Chen at Shanghai Jiao Tong University School of Medicine for providing plasmids.

Funding

This work was supported in part by grants from the National Key Research and Development Program of China (n. 2017YFA0505200), National Natural Science Foundation of China (8167010684, 81570118), Shanghai Commission of Science and Technology (16ZR1421400), and the Science and Technology Committee of Shanghai (15401901800).

References

- Maiso P, Huynh D, Moschetta M, et al. Metabolic signature identifies novel targets for drug resistance in multiple myeloma. *Cancer Res.* 2015;75(10):2071-2082.
- Ponting CP, Oliver PL, Reik W. Evolution and functions of long noncoding RNAs. *Cell.* 2009;136(4):629-641.
- Mercer TR, Dinger ME, Mattick JS. Long non-coding RNAs: insights into functions. *Nat Rev Genet.* 2009;10(3):155-159.
- Kornienko AE, Guenzl PM, Barlow DP, Pauler FM. Gene regulation by the act of long non-coding RNA transcription. *BMC Biol.*

- 2013;11:59.
5. Tsai MC, Spitale RC, Chang HY. Long intergenic noncoding RNAs: new links in cancer progression. *Cancer Res.* 2011;71(1):3-7.
 6. Gibb EA, Brown CJ, Lam WL. The functional role of long non-coding RNA in human carcinomas. *Mol Cancer.* 2011;10:38.
 7. Spizzo R, Almeida MI, Colombatti A, Calin GA. Long non-coding RNAs and cancer: a new frontier of translational research? *Oncogene.* 2012;31(43):4577-4587.
 8. Huang G, Zhou Z, Wang H, Kleinerman ES. CAPER-alpha alternative splicing regulates the expression of vascular endothelial growth factor(1)(6)(5) in Ewing sarcoma cells. *Cancer.* 2012;118(8):2106-2116.
 9. Jung DJ, Na SY, Na DS, Lee JW. Molecular cloning and characterization of CAPER, a novel coactivator of activating protein-1 and estrogen receptors. *J Biol Chem.* 2002;277(2):1229-1234.
 10. Dowhan DH, Hong EP, Auboeuf D, et al. Steroid hormone receptor coactivation and alternative RNA splicing by U2AF65-related proteins CAPERalpha and CAPERbeta. *Mol Cell.* 2005;17(3):429-439.
 11. Kang YK, Putluri N, Maity S, et al. CAPER is vital for energy and redox homeostasis by integrating glucose-induced mitochondrial functions via ERR-alpha-Gabpa and stress-induced adaptive responses via NF-kappaB-cMYC. *PLoS Genet.* 2015;11(4):e1005116.
 12. Han T, Goralski M, Gaskill N, et al. Anticancer sulfonamides target splicing by inducing RBM39 degradation via recruitment to DCAF15. *Science.* 2017;356(6336).
 13. Sillars-Hardebol AH, Carvalho B, Tijssen M, et al. TPX2 and AURKA promote 20q amplicon-driven colorectal adenoma to carcinoma progression. *Gut.* 2012;61(11):1568-1575.
 14. Guttman M, Donaghey J, Carey BW, et al. lincRNAs act in the circuitry controlling pluripotency and differentiation. *Nature.* 2011;477(7364):295-300.
 15. Kogo R, Shimamura T, Mimori K, et al. Long noncoding RNA HOTAIR regulates polycomb-dependent chromatin modification and is associated with poor prognosis in colorectal cancers. *Cancer Res.* 2011;71(20):6320-6326.
 16. Mai S, Qu X, Li P, Ma Q, Cao C, Liu X. Global regulation of alternative RNA splicing by the SR-rich protein RBM39. *Biochim Biophys Acta.* 2016;1859(8):1014-1024.
 17. McInturff AM, Cody MJ, Elliott EA, et al. Mammalian target of rapamycin regulates neutrophil extracellular trap formation via induction of hypoxia-inducible factor 1 alpha. *Blood.* 2012;120(15):3118-3125.
 18. Zhu Q, Wang H, Jiang B, et al. Loss of ATF3 exacerbates liver damage through the activation of mTOR/p70S6K/ HIF-1alpha signaling pathway in liver inflammatory injury. *Cell Death Dis.* 2018;9(9):910.
 19. Qu A, Taylor M, Xue X, et al. Hypoxia-inducible transcription factor 2alpha promotes steatohepatitis through augmenting lipid accumulation, inflammation, and fibrosis. *Hepatology.* 2011;54(2):472-483.
 20. Ulitsky I, Bartel DP. lincRNAs: genomics, evolution, and mechanisms. *Cell.* 2013;154(1):26-46.
 21. Qin W, Li X, Xie L, et al. A long non-coding RNA, APOA4-AS, regulates APOA4 expression depending on HuR in mice. *Nucleic Acids Res.* 2016;44(13):6423-6433.
 22. Villegas VE, Zaphiropoulos PG. Neighboring gene regulation by antisense long non-coding RNAs. *Int J Mol Sci.* 2015;16(2):3251-3266.
 23. Glisovic T, Bachorik JL, Yong J, Dreyfuss G. RNA-binding proteins and post-transcriptional gene regulation. *FEBS Lett.* 2008;582(14):1977-1986.
 24. Kim MY, Hur J, Jeong S. Emerging roles of RNA and RNA-binding protein network in cancer cells. *BMB Rep.* 2009;42(3):125-130.
 25. Nisole S, Stoye JP, Saib A. TRIM family proteins: retroviral restriction and antiviral defence. *Nat Rev Microbiol.* 2005;3(10):799-808.
 26. Liu B, Sun L, Liu Q, et al. A cytoplasmic NF-kappaB interacting long noncoding RNA blocks IkappaB phosphorylation and suppresses breast cancer metastasis. *Cancer Cell.* 2015;27(3):370-381.
 27. Taniue K, Kurimoto A, Sugimasa H, et al. Long noncoding RNA UPAT promotes colon tumorigenesis by inhibiting degradation of UHRF1. *Proc Natl Acad Sci U S A.* 2016;113(5):1273-1278.
 28. Zheng J, Huang X, Tan W, et al. Pancreatic cancer risk variant in LINC00673 creates a miR-1231 binding site and interferes with PTPN11 degradation. *Nat Genet.* 2016;48(7):747-757.

Identification of PIKfyve kinase as a target in multiple myeloma



Cecilia Bonolo de Campos,¹ Yuan Xiao Zhu,¹ Nikolai Sepetov,² Sergei Romanov,² Laura Ann Bruins,¹ Chang-Xin Shi,¹ Caleb K. Stein,¹ Joachim L. Petit,¹ Alysia N. Polito,¹ Meaghen E. Sharik,¹ Erin W. Meermeier,¹ Gregory J. Ahmann,¹ Ilse D. Lopez Armenta,¹ Jonas Kruse,¹ P. Leif Bergsagel,¹ Marta Chesi,¹ Nathalie Meurice,¹ Esteban Braggio¹ and A. Keith Stewart¹

¹Division of Hematology/Oncology, Mayo Clinic Arizona, Scottsdale, AZ and ²Nanosyn Inc., Santa Clara, CA, USA

ABSTRACT

The cellular cytotoxicity of APY0201, a PIKfyve inhibitor, against multiple myeloma was initially identified in an unbiased *in vitro* chemical library screen. The activity of APY0201 was confirmed in all 25 cell lines tested and in 40% of 100 *ex vivo* patient-derived primary samples, with increased activity in primary samples harboring trisomies and lacking t(11;14). The broad anti-multiple myeloma activity of PIKfyve inhibitors was further demonstrated in confirmatory screens and showed the superior potency of APY0201 when compared to the PIKfyve inhibitors YM201636 and apilimod, with a mid-point half maximal effective concentration (EC₅₀) at nanomolar concentrations in, respectively, 65%, 40%, and 5% of the tested cell lines. Upregulation of genes in the lysosomal pathway and increased cellular vacuolization were observed *in vitro* following APY0201 treatment, although these cellular effects did not correlate well with responsiveness. We confirm that PIKfyve inhibition is associated with activation of the transcription factor EB, a master regulator of lysosomal biogenesis and autophagy. Furthermore, we established an assay measuring autophagy as a predictive marker of APY0201 sensitivity. Overall, these findings indicate promising activity of PIKfyve inhibitors secondary to disruption of autophagy in multiple myeloma and suggest a strategy to enrich for likely responders.

Introduction

Although the survival outcomes of patients with multiple myeloma (MM) have improved significantly, in the majority of patients the disease remains characterized by recurrent episodes of relapse. Identification of vulnerable targets, particularly those targeting plasma cell biology, is thus an attractive approach aiming towards advances of therapeutic strategies. Consequently, we utilized an *ex vivo* chemo-genomics screening approach to identify potentially unrecognized targets in this disease. As part of this study, and somewhat unexpectedly, PIKfyve was identified as a vulnerable target in MM.

PIKfyve, first described in 1999,¹ is a mammalian protein and lipid kinase that controls complex and distinct cellular functions (reviewed by Shisheva *et al.*²). PIKfyve phosphorylation of protein substrates includes autophosphorylation³ while lipid kinase activity generates two phosphorylated species of phosphatidylinositol (PtdIns):-5-P and -3,5-P2.⁴ PtdIns-5-P plays crucial roles in remodeling the actin cytoskeleton, endocytosis, and nuclear signaling, and is suggested to be a critical signal in innate immune responses. PtdIns-3,5-P2 is involved mainly in intracellular trafficking and lysosomal acidification and is thus crucial for the regulation of macroautophagy (herein denominated autophagy).⁵ Apilimod, initially identified in functional screens as negatively interfering with the production of interleukin (IL)-12 and IL-23⁶ and used in clinical trials of the treatment of inflammatory diseases⁷⁻¹⁰ was subsequently characterized as a PIKfyve inhibitor.¹¹ Interestingly, apilimod inhibition has recently been described as a potentially useful therapeutic approach for the treatment of non-Hodgkin lymphoma (NHL).¹²

Haematologica 2020
Volume 105(6):1641-1649

Correspondence:

A. KEITH STEWART
stewart.keith@mayo.edu

Received: March 21, 2019.

Accepted: September 26, 2019.

Pre-published: October 3, 2019.

doi:10.3324/haematol.2019.222729

Check the online version for the most updated information on this article, online supplements, and information on authorship & disclosures: www.haematologica.org/content/105/6/1641

©2020 Ferrata Storti Foundation

Material published in *Haematologica* is covered by copyright. All rights are reserved to the Ferrata Storti Foundation. Use of published material is allowed under the following terms and conditions:

<https://creativecommons.org/licenses/by-nc/4.0/legalcode>.

Copies of published material are allowed for personal or internal use. Sharing published material for non-commercial purposes is subject to the following conditions:

<https://creativecommons.org/licenses/by-nc/4.0/legalcode>, sect. 3. Reproducing and sharing published material for commercial purposes is not allowed without permission in writing from the publisher.



Other novel compounds targeting the PIKfyve kinase, APY0201, YM201636, AS2677131, AS2795440, and MF4, have followed.¹³⁻¹⁶ Here we report that APY0201 and other PIKfyve inhibitors are effective inhibitors of MM cell viability in *in vitro* and *ex vivo* models of MM, explore their mechanisms of action, and describe the development of a predictive assay for PIKfyve sensitivity.

Methods

PIKfyve inhibitor sensitivity

APY0201 was included in a 76-drug panel high throughput screen and evaluated in a 7-point, 10-fold dilution of drug concentration, starting at 10 μ M. Twenty-five human MM cell lines (HMCL) and 15 NHL cell lines were incubated for 24 or 72 h. Cellular viability was assessed with the CellTiter Glo (Promega) assay for all dose-response curves. Mid-point half maximal effective concentrations (herein denominated EC₅₀), maximum inhibition, and area under the curve (AUC) were calculated.¹⁷

Twenty HMCL were treated with a 20-point 2-fold dilution of drug concentration, starting at 40 μ M, and incubated for 72 h with APY0201 (MedChemExpress, HY-15982, Monmouth Junction, NJ, USA), apilimod (Santa Cruz Biotechnology, sc-480051, Dallas, TX, USA), and YM201636 (SelleckChem, S1219, Houston, TX, USA).

Ex vivo sensitivity to APY0201 was assessed after 24 h incubation in 100 purified patient-derived MM samples (through magnetic bead sorting for CD138⁺ cells; average purity greater than 95%). Fifteen samples were also screened against APY0201 and apilimod in a 14-point, 3-fold dilution of drug concentration, starting at 50 μ M, and incubated for 72 h. Leukocytes from whole bone marrow samples were incubated for 24 h with increasing concentrations of APY0201 to measure cytotoxicity, as described previously.¹⁸ Written informed consent was obtained from the patients and samples were collected and stored under Mayo Clinic Institutional Review Board approval (IRB 919-04, 2207-02, 15-009436, and 18-003198). This study was conducted in accordance with the Declaration of Helsinki.

Immunoblotting

Anti- β -actin (#A00702-100) antibody was purchased from GeneScript (Piscataway, NJ, USA), anti-Lamp-1 (#ab25630) was purchased from Abcam (Cambridge, MA, USA), anti-SQSTM1 (#sc-28359) was purchased from Santa Cruz Biotechnology (Dallas, TX, USA), and anti-cathepsin A (#AF1049) and anti-cathepsin D (#AF1014) were purchased from R&D Systems (Minneapolis, MN, USA). Antibodies against β -tubulin (#2128), Beclin1 (#3495), Caspase 3 (#9662), GAPDH (#2118), Lamin A/C (#4777), LC3A/B (#12741), PARP (#9542), and transcription factor EB (TFEB, #4240) were purchased from Cell Signaling Technology (Danvers, MA, USA).

Autophagy organelle formation

Vacuolar phenotype was evaluated by live cell differential interference contrast (DIC) imaging. Acidic vacuoles were identified with the LysoSensor Yellow/Blue DND-160 probe (#L7545, Thermo Fisher Scientific, Waltham, MA, USA). HMCL were incubated with 20 μ L of the Premo Autophagy Tandem Sensor RFP-GFP-LC3 kit (#P36239, Thermo Fisher Scientific) for 48 h with subsequent addition of dimethylsulfoxide (DMSO) control or APY0201 for 18 h. The Autophagy Detection Kit (Abcam #ab139484) was used according to the manufacturers' recommendations. Cellular viability was measured at 72 h.

mRNA sequencing

HMCL were treated with 100 nM and patients' samples with 50 and 500 nM of APY0201, and DMSO as a control, for 24 h; the cells were then harvested, and total RNA was extracted. An internally developed RNA-sequencing analysis workflow (MAPRSeq,¹⁹ v3.0.1) was used to perform comprehensive analysis of raw RNA sequencing paired-end reads, which were aligned by a fast and splice-aware aligner (STAR,²⁰ v 2.5.2b) to human genome build hg38. Quality control was performed with RSeQC (v3.0.0).²¹ Gene expression was quantified with featureCounts²² from the Subread package (<http://subread.sourceforge.net/>, v1.5.1). Genes were determined as differentially expressed based on log-fold change >1, and the Enrichr platform²³ was used to identify involved pathways. The data have been deposited in the National Center for Biotechnology Information's (NCBI) Gene Expression Omnibus (GEO),²⁴ accessible through GEO series accession number GSE134598.

Results

Identification of PIKfyve as a potential target in multiple myeloma and non-Hodgkin lymphoma

Medium throughput screening on MM and NHL cell lines was first conducted at Nanosyn Inc. (Santa Clara, CA, USA) using a panel of known Food and drug Administration-approved oncology drugs, kinase inhibitors, and epigenetic compounds assembled by the investigators. A more refined panel of 76 drugs was then selected and sensitivity to the single agents was evaluated in 25 MM and 15 NHL cell lines. We observed a dose dependent inhibition of cellular viability in all of the 25 HMCL exposed to the PIKfyve inhibitor APY0201 after 72 h incubation, with a median EC₅₀ of 55 nM and a median maximum inhibition of cellular viability of 81% (dose-response curves are shown in *Online Supplementary Figure S1*). These results prompted a confirmatory validation screen of 20 HMCL treated with APY0201 and two additional PIKfyve inhibitors, YM201636 and apilimod, with an increased dose range. Dose-dependent inhibition of cellular viability was observed in this confirmatory screen in 20 HMCL with all three PIKfyve inhibitors after 72 h incubation. APY0201 was the most potent PIKfyve inhibitor, followed by YM201636 and apilimod (Table 1, *Online Supplementary Figures S2-S4* and *Online Supplementary Table S1*).

In NHL cell lines the effect was similar; after 72 h incubation, APY0201 was the most potent PIKfyve inhibitor evaluated, with 14 of 15 tested lines (93%) having an EC₅₀ in the nanomolar range (median 76 nM). For YM201636, only 37.5% of eight tested NHL cell lines were sensitive at nanomolar concentrations with a median EC₅₀ of 530 nM. Finally, for apilimod, only one of eight tested NHL lines (12.5%) had nanomolar activity with an EC₅₀ of 405 nM (*Online Supplementary Figures S5* and *S6* and *Online Supplementary Table S2*).

Ex vivo anti-myeloma activity of multiple PIKfyve inhibitors

We next tested 100 *ex vivo* primary CD138⁺-selected patients' samples. Dose-dependent sensitivities for APY0201 were observed in 40% of these *ex vivo* samples at 24 h, with 47% of the responsive samples exhibiting an EC₅₀ lower than 100 nM (19% of all tested samples). The

sensitivity to both APY0201 and apilimod was then examined in 15 *ex vivo* primary patients' samples after 72 h incubation, and more significant anti-MM activity was noted. Over 90% of the primary patients' samples showed dose-dependent inhibition of cellular viability in response to both drugs. APY0201 was considered the more potent PIKfyve inhibitor, with 71% of the samples exhibiting sensitivity in the nanomolar range (median EC₅₀ 179 nM), while for apilimod, 93% of the samples exhibited sensitivity in the micromolar range (median EC₅₀ 22618 nM) (Table 2 and *Online Supplementary Table S3*).

The cytotoxicity of APY0201 for different leukocyte populations was evaluated in two primary patients' samples with increasing drug concentrations. The plasma cell population of the first sample was sensitive to APY0201, with a marked decrease in cellular viability when incubated with the highest dose of the drug (*Online Supplementary Figure S7A*); the second sample was considered resistant (*Online Supplementary Figure S7B*). We did not observe any significant off-target effect of APY0201 in the T and B lymphocyte populations in either sample, while some off-target effects were noted in the population composed of monocytes, macrophages, and granulocytes.

Ploidy and t(11;14) are biomarkers of sensitivity

In HMCL, APY0201 was active regardless of the presence or absence of IgH translocations, TP53 deletion, CKS1B gain, monosomy 13, and MYC rearrangements (*Online Supplementary Figure S8*). We then evaluated possible associations between APY0201 sensitivity in primary patients' samples and clinical findings. We examined different disease stages (monoclonal gammopathy of undetermined significance, smoldering MM, and MM), disease status (newly diagnosed or relapsed), fluorescence *in situ* hybridization cytogenetics [t(11;14), t(4;14), t(14;16), t(6;14), deletion of 17p, CKS1B duplication, MYC rearrangement, monosomy 13, and trisomies of one or more odd-numbered chromosomes], flow cytometry analysis (hyperdiploid status and S-phase), and hyperdiploidy according to Wuillemme *et al.*²⁵ Despite the limited sample size, primary patients' samples lacking trisomies (Fisher test, P=0.0232) and harboring t(11;14) (Fisher test, P=0.0189) were more frequently classified as inactive to APY0201 in the *ex vivo* drug screen (Figure 1A, B). With high-risk patients defined as those with t(4;14), t(14;16), deletion of 17p, or CKS1B duplication, no discernible difference in PIKfyve sensitivity was observed between patients with high- or low-risk genetics.

Data publicly reported from the CoMMpass project (these data were generated as part of the Multiple Myeloma Research Foundation Personalized Medicine Initiatives; <https://research.themmr.org> and www.themmr.org) showed lower PIKfyve expression levels in hyperdiploid samples when compared to non-hyperdiploid samples (*t*-test, P=0.0003) and in samples lacking t(11;14) when compared to samples harboring the translocation (*t*-test, P<0.0001). These findings were also confirmed in a cohort of 487 primary MM samples (Mann-Whitney test, P<0.0001) (*unpublished data*). We hypothesize that increased PIKfyve expression levels may be associated with increased resistance to PIKfyve inhibitors, with higher concentrations of the inhibitors necessary to activate TFEB. However, further studies are needed to support this hypothesis.

Upregulation of lysosomal pathways *in vitro* and *ex vivo*

To further elucidate the anti-MM mechanism of PIKfyve inhibitors, we evaluated the mRNA-sequencing profiles of five HMCL with low, intermediate and high sensitivities to APY0201. When comparing RNA expression profiles from each HMCL treated with APY0201 for 24 h with its untreated control using the Enrichr platform, gene targets of the lysosomal pathway were upregulated in all five HMCL (P≤0.01), corroborating previous findings.²⁶ This is consistent with previous data from B-NHL suggesting that apilimod impaired lysosomal function and consequent degradation of the autophagosomal cargo.¹²

Three primary patients' samples identified as sensitive to APY0201 (EC₅₀ of 56.29, 101.14, and 103.36) and one resistant sample, lacking a dose-response curve (*Online Supplementary Figure S9*), were sent for mRNA-sequencing analysis. The three sensitive patients' samples harbored

Table 1. Cellular viability inhibition of 20 human myeloma cell lines after 72 h of incubation with three PIKfyve inhibitors.

Mid-point EC ₅₀	APY0201		HMCL YM201636		Apilimod	
	Samples	%	Samples	%	Samples	%
<100 nM	5/20	25	0/20	0	0/20	0
100-1000 nM	8/20	40	8/20	40	1/20	5
>1000 nM	7/20	35	12/20	60	19/20	95

EC₅₀: half maximal effective concentration; HMCL: human myeloma cell lines.

Table 2. Cellular viability inhibition of *ex vivo* primary patients' samples after 24 and 72 h incubation with APY0201 and apilimod.

Mid-point EC ₅₀	<i>Ex vivo</i> Primary Patients' Samples					
	APY0201		APY0201		Apilimod	
	24 Hour Incubation		72 Hour Incubation		72 Hour Incubation	
	Samples	%	Samples	%	Samples	%
<10 nM	2/100	2	3/14	21.4	0/15	0.0
10-100 nM	17/100	17.0	2/14	14.3	0/15	0.0
100-1000 nM	11/100	11.0	5/14	35.7	1/15	6.7
>1000 nM	10/100	10.0	3/14	21.4	14/15	93.3
Inactive	60/100	60.0	1/14	7.2	0/15	0.0

EC₅₀: half maximal effective concentration.

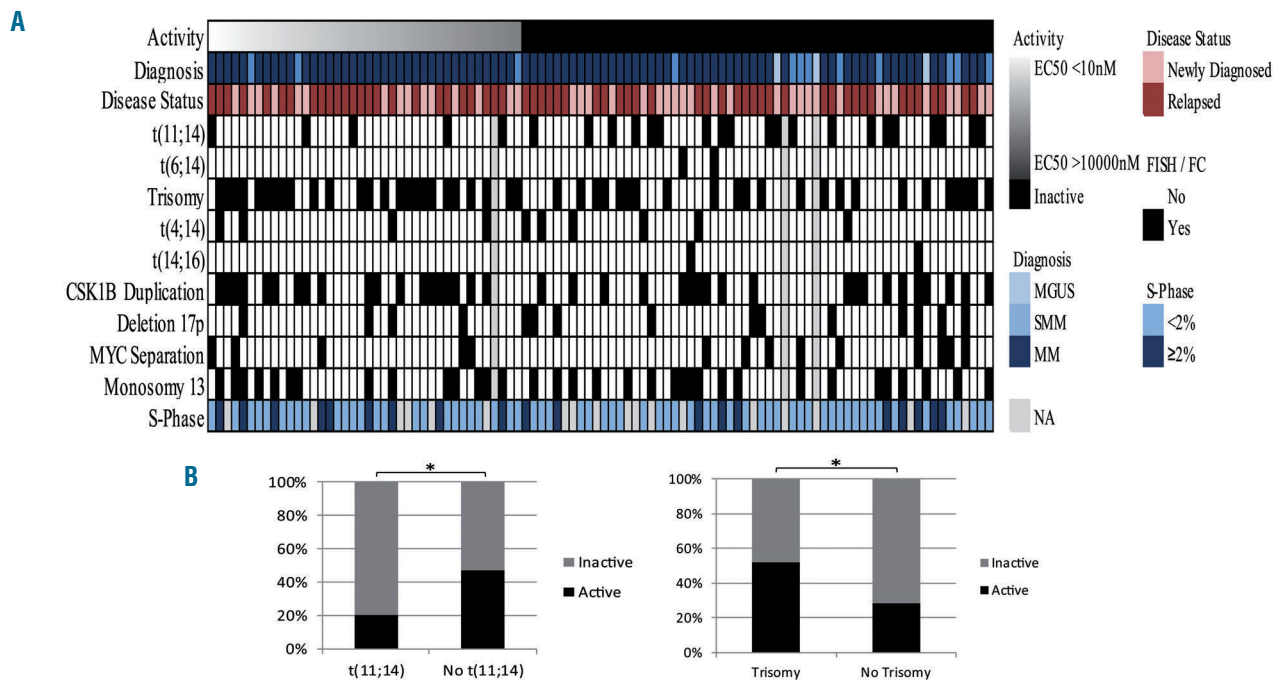


Figure 1. A global overview of clinical data from 100 multiple myeloma patients with *ex vivo* samples tested for APY0201 activity. (A) Clinical data including diagnosis (monoclonal gammopathy of undetermined significance, smoldering multiple myeloma and multiple myeloma), disease status (newly diagnosed or relapsed), fluorescence *in situ* hybridization data (t(11;14), t(6;14), trisomies of one or more odd-numbered chromosomes, t(4;14), t(14;16), CSK1B duplication, deletion of 17p, MYC rearrangements, and monosomy 13), and S-phase status from flow cytometry analysis. Missing data are shown in gray. (B) Primary patients' samples with trisomies of one or more odd-numbered chromosomes ($P=0.0182$) and lack of t(11;14) ($P=0.0168$) had increased *ex vivo* sensitivity to APY0201. EC₅₀: half maximal effective concentration; FISH: fluorescence *in situ* hybridization; FC: flow cytometry; MGUS: monoclonal gammopathy of undetermined significance; SMM: smoldering multiple myeloma; MM: multiple myeloma

trisomies of one or more odd-numbered chromosomes, further supporting an increased sensitivity of hyperdiploid MM to APY0201. As demonstrated in HMCL, incubation with APY0201 at 500 nM for 24 h led to upregulation of the lysosomal pathway in both sensitive and resistant primary patients' samples ($P \leq 0.01$). The transcriptional upregulation of lysosomal biogenesis in HMCL and in primary patients' samples warranted further assays to evaluate the functional consequences of PIKfyve inhibition on lysosomes and autophagy.

Of interest *CCL3* was the single most upregulated gene across all five HMCL and all four primary patients' samples following APY0201 treatment for 24 h. MM cells constitutively secrete *CCL3* (also known as MIP-1 α) and the chemokine has been directly related to osteolytic bone lesions and poor prognosis by stimulating the proliferation, migration and survival of MM cells (reviewed by Aggarwal *et al.*²⁷). In MM harboring t(4;14), we have previously demonstrated that *CCL3* is downregulated by inhibition of *FGFR3* and is regulated by the RAS-MAPK pathway, with overactivation of RAS-MAPK upregulating *CCL3*.²⁸ This counter-intuitive link between PIKfyve inhibition, lysosomal pathways and *CCL3* upregulation deserves further exploration beyond the scope of this report.

APY0201 activated TFEB, a master regulator of lysosomal biogenesis and autophagy, and promoted cellular vacuolization

Higher basal protein levels of TFEB, a regulator of lysosomal function and autophagy,²⁹ was shown in two HMCL (KMS26 and JJN3) most sensitive to APY0201

when compared to the two most resistant HMCL (RPMI-8226 and EJM), corroborating previous data associating TFEB overexpression with sensitivity to apilimod in B-cell NHL (Figure 2A, B).¹² Following treatment with APY0201 for 6 h, activation of TFEB, found in its dephosphorylated state, was observed independently of the HMCL sensitivity profile to the compound. Nuclear translocation of TFEB following PIKfyve exposure was subsequently confirmed in a subcellular localization immunoblotting assay (Figure 2C, D). Dephosphorylated TFEB translocates from the cytoplasm to the nucleus to regulate the expression of target genes associated with autophagy.³⁰ Therefore, these findings further supported an APY0201-induced autophagy disturbance through PIKfyve inhibition in MM.

Treatment with APY0201 led to the formation of enlarged intracellular vacuoles in all three HMCL (KMS26, L363, and EJM), independently of drug sensitivity (Figure 2E). The endolysosomal swelling phenotype has been widely related to the disruption of PIKfyve activity^{11–13,15,16,26,31} due to the role of the kinase in vacuole maturation after lysosome fusion has occurred.³¹ Vacuolation could therefore be a phenotypic biomarker of PIKfyve inhibition and consequent reduction of PtdIns-3,5-P2.¹⁴ The acidic nature of the vacuoles was further examined with LysoSensor staining. Blue fluorescence found in more neutral environments was observed in the vacuoles of all four treated HMCL (2 sensitive and 2 resistant to APY0201), indicating the prevalence of less acidic vacuolar content and, therefore, suggesting impaired lysosomal function. However, yellow fluores-

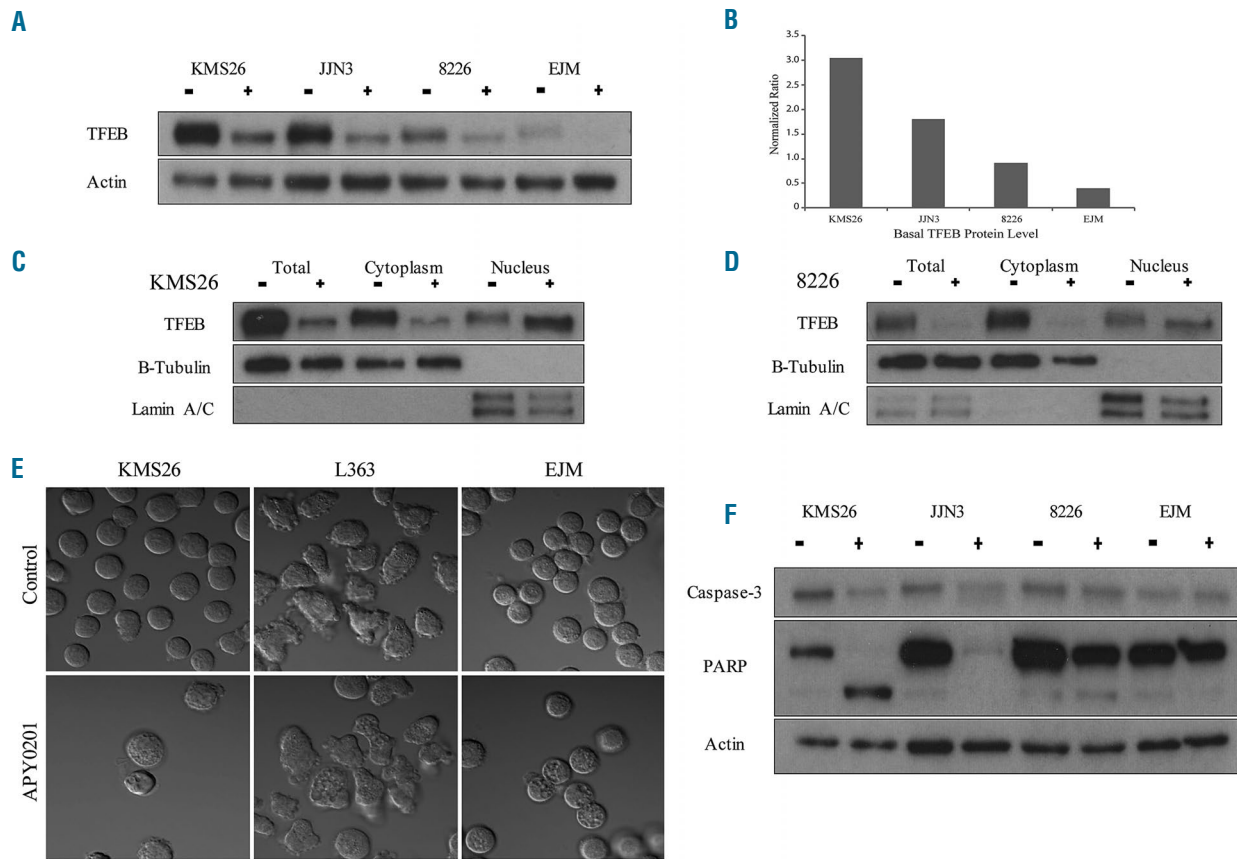


Figure 2. APY0201 treatment leads to activation of TFEB, a vacuolar phenotype, and cell death by apoptosis in human myeloma cell lines. (A) Two sensitive (KMS26 and JJN3) and two resistant (RPMI-8226 and EJM) human myeloma cell lines (HMCL) were treated with dimethylsulfoxide (DMSO) or 100 nM of APY0201. Cell lysates were harvested after 6 h of incubation with the drug and immunoblotting was performed to determine the level of transcription factor EB (TFEB) protein. (B) Basal TFEB level was correlated to sensitivity. Two HMCL were treated with DMSO or 100 nM of APY0201 after 6 h for KMS26 (C) and 24 h for RPMI-8226 (D) with immunoblotting performed to determine the subcellular localization of TFEB. (E) Three HMCL were or were not treated with APY0201 at 100 nM and live cell differential interference contrast (DIC) imaging was performed after 48 h with a confocal microscope Zeiss LSM 800 (63X). (F) Four HMCL were treated with DMSO (-) or 100 nM of APY0201 (+) for 48 h prior to immunoblotting for caspase-3 and poly (ADP-ribose) polymerase (PARP) protein.

cence found in more acidic environments prevailed in the vacuoles of the two resistant HMCL, RPMI-8226 and EJM, indicating a partial maintenance of a more acidic content after APY0201 exposure, which is necessary for autophagic flux maintenance (*Online Supplementary Figure S10*). The galectin puncta assay was performed to determine whether lysosomal cell death was critical in the APY0201-induced cytotoxicity. Lysosomal cell death is promoted by leakage of lysosomal contents following permeabilization of the lysosomal membrane;³² however, no evidence of lysosomal membrane permeabilization was observed (*data not shown*). APY0201 apoptosis-mediated cellular toxicity was demonstrated by immunoblotting of Caspase-3 and PARP cleavage in the sensitive HMCL, KMS26 and JJN3, but not in the two resistant HMCL, RPMI-8226 and EJM (Figure 2F).

Multiple myeloma cells resistant to PIKfyve inhibitors partially maintain autophagic flux

To further evaluate autophagic flux, we examined key components of lysosomes and autophagosomes. An accumulation of the inactive precursor procathepsin D was observed in all four HMCL and of procathepsin A both in sensitive KMS26, JJN3, and in resistant EJM cells following

incubation with APY0201 (Figure 3A), demonstrating a decrease in maturation of lysosomal proteases independent of APY0201 sensitivity. All treated HMCL exhibited an increase in LC3 A/B-II, a protein present in autophagosomes and autophagolysosomes; as well as lysosome-associated membrane protein 1 (Lamp-1), a protein present in lysosomes and autophagolysosomes. An increase in sequestosome 1 (SQSTM1)/p62 protein levels was also demonstrated in all four HMCL, further highlighting impaired autophagic protein degradation (Figure 3B). We therefore confirmed that lysosomal function, and consequently autophagy, was disrupted following PIKfyve inhibition and did not seem to predict drug sensitivity.

However, Beclin-1, a promoter of autophagy was decreased in KMS26 and JJN3 (the two HMCL sensitive to PIKfyve inhibitors) and discretely increased in RPMI-8226 and EJM (the two PIKfyve inhibitor-resistant HMCL) (Figure 3B). The SQSTM1:Beclin1 protein level ratio was then used as an autophagy indicator, with decreased SQSTM1 and increased Beclin-1 indicative of increased autophagic flux, as described previously.³³ A higher ratio was found in the sensitive HMCL (KMS26 and JJN3) when compared to the resistant HMCL (Figure 3C), which demonstrates impaired autophagic flux in drug-sensitive

HMCL. Further evaluation with the LC3-fluorescent protein showed a reduction of the acid-sensitive green fluorescent protein and maintenance of the acid-insensitive red fluorescent protein in the representative resistant HMCL, EJM, when compared to the sensitive HMCL, JN3, after 18 h of treatment with APY0201, indicating maturation of autophagosomes to autophagolysosomes in the resistant HMCL (Figure 3D, E).

Finally, we performed a cellular viability assay treating the two representative resistant HMCL, RPMI-8226 and EJM, with 1 nM and 2 nM of the autophagy inhibitor bafilomycin A1, respectively, showing synergistic anti-

MM activity (Figure 3F, G). In summary, these findings demonstrate the key role of autophagic flux disruption in MM cytotoxicity caused by PIKfyve inhibitors (Figure 4). Resistant HMCL maintain functional autophagy more efficiently, representing a mechanism of resistance to these drugs.

APY0201 sensitivity *in vitro* and *ex vivo* was predicted with the autophagy detection kit

Since anti-MM activity of APY0201 was associated with disruption of lysosome function and autophagy, we explored an autophagy detection assay, as a biomarker to

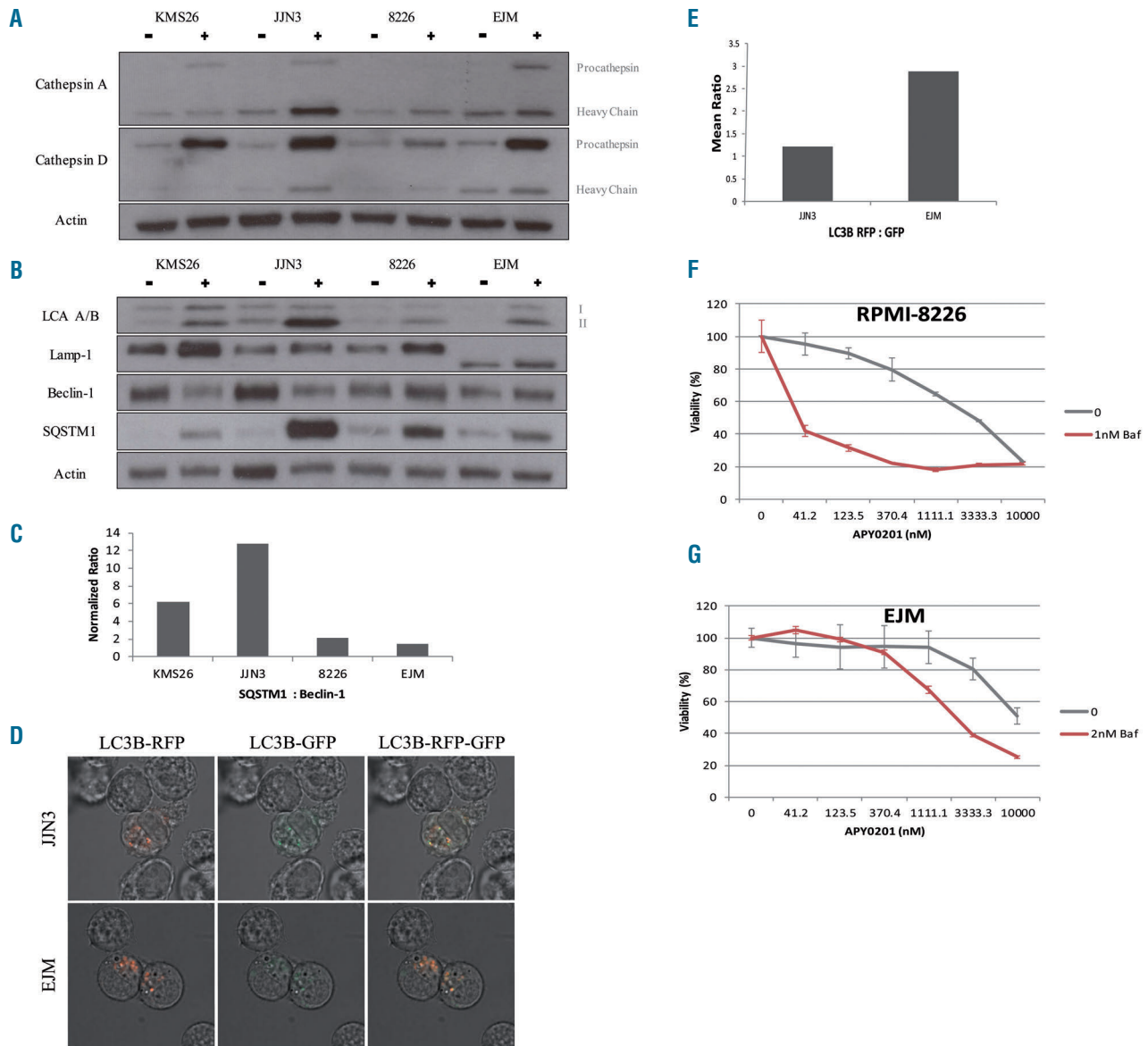


Figure 3. APY0201 treatment leads to an increase in inactive precursors of lysosomal proteases and in autophagy organelles but decreased autophagic flux in sensitive human myeloma cell lines. Four human myeloma cell lines (HMCL) were treated with dimethylsulfoxide (DMSO) or 100 nM of APY0201. Cell lysates were harvested after 48 h of drug incubation and immunoblotting was performed to determine the levels of cathepsin A and D proteins (A) and Beclin-1, LC3 A/B, lysosome-associated membrane protein 1 (Lamp-1), and sequestosome 1 (SQSTM1)/p62 protein levels (B). (C) The ratio of SQSTM1:Beclin1 protein levels in two sensitive (KMS26 and JN3) and two resistant (RPMI-8226 and EJM) HMCL following 48 h of incubation with APY0201. (D) LC3 acid-sensitive green fluorescent protein (GFP) and -insensitive red fluorescent protein (RFP) in representative sensitive and resistant HMCL (JN3 and EJM, respectively) after 18 h of treatment with 100 nM of APY0201; images were obtained with a Zeiss LSM 800 confocal microscope (63X) and processed with Zen Blue software. (E) Mean LC3 RFP:GFP ratio in JN3 and EJM. (F) Treatment of the RPMI-8226 resistant HMCL with APY0201 with and without 1 nM of bafilomycin A1 after 48 h. (G) Treatment of the EJM-resistant HMCL with APY0201 with and without 2 nM of bafilomycin A1 after 48 h.

predict sensitivity to APY0201. A more pronounced autophagy signal occurred when three HMCL sensitive to APY0201 (KMS26, JN3, and FR4) were treated with the PIKfyve inhibitor for 18 h than when three resistant HMCL

(EJM, KMS28PE, RPMI-8226) were so treated (Figure 5A). A decrease in cellular viability was confirmed as shown. The increased autophagy signal further demonstrates the disruption of autophagy in sensitive HMCL.³⁴

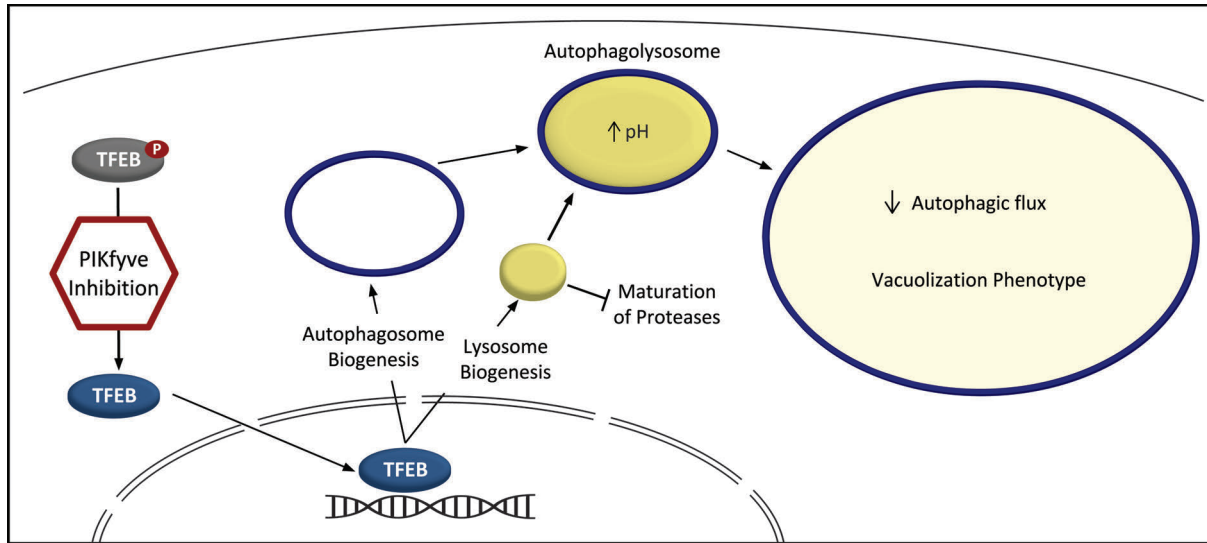


Figure 4. Proposed mechanism of action of PIKfyve inhibitors. PIKfyve inhibition following treatment with APY0201, activates transcription factor EB (TFEB) through dephosphorylation leading to upregulation of autophagosome and lysosome biogenesis. Lysosomal function is disrupted by a decrease in the maturation of proteases and a less acidic pH. Autophagic flux is therefore disrupted, leading to the vacuolization phenotype. We observed that resistant cell lines are able to maintain a more acidic pH and maintain, at least partially, autophagic flux.

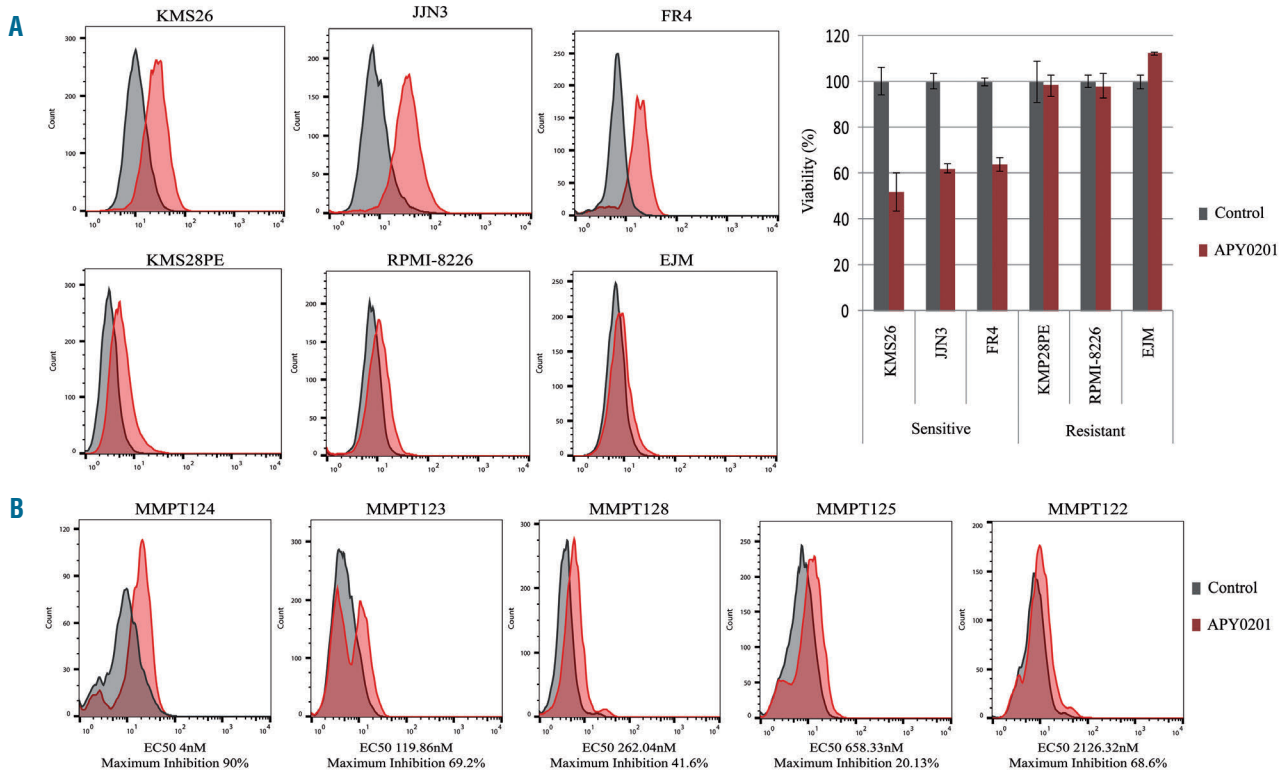


Figure 5. APY0201-mediated increase in autophagic vesicles and cellular toxicity. (A) Three sensitive (KMS26, JN3, FR4) and three resistant (EJM, KMS28PE, RPMI-8226) human multiple myeloma cell lines treated or not with APY0201 at 100 nM for 18 h. Histogram representation of the green detection reagent detected by flow cytometry and 3-(4,5-dimethylthiazol)-2,5-diphenyl tetrazolium bromide (MTT) assay performed following 72 h of incubation with the compound to determine cell viability. (B) The APY0201-mediated increase in autophagic vesicles in primary patients' samples treated or not with the compound for 18 h was inversely proportional to the mid-point half maximal effective concentration (EC₅₀).

Similarly, in primary patients' samples, an APY0201-mediated increase in autophagic vacuoles was inversely proportional to the EC₅₀ for the PIKfyve inhibitor APY0201 (Figure 5B). Analogous findings were also seen when HMCL and primary patients' samples were treated for 18 h with apilimod (*data not shown*). This could, therefore, be an efficient and fast assay to predict PIKfyve inhibitor response in MM patients.

Discussion

Although the clinical outcome of MM patients with current therapy protocols has improved markedly,^{35,36} most patients ultimately relapse.³⁷ The identification of novel anti-MM agents therefore remains an important step towards disease control. We first identified the PIKfyve inhibitor APY0201 as a promising anti-MM therapeutic in a preliminary screen and included the PIKfyve inhibitor in a 76-drug panel used for more intensive drug screening for sensitivity. Following 24 h incubation of 25 HMCL and 100 *ex vivo* primary patients' samples with APY0201, this drug was demonstrated to have activity in >90% and 40%, respectively. PIKfyve inhibition was then validated with three different PIKfyve inhibitors, APY0201, YM201636, and apilimod, generating dose-dependent responses in 20 HMCL, while APY0201 and apilimod showed activity in >90% of *ex vivo* patients' samples with a longer 72 h incubation.

The PIKfyve selectivity of apilimod had been demonstrated when this drug was profiled against several kinases and no off-target activity was detected,^{12,38} while the specificity of APY0201 was demonstrated against all tested kinases, G-protein-coupled receptors, ion channels, and enzymes, with APY0201 showing superior selectivity over apilimod.¹⁴ YM201636 is less selective, inhibiting PIKfyve and insulin-induced activation of class IA PI3 kinase.³⁹ Our findings clearly demonstrated increased inhibition of cellular viability with APY0201, when compared to YM201636 and apilimod, in HMCL, NHL cell lines, and primary *ex vivo* patients' samples.

PIKfyve negatively regulates TFEB,²⁶ and PIKfyve inhibitor sensitivity has been correlated with higher baseline levels of TFEB, a master regulator of the function of lysosomes and autophagy.²⁹ Following APY0201 treatment, TFEB was found in a dephosphorylated state which correlated with its translocation to the nucleus in representative sensitive and resistant HMCL, as previously noted by others.^{12,40} A PtdIns-3,5-P2-dependent regulation of the activation and nuclear translocation of TFEB has also been previously demonstrated.⁴⁰ In addition, the endolysosomal swelling phenotype associated with loss of PIKfyve function has been linked to a concomitantly reduced number and increased volume of autophagy

organelles after coalescence.²⁶ These findings clearly link PIKfyve inhibitors with lysosomal and autophagic disruption and were confirmed in our analysis.

Impaired lysosomal degradation of autophagic cargo induced by apilimod driving cell death was suggested in B-NHL.³⁸ However, we found an accumulation of lysosomal protease precursors, autophagosome and lysosome protein markers, intracellular vacuolization, as well as transcriptomic increases in the lysosome pathway in representative HMCL both sensitive and resistant to APY0201. This indicated that PIKfyve-induced cell death in MM could not be fully explained by the model of apilimod's mechanism of action in B-NHL,³⁸ whereby PIKfyve inhibition led to impaired lysosomal homeostasis with nuclear translocation of TFEB and vacuole formation, causing cell death. We theorize and provide supporting evidence that one mechanism of resistance to the PIKfyve inhibitor APY0201 in HMCL is by partially maintaining autophagic flux, which decelerates significant imbalances in membrane trafficking and the resulting metabolic alterations.

Autophagy is critical in plasma cell ontogenesis for sustainable immunoglobulin synthesis and endoplasmic reticulum capacity, increasing cellular viability, which may be even more important in plasma cell dyscrasias.⁴¹ Higher basal protein levels of TFEB were shown in HMCL sensitive to APY0201; therefore, since TFEB overexpression has been associated with increased autophagic flux,⁴² basal autophagic flux in HMCL could be directly related to the sensitivity to PIKfyve inhibition. MM cells are notably dependent on autophagy for their survival,^{43,44} thus targeting autophagy via PIKfyve inhibition could represent an effective treatment option for MM.

A phase 1 clinical trial with apilimod in B-cell malignancies is in progress, with preliminary results showing promising early antitumor activity in heavily pretreated patients and a favorable safety profile at doses of ≤125 mg BID.⁴⁵ *Ex vivo* drug screening is suggested to enrich MM patients sensitive to PIKfyve inhibitors in future clinical trials. Detection of autophagy in response to drug exposure is also a promising test to predict sensitivity, although additional validation is necessary. In addition, we anticipate greater sensitivity to PIKfyve inhibitors in patients with trisomies of one or more odd-numbered chromosomes and less sensitivity in MM samples harboring t(11;14).

In summary, we demonstrated promising anti-myeloma activity *in vitro* and *ex vivo* as a result of inhibition of PIKfyve, a novel therapeutic target in MM. PIKfyve inhibitors disrupt lysosomal function and, consequently, autophagic flux, and the high basal necessity of autophagy in plasma cells and MM cells indicate the clinical potential of this novel target in anti-MM strategies. PIKfyve inhibition should be further evaluated in MM.

References

- Shisheva A, Sbrissa D, Ikononov O. Cloning, characterization, and expression of a novel Zn²⁺-binding FYVE finger-containing phosphoinositide kinase in insulin-sensitive cells. *Mol Cell Biol.* 1999;19(1):623-634.
- Shisheva A. PIKfyve: partners, significance, debates and paradoxes. *Cell Biol Int.* 2008;32(6):591-604.
- Sbrissa D, Ikononov OC, Shisheva A. PIKfyve lipid kinase is a protein kinase: downregulation of 5'-phosphoinositide product formation by autophosphorylation. *Biochemistry.* 2000;39(51):15980-15989.
- Sbrissa D, Ikononov OC, Shisheva A. PIKfyve, a mammalian ortholog of yeast Fab1p lipid kinase, synthesizes 5-phosphoinositides. *J Biol Chem.* 1999;274(31):21589-21597.
- Hasegawa J, Strunk BS, Weisman LS. PI5P and PI(3,5)P₂: minor, but essential phosphoinositides. *Cell Struct Funct.* 2017; 42:49-60.
- Wada Y, Lu R, Zhou D, et al. Selective abrogation of Th1 response by STA-5326, a potent IL-12/IL-23 inhibitor. *Blood.*

- 2007;109(3):1156-1164.
7. Wada Y, Cardinale I, Khatcherian A, et al. Apilimod inhibits the production of IL-12 and IL-23 and reduces dendritic cell infiltration in psoriasis. *PLoS One*. 2012;7(4):e35069.
 8. Krausz S, Boumans MJH, Gerlag DM, et al. A phase IIa, randomized, double-blind, placebo-controlled trial of apilimod mesylate, an interleukin-12/interleukin-23 inhibitor, in patients with rheumatoid arthritis. *Arthritis Rheum*. 2012;64(6):1750-1755.
 9. Sands BE, Jacobson EW, Sylwestrowicz T, et al. Randomized, double-blind, placebo-controlled trial of the oral interleukin-12/23 inhibitor apilimod mesylate for treatment of active Crohn's disease. *Inflamm Bowel Dis*. 2010;16(7):1209-1218.
 10. Burakoff R, Barish CF, Riff D, et al. A phase 1/2A trial of STA5326, an oral interleukin-12/23 inhibitor, in patients with active moderate to severe Crohn's disease. *Inflamm Bowel Dis*. 2006;12(7):558-565.
 11. Cai X, Xu Y, Cheung AK, et al. PIKfyve, a class III PI kinase, is the target of the small molecular IL-12/IL-23 inhibitor apilimod and a player in toll-like receptor signaling. *Chem Biol*. 2013;20(7):912-921.
 12. Gayle S, Landrette S, Beeharry N, et al. Identification of apilimod as a first-in-class PIKfyve kinase inhibitor for treatment of B-cell non-Hodgkin lymphoma. *Blood*. 2017;129(13):1768-1778.
 13. Jefferies HBJ, Cooke FT, Jat P, et al. A selective PIKfyve inhibitor blocks PtdIns(3,5)P₂ production and disrupts endomembrane transport and retroviral budding. *EMBO Rep*. 2008;9(2):164-170.
 14. Hayakawa N, Noguchi M, Takeshita S, et al. Structure-activity relationship study, target identification, and pharmacological characterization of a small molecular IL-12 /23. *Bioorg Med Chem*. 2014;22(11):3021-3029.
 15. Terajima M, Kaneko-Kobayashi Y, Nakamura N, et al. Inhibition of c-Rel DNA binding is critical for the anti-inflammatory effects of novel PIKfyve inhibitor. *Eur J Pharmacol*. 2016;780:93-105.
 16. de Lartigue J, Polson H, Feldman M, et al. PIKfyve regulation of endosome-linked pathways. *Traffic*. 2009;10(7):883-893.
 17. Meurice N, Petit J, De Campos C, et al. "Direct to drug" screening as a route to individualized therapy in multiple myeloma. *Blood*. 2017;130(Suppl 1):3080.
 18. Seckinger A, Delgado JA, Moser S, et al. Target expression, generation, preclinical activity, and pharmacokinetics of the BCMA-T cell bispecific antibody EM801 for multiple myeloma treatment. *Cancer Cell*. 2017;31(3):396-410.
 19. Kalari KR, Nair AA, Bhavsar JD, et al. MAP-Seq: Mayo analysis pipeline for RNA sequencing. *BMC Bioinformatics*. 2014;15:224-15234.
 20. Dobin A, Davis CA, Schlesinger F, et al. STAR: ultrafast universal RNA-seq aligner. *Bioinformatics*. 2013;29(1):15-21.
 21. Wang L, Wang S, Li W. RSeQC: quality control of RNA-seq experiments. *Bioinformatics*. 2012;28(16):2184-2185.
 22. Liao Y, Smyth GK, Shi W. FeatureCounts: an efficient general purpose program for assigning sequence reads to genomic features. *Bioinformatics*. 2014;30(7):923-930.
 23. Kuleshov M V, Jones MR, Rouillard AD, et al. Enrichr: a comprehensive gene set enrichment analysis web server 2016 update. *Nucleic Acids Res*. 2016;44:90-97.
 24. Edgar R, Domrachev M, Lash AE. Gene Expression Omnibus: NCBI gene expression and hybridization array data repository. *Nucleic Acids Res*. 2002;30(1):207-210.
 25. Wuilleme S, Robillard N, Lodé L, et al. Ploidy, as detected by fluorescence in situ hybridization, defines different subgroups in multiple myeloma. *Leukemia*. 2005;19(2):275-278.
 26. Choy CH, Saffi G, Gray MA, et al. Lysosome enlargement during inhibition of the lipid kinase PIKfyve proceeds through lysosome coalescence. *J Cell Sci*. 2018;131(10).
 27. Aggarwal R, Ghobrial IM, Roodman GD. Chemokines in multiple myeloma. *Exp Hematol*. 2006;34(10):1289-1295.
 28. Masih-Khan E, Trudel S, Heise C, et al. MIP-1alpha (CCL3) is a downstream target of FGFR3 and RAS-MAPK signaling in multiple myeloma. *Blood*. 2006;108(10):3465-3471.
 29. Napolitano G, Ballabio A. TFEB at a glance. *J Cell Sci*. 2016;129(13):2475-2481.
 30. Settembre C, Ballabio A. TFEB regulates autophagy: an integrated coordination of cellular degradation and recycling processes. *Autophagy*. 2011;7(11):1379-1381.
 31. Krishna S, Palm W, Lee Y, et al. PIKfyve regulates vacuole maturation and nutrient recovery following engulfment. *Dev Cell*. 2016;38(5):536-547.
 32. Aits S, Jaattela M. Lysosomal cell death at a glance. *J Cell Sci*. 2013;126(9):1905-1912.
 33. Kara NZ, Toker L, Agam G, et al. Trehalose induced antidepressant-like effects and autophagy enhancement in mice. *Psychopharmacology*. 2013;229(2):367-375.
 34. Klionsky DJ, Abdelmohsen K, Abe A, et al. Guidelines for the use and interpretation of assays for monitoring autophagy (3rd edition). *Autophagy*. 2016;12(1):1-222.
 35. Sonneveld P. Management of multiple myeloma in the relapsed/refractory patient. *Hematol Am Soc Hematol Educ Progr*. 2017;2017(1):508-517.
 36. Manier S, Salem KZ, Park J, et al. Genomic complexity of multiple myeloma and its clinical implications. *Nat Rev Clin Oncol*. 2016;13:100-113.
 37. Laubach J, Garderet L, Mahindra A, et al. Management of relapsed multiple myeloma: recommendations of the International Myeloma Working Group. *Leukemia*. 2016;30(5):1005-1017.
 38. Gayle S, Landrette S, Beeharry N, et al. B-cell non-Hodgkin lymphoma: selective vulnerability to PIKfyve inhibition. *Autophagy*. 2017;13(6):1082-1083.
 39. Ikonomov OC, Sbrissa D, Shisheva A. YM201636, an inhibitor of retroviral budding and PIKfyve-catalyzed PtdIns(3,5)P₂ synthesis, halts glucose entry by insulin in adipocytes. *Biochem Biophys Res Commun*. 2009;382(3):566-570.
 40. Wang W, Gao Q, Yang M, et al. Up-regulation of lysosomal TRPML1 channels is essential for lysosomal adaptation to nutrient starvation. *Proc Natl Acad Sci U S A*. 2015;112(11):1373-1381.
 41. Pengo N, Scolari M, Oliva L, et al. Plasma cells require autophagy for sustainable immunoglobulin production. *Nat Immunol*. 2013;14(3):298-305.
 42. Settembre C, Polito VA, Garcia M, et al. TFEB links autophagy to lysosomal biogenesis. *Science*. 2011;332(6036):1429-1433.
 43. Milan E, Fabbri M, Cenci S. Autophagy in plasma cell ontogeny and malignancy. *J Clin Immunol*. 2016;36(Suppl 1):S18-S24.
 44. Milan E, Perini T, Resnati M, et al. A plastic SQSTM1/p62-dependent autophagic reserve maintains proteostasis and determines proteasome inhibitor susceptibility in multiple myeloma cells. *Autophagy*. 2015;11(7):1161-1178.
 45. Harb WA, Diefenbach CS, Lakhani N, et al. Phase 1 clinical safety, pharmacokinetics (PK), and activity of apilimod dimesylate (LAM-002A), a first-in-class inhibitor of phosphatidylinositol-3-phosphate 5-kinase (PIKfyve), in patients with relapsed or refractory B-cell malignancies. *Blood*. 2017;130(Suppl 1):4119.



Ferrata Storti Foundation

Health-related quality of life in transplant ineligible newly diagnosed multiple myeloma patients treated with either thalidomide or lenalidomide-based regimen until progression: a prospective, open-label, multicenter, randomized, phase 3 study

Haematologica 2020
Volume 105(1):1650-1659

Lene Kongsgaard Nielsen,^{1*} Claudia Stege,^{2*} Birgit Lissenberg-Witte,³ Bronno van der Holt,⁴ Ulf-Henrik Mellqvist,⁵ Morten Salomo,⁶ Gerard Bos,⁷ Mark-David Levin,⁸ Heleen Visser-Wisselaar,⁴ Markus Hansson,⁹ Annette van der Velden,¹⁰ Wendy Deenik,¹¹ Juleon Coenen,¹² Maja Hinge,¹³ Saskia Klein,¹⁴ Bea Tanis,¹⁵ Damian Szatkowski,¹⁶ Rolf Brouwer,¹⁷ Matthijs Westerman,¹⁸ Rineke Leys,¹⁹ Harm Sinnige,²⁰ Einar Haukås,²¹ Klaas van der Hem,²² Marc Durian,²³ Peter Gimsing,²⁴ Niels van de Donk,² Pieter Sonneveld,²⁵ Anders Waage,²⁶ Niels Abildgaard¹ and Sonja Zweegman²

¹Quality of Life Research Center, Department of Haematology, Odense University Hospital, Odense, Denmark; ²Amsterdam UMC, Vrije Universiteit Amsterdam, Department of Hematology, Cancer Center Amsterdam, Amsterdam, the Netherlands; ³Amsterdam UMC, Vrije Universiteit Amsterdam, Department of Epidemiology and Biostatistics, Amsterdam, the Netherlands; ⁴HOVON Data Center, Department of Hematology, Erasmus MC Cancer Institute, Rotterdam, the Netherlands; ⁵Section of Hematology and Coagulation, Department of Medicine, Sahlgrenska University Hospital, Gotheborg, Sweden; ⁶Department of Haematology, Rigshospitalet, Copenhagen, Denmark; ⁷Department of Haematology, Maastricht University Medical Center, Maastricht, the Netherlands; ⁸Department of Internal Medicine, Albert Schweitzer Hospital, Dordrecht, the Netherlands; ⁹Department of Haematology and Wallenberg Center for Molecular Medicine, Skåne University Hospital, Lund University, Lund, Sweden; ¹⁰Department of Internal Medicine, Martini Ziekenhuis, Groningen, the Netherlands; ¹¹Department of Internal Medicine, Tergooi Ziekenhuis, Hilversum, the Netherlands; ¹²Department of Internal Medicine, Isala, Zwolle, the Netherlands; ¹³Department of Internal Medicine, Division of Hematology, Vejle Hospital, Vejle, Denmark; ¹⁴Department of Internal Medicine, Meander Medisch Centrum, Amersfoort, the Netherlands; ¹⁵Department of Internal Medicine, Groene Hart Ziekenhuis, Gouda, the Netherlands; ¹⁶Department of Oncology, Haematology and Palliative Care, Førde Central Hospital, Førde, Norway; ¹⁷Department of Internal Medicine, Reinier de Graaf Ziekenhuis, Delft, the Netherlands; ¹⁸Department of Internal Medicine, Northwest Clinics, Alkmaar, the Netherlands; ¹⁹Department of Internal Medicine, Maasstad Ziekenhuis, Rotterdam, the Netherlands; ²⁰Department of Internal Medicine, Jeroen Bosch Ziekenhuis, Den Bosch, the Netherlands; ²¹Department of Haematology, Stavanger University Hospital, Stavanger, Norway; ²²Department of Internal Medicine, Zaans Medisch Centrum, Zaandam, the Netherlands; ²³Department of Internal Medicine, Tweesteden Ziekenhuis, Tilburg, the Netherlands; ²⁴Department of Haematology, Rigshospitalet, Copenhagen, Denmark; ²⁵Department of Haematology, Erasmus Medical Center Cancer Center, Rotterdam, the Netherlands and ²⁶Department of Haematology, St Olavs Hospital and Norwegian University of Science and Technology, Trondheim, Norway

*LKN and CS contributed equally as co-first authors.

Correspondence:

LENE KONGSGAARD NIELSEN
lene.kongsgaard.nielsen@rsyd.dk

Received: April 19, 2019.

Accepted: September 11, 2019.

Pre-published: September 12, 2019.

doi:10.3324/haematol.2019.222299

Check the online version for the most updated information on this article, online supplements, and information on authorship & disclosures: www.haematologica.org/content/105/6/1650

©2020 Ferrata Storti Foundation

Material published in *Haematologica* is covered by copyright. All rights are reserved to the Ferrata Storti Foundation. Use of published material is allowed under the following terms and conditions:

<https://creativecommons.org/licenses/by-nc/4.0/legalcode>.

Copies of published material are allowed for personal or internal use. Sharing published material for non-commercial purposes is subject to the following conditions:

<https://creativecommons.org/licenses/by-nc/4.0/legalcode>,

sect. 3. Reproducing and sharing published material for commercial purposes is not allowed without permission in writing from the publisher.



ABSTRACT

Data on the impact of long term treatment with immunomodulatory drugs (IMiD) on health-related quality of life (HRQoL) is limited. The HOVON-87/NMSG18 study was a randomized, phase 3 study in newly diagnosed transplant ineligible patients with multiple myeloma, comparing melphalan-prednisolone in combination with thalidomide or lenalidomide, followed by maintenance therapy until progression (MPT-T or MPR-R). The EORTC QLQ-C30 and MY20 questionnaires were completed at baseline, after three and nine induction cycles and six and 12 months of maintenance therapy. Linear mixed models and minimal important differences were used for evaluation. 596 patients participated in HRQoL reporting. Patients reported clinically relevant improvement in

global quality of life (QoL), future perspective and role and emotional functioning, and less fatigue and pain in both arms. The latter being of large effect size. In general, improvement occurred after 6-12 months of maintenance only and was independent of the World Health Organisation performance at baseline. Patients treated with MPR-R reported clinically relevant worsening of diarrhea, and patients treated with MPT-T reported a higher incidence of neuropathy. Patients who remained on lenalidomide maintenance therapy for at least three months reported clinically meaningful improvement in global QoL and role functioning at six months, remaining stable thereafter. There were no clinically meaningful deteriorations, but patients on thalidomide reported clinically relevant worsening in neuropathy. In general, HRQoL improves both during induction and maintenance therapy with immunomodulatory drugs. The side effect profile of treatment did not negatively affect global QoL, but it was, however, clinically relevant for the patients. (*Clinicaltrials.gov* identifier: NTR1630).

Introduction

Multiple myeloma (MM) is a malignancy of the plasma cells in the bone marrow. Patients with MM are at high risk of developing bone destructions and fractures, hypercalcaemia, renal failure and anemia.^{1,2} Compared to patients with other hematological malignancies, patients with MM report a higher incidence and severity of symptoms with a reduced health-related quality of life (HRQoL) as a consequence.³⁻⁵ However, there is limited data on the effect of first line treatment on HRQoL in transplant ineligible, newly diagnosed patients with MM (NDMM), especially throughout maintenance treatment.⁶ In several of these trials, the immunomodulatory drugs (IMiDs) thalidomide and/or lenalidomide were investigated.⁷⁻¹³ HRQoL during treatment with thalidomide and lenalidomide were compared head to head in the FIRST and the ECOG E1A06 trials only.^{10,14}

The FIRST trial compared continuous therapy with lenalidomide and dexamethasone (Rd), with Rd for 18 months, and melphalan-prednisone-thalidomide (MPT) for 18 months.¹⁴ Clinically relevant changes were published only for six HRQoL scales.⁹ These were preselected as they were perceived to be clinically relevant. Both Rd and MPT resulted in a statistically significant improvement in all subscales, except side effects of treatment that worsened over time in both arms. There were no differences between arms in global quality of life (QoL), physical functioning, pain and fatigue; although Rd treated patients reported significantly less side effects of treatment and less disease symptoms at three months compared to MPT. A *post hoc* prediction model was developed, suggesting that HRQoL was at least maintained or further improved beyond 18 months. Unfortunately, the effect of Rd continuous *versus* 18 months only on HRQoL cannot be deduced with certainty from this study, as HRQoL data beyond 18 months was lacking.¹³

In contrast to the FIRST trial, in the ECOG E1A06 trial, the Functional Assessment of Cancer Therapy-Neurotoxicity Trial Outcome Index (FACT-Ntx TOI) score was used for HRQoL evaluation, instead of the European Organisation for Research and Treatment of Cancer (EORTC) QLQ-C30. It was shown that melphalan-prednisone-lenalidomide (MPR) followed by lenalidomide maintenance (MPR-R) resulted in a superior HRQoL after 12 months only, compared to MPT followed by thalidomide maintenance (MPT-T).¹⁰ However, the HRQoL effects of lenalidomide and thalidomide maintenance therapies were not investigated separately.

The effect of MPR-R on HRQoL might be deduced from the MM-015 trial, comparing MPR-R, MPR and melphalan-prednisolone (MP).^{11,15} After six months of maintenance, patients who actually received MPR-R therapy reported a statistically significant improvement in HRQoL in 5 of 6 subscales, *versus* in 2 of 6 subscales only in MP and MPR treated patients. However, also from this study, HRQoL data beyond six months of maintenance therapy is lacking.^{6,11}

Recently, the data from the MRC IX study showed that maintenance therapy with thalidomide resulted in an inferior global QoL after three months with a persistent trend for detriment at six and 12 months.¹² This is important as, especially after achieving disease control with induction therapy, long-term continuation of maintenance therapy may turn the pros of maintenance therapy into cons because of side effects that negatively affect HRQoL. The data on lenalidomide maintenance therapy, however, is limited.^{10,11,13,16} Data from a prospective observational cohort study showed no negative impact of lenalidomide maintenance therapy following autologous stem cell transplantation.¹⁶ To the best of our knowledge, prospective analyses after six months of maintenance therapy in non-transplant eligible patients with NDMM are lacking. Only the *post hoc* analysis of the FIRST trial is available.¹³

We here report data on all the collected HRQoL subscales from the open-label, randomized HOVON-87/NMSG18 study, thereby providing HRQoL data, not only during induction, but also during maintenance therapy with lenalidomide and thalidomide therapy.¹⁷ Although currently both IMiD-based regimens are mainly replaced by Rd continuously, either combined with bortezomib during induction or not, the impact of long term lenalidomide on HRQoL is of interest. In addition, we discuss methods to account for the impact of differences in discontinuation rate due to toxicity between the two arms on the outcome of HRQoL analysis.

Methods

Study design

Study details have been published previously.¹⁷ In brief, symptomatic patients with NDMM >65 years of age or transplant ineligible patients ≤65 years were included. Patients were randomized between nine 28-day induction cycles of MPT, followed by thalidomide maintenance (MPT-T) or nine 28-day induction cycles of MPR followed by lenalidomide maintenance

(MPR-R). Maintenance treatment was given until progression, intolerable side effects or other conditions that required treatment discontinuation. The study protocol was approved by the Ethics Committee, and written informed consent was obtained from all participants. The study was registered at www.trialregister.nl as NTR1630.

Health-related quality of life assessments

Participation in the HRQoL reporting was optional. Questionnaires were given to the patients at baseline (T0), after induction cycle 3 (T1) and cycle 9 (T2), and after six (T3) and 12 (T4) months of maintenance therapy.

For HRQoL assessment, two EORTC QoL questionnaires were used; the QLQ-C30 and the Myeloma specific QLQ-MY20.^{18,19} The QLQ-C30 contains five functional scales, nine symptom scales and one global QoL scale.^{20,21} The QLQ-MY20 contains two functional and two symptom scales. For the evaluation of peripheral neuropathy, question 13 of the QLQ-MY20 “*Did you have tingling hands or feet?*” was used. The EORTC manual²¹ was used to calculate all HRQoL scales. A detailed description of the questionnaires and neuropathy scale, data collection and assignment of the questionnaires to T0-T4 is found in the *Online Supplementary Material and Methods*.

Statistical analyses

Change in HRQoL over time was assessed by linear mixed models, both “within arms” and “between arms”, from T0 to T4, as well as from T2 to T4 for patients who had at least three months of maintenance therapy. A *P*-value <0.005 was considered statistically significant as multiple subscales were tested. Model estimates were used for *post hoc* comparisons of changes from baseline.²¹ A change in mean HRQoL score was defined as clinically meaningful if it was above the minimal important difference (MID) threshold using distribution-based MID calculated for both QLQ-C30 and MY20 subscales.²² MID between arms was defined as >5 points difference at a specific time point.²² For QLQ-C30 subscales, an additional anchor-based method by Cocks was used, assessing whether HRQoL changes and differences were of small, medium or large effect.^{23,24} Details are described in the *Online Supplementary Material and Methods*.

To check for effect modification by the World Health Organisation (WHO) performance, sex, age and treatment response, linear mixed models included fixed effects for time, WHO, sex, age, treatment response and their two-way interaction and a random slope for subject.

HRQoL questionnaires were not systematically collected from patients who discontinued treatment, which might introduce a bias when comparing HRQoL. Therefore, we investigated the impact of missing data due to treatment discontinuation on changes in HRQoL over time. We compared HRQoL of i) patients on and off protocol matched by timing, ii) patients who discontinued therapy before or after start of maintenance, and iii) patients who discontinued therapy because of peripheral neuropathy *versus* patients still on protocol until 12 months maintenance therapy. For a detailed description, see the *Online Supplementary Appendix Materials and Methods*.

For statistical analysis, SPSS version 22.0 was used.

Results

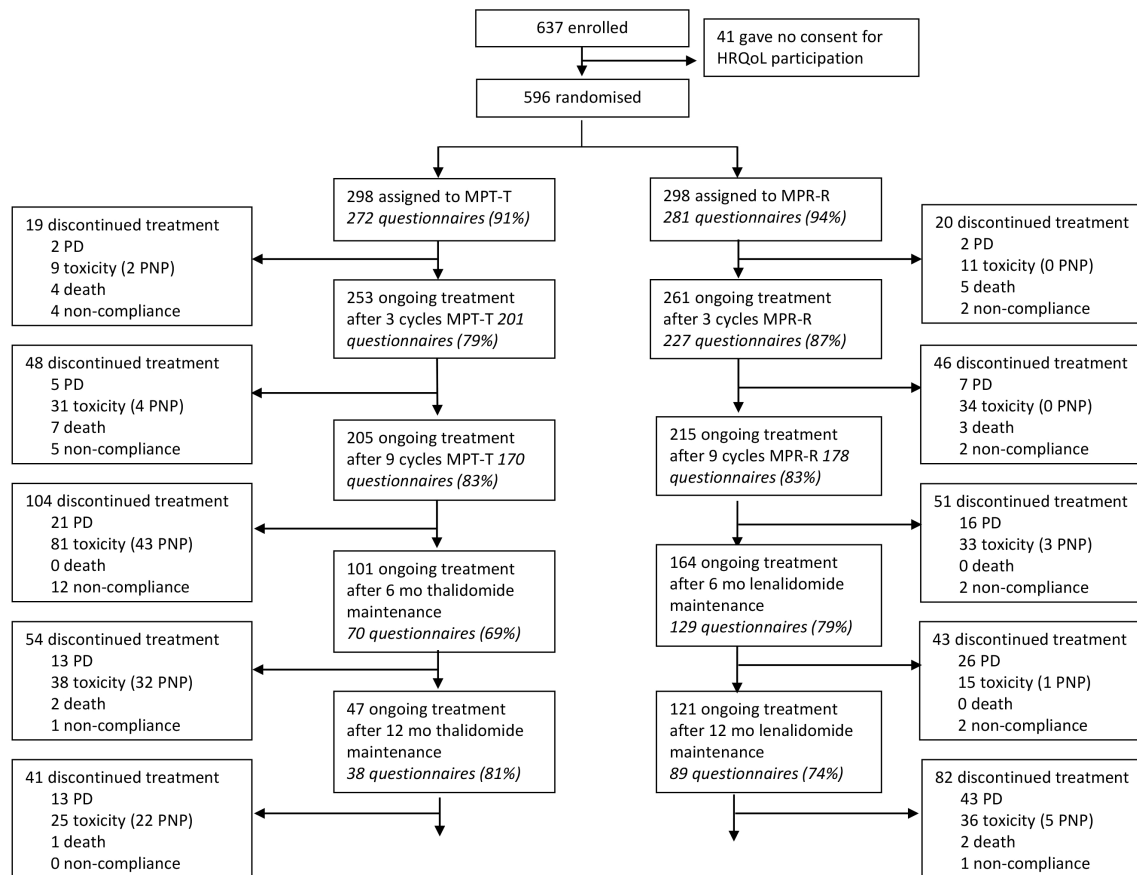
Ninety-four percent (596) of the 637 patients included in the HOVON-87/NSMG18 trial gave informed consent for participation in the HRQoL study. Only patients who filled out a baseline questionnaire were included in the

Table 1. Demographic characteristics of the patients included in the health-related quality of life analysis.

Demographic characteristics	MPT-T (N=272)	MPR-R (N=281)
Median age, years (IQR)	72 (69-77)	73 (69-77)
Age ≥ 76 years, N (%)	90 (33%)	98 (35%)
Sex, N (%)		
Male	133 (49%)	164 (58%)
Female	139 (51%)	117 (42%)
WHO performance, N (%)		
0	89 (33%)	107 (38%)
1	132 (49%)	124 (44%)
2	39 (14%)	40 (14%)
3	5 (2%)	5 (2%)
Unknown	6 (2%)	5 (2%)
M-protein subtype, N (%)		
IgG	177 (65%)	176 (63%)
IgA	73 (27%)	69 (25%)
IgD	4 (2%)	1 (<0.5%)
Light chain only	17 (6%)	34 (12%)
Unknown	0 (0%)	1 (<0.5%)
ISS, N (%)		
I	61 (23%)	78 (28%)
II	134 (49%)	136 (48%)
III	74 (27%)	65 (23%)
Unknown/missing	3 (1%)	2 (1%)
Lytic bone lesions, N (%)		
None	86 (32%)	89 (32%)
1	25 (9%)	19 (7%)
2	15 (6%)	19 (7%)
3 or more	141 (52%)	150 (53%)
Unknown/missing	5 (2%)	4 (1%)
FISH performed, N (%)		
Yes	206 (76%)	220 (78%)
FISH abnormality if performed, N (%)		
17p13 loss	23/188 (12%)	16/196 (8%)
t(4;14)(p16;q32)	18/199 (9%)	17/216 (8%)
t(14;16)(q32;q23)	2/170 (1%)	10/192 (5%)
1q21 gain	56/146 (38%)	58/165 (35%)

MPTT: melphalan-prednisone-thalidomide induction and thalidomide maintenance therapy; MPR-R: melphalan-prednisone-lenalidomide induction and lenalidomide maintenance therapy; n: number of patients; IQR: interquartile range, WHO: World Health Organisation; ISS: International Staging System; FISH: fluorescence *in situ* hybridization.

HRQoL analysis; 272 patients in MPT-T *versus* 281 patients in MPR-R. The patient- and disease characteristics of the HRQoL cohort (Table 1) were comparable to the original study population.¹⁷ The patient flow and drop-out during study are presented in the CONSORT diagram in Figure 1. Fewer patients in the MPT-T arm started maintenance compared to patients in the MPR-R arm, 146 (54%) *versus* 174 (62%). In addition, more patients discontinued MPT-T than MPR-R (first year discontinuation rate; 68% *vs.* 30%; *P*<0.001). The main reason for discontinuation was peripheral neuropathy for thalidomide and hematological toxicity for lenalidomide.¹⁷ A graphic presentation of the number of patients on protocol and the number of completed questionnaires at each scheduled time point, ranging from 69-87%, is presented in the *Online Supplementary Figure S1*. At baseline, no significant differences existed between the treatment arms (*Online Supplementary Table S1*).



HRQoL: health-related quality of life; MPT(-T): melphalan-prednisone-thalidomide (+thalidomide maintenance); MPR(-R): melphalan-prednisone-lenalidomide(+lenalidomide maintenance); PD: progressive disease; PNP: peripheral neuropathy

Figure 1. Consort diagram. Consort diagram of the number of patients participating in the health-related quality of life (HRQoL) study, the number of answered questionnaires and the number of patients off protocol and reason for treatment discontinuation.

Percentage of patients reaching a clinically meaningful change in HRQoL

In both arms, clinically relevant improvement in global QoL was more prominent than deterioration (Figure 2). During MPT induction therapy, improvement occurred in 48% of patients *versus* deterioration in 32%. With MPR induction improvement was reported in 52% of patients *versus* in 28% deterioration. After 1 year of thalidomide maintenance, 54% of patients improved *versus* 32% deteriorated. For lenalidomide maintenance these figures were 61% *versus* 19%, respectively. The results for all other subscales are presented in Figure 2. Clinically relevant deterioration in peripheral neuropathy was significantly more frequently reported in the patients treated with MPT-T than in the patients treated with MPR-R, both after induction (55% *vs.* 27%; $P < 0.001$) and after maintenance (63% *vs.* 31%; $P = 0.003$). A significantly higher percentage of patients treated with MPR reported clinically relevant worsening of diarrhea, compared to MPT, however after induction only (31% *vs.* 9%; $P < 0.001$).

Changes in HRQoL within each treatment arm during induction and maintenance

In both arms, a significant improvement in HRQoL over time was observed for the majority of scales, irrespective

of the received treatment. Global QoL, role and emotional functioning, fatigue, pain, and future perspective improved clinically relevant in both arms. In addition, patients who were treated with thalidomide reported a clinically relevant improvement in social functioning, insomnia and appetite loss, while physical functioning improved in patients who were treated with lenalidomide (see *Online Supplementary Table S2* for significant changes over time; see Figure 3 and *Online Supplementary Figure S2* for clinical meaningful changes within arms). Overall, these HRQoL changes corresponded to medium clinical effects, except for pain reduction, which corresponded to a large clinical effect.²⁴ In both arms, pain reduction was observed, irrespective of the number of bone lesions (0 *vs.* 1-2 *vs.* ≥ 3) (*Online Supplementary Figure S3*). In general, clinically meaningful improvement occurred from T3 and T4 onwards only (*i.e.* after six and 12 months of maintenance therapy). In contrast, global QoL, future perspective and pain improved already during induction therapy and was sustained throughout the whole treatment (Figure 3 and *Online Supplementary Figure S2*). Patients treated with MPT-T reported a statistically significant, but not clinically meaningful increase (small effect according to Cocks²⁴) in constipation and side effects of treatment ($P = 0.003$ and $P < 0.001$ respectively, see Figure 3, *Online Supplementary*

Table S2 and Online Supplementary Figure S2). Patients treated with MPR-R reported a statistically significant and clinically meaningful increase (small effect according to Cocks)²⁴ in diarrhea ($P < 0.001$, see Figure 3 and Online Supplementary Table S2). Peripheral neuropathy worsened in both arms (both $P < 0.001$, see Online Supplementary Table S2), being clinically meaningful in patients treated with thalidomide only (Figure 3).

Clinically relevant differences between arms in HRQoL course during induction and maintenance

During treatment, clinically meaningful differences occurred between arms in 13 of 21 scales (Figure 3 and Online Supplementary Figure S2). Patients treated with MPT-T reported less diarrhea at all follow-up time points (difference between arms was of medium clinical effect, according to Cocks²³), pain at T1, fatigue at T2, and insomnia and appetite loss at T1 and T4. MPR-R treated patients reported better future perspective, physical and role functioning at T4, better cognitive functioning at T1 and T4, and body image at T3, compared to the patients treated with MPT-T. In addition, patients treated with MPT-T reported more side effects of treatment at T3 and T4 and

more constipation and peripheral neuropathy at all follow-up time points. According to the definition of Cocks, all the differences between the arms were of small clinical effect at the largest, except where stated differently (Online Supplementary Table S2).²³

Changes in HRQoL within and between treatment arms during maintenance only

We performed an analysis of a subset of 242 patients who started and continued maintenance treatment for at least three months and of whom a T2 questionnaire was available: 95 of 146 patients who started with thalidomide maintenance therapy (65%) and 147 of 174 patients who started with lenalidomide maintenance therapy (84%). At the start of maintenance, there was already a significant difference in HRQoL in constipation, side effects of treatment and neuropathy (less in MPR treated patients) and diarrhea (less in MPT treated patients) (Online Supplementary Table S1). During maintenance treatment, a statistically significant reduction in appetite loss was reported in both arms (thalidomide $P = 0.003$, lenalidomide $P < 0.001$). In addition, during lenalidomide maintenance, a

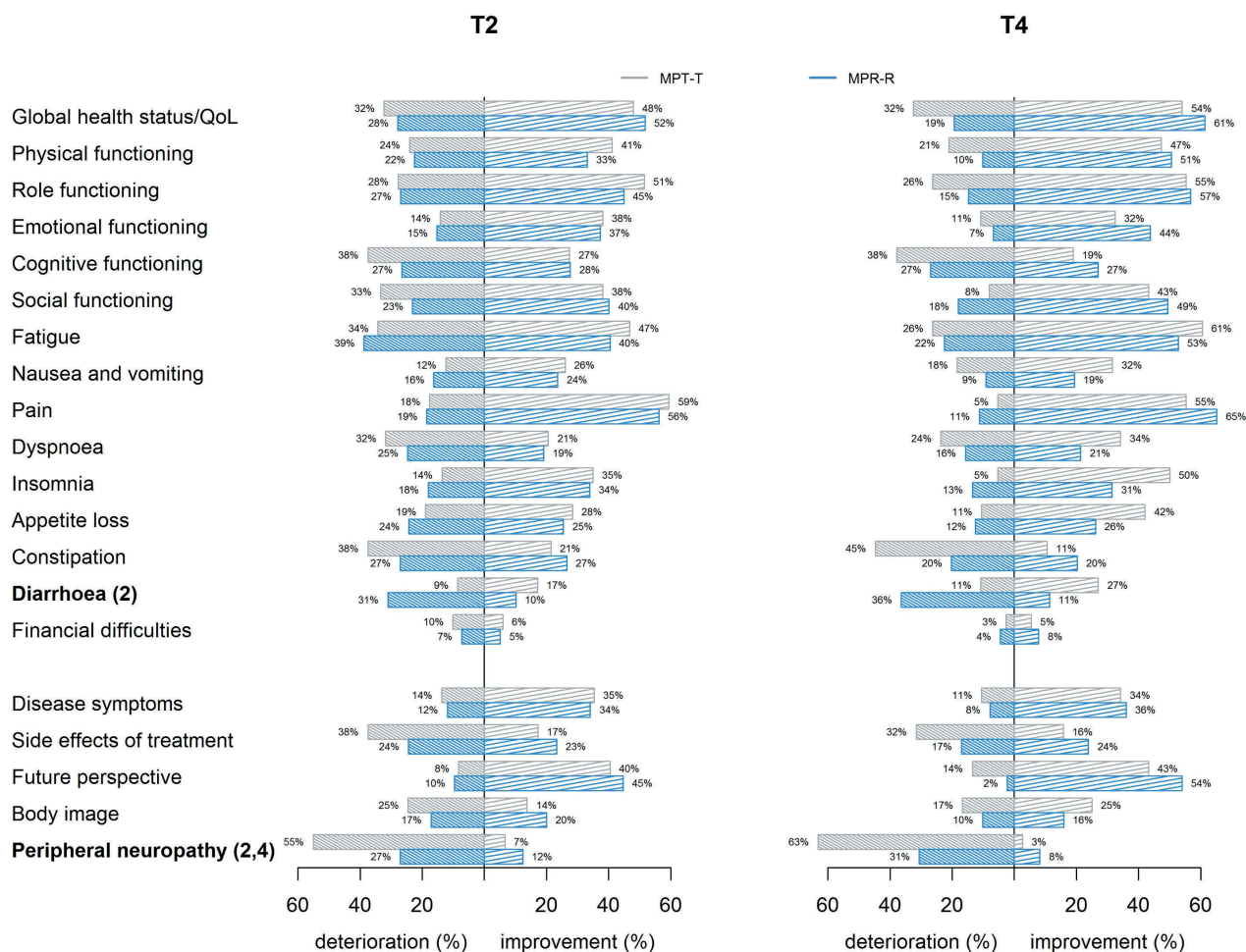


Figure 2. Responders. The percentage of patients reaching a clinically relevant change in health-related quality of life (HRQoL), e.g. reaching the minimal important difference (MID) threshold for within group change during the induction phase (T2) and induction and maintenance phase together (T4). A significant difference between the arms with respect to the percentage of patients improving or deteriorating by more than the MID was observed for diarrhoea and peripheral neuropathy at T2 and for peripheral neuropathy at T4.

significant improvement was observed in global QoL ($P=0.003$, clinically relevant at T3), physical- ($P<0.001$) and role functioning ($P<0.001$, clinically relevant at T4), fatigue ($P<0.001$) and dyspnea ($P=0.004$). In contrast, no significant improvement occurred during thalidomide maintenance. There was even statistically significant worsening of peripheral neuropathy symptoms ($P<0.001$, clinically relevant at both T3 and T4) (*Online Supplementary Table S3 and Online Supplementary Figure S4*). Between arms, there were clinically meaningful differences in physical and role functioning (better with lenalidomide), in appetite loss

(worse with lenalidomide) and in neuropathy (worse with thalidomide) (*Online Supplementary Table S4 and Online Supplementary Figure S4*). All differences in QLQ-C30 scales were of small effect size (of note for neuropathy, no effect sizes are available).²³

Analyses to account for missing data due to different discontinuation rates between arms

Because more patients in the thalidomide arm discontinued treatment compared to the lenalidomide arm¹⁷, HRQoL of patients on protocol in the thalidomide arm

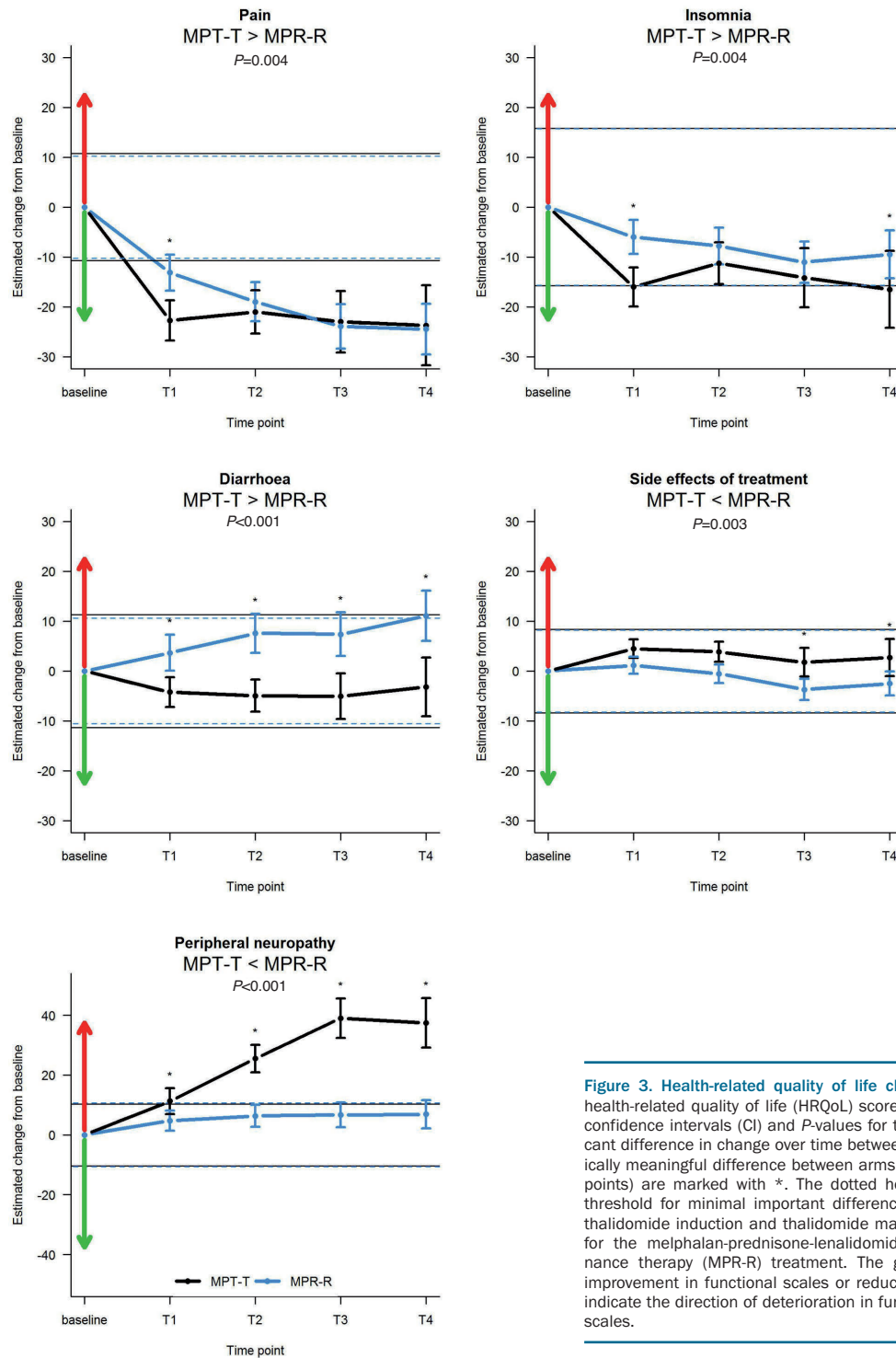


Figure 3. Health-related quality of life change over time. Estimated change in health-related quality of life (HRQoL) score from baseline with corresponding 95% confidence intervals (CI) and P-values for the five scales with a statistically significant difference in change over time between treatment arms. Time points with clinically meaningful difference between arms (minimal important difference [MID] >5 points) are marked with *. The dotted horizontal line represents the calculated threshold for minimal important difference, the black for melphalan-prednisone-thalidomide induction and thalidomide maintenance therapy (MPT-T) and the blue for the melphalan-prednisone-lenalidomide induction and lenalidomide maintenance therapy (MPR-R) treatment. The green arrows indicate the direction of improvement in functional scales or reduction in symptom scales. The red arrows indicate the direction of deterioration in functional scales or worsening of symptom scales.

could have been overestimated and toxicities underestimated. We performed additional analyses to exclude such a potential bias. Although it was not required, a questionnaire was available after treatment discontinuation (“off protocol” questionnaires) from 90 patients (53 MPT-T and 37 MPR-R), of which 84 could be matched with questionnaires from patients on protocol with comparable age, WHO, disease status, treatment arm and period. The global QoL for patients on protocol was comparable to patients off protocol (mean score 59.9 vs. 66.3 points, respectively, $P=0.043$; *Online Supplementary Table S5*). Secondly, in general, the HRQoL course did not differ between patients who discontinued therapy early ($\leq T2$, *e.g.* during induction) and those who discontinued therapy late or never ($>T2$, *e.g.* from start maintenance; *Online Supplementary Table S6* and *Online Supplementary Figure S6*). Lastly, global QoL over time did not differ between patients discontinuing treatment due to investigator-reported peripheral neuropathy and patients continuing treatment until 12 months of maintenance therapy ($P<0.001$; *Online Supplementary Table S7* and *Online Supplementary Figure S6*). These analyses support the absence of bias in our analyses.

Effect modification of HRQoL change by baseline WHO performance, gender, age and treatment response

Baseline WHO performance status appeared to be an effect modifier of HRQoL change during treatment for 7 of 21 scales in MPT-T treated- and in 12 of 21 scales in MPR-R treated patients (Figure 4 for global QoL and *Online Supplementary Table S8* and *Online Supplementary Figure S8* for other subscales). A low performance status (WHO score ≥ 2) was associated with a statistically significant overall lower HRQoL at baseline (*data not shown*), which became comparable to the HRQoL of patients with

baseline WHO performance status 0-1 during treatment (*Online Supplementary Table S8* and *Online Supplementary Figure S7*). Sex, age (≤ 75 years vs. >75 years) and treatment response (\geq partial response vs. stable/progressive disease) did not modify HRQoL course (*data not shown*). The only exception was observed for patients treated with MPT-T ≤ 75 years of age, who experienced more peripheral neuropathy during treatment compared to those >75 years (*Online Supplementary Table S9* and *Online Supplementary Figure S8*).

Patient- versus investigator-reported peripheral neuropathy

Figure 5 shows the patient-reported peripheral neuropathy, as described in the method section, in comparison to the investigator-reported CTCAE score at the given time point. After dichotomizing peripheral neuropathy to “no” or “mild” peripheral neuropathy versus “moderate” or “severe neuropathy”, the kappa between patient-reported and investigator-reported peripheral neuropathy was 0.33 (95% CI: 0.29–0.36). In 213 of 1,599 (13.3%) evaluable questionnaires a discordance was found between neuropathy grades reported by the patients versus investigators. In 76% of the cases, the investigator interpreted the grade of neuropathy lower than experienced by the patient.

Discussion

IMiD-based first line treatment of elderly non-transplant eligible patients with NDMM improves both progression free and overall survival.²⁵⁻²⁸ We here show that patients also perceive clinically relevant HRQoL benefits of induction therapy with thalidomide and lenalidomide

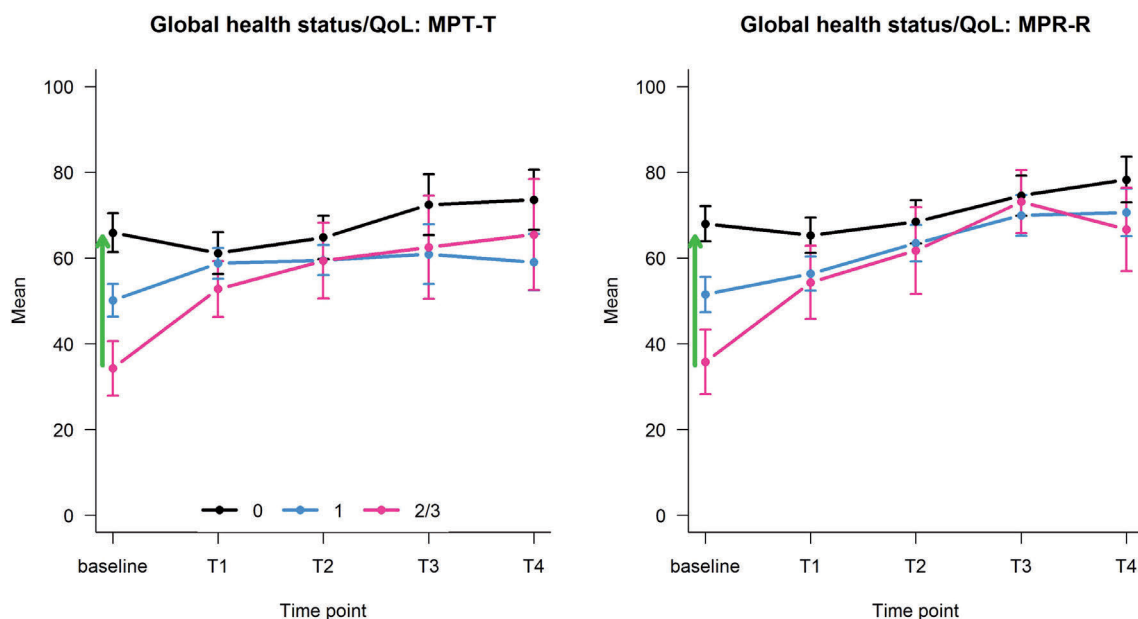


Figure 4. Effect modification of global quality of life by World Health Organisation status. Mean global quality of life (QoL) course over time with corresponding 95% confidence intervals (CI) for each time point for (A) melphalan-prednisone-thalidomide induction and thalidomide maintenance therapy (MPT-T) and (B) patients treated with melphalan-prednisone-lenalidomide induction and lenalidomide maintenance therapy (MPR-R), differentiated by baseline World health organisation (WHO) performance status 0 versus 1 versus 2/3. The black curve represents patients with baseline WHO status 0, the blue curve the patients with WHO status 1 and the pink curve the patients with WHO status 2/3. The green arrows indicate the direction of improvement in functional scales and reduction in symptom scales.

followed by maintenance therapy. Importantly, there was a clinically relevant decrease in pain, defined as large by Cocks *et al.*, in both arms. Clinically meaningful diarrhea developed in approximately 30% of patients during lenalidomide treatment, being of medium clinical effect and significantly higher than in patients treated with thalidomide. Importantly, in patients who reached maintenance, there was no clinically relevant further deterioration of diarrhea during MPR-R therapy. In contrast, clinically meaningful peripheral neuropathy developed in approximately 60% of patients during thalidomide treatment, being significantly higher than in lenalidomide-treated patients, both during induction and maintenance.

In general, the improvement in HRQoL subscales reached clinical relevance after six and 12 months of maintenance therapy only, with the exception of global QoL, future perspective and pain, which improved early during induction therapy and sustained during treatment. A sub-analysis of patients who started maintenance therapy and were treated for at least three months, showed that lenalidomide resulted in a clinically meaningful improvement in global QoL and role functioning over time, without any clinically meaningful deteriorations. In contrast, there was no clinical benefit of thalidomide maintenance treatment, only clinically relevant worsening of peripheral neuropathy occurred.

Importantly, patients with a poor WHO performance status of ≥ 2 at baseline reached similar HRQoL during treatment, compared to patients with a better WHO performance status at baseline, irrespective of the treatment arm. Although this could be explained by regression to the mean, indicating that the most pronounced improvement can be achieved in patients with the worst HRQoL, it is reasonable to suppose that the performance status can be negatively affected by the disease and therefore that treatment also improves HRQoL of the physically most compromised patients. Therefore, treatment should not be automatically withheld from those patients.

Our findings are in line with previous data on HRQoL describing improvement in QoL during treatment.⁶ In addition, we provide data about HRQoL during up to 1 year maintenance therapy with lenalidomide and thalidomide, being rarely reported in the current literature.^{10-13,16} In view of the continuous lenalidomide treatment approaches, our data showing clinically meaningful improvement of global QoL during maintenance therapy is important for clinical practice. In the FIRST trial, no such improvement was reported; the global QoL remained stable, which might have been attributed to the higher dose of lenalidomide and the continuation of dexamethasone, known to be associated with side effects that can hamper QoL.⁹ In the MM-015 trial, a statistically significant, but not clinically relevant deterioration in global QoL after six months of maintenance therapy was observed.¹¹ This cannot be accounted for by a difference in the percentage of patients starting maintenance, the dose of lenalidomide, response rates or different QoL evaluation methods. The fact that thalidomide maintenance has only limited impact on global QoL is in line with the data of the HOVON 49 and the MRC IX data. The latter even show an inferior global QoL at three months with a trend to further deterioration during maintenance treatment.^{8,12}

A limitation of our and HRQoL studies of patients with MM in general, is the fact that firstly, long term data reflect a subset of patients who tolerate remaining in treat-

ment. Secondly, we collected no data after discontinuation of the study although such results would rather reflect the outcome of subsequent therapies.²⁹ Therefore, biases are common, and comparisons between therapies with different toxicities and discontinuation rates are difficult. Especially, as missing data are not missing at random when related to toxicity and cannot be corrected for.³⁰ Such bias might be present in our sub-analyses of patients starting maintenance therapy, showing benefit for patients treated with lenalidomide only. Therefore, this can only be concluded for those patients who did benefit from MPR induction and were able to continue lenalidomide. In addition, the low number of patients continuing thalidomide might be the cause of a lack of finding statistically significant changes in their HRQoL during maintenance.

Interestingly, the higher incidence of peripheral neuropathy with thalidomide, both clinically meaningful to patients and according to CTCAE reported by physicians, did not translate into an inferior global QoL, neither in our study nor the FIRST trial.⁹ Via several analyses, we excluded a bias in global QoL evaluation due to missing HRQoL questionnaires from patients who discontinued treatment because of peripheral neuropathy. The fact that peripheral neuropathy did not negatively affect HRQoL was surprising. The opposite has been reported.³¹ Our observation might be explained by response shift, which is a well-known phenomenon in longitudinal QoL research. It reflects the probability that a patient's standards and values change over time.³² Patients with MM might adapt to their worsening function and increased symptoms and thereby not allow these aspects to affect their global QoL.³³ However, it cannot be excluded that the global QoL scale of the EORTC QLQ-C30 questionnaire has limitations in detecting the negative impact of toxicity on HRQoL. This discussion was addressed in a meta-analysis by Schuurhuizen and colleagues,³⁴ who also reported sim-

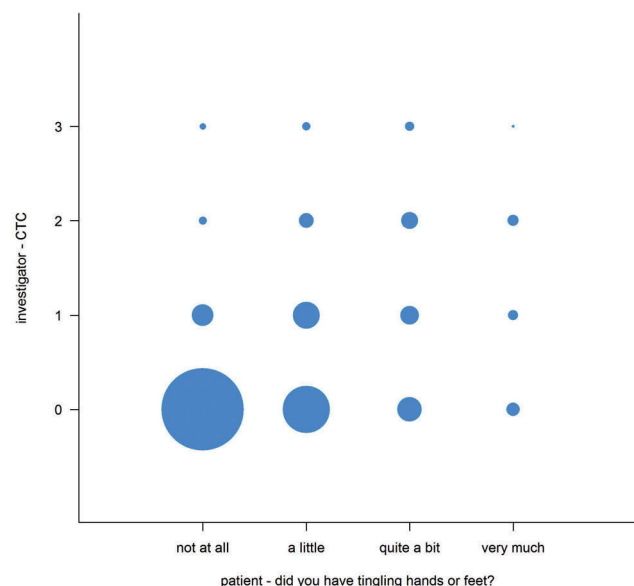


Figure 5. Patient- versus investigator-reported peripheral neuropathy. Patient-reported peripheral neuropathy compared to investigator-reported peripheral neuropathy assessed by National Cancer Institute Common Terminology Criteria for Adverse Events (CTCAE) version 3.0. The surface of the circles reflects the absolute number of patients plus investigators.

ilar global QoL in experimental *versus* control arms in patients with colorectal cancer, despite higher toxicity rates in the former. The authors question whether the global QoL assessment, using the very brief two-item global QoL scale, has sufficient measurement precision to detect a difference in global QoL over time. However, this has been challenged by others stating that QoL is a complex and multidimensional concept, not caused by side effects only.³⁵ Importantly, both those in favor and those against the limitations of the global QoL scale indicate the need for development for more sensitive patient-reported QoL instruments.³⁶ This is also supported by our data on peripheral neuropathy. We defined 'tingling' of hands or feet as peripheral neuropathy. Although this approach is not validated, we found a discrepancy between patient and physician-reported neuropathy in 13% of questionnaires, the majority (76%) being explained by lower reporting by physicians, which has been reported previously, both for neuropathy and other symptoms.³⁷⁻³⁹ The use of the EORTC QLQ-CIPN20 questionnaire might improve concordance between patients and physicians.⁴⁰ The need for flexible and tailored patient reported outcome (PRO) measurements has recently also been advocated by Thanarajasingam and colleagues and these have

been developed by the EORTC.^{36,41} Furthermore, the PRO version of the Common Terminologies Criteria for Adverse Events (PRO-CTCAE) for self-reported toxicities developed by the National Institute of Health is another valuable tool.^{42,43}

In conclusion, we found that the treatment with MPT-T and MPR-R improved HRQoL in elderly patients with NDMM and in general is clinically meaningful to the patients during maintenance therapy only. This supports the current paradigm of continuous treatment, not only improving survival, but also maintaining, and even improving, specific subscales of HRQoL. Although clinically relevant diarrhea developed in patients treated with lenalidomide, this did not negatively affect the global QoL during induction and maintenance. Moreover, currently it is known that bile acid malabsorption plays an important role, which can be treated with bile acid sequestrants.⁴⁴ Clinically significant peripheral neuropathy precluded long term thalidomide treatment in the majority of patients and appeared not to improve HRQoL in those patients who continued therapy.

Funding

Dutch Cancer Society KWF VU-2008 4246, Celgene.

References

- Rajkumar SV, Dimopoulos MA, Palumbo A, et al. International Myeloma Working Group updated criteria for the diagnosis of multiple myeloma. *Lancet Oncol*. 2014;15(12):e538-548.
- Kyle RA, Rajkumar SV. Multiple myeloma. *Blood*. 2008;111(6):2962-2972.
- Jordan K, Proskorovsky I, Lewis P, et al. Effect of general symptom level, specific adverse events, treatment patterns, and patient characteristics on health-related quality of life in patients with multiple myeloma: results of a European, multicenter cohort study. *Support Care Cancer*. 2014; 22(2):417-426.
- Johnsen AT, Tholstrup D, Petersen MA, Pedersen L, Groenvold M. Health related quality of life in a nationally representative sample of haematological patients. *Eur J Haematol*. 2009;83(2):139-148.
- Priscilla D, Hamidin A, Azhar MZ, Noorjan KON, Salmiah MS, Bahariah K. Quality of life among patients with hematological cancer in a Malaysian hospital. *Med J Malaysia*. 2011;66(2):117-120.
- Nielsen LK, Jarden M, Andersen CL, Frederiksen H, Abildgaard N. A systematic review of health-related quality of life in longitudinal studies of myeloma patients. *Eur J Haematol*. 2017;99(1):3-17.
- Waage A, Gimsing P, Fayers P, et al. Melphalan and prednisone plus thalidomide or placebo in elderly patients with multiple myeloma. *Blood*. 2010;116(9):1405-1412.
- Verelst SG, Termorshuizen F, Uyl-de Groot CA, et al. Effect of thalidomide with melphalan and prednisone on health-related quality of life (HRQoL) in elderly patients with newly diagnosed multiple myeloma: a prospective analysis in a randomized trial. *Ann Hematol*. 2011;90(12):1427-1439.
- Delforge M, Minuk L, Eisenmann JC, et al. Health-related quality-of-life in patients with newly diagnosed multiple myeloma in the FIRST trial: lenalidomide plus low-dose dexamethasone versus melphalan, prednisone, thalidomide. *Haematologica*. 2015; 100(6):826-833.
- Stewart AK. Melphalan, prednisone, and thalidomide vs melphalan, prednisone, and lenalidomide (ECOG E1A06) in untreated multiple myeloma. *Blood*. 2015;126(11):1294-1301.
- Dimopoulos MA, Delforge M, Hajek R, et al. Lenalidomide, melphalan, and prednisone, followed by lenalidomide maintenance, improves health-related quality of life in newly diagnosed multiple myeloma patients aged 65 years or older: results of a randomized phase III trial. *Haematologica*. 2013;98(5):784-788.
- Royle KL, Gregory WM, Cairns DA, et al. Quality of life during and following sequential treatment of previously untreated patients with multiple myeloma: findings of the Medical Research Council Myeloma IX randomised study. *Br J Haematol*. 2018;182(6):816-829.
- Vogl DT, Delforge M, Song K, et al. Long-term health-related quality of life in transplant-ineligible patients with newly diagnosed multiple myeloma receiving lenalidomide and dexamethasone. *Leuk Lymphoma*. 2018;59(2):398-405.
- Benboubker L, Dimopoulos MA, Dispenzieri A, et al. Lenalidomide and dexamethasone in transplant-ineligible patients with myeloma. *N Engl J Med*. 2014; 371(10):906-917.
- Dimopoulos MA, Palumbo A, Hajek R, et al. Factors that influence health-related quality of life in newly diagnosed patients with multiple myeloma aged > 65 years treated with melphalan, prednisone and lenalidomide followed by lenalidomide maintenance: Results of a randomized trial. *Leuk Lymphoma*. 2014;55(7):1489-1497.
- Abonour R, Wagner L, Durie BGM, et al. Impact of post-transplantation maintenance therapy on health-related quality of life in patients with multiple myeloma: data from the Connect(R) MM Registry. *Ann Hematol*. 2018;97(12):2425-2436.
- Zweegman S, van der Holt B, Mellqvist UH, et al. Melphalan, prednisone, and lenalidomide versus melphalan, prednisone, and thalidomide in untreated multiple myeloma. *Blood*. 2016;127(9):1109-1116.
- Cocks K, Cohen D, Wisløff F, et al. An international field study of the reliability and validity of a disease-specific questionnaire module (the QLQ-MY20) in assessing the quality of life of patients with multiple myeloma. *Eur J Cancer*. 2007;43(11):1670-1678.
- Aaronson NK, Ahmedzai S, Bergman B, et al. The European Organization for Research and Treatment of Cancer QLQ-C30: a quality-of-life instrument for use in international clinical trials in oncology. *J Natl Cancer Inst*. 1993;85(5):365-376.
- Giesinger JM, Kieffer JM, Fayers PM, et al. Replication and validation of higher order models demonstrated that a summary score for the EORTC QLQ-C30 is robust. *J Clin Epidemiol*. 2016;69:79-88.
- Fayers P, Aaronson NK, Bjordal K, Groenvold M, Curran D, Bottomley A, on behalf of the EORTC Quality of Life Group. The EORTC QLQ-C30 Scoring Manual (3rd Edition). European Organisation for Research and Treatment of Cancer, Brussels 2001.
- King MT. A point of minimal important difference (MID): a critique of terminology and methods. *Expert Rev Pharmacoecon Outcomes Res*. 2011;11(2):171-184.
- Cocks K, King MT, Velikova G, Martyn St-James M, Fayers PM, Brown JM. Evidence-based guidelines for determination of sample size and interpretation of the European Organisation for the Research and Treatment of Cancer Quality of Life

- Questionnaire Core 30. *J Clin Oncol*. 2011;29(1):89-96.
24. Cocks K, King MT, Velikova G, et al. Evidence-based guidelines for interpreting change scores for the European Organisation for the Research and Treatment of Cancer Quality of Life Questionnaire Core 30. *Eur J Cancer*. 2012; 48(11):1713-1721.
 25. Facon T, Mary JY, Hulin C, et al. Melphalan and prednisone plus thalidomide versus melphalan and prednisone alone or reduced-intensity autologous stem cell transplantation in elderly patients with multiple myeloma (IFM 99-06): a randomised trial. *Lancet*. 2007;370(9594):1209-1218.
 26. Hulin C, Facon T, Rodon P, et al. Efficacy of melphalan and prednisone plus thalidomide in patients older than 75 years with newly diagnosed multiple myeloma: IFM 01/01 trial. *J Clin Oncol*. 2009;27(22):3664-3670.
 27. Wijermans P, Schaafsma M, Termorshuizen F, et al. Phase III study of the value of thalidomide added to melphalan plus prednisone in elderly patients with newly diagnosed multiple myeloma: the HOVON 49 Study. *J Clin Oncol*. 2010;28(19):3160-3166.
 28. Palumbo A, Hajek R, Delforge M, et al. Continuous lenalidomide treatment for newly diagnosed multiple myeloma. *N Engl J Med*. 2012;366(19):1759-1769.
 29. Nielsen LK, Abildgaard N, Jarden M, Klausen TW. Methodological aspects of health-related quality of life measurement and analysis in patients with multiple myeloma. *Br J Haematol* 2019;185(1): 11-24.
 30. Sterne JA, White IR, Carlin JB, et al. Multiple imputation for missing data in epidemiological and clinical research: potential and pitfalls. *BMJ*. 2009;338:b2393.
 31. Beijers AJ, Vreugdenhil G, Oerlemans S, et al. Chemotherapy-induced neuropathy in multiple myeloma: influence on quality of life and development of a questionnaire to compose common toxicity criteria grading for use in daily clinical practice. *Support Care Cancer*. 2015;24(6):2411-2420.
 32. Sprangers MA, Schwartz CE. Integrating response shift into health-related quality of life research: a theoretical model. *Soc Sci Med*. 1999;48(11):1507-1515.
 33. Kvam AK, Wisloff F, Fayers PM. Minimal important differences and response shift in health-related quality of life; a longitudinal study in patients with multiple myeloma. *Health Qual Life Outcomes*. 2010;8:79.
 34. Schuurhuizen C, Braamse AMJ, Konings I, et al. Does severe toxicity affect global quality of life in patients with metastatic colorectal cancer during palliative systemic treatment? A systematic review. *Ann Oncol*. 2017;28(3):478-486.
 35. Bottomley A, Pe M, Sloan J, et al. Analysing data from patient-reported outcome and quality of life endpoints for cancer clinical trials: a start in setting international standards. *Lancet Oncol*. 2016;17(11):e510-e514.
 36. Thanarajasingam G, Minasian LM, Baron F, et al. Beyond maximum grade: modernising the assessment and reporting of adverse events in haematological malignancies. *Lancet Haematol*. 2018;5(11):e563-e598.
 37. Di Maio M, Gallo C, Leighl NB, et al. Symptomatic toxicities experienced during anticancer treatment: agreement between patient and physician reporting in three randomized trials. *J Clin Oncol*. 2015;33(8):910-915.
 38. Basch E, Iasonos A, McDonough T, et al. Patient versus clinician symptom reporting using the National Cancer Institute Common Terminology Criteria for Adverse Events: results of a questionnaire-based study. *Lancet Oncol*. 2006;7(11):903-909.
 39. Gravis G, Marino F, Joly F, et al. Patients' self-assessment versus investigators' evaluation in a phase III trial in non-castrate metastatic prostate cancer (GETUG-AFU 15). *Eur J Cancer*. 2014;50(5):953-962.
 40. Le-Rademacher J, Kanwar R, Seisler D, et al. Patient-reported (EORTC QLQ-CIPN20) versus physician-reported (CTCAE) quantification of oxaliplatin- and paclitaxel/carboplatin-induced peripheral neuropathy in NCCTG/Alliance clinical trials. *Support Care Cancer*. 2017;25(11):3537-3544.
 41. Kulis D, Bottomley A, Whittaker C, et al. The use of the Eortc item library to supplement Eortc quality of life instruments. *Value in Health*. 2017;20(9).
 42. Kluetz PG, Chingos DT, Basch EM, Mitchell SA. Patient-Reported Outcomes in Cancer Clinical Trials: Measuring Symptomatic Adverse Events With the National Cancer Institute's Patient-Reported Outcomes Version of the Common Terminology Criteria for Adverse Events (PRO-CTCAE). *Am Soc Clin Oncol Educ Book*. 2016; (36):67-73.
 43. Basch E, Reeve BB, Mitchell SA, et al. Development of the National Cancer Institute's patient-reported outcomes version of the common terminology criteria for adverse events (PRO-CTCAE). *J Natl Cancer Inst*. 2014;106(9).
 44. Pawlyn C, Khan MS, Muls A, et al. Lenalidomide-induced diarrhea in patients with myeloma is caused by bile acid malabsorption that responds to treatment. *Blood*. 2014;124(15):2467-2468.



Ferrata Storti Foundation

Glycoprotein Ib clustering in platelets can be inhibited by α -linolenic acid as revealed by cryo-electron tomography

Simona Stivala,^{1*} Simona Sorrentino,^{2*} Sara Gobbato,¹ Nicole R. Bonetti,^{1,3} Giovanni G. Camici,^{1,4,5} Thomas F. Lüscher,¹ Ohad Medalia^{2,6} and Jürg H. Beer^{1,3}

¹Laboratory for Platelet Research, Center for Molecular Cardiology, University of Zurich, Zurich, Switzerland; ²Department of Biochemistry, University of Zurich, Zurich, Switzerland; ³Internal Medicine, Cantonal Hospital of Baden, Baden, Switzerland; ⁴University Heart Center, University Hospital Zurich, Zurich, Switzerland; ⁵Department of Research and Education, University Hospital Zurich, Zurich, Switzerland and ⁶Department of Life Sciences and the National Institute for Biotechnology in the Negev, Ben-Gurion University, Beer-Sheva, Israel

*SSt and SSo contributed equally as co-first authors

Haematologica 2020
Volume 105(6):1660-1666

ABSTRACT

Platelet adhesion to the sub-endothelial matrix and damaged endothelium occurs through a multi-step process mediated in the initial phase by glycoprotein Ib binding to von Willebrand factor (vWF), which leads to the subsequent formation of a platelet plug. The plant-derived ω -3 fatty acid α -linolenic acid is an abundant alternative to fish-derived n-3 fatty acids and has anti-inflammatory and antithrombotic properties. In this study, we investigated the impact of α -linolenic acid on human platelet binding to vWF under high-shear flow conditions (mimicking blood flow in stenosed arteries). Pre-incubation of fresh human blood from healthy donors with α -linolenic acid at dietary relevant concentrations reduced platelet binding and rolling on vWF-coated microchannels at a shear rate of 100 dyn/cm². Depletion of membrane cholesterol by incubation of platelet-rich plasma with methyl- β cyclodextrin abrogated platelet rolling on vWF. Analysis of glycoprotein Ib by applying cryo-electron tomography to intact platelets revealed local clusters of glycoprotein Ib complexes upon exposure to shear force: the formation of these complexes could be prevented by treatment with α -linolenic acid. This study provides novel findings on the rapid local rearrangement of glycoprotein Ib complexes in response to high-shear flow and highlights the mechanism of *in vitro* inhibition of platelet binding to and rolling on vWF by α -linolenic acid.

Correspondence:

JÜRIG H. BEER
hansjuerg.beer@ksb.ch

Received: March 5, 2019.

Accepted: August 14, 2019.

Pre-published: August 22, 2019.

doi:10.3324/haematol.2019.220988

Check the online version for the most updated information on this article, online supplements, and information on authorship & disclosures: www.haematologica.org/content/105/6/1660

©2020 Ferrata Storti Foundation

Material published in Haematologica is covered by copyright. All rights are reserved to the Ferrata Storti Foundation. Use of published material is allowed under the following terms and conditions:

<https://creativecommons.org/licenses/by-nc/4.0/legalcode>.

Copies of published material are allowed for personal or internal use. Sharing published material for non-commercial purposes is subject to the following conditions:

<https://creativecommons.org/licenses/by-nc/4.0/legalcode>,

sect. 3. Reproducing and sharing published material for commercial purposes is not allowed without permission in writing from the publisher.



Introduction

The first event leading to the formation of a platelet plug is mediated by the glycoprotein Ib-IX complex (GpIb-IX), the second most-abundant platelet receptor after the integrin α IIb β 3.¹⁻³ Platelet binding to von Willebrand factor (vWF) is tightly controlled in order to occur only at sites of bleeding but not in the normal circulation, where it would cause thrombosis. This regulation involves activation of vWF only at high flow rates and binding of GpIb to the A1 domain of vWF through a two-step mechanism, in which a vWF multimer first elongates, then the A1 domain transitions to a high-affinity state.^{4,6} The role of high-shear flow in the pathogenesis of thrombosis is particularly relevant under pathological conditions such as in stenosed, atherosclerotic arteries, where shear stress can increase above 100 dyn/cm² (shear rate >4000/s).^{7,8} Because of its pivotal role in initiating platelet adhesion, GpIb represents a promising antithrombotic target.

Omega-3 fatty acids (n-3 FA) are a class of naturally occurring polyunsaturated fatty acids that include the plant-derived α -linolenic acid (ALA), whose cardioprotective effects have been shown by us and others,⁹⁻¹² which is readily available and marine-derived n-3 FA, whose use is restricted by limited fishery resources and sea pollution.¹³⁻¹⁵ n-3 FA modulate cellular responses through incorporation into plasma

membranes and reduction in the formation of typical protein complexes/lipid rafts, among other effects.¹⁶⁻¹⁸ Based on our previous observations that ALA reduces platelet reactivity,^{10,19} and on studies showing the presence of GpIb in lipid rafts,²⁰⁻²² we hypothesized that ALA might interfere with the distribution of GpIb on the plasma membrane in high-shear flow and, therefore, alter binding to vWF.

Methods

Blood samples

Blood from healthy volunteers was obtained from the Blood Center of the Swiss Red Cross at the Cantonal Hospital Baden with informed consent according to the Declaration of Helsinki. The study was approved by the Institutional Review Board. EDTA or citrated blood was kept at room temperature until assays were performed (within 2 h of drawing). Blood was incubated with vehicle (0.1% ethanol) or ALA 30 μ M for 1 h at room temperature before being used for subsequent experiments. The n-3 FA dose was chosen based on a previous study showing this to be a dietary reachable concentration.²³ Platelet adhesion to vWF was performed on a Bioflux 200 system (Fluxion Bioscience, San Francisco, CA, USA) according to the manufacturer's protocol (see the *Online Supplementary Data* file for details).

Immunofluorescence staining for ground state depletion microscopy

Washed platelets isolated from vehicle or ALA-treated samples were fixed with 4% paraformaldehyde for 15 min, then spun on a 1.5 coverslip in a Cytospin (Thermo Fisher Scientific, Waltham, MA, USA) and stained for ground state depletion (GSD) microscopy. For details, see the *Online Supplementary Data* file.

Flow cytometric analysis of von Willebrand factor binding

Platelet-rich plasma or washed platelets from vehicle- or ALA-treated blood samples were fixed with 4% paraformaldehyde for 15 min, then incubated with 1% bovine serum albumin (BSA) in phosphate-buffered saline (PBS) containing a rabbit anti-human vWF antibody (1:500, Dako A0082) and an anti-GpIb α -APC (BD Bioscience, San Jose, CA, USA) for 1 h. In some experiments, exogenous human vWF (100 μ g/mL, Hematologic Technologies) was added to washed platelets. Samples were washed three times in 1% BSA in PBS and then stained with anti-rabbit 488 (1:250, Jackson ImmunoResearch, West Grove, PA, USA) for 30 min. After three washes in 1% BSA in PBS, samples were resuspended in 300 μ L PBS and analyzed on a LSR Fortessa (BD Bioscience).

Cryo-electron tomography

Resting and sheared platelets in Tyrode buffer were seeded on gold grids coated with a silicon mesh (R 1/4, 200 mesh, Quantifoil, Jena, Germany). Platelets were allowed to adhere for 10 min and then fixed with 4% formaldehyde for 5 min at room temperature, before being processed for cryo-ET. GpIb and integrin α IIb β 3 receptors were detected by immunogold labeling (details are given in the *Online Supplementary Data*). Data were acquired using an FEI Titan Krios. Tomograms were acquired with a magnification of 42,000 \times corresponding to a pixel size of 0.34 nm. The receptor density was analyzed using MATLAB scripts and the receptor distributions were plotted and statistically analyzed by OriginLab software (Northampton, MA, USA).

Statistical analysis

Data are plotted as the mean \pm standard error of mean of at least three independent experiments. They were analyzed by a paired, two-tailed Student *t*-test with GraphPad Prism version 7 (GraphPad Software, La Jolla, CA, USA). *P* values <0.05 were considered statistically significant.

Results

Pre-incubation of blood with the n-3 FA ALA at dietary relevant concentrations²³ reduced the GpIb/vWF interaction under pathological high-shear flow (10,000 s^{-1} , corresponding to the flow rate in an 80% stenosed artery), as measured by the platelet-covered area (106,963 \pm 15,892 μ m² with vehicle vs. 75,519 \pm 16,254 μ m² with ALA) (Figure 1A, B and *Online Supplementary Videos S1 and S2*). Analysis of single fluorescently labeled platelets showed that their speed was doubled when pre-incubated with ALA (Figure 1C), while the distance traveled before stopping was increased (8.89 \pm 4.0 μ m with vehicle vs. 13.36 \pm 7.2 μ m with ALA) (Figure 1D, E).

It has been reported that GpIb resides in cholesterol-rich membrane domains termed lipid rafts,^{20,21,24,25} and that it appears to cluster in conditions of high-shear flow.²² In agreement with these findings, cholesterol depletion with methyl- β -cyclodextrin (M β CD), able to remove 50-90% of membrane cholesterol,²⁶ greatly reduced platelet adhesion to vWF, demonstrating the pivotal role of membrane cholesterol in GpIb-vWF adhesion under high-shear flow (188 \pm 16 μ m²) (Figure 1F).

To exclude that the reduced adhesion of ALA-treated platelets was due to lower levels of membrane GpIb, vehicle- and ALA-treated washed platelets were exposed to high-shear flow in a viscometer (10,000 s^{-1} for 1 min) and analyzed by flow cytometry. Levels of membrane GpIb were not different between vehicle- and ALA-treated platelets (Figure 2A); rather, pre-treatment with the n-3 FA preserved GpIb levels, as shown by higher fluorescence values, suggesting it had an inhibitory effect on GpIb cleavage, as previously shown by our group.¹⁹

Next, we analyzed whether the effect on GpIb-vWF binding was specific for GpIb, vWF, or both. Whole blood was pre-treated with ALA or vehicle for 1 h, followed by isolation of platelet-rich plasma and exposure to high-shear flow (10,000 s^{-1} for 1 min). Flow cytometric analysis of platelet-bound vWF showed that pathological high-shear flow was able to induce GpIb-vWF binding, and that this was not influenced by the presence of ALA (Figure 2B). When the same experiment was performed with washed platelets, we could not detect any platelet-bound vWF, demonstrating the plasmatic origin of the bound vWF (Figure 2C); however, addition of exogenous human vWF to washed platelets was able to restore vWF-platelet binding (Figure 2C). These results show that ALA has no effect on vWF itself, and suggest that its inhibitory effect is exerted through platelet GpIb and is specific for binding to anchored vWF (as typically exposed *in vivo* by endothelial cells after injury).

High resolution imaging of GpIb receptors at the plasma membrane of intact platelets was conducted using cryo-ET²⁷ (Figure 3A-C). Adherent platelets were incubated with anti-GpIb antibodies decorated with 6-nm gold-protein A and imaged with cryo-ET. The coordinates of the gold nanoclusters were identified (Figure 3A-C). While the

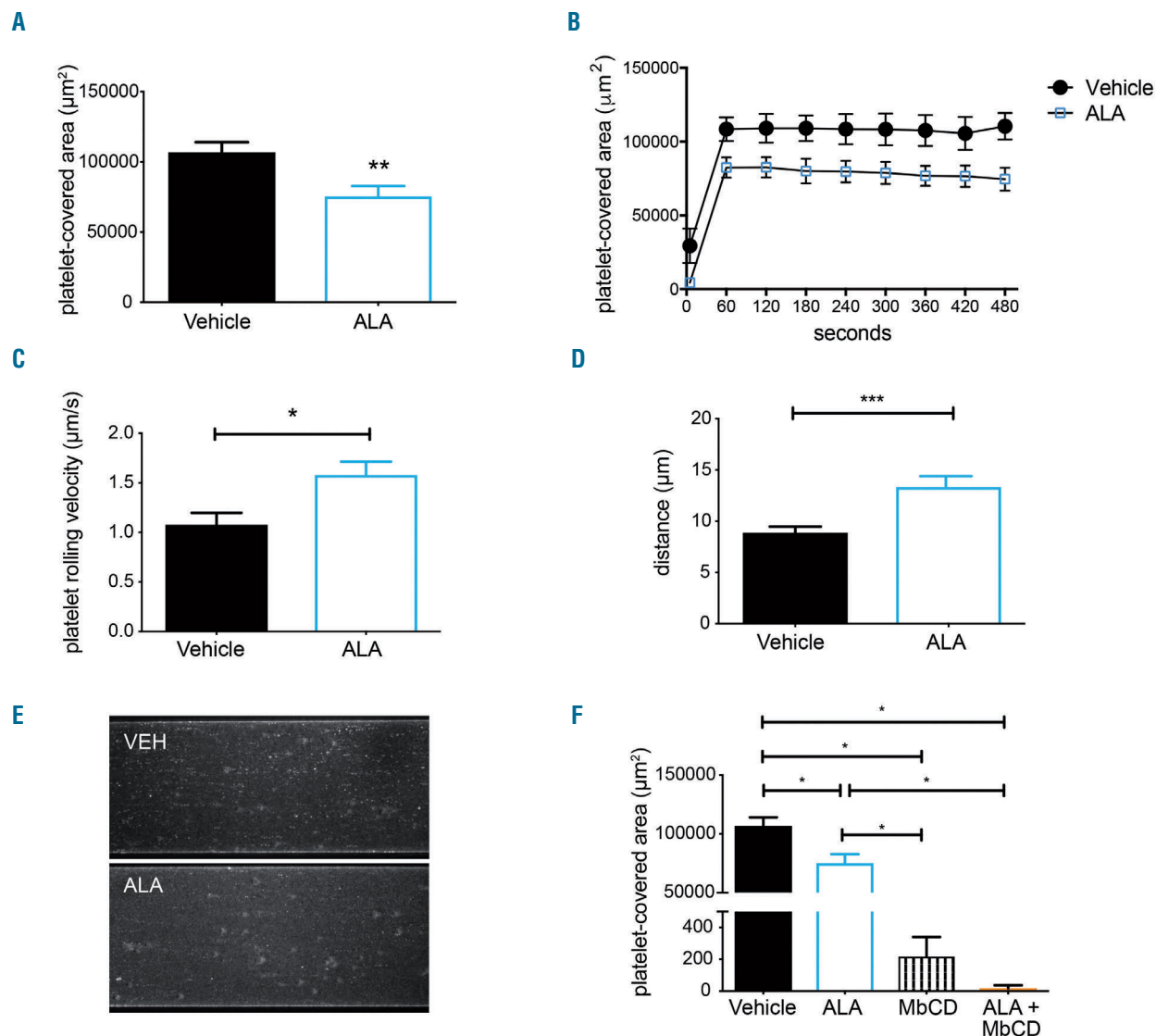


Figure 1. Platelet adhesion to von Willebrand factor is inhibited by α -linolenic acid. Blood collected into EDTA and pre-incubated with vehicle or α -linolenic acid (ALA) for 1 h was perfused on von Willebrand factor (vWF) at high-shear rate and platelet adhesion monitored by fluorescence microscopy. Platelet-covered area measured at the end of the perfusion (A) or every minute during the perfusion (B) was significantly reduced by the ALA treatment ($n=6$, $P=0.0039$). The first time-point in B corresponds to 5 s after the start of the flow. (C) Single platelet rolling velocity measurements showed an increased speed in the ALA-treated samples, and a correspondingly increased distance until firm adhesion (D) ($n=6$, $P=0.04$ for C and $P=0.0009$ for D). (E) Representative projection images of a vehicle (VEH)- or ALA-treated sample showing single platelets rolling over vWF. (F) Membrane cholesterol depletion by pre-incubation of EDTA-blood with methyl- β cyclodextrin MbCD completely abolished platelet adhesion to vWF ($n=6$, $P<0.0001$).

overall number of receptors per platelet did not differ significantly (115 ± 50 per μm^2 for the adherent platelets vs. 130 ± 50 per μm^2 in the case of the shear-activated platelets), the distribution of receptors varied. To quantify these changes, we analyzed the clustering properties of GpIb α by calculating, for each receptor, the number of receptors within a 50 nm radius. Figure 3E-G shows normal distributions of neighborhood receptors, with an average of 2.5 ± 1.8 neighbors for the adherent platelets, 3 ± 2.3 neighbors for the shear-activated platelets and 3 ± 1.8 for ALA-treated platelets. While the global distribution of receptors remained similar, 9% of the receptors (41/453) in the shear-activated platelets had ≥ 12 neighbors (Figure 3F), while in the case of platelets treated with ALA only 3.8% of receptors (14/366) had more than 12 neighbors (Figure 3G). As a control, we analyzed the density and

number of neighbors of the platelet integrin $\alpha\text{IIb}\beta 3$. This analysis showed a much higher density of integrin receptors (450 ± 180 per μm^2) and with many neighbors in comparison to the GpIb receptors (10 ± 5 per μm^2) (Figure 3D, H and *Online Supplementary Figure S3*), which is in agreement with the difference in abundance of the two receptors in platelets.²⁸

Analysis of immunofluorescent-stained GpIb α by GSD super-resolution microscopy also revealed that GpIb is abundantly expressed over the whole platelet membrane with small local points of high density (Figure 4A). To compare the GSD microscopy and cryo-ET findings, we adopted a recently developed strategy.²⁹ We used an assembly of the cryo-ET data into a $5\ \mu\text{m} \times 5\ \mu\text{m}$ collage in which the coordinates of the 6 nm gold-labeled GpIb were drawn as red dots and blurred to 20 nm resolution to

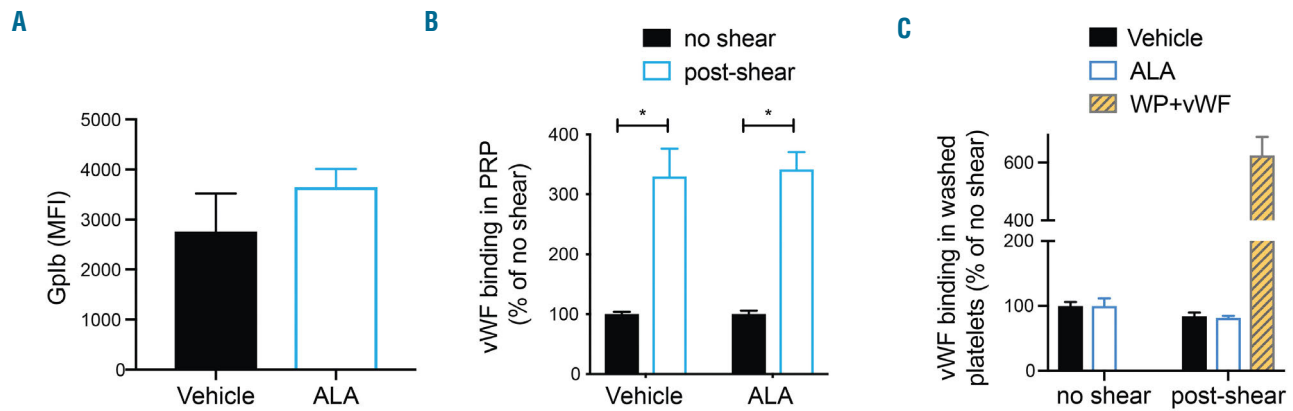


Figure 2. High-shear induces von Willebrand factor binding in platelet-rich plasma but not in washed platelets. (A) Washed platelets were exposed to high-shear flow and analyzed for GpIb abundance by flow cytometry, which did not reveal any difference between vehicle- and α -linolenic acid (ALA)-treated platelets ($n=3$). MFI: mean fluorescence intensity. (B) Platelet-rich plasma was either left untreated or exposed to high-shear flow, and platelet-bound von Willebrand factor (vWF) analyzed by flow cytometry. In both vehicle- and ALA-treated samples, high-shear flow induced vWF binding, as shown by a 3-fold increase compared to that of samples not exposed to the shear force ($n=3$, $P<0.05$). (C) Exposing washed platelets (WP) to high-shear flow did not lead to vWF binding; addition of exogenous human vWF before shear exposure resulted in robust binding ($n=3$).

match the GSD data (Figure 4B). The obtained synthetic model of platelet perimeter showed a distribution and appearance of the receptor in agreement with the fluorescence data, with a high density of GpIb throughout the membrane, but, interestingly, also local, small regions of more densely packed complexes (Figure 4B, arrowhead). Pre-treating blood with ALA did not cause a change in the distribution of membrane GpIb detected by total internal reflection fluorescence (TIRF), likely due to the small size of GpIb clusters, which is in the same range as the resolution of the technique (Figure 5).

Discussion

ALA is a plant-derived n-3 FA readily available in certain plant oils such as flaxseed, soybean and canola oil. Epidemiological studies have shown an inverse correlation between dietary ALA and cardiovascular events,^{11,30,31} although the molecular mechanisms of this protection are not completely known. Our group has investigated the molecular basis of several cardio-protective effects of ALA, showing that at least some of its effects are mediated by its action on endothelial cells, leukocytes and platelets.^{9,10,19} In this study, we have focused in particular on platelet adhesion to vWF under high-shear conditions, which represents the first step mediating platelet activation under arterial flow and is especially important in stenosed (atherosclerotic) arteries, where shear can reach extremely high values ($>5,000 \text{ s}^{-1}$).^{7,32,33}

Here we show for the first time that ALA is able to partially inhibit platelet adhesion to vWF under a shear flow of $10,000 \text{ s}^{-1}$, when whole blood is pre-incubated for 1 h with ALA at dietary relevant concentrations.²³ This is accompanied by an increase in speed and distance traveled by ALA-treated platelets, compared to vehicle-treated platelets (Figure 1), and extends previous results from our group showing a reduced aggregation of citrated platelets over collagen at low shear.¹⁹ The effect observed is specific to anchored vWF, since vWF binding upon exposure of platelet-rich plasma to high-shear flow could not be altered

by ALA pre-treatment (Figure 2). A similar inhibition of platelet adhesion was obtained with the longer, marine-derived n-3 FA eicosapentaenoic acid, while the saturated fatty acid stearic acid had no effect (*Online Supplementary Figure S4*). Although the inhibitory effect of ALA may seem small (25% reduction in platelet adhesion), its biological implications are important, since inhibition at this early step will reduce the number of platelets activated in response to GpIb engagement and subsequent signaling leading to thrombus formation. The additional inhibitory effects of ALA at the level of intracellular signaling and granule secretion will lead, overall, to a greater effect with a relevant biological significance on atherothrombosis.

Since platelet binding to vWF is mediated by the GpIb receptor, we employed state-of-the-art methods (super-resolution microscopy by GSD and cryo-ET) to analyze GpIb distribution on the platelet membrane at high-resolution.

The GpIb distribution analysis by cryo-ET suggests that a significant subpopulation of receptors clustered into a high number of neighbours in the shear activated (and to a lesser extent in the ALA-treated) platelets, indicating that platelet exposure to shear stress induces a local rearrangement of GpIb at the platelet plasma membrane, forming discrete small regions of high receptor density (Figure 3). These regions presumably represent high affinity “binding units” or even binding loci for anchoring multimeric vWF.

Our observations are in line with previous findings³⁴ showing that under high-shear stress platelets form local points of adhesion, termed “discrete adhesion points”, which are the putative regions of interaction between platelets/vWF. Our functional and structural data provide a high-resolution insight into the position of the GpIb receptors and support a model where high-shear stress induces a rapid, local rearrangement of GpIb receptors into small “clusters” of 15-20 complexes. This subpopulation of receptors may represent the previously described high-affinity binding units that interact with vWF and enable platelet rolling under arterial flow. Pre-incubation of platelets with ALA reduces the local clustering of GpIb receptors as shown by the virtual absence of larger complexes (GpIb with ≥ 17 neighbors) (Figure 3C, G). On the

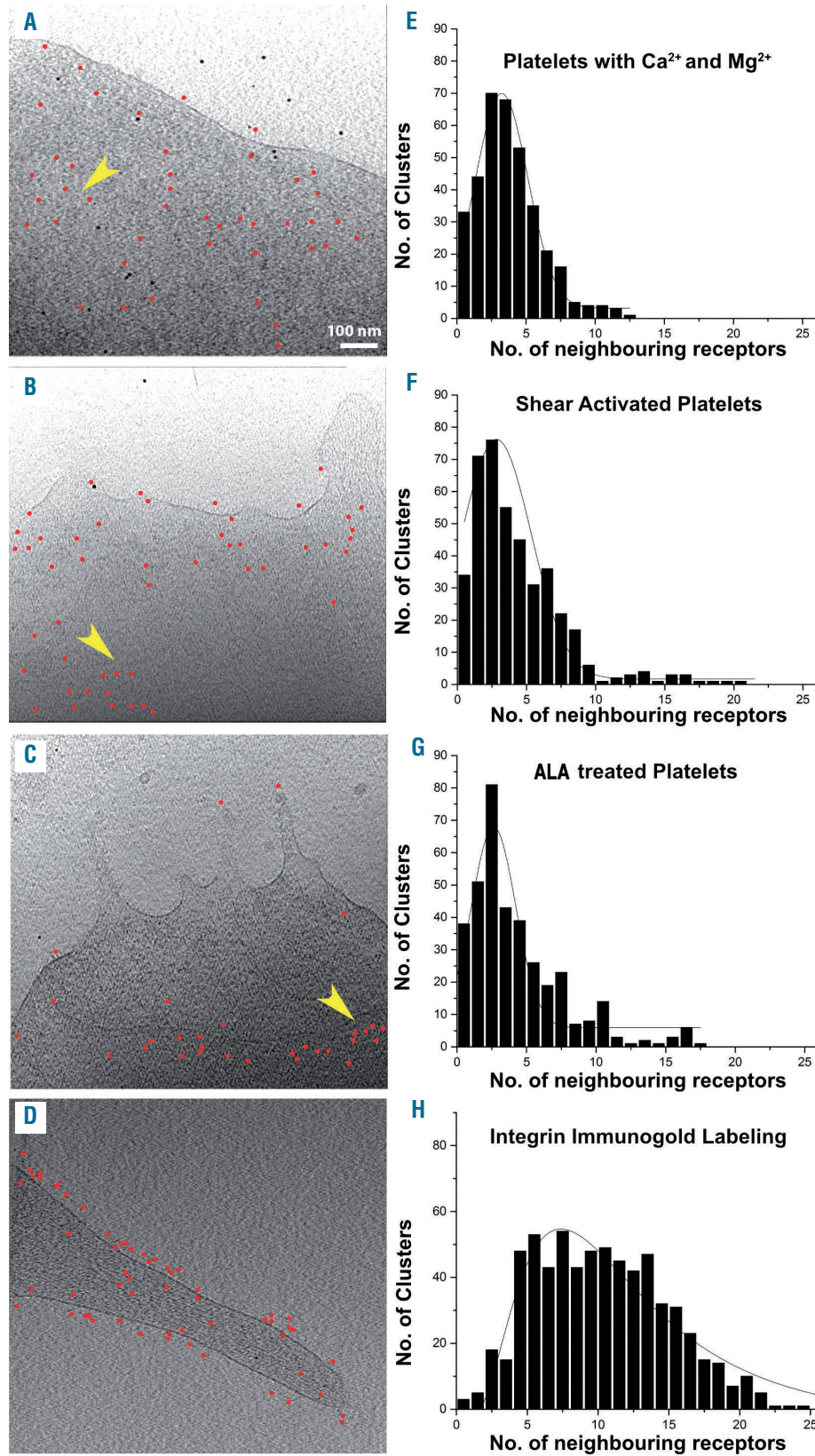


Figure 3. High-shear induces a local rearrangement of GpIb as revealed by cryo-electron tomography. (A-C) Immunogold labeling and (E-G) neighborhood analysis for the control (A, E), shear-activated (B, F) and α -linolenic acid (ALA)-treated shear-activated (C, G) platelets. (A-C): Projection images (~70 nm in thickness) obtained from tomograms of platelets on which GpIb α has been labeled with immunogold. The labeling was detected with protein G conjugated to 6 nm gold. To make the gold identification easier, the gold has been labeled with red circles. The yellow arrows indicate crowded neighborhoods in the pictures. All the projections have the same scale and the scale bar in A is 100 nm. (E-G) Analysis of the immunogold labeling. The three-dimensional coordinates of the 6 nm gold particles from six tomograms for each condition were selected and the distances to the “neighboring receptors” within a radius of 50 nm were calculated. The number of neighbors each receptor has is depicted in the histogram. (D) Integrin α IIb β 3 immunogold labeling was performed on spread platelets and (H) the same neighboring analysis performed.

functional side, this provides an explanation as to why adhesion is significantly inhibited by ALA pre-treatment while platelet rolling speed is increased (Figure 1A, C). Previous work has shown that ω -3 FA (of marine origin) can inhibit protein palmitoylation and, therefore, localization to lipid rafts.³⁵ Although in our experiments the pre-incubation time was too short to achieve an analog effect, long-term, nutritional supplementation with ALA may also inhibit GpIb localization to lipid rafts via reduced

palmitoylation and, consequently, reduce platelet adhesion to vWF even more through this additional mechanism.

Taken together, these data provide insight into the possible mechanism of the anti-thrombotic properties of n-3 FA in the early phase of thrombosis at sites of arterial stenosis or plaque. It may therefore represent the basis for a therapeutic approach that interferes with this process.

In conclusion, our structural data from intact platelets,

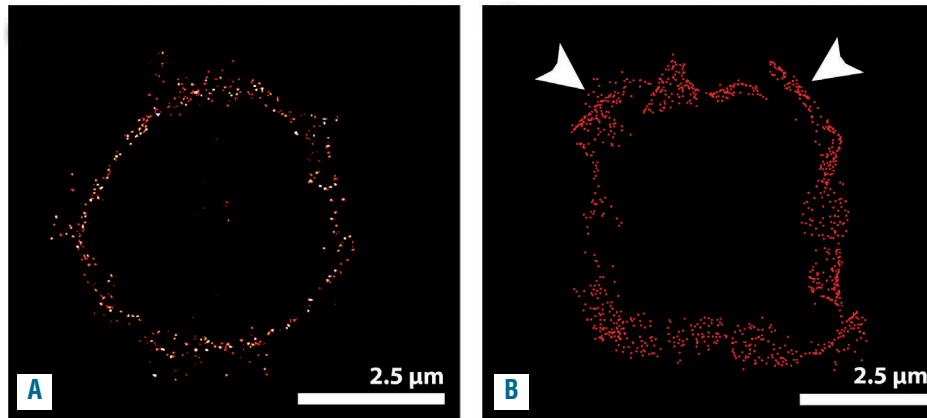


Figure 4. Comparison of GpIb labeling by super-resolution microscopy and cryo-electron tomography reveals a similar receptor distribution. (A) The GpIb receptors in shear-activated platelets were labeled and imaged by ground state depletion (GSD) as described in the Methods. (B) In order to compare the localization of the receptors determined by cryo-electron tomography and GSD microscopy, a synthetic model of platelet perimeter was generated by merging 17 tomograms from the gold-labeled platelets. The gold particle coordinates from the synthetic platelets were filtered to the same resolution as the GSD (20 nm), represented here in red. White arrowheads indicate local clustering areas. Scale bar: 2.5 μ m for both A and B.

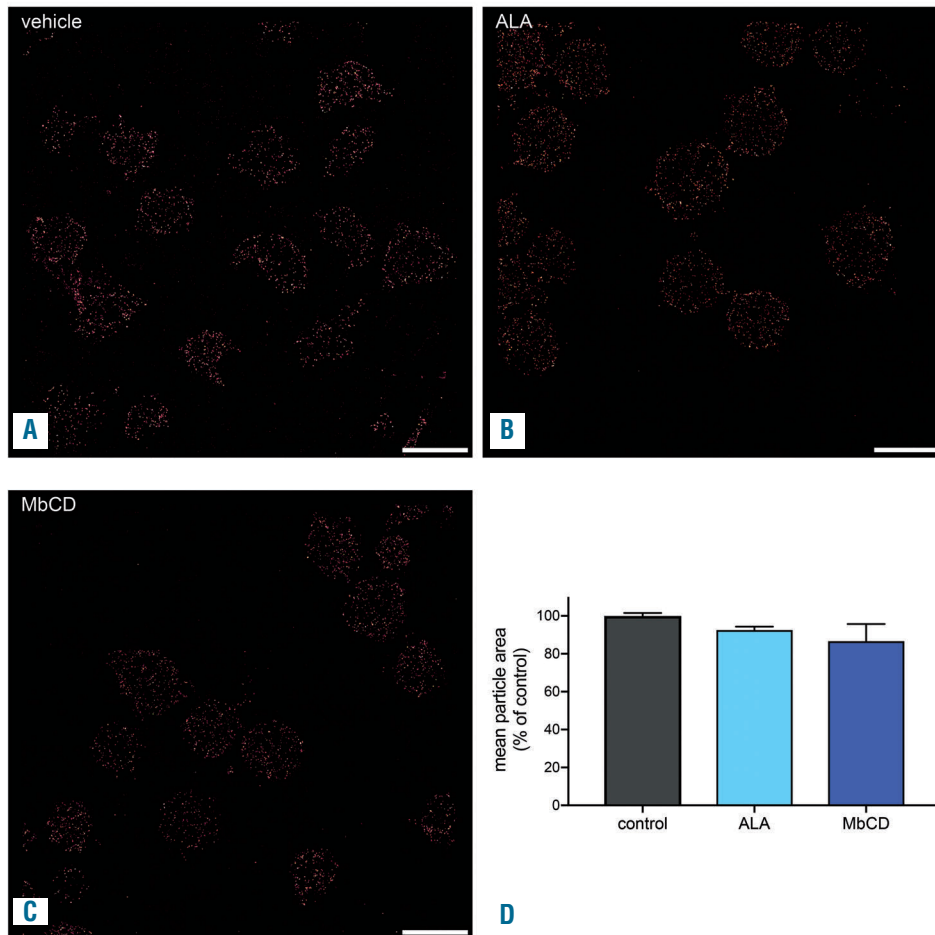


Figure 5. Analysis of GpIb distribution by total internal reflection microscopy. (A-D) Superresolution analysis of GpIb in platelets treated with vehicle (A), α -linolenic acid (ALA) (B) or methyl- β cyclodextrin (MbCD) (C) showed no detectable differences in the distribution of the receptor as measured by particle size (D). Scale bar: 2.5 μ m.

including cryo-ET and super-resolution microscopy, show that upon high-shear conditions platelet GpIb receptors reorganize into “clusters” of 10 to 20 complexes closer to each other than on resting platelets; functionally, we demonstrate that, through intervention with the plant-derived n-3 FA ALA, the size of these clusters is decreased, thereby reducing platelet adhesion to vWF under high-shear flow. This highlights the potential of ALA as an anti-thrombotic agent.

Acknowledgments

This work was supported by a grant from the Swiss National Foundation of Science, the Swiss Heart Foundation, the Kardio Foundation, Switzerland, and the Budai Foundation, Lichtenstein, to JHB (grant n. 310030_144152), and the Mäxi Foundation to OM. We are grateful to Prof. B. Collet, New York, for the generous gift of the *bD1* antibody against human GpIb. We also thank the Center for Microscopy and Image Analysis at the University of Zurich (ZMB). Switzerland.

References

- Canobbio I, Balduini C, Torti M. Signalling through the platelet glycoprotein Ib-V-IX complex. *Cell Signal*. 2004;16(12):1329-1344.
- Bergmeier W, Piffath CL, Goerge T, et al. The role of platelet adhesion receptor GPIbalpha far exceeds that of its main ligand, von Willebrand factor, in arterial thrombosis. *Proc Natl Acad Sci U S A*. 2006;103(45):16900-16905.
- Englund GD, Bodnar RJ, Li Z, Ruggeri ZM, Du X. Regulation of von Willebrand factor binding to the platelet glycoprotein Ib-IX by a membrane skeleton-dependent inside-out signal. *J Biol Chem*. 2001;276(20):16952-16959.
- Yago T, Lou J, Wu T, et al. Platelet glycoprotein Ib forms catch bonds with human WT vWF but not with type 2B von Willebrand disease vWF. *J Clin Invest*. 2008;118(9):3195-3207.
- Fu H, Jiang Y, Yang D, Scheiflinger F, Wong WP, Springer TA. Flow-induced elongation of von Willebrand factor precedes tension-dependent activation. *Nat Commun*. 2017;8(1):324.
- Butera D, Passam F, Ju L, et al. Autoregulation of von Willebrand factor function by a disulfide bond switch. *Sci Adv*. 2018;4(2):eaq1477.
- Sakariassen KS, Orning L, Turitto VT. The impact of blood shear rate on arterial thrombus formation. *Future Sci OA*. 2015;1(4):FSO30.
- Casa LDC, Deaton DH, Ku DN. Role of high shear rate in thrombosis. *J Vasc Surg*. 2015;61(4):1068-1080.
- Winnik S, Lohmann C, Richter EK, et al. Dietary α -linolenic acid diminishes experimental atherogenesis and restricts T cell-driven inflammation. *Eur Heart J*. 2011;32(20):2573-2584.
- Holy EW, Forestier M, Richter EK, et al. Dietary α -linolenic acid inhibits arterial thrombus formation, tissue factor expression, and platelet activation. *Arterioscler Thromb Vasc Biol*. 2011;31(8):1772-1780.
- Campos H, Baylin A, Willett WC. Alpha-linolenic acid and risk of nonfatal acute myocardial infarction. *Circulation*. 2008;118(4):339-345.
- Sala-Vila A, Guasch-Ferré M, Hu FB, et al. Dietary α -linolenic acid, marine ω -3 fatty acids, and mortality in a population with high fish consumption: findings from the PREvención con DIeta MEDiterránea (PREDIMED) study. *J Am Heart Assoc*. 2016;5(1):1-12.
- Guallar E, Sanz-Gallardo MI, van't Veer P, et al. Mercury, fish oils, and the risk of myocardial infarction. *N Engl J Med*. 2002;347(22):1747-1754.
- Mozaffarian D, Rimm EB. Fish intake, contaminants, and human health: evaluating the risks and the benefits. *JAMA*. 2006;296(15):1885-1899.
- Morris MC, Brockman J, Schneider JA, et al. Association of seafood consumption, brain mercury level, and APOE4 status with brain neuropathology in older adults. *JAMA*. 2016;60612(5):489-497.
- Shaikh SR, Jolly CA, Chapkin RS. n-3 Polyunsaturated fatty acids exert immunomodulatory effects on lymphocytes by targeting plasma membrane molecular organization. *Mol Aspects Med*. 2012;33(1):46-54.
- Shaikh SR, Rockett BD, Salameh M, Carraway K. Docosahexaenoic acid modifies the clustering and size of lipid rafts and the lateral organization and surface expression of MHC class I of EL4 cells. *J Nutr*. 2009;139(9):1632-1639.
- Chen W, Jump DB, Esselman WJ, Busik J V. Inhibition of cytokine signaling in human retinal endothelial cells through modification of caveolae/lipid rafts by docosahexaenoic acid. *Invest Ophthalmol Vis Sci*. 2007;48(1):18-26.
- Stivala S, Reiner MF, Lohmann C, Lüscher TF, Matter CM, Beer JH. Dietary α -linolenic acid increases the platelet count in ApoE^{-/-} mice by reducing clearance. *Blood*. 2013;122(6):1026-1033.
- Shrimpton CN, Borthakur G, Larrucea S, Cruz MA, Dong J-F, Lopez JA. Localization of the adhesion receptor glycoprotein Ib-IX-V complex to lipid rafts is required for platelet adhesion and activation. *J Exp Med*. 2002;196(8):1057-1066.
- Munday AD, Gaus K, López JA. The platelet glycoprotein Ib-IX-V complex anchors lipid rafts to the membrane skeleton: implications for activation-dependent cytoskeletal translocation of signaling molecules. *J Thromb Haemost*. 2010;8(1):163-172.
- Gitz E, Koopman CD, Giannas A, et al. Platelet interaction with von Willebrand factor is enhanced by shear-induced clustering of glycoprotein Iba. *Haematologica*. 2013;98(11):1810-1818.
- Harper CR, Edwards MJ, DeFilipis AP, Jacobson TA. Flaxseed oil increases the plasma concentrations of cardioprotective (n-3) fatty acids in humans. *J Nutr*. 2006;136(1):83-87.
- Canobbio I, Trionfani P, Guidetti GF, Balduini C, Torti M. Targeting of the small GTPase Rap2b, but not Rap1b, to lipid rafts is promoted by palmitoylation at Cys176 and Cys177 and is required for efficient protein activation in human platelets. *Cell Signal*. 2008;20(9):1662-1670.
- Bodin S, Tronchère H, Payrastre B. Lipid rafts are critical membrane domains in blood platelet activation processes. *Biochim Biophys Acta*. 2003;1610(2):247-257.
- Gousset K, Wolkers WF, Tsvetkova NM, et al. Evidence for a physiological role for membrane rafts in human platelets. *J Cell Physiol*. 2002;190(1):117-128.
- Sorrentino S, Studt JD, Horev MB, Medalia O, Sapra KT. Toward correlating structure and mechanics of platelets. *Cell Adhes Migr*. 2016;10(5):568-575.
- Lewandrowski U, Wortelkamp S, Lohrig K, et al. Platelet membrane proteomics: a novel repository for functional research. *Blood*. 2009;114(1):e10-e19.
- Turgay Y, Eibauer M, Goldman AE, et al. The molecular architecture of lamins in somatic cells. *Nature*. 2017;543(7644):261-264.
- Albert CM, Oh K, Whang W, et al. Dietary alpha-linolenic acid intake and risk of sudden cardiac death and coronary heart disease. *Circulation*. 2005;112(21):3232-3238.
- Djoussé L, Arnett DK, Carr JJ, et al. Dietary linolenic acid is inversely associated with calcified atherosclerotic plaque in the coronary arteries: the National Heart, Lung, and Blood Institute Family Heart Study. *Circulation*. 2005;111(22):2921-2926.
- Bark DL, Ku DN. Wall shear over high degree stenoses pertinent to atherothrombosis. *J Biomech*. 2010;43(15):2970-2977.
- Strony J, Beaudoin A, Brands D, Adelman B. Analysis of shear stress and hemodynamic factors in a model of coronary artery stenosis and thrombosis. *Am J Physiol*. 1993;265(5 Pt 2):H1787-1796.
- Reininger AJ, Heijnen HFG, Schumann H, Specht HM, Schramm W, Ruggeri ZM. Mechanism of platelet adhesion to von Willebrand factor and microparticle formation under high shear stress. *Blood*. 2006;107(9):3537-3545.
- Webb Y, Hermida-Matsumoto L, Resh MD. Inhibition of protein palmitoylation, raft localization, and T cell signaling by 2-bromopalmitate and polyunsaturated fatty acids. *J Biol Chem*. 2000;275(1):261-270.

Coactosin-like 1 integrates signaling critical for shear-dependent thrombus formation in mouse platelets

Inga Scheller,^{1,2} Simon Stritt,^{1,2,*} Sarah Beck,^{1,2} Bing Peng,³ Irina Pleines,^{1,2} Katrin G. Heinze,² Attila Braun,^{1,2} Oliver Otto,⁴ Robert Ahrends,³ Albert Sickmann,³ Markus Bender,^{1,2} and Bernhard Nieswandt^{1,2}

¹Institute of Experimental Biomedicine I, University Hospital, University of Würzburg, Würzburg; ²Rudolf Virchow Center, University of Würzburg, Würzburg; ³Leibniz-Institut für Analytische Wissenschaften - ISAS - e.V., Lipidomics, Dortmund and ⁴Center for Innovation Competence - Humoral Immune Reactions in Cardiovascular Diseases, Biomechanics, University of Greifswald, Greifswald, Germany.

*Current affiliation: Department of Immunology, Genetics and Pathology, Uppsala University, Uppsala, Sweden.



Haematologica 2020
Volume 105(6):1667-1676

ABSTRACT

Platelet aggregate formation is a multistep process involving receptor-mediated, as well as biomechanical, signaling cascades, which are highly dependent on actin dynamics. We have previously shown that actin depolymerizing factor (ADF)/n-cofilin and Twinfilin 2a, members of the ADF homology (ADF-H) protein family, have distinct roles in platelet formation and function. Coactosin-like 1 (Cotl1) is another ADF-H protein that binds actin and was also shown to enhance biosynthesis of pro-inflammatory leukotrienes (LT) in granulocytes. Here, we generated mice lacking Cotl1 in the megakaryocyte lineage (*Cotl1*^{-/-}) to investigate its role in platelet production and function. Absence of Cotl1 had no impact on platelet counts, platelet activation or cytoskeletal reorganization under static conditions *in vitro*. In contrast, Cotl1 deficiency markedly affected platelet aggregate formation on collagen and adhesion to immobilized von Willebrand factor at high shear rates *in vitro*, pointing to an impaired function of the platelet mechanoreceptor glycoprotein (GP) Ib. Furthermore, *Cotl1*^{-/-} platelets exhibited increased deformability at high shear rates, indicating that the GPIb defect may be linked to altered biomechanical properties of the deficient cells. In addition, we found that Cotl1 deficiency markedly affected platelet LT biosynthesis. Strikingly, exogenous LT addition restored defective aggregate formation of *Cotl1*^{-/-} platelets at high shear *in vitro*, indicating a critical role of platelet-derived LT in thrombus formation. *In vivo*, Cotl1 deficiency translated into prolonged tail bleeding times and protection from occlusive arterial thrombus formation. Together, our results show that Cotl1 in platelets is an integrator of biomechanical and LT signaling in hemostasis and thrombosis.

Introduction

Platelets are small anucleate cells that are essential for hemostasis and maintenance of vascular integrity, but are also implicated in thrombosis resulting in ischemia and infarction under pathological conditions.¹ The classic, simplified model of platelet-dependent arterial thrombus formation comprises sequential steps, involving platelet deceleration on the injured vessel wall *via* interaction of the platelet mechanoreceptor glycoprotein (GP) Ib with von Willebrand factor (vWF) immobilized on the injured vessel wall. This is followed by cellular activation *via* the collagen receptor GPVI and G protein-coupled receptors (GPCR) stimulated by soluble agonists such as ADP, thromboxane A₂ (TxA₂) or thrombin. The final common pathway of these activatory events is the functional upregulation of integrins, which mediate firm platelet adhesion and aggregation.

Correspondence:

BERNHARD NIESWANDT
bernhard.nieswandt@virchow.uni-wuerzburg.de

Received: April 29, 2019.

Accepted: September 26, 2019.

Pre-published: October 3, 2019.

doi:10.3324/haematol.2019.225516

Check the online version for the most updated information on this article, online supplements, and information on authorship & disclosures: www.haematologica.org/content/105/6/1667

©2020 Ferrata Storti Foundation

Material published in *Haematologica* is covered by copyright. All rights are reserved to the Ferrata Storti Foundation. Use of published material is allowed under the following terms and conditions:

<https://creativecommons.org/licenses/by-nc/4.0/legalcode>.

Copies of published material are allowed for personal or internal use. Sharing published material for non-commercial purposes is subject to the following conditions:

<https://creativecommons.org/licenses/by-nc/4.0/legalcode>, sect. 3. Reproducing and sharing published material for commercial purposes is not allowed without permission in writing from the publisher.



Critical determinants of thrombus formation are the locally prevailing rheological conditions. With increasing shear rate, e.g. during the development of stenosis, platelet adhesion and aggregate formation become increasingly dependent on GPIb-vWF interactions. At sites of very high, pathological shear rates and disturbed flow, occlusive arterial thrombus formation can be mediated predominantly by the GPIb-vWF interaction, does not involve visible platelet shape change or activation, and may thus be mediated, at least in part, by the biomechanical interaction of platelets.² In accordance with this, it was shown that vWF-mediated pulling at the GPIb α receptor under shear induces the unfolding of a juxtamembrane mechanosensitive domain, which might contribute to platelet mechanosensing under dynamic conditions and GPIb-induced intracellular signaling.³ Thus, it appears that platelet-mediated thrombus formation *in vivo* involves both agonist receptor and biomechanical signaling, the interplay of which is still poorly understood.

Platelets are produced by megakaryocytes (MK) in the bone marrow (BM) through a cytoskeleton-driven process. The critical role of the actin cytoskeleton for platelet production and function is illustrated by the association of mutations in genes encoding proteins that are involved in actin cytoskeletal organization, such as Diaphanous Related Formin 1 (*DIAPH1*),⁴ filamin A (*FLNA*),⁵ Wiskott Aldrich syndrom protein (*WASP*),⁶ actinin 1 (*ACTN1*),⁷ or tropomyosin 4 (*TPM4*)⁸ with platelet disorders in humans and mice. In circulating platelets, the actin cytoskeleton is essential to maintain cell morphology and to exert key functions upon activation, such as granule release, as well as the formation of filopodia and lamellipodia.⁹ However, the complex protein network orchestrating actin dynamics in platelets is not fully understood.

The ADF homology domain (ADF-H) is one of the best-characterized actin binding motifs. The ADF-H protein family comprises twinfilin (Twf), ADF/n-cofilin, Abp1/drebrin, and coactosin-like 1 (Cot1/CLP). We have previously shown that Twf2a and ADF/n-cofilin play distinct, critical roles in platelet formation and function.^{10,11} Although sharing less than 20% sequence identity with the other ADF-H family members, Cot1 is structurally highly homologous, suggesting a similar role for cytoskeletal dynamics.¹² Indeed, Cot1 binds F-actin, but does not interact with actin monomers.¹³ Furthermore, Cot1 was shown to prevent n-cofilin-mediated depolymerization of actin filaments, thereby promoting lamellipodia formation at the immune synapse.¹⁴ Besides its interaction with F-actin, Cot1 is implicated in the biosynthesis of leukotrienes (LT),¹⁵ lipid-derived pro-inflammatory mediators involved in a variety of inflammatory processes such as allergy or asthma. Cot1 was shown to interact with 5-lipoxygenase (5-LO), a key enzyme in LT biosynthesis that catalyzes two of the initial steps, namely the oxygenation of arachidonic acid (AA) to 5-HPETE and the subsequent dehydration into the epoxide LTA4.¹⁵⁻¹⁷ Platelet-stored LT have been shown to contribute to inflammatory responses, e.g. during lung inflammation.¹⁸ However, the mechanism underlying this contribution, as well as the precise role of LT for platelet function, have not been defined.

Here, we generated conditional knockout mice lacking Cot1 in the MK lineage. We found that Cot1 is critically required for stable platelet thrombus formation under con-

ditions of shear flow *in vitro* and *in vivo* by modulating the function of the mechanoreceptor GPIb, as well as platelet LT biosynthesis.

Methods

Animals

Cot1^{-/-} mice were generated by injection of embryonic stem cell clone *Cot1*^{tm1a(EUCOMM)Hmgui} into C57Bl/6 blastocysts. Germline transmission was confirmed by backcrossing of the chimeric mice with C57Bl/6 mice. *Cot1*^{+/-} mice were intercrossed with mice carrying Flp recombinase to generate *Cot1*^{fl/fl} mice, which were intercrossed with mice carrying Cre recombinase under control of the platelet factor 4 (P4) promoter to generate mice lacking Cot1 specifically in MK and platelets.¹⁹ For all experiments, 12- to 16-week old *Cot1*^{fl/fl;P4Cre} and *Cot1*^{fl/fl} littermate controls, maintained on a C57Bl/6 background, were used. All mice were derived from the following breeding strategy: *Cot1*^{fl/fl;P4Cre} X *Cot1*^{fl/fl}.

Animal studies

Animal studies were approved by the district government of Lower Franconia (AZ15_14; Bezirksregierung Unterfranken).

Further details of reagents and experimental procedures are given in the *Online Supplementary Appendix*.

Results

Cot1 deficiency does not affect platelet function under static conditions

Cot1^{fl/fl;P4Cre} mice (hereon referred to as *Cot1*^{-/-}) were viable and born in the expected Mendelian ratios. The absence of Cot1 in platelets was confirmed by western blotting (*Online Supplementary Figure S1A*). Cot1 deficiency did not affect either peripheral platelet count, size or ultrastructure (Figure 1A-C) nor the expression of prominent platelet surface receptors (*Online Supplementary Table S1*). This is in contrast to deficiency in the ADF-H protein family members Twf2a¹¹ or n-cofilin,¹⁰ which results in thrombocytopenia in mice. Thus, *Cot1*^{-/-} mice represent the first knockout mouse model of an ADF-H family member with apparently normal platelet biogenesis.

A common feature of ADF-H family members is their involvement in cytoskeletal dynamics. Consistently, n-cofilin deficiency resulted in impaired stimulus-dependent F-actin assembly, whereas Twf2a-deficient mice displayed increased actin dynamics.^{10,11} According to previous studies, n-cofilin and Cot1 are highly abundant in both human and mouse platelets,^{20,21} while Twf2 levels are slightly lower. The results for Twf1 and drebrin, which was not listed in the mouse dataset, suggest that they are expressed at a lower level. Importantly, both datasets indicate that the expression of ADF-H proteins is similar in human and mouse platelets.

We determined expression levels of the ADF-H members Twf1/2a and n-cofilin by western blotting, but could not detect differences in total expression levels of either protein between WT and *Cot1*^{-/-} platelets (Figure 1D and E). Strikingly, we observed a strong (2-fold) increase in expression of the (inactive) phosphorylated form of n-cofilin (Ser3) in *Cot1*^{-/-} platelets (***P*<0.001) (Figure 1E and F). Next, we analyzed the localization of Cot1 in resting and spread platelets (*Online Supplementary Figure S1B and C*). In line with previous observations,²² we

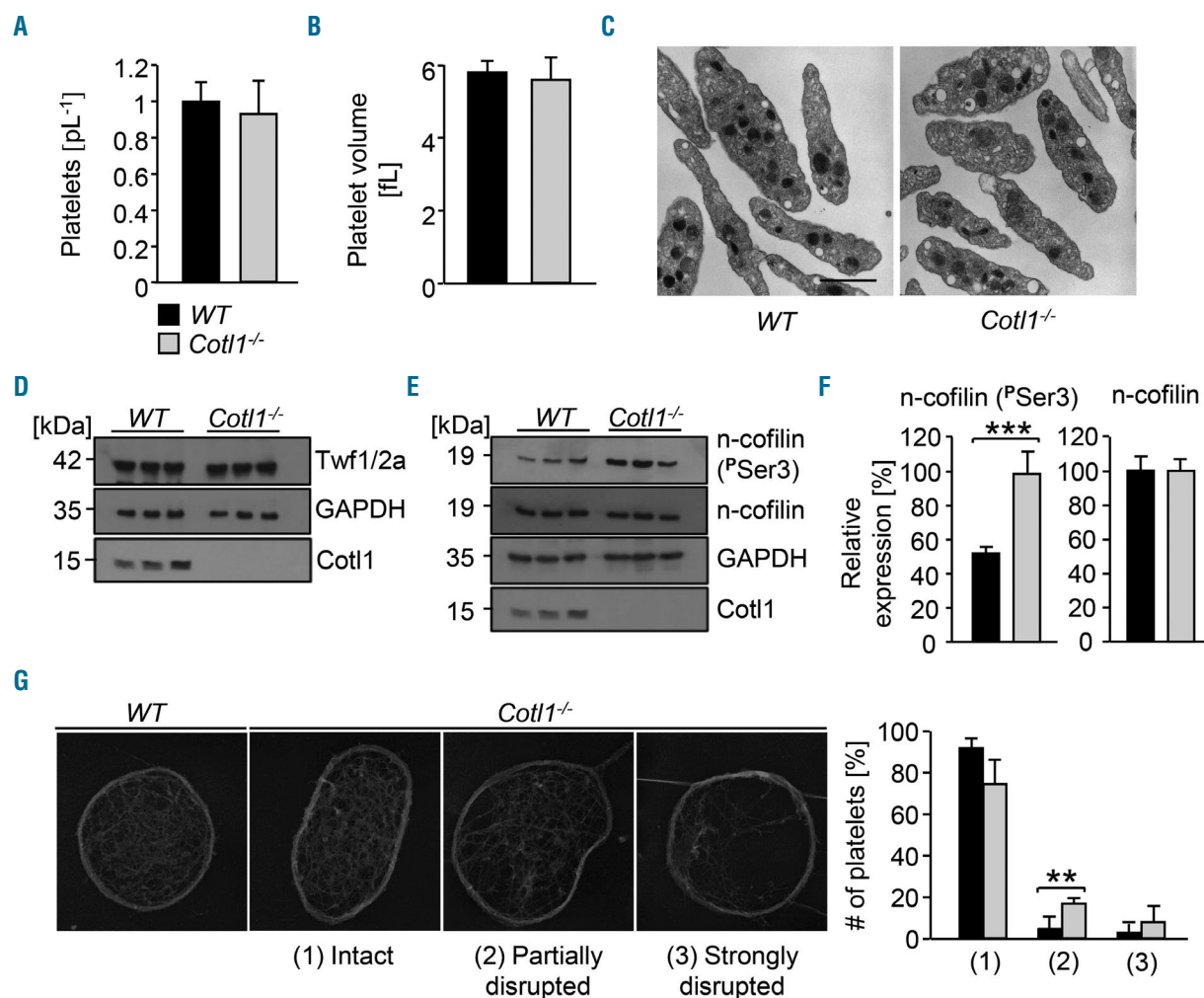


Figure 1. Cot11 is not essential for platelet formation and function under static conditions *in vitro*. (A and B) Platelet count (A) and size (B) were determined with an automated cell analyzer (SciVet). (C) Visualization of platelet size and structure using transmission electron microscopy (n=4). Scale bar, 2 μ m. (D-F) Platelets were left untreated, lysed, and processed for immunoblotting. Total twinfilin (D), phosphorylated n-cofilin and total n-cofilin (E) were probed with the respective antibodies and analyzed by densitometry (F). GAPDH served as loading control. Values are mean \pm standard deviation (SD) (n=3). (G) Images of the platelet cytoskeleton ultrastructure on poly-L-lysine. (Left) WT sample. (Right) *Cot11*^{-/-} sample. 0: intact, 1: partially disrupted, 2: strongly disrupted F-actin structures. Scale bar, 1 μ m. At least 158 platelets per genotype were analyzed.

observed a cytoplasmic localization which partially overlapped with that of F-actin and tubulin. When visualizing the F-actin ultrastructure in resting platelets by transmission electron microscopy (TEM),²³ we observed that the actin scaffold was disrupted in a significant proportion of *Cot11*-deficient platelets compared to the WT: (1) partially disrupted: *Cot11*^{-/-} 17.1% versus WT 4.9%, ***P*>0.01; (2) strongly disrupted: *Cot11*^{-/-} 8.2% vs. WT 3% (Figure 1G). However, we could not detect changes in resting F-actin levels or agonist-induced F-actin polymerization in *Cot11*^{-/-} platelets (Online Supplementary Figure S2A and B). In addition, although *Cot11* was recently described as a regulator of T-cell spreading at the immune synapse,¹⁴ *Cot11* deficiency in platelets did not affect their ability to spread on fibrinogen (Online Supplementary Figure S2C), as shown by normal morphology and distribution of F-actin and tubulin in the spread platelets (Online Supplementary Figure S2D and E).

Together, these results indicated that *Cot11* is not essential for platelet production or platelet actin remodeling.

Cot11 is required for platelet aggregate formation under flow conditions

We next studied the effect of *Cot11* deficiency on agonist-induced platelet activation. Flow cytometry was used to determine activation of the major platelet integrin α IIb β 3 as well as degranulation (P-selectin exposure) in response to a panel of standard agonists (Online Supplementary Figure S3A and B). In contrast to the hyper-reactivity of *Twf2a*-deficient platelets,¹¹ *Cot11*^{-/-} platelets displayed unaltered responses to agonists acting on both GPCR (thrombin, ADP, TxA₂ analog U46619) and (hem)ITAM signaling (collagen-related peptide (CRP), convulxin, rhodocytin) (Online Supplementary Figure S3A and B). Furthermore, washed *Cot11*^{-/-} platelets showed unaltered aggregation upon stimulation with thrombin, U46619, collagen and CRP as compared to the control (Online Supplementary Figure S4A). Similar results were obtained when using platelet-rich plasma (PRP) instead of washed platelets (Online Supplementary Figure S4B). These results demonstrated that *Cot11* is not required for platelet

activation and aggregation responses under static conditions *in vitro*.

In sharp contrast, however, *Cot11* deficiency markedly affected platelet aggregation and thrombus formation under shear flow conditions *in vitro*. We used a flow adhesion assay where the perfusion of whole anticoagulated *WT* blood over a collagen-coated surface leads to rapid platelet adhesion, activation and three-dimensional aggregate formation. While aggregate formation at low shear (150 s^{-1}) was comparable between *Cot11*^{-/-} and *WT* samples, we observed significantly reduced platelet adhesion, surface coverage and thrombus volume in blood from *Cot11*^{-/-} animals at medium and high shear rates ($1\,000\text{ s}^{-1}$, * $P < 0.05$; $3\,000\text{ s}^{-1}$, ** $P < 0.01$) (Figure 2A-C and *Online Supplementary Figure S5*). Strikingly, thrombus volume and platelet surface coverage were also significantly reduced in blood from *Cot11*^{-/-} mice when the flow adhesion assay was carried out in the presence of coagulation (*Online Supplementary Figure S6*).

Platelet adhesion and aggregate formation under medium and high shear rates is dependent on the interaction between the mechanoreceptor GPIb and immobilized vWF.²⁴ To investigate a possible involvement of *Cot11* in GPIb-mediated tethering/adhesion, we perfused blood from *WT* and *Cot11*^{-/-} animals over a vWF-coated surface at high shear ($3,000\text{ s}^{-1}$). The velocity of individual rolling *Cot11*^{-/-} platelets on immobilized vWF was comparable to the *WT* (Figure 2E, right); however, the number of adherent *Cot11*^{-/-} platelets was significantly reduced (** $P < 0.01$) (Figure 2D and E). Our results thus indicated that *Cot11* is required to ensure GPIb function during platelet adhesion and aggregate formation under conditions of high shear.

Growing experimental evidence suggests that signaling induced by the GPIb-vWF interaction involves mechanotransduction and transmission of forces to the actin cytoskeleton.^{25,26} Therefore, to assess the impact of *Cot11* deficiency on platelet biomechanical properties more generally, we subjected *Cot11*^{-/-} platelets to the recently described real-time deformability cytometry (RT-DC),²⁷ a method for continuous mechanical characterization of cells which are deformed by shear forces in a microfluidics chamber (Figure 2F). Strikingly, we found a significantly increased deformability of *Cot11*^{-/-} platelets (* $P < 0.05$) as compared to *WT* (Figure 2G and H, right). Importantly, we could exclude the possibility that the increased deformability was due to an increased platelet size; by contrast, the measured size of *Cot11*^{-/-} platelets in this assay was even slightly decreased as compared to the control (Figure 2H, left). Together, these results indicate that *Cot11* supports GPIb function and thus the formation of stable platelet aggregates under shear conditions, and that this function may, in part, be mediated by the modulation of platelet biomechanical properties.

Cot11 regulates leukotriene biosynthesis in platelets

Leukotrienes are pro-inflammatory lipid mediators mainly produced by immune competent cells such as leukocytes, e.g. mast cells, eosinophils, neutrophils, monocytes and basophils, and are implicated in a variety of inflammatory responses. Interestingly, besides its function as an actin-regulatory protein, *Cot11* was shown to bind and modulate the activity of the enzyme 5-lipoxygenase (5-LO).^{15,17,28} 5-LO catalyzes the two initial steps of LT biosynthesis: (1) the oxygenation of AA to 5-HPETE; and (2) the subsequent dehydration into leukotriene A₄ (LTA₄)

which is then further converted to LTB₄ (*Online Supplementary Figure S7*).^{29,30} Besides serving as substrate for LT biosynthesis, AA is converted to thromboxanes (TxA₂/B₂), prostacyclin (PGI₂), and prostaglandins (PGE₂/F₂) by cyclo-oxygenases in platelets (*Online Supplementary Figure S4*).^{31,32}

To investigate the effect of *Cot11* deficiency on LT production in platelets, we assessed the release of 5,12-diHETE and LTB₄ in the supernatant of washed CRP- or thrombin-stimulated platelets. Strikingly, the secretion of both lipid mediators was significantly reduced in *Cot11*^{-/-} platelets upon CRP activation as compared to *WT* controls and a similar tendency was observed for thrombin-stimulated platelets (* $P < 0.05$) (Figure 3A). Of note, the total AA amount was comparable to *WT* platelets, demonstrating that the abundance of this initial metabolite was not affected by *Cot11* deficiency (Figure 3A, left). To assess whether AA was consumed by other pathways, we analyzed TxB₂ levels by ELISA. Strikingly, we found significantly increased TxB₂ release in thrombin-stimulated and, to a lesser extent, CRP-stimulated *Cot11*^{-/-} platelets compared to the control (* $P < 0.05$), indicating that the excess of available AA in *Cot11*^{-/-} platelets was consumed by an upregulation of prostaglandin biosynthesis (*Online Supplementary Figure S8*).

To assess whether, indeed, *Cot11* directly influences 5-LO activity, lysates of CRP- or thrombin-stimulated platelets were probed for active 5-LO (S663 phosphorylation) by western blotting (Figure 3B). Of note, basal levels of active 5-LO were comparable between *Cot11*^{-/-} and *WT* platelets. Strikingly, while activation induced pronounced S663 phosphorylation in *WT* platelets, this process was significantly reduced in *Cot11*^{-/-} platelets (thrombin: * $P < 0.05$; CRP: ** $P < 0.01$) (Figure 3B and C). Together, these results demonstrated that *Cot11* directly influences 5-LO activity, ultimately resulting in reduced biosynthesis and, subsequently, release of LT from *Cot11*^{-/-} platelets.

Defective shear-dependent thrombus formation in Cot11-deficient mice is rescued by exogenous addition of leukotriene B₄

We next investigated whether the reduced release of lipid mediators in *Cot11*^{-/-} mice contributed to defective platelet aggregate formation of *Cot11*^{-/-} platelets under flow. We decided to focus on LTB₄, one of the end products of the LT biosynthesis pathway downstream of LTA₄, which was shown to stimulate neutrophil chemotaxis³³ and activation.³⁴ First, we tested whether LTB₄ was able to directly induce platelet activation. As LTB₄ was described to induce neutrophil aggregation and degranulation at concentrations of $0.1\text{ }\mu\text{M}$ ^{35,36} and leukocyte aggregation, chemotaxis and chemokinesis at a subnanomolar range of 0.39 nM ,³⁵ we used concentrations of $0.025\text{--}250\text{ nM}$ LTB₄ (Cayman Chemicals) in our assays. None of the tested LTB₄ concentrations induced platelet activation under static conditions *in vitro* (*Online Supplementary Figures S9A* and *S10A*). Likewise, LTB₄ addition did not further enhance integrin $\alpha\text{IIb}\beta\text{3}$ activation, degranulation or aggregation of *WT* or *Cot11*^{-/-} platelets (*Online Supplementary Figures S9B* and *S10B*).

Using the *in vitro* flow adhesion assay (Figure 2A-C), we next investigated the effect of LTB₄ on platelet aggregate formation under flow. Adding concentrations of 2.5 nM or higher interfered with aggregate formation ($1,700\text{ s}^{-1}$) in *WT* blood, whereas lower concentrations had no effect

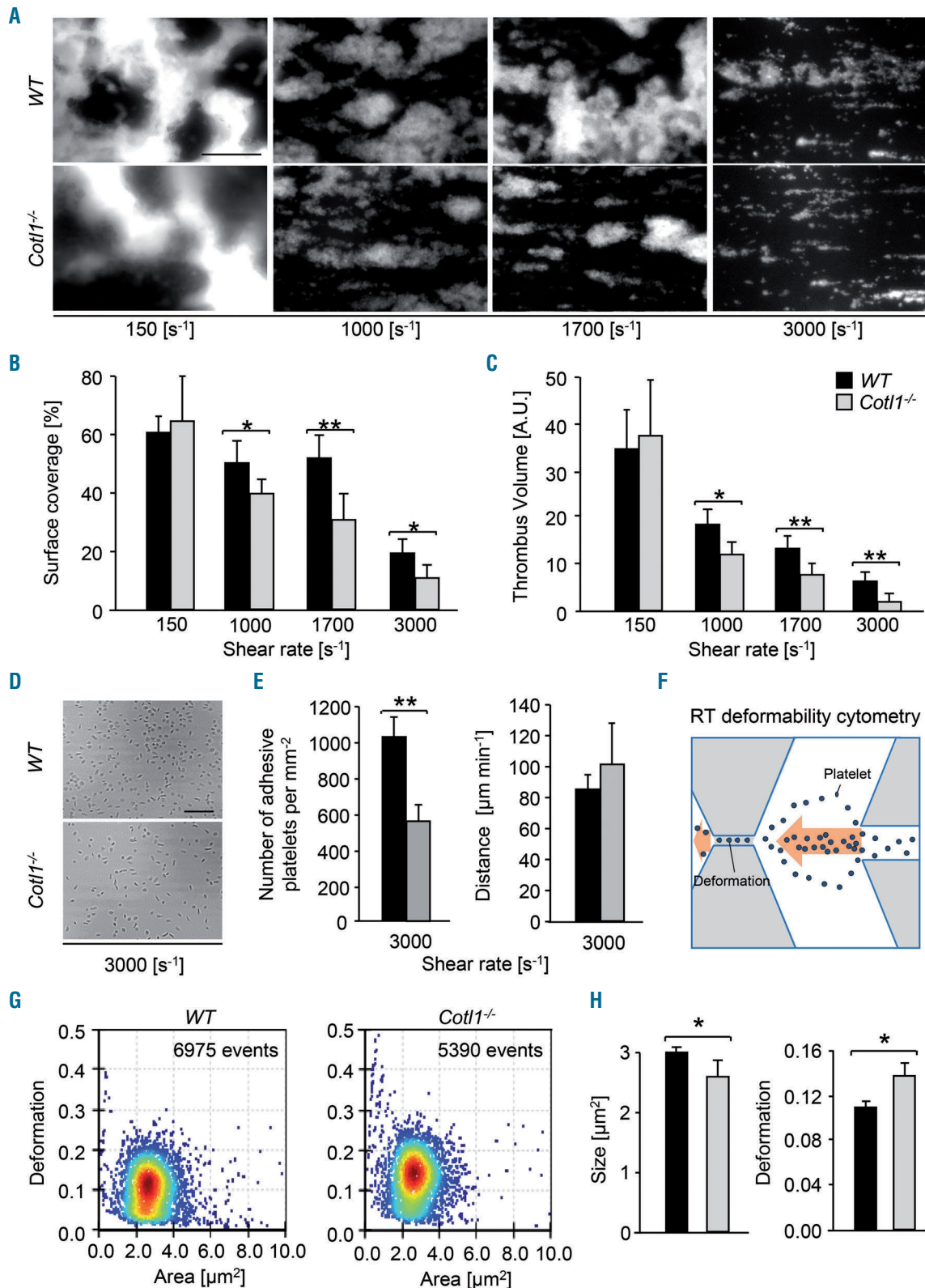


Figure 2. Cot11 is required for thrombus formation and stability at high shear. (A-C) Assessment of platelet adhesion (A and B) and aggregate formation (A and C) on Horm collagen (70 μg mL⁻¹) under flow (150-3 000 s⁻¹) in heparinized whole blood of WT and Cot11^{-/-} mice. Values are mean±standard deviation (SD) (n=12). Scale bar, 50 μm. (D and E) Heparinized whole blood of WT and Cot11^{-/-} mice was perfused over a von Willebrand factor (vWF)-coated cover slip for 4 minutes (min) at a shear rate of 3,000 s⁻¹. (D) Representative phase contrast images taken at the end of the perfusion time and (E) analysis of the number of adherent platelets per mm² ±SD (left), as well as the rolling velocity calculated from the distance a platelet covered per minute in μm ±SD (right) was performed. Images were acquired with a Zeiss Axiovert 200 inverted microscope (40x/0.6 oil objective). Images are representative of at least 12 animals per group. Scale bar, 50 μm. Unpaired Student t-test: **P<0.01; *P<0.05. (F-H) Real-time deformability cytometry (RT-DC),²⁷ a method for continuous mechanical characterization of cells which are deformed by deceleration at the stagnation point of fast extensional flow. (F) Scheme depicting the principle of real-time deformability cytometry (RT-DC). (G) Representative dot plots showing the relative deformation, as well as the (H) the size of washed WT and Cot11^{-/-} platelets. Values are mean±SD (n=3). *P<0.1; **P<0.01. A.U. : arbitrary units.

(Online Supplementary Figure S11A and B). Strikingly, pre-incubation with 0.25 nM LTB₄ could fully restore aggregate formation of *Cott1*^{-/-} platelets to WT levels (Figure 4A and B), indicating that the defect observed in untreated *Cott1*^{-/-} samples was caused by impaired platelet-derived LTB₄ production. To investigate whether LTB₄ has a more general function in this context, we analyzed two additional knockout mouse lines with a described defect in the flow adhesion assay: *Grb2*^{fl/fl;P4^{Cre}} (*Grb2*^{-/-}) mice have normal platelet counts but the platelets display a selective GPVI/ITAM activation defect.³⁷ *RhoA*^{fl/fl;P4^{Cre}} (*RhoA*^{-/-}) mice are thrombocytopenic and deficient platelets display

impaired G protein coupled receptor (GPCR) signaling.³⁸ Notably, the addition of LTB₄ to anticoagulated blood from *Grb2*^{-/-} mice resulted in moderately increased platelet surface coverage ($P=0.06$) as compared to untreated samples, but could not restore aggregate formation to WT levels (Online Supplementary Figure S12). Furthermore, LTB₄ addition had no effect on aggregate formation in platelet-count adjusted blood of *RhoA*^{-/-} mice (Online Supplementary Figure S13). Together, these findings demonstrated that addition of LTB₄ cannot compensate for defective platelet aggregate formation under flow in the presence of prominent platelet activation/secretion defects. At the same

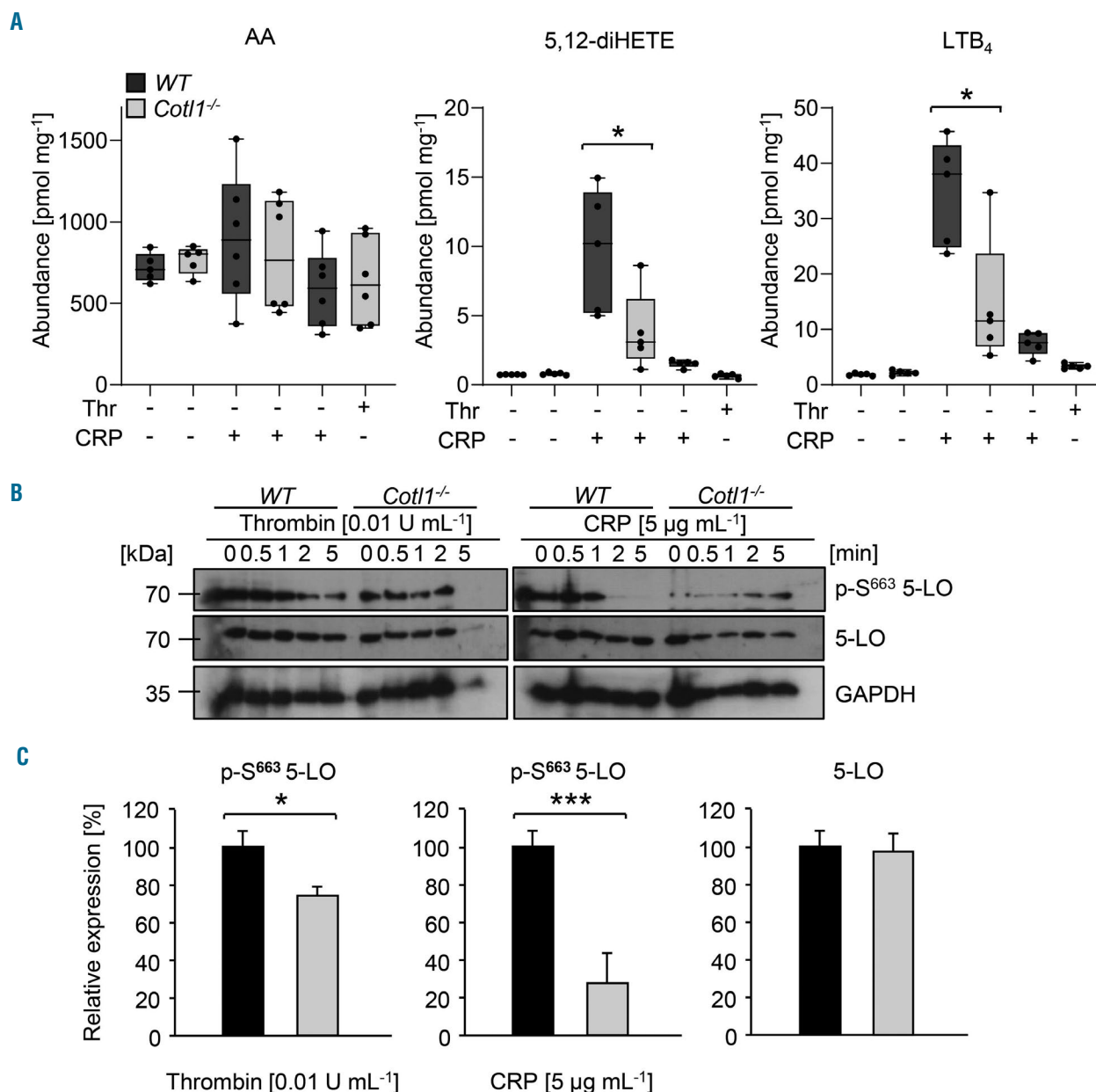


Figure 3. *Cott1* is a regulator of leukotriene biosynthesis in platelets. (A) For lipid mediator analysis platelets were either left untreated or stimulated with CRP [5 μg mL⁻¹] or thrombin [0.01 U mL⁻¹] for 5 minutes (min). Subsequently, samples were spun down, pellet and supernatant were separately shock-frozen in liquid nitrogen. Lipid abundance was assessed using liquid crystal mass spectrometry. Values are mean±standard deviation (SD) (n=15). (B and C) Platelets were either left untreated or stimulated with CRP [5 μg mL⁻¹] or thrombin [0.01 U mL⁻¹] for 5 min, lysed, and processed for immunoblotting. Total 5-LO, phospho-5-LO (S663) and GAPDH (B) were probed with the respective antibodies and analyzed by densitometry (C). Values are mean±SD (n=4).

time, our results emphasize that reduced LTB_4 production in $\text{Cot11}^{-/-}$ platelets, which display no obvious activation defect *per se*, significantly contributed to the impaired aggregate formation in the presence of shear.

Cot11 modulates thrombosis and hemostasis

To investigate whether the impaired shear-dependent aggregate formation translated into a phenotype *in vivo*, we subjected $\text{Cot11}^{-/-}$ mice to an experimental model of arterial thrombosis. Since it is well documented that collagen is a main driver of thrombus formation in bigger vessels, particularly in models of mechanical injury, we chose a model where the abdominal aorta is mechanically injured. This procedure triggers rapid platelet adhesion to the injured vessel wall, followed by the development of a large occlusive thrombus associated with dynamic changes in both shear and biomechanical forces acting on adhering platelets in the growing thrombus. Strikingly, $\text{Cot11}^{-/-}$ mice were profoundly protected from occlusive thrombus formation in this model (Figure 5A and B). In

WT mice, irreversible vessel occlusion was observed within 7 minutes (min) after injury (mean occlusion time 3.37 ± 0.72 min). In sharp contrast, while a progressive reduction in blood flow occurred during the first minutes after injury in $\text{Cot11}^{-/-}$ mice, indicative of beginning thrombus formation and increasing stenosis, blood flow afterwards normalized and 9 of 11 mice displayed normal blood flow through the injured vessel at the end of the observation period (30 min) ($***P < 0.001$). These results demonstrated that Cot11 is essential for occlusive arterial thrombus formation *in vivo*.

To assess the hemostatic function of $\text{Cot11}^{-/-}$ platelets, we performed a tail bleeding assay. Notably, while tail bleeding times were overall significantly increased in $\text{Cot11}^{-/-}$ mice (7.8 ± 12.2 min in $\text{Cot11}^{-/-}$ mice vs. 3.3 ± 1.8 min in WT; $*P < 0.05$) the hemostatic defect was rather mild given the profound protection in the arterial thrombosis model (Figure 5C), indicating that Cot11 may be particularly important in settings of pathological thrombus formation.

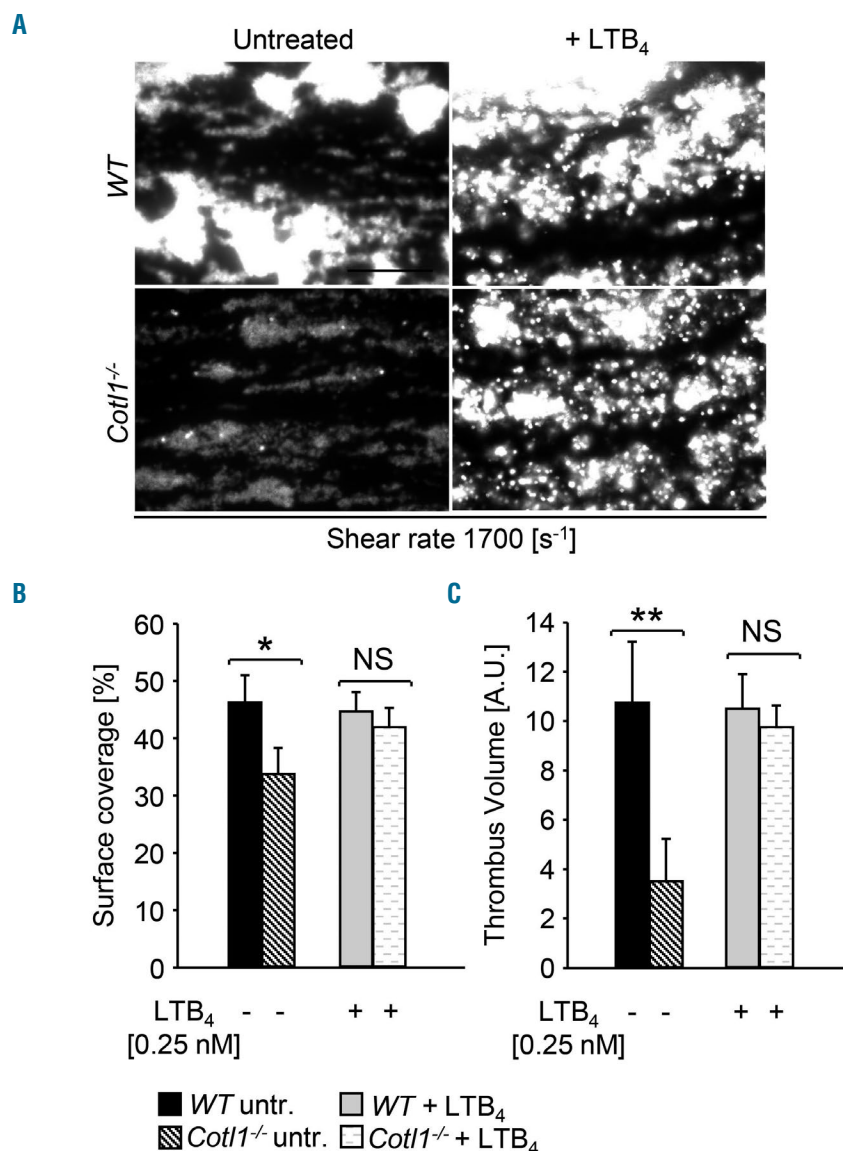


Figure 4. Defective shear-dependent thrombus formation in Cot11-deficient mice can be rescued by exogenous addition of leukotriene B₄. (A-C) Assessment of platelet adhesion (A and B) and aggregate formation in heparinized blood (A and C) on Horm collagen ($70 \mu\text{g mL}^{-1}$) under flow (1700 s^{-1}). WT and $\text{Cot11}^{-/-}$ samples were either left untreated or were pre-incubated for 5 minutes (min) with LTB_4 , [0.25 nM]. Images are representatives of at least 12 mice per group. Values are mean \pm standard deviation. Scale bar, 50 μm . $*P < 0.1$; $**P < 0.01$.

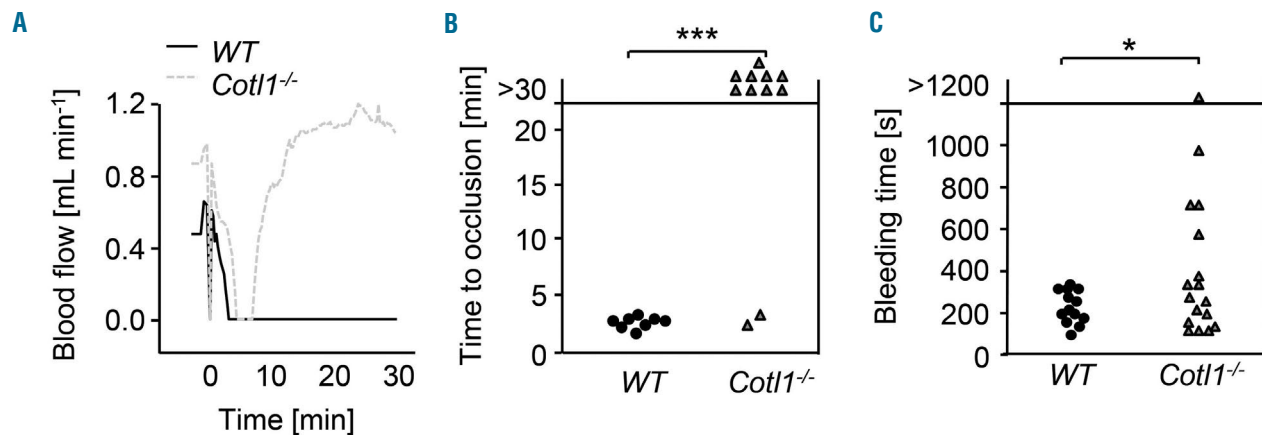


Figure 5. Cot1 modulates thrombosis and hemostasis. (A and B) Intravital thrombosis model. (A) Representative graph of blood flow of one WT and one Cot1^{-/-} mouse after mechanical injury of the abdominal aorta. (B) Occlusion times after mechanical injury of the abdominal aorta. Data are mean ± standard deviation of at least eight mice per group. (C) Tail bleeding times in WT and Cot1^{-/-} mice (filter paper method). Each symbol represents one individual. Unpaired Student t-test: ***P < 0.001; *P < 0.05.

Discussion

Here, we demonstrate for the first time that the small ADF-H-domain-containing actin-binding protein Cot1 has entirely different functions compared to the other protein family members ADF/n-cofilin and Twf, at least in platelets. Cot1 deficiency neither had an impact on thrombopoiesis or platelet function under static conditions *in vitro*, nor did it obviously affect actin reorganization. Strikingly, we could reveal a critical role of Cot1 for stable thrombus formation under conditions of shear *in vitro* and *in vivo*. Our results point to two distinct and so far undescribed roles of Cot1 in this process. On the one hand, the F-actin binding function of the protein is required for proper GPIb function and possibly shear-induced biomechanical signaling. On the other hand, the 5-LO enzyme-modulating function of Cot1 promotes the biosynthesis of LT, which positively modulate thrombus formation.

The crucial role of actin cytoskeletal rearrangements for platelet formation and reactivity has been demonstrated in a number of studies.^{5,7,8,10,11,39} While we have previously shown that lack of either Twf2a or n-cofilin in the MK lineage results in thrombocytopenia and distinct platelet function defects,^{10,11} deficiency of Cot1 did not affect circulating platelet counts. This may be explained by the distinct actin-binding properties and biological activities of each ADF-H member, which can be attributed to their different domain structure.¹² Hence, n-cofilin deficiency decreased stimulus-dependent F-actin assembly, whereas on the contrary, Twf2a-deficient mice displayed enhanced actin dynamics.^{10,11} Notably, we observed strongly elevated levels of phosphorylated (inactive) n-cofilin in Cot1-deficient platelets. This finding was unexpected given that, in T cells, Cot1 was shown to be required for spreading at the immune synapse by protecting F-actin from n-cofilin-mediated severing,¹⁴ which would suggest enhanced rather than reduced n-cofilin activity in the absence of Cot1. We still cannot explain this apparent discrepancy but can exclude the possibility that it was caused by a direct compensation by another ADF-H protein member since expression of Twf1/2a and n-cofilin were unaltered in Cot1^{-/-} compared to WT platelets.

Over the past few years, greater attention has been given to the critical influence of blood rheology and its dynamical changes on platelet adhesion and thrombus growth, including the relevance of mechanotransduction-based signaling *in vivo*. Best studied in this context is the platelet mechanoreceptor GPIb which plays a pivotal role for platelet adhesion, as well as thrombus formation at high shear.²⁴ We observed that the reduced aggregate formation of Cot1^{-/-} platelets on collagen under flow *in vitro* was most pronounced at high shear rates, where GPIb becomes increasingly important. Consistently, GPIb-mediated adhesion of Cot1^{-/-} platelets to vWF was significantly reduced. Together, this indicates an involvement of Cot1 in basic GPIb-mediated platelet responses.

The cytoplasmic domain of the GPIb α subunit is tightly linked to the actin cytoskeleton. This interaction is critical for the correct localization of GPIb in the plasma membrane⁴⁰ and probably also enables mechanotransduction upon binding of GPIb to its ligand vWF at high shear rates. To study whether the actin-regulating function of Cot1 in platelets may be specifically critical under shear conditions, we used a novel, quite general, approach to characterize platelet biomechanical properties by assessing their shear-induced deformability using RT-DC.²⁷ This assay has the advantage that, in contrast to other experimental approaches, the biomechanical function of a high cell number can be readily analyzed, and this increases the reliability of the results. Despite not detecting defects in actin assembly under static conditions, strikingly, we observed higher deformability of Cot1-deficient platelets in RT-DC measurements. Our results, therefore, clearly show that biomechanical properties are significantly altered in Cot1-deficient platelets, which may have a substantial influence on their function *in vivo*, possibly also affecting signaling of the mechanoreceptor GPIb.

Besides its interaction with F-actin, Cot1 is a binding partner of 5-LO, the key enzyme in LT biosynthesis,¹⁵ which is expressed in immune competent cells and platelets. LT are a group of inflammatory mediators derived from AA. Upon activation, intracellular Ca²⁺ levels increase, free AA is liberated from membrane phospholipids by phospholipases, and 5-LO is activated, leading to

the generation of intermediate LTA₄ and subsequently the production of the different LT types (*Online Supplementary Figure S7*).³⁵ Besides the cysteinyl (cysLT) LT (LTC₄, LTD₄, LTE₄), these also include LTB₄, which stimulates neutrophil chemotaxis,³⁵ enhances neutrophil-endothelial interactions,⁴¹ and stimulates neutrophil activation, leading to degranulation and the release of mediators, enzymes, and superoxides.³⁴ LTB₄ can also act on other cell types, e.g. by increasing interleukin (IL)-6 production by human monocytes.⁴² Platelet-derived LT were shown to contribute to inflammatory responses, e.g. during acute inflammation *via* activation of leukocytes,^{18,43} but only a few very early *in vitro* studies indicated an impact of LT directly on platelet aggregation.^{18,43}

A recent comprehensive analysis of the platelet lipidome by Peng *et al.* revealed that the AA/5-LO/LT pathway is significantly induced by platelet activation.⁴⁴ Therefore, to directly assess whether lack of Cot11 down-regulates 5-LO activity and hence LT biosynthesis, we characterized platelet lipid mediator levels using mass spectrometry.⁴⁴ Our data confirm previous findings from other cell types that Cot11 positively regulates 5-LO,¹⁷ as lack of Cot11 induced a shift from LT to prostaglandin biosynthesis downstream from AA, leading to reduced levels of LTA₄ and LTB₄, but higher levels of TxB₂ in the knock-out platelets. Interestingly, CRP (but not thrombin) was able to induce significant LTB₄ release in *WT* platelets. This is in line with findings by Peng *et al.* who observed that CRP, but not thrombin alone, was able to induce significant changes in the platelet lipidome.⁴⁴ Thus, our detailed study further shows that the AA/LTB₄ pathway is induced by GPVI/ITAM rather than GPCR signaling in platelets.

Strikingly, our results indicate that exogenous addition of LTB₄ could fully rescue the defective aggregate formation of Cot11-deficient platelets on collagen under flow *in vitro* (Figure 4). While this finding indicates that the exogenous addition of LT can compensate for the GPIb function defect in Cot11-deficient platelets, we cannot exclude that

GPIb signaling itself is involved in LT biosynthesis. Notably, exogenous addition of LTB₄ did not restore aggregate formation of RhoA- or Grb2-deficient platelets, which *per se* display significant activation/ secretion defects. These results show that LTB₄ secretion is required to fine-tune platelet function under flow rather than being a strong positive regulator of thrombus formation. However, LTB₄ addition could moderately increase aggregate formation of Grb2-deficient platelets, which display defective GPVI/ITAM signaling. This further suggests that LTB₄ is particularly relevant for platelet aggregate formation induced through the GPIb/GPVI/ITAM axis. It will be important to dissect the detailed signaling mechanisms leading to LT generation, as well as the precise role of LT and their signaling pathways for platelet thrombus formation *in vivo* in future studies.

Taken together, our study reveals that Cot11 modulates biomechanical properties of platelets and acts as a signaling integrator in thrombotic processes. Given that both GPIb and LT represent potential therapeutic targets for a number of thrombo-inflammatory and autoimmune diseases, our findings may contribute to a better understanding of the molecular pathways orchestrating these processes.

Acknowledgments

We thank Stefanie Hartmann for excellent technical assistance and the microscopy platform of the Bioimaging Center (Rudolf Virchow Centre) for providing technical infrastructure and support. This work was supported by the Deutsche Forschungsgemeinschaft (DFG, German Research Foundation) (NI 556/11-2 to BN and project number 374031971 – TRR 240). MB is supported by an Emmy Noether grant of the DFG (BE5084/3-1). OO gratefully acknowledges support from the German Ministry of Education and Research (ZIK grant to OO under grant agreement 03Z22CN11). RA received further support from the Federal Ministry of Education and Research (BMBF) in the German Network Bioinformatics Infrastructure (de.NBI) initiative (grants n. 031L0108A and n. 031 A 534B).

References

- Ruggeri ZM. Platelets in atherothrombosis. *Nat Med.* 2002;8(11):1227-1234.
- Jackson SP, Nesbitt WS, Kulkarni S. Signaling events underlying thrombus formation. *J Thromb Haemost.* 2003;1(7):1602-1612.
- Zhang W, Deng W, Zhou L, et al. Identification of a juxtamembrane mechanosensitive domain in the platelet mechanosensor glycoprotein Ib-IX complex. *Blood.* 2015;125(3):562-569.
- Stritt S, Nurden P, Turro E, et al. A gain-of-function variant in *DIAPH1* causes dominant macrothrombocytopenia and hearing loss. *Blood.* 2016;127(23):2903-2914.
- Nurden P, Debili N, Coupry I, et al. Thrombocytopenia resulting from mutations in filamin A can be expressed as an isolated syndrome. *Blood.* 2011;118(22):5928-5937.
- Thrasher AJ, Burns SO. WASP: a key immunological multitasker. *Nat Rev Immunol.* 2010;10(3):182-192.
- Kunishima S, Okuno Y, Yoshida K, et al. ACTN1 mutations cause congenital macrothrombocytopenia. *Am J Hum Genet.* 2013;92(3):431-438.
- Pleines I, Woods J, Chappaz S, et al. Mutations in tropomyosin 4 underlie a rare form of human macrothrombocytopenia. *J Clin Invest.* 2017;127(3):814-829.
- Hartwig JH. Mechanisms of actin rearrangements mediating platelet activation. *J Cell Biol.* 1992;118(6):1421-1442.
- Bender M, Eckly A, Hartwig JH, et al. ADF/n-cofilin-dependent actin turnover determines platelet formation and sizing. *Blood.* 2010;116(10):1767-1775.
- Stritt S, Beck S, Becker IC, et al. Twinfilin 2a regulates platelet reactivity and turnover in mice. *Blood.* 2017;130(15):1746-1756.
- Hellman M, Paavilainen VO, Naumanen P, Lappalainen P, Annala A, Permi P. Solution structure of coactosin reveals structural homology to ADF/cofilin family proteins. *FEBS Lett.* 2004;576(1-2):91-96.
- Provost P, Doucet J, Stock A, Gerisch G, Samuelsson B, Rådmark O. Coactosin-like protein, a human F-actin-binding protein: critical role of lysine-75. *Biochem J.* 2001;359(Pt 2):255-263.
- Kim J, Shapiro MJ, Bamidele AO, et al. Coactosin-Like 1 Antagonizes Cofilin to Promote Lamellipodial Protrusion at the Immune Synapse. *PLoS One.* 2014;9(1):e85090.
- Provost P, Doucet J, Hammarberg T, Gerisch G, Samuelsson B, Rådmark O. 5-Lipoxygenase Interacts with Coactosin-like Protein. *J Biol Chem.* 2001;276(19):16520-16527.
- Esser J, Rakonjac M, Hofmann B, et al. Coactosin-like protein functions as a stabilizing chaperone for 5-lipoxygenase: role of tryptophan 102. *Biochem J.* 2010;425(1):265-274.
- Rakonjac M, Fischer L, Provost P, et al. Coactosin-like protein supports 5-lipoxygenase enzyme activity and up-regulates leukotriene A(4) production. *Proc Natl Acad Sci U S A.* 2006;103(35):13150-13155.
- Evangelista V, Celardo A, Dell'Elba G, et al. Platelet contribution to leukotriene production in inflammation: *in vivo* evidence in the rabbit. *Thromb Haemost.* 1999;81(3):442-448.
- Tiedt R, Schomber T, Hao-Shen H, Skoda RC. *em>P4-Cre transgenic mice*

- allow the generation of lineage-restricted gene knockouts for studying megakaryocyte and platelet function *in vivo*. *Blood*. 2007;109(4):1503-1506.
20. Burkhart JM, Vaudel M, Gambaryan S, et al. The first comprehensive and quantitative analysis of human platelet protein composition allows the comparative analysis of structural and functional pathways. *Blood*. 2012;120(15):e73-82.
 21. Zeiler M, Moser M, Mann M. Copy number analysis of the murine platelet proteome spanning the complete abundance range. *Mol Cell Proteomics*. 2014;13(12):3435-3445.
 22. Provost P, Doucet J, Stock A, Gerisch G, Samuelsson B, Rådmark O. Coactosin-like protein, a human F-actin-binding protein: critical role of lysine-75. *Biochem J*. 2001;359(Pt 2):255-263.
 23. Spindler M, van Eeuwijk JMM, Schurr Y, et al. ADAP deficiency impairs megakaryocyte polarization with ectopic proplatelet release and causes microthrombocytopenia. *Blood*. 2018;132(6):635-646.
 24. Turitto VT, Weiss HJ, Baumgartner HR. The effect of shear rate on platelet interaction with subendothelium exposed to citrated human blood. *Microvasc Res*. 1980;19(3):352-365.
 25. Feghhi S, Munday AD, Tooley WW, et al. Glycoprotein Ib-IX-V Complex Transmits Cytoskeletal Forces That Enhance Platelet Adhesion. *Biophys J*. 2016;111(3):601-608.
 26. Hansen CE, Qiu Y, McCarty OJT, Lam WA. Platelet Mechanotransduction. *Ann Rev Biomed Eng*. 2018;20(1):253-275.
 27. Otto O, Rosendahl P, Mietke A, et al. Real-time deformability cytometry: on-the-fly cell mechanical phenotyping. *Nat Met*. 2015;12(3):199-202.
 28. Provost P, Samuelsson B, Rådmark O. Interaction of 5-lipoxygenase with cellular proteins. *Proc Natl Acad Sci U S A*. 1999;96(5):1881-1885.
 29. Samuelsson B, Dahlen S, Lindgren J, Rouzer C, Serhan C. Leukotrienes and lipoxins: structures, biosynthesis, and biological effects. *Science*. 1987;237(4819):1171-1176.
 30. Samuelsson B. Leukotrienes: mediators of immediate hypersensitivity reactions and inflammation. *Science*. 1983;220(4597):568-575.
 31. Hamberg M, Samuelsson B. Detection and Isolation of an Endoperoxide Intermediate in Prostaglandin Biosynthesis. *Proc Natl Acad Sci U S A*. 1973;70(3):899-903.
 32. Nugteren DH, Hazelhof E. Isolation and properties of intermediates in prostaglandin biosynthesis. *Biochim Biophys Acta Lipids Lipid Metab*. 1973;326(3):448-461.
 33. Palmer RMJ, Stepney RJ, Higgs GA, Eakins KE. Chemokinetic activity of arachidonic acid lipoxygenase products on leucocytes of different species. *Prostaglandins*. 1980;20(2):411-418.
 34. Sha'Afi RI, Naccache PH, Molski TFP, Borgeat P, Goetzl EJ. Cellular regulatory role of leukotriene B4: Its effects on cation homeostasis in rabbit neutrophils. *J Cell Physiol*. 1981;108(3):401-408.
 35. Ford-Hutchinson AW. Leukotriene B4 in inflammation. *Crit Rev Immunol*. 1990;10(1):1-12.
 36. McMillan RM, Foster SJ. Leukotriene B4 and inflammatory disease. *Agents Actions*. 1988;24(1):114-119.
 37. Dutting S, Vogtle T, Morowski M, et al. Growth factor receptor-bound protein 2 contributes to (hem)immunoreceptor tyrosine-based activation motif-mediated signaling in platelets. *Circ Res*. 2014;114(3):444-453.
 38. Pleines I, Hagedorn I, Gupta S, et al. Megakaryocyte-specific RhoA deficiency causes macrothrombocytopenia and defective platelet activation in hemostasis and thrombosis. *Blood*. 2012;119(4):1054-1063.
 39. Bender M, Stritt S, Nurden P, et al. Megakaryocyte-specific Profilin1-deficiency alters microtubule stability and causes a Wiskott-Aldrich syndrome-like platelet defect. *Nat Commun*. 2014;5(4746).
 40. Nakamura F, Pudas R, Heikkinen O, et al. The structure of the GPIb-filamin A complex. *Blood*. 2006;107(5):1925.
 41. Hoover RL, Karnovsky MJ, Austen KF, Corey EJ, Lewis RA. Leukotriene B4 action on endothelium mediates augmented neutrophil/endothelial adhesion. *Proc Natl Acad Sci U S A*. 1984;81(7):2191-2193.
 42. Brach MA, De Vos S, Arnold C, Gräß H-J, Mertelsmann R, Herrmann F. Leukotriene B4 transcriptionally activates interleukin-6 expression involving NK- κ B and NF-IL6. *European J Immunol*. 1992;22(10):2705-2711.
 43. Maclouf J, de Lacroix BF, Borgeat P. Stimulation of leukotriene biosynthesis in human blood leukocytes by platelet-derived 12-hydroperoxy-icosatetraenoic acid. *Proc Natl Acad Sci U S A*. 1982;79(19):6042-6046.
 44. Peng B, Geue S, Coman C, et al. Identification of key lipids critical for platelet activation by comprehensive analysis of the platelet lipidome. *Blood*. 2018;81(7):e1-e12.

LIM-only protein FHL2 attenuates vascular tissue factor activity, inhibits thrombus formation in mice and *FHL2* genetic variation associates with human venous thrombosis

Chantal Kroone,¹ Mariska Vos,² Timo Rademakers,³ Marijke Kuijpers,⁴ Mark Hoogenboezem,³ Jaap van Buul,³ Johan W.M. Heemskerk,⁴ Wolfram Ruf,^{5,6} Astrid van Hylckama Vlieg,⁷ Henri H. Versteeg,¹ Marie-José Goumans,⁸ Carlie J.M. de Vries,^{2#} and Kondababu Kurakula,^{2,8#} INVENT Consortium

¹The Eindhoven Laboratory for Experimental Vascular Medicine, Leiden University Medical Center (UMC), Leiden, the Netherlands; ²Department of Medical Biochemistry, Amsterdam Cardiovascular Sciences, Amsterdam UMC, University of Amsterdam, Amsterdam, the Netherlands; ³Department of Molecular Cell Biology, Sanquin Research, Amsterdam, the Netherlands; ⁴Department of Biochemistry, Cardiovascular Research Institute Maastricht (CARIM), Maastricht UMC, Maastricht, The Netherlands; ⁵Department of Immunology and Microbiology, The Scripps Research Institute, La Jolla, CA, USA; ⁶Center for Thrombosis and Hemostasis Mainz, Germany; ⁷Department of Clinical Epidemiology, Leiden UMC, Leiden, the Netherlands and ⁸Department of Cell and Chemical Biology, Leiden University Medical Center, Leiden, the Netherlands

*CMdV and KK contributed equally as co-senior authors.

ABSTRACT

Bleeding disorders and thrombotic complications are major causes of morbidity and mortality with many cases being unexplained. Thrombus formation involves aberrant expression and activation of tissue factor (TF) in vascular endothelial and smooth muscle cells. Here, we sought to identify factors that modulate *TF* gene expression and activity in these vascular cells. The LIM-only protein FHL2 is a scaffolding protein that modulates signal transduction pathways with crucial functions in endothelial and smooth muscle cells. However, the role of FHL2 in TF regulation and thrombosis remains unexplored. Using a murine model of venous thrombosis in mesenteric vessels, we demonstrated that FHL2 deficiency results in exacerbated thrombus formation. Gain- and loss-of-function experiments revealed that *FHL2* represses TF expression in endothelial and smooth muscle cells through inhibition of the transcription factors nuclear factor κ B and activating protein-1. Furthermore, we observed that FHL2 interacts with the cytoplasmic tail of TF. In line with our *in vivo* observations, *FHL2* decreases TF activity in endothelial and smooth muscle cells whereas *FHL2* knockdown or deficiency results in enhanced TF activity. Finally, the *FHL2* single nucleotide polymorphism rs4851770 was associated with the risk of venous thrombosis in a large population of venous thrombosis cases and control subjects from 12 studies (INVENT consortium). Altogether, our results highlight functional involvement of FHL2 in TF-mediated coagulation and identify *FHL2* as a novel gene associated with venous thrombosis in humans.

Introduction

Thrombosis is a common pathology underlying venous thromboembolism (VTE), as well as ischemic heart disease and ischemic stroke, and is a leading cause of morbidity and mortality worldwide.¹ Thrombus formation involves platelet activation and aggregation as well as local, vascular tissue factor (TF) expression and activation, which may result in occlusion of blood vessels and ischemic events.^{2,6} The expression of TF, a transmembrane protein, is highly induced in both vascular smooth muscle cells (SMC) and endothelial cells (EC) in response to



Haematologica 2020
Volume 105(6):1677-1685

Correspondence:

KONDABABU KURAKULA
k.b.kurakula@lumc.nl

Received: July 25, 2018.

Accepted: August 26, 2019.

Pre-published: August 29, 2019.

doi:10.3324/haematol.2018.203026

Check the online version for the most updated information on this article, online supplements, and information on authorship & disclosures: www.haematologica.org/content/105/6/1677

©2020 Ferrata Storti Foundation

Material published in *Haematologica* is covered by copyright. All rights are reserved to the Ferrata Storti Foundation. Use of published material is allowed under the following terms and conditions:

<https://creativecommons.org/licenses/by-nc/4.0/legalcode>.

Copies of published material are allowed for personal or internal use. Sharing published material for non-commercial purposes is subject to the following conditions:

<https://creativecommons.org/licenses/by-nc/4.0/legalcode>, sect. 3. Reproducing and sharing published material for commercial purposes is not allowed without permission in writing from the publisher.



vascular injury.⁷⁻¹⁰ Upon injury to the vessel wall, TF is exposed to blood coagulation factors. The TF-factor VIIa complex catalyzes the proteolytic activation of coagulation factor X, leading to generation of the multi-purpose enzyme thrombin, which converts fibrinogen into fibrin, activates platelets, induces thrombus formation, and initiates protease-activated receptor (PAR) signaling.^{11,12} It has been demonstrated that TF expression is induced on vascular cells such as EC and SMC as well as on immune cells such as monocytes and may play a pivotal role in a variety of pathological conditions, including acute coronary syndromes, thrombosis, sickle cell disease, diabetes, anti-phospholipid antibody syndrome, septic shock, and cancer.^{2,4,15-20} Furthermore, TF is detectable in macrophages, pericytes and adventitial fibroblasts of normal arteries.²¹

Inflammatory mediators such as tumor necrosis factor- α (TNF- α) and pro-thrombotic factors promoting thrombus formation (for example thrombin) have been shown to increase TF expression in vascular cells including EC and SMC.²²⁻²⁴ The regulation of TF transcription in EC and SMC, and circulating cells has been described extensively and involves numerous transcription factors such as activating protein-1 (AP-1) and nuclear factor- κ B (NF κ B).^{25,26} In order to identify individuals at risk of thrombosis and to design innovative therapeutic strategies inhibiting thrombus formation in the above-mentioned pathological conditions, it is crucial to identify key factors regulating TF expression and activity in EC and SMC.

LIM-only protein FHL2 is a member of the four and a half LIM (FHL) protein family and is composed of an N-terminal half LIM domain followed by four complete LIM domains.²⁷⁻³¹ LIM domains contain double zinc finger structures that mediate protein-protein interactions and, unlike other zinc finger structures, show no affinity for DNA. Rather, FHL2 has been shown to interact with a plethora of proteins including nuclear receptors such as Nur77, liver X receptors, androgen receptor, estrogen receptor, and other transcription factors such as AP-1 and NF κ B.²⁷⁻³¹ FHL2 is a multifunctional protein and acts as a transcriptional coactivator or corepressor in a cell- and context-dependent manner. Cumulative evidence shows that FHL2 is implicated in a range of physiological and pathological processes, such as cell proliferation, differentiation, migration, and apoptosis, bone formation, wound healing and inflammation.²⁷⁻³¹ FHL2 is highly expressed in vascular cells including EC and SMC,²⁸⁻³¹ which is relevant for the current study.

In this study, we investigated the impact of FHL2 on venous thrombosis using ferric chloride (FeCl₃)-induced vascular injury of murine mesenteric vessels. We also demonstrated that FHL2 inhibits TF expression and activity in EC and SMC. Insight into the molecular mechanisms governing this regulation involves evidence that FHL2 regulates TF gene expression in an AP-1- and NF κ B-dependent manner. Furthermore, we found that FHL2 physically interacts with TF, together modulating local thrombus formation in mice in response to vascular injury. Finally, we identified that the single nucleotide polymorphism (SNP) rs4851770 in the *FHL2* gene is associated with venous thrombosis in humans.

Methods

The methods are described in detail in the *Online Supplement*.

In vivo thrombosis in mesenteric veins

Five-week old male *FHL2*-knockout (KO) mice and respective wildtype (WT) littermate mice (C57BL/6; n=8 per group) were anesthetized by isoflurane (2% for induction, 1.6-1.8% to maintain anesthesia during imaging) and thrombus formation in the mesenteric veins was provoked as described previously.³² Animals were handled in accordance with national and European animal experimental protocols.

Cell culture and transfection

HEK293T, human umbilical vein endothelial cells (HUVEC), murine and human SMC, and murine macrophages were cultured as described previously.^{28-30,33,34} Human microvascular endothelial cells (HMEC-1) were cultured in MCDB131 medium (Gibco, Blijswijk, the Netherlands) supplemented with 10% fetal calf serum, epidermal growth factor, penicillin/streptomycin, and L-glutamine. The human endothelial cell line ECRF was cultured in EGM2 medium (Lonza, Basel, Switzerland).

Real-time polymerase chain reaction, western blot, protein stability and co-immunoprecipitation assays

Real-time polymerase chain reaction analysis, western blot, protein stability and co-immunoprecipitation assays were performed as described previously.^{28,29}

FHL2 knockdown

Recombinant lentiviral particles encoding *FHL2* and short hairpin RNA (shRNA) targeting *FHL2* were produced, concentrated, and titrated as described previously.²⁴

Tissue factor activity and luciferase assays

TF activity in HUVEC and SMC was assayed as previously described.³⁵

Luciferase assays were performed as described previously using TF-promoter luciferase reporter plasmids and full-length *FHL2* or *FHL2* variants.^{28,29,36}

Single nucleotide polymorphism association in patients with venous thromboembolism

To study the association between *FHL2* and VTE, a two-step validation study was designed, consisting of discovery and replication phases. For the discovery phase, 18 *FHL2* SNP (listed in Table 1) were tested. In collaboration with the International Network against Venous Thrombosis (INVENT) consortium, the association between these candidate SNP and venous thrombosis was assessed. Details about the design of the INVENT genome-wide association study have been previously published.³⁷ To obtain replication evidence, SNP rs4851770 ($P < 0.000201$) was selected for genotyping in The Thrombophilia, Hypercoagulability and Environmental Risks in Venous Thromboembolism (THE-VTE) case-control study including 676 patients with a first objectively diagnosed episode of deep venous thrombosis aged 18-70 years and 368 control subjects. This two-center, case-control study has been previously described.³⁸ Human studies were performed with patients' consent and approval from the institutional review boards of participating research centers and hospitals.

Statistical analysis

All statistical analyses were carried out with GraphPad Prism software (GraphPad Software, San Diego, CA, USA). Comparisons between two groups were done with the Student *t* test for unpaired variables. Comparisons between more than two

groups were tested by analysis of variance (ANOVA). Data are reported as mean ± standard deviation. *P* values <0.05 were considered statistically significant.

The *P* values obtained from the INVENT genome-wide association study were corrected using the Bonferroni adjustment. In the THE-VTE study, the association of the genotyped SNP with the risk of a first venous thrombosis was assessed by calculating odds ratios (OR) with corresponding 95% confidence intervals (95% CI) adjusted for age and sex, using SPSS (SPSS Inc, Chicago, IL, USA). Analyses were performed in the overall group of patients and after stratification into groups with provoked or unprovoked first venous thrombosis. An unprovoked venous thrombosis was defined as an event in the absence of surgery, plaster cast, injury,

immobilization for more than four consecutive days, hospitalization, pregnancy or postpartum status, or hormone use in the 3 months prior to the event.³⁷

Results

FHL2-deficient mice show enhanced thrombus formation upon vascular injury

We previously reported that FHL2 deficiency causes enhanced arterial lesion formation in the murine model of carotid artery ligation.³⁰ Interestingly, even 4 weeks after ligation, thrombus formation was observed in sections of

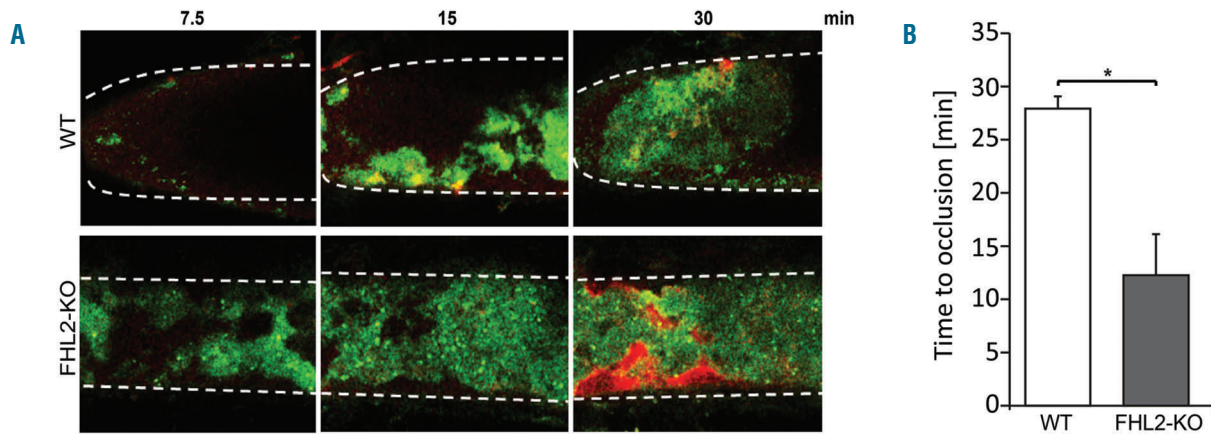


Figure 1. FHL2-deficient mice show enhanced thrombus formation upon vascular injury. Ferric chloride (FeCl₃)-induced thrombus formation in wildtype (WT) and FHL2-deficient (*FHL2*-KO) mice. (A) Representative photomicrographs are shown at different time points after injury in mesenteric vessels of WT and *FHL2*-KO mice. Platelets were visualized with a fluorescently labeled antibody (green) and labeled fibrinogen was injected to visualize fibrin formation in the thrombus (red). (B) The time to occlusion was assessed, revealing a 2.3-fold faster occlusion in *FHL2*-KO mice compared to WT animals. Data represent means ± standard deviation. **P*<0.05; n=8.

Table 1. FHL2 single nucleotide polymorphism analyses in the INVENT cohort.

Gene: <i>FHL2</i>	SNP	Chr:Pos	EA/NEA	BETA	SE	<i>P</i>
	rs11124029	2:105977761	G/A	0.032368	0.030102	0.282235
	rs3087523	2:105977776	G/A	-0.022763	0.035866	0.525667
	rs2278501	2:105979506	T/C	0.001005	0.023185	0.965399
	rs2278502	2:105979730	C/A	0.024248	0.024195	0.316255
	rs2576778	2:105982753	G/A	0.013155	0.02822	0.641123
	rs880427	2:105985228	G/A	0.024726	0.024537	0.313577
	rs4640402	2:105999009	A/C	0.011695	0.02346	0.618169
	rs4851765	2:106012632	T/C	0.030595	0.024279	0.207594
	rs11891016	2:106013216	C/T	0.031439	0.024313	0.195951
	rs11884297	2:106013248	C/T	-0.015773	0.025252	0.532232
	rs4374396	2:106024451	A/G	0.009225	0.023494	0.694594
	<i>rs2376740</i>	<i>2:106032291</i>	<i>C/T</i>	<i>-0.056017</i>	<i>0.02413</i>	<i>0.02028</i>
	<i>rs1914748</i>	<i>2:106035580</i>	<i>C/T</i>	<i>0.05547</i>	<i>0.023114</i>	<i>0.016425</i>
	rs4851770	2:106046333	C/T	-0.086598	0.023279	0.000201
	<i>rs6750100</i>	<i>2:106046789</i>	<i>A/G</i>	<i>0.056783</i>	<i>0.02598</i>	<i>0.028863</i>
	rs4851772	2:106051956	A/G	-0.005646	0.038529	0.883475
	rs7583367	2:106053343	G/T	-0.039482	0.023328	0.090562
	rs10177620	2:106083368	A/G	-0.031521	0.025241	0.211709

SNP: single nucleotide polymorphism. Chr:Pos: chromosome: position; EA_ effect allele; NEA: non-effect allele; SE: standard error SNP with a *P* value <0.05 are shown in italics. The SNP that is significantly associated after Bonferroni correction is in bold.

the ligated arteries in five of 14 *FHL2*-KO mice, whereas such structures were absent in the vascular lesions of WT mice (*data not shown*). We therefore hypothesized that *FHL2* may be involved in thrombus formation. To substantiate this hypothesis, we performed FeCl_3 -induced thrombosis experiments in WT and *FHL2*-KO mice. Upon

FeCl_3 -induced vascular injury, the blood flow in mesenteric veins was imaged by intravital microscopy to assess thrombus formation. Platelets were visualized with an anti-GPIIb β antibody and fluorescent fibrinogen was injected to monitor fibrin accumulation (Figure 1A). The time from vessel injury to formation of a stable occlusive

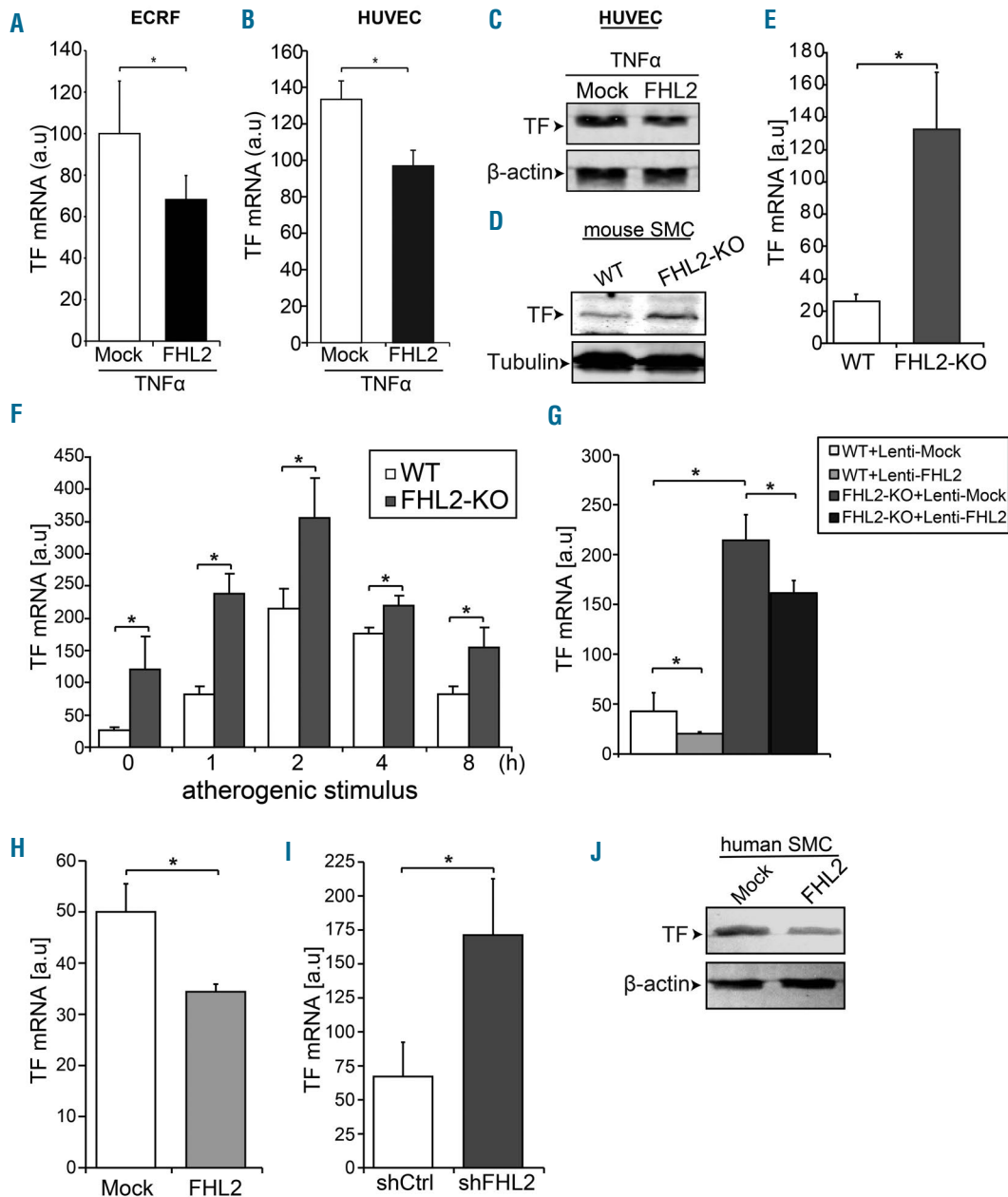


Figure 2. *FHL2* modulates tissue factor expression in endothelial cells and smooth muscle cells. (A) Tissue factor (TF) mRNA levels were determined by real-time quantitative polymerase chain reaction (qRT-PCR) in ECRF cells (A) and in human umbilical vein endothelial cells (HUVEC) (B) transduced with control lentivirus (Mock) or *FHL2*-encoding virus after treatment with tumor necrosis factor- α (TNF α) (C) Western blot analysis of TF protein expression in HUVEC following ectopic expression of *FHL2* and stimulation with TNF α . (D) Western blot analysis of TF in aortic smooth muscle cells (SMC) derived from wildtype (WT) and *FHL2*-knockout (KO) mice. Tubulin was used as a loading control. (E) To assess mRNA expression of TF in the aortic SMC isolated from WT and *FHL2*-KO mice, qRT-PCR was performed. (F) TF mRNA levels were determined by qRT-PCR in WT and *FHL2*-KO SMC stimulated with macrophage-conditioned medium (an atherogenic stimulus, see Methods) for the indicated time periods. (G) WT and *FHL2*-KO SMC were transduced with lentiviral particles encoding control (Mock) or *FHL2* and assayed for TF mRNA expression by qRT-PCR. (H) Gain-of-function and (I) knockdown of *FHL2* in human SMC, after which mRNA expression of TF was determined. Data represent means \pm standard deviation (SD). * $P < 0.05$. shCtrl, short-hairpin control. a.u., arbitrary units. (J) Human SMC were transduced with lentiviral particles encoding control (Mock) or *FHL2* and western blot analysis was performed to assess TF protein levels. In all qRT-PCR experiments acidic ribosomal phosphoprotein P0 was determined as an internal control for cDNA content of the samples and data are represented as means \pm SD. * $P < 0.05$. Western blot analyses were performed to assess TF protein levels and β -actin was used as a loading control. n=3

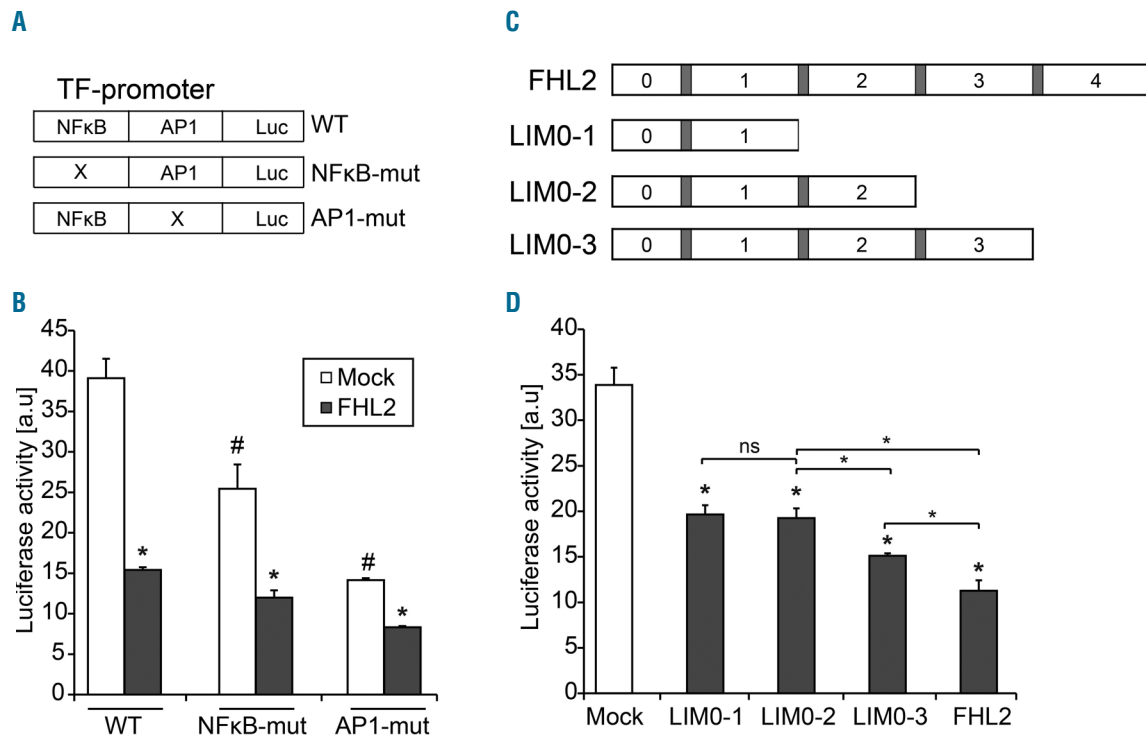


Figure 3. FHL2-mediated regulation of tissue factor promoter luciferase reporter. (A) Schematic representation of the normal (WT) and mutant human tissue factor (TF) promoter-reporter constructs that were used. (B) Transient co-transfection of 293T cells was performed with either TF-Luc (WT), NFκB mut-Luc and AP-1 mut-Luc in combination with either a control plasmid (Mock) or a plasmid encoding *FHL2* and luciferase activity was measured after stimulating the cells with phorbol myristate acetate (PMA). (C) Schematic representation of the *FHL2* variants that were tested. (D) The effect of *FHL2* variants on TF promoter activity was assayed following PMA stimulation in comparison with mock-plasmid transfected cells (Mock). Luciferase activity was normalized to Renilla. Data represent means ± standard deviation. **P*<0.05. a.u., arbitrary units. n=3

thrombus (time to occlusion) was 2.3-fold shorter in *FHL2*-KO mice, suggesting that FHL2 has an inhibitory function in thrombus formation following vascular injury (Figure 1B). Enhanced fibrin formation was observed in vessels of *FHL2*-KO animals and was visible as intense red fluorescence (*Online Supplementary Figure S4*). Since FeCl₃-induced thrombus formation involves TF expression and activity in the vessel wall,³⁹ we next studied the impact of FHL2 on this aspect in EC and SMC.

FHL2 deficiency enhances tissue factor expression

Given that TF expression in SMC is required for FeCl₃-induced vascular injury, we hypothesized that FHL2 may have a function in modulating TF expression in EC and SMC.⁴⁰ We therefore determined TF expression in the endothelial cell line ECRF and in HUVEC following over-expression of FHL2. Ectopic expression of FHL2 reduced TNFα-induced TF mRNA and protein expression in ECRF cells and HUVEC (Figure 2A-C; *Online Supplementary Figure S2A*). Similar results were observed in human microvascular endothelial cells (*data not shown*).

Next, we cultured SMC of WT and *FHL2*-KO mice and assessed the expression of TF. TF mRNA expression was significantly higher in SMC cultured from *FHL2*-KO than in those from WT mice (Figure 2D-E; *Online Supplementary Figure S2C*). The expression of TF in SMC was increased in response to a conditioned medium of macrophages stimulated with oxidized low density lipoproteins, which may be considered as an atherogenic stimulus.³⁵ Also under these conditions TF expression was higher in *FHL2*-

Table 2. Validation of results of the single nucleotide polymorphism rs4851770 in the THE VTE cohort.

	Patients	Controls	OR (95% CI)*
All			
TT	145 (21.5%)	84 (22.5%)	1 [ref]
CT	340 (50.4%)	200 (53.5%)	1.00 (0.72 – 1.38)
CC	190 (28.1%)	90 (24.1%)	1.21 (0.83 – 1.75)
Unprovoked			
TT	58 (17.3%)	84 (22.5%)	1 [ref]
CT	180 (53.6%)	200 (53.5%)	1.25 (0.82 – 1.89)
CC	98 (29.2%)	90 (24.1%)	1.53 (0.96 – 2.45)

OR: odds ratio; 95% CI: 95% confidence interval. *OR adjusted for age and sex.

KO SMC than in WT cells (Figure 2F). Subsequently, gain-of-function experiments were performed in both WT and *FHL2*-KO SMC (*FHL2* expression is shown in *Online Supplementary Figure S2D*). FHL2 downregulated TF expression in both WT and *FHL2*-KO SMC (Figure 2G). Similarly, in human SMC the expression of TF mRNA and protein decreased following ectopic FHL2 expression (Figure 2H, J; *Online Supplementary Figure S2B*), whereas knockdown of FHL2 in human SMC resulted in enhanced expression of TF mRNA (Figure 2I; FHL2 expression is shown in *Online Supplementary Figure S2E*). Furthermore, we confirmed increased TF expression in *FHL2*-KO mice in RNA samples from isolated carotid arteries after carotid artery ligation for 1, 2 and 4 weeks and in intact, isolated

mouse aorta to rule out confounding tissue culture-related effects (Online Supplementary Figure S3A, B). We also demonstrated that bone-marrow derived macrophages from *FHL2*-KO mice showed increased mRNA levels of TF under basal, lipopolysaccharide-, and interleukin-4-stimulated conditions compared to macrophages derived from WT mice (Online Supplementary Figure S3C). Together, these data indicate that FHL2 inhibits TF expression in EC, SMC and macrophages.

FHL2 regulates tissue factor expression through inhibition of nuclear factor κ B and activating protein-1

FHL2 does not bind DNA directly but is known to affect the activity of genuine transcription factors such as NF κ B and AP-1. The TF promoter contains functional binding motifs for NF κ B and AP-1.^{25,26} To elucidate the mechanism by which FHL2 suppresses transcription of the TF gene, we performed transient transfections with WT and mutant TF promoter-reporter constructs in HEK293T cells

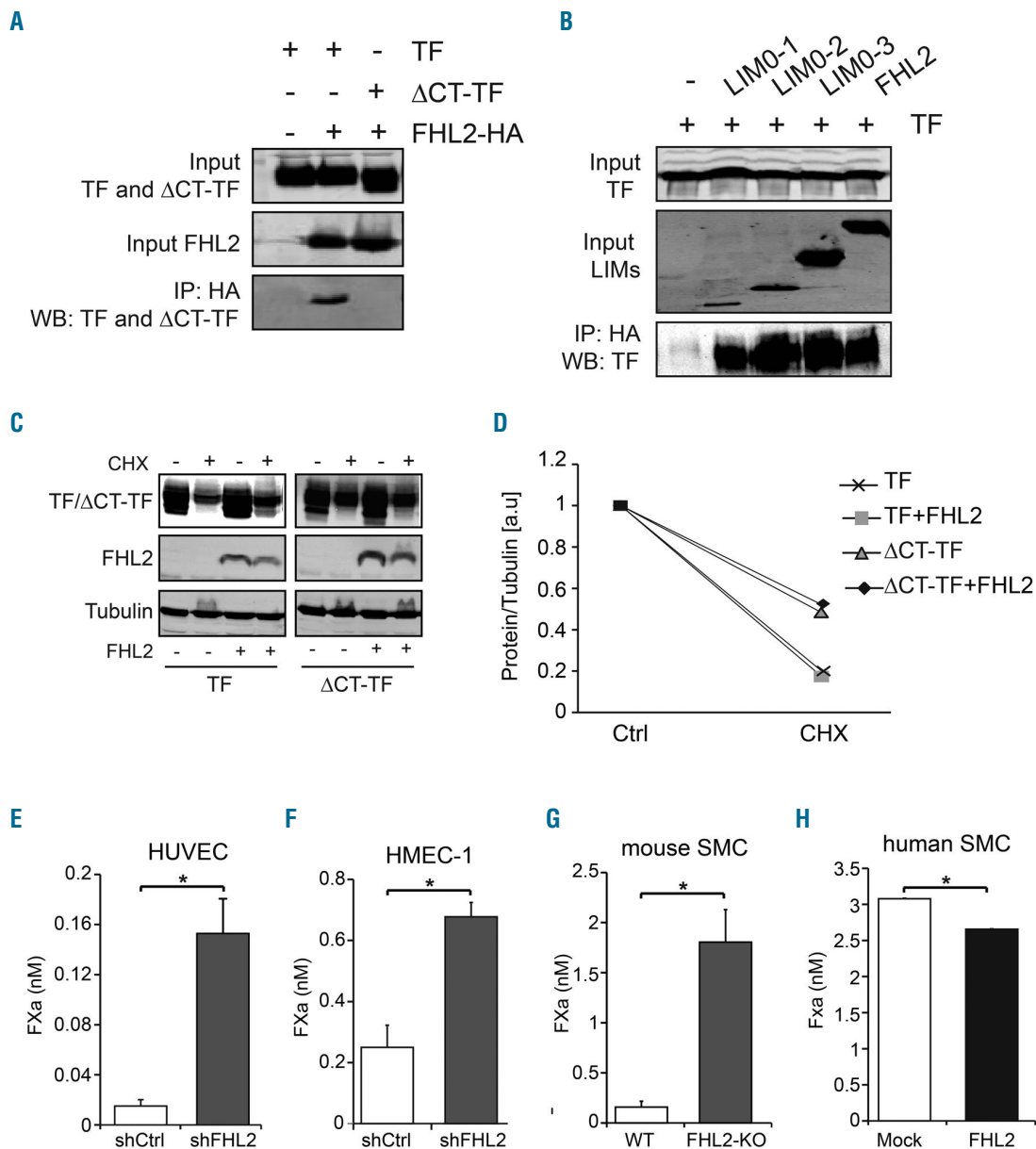


Figure 4. FHL2 physically interacts with tissue factor and inhibits tissue factor pro-coagulant activity. (A) HEK 293T cells were co-transfected with expression vectors encoding HA-tagged *FHL2* and full-length tissue factor (TF) or TF lacking the intracellular cytoplasmic TF domain (Δ CT-TF), as indicated. Whole cell extracts were immunoprecipitated using the anti-HA antibody (IP: HA) and analyzed by western blotting (WB) with an anti-TF antibody (WB: TF and Δ CT-TF). Input of TF (Input TF and Δ CT-TF) and FHL2 (Input FHL2) were revealed on a separate blot. (B) HEK293T cells were co-transfected with expression vectors encoding HA-tagged *FHL2* variants and TF, as indicated. After immunoprecipitation with the anti-HA antibody (IP: HA) the samples were analyzed by western blotting with anti-TF antibody (WB: TF). Input samples were probed for *FHL2* variants (Input LIMs) and TF (Input TF). (C, D) HEK293T cells were transfected with expression plasmids coding for TF or Δ CT-TF with or without FHL2. Cells were treated with cycloheximide (CHX) to block *de novo* protein synthesis for 16 h. Tubulin was used as the loading control. Western blot analysis (C) and quantification of western blots (D); a.u., arbitrary units. (E, F) Human umbilical vein endothelial cells (HUVEC) and human micro-vascular endothelial cells (HMEC-1) were transduced with lentivirus encoding control shRNA (shCtrl) or shFHL2 followed by serum-starvation and treatment with tumor necrosis factor- α (TNF α). The generation of activated factor X (FXa) was measured. (G) FXa generation was assayed in smooth muscle cells (SMC) derived from WT and FHL2-KO mice following treatment with ionomycin. (H) FXa generation was assayed in human SMC upon ectopic expression of FHL2 or transduced with control lentivirus (Mock) and treatment with TNF α . n=3.

(Figure 3A). FHL2 expression decreased the luciferase activity of the WT TF-promoter reporter (Figure 3B). TF promoter constructs with either a disrupted NF κ B response element or a mutated AP-1 element exhibited lower basal luciferase activity (Figure 3B) and FHL2-mediated inhibition of luciferase activity of the WT-promoter (61%) was stronger than that of the NF κ B- or AP-1-mutated promoter (52% and 43%, respectively) (Figure 3B). These data suggest that FHL2 affects the transcriptional activity of both NF κ B and AP-1 to downregulate TF-promoter activity in these cells. To assess whether activation of EC affects cellular localization of FHL2, we stimulated EC with TNF- α (50 ng/mL) and observed enhanced nuclear localization, which may contribute to the changed modulation of transcription factor activity by FHL2 (*Online Supplementary Figure S4*). To determine which domain of FHL2 is essential to inhibit TF-promoter activity, deletion mutants of FHL2²⁸ (Figure 3C) were tested in TF-promoter luciferase assays. The first one and a half LIM-domain (LIM0-1) already exhibited partial inhibition (41%) with the LIM0-2 variant having similar effects, while LIM0-3 (55% inhibition) and FHL2 were more potent inhibitors of TF-promoter activity (Figure 3D). Of note, overexpression of individual LIM domains of FHL2 had no effect on TF promoter activity (*data not shown*) indicating that at least one and a half LIM domains of FHL2 are required to elicit decreased TF-promoter activity.

FHL2 physically interacts with tissue factor

To investigate whether inhibition of TF by FHL2 is also attributable to this latter's physical interaction with TF, we performed co-immunoprecipitation experiments. Full-length TF co-immunoprecipitated efficiently with HA-tagged FHL2 from whole cell extracts using an anti-HA antibody (Figure 4A), whereas Δ CT-TF, which lacks the intracellular cytoplasmic TF domain, failed to bind FHL2 (Figure 4A), indicating that FHL2 requires the relatively short cytoplasmic tail of TF for its interaction. Pull-down assays using FHL2 deletion mutants (Figure 3C) revealed that all variants of FHL2 bind TF (Figure 4B). It is known that FHL2 can enhance protein stability and to measure

the effect of FHL2 on TF protein stability, we exposed cells to cycloheximide and determined the half-life of full-length TF and Δ CT-TF mutant proteins. The Δ CT-TF variant was more stable than full-length TF, but TF protein levels were not influenced by FHL2 (Figure 4C, D). We concluded that FHL2 interacts with TF but does not affect TF protein stability.

FHL2 modulates tissue factor procoagulant activity

Having established that FHL2 interacts with TF and regulates TF expression in EC and SMC, we sought to examine the impact of FHL2 on the activity of TF in cultured EC and murine and human SMC, by assessing the potential of these cells to generate factor Xa (FXa). Knockdown of FHL2 in HUVEC and HMEC-1 resulted in enhanced TNF α -induced FXa generation compared to control (Figure 4E, F). In a similar fashion, FHL2-deficient mouse SMC showed higher ionomycin-induced FXa generation than WT SMC (Figure 4G). Ectopic expression of FHL2 resulted in a modest decrease of TNF α -induced FXa generation compared to that of control-transduced cells (Figure 4H). Of note, following FHL2 knockdown in HMEC-1, we found, in the same cell lysates, that TF protein levels were increased 1.5-fold and that FXa generation was increased even more, 3-fold (*Online Supplementary Figure S5A, B*). These data indicate that FHL2 may regulate TF activity partly by binding the intracellular domain of TF and by modulating TF gene expression. Figure 5 is a schematic summary of our data.

Genetic variation in the FHL2 gene is associated with venous thrombosis in humans

Having established that FHL2 reduces TF activity in EC and SMC, we reasoned that genetic variation in FHL2 may affect venous thrombosis in man. We therefore analyzed 18 FHL2 SNP and venous thrombosis risk in the INVENT consortium (Table 1). We observed that the FHL2 polymorphism rs4851770 was associated with thrombosis risk with a *P*-value of 2×10^{-4} , even after correction for multiple testing. No association was found between other tested SNP in the FHL2 gene and risk of venous thrombosis

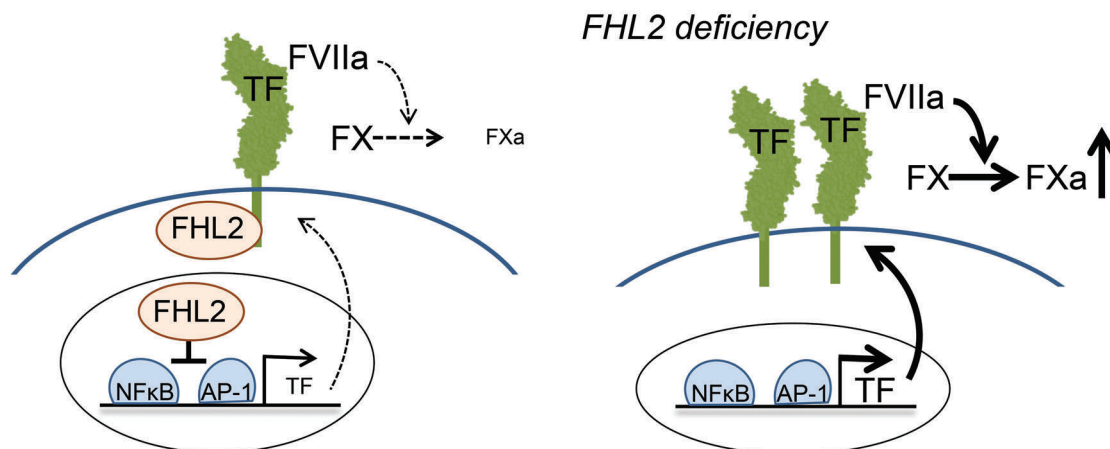


Figure 5. Schematic representation of FHL2 function in the modulation of tissue factor activity. The left panel shows the normal situation in which FHL2 inhibits tissue factor (TF) expression in activated endothelial cells (EC) and smooth muscle cells (SMC), whereas the right panel represents the effect of FHL2 deficiency, which results in enhanced TF expression and increased activity.

(Table 1). Next, we sought for replication in the THE-VTE study. Individuals homozygous for the rs4851770C allele had a mildly increased risk of venous thrombosis compared with individuals homozygous for the T-allele (OR: 1.2; 95% CI: 0.7-1.4). The risk of idiopathic venous thrombosis was more pronounced (OR:1.53 (95% CI: 0.96 - 2.45) (Table 2).

Discussion

Thrombosis-associated pathologies, such as VTE, myocardial infarction and stroke, are major causes of morbidity and mortality worldwide. TF is a key player in the extrinsic pathway of coagulation¹⁴ and although many experimental studies have helped us to understand the coagulation process, the regulation of TF expression and activity is incompletely understood. In the current study, we demonstrated that deficiency of FHL2 exacerbates thrombus formation in response to FeCl₃-induced vascular injury. We revealed that FHL2 inhibits the expression of TF in activated vascular cells, including EC and SMC. Furthermore, we showed that FHL2 interacts with the intracellular domain of TF and inhibits TF activity. Additionally, we found that the *FHL2* rs4851770 polymorphism is associated with venous thrombosis in humans.

We previously demonstrated that *FHL2*-KO mice develop larger SMC-rich lesions in the murine carotid artery ligation model and here we observed that these lesions comprised, even 4 weeks after ligation, more thrombi than lesions in WT mice.³⁰ The carotid artery ligation model is, however, not suitable for quantitative assessment of changes in venous thrombosis. For that reason, in this study we used the FeCl₃-induced vascular injury model and established that *FHL2*-KO mice do indeed show exacerbated venous thrombus formation compared to WT mice.

SMC are the major source of TF in the FeCl₃-induced model of vascular injury. Although there are some contrasting data on TF expression in EC, many studies demonstrated that TF is highly induced in endothelium under inflammatory conditions. Moreover, enhanced activity of TF is transient and directly correlates with increased mRNA levels.^{22,24} In the current study we found that overexpression of FHL2 inhibits TF expression, whereas FHL2 deficiency results in higher TF levels and activity. These observations were corroborated in HUVEC and microvascular HMEC-1 cells indicating that FHL2-mediated regulation of TF is not limited to larger vessels but may also occur in microvessels.

Thrombin is generated after TF exposure and is known to promote vascular neointima formation through multiple mechanisms, including activation of platelets and induction of SMC proliferation.^{41,42} Given that FHL2 inhibits SMC proliferation^{28,30} and our current observation that the level of active TF is increased in SMC deficient in FHL2, we hypothesize the following mechanism: in *FHL2*-KO mice enhanced TF expression promotes thrombin generation that in turn accelerates SMC proliferation causing enhanced lesion formation in the carotid artery ligation model. In addition to increased TF expression levels, we also observed that *FHL2*-KO SMC produce more pro-inflammatory cytokines than WT SMC, which may

also contribute to the pro-thrombotic phenotype of *FHL2*-KO mice (*data not shown*). Further studies are warranted to investigate the hypothesis that thrombin actually mediates the increased SMC-rich lesion formation observed in *FHL2*-KO mice.

It is well established that the human *TF* gene contains binding sites for the transcription factors NFκB, AP-1, Sp-1 and Egr-1.^{25,26} Interestingly, it has been reported that FHL2 is associated with these four transcription factors in multiple cell types in distinct contexts.^{29,31,43} Here, we demonstrated that FHL2 regulates TF-promoter activity through modulation of both NFκB and AP-1. The relative contribution of FHL2 in regulation of the activity of Egr-1 and Sp1 on the TF promoter is difficult to assess, because deletion of the respective response elements completely abrogates the activity of this promoter, as has been shown before. We found that FHL2 physically interacts with full-length TF, but not with the cytoplasmic tail-deleted mutant of TF (ΔCT-TF) indicating that FHL2 interacts intracellularly at the cell membrane with TF. This finding may relate to the interaction of FHL2 with several integrin units such as α_vβ₁, which form a complex with TF.^{44,45} It is not unlikely that FHL2 either stabilizes or abolishes the integrin α_vβ₁-TF complex, thereby affecting downstream signaling. Further studies are required to investigate the exact role of FHL2 in such TF complexes.

We explored the association between *FHL2* polymorphisms (Table 1) and venous thrombosis risk demonstrating that rs4851770 is associated. FHL2 was not previously known as a direct thrombo-modulator, although it has been shown to modulate the thrombosis-associated genes PAI-1⁴⁶ and eNOS.⁴⁷ At present, we can only speculate on the functional implication of the *FHL2* polymorphism rs4851770 in venous thrombosis. We postulate that this polymorphism affects the binding of specific transcription factors on the *FHL2* promoter, resulting in modulation of FHL2 expression and, as a consequence, regulates TF activity.

In summary, we demonstrated that FHL2 is a novel regulator of TF in vascular EC and SMC. Furthermore, we report that FHL2 regulates TF promoter activity partly through NFκB and AP-1. Finally, we showed that FHL2 physically interacts with full-length TF. This work reinforces the biological significance of FHL2 as a regulator of venous thrombosis, which may be of significance to identify individuals at risk of VTE, and suggest that enhancement of FHL2 expression may even be a target for intervention.

Acknowledgments

We thank Kamran Bakhtiari and Joost C.M. Meijers (Dept. of Plasma Proteins, Sanquin Research, Amsterdam, the Netherlands) for assistance with the TF activity assays. We also thank Dr. Nigel Mackman (University of North Carolina) for TF-promoter luciferase reporter plasmids.

Funding

This work was supported by the research program of the BioMedical Materials Institute, co-funded by the Dutch Ministry of Economic Affairs as a part of Project P1.02 NEXTREAM. This work was also supported by the Rembrandt Institute for Cardiovascular Research (RICS grant 2013), the Netherlands CardioVascular Research Initiative: the Dutch Heart Foundation (CVON: 2012-08) and the Dutch Lung Foundation (5.2.17.198JO).

References

- Raskob GE, Angchaisuksiri P, Blanco AN, et al. Thrombosis: a major contributor to the global disease burden. *J Thromb Haemost*. 2014;12(10):1580-1590.
- Aras O, Shet A, Bach RR, et al. Induction of microparticle- and cell-associated intravascular tissue factor in human endotoxemia. *Blood*. 2004;103(12):4545-4553.
- Cimmino G, Ciccarelli G, Golino P. Role of tissue factor in the coagulation network. *Semin Thromb Hemost*. 2015;41(7):708-717.
- Kakkar AK, DeRuvo N, Chinswangwatanakul V, Tebbutt S, Williamson RC. Extrinsic-pathway activation in cancer with high factor VIIa and tissue factor. *Lancet*. 1995;346(8981):1004-1005.
- Lijfering WM, Rosendaal FR, Cannegieter SC. Risk factors for venous thrombosis - current understanding from an epidemiological point of view. *Br J Haematol*. 2010;149(6):824-833.
- Rosendaal FR. Venous thrombosis: a multi-causal disease. *Lancet*. 1999;353(9159):1167-1173.
- Drake TA, Cheng J, Chang A, Taylor FB, Jr. Expression of tissue factor, thrombomodulin, and E-selectin in baboons with lethal *Escherichia coli* sepsis. *Am J Pathol*. 1993;142(5):1458-1470.
- Lupu C, Westmuckett AD, Peer G, et al. Tissue factor-dependent coagulation is preferentially up-regulated within arterial branching areas in a baboon model of *Escherichia coli* sepsis. *Am J Pathol*. 2005;167(4):1161-1172.
- Song D, Ye X, Xu H, Liu SF. Activation of endothelial intrinsic NF- κ B pathway impairs protein C anticoagulation mechanism and promotes coagulation in endotoxemic mice. *Blood*. 2009;114(12):2521-2529.
- Pawlinski R, Mackman N. Cellular sources of tissue factor in endotoxemia and sepsis. *Thromb Res*. 2010;125 Suppl 1:S70-S73.
- Posma JJ, Posthuma JJ, Spronk HM. Coagulation and non-coagulation effects of thrombin. *J Thromb Haemost*. 2016;14(10):1908-1916.
- Breitenstein A, Tanner FC, Luscher TF. Tissue factor and cardiovascular disease: quo vadis? *Circ J*. 2010;74(1):3-12.
- Gertz SD, Fallon JT, Gallo R, et al. Hirudin reduces tissue factor expression in neointima after balloon injury in rabbit femoral and porcine coronary arteries. *Circulation*. 1998;98(6):580-587.
- Moons AH, Levi M, Peters RJ. Tissue factor and coronary artery disease. *Cardiovasc Res*. 2002;53(2):313-325.
- Speidel CM, Eisenberg PR, Ruf W, Edgington TS, Abendschein DR. Tissue factor mediates prolonged procoagulant activity on the luminal surface of balloon-injured aortas in rabbits. *Circulation*. 1995;92(11):3323-3330.
- van der Wal AC, Li X, de Boer OJ. Tissue factor expression in the morphologic spectrum of vulnerable atherosclerotic plaques. *Semin Thromb Hemost*. 2006;32(1):40-47.
- Lopez-Pedraza C, Buendia P, Barbarroja N, Siendones E, Velasco F, Cuadrado MJ. Antiphospholipid-mediated thrombosis: interplay between anticardiolipin antibodies and vascular cells. *Clin Appl Thromb Hemost*. 2006;12(1):41-45.
- Khechai F, Ollivier V, Bridey F, Amar M, Hakim J, de Prost D. Effect of advanced glycation end product-modified albumin on tissue factor expression by monocytes. Role of oxidant stress and protein tyrosine kinase activation. *Arterioscler Thromb Vasc Biol*. 1997;17(11):2885-2890.
- Reverter JC, Tassies D, Font J, et al. Hypercoagulable state in patients with antiphospholipid syndrome is related to high induced tissue factor expression on monocytes and to low free protein s. *Arterioscler Thromb Vasc Biol*. 1996;16(11):1319-1326.
- Solovey A, Gui L, Key NS, Heibel RP. Tissue factor expression by endothelial cells in sickle cell anemia. *J Clin Invest*. 1998;101(9):1899-1904.
- Osterud B, Bjorklid E. Sources of tissue factor. *Semin Thromb Hemost*. 2006;32(1):11-23.
- Colucci M, Balconi G, Lorenzet R, et al. Cultured human endothelial cells generate tissue factor in response to endotoxin. *J Clin Invest*. 1983;71(6):1893-1896.
- Nawroth PP, Handley DA, Esmen CT, Stern DM. Interleukin 1 induces endothelial cell procoagulant while suppressing cell-surface anticoagulant activity. *Proc Natl Acad Sci U S A*. 1986;83(10):3460-3464.
- Scarpati EM, Sadler JE. Regulation of endothelial cell coagulant properties. Modulation of tissue factor, plasminogen activator inhibitors, and thrombomodulin by phorbol 12-myristate 13-acetate and tumor necrosis factor. *J Biol Chem*. 1989;264(34):20705-20713.
- Mackman N. Regulation of the tissue factor gene. *FASEB J*. 1995;9(10):883-889.
- Mackman N, Morrissey JH, Fowler B, Edgington TS. Complete sequence of the human tissue factor gene, a highly regulated cellular receptor that initiates the coagulation protease cascade. *Biochemistry*. 1989;28(4):1755-1762.
- Johannessen M, Moller S, Hansen T, Moens U, Van GM. The multifunctional roles of the four-and-a-half-LIM only protein FHL2. *Cell Mol Life Sci*. 2006;63(3):268-284.
- Kurakula K, Sommer D, Sokolovic M, et al. LIM-only protein FHL2 is a positive regulator of liver X receptors in smooth muscle cells involved in lipid homeostasis. *Mol Cell Biol*. 2015;35(1):52-62.
- Kurakula K, van der Wal E, Geerts D, van Tiel CM, de Vries CJ. FHL2 protein is a novel co-repressor of nuclear receptor Nur77. *J Biol Chem*. 2011;286(52):44336-44343.
- Kurakula K, Vos M, Otermin Rubio I, et al. The LIM-only protein FHL2 reduces vascular lesion formation involving inhibition of proliferation and migration of smooth muscle cells. *PLoS One*. 2014;9(4):e94931.
- Tran MK, Kurakula K, Koenis DS, de Vries CJ. Protein-protein interactions of the LIM-only protein FHL2 and functional implications of the interactions relevant in cardiovascular disease. *Biochim Biophys Acta*. 2016;1863(2):219-228.
- Kuijpers MJ, de Witt S, Nergiz-Unal R, et al. Supporting roles of platelet thrombospondin-1 and CD36 in thrombus formation on collagen. *Arterioscler Thromb Vasc Biol*. 2014;34(6):1187-1192.
- de Vries CJ, van Achterberg TA, Horrevoets AJ, ten Cate JW, Pannekoek H. Differential display identification of 40 genes with altered expression in activated human smooth muscle cells. Local expression in atherosclerotic lesions of smags, smooth muscle activation-specific genes. *J Biol Chem*. 2000;275(31):23939-23947.
- Kurakula K, Vos M, van Eijk M, Smits HH, de Vries CJ. LIM-only protein FHL2 regulates experimental pulmonary *Schistosoma mansoni* egg granuloma formation. *Eur J Immunol*. 2015;45(11):3098-3106.
- van den Hengel LG, Osanto S, Reitsma PH, Versteeg HH. Murine tissue factor coagulant activity is critically dependent on the presence of an intact allosteric disulfide. *Haematologica*. 2013;98(1):153-158.
- Mackman N, Fowler BJ, Edgington TS, Morrissey JH. Functional analysis of the human tissue factor promoter and induction by serum. *Proc Natl Acad Sci U S A*. 1990;87(6):2254-2258.
- Germain M, Chasman DI, de Haan H, et al. Meta-analysis of 65,734 individuals identifies TSPAN15 and SLC44A2 as two susceptibility loci for venous thromboembolism. *Am J Hum Genet*. 2015;96(4):532-542.
- van Hyleckama Vlieg A, Baglin CA, Luddington R, MacDonald S, Rosendaal FR, Baglin TP. The risk of a first and a recurrent venous thrombosis associated with an elevated D-dimer level and an elevated thrombin potential: results of the THE-VTE study. *J Thromb Haemost*. 2015;13(9):1642-1652.
- Kuijpers MJ, Munnix IC, Cosemans JM, et al. Key role of platelet procoagulant activity in tissue factor- and collagen-dependent thrombus formation in arterioles and venules in vivo differential sensitivity to thrombin inhibition. *Microcirculation*. 2008;15(4):269-282.
- Wang L, Miller C, Swarthout RE, Rao M, Mackman N, Taubman MB. Vascular smooth muscle-derived tissue factor is critical for arterial thrombosis after ferric chloride-induced injury. *Blood*. 2009;113(3):705-713.
- Martorell L, Martinez-Gonzalez J, Rodriguez C, Gentile M, Calvayrac O, Badimon L. Thrombin and protease-activated receptors (PARs) in atherothrombosis. *Thromb Haemost*. 2008;99(2):305-315.
- Oltrona L, Speidel CM, Recchia D, Wickline SA, Eisenberg PR, Abendschein DR. Inhibition of tissue factor-mediated coagulation markedly attenuates stenosis after balloon-induced arterial injury in minipigs. *Circulation*. 1997;96(2):646-652.
- Guo Z, Zhang W, Xia G, et al. Sp1 upregulates the four and half lim 2 (FHL2) expression in gastrointestinal cancers through transcription regulation. *Mol Carcinog*. 2010;49(9):826-836.
- Dorfleutner A, Hintermann E, Tarui T, Takada Y, Ruf W. Cross-talk of integrin α 3 β 1 and tissue factor in cell migration. *Mol Biol Cell*. 2004;15(10):4416-4425.
- Wixler V, Geerts D, Laplantine E, et al. The LIM-only protein DRAL/FHL2 binds to the cytoplasmic domain of several alpha and beta integrin chains and is recruited to adhesion complexes. *J Biol Chem*. 2000;275(43):33669-33678.
- Xia T, Levy L, Levillayer F, et al. The four and a half LIM-only protein 2 (FHL2) activates transforming growth factor β (TGF- β) signaling by regulating ubiquitination of the E3 ligase Arkadia. *J Biol Chem*. 2013;288(3):1785-1794.
- Hayashi H, Nakagami H, Takami Y, et al. FHL-2 suppresses VEGF-induced phosphatidylinositol 3-kinase/Akt activation via interaction with sphingosine kinase-1. *Arterioscler Thromb Vasc Biol*. 2009;29(6):909-914.



Ferrata Storti Foundation

Placenta-derived extracellular vesicles induce preeclampsia in mouse models

Cha Han,^{1,2*} Chenyu Wang,^{3*} Yuanyuan Chen,¹ Jiwei Wang,⁴ Xin Xu,² Tristan Hilton,² Wei Cai,³ Zilong Zhao,⁵ Yingang Wu,⁶ Ke Li,¹ Katie Houck,² Li Liu,⁵ Anil K. Sood,⁷ Xiaoping Wu,² Fengxia Xue,¹ Min Li,^{3*} Jing-fei Dong^{2,8} and Jianning Zhang⁵

¹Department of Obstetrics and Gynecology, Tianjin Medical University General Hospital, Tianjin, China; ²Bloodworks Research Institute, Seattle, WA, USA; ³Institute of Pathology, School of Medical Sciences and Gansu Provincial Key Laboratory of Preclinical Study for New Drug Development, Lanzhou University, Lanzhou, China; ⁴Department of Neurosurgery, Tianjin Key Laboratory of Cerebral Vascular and Neurodegenerative Diseases, Tianjin Huanhu Hospital, Tianjin, China; ⁵Department of Neurosurgery, Tianjin Medical University General Hospital and Tianjin Neurological Institute, Tianjin, China; ⁶Department of Neurosurgery, the First Affiliated Hospital, Division of Life Sciences and Medicine, University of Science and Technology of China, Hefei, China; ⁷Department of Gynecologic Oncology and Reproductive Medicine, Division of Surgery, MD Anderson Cancer Center, University of Texas, Houston, TX, USA and ⁸Division of Hematology, Department of Medicine, University of Washington, School of Medicine, Seattle, WA, USA.

*CH and CW contributed equally as co-first author.

Haematologica 2020
Volume 105(6):1686-1694

Correspondence:

MIN LI
limin@lzu.edu.cn

JIANING ZHANG
jianningzhang@hotmail.com

JING-FEI DONG
jfdong@bloodworksnw.org

Received: May 6, 2019.

Accepted: August 22, 2019.

Pre-published: August 22, 2019.

doi:10.3324/haematol.2019.226209

Check the online version for the most updated information on this article, online supplements, and information on authorship & disclosures: www.haematologica.org/content/105/6/1686

©2020 Ferrata Storti Foundation

Material published in Haematologica is covered by copyright. All rights are reserved to the Ferrata Storti Foundation. Use of published material is allowed under the following terms and conditions:

<https://creativecommons.org/licenses/by-nc/4.0/legalcode>.

Copies of published material are allowed for personal or internal use. Sharing published material for non-commercial purposes is subject to the following conditions:

<https://creativecommons.org/licenses/by-nc/4.0/legalcode>,

sect. 3. Reproducing and sharing published material for commercial purposes is not allowed without permission in writing from the publisher.



ABSTRACT

Preeclampsia is a pregnancy-induced condition that impairs the mother's health and results in pregnancy termination or premature delivery. Elevated levels of placenta-derived extracellular vesicles (pcEV) in the circulation have been consistently associated with preeclampsia, but whether these vesicles induce preeclampsia or are the product of preeclampsia is not known. Guided by a small cohort study of preeclamptic patients, we examined the impact of pcEV on the pathogenesis of preeclampsia in mouse models. We detected pcEV in pregnant C56BL/6J mice with a peak level of $3.8 \pm 0.9 \times 10^7$ /mL at 17-18 days post-coitum. However, these pregnant mice developed hypertension and proteinuria only after being infused with vesicles purified from injured placenta. These extracellular vesicles released from injured placenta disrupted endothelial integrity and induced vasoconstriction. Enhancing the clearance of extracellular vesicles prevented the development of the extracellular vesicle-induced preeclampsia in mice. Our results demonstrate a causal role of pcEV in preeclampsia and identify microvesicle clearance as a new therapeutic strategy for the treatment of this pregnancy-associated complication.

Introduction

Preeclampsia is a pregnancy-induced pathology characterized by poor placentation and endothelial dysfunction. Its primary clinical presentations include new-onset hypertension and proteinuria that resolve or are significantly improved after delivery or pregnancy termination.^{1,2} Preeclampsia can progress into eclampsia, potentially resulting in maternal and fetal death. Extensive clinical and laboratory studies have demonstrated that preeclampsia is triggered by placenta-derived mediators³ produced after placental ischemia and reperfusion injury, which could result from placental spiral artery remodeling disorders.^{4,5} One of these mediators is placenta-derived extracellular vesicles (pcEV), which are released into the maternal circulation, typically reaching a peak level in late pregnancy.^{6,8} These pcEV are constitutively released during normal pregnancy and are necessary for inducing maternal adaptive changes such as tolerance.⁹ However, excessive shedding of pcEV often indicates placental pathologies that contribute to the pathogenesis of preeclampsia.

Significantly elevated plasma levels of pcEV have been consistently associated with the development and severity of preeclampsia.^{10,11}

The pcEV found in patients with preeclampsia are heterogeneous in their cells of origin, size, and cargo contents, and thus possess diverse activities, some of which may not be apparent or detectable in their parental cells. Despite this heterogeneity, extracellular vesicles (EV) from syncytiotrophoblasts are widely used as the surrogate marker for detecting pcEV in the maternal circulation,^{12,13} even though there is no evidence in the literature that these pcEV directly cause preeclampsia. Placental cells vesiculate when the placenta is subjected to ischemic and hypoxic injuries that result in cell apoptosis and tissue necrosis.¹⁴⁻¹⁷ These injuries can also occur when trophoblasts are unable to infiltrate the wall of the placenta's spiral artery to gradually replace the endothelium in a process called "blood vessel recasting".¹⁴⁻¹⁷

Once released into the circulation, pcEV can cause endothelial injury,¹⁸⁻²⁰ systemic inflammation,^{21,22} and coagulation dysfunction,²³ all of which are hallmark events of preeclampsia. Despite extensive studies on the causes and mechanisms of placental injuries, key questions remain as to whether pcEV released from injured placenta directly induce the hypertension and proteinuria that define preeclampsia or are merely the products of preeclampsia. If the former holds true, could accelerating or enhancing the clearance of pcEV prevent preeclampsia or reduce its severity? Here we report the results of a study designed to answer these questions by analyzing blood samples from preeclamptic patients, studying new mouse models of preeclampsia, and conducting *in vitro* experiments.

Methods

Study of patients

Pregnant women were recruited from Tianjin Medical University General Hospital after they had given informed consent to participate in the study. Blood samples were collected from patients with preeclampsia at the diagnosis of their condition, before the administration of magnesium sulfate or anti-hypertensive medications, and analyzed for plasma levels of pcEV (*Online Supplementary Methods*). This study was approved by the Ethics Committee of Tianjin Medical University General Hospital.

Mouse models

We used three complementary models to study the role of pcEV in the development of preeclampsia (*Online Supplementary Methods*). The first model was designed to study whether increasing circulating pcEV in pregnant mice induced preeclampsia. For this study, we defined a mouse preeclampsia phenotype by hypertension, proteinuria, and kidney injury.¹ Blood pressure (BP) was measured at baseline, 17-18 days post-coitum (dpc), and 7-10 days postpartum using a noninvasive mouse tail-cuff BP analyzer (CODA; Kent Scientific Co., Torrington, CT, USA).²⁴ Urinary albumin and creatinine concentrations in a pooled urine sample collected over a 24-h period were measured and their ratio was calculated to define proteinuria (*Online Supplementary Methods*). The second model was used to study whether pcEV induced hypertension and proteinuria in non-pregnant C57BL/6J female mice. BP was measured 30 min after the pcEV infusion and 24 h urine samples were analyzed for proteinuria. The third model was used to specifically investigate the role of EV clearance.

Flow cytometry

Levels of pcEV in plasma samples from women with a normal pregnancy or preeclampsia were measured using a fluorescein isothiocyanate-conjugated antibody against placental alkaline phosphatase (PLAP; LifeSpan Biosciences, Inc., Seattle, WA, USA).^{11,14,20,25} For the mouse study, we used syncytin as the marker for pcEV because PLAP is not expressed in mouse placenta (*Online Supplementary Methods*).²⁶

Hematologic measurements

We used three tests to measure the procoagulant activity of pcEV: (i) a phosphatidylserine (PS)-dependent plasma-clotting assay that specifically measured microvesicle-mediated coagulation (*Online Supplementary Methods*);²⁷ (ii) platelet activation; and (iii) detection of plasma levels of the anionic phospholipid PS-expressing EV. Platelet activation and PS⁺ EV were detected by, respectively, a phycoerythrin-CD62p antibody (eBiosciences) and allophycocyanin-annexin V (eBiosciences) using flow cytometry.^{27,28}

Vascular leakage

We used an Evans blue extravasation test to measure pcEV-induced vascular leakage *in vivo* (*Online Supplementary Methods*).²⁸ We also measured the ability of pcEV to disrupt the integrity of cultured cells from the mouse endothelial line bEnd.3 (ATCC, Manassas, VA, USA) (*Online Supplementary Methods*).^{27,29}

Microvesicle-induced vasoconstriction and changes in cerebral blood flow

We measured vascular wall tension using a modified protocol (*Online Supplementary Methods*).³⁰ We also used non-invasive laser speckle contrast analysis (LASCA) technology to measure the impact of pcEV on cerebral blood flow. Cerebral blood flow was chosen because LASCA cannot accurately measure the blood flow of internal organs such as the kidney without surgery, which would have been a confounding injury that would have been difficult to stratify.

Statistical analysis

Quantitative data are expressed as percentages for categorical (frequency) variables or as the mean \pm standard error of the mean for continuous variables. For parametric data, a Shapiro-Wilk test was performed to test the distribution of the data. Data were analyzed using a paired *t*-test or one-way or repeated-measures analysis of variance, as specified for each dataset. A *P* value of less than 0.05 was considered to be statistically significant. For multiple comparisons, the Holm-Sidak method was used to control for family-wise error rate (Sigma plot V. 11.2).

Results

Placenta-derived extracellular vesicles were detected in preeclamptic women and pregnant mice

Among the 17 pregnant women (all first pregnancies) recruited into the study, ten were diagnosed as having preeclampsia between 28 and 38 weeks of gestation. Their information is listed in Table 1. Patients were excluded from the study if they had baseline hypertension and diabetes, developed pregnancy-associated diabetes, or were diagnosed as having eclampsia or HELLP syndrome. The women with preeclampsia developed hypertension and proteinuria and had earlier deliveries as compared to the women with normal pregnancies. Using PLAP as the surrogate marker, pcEV were detected in peripheral blood sam-

ples from all 17 pregnant women, but their levels were significantly higher in the preeclamptic patients than in the women with normal pregnancies at comparable gestational ages (Figure 1A). The levels of pcEV in patients with preeclampsia returned to the baseline during the postpartum period (Figure 1B).

This study of patients had a limited ability to investigate the underlying mechanisms of preeclampsia because it lacked manipulability of the clinical course and required extensive stratification of confounding clinical variables. To address these limitations, we conducted a mechanistic study in mouse models. We measured plasma levels of pcEV in pregnant mice using syncytin as the surrogate marker. Consistent with human data, plasma pcEV were detected in pregnant mice, reaching peak levels at 17-18 dpc, and rapidly returning to baseline during the postpartum period (Figure 1C-F). PcEV detection by the syncytin antibody was further validated using another placental marker, endoglin (Online Supplementary Figure S1). The levels of syncytin on pcEV were closely correlated with the

levels of annexin V⁺ microvesicles ($R^2 = 0.766$, $P < 0.001$) (Online Supplementary Figure S2), suggesting that most syncytin⁺ pcEV expressed anionic phospholipids. However,

Table 1. Clinical information of the pregnant women included in the study.

	PE	Normal pregnancy	P value*
Number	10	7	
Age (years) (mean±SD)	33.1 ± 4.2	31.4 ± 4.7	0.219
Time of blood drawing (day)	233 ± 21	233 ± 20	0.989
Systolic BP (mmHg)	166 ± 14	122 ± 7	< 0.001
Diastolic BP (mmHg)	104 ± 9	77 ± 8	< 0.001
Proteinuria (g/24 h)	5.37 ± 4.4	0.01 ± 0.0	< 0.001
Time of delivery (day)**	239 ± 23	270 ± 9	0.003

*Student t-test; **Nine of the ten women with preeclampsia had a Cesarean delivery, whereas all women with normal pregnancies had natural vaginal delivery. PE: preeclampsia; SD: standard deviation; BP: blood pressure.

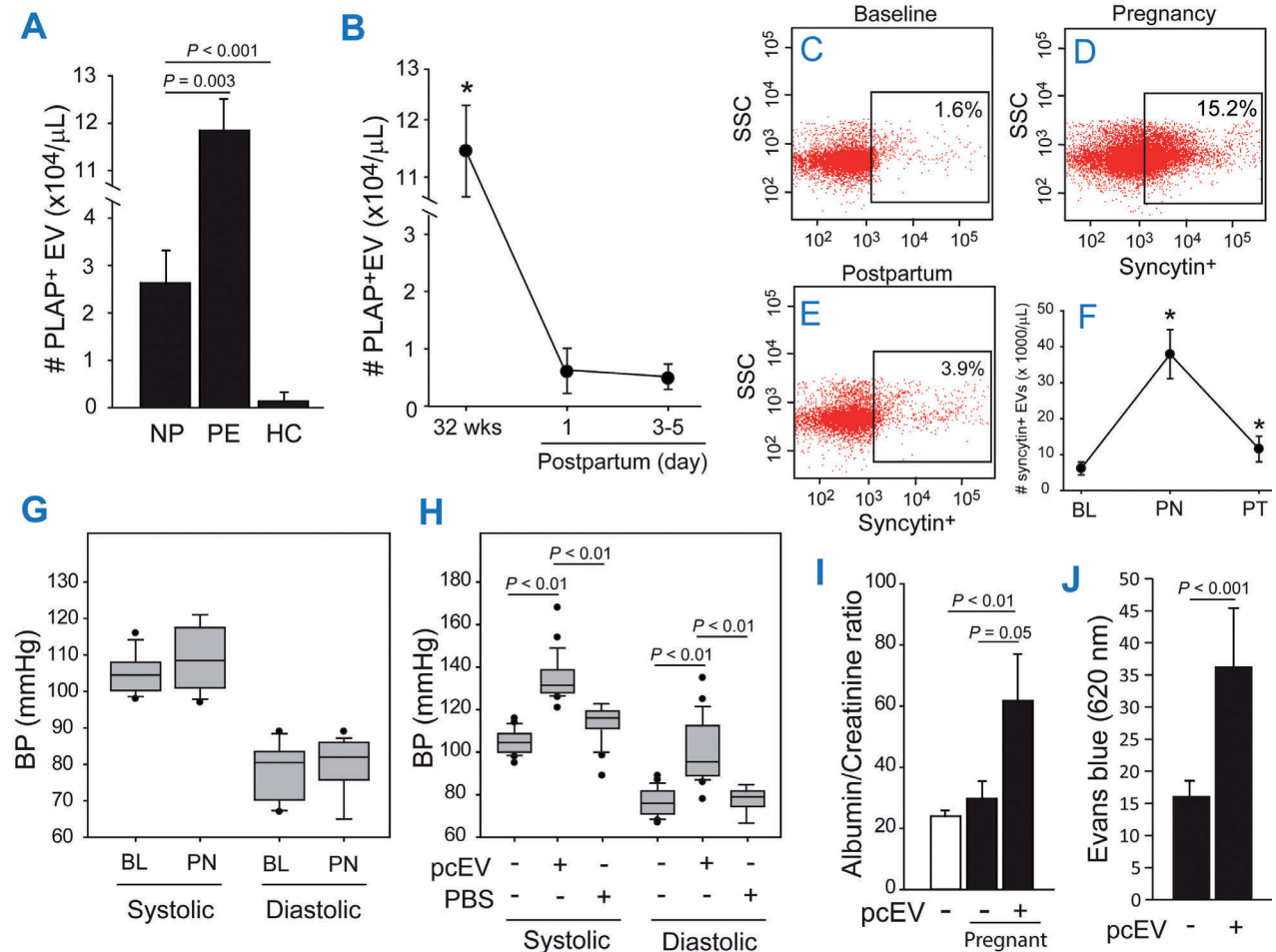


Figure 1. Placenta-derived extracellular vesicles in women with preeclampsia and in pregnant mice. (A) Plasma levels of placental alkaline phosphatase (PLAP)⁺ pcEV in women with normal pregnancy (NP, n=7), patients with preeclampsia (PE, n=10), and non-pregnant women (HC, n=5) (one-way analysis of variance, ANOVA). (B) Plasma levels of PLAP⁺ pcEV of PE patients at 32 weeks of pregnancy and during the postpartum period (one-way ANOVA with Tukey test, n=10, * $P < 0.01$ vs. postpartum). (C-E) Longitudinal changes of plasma syncytin⁺ pcEV of pregnant mice at baseline (BL), at 17-18 days post-coitus (dpc) (PN) and postpartum (PT). (C-E): Cytometry dot plots from a pregnant mouse. (F) Summary from 15 mice (one-way ANOVA, * $P < 0.001$, vs. BL and PT). (G) Blood pressure (BP) of C57BL/6J mice at BL and 17-18 dpc (n=30, paired t test). (H) BP and (I) proteinuria of pregnant C57 BL/6J mice (17-18 dpc) after infusion with 1×10^7 /mouse of pcEV (n=32, one-way ANOVA). (J) Renal vascular leakage detected by an Evans blue extravasation test in pregnant C57BL/6J mice infused with 1×10^7 pcEV/mouse or PBS (n=8, paired t test).

these pregnant mice did not develop hypertension or proteinuria. The levels of circulating pcEV in pregnant mice reached peak levels of $3.8 \pm 0.9 \times 10^7/\text{mL}$ (Figure 1F), which were comparable to those found in women with normal pregnancies ($2.6 \pm 1.3 \times 10^7/\text{mL}$), but significantly lower than those in the women with preeclampsia ($1.2 \pm 0.3 \times 10^8/\text{mL}$) (Figure 1A). We therefore intravenously infused pregnant mice with a single dose of pcEV ($1 \times 10^7/\text{mouse}$) purified from injured placenta. The pcEV generated using this protocol were similar to those detected in the peripheral blood of pregnant mice in terms of size and syncytin expression,³¹ but they expressed a higher level of anionic phospholipids

detected by annexin V (Online Supplementary Figure S3). The pregnant mice infused with injury-produced pcEV developed hypertension (Figure 1H) 30 min after the infusion and proteinuria was detected in urine samples collected over 24 h after the pcEV infusion (Figure 1I). The hypertension was not caused by an expansion of volume due to the pcEV infusion ($100 \mu\text{L}/\text{mouse}$), as an equal volume of phosphate-buffered saline (PBS) induced minimal BP changes. Consistent with the development of proteinuria, vascular leakage was detected by Evans blue extravasation in the kidneys of pregnant mice infused with pcEV (Figure 1J). These data demonstrate that a high level of circulating

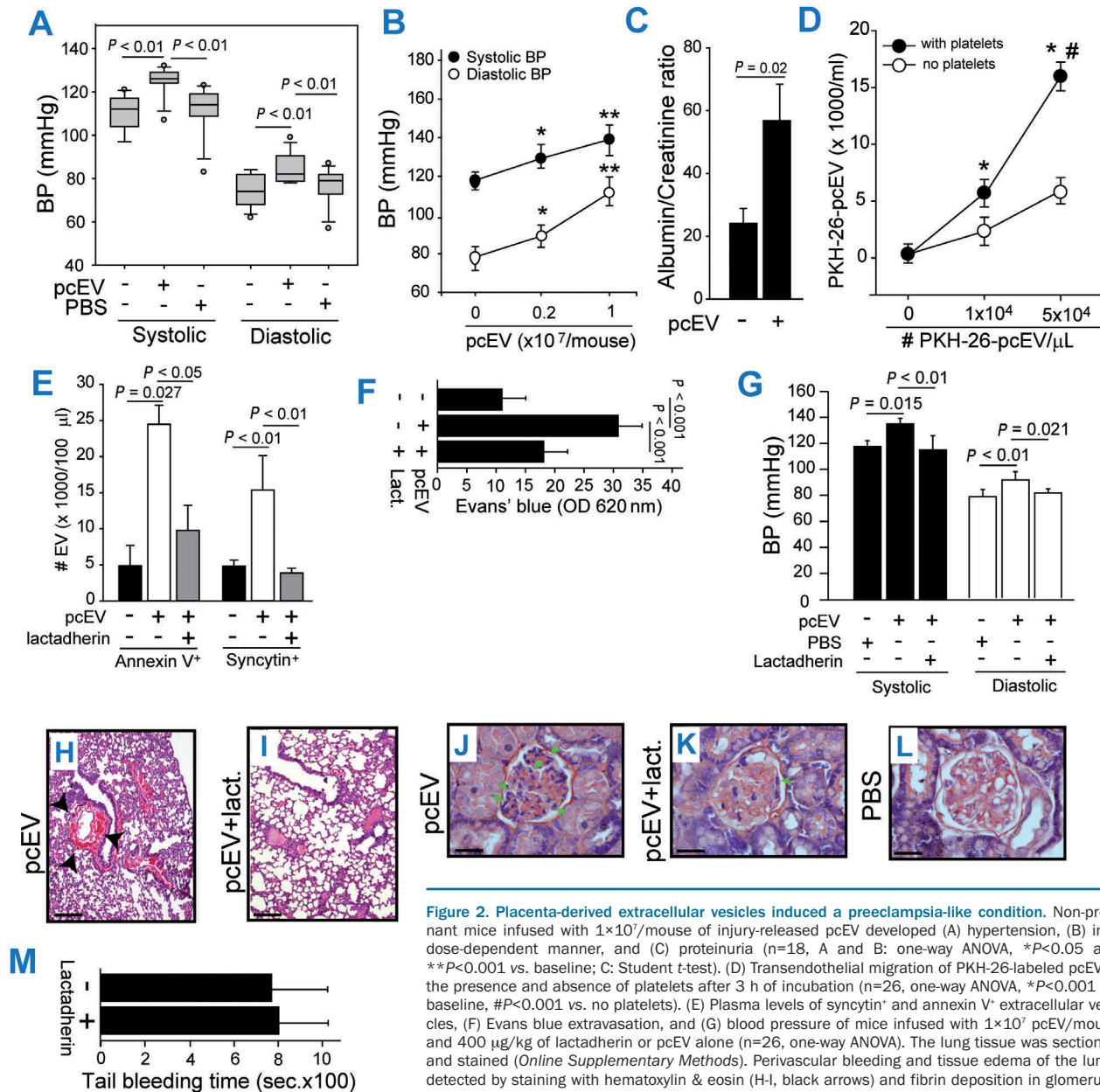


Figure 2. Placenta-derived extracellular vesicles induced a preeclampsia-like condition. Non-pregnant mice infused with $1 \times 10^7/\text{mouse}$ of injury-released pcEV developed (A) hypertension, (B) in a dose-dependent manner, and (C) proteinuria ($n=18$, A and B: one-way ANOVA, $*P < 0.05$ and $**P < 0.001$ vs. baseline; C: Student t-test). (D) Transendothelial migration of PKH-26-labeled pcEV in the presence and absence of platelets after 3 h of incubation ($n=26$, one-way ANOVA, $*P < 0.001$ vs. baseline, $\#P < 0.001$ vs. no platelets). (E) Plasma levels of syncytin⁺ and annexin V⁺ extracellular vesicles, (F) Evans blue extravasation, and (G) blood pressure of mice infused with 1×10^7 pcEV/mouse and 400 $\mu\text{g}/\text{kg}$ of lactadherin or pcEV alone ($n=26$, one-way ANOVA). The lung tissue was sectioned and stained (Online Supplementary Methods). Perivascular bleeding and tissue edema of the lungs detected by staining with hematoxylin & eosin (H-I, black arrows) and fibrin deposition in glomerular capillaries shown by phosphotungstic acid hematoxylin stain (J-L, green arrows) in pcEV-infused mice given lactadherin or phosphate-buffered saline (PBS) (representative images from 26 mice). (M) Tail bleeding of pcEV-infused mice given lactadherin or PBS ($n=26$, Student t-test). BP: blood pressure; EV: extracellular vesicles; Lact: lactadherin; OD: optical density.

pcEV from injured placenta could induce a preeclampsia-like phenotype in pregnant mice.

Placenta-derived extracellular vesicles directly induced hypertension and proteinuria

To examine the effect of pcEV specifically, without the confounding influences of pregnancy, we infused pcEV from injured placenta into non-pregnant C57 BL/6J female mice. These mice developed acute hypertension 30 min after the pcEV infusion in a dose-dependent manner (Figure 2A, B) and proteinuria was detected in 24-h urine samples (Figure 2C). Furthermore, these pcEV disrupted the integrity of cultured endothelial cells, especially in the presence of platelets (Figure 2D). These data suggest that pcEV can directly induce a preeclampsia-like phenotype, independent of other pregnancy-induced changes.

We then investigated whether the microvesicle-scavenging factor lactadherin²⁸ could prevent or reduce this

pcEV-induced preeclampsia-like condition. Mice infused with pcEV along with 400 µg/kg of lactadherin had lower levels of circulating annexin V⁺ microvesicles, including pcEV (Figure 2E), reduced renal vascular leakage (Figure 2F), and did not develop hypertension (Figure 2G), in contrast to mice that received pcEV alone. Lactadherin also prevented the perivascular bleeding and tissue edema found in the lungs of pcEV-infused mice (Figure 2H, I) and reduced the pcEV-induced hypercoagulable state that was defined by a shortened clotting time (Online Supplementary Figure S4A), platelet activation (Online Supplementary Figure S4B), the elevated level of annexin V⁺ EV (Online Supplementary Figure S4C), and extensive fibrin deposition in the glomerular capillary (Figure 2J, K), without prolonging the tail bleeding time (Figure 2M) or changing blood-cell counts and hematocrit (Online Supplementary Figure S5). The livers from mice infused with pcEV, but not those from mice infused with PBS, showed focal tissue necrosis

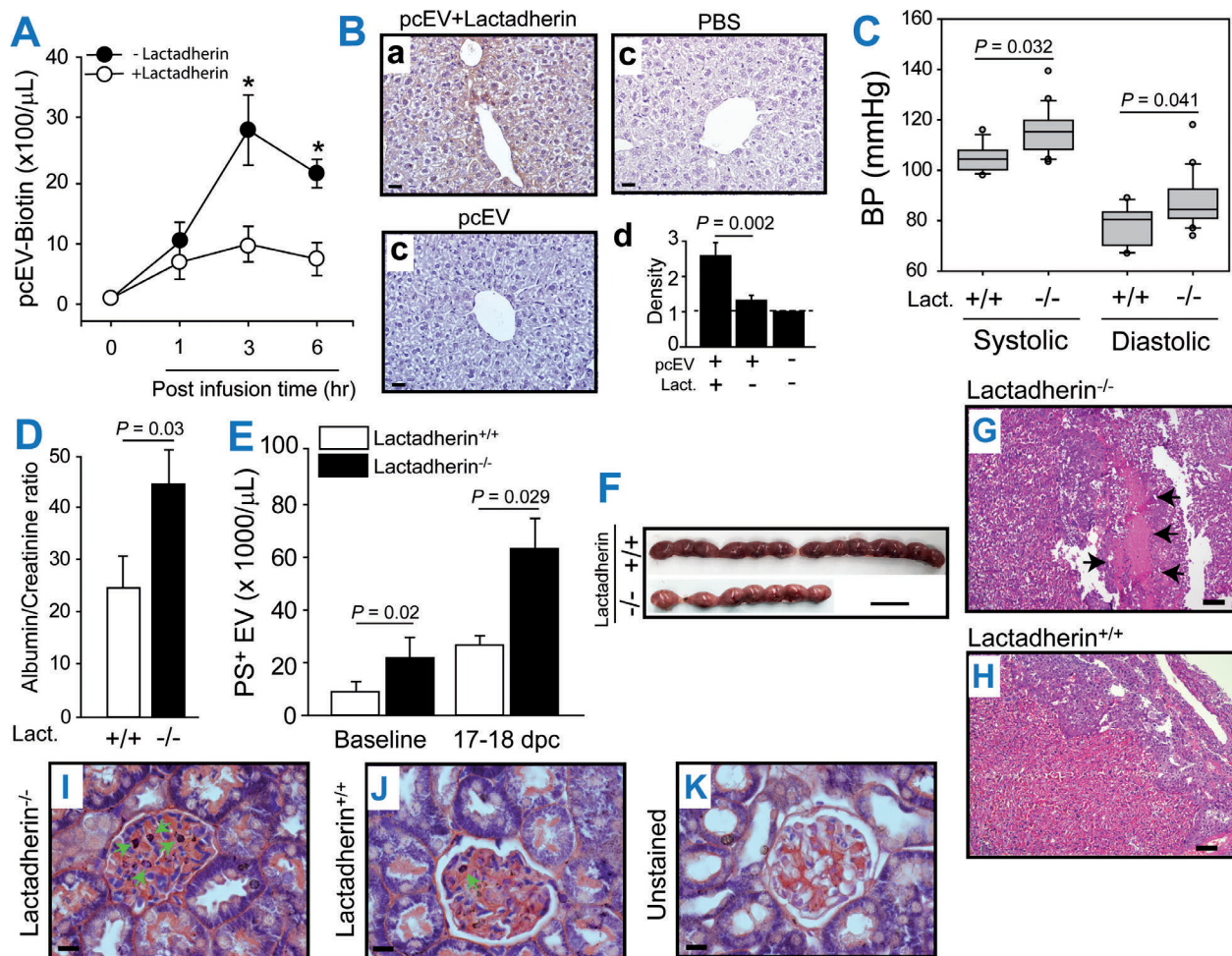


Figure 3. Prevention of a placenta-derived extracellular vesicle-induced preeclampsia-like condition by lactadherin. (A) Plasma levels of biotinylated pcEV in C57BL/6J mice infused with 1x10⁷/mouse of pcEV alone or combined with 400 µg/kg of lactadherin [n=10, one-way analysis of variance (ANOVA), *P<0.01 vs. baseline (BL)]. (B) Horseradish peroxidase streptavidin-stained liver tissue from mice infused with biotinylated pcEV alone, biotinylated pcEV in combination with lactadherin, and phosphate-buffered saline (a-c: representative images, d: optical densities of tissue scans, n=19, one-way ANOVA). (C) Blood pressure and (D) proteinuria of lactadherin^{-/-} and lactadherin^{+/+} mice measured at 17-18 days post-coitus (dpc) (n=8-24, Student t-test). (E) Plasma levels of phosphatidylserine⁺ microvesicles measured at BL and 17-18 dpc (n=16, Student t-test). (F) Placenta from lactadherin^{-/-} and lactadherin^{+/+} mice after 17-18 dpc. (G, H) Placenta at 17-18 dpc from lactadherin^{-/-} (G), not lactadherin^{+/+} (H) mice showing tissue necrosis (black arrows, bar = 100 µm). (I, J) Phosphotungstic acid hematoxylin stain for fibrin deposition in the glomerular capillaries of lactadherin^{-/-} mice (I, green arrows indicate fibrin) and not lactadherin^{+/+} mice (J). (K) Unstained background control. Images are representative of 39 mice. BP: blood pressure; PS: phosphatidylserine.

and infiltration by inflammatory cells; these changes were not detected in pcEV-infused mice that also received lactadherin (*Online Supplementary Figure S6*). In contrast to kidney tissues, intravascular fibrin deposition was very limited in the livers of pcEV-infused mice.

To measure directly whether lactadherin enhanced pcEV clearance, biotinylated pcEV (1×10^7 /mouse) were infused into non-pregnant C57BL/6J mice along with 400 $\mu\text{g}/\text{kg}$ of lactadherin or an equal volume of PBS. The plasma level of biotinylated pcEV reached a plateau 3 h after infusion (Figure 3A) but was significantly lower in mice that also received lactadherin (Figure 3A). The mice given pcEV and lactadherin had more extensive accumulation of biotinylated pcEV in their livers (Figure 3B).

Lactadherin-deficient mice developed unprovoked preeclampsia during pregnancy

To further validate the role of lactadherin in promoting EV clearance and preventing preeclampsia, we also exam-

ined lactadherin^{-/-} mice and their wildtype littermates (*Online Supplementary Figure S7*). At 17-18 dpc, lactadherin^{-/-} mice had higher BP (Figure 3C) and developed proteinuria (Figure 3D) without pcEV infusion, as required for pregnant C57BL/6J mice (Figure 1H). Plasma levels of PS-expressing EV recognized by annexin V were significantly higher in lactadherin^{-/-} mice than in their wildtype littermates at baseline, and they increased further during pregnancy (Figure 3E). There was no visible difference in the appearance of the fetuses and sizes of placenta between lactadherin^{-/-} and lactadherin^{+/+} mice at 17-18 dpc (*Online Supplementary Figure S8*), but the number of lactadherin^{-/-} litters was significantly less than the number of lactadherin^{+/+} litters (8.2 ± 1.7 vs. 11.5 ± 1.4 , Student *t*-test, $P < 0.05$) (Figure 3F). Hematoxylin & eosin stains of placental tissues frequently detected tissue necrosis in the trophoblast villi and decidua of lactadherin^{-/-} mice (Figure 3G,H). The lactadherin deficiency also resulted in more extensive fibrin deposition in glomerular capillaries, which occurred less in wildtype littermates (Figure 3I-K).

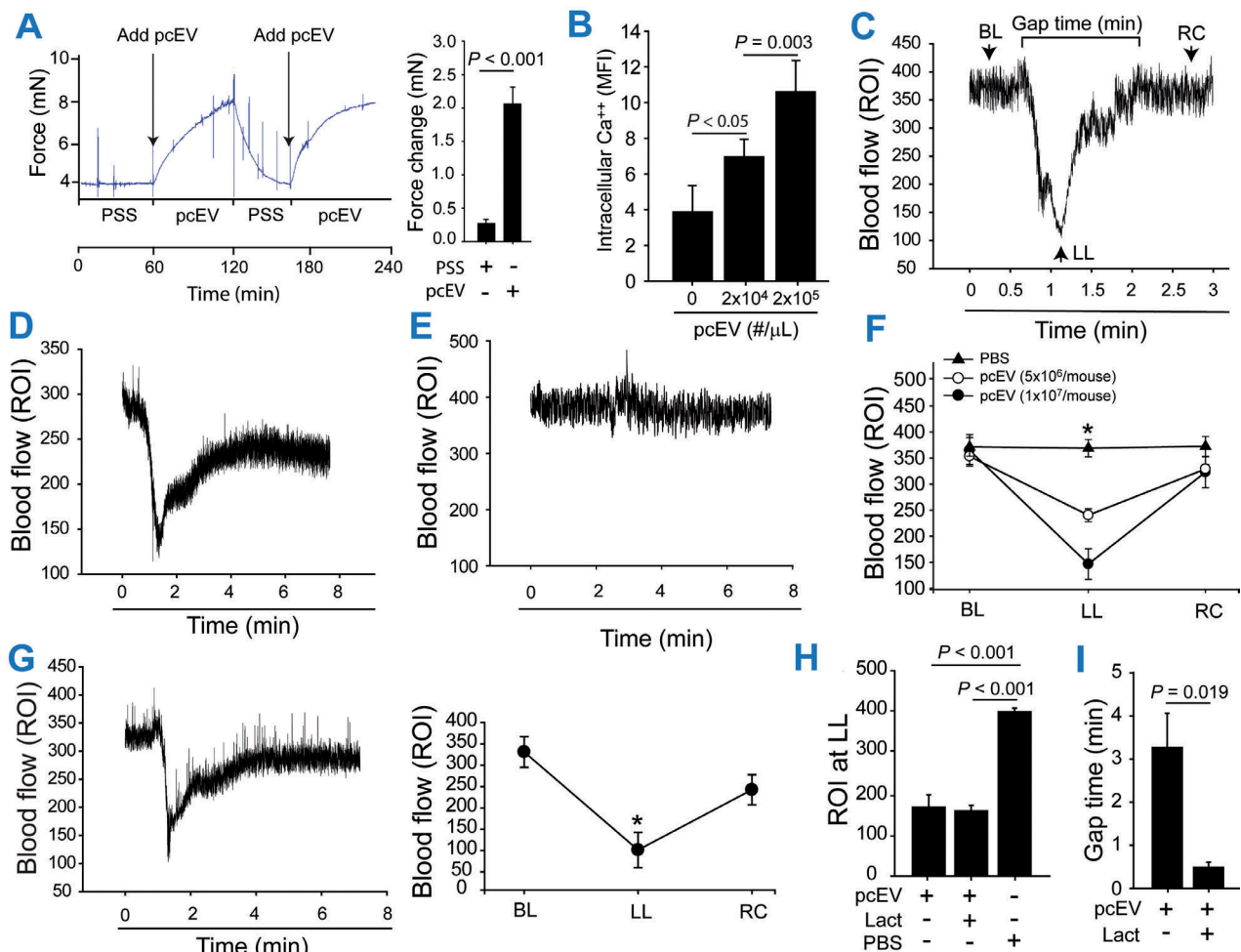


Figure 4. Placenta-derived extracellular vesicles induced vasoconstriction. (A) Placenta-derived extracellular vesicles (pcEV) ($2 \times 10^5/\mu\text{L}$) increase the vascular tension of the carotid artery (left: a myograph of pcEV-induced vasoconstriction; right: summary of effects in 20 experiments, Student *t*-test). (B) Calcium influx of cultured smooth muscle cells treated with pcEV [$n=12$, one-way analysis of variance (ANOVA)]. (C-F) pcEV (1×10^7 /mouse) but not phosphate-buffered saline (PBS) rapidly reduced cerebral blood flow as determined by laser speckle contrast analysis (LASCA) (BL: baseline; LL: lowest level, gap-time of flow reduction; and RC: flow recovery). The reduction is either fully (C) or partially (D) recovered (C-E: representative graphs; F: summary of 12 experiments, one-way ANOVA). (G) The cerebral blood flow of mice receiving extracellular vesicles purified from patients with preeclampsia (top: a representative graph, bottom: summary of 3 experiments, one-way ANOVA, $*P < 0.001$ vs. BL). The LL values (H) and gap-time (I) of pcEV-infused mice that also received 400 $\mu\text{g}/\text{kg}$ lactadherin or PBS ($n=12$, one-way ANOVA on ranks). ROI: region of interest; Lact: lactadherin.

Taken together, these results demonstrate that enhancing EV clearance prevented pcEV-induced hypertension, vascular leakage, and hypercoagulation.

Placenta-derived extracellular vesicles induced vasoconstriction

We used three complementary experiments to investigate how pcEV induce hypertension. First, pcEV increased the wall tension of the carotid artery (Figure 4A). The vasoconstriction was relaxed to the baseline level upon removal of pcEV and was induced again after reincubation with pcEV. Second, pcEV triggered the calcium influx of cultured smooth-muscle cells in a dose-dependent manner (Figure 4B). Third, a single-dose infusion of pcEV but not PBS induced a rapid and dose-dependent reduction of cerebral blood flow (Figure 4C-F). The reduction was transient, and the blood flow quickly recovered to either the pre-infusion level (Figure 4C) or a persistently low level (Figure 4D). This pcEV-induced reduction in blood flow was also detected in mice infused with total EV purified from plasma of patients with preeclampsia (Figure 4G). Lactadherin (400 $\mu\text{g}/\text{kg}$) given together with pcEV did not prevent the reduction of blood flow (Figure 4H) but significantly shortened its duration (Figure 4I). These data demonstrate that pcEV directly induced vasoconstriction by mobilizing intracellular calcium, resulting in the systemic reduction in microvascular blood flow.

Discussion

We have investigated the role of pcEV in the pathogenesis of preeclampsia by examining plasma samples from preeclamptic women, studying mouse models, and conducting *in vitro* experiments. Consistent with previous reports,^{10,11} we detected pcEV in blood samples of women in the late stage of pregnancy, but pcEV levels were significantly higher in patients with preeclampsia (Figure 1A) and rapidly returned to baseline during the postpartum period (Figure 1B). These clinical findings led us to study the activity of pcEV in new mouse models. These new mouse models offered advantages over previously used models because they did not require surgery, genetic manipulation, or pharmacological interventions. We made several novel observations that collectively define a causal role of pcEV in the pathogenesis of preeclampsia and a means to prevent it.

First, pregnant mice developed hypertension and proteinuria only after intravenous infusion of pcEV from injured placenta (Figures 1H), suggesting that preeclampsia can be induced either by a high level of circulating pcEV or by pcEV derived from injured placenta. Our results support the latter possibility because pcEV from injured placenta caused a preeclampsia-like condition in non-pregnant mice at a significantly lower number of 1×10^7 vesicles/mouse (Figure 2A, B) than the $3.8 \pm 0.9 \times 10^7$ vesicles/mouse found in pregnant mice (Figure 1F). These pcEV from injured placenta were similar in size and syncytin expression to those found in pregnant mice, but expressed a significantly high level of anionic phospholipids recognized by annexin V. These anionic phospholipids were strongly procoagulant and could also disrupt the integrity of the endothelium. In addition, syncytiotrophoblast EV from women with preeclampsia carry less endothelial nitric oxide synthase compared to those from

women with normal pregnancies²⁵ and thus have a reduced synthesis of the vasodilating factor nitric oxide. The fast development of hypertension in non-pregnant mice infused with pcEV (30 min after infusion) (Figures 2 and 3) is likely caused by the quick infusion of a large quantity of pcEV (< 5 min). In contrast, pcEV are probably released gradually during pregnancy and induce hypertension when they reach a critical threshold level in the circulation over a longer period of time.

Second, pcEV disrupted the endothelial barrier *in vitro*, especially in the presence of platelets to induce vascular leakage (Figure 2D), which could be responsible for pcEV-induced proteinuria (Figures 1I and 2C). The synergistic activity between pcEV and platelets is consistent with a recent study showing that EV activate maternal platelets to promote inflammation and a preeclampsia-like pathology,³² but how platelets enhance pcEV-induced endothelial injury remains to be investigated. Nevertheless, the pcEV-induced endothelial injury not only results in vascular leakage, but could also contribute to the development of hypertension by impairing the endothelium-dependent vasodilation machinery (e.g., endothelial nitric oxide synthase – nitric oxide pathway)^{30,33} and allowing pcEV to act directly on smooth muscle to trigger calcium-dependent vasoconstriction (Figure 4). Several calcium signaling pathways are involved in regulating smooth-muscle contractility,^{34,35} but the molecule(s) on pcEV that triggers one or all of these pathways remains to be identified. This vasoconstrictive activity is unlikely to be limited to pcEV because EV from injured endothelial cells also induce hypertension in pregnant mice in a platelet-dependent manner.³² The pcEV-induced vasoconstriction reduced blood flow (Figure 4C-F), potentially resulting in tissue ischemia that further propagates injury to the placenta and the endothelium.

Third, pcEV induced a systemic hypercoagulable state defined by shortened clotting time, platelet activation, and the expression of procoagulant PS (*Online Supplementary Figure S4*). This hypercoagulable state has been widely reported in patients with preeclampsia^{5,36,37} and causes extensive fibrin deposition in glomerular vessels (Figure 2J-L). The fibrin deposition could potentially induce vascular leakage and increase rigidity of the vessel wall, contributing to pcEV-induced renal dysfunction (i.e., proteinuria) and hypertension, respectively.³⁸ Surprisingly, fibrin deposition may be organ-specific because it was extensively detected in the kidney, but minimally in the liver vasculature (*Online Supplementary Figure S6*). Instead, focal tissue necrosis and infiltration of inflammatory cells were detected in the liver of pcEV-infused mice, but the cause of this tissue injury remains to be identified. Nevertheless, our findings are consistent with those of a recent cohort study, which showed that plasma samples from preeclamptic patients had elevated levels of EV from activated platelets and leukocytes as well as tissue factor-bearing EV, as compared to women with normal pregnancies.³⁹ However, another study found no association between preeclampsia and plasma levels of anionic phospholipid-expressing EV.⁴⁰

Finally, we have recently shown that lactadherin given intravenously promotes the phagocytosis of EV by coupling the vesicles to macrophages in the liver through their PS- and integrin-binding domains.²⁸ Here, we further show that lactadherin given intravenously also promotes the phagocytosis of pcEV (Figure 3A, B) and prevents pcEV-induced hypertension, proteinuria, and coagulation

(Figure 2). Lactadherin^{-/-} mice have elevated levels of PS-expressing EV (Figure 3E) and develop hypertension and proteinuria during pregnancy (Figure 3C, D). EV found in lactadherin^{-/-} mice before pregnancy likely come from platelets and endothelial cells, and could further propagate endothelial and placental injury, systemic inflammation, and coagulation.^{32,41} The findings in mice infused with exogenous lactadherin and those deficient in lactadherin raise several questions, (i) Could insufficient EV clearance induce placenta damage? (ii) Is intrinsically low EV-clearance activity a risk for preeclampsia and, if so, could it serve as a predictive marker? (iii) Could lactadherin be used as a treatment for preeclampsia? Human plasma contains ~1 ng/mL of lactadherin,⁴² which may be sufficient during homeostasis, but becomes insufficient to remove a large quantity of microvesicles that are substan-

tially and persistently released during pregnancy, especially in the condition of preeclampsia.

In summary, we demonstrated that pcEV from injured placenta induced a preeclampsia-like condition in mice by inducing endothelial injury, vasoconstriction, and hypercoagulation. This pcEV-induced condition was prevented by enhancing EV clearance. The rates of pcEV production and clearance could therefore be used for the risk assessment of preeclampsia and become new therapeutic targets for preeclampsia.

Funding

This study was supported by National Institutes of Health grants NS087296, HL119391 and HL125957 (to JFD), Natural Science Foundation of China State Key Program grant 81330029 (to JNZ) and research grant 81672399 (to ML).

References

- Tranquilli AL, Dekker G, Magee L, et al. The classification, diagnosis and management of the hypertensive disorders of pregnancy: a revised statement from the ISSHP. *Pregnancy Hypertens.* 2014;4(2):97-104.
- Phoa KY, Chedraui P, Perez-Lopez FR, et al. Perinatal outcome in singleton pregnancies complicated with preeclampsia and eclampsia in Ecuador. *J Obstet Gynaecol.* 2016;36(5):581-584.
- Redman CW, Tannetta DS, Dragovic RA, et al. Review: does size matter? Placental debris and the pathophysiology of preeclampsia. *Placenta.* 2012;33(Suppl):S48-54.
- Amaral LM, Wallace K, Owens M, LaMarca B. Pathophysiology and current clinical management of preeclampsia. *Curr Hypertens Rep.* 2017;19(8):61.
- Chaiworapongsa T, Chaemsaitong P, Yeo L, Romero R. Pre-eclampsia part 1: current understanding of its pathophysiology. *Nat Rev Nephrol.* 2014;10(8):466-480.
- Lok CA, Van der Post JA, Sturk A, Sargent IL, Nieuwland R. The functions of microparticles in preeclampsia. *Pregnancy Hypertens.* 2011;1(1):59-65.
- Guller S, Tang Z, Ma YY, Di Santo S, Sager R, Schneider H. Protein composition of microparticles shed from human placenta during placental perfusion: potential role in angiogenesis and fibrinolysis in preeclampsia. *Placenta.* 2011;32(1):63-69.
- Rusterholz C, Messerli M, Hoesli I, Hahn S. Placental microparticles, DNA, and RNA in preeclampsia. *Hypertens Pregnancy.* 2011;30(3):364-375.
- Mincheva-Nilsson L, Baranov V. Placenta-derived exosomes and syncytiotrophoblast microparticles and their role in human reproduction: immune modulation for pregnancy success. *Am J Reprod Immunol.* 2014;72(5):440-457.
- Germain SJ, Sacks GP, Sooranna SR, Sargent IL, Redman CW. Systemic inflammatory priming in normal pregnancy and preeclampsia: the role of circulating syncytiotrophoblast microparticles. *J Immunol.* 2007;178(9):5949-5956.
- Goswami D, Tannetta DS, Magee LA, et al. Excess syncytiotrophoblast microparticle shedding is a feature of early-onset preeclampsia, but not normotensive intrauterine growth restriction. *Placenta.* 2006;27(1):56-61.
- Dragovic RA, Collett GP, Hole P, et al. Isolation of syncytiotrophoblast microvesicles and exosomes and their characterisation by multicolour flow cytometry and fluorescence nanoparticle tracking analysis. *Methods.* 2015;87:64-74.
- Baig S, Kothandaraman N, Manikandan J, et al. Proteomic analysis of human placental syncytiotrophoblast microvesicles in preeclampsia. *Clin Proteomics.* 2014;11(1):40.
- Nakashima A, Yamanaka-Tatematsu M, Fujita N, et al. Impaired autophagy by soluble endoglin, under physiological hypoxia in early pregnant period, is involved in poor placentation in preeclampsia. *Autophagy.* 2013;9(3):303-316.
- Velicky P, Windsperger K, Petroczi K, et al. Pregnancy-associated diamine oxidase originates from extravillous trophoblasts and is decreased in early-onset preeclampsia. *Sci Rep.* 2018;8(1):6342.
- Saito S, Nakashima A. A review of the mechanism for poor placentation in early-onset preeclampsia: the role of autophagy in trophoblast invasion and vascular remodeling. *J Reprod Immunol.* 2014;101-102:80-88.
- Rusterholz C, Holzgreve W, Hahn S. Oxidative stress alters the integrity of cell-free mRNA fragments associated with placenta-derived syncytiotrophoblast microparticles. *Fetal Diagn Ther.* 2007;22(4):313-317.
- Brown CE, Flynn J, Carty DM, Scotland G, Delles C. Lb01.05: Vascular consequences of pre-eclampsia. *J Hypertens.* 2015;33(Suppl 1):e46.
- Cooper JC. The effect of placental syncytiotrophoblast microvillous membranes from normal and pre-eclamptic women on the growth of endothelial cells in vitro. *Br J Obstet Gynaecol.* 1994;101(6):559.
- Smarason AK, Sargent IL, Starkey PM, Redman CW. The effect of placental syncytiotrophoblast microvillous membranes from normal and pre-eclamptic women on the growth of endothelial cells in vitro. *Br J Obstet Gynaecol.* 1993;100(10):943-949.
- Al-Ofi E, Anumba DO, Coffelt S. OS006. Functional expression of endogenous ligands of Toll like receptor4 on monocytes and placentae from women during normal pregnancy and pre-eclampsia. *Pregnancy Hypertens.* 2012;2(3):178.
- Bobek G, Surmon L, Mirabito KM, Makris A, Hennessy A. Placental regulation of inflammation and hypoxia after TNF-alpha infusion in mice. *Am J Reprod Immunol.* 2015;74(5):407-418.
- Sergeeva ON, Chesnokova NP, Ponukalina EV, Rogozhina IE, Glukhova TN. [Pathogenetic relationship between endothelial dysfunction and disorders of blood coagulation potential in pregnancy complicated by pre-eclampsia]. *Vestn Ross Akad Med Nauk.* 2015(5):599-603.
- Doridot L, Passet B, Mehats C, et al. Preeclampsia-like symptoms induced in mice by fetoplacental expression of STOX1 are reversed by aspirin treatment. *Hypertension.* 2013;61(3):662-668.
- Motta-Mejia C, Kandzija N, Zhang W, et al. Placental vesicles carry active endothelial nitric oxide synthase and their activity is reduced in preeclampsia. *Hypertension.* 2017;70(2):372-381.
- Skynner MJ, Drage DJ, Dean WL, Turner S, Watt DJ, Allen ND. Transgenic mice ubiquitously expressing human placental alkaline phosphatase (PLAP): an additional reporter gene for use in tandem with beta-galactosidase (lacZ). *Int J Dev Biol.* 1999;43(1):85-90.
- Tian Y, Salsbery B, Wang M, et al. Brain-derived microparticles induce systemic coagulation in a murine model of traumatic brain injury. *Blood.* 2015;125(13):2151-2159.
- Zhou Y, Cai W, Zhao Z, et al. Lactadherin promotes microvesicle clearance to prevent coagulopathy and improves survival of severe TBI mice. *Blood.* 2018;131(5):563-572.
- Zhao Z, Wang M, Tian Y, et al. Cardiolipin-mediated procoagulant activity of mitochondria contributes to traumatic brain injury-associated coagulopathy in mice. *Blood.* 2016;127(2):2763-2772.
- Pascoal IF, Lindheimer MD, Nalbantian-Brandt C, Umans JG. Preeclampsia selectively impairs endothelium-dependent relaxation and leads to oscillatory activity in small omental arteries. *J Clin Invest.* 1998;101(2):464-470.
- Dupressoir A, Vernochet C, Bawa O, et al.

- Syncytin-A knockout mice demonstrate the critical role in placentation of a fusogenic, endogenous retrovirus-derived, envelope gene. *Proc Natl Acad Sci U S A.* 2009;106(29):12127-12132.
32. Kohli S, Ranjan S, Hoffmann J, et al. Maternal extracellular vesicles and platelets promote preeclampsia via inflammasome activation in trophoblasts. *Blood.* 2016;128(17):2153-2164.
 33. Pascoal IF, Umans JG. Effect of pregnancy on mechanisms of relaxation in human omental microvessels. *Hypertension.* 1996;28(2):183-187.
 34. Earley S, Brayden JE. Transient receptor potential channels in the vasculature. *Physiol Rev.* 2015;95(2):645-690.
 35. Ghigo A, Laffargue M, Li M, Hirsch E. PI3K and calcium signaling in cardiovascular disease. *Circ Res.* 2017;121(3):282-292.
 36. Bonnar J, McNicol GP, Douglas AS. Coagulation and fibrinolytic systems in preeclampsia and eclampsia. *Br Med J.* 1971;2(5752):12-16.
 37. Erez O, Romero R, Vaisbuch E, et al. Tissue factor activity in women with preeclampsia or SGA: a potential explanation for the excessive thrombin generation in these syndromes. *J Matern Fetal Neonatal Med.* 2018;31(12):1568-1577.
 38. Holdsworth SR, Tipping PG. Macrophage-induced glomerular fibrin deposition in experimental glomerulonephritis in the rabbit. *J Clin Invest.* 1985;76(4):1367-1374.
 39. Campello E, Spiezia L, Radu CM, et al. Circulating microparticles in umbilical cord blood in normal pregnancy and pregnancy with preeclampsia. *Thromb Res.* 2015;136(2):427-431.
 40. Katzenell S, Shomer E, Zipori Y, Zylberfisz A, Brenner B, Aharon A. Characterization of negatively charged phospholipids and cell origin of microparticles in women with gestational vascular complications. *Thromb Res.* 2012;130(3):479-484.
 41. Owens AP 3rd, Mackman N. Microparticles in hemostasis and thrombosis. *Circ Res.* 2011;108(10):1284-1297.
 42. Kishi C, Motegi SI, Ishikawa O. Elevated serum MFG-E8 level is possibly associated with the presence of high-intensity cerebral lesions on magnetic resonance imaging in patients with systemic lupus erythematosus. *J Dermatol.* 2017;44(7):783-788.

D' domain region Arg782-Cys799 of von Willebrand factor contributes to factor VIII binding

Małgorzata A. Przeradzka,¹ Josse van Galen,¹ Eduard H.T.M. Ebberink,¹ Arie J. Hoogendijk,¹ Carmen van der Zwaan,¹ Koen Mertens,¹ Maartje van den Biggelaar¹ and Alexander B. Meijer^{1,2}

¹Department of Molecular and Cellular Hemostasis, Sanquin Research, Amsterdam and

²Department of Biomolecular Mass Spectrometry and Proteomics, Utrecht Institute for Pharmaceutical Sciences, Utrecht University, Utrecht, the Netherlands



Haematologica 2020
Volume 105(6):1695-1703

ABSTRACT

In the complex with von Willebrand factor (VWF) factor VIII (FVIII) is protected from rapid clearance from circulation. Although it has been established that the FVIII binding site resides in the N-terminal D'-D3 domains of VWF, detailed information about the amino acid regions that contribute to FVIII binding is still lacking. In the present study, hydrogen-deuterium exchange mass spectrometry was employed to gain insight into the FVIII binding region on VWF. To this end, time-dependent deuterium incorporation was assessed in D'-D3 and the FVIII-D'-D3 complex. Data showed reduced deuterium incorporation in the D' region Arg782-Cys799 in the FVIII-D'-D3 complex compared to D'-D3. This implies that this region interacts with FVIII. Site-directed mutagenesis of the six charged amino acids in Arg782-Cys799 into alanine residues followed by surface plasmon resonance analysis and solid phase binding studies revealed that replacement of Asp796 affected FVIII binding. A marked decrease in FVIII binding was observed for the D'-D3 Glu787Ala variant. The same was observed for D'-D3 variants in which Asp796 and Glu787 were replaced by Asn796 and Gln787. Site-directed mutagenesis of Leu786, which together with Glu787 and Cys789 forms a short helical region in the crystal structure of D'-D3, also had a marked impact on FVIII binding. The combined results show that the amino acid region Arg782-Cys799 is part of a FVIII binding surface. Our study provides new insight into FVIII-VWF complex formation and defects therein that may be associated with bleeding caused by markedly reduced levels of FVIII.

Introduction

The multimeric glycoprotein von Willebrand factor (VWF) acts as a carrier protein for coagulation factor VIII (FVIII) in the circulation.¹ In the complex with VWF, FVIII is protected from rapid clearance from plasma.^{2,3} Multiple amino acid substitutions have been identified in VWF that impair FVIII-VWF complex formation. The associated reduced plasma levels of FVIII can result in the bleeding disorder referred to as von Willebrand disease type 2 Normandy (VWD type 2N).⁴ Most of the aberrant mutations in VWF involve substitutions of amino acid residues that have been proposed to affect the structural integrity of VWF.^{5,6} These substitutions provide therefore only limited information about the identity of the FVIII binding site on VWF.

Distinct protein domains can be identified in the primary amino acid sequence of VWF. These domains are arranged in the order: D'-D3-A1-A2-A3-D4-B-C1-C2-C2-CK.⁷ Zhou *et al.* have refined the domain organization within VWF. For D'-D3, they proposed that these domains can be further divided into TIL'-E'-VWD3-C8_3-TIL3-E3 subdomains.⁸ In plasma, VWF circulates as an ensemble of multimeric proteins of varying size. In these multimers, the VWF monomers are head-to-head and tail-to-tail connected *via* disulphide bridges between two D3 domains and two CK domains.⁹ FVIII also comprises multiple domains that together constitute a light chain of the domains A3-C1-C2 and a heavy chain comprising the domains A1-A2-

Correspondence:

ALEXANDER B. MEIJER
s.meijer@sanquin.nl

Received: March 20, 2019.

Accepted: September 25, 2019.

Pre-published: September 26, 2019.

doi:10.3324/haematol.2019.221994

Check the online version for the most updated information on this article, online supplements, and information on authorship & disclosures: www.haematologica.org/content/106/6/1695

©2020 Ferrata Storti Foundation

Material published in *Haematologica* is covered by copyright. All rights are reserved to the Ferrata Storti Foundation. Use of published material is allowed under the following terms and conditions:

<https://creativecommons.org/licenses/by-nc/4.0/legalcode>. Copies of published material are allowed for personal or internal use. Sharing published material for non-commercial purposes is subject to the following conditions: <https://creativecommons.org/licenses/by-nc/4.0/legalcode>, sect. 3. Reproducing and sharing published material for commercial purposes is not allowed without permission in writing from the publisher.



B.¹⁰ Because of limited proteolysis of the B domain, FVIII is heterogeneous in size with molecular weights ranging from 160 kDa to 330 kDa.^{11,12}

For effective binding to FVIII, VWF requires the presence of a short acidic amino acid region at the start of the FVIII A3 domain. This region, which includes sulphated tyrosine residues, is referred to as the $\alpha 3$ region.^{13,14} Next to this VWF binding region, hydrogen-deuterium exchange mass spectrometry (HDX-MS) and previous site-directed mutagenesis studies have identified binding sites for VWF in the C1 and C2 domain of FVIII as well.¹⁵⁻¹⁹ During activation of FVIII, the $\alpha 3$ region is removed from FVIII leading to the dissociation of the FVIII-VWF complex. Additional cleavages by thrombin generates activated FVIII that can perform its role in the coagulation cascade as a cofactor for activated factor IX ultimately leading to fibrin formation.²⁰

It has previously been established that the N-terminal D'-D3 domains of VWF comprise the binding site for FVIII. In 1987, limited proteolysis studies of VWF revealed that a VWF fragment comprising the residues 764-1036 harbors the interaction site for FVIII.²¹ Based on cryoelectron microscopy (cryo-EM) structures of FVIII in complex with D'-D3, it has later been shown that the main interactive region for FVIII resides in the D' domain.¹⁹ Recently, we have found that the presence of the VWD3 subdomain of the D3 domain is required to optimally support the interaction between D' and FVIII.²² Using a primary amine-directed chemical foot printing approach combined with mass spectrometry analysis, we have further demonstrated that Lys773 contributes to FVIII binding.²³ In the present study, we have employed HDX-MS combined with site-directed mutagenesis and protein binding studies to further explore the FVIII binding regions on VWF. The combined results show that the D' domain region Arg782-Cys799 is part of the FVIII binding interface.

Methods

Materials

Tris-HCl was from Invitrogen (Breda, the Netherlands), NaCl was obtained from Fagron (Rotterdam, the Netherlands) and HEPES was from Serva (Heidelberg, Germany), FreeStyle 293 expression medium was obtained from Gibco (Thermo Fisher Scientific). Tween-20 and D₂O was from Sigma-Aldrich (St Louis, MO, USA). Human serum albumin (HSA) was obtained from the Division of Products at Sanquin (Amsterdam, the Netherlands). All other chemicals were from Merck (Darmstadt, Germany), unless indicated otherwise.

Proteins

Antibody CLB-EL14 (EL14), CLB-Rag20, CLB-CAg12 (CAg 12) and HPC4 have been described before.^{22,24,25} D'-D3 fragment, FVIII lacking the B domain residues 746-1639 (referred to as FVIII throughout this paper) and VWF were obtained essentially as described before.²⁶⁻²⁸ Purified proteins were dialyzed against a buffer with 50 mM HEPES (pH 7.4), 150 mM NaCl, 10 mM CaCl₂, 50% (v/v) glycerol and stored at -20°C. Site-directed mutagenesis of the D'-D3 fragment was employed using Quik Change (Agilent Technologies) according to the manufacturer's instructions.

HDX-MS

D'-D3 was pre-incubated in presence or absence of FVIII in 1:1 molar ratio for 5 min at 4°C. Samples were subsequently diluted

ten times in deuterated binding buffer (98% D₂O) or standard binding buffer and incubated for 10 sec, 100 sec or 1,000 sec at 24°C. A detailed description is available in the *Online Supplementary Materials and Methods*.

Solid-phase competition assays

Recombinant VWF (1 μ g/mL) was immobilized overnight at 4°C in a buffer containing 50mM NaHCO₃ pH 9.8 in a 96-wells microtiter plate (Nunc Maxisorp). Increasing concentrations (0.3-900 nM) of D'-D3 and variants with single mutations were pre-incubated with 0.3 nM FVIII in a buffer containing 50 mM Tris, 150 mM NaCl, 2% human serum albumin, 0.1% Tween 20, pH 7.4 for 30 min at 37°C. These mixtures were transferred to the VWF coated plate and incubated for 2 hours at 37°C. Then, the plate was washed three times with 50 mM Tris (pH 7.4), 150 mM NaCl, 5mM CaCl₂, 0.1% Tween 20 after which FVIII bound to VWF was detected with an HRP-labeled monoclonal antibody (CAg 12).²⁶

Surface plasmon resonance analysis

Surface plasmon resonance (SPR) analysis was carried out using a Biacore T-200 biosensor system (GE Healthcare) as previously described.²² A monoclonal antibody to FVIII (EL14) was coupled to a CM5 sensor chip (GE Healthcare) to 5,000 response units (RU) density using the amino coupling activation method according to manufacturer's suggestions (GE Healthcare). Subsequently, 3,000 RU of FVIII were immobilized to the chip *via* EL14 antibody. Next, increasing concentrations of D'-D3 fragments were passed over the chip at a flow rate of 30 μ L/min in a buffer containing 20 mM HEPES (pH 7.4), 150 mM NaCl, 5 mM CaCl₂ and 0.05% Tween 20 at 25°C. An empty channel was utilized to correct for non-specific binding to the dextran matrix.

Results

HDX-MS on the isolated D'-D3 fragment of VWF

To facilitate identification of the FVIII binding residues within the D' domain (TIL'-E' subdomains), we made use of the D'-D3 monomer in which the cysteine residues involved in dimerization of the D3 domains (VWD3-C8_3-TIL3-E3 subdomains) were replaced by serine residues.²⁹ The D'-D3 fragment was transferred from H₂O to D₂O-containing buffer to assess time-dependent deuterium incorporation into the protein backbone. 178 peptides were identified covering 92% of the D'-D3 sequence (Figure 1A and *Online Supplementary Table S1*). For each peptide, we plotted the percentage of deuterium incorporation of the identified peptides at three different time points (Figure 1B). The overall result showed that almost all peptides from the N-terminal TIL' subdomain of D'-D3 exhibit limited to no change in deuterium incorporation at these time points. Only the peptide that includes the N-terminus of the TIL' subdomain showed increased deuterium incorporation. Apart from several peptides in the C8_3 subdomain of the D3 domain, most of the peptides in the other subdomains showed incorporation of deuterium in time. Peptides with the most marked change in deuterium incorporation correspond to unstructured regions in the recently published crystal structure of D'-D3.³⁰ This finding confirms that amino acid backbone hydrogens in unstructured regions exhibit an enhanced rate of hydrogen-deuterium exchange compared to structured regions. It further implies that these regions are unstructured in solution as can be predicted by the crystal structure.

D' region Arg782-Cys799 shows reduced deuterium incorporation in the presence of FVIII. HDX-MS was employed on the FVIII-D'-D3 complex

The complex was transferred to D₂O-containing buffer and the incorporation of deuterium was assessed at three

different time points. The obtained results were compared to the time-dependent deuterium incorporation in D'-D3 in the absence of FVIII. Most peptides originating from the FVIII-D'-D3 complex did not show a change in deuterium uptake compared to isolated D'-D3 (Figure 2 and *Online*

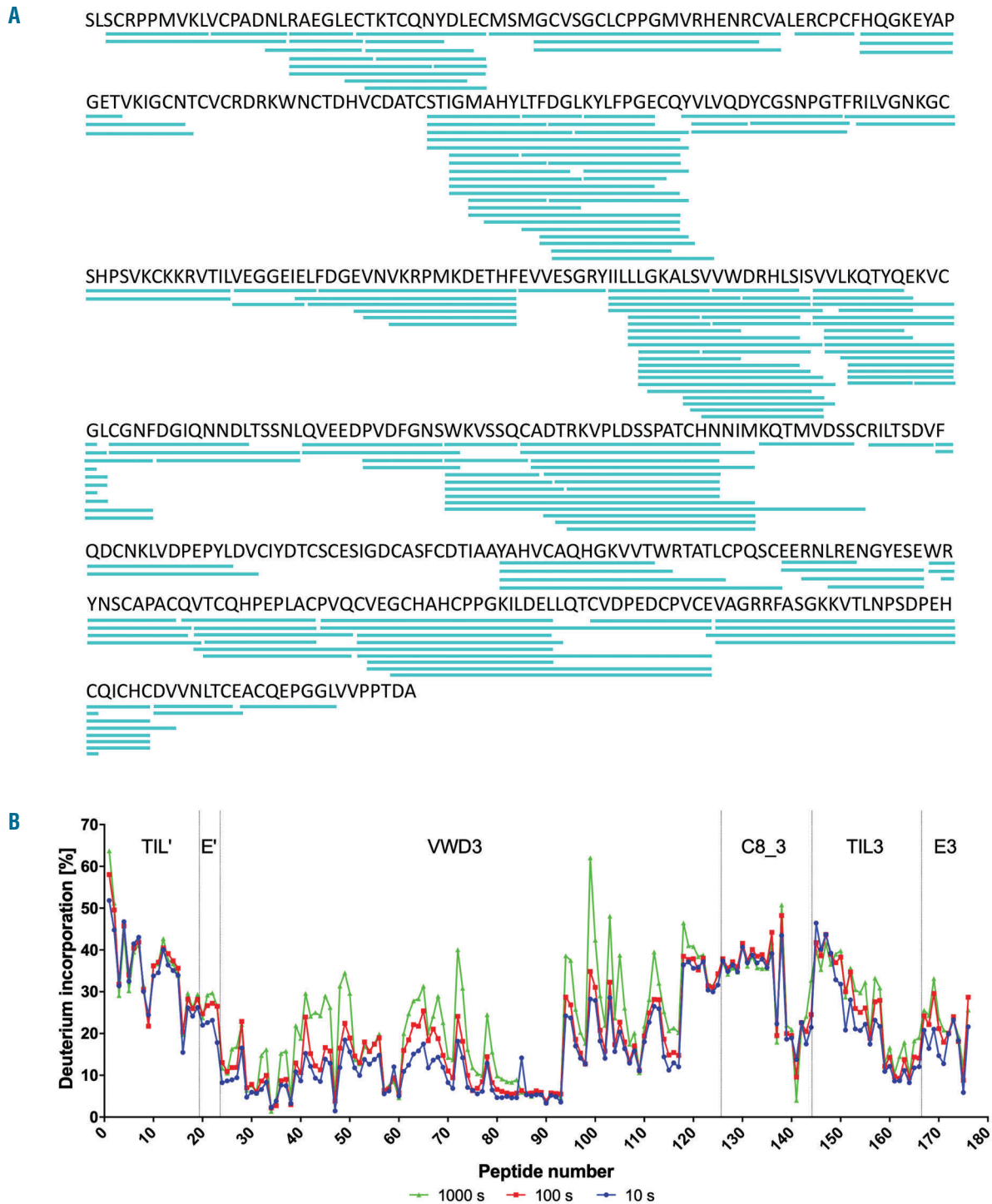


Figure 1. Hydrogen-deuterium exchange mass spectrometry analysis of the D'-D3 fragment. D'-D3 was incubated for 10 sec, 100 sec and 1000 sec in a deuterium buffer consisting of 20 mM HEPES (pH 7.4), 150 mM NaCl and 5 mM CaCl₂. D'-D3 was processed for hydrogen-deuterium exchange mass spectrometry (HDX-MS) analysis as described in the methods. (A) Shows the identified peptides as blue lines underneath the primary sequence of D'-D3. (B) Shows the percentage of deuterium incorporation for the individual identified peptides for the different incubation times with deuterium buffer. The sequence of the peptide's numbers, shown on the x-axis, is displayed in the *Online Supplementary Table S1*.

Supplementary Figure S1). Several overlapping peptides in the TIL' subdomain of D', however, did show a reduced deuterium incorporation in the complex. The peptide region that is shared by the overlapping peptides includes the amino acids Arg782-Cys799 (Figure 2B-C). The HDX-MS results suggest that the local hydrogen bonding network is altered in this VWF region upon FVIII binding implying that this region contributes to FVIII binding.

SPR analysis reveals that charged residues in D' region Arg782-Cys799 contribute to FVIII binding

Site-directed mutagenesis of the D'-D3 fragment was employed to verify the contribution of the region Arg782-Cys799 to FVIII binding. As electrostatic interactions have been proposed to mediate FVIII-VWF complex assembly,^{31,32} the charged amino acids in this region were replaced by alanine residues resulting in six new D'-D3 variants *i.e.* Arg782Ala, Glu784Ala, Glu787Ala, Lys790Ala, Asp796Ala and Glu798Ala. SPR analysis was performed to assess their FVIII binding efficiency. To this end, increasing concentrations of the D'-D3 variants were passed over FVIII that was immobilized *via* antibody EL14 to the surface of a CM5 sensor chip (Figure 3A-G). The Arg782Ala, Glu784Ala and Glu798Ala variants revealed association and dissociation binding responses that closely resembled those of the wild-type (WT) D'-D3. The Lys790Ala and Asp796Ala variants showed decreased binding responses compared to WT D'-D3. Almost no

binding was observed for the Glu787Ala variant. The association and dissociation responses revealed complex binding kinetics comprising at least two components. To estimate the binding affinities, we plotted the maximum binding response as a function of the D'-D3 variant concentration (Figure 3H). The concentration at which the half-maximum binding response is reached, represents an estimation of the average binding affinities ($\langle K_D \rangle$) of the involved components. Compared to the $\langle K_D \rangle$ obtained for the WT D'-D3 (~50 nM), results showed a more than four-fold increase in $\langle K_D \rangle$ for D'-D3 Asp796Ala (~190 nM) and a five-fold increase for D'-D3 Lys790Ala (~240 nM). These findings together show that charged amino acid residues in the region Arg782-Cys799 contribute to FVIII binding. A glutamic acid at position 787 appears most critical for effective interaction between FVIII and D'-D3.

A solid phase competition assay reveals that charged residues contribute to FVIII binding. The efficiency by which the D'-D3 variants were able to compete with VWF for FVIII binding was assessed using a competitive binding assay as also employed in previous studies.^{22,23} FVIII was incubated with immobilized VWF in the presence of increasing concentrations of the D'-D3 variants. Residual FVIII binding to immobilized VWF was assessed using an antibody against FVIII that does not interfere with the complex formation between FVIII and VWF (Figure 4). Results showed that about 50 nM of WT D'-D3 was

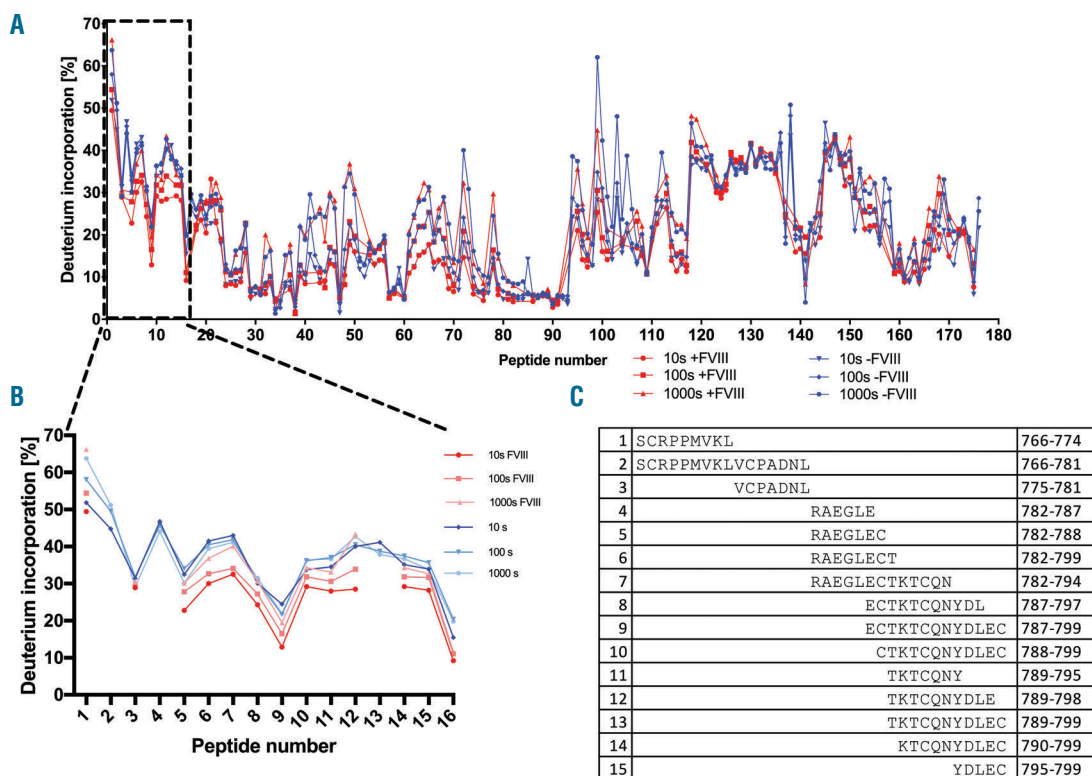


Figure 2. Hydrogen-deuterium exchange mass spectrometry analysis of the FVIII-D3 complex. The D'-D3 was incubated for 10 sec, 100 sec and 1000 sec in a deuterium buffer consisting of 20 mM HEPES (pH 7.4), 150 mM NaCl and 5 mM CaCl₂ in the presence and absence of coagulation factor VIII (FVIII). The proteins were processed for hydrogen-deuterium exchange mass spectrometry (HDX-MS) analysis as described in the methods. (A) Shows the percentage of deuterium incorporation of the identified peptides of the D'-D3 at the indicated incubation times in deuterium buffer in the presence and absence of FVIII. The sequence of the peptide numbers, shown on the x-axis, is displayed in the *Online Supplementary Table S1*. (B) Shows the percentage of time-dependent deuterium incorporation for the 15 identified peptides that cover part of the TIL' subdomain of D'. The sequence of the peptide numbers, shown on the x-axis, is displayed in (C).

required to reduce FVIII binding to immobilized VWF by 50%. For the Arg782Ala, Glu784Ala, and Glu798Ala variants of D'-D3 about 100 nM was required to reach the same effect. A markedly reduced competition efficiency was observed for the Asp796Ala variant as more than 800 nM was required to reduce the binding to 50%. Almost no competition was observed for D'-D3 Glu787Ala. The data further reveal a biphasic competition curve for the Lys790Ala variant. This implies that D'-D3 Lys790Ala may exist in two conformations that differentially interfere with complex formation between FVIII and VWF. We

therefore cannot make any reliable conclusions about the putative role of Lys790 for FVIII binding. Based on the results, we also constructed two new D'-D3 variants *i.e.* Glu787Gln and Asp796Asn and assessed their FVIII binding efficiency using SPR analysis. Results showed that changing the charged amino acids with their neutral counterpart also affected FVIII binding (*Online Supplementary Figure S2*). Changing Glu787 for a Gln in full-length VWF also revealed a major impact on FVIII using a solid phase binding assay (*Online Supplementary Figure S3*). The data together confirm the observation that amino acid residues

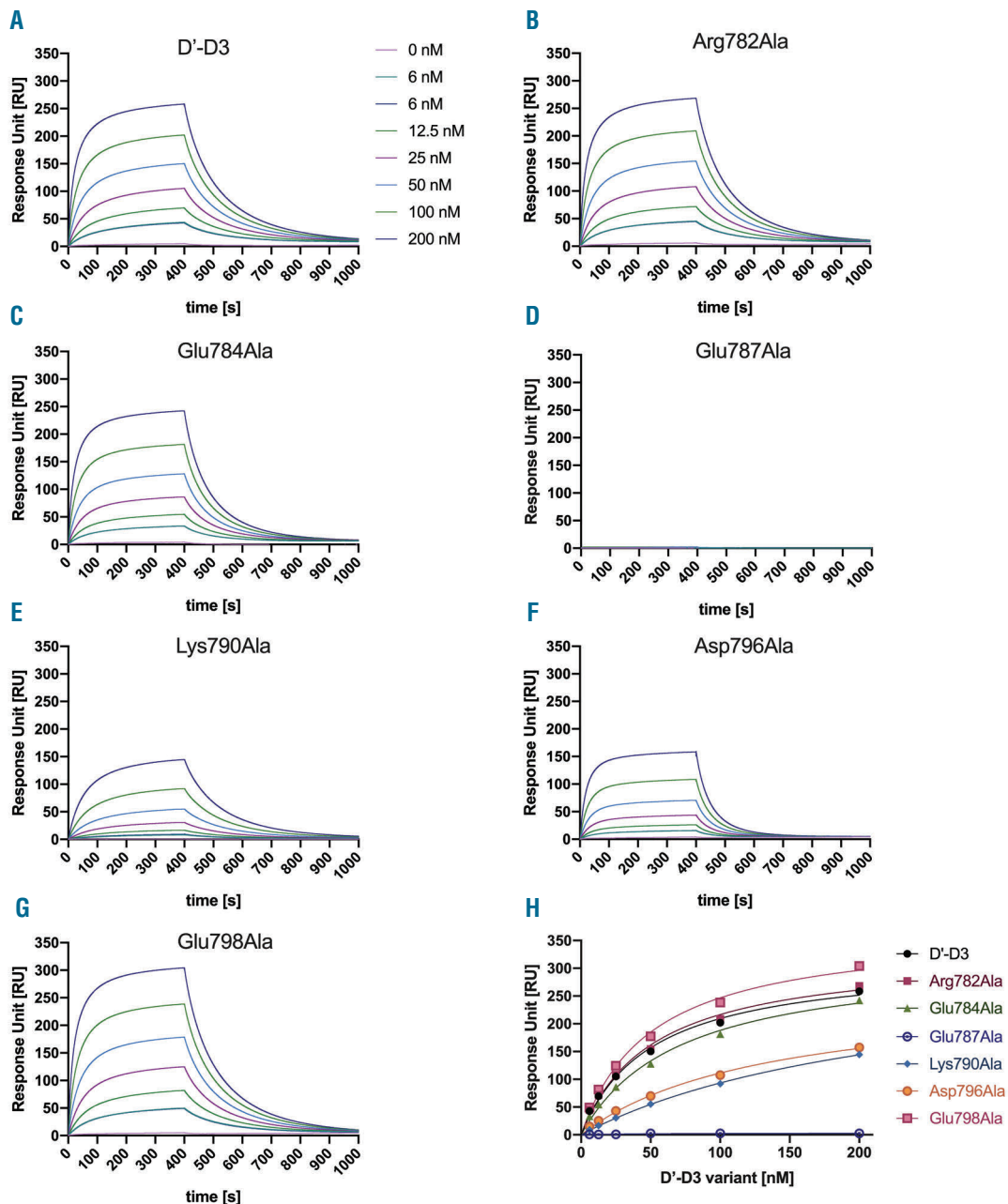


Figure 3. Surface plasmon resonance analysis of D'-D3 variants in interaction with FVIII. (A-G) Multiple concentrations (0-200 nM) of the indicated D'-D3 variants were passed over the coagulation factor VIII (FVIII) that was immobilized via antibody EL14 to the surface of a CM5 sensor chip. The binding response is represented in response units (RU) and was assessed in 20 mM HEPES (pH 7.4), 150 mM NaCl, 5 mM CaCl₂, 0.05% (v/v) Tween 20 at a flow rate of 30 μ L/min at 25°C. (H) Shows the maximum binding response in RU of the D'-D3 variants at a function of the employed concentration.

in the region Arg782-Cys799 are involved in FVIII binding. In particular, the glutamic acid residue at position 787 seems critical for the interaction between FVIII and D'-D3.

A leucine at position 786 is important for effective interaction with FVIII

Analysis of the crystal structure of D'-D3 shows that Glu787 is part of a short helical region that also includes Leu786 and Cys788 (Figure 5A).³⁰ We speculate Leu786 and Cys788 are critical to maintain the structural integrity of this helix, and therefore the spatial position of Glu787 in D'-D3. We therefore decided to destabilize this helical structure by replacing Leu786 for an alanine residue and study the effect thereof on FVIII binding. SPR analysis showed a markedly reduced FVIII binding response of the Leu786Ala variant with an estimated K_d of ~500 nM (Figure 5C). The competitive binding assay revealed that about 400 nM of the variant was required to reduce FVIII binding to VWF by 50% (Figure 5B). These findings together demonstrate an impaired FVIII binding efficiency of D'-D3 Leu786Ala. We propose therefore that the stability of the helical region may indeed be of importance for FVIII binding.

Discussion

The particularly high complexity of the molecular architecture of VWF has always posed a major challenge for the identification of the FVIII interactive regions within VWF. We therefore decided to utilize a short fragment of VWF that includes the FVIII binding site, *i.e.* D'-D3.² Previously, we have employed a primary amine-directed chemical footprinting approach on the FVIII-VWF complex and established that Lys773 contributes to FVIII binding.²³ This approach provided only information about the putative

role of the side-chains of lysine amino acid residues for FVIII-VWF complex formation. HDX-MS as utilized in this study has the potential to provide information about the putative role of all amino acids in D'-D3.³³

With HDX-MS, the replacement of amide hydrogen atoms of the protein backbone by deuterium atoms can be assessed upon the transfer of a protein complex from H₂O to D₂O. Sites where proteins interact can show a reduced time-dependent deuterium incorporation usually because of local changes in the hydrogen bonding network of the protein backbone. This methodology has proven to be particularly powerful in the identification of protein interaction sites.³⁴ Applying HDX-MS on the FVIII-D'-D3 complex showed reduced deuterium incorporation in amino acid region Arg782-Cys799 in the presence of FVIII (Figure 2). This result strongly suggest that it is involved in the interaction with FVIII. This region is also particularly rich in amino acid residues that are mutated in VWD type 2N (Figure 6). This corroborates the functional importance of this region.

The role of Arg782-Cys799 for FVIII binding was further confirmed by replacing the charged amino acid residues by alanine residues. Especially replacement of Glu787 proved detrimental for the interaction between D'-D3 and FVIII (Figures 3-4). A major impact on FVIII binding was also observed for the Glu787Gln variant of D'D3 and full-length VWF (*Online Supplementary Figure S2-3*). Patients with VWF type 2N have further been identified with a Glu787Lys variant of VWF.³⁵ These observations together demonstrate the importance of a glutamic acid at position 787. We cannot exclude that Glu787 may be critical for maintaining the local conformation of the D' domain. The crystal structure, however, reveals that Glu787 is exposed to the solvent and is not part of the internal protein core (Figure 5A).³⁰ We may therefore have identified one of the critical amino acids that directly

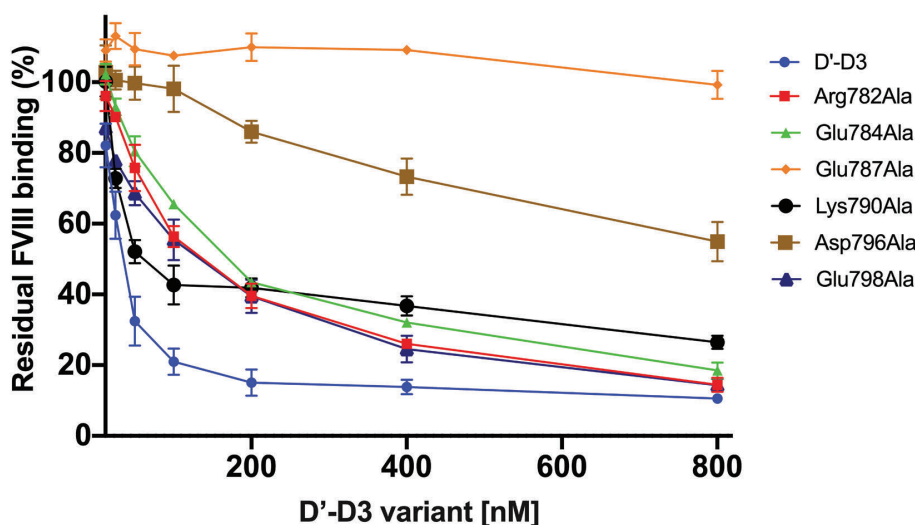


Figure 4. D'-D3 variants in competition with immobilized von Willebrand factor for binding FVIII. Coagulation factor VIII (FVIII) was incubated with increasing concentrations of the indicated D'-D3 variants in a buffer comprising 50 mM Tris (pH 7.4), 150 mM NaCl, 5mM CaCl₂, 2% human serum albumin and 0.1% Tween 20 at 37 °C. The protein mixtures were next incubated with immobilized von Willebrand factor (VWF) in the same buffer. Residual FVIII binding to immobilized VWF was assessed employing HRP-conjugated CAg12 antibody as described in the methods. Data represents mean \pm standard deviation (SD) of three independent experiments.

interacts with FVIII rather than being important for stabilizing the local conformation. The replacement of Leu786 by an alanine, most likely, alters the conformation of the short helical region 786-Leu-Glu-Cys-789 thereby repositioning Glu787 (Figure 5A). This can explain, in our view,

the altered FVIII binding efficiency of the Leu786Ala variant (Figure 5B-C). HDX-MS did not reveal reduced deuterium incorporation in peptides that include Lys773. This residue is part of a beta-sheet in which the amino backbone hydrogens tightly interact. Apparently, this second-

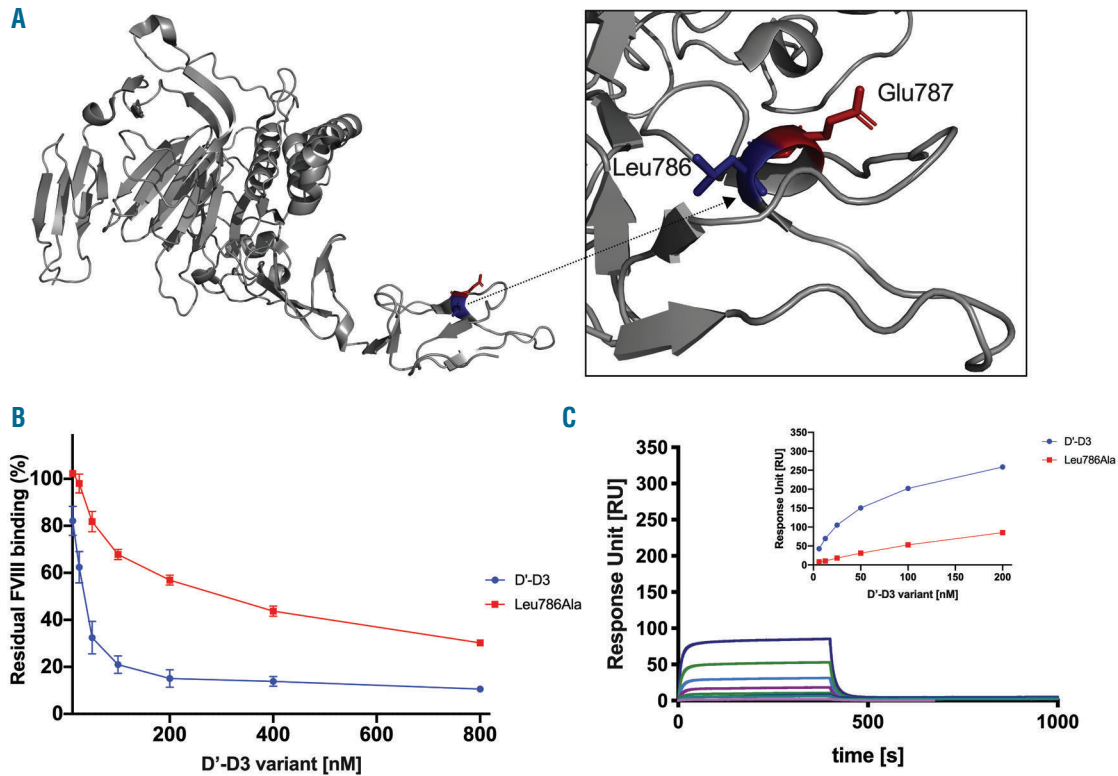


Figure 5. The FVIII binding efficiency of D'-D3 Leu786Ala. (A) Part of the crystal structure of D'-D3 (PDB entry: 6n29)30 with a zoom-in of the helical region comprising the residues 786-Leu-Glu-Cys-789. (B) Multiple concentrations of D'-D3 Leu786Ala were passed over coagulation factor VIII (FVIII) that was immobilized via antibody EL14 to the surface of a CM5 sensor chip. The binding response is indicated as response units (RU) and was assessed in 20 mM HEPES (pH 7.4), 150 mM NaCl, 5 mM CaCl₂, 0.05% (v/v) Tween 20 at a flow rate of 30 μ L/min at 25°C. (C) FVIII was pre-incubated with increasing concentrations of D'-D3 and D'-D3 Leu786Ala in a buffer comprising 50 mM Tris (pH 7.4), 150 mM NaCl, 5mM CaCl₂, 2% human serum albumin and 0.1% Tween 20 at 37 °C. The protein mixtures were next incubated with immobilized von Willebrand factor (VWF) in the same buffer. Residual FVIII binding to immobilized VWF was assessed employing HRP-conjugated CAg12 antibody as described in the methods. Data represents mean \pm standard deviation (SD) of three independent experiments.

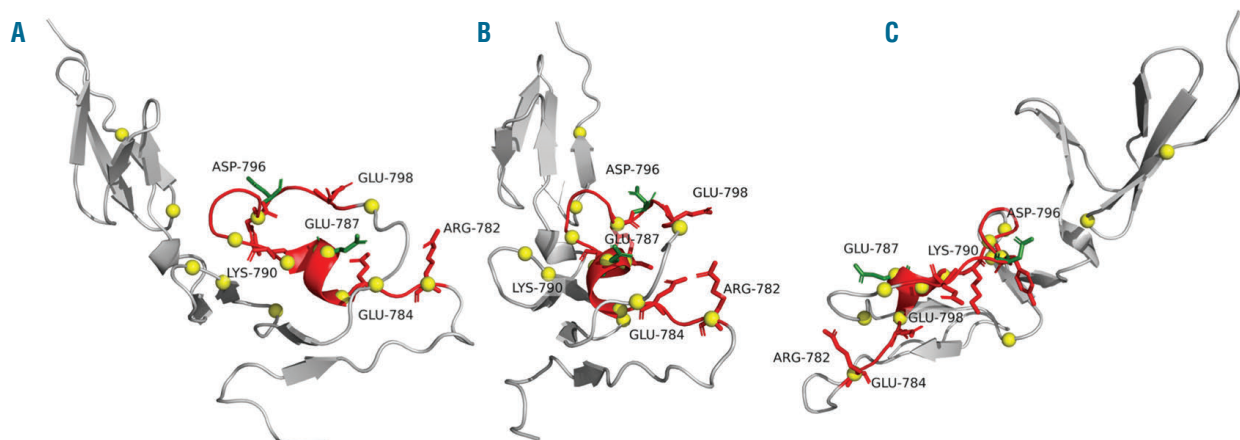


Figure 6. Amino acid region Arg782-Cys799 and sites involved in von Willebrand disease type 2 Normandy indicated in the crystal structure of TIL' subdomain. Shown is the TIL' subdomain of the crystal structure of the D'-D3 (PDB entry: 6n29) in a ribbon representation. (A-C) Present the same structure from different angles. Region Arg782-Cys799 is displayed in red. The yellow spheres indicated residues that have been mutated in the von Willebrand disease type 2 Normandy (VWD type 2N).³⁷

ary structure element does not change its conformation upon FVIII binding, which is required to detect altered deuterium incorporation.

Based on cryo-EM studies, Yee *et al.* proposed a model for the FVIII-D'-D3 complex. In this model the D' domain is in contact with the FVIII C1 domain.¹⁸ The contribution of the C1 domain to VWF binding has also been demonstrated with HDX-MS studies on FVIII in the presence and of the D'-D3.¹⁹ Because of the relatively low resolution of the structure, it was not possible to predict the orientation of the D' domain on FVIII. Results of this study now provide evidence that the region comprising Arg782-Lys790 may be oriented towards the C1 domain of FVIII. This sequence is part of a flat surface on the TIL' subdomain that may optimally interact with the C1 domain (*Online Supplementary Figure S4*).

How the sulphated acid a3 region at the start of the FVIII A3 domain interacts with D'-D3 remains, however, unclear from both the cryo-EM study and this study. Removal of this region upon activation of FVIII is the trigger for FVIII-VWF complex dissociation.¹² It has further

been shown that replacement of the sulphated tyrosine residue 1680 with a phenylalanine leads to a VWF binding defect.¹⁴ Recently, a well-designed nuclear magnetic resonance study was employed to assess the putative complex formation between the isolated a3 region and the isolated D' domain. Main changes in chemical shift were identified outside the region that was identified in our study, *i.e.* residues Val772, Asn819, Cys821 and Val 822, suggesting that the a3 region may interact with these residues. The isolated a3 binds the D' domain with a markedly reduced affinity compared to intact FVIII.³⁶ We have also found that the VWD3 subdomain of the D3 domain is required to support D' binding to FVIII as well.²² These notions show that the mechanism by which FVIII and VWF interact and the role of the a3 region therein remains a topic for further investigation.

Funding

This study has been funded by Product and Process Development, Sanquin, the Netherlands (PPOP-13-002) and by the Landsteiner foundation of blood research (LSBR 1882).

References

- Brinkhous KM, Sandberg H, Garris JB, et al. Purified human factor VIII procoagulant protein: Comparative hemostatic response after infusions into hemophilic and von Willebrand disease dogs. *Proc Natl Acad Sci U S A.* 1985;82(24):8752-8756.
- Yee A, Gildersleeve RD, Gu S, et al. A von Willebrand factor fragment containing the D'D3 domains is sufficient to stabilize coagulation factor VIII in mice. *Blood.* 2014;124(3):445-452.
- Pipe SW, Montgomery RR, Pratt KP, Lenting PJ, Lillicrap D. Life in the shadow of a dominant partner: the FVIII-VWF association and its clinical implications for hemophilia A. *Blood.* 2016;128(16):2007-2016.
- Mazurier C, Goudemand J, Hilbert L, et al. Type 2N von Willebrand disease: clinical manifestations, pathophysiology, laboratory diagnosis and molecular biology. *Best Pract Res Clin Haematol.* 2001;14(2):337-347.
- Jorieux S, Fressinaud E, Goudemand J, et al. Conformational changes in the D' domain of von Willebrand factor induced by CYS 25 and CYS 95 mutations lead to factor VIII binding defect and multimeric impairment. *Blood.* 2000;95(10):3139-3145.
- Jorieux S, Gaucher C, Goudemand J, Mazurier C. A Novel mutation in the D3 domain of von Willebrand factor markedly decreases its ability to bind Factor VIII and affects its multimerization. *Blood.* 1998; 92(12):4663-4670.
- Springer TA. Biology and physics of von Willebrand factor concatamers. *J Thromb Haemost.* 2011;9 Suppl 1:130-143.
- Zhou YF, Eng ET, Zhu J, et al. Sequence and structure relationships within von Willebrand factor. *Blood.* 2012;120(2):449-458.
- Marti T, Rösselet SJ, Titani K, Walsh KA. Identification of disulfide-bridged substructures within human von Willebrand factor. *Biochemistry.* 1987;26(25):8099-8109.
- Fay P. Factor VIII Structure and function. *Int J Hematol.* 2006;83(2):103-108.
- Stoilova-McPhie S, Villoutreix BO, Mertens K, Kembell-Cook G, Holzenburg A. 3-Dimensional structure of membrane-bound coagulation factor VIII: Modeling of the factor VIII heterodimer within a 3-dimensional density map derived by electron crystallography. *Blood.* 2002;99(4):1215-1223.
- Lenting PJ, van Mourik JA, Mertens K. The life cycle of coagulation factor VIII in view of its structure and function. *Blood.* 1997;92(11):3983-3996.
- Saenko EL, Scandella D. The acidic region of the factor VIII light chain and the C2 domain together form the high affinity binding site for von willebrand factor. *J Biol Chem.* 1997;272(29):18007-18014.
- Leyte A, van Schijndel HB, Niehrs C, et al. Sulfation of Tyr 1680 of human blood coagulation factor VIII is essential for the interaction of factor VIII with von Willebrand factor. *J Biol Chem.* 1991;266(2):740-746.
- Hamer R, Koedam J, Besser-visser N, et al. Factor VIII binds to von Willebrand factor via its 80,000 light chain. *Eur J Biochem.* 1987;166(1):37-43.
- Leyte A, Verbeet MP, Brodniewicz-Proba T, Van Mourik JA, Mertens K. The interaction between human blood-coagulation factor VIII and von Willebrand factor. Characterization of a high-affinity binding site on factor VIII. *Biochem J.* 1989;257(3):679-683.
- Lollar P, Hill-Eubanks DC, Parker CG. Association of the factor VIII light chain with von Willebrand factor. *J Biol Chem.* 1988;263(21):10451-10455.
- Yee A, Oleskie AN, Dosey AM, et al. Visualization of an N-terminal fragment of von Willebrand factor in complex with factor VIII. *Blood.* 2015;126(8):939-943.
- Chiu P-L, Bou-Assaf GM, Chhabra ES, et al. Mapping the interaction between factor VIII and von Willebrand factor by electron microscopy and mass spectrometry. *Blood.* 2015;126(8):935-938.
- Fay PJ. Activation of factor VIII and mechanisms of cofactor action. *Blood Rev.* 2004;18(1):1-15.
- Foster PA, Fulcher CA, Marti T, Titani K, Zimmerman TS. A major factor VIII binding domain resides within the amino-terminal 272 amino acid residues of von Willebrand factor. *J Biol Chem.* 1987;262(18):8443-8446.
- Przeradzka MA, Meems H, van der Zwaan C, et al. The D' domain of von Willebrand factor requires the presence of the D3 domain for optimal factor VIII binding. *Biochem J.* 2018;475(17):2819-2830.
- Castro-Núñez L, Bloem E, Boon-Spijker MG, et al. Distinct roles of Ser-764 and Lys-773 at the N terminus of von Willebrand factor in complex assembly with coagulation factor VIII. *J Biol Chem.* 2013;288(1):393-400.
- van den Biggelaar M, Meijer AB, Voorberg J, Mertens K. Intracellular cotrafficking of factor VIII and von Willebrand factor type 2N variants to storage organelles. *Blood.* 2009;113(13):3102-3109.
- Stel HV, Sakariassen KS, Scholte BJ, et al. Characterization of 25 Monoclonal antibodies to FVIII-von Willebrand factor: relationship between ristocetin-induced platelet aggregation and platelet adherence to subendothelium. *Blood.* 1984;63(6):1408-1415.
- Meems H, Van Den Biggelaar M, Rondaij M, et al. C1 domain residues Lys 2092 and Phe 2093 are of major importance for the endocytic uptake of coagulation factor VIII. *Int J Biochem Cell Biol.* 2011;43(8):1114-1121.
- Bloem E, Meems H, van den Biggelaar M, et al. Mass spectrometry-assisted study reveals that lysine residues 1967 and 1968 have opposite contribution to stability of activated factor VIII. *J Biol Chem.* 2012;287(8):5775-5783.
- van den Biggelaar M, Bouwens EAM, Voorberg J, Mertens K. Storage of factor VIII variants with impaired von Willebrand

- factor binding in Weibel-Palade bodies in endothelial cells. *PLoS One*. 2011;6(8):e24163.
29. Purvis AR, Gross J, Dang LT, et al. Two Cys residues essential for von Willebrand factor multimer assembly in the Golgi. *Proc Natl Acad Sci U S A*. 2007;104(40):15647-15652.
 30. Dong X, Leksa NC, Chhabra ES, et al. The von Willebrand factor D'D3 assembly and structural principles for factor VIII binding and concatemer biogenesis. *Blood*. 2019;133(14):1523-1533.
 31. Dimitrov JD, Christophe OD, Kang J, et al. Thermodynamic analysis of the interaction of factor VIII with von Willebrand factor. *Biochemistry*. 2012;51(20):4108-4116.
 32. Owen WG, Wagner RH. Antihemophilic factor: separation of an active fragment following dissociation by salts or detergents. *Thromb Diath Haemorrh*. 1972;27(3):502-515.
 33. Marcsisin SR, Engen JR. Hydrogen exchange mass spectrometry: what is it and what can it tell us? *Anal Bioanal Chem*. 2010;397(3):967-972.
 34. Morgan CR, Engen JR. Investigating solution-phase protein structure and dynamics by hydrogen exchange mass spectrometry. *Curr Protoc Protein Sci*. 2009;Chapter 17:Unit 17.6.1-17.
 35. Schneppenheim R, Budde U, Drewke E, et al. Results of a screening for von Willebrand disease type 2N in patients with suspected haemophilia A or von Willebrand disease type 1. *Thromb Haemost*. 1996;76(4):598-602.
 36. Dagil L, Troelsen KS, Bolt G, et al. Interaction Between the $\alpha 3$ Region of Factor VIII and the TIL'E' Domains of the von Willebrand Factor. *Biophys. J*. 2019;117(3):479-489.
 37. de Jong A, Eikenboom J. Von Willebrand disease mutation spectrum and associated mutation mechanisms. *Thromb Res*. 2017;159:65-75.



Ferrata Storti Foundation

Thrombotic biomarkers for risk prediction of malignant disease recurrence in patients with early stage breast cancer

Cinzia Giaccherini,^{1#} Marina Marchetti,^{1#} Giovanna Masci,² Cristina Verzeroli,¹ Laura Russo,¹ Luigi Celio,³ Roberta Sarmiento,⁴ Sara Gamba,¹ Carmen J. Tartari,¹ Erika Diani,¹ Alfonso Vignoli,¹ Paolo Malighetti,⁵ Daniele Spinelli,⁵ Carlo Tondini,⁶ Sandro Barni,⁷ Francesco Giuliani,⁹ Fausto Petrelli,⁷ Andrea D'Alessio,⁹ Giampietro Gasparini,⁴ Filippo De Braud,³ Armando Santoro,² Roberto Labianca¹⁰ and Anna Falanga,^{1,11} on behalf of the HYPERCAN Investigators**

Haematologica 2020
Volume 105(6):1704-1711

¹Immunohematology and Transfusion Medicine, Hospital Papa Giovanni XXIII, Bergamo; ²Oncology Unit, IRCCS Humanitas Institute, Rozzano; ³Oncology Unit, IRCCS National Cancer Institute, Milan; ⁴Oncology Unit, Hospital San Filippo Neri, Rome; ⁵Department of Management, Information and Production Engineering, University of Bergamo, Bergamo; ⁶Oncology Unit, Hospital Papa Giovanni XXIII, Bergamo; ⁷Oncology Unit, Hospital Treviglio-Caravaggio, Treviglio; ⁸Oncology Unit, IRCCS Cancer Institute Giovanni Paolo II, Bari; ⁹Medical Oncology and Internal Medicine, Policlinico San Marco, Zingonia-Bergamo; ¹⁰Department Oncology Bergamo Province, Hospital Papa Giovanni XXIII, Bergamo and ¹¹University of Milan Bicocca, School of Medicine and Surgery, Milan, Italy

#CG and MM contributed equally as co-first authors.

**A full list of the Investigators of the HYPERCAN (HYPERcoagulation in CANcer) Study Group appears in the Appendix 1.

ABSTRACT

In cancer patients, hypercoagulability is a common finding. It has been associated with an increased risk of venous thromboembolism, but also to tumor proliferation and progression. In this prospective study of a large cohort of breast cancer patients, we aimed to evaluate whether pre-chemotherapy abnormalities in hemostatic biomarkers levels: (i) are associated with breast cancer-specific clinico-pathological features; and (ii) can predict for disease recurrence. D-dimer, fibrinogen, prothrombin fragment 1+2, and FVIIa/antithrombin levels were measured in 701 early-stage resected breast cancer patients candidate to adjuvant chemotherapy and prospectively enrolled in the HYPERCAN study. Significant prognostic parameters for disease recurrence were identified by Cox regression multivariate analysis and used for generating a risk assessment model. Pre-chemotherapy D-dimer, fibrinogen, and prothrombin fragment 1+2 levels were significantly associated with tumor size and lymph node metastasis. After 3.4 years of follow up, 71 patients experienced a recurrence. Cox multivariate analysis identified prothrombin fragment 1+2, tumor size, and Luminal B HER2-negative or triple negative molecular subtypes as independent risk factors for disease recurrence. Based on these variables, we generated a risk assessment model that significantly differentiated patients at low- and high-risk of recurrence (cumulative incidence: 6.2 vs. 20.7%; Hazard Ratio=3.5; $P<0.001$). Our prospective clinical and laboratory data from the HYPERCAN study were crucial for generating a scoring model for assessing risk of disease recurrence in resected breast cancer patients, candidate to systemic chemotherapy. This finding stimulates future investigations addressing the role of plasma prothrombin fragment 1+2 in the management of breast cancer patients to provide the rationale for new therapeutic strategies. (The HYPERCAN study is registered at *clinicaltrials.gov* identifier 02622815.)

Correspondence:

ANNA FALANGA
annafalanga@yahoo.com

Received: June 7, 2019.

Accepted: September 24, 2019.

Pre-published: September 26, 2019.

doi:10.3324/haematol.2019.228981

Check the online version for the most updated information on this article, online supplements, and information on authorship & disclosures: www.haematologica.org/content/105/6/1704

©2020 Ferrata Storti Foundation

Material published in *Haematologica* is covered by copyright. All rights are reserved to the Ferrata Storti Foundation. Use of published material is allowed under the following terms and conditions:

<https://creativecommons.org/licenses/by-nc/4.0/legalcode>.

Copies of published material are allowed for personal or internal use. Sharing published material for non-commercial purposes is subject to the following conditions:

<https://creativecommons.org/licenses/by-nc/4.0/legalcode>,

sect. 3. Reproducing and sharing published material for commercial purposes is not allowed without permission in writing from the publisher.



Introduction

Cancer growth and dissemination is associated with the development of a subclinical hypercoagulable state in the host, detectable by coagulation laboratory tests.^{1,2} The pathogenesis of blood coagulation activation in cancer is complex and multifactorial. Among other factors, the expression of tumor cell clot-promoting properties, and the inflammatory response of the normal host cells to the tumor play a central role in the cancer-associated prothrombotic diathesis by leading to the activation of the blood clotting system.^{2,3} Importantly, tumor cells of different origin express different procoagulant profiles, and the clotting system can be triggered to various extents according to the type and stage of the malignant disease.⁴ Furthermore, the patient's hypercoagulable state worsens with cancer progression and metastatic spread, which supports the concept of a tight relationship between tumor burden and hemostatic abnormalities.⁵ All this contributes to an increased risk of thrombosis, and also affects the tumor biology by favoring tumor growth and metastasis.^{6,7}

Over the last three decades, several studies have evaluated the role of clotting activation biomarkers in relation to cancer outcomes, including disease progression, response to chemotherapy, and mortality.⁸⁻¹¹ As recently reviewed,¹² however, most of these studies were retrospective in nature and not always specifically designed to address the impact of thrombotic biomarkers on cancer outcomes. In addition, recruitment was often mono-institutional, and included small heterogeneous cohorts of patients with different treatments. Therefore, despite the encouraging results reported, new data coming from large prospective cohorts are needed. In this respect, breast cancer patients with limited resected disease are an important setting to test whether abnormal levels of circulating thrombotic biomarkers may represent a novel non-invasive factor for better prediction of disease recurrence (DR) risk.

Breast cancer, the most common cancer in women, is a highly heterogeneous disease presenting with a broad range of clinical and molecular characteristics, as well as variability in clinical progression. In recent years, information campaigns and large-scale prevention screening programs have contributed to an increase in the rate of early diagnosis,¹³ with a consequent improved rate of patients treated at an early stage of the disease.¹⁴ For the treatment choice, patients are classified according to intrinsic biological subtypes within the breast cancer spectrum, using clinico-pathological criteria, i.e. the immunohistochemical definition of estrogen receptor (ER) and progesterone receptor (PR), the detection of overexpression and/or amplification of the human epidermal growth factor receptor 2 (HER2) oncogene, and Ki-67 labeling index. This classification allows for a more personalized approach to the medical treatments, with favorable results. However, in spite of this, almost 10-15% of these patients still experience local or distant recurrences in the first five years from diagnosis,^{15,16} mainly in the high-risk category, characterized by worse prognostic factors in which the use of adjuvant systemic chemotherapy is justified.^{17,18} In this category, the identification of patients at the highest risk of relapse is an important area in which to improve personalized treatments and, ultimately, cancer care.

In the present study, we tested the predictive role of circulating clotting biomarkers on DR risk in a large patient cohort with resected high-risk breast cancer scheduled to receive post-surgical adjuvant chemotherapy enrolled in the ongoing prospective observational Italian multicenter HYPERCAN ("HYPERcoagulation and CANcer") study.¹⁹ Specifically, we investigated whether baseline levels of D-dimer, fibrinogen, prothrombin fragment 1+2 (F1+2), and FVIIa/antithrombin (FVIIa-AT) complex were associated with clinico-pathological characteristics of breast cancer, and whether these biomarkers might be effective in predicting DR in patients at an early stage of the disease.

Methods

Study design and study population

For the present study, we considered patients of both genders with a high-risk surgically treated breast cancer enrolled in the ongoing HYPERCAN study¹⁹ (*Online Supplementary Appendix*). The study protocol was approved by the local ethics committee. A data extraction from the HYPERCAN database was performed in January 2018. Patients enrolled from March 2012 to December 2015 were considered for the study. Of the 1,042 patients with resected breast cancer enrolled during this period, 953 had an adequate follow-up time. Data on ER/PR and HER2 positivity were available in 788 patients; in this subgroup, biomarkers data were available for 701 patients (*Online Supplementary Figure S1*). Median time of follow up at the time of the present analysis is 3.4 years.

Patient classification

Patients were categorized in subtypes according to tumor expression of ER, PR, ki67, and HER2 according to the American Society of Clinical Oncology (ASCO) - College of American Pathologist (CAP) guideline.²⁰ Data were derived from clinical pathology reports. ER/PR positivity defined the luminal groups, which included: Luminal A [i.e. HER2-negative (neg) and low Ki67]; Luminal B HER2-neg (i.e. HER2 negativity and high Ki67), and Luminal B HER2-positive (pos) (i.e. HER2-pos and any ki67). HER2-pos cancer subtype was defined by negativity for ER/PR and positivity for HER2, while triple negative (TN) cancer was defined by ER/PR and HER2 negativity.

Blood sampling and plasma preparation

Fasting peripheral venous blood was drawn at enrollment prior to start of systemic adjuvant chemotherapy using a 21-gauge needle into 6 mL vacutainer tubes containing 0.109 M citrate (9:1 vol/vol; Becton Dickinson) after discarding the first 2-3 mL of blood.²¹ Within two hours from collection, plasma was isolated by two sequential centrifugations at 2,600 rpm for 15 minutes (min)²² and stored at -80°C. All samples were anonymized and tested in blind at the Laboratory of Hemostasis and Thrombosis Center (Hospital Papa Giovanni XXIII, Bergamo, Italy).

Hypercoagulation biomarkers

Plasma levels of D-dimer (HemosIL D-dimerHS, Werfen Group) and fibrinogen (QFA thrombin, Werfen Group) were measured on an automated coagulometer analyzer (ACL TOP500, Werfen Group). F1+2 (Siemens Healthcare Diagnostics) and FVIIa-AT complex (Stago) were determined by commercial ELISA. Reference intervals for coagulation biomarkers were internally generated from a group of 200 apparently healthy controls (170 females; 30 males) with no chronic or acute diseases. Median age was 49 years (range, 35-64 years).

Outcome

The primary outcome of the present analysis was DR, defined as either loco-regional (limited to the ipsilateral breast or chest wall and/or axillary, infraclavicular, or supraclavicular lymph nodes) or distant metastasis.

Statistical analysis

Categorical data are summarized as frequencies and proportions, while for continuous variables, data are summarized as mean and standard deviation or median and 5th-95th percentile range, depending on their distribution. Differences between groups were tested by Pearson's χ^2 test, Student *t*-test or Mann-Whitney U-test. Survival functions were estimated using the Kaplan-Meier method, assuming as baseline time the beginning of chemotherapy, while survival analyses were performed using Cox's proportional hazard (PH) model. Statistical analysis was performed using SPSS v21.0 (IBM Corp).

Results

Characteristics of study population

Table 1 summarizes clinical and tumor histological characteristics of study patients (median age 52; range, 29-79 years). Breast-conserving resection was performed in 61% and mastectomy in 39%. HER-2 expression was positive in 203 and negative in 498 patient sample specimens, respectively. Most frequent molecular subtypes were Luminal B HER2-neg (33.4%) > Luminal A (22.7%) > Luminal B HER2-pos (20.3%) > TN (14.4%) > HER2-pos (8.6%) (4 missing data for ki67 =0.6%). According to histological subtype, the largest proportion was classified as invasive ductal carcinoma, diagnosed in 83% of patients. Lymph node involvement was found in 56% of patients. Based on primary tumor characteristics, ER/PR and HER2 status, age, and/or discretion of the treating physician, patients were candidates for systemic adjuvant chemotherapy. An anthracycline-based regimen was indicated for 35.1% of patients. The addition of taxane to an anthracycline regimen was considered in case of extensive disease burden or TN disease (50.8% of patients). A taxane-based regimen without anthracyclines was administered to 9.3% of patients. In case of comorbidities or patient preference, intravenous CMF (i.e. cyclophosphamide, methotrexate and 5-fluorouracil) was given (4.8% of patients). All 203 HER-2 positive breast cancers received (in addition to chemotherapy) trastuzumab every 21 days for one year. Four hundred and seventy-five patients with ER/PR positivity (n=535) received endocrine therapy according to their premenopausal state (data missing in 48 patients).

Disease recurrence

The Kaplan-Meier curve shown in Figure 1 describes the cumulative incidence of DR during four years of follow up. The incidence of DR in the group of patients was 2% (95%CI: 1-3) at one year, 6% (95%CI: 4.3-7.8) at two years, 9.5% (95%CI: 7.2-11.9) at three years, and 11.2% (95%CI:8.5-14) at four years. Specifically, 630 out of 701 patients included into the analysis remained disease-free, while 71 relapsed. Demographics and clinical characteristics of patients who developed DR and of those who remained disease-free are shown in Table 1. The group of patients who relapsed comprised 68 females and three males, with a median age of 52 years (range, 34-78 years).

Recurrences consisted of distant metastasis in 69% of cases, and loco-regional relapse in the remaining 31%. According to the molecular subtype, the majority of

Table 1. Characteristics of patients with resected breast cancer.

	All patients 701	No DR 630	DR 71	P
Gender				
Male	11 (1.6)	8 (1.3)	3 (4.2)	0.091
Female	690 (98.4)	622 (98.7)	68 (95.8)	
Age				
Median (5 th -95 th)	52 (37-73)	52 (36-72)	52 (37-76)	0.893
Stage				
IA	173 (24.7)	165 (26.2)	8 (11.3)	0.037*
IIA	225 (32.1)	209 (33.2)	16 (22.5)	
IIB	125 (17.8)	104 (16.5)	21 (29.6)	
IIIA	85 (12.1)	75 (11.9)	10 (14.1)	
IIIB	9 (1.3)	8 (1.3)	1 (1.4)	
IIIC	44 (6.3)	38 (6.0)	6 (8.4)	
Unknown	40 (5.7)	31 (4.9)	9 (12.7)	
Tumor size				
≤ 2 cm	80 (11.3)	76 (12.1)	4 (5.6)	0.011
2-5 cm	245 (35.0)	227 (36.0)	18 (25.4)	
≥ 5 cm	342 (48.8)	295 (46.8)	47 (66.2)	
Unknown	34 (4.9)	32 (5.1)	2 (2.8)	
N stage				
N0	287 (40.9)	268 (42.5)	19 (26.8)	0.020*
N1	268 (38.3)	236 (37.5)	32 (45.1)	
N2	77 (11.0)	70 (11.1)	7 (9.8)	
N3	48 (6.8)	40 (6.3)	8 (11.3)	
Unknown	21 (3.0)	16 (2.6)	5 (7.0)	
Histological type				
Ductal	580 (82.7)	526 (83.5)	54 (76.1)	0.193*
Lobular	56 (8.0)	49 (7.8)	7 (9.9)	
Mixed	4 (0.6)	3 (0.5)	1 (1.4)	
Others	44 (6.3)	38 (6.0)	6 (8.4)	
Unknown	17 (2.4)	14 (2.2)	3 (4.2)	
Grading				
G1	14 (2.0)	14 (2.2)	-	0.550*
G2	264 (37.7)	238 (37.8)	26 (36.6)	
G3	409 (58.3)	365 (57.9)	44 (62.0)	
Unknown	14 (2.0)	13 (2.1)	1 (1.4)	
Molecular subtype				
Luminal A	159 (22.7)	149 (23.7)	10 (14.1)	<0.001
Luminal B HER2-neg	234 (33.4)	201 (31.9)	33 (46.5)	
Luminal B HER2-pos	142 (20.3)	137 (21.7)	5 (7.0)	
HER2-pos	61 (8.6)	58 (9.2)	3 (4.2)	
Triple negative	101 (14.4)	82 (13.0)	19 (26.8)	
Unknown	4 (0.6)	3 (0.5)	1 (1.4)	
Surgery				0.047
Breast conserving	427 (61.0)	392 (62.2)	35 (49.3)	
Mastectomy	273 (38.9)	238 (37.8)	35 (49.3)	
Unknown	1 (0.1)	-	1 (1.4)	
ECOG-PS				
0	634 (90.4)	569 (90.3)	65 (91.6)	0.402
1	26 (3.7)	22 (3.5)	4 (5.6)	
Unknown	41 (5.9)	39 (6.2)	2 (2.8)	

Data are presented as number (percentage). *P* is statistical significance by Pearson's χ^2 test (or by Mann-Whitney test for age) for comparison between patients with disease recurrence (DR) and without relapse (no DR). χ^2 test performed on clustered groups (stage 1/2/3). χ^2 test performed on clustered groups (N0 vs. N1, N2, N3). χ^2 test performed on clustered groups (ductal vs. others). χ^2 test performed on clustered groups (G1/G2 vs. G3). HER2: human epidermal growth factor receptor 2; ECOG-PS: Eastern Cooperative Oncology Group Performance Status; N: number; neg: negative; pos: positive.

relapses occurred in Luminal B HER2-neg (n=33) and in TN (n=19), while the remaining were in Luminal A (n=10), in Luminal B HER2-pos (n=3), and in HER2-pos (n=3) patients; for one patient, this information was not available. The risk of recurrence was increased 4-fold ($P<0.01$) in patients with Luminal B HER2-neg and TN subtypes (HR=4.2, 95%CI: 2.3-7.8) compared to the remaining patients, with a DR cumulative incidence at four years of 17.6% (95%CI: 12.9-22.4) and 4.9% (95%CI: 2.4-7.5), respectively. Finally, the group of patients with DR was characterized by a higher proportion of subjects with tumor size ≥ 5 cm ($P=0.011$), infiltrated axillary lymph nodes ($P=0.020$), mastectomy ($P=0.047$), and Luminal B HER2-neg and TN molecular subtypes.

Hypercoagulation biomarkers and hematologic parameters

Patients had significantly higher plasma levels ($P<0.01$) of D-dimer, fibrinogen, and F1+2, compared to internal reference values obtained from a control group of healthy subjects (Figure 2). To exclude any influence of surgery [median time to blood sampling: 43 days (5th-95th range: 26-72 days)] on coagulation, the levels of each hemostatic marker were correlated with the time from surgery. The results showed no statistically significant correlation between time from surgery and each of the biomarkers (*data not shown*), even after sex and gender correction.

At enrollment, 12 patients were on thromboprophylaxis with anti-platelet agents (i.e. aspirin) and four with anticoagulants. To exclude any influence of thromboprophylaxis on thrombotic biomarker levels, we compared patients on aspirin (n=12) with those who were not (n=689), and no significant differences were found. The comparison of biomarkers between the anticoagulated (n=4) versus non-anticoagulated (n=697) subjects could not provide statistically reliable results due to the very small number of subjects on anticoagulants.

Hemochromocytometric tests showed most patients had low red blood cell count and hemoglobin levels as compared to the control reference range (Table 2).

Association of hypercoagulation biomarkers with tumor characteristics

Multivariate analyses were performed to search for any significant association between hypercoagulation biomarker levels, hematologic parameters and tumor characteristics. According to tumor-node-metastasis classification, tumor size was a significant determinant of D-dimer ($\beta=0.134$, $P=0.001$) and fibrinogen ($\beta=0.110$, $P=0.006$) levels, while lymph node involvement positivity was a significant predictor of D-dimer ($\beta=0.216$, $P<0.001$) and F1+2 ($\beta=0.112$, $P=0.004$) plasma levels. No significant associations were found between hypercoagulation biomarkers and tumor histological subtype or grading. Similarly, no significant associations were found between hematologic parameters and tumor characteristics.

Association between hypercoagulation biomarker abnormalities and disease recurrence

Plasma levels of hypercoagulation biomarkers and hematologic parameters according to DR occurrence are shown in Table 3. There was no statistical difference in levels of the D-dimer, FVIIa-AT and fibrinogen between patients who experienced a relapse as compared to patients who remained disease-free during follow up, while F1+2 levels were significantly higher in the group of relapsed patients ($P<0.05$). Interestingly, correlation analyses showed that pre-chemotherapy levels of fibrinogen were significantly and inversely associated with time to relapse ($\beta = -0.317$; $P=0.012$).

A receiver operating characteristic (ROC) curve analysis was performed to evaluate the contribution of F1+2 levels to predict DR at four years of follow up. The area under the curve was 0.595. Cut-off value was set at 202.5

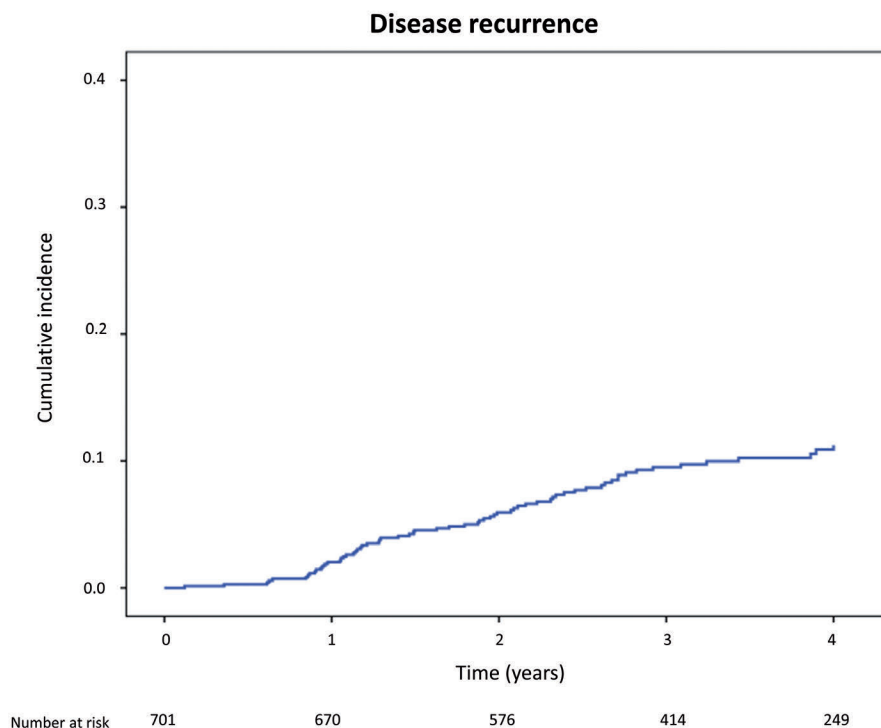


Figure 1. Cumulative incidence of disease recurrence in patients with resected breast cancer during four years follow up.

(pmol/L) (sensitivity=61%, specificity=53%). Kaplan-Meier analysis showed that in patients with F1+2 levels above the cut-off, cumulative incidence of DR was 14.7% (95%CI:10.2-19.2) and was significantly ($P<0.05$) higher than in patients with F1+2 levels \leq cut-off (8.7%; 95%CI: 5.4-12). A multivariate Cox regression analysis, stratified for age, was carried out testing for clinico-pathological covariates (Body Mass Index, smoking habit, infection, molecular subtype, tumor size, lymph node status, use of anticoagulant/anti-platelet agents, and type of surgery). After backward selection, only increased F1+2 value (HR 2; 95%CI: 1.1-3.6; $P=0.019$), tumor size \geq 5cm (HR 2.6; 95%CI:1.4-4.6; $P=0.001$), and having Luminal B HER2-neg or TN molecular subtypes (HR 3.9; 95%CI: 2.1-7.5; $P<0.001$) were identified as independent risk factors for DR.

To exclude any influence of the pre-analytical phase on biomarkers levels, we performed the multivariate Cox regression analysis stratifying for recruiting centers. Results confirmed F1+2, tumor size and molecular subtypes as significant independent risk factors for DR.

The co-efficients of the multivariate analysis for each independent co-variate were used to generate a risk assessment score, as follows: F1+2 > 202.5 pmol/L = +1, tumor

size \geq 5cm = +1.3, Luminal B HER2-neg and TN molecular subtypes = +2. After score calculation, a ROC curve analysis was performed to evaluate the contribution of score value for DR (Online Supplementary Figure S2). The area under the curve was 0.72. The risk groups were created using a cut-off value of 2.65 points (sensitivity=66%, specificity=67%). Kaplan Meier curves according to risk groups are shown in Figure 3. Cumulative incidence of DR was 6.2% (IC 95%: 3.6-8.7) and 20.7% (IC 95%: 14.8-26.6), in the low-risk (score<3) and high-risk (score \geq 3) groups, respectively (HR 3.5; 95%CI: 2.1-6.0; $P<0.001$).

Discussion

In this large, prospective cohort study of 701 patients with early stage, surgically resected, high-risk breast cancer, enrolled in the HYPERCAN study, we characterized the baseline hypercoagulability status before starting systemic chemotherapy and investigated the capacity of plasma thrombotic biomarkers to predict DR. This represents the first large prospective study specifically designed to assess hemostatic activation and its association with recurrence risk in breast cancer patients.

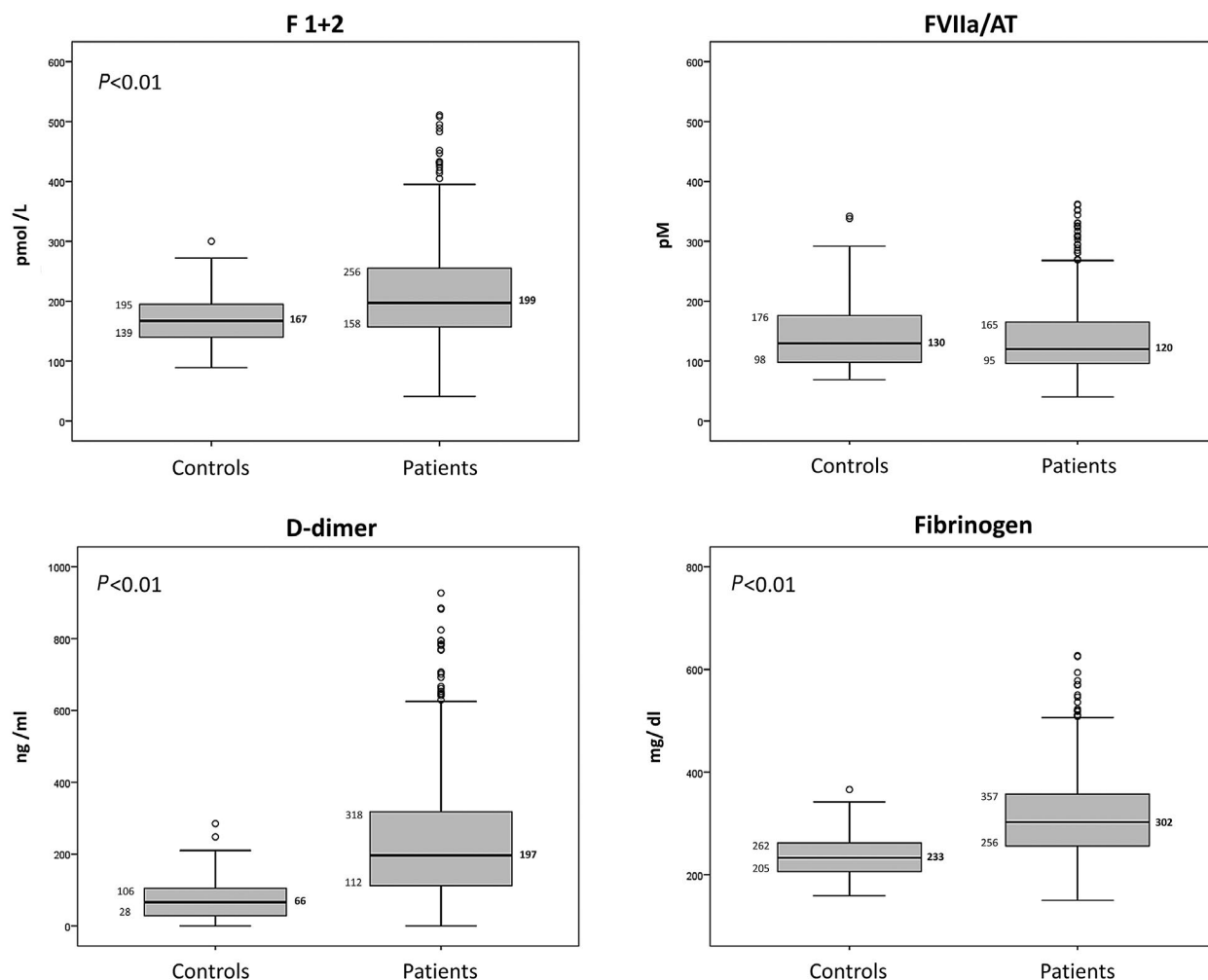


Figure 2. Distribution of F1+2, FVIIa-AT complex, D-dimer and fibrinogen values in patients compared to controls. The 25th, 50th and 75th percentile values are indicated for each biomarker and group. P-value calculated by Mann-Whitney test. AT: antithrombin; F1+2: prothrombin fragment 1+2.

In particular, we chose to study the role of fibrinogen, FVIIa-AT, F1+2, and D-dimer. Fibrinogen, a glycoprotein synthesized by the liver, is enzymatically converted to fibrin by thrombin during the coagulation process. In normal conditions, it circulates in plasma at high concentrations, and its levels increase in inflammatory states as part of the acute-phase response. Circulating levels of FVIIa-AT complexes reflect the degree of exposure of cellular tissue factor to blood; increased FVIIa-AT levels have been reported in a number of prothrombotic conditions, including solid and hematologic malignancies.²³ F1+2 is a peptide released during the proteolytic activation of prothrombin into active thrombin, and represents a parameter of *in vivo* thrombin formation, while D-dimer is the primary degradation product of cross-linked fibrin, representing an index of both coagulation and fibrinolysis activation. It has been suggested that fibrinogen is involved in several stages of cancer progression.²⁴ *In vivo*, in breast cancer patients, high fibrinogen levels have been associated with poorer overall survival^{25,26} and poor response to therapy,²⁷ while increase in D-dimer levels has been related to growth rate, tumor burden, progression rate, and survival.^{12,28}

In the present prospective cohort of patients with resected tumors and candidates to adjuvant therapy, we found the occurrence of a moderate, but significant, hypercoagulable state, as indicated by the increased plasma levels of fibrinogen, F1+2, and D-dimer. The lack of correlation between thrombotic biomarker levels and the time from surgery suggests involvement of a tumor-related mechanism in the hypercoagulability observed in these patients. Indeed, levels of thrombotic biomarkers, and particularly D-dimer and fibrinogen, positively and significantly correlated with tumor size and lymph node metastasis. The association with tumor characteristics might suggest an imprinting of the primary tumor on the coagulation system after resection, and might also represent the activity of residual occult circulating tumor cells on blood coagulation. In fact, it is well known that breast cancer cells can activate blood coagulation through several mechanisms,^{4,29,30} and *in vivo* studies in breast cancer patients show significant correlations between increased D-dimer levels with circulating tumor cells and number of metastasis,³¹ as well as with lymphovascular invasion, clinical stage, and lymph node involvement.³²

To understand the relevance of our observation in rela-

Table 2. Hematologic parameters in the study subjects.

	Patients	Reference range	Out of range
White blood cells (x10 ⁹ /L)	6.8 (2.0)	(4.2-9.4)	4% (<4.2) 9% (>9.4)
Red blood cells (x10 ¹² /L)	4.47 (0.51)	(4.7-5.82)	76% (<4.7) 0.5% (>5.82)
Hemoglobin (g/dL)	13.1 (1.3)	(14-17)	75% (<14)
Platelets (x10 ⁹ /L)	267 (80)	(150-400)	5% (>400)

Data of patients are shown as mean (standard deviation). Reference ranges are internally defined.

Table 3. Plasma levels of coagulation biomarkers according to disease recurrence.

	No-DR	DR	P
D-dimer (ng/mL)	196 (49-647)	224 (30-653)	0.270
FVIIa-AT (pM)	120 (70-269)	110 (62-335)	0.382
F 1+2 (pmol/L)	197 (117-385)	219 (114-628)	0.024
Fibrinogen (mg/dL)	298 (211-489)	321 (209-455)	0.909

Data are shown as median and range (5th-95th percentiles). P-value calculated by Mann-Whitney test. AT: antithrombin; F 1+2: prothrombin fragment 1+2; DR: disease recurrence.

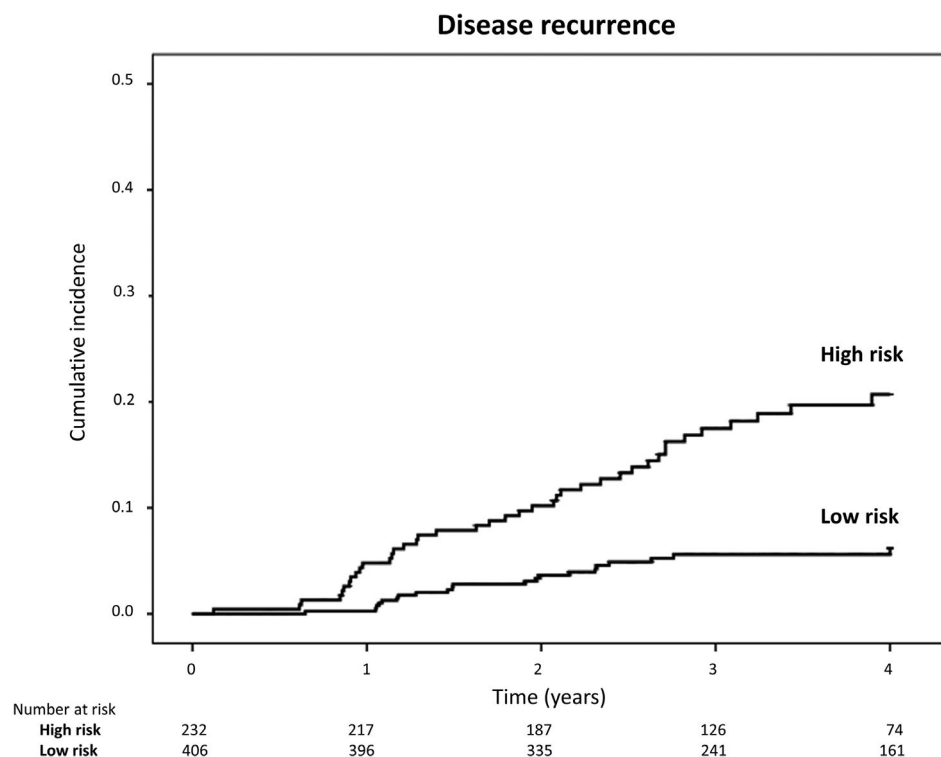


Figure 3. Kaplan-Meier analysis of disease recurrence cumulative incidence in patients according to risk-groups derived from the score (low-risk < 3, high-risk ≥ 3).

tion to the primary outcome of the study, we analyzed the patient thrombotic biomarkers according to DR. Relapses occurred in 71 patients, with distant metastasis in 69% and loco-regional metastasis in 31% of cases, respectively, providing a 10.8% cumulative incidence of DR after four years of follow up. As expected, most patients with DR belong to the Luminal B HER2-neg (46.5%) and TN (26.8%) subtypes. As regards thrombotic biomarkers, patients who subsequently experienced DR showed significantly ($P < 0.05$) higher circulating levels of F1+2, compared to disease-free subjects. Remarkably, high fibrinogen levels were significantly associated with shorter time to DR, also after age and gender correction by multivariate analysis. Recurrence can be considered to be the result of cancer cells that persist in the host after treatments and start to proliferate and disseminate after years of quiescence. Activation of the clotting system might represent the first sign of tumor cell proliferation, and increased levels of thrombotic biomarkers can be an echo of occult tumor cell action on the hemostatic system. This is probably what is happening in our population, as detected by hypercoagulability biomarkers. That blood clotting activation might be an overt sign of an occult cancer is supported by clinical studies in cancer-free subjects, showing that hypercoagulability is a risk factor for subsequent death from cancer.^{33,34} Analyses of hemostatic biomarkers in 19,303 male participants from three English cohorts followed for up to 30 years identified elevated circulating levels of fibrinogen and F1+2 as predictors of risk of smoking-related cancers.³⁵ In the setting of breast cancer, in a Scandinavian case-control study, high D-dimer and low antithrombin significantly predicted for breast cancer diagnosis,³⁶ while fibrinogen, in combination with cancer antigen 15-3 and platelet distribution width, distinguished breast cancer from benign breast disease in non-conclusive mammography patients.³⁷

Furthermore, we were able to combine a clotting biomarker with previously established breast cancer prognostic factors in order to improve the individual prediction recurrence in this high-risk population. In fact, we found that higher F1+2 values, TN and Luminal B HER2-neg molecular subtypes, and tumor size were independent risk factors for DR. Therefore, F1+2 might be very helpful to identify those subjects who deserve special attention and those who can instead avoid the side effects of sustained chemotherapy. Finally, the significant association between fibrinogen levels and time to DR suggests the potential utility of this marker in those subjects identified at greater risk of DR as a parameter indicative of time to DR.

Other authors have reported different results as regards the F1+2 prognostic role in breast cancer. Specifically, in a recently published study including 235 patients with stage I-IIA breast cancer, F1+2 was not predictive for disease-free survival.¹¹ This discrepancy may be due to different characteristics of that study: a single center study, involving a smaller cohort of patients with stage I and IIa breast cancer (whereas our study enrolls patients up to stage IIIC). In addition, in that study, the disease-free survival was evaluated in a subgroup of 62 patients and blood samples for biomarker testing were obtained before surgery, while our samples were collected in tumor-resected condition before starting chemotherapy.

One limitation of our study is that some data on factors which can have an impact on coagulation cascade, including treatments with corticosteroids, oral contraceptives,

and hormone replacement therapy, were not collected at the time of blood sampling. In any case, the hemostatic assays performed in this study directly represent the *in vivo* activity of the coagulation system, which already reflects all possible factors. In addition, at the time of this analysis, data on hormone therapy and radiotherapy were not available for all patients, and therefore were not included in the analysis. An evaluation of the contribution of these data on prognosis in these patients should be a subject of future study.

Several patients relapsed after a relatively long period of time and, therefore, the question may arise as to whether the time elapsed between blood collection and cancer relapse might be a source of uncontrolled confounding bias. This is a common limitation of prognostic biomarkers which aim to predict the cancer patient outcomes in order to decide on a best treatment option strategy. Validated genetic and biochemical prognostic biomarkers in early breast cancer provide a risk of DR for an event that may occur up to ten years later. In this study, we aimed to identify new prognostic biomarkers to help the selection of patients at highest risk of relapse at presentation, before planning the antitumor strategy. In this sense, we are consistent with the aim of the study, as our results identify a prognostic score based on the F1+2 applicable at presentation.

In conclusion, our prospective study is the first to demonstrate the utility of F1+2 as a potential circulating independent predictive biomarker for DR in a large cohort of patients with high-risk early breast cancer. Having reached this goal, we are now planning to validate the results in an independent cohort of patients. Our findings stimulate future investigations into the utility of longitudinal measurement of plasma F1+2 in the surveillance of women following surgery for primary breast cancer and to provide the rationale for new therapeutic strategies.

Appendix 1

The members of the HYPERCAN Study Group (all in Italy) are as follows: Investigators (by center) - Immunohematology and Transfusion Medicine, Hospital Papa Giovanni XXIII, Bergamo: Falanga A., Brevi S., Caldara G., Diani E., Gamba S., Giaccherini C., Marchetti M., Russo L., Schieppati F., Tartari C.J., Verzeroli C., Vignoli A.; Oncology Unit, IRCCS Humanitas Institute, Rozzano: Santoro A., Masci G.; Oncology Unit, IRCCS National Cancer Institute, Milan: De Braud F., Celio L., Nichetti F., Martinetti A.; Oncology Unit, Hospital Papa Giovanni XXIII, Bergamo: Tondini C.; Oncology Unit, Hospital San Filippo Neri, Rome: Gasparini G., Sarmiento R., Gennaro E., Meoni G.; Oncology Unit, Hospital San Giovanni, Rome: Minelli M.; Oncology Unit, Hospital Treviglio-Caravaggio, Treviglio: Barni S., Petrelli F., Ghilardi M.; Dept. of Management, Information and Production Engineering, University of Bergamo: Malighetti P., Spinelli D.; Dept. Oncology Bergamo Province, Hospital Papa Giovanni XXIII, Bergamo: Labianca R.; IRCCS Cancer Institute Giovanni Paolo II, Bari: Giuliani F.; Medical Oncology and Internal Medicine, Policlinico San Marco, Zingonia-Bergamo: D'Alessio A., Cecchini S.

Acknowledgments

The authors would like to thank "Associazione Italiana Ricerca sul Cancro" for grant "AIRC 5xmille n. 12237", and the CRO (Contract Research Organization) "High Research srl" for project management trial monitoring.

References

- Falanga A, Schieppati F, Russo D. Cancer Tissue Procoagulant Mechanisms and the Hypercoagulable State of Patients with Cancer. *Semin Thromb Hemost*. 2015;41(7):756-764.
- Falanga A, Marchetti M, Vignoli A. Coagulation and cancer: biological and clinical aspects. *J Thromb Haemost*. 2013;11(2):223-233.
- Falanga A, Russo L, Verzeroli C. Mechanisms of thrombosis in cancer. *Thromb Res*. 2013;131 Suppl 1:S59-62.
- Marchetti M, Diani E, ten Cate H, Falanga A. Characterization of the thrombin generation potential of leukemic and solid tumor cells by calibrated automated thrombography. *Haematologica*. 2012;97(8):1173-1180.
- Rickles FR, Falanga A. Activation of clotting factors in cancer. *Cancer Treat Res*. 2009;148:31-41.
- Falanga A, Panova-Noeva M, Russo L. Procoagulant mechanisms in tumour cells. *Best Pract Res Clin Haematol*. 2009;22(1):49-60.
- Adams GN, Rosenfeldt L, Frederick M, et al. Colon Cancer Growth and Dissemination Relies upon Thrombin, Stromal PAR-1, and Fibrinogen. *Cancer Res*. 2015;75(19):4235-4243.
- Guo R, Yang J, Liu X, Wu J, Chen Y. Increased von Willebrand factor over decreased ADAMTS-13 activity is associated with poor prognosis in patients with advanced non-small-cell lung cancer. *J Clin Lab Anal*. 2018;32(1).
- Falanga A, Marchetti M, Massi D, et al. Thrombophilic status may predict prognosis in patients with metastatic BRAFV600-mutated melanoma who are receiving BRAF inhibitors. *J Am Acad Dermatol*. 2016;74(6):1254-1256.e4.
- Ma C, Lu B, Diao C, et al. Preoperative neutrophil-lymphocyte ratio and fibrinogen level in patients distinguish between muscle-invasive bladder cancer and non-muscle-invasive bladder cancer. *Onco Targets Ther*. 2016;9:4917-4922.
- Mandoj C, Pizzuti L, Sergi D, et al. Observational study of coagulation activation in early breast cancer: development of a prognostic model based on data from the real world setting. *J Transl Med*. 2018;16(1):129.
- Falanga A, Marchetti M. Hemostatic biomarkers in cancer progression. *Thromb Res*. 2018;164 Suppl 1:S54-S61.
- Howlander N, Noone AM, Krapcho M et al. SEER cancer statistics review, 1975–2013. Bethesda, MD: National Cancer Institute. Available at http://seer.cancer.gov/csr/1975_2013/. 2016.
- American cancer society. Breast Cancer Facts & Figures 2017-2018. Available at <https://www.cancer.org/research/cancer-facts-statistics/breast-cancer-facts-figures.html>.
- Kennecke H, Yerushalmi R, Woods R, et al. Metastatic behavior of breast cancer subtypes. *J Clin Oncol*. 2010;28(20):3271-3277.
- Colleoni M, Sun Z, Price KN, et al. Annual Hazard Rates of Recurrence for Breast Cancer During 24 Years of Follow-Up: Results From the International Breast Cancer Study Group Trials I to V. *J Clin Oncol*. 2016;34(9):927-935.
- Gnant M, Harbeck N, Thomssen C. St. Gallen/Vienna 2017: A Brief Summary of the Consensus Discussion about Escalation and De-Escalation of Primary Breast Cancer Treatment. *Breast Care (Basel)*. 2017;12(2):102-107.
- National Comprehensive Cancer Network NCCN Clinical Practice Guidelines in Oncology: Breast Cancer. Fort Washington, PA: NCCN; 2017. Ver. 3.2017. Available at: https://www.nccn.org/professionals/physician_gls/pdf/breast.pdf. 2017.
- Falanga A, Santoro A, Labianca R, et al. Hypercoagulation screening as an innovative tool for risk assessment, early diagnosis and prognosis in cancer: the HYPERCAN study. *Thromb Res*. 2016;140 Suppl 1:S55-59.
- Wolff AC, Hammond ME, Hicks DG, et al. Recommendations for human epidermal growth factor receptor 2 testing in breast cancer: American Society of Clinical Oncology/College of American Pathologists clinical practice guideline update. *J Clin Oncol*. 2013;31(31):3997-4013.
- D'Alessio A, Marchetti M, Tartari CJ, et al. Long Term Low Molecular Weight Heparin Anticoagulant Therapy Modulates Thrombin Generation and D-dimer in Patients with Cancer and Venous Thromboembolism. *Cancer Invest*. 2017;35(7):490-499.
- Marchetti M, Tartari CJ, Russo L, et al. Phospholipid-dependent procoagulant activity is highly expressed by circulating microparticles in patients with essential thrombocythemia. *Am J Hematol*. 2014;89(1):68-73.
- Spiezia L, Campello E, Valle FD, Woodhams B, Simioni P. Factor VIIa-antithrombin complex: a possible new biomarker for activated coagulation. *Clin Chem Lab Med*. 2017;55(4):484-488.
- Palumbo JS, Kombrinck KW, Drew AF, et al. Fibrinogen is an important determinant of the metastatic potential of circulating tumor cells. *Blood*. 2000;96(10):3302-3309.
- Wen J, Yang Y, Ye F, et al. The preoperative plasma fibrinogen level is an independent prognostic factor for overall survival of breast cancer patients who underwent surgical treatment. *Breast*. 2015;24(6):745-750.
- Krenn-Pilkko S, Langsenlehner U, Stojakovic T, et al. An elevated preoperative plasma fibrinogen level is associated with poor disease-specific and overall survival in breast cancer patients. *Breast*. 2015;24(5):667-672.
- Liu YL, Lu Q, Liang JW, et al. High plasma fibrinogen is correlated with poor response to trastuzumab treatment in HER2 positive breast cancer. *Medicine*. 2015;94(5):e481.
- Dirix LY, Salgado R, Weytjens R, et al. Plasma fibrin D-dimer levels correlate with tumour volume, progression rate and survival in patients with metastatic breast cancer. *Br J Cancer*. 2002;86(3):389-395.
- Rousseau A, Van Dreden P, Mbemba E, et al. Cancer cells BXP3 and MCF7 differentially reverse the inhibition of thrombin generation by apixaban, fondaparinux and enoxaparin. *Thromb Res*. 2015;136(6):1273-1279.
- Rousseau A, Larsen AK, Van Dreden P, et al. Differential contribution of tissue factor and Factor XII to thrombin generation triggered by breast and pancreatic cancer cells. *Int J Oncol*. 2017;51(6):1747-1756.
- Mego M, Zuo Z, Gao H, et al. Circulating tumour cells are linked to plasma D-dimer levels in patients with metastatic breast cancer. *Thromb Haemost*. 2015;113(3):593-598.
- Pradhan S, Hassani I, Seeto WJ, Lipke EA. PEG-fibrinogen hydrogels for three-dimensional breast cancer cell culture. *J Biomed Mater Res A*. 2017;105(1):236-252.
- Folsom AR, Delaney JA, Lutsey PL, et al. Associations of factor VIIIc, D-dimer, and plasmin-antiplasmin with incident cardiovascular disease and all-cause mortality. *Am J Hematol*. 2009;84(6):349-353.
- Miller GJ, Bauer KA, Howarth DJ, et al. Increased incidence of neoplasia of the digestive tract in men with persistent activation of the coagulant pathway. *J Thromb Haemost*. 2004;2(12):2107-2114.
- Silvestris N, Scartozzi M, Graziano G, et al. Basal and bevacizumab-based therapy-induced changes of lactate dehydrogenases and fibrinogen levels and clinical outcome of previously untreated metastatic colorectal cancer patients: a multicentric retrospective analysis. *Expert Opin Biol Ther*. 2015;15(2):155-162.
- Tinholt M, Viken MK, Dahm AE, et al. Increased coagulation activity and genetic polymorphisms in the F5, F10 and EPCR genes are associated with breast cancer: a case-control study. *BMC Cancer*. 2014;14:845.
- Fu S, Yun ZY, Cui MM, et al. Cancer antigen 15-3, platelet distribution width, and fibrinogen in combination to distinguish breast cancer from benign breast disease in non-conclusive mammography patients. *Oncotarget*. 2017;8(40):67829-67836.



Ile73Asn mutation in protein C introduces a new N-linked glycosylation site on the first EGF-domain of protein C and causes thrombosis

Yeling Lu,^{1,2} Padmaja Mehta-D'souza,² Indranil Biswas,² Bruno O. Villoutreix,³ Xuefeng Wang,¹ Qiulan Ding,¹ and Alireza R. Rezaie^{2,4}

¹Department of Laboratory Medicine, Ruijin Hospital, Shanghai Jiaotong University School of Medicine, Shanghai, China; ²Cardiovascular Biology Research Program, Oklahoma Medical Research Foundation, Oklahoma City, OK, USA; ³Université Lille, Inserm, Institut Pasteur de Lille, U1177 - Drugs and Molecules for Living Systems, F-59000 Lille, France and ⁴Department of Biochemistry and Molecular Biology, University of Oklahoma Health Sciences Center, Oklahoma City, OK, USA

Haematologica 2020
Volume 105(6):1712-1722

ABSTRACT

Activated protein C exerts its anticoagulant activity by protein S-dependent inactivation of factors Va and VIIIa by limited proteolysis. We identified a venous thrombosis patient who has plasma protein C antigen level of 63% and activity levels of 44% and 23%, as monitored by chromogenic and clotting assays. Genetic analysis revealed the proband carries compound heterozygous mutations (c.344T>A, p.I73N and c.1181G>A, p.R352Q) in *PROC*. We individually expressed protein C mutations and discovered that thrombin-thrombomodulin activates both variants normally and the resulting activated protein C mutants exhibit normal amidolytic and proteolytic activities. However, while protein S-dependent catalytic activity of activated protein C-R352Q toward factor Va was normal, it was significantly impaired for activated protein C-I73N. These results suggest that the Ile to Asn substitution impairs interaction of activated protein C-I73N with protein S. This conclusion was supported by a normal anticoagulant activity for activated protein C-I73N in protein S-deficient but not in normal plasma. Further analysis revealed Ile to Asn substitution introduces a new glycosylation site on first EGF-like domain of protein C, thereby adversely affecting interaction of activated protein C with protein S. Activated protein C-R352Q only exhibited reduced activity in sub-physiological concentrations of Na⁺ and Ca²⁺, suggesting that this residue contributes to metal ion-binding affinity of the protease, with no apparent adverse effect on its function in the presence of physiological levels of metal ions. These results provide insight into the mechanism by which I73N/R352Q mutations in activated protein C cause thrombosis in proband carrying this compound heterozygous mutation.

Correspondence:

ALIREZA R. REZAIE
ray-rezaie@omrf.org

QIULAN DING
qiulan_ding@hotmail.com

Received: May 15, 2019.

Accepted: August 7, 2019.

Pre-published: August 8, 2019.

doi:10.3324/haematol.2019.227033

Check the online version for the most updated information on this article, online supplements, and information on authorship & disclosures: www.haematologica.org/content/105/6/1712

©2020 Ferrata Storti Foundation

Material published in *Haematologica* is covered by copyright. All rights are reserved to the Ferrata Storti Foundation. Use of published material is allowed under the following terms and conditions:

<https://creativecommons.org/licenses/by-nc/4.0/legalcode>.

Copies of published material are allowed for personal or internal use. Sharing published material for non-commercial purposes is subject to the following conditions:

<https://creativecommons.org/licenses/by-nc/4.0/legalcode>,

sect. 3. Reproducing and sharing published material for commercial purposes is not allowed without permission in writing from the publisher.



Introduction

Thrombin forms a complex with thrombomodulin (TM) on the endothelium to activate the vitamin K-dependent anticoagulant protein C zymogen to activated protein C (APC), thereby down-regulating thrombin generation by a feedback inhibition mechanism.¹ Activated protein C functions as an anticoagulant by degrading the procoagulant co-factors Va and VIIIa by limited proteolysis.² Protein C is a multi-domain glycoprotein composed of a non-catalytic light chain linked to the catalytic heavy chain by a single disulfide bond.^{3,4} The light chain harbors the vitamin K-dependent N-terminal γ -carboxyglutamic acid (Gla) domain followed by two epidermal growth factor (EGF)-like domains.⁴ The C-terminal catalytic heavy chain with a trypsin-like substrate specificity is preceded by an activation peptide, which is removed during the activation of protein C by the thrombin-TM

complex.^{1,5} Through its multi-domain structural feature, APC can function as an allosteric enzyme and its proteolytic activity is modulated by protein and metal ion co-factors binding to different domains of the protein.⁶⁻⁸ Protein S functions as a co-factor to promote the anticoagulant function of APC by binding to the light chain of the protease (primarily to Gla and EGF1 domains),⁹⁻¹² thereby stabilizing the active conformation of APC on negatively charged membrane surfaces in a topographical orientation in which the catalytic triad of the protease is aligned with scissile bonds of target co-factors Va and VIIIa for optimal cleavage.¹³⁻¹⁵ Similarly, binding of both monovalent and divalent cations to specific sites of APC on both light and heavy chains allosterically modulates the catalytic and anticoagulant function of APC on membrane surfaces.^{4,6-10}

Protein C deficiency exhibits autosomal dominant pattern of inheritance. The heterozygous deficiency of protein C increases risk of venous thromboembolism (VTE) and its homozygous deficiency is associated with purpura fulminans, which may be fatal if not treated by protein C replacement therapy.^{16,17} The complete protein C deficiency in knockout mice is lethal.¹⁸ There are two common types of protein C deficiency: type-I deficiency is characterized by both low antigen and activity levels, and type-II deficiency is characterized by only a lower activity level for APC.^{19,20} Protein C database (<http://www.hgmd.cf.ac.uk/ac/gene.php?gene=PROC>) analysis suggests that the mutations are scattered on both light and heavy chains and involve all functional domains of the protein (Gla, EGF1, EGF2 and catalytic domains). In this study, we have identified a compound heterozygous protein C deficient VTE patient whose plasma antigen (PC:Ag) level is 63% of the normal and activity (PC:A) levels are 23% and 44% of the normal as monitored by both clotting and chromogenic activity assays, respectively. Genetic analysis revealed that the proband carries compound heterozygous mutations (c.344T>A, p.I73N and c.1181G>A, p.R352Q) in *PROC*, inheriting the I73N mutation from her mother and R352Q mutation from her father. The first mutation is located on the N-terminal EGF1 and the second mutation is located on the catalytic domain of protein C. We individually expressed both protein C variants in mammalian cells and characterized their properties in established coagulation assays. We demonstrate that thrombin-TM activates both protein C variants normally and anticoagulant and amidolytic activities of the R352Q variant are normal; however, the anticoagulant activity of the I73N variant has been specifically and significantly impaired in the presence of protein S. Further analysis revealed that the basis for the protein S-dependent defect is that the Ile to Asn substitution introduces a novel N-linked glycosylation site on EGF1 of protein C, thereby interfering with interaction of the APC mutant with its co-factor.

Methods

Construction, expression, and purification of recombinant protein C derivatives

Expression, purification and activation of recombinant human wild-type protein (WT) C and the Ile73 to Asn (I73N) and Arg352 to Gln (R352Q; R187Q in chymotrypsin numbering)²¹ derivatives in human embryonic kidney cells have been described previously.²²⁻²⁴

A complete list and sources of reagents, together with details of the experimental methods used, are provided in the *Online Supplementary Appendix*.

Analysis of thrombin generation in plasma

Thrombin generation (TG) assay was performed with Thrombinoscope (Fluoroskan Ascent (Thermo Fisher Scientific, Waltham, MA, USA) using citrated human normal or protein C-deficient plasma reconstituted with either WT protein C or mutant protein C derivatives (60nM) as described.²⁵

Anticoagulant assays

Anticoagulant activities of APC derivatives in the absence and presence of different concentrations of protein S and/or different concentrations of PC/PS vesicles were monitored both in purified and plasma-based assay systems as described.^{24,25}

Endothelial cell permeability

Intracellular signaling activity of APC derivatives was evaluated in a permeability assay using EA.hy926 endothelial cells as described.²⁴ Cell permeability in response to thrombin [10nM for 10 minutes (min)] following treatment with APC derivatives [25nM for 3 hours (h)] was quantitated by spectrophotometric measurement of the flux of Evans blue-bound albumin across functional cell monolayers using a modified 2-compartment chamber model as described.²⁴

Statistical analysis

Data are expressed as mean±standard deviation from three or more experiments. Data were analyzed by Student *t*-test. *P*<0.05 was considered statistically significant.

Results

Case presentation

The proband is a 36-year old female (II-2) who was referred to the hematology clinic because of recurrent deep vein thrombosis (DVT) of the left lower limb (Figure 1A). Plasma levels of the proband's protein C revealed a combined type-I/type-II deficiency as evidenced by a moderately lower protein C antigen level based on the ELISA, but a significantly lower activity level based on the chromogenic assay, and an even more pronounced lower activity level based on aPTT (Figure 1C). Results of other routine coagulation and thrombophilia screening assays were normal (*data not shown*). Genetic analysis identified a compound heterozygous missense mutation (c.344T>A, p.I73N and c.1181G>A, p.R352Q) in *PROC* (Figure 1B). Further genetic analysis using blood samples from the proband's parents revealed that she has inherited I73N mutation from her mother and R352Q mutation from her father (Figure 1B). Both I73N and R352Q are novel mutations in *PROC*, though a thrombosis patient with type-II protein C deficiency carrying a R352W mutation has been reported previously.¹⁹ To understand the molecular defect causing recurrent thrombosis in this patient, we expressed both I73N and R352Q protein C variants in mammalian cells for further characterization.

Characterization of recombinant protein C mutants

Following expression, protein C derivatives were purified by a combination of immunoaffinity and ion exchange chromatography as described.²² Recombinant zymogens were activated by thrombin and APC deriva-

tives were separated from thrombin on the Mono Q column as described.²² Concentrations of APC derivatives, as determined by active-site titration, were within 90-100% of those expected based on zymogen concentrations as determined from absorbance at 280 nm. SDS-PAGE analysis indicated APC derivatives have been purified to near homogeneity, with the heavy chains of both APC-I73N and APC-R352Q migrating as triple bands representing α , β and γ subforms of protein C (Figure 2A), which are glycosylation variants of the protein also observed in APC-WT.²⁶ Triplet bands of APC-I73N migrated as diffused bands, but slower than those observed with APC-WT and APC-R352Q (Figure 2A). SDS-PAGE analysis under reducing conditions revealed the higher molecular mass of APC-I73N under non-reducing conditions is due to its light chain, which migrated slower than light chains of other two APC derivatives (Figure 2A). As expected, heavy chains of all three APC derivatives migrated with near similar apparent molecular masses under reducing conditions (Figure 2A). Analysis of the cDNA sequence of protein C revealed that Ile73 to Asn mutation creates a potential new N-linked glycosylation (⁷⁵Asn-Gly-Ser⁷⁵) site on EGF1-domain of protein C, suggesting the glycosylation of this mutant residue is responsible for the higher molecular mass of the protein (Figure 2A). In agreement with this observation, treatment with PNGase F, which catalyzes the cleavage of N-linked oligosaccharides, eliminated the diffused nature of bands as well as differences in molecular masses observed between APC-WT and APC-I73N (Figure 2A, right). As expected, SDS-PAGE analysis of WT and I73N protein C zymogens indicated both pro-

teins also migrate as triplet bands representing α , β and γ subforms of protein C and similar to APC derivatives, I73N zymogen migrated slower than WT protein under non-reducing conditions (Figure 2C). Analysis of zymogen derivatives under reducing conditions indicated a fraction of both proteins (a larger fraction with I73N) is not processed at the dibasic cleavage site,²⁷ thus migrating as single chains (Figure 2C). The single chain I73N zymogen migrated much slower than the single chain WT under reducing conditions (Figure 2C), most likely due to the additional glycan chain in the light chain of the mutant protein. Previously, we have demonstrated the single chain APC has normal amidolytic and anticoagulant activity.²⁷ Noting the compound heterozygous nature of protein C mutation, the relative contribution of each mutation to lower PC:Ag in the proband's plasma remains unknown.

Amidolytic activity of APC derivatives toward SpPCa is presented in Figure 2D. Kinetic analysis indicated APC-WT, APC-I73N, and APC-R352Q cleave SpPCa with similar kinetic parameters in TBS/Ca²⁺ ($K_{m(app)}=220-240\mu\text{M}$ and $k_{cat}=19-22\text{s}^{-1}$), suggesting neither mutation has an adverse effect on folding and/or reactivity of the catalytic pocket.

Analysis of protein C activation

Analysis of the initial rate of protein C activation indicated relative to WT, thrombin activates both variants with similar or improved rates. Thus, in EDTA containing TBS, the rate of protein C activation by thrombin was improved 1.5- and 2-fold for I73N and R352Q, respectively (Figure 2E). However, the initial rate of activation by

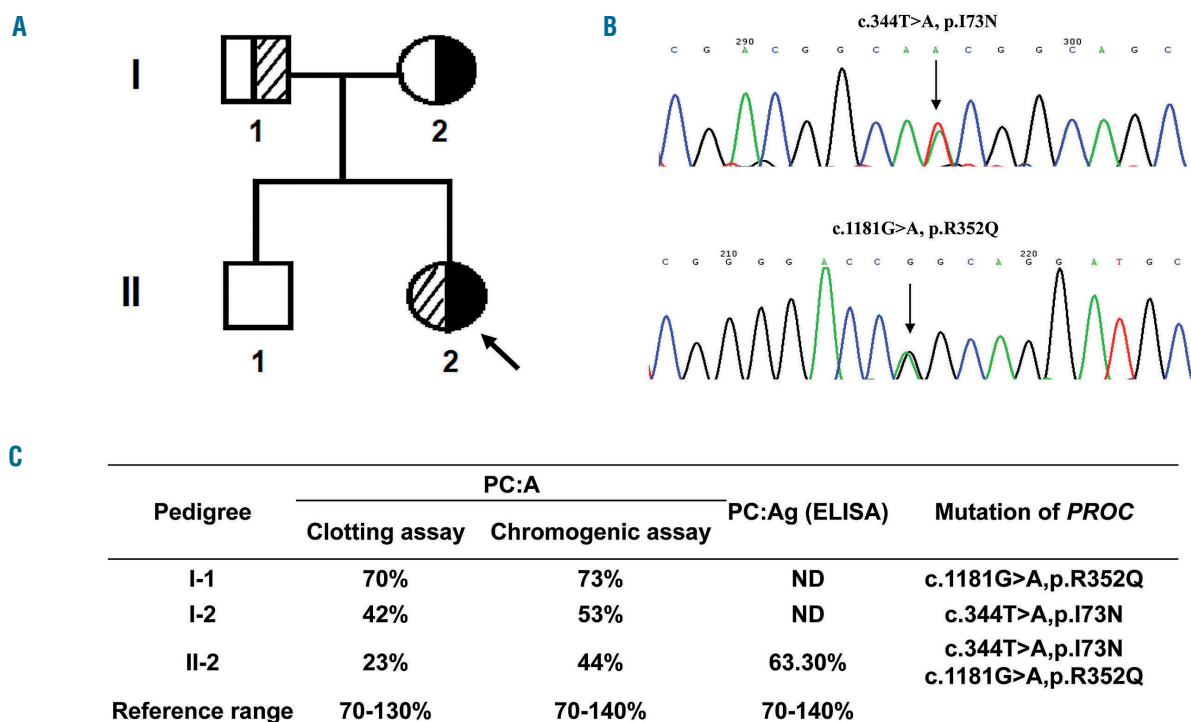


Figure 1. Genotype and phenotype analysis of the proband and her parents. (A) The pedigree of the family members of the proband (II-2). (B) Genetic analysis showing the proband carries compound heterozygous c.344T>A (p.I73N) and c.1181G>A (p.R352Q) mutations in the *PROC* gene. (C) Clinical data obtained by coagulation assays are shown for the proband and her parents. The PC:Ag data for the proband's parents were not available. ND: not determined.

thrombin-sTM in TBS/Ca²⁺ was essentially identical for all protein C derivatives (Figure 2F), further confirming a proper folding of recombinant proteins.

Anticoagulant activity

Anticoagulant activity of APC derivatives was evaluated in both the absence and presence of protein S. APC concentration-dependence of FVa degradation suggested both variants have normal anticoagulant activity toward FVa in the absence of protein S (Figure 3A). However, APC concentration-dependence of FVa degradation in the presence of protein S revealed while the anticoagulant activity of APC-R352Q is the same as APC-WT, it has been significantly impaired for APC-I73N in the presence of the co-factor (Figure 3B). Essentially identical results were obtained if anticoagulant activities of APC derivatives were evaluated by aPTT using normal and protein S-deficient plasma. Thus, all APC derivatives exhibited identical prolongation of clotting time in protein S-deficient plasma (Figure 3C); however, while the activity of APC-R352Q in the normal plasma was similar to APC-WT, it was significantly decreased for APC-I73N (Figure 3D). These results suggest APC-I73N may bind protein S with weaker affinity.

Since Ile73 is located on EGF1-domain of APC near the membrane-binding Gla-domain, both PC/PS concentration-dependence and protein S concentration-dependence

of FVa inactivation by APC-WT and APC-I73N were investigated to determine the basis for the lower protein S-dependent anticoagulant activity of the mutant. PC/PS concentration-dependence of FVa inactivation in the absence of protein S was essentially identical for both APC-WT and APC-I73N, yielding $K_{d(\text{app})}$ values of $\sim 1.7 \mu\text{M}$ PC/PS for both proteases (*data not shown*). However, PC/PS concentration-dependence of FVa inactivation in the presence of a fixed concentration of protein S (20nM) indicated 2-fold weaker affinity of APC-I73N for phospholipids ($K_{d(\text{app})} = 2 \mu\text{M}$; vs. APC-WT $K_{d(\text{app})} = 1 \mu\text{M}$, $n=3$, $P<0.05$) (Figure 4A). A similar low dissociation constant for the APC-protein S interaction in the kinetic assay has been reported.²⁸ Protein S concentration-dependence in the presence of a fixed concentration of PC/PS (25 μM) indicated a similar weaker affinity for protein S by APC-I73N, suggesting the mutant interacts with protein S with weaker affinity (Figure 4B). Nevertheless, increasing the concentration of protein S did not overcome the catalytic defect of APC-I73N (Figure 4B). Since APC-R352Q exhibited similar anticoagulant activity in FVa degradation and aPTT assays (Figure 3), co-factor concentration-dependence studies were not conducted with this mutant.

Anticoagulant activities of APC-WT and APC-I73N toward FVa Leiden were also evaluated in both the absence and presence of protein S. In FVa Leiden, the APC recognition site, Arg506 is mutated to Gln; however,

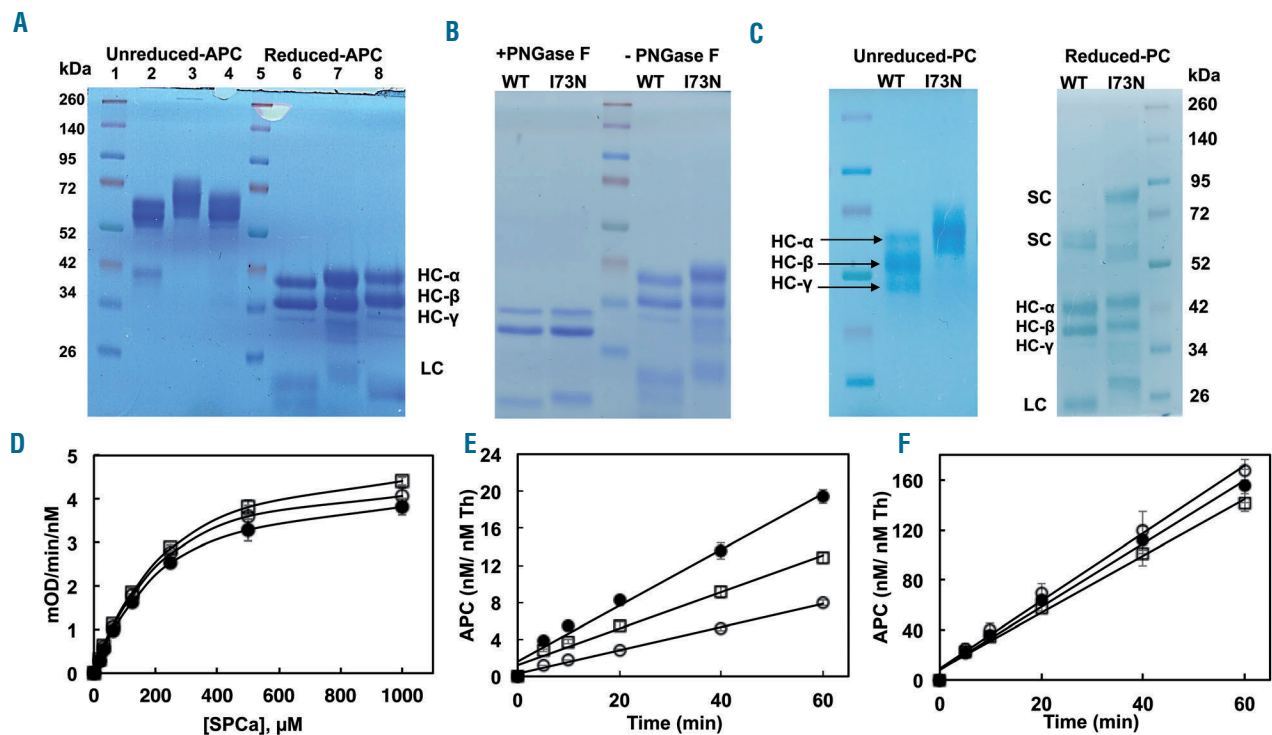


Figure 2. Characterization of recombinant activated protein C (APC) derivatives. (A) SDS-PAGE analysis of recombinant APC-wild type (WT), APC-I73N and APC-R352Q (lanes 2, 3 and 4, respectively), fractionated on a 10% gel under non-reducing and reducing conditions (lanes 6, 7 and 8, respectively). Lanes 1 and 5 represent molecular mass standards in kDa. (B) PNGase F treatment of APC-WT and APC-I73N under reducing conditions fractionated on 10% gel. (C) SDS-PAGE analysis of protein C-WT, protein C-I73N fractionated on a 8.75% gel under non-reducing and reducing conditions. HC- α : heavy chain α ; HC- β : heavy chain β ; HC- γ : heavy chain γ ; LC: light chain; SC: single chain. (D) Amidolytic activity of APC-WT (O), APC-I73N (●), and APC-R352Q (□) (5 nM each) toward the chromogenic substrate SpCa was monitored as described in "Methods". (E) Time course of activation protein C-WT (O), protein C-I73N (●), and protein C-R352Q (□) (1 μM each) by thrombin (10 nM) was monitored in TBS buffer lacking Ca²⁺. (F) The same as (E) except that the activation of protein C derivatives by the thrombin-sTM complex (1 nM thrombin and 50 nM sTM) was monitored in TBS/Ca²⁺. At indicated time intervals, the activity of thrombin was inhibited by antithrombin and the rate of APC generation was determined by an amidolytic activity as described in "Methods". Data are derived from at least three independent measurements (\pm standard deviation). The solid lines in (D) are computer fits of data to the Michaelis-Menten equation, and those in (E) and (F) fits of data to a linear equation. min: minutes.

Arg306 site is intact.^{29,30} Results indicated both APC-WT and APC-I73N inactivate FVa Leiden with similar rates in the absence of protein S (Figure 4C). However, the anticoagulant activity of APC-I73N toward FVa Leiden was significantly impaired in the presence of protein S (Figure 4D). These results suggest the co-factor function of protein S in promoting the catalytic efficiency of APC-I73N toward Arg306 has been impaired.

Anti-inflammatory signaling activity

Anti-inflammatory signaling activity of APC derivatives was evaluated in thrombin-mediated permeability assay as described.²⁴ Results suggest both APC-I73N and APC-R352Q exhibit normal signaling activities in the permeability assay, suggesting neither mutation adversely affects the anti-inflammatory function of APC (Figure 5A).

Interaction of APC-R352Q with Na⁺

Arg352 (residue 187 in chymotrypsin numbering)²¹ is located on a loop near the S1 specificity pocket (Asp189).⁵ This loop is allosterically linked to the Na⁺-binding 225-loop in both thrombin and factor Xa,³¹⁻³³ thus contributing to affinity of Na⁺ binding. To determine whether this loop in APC contributes to Na⁺-binding properties of APC, the amidolytic activity of this mutant was monitored in the presence of increasing concentrations of Na⁺ in both the absence and presence of Ca²⁺. Results demonstrated the

affinity of APC-R352Q for Na⁺ was impaired approximately 2-fold in both the absence and presence of Ca²⁺ (Figure 5B and C). $K_{d(app)}$ values, as determined from non-linear regression analysis of the saturable-dependence of the chromogenic substrate activity of APC-R352Q as a function of increasing concentrations of Na⁺, were 35mM in the absence and 2.8mM in the presence of Ca²⁺ (n=3, $P<0.01$). The same values for APC-WT were 18.7mM in the absence and 1.4mM in the presence of Ca²⁺ (n=3, $P<0.005$). Thus, similar to other coagulation proteases, 189-loop contributes to ligation of Na⁺ in the 225-loop of APC.

Thrombin generation assay

Anticoagulant activity of APC mutants was evaluated by thrombin generation assay using both normal and protein C-deficient plasma. In normal plasma, both APC-WT and APC-R352Q exhibited identical thrombin generation inhibitory profiles at concentrations of 5nM (Figure 6A) and 10nM (Figure 6B). By contrast, identical concentrations of APC-I73N showed significantly impaired activity (Figure 6A and B). Similar results were obtained when thrombin generation assay was conducted in the presence of sTM (2nM and 5nM) utilizing protein C-deficient plasma supplemented with a near physiological concentration of protein C derivatives and a tissue factor concentration of 1pM to initiate clotting. Results in the presence of both

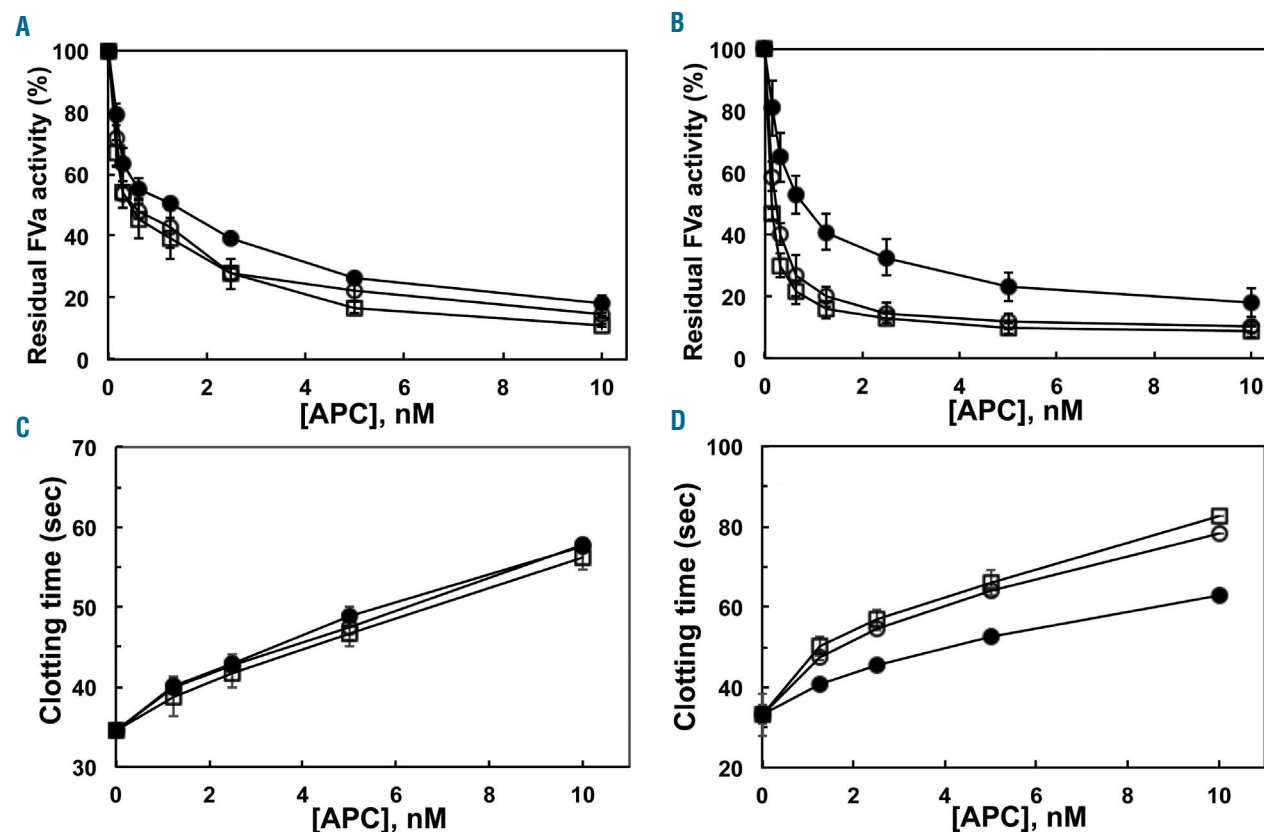


Figure 3. Assessment of the anticoagulant activity of activated protein C (APC) derivatives in the absence and presence of protein S. (A) Degradation of human FVa (2.5 nM) by increasing concentrations of APC-wild type (WT) (O), APC-I73N (●) and APC-R352Q (□) was carried out on PC/PS vesicles (25 μM) in TBS/Ca²⁺ in a 96-well assay plate. Following a 10-minute (min) incubation at room temperature, the remaining co-factor activity of FVa was determined by a prothrombinase assay (5 nM FXa and 1 μM prothrombin for 1 min) as described in "Methods". (B) The same as (A) except that the APC concentration dependence of FVa degradation was carried out in the presence of protein S (50 nM) for 1 min. (C) The anti-clotting activities of APC-WT (O), APC-I73N (●) and APC-R352Q (□) were determined in protein S-deficient plasma by an aPTT assay as a function of increasing concentrations of APC at 37 °C as described in "Methods". (D) The same as (C) except that the anti-clotting activities of the proteases were evaluated in normal plasma. sec: seconds.

concentrations of sTM confirmed the anticoagulant activity of protein C-I73N has been significantly impaired (Figure 7A and B). The lower activity of the protein C mutant is not due to its lower activation rate by thrombin-TM as demonstrated in the purified system (Figure 2F).

Discussion

We have demonstrated in this study that the I73N substitution may be responsible for the recurrent DVT in the proband who is a compound heterozygote for I73N and R352Q mutations in *PROC*. In order to decipher the molecular basis of the anticoagulant defect, we expressed each mutant separately and characterized their properties in coagulation assays. We discovered the I73N substitution introduces a potential new N-linked glycosylation site on EGF1-domain of protein C. This modification does not interfere with the activation of the mutant by thrombin-TM. However, the anticoagulant activity of APC-I73N was significantly decreased in both purified and plasma-based assays. Further analysis revealed APC-I73N exhibits

weaker affinity for protein S. This conclusion is derived from the observation that APC-I73N exhibited normal activity toward FVa in the absence of protein S, but impaired activity in the presence of the co-factor. In support of this hypothesis, the anticoagulant activity of APC-I73N was normal in the protein S-deficient plasma, but reduced in the normal plasma. Furthermore, in thrombin generation assays, inhibitory activities of APC-I73N (normal plasma) and protein C-I73N (protein C-deficient plasma supplemented with sTM) were markedly decreased. In contrast to I73N, the R352Q mutation did not impair the catalytic activity of APC in any of coagulation assays, strongly indicating the molecular defect leading to recurrent DVT in the proband carrying the two mutations is primarily due to the I73N substitution. It should be noted that neither mutation adversely affected the anti-inflammatory signaling function of APC.

Activated protein C is a Na^+ -binding protease and the R352Q mutation led to an approximately 2-fold lower affinity for interaction with the monovalent cation in both the absence and presence of Ca^{2+} . We have previously demonstrated an allosteric linkage between the two metal

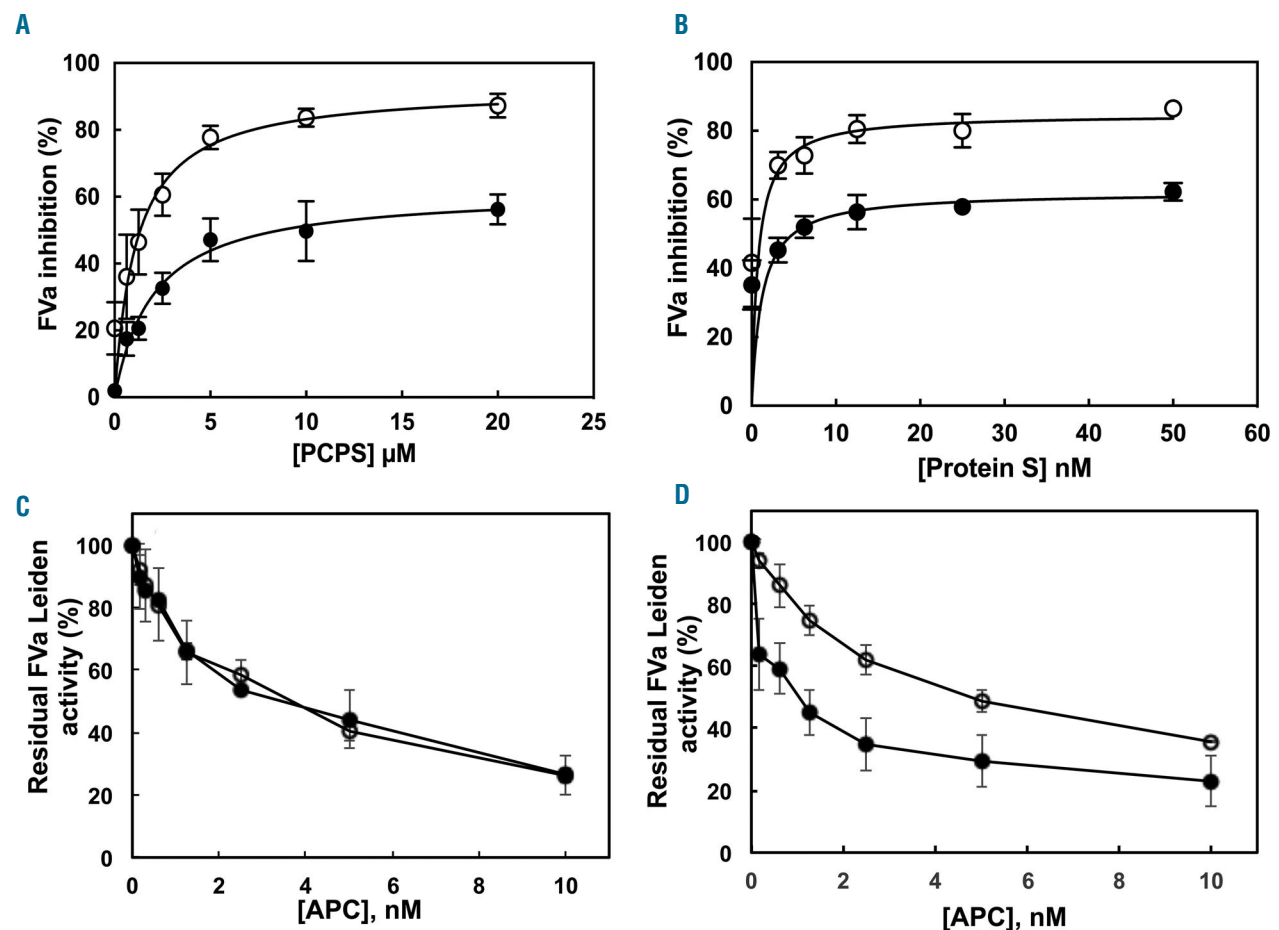


Figure 4. Assessment of the anticoagulant activity of activated protein C (APC) derivatives in the presence of increasing concentrations of PC/PS and protein S. (A) The degradation of human FVa (2.5 nM) by APC-wild type (WT) (O) and APC-I73N (●) in the presence of protein S (20 nM) was carried out as a function of increasing concentrations of PC/PS vesicles as described in "Methods". (B) The same as (A) except that FVa degradation by APC-WT (O) and APC-I73N (●) on PC/PS vesicles (25 μM) was carried out as a function of increasing concentrations of protein S. (C) The degradation of FVa Leiden (2.5 nM) by increasing concentrations of APC-WT (O) and APC-I73N (●) was carried out on PC/PS vesicles (25 μM) in TBS/Ca²⁺ in a 96-well assay plate. Following 10-minute (min) incubation at room temperature, the remaining co-factor activity of FVa Leiden was determined by a prothrombinase assay (10 nM FXa and 1 μM prothrombin for 1 min) as described in "Methods". (D) The same as (C) except that the APC concentration dependence of FVa Leiden degradation was carried out in the presence of protein S (50 nM) for 1 min.

ion binding loops, located in the C-terminal protease domain, modulates the catalytic activity of APC.⁶ We showed that binding of Ca^{2+} to 70-80-loop (chymotrypsin numbering)²¹ dramatically increases the affinity of Na^+ for its specific site on 225-loop of APC. A similar Ca^{2+} -dependent enhancement in Na^+ affinity for APC-R352Q was observed ($K_{d(\text{app})}$ of 35mM and 2.8mM in the absence and presence of Ca^{2+} , respectively). These dissociation constants are approximately 2-fold higher when compared to Na^+ binding to APC-WT ($K_{d(\text{app})}$ of 18.7mM and 1.4mM in the absence and presence of Ca^{2+} , respectively). These results suggest Arg352 contributes to high-affinity interaction of Na^+ with 225-loop of APC, which has been determined to be a monovalent cation-binding loop in all coagulation proteases.³⁴ This residue is located near the S1 specificity site (Asp189) on an exposed surface loop (185-189-loop) immediately below 225-loop.⁵ In the case of thrombin and factor Xa, mutagenesis studies have indicated that residues of 185-189-loop are critical for catalytic activity and monovalent cation-binding specificity of these proteases.³¹⁻³⁴ Thus, it appears that this loop makes a similar contribution to interaction of Na^+ with APC. However, noting the high physiological concentration of Na^+ in plasma and its high affinity for interaction with APC, a 2-fold lower affinity of Na^+ for APC-R352Q has no physiological relevance. The normal activity of the mutant protein C/APC in the coagulation assays is consistent with this conclusion. Thus, the basis for the type-II protein C

deficiency observed with R352W mutation may be due to distortion of the active-site conformation of APC because of the large and hydrophobic nature of the Trp side-chain.³⁵

The mechanism by which I73N mutation adversely affects the protein S-dependent anticoagulant function of APC is not fully understood. Similar to APC, protein S is a vitamin K-dependent protein which binds to negatively charged phospholipids. The affinity of protein S for phospholipid membranes is significantly higher than that of APC. It has been hypothesized that a co-factor function for protein S in the anticoagulant pathway is to stabilize the interaction of APC on phospholipid membranes in the vicinity of FVa/FVIIIa for optimal interaction and proteolytic degradation of these procoagulant co-factors.^{9,12,28} Furthermore, there is some evidence to suggest an interaction with protein S is also associated with topographical changes in the active-site of APC, thereby aligning it with scissile bonds of co-factors on the membrane surface.¹³⁻¹⁵ Analysis of protein S and PC/PS concentration-dependence of FVa degradation by APC indicated an approximately 2-fold weaker affinity for the mutant with protein S on PC/PS vesicles. While there was no difference in PC/PS concentration-dependence of FVa inactivation between APC-WT and APC-I73N in the absence of protein S, the apparent dissociation constant for interaction with PC/PS in the presence of the co-factor was increased from 1 μM for WT to 2 μM for the mutant. These results

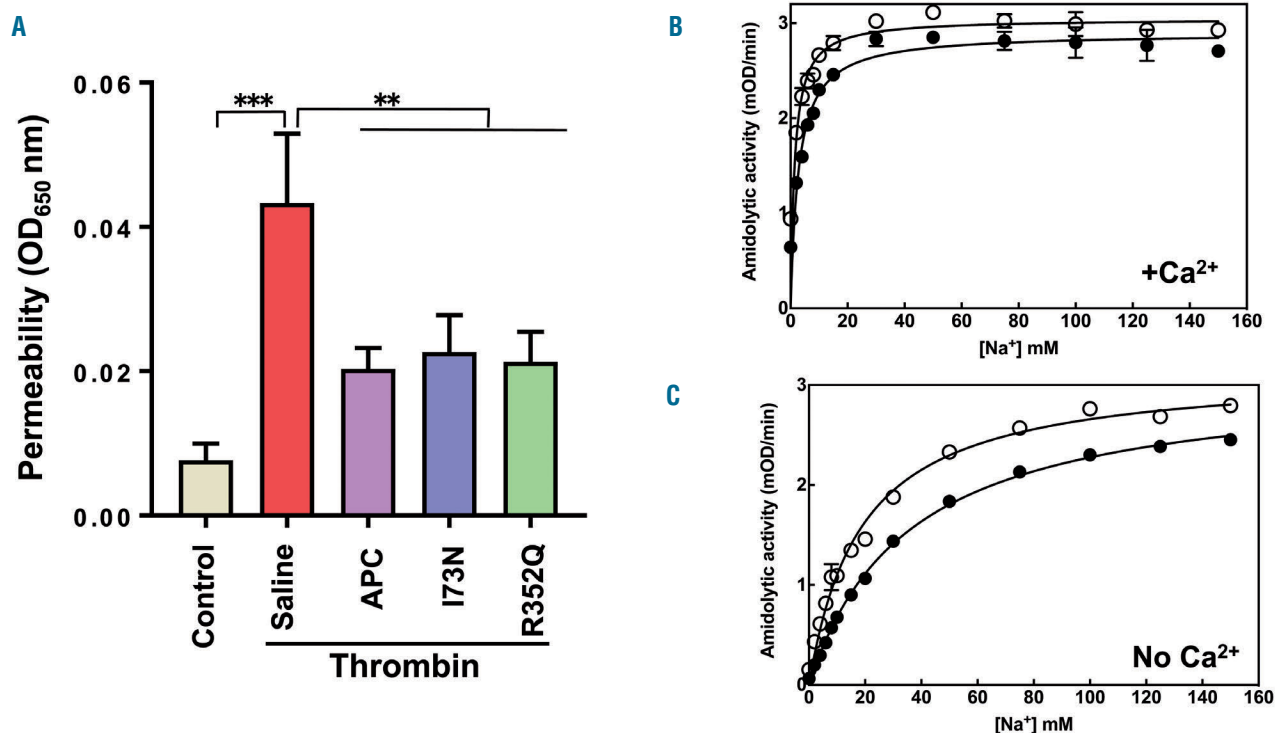


Figure 5. Analysis of the barrier-protective activity of activated protein C (APC) derivatives and assessment of the interaction of APC-R352Q with Na^+ . (A) The barrier-protective signaling activity of APC derivatives was evaluated by an established permeability assay. The EA.hy926 cells were treated with saline (as a negative control) and APC derivatives (25 nM for 3 hours) followed by inducing permeability with thrombin [10 nM for 10 minutes (min)]. The barrier-protective effect of APC derivatives was quantitated by spectrophotometric measurement of the flux of Evans blue-bound albumin across functional cell monolayers as described in "Methods". $**P < 0.01$ and $P^{***} < 0.001$. (B) The amidolytic activity of APC-WT (O) and APC-I73N (●) toward the chromogenic substrate SpPCa was monitored in the presence of 2.5 mM CaCl_2 in Tris-HCl (pH, 7.4) as a function of increasing Na^+ concentrations, keeping the total ionic strength constant at 0.2 M. (C) The same as (A) except that the amidolytic activities were monitored in the absence of Ca^{2+} .

confirm the previous hypothesis that a co-factor function for protein S is to enhance the affinity of APC for negatively charged membranes. It was interesting to note that the defect in the anticoagulant function of APC-I73N toward FVa in the presence of excess protein S was not

recovered, possibly suggesting that co-factor-mediated topographical changes in the active-site pocket that is required for optimal recognition of FVa scissile bond(s) by APC has also been adversely affected for mutant.

Activated protein C sequentially cleaves two peptide

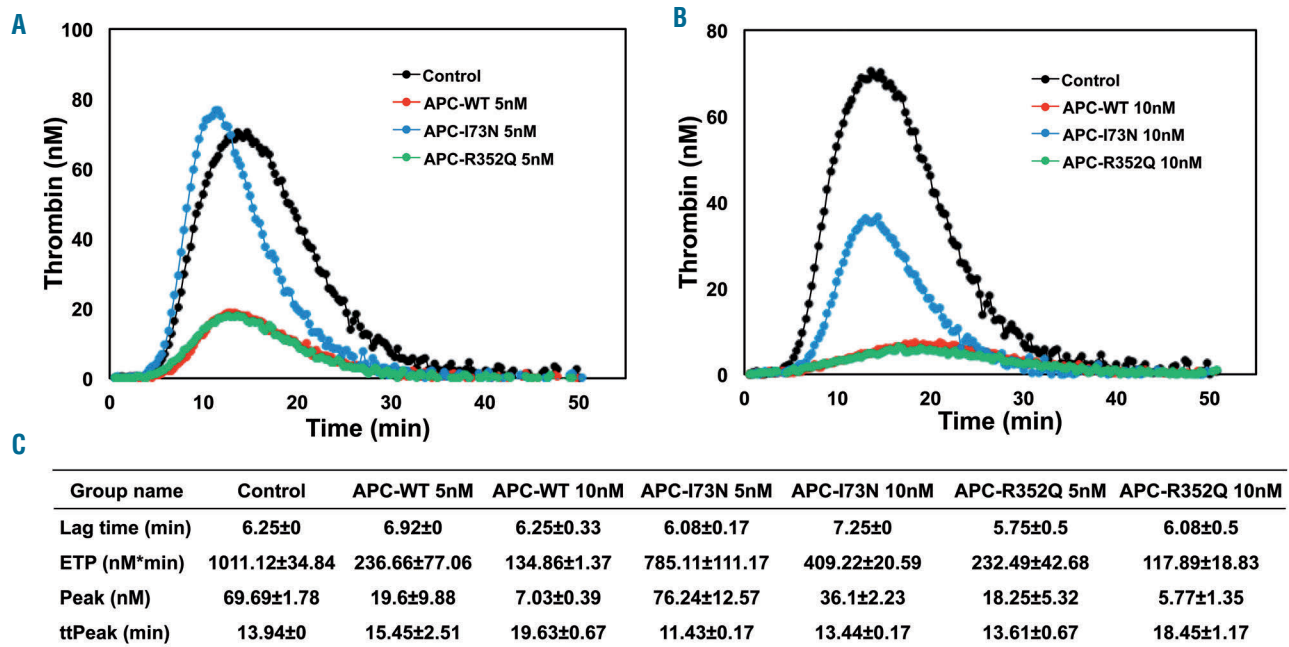


Figure 6. Assessment of the activated protein C (APC)-mediated inhibition of thrombin generation. Citrated normal plasma (80 μ L) was incubated with 20 μ L PPP-Reagent Low (1 pM TF) and APC-WT (red circles), APC-I73N (blue circles) or APC-R352Q (green circles): 5 nM APC in (A) and 10 nM APC in (B) or buffer control (black circles). The kinetics of thrombin generation was monitored by measuring the hydrolysis of a fluorogenic thrombin substrate. (C) The lag time (LT, min), peak height (Peak, nM), time to peak (ttPeak, min) and endogenous thrombin potential (ETP, nM*min) were deduced from thrombin generation curves as described in "Methods". min: minutes.

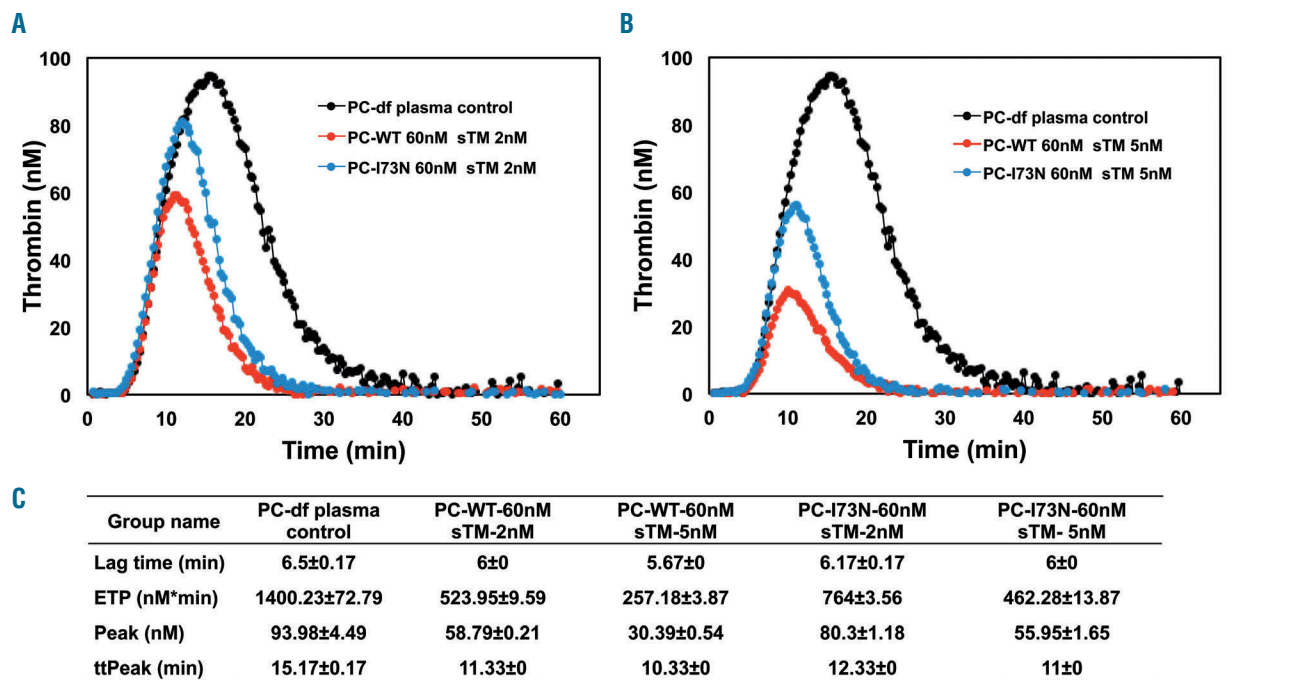


Figure 7. Assessment of the activated protein C (APC)-mediated inhibition of thrombin generation in protein C-deficient plasma. Citrated protein C-deficient plasma (80 μ L) was supplemented with buffer control (black circles), protein C-wild type (WT) (red circles), or protein C-I73N (blue circles) (60 nM each) and either 2 nM sTM (A) or 5 nM sTM (B) and incubated with 20 μ L PPP-Reagent Low (1 pM TF). The kinetics of thrombin generation were monitored by measuring the hydrolysis of a fluorogenic thrombin substrate. (C) The lag time [LT, minutes (min)], peak height (Peak, nM), time to peak (ttPeak, min) and endogenous thrombin potential (ETP, nM*min) were deduced from thrombin generation curves as described in "Methods". min: minutes.

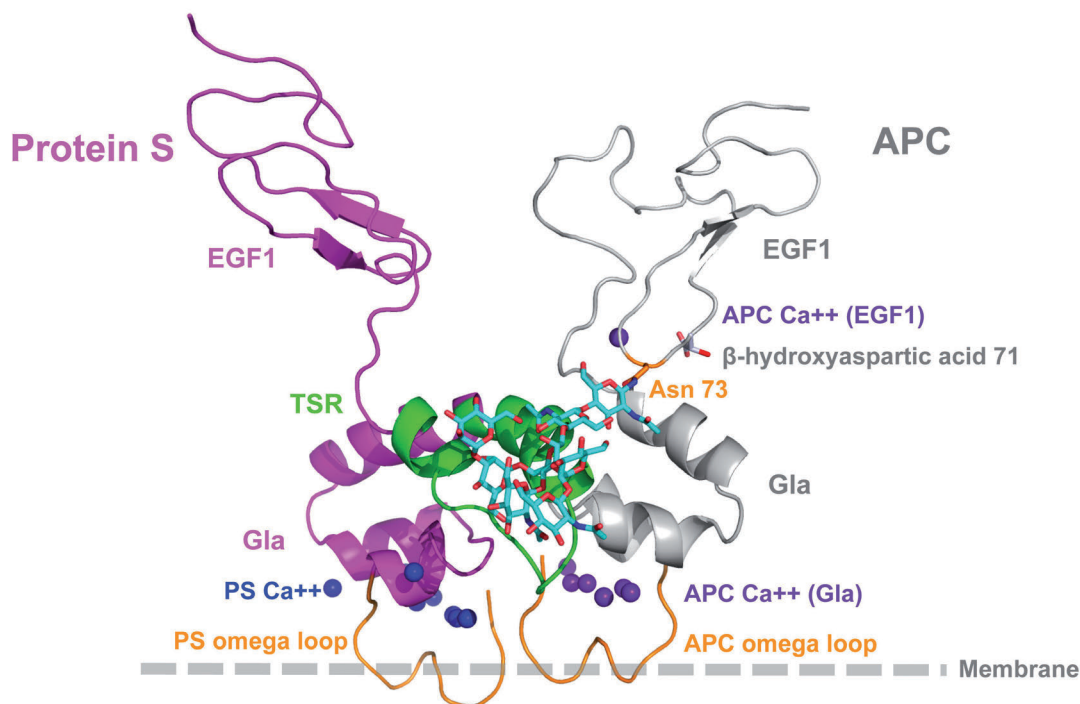


Figure 8. Computational model of the activated protein C (APC)-protein S complex. Molecular models of APC Gla-EGF1 (gray) and PS Gla-TSR-EGF1 (magenta and green) domains were docked as previously described.²⁵ The overall orientation agrees with several previous mutations that were modeled in the APC and protein S complex while positioning the two membrane binding omega loops side by side anchored in the phospholipid membrane. Following replacement of Ile73 with Asn, several rotamers were tested interactively and most of them could fit in the structure without creating steric clashes. An orientation of Asn representing most of the low energy rotamers was selected and a glycan was grafted and energy minimized: cyan with heteroatoms in blue (N) and red (O). The carbohydrate chain points toward the TSR and Gla domains of protein S. A key APC residue for calcium binding at position 71 (β -hydroxyaspartic acid) and the Ca^{++} ion are also shown (see main text for more details). The figure was generated using PyMol molecular graphic program (Schrodinger, Cambridge, MA, USA).

bonds after Arg506 and Arg306 to inactivate FVa.³⁶⁻³⁸ Unlike cleavage of the Arg506 site, which is faster and membrane-independent, the APC cleavage of Arg306 is slower and membrane-dependent.³⁶⁻³⁸ Thus, it has been hypothesized that the co-factor function of protein S preferentially improves cleavage of Arg306 to a greater extent than the cleavage of Arg506.^{37,38} To determine whether the defective protein S-dependent activity of APC-I73N is due to a slower cleavage of the Arg306 site, the anticoagulant activity of the mutant toward FVa-Leiden was compared to APC-WT. In FVa-Leiden, Arg506 is mutated to Gln so the anticoagulant activity of APC is only monitoring cleavage of Arg306. The findings that both APC-WT and APC-I73N inactivated FVa-Leiden with similar rates in the absence of protein S but the activity of APC-I73N in the presence of protein S was markedly impaired, suggest that the co-factor function of protein S in promoting the catalytic efficiency of APC-I73N toward the Arg306 site of FVa has been adversely affected. Nevertheless, these results do not exclude the possibility that the protein S-dependent activity of APC-I73N toward cleavage of Arg506 has also been impaired.

Previous results have indicated that APC may interact with specific sites within three regions of protein S including Gla-domain, thrombin-sensitive region (TSR), and EGF1-domain.⁸⁻¹² In a recent study, we identified a DVT patient who had a mutation on residue 74 (Gly74 to Ser substitution) of APC EGF1-domain, and similar to the patient in the current study, a protein S-dependent anticoagulant defect in the APC mutant was determined to be

responsible for thrombosis in the patient.²⁵ A computational docking model of the APC Gla-EGF1 and protein S Gla-TSR-EGF1 in this previous study indicated that the substitution of Gly74 with Ser may impose steric constraints for interaction between APC and protein S.²⁵ In the current study, we used the same computational approach and introduced a standard N-glycan chain at Asn73, which is solvent exposed in the mutant APC. Several rotamers were tested and all low energy conformations positioned the Asn73 side-chain toward the solvent in the direction of the docked protein S (Figure 8). Based on this computational model, we hypothesize that the carbohydrate side chain of the mutant Asn would be oriented toward TSR and Gla domains of protein S (Figure 8), thereby impeding a proper interaction between the two proteins. It should be noted that due to a low resolution of this molecular model and the flexibility of the loop carrying the mutation, the exact orientation of the glycan chain in EGF1 of the mutant APC cannot be predicted with any great certainty. However, results of coagulation assays strongly suggest that this glycan interferes with the interaction between EGF1-domain of APC and one of the three regions of protein S (Gla-TSR-EGF1) which have been identified as interactive-sites on the co-factor by molecular modeling and mutagenesis studies. Another potential mechanism through which glycosylation can impede the interaction of APC-I73N with protein S is by altering the Ca^{2+} affinity of EGF1-domain. The high affinity EGF1 Ca^{2+} binding site of APC (K_d approx. 100 μM) is centered around β -hydroxyaspartic acid at position 71.³⁹ Ca^{2+} bind-

ing to this site makes a key contribution to APC interaction with protein S.³⁹ Due to close proximity of residue 73 to this functionally important metal ion binding-site, it is possible a glycosylated Asn73 impairs the affinity of APC-I73N for protein S by altering the affinity of EGF1 for Ca²⁺. Since this site has a much higher affinity for Ca²⁺ than the Gla-domain of APC (Kd low mM range), evaluating the effect of mutagenesis on the affinity of EGF1-domain for Ca²⁺ was not feasible by functional assays.

In summary, our results strongly suggest that substitution of Ile73 with Asn introduces a new N-linked glycosylation site on EGF1-domain of APC. This modification in the compound heterozygote patient leads to a weaker affinity of APC-I73N for protein S, thereby causing anticoagulant defect and recurrent DVT. Noting the anticoagulant defect is observed only in the presence of protein S, results further suggest the I73N mutation would be most harmful under conditions where the co-factor level is low (i.e. pregnancy, oral contraceptive use, etc.).^{40,41} This hypothesis is consistent with the observation that recurrent DVT in the affected patient was associated with pregnancy (28th week, left lower limb DVT), during the postpar-

tum period (3rd and 4th weeks, lower limb DVT and mesenteric venous thrombosis, respectively) and when taking oral contraceptives (mesenteric venous thrombosis after finishing one year of anticoagulant therapy). The I73N mutation does not adversely affect the anti-inflammatory signaling function of APC. Molecular modeling predicts the newly attached N-linked glycan on Asn73 can impede with the proper interaction of APC EGF1-domain with Gla-TSR-EGF1 domains of protein S on the membrane surface. This modification appears to not only weaken the affinity of APC for protein S but also adversely affect functionally important protein S-dependent topographical changes in the active-site of APC, thereby impairing its anticoagulant function on the membrane surface.

Acknowledgments

This study was supported by an institutional fund from OMRF and grants awarded by the National Heart, Lung, and Blood Institute of the National Institutes of Health HL101917 and HL062565 to ARR; and The General Program of National Natural Science Foundation of China (81570114) to QD and (81870107) to YL.

References

1. Esmon CT. Molecular events that control the protein C anticoagulant pathway. *Thromb Haemost.* 1993;70(1):29-35.
2. Walker FJ, Fay PJ. Regulation of blood coagulation by the protein C system. *FASEB J.* 1992;6(8):2561-2567.
3. Foster D, Davie EW. Characterization of a cDNA coding for human protein C. *Proc Natl Acad Sci. (USA)* 1984;81(15):4766-4770.
4. Stenflo J. Structure-function relationships of epidermal growth factor modules in vitamin K-dependent clotting factors. *Blood.* 1991;78(7):1637-1651.
5. Mather T, Oganessyan V, Hof P, et al. The 2.8 Å crystal structure of Gla-domainless activated protein C. *EMBO J.* 1996;15(24):6822-6831.
6. He X, Rezaie AR. Identification and characterization of the sodium-binding site of activated protein C. *J Biol Chem.* 1999;274(8):4970-4976.
7. Yang L, Prasad S, Di Cera E, Rezaie AR. The conformation of the activation peptide of protein C is influenced by Ca²⁺ and Na⁺ binding. *J Biol Chem.* 2004;279(37):38519-38524.
8. Preston RJ, Ajzner E, Razzari C, et al. Multifunctional specificity of the protein C/activated protein C Gla domain. *J Biol Chem.* 2006;281(39):28850-28857.
9. Norstrom EA, Steen M, Tran S, Dahlbäck B. Importance of protein S and phospholipid for activated protein C-mediated cleavage in factor Va. *J Biol Chem.* 2003;278(27):24904-24911.
10. Ahnström J, Andersson HM, Canis K, et al. Activated protein C cofactor function of protein S: a novel role for a γ-carboxyglutamic acid residue. *Blood.* 2011;117(24):6685-6693.
11. Villoutreix BO, Teleman O, Dahlbäck B. A theoretical model for the Gla-TSR-EGF-1 region of the anticoagulant cofactor protein S: from biostructural pathology to species-specific cofactor activity. *J Comput. Aided Mol Des.* 1997;11(3):293-304.
12. Andersson HM, Arantes MJ, Crawley JT, et al. Activated protein C cofactor function of protein S: a critical role for Asp95 in the EGF1-like domain. *Blood.* 2010;115(23):4878-4885.
13. Yegneswaran S, Wood GM, Esmon CT, Johnson AE. Protein S alters the active site location of activated protein C above the membrane surface. A fluorescence resonance energy transfer study of topography. *J Biol Chem.* 1997;272(40):25013-25021.
14. Yegneswaran S, Smirnov MD, Safa O, Esmon NL, Esmon CT, Johnson AE. Relocating the active site of activated protein C eliminates the need for its protein S cofactor. A fluorescence resonance energy transfer study. *J Biol Chem.* 1999;274(9):5462-5468.
15. Hackeng TM, Yegneswaran S, Johnson AE, Griffin JH. Conformational changes in activated protein C caused by binding of the first epidermal growth factor-like module of protein S. *Biochem J.* 2000;349 Pt 3:757-764.
16. Dahlbäck B. The protein C anticoagulant system: inherited defects as basis for venous thrombosis. *Thromb. Res.* 1995;77(1):1-43.
17. Griffin JH, Evatt B, Zimmerman TS, et al. Deficiency of protein C in congenital thrombotic disease. *J Clin Invest.* 1981;68(5):1370-1373.
18. Jalbert LR, Rosen ED, Moons L, et al. Inactivation of the gene for anticoagulant protein C causes lethal perinatal consumptive coagulopathy in mice. *J Clin Invest.* 1998;102(8):1481-1488.
19. Reitsma PH, Poort S, Bernardi F, et al. Protein C deficiency: a database of mutations. *Thromb Haemost.* 1993;69(1):77-84.
20. Mackie I, Cooper P, Lawrie A, Kitchen S, Gray E, Laffan M. Guidelines on the laboratory aspects of assays used in haemostasis and thrombosis. *Int J Lab Hematol.* 2013;35(1):1-13.
21. Bode W, Mayr I, Baumann U, Huber R, Stone SR, Hofsteenge J. The refined 1.9 Å crystal structure of human α-thrombin: interaction with D-Phe-Pro-Arg chloromethylketone and significance of the Tyr-Pro-Pro-Trp insertion segment. *EMBO J.* 1989;8(11):3467-3475.
22. Yang L, Manithody C, Rezaie AR. Contribution of basic residues of the 70-80-loop to heparin binding and anticoagulant function of activated protein C. *Biochemistry.* 2002;41(19):6149-6157.
23. Yang L, Rezaie AR. Calcium-binding sites of the thrombin-thrombomodulin-protein C complex: possible implications for the effect of platelet factor 4 on the activation of vitamin K-dependent coagulation factors. *Thromb Haemost.* 2007;97(6):899-906.
24. Ding Q, Yang L, Dinarvand P, Wang X, Rezaie AR. Protein C Thr315Ala variant results in gain of function but manifests as type II deficiency in diagnostic assays. *Blood.* 2015;125(15):2428-2434.
25. Chen C, Yang L, Villoutreix BO, Wang X, Ding Q, Rezaie AR. Gly74Ser mutation in protein S-dependent anticoagulant function. *Thromb Haemost.* 2017;117(7):1358-1369.
26. Grinnell BW, Walls JD, Gerlitz B. Glycosylation of human protein C affects its secretion, processing, functional activities, and activation by thrombin. *J Biol Chem.* 1991;266(15):9778-9785.
27. Rezaie AR, Esmon CT. Tryptophans 231 and 234 in protein C report the Ca(2+)-dependent conformational change required for activation by the thrombin-thrombomodulin complex. *Biochemistry.* 1995;34(38):12221-12226.
28. Walker FJ. Regulation of activated protein C by protein S. The role of phospholipid in factor Va inactivation. *J Biol Chem.* 1981;256(21):11128-11131.
29. Dahlbäck B, Carlsson M, Svensson PJ. Familial thrombophilia due to a previously unrecognized mechanism characterized by poor anticoagulant response to activated protein C: prediction of a cofactor to activated protein C. *Proc Natl Acad Sci U S A.*

- 1993;90(3):1004-1008.
30. Bertina RM, Koeleman BP, Koster T, et al. Mutation in blood coagulation factor V associated with resistance to activated protein C. *Nature*. 1994;369(6475):64-67.
 31. Pineda AO, Zhang E, Guinto ER, Savvides SN, Tulinsky A, Di Cera E. Crystal structure of the thrombin mutant D221A/D222K: the Asp222:Arg187 ion-pair stabilizes the fast form. *Biophys Chem*. 2004;112(2-3):253-256.
 32. Qureshi SH, Yang L, Manithody C, Iakhiaev AV, Rezaie AR. Mutagenesis studies toward understanding allostery in thrombin. *Biochemistry*. 2009;48(34):8261-8270.
 33. Rezaie AR, Kittur FS. The critical role of the 185-189-loop in the factor Xa interaction with Na⁺ and factor Va in the prothrombinase complex. *J Biol Chem*. 2004;279(46):48262-48269.
 34. Dang QD, Di Cera E. Residue 225 determines the Na⁺-induced allosteric regulation of catalytic activity in serine proteases. *Proc Natl Acad Sci U S A*. 1996;93(20):10653-10656.
 35. Greengard JS, Fisher CL, Villoutreix B, Griffin JH. Structural basis for type I and type II deficiencies of antithrombotic plasma protein C: patterns revealed by three-dimensional molecular modelling of mutations of the protease domain. *Proteins*. 1994;18(4):367-380.
 36. Kalafatis M, Mann KG. Role of the membrane in the inactivation of factor Va by activated protein C. *J Biol Chem*. 1993;268(36):27246-27257.
 37. Nicolaes GA, Tans G, Thomassen MC, et al. Peptide bond cleavages and loss of functional activity during inactivation of factor Va and Factor VaR506Q by activated protein C. *J Biol Chem*. 1995;270(36):21158-21166.
 38. Rosing J, Hoekema L, Nicolaes GA, et al. Effects of protein S and factor Xa on peptide bond cleavages during inactivation of factor Va and factor VaR506Q by activated protein C. *J Biol Chem*. 1995;270(46):27852-27858.
 39. Ohlin AK, Landes G, Bourdon P, Oppenheimer C, Wydro R, Stenflo J. Beta-hydroxyaspartic acid in the first epidermal growth factor-like domain of protein C. Its role in Ca²⁺ binding and biological activity. *J Biol Chem*. 1988;263(35):19240-19248.
 40. Boerger LM, Morris PC, Thurnau GR, Esmon CT, Comp PC. Oral contraceptives and gender affect protein S status. *Blood*. 1987;69(2):692-694.
 41. Comp PC, Thurnau GR, Welsh J, Esmon CT. Functional and immunologic protein S levels are decreased during pregnancy. *Blood*. 1986;68(4):881-885.

Allogeneic stem cell transplantation in second complete remission for core binding factor acute myeloid leukemia: a study from the Acute Leukemia Working Party of the European Society for Blood and Marrow Transplantation

Kazimierz Halaburda,^{1*} Myriam Labopin,^{2,3*} Audrey Mailhol,² Gerard Socié,⁴ Charles Craddock,⁵ Mahmoud Aljurf,⁶ Dietrich Beelen,⁷ Jan J. Cornelissen,⁸ Jean-Henri Bourhis,⁹ H el ene Labussiere-Wallet,¹⁰ Didier Blaise,¹¹ Tobias Gedde-Dahl,¹² Maria Gillece,¹³ Ibrahim Yakoub-Agha,¹⁴ Ghulam Mufti,¹⁵ Jordi Esteve,¹⁶ Mohamad Mohty^{2,3} and Arnon Nagler^{2,17*}

¹Institute of Haematology and Transfusion Medicine, Warsaw, Poland; ²EBMT Paris Study Office, Paris, France; ³Saint Antoine Hospital, Paris, France; ⁴St. Louis Hospital, Paris, France; ⁵Queen Elizabeth Hospital, Birmingham, UK; ⁶King Faisal Hospital, Riyadh, Saudi Arabia; ⁷University Hospital, Essen, Germany; ⁸Erasmus MC Cancer Institute, Rotterdam, the Netherlands; ⁹Gustave Roussy Institut de Canc erologie, Villejuif, France; ¹⁰Hospices Civils de Lyon, Centre Hospitalier Lyon Sud, Lyon, France; ¹¹Institut Paoli Calmettes, Marseille, France; ¹²Oslo University Hospital, Oslo, Norway; ¹³St James's Institute of Oncology, Leeds, UK; ¹⁴CHU de Lille, LIRIC, INSERM U995, Universit  de Lille, 59000 Lille, France; ¹⁵GKT School of Medicine, London, UK; ¹⁶Hospital Clinic, Barcelona, Spain and ¹⁷Chaim Sheba Medical Center, Tel Hashomer, Israel

*KH, ML and AN contributed equally as co-first authors.

ABSTRACT

Core binding factor acute myeloid leukemia (AML) comprises two subtypes with distinct cytogenetic abnormalities of either t(8;21)(q22;q22) or inv(16)(p13q22)/t(16;16)(p13;q22). Since long-term response to chemotherapy in these leukemias is relatively good, allogeneic hematopoietic stem cell transplantation is considered in patients who relapse and achieve second complete remission. To evaluate the outcomes of allogeneic transplantation in this indication, we studied 631 patients reported to the European Society for Blood and Marrow Transplantation Registry between the years 2000 and 2014. Leukemia-free survival probabilities at two and five years were 59.1% and 54.1%, while overall survival probabilities were 65% and 58.2%, respectively. The incidence of relapse and risk of non-relapse mortality at the same time points were 19.8% and 22.5% for relapse and 20.9% and 23.3% for non-relapse mortality, respectively. The most important adverse factors influencing leukemia-free and overall survival were: leukemia with t(8;21), presence of three or more additional chromosomal abnormalities, and Karnofsky performance score <80. Relapse risk was increased in t(8;21) leukemia and associated with additional cytogenetic abnormalities as well as reduced intensity conditioning. Measurable residual disease in molecular evaluation before transplantation was associated with increased risk of relapse and inferior leukemia-free survival.

Introduction

Core binding factor (CBF) leukemia represents up to 12% of all newly diagnosed adult acute myeloid leukemia (AML).¹ Chromosomal markers of CBF AML include t(8;21)(q22;q22) and inv(16)(p13q22) or less frequently t(16;16)(p13;q22), further described jointly as inv(16). As a result of chromosomal abnormalities, fusion transcripts *RUNX1-RUNX1T1* in t(8;21) and *CBFB-MYH11* in inv(16) emerge. The tran-



Ferrata Storti Foundation

Haematologica 2020
Volume 105(6):1723-1730

Correspondence:

KAZIMIERZ HALABURDA
khalab30@wp.pl

Received: March 22, 2019.

Accepted: August 14, 2019.

Pre-published: August 22, 2019.

doi:10.3324/haematol.2019.222810

Check the online version for the most updated information on this article, online supplements, and information on authorship & disclosures: www.haematologica.org/content/105/6/1723

 2020 Ferrata Storti Foundation

Material published in *Haematologica* is covered by copyright. All rights are reserved to the Ferrata Storti Foundation. Use of published material is allowed under the following terms and conditions:

<https://creativecommons.org/licenses/by-nc/4.0/legalcode>.

Copies of published material are allowed for personal or internal use. Sharing published material for non-commercial purposes is subject to the following conditions:

<https://creativecommons.org/licenses/by-nc/4.0/legalcode>, sect. 3. Reproducing and sharing published material for commercial purposes is not allowed without permission in writing from the publisher.



scripts represent molecular attributes of CBF AML and are driver mutations for leukemogenesis. They disrupt normal hematopoiesis dependent on core binding factor subunit α (*RUNX1*) and β (*CBFB*) by silencing tumor suppressor genes leading to neoplastic transformation.² Accompanying secondary gene mutations (mutations of *NRAS*, *KIT*, *NF1*, *FLT3*, *KRAS*, *ASXL1* & *2*), additional cytogenetic abnormalities, and clinical features at diagnosis (age, white blood cell and blast counts, extramedullary involvement) affect treatment outcomes, but general prognosis in CBF AML remains favorable.^{3,4} Indeed, current induction chemotherapy standards lead to a complete remission (CR) rate of 87-89%, involving a high proportion of younger patients.^{5,6} Repeated high or intermediate-dose cytarabine consolidation provides long-term disease control in a large proportion of patients. Conventional chemotherapy results in long-term survival in 53-64% of patients. The major reason for treatment failure in CBF AML is relapse, reported in 30-50% of patients.^{7,8} Given the relatively favorable results of chemotherapy, patients with CBF leukemia are not usually candidates for allogeneic hematopoietic stem cell transplantation (HSCT) in first CR (CR1). However, CBF AML is a heterogeneous group of malignancies. Several variables, including type of CBF subunit involved, age, additional molecular or cytogenetic abnormalities, and dynamics of measurable residual disease (MRD) are known to influence the outcomes and contribute to disease recurrence.⁷⁻¹¹ HSCT is recognized as a standard procedure in patients who relapse and subsequently achieve CR2.^{4,12} To evaluate the results of HSCT in CBF AML patients in CR2, we decided to perform a retrospective study using registry data from the Acute Leukemia Working Party (ALWP) of the European Society for Blood and Marrow Transplantation (EBMT). The EBMT is a non-profit, scientific society representing more than 600 transplant centers, mainly in Europe. Member centers are required to report all consecutive stem cell transplantations and follow ups once a year. Data are entered, managed, and maintained in a central database with internet access; each EBMT center is represented in this database. Audits are routinely performed to determine accuracy of data. Before transplantation, patients or legal guardians provide informed consent authorizing the use of their anonymized personal information for research purposes.

Methods

Patients and data selection

The study was approved by the ALWP Institutional Review Board and included all adult patients undergoing HSCT in the period from the year 2000 to 2014 reported to the EBMT. The centers were asked by survey to provide data on all patients with t(8;21) or inv(16) to verify the cytogenetic aberrations and to update the transplantation outcomes using designated clinical forms. The patients had to have *de novo* CBF AML, with classical cytogenetics confirmation of t(8;21) or inv(16) at initial diagnosis, undergoing HSCT in hematologic CR2, defined as less than 5% blasts in the bone marrow (BM) and absence of extramedullary involvement, and regardless of current peripheral blood (PB) counts (i.e. *bona fide* CR or CR with incomplete hematologic recovery). All patients received BM or PB transplantation (BMT, PBSCT) from matched sibling (MSD) or unrelated donors (UD) after myeloablative (MAC) or reduced intensity (RIC) conditioning, as defined by the

EBMT criteria.¹³ The variables selected to assess outcomes were: age, type of AML, white blood cell count, presence of extramedullary involvement at diagnosis, additional cytogenetic abnormalities, time from diagnosis to CR1, duration of CR1, time from diagnosis and from CR2 to transplantation, molecular remission status at transplantation, Karnofsky performance score (KPS) at transplantation, sex matching of patients and donors, cytomegalovirus (CMV) serological status of patients and donors, year of transplantation, type of the donor, source of stem cells, conditioning intensity, and *in vivo* T-cell depletion.

End points and statistical analysis

The primary end point was leukemia-free survival (LFS). Secondary end points were: overall survival (OS), relapse incidence (RI), non-relapse mortality (NRM), graft-*versus*-host disease-free and leukemia-free survival (GRFS), as well as acute and chronic graft-*versus*-host disease (aGvHD and cGvHD). LFS was defined as survival without any symptoms of disease recurrence. OS was defined as probability of survival from transplantation to the last follow up. Relapse was defined as presence of >5% blasts in the BM or extramedullary disease after transplantation. NRM was defined as mortality from any cause not related to disease recurrence and GRFS was defined as survival without leukemia, aGvHD grade III-IV or extensive cGvHD.¹⁴ Minimal residual disease (MRD) was measured in the BM during the interval between last chemotherapy and transplantation. Real-time quantitative polymerase chain reaction (RT-qPCR) was used for *RUNX1-RUNX1T1* and *CBFB-MYH11* quantification. MRD results were reported by the centers as absent (MRDneg) or present (MRDpos) in line with their local guidelines. Acute GvHD was graded according to Glucksberg criteria.¹⁵ Surviving patients were censored at last follow up. Probabilities of LFS, OS, and GRFS were calculated using Kaplan-Meier estimates. Cumulative incidence functions (CIF) were used to determine RI and NRM in a competing risk setting with each other. Univariate analyses were performed using Gray's test for CIF and the log-rank test for LFS and OS. For all univariate analyses, continuous variables were categorized and the median was used as cut-off point. Associations of patient and transplantation characteristics with outcomes were evaluated in multivariate analysis using Cox proportional hazards model. Multivariate models were built by using stepwise selection procedure. Results were expressed as the hazard ratio (HR) with 95% Confidence Interval (CI). All tests were two-sided. The type-1 error rate was fixed at 0.05 for determination of factors associated with time to event outcomes. Statistical analyses were performed with SPSS 24 (SPSS Inc. /IBM, Armonk, NY, USA) and R 1.3.0 (R Development Core Team, Vienna, Austria) software packages.

Results

The detailed characteristics of the 631 patients from 181 transplant centers who met the study inclusion criteria are shown in Table 1. Three hundred and sixty-six patients (58%) harbored inv(16) and 265 (42%) t(8;21). The two groups were compared for essential patient and transplant characteristics (*Online Supplementary Table S1*). The differences included: sex of the patients [with more males in the t(8;21) group], time from diagnosis to transplantation [which was longer in the t(8;21) group], and time from diagnosis to CR1 [which was also longer in the t(8;21) group]. Altogether there were 361 (57%) males and 270 (43%) females. Median age at transplantation was 41.7 years [range 18-73, interquartile range (IQR) 31.3-51.2],

Table 1. Patients' and transplant characteristics. Percentage values in parentheses refer to reported data.

Number of patients	631
Median follow up, months (range)	59.6 (0.9 - 201)
Median year of transplantation (range)	2010 (2000-2014)
Type of AML	
inv(16)	366(58%)
t(8;21)	265(42%)
Median age at transplantation, years (range; IQR)	41.7 (18 -73; 31.3-51.2)
Median CR1 duration, days (range; IQR)	318 (6-2380; 246-474)
Median time from diagnosis to transplantation, months (range; IQR)	17 (3.5-222.9; 14-22.5)
Sex	
Male	361(57.2%)
Female	270(42.8%)
Donors	
Matched siblings	264(42%)
Unrelated	367(58%)
Additional chromosomal abnormalities	
No abnormality reported	497(79%)
3 or more abnormalities	32(5%)
Abn5	2(0.3%)
Abn7	10(1.6%)
Del 9	5(0.8%)
Del X or Y	18(2.9%)
Trisomy 22	9(1.4%)
Trisomy 8	10(1.6%)
Hyperdiploidy	4(0.6%)
Hypodiploidy	7(1.1%)
Undefined/other abnormalities	34(5.3%)
Molecular remission at transplantation	
Molecular CR	343(73.3%)
No molecular CR	125(26.7%)
Missing	163
Karnofsky performance score	
<80	16(2.8%)
≥80	559(97.2%)
Missing	56
Conditioning intensity	
Myeloablative	424(67.5%)
Reduced intensity	204(32.5%)
Missing	3
Source of stem cells	
Bone marrow	117(18.5%)
Peripheral blood	514(81.5%)
GvHD prophylaxis	
CsA based	584(92.6%)
Tacrolimus based	26(4%)
PTCY	6(1%)
Other	10(1.6%)
Missing	5(0.8%)
<i>In vivo</i> T-cell depletion	
Yes	325(51.8%)
No	302(48.2%)
Missing	4
Donor sex	
Male	369(59.4%)
Female	252(40.6%)
Missing	10
Female to male transplantation	133(21.2%)
CMV serology	
Patient CMV IgG positive	387(63%)
Donor CMV IgG positive	305(49.9%)

continued in next column

Engraftment	
Yes	619(98.7%)
No	8(1.3%)
Missing	4
aGvHD grade II-IV	
Yes	171(27.9%)
No	443(72.1%)
Missing	17
cGvHD	
Yes	279(46.7%)
No	318(53.3%)
Missing	34

AML: acute myeloid leukemia; IQR: interquartile range; CR1: first complete remission; abn 5: abnormalities of chromosome 5; abn 7: abnormalities of chromosome 7; del 9 complete or partial deletion of chromosome 9; del X or Y, deletion of chromosome X or Y; trisomy 22: trisomy of chromosome 22; trisomy 8: trisomy of chromosome 8; CR: complete remission; GvHD: graft-versus-host disease; CsA: cyclosporine A; PTCY: post-transplant cyclophosphamide; CMV IgG: cytomegalovirus-specific immunoglobulin G antibody; aGvHD: acute graft-versus-host disease; cGvHD: chronic graft-versus-host disease.

and the median year of transplantation was 2010. Nearly half of the procedures were performed between the years 2010 and 2014. Additional analysis of transplantation intervals 2000-2005, 2006-2009, and 2010-2014 periods did not reveal any significant differences in outcomes. Twenty-one percent of patients had additional cytogenetic aberrations detected at diagnosis. The most frequent of them was presence of three or more abnormalities (32.5%). There was a low frequency of reports of accompanying molecular abnormalities (cKIT mutations, FLT3-ITD, NRAS mutations and KRAS mutations) which precluded subset evaluation. The most frequent available information on co-mutation pattern was FLT3-ITD, which was reported in 26 patients, with a similar distribution between the inv(16) and the t(8;21) groups (14 and 12 patients, respectively). Three hundred and forty-three (73.3%) patients were MRDneg, while 125 (26.7%) were MRDpos before transplantation. There was a trend for higher frequency of MRDpos patients in the t(8;21) compared to the inv(16) subgroup ($P=0.06$) (*Online Supplementary Table S1*). Further analysis showed significant differences in terms of LFS, OS, and relapse in favor of inv(16) compared to t(8;21) AML in MRDneg but not MRDpos patients (*Online Supplementary Table S2*). Engraftment was achieved in 619 (98.7%) patients.

Leukemia-free survival

The 2- and 5-year probability of LFS was 59.1% (95%CI: 55.2-63.1) and 54.1% (95%CI: 50-58.2), respectively. In univariate analysis, LFS was significantly higher for patients with inv(16) compared to patients with t(8;21) (63.8% vs. 52.5%, $P=0.003$) (Figure 1A). Presence of three or more additional cytogenetic abnormalities at diagnosis resulted in worse LFS (37.5% vs. 60.4%, $P=0.002$). For MRDpos patients, the probability of LFS was 49% compared to 61.6% for patients who were MRDneg ($P=0.046$) (Figure 2A). Performance status was also an important factor, with 2-year LFS probability of 59.9% for patients with KPS ≥80 versus 37.5% for those with KPS <80 ($P=0.003$). The results of the univariate analysis are provided in *Online Supplementary Table S3*. In multivariate analysis, the type of CBF AML [t(8;21) versus inv(16)] was an independent factor for LFS (HR=1.40, 95%CI: 1.05-1.86, $P=0.022$) as was presence of three or more additional cyto-

Table 2. Multivariate analysis using Cox proportional hazards model. Variables with $P < 0.15$ in univariate analysis were included in the model.

		P	HR	95% CI
LFS	t(8;21) <i>vs.</i> inv(16)	0.022	1.40	1.05-1.86
	≥3 chromosomal abnormalities <i>vs.</i> no	0.004	2.09	1.27-3.42
	Molecular MRDneg <i>vs.</i> MRDpos	0.080	0.76	0.55-1.03
	KPS ≥ 80 <i>vs.</i> < 80	0.006	0.32	0.14-0.73
OS	t(8;21) <i>vs.</i> inv(16)	0.00002	1.76	1.35-2.28
	≥3 chromosomal abnormalities <i>vs.</i> no	0.037	1.68	1.03-2.72
	KPS ≥ 80 <i>vs.</i> < 80	0.002	0.36	0.19-0.68
RI	t(8;21) <i>vs.</i> inv(16)	0.002	1.89	1.26-2.84
	≥3 chromosomal abnormalities <i>vs.</i> no	0.011	2.31	1.23-4.40
	Time from diagnosis to transplantation (>median>)	0.023	0.97	0.94-0.99
	RIC <i>vs.</i> MAC	0.017	1.64	1.09-2.47
	Molecular MRDneg <i>vs.</i> MRDpos	0.043	0.65	0.42-0.99
NRM	KPS ≥ 80 <i>vs.</i> < 80	0.001	0.29	0.14-0.59
GRFS	Molecular MRDneg <i>vs.</i> MRDpos	0.054	0.77	0.60-1.00
	≥3 chromosomal abnormalities <i>vs.</i> no	0.031	1.61	1.04-2.47
	<i>In vivo</i> TCD <i>vs.</i> no	0.027	0.76	0.60-0.97
	Donor CMV IgG negative <i>vs.</i> positive	0.058	0.79	0.99-1.61
aGvHD II-IV	RIC <i>vs.</i> MAC	0.011	0.64	0.45-0.90
cGvHD	<i>In vivo</i> TCD <i>vs.</i> no	<10-5	0.56	0.43-0.72
	Donor CMV IgG positive <i>vs.</i> negative	0.004	1.45	1.13-1.87
	PBSCT <i>vs.</i> BMT	0.003	1.72	1.20-2.46

LFS: leukemia-free survival; MRDneg: minimal residual disease negative; MRDpos: minimal residual disease positive; KPS: Karnofsky performance score; OS: overall survival; RI: relapse incidence; RIC: reduced intensity conditioning; MAC: myeloablative conditioning; NRM: non-relapse mortality; GRFS: graft-*versus*-host disease-free, relapse-free survival; CMV IgG: cytomegalovirus-specific immunoglobulin G antibody; TCD: T-cell depletion; aGvHD II-IV: acute graft-*versus*-host disease, grades II to IV; cGvHD: chronic graft-*versus*-host disease; PBSCT: peripheral blood stem cell transplantation; BMT: bone marrow transplantation.

genetic abnormalities (HR=2.09, 95%CI: 1.27-3.42, $P=0.004$), and KPS ≥80 (HR=0.32; 95%CI: 0.14-0.73, $P=0.32$). In multivariate analysis, MRDneg was not an independent prognostic factor for LFS (HR=0.76; 95%CI: 0.55-1.03, $P=0.08$) (Table 2).

Overall survival

Two- and 5-year OS probability for the whole group was 65% (95%CI: 61.2-68.9) and 58.2% (95%CI: 54.1-62.3), respectively. In univariate analysis, patients with t(8;21) AML had a lower probability of OS compared to those with inv(16) (57% *vs.* 70.5%, $P=0.0003$) (Figure 1B). Three or more additional cytogenetic abnormalities was associated with lower OS (49.6% *vs.* 65.9%, $P=0.013$). Performance status at transplantation influenced OS. OS of patients with KPS≥80 was 66.1% *versus* 37.5% in those with KPS<80 ($P=0.003$) (Online Supplementary Table S3). MRDneg was not significantly associated with OS (Figure 2B). Multivariate analysis confirmed the findings of the univariate analysis. AML with t(8; 21), additional cytogenetic abnormalities, and KPS <80 were the three independent prognostic factors for significantly worse OS with HR 1.76 (95%CI: 1.35-2.28, $P=0.00002$), HR 1.68 (95%CI: 1.03-2.72, $P=0.037$), and HR 0.36 for KPS ≥80 (95%CI: 0.19-0.68, $P=0.002$), respectively (Table 2). In multivariate analysis, MRD status was not an independent prognostic factor for OS (59.9%; 95%CI: 50.8-68.9 *vs.* 65.8%; 95%CI: 60.7-71, $P=0.47$). Age at HSCT (below or above the median) did not affect OS (66.5%; 95%CI: 61.1-71 *vs.* 63.6%; 95%CI: 58.1-69, $P=0.39$).

Relapse incidence

The risk of relapse at two and at five years was estimated at 19.8% (95%CI: 16.7-23.1) and 22.5% (95%CI: 19.2-26). In patients with t (8; 21), the risk of relapse at two

years was significantly higher: 25.8% *versus* 15.6% in those with inv (16) ($P=0.009$) (Figure 1C). The risk of relapse was higher in patients with three or more additional chromosomal aberrations (34.4% *vs.* 19%, $P=0.03$). In the whole cohort, MRDneg patients had a significantly decreased risk of relapse compared to MRDpos patients (16.2% *vs.* 29.3%, $P=0.003$) (Figure 2C). In patients with CR1 shorter than the median (318 days), the risk of relapse after transplantation was higher (26.4% *vs.* 13%, $P < 0.001$). Time from diagnosis to transplantation was also significant. In patients receiving HSCT within a shorter time than the median (17 months from diagnosis), the risk of relapse was higher (26.4% *vs.* 13.1%, $P < 0.001$). Conditioning intensity was also important. Patients receiving RIC experienced more leukemia relapses compared to those receiving MAC (25.9% *vs.* 17%, $P=0.002$). Finally, *in vivo* T-cell depletion led to more recurrences (22.6% *vs.* 16.7% in patients transplanted without T-cell depletion ($P=0.02$)) (Online Supplementary Table S3). In multivariate analysis, t(8; 21) *versus* inv(16), presence of three or more additional chromosomal abnormalities, time from diagnosis to transplantation (> *vs.* ≤ median), MRDneg, and RIC were independent significant prognostic factors for relapse. The corresponding HR values for those factors were 1.89 (95%CI: 1.26-2.84, $P=0.002$), 2.31 (95%CI: 1.23-4.4, $P=0.011$), 0.97 (95%CI: 0.94-0.99, $P=0.023$), 0.65 (95%CI: 0.42-0.99, $P=0.043$), and 1.64 (95%CI: 1.09-2.47, $P=0.017$), respectively. *In vivo* T-cell depletion was not confirmed to be an independent risk factor for relapse in multivariate analysis (Table 2).

Non-relapse mortality

The 2- and 5-year incidence of NRM was 20.9% (95%CI: 17.7-24.2) and 23.3% (95%CI: 19.9-26.8), respectively. In univariate analysis, KPS <80 *versus* ≥80 was

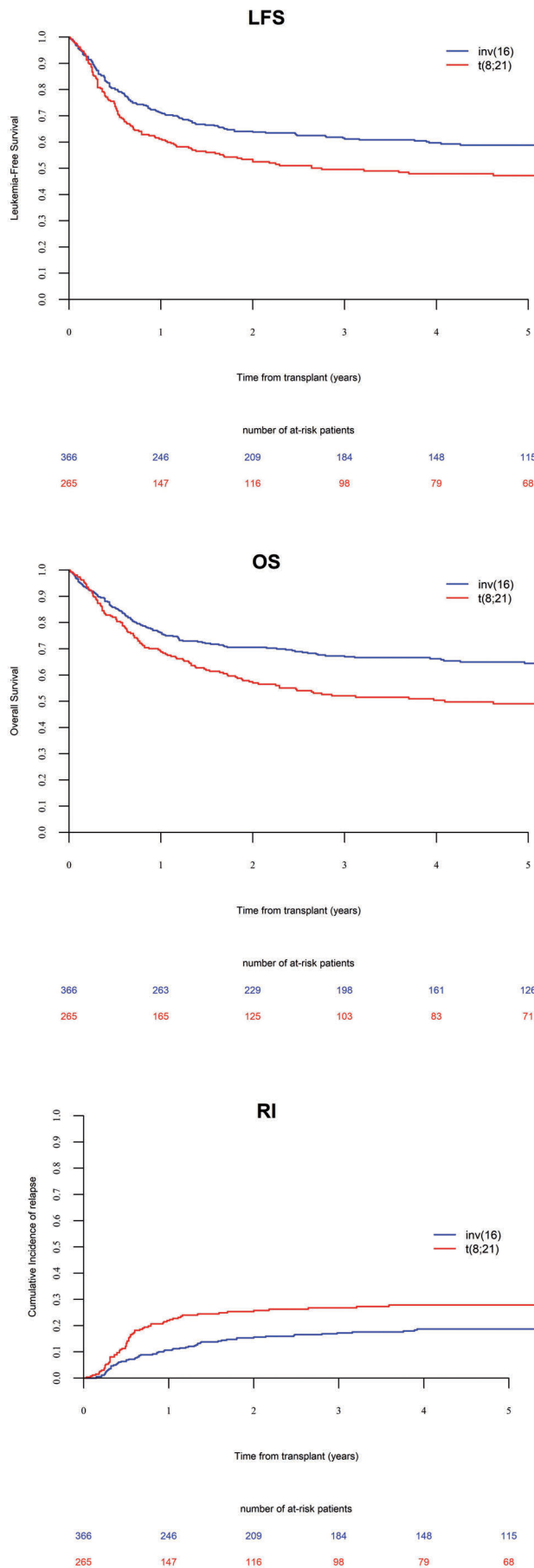


Figure 1. Leukemia-free survival (LFS), overall survival (OS), and relapse incidence (RI) in patients with core-binding factor acute myeloid leukemia (CBF AML) transplanted in second complete remission for patients with inv(16) versus t(8;21). 2-year probability of LFS: 63.8% (95% CI: 58.8-68.8) vs. 52.5% (95% CI: 46.2-58.8), $P=0.003$. 2-year probability of OS: 70.5% (95% CI: 65.8-75.3) vs. 57% (95% CI: 50.7-63.2), $P=0.0003$. 2-year risk of relapse: 15.6% (95% CI: 12-19.6) vs. 25.8% (95% CI: 20.5-31.4), $P=0.009$.

strongly associated with NRM (50% vs. 19.8%, $P=0.002$). Patients in whom CR1 duration was shorter than the median, or those who were transplanted at a shorter time from diagnosis than the median, experienced decreased NRM (17.1% vs. 25.8%, $P=0.007$ and 18% vs. 24%, $P=0.01$, respectively) (*Online Supplementary Table S3*). In multivariate analysis, only performance status was an independent risk factor for NRM; HR 0.29 (95%CI: 0.14-0.59, $P=0.001$) for patients with KPS ≥ 80 versus those with KPS < 80 (Table 2).

Graft-versus-host disease and leukemia-free survival

The 2- and 5-year probability of GRFS was 40.2% (95%CI: 36.2-44.2) and 34.6% (95% CI: 30.6-38.6), respectively. The 2-year probability of GRFS for patients with inv (16) was higher than for those with t(8; 21) (44.1% vs. 34.7%, $P=0.049$). Presence of three or more additional chromosomal aberrations was significantly associated with worse GRFS (20% vs. 41.3%, $P=0.01$). Patients who were MRDneg before transplantation had a higher probability of GRFS (42.9% vs. 29.2%, $P=0.02$). Similarly, those who received *in vivo* T-cell depletion had a higher GRFS (46.1% vs. 33.9%, $P=0.004$). Finally, there was a trend for better GRFS in patients transplanted from CMV seronegative versus seropositive donors (41.8% vs. 38.4%, $P=0.07$) (*Online Supplementary Table S3*). In multivariate analysis, factors independently associated with GRFS were three or more cytogenetic abnormalities and *in vivo* T-cell depletion (HR 1.61; 95%CI: 1.04-2.47, $P=0.03$ and HR 0.76; 95%CI: 0.6-0.97, $P=0.027$, respectively). Transplantation from CMV negative donors and MRDneg status were associated with a trend for better GRFS (HR0.79; 95%CI: 0.62-1, $P=0.058$ and HR 0.77; 95%CI: 0.6-1.0, $P=0.054$, respectively) (Table 2).

Graft-versus-host disease

The incidence of aGvHD grades II to IV and III-IV was 28% (95%CI: 24.5-31.6) and 9.5% (95%CI: 7.3-12), respectively. In univariate analysis, transplantation from MSD compared to UD was associated with lower incidence of grade II-IV aGvHD (24.1% vs. 30.8%, $P=0.049$). Grade II-IV aGvHD was higher in patients transplanted with BM vs. PB grafts (36% vs. 26.1%, $P=0.04$). MAC in comparison to RIC was associated with increased incidence of aGvHD grade II-IV (30.8% vs. 21.6%, $P=0.01$). *In vivo* T-cell depletion reduced grade II-IV (23.6% vs. 32.7%, $P=0.01$) and grade III-IV (5.7% vs. 13.6%, $P=0.009$) aGVHD incidence (*Online Supplementary Table S3*). In multivariate analysis, only intensity of conditioning regimen (RIC vs. MAC) was an independent prognostic factor for aGvHD grade II-IV: HR 0.64 (95%CI: 0.45-0.9), $P=0.011$ (Table 2).

The incidence of cGvHD at two and five years post transplant was 46.7% (95%CI: 42.5-50.8) and 48.4% (95%CI: 44-52.4), respectively. Transplantation from

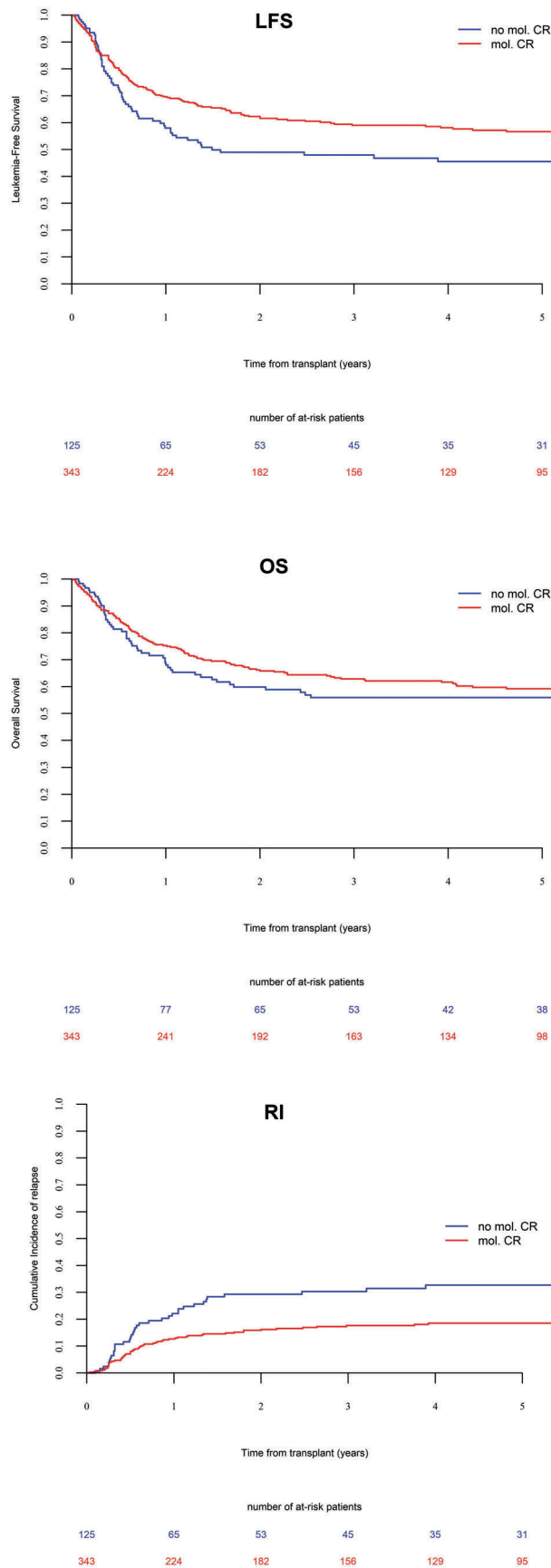


Figure 2. Leukemia-free survival (LFS), overall survival (OS), and relapse incidence (RI) in patients with core-binding factor acute myeloid leukemia in patients without versus with molecular remission pre-transplant. 2-year probability of LFS: 49% (95%CI: 39.8-58.2) vs. 61.6% (95%CI: 56.3-66.9), $P=0.046$. 2-year probability of OS: 59.9% (95%CI: 50.8-68.9) vs. 65.8% (95%CI: 60.7-71), $P=0.47$. 2-year risk of relapse: 29.3% (95%CI: 21.2-37.8) vs. 16.2% (95%CI: 12.4-20.4), $P=0.003$.

Table 3. Mortality during follow up.

Causes of death	Number
Total	257
Original disease	83
Infection	62
Graft-versus-host disease	59
Other related to transplantation	21
Interstitial pneumonitis	9
Sinusoidal obstruction syndrome	5
Hemorrhage	4
Second malignancy	4
Cardiac toxicity	2
Missing	8

female versus male donors was associated with increased risk of cGvHD (52.1% vs. 43.4%, $P=0.01$); the same was true for female to male transplantations versus other combinations (55.2% vs. 44.5%, $P=0.03$). Transplantation from CMV positive versus CMV negative donors also correlated with increased risk of cGvHD (53.2% vs. 40.5%, $P=0.002$). BM versus PB grafts resulted in lower incidence of cGVHD (37.1% vs. 49.1%, $P=0.04$). *In vivo* T-cell depletion decreased risk of cGVHD (37.7% vs. 55.9%, $P<0.001$) (Online Supplementary Table S3). In multivariate analysis, *in vivo* T-cell depletion was an independent factor for decreased risk of cGVHD (HR=0.56; 95%CI: 0.43-0.72, $P<0.001$), while PBSCT and CMV donor seropositivity were associated with increased risk of cGVHD (HR=1.72; 95%CI: 1.2-2.46, $P=0.003$ and HR=1.45; 95%CI: 1.13-1.87, $P=0.004$, respectively) (Table 2).

Mortality

During follow up, 257 of 631 patients died. The main causes of death were recurrence of the original disease, infection, and GvHD (Table 3).

Discussion

This retrospective analysis of HSCT in CBF AML in second hematologic CR was based on a large number of patients reported to the EBMT. Chemotherapy alone after relapse in patients with favorable risk AML is able to produce 5-year survival in 42-44% of patients.^{16,17} Allogeneic HSCT is recommended by leading organizations in Europe and the USA as consolidation treatment for AML patients achieving CR2.¹³ In our study, the results of transplantation in terms of OS and LFS were a little worse than those described previously for patients with CBF AML transplanted in CR1 and comparable with published outcomes of HSCT performed in CR2.^{19,20} Similarly to those

studies, in our group, patients with *inv(16)* had a higher probability of LFS, OS, and a lower risk of relapse than those with *t(8;21)*. Interestingly, these end points reported in most papers for patients treated with chemotherapy alone are not usually different for *inv(16)* and *t(8;21)* AML. On the other hand, the MD Anderson study, for example, pointed out that patients diagnosed with *t(8;21)* have a worse prognosis than those with *inv(16)*.⁵

Response to chemotherapy with clearance of *RUNX1-RUNX1T1* and *CBFB-MYH11* evaluated with RT-qPCR, as well as additional molecular aberrations detected at diagnosis, but not type of CBF AML *per se*, are most frequently emphasized as the factors determining outcome in chemotherapy-treated patients.^{9,21,22} Presence of MRD assessed with flow cytometry in AML before transplantation is a recognized risk factor for inferior outcome.²³ Molecular evaluation of MRD in CBF AML before transplantation has not been extensively studied to date. In our cohort, MRDneg patients had a significantly decreased risk of relapse compared with MRDpos patients (HR=0.65, *P*=0.043); this translated into a trend for improved LFS (HR=0.76, *P*=0.08) and GRFS (HR=0.77, *P*=0.054) but showed no significant influence on OS (*P*=0.47). Data analysis revealed that MRDpos patients more frequently received donor lymphocyte infusions or subsequent transplants after relapse than MRDneg patients. Those therapeutic interventions, and probably lack of statistical power, may explain why we did not find a significant difference in OS in favor of MRDneg patients. The results of our study indicate that even patients who are MDRpos can expect survival advantage from transplantation compared to those who are treated with chemotherapy alone.⁹ A recent paper showed that evaluation of *RUNX1-RUNX1T1* was useful to predict relapse not only before but also after HSCT.²⁴ It should be emphasized that the kinetics of relapse in *inv(16)* and *t(8;21)* patients differ, and the latter group requires more frequent molecular testing.²⁵

According to the 2017 European Leukemia Net and National Comprehensive Cancer Network guidelines, additional cytogenetic aberrations in CBF AML do not modify disease risk.^{4,26} In our study group, the presence of concurrent three or more chromosomal abnormalities had a marked deleterious effect on relapse (HR=2.31, *P*=0.011), LFS (HR=2.09, *P*=0.004), and even OS (HR=1.68, *P*=0.037) after HSCT. Indeed, earlier reports documented worse outcomes in newly diagnosed CBF AML patients with three or more cytogenetic abnormalities.⁵ This finding may indicate a more complex clonal evolution, and could support the adoption of anticipated measures to avoid relapse, such as indication of transplantation in first remission.

Not surprisingly, in our study, performance status was a strong independent risk factor for NRM, LFS, and OS. Thus, patients with KPS ≥ 80 had decreased NRM and improved LFS and OS, which was similar to the findings of previous studies.²⁷

The intensity of conditioning regimen in the current analysis favored MAC over RIC in terms of relapse. Comparable findings were described in a recent EBMT ALWP study in patients transplanted for secondary AML with additional benefit of higher probability of LFS and OS in individuals receiving MAC.²⁸ The results of an

American phase III prospective randomized trial of MAC *versus* RIC in AML and myelodysplastic syndrome patients published in 2017 also revealed statistically higher relapse rates and worse LFS with a trend for decreased OS after RIC.²⁹ In contrast, in a German randomized study including AML patients published a few years earlier, RIC and MAC yielded identical results for both types of conditioning, even in terms of disease recurrence.³⁰ In our cohort, conditioning intensity had no significant impact on LFS or OS. In the German trial, MAC was also a predictor for aGvHD. Similarly, in our study, MAC was the only independent risk factor for clinically significant, grade II-IV aGvHD. The same correlation had been described previously, and is supported by the concept of a more pronounced inflammatory reaction after MAC.³¹

Independent factors influencing cGvHD in our study were: *in vivo* TCD, the use of PBSC *versus* BM, and transplantation from CMV seropositive donors; these findings are in agreement with previous literature.^{32,33} Only recently, possible mechanisms linking CMV immunity and cGvHD were studied in HSCT recipients. In patients with cGvHD, a higher proportion of donor-origin high-affinity CMV-specific cytotoxic T lymphocytes was demonstrated.³⁴ The composite end point described as GRFS represents the most desirable outcome of HSCT. In our study, 2- and 5-year probabilities of GRFS were 40.2% and 34.6%, respectively. Recently, a large analysis of 5,059 AML patients from the EBMT database defined transplantation from unrelated donors, PB stem cell transplants, and unfavorable cytogenetics as prognostic factors for worse GRFS. In contrast, *in vivo* TCD was associated with better results and was the main beneficial factor for GRFS.³⁵ In our cohort, type of donor and source of stem cells did not have a significant impact on GRFS, which may be due to a considerably smaller study sample. Adverse cytogenetics decreased, while *in vivo* TCD increased the probability of GRFS in our patients, which is in line with the results of the above-mentioned study.

Our registry-based, retrospective study has various well-known limitations. For example, due to low reporting, we were not able to investigate the prognostic impact of additional genetic co-mutations frequently observed in CBF-AML, such as mutations in signaling pathways KIT, NRAS, KRAS and FLT3.³⁶

The most important findings of our study show that HSCT in CBF AML in CR2 was able to cure a large proportion of patients, with 2-year and 5-year OS 65% and 58.2%, respectively. The survival of patients with *inv(16)* was better than those with *t(8;21)*; an observation which confirms a substantial underlying difference between the two CBF AML subtypes also in the transplant setting. Based on our results, CBF AML patients should receive MAC rather than RIC, if eligible. Although patients who were MRDneg had lower risk of relapse and higher probability of survival without recurrence of leukemia, a significant proportion of MRDpos patients obtained durable response following HSCT. In view of our study, lack of MRD clearance should not be considered a contraindication for allogeneic transplantation.

Acknowledgments

The authors would like to thank all colleagues from 184 reporting centers for providing data for the analysis.

References

- Grimwade D, Walker H, Oliver F, et al. The importance of diagnostic cytogenetics on outcome in AML: analysis of 1,612 patients entered into the MRC AML 10 Trial. *Blood*. 1998;92(7):2322-2333.
- Solh M, Yohe S, Weidorf D, Ustun C. Core-binding factor acute myeloid leukemia: heterogeneity, monitoring and therapy. *Am J Hematol*. 2014;89(12):1121-1131.
- Papaemmanuil E, Gerstung M, Bullinger L, et al. Genomic classification and prognosis in acute myeloid leukemia. *N Engl J Med*. 2016;374(23):2209-2221.
- Döhner H, Estey E, Grimwade D, et al. Diagnosis and management of AML in adults: 2017 ELN recommendations from an international expert panel. *Blood*. 2017;129(4):424-447.
- Appelbaum FR, Kopecky KJ, Tallman MS, et al. The clinical spectrum of adult acute myeloid leukaemia associated with core binding factor translocations. *Br J Haematol*. 2006;135(2):165-173.
- Schlenk RF, Benner A, Krauter J, et al. Individual patient data-based meta-analysis of patients aged 16 to 60 years with core binding factor acute myeloid leukemia: a survey of the German Acute Myeloid Leukemia Intergroup. *J Clin Oncol*. 2004;22(18):3741-3750.
- Marcucci G, Mrózek K, Ruppert AS, et al. Prognostic factors and outcome of core binding factor acute myeloid leukemia patients with t(8;21) differ from those of patients with inv(16): a Cancer and Leukemia Group B study. *J Clin Oncol*. 2005;23(24):5705-5717.
- Mosna F, Papayannidis C, Martinelli G, et al. Complex karyotype, older age, and reduced first-line dose intensity determine poor survival in core binding factor acute myeloid leukemia patients with long-term follow-up. *Am J Hematol*. 2015;90(6):515-523.
- Jourdan E, Boissel N, Chevret S, et al. Prospective evaluation of gene mutations and minimal residual disease in patients with core binding factor acute myeloid leukemia. *Blood*. 2013;121(12):2213-2223.
- Liu Yin JA, O'Brien MA, Hills RK, Daly SB, Wheatley K, Burnett AK. Minimal residual disease monitoring by quantitative RT-PCR in core binding factor AML allows risk stratification and predicts relapse: results of the United Kingdom MRC AML-15 trial. *Blood*. 2012;120(14):2826-2835.
- Cairoli R, Beghini A, Turrini M, et al. Old and new prognostic factors in acute myeloid leukemia with deranged core-binding factor beta. *Am J Hematol*. 2013;88(7):594-600.
- Sureda A, Bader P, Cesaro S, et al. Indications for allo- and auto-SCT for haematological diseases, solid tumors and immune disorders: current practice in Europe, 2015. *Bone Marrow Transplant*. 2015;50(8):1037-1056.
- Bacigalupo A, Ballen K, Rizzo D, et al. Defining the intensity of conditioning regimens: working definitions. *Biol Blood Marrow Transplant*. 2009;15(12):1628-1633.
- Ruggeri A, Labopin M, Ciceri F, Mohty M, Nagler A. Definition of GvHD-free, relapse-free survival for registry-based studies: an ALWP-EBMT analysis on patients with AML in remission. *Bone Marrow Transplant*. 2016;51(4):610-611.
- Glucksberg H, Storb R, Fefer A, et al. Clinical manifestations of graft-versus-host disease in human recipients of marrow from HLA-matched sibling donors. *Transplantation*. 1974;18(4):295-304.
- Hospital MA, Prebet T, Bertoli S, et al. Core-binding factor acute myeloid leukemia in first relapse: a retrospective study from the French AML intergroup. *Blood*. 2014;124(8):1312-1319.
- Burnett AK, Goldstone A, Hills RK, et al. Curability of patients with acute myeloid leukemia who did not undergo transplantation in first remission. *J Clin Oncol*. 2013;31(10):1293-1301.
- Hübel K, Weingart O, Naumann F, et al. Allogeneic stem cell transplant in adult patients with acute myelogenous leukemia: a systematic analysis of international guidelines and recommendations. *Leuk Lymph*. 2011;52(3):444-457.
- Joon JH, Kim JW, Jeon YW, et al. Identification of molecular and cytogenetic risk factors for unfavorable core-binding factor-positive adult AML with post-remission treatment outcome analysis including transplantation. *Bone Marrow Transpl*. 2014;49(12):1466-1474.
- Kuwatsuka W, Miyamura K, Suzuki R, et al. Hematopoietic stem cell transplantation for core binding factor acute myeloid leukemia: t(8;21) and inv(16) represent different clinical outcomes. *Blood*. 2009;113(9):2096-2103.
- Hoyos M, Nomdedeu JF, Esteve J, et al. Core binding factor acute myeloid leukemia: the impact of age, leukocyte count, molecular findings, and minimal residual disease. *Eur J Haematol*. 2013;91(3):209-218.
- Duployez N, Marceau-Renaut A, Boissel N, et al. Comprehensive mutational profiling of core binding factor acute myeloid leukemia. *Blood*. 2016;127(20):2451-2459.
- Walter RB, Buckley SA, Pagel JM, et al. Significance of minimal residual disease before myeloablative allogeneic hematopoietic cell transplantation for AML in first and second complete remission. *Blood*. 2013;122(10):1813-1821.
- Qin YZ, Wang Y, Xu LP, et al. The dynamics of RUNX1-RUNX1T1 transcript levels after allogeneic hematopoietic stem cell transplantation predict relapse in patients with t(8;21) acute myeloid leukemia. *J Hematol Oncol*. 2017;10(1):44.
- Ommen HB, Schnittger S, Jovanovic JV, et al. Strikingly different molecular relapse kinetics in NPM1c, PML-RARA, RUNX1-RUNX1T1, and CBFβ-MYH11 acute myeloid leukemias. *Blood*. 2010;115(2):198-205.
- O'Donnell MR, Tallman MS, Abboud CN, et al. NCCN Guidelines version 2.2018. Acute myeloid leukemia. Cited 2018, 15 Sept. Available from https://www.nccn.org/professionals/physician_gls/pdf/aml.pdf
- Sorrer M, Storer B, Sandmaier BM, et al. Hematopoietic cell transplantation-comorbidity index and Karnofsky performance status are independent predictors of morbidity and mortality after allogeneic nonmyeloablative hematopoietic cell transplantation. *Cancer*. 2008;112(9):1992-2001.
- Sengsayadeth S, Gatwood KS, Boumendil A, et al. Conditioning intensity in secondary AML with prior myelodysplastic syndrome/myeloproliferative disorders: an EBMT ALWP study. *Blood Adv*. 2018;2(16):2127-2135.
- Scott BL, Pasquini MC, Logan BR, et al. Myeloablative versus reduced-intensity hematopoietic cell transplantation for acute myeloid leukemia and myelodysplastic syndromes. *J Clin Oncol*. 2017;35(11):1154-1161.
- Bornhäuser M, Kienast J, Trensche R, et al. Reduced-intensity conditioning versus standard conditioning before allogeneic haemopoietic cell transplantation in patients with acute myeloid leukaemia in first complete remission: a prospective, open-label randomised phase 3 trial. *Lancet Oncol*. 2012;13(10):1035-1044.
- Couriel DR, Saliba RM, Giral S, et al. Acute and chronic graft-versus-host disease after ablative and nonmyeloablative conditioning for allogeneic hematopoietic transplantation. *Biol Blood Marrow Transplant*. 2004;10(3):178-185.
- Jacobsen N, Badsberg JH, Lönnqvist B, et al. Graft-versus-leukaemia activity associated with CMV-seropositive donor, post-transplant CMV infection, young donor age and chronic graft-versus-host disease in bone marrow allograft recipients. *The Nordic Bone Marrow Transplantation Group*. *Bone Marrow Transplant*. 1990;5(6):413-418.
- Ljungman P, Brand R, Hoek J, et al. Donor cytomegalovirus status influences the outcome of allogeneic stem cell transplant: a study by the European group for blood and marrow transplantation. *Clin Infect Dis*. 2014;59(4):473-481.
- Poiret T, Axelsson-Robertson R, Remberger M, et al. Cytomegalovirus-specific CD8+ T-cells with different T-cell receptor affinities segregate T-cell phenotypes and correlate with chronic graft-versus-host disease in patients post-hematopoietic stem cell transplantation. *Front Immunol*. 2018;9:760.
- Battipaglia G, Ruggeri A, Labopin M, et al. Refined graft-versus-host disease/relapse-free survival in transplant from HLA-identical related or unrelated donors in acute myeloid leukemia. *Bone Marrow Transplant*. 2018;53(10):1295-1303.
- Faber ZJ, Chen X, Gedman AL, et al. The genomic landscape of core-binding factor acute myeloid leukemias. *Nat Genet*. 2016;48(12):1551-1556.

Yttrium-90-labeled anti-CD45 antibody followed by a reduced-intensity hematopoietic cell transplantation for patients with relapsed/refractory leukemia or myelodysplasia

Phuong Vo,^{1,2} Ted A. Gooley,^{1,2} Joseph G. Rajendran,³ Darrell R. Fisher,⁴ Johnnie J. Orozco,^{1,2} Damian J. Green,^{1,2} Ajay K. Gopal,^{1,2} Robyn Haaf,¹ Margaret Nartea,¹ Rainer Storb,^{1,2} Frederick R. Appelbaum,^{1,2} Oliver W. Press,^{1,2,†} John M. Pagel^{5*} and Brenda M. Sandmaier^{1,2}

¹Division of Clinical Research, Fred Hutchinson Cancer Research Center, Seattle; ²Department of Medicine, University of Washington, Seattle; ³Department of Radiology, University of Washington, Seattle; ⁴Versant Medical Physics and Radiation Safety, Richland and ⁵Swedish Cancer Institute, Seattle, WA, USA

*Current address: Swedish Medical Center, Seattle, WA, USA

†Posthumous.



Ferrata Storti Foundation

Haematologica 2020

Volume 105(6):1731-1737

ABSTRACT

Outcomes of patients with persistent high-risk leukemia or myelodysplasia prior to allogeneic hematopoietic cell transplantation are dismal. We therefore conducted a phase I trial evaluating the use of CD45-targeted radiotherapy preceding hematopoietic cell transplantation with the goal of improving outcomes for this high-risk scenario. Fifteen patients, median age 62 (range 37-76) years, were treated: ten with advanced acute myeloid leukemia, five with high-risk myelodysplastic syndrome. All patients had evidence of disease prior to treatment including nine with marrow blast counts ranging from 7-84% and six with minimal residual disease. Patients received escalating doses of yttrium-90-labeled anti-CD45 antibody followed by fludarabine and 2 Gy total body irradiation prior to human leukocyte antigen-matched, related or unrelated hematopoietic cell transplantation. Although a maximum dose of 30 Gy was delivered to the liver, no dose-limiting toxicity was observed. Therefore, the maximum-tolerated dose could not be estimated. Treatment led to complete remission in 13 patients (87%). All patients engrafted by day 28. Six patients relapsed, median of 59 (range 6-351) days, after transplantation. The 1-year estimate of relapse was 41%. Eight patients (53%) are surviving with median follow up of 1.8 (range 0.9-5.9) years. Estimated overall survival at one and two years was 66% and 46%, respectively, with progression-free survival estimated to be 46% at each time point. In conclusion, the combination of ⁹⁰Y-DOTA-BC8 with an allogeneic hematopoietic cell transplantation regimen was feasible and tolerable. This approach appears promising in this high-risk leukemia/myelodysplasia patient population with active disease. (Trial registered at *clinicaltrials.gov* identifier: NCT01300572.)

Introduction

Allogeneic hematopoietic cell transplantation (HCT) is a commonly used therapy for patients with refractory/relapsed acute leukemia and myelodysplastic syndrome (MDS) with unfavorable genetics. Although HCT is the most effective treatment for these patients, the procedure is associated with significant toxicities, especially for elderly patients. Reduced-intensity preparative regimens have been developed as an alternative approach for older patients and those with comorbidities that might prevent them from undergoing a myeloablative HCT. Standard reduced-intensity conditioning regimens, however, have been commonly associated with higher relapse rates

Correspondence:

BRENDA M. SANDMAIER
bsandmai@fredhutch.org

Received: June 13, 2019.

Accepted: October 3, 2019.

Pre-published: October 3, 2019.

doi:10.3324/haematol.2019.229492

Check the online version for the most updated information on this article, online supplements, and information on authorship & disclosures: www.haematologica.org/content/105/6/1731

©2020 Ferrata Storti Foundation

Material published in *Haematologica* is covered by copyright. All rights are reserved to the Ferrata Storti Foundation. Use of published material is allowed under the following terms and conditions:

<https://creativecommons.org/licenses/by-nc/4.0/legalcode>.

Copies of published material are allowed for personal or internal use. Sharing published material for non-commercial purposes is subject to the following conditions:

<https://creativecommons.org/licenses/by-nc/4.0/legalcode>, sect. 3. Reproducing and sharing published material for commercial purposes is not allowed without permission in writing from the publisher.



in patients with an advanced burden of active leukemia at the time of transplantation.¹ We previously combined iodine-131-labeled anti-CD45 monoclonal antibody (¹³¹I-BC8) with a reduced-intensity conditioning regimen to decrease relapse in older patients with advanced or refractory myeloid malignancies.² While the study was not designed to examine potential efficacy, the 3-year disease-free survival was 38% for 58 patients with active relapsed/refractory leukemia, a rate superior to historical experience where the 3-year overall and disease-free survival estimates of these patients were only 23% and 13%, respectively.^{1,3} Furthermore, 86% of the patients had acute myeloid leukemia (AML) in active relapse or MDS with more than 5% blasts in their marrow by morphology at the time of HCT. All patients achieved a complete remission as well as 100% donor chimerism in the CD3 and CD33 compartments by day 28. The maximum-tolerated dose (MTD) was estimated to be 24 Gy delivered by ¹³¹I-BC8 to the normal organ receiving the highest dose (liver), with renal insufficiency and cardiopulmonary toxicities being dose-limiting.

We used ¹³¹I as the therapeutic radionuclide in our prior clinical studies because it was readily available, there was extensive experience with its medical use, the technology for directly radiolabeling antibodies with iodine has been well established, and its gamma-ray component allowed direct determination of labeled antibody biodistribution in the patient after a tracer infusion. However, the high abundance gamma radiation component of ¹³¹I requires that patients be treated and sequestered in radiation isolation and poses a potential radiation exposure risk for staff and family, presenting a major limitation to the wide-spread exportability of this modality. As an alternative, yttrium-90 (⁹⁰Y) has been explored as a pure β -emitter that has been available in high specific activity and purity. Moreover, the β particles from ⁹⁰Y have a high energy ($E_{max} = 2.28$ MeV) with greater tissue penetrating range (up to 11 mm) that may be more favorable for near-uniform deposition of radiation energy in tumor masses.⁴

In this current study, we evaluated the safety and potential efficacy of ⁹⁰Y-labeled anti-CD45 antibody (⁹⁰Y-DOTA-BC8) followed by a standard reduced-intensity regimen with fludarabine (FLU) and 2 Gy total body irradiation (TBI) as a means of developing an improved HCT strategy for high-risk acute leukemia or MDS patients.

Methods

Patient and donor selection

Patients aged 18 years and older were eligible if they had advanced AML (beyond first remission, primary refractory, relapsed with >5% marrow blasts by morphology, or evolved from previous myeloproliferative neoplasm or MDS), MDS with >5% blasts in the marrow, or chronic myelomonocytic leukemia-2, and if they had an HLA-matched donor. Patients were excluded if they had evidence of major organ dysfunction, seropositivity for human immunodeficiency virus, allergies to mouse protein, or human antibody specific for mouse immunoglobulin (HAMA). All patients signed consent forms approved by the institutional review board of Fred Hutchinson Cancer Research Center. (NCI Clinical Trials Network registration: *clinicaltrials.gov identifier: NCT01300572*.)

Treatment plan

The patients received an infusion of 0.5 mg/kg ideal body

weight of anti-CD45 antibody (DOTA-BC8) trace-labeled with 5-10 mCi of the imaging radionuclide indium-111 (¹¹¹In), which provides gamma photons (0.171 and 0.245 MeV) for imaging (not provided by ⁹⁰Y), to evaluate the biodistribution of the anti-CD45 antibody and calculate the radiation-absorbed doses delivered to normal organs and the whole body, as described previously.² The subsequent therapy infusion of ⁹⁰Y-DOTA-BC8 was calculated to not exceed a maximum value dose to the critical normal organ. The therapy dose was administered on approximately day -12 of the preparative regimen. FLU 30 mg/kg/day was given intravenously (i.v.) on days -4 through -2, followed by TBI (2 Gy) and subsequent infusion of unmanipulated, G-CSF-mobilized peripheral blood stem cells on day 0. Mycophenolate mofetil and cyclosporine was given for graft-versus-host-disease (GvHD) prophylaxis.⁵

Dose-adjustment schema and statistical analysis

The primary objective of this study was to estimate the MTD of ⁹⁰Y-DOTA-BC8 used in combination with FLU/2-Gy TBI. The MTD was defined as the radiation dose to the normal organ associated with a dose-limiting toxicity (DLT) rate of 25% using Bearman criteria, developed specifically for HCT patients.⁶ A DLT was defined as a Bearman grade III or IV regimen-related toxicity occurring up to day 100 after HCT.⁶ A two-stage approach described by Storer *et al.* was planned for dose adjustment.⁷ In stage I, single patient cohorts were enrolled, and each successive patient received 2 Gy more radiation to the dose-limiting normal organ than the previous patient until the first DLT was observed. Dose escalation could proceed only if the patient receiving the previous dose was observed for at least 30 days after HCT; if not, the newly enrolled patient had to be treated at the same dose level as the previous patient. If a DLT was observed, stage II would be initiated at the next lower dose level, treating patients in cohorts of four patients each; this cohort size was dictated by the target DLT rate of 25%.

Secondary objectives included evaluation of potential efficacy in the context of a dose-finding study. Overall survival (OS) and relapse-free survival (RFS) were estimated according to the Kaplan-Meier method, and relapse and non-relapse mortality (NRM) were summarized using cumulative incidence estimates. NRM was considered a competing risk for relapse, and relapse was treated as a competing risk for NRM.

Results

Patients' characteristics

Sixteen patients with high-risk leukemia/MDS were enrolled to the study. One patient was withdrawn from the study due to HAMA seroconversion after receiving the ¹¹¹In-DOTA-BC8 test dose. Thus, fifteen patients, median age 62 years (range 37-76 years) years, were treated: ten patients had advanced AML and five had high-risk MDS. At the time of HCT, nine patients had refractory active diseases (pre-HCT marrow blast range 7-83.9%), while six had minimal residual disease documented by flow cytometry and cytogenetics (Table 1). Among the ten AML patients, three patients with *de novo* AML had relapsed disease and were refractory to a median of four lines of previous chemo-induction (range 3-6). Seven patients with secondary AML had received a median of three (range 1-6) induction chemotherapies prior to the HCT. Three of the 15 patients had failed previous allo-HCT. According to Southwest Oncology Group criteria,⁸ eight patients had high-risk/unfavorable cytogenetic

abnormalities, and the remaining seven patients had intermediate-risk cytogenetic abnormalities. The median HCT-comorbidity index of the 15 treated patients was three (range 0-7).

Three patients had HLA-matched related donors, and 12 had unrelated donors, of which ten were 10/10 HLA-matched, one was HLA-A antigen mismatched, and one had an allele mismatch at HLA-DQ.

The patients received an average of 78.6 mCi of ⁹⁰Y (range 22.8-151.2 mCi), with average delivered doses of 10.5 Gy to marrow, 70 Gy to spleen, and 17.9 Gy to liver through complete radionuclide decay. Although a maximum dose of 30 Gy was delivered to the liver, no DLT was observed; therefore, the MTD could not be estimated. Despite the lack of any DLT observed among the 15 patients treated, the BC8 antibody was not labeled with higher amounts of ⁹⁰Y that would deliver more than 30 Gy to any critical normal organ because of concerns of potential damage to the antibody avidity and function.

Dosimetry, biodistribution and engraftment

Since the biokinetics of ⁹⁰Y-labeled anti-CD45 antibody vary substantially from one patient to another, treatment planning based on individualized patient dosimetry enables a therapy that maximizes therapeutic efficacy without exceeding normal organ toxicity. The mean absorbed dose per unit administered activity (cGy/mCi ± standard deviation) for the 15 treated patients was: 15.25±7.05 to the bone marrow, 24.99 ± 6.76 to liver, 106.1 ± 33.19 to spleen, 8.14 ± 4.79 to kidney, 6.69 ± 19.5 to lung, and 2.16 ± 0.55 to the total body (Figure 1 and *Online Supplementary Table S1*). The calculated absorbed doses of ⁹⁰Y to liver, marrow and spleen are summarized in Table 2.

Median CD34⁺ cell dose of the 15 transplanted patients was 9.03 (range 2.14-15.86) x10⁶/kg. Median time to neutrophil engraftment [absolute neutrophil count (ANC) >0.5 x 10⁹/L for 3 consecutive days] was 15 (range 12-26) days. Median time to platelet engraftment (platelets >20 x10⁹/L for 7 consecutive days without transfusion support) was 16.5 (range 12-74) days. All patients engrafted with median donor-derived CD3 chimerisms of 99% and

CD33 chimerisms of 100% by day 28, with 100% median donor-derived CD3 and CD33 chimerisms for both by day 84 after HCT.

Table 1. Characteristics of 15 patients who received a therapeutic dose of ⁹⁰Y-DOTA-BC8.

Median age, [years (range)]	62 (37-76)
Sex	
Male	8
Female	7
Diagnosis at HCT	
AML, total n	10
Secondary AML, total n	7
Refractory disease	1
In CR1 with (+) MRD	4
In CR2 with (+) MRD	1
Rel 1	1
Primary AML, total n	3
Rel 1	1
Rel 2	2
MDS-RAEB, total n	4
Refractory disease	3
In CR1 with (+) MRD	1
Untreated CMML	1
History of previous allo-HCT	
Cytogenetic risk	
Intermediate	7
High/unfavorable	8
Donor status	
Related	3
Unrelated	12
Median n. pre-HCT induction chemotherapy [n, (range)]	
AML	
Secondary	3 (1-6)
Primary	4 (3-6)
MDS-RAEB	1 (1-2)
CMML	0

HCT: allogeneic hematopoietic cell transplantation; AML: acute myeloid leukemia; CR1: first complete remission; CR2: second CR; MRD: measurable residual disease; CR: complete remission; Rel: relapse; MDS-RAEB: myelodysplastic syndrome-refractory anemia with excess blasts; CMML: chronic myelomonocytic leukemia; n: number.

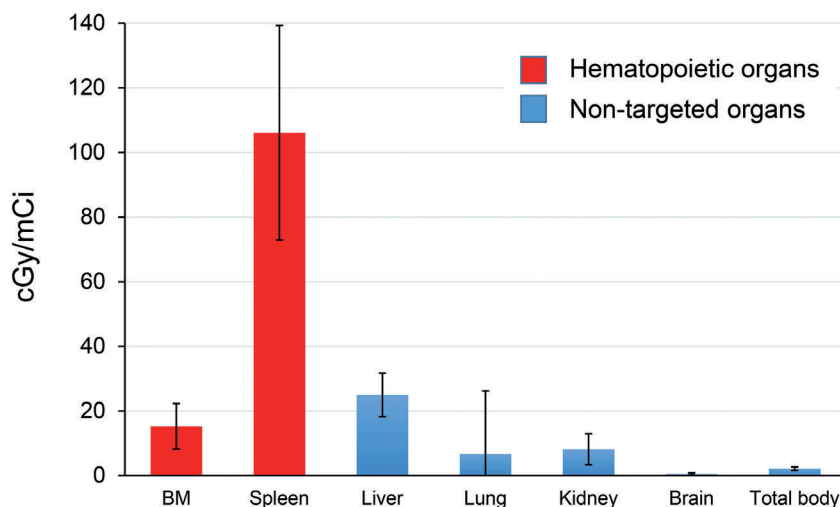


Figure 1. Estimated radiation absorbed doses per millicurie of ⁹⁰Y administered for 15 patients who received a therapeutic dose of ⁹⁰Y-DOTA-BC8.

Table 2. ⁹⁰Y activity administered and total radiation absorbed doses* to dose-limiting organ (liver), marrow, and spleen.

Dose level (targeted dose, † Gy)	Patient number	Therapy dose delivered, mCi (MBq)	Dose to liver, cGy	Dose to marrow, cGy	Dose to spleen, cGy
1 (6)	1	22.80 (843.60)	570	247.38	2508
2 (8)	2	27.06 (1001.22)	838.86	534.43	2814.24
3 (10)	3	30.30 (1121.10)	951.42	601.45	3120.9
4 (12)	4	45.50 (1683.50)	978.25	51.87	3676.4
5 (14)	5	38.40 (1420.80)	1413.12	1019.52	7219.2
6 (16)	6	53.70 (1986.90)	1594.89	622.92	0‡
6 (16)	7	65.10 (2408.70)	1660.05	823.51	6379.8
7 (18)	8	128.30 (4747.10)	1783.37	1321.49	6568.96
8 (20)	9	70.80 (2619.60)	1932.84	730.65	7929.6
9 (22)	10	141.20 (5224.40)	2230.96	3897.12	14402.4
10 (24)	11	112.40 (4158.80)	2326.68	1354.42	9891.2
10 (24)	12	151.20 (5594.40)	2358.72	1670.76	8542.8
11 (26)	13	81.50 (3015.50)	2583.55	1662.6	0‡
12 (28)	14	104.00 (3848.00)	2797.6	1632.8	12376
13 (30)	15	104.70 (3873.90)	2858.31	961.14	13506.3

*Among patients who received a therapeutic dose of ⁹⁰Y-DOTA-BC8. †Targeted radiation dose to normal organ receiving highest dose (liver). ‡Patients with splenectomy.

Toxicities and graft-versus-host disease

Despite premedication, grade 1-2 antibody-related infusion reactions (e.g. fever and chills) were observed in 6 of 15 patients; however, the reactions resolved by the end of each infusion. Notably, no grade 4 Common Toxicity Criteria Adverse Event (CTCAE) was observed. Ten (67%) patients experienced grade 3 non-hematologic events (Table 3). Hepatic veno-occlusive disease was not observed, despite delivering an average of 17.9 Gy to the liver. Ten patients (67%) developed grade II-IV acute GvHD (grade II: n=8; III: n=1; IV: n=1) (Table 4). Five patients (33%) developed chronic GvHD, most commonly involving skin and mouth.

Overall and relapse-free survival, non-relapse mortality, and relapse

Treatment led to complete remission in 13 patients (87%) based on a day-28 BM evaluation, whereas two patients had persistent disease documented by peripheral blood flow cytometry assessment on day 6 and day 20 after HCT (Table 5). Of note, the two patients with persistent disease had 83.9% and 70% marrow blasts before transplant, respectively. One of these two patients had also failed a previous allogeneic HCT. Among the 15 patients who received a therapy dose infusion of ⁹⁰Y-DOTA-BC8, eight patients are still alive with a median follow up of 1.8 (range 0.9-5.9) years. Estimated OS at one and two years were 66% (confidence interval, CI: 36-84) and 46% (CI: 17-71), respectively, with RFS estimated to be 46% (CI: 20-68) at each of these time points. The 1-year estimate of relapse was 41% (16-65%). Figure 2 summarizes the probabilities of OS, RFS, and relapse among all 15 patients. Six patients relapsed, five of whom subsequently died due to progression of disease. The median time to relapse among these six patients was 59 days (range 6-351 days). One patient died from grade IV steroid-refractory GvHD in remission at day 71, which resulted in a 6.6% day-100 NRM. One patient died also in remission from acute renal failure seven months after HCT while receiving foscarnet for cytomegalovirus reactivation.

Table 3. Grades 3 and 4 non-hematologic adverse events of the 15 patients who received a therapeutic dose of ⁹⁰Y-DOTA-BC8.

NCI CTCAE term	Grade 3	Grade 4
Febrile neutropenia	7	0
Infection	2	0
Blood bilirubin increased	2	0
Hyperglycemia	1	0
Rash	4	0
Skeletal muscular pain	4	0
Hypoxia	1	0
Atrial fibrillation	1	0
Nausea/vomiting	3	0
Diarrhea	2	0
Hematoma	1	0
Mucositis	1	0
Hematoma	1	0
Edema	1	0

NCI CTCAE: National Cancer Institute Common Terminology Criteria for Adverse Events, version 4.0.

Discussion

Although allogeneic HCT is an important and frequently used treatment for advanced AML and high-risk MDS, many patients have recurrent disease.^{9,10} In a randomized study of patients with AML in first complete remission, the relapse rate was 12% after 15.75 Gy TBI, compared with 35% after 12 Gy TBI.¹¹ Although this study showed improved leukemia control with escalated doses of TBI, the higher doses of TBI were associated with increased NRM, resulting in no improvement in survival. The finding also confirmed that the high-dose TBI preparative regimens were at the limit of normal organ tolerance.

The results reported from studies that used reduced-intensity conditioning suggest that a graft-versus-malignancy

nancy effect is most effective in patients with a low burden of malignant cells.^{1,12,13} In a study of 274 patients who had allogeneic HCT after non-myeloablative conditioning using FLU and 2 Gy TBI for the treatment of AML, patients in first and second complete remission had better 5-year survival rates than patients with more advanced disease (37% and 34% vs. 18%, respectively). Most treatment failures were caused by recurrent AML.¹⁴ These data suggest that a graft-versus-leukemia effect alone may be inadequate for patients with AML/MDS in relapse or with refractory disease, whereas additional targeted antileukemic therapy may be beneficial. Our group previously explored the safety and feasibility of ¹³¹I-BC8 antibody to deliver targeted radiation to malignant cells in the marrow and spleen, and combined this approach with the non-myeloablative conditioning regimen of 2 Gy TBI and FLU in patients with advanced myeloid malignancies.^{2,15}

While results were encouraging, one major limitation of this approach was the medium energy gamma component of ¹³¹I and 8-day physical half-life that required patients to be treated in radiation isolation due to the exposure risk for staff and family. ⁹⁰Y was selected as the therapeutic radionuclide for this current clinical trial because it is a pure β-emitter that is available in high specific activity and purity. Moreover, the β particles from ⁹⁰Y have a high energy (E_{max} = 2.28 MeV) with greater tissue penetrating range (up to 11 mm) than β particles from ¹³¹I, characteristics that may be more favorable for therapy of large tumor masses.⁴ Finally, replacement of ¹³¹I with ⁹⁰Y may be more feasible for studies at additional centers.

As a phase I dose-finding trial, the current study was not designed to determine the efficacy of the conditioning regimen of ⁹⁰Y-DOTA-BC8 combined with FLU/TBI. However, the experience reported in this dose-escalation study suggests that the delivery of supplemental doses of ⁹⁰Y-DOTA-BC8 could improve 2-year OS and RFS of very high-risk AML/MDS patients to 46% and 46%, respectively, compared with patients who received HCT with the use of the FLU/TBI conditioning regimen alone.^{1,3,14} Although the estimated probability of relapse at one year remains high at 41%, these results are encouraging, considering that all of the patients in our study had either active AML/MDS or measurable residual disease (MRD) prior to the beginning of the conditioning regimen. Patients with detectable disease have historically dismal

Table 4. Acute graft-versus-host disease overall grading with organ staging of the 15 patients.

Grade/stage	Overall (n)	Gut (n)	Liver (n)	Skin (n)
I/1	1	9	2	1
II/2	8	0	0	2
III/3	1	0	1	4
IV/4	1	1	0	0

Table 5. Outcomes of the 15 patients who received a therapeutic dose of ⁹⁰Y-DOTA-BC8.

Pt n.	Age/Gender	Diagnosis at HCT	Disease status at transplant	Pre-HCT BM/PB blast (%)	Cytogenetic risk*	CR [†] Achievement post HCT	Donor status	Grade acute GvHD	Current status, days after HCT
1	51/M	Relapsed secondary AML	Active disease	83.9/0	high	No	URD	0	Persistent disease; died day 23
2	69/M	Refractory secondary AML	MRD (+)	0/0 [‡]	high	Yes	URD [§]	2	Alive and in CR: 2137 d
3	74/M	MDS-RAEB	MRD (+)	1.4/0	Int.	Yes	URD	0	Died day 218 due to renal failure (in CR)
4	76/M	MDS-RAEB	Active disease	13.6/0	Int.	Yes	URD	4	Died day 80 due to steroid refractory aGvHD (in CR)
5	52/F	Refractory secondary AML	MRD (+)	3.5/0	Int.	Yes	URD	2	Died day 694 due to relapse
6	65/M	Refractory secondary AML	MRD (+)	0.22/1.1	Int.	Yes	URD	2	Alive and in CR: 1234 d
7	48/F	Relapsed secondary AML	MRD (+)	0.17/0	high	Yes, with MRD	URD	2	Died day 395 due to relapse
8	60/M	Refractory secondary AML	Active disease	17.6/3.6	high	Yes	URD	0	Alive and in CR: 767 d
9	56/F	Relapse/refractory AML	Active disease	31.6/0	Int.	Yes	URD	2	Alive and in CR: 727 d
10	37/F	Relapse/refractory AML	Active disease	70.0/0	Int.	No	URD	3	Persistent disease; died day 109
11	71/M	MDS-RAEB	Active disease	7.0/0	high	Yes, with MRD	RD	0	Alive, on azacytidine, achieved CR with MRD (-): 583 d
12	72/M	Secondary AML	MRD (+)	2.5/1.5	high	Yes	URD	2	Died day 318 due to relapse
13	65/F	Untreated CMML	Active disease	0.89/0	Int.	Yes	RD	2	Alive: relapsed on day 351. Currently on azacytidine and now CR with MRD (-)
14	62/F	MDS-RAEB	Active disease	11.4/0.38	high	Yes	RD	1	Alive and in CR: 394 d
15	37/F	Relapse/refractory AML	Active disease	43.0/4.0	high	Yes, with MRD	URD	2	Alive and in CR with MRD (+): 316 d

BM: bone marrow; CMML: chronic myelomonocytic leukemia; CR: complete remission; F: female; Int.: intermediate; M: male; MDS-RAEB: myelodysplastic syndrome-refractory anemia with excess blast; MRD: measurable residual disease; PB: peripheral blood; RD: HLA-matched related donor; URD: unrelated donor. *According to Southwest Oncology Group criteria.⁸ [†]Protocol-defined CR as bone marrow with blasts <5% by morphology with blood count recovery. [‡]MRD by cytogenetics. [§]Patient had a DQ allele mismatch unrelated donor. ^{||}Patient had an HLA-A antigen mismatch unrelated donor.

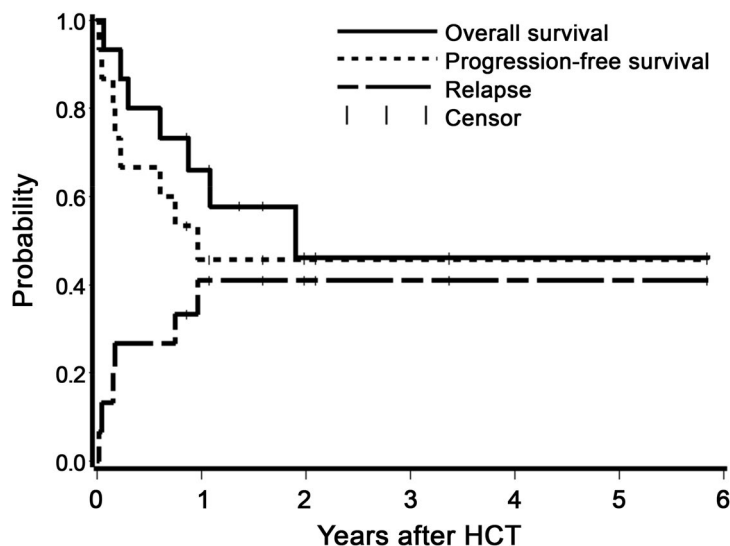


Figure 2. Estimates of the probability of overall survival, relapse-free survival, and relapse among all patients who received a therapeutic dose of ^{90}Y -DOTA-BC8 followed by total body irradiation/fludarabine. HCT: allogeneic hematopoietic cell transplantation.

outcomes even with myeloablative HCT, with 3-year estimates of relapse of 65%.^{3,16} Our study establishes proof of principle that radioimmunoconjugates can deliver supplemental doses of radiation to sites of leukemic involvement and have the potential to improve the cure rate by decreasing the risk of relapse in these high-risk patients.

More importantly, the results presented here show the feasibility of using ^{90}Y -DOTA-BC8 combined with reduced-intensity allogeneic HCT for patients with high-risk MDS and AML. Engraftment was not delayed after delivery of ^{90}Y -DOTA-BC8, and infusion-related toxicities were mild and manageable. Intensified conditioning with ^{90}Y -DOTA-BC8 resulted in few toxicities beyond those expected with FLU and TBI alone with no grade 4 adverse events reported. Most commonly seen grade 3 adverse events were neutropenic fever with or without identified sources of infection and constitutional symptoms. There was one case of NRM in the first 100 days after transplantation that was not attributed to the investigational therapy among the 15 patients treated. Taken altogether, these findings suggest that this transplantation-conditioning strategy has acceptable toxicity profiles while complementing the efficacy of reduced-intensity conditioning, and demonstrates the potential exportability of this approach to other patient populations with hematologic malignancies.

The overall incidence of grades II to IV acute GvHD in this study was 67%. This incidence is similar to that seen with FLU or TBI alone at our center.¹⁷ The incidence of chronic GvHD (33%) in the current study is comparable to that among patients who received reduced intensity conditioning without targeted radiotherapy, suggesting that the radiolabeled antibody has no demonstrative effect on the risk of chronic GvHD.^{18,19}

Although we previously estimated an MTD of 24 Gy in our study using ^{131}I -BC8,² no grade III or IV DLT were observed when the same antibody was conjugated to ^{90}Y , despite targeted doses of up to 30 Gy to the liver (median dose 19 Gy), suggesting that higher doses of radiation may be tolerated in the marrow or spleen. Nonetheless, theoretical concerns persist about both the short- and long-term consequences of ^{90}Y at higher doses due to its long path-

length. After treating these 15 patients, grant funding was exhausted, and in seeking renewed funding, we chose instead to pursue α emitters for two reasons. First, given the lack of DLT even after reaching 30 Gy to liver, it seemed unlikely that we would be able to load enough ^{90}Y onto the amount of antibody that provides optimal biodistribution without damaging the antibody itself.²⁰ Secondly, α -emitting radionuclides have a higher linear energy transfer that is coupled with a short path length capable of killing the target cells with only a few cell traversals, thereby potentially providing even greater specificity at high radiation doses.²¹ Ongoing studies are evaluating the use of an α emitter, astatine-211, conjugated to anti-CD45 antibody BC8 as part of an HCT conditioning regimen for patients with advanced leukemia or high-risk MDS.

In summary, the delivery of supplemental radiation to bone marrow and spleen by ^{90}Y -DOTA-BC8 was well tolerated when combined with FLU/TBI in patients undergoing HCT for advanced AML and high-risk MDS who were not candidates for myeloablative HCT. The encouraging results from this study support more clinical trials using radioimmunotherapy as part of the conditioning regimen for allo-HCT. The antileukemic potential of this approach, combined with the promise of reduced toxicity, may improve outcomes after allogeneic HCT for patients with advanced hematologic malignancies.

Acknowledgments

The authors thank the patients who participated in the clinical trial. They also thank their colleagues in the transplant services, the research staff, and clinical staff. We greatly appreciate Monina Almeda's assistance in data management and regulatory support, and Helen Crawford's assistance with manuscript preparation.

Funding

Research funding was provided by the National Institutes of Health, Bethesda, MD, grants, P01 CA044991, P01 CA078902, and P30 CA015704 from the National Cancer Institute. The content is solely the responsibility of the authors and does not necessarily represent the official views of the National Institutes of Health nor its subsidiary Institutes and Centers.

References

- Kahl C, Storer BE, Sandmaier BM, et al. Relapse risk among patients with malignant diseases given allogeneic hematopoietic cell transplantation after nonmyeloablative conditioning. *Blood*. 2007;110(7):2744-2748.
- Pagel JM, Gooley TA, Rajendran J, et al. Allogeneic hematopoietic cell transplantation after conditioning with 131I-anti-CD45 antibody plus fludarabine and low-dose total body irradiation for elderly patients with advanced acute myeloid leukemia or high-risk myelodysplastic syndrome. *Blood*. 2009;114(27):5444-5453.
- Araki D, Wood BL, Othus M, et al. Allogeneic hematopoietic cell transplantation for acute myeloid leukemia: Time to move toward a minimal residual disease-based definition of complete remission? *J Clin Oncol*. 2016;34(4):329-336.
- O'Donoghue JA. Optimal therapeutic strategies for radioimmunotherapy. *Recent Results Cancer Res*. 1996;141:77-99.
- McSweeney PA, Niederwieser D, Shizuru JA, et al. Hematopoietic cell transplantation in older patients with hematologic malignancies: replacing high-dose cytotoxic therapy with graft-versus-tumor effects. *Blood*. 2001;97(11):3390-3400.
- Bearman SI, Appelbaum FR, Buckner CD, et al. Regimen-related toxicity in patients undergoing bone marrow transplantation. *J Clin Oncol*. 1988;6(10):1562-1568.
- Storer BE. Small-sample confidence sets for the MTD in a phase I clinical trial. *Biometrics*. 1993;49(4):1117-1125.
- Slovak ML, Kopecky KJ, Cassileth PA, et al. Karyotypic analysis predicts outcome of preremission and postremission therapy in adult acute myeloid leukemia: a Southwest Oncology Group/Eastern Cooperative Oncology Group study. *Blood*. 2000;96(13):4075-4083.
- Sierra J, Storer B, Hansen JA, et al. Transplantation of marrow cells from unrelated donors for treatment of high-risk acute leukemia: the effect of leukemic burden, donor HLA-matching, and marrow cell dose. *Blood*. 1997;89(11):4226-4235.
- Miller CB, Zehnbauser BA, Piantadosi S, Rowley SD, Jones RJ. Correlation of occult clonogenic leukemia drug sensitivity with relapse after autologous bone marrow transplantation. *Blood*. 1991;78(4):1125-1131.
- Clift RA, Buckner CD, Appelbaum FR, et al. Allogeneic marrow transplantation in patients with acute myeloid leukemia in first remission: A randomized trial of two irradiation regimens. *Blood*. 1990;76(9):1867-1871.
- Laport GG, Sandmaier BM, Storer BE, et al. Reduced-intensity conditioning followed by allogeneic hematopoietic cell transplantation for adult patients with myelodysplastic syndrome and myeloproliferative disorders. *Biol Blood Marrow Transplant*. 2008;14(2):246-255.
- Sorrer ML, Storer BE, Sandmaier BM, et al. Five-year follow-up of patients with advanced chronic lymphocytic leukemia treated with allogeneic hematopoietic cell transplantation after nonmyeloablative conditioning. *J Clin Oncol*. 2008;26(30):4912-4920.
- Gyurkocza B, Storb R, Storer BE, et al. Nonmyeloablative allogeneic hematopoietic cell transplantation in patients with acute myeloid leukemia. *J Clin Oncol*. 2010;28(17):2859-2867.
- Mawad R, Gooley TA, Rajendran JG, et al. Radiolabeled anti-CD45 antibody with reduced-intensity conditioning and allogeneic transplantation for younger patients with advanced acute myeloid leukemia or myelodysplastic syndrome. *Biol Blood Marrow Transplant*. 2014;20(9):1363-1368.
- Walter RB, Gyurkocza B, Storer BE, et al. Comparison of minimal residual disease as outcome predictor for AML patients in first complete remission undergoing myeloablative or nonmyeloablative allogeneic hematopoietic cell transplantation. *Leukemia*. 2015;29(1):137-144.
- Mielcarek M, Burroughs L, Leisenring W, et al. Prognostic relevance of early-onset graft-versus-host disease following nonmyeloablative hematopoietic cell transplantation. *Br J Haematol*. 2005;129(3):381-391.
- Wong R, Giralt SA, Martin T, et al. Reduced-intensity conditioning for unrelated donor hematopoietic stem cell transplantation as treatment for myeloid malignancies in patients older than 55 years. *Blood*. 2003;102(8):3052-3059.
- Kroger N, Bornhauser M, Ehninger G, et al. Allogeneic stem cell transplantation after a fludarabine/busulfan-based reduced-intensity conditioning in patients with myelodysplastic syndrome or secondary acute myeloid leukemia. *Ann Hematol*. 2003;82(6):336-342.
- Salako QA, O'Donnell RT, DeNardo SJ. Effects of radiolysis on yttrium-90-labeled Lym-1 antibody preparations. *J Nucl Med*. 1998;39(4):667-670.
- Hall EJ, Giaccia AJ. *Radiobiology for the radiologist*. 6th ed. Philadelphia: Lippincott Williams & Wilkins, 2006.



Ferrata Storti Foundation

Genetic platelet depletion is superior in platelet transfusion compared to current models

Manuel Salzmann,¹ Waltraud C. Schrottmaier,¹ Julia B. Kral-Pointner,¹ Marion Mussbacher,¹ Julia Volz,³ Bastian Hoesel,¹ Bernhard Moser,¹ Sonja Bleichert,^{1,2} Susanne Morava,¹ Bernhard Nieswandt,³ Johannes A. Schmid¹ and Alice Assinger¹

¹Institute of Vascular Biology and Thrombosis Research, Medical University of Vienna, Vienna, Austria, ²Department of Surgery, General Hospital, Medical University Vienna, Vienna, Austria and ³Institute of Experimental Biomedicine, University Hospital and Rudolf Virchow Center, University of Würzburg, Würzburg, Germany

Haematologica 2020
Volume 105(6):1738-1749

ABSTRACT

Genetically modified mice have advanced our knowledge on platelets in hemostasis and beyond tremendously. However, mouse models harbor certain limitations, including availability of platelet specific transgenic strains, and off-target effects on other cell types. Transfusion of genetically modified platelets into thrombocytopenic mice circumvents these problems. Additionally, *ex vivo* treatment of platelets prior to transfusion eliminates putative side effects on other cell types. Thrombocytopenia is commonly induced by administration of anti-platelet antibodies, which opsonize platelets to cause rapid clearance. However, antibodies do not differentiate between endogenous or exogenous platelets, impeding transfusion efficacy. In contrast, genetic depletion with the inducible diphtheria toxin receptor (iDTR) system induces thrombocytopenia *via* megakaryocyte ablation without direct effects on circulating platelets. We compared the iDTR system with antibody-based depletion methods regarding their utility in platelet transfusion experiments, outlining advantages and disadvantages of both approaches. Antibodies led to thrombocytopenia within two hours and allowed the dose-dependent adjustment of the platelet count. The iDTR model caused complete thrombocytopenia within four days, which could be sustained for up to 11 days. Neither platelet depletion approach caused platelet activation. Only the iDTR model allowed efficient platelet transfusion by keeping endogenous platelet levels low and maintaining exogenous platelet levels over longer time periods, thus providing clear advantages over antibody-based methods. Transfused platelets were fully functional *in vivo*, and our model allowed examination of transgenic platelets. Using donor platelets from already available genetically modified mice or *ex vivo* treated platelets, may decrease the necessity of platelet-specific mouse strains, diminishing off-target effects and thereby reducing animal numbers.

Correspondence:

ALICE ASSINGER
alice.assinger@meduniwien.ac.at

Received: March 19, 2019.

Accepted: September 19, 2019.

Pre-published: September 19, 2019.

doi:10.3324/haematol.2019.222448

Check the online version for the most updated information on this article, online supplements, and information on authorship & disclosures: www.haematologica.org/content/105/6/1738

©2020 Ferrata Storti Foundation

Material published in *Haematologica* is covered by copyright. All rights are reserved to the Ferrata Storti Foundation. Use of published material is allowed under the following terms and conditions:

<https://creativecommons.org/licenses/by-nc/4.0/legalcode>.

Copies of published material are allowed for personal or internal use. Sharing published material for non-commercial purposes is subject to the following conditions:

<https://creativecommons.org/licenses/by-nc/4.0/legalcode>,

sect. 3. Reproducing and sharing published material for commercial purposes is not allowed without permission in writing from the publisher.



Introduction

Platelets are anucleate cells, which derive from bone marrow megakaryocytes. Beyond their central role in hemostasis, platelets fulfill important functions in inflammation and infection,¹ atherogenesis² and tissue regeneration.³ Genetically modified mice are valuable tools to investigate the role of platelet function in hemostasis and beyond in complex *in vivo* systems. However, ascertaining the specific contribution of platelets in global knockout mice can be challenging. Usage of the tissue-specific Cre/loxP system is one possibility to circumvent this problem and enables the investigation of a genetic modification in selected cell types. Mouse lines expressing Cre recombinase *via* the platelet- and megakaryocyte-specific platelet factor 4 (PF4)⁴ or the glycoprotein (GP) 1b α promoters⁵ are essential to delineate distinct platelet mediated effects in complex physiological and pathophysiological settings. However, crossing of mice is expensive and time-consuming

and loxP flanked genes of interest are not available in all cases.

An alternative to overcome these limitations is transfusion of genetically or pharmacologically modified platelets into platelet depleted mice. This allows research of altered platelets in a genetically unchanged environment. Additionally, platelets can be treated *ex vivo* before transfusion, eliminating putative side effects of the treatment on other cell types. Platelet depletion prior to platelet transfusion is frequently performed by administration of antibodies targeting platelet-specific epitopes although this harbors certain inherent limitations: Platelets are opsonized by antibodies and actively scavenged from the circulation. This could lead to immune reactions or activation of opsonized and agglomerated platelets. Most importantly though, antibody binding does not differ between endogenous and transfused platelets, which either negates transfusion or demands repeated cycles of depletion and transfusion, to maintain a stable population of exogenous platelets.

A solution to this limitation is provided by a novel model, in which an inducible diphtheria toxin (DT) receptor (iDTR) is expressed under the control of a platelet-specific PF4 Cre recombinase, rendering megakaryocytes susceptible to DT-induced termination of protein synthesis.⁶⁷ A single DT molecule in the cytoplasm is sufficient to kill an iDTR-expressing cell,⁸ whereas wild-type (WT) murine cells are highly insensitive towards DT,⁹ making megakaryocyte ablation exceptionally specific and efficient.

Here, we aimed to validate the platelet iDTR model and compared it with antibody-mediated platelet depletion methods regarding its use in platelet transfusion experiments. We show for the first time that the iDTR model can be successfully used in platelet transfusion and that it provides several advantages over antibody-mediated depletion by simplifying the experimental setup and refining platelet transfusion. Additionally, the iDTR model may help to avoid time consuming generation of tissue-specific mice and allows analysis of platelet-specific functions, in cases where only a full knockout of the gene of interest is available.

Methods

Detailed methods regarding genotyping, platelet function assays, and *in vivo* experiments can be found in the *Online Supplementary Materials and Methods*.

Mice

All experiments and animal studies were conducted according to institutional guidelines and were approved by the Animal Care and Use Committee of the Medical University of Vienna (BMWF-66.009/0246-WF/V/3b/2016).

All experimental procedures were conducted according to the SYRCLC's risk of bias tool for animal studies; *e.g.* groups were age matched littermates, and after initial scouting experiments, only female mice were used in all studies, to minimize a risk of bias; animals within the same cage were preferably taken into the same experiment; cages of iDTR^{Pit} mice were randomly selected for experiments; blinding was not applicable.

Platelet depletion

Megakaryocyte and consequently platelet depletion were

induced in iDTR^{Pit} mice by subcutaneous injections of 100 ng DT on days 0, 2 and 4, followed by 250 ng on days 7, 9 and 11. To prevent hematoma and scarring, mice were anesthetized with isoflurane (Abbot Laboratories) for subcutaneous injections after day 7. WT mice were platelet depleted by intravenous administration of 4 µg/g anti-mouse GPIbα (R300, Emfret Analytics), 0.2 µg/g anti-mouse platelet monoclonal antibody 6A6-IgG2A (originating from Dr R. Good, University of South Florida College of Medicine, Tampa, FL, USA) or intraperitoneal injection of 15 µL rabbit anti-mouse thrombocyte serum (AIA31440, Accurate Chemical & Scientific Corporation).

Platelet transfusion

DT treatment was started at day 7 and R300 treatment 12 hours prior to transfusion. Recipients were injected with 4.3x10⁸ washed platelets from WT or naïve male iDTR^{Pit} mice, labeled with anti GPIIb/IIIa DyLight649 (X649, Emfret Analytics) and blood samples were collected after 2, 14, 48 and 72 hours. Blood was labeled with anti-CD41-BV421 and analyzed using a CytoflexS flow cytometer with Cytexpert 2.2 software. Exogenous platelets were defined as CD41⁺ X649⁺ events, whereas endogenous platelets were CD41⁺ X649⁻.

Statistics

Calculations were performed using GraphPad Prism 8.02 software. Statistical significances are depicted as: **P*≤0.05, ***P*≤0.01, ****P*≤0.001, *****P*≤0.0001.

Comparison of two groups was done by unpaired t-test or Mann-Whitney test if data was not distributed normally. Two or more groups were compared to the respective control group using One-Way ANOVA with Dunnett correction. If all groups were compared with each other, Tukey correction was applied. Two groups with more than one condition were compared by Two-Way ANOVA and Sidak correction. For Figure 1D-E, H-I and Figure 4B-E individual area under the curves (AUC) were calculated and groups compared to the respective control using One-Way ANOVA with Dunnett correction.

Results

Selective killing of megakaryocytes leads to rapid platelet depletion

To selectively ablate megakaryocytes and induce thrombocytopenia, we crossed mice expressing iDTR downstream of a loxP-flanked stop cassette with a PF4 iCre strain to generate mice with megakaryocytes expressing iDTR (iDTR^{Pit}) (Figure 1A). Naïve iDTR^{Pit} mice did not show any obvious alterations in bone marrow or megakaryocyte morphology (*Online Supplementary Figure S1A*), nor was the megakaryocyte count affected (*Online Supplementary Figure S1B*). For platelet depletion, we administered DT in a weekly routine with 100 ng being injected subcutaneously on days 0, 2 and 4. The dosage was increased at day 7 to 250 ng to avoid rebound effects and maintain efficient thrombocytopenia (Figure 1B), as megakaryocyte count return to basal levels within two days after last 100 ng injection (*Online Supplementary Figure S1C*). As controls we injected PBS into iDTR^{Pit} mice and DT into WT mice. Megakaryocytes were already remarkably depleted on day 2 (*Online Supplementary Figure S1D*) and undetectable from day 4 till day 7 (Figure 1C). Platelet count decreased over time in DT-treated iDTR^{Pit} mice, reaching a nadir with day 4, and remained low until day 12 (Figure 1D). Platelet counts of control groups remained unaffected. In parallel, mean platelet size increased in the

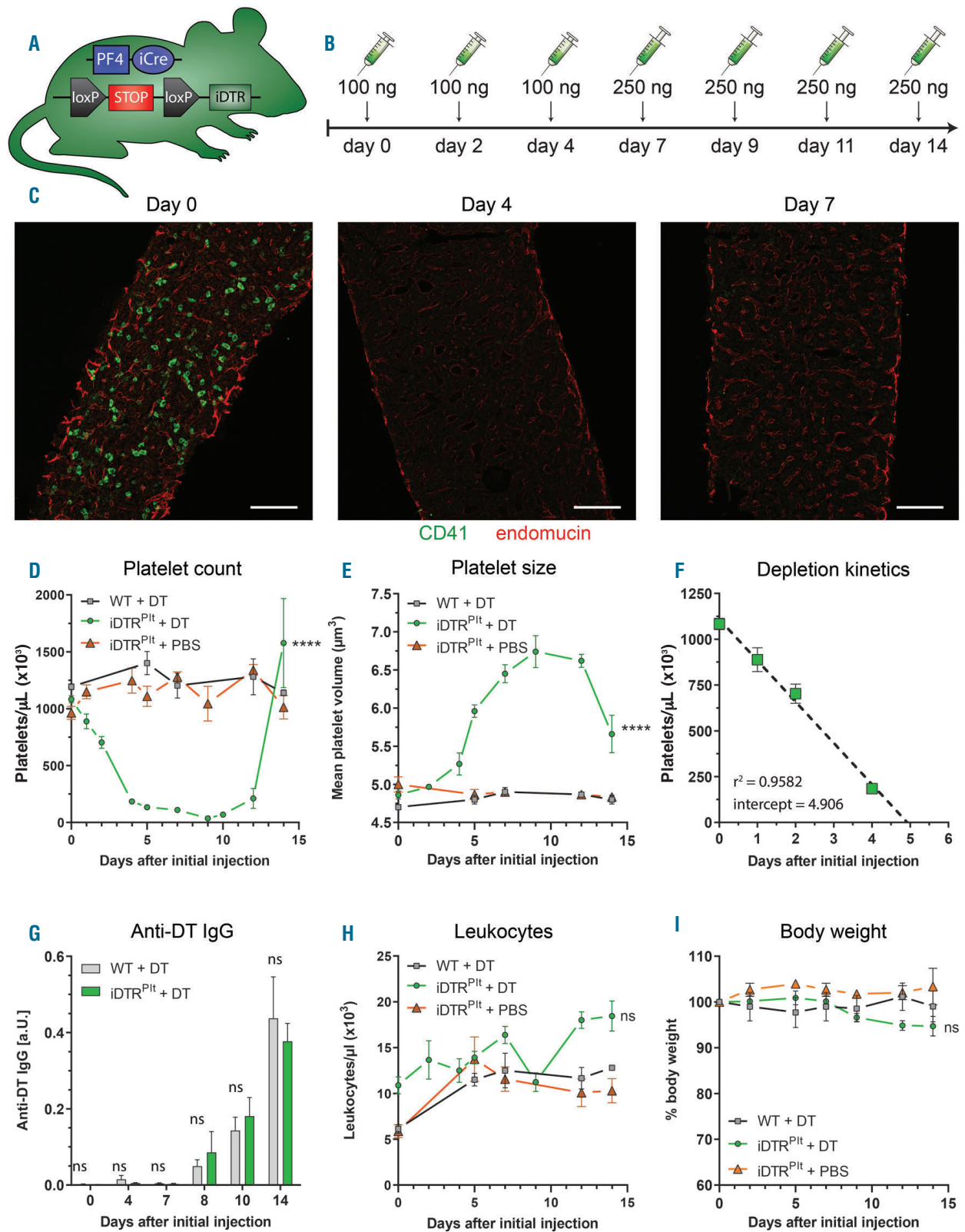


Figure 1. Depletion of megakaryocytes and platelets with diphtheria toxin. (A) Genetic scheme of PF4-iCre iDTR mice, termed iDTR^{Pit} mice. (B) Graphical overview of diphtheria toxin (DT) administration scheme. (C) Femora of untreated and mice treated for four and seven days with DT. Bone marrow was stained for endothelial cells (endomucin, red) and megakaryocytes (CD41, green). Scale bar: 200 μm . (D) Platelet counts and (E) mean platelet volume after indicated days of DT treatment. (F) Linear regression of decrease in platelet counts of iDTR^{Pit} mice within first four days of DT treatment. 95% confidence interval of X-intercept: 4.563-5.318. (D-F) Curves of groups were compared to that of iDTR^{Pit} + DT (n=3-8). (G) Titer of anti-DT IgG after indicated times of treatment, normalized to a DT-boosted mouse (n=4-17). (H) Leukocyte counts and (I) body weight after indicated days of DT treatment. (H-I) Curves of groups were compared to that of iDTR^{Pit} + DT (n=3-8).

remaining platelet population during DT treatment (Figure 1E). Notably, linear regression of platelet counts until day 4 revealed that their decrease corresponded to their reported lifespan (Figure 1F) of 4.8 days.¹⁰ Platelets were therefore not directly affected by DT treatment and thrombocytopenia was induced by megakaryocyte depletion rather than platelet ablation. Examining a putative immune response against DT, we quantified DT-specific immunoglobulin G (IgG) generated during treatment. Antibodies were detectable from day 8 onwards, with no significant difference between iDTR^{Pit} and WT mice, indicating that presence of iDTR on platelets did not alter the adaptive immune response (Figure 1G). Furthermore, leukocyte count remained unaffected in thrombocytopenic iDTR^{Pit} mice (Figure 1H). Upon prolonged platelet depletion mice displayed an increased burden of hematoma and impaired wound healing, with body weight being slightly, but not significantly decreased (Figure 1I). We also observed that male mice fared worse than females (*data not shown*). Therefore, only female mice were used in further experiments.

Presence of iDTR does not affect platelet function

To monitor potential off-target effects of iDTR expression on platelet physiology, we performed blood counts as well as platelet function assays. Untreated iDTR^{Pit} mice

displayed normal blood cell counts with no significant differences in platelet, leukocyte and erythrocyte numbers compared to WT mice (Figure 2A-C) although mean platelet volume (MPV) was slightly increased (Figure 2D). However, this did neither affect the hemostatic platelet function, nor the interaction with leukocytes. Light transmission aggregometry revealed no alterations in aggregation upon stimulation with thrombin or collagen I (Figure 2E-F and Figure 3D). Further, platelet activation was evaluated by stimulating the major platelet activation receptors PAR4 with PAR4-activating peptide (PAR4-AP), GPVI with convulxin (CVX), and P2Y_{1/12} with ADP (Figure 3A). Expression of iDTR on platelets did not affect surface expression of the degranulation marker P-selectin (CD62P) when compared to WT littermate controls (Figures 3B), nor did it influence activation of GPIIb/IIIa (Figure 3C). As an example for non-classical functions of platelets, we evaluated their ability to form aggregates with monocytes and neutrophils which was also unaltered by iDTR expression (Figure 3E-H). These data indicate that physiological platelet function is preserved in naive iDTR^{Pit} mice.

Comparison of platelet depletion strategies

Next, we compared the iDTR model with antibody-based depletion methods in terms of platelet activation. Blood samples were taken prior to platelet depletion

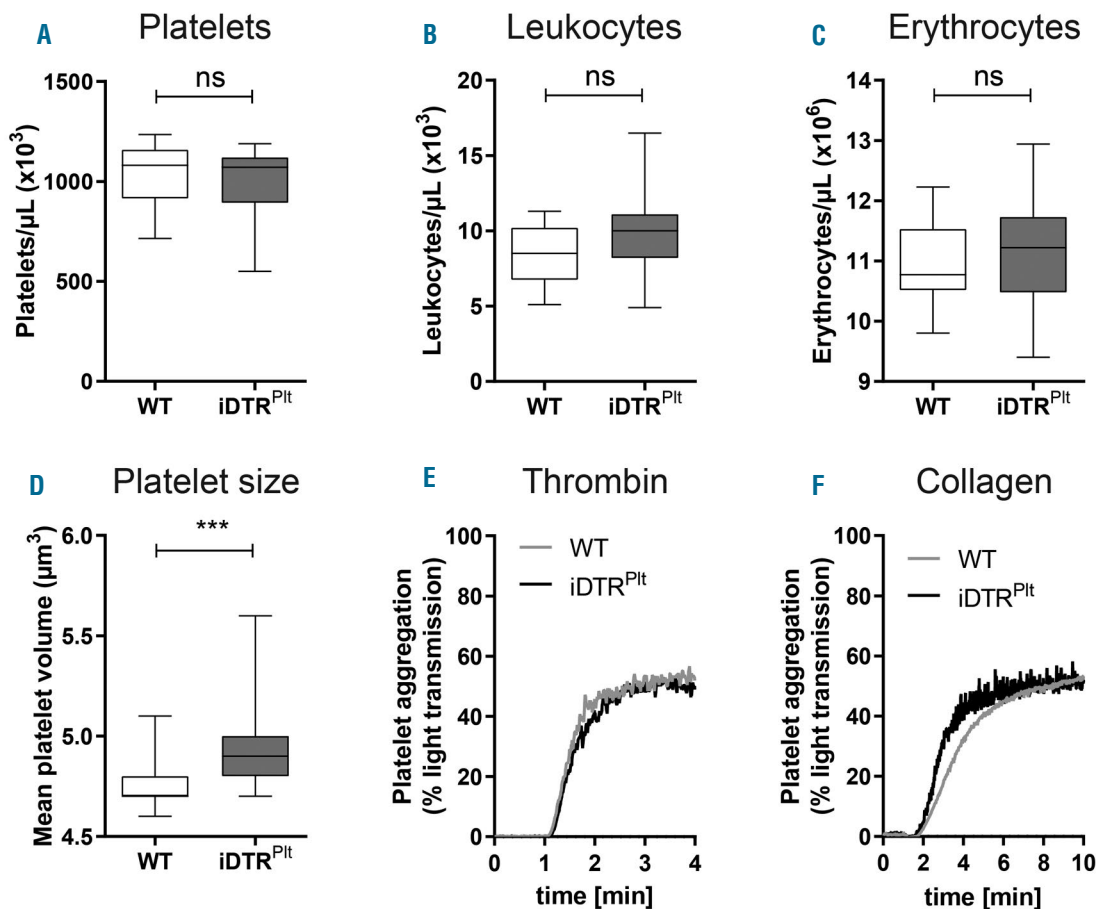


Figure 2. iDTR expression does not alter blood counts or platelet aggregation. Comparison of blood count: (A) platelets, (B) leukocytes, (C) erythrocytes and (D) mean platelet volume ($n=13-14$). Representative aggregation curves of washed platelets stimulated with thrombin (E) or (F) collagen I.

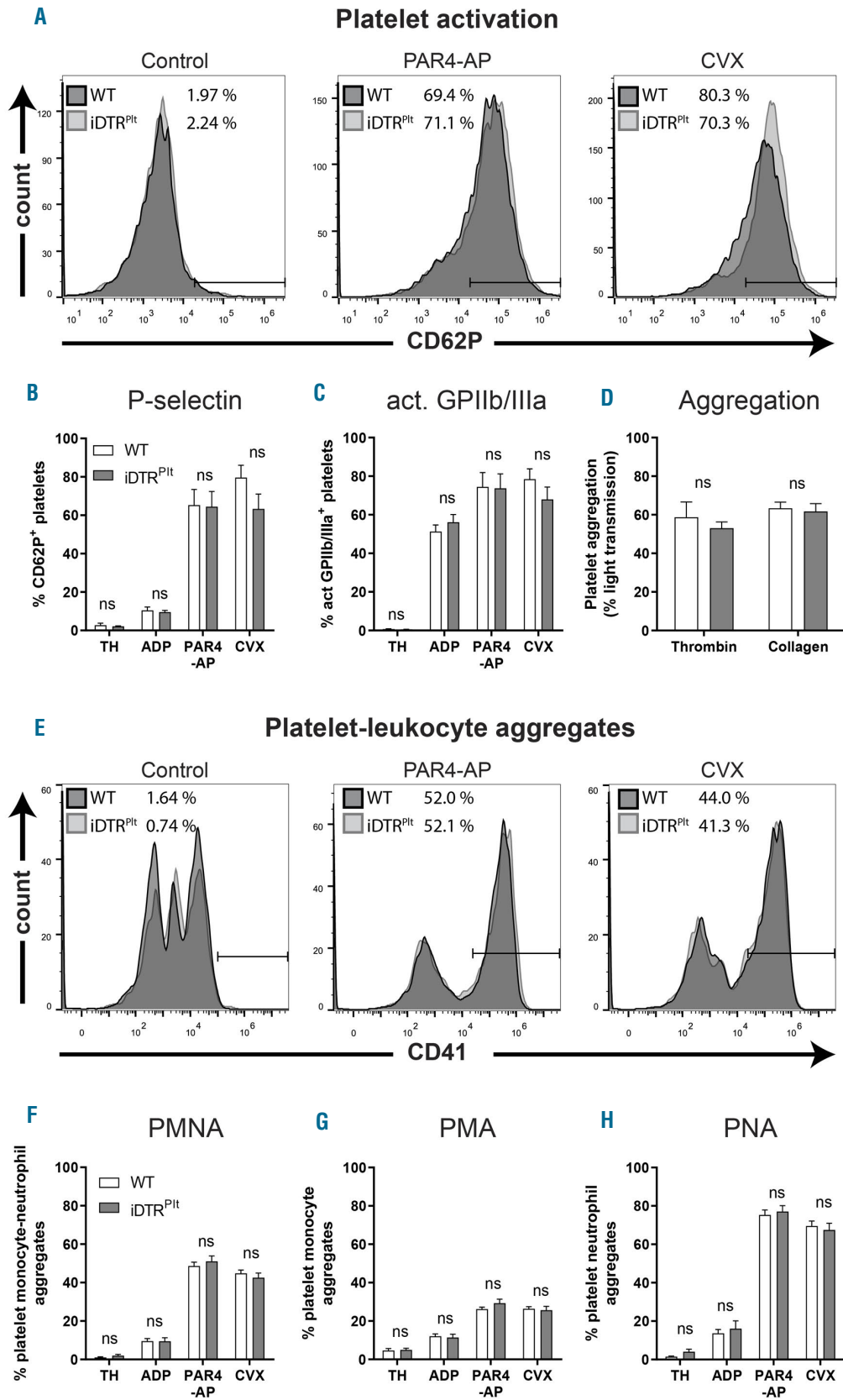


Figure 3. Expression of iDTR does not change platelet function. (A) Representative histograms showing CD62P expression of CD41⁺ cells in diluted whole blood, stimulated with PAR4 agonist peptide (PAR4-AP), or convulxin (CVX), or treated with Tyrode's HEPES buffer (TH). (B) Percentage CD62P⁺ and (C) activated GPIIb/IIIa⁺ of CD41⁺ events in diluted whole blood, stimulated with ADP, PAR4-AP or CVX (n=7-8). (D) Light transmission aggregometry of washed platelets stimulated with thrombin or collagen I (n=3-5). (E) Representative histograms of CD41 expression of CD11b⁺, CD45⁺ events in blood, stimulated with PAR4-AP or CVX. (F) Percentage CD41⁺ of CD11b⁺, CD45⁺ events in whole blood, stimulated with ADP, PAR4-AP or CVX. (G) Sub classification into CD41⁺ side scatter medium monocytes and (H) side scatter high neutrophils (n=8).

induction and two days or two hours after the first DT or antibody/rabbit anti-mouse thrombocyte serum treatment, respectively. Additionally, platelet activation was assayed at time points of stable platelet depletion, *i.e.* seven days after DT injection or 12 hours after antibody injection, as well as three days afterwards (Figure 4A). Different anti-platelet antibodies were applied and compared with the iDTR system: while the antibodies anti-GPIIb α (R300) and 6A6-IgG2A rapidly induced stable thrombocytopenia of different degree within two hours, anti-mouse thrombocyte serum gradually reduced platelet counts to $10.8\pm 9.8\%$ within 12 hours (Figure 4B). Depletion with antibodies or serum did not significantly increase the expression of P-selectin on the remaining platelets, but seven days after first DT administration, the remaining $0.2\pm 0.2\%$ platelets of iDTR^{Plt} mice showed

slightly increased reactivity (Figure 4C). However, in comparison with a positive control of PAR4-AP stimulated blood, platelet activation in iDTR^{Plt} mice was still minor. As expected, thrombocytopenia resulted in decreased plasma CXCL4 concentrations compared to basal levels when using R300, serum or the iDTR model (Figure 4D), underlining the lack of platelet activation upon induced thrombocytopenia. This is also reflected by normal platelet-leukocyte-aggregate (PLA) formation (Figure 4E).

The iDTR model outperforms antibody-based platelet depletion in transfusion studies

As a next step, we compared the iDTR model with antibody-based platelet depletion as a potential tool for platelet transfusion. DT treatment started seven days and R300 (4 $\mu\text{g}/\text{mL}$) was administered 12 hours prior to trans-

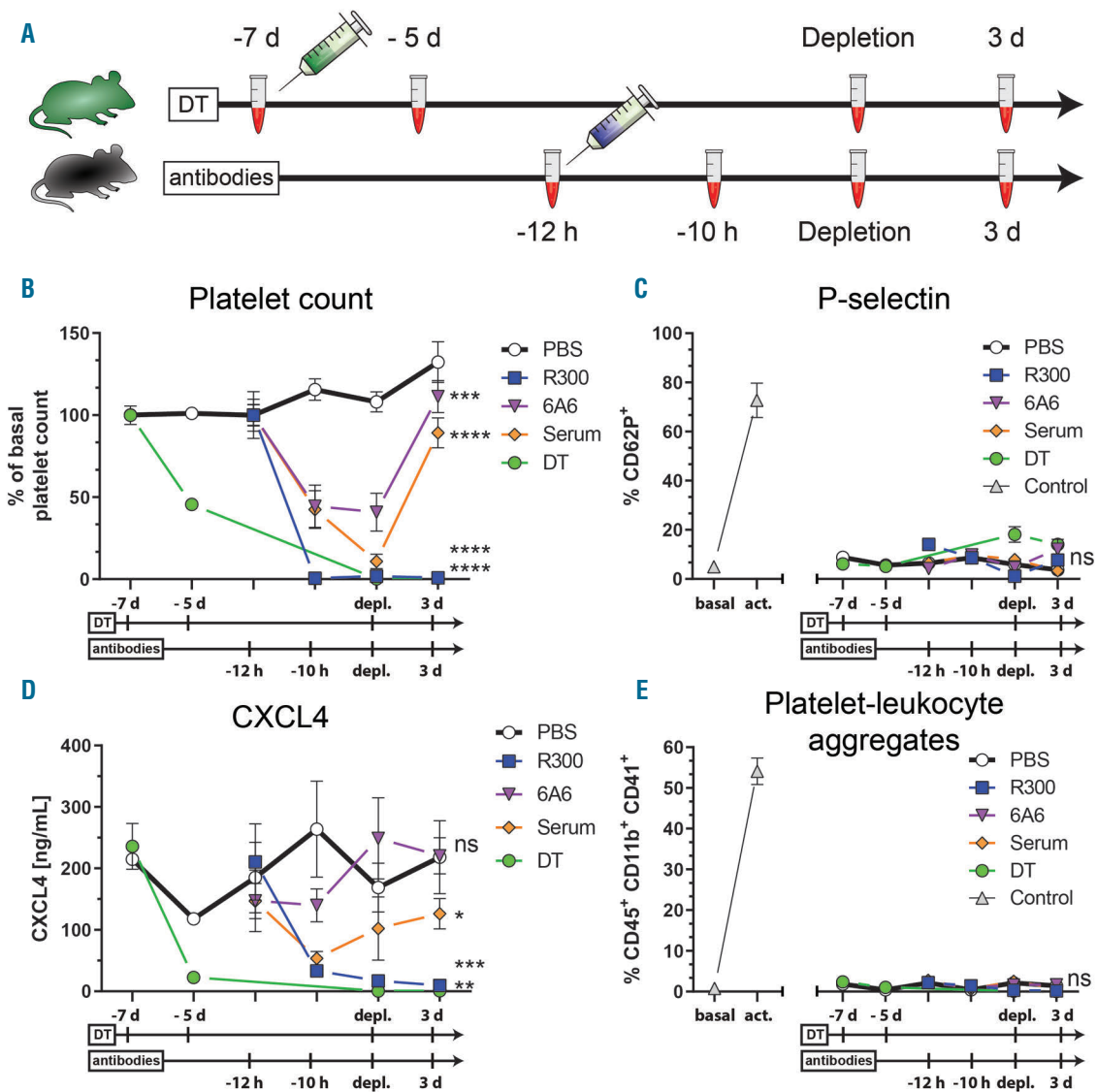


Figure 4. Neither antibody-based nor diphtheria toxin-induced thrombocytopenia cause platelet activation. (A) Graphical overview of depletion comparison. Diphtheria toxin (DT) treatment started seven days (d) prior to stable depletion and R300 treatment 12 hours (h) prior to stable depletion. Blood sampling time points are indicated as reaction tubes. (B) Percentage of platelet counts, relative to initial counts. (C) Percentage CD62P⁺ of CD41⁺ events in diluted whole blood, with PAR4-AP-activated positive controls. (D) CXCL4 plasma concentrations. (E) Percentage CD45⁺ of CD11b⁺, CD45⁺ events in whole blood, with PAR4-AP activated positive controls (n=4-5).

fusion. Efficacy of transfusion was analyzed 2, 24, 48 and 72 hours after platelet injection (Figure 5A). To differentiate between endogenous and transfused platelets, platelets were labeled *ex vivo* with a fluorescent antibody directed against murine GPIIb β . Platelet counts dropped to $0.2 \pm 0.05\%$ of baseline in iDTR^{Pit} mice and to $0.5 \pm 0.2\%$ in R300-treated mice. Theoretically, transfusion of all platelets, calculated by estimating a blood volume of 77-80 $\mu\text{L/g}$ mouse,^{11,12} would have reached 62.5-65% of basal platelets counts. In iDTR^{Pit} mice, platelet transfusion

raised platelet counts to $34.8 \pm 19.2\%$ after two hours, whereas $33.6 \pm 18.7\%$ of platelets were of exogenous origin. In contrast, platelet counts of R300-treated mice remained at $0.5 \pm 0.2\%$ after transfusion, with $0.1 \pm 0.1\%$ of platelets being of exogenous origin. Counts of endogenous platelets remained stable in iDTR^{Pit} mice, while R300 treatment was unable to maintain thrombocytopenia at day 3 (Figure 5B). Lower concentrations of R300 mitigated depletion and enhanced transfusion efficacy, indicating that excess antibody removed newly transfused platelets

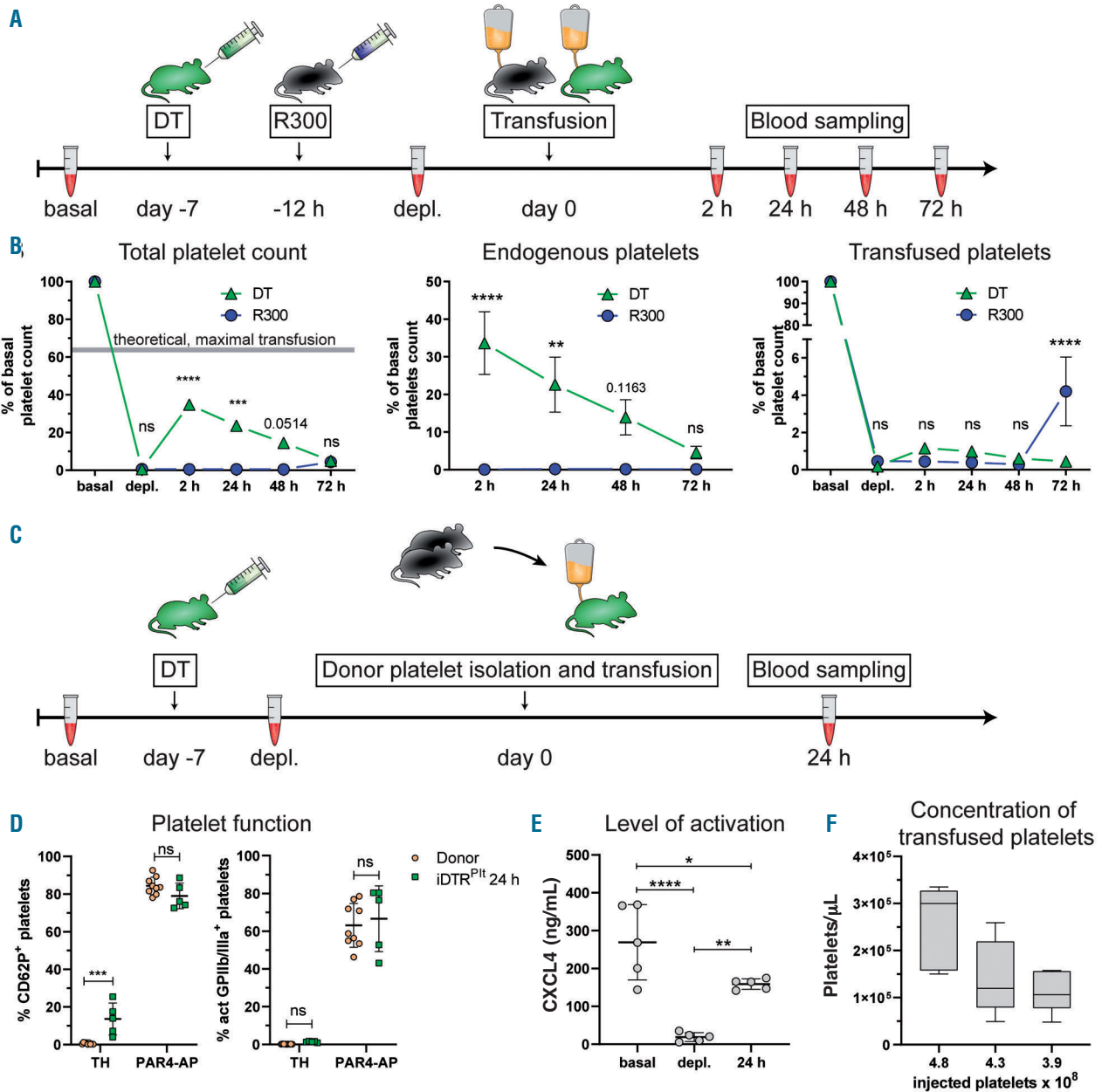


Figure 5. Platelet transfusion efficacy and donor platelet function analysis of iDTR^{Pit} mice. (A) Graphical overview for comparison of platelet transfusion. Diphtheria toxin (DT) treatment started seven days prior to transfusion and R300 treatment 12 hours (h) prior to transfusion. Blood was taken at basal and depleted state, and 2, 24, 48 and 72 hours after transfusion. (B) Percentage of total, endogenous and transfused platelet counts, relative to initial counts. Transfused platelets were labeled with an anti-GPIIb β -Dylight649 antibody. Theoretical, maximal transfusion is depicted as grey area (n=5). (C) Graphical overview of donor platelet function evaluation. DT treatment started seven days prior to transfusion and blood was taken at basal and depleted state, and 24 hours after transfusion. (D) Comparison of percentage of CD62P⁺ and activated GPIIb/IIIa⁺ platelets in whole blood, freshly drawn from donors and after circulating for 24 hours in iDTR^{Pit} mice (n=4-9). (E) Concentration of plasma CXCL4 of iDTR^{Pit} mice at basal and depleted levels, and 24 hours after platelet transfusion (n=5). (F) Concentration of circulating exogenous platelets after transfusion of indicated numbers of platelets (n=5-10).

(*Online Supplementary Figure S2A-B*). Platelet isolation did not lead to increased basal activation but reduces the responsiveness of washed platelets to PAR4 stimulation as compared to whole blood (*Online Supplementary Figure S2C*). These data indicate that genetic ablation of platelets results in a much higher platelet transfusion efficacy. In antibody-mediated models, even upon adjustment of platelet depletion, transfusion efficacy is lower and purity of circulating exogenous platelets cannot be maintained.

Transfused platelets are fully functional

Next, we examined the function of transfused platelets. The activation status and platelet reactivity of donor platelets was analyzed immediately after blood drawing and 24 hours after transfusion into platelet-depleted iDTR^{Pit} mice (Figure 5C). While donor platelets showed low levels of platelet activation marker (surface expression of CD62P and GPIIb/IIIa activation) before transfusion, surface expression of CD62P was slightly - though significantly - increased 24 hours after transfusion. In contrast, GPIIb/IIIa activation remained at the initial level (Figure 5D). Donor platelets were fully responsive to PAR4 stimulation after 24 hours of circulation (Figure 5D). In addition, we evaluated plasma levels of CXCL4 to indirectly determine indications for *in vivo* platelet activation. As shown in Figure 4D, depletion of platelets led to a profound reduction of CXCL4 in plasma. Transfusion of platelets increased CXCL4 concentration although it did not reach basal levels, which can be explained by the reduced number of platelets. Noteworthy, basal CXCL4 levels with each mouse's endogenous platelets, had a higher variation than those 24 hours later where all iDTR^{Pit} mice received platelets from the same pool (Figure 5E). These data indicate that transfused platelets did not become activated *in vivo*. Of note, concentrations of transfused platelets slightly differed between experiments, and higher concentrations of donor platelets were always reflected by higher platelet counts (Figure 5F). Therefore, concentration of transfused platelets can be adjusted in the circulation, dependent on the number of platelets injected.

Transfused platelets are fully functional *in vivo*

Finally, we verified that transfused platelets are fully functional *in vivo* by analyzing their function in mouse models of inflammation and thrombosis. Moreover, we verified the applicability of our model for examination of genetically modified platelets. First, we checked if platelet transfusion can rescue macrophage recruitment in thrombocytopenic iDTR^{Pit} mice upon sterile inflammation. After seven days of DT treatment iDTR^{Pit} mice received platelet transfusion, and peritonitis was induced by thioglycollate injection. Three days later, peritoneal macrophages were isolated, and the number of recruited cells was compared between WT, iDTR^{Pit} and iDTR^{Pit} mice that received platelet transfusion (Figure 6A). Compared to WT mice, thrombocytopenic iDTR^{Pit} mice showed a significant reduction in recruited peritoneal leukocytes; the majority were F4/80 positive macrophages, which was restored by platelet transfusion. In thrombocytopenic mice, leukocyte recruitment was reduced to 30.9% of WT counts. Platelet transfusion reverted macrophage counts back to 92.1% of WT levels, thus confirming that transfused platelets successfully fostered macrophages extravasation to the site of inflammation (Figure 6B-D). Imaging of fluorescently labeled lavage cells confirmed expression of CD45 and

F4/80, thus verifying their identity as macrophages (*Online Supplementary Figure S3A*). Moreover, the activation state and reactivity of platelets transfused into iDTR^{Pit} was not significantly changed after thioglycollate treatment as compared to those of WT mice (*Online Supplementary Figure S3B*).

Lastly, we monitored thrombus formation in platelet-depleted iDTR^{Pit} mice that received donor platelets from *Nbeal2* knockout mice (*Nbeal2*^{-/-}) in a FeCl₃-induced vessel injury model. Knockout of *Nbeal2* leads to α -granule deficiency and thereby severe deficiencies in platelet function and *in vivo* thrombus formation.¹³ FeCl₃ induced thrombus formation in mesenteric arterioles was monitored intravitaly in DT treated iDTR^{Pit} mice that received either *Nbeal2*^{+/+} or *Nbeal2*^{-/-} platelets (Figure 6E). While *Nbeal2*^{+/+} platelets were able to form an occlusive thrombus reaching from vessel wall to vessel wall within 21.4±8.7 minutes, thrombus formation was severely impaired in mice receiving *Nbeal2*^{-/-} platelets (Figure 6F-G and *Online Supplementary Video S1-2*), thus confirming the genetically modified platelet's phenotype¹⁴ in an otherwise unaltered environment.

Discussion

In this study, we compared advantages and disadvantages of genetic and antibody-based platelet depletion methods. Antibody-based methods allow controlled adjustment of thrombocytopenia, while the genetic model selectively targets only endogenous megakaryocytes and platelets and is therefore superior when combined with platelet transfusion.

Antibody-based methods directly and indiscriminately target murine platelet epitopes and cause rapid clearance of platelets from the circulation. Contrarily, genetic depletion with the iDTR system works *via* ablation of megakaryocytes, as a cell type-specific Cre, the PF4-iCre4, controls the expression of iDTR.¹⁵ Thus, megakaryocytes are selectively killed upon DT administration, which prevents endogenous platelet production. Additionally, the decrease of platelet counts corresponded well to the reported lifespan of murine platelets of about 4.8 days,¹⁰ which is in line with the assumption that platelets are naturally used up^{7,16,17} rather than being actively killed by DT.

In general, the expression of a protein that is normally absent in a cell might lead to an alteration of cellular functions. Thus, we found it important to investigate whether iDTR expressing platelets exhibit normal physiological functions, an aspect that is also important for platelet transfusion experiments. To the best of our knowledge, our study is the first to thoroughly analyze platelet function of mice expressing iDTR in megakaryocytes and thus also on the platelet surface. We tested the classical platelet activators thrombin and collagen, as well as agonists that selectively trigger P2Y_{1/12}, PAR4 and GPVI receptors. The fact that iDTR-expressing platelets did not show any noteworthy difference in activation, granule secretion, and aggregation compared to controls supports the notion that these platelets can be considered normal and thus do not cause any unwanted side-effects. As a non-classical function, we analyzed platelet-leukocyte aggregate formation, but were unable to detect any alterations to WT mice.

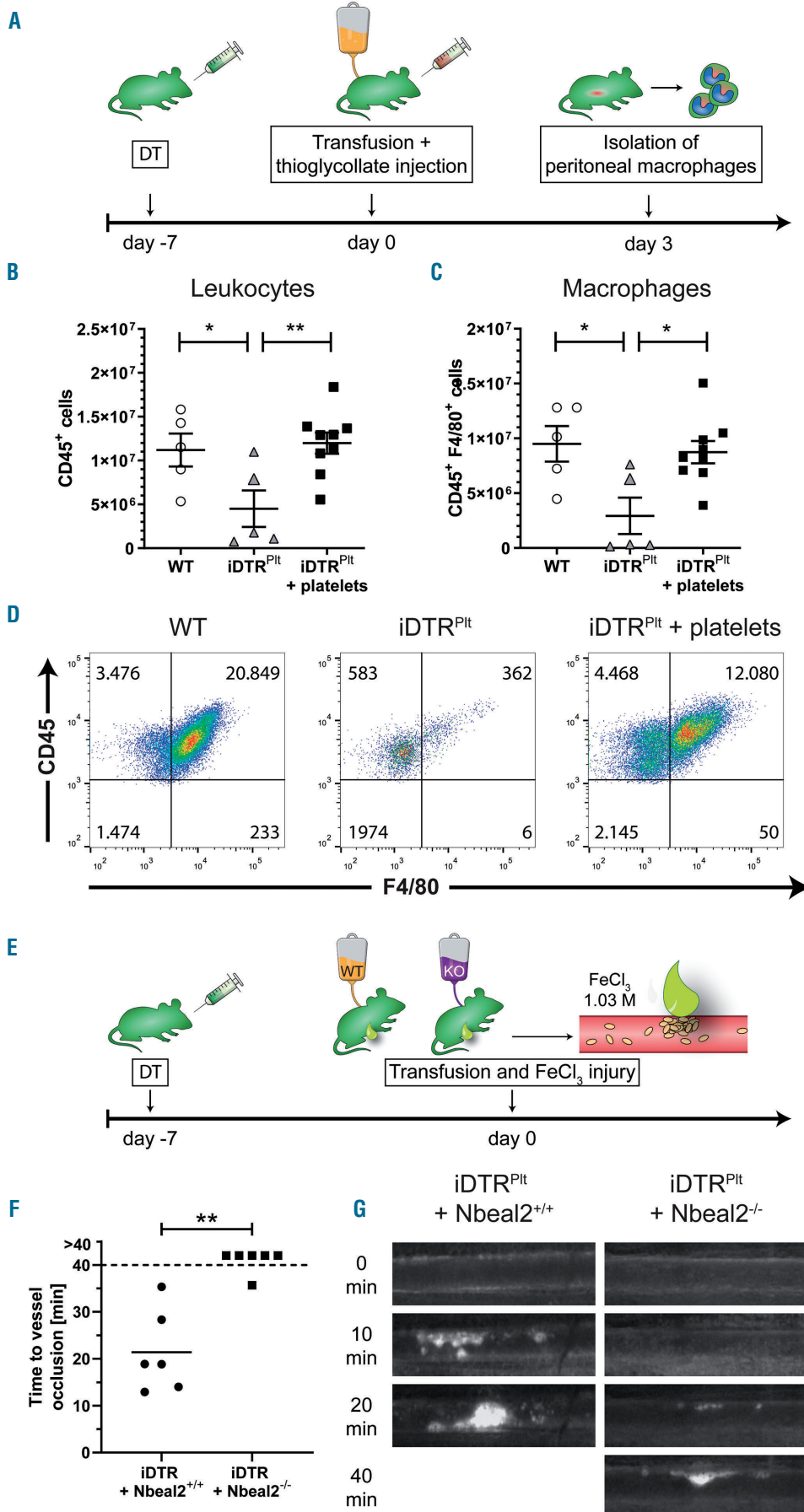


Figure 6. Platelet function and phenotype remains intact after transfusion. (A) Time plan of macrophage recruitment after sterile peritonitis. Seven days after diphtheria toxin (DT) treatment of wild-type (WT) and iDTR^{Pit} mice, one group of iDTR^{Pit} mice received platelet transfusion, followed by thioglycollate injection. After three days peritoneal macrophages were isolated and quantified. (B) Recruited CD45⁺ cells and (C) CD45⁺ F4/80⁺ cells per mouse (n=5-9, mean ± standard error of the mean [SEM]). (D) Representative blots of peritoneal lavage cells of WT mice, iDTR^{Pit} mice and iDTR^{Pit} mice with platelet transfusion. (E) Graphical overview of FeCl₃ induced thrombus formation experiments. Seven days after DT treatment of iDTR^{Pit} mice, one group received Nbeal2^{+/+} and the other Nbeal2^{-/-} platelets, followed by induction of a thrombus in mesenteric arterioles by topical application of FeCl₃. (F) Time to stable vessel occlusion. Each symbol represents a mesenteric arteriole. (G) Representative images of thrombus formation in arterioles (n=6).

However, MPV was slightly but significantly increased, adding to the contradictory discussion in the literature. While some studies failed to observe a difference during depletion,⁷ we, like others,¹⁶ detected an increase of MPV during the thrombocytopenic phase. We hypothesize that the few “remaining” platelets were freshly produced by megakaryocytes that were not yet eliminated. These young platelets are reported to have a higher MPV¹⁸ and

are therefore thought to be more reactive.¹⁹ Clinically, MPV distinguishes between different etiologies of thrombocytopenia.²⁰ Thus, it may be a more sensitive biomarker than platelet count in a variety of disorders, yet it is discussed controversially for different diseases. MPV is higher in patients with acute coronary syndrome (ACS), compared to those with non-cardiac chest pain,²¹ associates with poor prognosis after ACS²¹ and closely correlates

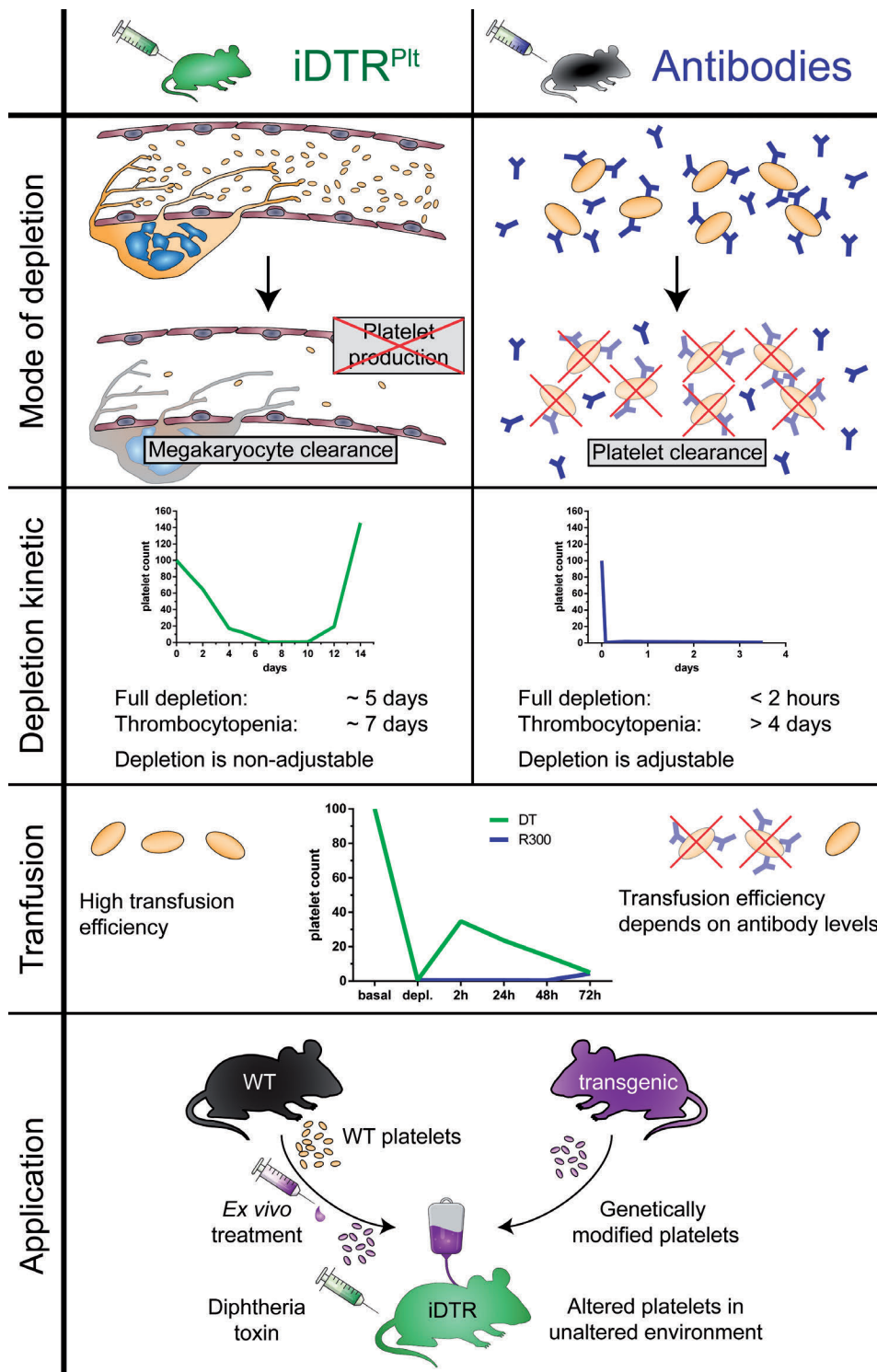


Figure 7. Comparison of platelet depletion methods. Depletion principle, depletion kinetic and transfusion efficacy are depicted for the iDTR and antibody-based models, as well as possible applications of the iDTR model.

with arterial stiffness.²² However, diagnosis of coronary artery disease does not associate with MPV.²³ Further, viruses can alter MPV in both directions, depending on the virus species,^{24,25} and a high MPV can be used to differentiate between gastric ulcer and gastric cancer.²⁶

In addition to increased MPV, we also measured increased P-selectin expression of the remaining platelets at day 7 of depletion, an observation also reported by others.⁷ Nevertheless, plasma CXCL4 levels, a surrogate marker for platelet degranulation, were not increased, further underlining that platelets were not activated in circulation.

Like the iDTR system, also antibody-based methods, which induce active and rapid clearance of platelets, did not lead to increased plasma CXCL4 levels or platelet activation. In contrast to the iDTR model, antibody-based methods have the advantage that the amount of injected antibody can be fine-tuned to adjust the degree of thrombocytopenia. The iDTR model completely inhibits platelet production, thus thrombocytopenia cannot be adjusted by titrating DT concentration. This is evident from a rebound effect with rapidly increasing platelet counts after reappearance of megakaryocytes. This phenomenon was also observed by others either after short term treatment, where it was used to study young, reticulated platelets.¹⁶ In contrast, others were able to keep platelet counts stably low until day 17 using a single injection of 400 ng DT,⁷ whereas we observed a rebound at day 14. The reason for this discrepancy is currently unclear. Additionally, continuous depletion of platelets with the iDTR model has been reported for six weeks.²⁷ However, at day 12-14 we already observed hematomata and impaired wound healing, thus we decided to anesthetize mice for subcutaneous injections to reduce the risk of injuries. Additionally, we observed that female mice tolerated the treatment better than males. This suggests that females are more suitable as recipients during transfusion experiments, whereas untreated males can be readily used as platelet donors.

However, regarding platelet transfusions, the iDTR^{Pit} model shows a significantly better performance than antibody-based models. In the latter, newly transfused platelets are rapidly depleted by an excess of circulating antibodies, which decreases transfusion efficacy and shortens thrombocytopenia by removing the depleting

antibodies. This became evident, when endogenous platelet counts of R300 antibody-treated mice increased again at day 3 after transfusion although the dosage of antibody used in our transfusion experiment ensured stable platelet depletion over 3.5 days. In contrast to antibody-based platelet depletion, endogenous platelet counts of iDTR^{Pit} mice remained unaffected by the introduction of new platelets, further demonstrating the superiority of the iDTR system.

Finally, we could show that transfused platelets were fully functional by quantifying macrophage recruitment after induction of sterile peritonitis. Platelets are immunomodulatory cells and play a pivotal role in recruiting leukocytes to the site of inflammation.²⁸

In conclusion we were able to delineate advantages and disadvantages of different platelet depletion methods (as summarized in Figure 6). While the iDTR model targets platelets indirectly *via* megakaryocytes, antibody-based models deplete platelets directly. Hence, stable thrombocytopenia is reached with antibodies and anti-mouse thrombocyte serum within 2 or 12 hours, respectively, while the iDTR model takes about five days. Antibody-based methods allow adjustment of platelet counts, depending on the amount of used reagent, whereas the iDTR model results in almost complete thrombocytopenia which may be disadvantageous in certain experimental settings. However, the iDTR model is much more efficient in platelet transfusion compared to antibody based methods, in which freshly transfused platelets and endogenous platelets are scavenged to the same degree.

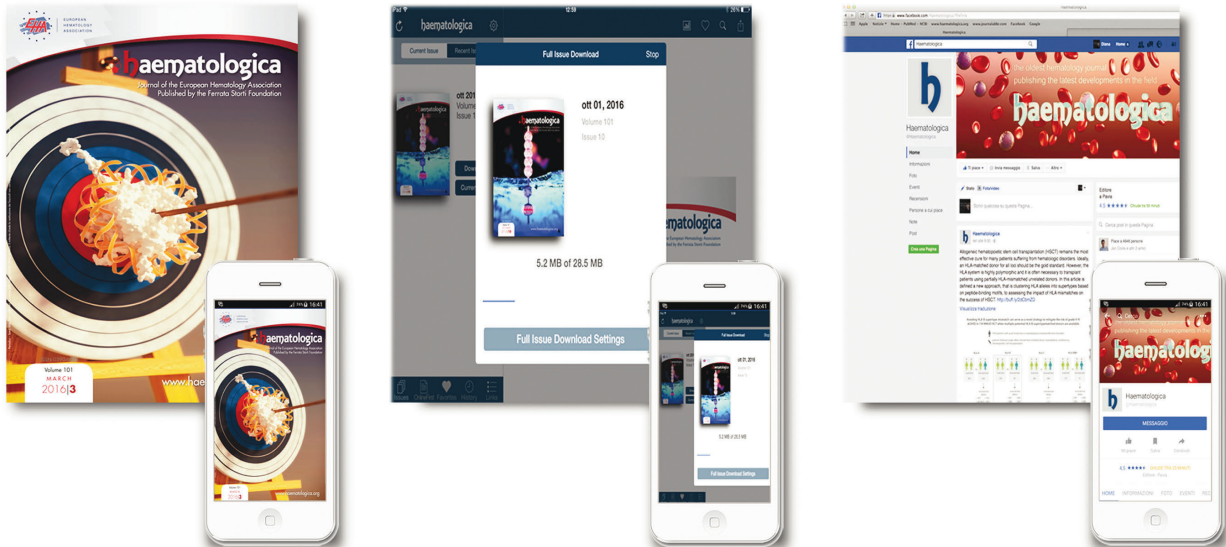
Altogether, the iDTR model refines platelet transfusion and simplifies its experimental setup, thus reducing the number of required animals. The possibility to transfuse *ex vivo*-treated platelets or platelets from any global knockout or knockin mouse strain replaces the need to generate lineage-specific conditional mouse strains, further reducing required animal numbers. Moreover, as transfusion of human megakaryocytes²⁹ and platelets³⁰ into mice has been successfully established, the iDTR model could be potentially useful to evaluate platelet concentrate preparations and storage conditions for clinical applications. Therefore, employing the iDTR-model for platelet depletion and transfusion experiments can facilitate multiple angles of platelet research.

References

- Assinger A, Kral JB, Yaiw KC, et al. Human cytomegalovirus-platelet interaction triggers toll-like receptor 2-dependent proinflammatory and proangiogenic responses. *Arterioscler Thromb Vasc Biol.* 2014;34(4):801-809.
- Linden MD, Jackson DE. Platelets: pleiotropic roles in atherogenesis and atherothrombosis. *Int J Biochem Cell Biol.* Vol. 42. Netherlands: 2010 Elsevier Ltd. 2010:1762-1766.
- Starlinger P, Haegele S, Offensperger F, et al. The profile of platelet alpha-granule released molecules affects postoperative liver regeneration. *Hepatology.* 2016;63(5):1675-1688.
- Tiedt R, Schomber T, Hao-Shen H, Skoda RC. Pf4-Cre transgenic mice allow the generation of lineage-restricted gene knockouts for studying megakaryocyte and platelet function in vivo. *Blood.* 2007;109(4):1503-1506.
- Nagy Z, Vogtle T, Geer MJ, et al. The Gp1ba-Cre transgenic mouse: a new model to delineate platelet and leukocyte functions. *Blood.* 2019;133(4):331-343.
- Honjo T, Nishizuka Y, Kato I, Hayaishi O. Adenosine diphosphate ribosylation of aminoacyl transferase II and inhibition of protein synthesis by diphtheria toxin. *J Biol Chem.* 1971;246(13):4251-4260.
- Wuescher LM, Takashima A, Worth RG. A novel conditional platelet depletion mouse model reveals the importance of platelets in protection against *Staphylococcus aureus* bacteremia. *J Thromb Haemost.* 2015;13(2):303-313.
- Yamaizumi M, Mekada E, Uchida T, Okada Y. One molecule of diphtheria toxin fragment A introduced into a cell can kill the cell. *Cell.* 1978;15(1):245-250.
- Chang T, Neville DM, Jr. Demonstration of diphtheria toxin receptors on surface membranes from both toxin-sensitive and toxin-resistant species. *J Biol Chem.* 1978;253(19):6866-6871.
- Manning KL, Novinger S, Sullivan PS, McDonald TP. Successful determination of platelet lifespan in C3H mice by *in vivo* biotinylation. *Lab Anim Sci.* 1996;46(5):545-548.
- Harkness JE, Wagner JE. *The Biology and Medicine of Rabbits and Rodents* (ed 3rd). Philadelphia: Lea & Febiger. 1989.
- Mitruka BM. Clinical biochemical and hematological reference values in normal experimental animals and normal humans

- (ed 2nd ed.). New York: Masson Pub. USA. c1981.
13. Kahr WH, Lo RW, Li L, et al. Abnormal megakaryocyte development and platelet function in Nbeal2(-/-) mice. *Blood*. 2013; 122(19):3349-3358.
 14. Deppermann C, Cherpokova D, Nurden P, et al. Gray platelet syndrome and defective thrombo-inflammation in Nbeal2-deficient mice. *J Clin Invest*. 2013 July 1. [Epub ahead of print]
 15. Buch T, Heppner FL, Tertilt C, et al. A Cre-inducible diphtheria toxin receptor mediates cell lineage ablation after toxin administration. *Nat Methods*. 2005;2(6):419-426.
 16. Angenieux C, Maitre B, Eckly A, Lanza F, Gachet C, de la Salle H. Time-Dependent Decay of mRNA and Ribosomal RNA during Platelet Aging and Its Correlation with Translation Activity. *PLoS One*. 2016;11(1):e0148064.
 17. Miyachi H, Reinhardt JW, Otsuru S, et al. Bone marrow-derived mononuclear cell seeded bioresorbable vascular graft improves acute graft patency by inhibiting thrombus formation via platelet adhesion. *Int J Cardiol*. 2018;266:61-66.
 18. Balduini CL, Noris P, Spedini P, Belletti S, Zambelli A, Da Prada GA. Relationship between size and thiazole orange fluorescence of platelets in patients undergoing high-dose chemotherapy. *Br J Haematol*. 1999;106(1):202-207.
 19. Guthikonda S, Alviar CL, Vaduganathan M, et al. Role of reticulated platelets and platelet size heterogeneity on platelet activity after dual antiplatelet therapy with aspirin and clopidogrel in patients with stable coronary artery disease. *J Am Coll Cardiol*. 2008; 52(9):743-749.
 20. Schmoeller D, Picarelli MM, Paz Munhoz T, Poli de Figueiredo CE, Staub HL. Mean platelet volume and immature platelet fraction in autoimmune Disorders. *Front Med (Lausanne)*. 2017;4:146.
 21. Leader A, Pereg D, Lishner M. Are platelet volume indices of clinical use? A multidisciplinary review. *Ann Med*. 2012;44(8):805-816.
 22. Panova-Noeva M, Arnold N, Hermanns MI, et al. Mean platelet volume and arterial stiffness - clinical relationship and common genetic variability. *Sci Rep*. 2017;7:40229.
 23. Ball S, Arevalo M, Wongsangsak S, Dennis JA, Nugent K. Implications of mean platelet volume in health and disease: A large population study on data from National Health and Nutrition Examination Survey. *Thromb Res*. 2019;175:90-94.
 24. Lv L, Li Y, Fan X, Xie Z, Liang H, Shen T. HCV coinfection aggravated the decrease of platelet counts, but not mean platelet volume in chronic HIV-infected patients. *Sci Rep*. 2018;8(1):17497.
 25. Assinger A. Platelets and infection - an emerging role of platelets in viral infection. *Front Immunol*. 2014;5:649.
 26. Yun ZY, Li N, Zhang X, et al. Mean platelet volume, platelet distribution width and carcinoembryonic antigen to discriminate gastric cancer from gastric ulcer. *Oncotarget*. 2017;8(37):62600-62605.
 27. Bruns I, Lucas D, Pinho S, et al. Megakaryocytes regulate hematopoietic stem cell quiescence through CXCL4 secretion. *Nat Med*. 2014;20(11):1315-1320.
 28. Badmya S, Schrottmaier WC, Kral JB, et al. Platelets mediate oxidized low-density lipoprotein-induced monocyte extravasation and foam cell formation. *Arterioscler Thromb Vasc Biol*. 2014;34(3):571-580.
 29. Wang Y, Hayes V, Jarocha D, et al. Comparative analysis of human ex vivo-generated platelets vs megakaryocyte-generated platelets in mice: a cautionary tale. *Blood*. 2015;125(23):3627-3636.
 30. Huo Y, Schober A, Forlow SB, et al. Circulating activated platelets exacerbate atherosclerosis in mice deficient in apolipoprotein E. *Nat Med*. 2003;9(1):61-67.

RESEARCH, READ & CONNECT



We reach more than
6 hundred thousand readers each year

The first Hematology Journal in Europe

Impressions YTD

9,621,645

Digital Readers

4,431

Total Audience

554,484

Worldwide rank

7th

Impact factor

7.570

Total citations

16,255



Journal of the Ferrata Storti Foundation

